



Chemical Kinetics and Photochemical Data for Use in Atmospheric Studies

Evaluation Number 17

NASA Panel for Data Evaluation:

S. P. Sander
R. R. Friedl
NASA/Jet Propulsion Laboratory

J. R. Barker
University of Michigan

D. M. Golden
Stanford University

M. J. Kurylo
**Goddard Earth Sciences, Technology and
Research Program**

P. H. Wine
Georgia Institute of Technology

J. P. D. Abbatt
University of Toronto

J. B. Burkholder
NOAA Earth System Research Laboratory

C. E. Kolb
Aerodyne Research, Inc.

G. K. Moortgat
Max-Planck Institute for Chemistry

R. E. Huie
V. L. Orkin
**National Institute of Standards and
Technology**

**National Aeronautics and
Space Administration**

**Jet Propulsion Laboratory
California Institute of Technology
Pasadena, California**

June 10, 2011

The research described in this publication was carried out by the Jet Propulsion Laboratory, California Institute of Technology, under a contract with the National Aeronautics and Space Administration.

Reference herein to any specific commercial product, process, or service by trade name, trademark, manufacturer, or otherwise, does not constitute or imply its endorsement by the United States Government or the Jet Propulsion Laboratory, California Institute of Technology. Copyright 2010. All rights reserved.

ABSTRACT

This is the seventeenth in a series of evaluated sets of rate constants and photochemical cross sections compiled by the NASA Panel for Data Evaluation.

The data are used primarily to model stratospheric and upper tropospheric processes, with particular emphasis on the ozone layer and its possible perturbation by anthropogenic and natural phenomena.

Copies of this evaluation are available in electronic form and may be printed from the following Internet URL:

<http://jpldataeval.jpl.nasa.gov/>

This evaluation should be cited using the following format:

Sander, S. P., J. Abbatt, J. R. Barker, J. B. Burkholder, R. R. Friedl, D. M. Golden, R. E. Huie, C. E. Kolb, M. J. Kurylo, G. K. Moortgat, V. L. Orkin and P. H. Wine "Chemical Kinetics and Photochemical Data for Use in Atmospheric Studies, Evaluation No. 17," JPL Publication 10-6, Jet Propulsion Laboratory, Pasadena, 2011 <http://jpldataeval.jpl.nasa.gov>.

TABLE OF CONTENTS

INTRODUCTION	vi
1.1 Basis of the Recommendations	viii
1.2 Scope of the Evaluation.....	viii
1.3 Format of the Evaluation.....	ix
1.4 Computer Access	ix
1.5 Data Formats	ix
1.6 Units.....	ix
1.7 Noteworthy Changes in this Evaluation	ix
1.8 Acknowledgements	xii
1.9 References	xii
SECTION 1. BIMOLECULAR REACTIONS	1-1
1.1 Introduction	1-1
1.2 Uncertainty Estimates	1-2
1.3 Notes to Table 1	1-35
1.4 References	1-132
SECTION 2. TERMOLICULAR REACTIONS	2-1
2.1 Introduction	2-1
2.2 Low-Pressure-Limiting Rate Constant, $k_o^x(T)$	2-2
2.3 Temperature Dependence of Low-Pressure Limiting Rate Constants: T^n	2-2
2.4 High-Pressure-Limit Rate Constants, $k_\infty(T)$	2-3
2.5 Temperature Dependence of High-Pressure-Limiting Rate Constants: T^m	2-3
2.6 Uncertainty Estimates	2-3
2.7 Notes to Table 2	2-8
2.8 References	2-20
SECTION 3. EQUILIBRIUM CONSTANTS	3-1
3.1 Format	3-1
3.2 Definitions.....	3-1
3.3 Notes to Table 3	3-5
3.4 References	3-10
SECTION 4. PHOTOCHEMICAL DATA	4-1
4.1 Format and Error Estimates.....	4-5
4.2 Halocarbon Absorption Cross Sections and Quantum Yields	4-6
4.3 Web Access to Recommended Data in Text and Graphical Formats.....	4-6
4.4 References	4-11
4A O_x Photochemistry.....	4A-1
References for Section 4A.....	4A-13
4B HO_x Photochemistry	4B-1
References for Section 4B.....	4B-8
4C NO_x Photochemistry	4C-1
References for Section 4C.....	4C-24
4D Organic Photochemistry.....	4D-1
References for Section 4D.....	4D-50
4E FO_x Photochemistry.....	4E-1
References for Section 4E.....	4E-21
4F ClO_x Photochemistry.....	4F-1
References for Section 4F.....	4F-63

4G	BrO _x Photochemistry.....	4G-1
	References for Section 4G.....	4G-51
4H	IO _x Photochemistry.....	4H-1
	References for Section 4H.....	4H-32
4I	SO _x Photochemistry.....	4I-1
	References for Section 4I.....	4I-7
4J	Metal Photochemistry.....	4J-1
	References for Section 4J.....	4J-5
SECTION 5. HETEROGENEOUS CHEMISTRY		5-1
5.1	Introduction	5-1
5.2	Surface Types—Acid/Water, Liquids and Solids	5-2
5.3	Surface Types—Soot and Alumina.....	5-2
5.4	Surface Types—Solid Alkali Halide Salts and Aqueous Salt Solutions	5-4
5.5	Surface Composition and Morphology	5-4
5.6	Surface Porosity	5-5
5.7	Temperature Dependences of Parameters	5-5
5.8	Solubility Limitations.....	5-5
5.9	Data Organization	5-6
5.10	Parameter Definitions.....	5-6
5.11	Mass Accommodation Coefficients and Reversible Uptake Data for Surfaces Other Than Soot.....	5-12
5.12	Notes to Table 5-1	5-15
5.13	Gas/Surface Reaction Probabilities for Surfaces Other Than Soot	5-28
5.14	Notes to Table 5-2.....	5-34
5.15	Soot Surface Uptake Coefficients	5-63
5.16	Notes to Table 5-3.....	5-63
5.17	Henry's Law Constants for Pure Water	5-66
5.18	Notes to Table 5-4.....	5-70
5.19	Ion-Specific Schumpe Parameters.....	5-77
5.20	Henry's Law Constants for Acids	5-78
5.21	Notes to Table 5-6.....	5-79
5.22	References	5-83
APPENDIX A. GAS-PHASE ENTROPY AND ENTHALPY VALUES FOR SELECTED SPECIES AT 298.15 K AND 100 KPA		A-1

I. INTRODUCTION

This compilation of kinetic and photochemical data is the 17th evaluation prepared by the NASA Panel for Data Evaluation. The Panel was established in 1977 by the NASA Upper Atmosphere Research Program Office for the purpose of providing a critical tabulation of the latest kinetic and photochemical data for use by modelers in computer simulations of atmospheric chemistry. Table I-1 lists this publication's editions:

Table I-1: Editions of this Publication

	Edition	Reference
1	NASA RP 1010, Chapter 1	Hudson et al. [1]
2	JPL Publication 79-27	DeMore et al. [2]
3	NASA RP 1049, Chapter 1	Hudson and Reed [3]
4	JPL Publication 81-3	DeMore et al. [4]
5	JPL Publication 82-57	DeMore et al. [5]
6	JPL Publication 83-62	DeMore et al. [6]
7	JPL Publication 85-37	DeMore et al. [7]
8	JPL Publication 87-41	DeMore et al. [8]
9	JPL Publication 90-1	DeMore et al. [9]
10	JPL Publication 92-20	DeMore et al. [10]
11	JPL Publication 94-26	DeMore et al. [11]
12	JPL Publication 97-4	DeMore et al. [12]
13	JPL Publication 00-3	Sander et al. [13]
14	JPL Publication 02-25	Sander et al. [14]
15	JPL Publication 06-2	Sander et al. [15]
16	JPL Publication 09-31	Sander et al. [16]
17	JPL Publication 10-6	Sander et al. [17]

In addition to the current edition, several previous editions are available for download from the website.

Panel members, and their major responsibilities for the current evaluation are listed in Table I-2.

Table I-2: Panel Members and their Major Responsibilities for the Current Evaluation

Panel Members	Responsibility
S. Sander, Chairman	NO _x reactions, editorial review
V. Orkin M. Kurylo	Reactions of OH with halocarbons
D. Golden, J. Barker	Three-body reactions, equilibrium constants, editorial review
R. Huie	Aqueous chemistry, thermodynamic parameters
C. Kolb, J. Abbatt	Heterogeneous chemistry, Na chemistry
R. Friedl	Inorganic ClO _x , BrO _x reactions
J. Burkholder	O _x , HO _x reactions
G. K. Moortgat, J. Burkholder	Photochemistry
P. H. Wine	SO _x reactions, isoprene chemistry

As shown above, each Panel member concentrates his efforts on a given area or type of data. Nevertheless, the Panel's final recommendations represent a consensus of the entire Panel. Each member reviews the basis for all recommendations, and is cognizant of the final decision in every case.

Address communications regarding particular reactions to the appropriate panel member:

S. P. Sander
R. R. Friedl
NASA/Jet Propulsion Laboratory
M/S 183-901
4800 Oak Grove Drive
Pasadena, CA 91109
Stanley.Sander@jpl.nasa.gov
Randall.Friedl@jpl.nasa.gov

D. M. Golden
Department of Mechanical Engineering
Stanford University
Bldg 520
Stanford, CA 94305
david.golden@stanford.edu

M. J. Kurylo
Goddard Earth Sciences, Technology, and
Research (GESTAR) Program
NASA Goddard Space Flight Center
Universities Space Research Association
Mail Stop 610.6
8800 Greenbelt Road
Greenbelt, MD 20771
Michael.J.Kurylo@nasa.gov

J. P. D. Abbatt
Department of Chemistry
University of Toronto
80 St. George Street
Toronto, ON M5S 3H6 CANADA
jabbatt@chem.utoronto.ca

C. E. Kolb
Aerodyne Research Inc.
45 Manning Rd.
Billerica, MA 01821
kolb@aerodyne.com

J. R. Barker
Department of Atmospheric, Oceanic, and
Space Sciences
1520 Space Research Building
University of Michigan
2455 Hayward Street
Ann Arbor, MI 48109-2143
jrbarker@umich.edu

G. K. Moortgat
Max-Planck-Institut für Chemie
Atmospheric Chemistry Division
Postfach 3060
55020 Mainz
Germany
Geert.Moortgat@mpic.de

V. L. Orkin , R. E. Huie
Chemical and Biochemical Reference Data
Division
National Institute of Standards and
Technology (NIST)
100 Bureau Drive, Stop 8320
Gaithersburg, MD 20899-8320
Vladimir.Orkin@nist.gov
rehuie@verizon.net

P. H. Wine
School of Chemistry and Biochemistry
Georgia Institute of Technology
901 Atlantic Dr. NW
Atlanta, GA 30332-0400
paul.wine@chemistry.gatech.edu

J. B. Burkholder
Chemical Sciences Division, R/CSD6
Earth System Research Laboratory
National Oceanic and Atmospheric
Administration (NOAA)
325 Broadway
Boulder, CO 80305-3328
James.B.Burkholder@noaa.gov

I.1 Basis of the Recommendations

The recommended rate data and cross sections are based on laboratory measurements. In order to provide recommendations that are as up-to-date as possible, preprints and written private communications are accepted, but only when it is expected that they will appear as published journal articles. Under no circumstances are rate constants adjusted to fit observations of atmospheric concentrations. The Panel considers the question of consistency of data with expectations based on the theory of reaction kinetics, and when a discrepancy appears to exist this fact is pointed out in the accompanying note. The major use of theoretical extrapolation of data is in connection with three-body reactions, in which the required pressure or temperature dependence is sometimes unavailable from laboratory measurements, and can be estimated by use of appropriate theoretical treatment. In the case of important rate constants for which no experimental data are available, the panel may provide estimates of rate constant parameters based on analogy to similar reactions for which data are available.

I.2 Scope of the Evaluation

In the past (releases 1-12 of this evaluation) it has been the practice of the Panel to reevaluate the entire set of reactions with individual Panel members taking responsibility for specific chemical families or processes. In recent years, the upper troposphere and lower stratosphere (UT/LS) have become the primary areas of focus for model calculations and atmospheric measurements related to studies of ozone depletion and climate change. Because the UT/LS is a region of relatively high chemical and dynamical complexity, a different approach has been adopted for future releases of the evaluation. Specifically, the entire reaction set of the data evaluation will no longer be re-evaluated for each release. Instead, specific subsets will be chosen for re-evaluation, with several Panel members working to develop recommendations for a given area. This approach will make it possible to treat each subset in greater depth, and to expand the scope of the evaluation to new areas. It is the aim of the Panel to consider the entire set of kinetics, photochemical and thermodynamic parameters every three review cycles. Each release of the evaluation will contain not only the new evaluations, but also recommendations for every process that has been considered in the past. In this way, the tables for each release will constitute a complete set of recommendations.

It is recognized that important new laboratory data may be published that lie outside the specific subset chosen for re-evaluation. In order to ensure that these important data receive prompt consideration, each evaluation will also have a “special topics” category. Feedback from the atmospheric modeling community is solicited in the selection of reactions for this category.

For the current evaluation, the specific subsets include the following:

- Reactions of $O(^1D)$
- Reactions of OH with halocarbons
- Reactions of sulfur compounds
- Initial steps in isoprene oxidation
- Photochemistry of O_3 , organic compounds and halogen oxides
- Heterogeneous processes on liquid water, water ice, alumina and solid alkali halide salts
- Gas-liquid solubility (Henry's Law Constants and Schumpe Parameters)
- Thermodynamic parameters (entropy and enthalpy of formation)

I.3 Format of the Evaluation

Changes or additions to the data tables are indicated by shading. A new entry is completely shaded, whereas a changed entry is shaded only where it has changed. In some cases only the note has been changed, in which case the corresponding note number in the table is shaded.

I.4 Computer Access

This document is available online in the form of individual chapters and as a complete document in Adobe PDF (Portable Data File) format. Files may be downloaded from <http://jpldataeval.jpl.nasa.gov/>. This document is not available in printed form from JPL.

The tables of recommended cross sections from this evaluation can be downloaded from the spectral atlas of the Max-Planck Institute for Chemistry at: <http://www.atmosphere.mpg.de/enid/2295>

To receive email notification concerning releases of new publications and errata, a mailing list is available. To subscribe, send a blank message to join-jpl-dataeval@list.jpl.nasa.gov with “Subscribe” (without quotes) in the subject line.

For more information, contact Stanley Sander (Stanley.Sander@jpl.nasa.gov).

I.5 Data Formats

In Table 1 (Rate Constants for Bimolecular Reactions) the reactions are grouped into the classes O_x, HO_x, NO_x, Organic Compounds, FO_x, ClO_x, BrO_x, IO_x, SO_x and Metal Reactions. The data in Table 2 (Rate Constants for Association Reactions) are presented in the same order as the bimolecular reactions. The presentation of photochemical cross section data follows the same sequence.

I.6 Units

Rate constants are given in units of concentration expressed as molecules per cubic centimeter and time in seconds. That is, for first-, second-, and third-order reactions, units of *k* are s⁻¹, cm³ molecule⁻¹ s⁻¹, and cm⁶ molecule⁻² s⁻¹, respectively. Cross sections are expressed as cm² molecule⁻¹, base e.

I.7 Noteworthy Changes in this Evaluation

I.7.1 Bimolecular Reactions (Section 1)

The uncertainties for all O(¹D) and HO_x rate coefficients in Table 1 have been evaluated and recommendations, at the 1σ level, that are representative of the available experimental data are reported. O(¹D) reactions that include a combination of physical quenching of O(¹D) to the ground electronic state, O(³P), as well as chemical reaction are identified with “Quenching and Reaction” given as the reaction products. The notes for these reactions contain a summary of the available branching ratio data to be used in atmospheric model calculations. Upper limits for O(¹D) + perfluorocarbon (PFCs) and SF₅CF₃ rate coefficients are now reported in Table 1. The rate coefficient for the HO₂ + HO₂ reaction has been revised and an entry for the HO₂ reaction with the HO₂-H₂O adduct, which is predicted to be present at significant levels in the atmosphere, has been added to Table 1.

A comprehensive review of the reactions of industrial and naturally occurring halogenated hydrocarbons with OH radicals was conducted for this evaluation. A number of reactions between OH and halogenated hydrocarbons listed in the Annex C to the Montreal Protocol, the IPCC Reports, and the Scientific Assessment of Ozone Depletion: 2010 were added to this evaluation along with those for CH₃CHO, C₂H₅OH and CH₃C(O)OH. The reactions of isoprene with OH, Cl, and Br were added as

well. In doing so, attempts were made to understand and reconcile apparent differences between the results of absolute and relative rate measurements for some of the reactions. Relative rate constants were “renormalized” using the revised recommendations for the reference reactions. Thus, the re-evaluation procedure was an iterative one, since relative rate studies themselves were often included as the basis for the rate constant recommendations of these very reference reactions. The recommendations were then checked for self-consistency by seeing if ratios of the recommended rate constants were in agreement with published relative rate measurements. In some cases, disparities may seem to exist. However, it should be recognized that the focus of this re-evaluation was generating recommended rate constants over the temperature range of atmospheric importance (i.e., below 300 K). In a number of cases the temperature dependence of the rate constants noticeably deviates from the standard two-parameter Arrhenius expression when measured over a wider temperature range. In such cases, an Arrhenius expression was fit to the data obtained over the temperature range below 300 K and the recommended parameters, A and E/R, should not be used to calculate the rate constant at higher temperatures. Finally, uncertainty factors (f and g) were carefully reviewed in an attempt to reasonably narrow the rate constant uncertainties for modeling purposes. Previous uncertainty limits were overly conservative in some cases. Finally, in addition to the chemicals mentioned above, several other reactions were reviewed and added to this evaluation.

The section on SO_x reactions has been updated to include all literature through 2009. Fourteen reactions that appeared in Table 1 of Evaluation 15 (JPL 06-2) have been re-evaluated, including reactions of CH₃SCH₃ with OH, NO₃, Cl, IO, and O₃. Reactions of SO₂F₂ are included in Table 1 for the first time, as are the reactions of OH with CH₃SCH₂Cl, Cl₂ with CH₃SCH₃, and BrO with CH₃SH.

Evaluations for reactions of OH, O₃, NO₃, Cl, and Br with CH₂=C(CH₃)CH=CH₂ (isoprene) are included in Table 1 for the first time.

I.7.2 Photochemical Data (Section 4)

Notes have been revised and updated in each sub-section as indicated in Table 4-1.

Photodissociation product channels and energy thresholds, based on the heats of formation given in Appendix A, are reported where possible. The notes for O₂, O₃, and H₂O have been revised to include a more comprehensive review of the literature. New entries have been added in the Organic, FO_x, BrO_x, SO_x, and Metal Photochemistry sub-sections. On the basis of several recent studies, the recommendation for the ClOOCl UV absorption cross sections and photolysis quantum yields, which are important for modeling polar stratospheric ozone depletion, has been revised

I.7.3 Heterogeneous Chemistry (Section 5)

Uptake studies of volatile organic species (VOCs) on water ice surfaces have been included in this evaluation for the first time and uptake of acid gases and their precursors on ice have been updated. Some important uptake processes occurring on alumina, liquid water, sulfuric acid solutions, solid salt, and salt solutions have also been added or updated. The compilation of Henry’s law parameters for pure water has been extended to include a number of additional oxygenated organic and halo-organic compounds. The compilation of Henry’s law parameters for sulfuric acid solutions has also been extended.

I.7.4 Thermodynamic Parameters (Appendix A)

There has been a major overhaul of the Table of Thermodynamic Properties for this update. Compared with JPL 06-2, the table has expanded considerably: from 342 individual species to 655, including a complete section on alkali metal compounds, new halogen oxides, new sulfur species, more

oxygenates and their radicals, and more isomers. The table was redesigned to include enthalpy values at 0 K and all values are now only in Joules. Most entries now have notes associated with the values, giving information ranging from a simple statement of the source of the data to an extensive discussion of controversy about the chosen value. This has resulted in a significant expansion of the total length of the table. An effort was made to ensure that the thermodynamic values recorded in this table are consistent with the equilibrium constant values recommended in Table 3 of JPL 10-6.

I.8 Acknowledgements

The Panel wishes to acknowledge the assistance of Kyle Bayes (JPL) and Kathleen Tanner (Georgia Tech). We also acknowledge the technical support provided by Rose Kendall (CSC), Kathy Thompson (CSC) and Tom Wilson (JPL). Financial support from the NASA Upper Atmosphere Research and Tropospheric Chemistry Programs is gratefully acknowledged.

I.9 References

1. Chlorofluoromethanes and the Stratosphere. In NASA Reference Publication 1010; R. D. Hudson, Ed.; NASA: Washington, D.C, 1977.
2. DeMore, W. B., L. J. Stief, F. Kaufman, D. M. Golden, R. F. Hampson, M. J. Kurylo, J. J. Margitan, M. J. Molina and R. T. Watson "Chemical Kinetics and Photochemical Data for Use in Stratospheric Modeling, Evaluation Number 2," JPL Publication 79-27, Jet Propulsion Laboratory, California Institute of Technology, Pasadena, CA, 1979
3. The Stratosphere: Present and Future. In NASA Reference Publication 1049; R. D. Hudson and E. I. Reed, Eds.; NASA: Washington, D.C, 1979.
4. DeMore, W. B., D. M. Golden, R. F. Hampson, M. J. Kurylo, J. J. Margitan, M. J. Molina, L. J. Stief and R. T. Watson "Chemical Kinetics and Photochemical Data for Use in Stratospheric Modeling, Evaluation Number 4," JPL Publication 81-3, Jet Propulsion Laboratory, California Institute of Technology, Pasadena CA, 1981
5. DeMore, W. B., D. M. Golden, R. F. Hampson, C. J. Howard, M. J. Kurylo, M. J. Molina, A. R. Ravishankara and R. T. Watson "Chemical Kinetics and Photochemical Data for Use in Stratospheric Modeling, Evaluation Number 5," JPL Publication 82-57, Jet Propulsion Laboratory, California Institute of Technology, Pasadena CA, 1982
6. DeMore, W. B., D. M. Golden, R. F. Hampson, C. J. Howard, M. J. Kurylo, M. J. Molina, A. R. Ravishankara and R. T. Watson "Chemical Kinetics and Photochemical Data for Use in Stratospheric Modeling, Evaluation Number 6," JPL Publication 83-62, Jet Propulsion Laboratory, California Institute of Technology, Pasadena CA, 1983
7. DeMore, W. B., D. M. Golden, R. F. Hampson, C. J. Howard, M. J. Kurylo, J. J. Margitan, M. J. Molina, A. R. Ravishankara and R. T. Watson "Chemical Kinetics and Photochemical Data for Use in Stratospheric Modeling, Evaluation Number 7," JPL Publication 85-37, Jet Propulsion Laboratory, California Institute of Technology, Pasadena CA, 1985
8. DeMore, W. B., D. M. Golden, R. F. Hampson, C. J. Howard, M. J. Kurylo, M. J. Molina, A. R. Ravishankara and S. P. Sander "Chemical Kinetics and Photochemical Data for Use in Stratospheric Modeling, Evaluation Number 8," JPL Publication 87-41, Jet Propulsion Laboratory, California Institute of Technology, Pasadena CA, 1987
9. DeMore, W. B., D. M. Golden, R. F. Hampson, C. J. Howard, M. J. Kurylo, M. J. Molina, A. R. Ravishankara and S. P. Sander "Chemical Kinetics and Photochemical Data for Use in Stratospheric Modeling, Evaluation Number 9," JPL Publication 90-1, Jet Propulsion Laboratory, California Institute of Technology, Pasadena CA, 1990
10. DeMore, W. B., D. M. Golden, R. F. Hampson, C. J. Howard, M. J. Kurylo, M. J. Molina, A. R. Ravishankara and S. P. Sander "Chemical Kinetics and Photochemical Data for Use in Stratospheric Modeling, Evaluation Number 10," JPL Publication 92-20, Jet Propulsion Laboratory, California Institute of Technology, Pasadena, CA, 1992
11. DeMore, W. B., D. M. Golden, R. F. Hampson, C. J. Howard, M. J. Kurylo, M. J. Molina, A. R. Ravishankara and S. P. Sander "Chemical Kinetics and Photochemical Data for Use in Stratospheric Modeling, Evaluation Number 11," JPL Publication 94-26, Jet Propulsion Laboratory, California Institute of Technology, Pasadena, CA, 1994
12. DeMore, W. B., S. P. Sander, D. M. Golden, R. F. Hampson, M. J. Kurylo, C. J. Howard, A. R. Ravishankara, C. E. Kolb and M. J. Molina "Chemical Kinetics and Photochemical Data for Use in Stratospheric Modeling, Evaluation Number 12," JPL Publication 97-4, Jet Propulsion Laboratory, California Institute of Technology, Pasadena, CA, 1997 <http://jpldataeval.jpl.nasa.gov>.
13. Sander, S. P., R. R. Friedl, W. B. DeMore, D. M. Golden, M. J. Kurylo, R. F. Hampson, R. E. Huie, G. K. Moortgat, A. R. Ravishankara, C. E. Kolb and M. J. Molina "Chemical Kinetics and Photochemical Data for Use in

Stratospheric Modeling, Evaluation Number 13," JPL Publication 00-3, Jet Propulsion Laboratory, California Institute of Technology, Pasadena, CA, 2000 <http://jpldataeval.jpl.nasa.gov>.

14. Sander, S. P., B. J. Finlayson-Pitts, R. R. Friedl, D. M. Golden, R. E. Huie, C. E. Kolb, M. J. Kurylo, M. J. Molina, G. K. Moortgat, V. L. Orkin and A. R. Ravishankara "Chemical Kinetics and Photochemical Data for Use in Atmospheric Studies, Evaluation Number 14," JPL Publication 02-25, Jet Propulsion Laboratory, Pasadena, 2002 <http://jpldataeval.jpl.nasa.gov>.
15. Sander, S. P., B. J. Finlayson-Pitts, R. R. Friedl, D. M. Golden, R. E. Huie, H. Keller-Rudek, C. E. Kolb, M. J. Kurylo, M. J. Molina, G. K. Moortgat, V. L. Orkin, A. R. Ravishankara and P. H. Wine "Chemical Kinetics and Photochemical Data for Use in Atmospheric Studies, Evaluation Number 15," JPL Publication 06-2, Jet Propulsion Laboratory, Pasadena, 2006 <http://jpldataeval.jpl.nasa.gov>.
16. Sander, S. P., J. Abbatt, J. R. Barker, J. B. Burkholder, R. R. Friedl, D. M. Golden, R. E. Huie, C. E. Kolb, M. J. Kurylo, G. K. Moortgat, V. L. Orkin and P. H. Wine "Chemical Kinetics and Photochemical Data for Use in Atmospheric Studies, Evaluation No. 16," JPL Publication 09-24, Jet Propulsion Laboratory, Pasadena, 2009 <http://jpldataeval.jpl.nasa.gov>.
17. Sander, S. P., J. Abbatt, J. R. Barker, J. B. Burkholder, R. R. Friedl, D. M. Golden, R. E. Huie, C. E. Kolb, M. J. Kurylo, G. K. Moortgat, V. L. Orkin and P. H. Wine "Chemical Kinetics and Photochemical Data for Use in Atmospheric Studies, Evaluation No. 17," JPL Publication 10-6, Jet Propulsion Laboratory, Pasadena, 2011 <http://jpldataeval.jpl.nasa.gov>.

SECTION 1. BIMOLECULAR REACTIONS

Table of Contents

SECTION 1. BIMOLECULAR REACTIONS	1-1
1.1 Introduction	1-1
1.2 Uncertainty Estimates	1-2
1.3 Notes to Table 1.....	1-35
1.4 References	1-132

Tables

Table 1-1. Rate Constants for Second-Order Reactions	1-5
--	-----

Figures

Figure 1. Symmetric and Asymmetric Error Limits	1-3
---	-----

1.1 Introduction

In Table 1 (Rate Constants for Second-Order Reactions) the reactions are grouped into the classes O_x , $O(^1D)$, Singlet O_2 , HO_x , NO_x , Organic Compounds, FO_x , ClO_x , BrO_x , IO_x , SO_x and Metals. Some of the reactions in Table 1 are actually more complex than simple two-body reactions. To explain the pressure and temperature dependences occasionally seen in reactions of this type, it is necessary to consider the bimolecular class of reactions in terms of two subcategories, direct (concerted) and indirect (nonconcerted) reactions.

A direct or concerted bimolecular reaction is one in which the reactants A and B proceed to products C and D without the intermediate formation of an AB adduct that has appreciable bonding, i.e., there is no bound intermediate; only the transition state $(AB)^\ddagger$ lies between reactants and products.



The reaction of OH with CH_4 forming $H_2O + CH_3$ is an example of a reaction of this class.

Very useful correlations between the expected structure of the transition state $[AB]^\ddagger$ and the A-Factor of the reaction rate constant can be made, especially in reactions that are constrained to follow a well-defined approach of the two reactants in order to minimize energy requirements in the making and breaking of bonds. The rate constants for these reactions are well represented by the Arrhenius expression $k = A \exp(-E/RT)$ in the 200–300 K temperature range. These rate constants are not pressure dependent.

The indirect or nonconcerted class of bimolecular reactions is characterized by a more complex reaction path involving a potential well between reactants and products, leading to a bound adduct (or reaction complex) formed between the reactants A and B:



The intermediate $[AB]^*$ is different from the transition state $[AB]^\ddagger$, in that it is a bound molecule which can, in principle, be isolated. (Of course, transition states are involved in all of the above reactions, both forward and backward, but are not explicitly shown.) An example of this reaction type is $ClO + NO$, which normally produces $Cl + NO_2$. Reactions of the nonconcerted type can have a more complex temperature dependence and can exhibit a pressure dependence if the lifetime of $[AB]^*$ is comparable to the rate of collisional deactivation of $[AB]^*$. This arises because the relative rate at which $[AB]^*$ goes to products C + D vs. reactants A + B is a sensitive function of its excitation energy. Thus, in reactions of this type, the distinction between the bimolecular and termolecular classification becomes less meaningful, and it is especially necessary to study such reactions under the temperature and pressure conditions in which they are to be used in model calculation, or, alternatively, to develop a reliable theoretical basis for

extrapolation of data. In several cases where sufficient data exist, reactions of this type are treated in Table 2.

The rate constant tabulation for second-order reactions (Table 1) is given in Arrhenius form:

$$k(T) = A \cdot \exp\left(-\frac{E/R}{T}\right)$$

and contains the following information:

1. Reaction stoichiometry and products (if known). The pressure dependences are included, where appropriate.
2. Arrhenius A-factor: **A**
3. Temperature dependence (“activation temperature”): **E/R**
4. Rate constant at 298 K: **k(298 K)**
5. Rate constant uncertainty factor at 298 K: **f(298 K)** (see below)
6. A parameter used to calculate the rate constant uncertainty at temperatures other than 298 K: **g** (see below)
7. Index number for a detailed note containing references to the literature, the basis of recommendation and in several cases, alternative methods to calculate the rate constant.

For a few reactions, the A-factor, E/R and k(298 K) are italicized. These represent estimates by the Panel in cases where there are no literature data or where the existing data are judged to be of insufficient quality to base a recommendation.

1.2 Uncertainty Estimates

For bimolecular rate constants in Table 1, an estimate of the uncertainty at any given temperature, f(T), may be obtained from the following expression:

$$f(T) = f(298 \text{ K}) \exp\left|g\left(\frac{1}{T} - \frac{1}{298}\right)\right|$$

Note that the exponent is an absolute value. An upper or lower bound (corresponding approximately to one standard deviation) of the rate constant at any temperature T can be obtained by multiplying or dividing the recommended value of the rate constant at that temperature by the factor f(T). The quantity f(298 K) is the uncertainty in the rate constant at T = 298 K. The quantity g has been defined in this evaluation for use with f(298 K) in the above expression to obtain the rate constant uncertainty at different temperatures. It should not be interpreted as the uncertainty in the Arrhenius activation temperature (E/R). Both uncertainty factors, f(298 K) and g, do not necessarily result from a rigorous statistical analysis of the available data. Rather, they are chosen by the evaluators to construct the appropriate uncertainty factor, f(T), shown above.

This approach is based on the fact that rate constants are almost always known with minimum uncertainty at room temperature. The overall uncertainty normally increases at other temperatures, because there are usually fewer data at other temperatures. In addition, data obtained at temperatures far distant from 298 K may be less accurate than at room temperature due to various experimental difficulties.

The uncertainty represented by f(T) is normally symmetric; i.e., the rate constant may be greater than or less than the recommended value, k(T), by the factor f(T). In a few cases in Table 1 asymmetric uncertainties are given in the temperature coefficient. For these cases, the factors by which a rate constant is to be multiplied or divided to obtain, respectively, the upper and lower limits are not equal, except at 298 K where the factor is simply f(298 K). Explicit equations are given below for the case where g is given as (+a, -b):

For T > 298 K, multiply by the factor

$$f(298 \text{ K}) e^{a\left(\frac{1}{298} - \frac{1}{T}\right)}$$

and divide by the factor

$$f(298\text{ K})e^{\left[b\left(\frac{1}{298}-\frac{1}{T}\right)\right]}$$

For $T < 298\text{ K}$, multiply by the factor

$$f(298\text{ K})e^{\left[b\left(\frac{1}{T}-\frac{1}{298}\right)\right]}$$

and divide by the factor

$$f(298\text{ K})e^{\left[a\left(\frac{1}{T}-\frac{1}{298}\right)\right]}$$

Examples of symmetric and asymmetric error limits are shown in Figure 1.

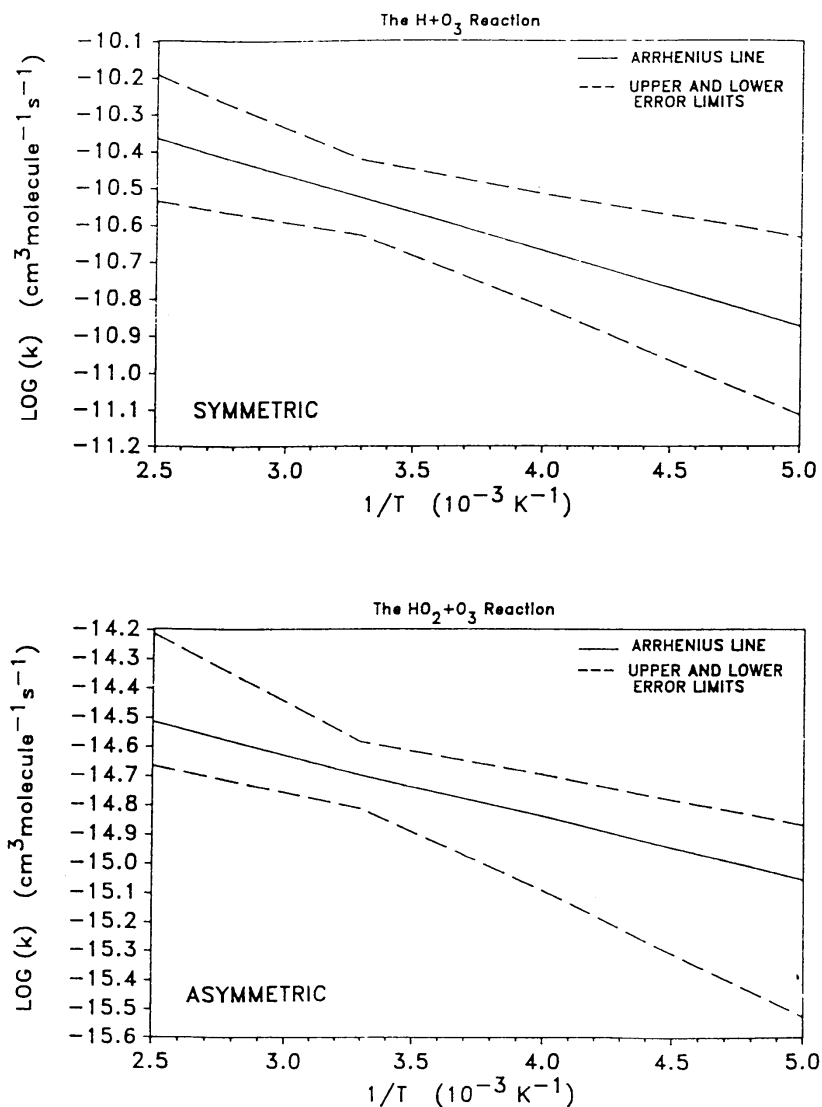


Figure 1. Symmetric and Asymmetric Error Limits

The assigned uncertainties represent the subjective judgment of the Panel. They are not determined by a rigorous, statistical analysis of the database, which generally is too limited to permit such an analysis. Rather, the uncertainties are based on knowledge of the techniques, the difficulties of the experiments, and the potential for systematic errors.

There is obviously no way to quantify these “unknown” errors. The spread in results among different techniques for a given reaction may provide some basis for an uncertainty, but the possibility of the same, or compensating, systematic errors in all the studies must be recognized.

Furthermore, the probability distribution may not follow the normal Gaussian form. For measurements subject to large systematic errors, the true rate constant may be much further from the recommended value than would be expected based on a Gaussian distribution with the stated uncertainty. As an example, in the past the recommended rate constants for the reactions $\text{HO}_2 + \text{NO}$ and $\text{Cl} + \text{ClONO}_2$ changed by factors of 30–50. These changes could not have been allowed for with any reasonable values of σ in a Gaussian distribution.

Table 1-1. Rate Constants for Second-Order Reactions

Reaction	A-Factor ^a	E/R	k(298 K) ^a	f(298 K) ^b	g	Notes
O_x Reactions						
$O + O_2 \xrightarrow{M} O_3$	(See Table 2)					
$O + O_3 \rightarrow O_2 + O_2$	8.0×10^{-12}	2060	8.0×10^{-15}	1.10	200	A1
O(¹D) Reactions						A2
$O(^1D) + O_2 \rightarrow O + O_2$	3.3×10^{-11}	-55	3.95×10^{-11}	1.1	10	A3
$O(^1D) + O_3 \rightarrow O_2 + O_2$	1.2×10^{-10}	0	1.2×10^{-10}	1.2	50	A4
$\rightarrow O_2 + O + O$	1.2×10^{-10}	0	1.2×10^{-10}	1.2	50	A4
$O(^1D) + H_2 \rightarrow OH + H$	1.2×10^{-10}	0	1.2×10^{-10}	1.15	50	A5
$O(^1D) + H_2O \rightarrow OH + OH$	1.63×10^{-10}	-60	2.0×10^{-10}	1.08	20	A6
$O(^1D) + N_2 \rightarrow O + N_2$	2.15×10^{-11}	-110	3.1×10^{-11}	1.10	20	A7
$O(^1D) + N_2 \xrightarrow{M} N_2O$	(See Table 2-1)					
$O(^1D) + N_2O \rightarrow$ Overall $\rightarrow N_2 + O_2$ $\rightarrow NO + NO$	1.19×10^{-10} 4.63×10^{-11} 7.25×10^{-11}	-20	1.27×10^{-10} 4.95×10^{-11} 7.75×10^{-11}	1.10 1.10 1.10	25 25 25	A8
$O(^1D) + NH_3 \rightarrow OH + NH_2$	2.5×10^{-10}	0	2.5×10^{-10}	1.20	25	A9
$O(^1D) + CO_2 \rightarrow O + CO_2$	7.5×10^{-11}	-115	1.1×10^{-10}	1.15	20	A10
$O(^1D) + CH_4 \rightarrow$ Overall $\rightarrow CH_3 + OH$ $\rightarrow CH_3O \text{ or } CH_2OH + H$ $\rightarrow CH_2O + H_2$	1.75×10^{-10} 1.31×10^{-10} 0.35×10^{-10} 0.09×10^{-10}	0	1.75×10^{-10} 1.31×10^{-10} 0.35×10^{-10} 0.09×10^{-10}	1.15 1.15 1.15 1.15	25 25 25 25	A11
$O(^1D) + HCl \rightarrow$ Quenching and Reaction	1.5×10^{-10}	0	1.5×10^{-10}	1.10	25	A12
$O(^1D) + HF \rightarrow$ Quenching and Reaction	5.0×10^{-11}	0	5.0×10^{-11}	1.50	25	A13
$O(^1D) + NF_3 \rightarrow$ Quenching and Reaction	2.05×10^{-11}	-50	2.4×10^{-11}	1.20	25	A14
$O(^1D) + HBr \rightarrow$ Quenching and Reaction	1.5×10^{-10}	0	1.5×10^{-10}	1.50	25	A15

Reaction	A-Factor ^a	E/R	k(298 K) ^a	f(298 K) ^b	g	Notes
O(¹ D) + Cl ₂ → Quenching and Reaction	2.7×10 ⁻¹⁰	0	2.7×10 ⁻¹⁰	1.10	25	A16
O(¹ D) + CCl ₂ O → Quenching and Reaction	2.2×10 ⁻¹⁰	-30	2.4×10 ⁻¹⁰	1.10	25	A17
O(¹ D) + CCIFO → Quenching and Reaction	1.9×10 ⁻¹⁰	0	1.9×10 ⁻¹⁰	1.50	25	A18
O(¹ D) + CF ₂ O → Quenching and Reaction	7.4×10 ⁻¹¹	0	7.4×10 ⁻¹¹	1.50	25	A19
O(¹ D) + CCl ₄ → Quenching and Reaction (CFC-10)	3.3×10 ⁻¹⁰	0	3.3×10 ⁻¹⁰	1.2	50	A20
O(¹ D) + CH ₃ Br → Quenching and Reaction	1.8×10 ⁻¹⁰	0	1.8×10 ⁻¹⁰	1.15	50	A21
O(¹ D) + CH ₂ Br ₂ → Quenching and Reaction	2.7×10 ⁻¹⁰	0	2.7×10 ⁻¹⁰	1.20	25	A22
O(¹ D) + CHBr ₃ → Quenching and Reaction	6.6×10 ⁻¹⁰	0	6.6×10 ⁻¹⁰	1.30	25	A23
O(¹ D) + CH ₃ F → Quenching and Reaction (HFC-41)	1.5×10 ⁻¹⁰	0	1.5×10 ⁻¹⁰	1.15	50	A24
O(¹ D) + CH ₂ F ₂ → Quenching and Reaction (HFC-32)	5.1×10 ⁻¹¹	0	5.1×10 ⁻¹¹	1.20	50	A25
O(¹ D) + CHF ₃ → Quenching and Reaction (HFC-23)	9.1×10 ⁻¹²	0	9.1×10 ⁻¹²	1.10	50	A26
O(¹ D) + CHCl ₂ F → Quenching and Reaction (HCFC-21)	1.9×10 ⁻¹⁰	0	1.9×10 ⁻¹⁰	1.15	50	A27
O(¹ D) + CHClF ₂ → Quenching and Reaction (HCFC-22)	1.0×10 ⁻¹⁰	0	1.0×10 ⁻¹⁰	1.15	50	A28
O(¹ D) + CHF ₂ Br → Quenching and Reaction	1.75×10 ⁻¹⁰	-70	2.2×10 ⁻¹⁰	1.15	25	A29
O(¹ D) + CCl ₃ F → Quenching and Reaction (CFC-11)	2.3×10 ⁻¹⁰	0	2.3×10 ⁻¹⁰	1.2	50	A30
O(¹ D) + CCl ₂ F ₂ → Quenching and Reaction (CFC-12)	1.4×10 ⁻¹⁰	0	1.4×10 ⁻¹⁰	1.25	50	A31
O(¹ D) + CCIF ₃ → Quenching and Reaction (CFC-13)	8.7×10 ⁻¹¹	0	8.7×10 ⁻¹¹	1.20	50	A32
O(¹ D) + CClBrF ₂ → Quenching and Reaction (Halon-1211)	1.5×10 ⁻¹⁰	0	1.5×10 ⁻¹⁰	1.20	50	A33
O(¹ D) + CBr ₂ F ₂ → Quenching and Reaction (Halon-1202)	2.2×10 ⁻¹⁰	0	2.2×10 ⁻¹⁰	1.20	50	A34
O(¹ D) + CBrF ₃ → Quenching and Reaction (Halon-1301)	1.0×10 ⁻¹⁰	0	1.0×10 ⁻¹⁰	1.20	50	A35

Reaction	A-Factor ^a	E/R	k(298 K) ^a	f(298 K) ^b	g	Notes
$O(^1D) + CF_4 \rightarrow CF_4 + O$ (PFC-14)			$<2 \times 10^{-14}$			A36
$O(^1D) + CH_3CH_2F \rightarrow$ Quenching and Reaction (HFC-161)	2.6×10^{-10}	0	2.6×10^{-10}	1.20	25	A37
$O(^1D) + CH_3CHF_2 \rightarrow$ Quenching and Reaction (HFC-152a)	1.75×10^{-10}	0	1.75×10^{-10}	1.20	50	A38
$O(^1D) + CH_3CCl_2F \rightarrow$ Quenching and Reaction (HCFC-141b)	2.6×10^{-10}	0	2.6×10^{-10}	1.20	50	A39
$O(^1D) + CH_3CClF_2 \rightarrow$ Quenching and Reaction (HCFC-142b)	2.2×10^{-10}	0	2.2×10^{-10}	1.20	50	A40
$O(^1D) + CH_3CF_3 \rightarrow$ Quenching and Reaction (HFC-143a)	4.4×10^{-11}	0	4.4×10^{-11}	1.50	25	A41
$O(^1D) + CH_2ClCClF_2 \rightarrow$ Quenching and Reaction (HCFC-132b)	1.6×10^{-10}	0	1.6×10^{-10}	1.50	50	A42
$O(^1D) + CH_2ClCF_3 \rightarrow$ Quenching and Reaction (HCFC-133a)	1.2×10^{-10}	0	1.2×10^{-10}	1.25	50	A43
$O(^1D) + CH_2FCF_3 \rightarrow$ Quenching and Reaction (HFC-134a)	4.9×10^{-11}	0	4.9×10^{-11}	1.15	50	A44
$O(^1D) + CHCl_2CF_3 \rightarrow$ Quenching and Reaction (HCFC-123)	2.0×10^{-10}	0	2.0×10^{-10}	1.20	50	A45
$O(^1D) + CHClCF_3 \rightarrow$ Quenching and Reaction (HCFC-124)	8.6×10^{-11}	0	8.6×10^{-11}	1.20	50	A46
$O(^1D) + CHF_2CF_3 \rightarrow$ Quenching and Reaction (HFC-125)	1.2×10^{-10}	0	1.2×10^{-10}	1.15	50	A47
$O(^1D) + CCl_3CF_3 \rightarrow$ Quenching and Reaction (CFC-113a)	2×10^{-10}	0	2×10^{-10}	1.50	50	A48
$O(^1D) + CCl_2FCClF_2 \rightarrow$ Quenching and Reaction (CFC-113)	2×10^{-10}	0	2×10^{-10}	1.50	50	A49
$O(^1D) + CCl_2FCF_3 \rightarrow$ Quenching and Reaction (CFC-114a)	1×10^{-10}	0	1×10^{-10}	1.50	50	A50
$O(^1D) + CClF_2CClF_2 \rightarrow$ Quenching and Reaction (CFC-114)	1.3×10^{-10}	0	1.3×10^{-10}	1.20	50	A51
$O(^1D) + CClF_2CF_3 \rightarrow$ Quenching and Reaction (CFC-115)	5×10^{-11}	0	5×10^{-11}	1.20	25	A52
$O(^1D) + CBrF_2CBrF_2 \rightarrow$ Quenching and Reaction	1.6×10^{-10}	0	1.6×10^{-10}	1.20	50	A53

Reaction	A-Factor ^a	E/R	k(298 K) ^a	f(298 K) ^b	g	Notes
(Halon-2402)						
$O(^1D) + CF_3CF_3 \rightarrow$ Quenching and Reaction (PFC-116)			$<1.5 \times 10^{-13}$			A54
$O(^1D) + CHF_2CF_2CF_2CHF_2 \rightarrow$ Quenching and Reaction (HFC-338pcc)	1.8×10^{-11}	0	1.8×10^{-11}	1.30	50	A55
$O(^1D) + c-C_4F_8 \rightarrow$ Quenching and Reaction			$<8 \times 10^{-13}$			A56
$O(^1D) + CF_3CHFCHFCF_2CF_3 \rightarrow$ Quenching and Reaction (HFC-43-10mee)	2.1×10^{-10}	0	2.1×10^{-10}	2	50	A57
$O(^1D) + C_5F_{12} \rightarrow$ Quenching and Reaction (PFC-41-12)			$<4 \times 10^{-13}$			A58
$O(^1D) + C_6F_{14} \rightarrow$ Quenching and Reaction (PFC-51-14)			$<1 \times 10^{-12}$			A59
$O(^1D) + 1,2-(CF_3)_2C-C_4F_6 \rightarrow$ Quenching and Reaction			$<3 \times 10^{-13}$			A60
$O(^1D) + C_4F_{10} \rightarrow$ Quenching and Reaction			$<5 \times 10^{-13}$			A61
$O(^1D) + SF_6 \rightarrow$ Quenching and Reaction			$<1.8 \times 10^{-14}$			A62
$O(^1D) + SO_2 \rightarrow$ Quenching and Reaction	2.2×10^{-10}	0	2.2×10^{-10}	1.30	30	A63
$O(^1D) + SO_2F_2 \rightarrow$ Quenching and Reaction	9×10^{-11}	-100	1.25×10^{-10}	1.30	30	A64
$O(^1D) + SF_5CF_3 \rightarrow$ Quenching and Reaction			$<2 \times 10^{-13}$			A65
Singlet O₂ Reactions						
$O_2(^1\Delta) + O \rightarrow$ products			$<2 \times 10^{-16}$			A66
$O_2(^1\Delta) + O_2 \rightarrow$ products	3.6×10^{-18}	220	1.7×10^{-18}	1.2	100	A67
$O_2(^1\Delta) + O_3 \rightarrow O + 2O_2$	5.2×10^{-11}	2840	3.8×10^{-15}	1.2	500	A68
$O_2(^1\Delta) + H_2O \rightarrow$ products			4.8×10^{-18}	1.5		A69
$O_2(^1\Delta) + N \rightarrow NO + O$			$<9 \times 10^{-17}$			A70
$O_2(^1\Delta) + N_2 \rightarrow$ products			$<10^{-20}$			A71
$O_2(^1\Delta) + CO_2 \rightarrow$ products			$<2 \times 10^{-20}$			A72

Reaction	A-Factor ^a	E/R	k(298 K) ^a	f(298 K) ^b	g	Notes
$O_2(^1\Sigma) + O \rightarrow \text{products}$			8×10^{-14}	5.0		A73
$O_2(^1\Sigma) + O_2 \rightarrow \text{products}$			3.9×10^{-17}	1.5		A74
$O_2(^1\Sigma) + O_3 \rightarrow \text{products}$	3.5×10^{-11}	135	2.2×10^{-11}	1.15	50	A75
$O_2(^1\Sigma) + H_2 \rightarrow \text{products}$ $O_2(^1\Sigma) + H_2 \rightarrow 2 OH$	6.4×10^{-12}	600	8.5×10^{-13} $< 4 \times 10^{-17}$ (see note)	1.15	100	A76
$O_2(^1\Sigma) + H_2O \rightarrow O_2 + H_2O$	3.9×10^{-12}	-125	5.9×10^{-12}	1.3	100	A77
$O_2(^1\Sigma) + N \rightarrow \text{products}$			$< 10^{-13}$			A78
$O_2(^1\Sigma) + N_2 \rightarrow \text{products}$	1.8×10^{-15}	-45	2.1×10^{-15}	1.1	100	A79
$O_2(^1\Sigma) + N_2O \rightarrow \text{products}$ $O_2(^1\Sigma) + N_2O \rightarrow NO + NO_2$	7.0×10^{-14}	-75	9.0×10^{-14} $< 2 \times 10^{-17}$ (see Note)	1.3	50	A80
$O_2(^1\Sigma) + CO_2 \rightarrow \text{products}$	4.2×10^{-13}	0	4.2×10^{-13}	1.2	200	A81
HO_x Reactions						
$O + OH \rightarrow O_2 + H$	1.8×10^{-11}	-180	3.3×10^{-11}	1.15	50	B1
$O + HO_2 \rightarrow OH + O_2$	3.0×10^{-11}	-200	5.9×10^{-11}	1.05	50	B2
$O + H_2O_2 \rightarrow OH + HO_2$	1.4×10^{-12}	2000	1.7×10^{-15}	1.2	100	B3
$H + O_2 \xrightarrow{M} HO_2$	See Table 2-1					
$H + O_3 \rightarrow OH + O_2$	1.4×10^{-10}	470	2.9×10^{-11}	1.1	40	B4
$H + HO_2 \rightarrow 2 OH$	7.2×10^{-11}	0	7.2×10^{-11}	1.2	100	B5
$\quad \rightarrow O + H_2O$	1.6×10^{-12}	0	1.6×10^{-12}	1.5	100	
$\quad \rightarrow H_2 + O_2$	6.9×10^{-12}	0	6.9×10^{-12}	1.4	100	
$OH + O_3 \rightarrow HO_2 + O_2$	1.7×10^{-12}	940	7.3×10^{-14}	1.15	50	B6
$OH + H_2 \rightarrow H_2O + H$	2.8×10^{-12}	1800	6.7×10^{-15}	1.05	100	B7
$OH + HD \rightarrow \text{products}$	5.0×10^{-12}	2130	4.0×10^{-15}	1.15	50	B8
$OH + OH \rightarrow H_2O + O$ $\quad \xrightarrow{M} H_2O_2$	1.8×10^{-12} See Table 2-1	0	1.8×10^{-12}	1.25	50	B9
$OH + HO_2 \rightarrow H_2O + O_2$	4.8×10^{-11}	-250	1.1×10^{-10}	1.15	50	B10

Reaction	A-Factor ^a	E/R	k(298 K) ^a	f(298 K) ^b	g	Notes
$\text{OH} + \text{H}_2\text{O}_2 \rightarrow \text{H}_2\text{O} + \text{HO}_2$	See Note					<u>B11</u>
$\text{HO}_2 + \text{O}_3 \rightarrow \text{OH} + 2\text{O}_2$	1.0×10^{-14}	490	1.9×10^{-15}	1.15	80	<u>B12</u>
$\text{HO}_2 + \text{HO}_2 \rightarrow \text{H}_2\text{O}_2 + \text{O}_2$	3.0×10^{-13}	-460	1.4×10^{-12}	1.15	100	<u>B13</u>
$\xrightarrow{\text{M}} \text{H}_2\text{O}_2 + \text{O}_2$	$2.1 \times 10^{-33} [\text{M}]$	-920	$4.6 \times 10^{-32} [\text{M}]$	1.2	200	
$\text{HO}_2 + \text{HO}_2 \cdot \text{H}_2\text{O} \rightarrow \text{products}$	5.4×10^{-11}	410	1.4×10^{-11}	2	100	<u>B14</u>
NO_x Reactions						
$\text{O} + \text{NO} \xrightarrow{\text{M}} \text{NO}_2$	(See Table 2-1)					
$\text{O} + \text{NO}_2 \rightarrow \text{NO} + \text{O}_2$	5.1×10^{-12}	-210	1.04×10^{-11}	1.1	20	<u>C 1</u>
$\text{O} + \text{NO}_2 \xrightarrow{\text{M}} \text{NO}_3$	(See Table 2-1)					
$\text{O} + \text{NO}_3 \rightarrow \text{O}_2 + \text{NO}_2$	1.0×10^{-11}	0	1.0×10^{-11}	1.5	150	<u>C 2</u>
$\text{O} + \text{N}_2\text{O}_5 \rightarrow \text{products}$			$<3.0 \times 10^{-16}$			<u>C 3</u>
$\text{O} + \text{HNO}_3 \rightarrow \text{OH} + \text{NO}_3$			$<3.0 \times 10^{-17}$			<u>C 4</u>
$\text{O} + \text{HO}_2\text{NO}_2 \rightarrow \text{products}$	7.8×10^{-11}	3400	8.6×10^{-16}	3.0	750	<u>C 5</u>
$\text{H} + \text{NO}_2 \rightarrow \text{OH} + \text{NO}$	4.0×10^{-10}	340	1.3×10^{-10}	1.3	300	<u>C 6</u>
$\text{OH} + \text{NO} \xrightarrow{\text{M}} \text{HONO}$	(See Table 2-1)					
$\text{OH} + \text{NO}_2 \xrightarrow{\text{M}} \text{HNO}_3$	(See Table 2-1)					
$\text{OH} + \text{NO}_3 \rightarrow \text{products}$			2.2×10^{-11}	1.5		<u>C 7</u>
$\text{OH} + \text{HONO} \rightarrow \text{H}_2\text{O} + \text{NO}_2$	1.8×10^{-11}	390	4.5×10^{-12}	1.5	+200 –	<u>C 8</u>
$\text{OH} + \text{HNO}_3 \rightarrow \text{H}_2\text{O} + \text{NO}_3$	(See Note)			1.2		<u>C 9</u>
$\text{OH} + \text{HO}_2\text{NO}_2 \rightarrow \text{products}$	1.3×10^{-12}	-380	4.6×10^{-12}	1.3	+270 –500	<u>C10</u>
$\text{OH} + \text{NH}_3 \rightarrow \text{H}_2\text{O} + \text{NH}_2$	1.7×10^{-12}	710	1.6×10^{-13}	1.2	200	<u>C11</u>
$\text{HO}_2 + \text{NO} \rightarrow \text{NO}_2 + \text{OH}$	3.3×10^{-12}	-270	8.0×10^{-12}	1.15	20	<u>C12</u>
$\text{H}_2\text{O} + \text{NO}_2^* \rightarrow \text{OH} + \text{HONO}$		see note				<u>C13</u>
$\text{HO}_2 + \text{NO}_2 \xrightarrow{\text{M}} \text{HO}_2\text{NO}_2$	(See Table 2-1)					
$\text{HO}_2 + \text{NO}_2 \rightarrow \text{HONO} + \text{O}_2$	(See Note)					<u>C14</u>

Reaction	A-Factor ^a	E/R	k(298 K) ^a	f(298 K) ^b	g	Notes
$\text{HO}_2 + \text{NO}_3 \rightarrow \text{products}$			3.5×10^{-12}	1.5		C15
$\text{HO}_2 + \text{NH}_2 \rightarrow \text{products}$			3.4×10^{-11}	2.0		C16
$\text{N} + \text{O}_2 \rightarrow \text{NO} + \text{O}$	1.5×10^{-11}	3600	8.5×10^{-17}	1.25	400	C17
$\text{N} + \text{O}_3 \rightarrow \text{NO} + \text{O}_2$			$<2.0 \times 10^{-16}$			C18
$\text{N} + \text{NO} \rightarrow \text{N}_2 + \text{O}$	2.1×10^{-11}	-100	3.0×10^{-11}	1.3	100	C19
$\text{N} + \text{NO}_2 \rightarrow \text{N}_2\text{O} + \text{O}$	5.8×10^{-12}	-220	1.2×10^{-11}	1.5	100	C20
$\text{NO} + \text{O}_3 \rightarrow \text{NO}_2 + \text{O}_2$	3.0×10^{-12}	1500	1.9×10^{-14}	1.1	200	C21
$\text{NO} + \text{NO}_3 \rightarrow 2\text{NO}_2$	1.5×10^{-11}	-170	2.6×10^{-11}	1.3	100	C22
$\text{NO}_2 + \text{O}_3 \rightarrow \text{NO}_3 + \text{O}_2$	1.2×10^{-13}	2450	3.2×10^{-17}	1.15	150	C23
$\text{NO}_2 + \text{NO}_3 \rightarrow \text{NO} + \text{NO}_2 + \text{O}_2$ $\text{NO}_2 + \text{NO}_3 \xrightarrow{\text{M}} \text{N}_2\text{O}_5$	(See Note) (See Table 2-1)					C24
$\text{NO}_3 + \text{NO}_3 \rightarrow 2\text{NO}_2 + \text{O}_2$	8.5×10^{-13}	2450	2.3×10^{-16}	1.5	500	C25
$\text{NH}_2 + \text{O}_2 \rightarrow \text{products}$			$<6.0 \times 10^{-21}$			C26
$\text{NH}_2 + \text{O}_3 \rightarrow \text{products}$	4.3×10^{-12}	930	1.9×10^{-13}	3.0	500	C27
$\text{NH}_2 + \text{NO} \rightarrow \text{products}$	4.0×10^{-12}	-450	1.8×10^{-11}	1.3	150	C28
$\text{NH}_2 + \text{NO}_2 \rightarrow \text{products}$	2.1×10^{-12}	-650	1.9×10^{-11}	3.0	250	C29
$\text{NH} + \text{NO} \rightarrow \text{products}$	4.9×10^{-11}	0	4.9×10^{-11}	1.5	300	C30
$\text{NH} + \text{NO}_2 \rightarrow \text{products}$	3.5×10^{-13}	-1140	1.6×10^{-11}	2.0	500	C31
$\text{O}_3 + \text{HNO}_2 \rightarrow \text{O}_2 + \text{HNO}_3$			$<5.0 \times 10^{-19}$			C32
$\text{N}_2\text{O}_5 + \text{H}_2\text{O} \rightarrow 2\text{HNO}_3$			$<2.0 \times 10^{-21}$			C33
$\text{N}_2(\text{A},\text{v}) + \text{O}_2 \rightarrow \text{products}$			$2.5 \times 10^{-12}, \text{v}=0$	1.5		C34
$\text{N}_2(\text{A},\text{v}) + \text{O}_3 \rightarrow \text{products}$			$4.1 \times 10^{-11}, \text{v}=0$	2.0		C34
Reactions of Organic Compounds						
$\text{O} + \text{CH}_3 \rightarrow \text{products}$	1.1×10^{-10}	0	1.1×10^{-10}	1.3	250	D 1
$\text{O} + \text{HCN} \rightarrow \text{products}$	1.0×10^{-11}	4000	1.5×10^{-17}	10	1000	D 2

Reaction	A-Factor ^a	E/R	k(298 K) ^a	f(298 K) ^b	g	Notes
$O + C_2H_2 \rightarrow \text{products}$	3.0×10^{-11}	1600	1.4×10^{-13}	1.3	250	D 3
$O + H_2CO \rightarrow \text{products}$	3.4×10^{-11}	1600	1.6×10^{-13}	1.25	250	D 4
$O + CH_3CHO \rightarrow CH_3CO + OH$	1.8×10^{-11}	1100	4.5×10^{-13}	1.25	200	D 5
$O_2 + HOCO \rightarrow HO_2 + CO_2$			2×10^{-12} (See Note)	2		D 6
$O_3 + C_2H_2 \rightarrow \text{products}$	1.0×10^{-14}	4100	1.0×10^{-20}	3	500	D 7
$O_3 + C_2H_4 \rightarrow \text{products}$	1.2×10^{-14}	2630	1.7×10^{-18}	1.25	100	D 8
$O_3 + C_3H_6 \rightarrow \text{products}$	6.5×10^{-15}	1900	1.1×10^{-17}	1.15	200	D 9
$O_3 + CH_2=C(CH_3)CH=CH_2 \rightarrow \text{products}$	1.0×10^{-14}	1970	1.3×10^{-17}	1.1	150	D10
$OH + CO \rightarrow \text{Products}$	(See Table 2-1)					D11
$OH + CH_4 \rightarrow CH_3 + H_2O$	2.45×10^{-12}	1775	6.3×10^{-15}	1.1	100	D12
$OH + ^{13}CH_4 \rightarrow ^{13}CH_3 + H_2O$	(See Note)					D13
$OH + CH_3D \rightarrow \text{products}$	3.5×10^{-12}	1950	5.0×10^{-15}	1.15	200	D14
$OH + H_2CO \rightarrow H_2O + HCO$	5.5×10^{-12}	-125	8.5×10^{-12}	1.15	50	D15
$OH + CH_3OH \rightarrow \text{products}$	2.9×10^{-12}	345	9.1×10^{-13}	1.10	60	D16
$OH + CH_3OOH \rightarrow \text{products}$	3.8×10^{-12}	-200	7.4×10^{-12}	1.4	150	D17
$OH + HC(O)OH \rightarrow \text{products}$	4.0×10^{-13}	0	4.0×10^{-13}	1.2	100	D18
$OH + HC(O)C(O)H \rightarrow \text{products}$	1.15×10^{-11}	0	1.15×10^{-11}	1.5	200	D19
$OH + HOCH_2CHO \rightarrow \text{products}$	1.1×10^{-11}	0	1.1×10^{-11}	1.2	200	D20
$OH + HCN \rightarrow \text{products}$	1.2×10^{-13}	400	3.1×10^{-14}	3	150	D21
$OH + C_2H_2 \xrightarrow{M} \text{products}$	(See Table 2)					
$OH + C_2H_4 \xrightarrow{M} \text{products}$	(See Table 2)					
$OH + C_2H_6 \rightarrow H_2O + C_2H_5$	7.66×10^{-12}	1020	2.5×10^{-13}	1.07	50	D22
$OH + CH_3CHO \rightarrow \text{products}$	4.63×10^{-12}	-350	1.5×10^{-11}	1.05	20	D23
$OH + CH_3CH_2OH \rightarrow \text{products}$	3.35×10^{-12}	0	3.35×10^{-12}	1.05	20	D24
$OH + CH_3C(O)OH \rightarrow \text{products}$	3.15×10^{-14}	-920	6.9×10^{-13}	1.15	100	D25

Reaction	A-Factor ^a	E/R	k(298 K) ^a	f(298 K) ^b	g	Notes
OH + C ₃ H ₈ → products	8.7×10 ⁻¹²	615	1.1×10 ⁻¹²	1.05	50	D26
OH + C ₂ H ₅ CHO → C ₂ H ₅ CO + H ₂ O	4.9×10 ⁻¹²	-405	1.9×10 ⁻¹¹	1.05	80	D27
OH + 1-C ₃ H ₇ OH → products	4.4×10 ⁻¹²	-70	5.6×10 ⁻¹²	1.05	80	D28
OH + 2-C ₃ H ₇ OH → products	3.0×10 ⁻¹²	-180	5.5×10 ⁻¹²	1.05	80	D29
OH + C ₂ H ₅ C(O)OH → products	1.2×10 ⁻¹²	0	1.2×10 ⁻¹²	1.1	200	D30
OH + CH ₃ C(O)CH ₃ → H ₂ O + CH ₃ C(O)CH ₂ → CH ₃ + CH ₃ C(O)OH	See Note		< 2% of k			D31
OH + CH ₂ =C(CH ₃)CH=CH ₂ → products	3.1×10 ⁻¹¹	-350	1.0×10 ⁻¹⁰	1.1	100	D32
OH + CH ₃ CN → products	7.8×10 ⁻¹³	1050	2.3×10 ⁻¹⁴	1.5	200	D33
OH + CH ₃ ONO ₂ → products	8.0×10 ⁻¹³	1000	2.8×10 ⁻¹⁴	1.7	200	D34
OH + CH ₃ C(O)O ₂ NO ₂ (PAN) → products			<4 × 10 ⁻¹⁴			D35
OH + C ₂ H ₅ ONO ₂ → products	1.0×10 ⁻¹²	490	2.0×10 ⁻¹³	1.4	150	D36
OH + 1-C ₃ H ₇ ONO ₂ → products	7.1×10 ⁻¹³	0	7.1×10 ⁻¹³	1.5	200	D37
OH + 2-C ₃ H ₇ ONO ₂ → products	1.2×10 ⁻¹²	320	4.1×10 ⁻¹³	1.5	200	D38
HO ₂ + CH ₂ O → adduct	6.7×10 ⁻¹⁵	-600	5.0×10 ⁻¹⁴	5	600	D39
HO ₂ + CH ₃ O ₂ → CH ₃ OOH + O ₂	4.1×10 ⁻¹³	-750	5.2×10 ⁻¹²	1.3	150	D40
HO ₂ + C ₂ H ₅ O ₂ → C ₂ H ₅ OOH + O ₂	7.5×10 ⁻¹³	-700	8.0×10 ⁻¹²	1.5	250	D41
HO ₂ + CH ₃ C(O)O ₂ → products	4.3×10 ⁻¹³	-1040	1.4×10 ⁻¹¹	2	500	D42
HO ₂ + CH ₃ C(O)CH ₂ O ₂ → products	8.6×10 ⁻¹³	-700	9.0×10 ⁻¹²	2	300	D43
NO ₃ + CO → products			<4.0×10 ⁻¹⁹			D44
NO ₃ + CH ₂ O → products			5.8×10 ⁻¹⁶	1.3		D45
NO ₃ + CH ₃ CHO → products	1.4×10 ⁻¹²	1900	2.4×10 ⁻¹⁵	1.3	300	D46
CH ₃ + O ₂ → products			<3.0×10 ⁻¹⁶			D47
CH ₃ + O ₂ \xrightarrow{M} CH ₃ O ₂	(See Table 2-1)					
CH ₃ + O ₃ → products	5.4×10 ⁻¹²	220	2.6×10 ⁻¹²	2	150	D48

Reaction	A-Factor ^a	E/R	k(298 K) ^a	f(298 K) ^b	g	Notes
$\text{HCO} + \text{O}_2 \rightarrow \text{CO} + \text{HO}_2$	5.2×10^{-12}	0	5.2×10^{-12}	1.4	100	D49
$\text{CH}_2\text{OH} + \text{O}_2 \rightarrow \text{CH}_2\text{O} + \text{HO}_2$	9.1×10^{-12}	0	9.1×10^{-12}	1.3	200	D50
$\text{CH}_3\text{O} + \text{O}_2 \rightarrow \text{CH}_2\text{O} + \text{HO}_2$	3.9×10^{-14}	900	1.9×10^{-15}	1.5	300	D51
$\text{CH}_3\text{O} + \text{NO} \rightarrow \text{CH}_2\text{O} + \text{HNO}$ $\text{CH}_3\text{O} + \text{NO} \xrightarrow{\text{M}} \text{CH}_3\text{ONO}$	(See Note) (See Table 2-1)					D52
$\text{CH}_3\text{O} + \text{NO}_2 \rightarrow \text{CH}_2\text{O} + \text{HONO}$	1.1×10^{-11}	1200	2.0×10^{-13}	5	600	D53
$\text{CH}_3\text{O} + \text{NO}_2 \xrightarrow{\text{M}} \text{CH}_3\text{ONO}_2$	(See Table 2-1)					
$\text{CH}_3\text{O}_2 + \text{O}_3 \rightarrow \text{products}$	2.9×10^{-16}	1000	1.0×10^{-17}	3	500	D54
$\text{CH}_3\text{O}_2 + \text{CH}_3\text{O}_2 \rightarrow \text{products}$	9.5×10^{-14}	-390	3.5×10^{-13}	1.2	100	D55
$\text{CH}_3\text{O}_2 + \text{NO} \rightarrow \text{CH}_3\text{O} + \text{NO}_2$	2.8×10^{-12}	-300	7.7×10^{-12}	1.15	100	D56
$\text{CH}_3\text{O}_2 + \text{NO}_2 \xrightarrow{\text{M}} \text{CH}_3\text{O}_2\text{NO}_2$	(See Table 2-1)					
$\text{CH}_3\text{O}_2 + \text{CH}_3\text{C(O)O}_2 \rightarrow \text{products}$	2.0×10^{-12}	-500	1.1×10^{-11}	1.5	250	D57
$\text{CH}_3\text{O}_2 + \text{CH}_3\text{C(O)CH}_2\text{O}_2 \rightarrow \text{products}$	7.5×10^{-13}	-500	4.0×10^{-12}	2	300	D58
$\text{C}_2\text{H}_5 + \text{O}_2 \rightarrow \text{C}_2\text{H}_4 + \text{HO}_2$ $\text{C}_2\text{H}_5 + \text{O}_2 \xrightarrow{\text{M}} \text{C}_2\text{H}_5\text{O}_2$	(See Table 2-1)		$< 2.0 \times 10^{-14}$			D59
$\text{C}_2\text{H}_5\text{O} + \text{O}_2 \rightarrow \text{CH}_3\text{CHO} + \text{HO}_2$	6.3×10^{-14}	550	1.0×10^{-14}	1.5	200	D60
$\text{C}_2\text{H}_5\text{O} + \text{NO} \xrightarrow{\text{M}} \text{products}$	(See Table 2-1)					
$\text{C}_2\text{H}_5\text{O} + \text{NO}_2 \xrightarrow{\text{M}} \text{products}$	(See Table 2-1)					
$\text{C}_2\text{H}_5\text{O}_2 + \text{C}_2\text{H}_5\text{O}_2 \rightarrow \text{products}$	6.8×10^{-14}	0	6.8×10^{-14}	2	300	D61
$\text{C}_2\text{H}_5\text{O}_2 + \text{NO} \rightarrow \text{products}$	2.6×10^{-12}	-365	8.7×10^{-12}	1.2	150	D62
$\text{CH}_3\text{C(O)O}_2 + \text{CH}_3\text{C(O)O}_2 \rightarrow \text{products}$	2.9×10^{-12}	-500	1.5×10^{-11}	1.5	150	D63
$\text{CH}_3\text{C(O)O}_2 + \text{NO} \rightarrow \text{products}$	8.1×10^{-12}	-270	2.0×10^{-11}	1.5	100	D64
$\text{CH}_3\text{C(O)O}_2 + \text{NO}_2 \xrightarrow{\text{M}} \text{products}$	(See Table 2-1)					
$\text{CH}_3\text{C(O)CH}_2\text{O}_2 + \text{NO} \rightarrow \text{products}$	2.9×10^{-12}	-300	8.0×10^{-12}	1.5	300	D65
$\text{CH}_2=\text{C}(\text{CH}_3)\text{CH}=\text{CH}_2 + \text{NO}_3 \rightarrow \text{products}$	3.3×10^{-12}	450	7.3×10^{-13}	1.25	100	D66

Reaction	A-Factor ^a	E/R	k(298 K) ^a	f(298 K) ^b	g	Notes
FO_x Reactions						
O + FO → F + O ₂	2.7×10 ⁻¹¹	0	2.7×10 ⁻¹¹	3.0	250	E 1
O + FO ₂ → FO + O ₂	5.0×10 ⁻¹¹	0	5.0×10 ⁻¹¹	5.0	250	E 2
OH + CH ₃ F → CH ₂ F + H ₂ O (HFC-41)	2.5×10 ⁻¹²	1430	2.1×10 ⁻¹⁴	1.15	150	E 3
OH + CH ₂ F ₂ → CHF ₂ + H ₂ O (HFC-32)	1.7×10 ⁻¹²	1500	1.1×10 ⁻¹⁴	1.15	150	E 4
OH + CHF ₃ → CF ₃ + H ₂ O (HFC-23)	5.2×10 ⁻¹³	2210	3.1×10 ⁻¹⁶	1.15	100	E 5
OH + CH ₃ CH ₂ F → products (HFC-161)	2.5×10 ⁻¹²	730	2.2×10 ⁻¹³	1.15	150	E 6
OH + CH ₃ CHF ₂ → products (HFC-152a)	8.7×10 ⁻¹³	975	3.3×10 ⁻¹⁴	1.07	50	E 7
OH + CH ₂ FCH ₂ F → CHFCH ₂ F + H ₂ O (HFC-152)	1.05×10 ⁻¹²	710	9.7×10 ⁻¹⁴	1.07	100	E 8
OH + CH ₃ CF ₃ → CH ₂ CF ₃ + H ₂ O (HFC-143a)	1.1×10 ⁻¹²	2010	1.3×10 ⁻¹⁵	1.1	100	E 9
OH + CH ₂ FCH ₂ F → products (HFC-143)	3.9×10 ⁻¹²	1620	1.7×10 ⁻¹⁴	1.2	200	E10
OH + CH ₂ FCF ₃ → CHFCH ₂ F + H ₂ O (HFC-134a)	1.05×10 ⁻¹²	1630	4.4×10 ⁻¹⁵	1.1	200	E11
OH + CHF ₂ CH ₂ F → CF ₂ CH ₂ F + H ₂ O (HFC-134)	1.6×10 ⁻¹²	1660	6.1×10 ⁻¹⁵	1.2	200	E12
OH + CHF ₂ CF ₃ → CF ₂ CF ₃ + H ₂ O (HFC-125)	6.0×10 ⁻¹³	1700	2.0×10 ⁻¹⁵	1.2	150	E13
OH + CH ₃ CHFCH ₃ → products (HFC-281ea)	3.0×10 ⁻¹²	490	5.8×10 ⁻¹³	1.2	100	E14
OH + CH ₃ CH ₂ CF ₃ → products (HFC-263fb)	3.7×10 ⁻¹²	1290	4.9×10 ⁻¹⁴	1.15	100	E15
OH + CH ₂ FCF ₂ CH ₂ F → products (HFC-245ca)	2.1×10 ⁻¹²	1620	9.2×10 ⁻¹⁵	1.2	150	E16
OH + CHF ₂ CH ₂ CHF ₂ → products (HFC-245ea)	1.53×10 ⁻¹²	1340	1.7×10 ⁻¹⁴	1.1	150	E17
OH + CH ₂ FCH ₂ CF ₃ → products (HFC-245eb)	1.16×10 ⁻¹²	1260	1.7×10 ⁻¹⁴	1.15	100	E18
OH + CHF ₂ CH ₂ CF ₃ → products (HFC-245fa)	6.1×10 ⁻¹³	1330	7.0×10 ⁻¹⁵	1.2	150	E19
OH + CH ₂ FCF ₂ CF ₃ → CHFCH ₂ CF ₃ + H ₂ O (HFC-236cb)	1.05×10 ⁻¹²	1630	4.4×10 ⁻¹⁵	2.0	200	E20
OH + CHF ₂ CH ₂ CF ₃ → products (HFC-236ea)	9.4×10 ⁻¹³	1550	5.2×10 ⁻¹⁵	1.2	200	E21
OH + CF ₃ CH ₂ CF ₃ → CF ₃ CHCF ₃ + H ₂ O (HFC-236fa)	1.45×10 ⁻¹²	2500	3.3×10 ⁻¹⁶	1.15	150	E22
OH + CF ₃ CH ₂ CF ₃ → CF ₃ CFCH ₂ F + H ₂ O (HFC-227ea)	6.3×10 ⁻¹³	1800	1.5×10 ⁻¹⁵	1.15	150	E23

Reaction	A-Factor ^a	E/R	k(298 K) ^a	f(298 K) ^b	g	Notes
OH + CH ₃ CF ₂ CH ₂ CF ₃ → products (HFC-365mfc)	1.8×10 ⁻¹²	1660	6.9×10 ⁻¹⁵	1.3	100	E24
OH + CF ₃ CH ₂ CH ₂ CF ₃ → products (HFC-356mff)	3.4×10 ⁻¹²	1820	7.6×10 ⁻¹⁵	1.2	300	E25
OH + CH ₂ FCH ₂ CF ₂ CF ₃ → products (HFC-356mcf)	1.7×10 ⁻¹²	1100	4.2×10 ⁻¹⁴	1.3	150	E26
OH + CHF ₂ CF ₂ CF ₂ CF ₂ H → products (HFC-338pcc)	7.7×10 ⁻¹³	1540	4.4×10 ⁻¹⁵	1.2	150	E27
OH + CF ₃ CH ₂ CF ₂ CH ₂ CF ₃ → products (HFC-458mfcf)	1.1×10 ⁻¹²	1800	2.6×10 ⁻¹⁵	1.5	200	E28
OH + CF ₃ CHFCHFCF ₂ CF ₃ → products (HFC-43-10mee)	5.2×10 ⁻¹³	1500	3.4×10 ⁻¹⁵	1.2	150	E29
OH + CF ₃ CF ₂ CH ₂ CH ₂ CF ₂ CF ₃ → products (HFC-55-10-mcff)	3.5×10 ⁻¹²	1800	8.3×10 ⁻¹⁵	1.5	300	E30
OH + CH ₂ =CHF → products	1.77×10 ⁻¹²	-310	5.0×10 ⁻¹²	1.07	50	E31
OH + CH ₂ =CF ₂ → products	1.75×10 ⁻¹²	-140	2.8×10 ⁻¹²	1.1	20	E32
OH + CF ₂ =CF ₂ → products	3.4×10 ⁻¹²	-320	1.0×10 ⁻¹¹	1.15	100	E33
OH + CH ₂ =CHCH ₂ F → products	6.0×10 ⁻¹²	-290	1.6×10 ⁻¹¹	1.3	100	E34
OH + CH ₂ =CHCF ₃ → products	7.9×10 ⁻¹³	-180	1.45×10 ⁻¹²	1.1	50	E35
OH + CH ₂ =CFCF ₃ → products	1.1×10 ⁻¹²	0	1.1×10 ⁻¹²	1.05	0	E36
OH + <i>E</i> -CHF=CHCF ₃ → products	6.1×10 ⁻¹³	-40	7.0×10 ⁻¹³	1.1	0	E37
OH + <i>E</i> -CHF=CFCF ₃ → products	1.65×10 ⁻¹²	-100	2.3×10 ⁻¹²	1.3	50	E38
OH + <i>Z</i> -CHF=CFCF ₃ → products	7.5×10 ⁻¹³	-165	1.3×10 ⁻¹²	1.07	50	E39
OH + CF ₂ =CFCF ₃ → products	8.0×10 ⁻¹³	-300	2.2×10 ⁻¹²	1.1	50	E40
OH + CH ₂ =CHCF ₂ CF ₃ → products	7.6×10 ⁻¹³	-180	1.4×10 ⁻¹²	1.2	50	E41
OH + CF ₃ OH → CF ₃ O + H ₂ O			<2×10 ⁻¹⁷			E42
OH + CH ₂ FCH ₂ OH → products	1.86×10 ⁻¹²	200	9.5×10 ⁻¹³	1.05	50	E43
OH + CHF ₂ CH ₂ OH → products	1.4×10 ⁻¹²	500	2.6×10 ⁻¹³	1.05	100	E44
OH + CF ₃ CH ₂ OH → products	1.04×10 ⁻¹²	700	9.9×10 ⁻¹⁴	1.05	100	E45
OH + CF ₃ CF ₂ CH ₂ OH → products	1.15×10 ⁻¹²	730	1.0×10 ⁻¹³	1.05	100	E46
OH + (CF ₃) ₂ CHOH → products	5.1×10 ⁻¹³	900	2.5×10 ⁻¹⁴	1.2	200	E47
OH + CF ₃ CF ₂ CF ₂ CF ₂ CH ₂ OH → products	1.16×10 ⁻¹²	730	1.0×10 ⁻¹³	1.1	200	E48

Reaction	A-Factor ^a	E/R	k(298 K) ^a	f(298 K) ^b	g	Notes
OH + CH ₃ OCHF ₂ → products (HFE-152a)	6.0×10 ⁻¹²	1530	3.5×10 ⁻¹⁴	1.3	200	E49
OH + CH ₃ OCF ₃ → CH ₂ OCF ₃ + H ₂ O (HFE-143a)	1.84×10 ⁻¹²	1500	1.2×10 ⁻¹⁴	1.1	150	E50
OH + CHF ₂ OCHF ₂ → CF ₂ OCHF ₂ + H ₂ O (HFE-134)	1.1×10 ⁻¹²	1830	2.4×10 ⁻¹⁵	1.15	150	E51
OH + CHF ₂ OCF ₃ → CF ₂ OCF ₃ + H ₂ O (HFE-125)	4.6×10 ⁻¹³	2040	4.9×10 ⁻¹⁶	1.2	200	E52
OH + CH ₃ OCHF ₂ CF ₃ → products	1.62×10 ⁻¹²	690	1.6×10 ⁻¹³	1.15	50	E53
OH + CH ₃ OCF ₂ CHF ₂ → products	1.7×10 ⁻¹²	1300	2.2×10 ⁻¹⁴	1.3	200	E54
OH + CH ₃ OCF ₂ CF ₃ → products	1.1×10 ⁻¹²	1370	1.1×10 ⁻¹⁴	1.2	150	E55
OH + CHF ₂ OCH ₂ CF ₃ → products (HFE-245fa)	2.9×10 ⁻¹²	1660	1.1×10 ⁻¹⁴	1.15	200	E56
OH + CHF ₂ OCHF ₂ CF ₃ → products	2.4×10 ⁻¹²	1800	5.7×10 ⁻¹⁵	1.4	200	E57
OH + CHF ₂ OCF ₂ CHF ₂ → products	5.8×10 ⁻¹³	1600	2.7×10 ⁻¹⁵	1.2	50	E58
OH + CF ₃ OCHF ₂ CF ₃ → products	3.6×10 ⁻¹³	1700	1.2×10 ⁻¹⁵	1.15	100	E59
OH + CH ₃ OCF ₂ CF ₂ CF ₃ → products	1.4×10 ⁻¹²	1440	1.1×10 ⁻¹⁴	1.15	150	E60
OH + CH ₃ OCF(CF ₃) ₂ → products	1.3×10 ⁻¹²	1330	1.5×10 ⁻¹⁴	1.15	100	E61
OH + CH ₃ OC ₄ F ₉ → products	1.3×10 ⁻¹²	1400	1.2×10 ⁻¹⁴	1.15	150	E62
OH + CHF ₂ OCH ₂ CF ₂ CHF ₂ → products	1.8×10 ⁻¹²	1410	1.6×10 ⁻¹⁴	1.3	200	E63
OH + CHF ₂ OCH ₂ CF ₂ CF ₃ → products	1.6×10 ⁻¹²	1510	1.0×10 ⁻¹⁴	1.3	200	E64
OH + CHF ₂ OCH(CF ₃) ₂ → products	1.03×10 ⁻¹²	1760	2.8×10 ⁻¹⁵	1.2	150	E65
OH + CH ₃ CH ₂ OCF ₂ CHF ₂ → products	2.1×10 ⁻¹²	670	2.2×10 ⁻¹³	1.1	100	E66
OH + CF ₃ CH ₂ OCH ₂ CF ₃ → products	2.8×10 ⁻¹²	890	1.4×10 ⁻¹³	1.1	100	E67
OH + CF ₃ CH ₂ OCF ₂ CHF ₂ → products (HFE-347pcf2)	1.32×10 ⁻¹²	1470	9.5×10 ⁻¹⁵	1.1	50	E68
OH + CHF ₂ OCF ₂ OCHF ₂ → products	1.0×10 ⁻¹²	1800	2.4×10 ⁻¹⁵	1.4	200	E69
OH + CHF ₂ OCF ₂ CF ₂ OCHF ₂ → products	2.0×10 ⁻¹²	1800	4.7×10 ⁻¹⁵	1.5	200	E70
OH + CHF ₂ OCF ₂ CF ₂ OCF ₂ OCHF ₂ → products	1.9×10 ⁻¹²	1800	4.6×10 ⁻¹⁵	1.5	200	E71
F + O ₂ \xrightarrow{M} FO ₂	(See Table 2-1)					
F + O ₃ → FO + O ₂	2.2×10 ⁻¹¹	230	1.0×10 ⁻¹¹	1.5	200	E72

Reaction	A-Factor ^a	E/R	k(298 K) ^a	f(298 K) ^b	g	Notes
$F + H_2 \rightarrow HF + H$	1.4×10^{-10}	500	2.6×10^{-11}	1.2	200	E73
$F + H_2O \rightarrow HF + OH$	1.4×10^{-11}	0	1.4×10^{-11}	1.3	200	E74
$F + NO \xrightarrow{M} FNO$	(See Table 2-1)					
$F + NO_2 \xrightarrow{M} FNO_2$	(See Table 2-1)					
$F + HNO_3 \rightarrow HF + NO_3$	6.0×10^{-12}	-400	2.3×10^{-11}	1.3	200	E75
$F + CH_4 \rightarrow HF + CH_3$	1.6×10^{-10}	260	6.7×10^{-11}	1.4	200	E76
$FO + O_3 \rightarrow \text{products}$			$<1 \times 10^{-14}$			E77
$FO + NO \rightarrow NO_2 + F$	8.2×10^{-12}	-300	2.2×10^{-11}	1.5	200	E78
$FO + NO_2 \xrightarrow{M} FONO_2$	(See Table 2-1)					
$FO + FO \rightarrow 2F + O_2$	1.0×10^{-11}	0	1.0×10^{-11}	1.5	250	E79
$FO_2 + O_3 \rightarrow \text{products}$			$<3.4 \times 10^{-16}$			E80
$FO_2 + NO \rightarrow FNO + O_2$	7.5×10^{-12}	690	7.5×10^{-13}	2.0	400	E81
$FO_2 + NO_2 \rightarrow \text{products}$	3.8×10^{-11}	2040	4.0×10^{-14}	2.0	500	E82
$FO_2 + CO \rightarrow \text{products}$			$<5.1 \times 10^{-16}$			E83
$FO_2 + CH_4 \rightarrow \text{products}$			$<2 \times 10^{-16}$			E84
$CF_3 + O_2 \xrightarrow{M} CF_3O_2$	(See Table 2-1)					
$CF_3O + M \rightarrow F + CF_2O + M$	(See Table 2-1)					
$CF_3O + O_2 \rightarrow FO_2 + CF_2O$	$<3 \times 10^{-11}$	5000	$<1.5 \times 10^{-18}$	1.3	-	E85
$CF_3O + O_3 \rightarrow CF_3O_2 + O_2$	2×10^{-12}	1400	1.8×10^{-14}		600	E86
$CF_3O + H_2O \rightarrow OH + CF_3OH$	3×10^{-12}	>3600	$<2 \times 10^{-17}$	1.2	-	E87
$CF_3O + NO \rightarrow CF_2O + FNO$	3.7×10^{-11}	-110	5.4×10^{-11}		70	E88
$CF_3O + NO_2 \rightarrow \text{products}$	(See Note)					E89
$\xrightarrow{M} CF_3ONO_2$	(See Table 2-1)					
$CF_3O + CO \rightarrow \text{products}$			$<2 \times 10^{-15}$			E90
$\xrightarrow{M} CF_3OCO$	(See Table 2-1)					

Reaction	A-Factor ^a	E/R	k(298 K) ^a	f(298 K) ^b	g	Notes
$\text{CF}_3\text{O} + \text{CH}_4 \rightarrow \text{CH}_3 + \text{CF}_3\text{OH}$	2.6×10^{-12}	1420	2.2×10^{-14}	1.1	200	E91
$\text{CF}_3\text{O} + \text{C}_2\text{H}_6 \rightarrow \text{C}_2\text{H}_5 + \text{CF}_3\text{OH}$	4.9×10^{-12}	400	1.3×10^{-12}	1.2	100	E92
$\text{CF}_3\text{O}_2 + \text{O}_3 \rightarrow \text{CF}_3\text{O} + 2\text{O}_2$			$<3 \times 10^{-15}$			E93
$\text{CF}_3\text{O}_2 + \text{CO} \rightarrow \text{CF}_3\text{O} + \text{CO}_2$			$<5 \times 10^{-16}$			E94
$\text{CF}_3\text{O}_2 + \text{NO} \rightarrow \text{CF}_3\text{O} + \text{NO}_2$	5.4×10^{-12}	-320	1.6×10^{-11}	1.1	150	E95
$\text{CF}_3\text{O}_2 + \text{NO}_2 \xrightarrow{\text{M}} \text{CF}_3\text{O}_2\text{NO}_2$	(See Table 2-1)					
ClO_x Reactions						
$\text{O} + \text{ClO} \rightarrow \text{Cl} + \text{O}_2$	2.8×10^{-11}	-85	3.7×10^{-11}	1.05	50	F 1
$\text{O} + \text{OCIO} \rightarrow \text{ClO} + \text{O}_2$	2.4×10^{-12}	960	1.0×10^{-13}	2.0	300	F 2
$\text{O} + \text{OCIO} \xrightarrow{\text{M}} \text{ClO}_3$	(See Table 2-1)					
$\text{O} + \text{Cl}_2\text{O} \rightarrow \text{ClO} + \text{ClO}$	2.7×10^{-11}	530	4.5×10^{-12}	1.2	100	F 3
$\text{O} + \text{HCl} \rightarrow \text{OH} + \text{Cl}$	1.0×10^{-11}	3300	1.5×10^{-16}	1.5	350	F 4
$\text{O} + \text{HOCl} \rightarrow \text{OH} + \text{ClO}$	1.7×10^{-13}	0	1.7×10^{-13}	3.0	300	F 5
$\text{O} + \text{ClONO}_2 \rightarrow \text{products}$	3.6×10^{-12}	840	2.1×10^{-13}	1.2	100	F 6
$\text{O}_3 + \text{OCIO} \rightarrow \text{products}$	2.1×10^{-12}	4700	3.0×10^{-19}	2.5	1000	F 7
$\text{O}_3 + \text{Cl}_2\text{O}_2 \rightarrow \text{products}$			$<1.0 \times 10^{-19}$			F 8
$\text{OH} + \text{Cl}_2 \rightarrow \text{HOCl} + \text{Cl}$	2.6×10^{-12}	1100	6.5×10^{-14}	1.1	200	F 9
$\text{OH} + \text{ClO} \rightarrow \text{Cl} + \text{HO}_2$ $\rightarrow \text{HCl} + \text{O}_2$	7.4×10^{-12} 6.0×10^{-13}	-270 -230	1.8×10^{-11} 1.3×10^{-12}	1.2 1.7	50 100	F10
$\text{OH} + \text{OCIO} \rightarrow \text{HOCl} + \text{O}_2$	1.4×10^{-12}	-600	1.0×10^{-11}	1.5	150	F11
$\text{OH} + \text{Cl}_2\text{O} \rightarrow \text{HOCl} + \text{ClO}$	4.7×10^{-12}	-140	7.5×10^{-12}	1.2	100	F12
$\text{OH} + \text{Cl}_2\text{O}_2 \rightarrow \text{HOCl} + \text{ClOO}$	6.0×10^{-13}	-670	5.7×10^{-12}	1.3	100	F13
$\text{OH} + \text{HCl} \rightarrow \text{H}_2\text{O} + \text{Cl}$	1.8×10^{-12}	250	7.8×10^{-13}	1.1	50	F14
$\text{OH} + \text{HOCl} \rightarrow \text{H}_2\text{O} + \text{ClO}$	3.0×10^{-12}	500	5.0×10^{-13}	3.0	500	F15
$\text{OH} + \text{ClONO}_2 \rightarrow \text{HOCl} + \text{NO}_2$	2.4×10^{-12}	1250	3.6×10^{-14}	2.0	300	F16
$\text{OH} + \text{ClONO}_2 \rightarrow \text{products}$	1.2×10^{-12}	330	3.9×10^{-13}	1.5	200	F17

Reaction	A-Factor ^a	E/R	k(298 K) ^a	f(298 K) ^b	g	Notes
$\text{OH} + \text{CH}_3\text{Cl} \rightarrow \text{CH}_2\text{Cl} + \text{H}_2\text{O}$	2.4×10^{-12}	1250	3.6×10^{-14}	1.15	100	F18
$\text{OH} + \text{CH}_2\text{Cl}_2 \rightarrow \text{CHCl}_2 + \text{H}_2\text{O}$	1.9×10^{-12}	870	1.0×10^{-13}	1.15	100	F19
$\text{OH} + \text{CHCl}_3 \rightarrow \text{CCl}_3 + \text{H}_2\text{O}$	2.2×10^{-12}	920	1.0×10^{-13}	1.15	150	F20
$\text{OH} + \text{CCl}_4 \rightarrow \text{products}$	$\sim 1.0 \times 10^{-12}$	>2300	$< 5.0 \times 10^{-16}$	–	–	F21
$\text{OH} + \text{CH}_2\text{FCl} \rightarrow \text{CHClF} + \text{H}_2\text{O}$ (HCFC-31)	2.4×10^{-12}	1210	4.1×10^{-14}	1.15	200	F22
$\text{OH} + \text{CHFCl}_2 \rightarrow \text{CFCl}_2 + \text{H}_2\text{O}$ (HCFC-21)	1.2×10^{-12}	1100	3.0×10^{-14}	1.2	150	F23
$\text{OH} + \text{CHF}_2\text{Cl} \rightarrow \text{CF}_2\text{Cl} + \text{H}_2\text{O}$ (HCFC-22)	1.05×10^{-12}	1600	4.8×10^{-15}	1.1	150	F24
$\text{OH} + \text{CFCl}_3 \rightarrow \text{products}$ (CFC-11)	$\sim 1.0 \times 10^{-12}$	>3700	$< 5.0 \times 10^{-18}$			F25
$\text{OH} + \text{CF}_2\text{Cl}_2 \rightarrow \text{products}$ (CFC-12)	$\sim 1.0 \times 10^{-12}$	>3600	$< 6.0 \times 10^{-18}$			F26
$\text{OH} + \text{CH}_2\text{ClCH}_3 \rightarrow \text{products}$	5.4×10^{-12}	800	3.7×10^{-13}	1.2	100	F27
$\text{OH} + \text{CH}_3\text{CCl}_3 \rightarrow \text{CH}_2\text{CCl}_3 + \text{H}_2\text{O}$	1.64×10^{-12}	1520	1.0×10^{-14}	1.15	100	F28
$\text{OH} + \text{CH}_3\text{CFCl}_2 \rightarrow \text{CH}_2\text{CFCl}_2 + \text{H}_2\text{O}$ (HCFC-141b)	1.25×10^{-12}	1600	5.8×10^{-15}	1.15	150	F29
$\text{OH} + \text{CH}_3\text{CF}_2\text{Cl} \rightarrow \text{CH}_2\text{CF}_2\text{Cl} + \text{H}_2\text{O}$ (HCFC-142b)	1.3×10^{-12}	1770	3.4×10^{-15}	1.2	150	F30
$\text{OH} + \text{CH}_2\text{ClCF}_2\text{Cl} \rightarrow \text{CHClCF}_2\text{Cl} + \text{H}_2\text{O}$ (HCFC-132b)	3.6×10^{-12}	1600	1.7×10^{-14}	1.5	200	F31
$\text{OH} + \text{CH}_2\text{ClCF}_3 \rightarrow \text{CHClCF}_3 + \text{H}_2\text{O}$ (HCFC-133a)	1.43×10^{-12}	1400	1.3×10^{-14}	1.3	150	F32
$\text{OH} + \text{CHCl}_2\text{CF}_2\text{Cl} \rightarrow \text{CCl}_2\text{CF}_2\text{Cl}$ (HCFC-122) + H_2O	7.7×10^{-13}	810	5.1×10^{-14}	1.2	150	F33
$\text{OH} + \text{CHFClCFCl}_2 \rightarrow \text{CFCICFCl}_2$ (HCFC-122a) + H_2O	7.1×10^{-13}	1140	1.6×10^{-14}	1.3	150	F34
$\text{OH} + \text{CHCl}_2\text{CF}_3 \rightarrow \text{CCl}_2\text{CF}_3 + \text{H}_2\text{O}$ (HCFC-123)	6.3×10^{-13}	850	3.6×10^{-14}	1.2	100	F35
$\text{OH} + \text{CHFClCF}_2\text{Cl} \rightarrow \text{CFCICF}_2\text{Cl} + \text{H}_2\text{O}$ (HCFC-123a)	8.6×10^{-13}	1250	1.3×10^{-14}	1.3	200	F36
$\text{OH} + \text{CHFClCF}_3 \rightarrow \text{CFCICF}_3 + \text{H}_2\text{O}$ (HCFC-124)	7.1×10^{-13}	1300	9.0×10^{-15}	1.15	100	F37
$\text{OH} + \text{CH}_3\text{CF}_2\text{CFCl}_2 \rightarrow \text{products}$ (HCFC-243cc)	7.7×10^{-13}	1720	2.4×10^{-15}	1.3	200	F38
$\text{OH} + \text{CHCl}_2\text{CF}_2\text{CF}_3 \rightarrow \text{products}$ (HCFC-225ca)	6.3×10^{-13}	960	2.5×10^{-14}	1.2	200	F39
$\text{OH} + \text{CHFClCF}_2\text{CF}_2\text{Cl} \rightarrow \text{products}$ (HCFC-225cb)	5.5×10^{-13}	1230	8.9×10^{-15}	1.2	150	F40
$\text{OH} + \text{CF}_3\text{CH}_2\text{CFCl}_2 \rightarrow \text{CF}_3\text{CHCFCl}_2 + \text{H}_2\text{O}$	1.8×10^{-12}	2300	8.0×10^{-16}	1.5	200	F41
$\text{OH} + \text{CH}_2=\text{CHCl} \rightarrow \text{products}$	1.3×10^{-12}	–500	6.9×10^{-12}	1.2	100	F42

Reaction	A-Factor ^a	E/R	k(298 K) ^a	f(298 K) ^b	g	Notes
OH + CH ₂ =CCl ₂ → products	1.9×10 ⁻¹²	-530	1.1×10 ⁻¹¹	1.15	150	F43
OH + CHCl=CCl ₂ → products	8.0×10 ⁻¹³	-300	2.2×10 ⁻¹²	1.2	100	F44
OH + CCl ₂ =CCl ₂ → products	4.7×10 ⁻¹²	990	1.7×10 ⁻¹³	1.2	200	F45
OH + CHF ₂ OCHClCF ₃ → products	1.1×10 ⁻¹²	1275	1.5×10 ⁻¹⁴	1.1	50	F46
OH + CH ₃ OCl → products	2.5×10 ⁻¹²	370	7.1×10 ⁻¹³	2.0	150	F47
OH + CCl ₃ CHO → H ₂ O + CCl ₃ CO	9.1×10 ⁻¹²	580	1.3×10 ⁻¹²	1.3	200	F48
HO ₂ + Cl → HCl + O ₂	1.4×10 ⁻¹¹	-270	3.5×10 ⁻¹¹	1.2	100	F49
→ OH + ClO	3.6×10 ⁻¹¹	375	1.0×10 ⁻¹¹	1.4	150	
HO ₂ + ClO → HOCl + O ₂	2.6×10 ⁻¹²	-290	6.9×10 ⁻¹²	1.2	150	F50
H ₂ O + ClONO ₂ → products			<2.0×10 ⁻²¹			F51
NO + OClO → NO ₂ + ClO	2.5×10 ⁻¹²	600	3.4×10 ⁻¹³	2.0	300	F52
NO + Cl ₂ O ₂ → products			<1.0×10 ⁻¹⁵			F53
NO ₃ + OClO \xrightarrow{M} O ₂ ClONO ₂	(See Table 2-1)					
NO ₃ + HCl → HNO ₃ + Cl			<5.0×10 ⁻¹⁷			F54
HO ₂ NO ₂ + HCl → products			<1.0×10 ⁻²¹			F55
Cl + O ₂ \xrightarrow{M} ClOO	(See Table 2-1)					
Cl + O ₃ → ClO + O ₂	2.3×10 ⁻¹¹	200	1.2×10 ⁻¹¹	1.15	50	F56
Cl + H ₂ → HCl + H	3.05×10 ⁻¹¹	2270	1.5×10 ⁻¹⁴	1.1	100	F57
Cl + H ₂ O ₂ → HCl + HO ₂	1.1×10 ⁻¹¹	980	4.1×10 ⁻¹³	1.3	300	F58
Cl + NO \xrightarrow{M} NOCl	(See Table 2-1)					
Cl + NO ₂ \xrightarrow{M} ClONO (ClONO ₂)	(See Table 2-1)					
Cl + NO ₃ → ClO + NO ₂	2.4×10 ⁻¹¹	0	2.4×10 ⁻¹¹	1.5	400	F59
Cl + N ₂ O → ClO + N ₂	(See Note)					F60
Cl + HNO ₃ → products			<2.0×10 ⁻¹⁶			F61
Cl + HO ₂ NO ₂ → products			<1×10 ⁻¹³			F62

Reaction	A-Factor ^a	E/R	k(298 K) ^a	f(298 K) ^b	g	Notes
$\text{Cl} + \text{CO} \xrightarrow{\text{M}} \text{ClCO}$	(See Table 2-1)					
$\text{Cl} + \text{CH}_4 \rightarrow \text{HCl} + \text{CH}_3$	7.3×10^{-12}	1280	1.0×10^{-13}	1.05	50	F63
$\text{Cl} + \text{CH}_3\text{D} \rightarrow \text{products}$	7.0×10^{-12}	1380	6.8×10^{-14}	1.07	50	F64
$\text{Cl} + \text{H}_2\text{CO} \rightarrow \text{HCl} + \text{HCO}$	8.1×10^{-11}	30	7.3×10^{-11}	1.15	100	F65
$\text{Cl} + \text{HC(O)OH} \rightarrow \text{products}$			2.0×10^{-13}	1.5		F66
$\text{Cl} + \text{CH}_3\text{O}_2 \rightarrow \text{products}$			1.6×10^{-10}	1.5		F67
$\text{Cl} + \text{CH}_3\text{OH} \rightarrow \text{CH}_2\text{OH} + \text{HCl}$	5.5×10^{-11}	0	5.5×10^{-11}	1.2	100	F68
$\text{Cl} + \text{CH}_3\text{OOH} \rightarrow \text{products}$			5.7×10^{-11}	2.0		F69
$\text{Cl} + \text{CH}_3\text{ONO}_2 \rightarrow \text{products}$	1.3×10^{-11}	1200	2.3×10^{-13}	1.5	300	F70
$\text{Cl} + \text{C}_2\text{H}_2 \xrightarrow{\text{M}} \text{ClC}_2\text{H}_2$	(See Table 2-1)					
$\text{Cl} + \text{C}_2\text{H}_4 \xrightarrow{\text{M}} \text{ClC}_2\text{H}_4$	(See Table 2-1)					
$\text{Cl} + \text{C}_2\text{H}_6 \rightarrow \text{HCl} + \text{C}_2\text{H}_5$	7.2×10^{-11}	70	5.7×10^{-11}	1.07	20	F71
$\text{Cl} + \text{C}_2\text{H}_5\text{O}_2 \rightarrow \text{ClO} + \text{C}_2\text{H}_5\text{O}$ $\rightarrow \text{HCl} + \text{C}_2\text{H}_4\text{O}_2$			7.4×10^{-11} 7.7×10^{-11}	2.0 2.0		F72
$\text{Cl} + \text{CH}_3\text{CH}_2\text{OH} \rightarrow \text{products}$	9.6×10^{-11}	0	9.6×10^{-11}	1.2	100	F73
$\text{Cl} + \text{CH}_3\text{C(O)OH} \rightarrow \text{products}$			2.8×10^{-14}	2.0		F74
$\text{Cl} + \text{CH}_3\text{CN} \rightarrow \text{products}$	1.6×10^{-11}	2140	1.2×10^{-14}	2.0	300	F75
$\text{Cl} + \text{C}_2\text{H}_5\text{ONO}_2 \rightarrow \text{products}$	1.5×10^{-11}	400	3.9×10^{-12}	1.5	200	F76
$\text{Cl} + \text{CH}_3\text{CO}_3\text{NO}_2 \rightarrow \text{products}$			$<1 \times 10^{-14}$			F77
$\text{Cl} + \text{C}_3\text{H}_8 \rightarrow \text{HCl} + \text{CH}_3\text{CHCH}_3$ $\rightarrow \text{HCl} + \text{CH}_2\text{CH}_2\text{CH}_3$	6.54×10^{-11} 7.85×10^{-11}		8.0×10^{-11} 6.0×10^{-11}	1.1 1.05	20 20	F78
$\text{Cl} + \text{CH}_3\text{C(O)CH}_3 \rightarrow \text{CH}_3\text{C(O)CH}_2 + \text{HCl}$	7.7×10^{-11}	1000	2.7×10^{-12}	1.3	500	F79
$\text{Cl} + \text{CH}_2=\text{C}(\text{CH}_3)\text{CH}=\text{CH}_2 \rightarrow \text{products}$	7.7×10^{-11}	-500	4.1×10^{-10}	1.15	100	F80
$\text{Cl} + \text{C}_2\text{H}_5\text{CO}_3\text{NO}_2 \rightarrow \text{products}$			1.1×10^{-12}	2.0		F81
$\text{Cl} + 1\text{-C}_3\text{H}_7\text{ONO}_2 \rightarrow \text{products}$			2.3×10^{-11}	1.5		F82

Reaction	A-Factor ^a	E/R	k(298 K) ^a	f(298 K) ^b	g	Notes
Cl + 2-C ₃ H ₇ ONO ₂ → products			4.0×10 ⁻¹²	2.0		F83
Cl + OCIO → ClO + ClO	3.4×10 ⁻¹¹	-160	5.8×10 ⁻¹¹	1.25	200	F84
Cl + ClOO → Cl ₂ + O ₂	2.3×10 ⁻¹⁰	0	2.3×10 ⁻¹⁰	2.0	200	F85
→ ClO + ClO	1.2×10 ⁻¹¹	0	1.2×10 ⁻¹¹	2.0	200	
Cl + Cl ₂ O → Cl ₂ + ClO	6.2×10 ⁻¹¹	-130	9.6×10 ⁻¹¹	1.2	130	F86
Cl + Cl ₂ O ₂ → products	7.6×10 ⁻¹¹	9.4×10 ⁻¹¹	1.0×10 ⁻¹⁰	1.2	100	F87
Cl + HOCl → products	3.4×10 ⁻¹²	130	2.2×10 ⁻¹²	1.3	200	F88
Cl + ClNO → NO + Cl ₂	5.8×10 ⁻¹¹	-100	8.1×10 ⁻¹¹	1.5	200	F89
Cl + ClONO ₂ → products	6.5×10 ⁻¹²	-135	1.0×10 ⁻¹¹	1.1	50	F90
Cl + CH ₃ Cl → CH ₂ Cl + HCl	2.17×10 ⁻¹¹	1130	4.9×10 ⁻¹³	1.07	50	F91
Cl + CH ₂ Cl ₂ → HCl + CHCl ₂	7.4×10 ⁻¹²	910	3.5×10 ⁻¹³	1.07	100	F92
Cl + CHCl ₃ → HCl + CCl ₃	3.310 ⁻¹²	990	1.2×10 ⁻¹³	1.15	100	F93
Cl + CH ₃ F → HCl + CH ₂ F (HFC-41)	1.96×10 ⁻¹¹	1200	3.5×10 ⁻¹³	1.15	150	F94
Cl + CH ₂ F ₂ → HCl + CHF ₂ (HFC-32)	4.9×10 ⁻¹²	1500	3.2×10 ⁻¹⁴	1.5	200	F95
Cl + CHF ₃ → HCl + CF ₃ (HFC-23)			<5.0×10 ⁻¹⁶			F96
Cl + CH ₂ FCI → HCl + CHFCl (HCFC-31)	5.9×10 ⁻¹²	1200	1.05×10 ⁻¹³	1.1	200	F97
Cl + CHFCl ₂ → HCl + CFCl ₂ (HCFC-21)	6.0×10 ⁻¹²	1700	2.0×10 ⁻¹⁴	1.2	200	F98
Cl + CHF ₂ Cl → HCl + CF ₂ Cl (HCFC-22)	5.6×10 ⁻¹²	2430	1.6×10 ⁻¹⁵	1.15	200	F99
Cl + CH ₃ CCl ₃ → CH ₂ CCl ₃ + HCl	3.23×10 ⁻¹²	1770	8.5×10 ⁻¹⁵	1.2	200	F100
Cl + CH ₃ CH ₂ F → HCl + CH ₃ CHF (HFC-161)	1.82×10 ⁻¹¹	330	6.0×10 ⁻¹²	1.1	100	F101
→ HCl + CH ₂ CH ₂ F	1.4×10 ⁻¹¹	940	6.0×10 ⁻¹³	1.15	100	
Cl + CH ₃ CHF ₂ → HCl + CH ₃ CF ₂ (HFC-152a)	5.8×10 ⁻¹²	950	2.4×10 ⁻¹³	1.1	100	F102
→ HCl + CH ₂ CHF ₂	6.25×10 ⁻¹²	2320	2.6×10 ⁻¹⁵	1.15	200	
Cl + CH ₂ FCH ₂ F → HCl + CHFCH ₂ F (HFC-152)	2.27×10 ⁻¹¹	1050	6.7×10 ⁻¹³	1.15	200	F103
Cl + CH ₃ CFCl ₂ → HCl + CH ₂ CFCl ₂ (HCFC-141b)	3.4×10 ⁻¹²	2200	2.1×10 ⁻¹⁵	1.15	200	F104

Reaction	A-Factor ^a	E/R	k(298 K) ^a	f(298 K) ^b	g	Notes
Cl + CH ₃ CF ₂ Cl → HCl + CH ₂ CF ₂ Cl (HCFC-142b)	1.35x10 ⁻¹²	2400	4.3x10 ⁻¹⁶	1.15	200	F105
Cl + CH ₃ CF ₃ → HCl + CH ₂ CF ₃ (HFC-143a)	1.44x10 ⁻¹¹	3940	2.6x10 ⁻¹⁷	3.0	300	F106
Cl + CH ₂ FCHF ₂ → HCl + CH ₂ FCF ₂ (HFC-143)	6.8x10 ⁻¹²	1670	2.5x10 ⁻¹⁴	1.3	200	F107
→ HCl + CHFCHF ₂	9.1x10 ⁻¹²	1770	2.4x10 ⁻¹⁴	1.3	200	
Cl + CH ₂ ClCF ₃ → HCl + CHClCF ₃ (HCFC-133a)	1.83x10 ⁻¹²	1680	6.5x10 ⁻¹⁵	1.2	200	F108
Cl + CH ₂ FCF ₃ → HCl + CHF ₂ CF ₃ (HFC-134a)	2.4x10 ⁻¹²	2200	1.5x10 ⁻¹⁵	1.1	200	F109
Cl + CHF ₂ CHF ₂ → HCl + CF ₂ CHF ₂ (HCF-134)	7.0x10 ⁻¹²	2430	2.0x10 ⁻¹⁵	1.2	200	F110
Cl + CHCl ₂ CF ₃ → HCl + CCl ₂ CF ₃ (HCFC-123)	5.0x10 ⁻¹²	1800	1.2x10 ⁻¹⁴	1.15	200	F111
Cl + CHFClCF ₃ → HCl + CFCICF ₃ (HCFC-124)	1.13x10 ⁻¹²	1800	2.7x10 ⁻¹⁵	1.2	200	F112
Cl + CHF ₂ CF ₃ → HCl + CF ₂ CF ₃ (HFC-125)	1.8x10 ⁻¹²	2600	3.0x10 ⁻¹⁶	1.5	300	F113
Cl + C ₂ Cl ₄ \xrightarrow{M} C ₂ Cl ₅	(See Table 2-1)					
ClO + O ₃ → ClOO + O ₂			<1.4x10 ⁻¹⁷			F114
→ OCIO + O ₂	1.0x10 ⁻¹²	>4000	<1.0x10 ⁻¹⁸			
ClO + H ₂ → products	~1.0x10 ⁻¹²	>4800	<1.0x10 ⁻¹⁹			F115
ClO + NO → NO ₂ + Cl	6.4x10 ⁻¹²	-290	1.7x10 ⁻¹¹	1.15	100	F116
ClO + NO ₂ \xrightarrow{M} ClONO ₂	(See Table 2-1)					
ClO + NO ₃ → ClOO + NO ₂	4.7x10 ⁻¹³	0	4.7x10 ⁻¹³	1.5	400	F117
ClO + N ₂ O → products	~1.0x10 ⁻¹²	>4300	<6.0x10 ⁻¹⁹			F118
ClO + CO → products	~1.0x10 ⁻¹²	>3700	<4.0x10 ⁻¹⁸			F119
ClO + CH ₄ → products	~1.0x10 ⁻¹²	>3700	<4.0x10 ⁻¹⁸			F120
ClO + H ₂ CO → products	~1.0x10 ⁻¹²	>2100	<1.0x10 ⁻¹⁵			F121
ClO + CH ₃ O ₂ → products	3.3x10 ⁻¹²	115	2.2x10 ⁻¹²	1.5	115	F122
ClO + ClO → Cl ₂ + O ₂	1.0x10 ⁻¹²	1590	4.8x10 ⁻¹⁵	1.5	300	F123
→ ClOO + Cl	3.0x10 ⁻¹¹	2450	8.0x10 ⁻¹⁵	1.5	500	
→ OCIO + Cl	3.5x10 ⁻¹³	1370	3.5x10 ⁻¹⁵	1.5	300	

Reaction	A-Factor ^a	E/R	k(298 K) ^a	f(298 K) ^b	g	Notes
$\text{ClO} + \text{ClO} \xrightarrow{\text{M}} \text{Cl}_2\text{O}_2$	(See Table 2-1)					
$\text{ClO} + \text{OCIO} \xrightarrow{\text{M}} \text{Cl}_2\text{O}_3$	(See Table 2-1)					
$\text{HCl} + \text{ClONO}_2 \rightarrow \text{products}$			$<1.0 \times 10^{-20}$			<u>F124</u>
$\text{CH}_2\text{Cl} + \text{O}_2 \xrightarrow{\text{M}} \text{CH}_2\text{ClO}_2$	(See Table 2-1)					
$\text{CHCl}_2 + \text{O}_2 \xrightarrow{\text{M}} \text{CHCl}_2\text{O}_2$	(See Table 2-1)					
$\text{CCl}_3 + \text{O}_2 \xrightarrow{\text{M}} \text{CCl}_3\text{O}_2$	(See Table 2-1)					
$\text{CFCl}_2 + \text{O}_2 \xrightarrow{\text{M}} \text{CFCl}_2\text{O}_2$	(See Table 2-1)					
$\text{CF}_2\text{Cl} + \text{O}_2 \xrightarrow{\text{M}} \text{CF}_2\text{ClO}_2$	(See Table 2-1)					
$\text{CCl}_3\text{O}_2 + \text{NO}_2 \xrightarrow{\text{M}} \text{CCl}_3\text{O}_2\text{NO}_2$	(See Table 2-1)					
$\text{CFCl}_2\text{O}_2 + \text{NO}_2 \xrightarrow{\text{M}} \text{CFCl}_2\text{O}_2\text{NO}_2$	(See Table 2-1)					
$\text{CF}_2\text{ClO}_2 + \text{NO}_2 \xrightarrow{\text{M}} \text{CF}_2\text{ClO}_2\text{NO}_2$	(See Table 2-1)					
$\text{CH}_2\text{ClO} + \text{O}_2 \rightarrow \text{CHClO} + \text{HO}_2$			6×10^{-14}	5		<u>F125</u>
$\text{CH}_2\text{ClO}_2 + \text{HO}_2 \rightarrow \text{CH}_2\text{ClO}_2\text{H} + \text{O}_2$	3.3×10^{-13}	-820	5.2×10^{-12}	1.5	200	<u>F126</u>
$\text{CH}_2\text{ClO}_2 + \text{NO} \rightarrow \text{CH}_2\text{ClO} + \text{NO}_2$	7×10^{-12}	-300	1.9×10^{-11}	1.5	200	<u>F127</u>
$\text{CCl}_3\text{O}_2 + \text{NO} \rightarrow \text{CCl}_2\text{O} + \text{NO}_2 + \text{Cl}$	7.3×10^{-12}	-270	1.8×10^{-11}	1.3	200	<u>F128</u>
$\text{CCl}_2\text{FO}_2 + \text{NO} \rightarrow \text{CClFO} + \text{NO}_2 + \text{Cl}$	4.5×10^{-12}	-350	1.5×10^{-11}	1.3	200	<u>F129</u>
$\text{CClF}_2\text{O}_2 + \text{NO} \rightarrow \text{CF}_2\text{O} + \text{NO}_2 + \text{Cl}$	3.8×10^{-12}	-400	1.5×10^{-11}	1.2	200	<u>F130</u>
BrO_x Reactions						
$\text{O} + \text{BrO} \rightarrow \text{Br} + \text{O}_2$	1.9×10^{-11}	-230	4.1×10^{-11}	1.5	150	<u>G 1</u>
$\text{O} + \text{HBr} \rightarrow \text{OH} + \text{Br}$	5.8×10^{-12}	1500	3.8×10^{-14}	1.3	200	<u>G 2</u>
$\text{O} + \text{HOBr} \rightarrow \text{OH} + \text{BrO}$	1.2×10^{-10}	430	2.8×10^{-11}	3.0	300	<u>G 3</u>
$\text{O} + \text{BrONO}_2 \rightarrow \text{NO}_3 + \text{BrO}$	1.9×10^{-11}	-215	3.9×10^{-11}	1.25	40	<u>G 4</u>
$\text{OH} + \text{Br}_2 \rightarrow \text{HOBr} + \text{Br}$	2.1×10^{-11}	-240	4.6×10^{-11}	1.1	50	<u>G 5</u>
$\text{OH} + \text{BrO} \rightarrow \text{products}$	1.7×10^{-11}	-250	3.9×10^{-11}	1.4	100	<u>G 6</u>
$\text{OH} + \text{HBr} \rightarrow \text{H}_2\text{O} + \text{Br}$	5.5×10^{-12}	-200	1.1×10^{-11}	1.1	100	<u>G 7</u>

Reaction	A-Factor ^a	E/R	k(298 K) ^a	f(298 K) ^b	g	Notes
$\text{OH} + \text{CH}_3\text{Br} \rightarrow \text{CH}_2\text{Br} + \text{H}_2\text{O}$	2.35×10^{-12}	1300	3.0×10^{-14}	1.1	100	G 8
$\text{OH} + \text{CH}_2\text{Br}_2 \rightarrow \text{CHBr}_2 + \text{H}_2\text{O}$	2.0×10^{-12}	840	1.2×10^{-13}	1.15	150	G 9
$\text{OH} + \text{CHBr}_3 \rightarrow \text{CBr}_3 + \text{H}_2\text{O}$	1.35×10^{-12}	600	1.8×10^{-13}	1.5	100	G10
$\text{OH} + \text{CHF}_2\text{Br} \rightarrow \text{CF}_2\text{Br} + \text{H}_2\text{O}$	1.0×10^{-12}	1380	1.0×10^{-14}	1.1	100	G11
$\text{OH} + \text{CH}_2\text{ClBr} \rightarrow \text{CHClBr} + \text{H}_2\text{O}$	2.4×10^{-12}	920	1.1×10^{-13}	1.1	100	G12
$\text{OH} + \text{CF}_2\text{Br}_2 \rightarrow \text{products}$ (Halon-1202)	$\sim 1 \times 10^{-12}$	>2200	$< 5.0 \times 10^{-16}$			G13
$\text{OH} + \text{CF}_3\text{Br} \rightarrow \text{products}$ (Halon-1301)	$\sim 1 \times 10^{-12}$	>3600	$< 6.0 \times 10^{-18}$			G14
$\text{OH} + \text{CF}_2\text{ClBr} \rightarrow \text{products}$ (Halon-1211)	$\sim 1 \times 10^{-12}$	>2600	$< 1.5 \times 10^{-16}$			G15
$\text{OH} + \text{CH}_2\text{BrCH}_3 \rightarrow \text{products}$	2.9×10^{-12}	640	3.4×10^{-13}	1.2	150	G16
$\text{OH} + \text{CH}_2\text{BrCF}_3 \rightarrow \text{CHBrCF}_3 + \text{H}_2\text{O}$	1.4×10^{-12}	1340	1.6×10^{-14}	1.2	150	G17
$\text{OH} + \text{CHFBrCF}_3 \rightarrow \text{CFBrCF}_3 + \text{H}_2\text{O}$	7.3×10^{-13}	1120	1.7×10^{-14}	1.2	100	G18
$\text{OH} + \text{CHClBrCF}_3 \rightarrow \text{CClBrCF}_3 + \text{H}_2\text{O}$	1.1×10^{-12}	940	4.7×10^{-14}	1.2	150	G19
$\text{OH} + \text{CHFCICF}_2\text{Br} \rightarrow \text{CFCICF}_2\text{Br} + \text{H}_2\text{O}$	8.4×10^{-13}	1220	1.4×10^{-14}	1.3	200	G20
$\text{OH} + \text{CF}_2\text{BrCF}_2\text{Br} \rightarrow \text{products}$ (Halon-2402)	$\sim 1 \times 10^{-12}$	>3600	$< 6 \times 10^{-18}$			G21
$\text{OH} + \text{CH}_2\text{BrCH}_2\text{CH}_3 \rightarrow \text{products}$	3.0×10^{-12}	330	1.0×10^{-12}	1.05	50	G22
$\text{OH} + \text{CH}_3\text{CHBrCH}_3 \rightarrow \text{products}$	1.85×10^{-12}	270	7.5×10^{-13}	1.05	50	G23
$\text{HO}_2 + \text{Br} \rightarrow \text{HBr} + \text{O}_2$	4.8×10^{-12}	310	1.7×10^{-12}	1.3	150	G24
$\text{HO}_2 + \text{BrO} \rightarrow \text{products}$	4.5×10^{-12}	-460	2.1×10^{-11}	1.15	100	G25
$\text{NO}_3 + \text{HBr} \rightarrow \text{HNO}_3 + \text{Br}$			$< 1.0 \times 10^{-16}$			G26
$\text{Cl} + \text{CH}_3\text{Br} \rightarrow \text{HCl} + \text{CH}_2\text{Br}$	1.4×10^{-11}	1030	4.4×10^{-13}	1.05	50	G27
$\text{Cl} + \text{CH}_2\text{Br}_2 \rightarrow \text{HCl} + \text{CHBr}_2$	6.3×10^{-12}	800	4.3×10^{-13}	1.1	50	G28
$\text{Cl} + \text{CHBr}_3 \rightarrow \text{CBr}_3 + \text{HCl}$	4.85×10^{-12}	850	2.8×10^{-13}	1.3	200	G29
$\text{Cl} + \text{CH}_2\text{ClBr} \rightarrow \text{HCl} + \text{CHClBr}$	6.8×10^{-12}	870	3.7×10^{-13}	1.2	100	G30
$\text{Br} + \text{O}_3 \rightarrow \text{BrO} + \text{O}_2$	1.6×10^{-11}	780	1.2×10^{-12}	1.15	100	G31
$\text{Br} + \text{H}_2\text{O}_2 \rightarrow \text{HBr} + \text{HO}_2$	1.0×10^{-11}	>3000	$< 5.0 \times 10^{-16}$			G32

Reaction	A-Factor ^a	E/R	k(298 K) ^a	f(298 K) ^b	g	Notes
$\text{Br} + \text{NO}_2 \xrightarrow{\text{M}} \text{BrNO}_2$	(See Table 2-1)					
$\text{Br} + \text{NO}_3 \rightarrow \text{BrO} + \text{NO}_2$			1.6×10^{-11}	2.0		G33
$\text{Br} + \text{H}_2\text{CO} \rightarrow \text{HBr} + \text{HCO}$	1.7×10^{-11}	800	1.1×10^{-12}	1.2	125	G34
$\text{Br} + \text{CH}_2=\text{C}(\text{CH}_3)\text{CH}=\text{CH}_2 \xrightarrow{\text{M}} \text{X} \xrightarrow{\text{O}_2} \text{products}$	(see note)					G35
$\text{Br} + \text{OCIO} \rightarrow \text{BrO} + \text{ClO}$	2.6×10^{-11}	1300	3.4×10^{-13}	2.0	300	G36
$\text{Br} + \text{Cl}_2\text{O} \rightarrow \text{BrCl} + \text{ClO}$	2.1×10^{-11}	470	4.3×10^{-12}	1.3	150	G37
$\text{Br} + \text{Cl}_2\text{O}_2 \rightarrow \text{products}$	5.9×10^{-12}	170	3.3×10^{-12}	1.3	200	G38
$\text{BrO} + \text{O}_3 \rightarrow \text{products}$	$\sim 1.0 \times 10^{-12}$	>3200	$< 2.0 \times 10^{-17}$			G39
$\text{BrO} + \text{NO} \rightarrow \text{NO}_2 + \text{Br}$	8.8×10^{-12}	-260	2.1×10^{-11}	1.15	130	G40
$\text{BrO} + \text{NO}_2 \xrightarrow{\text{M}} \text{BrONO}_2$	(See Table 2-1)					
$\text{BrO} + \text{NO}_3 \rightarrow \text{products}$			1.0×10^{-12}	3.0		G41
$\text{BrO} + \text{ClO} \rightarrow \text{Br} + \text{OCIO}$	9.5×10^{-13}	-550	6.0×10^{-12}	1.2	100	G42
$\quad \rightarrow \text{Br} + \text{ClOO}$	2.3×10^{-12}	-260	5.5×10^{-12}	1.2	100	
$\quad \rightarrow \text{BrCl} + \text{O}_2$	4.1×10^{-13}	-290	1.1×10^{-12}	1.2	100	
$\text{BrO} + \text{BrO} \rightarrow \text{products}$	1.5×10^{-12}	-230	3.2×10^{-12}	1.15	150	G43
$\text{OBrO} + \text{O}_3 \rightarrow \text{Products}$			$< 1.5 \times 10^{-15}$			G44
$\text{OBrO} + \text{NO} \rightarrow \text{Products}$	2.4×10^{-13}	-610	1.8×10^{-12}	3	200	G45
$\text{CH}_2\text{BrO}_2 + \text{NO} \rightarrow \text{CH}_2\text{O} + \text{NO}_2 + \text{Br}$	4×10^{-12}	-300	1.1×10^{-11}	1.5	200	G46
IO_x Reactions						
$\text{O} + \text{I}_2 \rightarrow \text{IO} + \text{I}$	1.4×10^{-10}	0	1.4×10^{-10}	1.4	250	H 1
$\text{O} + \text{IO} \rightarrow \text{O}_2 + \text{I}$			1.2×10^{-10}	2.0		H 2
$\text{OH} + \text{I}_2 \rightarrow \text{HOI} + \text{I}$			1.8×10^{-10}	2.0		H 3
$\text{OH} + \text{HI} \rightarrow \text{H}_2\text{O} + \text{I}$			3.0×10^{-11}	2.0		H 4
$\text{OH} + \text{CH}_3\text{I} \rightarrow \text{H}_2\text{O} + \text{CH}_2\text{I}$	2.9×10^{-12}	1100	7.2×10^{-14}	1.5	300	H 5
$\text{OH} + \text{CF}_3\text{I} \rightarrow \text{HOI} + \text{CF}_3$	2.5×10^{-11}	2070	2.4×10^{-14}	1.3	200	H 6

Reaction	A-Factor ^a	E/R	k(298 K) ^a	f(298 K) ^b	g	Notes
$\text{HO}_2 + \text{I} \rightarrow \text{HI} + \text{O}_2$	1.5×10^{-11}	1090	3.8×10^{-13}	2.0	500	H 7
$\text{HO}_2 + \text{IO} \rightarrow \text{HOI} + \text{O}_2$			8.4×10^{-11}	1.5		H 8
$\text{NO}_3 + \text{HI} \rightarrow \text{HNO}_3 + \text{I}$	(See Note)					H 9
$\text{Cl} + \text{CH}_3\text{I} \rightarrow \text{CH}_2\text{I} + \text{HCl}$	2.9×10^{-11}	1000	1.0×10^{-12}	1.5	250	H10
$\text{I} + \text{O}_3 \rightarrow \text{IO} + \text{O}_2$	2.3×10^{-11}	870	1.2×10^{-12}	1.2	200	H11
$\text{I} + \text{NO} \xrightarrow{\text{M}} \text{INO}$	(See Table 2-1)					
$\text{I} + \text{NO}_2 \xrightarrow{\text{M}} \text{INO}_2$	(See Table 2-1)					
$\text{I} + \text{BrO} \rightarrow \text{IO} + \text{Br}$			1.2×10^{-11}	2.0		H12
$\text{IO} + \text{NO} \rightarrow \text{I} + \text{NO}_2$	9.1×10^{-12}	-240	2.0×10^{-11}	1.2	150	H13
$\text{IO} + \text{NO}_2 \xrightarrow{\text{M}} \text{IONO}_2$	(See Table 2-1)					
$\text{IO} + \text{ClO} \rightarrow \text{products}$	5.1×10^{-12}	-280	1.3×10^{-11}	2.0	200	H14
$\text{IO} + \text{BrO} \rightarrow \text{products}$			6.9×10^{-11}	1.5		H15
$\text{IO} + \text{IO} \rightarrow \text{products}$	1.5×10^{-11}	-500	8.0×10^{-11}	1.5	500	H16
$\text{INO} + \text{INO} \rightarrow \text{I}_2 + 2\text{NO}$	8.4×10^{-11}	2620	1.3×10^{-14}	2.5	600	H17
$\text{INO}_2 + \text{INO}_2 \rightarrow \text{I}_2 + 2\text{NO}_2$	2.9×10^{-11}	2600	4.7×10^{-15}	3.0	1000	H18
SO_x Reactions						
$\text{O} + \text{SH} \rightarrow \text{SO} + \text{H}$			1.6×10^{-10}	5.0		I 1
$\text{O} + \text{CS} \rightarrow \text{CO} + \text{S}$	2.7×10^{-10}	760	2.1×10^{-11}	1.1	250	I 2
$\text{O} + \text{H}_2\text{S} \rightarrow \text{OH} + \text{SH}$	9.2×10^{-12}	1800	2.2×10^{-14}	1.7	550	I 3
$\text{O} + \text{OCS} \rightarrow \text{CO} + \text{SO}$	2.1×10^{-11}	2200	1.3×10^{-14}	1.15	150	I 4
$\text{O} + \text{CS}_2 \rightarrow \text{CS} + \text{SO}$	3.2×10^{-11}	650	3.6×10^{-12}	1.2	150	I 5
$\text{O} + \text{SO}_2 \xrightarrow{\text{M}} \text{SO}_3$	(See Table 2-1)					
$\text{O} + \text{CH}_3\text{SCH}_3 \rightarrow \text{CH}_3\text{SO} + \text{CH}_3$	1.3×10^{-11}	-410	5.0×10^{-11}	1.1	100	I 6
$\text{O} + \text{CH}_3\text{SSCH}_3 \rightarrow \text{CH}_3\text{SO} + \text{CH}_3\text{S}$	3.9×10^{-11}	-290	1.03×10^{-10}	1.1	100	I 7
$\text{O} + \text{CH}_3\text{S(O)CH}_3 \rightarrow \text{products}$	2.0×10^{-12}	-440	8.8×10^{-12}	1.2	200	I 8

Reaction	A-Factor ^a	E/R	k(298 K) ^a	f(298 K) ^b	g	Notes
$O_3 + H_2S \rightarrow \text{products}$			$<2.0 \times 10^{-20}$			I9
$O_3 + CH_3SCH_3 \rightarrow \text{products}$			$<1.5 \times 10^{-19}$			I10
$O_3 + SO_2 \rightarrow SO_3 + O_2$	3.0×10^{-12}	>7000	$<2.0 \times 10^{-22}$			I11
$O_3 + SO_2F_2 \rightarrow \text{products}$			$<1.0 \times 10^{-23}$			I12
$OH + H_2S \rightarrow SH + H_2O$	6.1×10^{-12}	75	4.7×10^{-12}	1.1	75	I13
$OH + OCS \rightarrow \text{products}$	1.1×10^{-13}	1200	1.9×10^{-15}	2.0	500	I14
$OH + CS_2 \rightarrow SH + OCS$			$<2.0 \times 10^{-15}$			I15
$OH + CS_2 \xrightarrow{O_2} CS_2OH \rightarrow \text{products}$	(See Note)	(See Note)	1.2×10^{-12} at $P_{air} = 1 \text{ atm}$	1.25		I16
$CS_2OH + O_2 \rightarrow \text{products}$	2.8×10^{-14}	0	2.8×10^{-14}	1.2	100	I17
$OH + CH_3SH \rightarrow CH_3S + H_2O$	9.9×10^{-12}	-360	3.3×10^{-11}	1.07	75	I18
$OH + CH_3SCH_3 \rightarrow H_2O + CH_2SCH_3$	1.2×10^{-11}	280	4.7×10^{-12}	1.1	100	I19
$OH + CH_3SCH_3 \xrightleftharpoons[M]{O_2} (CH_3)_2SOH \rightarrow \text{products}$	(See Note)	(See Note)	2.0×10^{-12} at $P_{air} = 1 \text{ atm}$	1.2		I20
$(CH_3)_2SOH + O_2 \rightarrow \text{products}$	8.5×10^{-13}	0	8.5×10^{-13}	1.25	0	I21
$OH + CH_3SCH_2Cl \rightarrow \text{products}$			2.5×10^{-12}	2.0		I22
$OH + CH_3SSCH_3 \rightarrow \text{products}$	6.0×10^{-11}	-400	2.3×10^{-10}	1.2	200	I23
$OH + CH_3S(O)CH_3 \rightarrow \text{products}$	6.1×10^{-12}	-800	8.9×10^{-11}	1.2	500	I24
$OH + CH_3S(O)OH \rightarrow \text{products}$			9.0×10^{-11}	1.4		I25
$OH + S \rightarrow H + SO$			6.6×10^{-11}	3.0		I26
$OH + SO \rightarrow H + SO_2$	2.7×10^{-11}	-335	8.3×10^{-11}	1.2	150	I27
$OH + SO_2 \xrightarrow{M} HOSO_2$	(See Table 2-1)					
$OH + SO_2F_2 \rightarrow \text{products}$			$<1.0 \times 10^{-16}$			I28
$HO_2 + H_2S \rightarrow \text{products}$			$<3.0 \times 10^{-15}$			I29
$HO_2 + CH_3SH \rightarrow \text{products}$			$<4.0 \times 10^{-15}$			I29
$HO_2 + CH_3SCH_3 \rightarrow \text{products}$			$<5.0 \times 10^{-15}$			I29

Reaction	A-Factor ^a	E/R	k(298 K) ^a	f(298 K) ^b	g	Notes
$\text{HO}_2 + \text{SO}_2 \rightarrow \text{products}$			$<1.0 \times 10^{-18}$			I30
$\text{NO}_2 + \text{SO}_2 \rightarrow \text{products}$			$<2.0 \times 10^{-26}$			I31
$\text{NO}_3 + \text{H}_2\text{S} \rightarrow \text{products}$			$<8.0 \times 10^{-16}$			I32
$\text{NO}_3 + \text{OCS} \rightarrow \text{products}$			$<1.0 \times 10^{-16}$			I33
$\text{NO}_3 + \text{CS}_2 \rightarrow \text{products}$			$<4.0 \times 10^{-16}$			I34
$\text{NO}_3 + \text{CH}_3\text{SH} \rightarrow \text{products}$	4.4×10^{-13}	-210	8.9×10^{-13}	1.25	210	I35
$\text{NO}_3 + \text{CH}_3\text{SCH}_3 \rightarrow \text{CH}_3\text{SCH}_2 + \text{HNO}_3$	1.9×10^{-13}	-530	1.1×10^{-12}	1.1	150	I36
$\text{NO}_3 + \text{CH}_3\text{SSCH}_3 \rightarrow \text{products}$	1.3×10^{-12}	270	5.3×10^{-13}	1.4	270	I37
$\text{NO}_3 + \text{CH}_3\text{S(O)CH}_3 \rightarrow \text{products}$			2.9×10^{-13}	1.6		I38
$\text{NO}_3 + \text{SO}_2 \rightarrow \text{products}$			$<7.0 \times 10^{-21}$			I39
$\text{N}_2\text{O}_5 + \text{CH}_3\text{SCH}_3 \rightarrow \text{products}$			$<1.0 \times 10^{-17}$			I40
$\text{CH}_3\text{O}_2 + \text{SO}_2 \rightarrow \text{products}$			$<5.0 \times 10^{-17}$			I41
$\text{F} + \text{CH}_3\text{SCH}_3 \rightarrow \text{products}$			2.4×10^{-10}	2.0		I42
$\text{Cl} + \text{H}_2\text{S} \rightarrow \text{HCl} + \text{SH}$	3.7×10^{-11}	-210	7.4×10^{-11}	1.2	100	I43
$\text{Cl} + \text{SO}_2\text{F}_2 \rightarrow \text{products}$			$<1.5 \times 10^{-18}$			I44
$\text{Cl} + \text{OCS} \rightarrow \text{products}$			$<1.0 \times 10^{-16}$			I45
$\text{Cl} + \text{CS}_2 \rightarrow \text{products}$	(See Table 2-1)					
$\text{CS}_2\text{Cl} + \text{O}_2 \rightarrow \text{products}$			$<2.5 \times 10^{-16}$			I46
$\text{Cl} + \text{CH}_3\text{SH} \rightarrow \text{CH}_3\text{S} + \text{HCl}$	1.2×10^{-10}	-150	2.0×10^{-10}	1.1	100	I47
$\text{Cl} + \text{CH}_3\text{SCH}_3 \rightarrow \text{CH}_3\text{SCH}_2 + \text{HCl}$	9.4×10^{-11}	-190	1.8×10^{-10}	+1.2/ -2.5	0	I48
$\text{Cl} + \text{CH}_3\text{SCH}_3 \rightarrow \text{products} \text{ (P = 1 atm)}$	3.5×10^{-10}	0	3.5×10^{-10}	1.2	0	
$(\text{CH}_3)_2\text{SCI} + \text{O}_2 \rightarrow \text{products}$			$<4.0 \times 10^{-18}$			I49
$(\text{CH}_3)_2\text{SCI} + \text{NO} \rightarrow \text{products}$			1.2×10^{-11}	1.25		I49
$(\text{CH}_3)_2\text{SCI} + \text{NO}_2 \rightarrow \text{products}$			2.7×10^{-11}	1.25		I49
$\text{Cl} + \text{CH}_3\text{S(O)CH}_3 \rightarrow \text{CH}_3\text{S(O)CH}_2 + \text{HCl}$	1.4×10^{-11}	0	1.4×10^{-11}	1.2	150	I50

Reaction	A-Factor ^a	E/R	k(298 K) ^a	f(298 K) ^b	g	Notes
$\text{Cl} + \text{CH}_3\text{S}(\text{O})\text{CH}_3 \xrightarrow{\text{M}} \text{CH}_3(\text{Cl})\text{S}(\text{O})\text{CH}_3$	(See Note)					I50
$\text{CH}_3(\text{Cl})\text{S}(\text{O})\text{CH}_3 + \text{O}_2 \rightarrow \text{products}$			$<3.0 \times 10^{-18}$			I51
$\text{CH}_3(\text{Cl})\text{S}(\text{O})\text{CH}_3 + \text{NO} \rightarrow \text{products}$			1.2×10^{-11}	1.5		I51
$\text{CH}_3(\text{Cl})\text{S}(\text{O})\text{CH}_3 + \text{NO}_2 \rightarrow \text{products}$			2.1×10^{-11}	1.5		I51
$\text{Cl}_2 + \text{CH}_3\text{SCH}_3 \rightarrow \text{products}$			$<5.0 \times 10^{-14}$			I52
$\text{ClO} + \text{OCS} \rightarrow \text{products}$			$<2.0 \times 10^{-16}$			I53
$\text{ClO} + \text{CH}_3\text{SCH}_3 \rightarrow \text{products}$	2.1×10^{-15}	-340	6.6×10^{-15}	1.5	300	I54
$\text{ClO} + \text{CH}_3\text{S}(\text{O})\text{CH}_3 \rightarrow \text{products}$			$<2.0 \times 10^{-14}$			I55
$\text{ClO} + \text{SO} \rightarrow \text{Cl} + \text{SO}_2$	2.8×10^{-11}	0	2.8×10^{-11}	1.3	50	I56
$\text{ClO} + \text{SO}_2 \rightarrow \text{Cl} + \text{SO}_3$			$<4.0 \times 10^{-18}$			I53
$\text{Br} + \text{H}_2\text{S} \rightarrow \text{HBr} + \text{SH}$	1.4×10^{-11}	2750	1.4×10^{-15}	2.0	300	I57
$\text{Br} + \text{CH}_3\text{SH} \rightarrow \text{CH}_3\text{S} + \text{HBr}$	9.2×10^{-12}	390	2.5×10^{-12}	2.0	100	I57
$\text{Br} + \text{CH}_3\text{SCH}_3 \rightarrow \text{CH}_3\text{SCH}_2 + \text{HBr}$	9.0×10^{-11}	2390	3.0×10^{-14}	1.4	150	I58
$\text{Br} + \text{CH}_3\text{SCH}_3 \xrightarrow{\text{M}} (\text{CH}_3)_2\text{SBr}$	(See Table 2-1)					
$\text{Br} + \text{CH}_3\text{S}(\text{O})\text{CH}_3 \rightarrow \text{products}$			1.2×10^{-14}	1.5		I59
$\text{BrO} + \text{CH}_3\text{SH} \rightarrow \text{products}$	(see note)					I60
$\text{BrO} + \text{CH}_3\text{SCH}_3 \rightarrow \text{products}$	1.4×10^{-14}	-950	3.4×10^{-13}	1.25	200	I61
$\text{BrO} + \text{CH}_3\text{SSCH}_3 \rightarrow \text{products}$			1.5×10^{-14}	2.0		I62
$\text{BrO} + \text{CH}_3\text{S}(\text{O})\text{CH}_3 \rightarrow \text{products}$			1.0×10^{-14}	2.0		I63
$\text{BrO} + \text{SO} \rightarrow \text{Br} + \text{SO}_2$			5.7×10^{-11}	1.4		I64
$\text{IO} + \text{CH}_3\text{SH} \rightarrow \text{products}$			6.6×10^{-16}	2.0		I65
$\text{IO} + \text{CH}_3\text{SCH}_3 \rightarrow \text{products}$	2.4×10^{-12}	1470	1.7×10^{-14}	1.5	400	I66
$\text{S} + \text{O}_2 \rightarrow \text{SO} + \text{O}$	2.3×10^{-12}	0	2.3×10^{-12}	1.2	200	I67
$\text{S} + \text{O}_3 \rightarrow \text{SO} + \text{O}_2$			1.2×10^{-11}	2.0		I68
$\text{SO} + \text{O}_2 \rightarrow \text{SO}_2 + \text{O}$	1.25×10^{-13}	2190	8.0×10^{-17}	1.3	350	I69

Reaction	A-Factor ^a	E/R	k(298 K) ^a	f(298 K) ^b	g	Notes
$\text{SO} + \text{O}_3 \rightarrow \text{SO}_2 + \text{O}_2$	3.4×10^{-12}	1100	8.4×10^{-14}	1.1	150	170
$\text{SO} + \text{NO}_2 \rightarrow \text{SO}_2 + \text{NO}$	1.4×10^{-11}	0	1.4×10^{-11}	1.2	50	171
$\text{SO} + \text{OCIO} \rightarrow \text{SO}_2 + \text{ClO}$			1.9×10^{-12}	3.0		172
$\text{SO}_3 + 2 \text{H}_2\text{O} \rightarrow \text{products}$	(See Note)	(See Note)	(See Note)	1.2	200	173
$\text{SO}_3 + \text{NH}_3 \rightarrow \text{products}$	(See Table 2-1)					
$\text{SO}_3 + \text{NO}_2 \rightarrow \text{products}$			1.0×10^{-19}	10.0		174
$\text{SH} + \text{O}_2 \rightarrow \text{OH} + \text{SO}$			$< 4.0 \times 10^{-19}$			175
$\text{SH} + \text{O}_3 \rightarrow \text{HSO} + \text{O}_2$	9.0×10^{-12}	280	3.5×10^{-12}	1.2	200	176
$\text{SH} + \text{H}_2\text{O}_2 \rightarrow \text{products}$			$< 5.0 \times 10^{-15}$			177
$\text{SH} + \text{NO} \xrightarrow{\text{M}} \text{HSNO}$	(See Table 2-1)					
$\text{SH} + \text{NO}_2 \rightarrow \text{HSO} + \text{NO}$	3.0×10^{-11}	-250	7.0×10^{-11}	1.1	50	178
$\text{SH} + \text{N}_2\text{O} \rightarrow \text{HSO} + \text{N}_2$			$< 5.0 \times 10^{-16}$			179
$\text{SH} + \text{Cl}_2 \rightarrow \text{ClSH} + \text{Cl}$	1.4×10^{-11}	690	1.4×10^{-12}	1.15	200	180
$\text{SH} + \text{BrCl} \rightarrow \text{products}$	2.3×10^{-11}	-350	7.4×10^{-11}	2.0	200	181
$\text{SH} + \text{Br}_2 \rightarrow \text{BrSH} + \text{Br}$	6.0×10^{-11}	-160	1.0×10^{-10}	2.0	160	181
$\text{SH} + \text{F}_2 \rightarrow \text{FSH} + \text{F}$	4.3×10^{-11}	1390	4.0×10^{-13}	2.0	200	181
$\text{HSO} + \text{O}_2 \rightarrow \text{products}$			$< 2.0 \times 10^{-17}$			182
$\text{HSO} + \text{O}_3 \rightarrow \text{products}$			1.0×10^{-13}	1.3		183
$\text{HSO} + \text{NO} \rightarrow \text{products}$			$< 1.0 \times 10^{-15}$			184
$\text{HSO} + \text{NO}_2 \rightarrow \text{HSO}_2 + \text{NO}$			9.6×10^{-12}	2.0		184
$\text{HSO}_2 + \text{O}_2 \rightarrow \text{HO}_2 + \text{SO}_2$			3.0×10^{-13}	3.0		185
$\text{HOSO}_2 + \text{O}_2 \rightarrow \text{HO}_2 + \text{SO}_3$	1.3×10^{-12}	330	4.3×10^{-13}	1.15	200	186
$\text{CS} + \text{O}_2 \rightarrow \text{OCS} + \text{O}$			2.9×10^{-19}	2.0		187
$\text{CS} + \text{O}_3 \rightarrow \text{OCS} + \text{O}_2$			3.0×10^{-16}	3.0		188
$\text{CS} + \text{NO}_2 \rightarrow \text{OCS} + \text{NO}$			7.6×10^{-17}	3.0		188

Reaction	A-Factor ^a	E/R	k(298 K) ^a	f(298 K) ^b	g	Notes
$\text{CH}_3\text{S} + \text{O}_2 \rightarrow \text{products}$			$<3.0 \times 10^{-18}$			<u>189</u>
$\text{CH}_3\text{S} + \text{O}_3 \rightarrow \text{products}$	1.5×10^{-12}	-360	5.0×10^{-12}	1.15	100	<u>190</u>
$\text{CH}_3\text{S} + \text{NO} \rightarrow \text{products}$			$<1.0 \times 10^{-13}$			<u>191</u>
$\text{CH}_3\text{S} + \text{NO} \xrightarrow{\text{M}} \text{products}$	(See Table 2-1)					
$\text{CH}_3\text{S} + \text{NO}_2 \rightarrow \text{CH}_3\text{SO} + \text{NO}$	3.0×10^{-11}	-240	6.7×10^{-11}	1.2	150	<u>192</u>
$\text{CH}_2\text{SH} + \text{O}_2 \rightarrow \text{products}$			6.5×10^{-12}	2.0		<u>193</u>
$\text{CH}_2\text{SH} + \text{O}_3 \rightarrow \text{products}$			3.5×10^{-11}	2.0		<u>194</u>
$\text{CH}_2\text{SH} + \text{NO} \rightarrow \text{products}$			1.9×10^{-11}	2.0		<u>195</u>
$\text{CH}_2\text{SH} + \text{NO}_2 \rightarrow \text{products}$			5.2×10^{-11}	2.0		<u>196</u>
$\text{CH}_3\text{SO} + \text{O}_3 \rightarrow \text{products}$			4.0×10^{-13}	1.5		<u>197</u>
$\text{CH}_3\text{SO} + \text{NO}_2 \rightarrow \text{CH}_3\text{SO}_2 + \text{NO}$			1.2×10^{-11}	1.2		<u>198</u>
$\text{CH}_3\text{SOO} + \text{O}_3 \rightarrow \text{products}$			$<8.0 \times 10^{-13}$			<u>199</u>
$\text{CH}_3\text{SOO} + \text{NO} \rightarrow \text{products}$	1.1×10^{-11}	0	1.1×10^{-11}	2.0	100	199
$\text{CH}_3\text{SO}_2 + \text{NO}_2 \rightarrow \text{products}$	2.2×10^{-11}	0	2.2×10^{-11}	2.0	100	<u>100</u>
$\text{CH}_3\text{SCH}_2 + \text{O}_2 \xrightarrow{\text{M}} \text{CH}_3\text{SCH}_2\text{O}_2$	(See Table 2-1)					
$\text{CH}_3\text{SCH}_2 + \text{NO}_3 \rightarrow \text{products}$			3.0×10^{-10}	2.0		<u>101</u>
$\text{CH}_3\text{SCH}_2\text{O}_2 + \text{NO} \rightarrow \text{CH}_3\text{S} + \text{CH}_2\text{O} + \text{NO}_2$	4.9×10^{-12}	-260	1.2×10^{-11}	1.3	200	<u>102</u>
$\text{CH}_3\text{SCH}_2\text{O}_2 + \text{CH}_3\text{SCH}_2\text{O}_2 \rightarrow \text{products}$			1.0×10^{-11}	1.25		<u>103</u>
$\text{CH}_3\text{SS} + \text{O}_3 \rightarrow \text{products}$			4.6×10^{-13}	2.0		<u>104</u>
$\text{CH}_3\text{SS} + \text{NO}_2 \rightarrow \text{products}$			1.8×10^{-11}	2.0		<u>105</u>
$\text{CH}_3\text{SSO} + \text{NO}_2 \rightarrow \text{products}$			4.5×10^{-12}	2.0		105
Sodium Reactions						
$\text{Na} + \text{O}_2 \xrightarrow{\text{M}} \text{NaO}_2$	(See Table 2-1)					
$\text{Na} + \text{O}_3 \rightarrow \text{NaO} + \text{O}_2$	1.0×10^{-9}	95	7.3×10^{-10}	1.2	50	<u>J 1</u>
$\rightarrow \text{NaO}_2 + \text{O}$			$<4.0 \times 10^{-11}$			<u>J 1</u>

Reaction	A-Factor ^a	E/R	k(298 K) ^a	f(298 K) ^b	g	Notes
$\text{Na} + \text{N}_2\text{O} \rightarrow \text{NaO} + \text{N}_2$	2.8×10^{-10}	1600	1.3×10^{-12}	1.2	400	<u>J 2</u>
$\text{Na} + \text{Cl}_2 \rightarrow \text{NaCl} + \text{Cl}$	7.3×10^{-10}	0	7.3×10^{-10}	1.3	200	<u>J 3</u>
$\text{NaO} + \text{O} \rightarrow \text{Na} + \text{O}_2$	4.4×10^{-10}	0	4.4×10^{-10}	1.5	200	<u>J 4</u>
$\text{NaO} + \text{O}_2 \xrightarrow{\text{M}} \text{NaO}_3$	(See Table 2-1)					
$\text{NaO} + \text{O}_3 \rightarrow \text{NaO}_2 + \text{O}_2$	1.1×10^{-9}	570	1.6×10^{-10}	1.5	300	<u>J 5</u>
$\quad \quad \quad \rightarrow \text{Na} + 2\text{O}_2$	6.0×10^{-11}	0	6.0×10^{-11}	3.0	800	J 5
$\text{NaO} + \text{H}_2 \rightarrow \text{NaOH} + \text{H}$	2.6×10^{-11}	0	2.6×10^{-11}	2.0	600	<u>J 6</u>
$\text{NaO} + \text{H}_2\text{O} \rightarrow \text{NaOH} + \text{OH}$	4.3×10^{-10}	500	8.0×10^{-11}	1.5	200	<u>J 7</u>
$\text{NaO} + \text{NO} \rightarrow \text{Na} + \text{NO}_2$	1.5×10^{-10}	0	1.5×10^{-10}	4.0	400	<u>J 8</u>
$\text{NaO} + \text{CO}_2 \xrightarrow{\text{M}} \text{NaCO}_3$	(See Table 2-1)					
$\text{NaO} + \text{HCl} \rightarrow \text{products}$	2.8×10^{-10}	0	2.8×10^{-10}	3.0	400	<u>J 9</u>
$\text{NaO}_2 + \text{O} \rightarrow \text{NaO} + \text{O}_2$	2.2×10^{-11}	0	2.2×10^{-11}	5.0	600	<u>J 10</u>
$\text{NaO}_2 + \text{NO} \rightarrow \text{NaO} + \text{NO}_2$			$<10^{-14}$			<u>J 11</u>
$\text{NaO}_2 + \text{HCl} \rightarrow \text{products}$	2.3×10^{-10}	0	2.3×10^{-10}	3.0	400	<u>J 12</u>
$\text{NaOH} + \text{HCl} \rightarrow \text{NaCl} + \text{H}_2\text{O}$	2.8×10^{-10}	0	2.8×10^{-10}	3.0	400	<u>J 13</u>
$\text{NaHCO}_3 + \text{H} \rightarrow \text{Na} + \text{H}_2\text{O} + \text{CO}_2$	1.4×10^{-11}	1000	5×10^{-13}	2.0	100	<u>J 14</u>
$\text{NaOH} + \text{CO}_2 \xrightarrow{\text{M}} \text{NaHCO}_3$	(See Table 2-1)					

Shaded areas indicate changes or additions since JPL 06-2/JPL 09-31. Italicized entries denote estimates.

^a Units are $\text{cm}^3 \text{ molecule}^{-1} \text{ s}^{-1}$.

^b f(298 K) is the uncertainty factor at 298 K. To calculate the uncertainty at other temperatures, use the expression:

$$f(T) = f(298) \exp \left| g \left(\frac{1}{T} - \frac{1}{298} \right) \right|$$

Note that the exponent is absolute value.

1.3 Notes to Table 1

JPL Publication numbers for the most recent revision of the table entry and note are given at the end of each note.

- A1. $O + O_3$. The recommended rate expression is from Wine et al. [1626] and is a linear least-squares fit of all data (unweighted) from Davis et al. [400], McCrumb and Kaufman [986], West et al. [1595], Arnold and Comes [38], and Wine et al. [1626]. (Table: 83-62, Note: 83-62) [Back to Table](#)
- A2. $O(^1D)$ Reactions. In general, the rate coefficients given in Table 1 are for the disappearance of $O(^1D)$, which includes physical quenching or deactivation and chemical reaction. Where information is available, the rate coefficient for a specific channel is given. The details of deriving a recommended rate coefficient are given in the note for that reaction. In deriving recommended values, direct measurements are used whenever possible. However, rate coefficients measured via relative rate techniques have been considered for checking consistency in measured elementary reaction rate coefficients. The ratios of the rate coefficients for $O(^1D)$ reactions measured using the same method (and often the same apparatus) may be more accurate and precise than the individual rate coefficients quoted in Table 1. The ratios of rate coefficients can be obtained from the original references. The weight of the evidence indicates that the results from Heidner and Husain [628], Heidner et al. [627] and Fletcher and Husain [511, 512] contain systematic errors and therefore are not considered in the determination of the recommendations.

Products of the reactive channels for the $O(^1D) +$ halomethane reactions may include $CX_3O + X$, $CX_2O + X_2$ (or $2X$), and $CX_3 + XO$, where $X = H, F, Cl$, or Br in various combinations. Bromine, chlorine and hydrogen are more easily displaced than fluorine from halocarbons. Where information is available, the rate coefficient for a specific reactive channel and physical quenching is given. (Note: 10-6) [Back to Table](#)

- A3. $O(^1D) + O_2$. The recommended 298 K rate coefficient was derived from the studies of Blitz et al. [170], Amimoto et al. [24, 25], Lee and Slanger [874, 875], Davidson et al. [392, 393], Dunlea and Ravishankara [462], Streit et al. [1376], Strekowski et al. [1380] and Takahashi et al. [1408]. The temperature dependence was computed by normalizing the results of Strekowski et al., Dunlea and Ravishankara, and Streit et al. to the 298 K value recommended here. The deactivation of $O(^1D)$ by O_2 leads to the production of $O_2(^1\Sigma)$ with an efficiency of $80 \pm 20\%$. (Noxon [1105], Biedenapp and Bair [154], Snelling [1341], and Lee and Slanger [874]). $O_2(^1\Sigma)$ is produced in the $v=0, 1$, and 2 vibrational levels in the amounts 60%, 40%, and <3%, respectively (Gauthier and Snelling [537] and Lee and Slanger [874]). The fractional deactivation of $O(^1D)$ that leads to the excitation of $O_2(^3\Sigma)$ to $O_2(^1\Delta)$ is expected to be ~20%. (Table: 06-2, Note: 10-6, Evaluated: 10-6) [Back to Table](#)
- A4. $O(^1D) + O_3$. The room temperature rate coefficient was derived from the results of Davidson et al. [392, 393], Streit et al. [1376], Amimoto et al. [24, 25], Wine and Ravishankara [1627-1629], Talukdar and Ravishankara [1423] and Dunlea and Ravishankara [462]. The reaction of $O(^1D)$ with O_3 gives $O_2 + O_2$ or $O_2 + O + O$ as products. Davenport et al. [387] and Amimoto et al. [25] report that, on average, one ground state O atom is produced per $O(^1D)$ reacting with O_3 . Dunlea et al. [464] have shown that the yield of $O(^3P)$ in this reaction is close to, but not exactly, unity. Dunlea et al. suggest a small but significant decrease in the O atom yield with decreasing temperature. A unity yield of $O(^3P)$, at all temperatures, is recommended. (Table: 06-2, Note: 10-6, Evaluated: 10-6) [Back to Table](#)
- A5. $O(^1D) + H_2$. The recommendation is based on the room temperature rate coefficient data from Davidson et al. [392, 393], Force and Wiesenfeld [517, 518], Wine and Ravishankara [1628], Talukdar and Ravishankara [1423], Blitz et al. [170], and Vranckx et al. [1528]. Davidson et al. (200 – 350 K) and Vranckx et al. (227 – 453 K) report that k is independent of temperature. Wine and Ravishankara [1628] and Vranckx et al. [1528] report the yield of $O(^3P)$ to be <4.9% and 0.7%, respectively. Hence, the major products of this reaction are $H + OH$. Koppe et al. [818] report a 2.7 times larger rate coefficient at a collisional energy of 0.12 eV. This does not agree with the observations of Davidson et al. [393] and Vranckx et al. who reported that k is independent of

temperature and Matsumi et al. [980] who report no change in k when translationally hot $O(^1D)$ was moderated with Ar. (Table: 10-6, Note: 10-6, Evaluated: 10-6) [Back to Table](#)

- A6. $O(^1D) + H_2O$. The recommended $k(298\text{ K})$ is based on the results of Davidson et al. [393], Amimoto et al. [24], Wine and Ravishankara [1627, 1628], Gericke and Comes [541], Dunlea and Ravishankara [463], Carl [259], and Takahashi et al. [1408], but is weighted towards the study of Dunlea and Ravishankara because the latter study used several different methods to quantify the water vapor concentration. The results of Lee and Slanger [875] and Dillon et al. [433] are consistent with the recommended value. The temperature dependence of this rate coefficient is derived from the data of Streit et al. [1376] and Dunlea and Ravishankara, after normalizing the results from the two studies to the $k(298\text{ K})$ value recommended here. The $O_2 + H_2$ product yield was measured by Zellner et al. [1676] to be $(1 + 0.5/-1)\%$ and Glinski and Birks [563] to be $(0.6 + 0.7/-0.6)\%$. The yield of $O(^3P)$ from $O(^1D) + H_2O$ is reported to be less than $(4.9 \pm 3.2)\%$ by Wine and Ravishankara [1628], $(2 \pm 1)\%$ by Takahashi et al. [1409], and $<0.3\%$ by Carl [259]. The recommended yield of OH in this reaction is 2.0. To calculate the rates of OH production via $O(^1D)$ reactions in the atmosphere, the quantities of interest are the ratios of the rate coefficients for the reaction of $O(^1D)$ with H_2O to those with N_2 and O_2 . Ratio data are given in the original references for this reaction. (Table 09-31, Note: 09-31) [Back to Table](#)
- A7. $O(^1D) + N_2$. The rate coefficient recommendation for this reaction is taken from Ravishankara et al. [1206], which included the results from Strekowski et al. [1380], Blitz et al. [170], and Dunlea and Ravishankara [462] in their analysis. The more recent results from Takahashi et al. [1408] and Dillon et al. [433] are in agreement with the recommendation. Strekowski et al. reported the rate coefficient for $O(^1D)$ removal by air and their results are in excellent agreement with the value derived using the current recommendation for $O(^1D)$ removal by N_2 and O_2 . (Table: 06-2, Note: 10-6, Evaluated: 10-6) [Back to Table](#)
- A8. $O(^1D) + N_2O$. This reaction has two channels, one producing $2NO$ and the other producing $N_2 + O_2$. For atmospheric calculations of NO_x production, the rate coefficient for the channel that produces NO is critical, while the overall rate coefficient is important for deriving the loss rate of N_2O . The recommendation for the overall room temperature rate coefficient for the removal of $O(^1D)$ by N_2O was derived from a weighted average of the results from Davidson et al. [390], Amimoto et al. [24], Wine and Ravishankara [1628], Blitz et al. [170], Dunlea and Ravishankara [462], Carl [259], Takahashi et al. [1408], Dillon et al. [433], and Vranckx et al. [1527]. The temperature dependence of the rate coefficient was derived from the results of Davidson et al. (204 – 359 K), Dunlea and Ravishankara (220 – 370 K), and Vranckx et al. (227 – 715 K); only data at $<400\text{ K}$ were considered in the evaluation, after normalization to the $k(298\text{ K})$ value recommended here for the overall rate coefficient. The recommended rate coefficients for the $N_2 + O_2$ and $2NO$ product channels were evaluated for 298 K, the only temperature at which such data are available. The branching ratio, R , $k(NO + NO)/k(\text{Total})$ is taken from Cantrell et al. [255] who reported $R = 0.57$ as well as an analysis of all measurements from 1957–1994 that led them to recommend $R = 0.61 \pm 0.06$, where the uncertainty is the 95% confidence interval. Their recommended branching ratio agrees well with earlier measurements of the quantum yield from N_2O photolysis (Calvert and Pitts [242]). Dependencies of the branching ratio on $O(^1D)$ translational energy and temperature are at present not clearly resolved. The recommended rate coefficients for the two channels as a function of temperature were derived assuming that the branching ratio for the two channels is invariant with temperature.

The yield of $O(^3P)$ from $O(^1D) + N_2O$ (physical quenching or chemical deactivation) has been determined to be <0.04 , 0.04 ± 0.02 , 0.056 ± 0.009 , and 0.005 ± 0.002 by Wine and Ravishankara [1628], Nishida et al. [1100], Carl [259] and Vranckx et al. [1527] at 298 K, respectively. Vranckx et al. report a slight increase in the $O(^3P)$ yield with increasing temperature (248 – 600 K) and their reported yield supercedes the anomalously high value reported by Carl [259] from the same laboratory. A recommended $O(^3P)$ yield of <0.01 is based on the Vranckx et al. study. A direct measurement of the NO yield from the $O(^1D) + N_2O$ reaction in synthetic air by Greenblatt and Ravishankara [578] and the re-analysis by Dunlea and Ravishankara [462] agrees very well with the value predicted using the recommended $O(^1D)$ rate coefficients for N_2 , O_2 , and N_2O and the $O(^1D) + N_2O$ product branching ratio to give $NO + NO$. Better reactive channel branching ratio

measurements at stratospheric temperatures and/or measurements of the NO yield in this reaction as a function of temperature below 298 K would be useful. The uncertainty for this reaction includes factors for both the overall rate coefficient and the branching ratio. (Table 09-31, Note: 09-31) [Back to Table](#)

- A9. $O(^1D) + NH_3$. The recommended rate coefficient and temperature dependence is taken from Davidson et al. [393]. Sanders et al. [1256] have detected the products $NH(a^1\Delta)$ and OH formed in the reaction. They report that the yield of $NH(a^1\Delta)$ is in the range 3–15% of the amount of the OH detected. (Table: 82-57, Note: 10-6, Evaluated: 10-6) [Back to Table](#)
- A10. $O(^1D) + CO_2$. $k(298\text{ K})$ was derived from the studies of Davidson et al. [393], Streit et al. [1376], Amimoto et al. [24], Dunlea and Ravishankara [462], Shi and Barker [1298], and Blitz et al. [170]. Temperature dependence was computed after normalizing the results of Dunlea and Ravishankara and Streit et al. (only the data in the range of 200 to 354 K) to the value of $k(298\text{ K})$ recommended here. The rate coefficient at 195 K reported by Blitz et al. is consistent with the recommendation.
- This reaction produces $O(^3P)$ and CO_2 , and is expected to proceed through the formation of a CO_3 complex (see for example DeMore and Dede, [418]). This complex formation leads to isotopic scrambling (See for example Perri et al. [1156]). There appears to be a small, but non-negligible, channel for $O(^1D)$ quenching. A reactive channel to give CO and O_2 has been reported ([1283]), but needs better quantification. (Table: 06-2, Note: 06-2) [Back To Table](#)
- A11. $O(^1D) + CH_4$. The recommended overall rate coefficient for the removal of $O(^1D)$ by CH_4 at room temperature is a weighted average of the results from Davidson et al. [393], Blitz et al. [170], Dillon et al. [432], and Vranckx et al. [1526]. The temperature dependence of the rate coefficient was derived from the results of Davidson et al. (198 – 357 K), Dillon et al. (223 – 297 K), and Vranckx et al. (227 – 450 K). The recommended rate coefficients for the product channels (a) $CH_3 + OH$, (b) CH_3O or $CH_2OH + H$ and (c) $CH_2O + H_2$ were evaluated for 298 K, the only temperature at which such data are available. Lin and DeMore [919] analyzed the final products of N_2O/CH_4 photolysis mixtures and concluded that (a) accounted for about 90% and CH_2O and H_2 (c) accounted for about 9%. Casavecchia et al. [262] used a molecular beam experiment to observe H and CH_3O (or CH_2OH) products. They reported that the yield of H_2 was <25% of the yield of H from channel (b). Satyapal et al. [1262] observed the production of H atoms in a pulsed laser experiment and reported an H atom yield of $25 \pm 8\%$. Matsumi et al. [979] reported the H atom yield in low pressure gas mixtures to be $(15 \pm 3)\%$. Chen et al. [279] used laser infrared kinetic spectroscopy to study product formation and report yields of $67 \pm 5\%$, $30 \pm 10\%$, and 5% for channels a, b, and c, respectively. The yield of $O(^3P)$ via the physical quenching of $O(^1D)$ by CH_4 has been reported by several groups. Wine and Ravishankara [1628], Matsumi et al. [970], and Takahashi et al. [1409] reported $O(^3P)$ yields of <4.3%, <5%, and <1%, respectively. Vranckx et al. [1526] reported the most sensitive $O(^3P)$ yield measurement to date and obtained a yield of 0.002 ± 0.003 . We recommend the following branching ratios (a) $(75 \pm 15)\%$, (b) $(20 \pm 10)\%$, (c) $(5 \pm 5)\%$ and it is assumed that the branching ratio for the three channels is invariant with temperature. The uncertainties are based on the evaluation of the overall rate coefficient. (Table 09-31, Note: 09-31) [Back to Table](#)
- A12. $O(^1D) + HCl$. The recommended room temperature rate coefficient is based on the measurements of Davidson et al. [393], Wine et al. [1634] and Chichinin [298]. The temperature dependence is based on the measurements of Davidson et al. Product studies by Wine et al. indicate: $O(^3P) + HCl$ ($9 \pm 5\%$); $H + ClO$ ($24 \pm 5\%$); and $OH + Cl$ ($67 \pm 10\%$). Takahashi et al. [1409] report that the $O(^3P)$ yield is $(15 \pm 4)\%$. Chichinin [299] report the $H + ClO$ channel to be $(18 \pm 4)\%$. (Table: 06-2, Note: 06-2, Evaluated: 10-6) [Back to Table](#)
- A13. $O(^1D) + HF$. The recommended value of $k(298\text{ K})$ is based on the one reported value of Sorokin et al. [1346]. It is assumed that the rate coefficient is independent of temperature. The possible products of this reaction are: $HF + O(^3P)$ and $F + OH$. The channel to give $H + FO$ is endothermic and, hence, considered to be unimportant. (Table: 06-2, Note: 06-2) [Back to Table](#)
- A14. $O(^1D) + NF_3$. The recommended value for $k(298\text{ K})$ is based on the results of Zhao et al. [1689]. The $k(298\text{ K})$ value reported by Sorokin et al. [1346] is a factor of two lower. The temperature dependence of the rate coefficient is based on the measurements of Zhao et al. Sorokin et al. and Zhao et al. report that 70 and >95%, respectively, of the $O(^1D)$ - NF_3 collisions lead to removal of

NF₃, i.e., products other than O(³P) + NF₃. The identity of the reaction products is not known. (Table: 10-6, Note: 10-6, Evaluated: 10-6) [Back to Table](#)

- A15. O(¹D) + HBr. The recommended rate coefficient at 298 K was taken from Wine et al. [1634]. There are no reports on the temperature dependence of this rate coefficient. Because it is close to a collisional rate coefficient, the rate coefficient is assumed to be temperature independent. On the basis of O(³P) and H(²S) atom detection, Wine et al. reported physical quenching, HBr + O(³P), in this reaction to be (20 ± 7)% and the H + BrO reactive product channel to be <4.5%. In a crossed molecular beam study of this reaction, Balucani et al. [84] found the BrO yield to be >(14 ± 6)%. Using transient UV absorption spectroscopy, Cronkhite et al. [372] found the BrO yield to be (20 ± 4)%. The balance of the reaction leads to the formation of Br + OH products. (Table: 87-41, Note: 10-6, Evaluated: 10-6) [Back to Table](#)
- A16. O(¹D) + Cl₂. The recommended k(298 K) is based on the reports of Wine et al. [1624] and Sorokin et al. [1346]. There are no reports on the temperature dependence of this rate coefficient. The rate coefficient is assumed to be temperature independent because k(298 K) is close to a collisional rate coefficient. Sorokin et al. and Wine et al. report that the branching ratio to produce ClO + Cl is 0.75 based on the measured O(³P) yield. The Cl atom measurements of Chichinin [298] are consistent with a ClO + Cl yield of 0.7. These values are in excellent agreement with the directly measured ClO yield of (74 ± 15)% by Takahashi et al. [1409]. An indirect study by Freudenstein and Biedenkapp [521] is in reasonable agreement on the yield of ClO. Though energetically allowed, the formation of Cl₂O is expected to be negligible under atmospheric pressure and temperature conditions. (Table: 06-2, Note: 10-6, Evaluated: 10-6) [Back to Table](#)
- A17. O(¹D) + CCl₂O. The recommended value of k(298 K) is derived from the values reported by Chichinin [298] and Strekowski et al. [1378]. The value of Fletcher and Husain, reduced by a factor of 2 to account for the systematic errors in their measurement method, is in reasonable agreement with the recommended value. The relative rate study of Jayanty et al. [727] is also consistent with the recommended value. The temperature dependence is taken from Strekowski et al. There are three possible reactive channels: CO + ClO + Cl; CO₂ + 2 Cl; CO₂ + Cl₂. In the stratosphere, all these processes will lead to CO₂ and ClO. Chichinin reports that the above 3 reactions account for 80% of O(¹D) loss with 20% leading to O(³P). The rate coefficient for the loss of COCl₂ via reaction with O(¹D) is expected to be more than 80% for the overall rate coefficient recommended here. (Table: 06-2, Note: 06-2) [Back to Table](#)
- A18. O(¹D) + CCIFO. The recommended rate constant is derived from data of Fletcher and Husain [513]. For consistency, the recommended value was derived using a scaling factor (0.5) that corrects for the difference between rate constants from the Husain laboratory and the recommendations for other O(¹D) rate constants given in this evaluation. This reaction has only been studied at 298 K. Based on consideration of similar O(¹D) reactions, it is assumed that E/R equals zero and the A-factor has been set equal to k(298 K). (Table: 82-57, Note: 10-6) [Back to Table](#)
- A19. O(¹D) + CF₂O. The recommendation is from the data of Wine and Ravishankara [1629]. Their result is preferred over the value of Fletcher and Husain [513] because it appears to follow the pattern of decreased reactivity with increased fluorine substitution observed for other halocarbons. This reaction has only been studied at 298 K. Based on consideration of similar O(¹D) reactions, it is assumed that E/R equals zero and the A-factor has been set equal to k(298 K). (Table: 82-57, Note: 10-6) [Back to Table](#)
- A20. O(¹D) + CCl₄. The recommended rate coefficient is based on the room temperature data from Davidson et al. [392] and Force and Wiesenfeld [517]. The rate coefficient is assumed to be temperature independent based on comparison with other O(¹D) reactions. Force and Wiesenfeld [517] reported this reaction to be (14 ± 6)% quenching and (86 ± 6)% reaction. Takahashi et al. [1409] report a ClO yield of (90 ± 19)% in good agreement with the Force and Wiesenfeld study. (Table: 82-57, Note: 10-6) [Back to Table](#)
- A21. O(¹D) + CH₃Br. The recommended rate coefficient at 298 K is taken from Thompson and Ravishankara [1434]. There are no reports on the temperature dependence of this rate coefficient and it is assumed to be temperature independent. Thompson and Ravishankara report that the yield of O(³P) from physical quenching is 0 ± 7%. Using transient UV absorption spectroscopy,

- Cronkhite et al. [372] measured the BrO yield to be $(44 \pm 5)\%$. (Table: 94-26, Note: 10-6, Evaluated: 10-6) [Back to Table](#)
- A22. $O(^1D) + CH_2Br_2$. The recommendation is based on data from Thompson and Ravishankara [1434]. They report that the yield of $O(^3P)$ from physical quenching is $(5 \pm 7)\%$. (Table: 94-26, Note: 94-26) [Back to Table](#)
- A23. $O(^1D) + CHBr_3$. The recommendation is based on data from Thompson and Ravishankara [1434]. The rate coefficient is somewhat large compared to analogous compounds. They report that the yield of $O(^3P)$ from physical quenching is $(32 \pm 8)\%$. (Table: 94-26, Note: 94-26) [Back to Table](#)
- A24. $O(^1D) + CH_3F$ (HFC-41). The recommendation is the average of measurements of Force and Wiesenfeld [517] and Schmoltner et al. [1275]. The $O(^3P)$ product yield was reported to be $(25 \pm 3)\%$ by Force and Wiesenfeld, $(11 \pm 5)\%$ by Schmoltner et al., and $(19 \pm 5)\%$ by Takahashi et al. [1409]. Burks and Lin [223] reported observing vibrationally excited HF as a product. Park and Wiesenfeld [1143] observed OH. (Table: 94-26, Note: 97-4) [Back to Table](#)
- A25. $O(^1D) + CH_2F_2$ (HFC-32). The recommendation is based upon the measurement of Schmoltner et al. [1275], who reported that the yield of $O(^3P)$ is $(70 \pm 11)\%$. Green and Wayne [576] measured the loss of CH_2F_2 relative to the loss of N_2O . Their value when combined with our recommendation for $O(^1D) + N_2O$ yields a rate coefficient for reactive loss of CH_2F_2 that is about three times the result of Schmoltner et al. Burks and Lin [223] reported observing vibrationally excited HF as a product. (Table: 94-26, Note: 94-26) [Back to Table](#)
- A26. $O(^1D) + CHF_3$ (HFC-23). The recommendation is the average of measurements of Force and Wiesenfeld [517] and Schmoltner et al. [1275]. The $O(^3P)$ product yield was reported to be $(77 \pm 15)\%$ by Force and Wiesenfeld and $(102 \pm 3)\%$ by Schmoltner et al. Although physical quenching is the dominant process, detectable yields of vibrationally excited HF have been reported by Burks and Lin [223] and Aker et al. [18], which indicate the formation of $HF + CF_2O$ products. (Table: 94-26, Note: 94-26) [Back to Table](#)
- A27. $O(^1D) + CHCl_2F$ (HCFC-21). The recommendation is based on the total rate coefficient (physical quenching and reaction) measurements of Davidson et al. [392] over the temperature range 188 – 343 K. Takahashi et al. [1409] report the yield of ClO to be $(74 \pm 15)\%$. (Table: 90-1, Note: 10-6) [Back to Table](#)
- A28. $O(^1D) + CHClF_2$ (HCFC-22). The recommendation is based on the rate coefficient measurements of Davidson et al. [392] and Warren et al. [1579]. Davidson et al. determined the rate coefficient to have no temperature dependence between 173 and 343 K. A measurement of the rate of reaction (halocarbon removal) relative to the rate of reaction with N_2O by Green and Wayne [576] agrees very well with this value when the current $O(^1D) + N_2O$ recommendation is used to obtain an absolute value. A relative measurement by Atkinson et al. [57] gives a rate coefficient about a factor of two higher. Addison et al. [10] reported the following product yields: ClO $(55 \pm 10)\%$, CF_2 $(45 \pm 10)\%$, $O(^3P)$ $(28 \pm 10/-15)\%$, and OH 5%, where the $O(^3P)$ comes from a branch yielding CF_2 and HCl. Warren et al. [1579] also report a yield of $O(^3P)$ of $(28 \pm 6)\%$, which they interpret to be the product of physical quenching. (Table: 92-20, Note: 10-6) [Back to Table](#)
- A29. $O(^1D) + CHF_2Br$. The recommended rate coefficient at room temperature and its temperature dependence are based on the study of Strekowski et al. [1379] (211 – 425 K) which is the only available investigation of this reaction. They report a branching ratio for $O(^3P)$ production of ~40% independent of temperature and a branching ratio for H atom production of ~2% at 298 K. Cronkhite et al. [372] report a BrO yield of $(39 \pm 7)\%$ at room temperature. Therefore, 60% of the reaction is expected to lead to destruction of CHF_2Br . (Table: 06-2, Note: 10-6, Evaluated: 10-6) [Back to Table](#)
- A30. $O(^1D) + CCl_3F$ (CFC-11). The recommended rate coefficient is based on the room temperature data from Davidson et al. [392] and Force et al. [517]. The rate coefficient is assumed to be temperature independent based on comparison with other $O(^1D)$ reactions. Force and Wiesenfeld [517] reported this reaction to be $(12 \pm 4)\%$ quenching and $(88 \pm 5)\%$ reaction. Takahashi et al. [1409] report a ClO yield of $(88 \pm 18)\%$ in good agreement with the Force and Wiesenfeld study. (Table: 92-20, Note: 10-6) [Back to Table](#)

- A31. $\text{O}(^1\text{D}) + \text{CCl}_2\text{F}_2$ (CFC-12). The recommended rate coefficient is based on the room temperature data from Davidson et al. [392] and Force et al. [517]. The rate coefficient is assumed to be temperature independent based on comparison with other $\text{O}(^1\text{D})$ reactions. Force and Wiesenfeld [517] report this reaction to be $(14 \pm 7)\%$ quenching and $(86 \pm 14)\%$ reaction. Takahashi et al. [1409] report a ClO yield of $(87 \pm 18)\%$ in good agreement with the Force and Wiesenfeld study. (Table: 92-20, Note: 10-6) [Back to Table](#)
- A32. $\text{O}(^1\text{D}) + \text{CClF}_3$ (CFC-13). The recommendation is based on the measurement by Ravishankara et al. [1211] who report $(31 \pm 10)\%$ physical quenching. Takahashi et al. [1409] report the yields of $\text{O}(^3\text{P})$ $(16 \pm 5)\%$ and ClO $(85 \pm 18)\%$. (Table: 92-20, Note: 97-4) [Back to Table](#)
- A33. $\text{O}(^1\text{D}) + \text{CClBrF}_2$ (Halon-1211). The recommended rate coefficient at room temperature, $k(298 \text{ K})$, is based on the data from Thompson and Ravishankara [1434]. There are no reports on the temperature dependence of this rate coefficient and it is assumed to be temperature independent. Thompson and Ravishankara report that the yield of $\text{O}(^3\text{P})$ from physical quenching is $(36 \pm 4)\%$. Cronkhite et al. [372] report a BrO yield of $(31 \pm 6)\%$ at room temperature. (Table: 94-26, Note: 10-6, Evaluated: 10-6) [Back to Table](#)
- A34. $\text{O}(^1\text{D}) + \text{CBr}_2\text{F}_2$ (Halon-1202). The recommendation is based on data from Thompson and Ravishankara [1434]. They report that the yield of $\text{O}(^3\text{P})$ from physical quenching is $(54 \pm 6)\%$. (Table: 94-26, Note: 94-26) [Back to Table](#)
- A35. $\text{O}(^1\text{D}) + \text{CBrF}_3$ (Halon-1301). The recommended rate coefficient at room temperature is based on data from Thompson and Ravishankara [1434]. There are no reports on the temperature dependence of this rate coefficient and it is assumed to be temperature independent. Thompson and Ravishankara report that the yield of $\text{O}(^3\text{P})$ from physical quenching is $(59 \pm 8)\%$. Lorenzen-Schmidt et al. [933] measured the CBrF_3 removal rate relative to N_2O and report that the rate coefficient for CBrF_3 destruction in this reaction is $(4.0 \pm 0.4) \times 10^{-11}$, which is in excellent agreement with the results of Thompson and Ravishankara. Cronkhite et al. [372] report a BrO yield of $(49 \pm 7)\%$ at room temperature. (Table: 94-26, Note: 10-6, Evaluated: 10-6) [Back to Table](#)
- A36. $\text{O}(^1\text{D}) + \text{CF}_4$ (CFC-14). The recommended rate coefficient upper limit is based on the work of Ravishankara et al. [1211], who report $(92 \pm 8)\%$ physical quenching. Force and Wiesenfeld [517] measured a quenching rate coefficient about 10 times larger. Shi and Barker [1298] report an upper limit that is consistent with the recommendation. The small rate coefficient for this reaction makes it vulnerable to interference from reactant impurities. For this reason only an upper limit for the rate coefficient is recommended. (Table: 92-20, Note: 10-6, Evaluated: 10-6) [Back to Table](#)
- A37. $\text{O}(^1\text{D}) + \text{CH}_3\text{CH}_2\text{F}$ (HFC-161). The recommendation is based on data from Schmoltner et al. [1275]. They report that the yield of $\text{O}(^3\text{P})$ from physical quenching is $(18 \pm 5)\%$. (Table: 94-26, Note: 94-26) [Back to Table](#)
- A38. $\text{O}(^1\text{D}) + \text{CH}_3\text{CHF}_2$ (HFC-152a). The recommended rate coefficient at room temperature is an average of the data from Warren et al. [1579] and Kono and Matsumi [817] which agree within 25%. There are no reports on the temperature dependence of this rate coefficient and it is assumed to be temperature independent. Warren et al. report that the yield of $\text{O}(^3\text{P})$ from physical quenching is $(54 \pm 7)\%$. Kono and Matsumi report that the yield of $\text{O}(^3\text{P})$ from physical quenching is $(34 \pm 6)\%$, the OH yield is $(15 \pm 2)\%$, and a large fraction of the reaction, $\sim 50\%$, leads to unidentified products. (Table: 10-6, Note: 10-6, Evaluated: 10-6) [Back to Table](#)
- A39. $\text{O}(^1\text{D}) + \text{CH}_3\text{CCl}_2\text{F}$ (HCFC-141b). The recommendation is based upon the measurement of Warren et al. [1579], who report $(31 \pm 5)\%$ physical quenching. (Table: 92-20, Note: 92-20) [Back to Table](#)
- A40. $\text{O}(^1\text{D}) + \text{CH}_3\text{CClF}_2$ (HCFC-142b). The recommendation is based upon the measurement of Warren et al. [1579], who report $(26 \pm 5)\%$ physical quenching. This agrees very well with Green and Wayne [576], who measured the loss of $\text{CH}_3\text{CF}_2\text{Cl}$ relative to the loss of N_2O , when the recommendation for N_2O is used. (Table: 92-20, Note: 92-20) [Back to Table](#)
- A41. $\text{O}(^1\text{D}) + \text{CH}_3\text{CF}_3$ (HFC-143a). The recommended rate coefficient at room temperature is taken from Kono and Matsumi [817]. There are no reports on the temperature dependence of this rate coefficient and it is assumed to be temperature independent. Kono and Matsumi report the yield of $\text{O}(^3\text{P})$ from physical quenching to be $(18 \pm 4)\%$, an OH yield of $(38 \pm 6)\%$, and $\sim 40\%$ of the reaction

occurs through unidentified product channels. That is 80% of the reaction leads to loss of CH_3CF_3 . The relative rate coefficient measurement by Green and Wayne [576], who measured the loss of CH_3CF_3 relative to N_2O , is in poor agreement with the results from Kono and Matsumi. Using the current recommendation for $\text{O}(^1\text{D}) + \text{N}_2\text{O}$ rate coefficient, the Green and Wayne rate coefficient for the loss of CH_3CF_3 would be $k(298\text{ K})$ of $6.4 \times 10^{-11} \text{ cm}^3 \text{ molecule}^{-1} \text{ s}^{-1}$. (Table: 10-6, Note: 10-6, Evaluated: 10-6) [Back to Table](#)

- A42. $\text{O}(^1\text{D}) + \text{CH}_2\text{ClCClF}_2$ (HCFC-132b). The recommendation is based upon the relative rate measurement of Green and Wayne [576], who measured the loss of $\text{CH}_2\text{ClCF}_2\text{Cl}$ relative to the loss of N_2O . The recommendation for N_2O is used to obtain the value given. It is assumed that there is no physical quenching. (Table: 90-1, Note: 90-1) [Back to Table](#)
- A43. $\text{O}(^1\text{D}) + \text{CH}_2\text{ClCF}_3$ (HCFC-133a). The recommendation is based upon the measurement of Warren et al. [1579], who report $(20 \pm 5)\%$ physical quenching. This agrees with Green and Wayne [576] who measured the loss of CH_2ClCF_3 relative to the loss of N_2O , when the recommendation for N_2O is used. (Table: 92-20, Note: 92-20) [Back to Table](#)
- A44. $\text{O}(^1\text{D}) + \text{CH}_2\text{FCF}_3$ (HFC-134a). The recommended rate coefficient at room temperature is based on data from Warren et al. [1579] and Kono and Matsumi [817], which are in excellent agreement. There are no reports on the temperature dependence of this rate coefficient and it is assumed to be temperature independent. Warren et al. [1579] report that the yield of $\text{O}(^3\text{P})$ from physical quenching is $(94 + 6/-1)\%$. Kono and Matsumi report that the yield of $\text{O}(^3\text{P})$ from physical quenching is $(65 \pm 6)\%$, the OH yield is $(24 \pm 4)\%$, and a small fraction of the reaction, $\sim 11\%$, leads to other products. The product yields reported in the Kono and Matsumi study are recommended considering that C–H bonds are usually reactive toward $\text{O}(^1\text{D})$. (Table: 92-20, Note: 10-6, Evaluated: 10-6) [Back to Table](#)
- A45. $\text{O}(^1\text{D}) + \text{CHCl}_2\text{CF}_3$ (HCFC-123). The recommendation is based upon measurements by Warren et al. [1579]. The relative rate measurement of Green and Wayne [576], who measured the loss of CHCl_2CF_3 relative to the loss of N_2O , agrees well with the recommendation when the recommendation for N_2O is used. Warren et al. report $(21 \pm 8)\%$ physical quenching. (Table: 92-20, Note: 92-20) [Back to Table](#)
- A46. $\text{O}(^1\text{D}) + \text{CHClFCF}_3$ (HCFC-124). The recommendation is based upon the measurement of Warren et al. [1579], who report $(31 \pm 10)\%$ physical quenching. (Table: 92-20, Note: 92-20) [Back to Table](#)
- A47. $\text{O}(^1\text{D}) + \text{CHF}_2\text{CF}_3$ (HFC-125). The recommended rate coefficient at room temperature is based on data from Warren et al. [1579] and Kono and Matsumi [817], which are in good agreement. This reaction is faster than one would predict by analogy to similar compounds, such as CH_2FCF_3 . There are no reports on the temperature dependence of this rate coefficient and it is assumed to be temperature independent. Warren et al. report that the yield of $\text{O}(^3\text{P})$ from physical quenching is $(85 + 15/-22)\%$. Kono and Matsumi report that the yield of $\text{O}(^3\text{P})$ from physical quenching is $(24 \pm 4)\%$, the OH yield is $(60 \pm 10)\%$, and a fraction of the reaction, $\sim 20\%$, leads to other products. Green and Wayne [576] measured the loss of CHF_2CF_3 relative to the loss of N_2O and report a rate coefficient $\sim 40\%$ of the recommended rate coefficient. The product yields reported in these studies are in poor agreement and no recommendation is given. (Table: 92-20, Note: 10-6, Evaluated: 10-6) [Back to Table](#)
- A48. $\text{O}(^1\text{D}) + \text{CCl}_3\text{CF}_3$ (CFC-113a). The recommendation is an estimate based on analogy to similar compounds. (Table: 92-20, Note: 92-20) [Back to Table](#)
- A49. $\text{O}(^1\text{D}) + \text{CCl}_2\text{FCClF}_2$ (CFC-113). The recommendation is an estimate based on analogy to similar compounds. (Table: 92-20, Note: 92-20) [Back to Table](#)
- A50. $\text{O}(^1\text{D}) + \text{CCl}_2\text{FCF}_3$ (CFC-114a). The recommendation is an estimate based on analogy to similar compounds. (Table: 92-20, Note: 92-20) [Back to Table](#)
- A51. $\text{O}(^1\text{D}) + \text{CClF}_2\text{CClF}_2$ (CFC-114). The recommendation is based on the measurement by Ravishankara et al. [1211], who report $(25 \pm 9)\%$ physical quenching. (Table: 92-20, Note: 92-20) [Back to Table](#)

- A52. $O(^1D) + CClF_2CF_3$ (CFC-115). The recommendation is based on the measurement by Ravishankara et al. [1211], who report $(70 \pm 7)\%$ physical quenching. (Table: 92-20, Note: 92-20) [Back to Table](#)
- A53. $O(^1D) + CBrF_2CBrF_2$ (Halon-2402). The recommendation is based on data from Thompson and Ravishankara [1434]. They report that the yield of $O(^3P)$ from physical quenching is $(25 \pm 7)\%$. Lorenzen-Schmidt et al. [933] measured the Halon removal rate relative to the N_2O removal rate and report that the rate coefficient for the Halon destruction path is $(8.8 \pm 1.2) \times 10^{-11}$, in fair agreement with the result of Thompson and Ravishankara. (Table: 94-26, Note: 97-4) [Back to Table](#)
- A54. $O(^1D) + CF_3CF_3$ (PFC-116). The recommendation is based on the work of Ravishankara et al. [1211] who report $(85 \pm 15)\%$ physical quenching. The small rate coefficient for this reaction makes it vulnerable to interference from reactant impurities. For this reason only an upper limit for the rate coefficient is recommended. (Table: 94-26, Note: 10-6, Evaluated: 10-6) [Back to Table](#)
- A55. $O(^1D) + CHF_2CF_2CF_2CHF_2$ (HFC-338pcc). The recommendation is based on data from Schmoltner et al. [1275]. They report that the yield of $O(^3P)$ from physical quenching is $(97 \pm 9)\%$. (Table: 94-26, Note: 94-26) [Back to Table](#)
- A56. $O(^1D) + c-C_4F_8$. The recommended rate coefficient for perfluorocyclobutane is based on the work of Ravishankara et al. [1211] who report $(100 \pm 15)\%$ physical quenching. The small rate coefficient for this reaction makes it vulnerable to interference from reactant impurities. For this reason only an upper limit for the rate coefficient is recommended. (Table: 92-20, Note: 10-6, Evaluated: 10-6) [Back to Table](#)
- A57. $O(^1D) + CF_3CHFCHFCF_2CF_3$ (HFC-43-10mee). The recommendation is based on data from Schmoltner et al. [1275]. The rate coefficients for this compound and CHF_2CF_3 do not follow the reactivity trend of other HFCs. Schmoltner et al. report that the yield of $O(^3P)$ from physical quenching is $(91 \pm 4)\%$. (Table: 94-26, Note: 94-26) [Back to Table](#)
- A58. $O(^1D) + C_5F_{12}$ (CFC-41-12). The recommendation is based on data from Ravishankara et al. [1211]. They report that the yield of $O(^3P)$ from physical quenching is $(79 \pm 12)\%$. The small rate coefficient for this reaction makes it vulnerable to interference from reactant impurities. For this reason only an upper limit for the rate coefficient is recommended. (Table: 94-26, Note: 10-6, Evaluated: 10-6) [Back to Table](#)
- A59. $O(^1D) + C_6F_{14}$ (PFC-51-14). The recommendation is based on data from Ravishankara et al. [1211]. They report the yield of $O(^3P)$ from physical quenching is $(75 \pm 9)\%$. The small rate coefficient for this reaction makes it vulnerable to interference from reactant impurities. For this reason only an upper limit for the rate coefficient is recommended. (Table: 94-26, Note: 10-6, Evaluated: 10-6) [Back to Table](#)
- A60. $O(^1D) + 1,2-(CF_3)_2C-C_4F_6$. The recommendation is based on data from Ravishankara et al. [1211]. They report the yield of $O(^3P)$ from physical quenching is $(84 \pm 16)\%$. The small rate coefficient for this reaction makes it vulnerable to interference from reactant impurities. For this reason only an upper limit for the rate coefficient is recommended. (Table: 94-26, Note: 10-6, Evaluated: 10-6) [Back to Table](#)
- A61. $O(^1D) + C_4F_{10}$. The recommendation is taken from the estimated upper limit for reactive loss given by Ravishankara et al. [1211]. The small rate coefficient for this reaction makes it vulnerable to interference from reactant impurities. For this reason only an upper limit for the rate coefficient is recommended. (Table: 10-6, Note: 10-6, Evaluated: 10-6) [Back to Table](#)
- A62. $O(^1D) + SF_6$. The recommendation is based on the work of Ravishankara et al. [1211] who report $(32 \pm 10)\%$ physical quenching. The small rate coefficient for this reaction makes it vulnerable to interference from reactant impurities. For this reason only an upper limit for the rate coefficient is recommended. (Table: 92-20, Note: 10-6, Evaluated: 10-6) [Back to Table](#)
- A63. $O(^1D) + SO_2$. The room temperature rate coefficient is taken from the work of Zhao et al. [1689], which is the only study for this reaction. Although no studies are available, the reaction rate coefficient is expected to have negligible temperature dependence. Zhao et al. reported the branching ratio for reactive loss to be $(76 \pm 12)\%$. (Table: 10-6, Note: 10-6, Evaluated: 10-6) [Back to Table](#)

- A64. $\text{O}(^1\text{D}) + \text{SO}_2\text{F}_2$. The recommendation is based on the measurements of Dillon et al. [433] and Zhao et al. [1689], which are in good agreement. Although Dillon et al. report a temperature independent rate coefficient over the temperature range 220 – 300 K, a weak negative temperature dependence is apparent in their data. Zhao et al. (199 – 351 K) report a negative temperature dependence, $E/R = -98$ K, that reproduces both data sets very well and is recommended. Dillon et al. reported that collisional quenching accounts for $(55 \pm 4)\%$ of the total rate coefficient, independent of temperature. The results from Zhao et al. are in agreement with this result but are less precise. (Table: 10-6, Note: 10-6, Evaluated: 10-6) [Back to Table](#)
- A65. $\text{O}(^1\text{D}) + \text{SF}_5\text{CF}_3$. Zhao et al. [1689], the only study of this reaction, report an upper limit for the room temperature rate coefficient. The determination of the small rate coefficient for this reaction makes it vulnerable to interference from reactant impurities. For this reason only an upper limit for the rate coefficient is recommended. (Table: 10-6, Note: 10-6, Evaluated: 10-6) [Back to Table](#)
- A66. $\text{O}_2(^1\Delta) + \text{O}$. The recommendation is based on the upper limit reported by Clark and Wayne [308]. (Table: 92-20, Note: 92-20) [Back to Table](#)
- A67. $\text{O}_2(^1\Delta) + \text{O}_2$. The recommendation is the average of eight room temperature measurements: Steer et al. [1361], Findlay and Snelling [503], Borrell et al. [181], Leiss et al. [879], Tachibana and Phelps [1401], Billington and Borrell [162], Raja et al. [1197], and Wildt et al. [1609]. The temperature dependence is derived from the data of Findlay and Snelling, and Billington and Borrell. Several other less direct measurements of the rate coefficient agree with the recommendation, including Clark and Wayne [309], Findlay et al. [502], and McLaren et al. [991]. Wildt et al. [1610] report observations of weak emissions in the near IR due to collision-induced radiation. Wildt et al. [1611] give rate coefficients for this process. (Table: 92-20, Note: 94-26) [Back to Table](#)
- A68. $\text{O}_2(^1\Delta) + \text{O}_3$. The recommendation is the average of the room temperature measurements of Clark et al. [307], Findlay and Snelling [504], Becker et al. [123], and Collins et al. [344]. Several less direct measurements agree well with the recommendation (McNeal and Cook [992], Wayne and Pitts [1591], and Arnold and Comes [39]). The temperature dependence is from Findlay and Snelling and Becker et al., who agree very well, although both covered a relatively small temperature range. An earlier study by Clark et al. covered a much larger range, and found a much smaller temperature coefficient. The reason for this discrepancy is not clear. The yield of $\text{O} + 2\text{O}_2$ products appears to be close to unity, based on many studies of the quantum yield of O_3 destruction near the peak of the Hartley band. For example, measurements of the number of O_3 molecules destroyed per photon absorbed: Von Ellenrieder et al. [1525], Ravishankara et al. [1216], Lissi and Heicklen [925], and references cited therein and measurements of O_3 loss and O atom temporal profiles in pulsed experiments Klais et al. [797] and Arnold and Comes [39]. Anderson et al. [33] report that the rate coefficient for atom exchange between $\text{O}_2(^1\Delta)$ and O_3 is $< 5 \times 10^{-16}$ at 300 K. (Table: 92-20, Note: 94-26) [Back to Table](#)
- A69. $\text{O}_2(^1\Delta) + \text{H}_2\text{O}$. The recommendation is the average of the measurements reported by Becker et al. [122] and Findlay and Snelling [503]. An earlier study by Clark and Wayne [309] reported a value about three times larger. (Table: 92-20, Note: 92-20) [Back to Table](#)
- A70. $\text{O}_2(^1\Delta) + \text{N}$. The recommendation is an upper limit based upon the measurement reported by Westenberg et al. [1604], who used ESR to detect $\text{O}_2(\text{X}^3\Sigma)$ and $\text{a}^1\Delta$, $\text{O}(^3\text{P})$ and $\text{N}(^4\text{S})$ with a discharge flow reactor. They used an excess of $\text{O}_2(^1\Delta)$ and measured the decay of N and the appearance of O at 195 and 300 K. They observed that the reaction of N with $\text{O}_2(^1\Delta)$ is somewhat slower than its reaction with $\text{O}_2(^3\Sigma)$. The recommended rate constant value for the latter provides the basis for the recommendation. Clark and Wayne [308, 310] and Schmidt and Schiff [1272] reported observations of an $\text{O}_2(^1\Delta)$ reaction with N that is about 30 times faster than the recommended limit. Schmidt and Schiff attribute the observed loss of $\text{O}_2(^1\Delta)$ in excess N to a rapid energy exchange with some constituent in discharged nitrogen, other than N. (Table: 92-20, Note: 92-20) [Back to Table](#)
- A71. $\text{O}_2(^1\Delta) + \text{N}_2$. The recommendation is based upon the measurements by Findlay et al. [502] and Becker et al. [122]. Other studies obtained higher values for an upper limit: Clark and Wayne [309] and Steer et al. [1361]. (Table: 92-20, Note: 92-20) [Back to Table](#)

- A72. $\text{O}_2(^1\Delta) + \text{CO}_2$. The recommendation is based on the measurements reported by Findlay and Snelling [503] and Leiss et al. [879]. Upper limit rate coefficients reported by Becker et al. [122], McLaren et al. [991], and Singh et al. [1315] are consistent with the recommendation. (Table: 92-20, Note: 92-20) [Back to Table](#)
- A73. $\text{O}_2(^1\Sigma) + \text{O}$. The recommendation is based on the measurement reported by Slinger and Black [1331]. (Table: 92-20, Note: 92-20) [Back to Table](#)
- A74. $\text{O}_2(^1\Sigma) + \text{O}_2$. The recommendation is the average of values reported by Martin et al. [974], Lawton et al. [858], and Lawton and Phelps [859], who are in excellent agreement. Measurements by Thomas and Thrush [1433], Chatha et al. [276], and Knickelbein et al. [806] are in reasonable agreement with the recommendation. Knickelbein et al. report an yield of $\text{O}_2(^1\Delta)$ product to be approximately unity. (Table: 92-20, Note: 92-20) [Back to Table](#)
- A75. $\text{O}_2(^1\Sigma) + \text{O}_3$. The recommendation is based upon the room temperature measurements of Gilpin et al. [557], Gauthier and Snelling [538], Slinger and Black [1331], Choo and Leu [301], Shi and Barker [1298], Turnipseed et al. [1483], and Dunlea et al. [465]. Measurements by Snelling [1341], Amimoto and Wiesenfeld [26], and Ogren et al. [1107] are in agreement with the recommendation. The value from the study of Biedenkapp and Bair [154] is lower than the recommended value. The temperature dependence is taken from the results of Dunlea et al., who measured the rate coefficient between 210 and 370 K. The results of Choo and Leu, which encompassed 295-362 K, are consistent with the recommended value. This reaction has multiple product channels. The yield of $\text{O} + 2\text{O}_2$ products is reported to be $(70 \pm 20)\%$ by Slinger and Black and Amimoto and Wiesenfeld. The remaining $\sim 30\%$ of the reaction is expected to lead to quenching to $\text{O}_2(^1\Delta$ or $^3\Sigma)$ while leaving ozone intact; the electronic state of O_2 that is produced in all these channels are not known. (Table: 06-2, Note: 06-2) [Back to Table](#)
- A76. $\text{O}_2(^1\Sigma) + \text{H}_2$. The rate coefficient for this reaction, at or around 298 K, has been measured by Kohse-Hoinghaus and Stuhl [814], Braithwaite et al. [192], Choo and Leu, [301], Singh and Setser, [1315], Wildt et al., [1609], Michelangeli et al., [1020], Borrell and Richards, [182], Hohmann et al. [662], and Talukdar et al. [1417]. $k(298\text{K})$ was derived from the results of all, but two, of the above studies. Results of Singh and Setser and Borrell and Richards, which are clearly outside of the range of values obtained by others, were not used.
- The temperature dependence of the rate coefficient was computed using the results of Braithwaite et al., Hohmann et al., and Talukdar et al. The results of Kohse-Hoinghaus and Stuhl were not included because it is assumed to be superseded by those of Hohmann et al. from the same group. It is suspected that the Kohse-Hoinghaus and Stuhl study was hampered by impurities in their system, as discussed in Talukdar et al.
- The rate coefficient for the reaction to produce 2 OH radicals is listed separately as an upper limit at 298 K and is based on the results of Talukdar et al. The same upper limit is shown to be valid even at 209 K. Therefore, this upper limit is recommended for all atmospheric calculations.
- This reaction could also produce $\text{O}(^3\text{P}) + \text{H}_2\text{O}$. However, there is no evidence for the formation of $\text{O}(^3\text{P})$ (Dunlea et al.[461]). Therefore, it is assumed that $\text{O}_2(^1\Sigma)$ is removed exclusively via quenching. The electronic state of O_2 that is produced is not known. (Table: 06-2, Note: 06-2) [Back to Table](#)
- A77. $\text{O}_2(^1\Sigma) + \text{H}_2\text{O}$. The recommendation is the average of room temperature measurements reported by Stuhl and Niki [1383], Aviles et al. [68], Shi and Barker [1298], and Dunlea et al. [465]. Measurements reported by O'Brien and Myers [1106] are lower likely due to an interference from $\text{O}_2(^1\Sigma)$ regeneration. The results of Derwent and Thrush [424], and Thomas and Thrush [1433] are in agreement with the recommendation. The value reported by Gauthier and Snelling [538] has a very large uncertainty and hence overlaps with the recommendation. It is not clear why the results of Filseth et al. are lower than all the other reported values; perhaps, they had an error in measuring water vapor concentration. The temperature dependence of the reaction is taken from the only reported value of Dunlea et al. Wildt et al. [1609] report that the yield of $\text{O}_2(^1\Delta)$ greater than 90%. There are no thermodynamically allowed reactive channels for this reaction. Therefore, the reaction products are written as $\text{O}_2 + \text{H}_2\text{O}$ [465]. (Table: 06-2, Note: 06-2) [Back to Table](#)

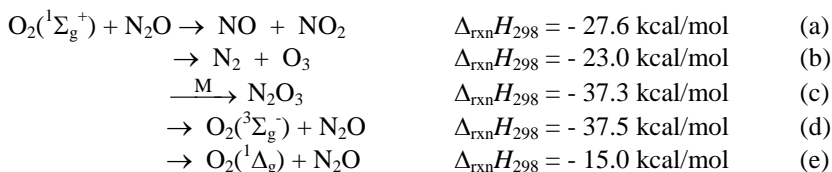
A78. $O_2(^1\Sigma) + N$. The recommendation is based on the limit reported by Slanger and Black [1331]. (Table: 92-20, Note: 92-20) [Back to Table](#)

A79. $O_2(^1\Sigma) + N_2$. The recommendation is the average of measurements reported by Izod and Wayne [719], Stuhl and Welge [1386], Filseth et al. [501], Martin et al. [974], Kohse-Höinghaus and Stuhl [814], Choo and Leu [301], Wildt et al. [1609], Shi and Barker [1298], and Dunlea et al. [465]. Less direct measurements reported by Noxon [1105], Myers and O'Brien [1038], and Chatha et al. [276] are consistent with the recommendation. The temperature dependence of the rate coefficient is derived from the results of Kohse-Höinghaus and Stuhl between 203 and 349 K and of Dunlea et al. between 210 and 370 K.

There are no exothermic reaction channels. The channel to produce 2 NO molecules is endothermic by 5.6 kcal mol⁻¹ at 298 K. (Table: 06-2, Note: 06-2) [Back to Table](#)

A80. $O_2(^1\Sigma) + N_2O$. The rate coefficient for the removal of $O_2(^1\Sigma)$ by N_2O at 298 K is derived from the studies of Filseth et al., [501, 1433] Borrell et al., [180] and Dunlea et al. [466]. The results of Gauthier and Snelling has a very large error bar and overlaps with the recommended value within their quoted error bars. The temperature dependence of this rate coefficient is taken from Dunlea et al., who are the only ones to report this value.

There are many possible reactive channels for this reaction:



Dunlea et al. have placed upper limits of $<2 \times 10^{-4}$, $<1 \times 10^{-3}$, and $<3 \times 10^{-3}$ for channel (a+c), channel (c), and overall N_2O loss from this reaction at 298 K. Based on these results, we recommend the upper limit for the NO_x production process in the table. The upper limit for NO_x production from this reaction noted in the table is assumed to be valid for all atmospheric temperatures. (Table: 06-2, Note: 06-2) [Back to Table](#)

A81. $O_2(^1\Sigma) + CO_2$. The recommendation is the average of measurements reported by Filseth et al. [501], Davidson et al. [391], Avilés et al. [68], Muller and Houston [1035], Choo and Leu [301], Wildt et al. [1609], Hohmann et al. [662], Dunlea and Ravishankara, and Shi and Barker [1298] at room temperature. The temperature dependence is from the work of Choo and Leu. Muller and Houston, and Singh and Setser [1315] give evidence that $O_2(^1\Delta)$ is a product. Wildt et al. report that the yield of $O_2(^1\Delta) \geq 90\%$. (Table: 92-20, Note: 06-2) [Back to Table](#)

B1. $O + OH$. The recommended rate coefficient was obtained from the studies of Westenberg et al. [1602] (228 – 340 K), Lewis and Watson [902] (221 – 499 K), Howard and Smith [678] (250 – 515 K), Smith and Stewart [1336] (158 – 294 K), and Robertson and Smith [1237] (136 – 377 K). The recommendation is consistent with earlier work near room temperature as reviewed by Lewis and Watson [902] and with the measurements of Brune et al. [203] (300 K), and Robertson and Smith [1238] (295 K). The ratio $k(O + HO_2)/k(O + OH)$ measured by Keyser [783] agrees with the recommended values. (Table: 10-6, Note: 10-6, Evaluated: 10-6) [Back to Table](#)

B2. $O + HO_2$. The recommended values are based on the results of studies over a range of temperatures by Keyser [782] and Nicovich and Wine [1071] and the room temperature studies of Sridharan et al. [1350], Ravishankara et al. [1216], and Brune et al. [203]. Earlier studies by Hack et al. [598] and Burrows et al. [224, 227] are not considered, because the $OH + H_2O_2$ reaction was important in these studies and the value used for its rate constant in their analyses has been shown to be in error. A study by Lii et al. [914] is also not considered because of the insensitivity of the observed to decays to $O + HO_2$. Data from Ravishankara et al. [1216] at 298 K show no dependence on pressure between 10 and 500 Torr N_2 . The ratio $k(O + HO_2)/k(O + OH)$ measured by Keyser [783] agrees with the rate constants recommended here. Sridharan et al. [1348] showed that the reaction products

correspond to abstraction of an oxygen atom from HO₂ by the O reactant. Keyser et al. [787] reported <1% O₂ (¹Δ) yield. (Table: 06-2, Note: 06-2) [Back to Table](#)

- B3. O + H₂O₂. There are two direct studies of the O + H₂O₂ reaction: Davis et al. [401] and Wine et al. [1626]. The recommended value is a fit to the combined data. An indirect measurement of the E/R by Roscoe [1241] is consistent with the recommendation. The A-factor for both data sets is quite low compared to similar atom-molecule reactions. A somewhat higher activation barrier reported by Albers et al. [21] over the temperature range 370–800 K is suggestive of a non-linear temperature dependence. (Table: 06-2, Note: 06-2) [Back to Table](#)
- B4. H + O₃. The recommendation is an average of the results of Lee et al. [866] and Keyser [778], which are in excellent agreement over the 200–400 K range. Results by Finlayson-Pitts, Seeley [1284] and Kleindienst [509] agree well with the present recommendations. An earlier study by Clyne and Monkhouse [329] is in very good agreement on the T dependence in the range 300–560 K but lies about 60% below the recommended values. Although we have no reason not to believe the Clyne and Monkhouse values, we prefer the two studies that are in excellent agreement, especially since they were carried out over the T range of interest. Reports of a channel forming HO₂ + O (Finlayson-Pitts and Kleindienst [509]: ~25%, and Force and Wiesenfeld [518]: ~40%) have been contradicted by other studies (Howard and Finlayson-Pitts [677]: <3%; Washida et al. [1582]: <6%; Finlayson-Pitts et al. [510]: <2%; and Dodonov et al. [445]: <0.3%). Secondary chemistry is believed to be responsible for the observed O-atoms in this system. Washida et al. [1583] measured a limit (<0.1%) for the production of singlet molecular oxygen in the reaction H + O₃. (Table: 06-2, Note: 06-2) [Back to Table](#)
- B5. H + HO₂. There are five studies of this reaction: Hack et al. [602], Hack et al. [600], Thrush and Wilkinson [1440], Sridharan et al. [1350] and Keyser [785]. Related early work and combustion studies are referenced in the Sridharan et al. paper. All five studies used discharge flow systems. It is difficult to obtain a direct measurement of the rate constant for this reaction because both reactants are radicals and the products OH and O are very reactive toward the HO₂ reactant. The recommendation is based on the kinetics and product data of Sridharan et al. and Keyser because their measurements were the most direct and required the fewest corrections. Keyser found the rate coefficient and product yields to be independent of temperature for 245 < T < 300 K. The other measurements, $(5.0 \pm 1.3) \times 10^{-11} \text{ cm}^3 \text{ molecule}^{-1} \text{ s}^{-1}$ by Thrush and Wilkinson [1440] and $(4.65 \pm 1) \times 10^{-11}$ by Hack et al. [600] are in reasonable agreement with the recommended value. Hislop and Wayne [653], Keyser et al. [787], and Michelangeli et al. [1020] reported on the yield of O₂ (b¹Σ) formed in the H₂ + O₂ channel as $(2.8 \pm 1.3) \times 10^{-4}$, $< 8 \times 10^{-3}$, and $< 2.1 \times 10^{-2}$, respectively as a fraction of the overall reaction. (Table: 06-2, Note: 06-2) [Back to Table](#)
- B6. OH + O₃. The recommended values are based on the results of studies over a range of temperatures by Anderson and Kaufman [31] (220 – 450 K), Ravishankara et al. [1215] (238 – 357 K), Smith et al. [1335] (240 – 295 K) and Nizkorodov et al. [1101] (191 – 314 K) and the room temperature measurements of Kurylo [833], Zahniser and Howard [1668], and Kulcke et al. [828]. The recommended E/R and k(298 K) values are based on averages of the individual E/R and k(298 K) values obtained in the above mentioned studies. The value reported by Kulcke et al. [828] has been corrected for a minor contribution from k(HO₂ + O₃). (Table: 02-25, Note: 10-6, Evaluated: 10-6) [Back to Table](#)
- B7. OH + H₂. The OH + H₂ reaction has been the subject of numerous studies. The recommendation is fixed to the average of eleven studies at 298 K: Greiner [582], Stuhl and Niki [1385], Westenberg and de Haas [1598], Smith and Zellner [1338], Atkinson et al. [59], Overend et al. [1134], Tully and Ravishankara [1472], Zellner and Steinert [1675], Ravishankara et al. [1209], Talukdar et al. [1418] and Orkin et al. [1124]. Temperature dependent studies of Orkin et al., Talukdar et al., and Ravishankara et al. find that the reaction does not follow a simple Arrhenius expression over a large range of temperature. The recommended temperature dependence is based on the average of E/R's determined in the above-mentioned studies for temperatures below 300 K. Accordingly, the recommended Arrhenius expression is only valid between 200 – 300 K. Even over this range the simple Arrhenius expression likely overestimates, near 250 K, and underestimates, near 200 K, the data by approximately 10%. (Table: 06-2, Note: 06-2) [Back to Table](#)

- B8. OH + HD. The recommendation is based on direct measurements made by Talukdar et al. [1418] using pulsed photolysis-laser induced fluorescence over the temperature range 248–418 K. The recommendation is in excellent agreement with the ratio $k(\text{OH} + \text{H}_2)/k(\text{OH} + \text{HD}) = 1.65 \pm 0.05$ at 298 K reported by Ehhalt et al. [477] when combined with the recommended $k(\text{OH} + \text{H}_2)$. (Table: 06-2, Note: 06-2) [Back to Table](#)
- B9. OH + OH. The recommendation for the OH + OH reaction is the average of eight measurements performed near 298 K at low bath gas pressures: Westenberg and de Haas [1599], McKenzie et al. [990], Clyne and Down [318], Trainor and von Rosenberg [1459], Farquharson and Smith [495], Wagner and Zellner [1530], Bedjanian et al. [127], and Bahng and MacDonald [77]. The rate coefficients reported in these studies fall in the range $(1.4 - 2.7) \times 10^{-12} \text{ cm}^3 \text{ molecule}^{-1} \text{ s}^{-1}$. Wagner and Zellner reported a slight positive temperature dependence of the rate coefficient in contrast with that reported by Bedjanian et al., who report a small negative temperature dependence. The earlier work of Wagner and Zellner may have been complicated by an increased contribution of the OH + H reaction due to an underestimate of its reaction rate. Theoretical calculations by Harding and Wagner [614] suggest that tunneling substantially influences the reaction rate coefficient. In taking account of the tunneling contribution, the rate coefficient is found to have a minimum value near room temperature. In view of the predicted behavior and given that the experimental data are consistent with each other, within the stated uncertainties, the recommendation is a temperature independent value for the rate coefficient over the temperature range 200 – 300 K. (Table: 10-6, Note: 10-6, Evaluated: 10-6) [Back to Table](#)
- B10. OH + HO₂. A study by Keyser [786] appears to resolve a discrepancy among low-pressure discharge flow experiments that all gave rate coefficients near $7 \times 10^{-11} \text{ cm}^3 \text{ molecule}^{-1} \text{ s}^{-1}$: Keyser [781], Thrush and Wilkinson [1441], Sridharan et al. [1349], [1351], Temps and Wagner [1428], and Rozenshtein et al. [1245], and atmospheric pressure studies that gave rate coefficients near 11×10^{-11} : Lii et al. [913], Hohanadel et al. [661], DeMore [410], Cox et al. [354], Burrows et al. [226], and Kurylo et al. [839]. Laboratory measurements using a discharge flow experiment and a chemical model analysis of the results by Keyser [786] demonstrate that the previous discharge flow measurements were probably subject to interference from small amounts of O and H. In the presence of excess HO₂ these atoms generate OH and result in a rate coefficient measurement that falls below the true value. The temperature dependence is from Keyser [786], who covered the range 254 to 382 K. A flow tube study by Schwab et al. [1280] reported $k = (8.0 \pm 3/-4) \times 10^{-11}$. These workers measured the concentrations of HO₂, OH, O, and H and used a computer model of the relevant reactions to test for interference. A flow tube study by Dransfeld and Wagner [456] employing an isotope labeled ¹⁸OH reactant obtained $k = (11 \pm 2) \times 10^{-11}$ in good agreement with the recommendation. They attributed about half of the reactive events to isotope scrambling because control experiments with ¹⁶OH gave $k = 6 \times 10^{-11}$. It should be noted that their control experiments were subject to the errors described by Keyser [786] due to the presence of small amounts of H and O, whereas their ¹⁸OH measurements were not. Kurylo et al. [839] found no evidence of significant scrambling in isotope studies of the OH and HO₂ reaction. An additional careful study of the reaction temperature dependence would be useful. Hippler and Troe [651] have analysed data for this reaction at temperatures up to 1250 K. In summary, this has historically been a difficult reaction to study. Earlier problems appear to have been resolved, as discussed above, and results now tend to converge on a central value, but the recommended value is still subject to a large uncertainty. (Table: 06-2, Note: 06-2) [Back to Table](#)
- B11. OH + H₂O₂. The rate coefficient for this reaction shows non-Arrhenius behavior between 96 and 1250 K with a minimum value near room temperature. Data from a number of studies are in relatively good agreement between 300 and 500 K after normalization to account for the H₂O₂ UV absorption cross section recommendation in this evaluation. Hippler and Troe [651] analyzed data for this reaction at temperatures up to 1250 K. The studies of Keyser [780] (245 – 423 K), Sridharan et al. [1352] (250 – 459 K), Wine et al. [1630] (273 – 410 K), Kurylo et al. [843] (250 – 370 K), Lamb et al. [847] (241 – 413 K), and Vaghjani et al. [1507] (273 – 410 K) show that the reaction displays a small positive temperature dependence ($E/R = \sim 160 \text{ K}$) over the 300 – 500 K range. Measurements at room temperature by Marinelli and Johnston [966], Riffault et al. [1235], Turnipseed et al. [1483], and Vakhtin et al. [1508] agree with the other studies. A value of $1.8 \times 10^{-12} \text{ cm}^3 \text{ molecule}^{-1} \text{ s}^{-1}$ is obtained by averaging the room temperature data. Lamb et al. and Vaghjani

report that k increases slightly with decreasing temperature for temperatures below 300 K while other studies show a slight positive temperature dependence. Vakhtin et al. used a pulsed Laval nozzle technique to study the reaction at very low temperatures (96 – 165 K) and report a significant increase in k with decreasing temperature. They suggest that the reaction mechanism includes the formation of a hydrogen-bonded complex. The recommendation is a temperature independent value of 1.8×10^{-12} with $f(298 \text{ K}) = 1.15$ and $g = 45$ over the temperature range of 200 – 300 K. (Table: 06-2, Note: 10-6, Evaluated: 10-6) [Back to Table](#)

- B12. $\text{HO}_2 + \text{O}_3$. The recommended values are based on results of studies over a range of temperatures by DeMore [408] at 231 to 334 K, Zahniser and Howard [1668] at 245 to 365 K, Manzanares et al. [957] at 298 K, Sinha et al. [1325] at 243 to 413 K, Wang et al. [1577] at 233 to 400 K and Herndon et al. [638] at 200 to 298 K. The data of Simonaitis and Heicklen [1310] and DeMore and Tschuikow-Roux [421] were not considered. The temperature dependence studies show varying degrees of curvature in the Arrhenius plots, with the E/R decreasing at lower temperature. This is especially evident in the low temperature data of Herndon et al. where a number of measures were taken to control potential kinetic complications. The recommended E/R and $k(298 \text{ K})$ values are based on averages of the individual E/R and $k(298 \text{ K})$ values. Furthermore, only data at temperatures less than 298 K were used for the E/R determination, accordingly the recommendation is not valid for $T > 298 \text{ K}$. Additional temperature dependence data are needed for this reaction over a larger range to more fully characterize the non-linear behavior of the rate constant. The mechanism of the reaction has been studied using ^{18}O labeled HO_2 by Sinha et al. [1325], who reported that the reaction occurs $75 \pm 10\%$ via H atom transfer at 297 K and by Nelson and Zahniser [1050], who reported branching ratios for H transfer vs O transfer over the range 226–355 K. They report that the H atom transfer decreases from $94 \pm 5\%$ at $226 \pm 11 \text{ K}$ to $88 \pm 5\%$ at $355 \pm 8 \text{ K}$. (Table: 00-3, Note: 00-3) [Back to Table](#)

- B13. $\text{HO}_2 + \text{HO}_2$. The overall rate coefficient for this reaction is the sum of a pressure-independent bimolecular component and a pressure-dependent termolecular component. Two separate expressions are given for these rate coefficients. Both components contribute to the overall loss of HO_2 under atmospheric conditions and have negative temperature dependencies. This reaction also has a dependence on H_2O that needs to be included in atmospheric model calculations. Christensen et al. [303, 304] found that kinetic studies that used CH_3OH as an HO_2 radical precursor were possibly complicated by the formation of a weakly bound reactive $\text{HO}_2\text{-CH}_3\text{OH}$ adduct, particularly at low temperatures. The magnitude of the CH_3OH effect on the measured rate coefficients is dependent on the CH_3OH concentration and temperature in the particular study.

The recommended bimolecular and termolecular expressions for the $\text{HO}_2 + \text{HO}_2$ reaction were obtained from a global fit of the rate coefficient data that had negligible complications due to the presence of CH_3OH . The analysis included data obtained at low-pressure ($< 30 \text{ Torr}$) from Thrush and Tyndall [1437, 1438] (7 – 20 Torr, 298 – 358 K), Simonaitis and Heicklen [1312] (5 – 770 Torr, 296 K), Sander [1249] (1 Torr, 298 K), Takacs and Howard [1405, 1406] (1 – 7 Torr, 252 – 391 K), Kurylo et al. [845] (25 – 600 Torr, 298 K), and Tang et al. [37] (30 Torr, 253 – 323 K) and data obtained at higher-pressure ($> 30 \text{ Torr}$) from Sander et al. [1253] (100 – 700 Torr, 298 K), Simonaitis and Heicklen [1312], Kurylo et al. [845], Christensen [304] (100 Torr, 222 – 295 K), Kircher and Sander [791] (100 – 700 Torr, 230 – 420 K) (only data above 298 K were used in the analysis), and Maricq and Sente [963] (200 Torr, 210 – 365 K). The rate coefficient data obtained using transient UV absorption detection of HO_2 [791, 845, 963, 1253, 1312] were scaled to the currently recommended HO_2 absorption cross sections. Rate coefficient studies of Kurylo et al., Sander et al. [1253], and Kircher and Sander found little difference of the measured rate coefficient when N_2 or O_2 was used as the bath gas. The recommended termolecular expression applies to $M = \text{air}$. The experimental data is reproduced to within $\pm 20\%$ using the recommended parameters. The rate coefficient data reported by Maricq and Sente are systematically 20% higher than the current recommendation. Systematic discrepancies also exist in the low-temperature rate coefficient data where the results from Christensen et al. are $\sim 25\%$ lower than the current recommendation at 222 K. Hamilton and Lii [607] and Sander et al. [1253] have reported the dependence of the rate coefficient on isotopic (H/D) substitution. Lightfoot et al. [911] reported rate coefficients at atmospheric pressure over the temperature range 298 – 777 K that are in agreement with the recommended value

at 298 K. This study indicates an upward curvature in the rate coefficient at temperatures above 500 K. A high temperature (750 – 1120 K) study by Hippler et al. [652] confirms the strong curvature. The current recommendation does not account for the non-Arrhenius behavior and is valid only for temperatures below 500 K.

Stone and Rowley [1375] reported rate coefficient data at 760 Torr over the temperature range 236 – 309 K that were later shown by Christensen et al. [303] to be systematically overestimated due to the use of very high concentrations of CH₃OH. The Stone and Rowley [1375] data were not included in the present evaluation. The rate coefficient data and temperature dependence reported by Cox and Burrows [353] is in general agreement with this recommendation. Data from Rozenshtein et al. [1245] are consistent with the low-pressure recommendation but they report no change in the rate coefficient with pressure up to 1 atm. Results reported by Thrush and Wilkinson [1439] and Dobis and Benson [443] are inconsistent with the recommendation.

The HO₂ + HO₂ reaction exhibits a dependence on H₂O concentration due to the formation of a weakly bound reactive HO₂·H₂O complex. English et al. [484] report a bond energy of 6.9 kcal mol⁻¹ for the complex (also see Table 3). There are numerous studies of the rate coefficient H₂O dependence (Hamilton [606], Hochenadel et al. [660], Hamilton and Lii [607], Cox and Burrows [353], DeMore [408], Lii et al. [915], Sander et al. [1253], Andersson et al. [34], Stone and Rowley [1375], English et al. [484], and Tang et al. [37]) that are in good agreement. The effective rate coefficient in the presence of H₂O can be obtained by multiplying the recommended rate coefficient by the factor given by Lii et al. [915] and Kircher and Sander [791]: $[1 + 1.4 \times 10^{-21} [\text{H}_2\text{O}] \exp(2200/T)]$.

The major reaction products at 300 K have been identified as H₂O₂ + O₂ by Su et al. [1388], Niki et al. [1089], Sander et al. [1253], and Simonaitis and Heicklen [1312]. (Table: 10-6, Note: 10-6, Evaluated: 10-6) [Back to Table](#)

- B14. HO₂ + HO₂-H₂O. The enhancement of the HO₂ + HO₂ reaction in the presence of H₂O vapor has been ascribed to the formation of a HO₂-H₂O complex and the higher reactivity of the complex over that of HO₂. The recommendation is based upon the studies of Kanno et al. [766, 767] who analyzed the enhancement of HO₂ decays in the presence of H₂O. Enhancement factors were obtained at 298, 325, and 350 K and a total pressure of 50 Torr N₂. A pressure dependence of the rate coefficient has not been measured and a pressure independent value is recommended. (Table: 10-6, Note: 10-6, Evaluated: 10-6) [Back to Table](#)
- C1. O + NO₂. The recommended values are based on the results of studies over a range of temperatures by Estupiñán et al. [487], Gierczak et al. [542], Ongstad and Birks [1116], Slinger et al. [1332] and Geers-Muller and Stuhl [539] and the room temperature study of Paulson et al. [1150]. In the most recent studies of Estupiñán et al. [487] and Gierczak et al. [542], special emphasis was placed on accurate measurement of the NO₂ concentration and on measurements at low temperatures. The results of earlier studies by Davis et al. [396] and Bemand et al. [144] were not used in deriving the recommended values either because of possible complications from decomposition of NO₂ at higher temperatures or lack of direct NO₂ detection. (Table: 06-2, Note: 06-2) [Back to Table](#)
- C2. O + NO₃. The recommendation is based on the study of Graham and Johnston [573] at 298 K and 329 K. While limited in temperature range, the data indicate no temperature dependence. Furthermore, by analogy with the reaction of O with NO₂, it is assumed that this rate constant is independent of temperature. Clearly, temperature-dependence studies are needed. (Table: 82-57, Note: 82-57) [Back to Table](#)
- C3. O + N₂O₅. The recommendation is based on the study by Kaiser and Japar [758]. (Table: 82-57, Note: 82-57) [Back to Table](#)
- C4. O + HNO₃. The upper limit reported by Chapman and Wayne [274] is accepted. (Table: 82-57, Note: 82-57) [Back to Table](#)
- C5. O + HO₂NO₂. The recommended value is based on the study of Chang et al. [272]. The large uncertainty in E/R and k at 298 K are due to the fact that the recommendation is based on a single study. (Table: 82-57, Note: 82-57) [Back to Table](#)

- C6. $\text{H} + \text{NO}_2$. The recommended value of k_{298} is derived from the studies of Wagner et al. [1532], Bemand and Clyne [142], Clyne and Monkhouse [329], Michael et al. [1015] and Ko and Fontijn [812]. The temperature dependence is from the studies of Wagner et al. and Ko and Fontijn. The data from Wategaonkar and Setser [1586] and Agrawalla et al. [17] were not considered. (Table: 92-20, Note: 92-20) [Back to Table](#)
- C7. $\text{OH} + \text{NO}_3$. The recommendation is derived from an average of the results of Boodaghians et al. [176], Mellouki et al. [1001], Becker et al. [119] and Mellouki et al. [1004]. There are no temperature dependence data. The reaction products are probably $\text{HO}_2 + \text{NO}_2$. (Table: 94-26, Note: 94-26) [Back to Table](#)
- C8. $\text{OH} + \text{HONO}$. The recommended rate expression is derived from the work of Jenkin and Cox [733], which supersedes the earlier room temperature study of Cox et al. [360]. Results from the Burkholder et al. [221] suggest that the reaction may have a small negative temperature dependence. (Table: 92-20, Note: 92-20) [Back to Table](#)
- C9. $\text{OH} + \text{HNO}_3$. The recent study of Brown et al. [202] furnishes the most comprehensive set of rate measurements for N_2 as the bath gas over a significant range of temperature (200–350 K) and pressure (20–500 torr). They analyzed their results in terms of the mechanism proposed by Smith et al. [1335], involving the formation of a bound, relatively long-lived $\text{HO}\cdot\text{HNO}_3$ complex, as well as the direct reaction channel. Studies of the effects of isotopic substitution on the reactions $\text{OD} + \text{DNO}_3$, $\text{OH} + \text{DNO}_3$, $\text{OD} + \text{HNO}_3$ and $^{18}\text{OH} + \text{HNO}_3$ by Brown et al. [201] support this mechanism and suggest that the structure of the intermediate consists of a H-bonded six-membered ring. Thus, the P dependence can be represented by combining a low pressure (bimolecular) limit, k_0 , with a Lindemann-Hinshelwood expression for the p-dependence:

$$k([\text{M}], T) = k_0 + \frac{k_3[\text{M}]}{1 + \frac{k_3[\text{M}]}{k_2}} \quad \left\{ \begin{array}{l} k_0 = 2.4 \times 10^{-14} \exp(460/T) \\ k_2 = 2.7 \times 10^{-17} \exp(2199/T) \\ k_3 = 6.5 \times 10^{-34} \exp(1335/T) \end{array} \right\}$$

The coefficients k_3 and k_2 are the termolecular and high pressure limits for the “association” channel. The value of k at high pressures is the sum $k_0 + k_2$.

This expression for $k([\text{M}], T)$ and the values of the Arrhenius parameters for k_0 , k_2 , and k_3 derived by Brown et al. [202] for N_2 as the bath gas constitute the recommended values for this rate coefficient. These recommended values are derived from a fit to the data of Brown et al. [202], Stachnik et al. [1355], Devolder et al. [425] and Margitan and Watson [961].

The reaction yield of NO_3 (per OH removed) is assumed to be unity at all temperatures for either reaction channel. These assumptions are supported by the isotopic studies of Brown et al. [201] and the theoretical calculations of Xia and Lin [1648]. (Table: 00-3, Note: 02-25) [Back to Table](#)

- C10. $\text{OH} + \text{HO}_2\text{NO}_2$. The recommendation for both k at 298 K and the Arrhenius expression is based upon the data of Trevor et al. [1461], Barnes et al. [88], C. A. Smith et al. [1335] and Barnes et al. [90]. Trevor et al. studied this reaction over the temperature range 246–324 K and reported a temperature invariant value of $4.0 \times 10^{-12} \text{ cm}^3 \text{ molecule}^{-1} \text{ s}^{-1}$, although a weighted least squares fit to their data yields an Arrhenius expression with an E/R value of $(193 \pm 193) \text{ K}$. In contrast, Smith et al. studied the reaction over the temperature range 240–300 K and observed a negative temperature dependence with an E/R value of $-(650 \pm 30) \text{ K}$. The early Barnes et al. study [88] was carried out only at room temperature and 1 torr total pressure while their later study was performed in the pressure range 1–300 torr N_2 and temperature range 268–295 K with no rate constant variation being observed. In addition, k_{298} derived in Barnes et al. [88] was revised upward in the later study from 4.1×10^{-12} to 5.0×10^{-12} due to a change in the rate constant for the reference reaction. The values of k at 298 K from the four studies are in excellent agreement. An unweighted least squares fit to the data from the above-mentioned studies yields the recommended Arrhenius expression. The less precise value for k at 298 K reported by Littlejohn and Johnston [926] is in fair agreement with the recommended value. The error limits on the recommended E/R are sufficient to encompass the results of both Trevor et al. and Smith et al. It should be noted that the values of k at 220 K deduced from the two studies differ by a factor of 2. Clearly, additional studies of k as a function of

temperature and the identification of the reaction products are needed. (Table 02-25, Note: 02-25)
[Back to Table](#)

- C11. $\text{OH} + \text{NH}_3$. The recommended value at 298 K is the average of the values reported by Stuhl [1381], Smith and Zellner [1339], Perry et al. [1159], Silver and Kolb [1302], Stephens [1363] and Diau et al. [427]. The values reported by Pagsberg et al. [1138] and Cox et al. [359] were not considered because these studies involved the analysis of a complex mechanism and the results are well outside the error limits implied by the above six direct studies. The results of Kurylo [833] and Hack et al. [596] were not considered because of their large discrepancies with the other direct studies (factors of 3.9 and 1.6 at room temperature, respectively). Because the Arrhenius plot displays considerable curvature, the temperature dependence is based only on the data below 300 K, i.e., the studies of Smith and Zellner [1339] and Diau et al. [427], and the A-factor has been selected to fit the recommended room temperature value. (Table: 92-20, Note: 92-20) [Back to Table](#)
- C12. $\text{HO}_2 + \text{NO}$. The recommendation for $\text{HO}_2 + \text{NO}$ is based on the average of eight measurements of the rate constant at room temperature and below: Howard and Evenson [676], Leu [896], Howard [673], Hack et al. [599], Jemi-Alade and Thrush [730], Seeley et al. [1286] Bohn and Zetsch [174] and Bardwell et al. [85]. All of these are in quite good agreement. The results of Imamura and Washida [711] were not considered due to the relatively large uncertainty limits reported in this study. An earlier study, Burrows et al. [224] has been disregarded because of an error in the reference rate constant, $k(\text{OH} + \text{H}_2\text{O}_2)$. The room temperature study of Rozenshtein et al. [1245] has also been disregarded due to an inadequate treatment of possible secondary reactions. The data of Glaschick-Schimpf et al. [558] were not considered because of complications associated with the HO_2 detection method. The data of Thrush and Wilkinson [1441] were not considered because it is a relative rate study. The recommended Arrhenius parameters are obtained from a fit to all the data. The recommended value of $k(298 \text{ K})$ is obtained from the Arrhenius line. (Table: 10-6, Note: 10-6, Evaluated: 10-6) [Back to Table](#)
- C13. $\text{NO}_2^* + \text{H}_2\text{O}$. The reaction of NO_2 with H_2O to produce OH and HONO is endothermic by about 40 kcal mole⁻¹ (ground state reactants and products). However, absorption of light by NO_2 at wavelengths less than 718 nm can exceed the thermodynamic threshold if all the NO_2 internal energy is available for reaction. Crowley and Carl [374] photolyzed $\text{NO}_2/\text{H}_2\text{O}$ mixtures in the 430-450 nm spectral region and observed an OH action spectrum that mimicked the absorption features of NO_2 . Because the dependence of the OH signal on photolysis laser energy was second order, they suggested that two-photon absorption of NO_2 produced $\text{O}(^1\text{D})$ in their experiment which reacted with water vapor to produce OH. The energetic threshold for $\text{O}(^1\text{D})$ production is 488 nm. When they performed the same experiment with 532 nm photolysis, no OH production was observed giving an upper limit for the OH branching fraction (reactive vs. unreactive quenching) of 7×10^{-5} . Li et al. [904] carried out laser pump/probe experiments at photolysis wavelengths between 560 and 640 nm in $\text{NO}_2/\text{H}_2\text{O}$ mixtures. In contrast to Crowley and Carl, they found significant OH production in this wavelength range. Their experiments showed a unity slope dependence of OH production on laser energy, suggesting a one-photon process. Overtone pumping was used to check for the presence of HONO and HNO_3 , which might be the source of the observed OH radicals. The rate constant for the $\text{NO}_2^* + \text{H}_2\text{O}$ reaction was determined to be $1.7 \times 10^{-13} \text{ cm}^3 \text{ molecule}^{-1} \text{ s}^{-1}$ for NO_2 excitation at 565, 590 and 612.5 nm with an overall uncertainty of $\pm 50\%$. This is large enough to have a significant impact on HO_x production in the troposphere. Carr et al. [260] performed a laser pump/probe experiment at 567.5 and 563.5 nm in $\text{NO}_2/\text{H}_2\text{O}$ mixtures. These experiments failed to detect OH formation, resulting in an upper limit of 6×10^{-5} for the reactive branching fraction.
- Although this reaction is potentially important, in view of the disagreement in the published results, the Panel makes no recommendation on this reaction until additional credible studies are carried out. (Table: 10-6, Note: 10-6, Evaluated: 10-6) [Back to Table](#)
- C14. $\text{HO}_2 + \text{NO}_2$. Tyndall et al. [1490] obtained an upper limit to the rate coefficient of $5 \times 10^{-16} \text{ cm}^3 \text{ molecule}^{-1} \text{ s}^{-1}$ based on static photolysis experiments with FTIR analysis at 296 K and 760 torr of N_2 . (Table: 97-4, Note: 97-4) [Back to Table](#)
- C15. $\text{HO}_2 + \text{NO}_3$. The recommendation for k_{298} is based on a weighted average of the data of Hall et al. [604], Mellouki et al. [1001], Becker et al. [119] and Mellouki et al. [1004]. There are insufficient

data on which to base the temperature dependence of the rate coefficient. The measured branching ratios for the $\text{OH} + \text{NO}_2 + \text{O}_2$ channel range from 0.57 to 1.0. The most direct measurement is derived from the study of Mellouki et al. [1004], which obtained a value of $1.0 \pm 0.0/-0.3$ at 298 K. (Table: 94-26, Note: 94-26) [Back to Table](#)

- C16. $\text{HO}_2 + \text{NH}_2$. There is a fairly good agreement on the value of k at 298 K between the direct study of Kurasawa and Lesclaux [831] and the relative studies of Cheskis and Sarkisov [295] and Pagsberg et al. [1138]. The recommended value is the average of the values reported in these three studies. The identity of the products is not known; however, Kurasawa and Lesclaux suggest that the most probable reaction channels give either $\text{NH}_3 + \text{O}_2$ or $\text{HNO} + \text{H}_2\text{O}$ as products. (Table: 83-62, Note: 83-62) [Back to Table](#)
- C17. $\text{N} + \text{O}_2$. The recommended expression is derived from a least squares fit to the data of Kistiakowsky and Volpi [793], Wilson [1620], Becker et al. [121], Westenberg et al. [1604], Clark and Wayne [310], Winkler et al. [1637] and Barnett et al. [100]. $k(298 \text{ K})$ is derived from the Arrhenius expression and is in excellent agreement with the average of all of the room temperature determinations. (Table: 90-1, Note: 90-1) [Back to Table](#)
- C18. $\text{N} + \text{O}_3$. The recommendation is based on the results of Barnett et al. [100]. The value of $(1.0 \pm 0.2) \times 10^{-16} \text{ cm}^3 \text{ molecule}^{-1} \text{ s}^{-1}$ reported by Barnett et al. should probably be considered an upper limit rather than a determination. The low values reported by Barnett et al., Stief et al. [1373] and Garvin and Broida [536] cast doubt on the much faster rates reported by Phillips and Schiff [1164], and Chen and Taylor [291]. (Table: 90-1, Note: 90-1) [Back to Table](#)
- C19. $\text{N} + \text{NO}$. The recommended temperature dependence is based on the discharge flow-resonance fluorescence studies of Wennberg and Anderson [1594], and the discharge flow-resonance fluorescence and flash photolysis-resonance fluorescence studies of Lee et al. [868]. There is relatively poor agreement between these studies and the results of Clyne and McDermid [326], Kistiakowsky and Volpi [794], Herron [639], Phillips and Schiff [1164], Lin et al. [917], Ishikawa et al. [716], Sugawara et al. [1392], Cheah and Clyne [277], Husain and Slater [699], Clyne and Ono [333], Brunning and Clyne [204] and Jeoung et al. [743]. (Table: 94-26, Note: 94-26) [Back to Table](#)
- C20. $\text{N} + \text{NO}_2$. The recommendation for k_{298} is from the discharge flow-resonance fluorescence study of Wennberg and Anderson [1594]. The latter study had significantly better sensitivity for $\text{N}(^4\text{S})$ than the discharge flow-resonance fluorescence study of Clyne and Ono [333], which obtained a value about four times smaller. The results of Husain and Slater [699] and Clyne and McDermid [326] are not considered. The temperature dependence is obtained from the study of Wennberg and Anderson. In the latter study, atomic oxygen was shown to be the principal reaction product, in agreement with Clyne and McDermid. A recent study by Iwata et al. [717] suggested an upper limit of $3.3 \times 10^{-13} \text{ cm}^3 \text{ molecule}^{-1} \text{ s}^{-1}$ for the corresponding reaction involving $\text{N}(^2\text{D})$ and $\text{N}(^2\text{P})$ atoms (sum of all reaction channels). (Table: 94-26, Note: 94-26) [Back to Table](#)
- C21. $\text{NO} + \text{O}_3$. The recommended values are based on the results of studies over a range of temperatures by Birks et al. [164], Lippmann et al. [922], Ray and Watson [1222], Michael et al. [1009], Borders and Birks [178] and Moonen et al. [1028] and the room temperature studies of Stedman and Niki [1359] and Bemand et al. [144]. The six temperature-dependent studies were given equal weighting in the recommendation by averaging over the E/R 's from each individual data set. Following the Moonen et al. recommendation, the 200-K data point from their study has been excluded from the fit. All of the temperature dependence studies show some curvature in the Arrhenius plot at temperatures below 298 K. Increasing scatter between the data sets is evident at the lower temperatures. Clough and Thrush [314], Birks et al., Schurath et al. [1279], and Michael et al. have reported individual Arrhenius parameters for the two primary reaction channels producing ground and excited molecular oxygen. (Table: 00-3, Note: 00-3) [Back to Table](#)
- C22. $\text{NO} + \text{NO}_3$. The recommendation is based on the studies of Hammer et al. [608], Sander and Kircher [1252] and Tyndall et al. [1491], which are in excellent agreement. (Table: 92-20, Note: 92-20) [Back to Table](#)

- C23. $\text{NO}_2 + \text{O}_3$. The recommended expression is derived from a least squares fit to the data of Davis et al. [399], Graham and Johnston [572], Huie and Herron [691], and Cox and Coker [355]. The data of Verhees and Adema [1515] and Stedman and Niki [1359] were not considered because of systematic discrepancies with the other studies. (Table: 90-1, Note: 90-1) [Back to Table](#)
- C24. $\text{NO}_2 + \text{NO}_3$. The existence of the reaction channel forming $\text{NO} + \text{NO}_2 + \text{O}_2$ has not been firmly established. However, studies of N_2O_5 thermal decomposition that monitor NO_2 (Daniels and Johnston [385]; Johnston and Tao [748]; Cantrell et al. [253]) and NO (Hjorth et al. [656], and Cantrell et al. [256]) require reaction(s) that decompose NO_3 into $\text{NO} + \text{O}_2$. The rate constant from the first three studies is obtained from the product kK_{eq} , where K_{eq} is the equilibrium constant for $\text{NO}_2 + \text{NO}_3 \rightarrow \text{N}_2\text{O}_5$, while for the latter two studies the rate constant is obtained from the ratio $k/k(\text{NO} + \text{NO}_3)$, where $k(\text{NO} + \text{NO}_3)$ is the rate constant for the reaction $\text{NO} + \text{NO}_3 \rightarrow 2\text{NO}_2$. Using K_{eq} and $k(\text{NO} + \text{NO}_3)$ from this evaluation, the rate expression that best fits the data from all five studies is $4.5 \times 10^{-14} \exp(-1260/T) \text{ cm}^3 \text{ molecule}^{-1} \text{ s}^{-1}$ with an overall uncertainty factor of 2. (Table: 92-20, Note: 92-20) [Back to Table](#)
- C25. $\text{NO}_3 + \text{NO}_3$. The recommendation for $k(298 \text{ K})$ is from the studies of Graham and Johnston [573] and Biggs et al. [158]. The temperature dependence is from Graham and Johnston. (Table: 94-26, Note: 94-26) [Back to Table](#)
- C26. $\text{NH}_2 + \text{O}_2$. This reaction has several product channels which are energetically possible, including $\text{NO} + \text{H}_2\text{O}$ and $\text{HNO} + \text{OH}$. With the exception of the studies of Hack et al. [595] and Jayanty et al. [726] and several studies at high temperature, there is no evidence for a reaction. The following upper limits have been measured ($\text{cm}^3 \text{ molecule}^{-1} \text{ s}^{-1}$): 3×10^{-18} (Lesclaux and Demissy [882]), 8×10^{-15} (Pagsberg et al. [1138]), 1.5×10^{-17} (Cheskis and Sarkisov [295]), 3×10^{-18} (Lozovsky et al. [941]), 1×10^{-17} (Patrick and Golden [1148]) and 7.7×10^{-18} (Michael et al. [1011]) and 6×10^{-21} (Tyndall et al. [1493]). The recommendation is based on the study of Tyndall et al., which was sensitive to reaction paths leading to the products NO , NO_2 and N_2O . The reaction forming NH_2O_2 cannot be ruled out, but is apparently not important in the atmosphere. (Table: 92-20, Note: 92-20) [Back to Table](#)
- C27. $\text{NH}_2 + \text{O}_3$. There is poor agreement among the recent studies of Cheskis et al. [294], $k(298) = 1.5 \times 10^{-13} \text{ cm}^3 \text{ s}^{-1}$, Patrick and Golden [1148], $k(298 \text{ K}) = 3.25 \times 10^{-13} \text{ cm}^3 \text{ s}^{-1}$, Hack et al. [594], $1.84 \times 10^{-13} \text{ cm}^3 \text{ s}^{-1}$, Bulatov et al. [214], $1.2 \times 10^{-13} \text{ cm}^3 \text{ s}^{-1}$, and Kurasawa and Lesclaux [832], $0.63 \times 10^{-13} \text{ cm}^3 \text{ s}^{-1}$. The very low value of Kurasawa and Lesclaux may be due to regeneration of NH_2 from secondary reactions (see Patrick and Golden), and it is disregarded here. The discharge flow value of Hack et al. is nearly a factor of two less than the recent Patrick and Golden flash photolysis value. The large discrepancy between Bulatov et al. and Patrick and Golden eludes explanation. The recommendation is the $k(298 \text{ K})$ average of these four studies, and E/R is an average of Patrick and Golden (1151 K) with Hack et al. (710 K). (Table: 90-1, Note: 90-1) [Back to Table](#)
- C28. $\text{NH}_2 + \text{NO}$. The recommended value for k at 298 K is the average of the values reported by Lesclaux et al. [884], Hancock et al. [609], Sarkisov et al. [1260], Stief et al. [1371], Andresen et al. [35], Whyte and Phillips [1605], Dreier and Wolfrum [457], Atakan et al. [44], Wolf et al. [1638], Diau et al. [428] and Imamura and Washida [711]. The results of Gordon et al. [569], Gehring et al. [540], Hack et al. [601] and Silver and Kolb [1303] were not considered because they lie at least 2 standard deviations from the average of the previous group. The results tend to separate into two groups. The flash photolysis results average $1.8 \times 10^{-11} \text{ cm}^3 \text{ molecule}^{-1} \text{ s}^{-1}$ (except for the pulse radiolysis study of Gordon et al.), while those obtained using the discharge flow technique average $0.9 \times 10^{-11} \text{ cm}^3 \text{ molecule}^{-1} \text{ s}^{-1}$. The apparent discrepancy cannot be due simply to a pressure effect as the pressure ranges of the flash photolysis and discharge flow studies overlapped and none of the studies observed a pressure dependence for k . Whyte and Phillips have suggested that the difference may be due to decomposition of the adduct NH_2NO , which occurs on the timescale of the flow experiments, but not the flash experiments. There have been many studies of the temperature dependence but most have investigated the regime of interest to combustion and only two have gone below room temperature (Hack et al. from 209–505 K and Stief et al. from 216–480 K. Each study reported k to decrease with increasing temperature. The recommended temperature dependence is taken from a fit to the Stief et al. data at room temperature and below. The reaction proceeds along a complex potential energy surface, which results in product branching ratios that are strongly dependent on

temperature. *Ab initio* calculations by Walch [1535] show the existence of four saddle points in the potential surface leading to $\text{N}_2 + \text{H}_2\text{O}$ without a reaction barrier. Elimination to form $\text{OH} + \text{HN}_2$ can occur at any point along the surface. While results from early studies on the branching ratio for OH formation differ significantly, the most recent studies (Hall et al., Dolson [447], Silver and Kolb [1306], Atakan et al., Stephens et al. [1362], Park and Lin [1145]) agree on a value around 0.1 at 300 K, with $\text{N}_2 + \text{H}_2\text{O}$ making up the balance. (Table: 97-4, Note: 97-4) [Back to Table](#)

- C29. $\text{NH}_2 + \text{NO}_2$. There have been four studies of this reaction (Hack et al. [601]; Kurasawa and Lesclaux [830]; Whyte and Phillips [1605]; and Xiang et al. [1649]). There is very poor agreement among these studies both for k at 298 K (factor of 2.3) and for the temperature dependence of k ($T^{3.0}$ and $T^{-1.3}$). The recommended values of k at 298 K and the temperature dependence of k are averages of the results reported in these four studies. Hack et al. have shown that the predominant reaction channel (>95%) produces $\text{N}_2\text{O} + \text{H}_2\text{O}$. Just as for the $\text{NH}_2 + \text{NO}$ reaction, the data for this reaction seem to indicate a factor of two discrepancy between flow and flash techniques, although the data base is much smaller. (Table: 85-37, Note: 87-41) [Back to Table](#)
- C30. $\text{NH} + \text{NO}$. The recommendation is derived from the room temperature results of Hansen et al. [612], Cox et al. [350] and Harrison et al. [616]. The temperature dependence is from Harrison et al. (Table: 92-20, Note: 92-20) [Back to Table](#)
- C31. $\text{NH} + \text{NO}_2$. The recommendation is derived from the temperature-dependence study of Harrison et al. [616]. (Table: 92-20, Note: 92-20) [Back to Table](#)
- C32. $\text{O}_3 + \text{HNO}_2$. Based on Kaiser and Japar [757] and Streit et al. [1377]. (Table: 82-57, Note: 82-57) [Back to Table](#)
- C33. $\text{N}_2\text{O}_5 + \text{H}_2\text{O}$. The recommended value at 298 K is based on the studies of Tuazon et al. [1467], Atkinson et al. [65] and Hjorth et al. [657]. Sverdrup et al. [1397] obtained an upper limit that is a factor of four smaller than that obtained in the other studies, but the higher upper limit is recommended because of the difficulty of distinguishing between homogeneous and heterogeneous processes in the experiment. See the heterogeneous chemistry section of this evaluation for additional rate data for this reaction. (Table: 85-37, Note: 90-1) [Back to Table](#)
- C34. $\text{N}_2(\text{A},v) + \text{O}_2$. Rate constants for the overall reaction for the $v=0, 1$ and 2 vibrational levels of $\text{N}_2(\text{A})$ have been made by Dreyer et al. [458], Zipf [1693], Piper et al. [1168], Iannuzzi and Kaufman [708], Thomas and Kaufman [1432] and De Sousa et al. [405]. The results of these studies are in relatively good agreement. The recommended values are (2.5 ± 0.4) , (4.0 ± 0.6) and $(4.5 \pm 0.6) (\times 10^{-12} \text{ cm}^3 \text{ molecule}^{-1} \text{ s}^{-1})$, from the work of De Sousa et al. The only temperature dependence data are from De Sousa et al., who obtained $k(T,v)=k(v,298\text{K})(T/300)^{0.55}$ for $v=0,1,2$. The observation of high N_2O production initially reported by Zipf [1693] has not been reproduced by other groups, and the branching ratio for this channel is probably less than 0.02 (Iannuzzi et al. [707], Black et al. [167], De Sousa et al. [405], Fraser and Piper [519]). The branching ratios for the other channels are poorly established, although there is strong evidence for the formation of both $\text{O}(^3\text{P})$ and $\text{O}_2(\text{B}^3\Sigma_u^-)$. (Table: 94-26, Note: 94-26) [Back to Table](#)
- C35. $\text{N}_2(\text{A},v) + \text{O}_3$. The only study is that of Bohmer and Hack [173], who obtained 298 K rate constants of 4.1 ± 1.0 , 4.1 ± 1.2 , 8.0 ± 2.3 , and $10 \pm 3.0 (\times 10^{-11} \text{ cm}^3 \text{ molecule}^{-1} \text{ s}^{-1})$ for the $v=0-3$ vibrational levels of $\text{N}_2(\text{A})$, respectively. This study determined that the NO channel accounts for about 20% of the reaction products. (Table: 94-26, Note: 94-26) [Back to Table](#)
- D1. $\text{O} + \text{CH}_3$. The recommended $k(298 \text{ K})$ is the weighted average of three measurements by Washida and Bayes [1584], Washida [1581], and Plumb and Ryan [1174]. The E/R value is based on the results of Washida and Bayes [1584], who found k to be independent of temperature between 259 and 341 K. (Table: 83-62, Note: 83-62) [Back to Table](#)
- D2. $\text{O} + \text{HCN}$. Because it is a very slow reaction, there are no studies of this reaction below 450 K. Davies and Thrush [394] studied this reaction between 469 and 574 K while Perry and Melius [1160] studied it between 540 and 900 K. Results of Perry and Melius are in agreement with those of Davies and Thrush. Our recommendation is based on these two studies. The higher-temperature ($T > 1000 \text{ K}$) combustion-related studies of Roth et al. [1242], Szekely et al. [1398], and Louge and Hanson [934] have not been considered. This reaction has two reaction pathways: $\text{O} + \text{HCN} \rightarrow \text{H} +$

NCO, $\Delta H = -2$ kcal/mol (k_a); and $O + HCN \rightarrow CO + NH$ (k_b), $\Delta H = -36$ kcal/mol. The branching ratio k_a/k_b for these two channels has been measured to be ~ 2 at $T = 860$ K. The branching ratio at lower temperatures, which is likely to vary significantly with temperature, is unknown. (Table: 87-41, Note: 92-20) [Back to Table](#)

- D3. $O + C_2H_2$. The value at 298 K is an average of ten measurements (Arrington et al. [40], Sullivan and Warneck [1396], Brown and Thrush [199], Hoyer mann et al. [679, 680], Westenberg and deHaas [1596], James and Glass [722], Stuhl and Niki [1384], Westenberg and deHaas [1601], and Aleksandrov et al. [23]). There is reasonably good agreement among these studies. Arrington et al. [40] did not observe a temperature dependence, an observation that was later shown to be erroneous by Westenberg and deHaas [1596]. Westenberg and deHaas [1596], Hoyer mann et al. [680] and Aleksandrov et al. [23] are the only authors who have measured the temperature dependence below 500 K. Westenberg and deHaas observed a curved Arrhenius plot at temperatures higher than 450 K. In the range 194–450 K, Arrhenius behavior provides an adequate description and the E/R obtained by a fit of the data from these three groups in this temperature range is recommended. The A-factor was calculated to reproduce $k(298\text{ K})$. This reaction can have two sets of products, i.e., $C_2HO + H$ or $CH_2 + CO$. Under molecular beam conditions C_2HO has been shown to be the major product. The study by Aleksandrov et al. using a discharge flow-resonance fluorescence method (under undefined pressure conditions) indicates that the $C_2HO + H$ channel contributes no more than 7% to the net reaction at 298 K, while a similar study by Vinckier et al. [1522] suggests that both CH_2 and C_2HO are formed. (Table: 82-57, Note: 82-57) [Back to Table](#)
- D4. $O + H_2CO$. The recommended values for A, E/R and $k(298\text{ K})$ are the averages of those determined by Klemm [802] (250 to 498 K) using flash photolysis-resonance fluorescence, by Klemm et al. [803] (298 to 748 K) using discharge flow-resonance fluorescence, and Chang and Barker [269] (296 to 436 K) using discharge flow-mass spectrometry techniques. All three studies are in good agreement. The $k(298\text{ K})$ value is also consistent with the results of Niki et al. [1085], Herron and Penzhorn [641], and Mack and Thrush [945]. Although the mechanism for $O + H_2CO$ has been considered to be the abstraction reaction yielding $OH + HCO$, Chang and Barker suggest that an additional channel yielding $H + HCO_2$ may be occurring to the extent of 30% of the total reaction. This conclusion is based on an observation of CO_2 as a product of the reaction under conditions where reactions such as $O + HCO \rightarrow H + CO_2$ and $O + HCO \rightarrow OH + CO$ apparently do not occur. This interesting suggestion needs independent confirmation. (Table: 82-57, Note: 82-57) [Back to Table](#)
- D5. $O + CH_3CHO$. The recommended $k(298\text{ K})$ is the average of three measurements by Cadle and Powers [237], Mack and Thrush [946], and Singleton et al. [1319], which are in good agreement. Cadle and Powers and Singleton et al. studied this reaction as a function of temperature between 298 and 475 K and obtained very similar Arrhenius parameters. The recommended E/R value was obtained by considering both sets of data. This reaction is known to proceed via H-atom abstraction (Mack and Thrush [946], Avery and Cvetanovic [67], and Singleton et al. [1319]). (Table: 87-41, Note: 87-41) [Back to Table](#)
- D6. $O_2 + HOCO$. HOCO is produced by the association of OH with CO (See Table 2). The rate coefficient for the reaction of O_2 with HOCO has been measured by Petty et al. [1162] and Nolte et al. [1102] and the recommendation is based on these measurements. There are no reports on the temperature dependence of this reaction; however, the value at 298 K would be appropriate for all atmospheric conditions. The products of this reaction are HO_2 , as shown by Nolte et al., and CO_2 , as seen in numerous previous studies where it has been known to be the product of the reaction of OH with CO in air. (Table: 06-2, Note: 06-2) [Back to Table](#)
- D7. $O_3 + C_2H_2$. The database for this reaction is not well established. Room temperature measurements (Cadle and Schadt [238]; DeMore [406]; DeMore [407]; Stedman and Niki [1358]; Pate et al. [1147]; and Atkinson and Aschmann [46]) disagree by as much as an order of magnitude. It is probable that secondary reactions involving destruction of ozone by radical products resulted in erroneously high values for the rate constants in several of the previous measurements. The present recommendation for $k(298\text{ K})$ is based on the room temperature value of Atkinson and Aschmann [46], which is the lowest value obtained and therefore perhaps the most accurate. The temperature dependence is estimated, based on an assumed A-factor of $10^{-14}\text{ cm}^3\text{ molecule}^{-1}\text{ s}^{-1}$ similar to that for

the $\text{O}_3 + \text{C}_2\text{H}_4$ reaction and corresponding to the expected five-membered ring structure for the transition state (DeMore [406, 407]). Further studies, particularly of the temperature dependence, are needed. Major products in the gas phase reaction are CO, CO_2 , and HCOOH , and chemically-activated formic anhydride has been proposed as an intermediate of the reaction (DeMore [407], and DeMore and Lin [419]). The anhydride intermediates in several alkyne ozonations have been isolated in low temperature solvent experiments (DeMore and Lin [419]). (Table: 90-1, Note: 90-1) [Back to Table](#)

- D8. $\text{O}_3 + \text{C}_2\text{H}_4$. The rate constant of this reaction is well established over a large temperature range, 178 to 360 K. The present recommendation is based on the data of DeMore [406], Stedman et al. [1360], Herron and Huie [640], Japar et al. [723, 724], Toby et al. [1447], Su et al. [1390], Adeniji et al. [11], Kan et al. [764], Atkinson et al. [53], and Bahta et al. [78]. (Table: 90-1, Note: 90-1) [Back to Table](#)
- D9. $\text{O}_3 + \text{C}_3\text{H}_6$. The rate constant of this reaction is well established over the temperature range 185 to 360 K. The present recommendation is based largely on the data of Herron and Huie [640], in the temperature range 235–362 K. (Note that a typographical error in Table 2 of that paper improperly lists the lowest temperature as 250 K, rather than the correct value, 235 K.) The recommended Arrhenius expression agrees within 25% with the low temperature (185–195 K) data of DeMore [406], and is consistent with, but slightly higher (about 10%) than the data of Treacy et al. [1460] and slightly lower (about 40%) than the data of Adeniji et al. [11] in the temperature range 260–294 K. Room temperature measurements of Cox and Penkett [365], Stedman et al. [1360], Japar et al. [723, 724], and Atkinson et al. [53] and Neeb and Moorgat [1047] are in good agreement (10% or better) with the recommendation. (Table: 06-2, Note: 06-2) [Back to Table](#)
- D10. $\text{O}_3 + \text{CH}_2=\text{C}(\text{CH}_3)\text{CH}=\text{CH}_2 \rightarrow \text{products}$. The recommendation is based on an unweighted fit to the temperature-dependent rate constants reported by Khamaganov & Hites [789] and Avzianova & Ariya [70], as well as the ambient temperature rate constants reported by Greene & Atkinson [579], Grosjean et al. [587], Grosjean & Grosjean [588], Neeb & Moortgat [1047], Klawatsch-Carrasco et al. [798], and Karl et al. [768]. In all of the above studies, measures were taken to prevent secondary consumption of reactants by OH radicals, which are known to be generated in ozone + alkene reactions. Results from early studies by Adeniji et al. [11], Atkinson et al. [51], and Treacy et al. [1460], while in reasonable agreement with other studies, are not used to arrive at the recommendation because OH radicals were not scavenged in those studies. Donahue et al. [454] have directly detected OH as a product of the O_3 + isoprene reaction, and OH yields have been reported in a number of studies where OH production was monitored indirectly by following the loss of an OH scavenger or the production of a product of an OH + scavenger reaction [51, 591, 592, 900, 1047, 1149, 1231]. At room temperature and atmospheric pressure of air, reported OH yields from seemingly careful studies range from 0.19 to 0.53 with an average value of 0.32. (Table: 10-6, Note: 10-6, Evaluated 10-6) [Back to Table](#)
- D11. $\text{OH} + \text{CO}$. See note for the $\text{OH} + \text{CO}$ reaction in Section 2. [Back to Table](#)
- D12. $\text{OH} + \text{CH}_4$. This reaction has been extensively studied. The most recent data are from Vaghjiani and Ravishankara [1506], Saunders et al. [1264], Finlayson-Pitts et al. [507], Dunlop and Tully [468], Mellouki et al. [1007], and Gierczak et al. [549], who measured the absolute rate coefficients for this reaction using discharge flow and pulsed photolysis techniques. Sharkey and Smith [1297] have reported a high value ($7.7 \times 10^{-15} \text{ cm}^3 \text{ molecule}^{-1} \text{ s}^{-1}$) for $k(298 \text{ K})$, and this value has not been considered here. The current recommendation for $k(298 \text{ K})$ was derived from the results of Vaghjiani and Ravishankara, Dunlop and Tully, Saunders et al., Mellouki et al., Finlayson-Pitts et al., and Gierczak et al. The temperature dependence of this rate coefficient has been measured by Vaghjiani and Ravishankara (223–420 K), Dunlop and Tully (above 298 K), Finlayson-Pitts et al. (278–378 K), and Mellouki et al. (233–343 K). Gierczak et al. have extended the measurements of k to 195 K, and it appears that the rate coefficient does not strictly follow an Arrhenius expression. The recommended E/R was obtained from these results using data below 300 K.

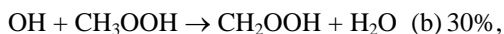
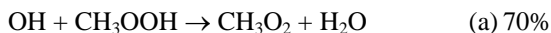
A more accurate representation of the rate constant as a function of temperature is obtained by using the three-parameter expression: $k = 2.80 \times 10^{-14} T^{0.667} \exp(-1575/T) \text{ cm}^3 \text{ molecule}^{-1} \text{ s}^{-1}$. This three-parameter fit may be preferred for lower stratosphere and upper troposphere calculations. A report

on this rate coefficient by Bonard et al. [175] agrees very well with the value recommended here. (Table: 97-4, Note: 06-2) [Back to Table](#)

- D13. $\text{OH} + {}^{13}\text{CH}_4$. This reaction has been studied relative to the $\text{OH} + \text{CH}_4$ reaction, since the ratio of the rate coefficients is the quantity needed for quantifying methane sources. Rust and Stevens [1246], Davidson et al. [389], and Cantrell et al. [257] have measured k_{12}/k_{13} at 298 K to be 1.003, 1.010, and 1.0055, respectively. Cantrell et al.'s data supersede the results of Davidson et al. The recommended value of 1.005 ± 0.002 is based on the results of Rust and Stevens and Cantrell et al. Cantrell et al. find k_{12}/k_{13} to be independent of temperature between 273 and 353 K. (Table: 92-20, Note: 92-20) [Back to Table](#)
- D14. $\text{OH} + \text{CH}_3\text{D}$. The rate coefficient for this reaction has been measured between 249 and 422 K using a pulsed laser photolysis-laser induced fluorescence system by Gierczak et al. [548]. The recommended values of $k(298\text{ K})$ and E/R are from this study. The recommendation agrees within about 10% at 298 K with the rate constant measured by DeMore [414] in a relative rate study over the temperature range 298–360 K. The difference, while small in an absolute sense, is nevertheless significant for the isotopic fractionation of atmospheric CH_3D and CH_4 by OH. An earlier result of Gordon and Mulac at 416 K [570] is in good agreement with the extrapolated data of both of these determinations. However, that measurement has not been explicitly included in this recommendation because the experiments were carried out at higher temperatures and therefore are less applicable to the atmosphere. The rate coefficients for the reactions of OH with other deuterated methanes have also been measured (Dunlop and Tully [468], Gierczak et al. [1418], Gordon and Mulac [570]). (Table: 94-26, Note: 94-26) [Back to Table](#)
- D15. $\text{OH} + \text{H}_2\text{CO}$. The value for $k(298\text{ K})$ is the average of those determined by Niki et al. [1094], Atkinson and Pitts [62], Stief et al. [1372], Yetter et al. [1658], Temps and Wagner [1429], and Sivakumaran et al. [1327]. The value reported by Morris and Niki [1031] is expected to be superseded by the later report of Niki et al. [1094], although it agrees within the stated uncertainty. There are two relative values that are not in agreement with the recommendations. The value of Niki et al. [1087] relative to the $\text{OH} + \text{C}_2\text{H}_4$ reaction is higher, while the value of Smith [1340] relative to the $\text{OH} + \text{OH}$ reaction is lower. The later report of Niki et al. [1094] is assumed to supersede the earlier rate constant. The rate coefficients reported by Zabarnick et al. [1663] at and above 298 K are consistently higher than those recommended here, but overlap within the combined uncertainty. The temperature dependence was calculated from the data of Stief et al. obtained below 298 K and from the data of Sivakumaran et al. below 330 K after normalizing the results of both studies to $k(298\text{ K})$ recommended here. There is a clear indication that the Arrhenius plot of this rate coefficient is curved with a positive activation energy at temperatures above ~330 K. It is therefore important that the recommended rate coefficients be used only in the 200-300 K temperature range. The abstraction reaction shown in the table is the major channel (Temps and Wagner [1429], Niki et al. [1093]); other channels may contribute to a small extent (Horowitz et al. [670]). There is no indication that this rate coefficient is pressure dependent at atmospheric pressures and temperatures. (Table: 06-2, Note: 06-2) [Back to Table](#)
- D16. $\text{OH} + \text{CH}_3\text{OH}$. The recommended value for $k(298\text{ K})$ is the average of direct studies by Overend and Paraskevopoulos [1133], Ravishankara and Davis [1204], Hagele et al. [603], Meier et al. [994], McCaulley et al. [985], Wallington and Kurylo [1557], Hess and Tully [644], Jimenez et al. [746], and Dillon et al. [431]. When these measurements were not at exactly 298 K, their values were recalculated for 298 K by using the E/R recommended here. Indirect measurements by Campbell et al. [244], Barnes et al. [89], Tuazon et al. [1468], Picquet et al. [1165], and Klopffer et al. [805] are in good agreement with the recommended value. The temperature dependence of k has been measured by Hagele et al., Meier et al., Greenhill and O'Grady, Wallington and Kurylo, Hess and Tully, Jimenez et al., and Crowley et al. The recommended value of E/R was calculated using the results obtained at temperature below 330 K by Wallington and Kurylo, Meier et al., Hess and Tully, Jimenez et al., and Crowley et al. The results of Greenhill and O'Grady are in reasonable agreement with the recommendation at and above 298 K, but are clearly lower than the recommendation below 298 K. Hess and Tully report a curved Arrhenius plot over the temperature range 298 – 1000 K, while Meier et al. do not observe such a curvature. This reaction has two pathways: abstraction of the H-atom from the methyl group to give $\text{CH}_2\text{OH} + \text{H}_2\text{O}$ or from the OH group to give $\text{CH}_3\text{O} +$

H₂O. The results of Hagele et al., Meier et al., and Hess and Tully suggest that H abstraction from the methyl group to give CH₂OH + H₂O is the dominant channel below room temperature. At 298 K, for example, the branching ratio for the formation of CH₂OH is about 0.85 and increases as the temperature decreases. In the Earth's atmosphere, the eventual products of OH + CH₃OH reaction are the same for both reaction channels: CH₂O and HO₂. (Table: 06-2, Note: 06-2) [Back to Table](#)

- D17. OH + CH₃OOH. The recommended value for k(298 K) is the average of the rate coefficients measured by Niki et al. [1092] and Vaghjiani and Ravishankara [1505], which differ by nearly a factor of two. Niki et al. measured the rate coefficient relative to that for OH with C₂H₄ ($= 8.0 \times 10^{-12} \text{ cm}^3 \text{ molecule}^{-1} \text{ s}^{-1}$) by monitoring CH₃OOH disappearance using an FTIR system. Vaghjiani and Ravishankara monitored the disappearance of OH, OD, and ¹⁸OH in excess CH₃OOH in a pulsed photolysis-LIF system. They measured k between 203 and 423 K and report a negative activation energy with E/R = -190 K; the recommended E/R is based on their results. The reaction of OH with CH₃OOH occurs via abstraction of H from the oxygen end to produce the CH₃OO radical and from the CH₃ group to produce the CH₂OOH radical, as originally proposed by Niki et al. and confirmed by Vaghjiani and Ravishankara. CH₂OOH is unstable and falls apart to CH₂O and OH within a few microseconds. The possible reaction of CH₂OOH with O₂ is unimportant under atmospheric conditions (Vaghjiani and Ravishankara). The recommended branching ratios are,



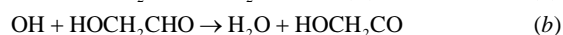
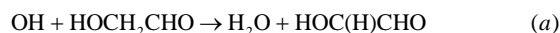
(from Vaghjiani and Ravishankara) and are nearly independent of temperature. (Table: 02-25, Note: 02-25) [Back to Table](#)

- D18. OH + HC(O)OH. The recommended value of k(298 K) is the average of those measured by Zetzsch and Stuhl [1678], Wine et al. [1621], Jolly et al. [749], Dagaut et al. [384], and Singleton et al. [1324]. The temperature dependence of k has been studied by Wine et al. and by Singleton et al., who observed k to be essentially independent of T.

Wine et al. found the rate coefficient for the OH + HC(O)OH reaction to be the same as that for OH + DC(O)OH reaction. Jolly et al. found the formic acid dimer to be unreactive toward OH, i.e., abstraction of the H atom attached to C was not the major pathway for the reaction. A comprehensive study of Singleton et al. showed that reactivity of HC(O)OH is essentially the same as that of DC(O)OH, but DC(O)OD reacts much slower than HC(O)OH and DC(O)OH. These observations show that the reaction proceeds via abstraction of the acidic H atom. Wine et al. and Jolly et al. also found that H atoms are produced in the reaction, which is consistent with the formation of HC(O)O, which would rapidly fall apart to CO₂ and H. End product studies are also consistent with the formation of CO₂ and H₂O in this reaction (Singleton et al. [1324]). The products of this reaction would be mostly HC(O)O and H₂O. The fate of HC(O)O in the atmosphere will be to give HO₂ either directly via reaction with O₂ or via thermal decomposition to H atom, which adds to O₂.

Wine et al. have suggested that, in the atmosphere, the formic acid could be hydrogen bonded to a water molecule and its reactivity with OH could be lowered because the hydrogen bonded water would obstruct the abstraction of the H atom. This suggestion needs to be checked. (Table: 02-25, Note: 02-25) [Back to Table](#)

- D19. OH + HC(O)C(O)H. The only available data are from the 298 K relative rate study of Plum et al. [1173] and the results are recommended here. Because the rate coefficient is so large, it is unlikely to have a substantial temperature dependence and an E/R of zero is recommended. This reaction is expected to proceed via H-abstraction to yield H₂O, CO and HCO. (Table: 06-2, Note: 06-2) [Back to Table](#)
- D20. OH + HOCH₂CHO. The available data are from relative rate studies at 298 K (Bacher et al. [74], Niki et al. [1095], and Mellouki et al. [951]). The recommendation is based on all these studies, which are in good agreement. Because the rate coefficient is very large, it is unlikely to have a substantial temperature dependence. Therefore, we recommend an E/R of zero. There are three possible sites for H-abstraction: the alcohol group, the CH₂ group and the carbonyl group. Of these, the likely pathways for abstraction are from the latter two sites:



Niki et al. have shown that the branching ratio for channel (b) is 0.8 and for channel (a) is 0.2. It is unlikely that the branching ratio changes significantly with temperature. (Table: 06-2, Note: 06-2) [Back to Table](#)

- D21. OH + HCN. This reaction is pressure dependent. The recommended value is the high pressure limit measured by Fritz et al. [526] using a laser photolysis-resonance fluorescence apparatus. Phillips [1163] studied this reaction using a discharge flow apparatus at low pressures and found the rate coefficient to have reached the high pressure limit at ~10 Torr at 298 K. Fritz et al.'s results contradict this finding. They agree with Phillip's measured value, within a factor of two, at 7 Torr, but they find k to increase further with pressure. The products of the reaction are unknown. (Table: 83-62, Note: 83-62) [Back to Table](#)
- D22. OH + C₂H₆. There are numerous studies of this reaction at 298 K (Greiner [581], Horne and Norrish [667], Greiner [583], Overend et al. [1134], Howard and Evenson [675], Leu [896], Lee and Tang [870], Tully et al. [1473], Jeong et al. [740], Smith et al. [1335], Baulch et al. [114], Schmidt et al. [1273], Edney et al. [475], Tully et al. [1471], Nielsen et al. [1080], Stachnik et al. [1355], Wallington et al. [1559], Bourmada et al. [186], Zabarnick et al. [1663], Abbatt et al. [2], Schiffman et al. [1268], Dobe et al. [440], Sharkey and Smith [1297], Finlayson-Pitts [507], Talukdar et al. [1421], Crowley et al. [373], Cavalli et al. [268], Donahue et al. [452], Clarke et al. [312], Heathfield et al. [624], and Li et al. [903]). The recommended value for k(298 K) is an average of the majority of the results reported at room temperature (Overend et al. [1134], Howard and Evenson [675], Leu [896], Lee and Tang [870], Tully et al. [1473], Smith et al. [1335], Baulch et al. [114], Schmidt et al. [1273], Tully et al. [1471], Stachnik et al. [1355], Wallington et al. [1559], Bourmada et al. [186], Zabarnick et al. [1663], Abbatt et al. [2], Schiffman et al. [1268], Dobe et al. [440], Finlayson-Pitts [507], Talukdar et al. [1421], Crowley et al. [373], Cavalli et al. [268], Donahue et al. [452], Clarke et al. [312], Heathfield et al. [624], and Li et al. [903]). The room temperature studies not used were either of lower precision (as evidenced by data scatter) or yielded somewhat higher rate constants. The temperature dependence of the rate coefficient below 298 K has been measured by Jeong et al. [740], Stachnik et al. [1355], Smith et al. [1335], Wallington et al. [1559], Talukdar et al. [1421], Crowley et al. [373], and Clarke et al. [312]. The last six of these studies are in good agreement (the data from Jeong et al. [740] exhibiting noticeable upward curvature below 298 K). Thus the recommended value for E/R is derived from a combined fit to the data below 300 K from the aforementioned six studies after each data set was normalized to the recommended value for k(298 K). (Table: 10-6, Note: 10-6, Evaluated: 10-6) [Back to Table](#)
- D23. OH + CH₃CHO. The recommended values for k(298 K) and E/R come from a combined fit to the data of Sivakumaran and Crowley [1326] and Zhu et al [1692] at T ≤ 300 K. There are 14 other studies of this reaction that provide the room temperature rate constant (Morris et al. [1033], Niki et al. [1087], Atkinson and Pitts [62], Kerr and Sheppard [775], Semmes et al. [1294], Michael et al. [1010], Dobe et al. [437], Balestra-Garcia et al. [81], Scollard et al. [1282], Tyndall et al. [1499], Taylor et al. [1426], D'Anna et al. [379], Wang et al. [1564], and Taylor et al. [1427]). The average value of k(298 K) from all of these studies is identical to that derived from the above fit. The study by Michael et al. [1010] also provided data down to 244 K. While these data are far more scattered than those from Sivakumaran and Crowley [1326] and Zhu et al [1692], they are encompassed by the 95% confidence limits of the recommendation. Measurements of H₂O formation yields were conducted by Wang et al. [1564], Butkovskaya et al. [230], and Vandenberk and Peeters [1510]. These investigators reported values of ~100%, (97.7 ± 4.7)%, and (89 ± 6)%, respectively at about room temperature. Butkovskaya et al. [230] report identical yields at both 298 K and 248 K. Tyndall et al. [1485] concluded that more than 90% of the reaction proceeds via H-atom abstraction based on no measurable detection of acetic acid formation. Cameron et al. [243] detected CH₃ and CH₃CO radicals and H-atoms. The major reaction pathway was determined to be CH₃CHO + OH → CH₃CO + H₂O with a measured yield of (93 ± 18)%. Butkovskaya et al. [230] detected CH₂CHO radicals to obtain a branching ratio for H-atom

abstraction from the CH₃ group of 5.1^{+2.4}_{-1.7}% . Vöhringer-Martinez et al. [1524] studied the effect of water vapor on the reaction rate constant at temperatures between 300 K and 60 K. They found little-to no effect at 300 K and enhancements approaching a factor of 2 at temperatures below 100 K. (Table: 10-6, Note: 10-6, Evaluated: 10-6) [Back to Table](#)

- D24. OH + C₂H₅OH. There are numerous studies of the reaction rate constant at room temperature (Campbell et al. [244], Overend and Paraskevopoulos [1133], Ravishankara and Davis [1204], Kerr and Stocker [776], Greenhill and O'Grady [580], Wallington and Kurylo [1557], Hess and Tully [643], Nelson et al. [1054], Picquet et al. [1165], Oh and Andino [1110], Sorensen et al. [1344], Jimenez et al. [746], Wu et al. [1646], Dillon et al. [431], Kovacs et al. [819], Rajakumar et al. [1198], Carr et al. [261], and Orkin et al. [1123]). The recommended k(298 K) is an average of the rate constants measured by Campbell et al. [244], Kerr and Stocker [776], Wallington and Kurylo [1557], Hess and Tully [643], Nelson et al. [1054], Sorensen et al. [1344], Jimenez et al. [746], Wu et al. [1646], Dillon et al. [431], Kovacs et al. [819], Rajakumar et al. [1198], and Orkin et al. [1123]. The room temperature studies not used were either of lower precision (as evidenced by data scatter) or yielded systematically higher or lower rate constants. Comprehensive studies of this reaction at sub-ambient temperatures were done by Jimenez et al. [746], Dillon et al. [431], and Orkin et al. [1123]. The last two studies resulted in indistinguishable rate constants at low temperatures and coincide with the recommended value of k(298 K). The analysis of the data at low temperatures suggests a temperature independent reaction rate constant between 210 K and 298 K.

This reaction has three possible product channels: (a) CH₃CH₂O + H₂O, (b) CH₃CHOH + H₂O, and (c) CH₂CH₂OH + H₂O. At room temperature, channel (b) is the major pathway accounting for (75% ± 15%) of the reaction (Meier et al. [995]) which is consistent with the thermochemistry of these three possible pathways. The branching ratio for channel (b) is expected to increase with decreasing temperature. (Table: 10-6, Note: 10-6, Evaluated: 10-6) [Back to Table](#)

- D25. OH + CH₃C(O)OH. The recommended values of k(298 K) and E/R are derived from a combined fit to the data of Singleton et al. [1323], Butkovskaya et al. [231], Crunaire et al. [375], Vimal and Stevens [1521], Khamaganov et al. [788], Huang et al. [688], and Huang et al. [687] at T ≤ 300 K. Data from these studies are in reasonable agreement below 300 K. However, above 300 K there is not a consistent picture of the temperature dependence of the rate constant with E/R values ranging from ~ -500 K to ~ -1000 K. In an earlier study by Dagaut et al. [384] at room temperature and above, an E/R value of +170 K was obtained. For this reason data from this study were not included in the combined fit, although k(298 K) from this study is in good agreement with recommended value. All studies required corrections for the presence of acetic acid dimer especially at temperatures below 298 K and they assumed no reactivity between OH and the dimer. This latter assumption is based on results from Singleton et al. [1323]. However, in the same study Singleton et al. [1323] found that the rate constant for the reaction of OH with the dimer of propionic acid is equal to or greater than that of the rate constant of OH with propionic acid monomer. This result suggests that uncertainties regarding the reactivity of acetic acid dimer may remain. Such uncertainties would propagate into uncertainties in the reactivity of the monomer, especially at lower temperatures.

Three studies give similar results for the reaction mechanism. Butkovskaya et al. [231] reported a yield of (64 ± 17)% over the temperature range of 300 - 249 K for H-atom abstraction from the carboxyl group, (OH + CH₃C(O)OH → CH₃ + CO₂ + H₂O). At room temperature, De Smedt et al. [1334] and Crunaire et al. [375] reported similar yields of (64 ± 14)% and (78 ± 13)%, respectively. Observations by Singleton et al. [1323] regarding the decrease in reactivity upon D substitution on the carboxylic site and no change in reactivity upon substitution on the methyl group, are reasonably consistent with these mechanistic studies. (Table: 10-6, Note: 10-6, Evaluated: 10-6) [Back to Table](#)

- D26. OH + C₃H₈. There are many measurements of the rate coefficients at 298 K. In this evaluation we have considered only the direct measurements (Greiner [583], Tully et al. [1473], Droege and Tully [459], Schmidt et al. [1273], Baulch et al. [114], Bradley et al. [189], Abbatt et al. [2], Schiffman et al. [1268], Talukdar et al. [1421], Mellouki et al. [1007], Donahue et al. [452], Clarke et al. [312] and Kozlov et al. [821]). The 298 K value is the average of these thirteen studies. Greiner, Tully et al. [1470], Droege and Tully, Talukdar et al., Mellouki et al., Donahue et al., Clarke et al. and

Kozlov et al. [821] have measured the temperature dependence of this reaction. Donahue and Clark [453] have shown that there is outstanding agreement between all of the data sets after correcting some of them for small offsets due to systematic calibration errors. Due to the significant curvature in the Arrhenius behavior over the studied temperature range, the recommended Arrhenius expression is only valid between 190 and 300 K. The recommended E/R is obtained from a composite fit to the four data sets (Kozlov et al., Clarke et al., Talukdar et al., and Mellouki et al.) at temperature below 300 K. Each data set was normalized to the recommended $k(298\text{ K})$. This reaction has two possible channels, i.e., abstraction of the primary and the secondary H-atom. Observations of both channels by Tully et al. and Droge and Tully indicate that the reaction exhibits non-Arrhenius behavior over a wide temperature range. The branching ratios were estimated from the latter study:

$$k_{\text{primary}} = 6.3 \times 10^{-12} \exp(-1050/T) \text{ cm}^3 \text{ molecule}^{-1} \text{ s}^{-1}$$

$$k_{\text{secondary}} = 6.3 \times 10^{-12} \exp(-580/T) \text{ cm}^3 \text{ molecule}^{-1} \text{ s}^{-1}$$

These numbers are in reasonable agreement with the older data of Greiner. The ratio of the rate coefficients for OH reactions with C_2H_6 and C_3H_8 has been measured by Finlayson-Pitts et al. [507] and DeMore and Bayes [417]. Our recommendations are in reasonable agreement with their ratios. (Table: 06-2, Note: 06-2) [Back to Table](#)

- D27. $\text{OH} + \text{C}_2\text{H}_5\text{CHO}$. The recommended value at 298 K is an average of the results from Niki et al. [1087], Audley et al. [66], Kerr and Sheppard [775], Semmes et al. [1294], Papagni [1141], Thevenet [1431], and D'Anna [379]. The temperature dependence has been measured by Thevenet. The E/R is taken from Thevenet and the A-factor is adjusted to reproduce $k(298\text{ K})$. Vandenberg and Peeters [1510] measured unity yields of H_2O from the reaction and conclude that the reaction proceeds exclusively by H-abstraction of the aldehydic H-atom. (Table: 06-2, Note: 06-2) [Back to Table](#)
- D28. $\text{OH} + 1\text{-C}_3\text{H}_7\text{OH}$. There have been a number of room temperature measurements that are in excellent agreement. The recommended value is an average of the results from absolute kinetics studies by Overend and Paraskevopoulos [1133], Wallington and Kurylo [1557], Nelson et al. [1054], and Yujing and Mellouki [1661]. Relative rate studies of Nelson et al., Oh and Andino [1109], Wu et al. [1646], and Cheema et al. [278] are in excellent agreement with the recommended value. The indirect study of Campbell [244] is consistent with, but 30% lower than the recommended value. The reaction is observed to be nearly temperature independent; Yujing and Mellouki find a slight positive temperature dependence while Cheema et al. find a small negative temperature dependence. The recommended E/R value is based on the direct study of Yujing and Mellouki. End product studies carried out by Azad and Andino [72] support predictions based on the structure-activity relationship that identify the primary reaction channels as hydrogen abstraction by the OH radical from the α (~75%) and β (~20%) carbons. (Table: 06-2, Note: 06-2) [Back to Table](#)
- D29. $\text{OH} + 2\text{-C}_3\text{H}_7\text{OH}$. The recommended value at 298 K is an average of the absolute measurements by Overend and Paraskevopoulos [1133], Wallington and Kurylo [1557], Nelson et al. [1054], Dunlop and Tully [467], and Yujing and Mellouki [1661]. A relative rate study by Lloyd et al. [929] is, within its wide error limits, consistent with the recommendation. The temperature dependence is observed to vary little with temperature below 400 K. Measurements over the range 293-745 K by Dunlop and Tully revealed a "bowl" shaped temperature dependence, with a minimum in the rate coefficient observed at 378 K. The recommended E/R is based on the measurements of Yujing and Mellouki and, on account of the complex reaction behavior, is valid only for temperatures below 400 K. Temperature dependent data of Dunlop and Tully and Wallington and Kurylo are, within the experimental uncertainties, consistent with the recommendation. By using isotopic substitution, Dunlop and Tully determined that the primary reaction channel below 400 K involves H atom abstraction by OH from the α -site. This result is in agreement with estimates based on the structure-activity relationship (Yujing and Mellouki [1661]). (Table: 06-2, Note: 06-2) [Back to Table](#)
- D30. $\text{OH} + \text{C}_2\text{H}_5\text{C(O)OH}$. Studies of this reaction have been confined to 298 K and above on account of the tendency of propionic acid to dimerize at lower temperatures and higher concentrations. Kinetic

isotope effects measured by Singleton et al. [1323] are consistent with a two channel mechanism proposed previously for OH reaction with acetic acid. In the propionic acid case, the channel involving direct abstraction of an alkyl hydrogen is predominant, thus accounting for the observed temperature independence of the rate constant. The recommended temperature independent rate constant, is based on an average of the results of Singleton et al. and Dagout et al. [384] taken at a variety of temperatures between 298 K and 446 K. An study room temperature measurement by Zetsch and Stuhl [1678] is ~30% higher, but consistent with the recommendation. Further studies below 298 K would be desirable in order to investigate possible non-Arrhenius behavior. (Table: 06-2, Note: 06-2) [Back to Table](#)

- D31. OH + CH₃C(O)CH₃. The rate coefficient for this reaction has been measured at temperatures close to 298 K by Cox et al. [362], Zetzsch [1677], Chiorboli et al. [300], Kerr and Stocker [776], Wallington and Kurylo [1558], LeCalve et al. [863], Wollenhaupt et al. [1639], Gierczak et al. [544] and Yamada et al. [1656]. Cox reported only an upper limit of $<5 \times 10^{-13}$ cm³ molecule⁻¹s⁻¹, which is consistent with this recommendation. The primary aim of Chiorboli et al. was to examine the atmospheric degradation of styrene, which produces acetone. They employed a relative rate measurement and reported a value of k(298 K) that is almost three times faster than the recommended value. Because of possible complications in their system, we have not included their results in arriving at the recommended value. Wallington and Kurylo, LeCalve et al., Wollenhaupt et al., Gierczak et al., and Yamada et al. have reported k as a function of temperature; all these studies directly measured the rate constant using the pulsed photolysis method where the temporal profile of OH was measured using resonance fluorescence or laser induced fluorescence. The extensive data of Wollenhaupt et al. and Gierczak et al. seem to show that this rate coefficient does not follow an Arrhenius expression. The results of LeCalve et al. and Wallington et al. are in general agreement with the results of Wollenhaupt et al. and Gierczak et al. The non-Arrhenius behavior was not evident in the results of Wallington et al. and LeCalve et al. because they measured the rate constant at a few temperatures and did not explore temperature below 240 K, where the curvature becomes increasingly evident. Yamada et al. measured k only above room temperature and their values are consistently lower than those of all the others noted above. As they noted in their paper, Yamada et al. did not measure the acetone concentration in the reactor and, thus, could have overestimated its concentration leading to consistently lower values of k. We have not included data of Yamada et al. (2003) in deriving the fit because of this possible systematic error and because they did not report k under atmospheric temperatures. The following recommendation reproduces all reported data, except that of Chiorboli et al. within the recommended uncertainty of 25% at all temperatures:

$$k(T) = 1.33 \times 10^{-13} + 3.82 \times 10^{-11} \exp(-2000/T) \text{ cm}^3 \text{ molecule}^{-1} \text{ s}^{-1}$$

This reaction can proceed via the abstraction of an H atom or via the formation of a complex that decomposes to give many different products, which include CH₃ + CH₃C(O)OH, CH₃OH + CH₃C(O), CH₄ + CH₃CO₂, and H₂O + CH₃C(O)CH₂. The branching ratios for the formation of different sets of products could vary with temperature. Wollenhaupt and Crowley (2000) have deduced that CH₃ radicals are produced with a yield of ~50% at 298 K and ~30% at 233 K. A similar branching ratio has also been reported by Vasvari et al. [1514]. The results of Gierczak et al. on the OH + CD₃C(O)CD₃ reaction, whose rate coefficient nearly obeys an Arrhenius expression between 240 and 400 K and is nearly an order of magnitude smaller than the non-deuterated analog at 250 K, suggest that H abstraction may be the dominant channel. Vandenberk et al. [1511], Tyndall et al. [1485], and Talukdar et al. [1419], clearly show that CH₃C(O)OH is a minor, if not negligible, product of this reaction and that the reaction proceeds to abstract an H atom. The results of Yamada et al. are consistent with this finding. Theoretical calculations of Henon et al. [634], and Vandenberk et al. [1511] also suggest that formation of acetic acid is negligible. We recommend that the products of this reaction be taken as H₂O and CH₃C(O)CH₂. (Table: 06-2, Note: 06-2) [Back to Table](#)

- D32. OH + CH₂=C(CH₃)CH=CH₂ → products. The recommendation is based on an un-weighted fit to the temperature-dependent rate constants reported by Kleindienst et al. [799], Chuong & Stevens [305], Campuzano-Jost et al. [245, 246], Gill & Hites [550], Park et al. [1144], Singh & Li [1316], and Hites & Turner [654] as well as the ambient temperature rate constants reported by Winer et al.

[1636] (based on data reported by Grimsrud et al. [586]), Cox et al. [362], Ohta [1112], Atkinson & Aschmann [47], Edney et al. [475], Stevens et al. [1364], McGivern et al. [987], Zhang et al. [1681], Iida et al. [710], and Karl et al. [768]. Only results obtained under (investigator-reported) high pressure limit conditions are considered. Data from the Laval nozzle study of Spangenberg et al. [1347] are not considered because the investigated T, P conditions are not relevant for application to atmospheric chemistry. Although the detailed pressure-dependence remains a subject of disagreement [305, 710, 768, 987, 1364], it is clear that the reaction is in its high pressure limit under all relevant atmospheric conditions. (Table: 10-6, Note: 10-6, Evaluated: 10-6) [Back to Table](#)

- D33. $\text{OH} + \text{CH}_3\text{CN}$. This rate coefficient has been measured as a function of temperature by Harris et al. [615] between 298 and 424 K, Kurylo and Knable [840] between 250 and 363 K, Rhasa [1229] between 295 and 520 K, and Hynes and Wine [703] between 256 and 388 K. In addition, the 298 K value has been measured by Poulet et al. [1180]. The 298 K results of Harris et al. are in disagreement with all other measurements and therefore have not been included. The recommended 298 K value is a weighted average of all other studies. The temperature dependence was computed using the results of Kurylo and Knable, the lower temperature values (i.e., 295–391 K) of Rhasa, and the data of Hynes and Wine. Three points are worth noting: (a) Rhasa observed a curved Arrhenius plot even in the temperature range of 295 to 520 K, and therefore extrapolation of the recommended expression could lead to large errors; (b) Hynes and Wine observed a pressure dependent increase of $k(298\text{ K})$ that levels off at about 1 atmosphere, and this observation is contradictory to the results of other investigations; (c) Hynes and Wine have carried out extensive pressure, temperature, O_2 concentration, and isotope variations in this reaction. Hynes and Wine postulate that the reaction proceeds via addition as well as abstraction pathways. They observe OH regeneration in the presence of O_2 . The recommended $k(298\text{ K})$ and E/R are applicable for only lower tropospheric conditions. Because of the unresolved questions of pressure dependence and reaction mechanism, the recommended value may not be applicable under upper tropospheric and stratospheric conditions. (Table: 92-20, Note: 92-20) [Back to Table](#)
- D34. $\text{OH} + \text{CH}_3\text{ONO}_2$. The rate coefficient for this reaction at 298 K has been measured by Kerr and Stocker [776], Nielsen et al. [1082], Gaffney et al. [529], Talukdar et al. [529], Kakesu et al. [762] and Shallcross et al. [1295]. The results of Kerr and Stocker and of Nielsen et al. are a factor of ten higher than those reported by the other groups. There are no obvious reasons for the reported differences but the lower values are preferred for a number of reasons. Firstly, Talukdar et al. have carried out a large number of checks which ruled out possible effects in their system due to the regeneration of OH via secondary reactions, to bath gas pressure, and to formation of an adduct that could undergo further reaction in the presence of oxygen. Secondly, the lower values are more consistent with reactivity predictions of Atkinson and Aschmann [50], who assumed that the series of nitrate reactions proceed by H-atom abstraction pathways. Kinetic measurements of Talukdar et al. performed with isotopically substituted hydroxyl radical (OH, ^{18}OH , and OD) and methyl nitrate (CH_3ONO_2 and CD_3ONO_2) are consistent with this reaction proceeding via an H-atom abstraction pathway. Accordingly, the recommended value of $k(298\text{ K})$ is based on an average of the values given by Gaffney et al., Talukdar et al., Kakesu et al. and Shallcross et al. Further verification of the reaction mechanism by identification of the products of the reaction is needed. The temperature dependence of the rate coefficient has been measured by Nielsen et al., Talukdar et al., and Shallcross et al. While Nielsen et al. report a negative activation energy, Talukdar et al. and Shallcross et al. report positive values. For the reasons given above, the temperature dependence recommended here is based on an average of Talukdar et al. and Shallcross et al. (Table: 06-2, Note: 06-2) [Back to Table](#)
- D35. $\text{OH} + \text{CH}_3\text{C}(\text{O})\text{O}_2\text{NO}_2$ (PAN). This reaction has been studied by four groups, Winer et al. [1635], Wallington et al. [1539], Tsalkani et al. [1462], and Talukdar et al. [1416]. Winer et al. obtained only an upper limit for the rate coefficient. Tsalkani et al. noted that their system was very ill-behaved and obtained a value of $k(298\text{ K})$ that is a factor of ~ 2 lower than that obtained by Wallington et al. The pulsed photolysis study of Wallington et al. yielded consistent results, but PAN was not directly measured and photodissociation of H_2O in the vacuum UV, where PAN absorbs strongly, was used as the OH source. The recent study of Talukdar et al. [1416] yielded much lower rate coefficients. These investigators measured the PAN concentration directly in their system, minimized secondary reactions due to the photodissociation of PAN, and carried out extensive tests for decomposition of

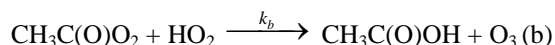
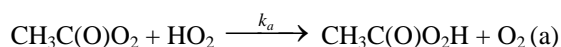
PAN, impurities, and secondary reactions. The recommended upper limit is a factor of two higher than the highest value measured by Talukdar et al. at 298 K and at 272 K. The quoted upper limit is expected to be valid at all atmospheric temperatures. The products of the reaction are not known. Further measurements of the rate coefficients and information on the reaction pathways are needed. (Table: 94-26, Note: 94-26) [Back to Table](#)

- D36. $\text{OH} + \text{C}_2\text{H}_5\text{ONO}_2$. The rate constant for this reaction at 298 K has been measured by Kerr and Stocker [776], Nielsen et al. [1082], Talukdar et al. [1420], Kakesu et al. [762], and Shallcross et al. [1295]. As in the case of the reaction of OH with CH_3ONO_2 , the results of Kerr and Stocker and of Nielsen et al. are larger (by a factor of 3) than those of the more recent studies. The reasons for the differences are not clear. Because of the exhaustive tests carried out (see the note for the $\text{OH} + \text{CH}_3\text{ONO}_2$ reaction), the values of Talukdar et al., Kakesu et al., and Shallcross et al. are recommended. Nielsen et al., Talukdar et al., and Shallcross et al. have measured the rate constant as a function of temperature. As with the $\text{OH} + \text{CH}_3\text{ONO}_2$ reaction, Nielsen et al. report a negative activation energy while Talukdar et al. and Shallcross et al. have observed a small positive activation energy. Talukdar et al. note that the rate coefficient for this reaction does not strictly follow Arrhenius behavior, consistent with the abstraction of both the primary and the secondary H atoms. Above 298 K, E/R values measured by Shallcross et al. and Talukdar et al. are in excellent agreement. Only Talukdar et al. have kinetics data below 298 K and the recommended E/R value was obtained by fitting the rate coefficients measured by Talukdar et al. at or below 298 K. The large uncertainty encompasses the results of Kerr and Stocker and Nielsen et al. (Table: 06-2, Note: 06-2) [Back to Table](#)
- D37. $\text{OH} + 1\text{-C}_3\text{H}_7\text{ONO}_2$. The reaction has been studied by Kerr and Stocker [776] and Atkinson and Aschmann [50] at room temperature and by Nielsen et al. [1082] between 298 and 368 K. The results of the three studies are in good agreement at room temperature. Nielsen et al. find that the reaction is temperature independent within the measurement uncertainty over the range studied. However as discussed above, the Nielsen et al. results for the analogous reactions of OH with CH_3ONO_2 and $\text{C}_2\text{H}_5\text{ONO}_2$, yield negative activation energies that disagree with the positive activation energies obtained by others. Judging from the E/R's for the analogous reactions, one might expect the E/R for this reaction to be on the order of 300 K. Accordingly, we place a large uncertainty on the recommended temperature dependence. A thorough investigation of the temperature dependence of this reaction is needed. (Table: 02-25, Note: 02-25) [Back to Table](#)
- D38. $\text{OH} + 2\text{-C}_3\text{H}_7\text{ONO}_2$. The reaction has been studied by Atkinson and Aschmann [50], Atkinson et al. [52] and Becker and Wirtz [125] at room temperature and by Talukdar et al. [1420] over the range 233 and 395 K. The results of Atkinson and Aschmann supersede those of Atkinson et al. There is fair agreement between the results of the three studies at room temperature, with roughly a factor of two spread in the values. The recommendation is based on an average of the room temperature values and the E/R measured by Talukdar et al. (Table: 02-25, Note: 02-25) [Back to Table](#)
- D39. $\text{HO}_2 + \text{CH}_2\text{O}$. There is sufficient evidence to suggest that HO_2 adds to CH_2O (Su et al. [1389, 1391], Veyret et al. [1518], Zabel et al. [1664], Barnes et al. [96], and Veyret et al. [1517]). The recommended $k(298\text{ K})$ is the average of values obtained by Su et al. [1389], Veyret et al. [1518], and Veyret et al. [1517]. The temperature dependence observed by Veyret et al. [1517] is recommended. The value reported by Barnes et al. at 273 K is consistent with this recommendation. The adduct $\text{HO}_2\cdot\text{CH}_2\text{O}$ seems to isomerize to HOCH_2OO reasonably rapidly and reversibly. There are significant discrepancies between measured values of the equilibrium constants for this reaction. (Table: 90-1, Note: 90-1) [Back to Table](#)
- D40. $\text{HO}_2 + \text{CH}_3\text{O}_2$. This recommendation is taken from the evaluated review of Tyndall et al. [1487]. The kinetics of this reaction have been studied by using UV absorption following pulsed photolytic production of the radicals. These authors first analyzed the available data for the products of the reaction and concluded that the major products are CH_3OOH and O_2 . They used this product yield information with their evaluated UV absorption cross sections for HO_2 and CH_3O_2 to reanalyze the UV absorption profiles measured in kinetics experiments by Dagaut et al. [382] and by Lightfoot et al. [912], the two groups that carried out the most extensive studies. They found that rate coefficients reported by these two groups need to be increased by ~20%. The recommended value is based on the average of the corrected data from these two groups. The temperature dependence was

evaluated by Tyndall et al. by assuming that the absorption cross sections of CH_3O_2 and HO_2 are independent of temperature at the wavelengths used for the kinetics studies. The products of this reaction are shown as $\text{CH}_3\text{OOH} + \text{O}_2$ in the table. However, Elrod et al. [482] have determined that the reaction also yields $\text{CH}_2\text{O} + \text{H}_2\text{O} + \text{O}_2$ with yields that range from 0.1 at 298 K to 0.3 at 220 K. In anticipation of further work, the recommended product yield for the CH_2O channel is zero. (Table: 02-25, Note: 06-2) [Back to Table](#)

- D41. $\text{HO}_2 + \text{C}_2\text{H}_5\text{O}_2$. The recommended value is the weighted average of those measured by Cattell et al. [266], Dagaut et al. [383], Fenter et al. [500], and Maricq and Sente [963]. In all experiments the rate coefficient was obtained by modeling the reaction system. Also, the calculated rate coefficients depended on the UV absorption cross sections of both $\text{C}_2\text{H}_5\text{O}_2$ and HO_2 . The absorption cross section of $\text{C}_2\text{H}_5\text{O}_2$ is not well-defined. The value reported by Dagaut et al. would be ~30% higher if the cross sections used by Maricq and Sente were used. The recommended E/R is derived from the measurements of Dagaut et al., Fenter et al., and Maricq and Sente. Wallington and Japar [1556] have shown that $\text{C}_2\text{H}_5\text{O}_2\text{H}$ and O_2 are the only products of this reaction. (Table: 94-26, Note: 94-26) [Back to Table](#)

- D42. $\text{HO}_2 + \text{CH}_3\text{C(O)O}_2$. This recommendation is taken from the evaluated review of Tyndall et al. [1487]. This reaction has two sets of products:



The majority of the reaction proceeds via channel (a), but there is clear evidence for channel (b). Tyndall et al. reevaluated the available data on end products of this reaction, particularly those of Crawford et al. [370], Moortgat et al. [1029], and Horie and Moortgat [666], and concluded that channel (a) contributes ~80% while channel (b) contributes ~20% at 298 K. They also concluded that $k_a/k_b = 37 \times \exp(-660/T)$ with a large uncertainty in this value. They derived the overall rate coefficient for this reaction, which has been measured only by following the radical concentrations via UV absorption. They based their recommendation mostly on the results of Moortgat et al. [1029] and Tomas et al. [1454]. (Table: 02-25, Note: 02-25) [Back to Table](#)

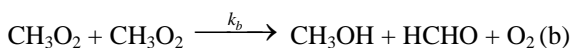
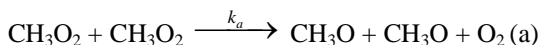
- D43. $\text{HO}_2 + \text{CH}_3\text{C(O)CH}_2\text{O}_2$. This recommendation is from Tyndall et al. [1487]. This reaction has been studied by only Bridier et al. [195] and Tyndall et al. based their recommendation on this one study. (Table: 02-25, Note: 02-25) [Back to Table](#)
- D44. $\text{NO}_3 + \text{CO}$. The upper limit is based on the results of Hjorth et al. [658], who monitored isotopically labeled CO loss in the presence of NO_3 by FTIR. Burrows et al. [228] obtained an upper limit of $4 \times 10^{-16} \text{ cm}^3 \text{ molecule}^{-1} \text{ s}^{-1}$, which is consistent with the Hjorth et al. study. Products are expected to be $\text{NO}_2 + \text{CO}_2$, if the reaction occurs. (Table: 87-41, Note: 92-20) [Back to Table](#)
- D45. $\text{NO}_3 + \text{CH}_2\text{O}$. There are three measurements of this rate coefficient at 298 K: Atkinson et al. [64], Cantrell et al. [258], and Hjorth et al. [659]. The value reported by Atkinson et al. [64], $k = (3.23 \pm 0.26) \times 10^{-16} \text{ cm}^3 \text{ molecule}^{-1} \text{ s}^{-1}$, is corrected to $5.8 \times 10^{-16} \text{ cm}^3 \text{ molecule}^{-1} \text{ s}^{-1}$ to account for the different value of the equilibrium constant for the $\text{NO}_3 + \text{NO}_2 \leftrightarrow \text{N}_2\text{O}_5$ reaction that was measured subsequent to this study by the same group using the same apparatus. This correction is in accordance with their suggestion (Tuazon et al. [1469]). The values reported by Cantrell et al. and Hjorth et al., $k = 6.3 \times 10^{-16} \text{ cm}^3 \text{ molecule}^{-1} \text{ s}^{-1}$ and $(5.4 \pm 1.1) \times 10^{-16} \text{ cm}^3 \text{ molecule}^{-1} \text{ s}^{-1}$, respectively, are in good agreement with the corrected value of Atkinson et al. The recommended value is the average of these three studies. Cantrell et al. have good evidence to suggest that HNO_3 and CHO are the products of this reaction. The temperature dependence of this rate coefficient is unknown, but comparison with the analogous $\text{NO}_3 + \text{CH}_3\text{CHO}$ reaction suggests a large E/R. (Table: 90-1, Note: 90-1) [Back to Table](#)
- D46. $\text{NO}_3 + \text{CH}_3\text{CHO}$. There are four measurements of this rate constant: Morris and Niki [1032], Atkinson et al. [64], Cantrell et al. [252], and Dlugokencky and Howard [436]. The value reported by Atkinson et al., $k = (1.34 \pm 0.28) \times 10^{-15} \text{ cm}^3 \text{ molecule}^{-1} \text{ s}^{-1}$, is corrected to $2.4 \times 10^{-15} \text{ cm}^3 \text{ molecule}^{-1} \text{ s}^{-1}$ as discussed for the $\text{NO}_3 + \text{H}_2\text{CO}$ reaction above and as suggested by Tuazon et al. [1469]. The recommended value is the average of the values obtained by Atkinson et al., Cantrell et

al., and Dlugokencky and Howard. The results of Morris and Niki agree with the recommended value when their original data are re-analyzed using a more recent value for the equilibrium constant for the reaction $\text{NO}_2 + \text{NO}_3 \leftrightarrow \text{N}_2\text{O}_5$ as shown by Dlugokencky and Howard. Dlugokencky and Howard have studied the temperature dependence of this reaction. Their measured value of E/R is recommended. The A-factor has been calculated to agree with the $k(298 \text{ K})$ recommended here. Morris and Niki, and Cantrell et al. observed the formation of HNO_3 and PAN in their studies, which strongly suggests that HNO_3 and CH_3CO are the products of this reaction. (Table: 87-41, Note: 87-41) [Back to Table](#)

- D47. $\text{CH}_3 + \text{O}_2$. This bimolecular reaction is not expected to be important, based on the results of Baldwin and Golden [80], who found $k < 5 \times 10^{-17} \text{ cm}^3 \text{ molecule}^{-1} \text{ s}^{-1}$ for temperatures up to 1200 K. Klais et al. [796] failed to detect OH (via $\text{CH}_3 + \text{O}_2 \rightarrow \text{CH}_2\text{O} + \text{OH}$) at 368 K and placed an upper limit of $3 \times 10^{-16} \text{ cm}^3 \text{ molecule}^{-1} \text{ s}^{-1}$ for this rate coefficient. Bhaskaran et al. [151] measured $k = 1 \times 10^{-11} \exp(-12,900/T) \text{ cm}^3 \text{ molecule}^{-1} \text{ s}^{-1}$ for $1800 < T < 2200 \text{ K}$. The latter two studies thus support the results of Baldwin and Golden. Studies by Selzer and Bayes [1293] and Plumb and Ryan [1174] confirm the low value for this rate coefficient. Previous studies of Washida and Bayes [1584] are superseded by those of Selzer and Bayes. Plumb and Ryan have placed an upper limit of $3 \times 10^{-16} \text{ cm}^3 \text{ molecule}^{-1} \text{ s}^{-1}$ based on their inability to find HCHO in their experiments. A study by Zellner and Ewig [1674] suggests that this reaction is important at combustion temperature but is unimportant for the atmosphere. (Table: 83-62, Note: 83-62) [Back to Table](#)
- D48. $\text{CH}_3 + \text{O}_3$. The recommended A-factor and E/R are those obtained from the results of Ogryzlo et al. [1108]. The results of Simonaitis and Heicklen [1311], based on an analysis of a complex system, are not used. Washida et al. [1583] used $\text{O} + \text{C}_2\text{H}_4$ as the source of CH_3 . Studies on the $\text{O} + \text{C}_2\text{H}_4$ reaction (Schmoltner et al. [1274], Kleinermanns and Luntz [800], Hunziker et al. [692], and Inoue and Akimoto [714]) have shown this reaction to be a poor source of CH_3 . Therefore, the results of Washida et al. are also not used. (Table: 83-62, Note: 83-62) [Back to Table](#)
- D49. $\text{HCO} + \text{O}_2$. The value of $k(298 \text{ K})$ is the average of the determinations by Washida et al. [1585], Shibuya et al. [1300], Veyret and Lesclaux [1516], Langford and Moore [853], Nesbitt et al. [1058], Temps et al. [1429], and Ninomiya et al. [1097]. There are three measurements of k where HCO was monitored via the intracavity dye laser absorption technique (Reilly et al. [1223], Nadochenko et al. [1039], and Gill et al. [551]). Even though these studies agree with the recent measurements of Nesbitt et al., the only recent measurement to obtain a low value, they have not been included in deriving the recommended value of $k(298 \text{ K})$. However, the uncertainty has been increased to overlap with those measurements. The main reason for not including them in the average is the possible depletion of O_2 in those static systems (as suggested by Veyret and Lesclaux). Also, these experiments were designed more for the study of photochemistry than kinetics. The temperature dependence of this rate coefficient has been measured by Veyret and Lesclaux, Timonen et al. [1446], and Nesbitt et al. While Timonen et al. obtain a slightly positive activation energy, Veyret and Lesclaux, and Nesbitt et al. measure slightly negative activation energy. It is very likely that the Arrhenius expression is curved. We recommend an E/R value of zero, with an uncertainty of 100 K. Veyret and Lesclaux preferred a T^n form ($k = 5.5 \times 10^{-11} T^{-(0.4 \pm 0.3)} \text{ cm}^3 \text{ molecule}^{-1} \text{ s}^{-1}$). Hsu et al. [681] suggest that this reaction proceeds via addition at low temperature and abstraction at higher temperatures. (Table: 02-25, Note: 02-25) [Back to Table](#)
- D50. $\text{CH}_2\text{OH} + \text{O}_2$. The rate coefficient was first measured directly by Radford [1192] by detecting the HO_2 product in a laser magnetic resonance spectrometer. The wall loss of CH_2OH could have introduced a large error in this measurement. Radford also showed that the previous measurement of Avramenko and Kolesnikova [69] was in error. Wang et al. [1575] measured a value of $1.4 \times 10^{-12} \text{ cm}^3 \text{ molecule}^{-1} \text{ s}^{-1}$ by detecting the HO_2 product. Recently, Dobe et al. [439], Grotheer et al. [589], Payne et al. [1152], Grotheer et al. [590] and Nesbitt et al. [1061] have measured $k(298 \text{ K})$ to be close to $1.0 \times 10^{-11} \text{ cm}^3 \text{ molecule}^{-1} \text{ s}^{-1}$ under conditions where wall losses are small. This reaction appears to exhibit a very complex temperature dependence. Based on the recent data of Grotheer et al. [590], and Nesbitt et al. [1061], k appears to increase from 200 K to approximately 250 K in an Arrhenius fashion, levels off at approximately 300 K, decreases from 300 to 500 K, and finally increases as temperature is increased. This complex temperature dependence is believed to be due to the formation of a $\text{CH}_2(\text{OH})\cdot\text{O}_2$ adduct which can isomerize to $\text{CH}_2\text{O}\cdot\text{HO}_2$ or decompose to

reactants. The $\text{CH}_2\text{O}\cdot\text{HO}_2$ isomer can also decompose to CH_2O and HO_2 or reform the original adduct. At temperatures less than 250 K, the data of Nesbitt et al. suggests an E/R value of ~ 1700 K. For atmospheric purposes, the value $E/R = 0$ is appropriate. (Table: 90-1, Note: 90-1) [Back to Table](#)

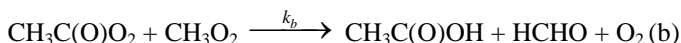
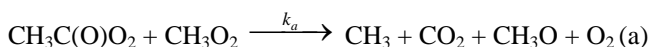
- D51. $\text{CH}_3\text{O} + \text{O}_2$. The recommended value for $k(298\text{ K})$ is the average of those reported by Lorenz et al. [932] and Wantuck et al. [1578]. The recommended E/R was obtained using the results of Gutman et al. [593] (413 to 608 K), Lorenz et al. [932] (298 to 450 K), and Wantuck et al. [1578] (298 to 498 K). These investigators have measured k directly under pseudo-first order conditions by following CH_3O via laser induced fluorescence. Wantuck et al. measured k up to 973 K and found the Arrhenius plot to be curved; only their lower temperature data are used in the fit to obtain E/R. The A factor has been adjusted to reproduce the recommended $k(298\text{ K})$. The previous high temperature measurements (Barker et al. [86] and Batt and Robinson [111]) are in reasonable agreement with the derived expression. This value is consistent with the 298 K results of Cox et al. [361], obtained from an end product analysis study, and with the upper limit measured by Sanders et al. [1257]. The A-factor appears low for a hydrogen atom transfer reaction. The reaction may be more complicated than a simple abstraction. At 298 K, the products of this reaction are HO_2 and CH_2O , as shown by Niki et al. [1090]. (Table: 87-41, Note: 87-41) [Back to Table](#)
- D52. $\text{CH}_3\text{O} + \text{NO}$. The reaction of CH_3O with NO proceeds mainly via addition to form CH_3ONO (Batt et al. [110], Wiebe and Heicklen [1608], Frost and Smith [527], and Ohmori et al. [1111]). However, a fraction of the energized CH_3ONO adducts decomposes to $\text{CH}_2\text{O} + \text{HNO}$, and appear to be a bimolecular channel. This reaction has been investigated by direct detection of CH_3O via laser-induced fluorescence (Zellner [1672]; Frost and Smith [527]; Ohmori et al. [1111]). End-product studies (Batt et al. [110], Wiebe and Heicklen [1608]) are generally consistent with this conclusion. Since the fraction of the CH_3ONO adduct that falls apart to $\text{CH}_2\text{O} + \text{HNO}$ decreases with increasing pressure and decreasing temperature, it is not possible to derive a "bimolecular" rate coefficient. A value of $k < 8 \times 10^{-12} \text{ cm}^3 \text{ molecule}^{-1} \text{ s}^{-1}$ can be deduced from the work of Frost and Smith [527] and Ohmori et al. [1111] for lower atmospheric conditions. (Table: 97-4, Note: 97-4) [Back to Table](#)
- D53. $\text{CH}_3\text{O} + \text{NO}_2$. The reaction of CH_3O with NO_2 proceeds mainly via the formation of CH_3ONO_2 . However, a fraction of the energized adducts fall apart to yield $\text{CH}_2\text{O} + \text{HNO}_2$. The bimolecular rate coefficient reported here is for the fraction of the reaction that yields CH_2O and HNO_2 . It is not meant to represent a bimolecular metathesis reaction. The recommended value was derived from the study of McCaulley et al. [985] and is discussed in the section on association reactions. (Table: 97-4, Note: 97-4) [Back to Table](#)
- D54. $\text{CH}_3\text{O}_2 + \text{O}_3$. This recommendation is from Tyndall et al. [1487]. Their recommendation is based mostly on the recent study by Tyndall et al. [1500]. The temperature dependence is based on the assumption that the only possible reaction which can occur is the O atom transfer from the CH_3O_2 radical and that the activation energy of $\sim 2 \text{ kcal mol}^{-1}$ for this O-atom transfer is similar to that in the $\text{HO}_2 + \text{O}_3$ reaction. (Table: 02-25, Note: 02-25) [Back to Table](#)
- D55. $\text{CH}_3\text{O}_2 + \text{CH}_3\text{O}_2$. This recommendation is from Tyndall et al. [1487]. There are two confirmed sets of products for this reaction.



The relative product yield, k_a/k_b , was evaluated by Tyndall et al. to be $(26.2 \pm 6.6) \times \exp((-1130 \pm 240)/T)$. They concluded that there was no evidence for the formation of the CH_3OOCH_3 . The kinetics of this reaction have been studied by using UV absorption following pulsed photolytic production of the radicals. Tyndall et al. used the values of k/σ measured by a large number of groups along with the σ values from their evaluation to calculate k . (σ is the absorption cross section of the radical at the wavelength at which it was monitored.) They only used the kinetics data obtained at wavelengths larger than 240 nm, since the absorption by HO_2 radicals that are unavoidably produced in these measurements can significantly contribute to the measured UV profiles at shorter wavelengths. They noted that the values of k/σ measured by various groups were

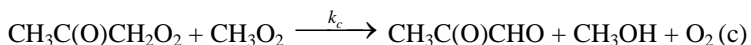
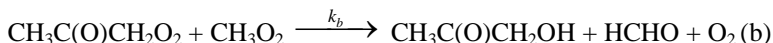
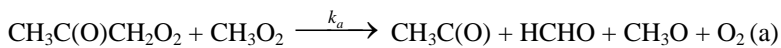
much more accurate than the values of σ measured by the same groups. The value of k obtained by this method was then corrected using the above branching ratio for the production of CH_3O that leads to the unavoidable occurrence of the $\text{CH}_3\text{O}_2 + \text{HO}_2$ side reaction; this side reaction consumes another CH_3O_2 radical. (Table: 02-25, Note: 02-25) [Back to Table](#)

- D56. $\text{CH}_3\text{O}_2 + \text{NO}$. This recommendation is from Tyndall et al. [1487]. They evaluated the available information to deduce that the main set of products under atmospheric conditions is $\text{CH}_3\text{O} + \text{NO}_2$. They noted, however, that a very small yield, $<0.5\%$, of CH_3ONO_2 is also possible. The rate coefficient for the reaction at 298 K and its temperature dependence is based on numerous direct studies of this reaction that have been reported. (Table: 02-25, Note: 02-25) [Back to Table](#)
- D57. $\text{CH}_3\text{O}_2 + \text{CH}_3\text{C}(\text{O})\text{O}_2$. This recommendation is from Tyndall et al. [1487]. This reaction has two sets of products:



Tyndall et al. reanalyzed the previously available data on the branching ratios for this reaction and concluded that the branching ratio for channel (a) was $k_a/k = 0.9 \pm 0.1$ and $k_b/k = 0.1 \pm 0.1$ at 298 K. They also concluded that branching ratios could not be derived for other temperatures from the existing data and therefore did not make a recommendation for the temperature dependence. The recommendation from Tyndall et al. is based on the work of Roehl et al. [1240] and Villenave et al. [1519]. Their recommended temperature dependence for the overall rate coefficient is based on analogy with other RO_2 reactions. (Table: 02-25, Note: 02-25) [Back to Table](#)

- D58. $\text{CH}_3\text{O}_2 + \text{CH}_3\text{C}(\text{O})\text{CH}_2\text{O}_2$. This recommendation is from Tyndall et al. [1487]. This reaction has three possible sets of products:



The branching ratios for these channels, $k_a/k = 0.3 \pm 0.1$, $k_b/k = 0.2 \pm 0.1$, and $k_c/k = 0.5 \pm 0.1$, are based on the work of Bridier et al. [195] and Jenkin et al. [734]. The overall rate coefficient for this reaction has been studied only at 298 K by Bridier et al. and the recommendation is based on this value. The recommended values of E/R and g are based on analogy with other RO_2 reactions. (Table: 02-25, Note: 02-25) [Back to Table](#)

- D59. $\text{C}_2\text{H}_5 + \text{O}_2$. This is a complex reaction that involves the formation of a $\text{C}_2\text{H}_5\text{O}_2$ adduct, which can either be stabilized by collisions or fall apart to HO_2 and C_2H_4 (Wagner et al. [1529], Bozzelli and Dean [188], and Kaiser et al. [759]). The fraction of the energized adducts that fall apart to give HO_2 and C_2H_4 will decrease with increasing pressure and decreasing temperature, i.e., as the $\text{C}_2\text{H}_5\text{O}_2$ formation increases. The C_2H_4 -formation channel cannot be separated from the addition reaction. We recommend a conservative upper limit as a guide to the extent of this reaction. This upper limit is applicable only for lower atmospheric pressure and temperature conditions. (Table: 94-26, Note: 94-26) [Back to Table](#)
- D60. $\text{C}_2\text{H}_5\text{O} + \text{O}_2$. The recommendation is based on the pulsed laser photolysis studies of Gutman et al. [593] and Hartmann et al. [617]. In both these studies, removal of $\text{C}_2\text{H}_5\text{O}$ in an excess of O_2 was directly monitored via laser induced fluorescence. Gutman et al. measured k at only two temperatures, while Hartmann et al. measured k at 5 temperatures between 295 and 411 K. The E/R is from Hartmann et al. The 298 K value deduced from an indirect study by Zabarnick and Hecklen [1662] is in reasonable agreement with the recommended value. (Table: 92-20, Note: 92-20) [Back to Table](#)
- D61. $\text{C}_2\text{H}_5\text{O}_2 + \text{C}_2\text{H}_5\text{O}_2$. $k(298 \text{ K})$ has been studied by Adachi et al. [8], Anastasi et al. [29], Munk et al. [1036], Cattell et al. [266], Anastasi et al. [28], Wallington et al. [1545], Bauer et al. [113], and

Fenter et al. [500]. All the above determinations used only UV absorption to monitor $\text{C}_2\text{H}_5\text{O}_2$ and hence measured k/σ , where σ is the absorption cross section of $\text{C}_2\text{H}_5\text{O}_2$ at the monitoring wavelength. These investigators also measured the σ that was used in evaluating the rate coefficient. There are large discrepancies in the measured values of σ . For this evaluation, we have used the cross sections recommended here and recalculated the values of k from each investigation. The recommended k is based on the results of Cattell et al., Wallington et al., Bauer et al., and Fenter et al. In all these experiments the observed rate coefficient is higher than the true rate coefficient because of secondary reactions involving HO_2 . HO_2 is formed by the reaction of $\text{CH}_3\text{CH}_2\text{O}$ with O_2 and it reacts with $\text{C}_2\text{H}_5\text{O}_2$ to enhance the observed rate coefficient (see Wallington et al. [1547] or Lightfoot et al. [910] for further discussion). Based on product branching ratios discussed below, which determine the magnitude of the necessary correction, the recommended rate coefficient is 0.6 times the average observed rate coefficient. The recommended value of E/R was obtained from the results of Anastasi et al., Wallington et al., Cattell et al., Bauer et al., and Fenter et al. The observed products (Niki et al. [1091]), suggest that at 298 K the channel to yield $2 \text{ C}_2\text{H}_5\text{O} + \text{O}_2$ accounts for about 60% of the reaction; the channel to yield $\text{CH}_3\text{CHO} + \text{C}_2\text{H}_5\text{OH} + \text{O}_2$ accounts for about 40% of the reaction; and the channel to yield $\text{C}_2\text{H}_5\text{O}_2\text{C}_2\text{H}_5 + \text{O}_2$ accounts for less than 5% of the reaction. These branching ratios were used to obtain the true rate coefficient from the observed rate coefficient. (Table: 94-26, Note: 94-26) [Back to Table](#)

- D62. $\text{C}_2\text{H}_5\text{O}_2 + \text{NO}$. The recommended $k(298 \text{ K})$ is obtained from the results of Plumb et al. [1176], Sehested et al. [1290], Daele et al. [381], Eberhard and Howard [471], and Maricq and Szenté [964]. The value reported by Adachi and Basco [7], which is a factor of three lower than the recommended value, was not used. The rate coefficient for the $\text{CH}_3\text{O}_2 + \text{NO}$ reaction measured by Basco and co-workers (Adachi et al. [8]) using the same apparatus is also much lower than the value recommended here. The recommended temperature dependence is derived from Eberhardt and Howard [471] and Maricq and Szenté [964], which are in good agreement. (Table: 97-4, Note: 97-4) [Back to Table](#)
- D63. $\text{CH}_3\text{C}(\text{O})\text{O}_2 + \text{CH}_3\text{C}(\text{O})\text{O}_2$. This reaction has been studied by Addison et al. [9], Basco and Parmar [109], Moortgat et al. [1029], Maricq and Szenté [964], and Roehl et al. [1240], using UV absorption techniques. The recommended value is obtained from the data of Moortgat et al., Maricq and Szenté, and Roehl et al. As pointed out by Moortgat et al., the six times lower value of k obtained by Addison et al. is likely due to the use of incorrect UV absorption cross sections for the peroxy radical. The k obtained by Basco and Parmar is ~ 2 times lower than the recommended value. This discrepancy is possibly due to neglecting the UV absorption of CH_3O_2 and other stable products in their data analysis (Moortgat et al., Maricq and Szenté). The recommended temperature dependence was calculated from the data of Moortgat et al. and Maricq and Szenté. Addison et al. reported the formation of O_3 , which was attributed to the reaction channel that produces $\text{CH}_3\text{C}(\text{O})\text{OCH}_2\text{C}(\text{O}) + \text{O}_3$. Moortgat et al. place an upper limit of 2% for this channel. The main products of this reaction appear to be $\text{CH}_3\text{C}(\text{O})\text{O} + \text{O}_2$. The $\text{CH}_3\text{C}(\text{O})\text{O}$ radicals rapidly decompose to give CH_3 and CO_2 . (Table: 97-4, Note: 97-4) [Back to Table](#)
- D64. $\text{CH}_3\text{C}(\text{O})\text{O}_2 + \text{NO}$. This recommendation is from Tyndall et al. [1487]. These authors have argued that the only set of products of importance in the atmosphere is the production of $\text{CH}_3 + \text{CO}_2 + \text{NO}_2$. This is because the alkoxy radical produced upon O abstraction from the peroxy radical by NO will be unstable towards decomposition to give CH_3 and CO_2 . The rate coefficient for the reaction was deduced primarily from direct studies, but was found to be consistent with the relative rate studies. In the relative rate studies, this rate coefficient was measured relative to the rate coefficient for the reaction of $\text{CH}_3\text{C}(\text{O})\text{O}_2$ with NO_2 . (Table: 02-25, Note: 10-6) [Back to Table](#)
- D65. $\text{CH}_3\text{C}(\text{O})\text{CH}_2\text{O}_2 + \text{NO}$. This recommendation is from Tyndall et al. [1487]. They deduced, based on the results of Sehested et al. [1287], Jenkin et al. [734], and Orlando et al. [1130], that the products of this reaction are $\text{CH}_3\text{C}(\text{O})\text{CH}_2\text{O} + \text{NO}_2$. The $\text{CH}_3\text{C}(\text{O})\text{CH}_2\text{O}$ radical decomposes rapidly to give $\text{CH}_3\text{C}(\text{O}) + \text{CH}_2\text{O}$. The only kinetics study of this reaction by Sehested et al. forms the basis for the rate coefficient at 298 K. This value is uncertain because of the corrections that had to be made in the study of Sehested et al. to account for the production of NO_2 , the monitored species, via the reaction of peroxy radicals (such as $\text{CH}_3\text{C}(\text{O})\text{O}_2$ and CH_3O_2) with NO. The temperature dependence of the reaction is derived based on analogy with other peroxy radical reactions. (Table: 02-25, Note: 02-25) [Back to Table](#)

- D66. $\text{NO}_3 + \text{CH}_2=\text{C}(\text{CH}_3)\text{CH}=\text{CH}_2 \rightarrow \text{products}$. The recommended 298 K rate constant is an unweighted average of room temperature results reported by Atkinson et al. [55, 56], Dlugokencky & Howard [436], Barnes et al. [93], Wille et al. [1612], Ellermann et al. [479], Berndt and Boge [148], Suh et al. [1393], and Stabel et al. [1353]. The recommended E/R is based on the single temperature dependence study by Dlugokencky & Howard [436]. The 298 K rate constant reported by Benter & Schindler [146] is not considered because (a) it is faster than all others in the literature and (b) it is superseded by a later study from the same group [1612]. (Table 10-6, Note: 10-6, Evaluated: 10-6) [Back to Table](#)
- E1. $\text{O} + \text{FO}$. The recommended value is based on results of the room temperature study of Bedzhanyan et al. [140]. The temperature dependence of the rate constant is expected to be small, as it is for the analogous ClO reaction. (Table: 94-26, Note: 94-26) [Back to Table](#)
- E2. $\text{O} + \text{FO}_2$. No experimental data. The rate constant for such a radical-atom process is expected to approach the gas collision frequency, and is not expected to exhibit a strong temperature dependence. (Table: 82-57, Note: 82-57) [Back to Table](#)
- E3. $\text{OH} + \text{CH}_3\text{F}$ (HFC-41). The recommended values for $k(298 \text{ K})$ and E/R are averages of these parameters derived from fits to the data of Schmoltner et al. [1275], Nip et al [1099], Hsu and DeMore [684], and DeMore [415] (with the relative rate constants from the last two studies recalculated based on the current recommendations for the rate constants for the $\text{OH} + \text{CH}_3\text{CHF}_2$ and $\text{OH} + \text{CH}_3\text{Cl}$ reference reactions, respectively.) The A factor was then calculated. The renormalization procedure for relative rate measurements referenced to the $\text{OH} + \text{CH}_3\text{CHF}_2$ reaction is discussed in the note for that reaction. The results of Howard and Evenson [674], Jeong and Kaufman [742], and Wallington and Hurley [1551] appear to be systematically lower than those of the other studies over the temperature region of interest and were not used to derive the recommended parameters. The results from the 298 K study by Kowalczyk et al.[820], although in good agreement with the recommended value for $k(298 \text{ K})$, also were not used since the results reported in this study for several halocarbons vary widely (ranging from 10% agreement with recommendations to as much as 3 orders of magnitude disagreement with recommendations). (Table: 10-6, Note: 10-6, Evaluated: 10-6) [Back to Table](#)
- E4. $\text{OH} + \text{CH}_2\text{F}_2$ (HFC-32). The recommended value of $k(298 \text{ K})$ is an average from the studies of Nip et al. [1099], Jeong and Kaufman [742], Talukdar et al. [1415], Hsu and DeMore [684] (recalculated based on the current recommendation for the rate constant for the $\text{OH} + \text{CH}_3\text{CHF}_2$ reference reaction, as described in the note for that reaction), and Szilagyi et al. [1399]. The recommended value for E/R is derived from an Arrhenius fit to the data from these same five studies below 400 K. The results of Howard and Evenson [674], Clyne and Holt [322], Bera and Hanrahan [147] and Kowalczyk et al.[820] are somewhat more scattered and were not used in deriving the recommended parameters. (Table: 10-6, Note: 10-6, Evaluated: 10-6) [Back to Table](#)
- E5. $\text{OH} + \text{CHF}_3$ (HFC-23). The recommended values for $k(298 \text{ K})$ is an average of the values reported in the absolute rate study of Schmoltner et al. [1275] and in the relative rate studies of Hsu and DeMore [684] (recalculated based on the current recommendation for the rate constant for the $\text{OH} + \text{CHF}_2\text{CF}_3$ reference reaction) and of Chen et al.[287] (2 studies recalculated based on the current recommendations for the rate constants for the $\text{OH} + \text{CHF}_2\text{CF}_3$ and $\text{OH} + \text{CHF}_2\text{Cl}$ reference reactions). The recommended value for E/R was from a combined fit to the data (at room temperature and below) of Schmoltner et al. [1275], Hsu and DeMore [684], and Chen et al.[287]. The results of Jeong and Kaufman [742], and Medhurst et al. [993], being predominantly above room temperature, were not used in deriving the recommended parameters. The results from Clyne and Holt [322] and Bera and Hanrahan [147] were also not used due to their inconsistency with the other studies. The room temperature values of Howard and Evenson [674] and Nip et al. [1099] are encompassed within the 2σ confidence limits. (Table: 10-6, Note: 10-6, Evaluated: 10-6) [Back to Table](#)
- E6. $\text{OH} + \text{CH}_3\text{CH}_2\text{F}$ (HFC-161). The recommended value for $k(298 \text{ K})$ is an average of the values from Nip et al. [1099], Schmoltner et al. [1275], and Kozlov et al. [821]. The value of E/R is based on a fit to the data from these three studies from room temperature and below. The relative rate study by Hsu and DeMore [684] reports a temperature dependence that is markedly different from those of

Schmoltnner et al. [1275] and Kozlov et al. [821], which are in excellent agreement. This difference is due to significantly lower rate constant values being obtained in the Hsu and DeMore study in the region near room temperature. Given the most recent results for the reaction of OH + CH₃CHF₂ (HFC-152a), it seems likely that the HFC-161 reaction also has two channels with different activation energies and that the temperature dependence below room temperature should be less than that recommended for HFC-152a, consistent with the present recommendation. Curvature in the Arrhenius plot is evident from the study by Kozlov et al. [821], which was conducted over an extended temperature range above and below room temperature. Singleton et al. [1321] determined that 85 ± 3% of the abstraction by OH is from the fluorine substituted methyl group at room temperature. Hence this curvature is quite possibly due to the increasing importance of hydrogen abstraction from the unsubstituted methyl group with increasing temperature. Due to such occurrence, the recommended parameters should not be used for calculating rate constants above room temperature. (Table: 02-25, Note: 02-25) [Back to Table](#)

- E7. OH + CH₃CHF₂ (HFC-152a). The recommended value for k(298 K) is an average of the values from Howard and Evenson [675], Handwerk and Zellner [611], Nip et al. [1099], Gierczak et al. [546] (two different absolute determinations), Hsu and DeMore [684] (two relative rate determinations which have been recalculated based on the current recommendations for the rate constants of the OH + CH₄ and OH + CH₃CCl₃ reference reactions), Kozlov et al [821], Wilson et al.[1618] (two relative rate determinations which have been recalculated based on the current recommendations for the rate constants of the OH + C₂H₆ and OH + *c*-C₃H₆ reference reactions), and Taketani et al.[1410] (two relative rate determinations which have been recalculated based on the current recommendations for the rate constants of the OH + C₂H₂ and OH + C₂H₄ reference reactions). There are systematic differences in the temperature dependencies determined in the absolute studies (particularly below room temperature) and relative studies (conducted at room temperature and above). Curvature in the Arrhenius plot (as suggested by the data of Gierczak et al. [546]) has been more clearly demonstrated by the study of Kozlov et al. [821] and seems to explain the earlier cited differences between the relative and absolute rate data. This curvature is likely due to the presence of two hydrogen-abstraction reaction channels. Hence, care must be taken in deriving a recommended rate expression suitable for atmospheric modeling (in the temperature region below room temperature).

In spite of the noticeable Arrhenius curvature over the temperature range from 480 K to 210 K, the data below 300 K can be well represented by a two-parameter Arrhenius expression. Thus, the recommended value for E/R is derived from a combined fit to the data (T ≤ 300 K) of Gierczak et al. and Kozlov et al. after normalization of the data sets to k(298 K). The studies by Clyne and Holt [322], Brown et al. [197], and Nielsen [1075] all yield systematically higher rate constants and were not used in deriving the recommended parameters. The study by Liu et al. [928] is superseded by that of Kozlov et al.

Clearly, in light of the observed Arrhenius curvature, the above procedure for deriving our recommendation for E/R below 300 K does not yield a parameter suitable for use in recalculating rate constants from relative rate studies in which the OH + CH₃CHF₂ reaction was the reference and which were conducted at temperatures above 300 K. Use of the below-room-temperature value for E/R for such purposes results in rate constant values that are systematically different from those determined relative to other reactions or determined by absolute techniques. For such renormalization purposes, one should use an Arrhenius expression derived from data over the appropriate temperature range. A fit to the absolute rate data of Gierczak et al. [546] and Kozlov et al. [821] between room temperature and 400 K yields the Arrhenius expression

$$k_{\text{abs}} = 2.36 \times 10^{-12} \exp(-1255/T) \text{ cm}^3 \text{ molecule}^{-1} \text{ s}^{-1}$$

This is in good agreement with the expression derived from the relative rate data of Hsu and DeMore [684]

$$k_{\text{rel}} = 2.1 \times 10^{-12} \exp(-1265/T) \text{ cm}^3 \text{ molecule}^{-1} \text{ s}^{-1}$$

The small difference in the pre-exponential factors results from a slight systematic difference in the actual rate constants determined in these three studies that is probably within the combined uncertainties of the determinations. Thus, the following expression derived from the above room

temperature E/R value and the recommended $k(298\text{ K})$ has been used for renormalization purposes in this evaluation.

$$k(T \geq 300\text{ K}) = 2.33 \times 10^{-12} \exp(-1260/T) \text{ cm}^3 \text{ molecule}^{-1} \text{ s}^{-1}$$

However, this expression should not be used below 298 K, as erroneous values for $\text{OH} + \text{CH}_3\text{CHF}_2$ reaction rate constants would be obtained. (Table: 10-6, Note: 10-6, Evaluated: 10-6) [Back to Table](#)

- E8. $\text{OH} + \text{CH}_2\text{FCH}_2\text{F}$ (HFC-152). The recommended value for $k(298\text{ K})$ is an average of the values from the absolute rate studies of Martin and Paraskevopoulos [973] and Kozlov et al. [821], and from the relative rate studies of Wilson et al. [1618] (three independent studies renormalized using the current recommendations for the reference reactions of OH with HFC-152a, cyclopropane, and ethane). The value for E/R is from a fit to the data of Kozlov et al. [821] at room temperature and below. The A factor was then calculated to agree with the recommended value for $k(298\text{ K})$. The data above room temperature from Kozlov et al. [821] are in excellent agreement with the three relative rate data sets of Wilson et al. [1618]. Together, they show a pronounced curvature in the Arrhenius plot, which may indicate the existence of different conformers for HFC-152, each with differing temperature populations and reactivities. (Table: 10-6, Note: 10-6, Evaluated: 10-6) [Back to Table](#)
- E9. $\text{OH} + \text{CH}_3\text{CF}_3$ (HFC-143a). The recommended value for $k(298\text{ K})$ is an average of the values from Martin and Paraskevopoulos [973], Orkin et al. [1117], Talukdar et al. [1415] (two different determinations), and Hsu and DeMore [684] (two relative rate determinations which have been recalculated based on the current recommendations for the rate constants of the $\text{OH} + \text{CH}_4$ and $\text{OH} + \text{CHF}_2\text{CF}_3$ reference reactions). The value for E/R is an average of the E/R values from the last three of these studies which are in excellent agreement (Martin and Paraskevopoulos having made measurements only at room temperature). The data of Clyne and Holt [322] were not used due to their inconsistency with the other studies. (Table: 02-25, Note: 02-25) [Back to Table](#)
- E10. $\text{OH} + \text{CH}_2\text{FCHF}_2$ (HFC-143). The recommended temperature dependence is based on results of the relative rate study of Barry et al. [105] normalized to the value of the rate constant for the reference reaction ($\text{OH} + \text{CH}_3\text{CCl}_3$) recommended in this evaluation. The value for $k(298\text{ K})$ is an average of the room temperature values of Martin and Paraskevopoulos [973] and Barry et al. The significantly higher values reported by Clyne and Holt [322] were not used in the derivation of the recommended parameters. (Table: 02-25, Note: 02-25) [Back to Table](#)
- E11. $\text{OH} + \text{CH}_2\text{FCF}_3$ (HFC-134a). The recommended value for $k(298\text{ K})$ is an average of the values from Martin and Paraskevopoulos [973], Bednarek et al. [135], Orkin and Khamaganov [1119], Leu and Lee [885], Gierczak et al. [546] (two different determinations), Liu et al. [928], and DeMore [413] (three determinations which have been recalculated based on the current recommendations for the rate constants for the reference reactions $\text{OH} + \text{CH}_4$, $\text{OH} + \text{CH}_3\text{CCl}_3$, and $\text{OH} + \text{CHF}_2\text{CF}_3$). The value for E/R is an average of the E/R values from the last five of these investigations (the studies by Martin and Paraskevopoulos and by Bednarek et al. being conducted only at room temperature). The 270 K result of Zhang et al. [1682] is in excellent agreement with the recommendation. The data of Jeong et al. [740], Brown et al. [197], and Clyne and Holt [322] were not used in deriving the recommended parameters. (Table: 02-25, Note: 02-25) [Back to Table](#)
- E12. $\text{OH} + \text{CHF}_2\text{CHF}_2$ (HFC-134). The preferred rate expression is based on results of the three relative rate measurements by DeMore [413] (which have been recalculated based on the current rate constant recommendations for the $\text{OH} + \text{CH}_3\text{CCl}_3$, $\text{OH} + \text{CH}_2\text{FCF}_3$, and $\text{OH} + \text{CHF}_2\text{CF}_3$ reference reactions). The room temperature value of Clyne and Holt [322] agrees within the 2σ confidence limits. (Table: 02-25, Note: 02-25) [Back to Table](#)
- E13. $\text{OH} + \text{CHF}_2\text{CF}_3$ (HFC-125). The recommended rate expression is derived from a combined fit to the temperature dependence data of Talukdar et al. [1415] and DeMore [413] and the room temperature data of Martin and Paraskevopoulos [973]. The data of Brown et al. [197] and Clyne and Holt [322] were not used in deriving the recommended parameters. (Table: 02-25, Note: 02-25) [Back to Table](#)
- E14. $\text{OH} + \text{CH}_3\text{CHFCH}_3$ (HFC-281ea). The recommended parameters were derived from a fit to the data of DeMore and Wilson [423] who conducted five independent relative rate determinations. Using infrared detection, these investigators based their determinations on the reference reactions of OH

with C_2H_6 , C_3H_8 , and $\text{C}_2\text{H}_5\text{Cl}$. Using gas chromatographic detection, they based their determinations on the reference reactions of OH with C_2H_6 and C_3H_8 . All of the data were recalculated based on the current recommendations for the reference rate constants. (Table: 02-25, Note: 02-25) [Back to Table](#)

- E15. $\text{OH} + \text{CH}_3\text{CH}_2\text{CF}_3$ (HFC-263fb). The recommended value for $k(298\text{ K})$ is an average of the values reported by Nelson et al. [1052] and by Rajakumar et al. [1199]. The temperature dependence is from a fit to the data of Rajakumar et al. [1199]. (Table: 10-6, Note: 10-6, Evaluated: 10-6) [Back to Table](#)
- E16. $\text{OH} + \text{CH}_2\text{FCF}_2\text{CHF}_2$ (HFC-245ca). The absolute rate constant results of Zhang et al. [1685] differ from the relative rate data (Hsu and DeMore [684]) by approximately 30 to 40% over the temperature region of measurement overlap. Both studies, however, derive nearly identical T-dependencies. The recommended rate expression, hence, averages both the $k(298\text{ K})$ and E/R values from these studies (with the results of Hsu and DeMore [684] recalculated using the current recommendation for the rate constant of the $\text{OH} + \text{CH}_4$ reference reaction). (Table: 02-25, Note: 02-25) [Back to Table](#)
- E17. $\text{OH} + \text{CHF}_2\text{CHFCHF}_2$ (HFC-245ea). Nelson et al. [1052] measured the room temperature rate constant for this reaction. Rajakumar et al. [1199] studied the temperature dependence in experiments conducted above and below room temperature. However, this study was complicated by the presence of a reactive impurity as demonstrated by some additional low temperature results obtained with a purified sample. The recommended value for E/R was derived from a fit to the original data from Rajakumar et al. [1199] corrected for the effect of reactive impurities at $T \geq 298\text{ K}$ and the data obtained with the purified sample below 298 K. The recommended value for $k(298\text{ K})$ is an average of the value obtained from this fit and the value reported by Nelson et al. [1052], which are in excellent agreement. (Table: 10-6, Note: 10-6, Evaluated: 10-6) [Back to Table](#)
- E18. $\text{OH} + \text{CH}_2\text{FCHFCF}_3$ (HFC-245eb). The recommended value for $k(298\text{ K})$ is an average of the values reported by Nelson et al. [1052] and by Rajakumar et al. [1199]. The recommended value for E/R was derived from a fit to the data from Rajakumar et al. [1199]. (Table: 10-6, Note: 10-6, Evaluated: 10-6) [Back to Table](#)
- E19. $\text{OH} + \text{CHF}_2\text{CH}_2\text{CF}_3$ (HFC-245fa). The recommended room temperature value is the mean of the values reported by Orkin et al. [1117] and Nelson et al. [1052], which are in good agreement. The temperature dependence is from Orkin et al. The A-factor has been calculated to fit the recommended room temperature value. (Table: 02-25, Note: 02-25) [Back to Table](#)
- E20. $\text{OH} + \text{CH}_2\text{FCF}_2\text{CF}_3$ (HFC-236cb). The recommended rate expression is estimated as being the same as that for the reaction of OH with CH_2FCF_3 (HFC-134a), since these reactions are expected to have very similar Arrhenius parameters. This estimate is preferred over the results reported by Garland et al. [533], the only published experimental study. The A-factor reported in that study is much lower than expected and the reported $E/R = 1107\text{ K}$ is lower than that reported for any similar halocarbon reaction. (Table: 10-6, Note: 10-6, Evaluated: 10-6) [Back to Table](#)
- E21. $\text{OH} + \text{CHF}_2\text{CHFCF}_3$ (HFC-236ea). The recommended value for $k(298\text{ K})$ averages the values reported by Hsu and DeMore [684] by a relative rate method (recalculated based on the current recommendation for the rate constant of the $\text{OH} + \text{CH}_4$ reference reaction) and by Nelson et al. [1052] by an absolute technique. The temperature dependence is from Hsu and DeMore [684], with the A-factor adjusted to fit the recommended room temperature value. The higher and somewhat more scattered values of Garland et al. [533] and Zhang et al. [1685] were not used in deriving the recommended expression. (Table: 02-25, Note: 02-25) [Back to Table](#)
- E22. $\text{OH} + \text{CF}_3\text{CH}_2\text{CF}_3$ (HFC-236fa). The recommended rate expression is derived from a combined fit to the data from the relative rate study of Hsu and DeMore [684] (recalculated based on the current recommendation for the rate constant for the reference reaction $\text{OH} + \text{CHF}_2\text{CF}_3$) and the absolute rate study of Gierczak et al. [547]. The higher results of Nelson et al. [1052] and of Garland and Nelson [534], which superseded the earlier results of Garland et al. [534], were not used. A relative rate determination at room temperature by Barry et al. [103] yields a rate constant in excellent agreement with the recommended value. However, the extremely small rate constant ratio measured

(relative to $\text{OH} + \text{CH}_3\text{CF}_2\text{CH}_2\text{CF}_3$) resulted in fairly large uncertainties. Hence this determination was not directly used in the evaluation. (Table: 02-25, Note: 02-25) [Back to Table](#)

- E23. $\text{OH} + \text{CF}_3\text{CHF}_2\text{CF}_3$ (HFC-227ea). The recommended rate expression is derived from a combined fit to the data (below 400 K) from the absolute studies of Nelson et al. [1048], Zellner et al. [1673], Zhang et al. [1685], and Tokuhashi et al. [1448], and from the relative rate studies of Hsu and DeMore [684] (two determinations which have been recalculated based on the current recommendations for the rate constants for the reference reactions $\text{OH} + \text{CH}_4$ and $\text{OH} + \text{CHF}_2\text{CF}_3$) and Wallington et al. [1552] (two determinations which have been recalculated based on the current recommendations for the rate constants for the reference reactions $\text{OH} + \text{C}_2\text{H}_4$ and $\text{OH} + \text{C}_2\text{H}_2$). (Table: 10-6, Note: 10-6, Evaluated: 10-6) [Back to Table](#)
- E24. $\text{OH} + \text{CH}_3\text{CF}_2\text{CH}_2\text{CF}_3$ (HFC-365mfc). The recommended value of $k(298 \text{ K})$ is an average of the values obtained from fits to the data from the absolute rate study of Mellouki et al. [1008] and of the relative rate study of Barry et al. [103] (renormalized to the current recommendation for the rate constant for the reference reaction $\text{OH} + \text{CH}_3\text{CCl}_3$). The value for E/R is an average of the values for this parameter from the same two studies. (Table: 10-6, Note: 10-6, Evaluated: 10-6) [Back to Table](#)
- E25. $\text{OH} + \text{CF}_3\text{CH}_2\text{CH}_2\text{CF}_3$ (HFC-356mff). The recommended value of $k(298 \text{ K})$ is an average of the values from Nelson et al. [1052] and Zhang et al. [1685]. The temperature dependence is from a fit to the data of Zhang et al. excluding the lowest temperature points (at 260 K), which are somewhat higher than an extrapolation from their other data would indicate. The A-factor has been calculated to fit the recommended room temperature value. (Table: 02-25, Note: 02-25) [Back to Table](#)
- E26. $\text{OH} + \text{CH}_2\text{FCH}_2\text{CF}_2\text{CF}_3$ (HFC-356mcf). The recommended parameters are based on a fit to the data of Nelson et al. [1052]. (Table: 02-25, Note: 02-25) [Back to Table](#)
- E27. $\text{OH} + \text{CHF}_2\text{CF}_2\text{CF}_2\text{CHF}_2$ (HFC-338pcc). The recommended values for both $k(298 \text{ K})$ and E/R are averages of these values taken from the individual fits to the data of Schmoltner et al. [1275] and Zhang et al. [1686]. (Table: 02-25, Note: 02-25) [Back to Table](#)
- E28. $\text{OH} + \text{CF}_3\text{CH}_2\text{CF}_2\text{CH}_2\text{CF}_3$ (HFC-458mfcf). The recommended values for both $k(298 \text{ K})$ and E/R are from a fit to the data of Nelson et al. [1052]. (Table: 02-25, Note: 02-25) [Back to Table](#)
- E29. $\text{OH} + \text{CF}_3\text{CHFCHFCF}_2\text{CF}_3$ (HFC-43-10mee). The recommended rate expression is derived from a combined fit to the data from Schmoltner et al. [1275] and Zhang et al. [1686]. (Table: 02-25, Note: 02-25) [Back to Table](#)
- E30. $\text{OH} + \text{CF}_3\text{CF}_2\text{CH}_2\text{CH}_2\text{CF}_2\text{CF}_3$ (HFC-55-10mccf). The recommended value for $k(298 \text{ K})$ is based on Nelson et al. [1052]. As expected, the rate constant is similar to that for $\text{CF}_3\text{CH}_2\text{CH}_2\text{CF}_3$. Hence the recommendation for E/R is estimated as being approximately the same as for this reaction, with the A-factor calculated to agree with $k(298 \text{ K})$. (Table: 02-25, Note: 02-25) [Back to Table](#)
- E31. $\text{OH} + \text{CH}_2=\text{CHF}$. The recommended parameters were derived from a fit to the data from Baasandorj et al. [73] who found the rate constant to be pressure independent between 20 and 600 Torr, indicating that the high pressure limit is achieved for the reaction of this fluorinated alkene. Since this is the simplest of the halogenated alkenes, it implies that the recommendations for all of the halogenated alkene reactions included in Table 1 represent the high pressure limits for the rate constants. The earlier results of Perry et al. [1157] are ca. 10% larger at room temperature; the agreement is better above room temperature. (Table: 10-6, Note: 10-6, Evaluated: 10-6) [Back to Table](#)
- E32. $\text{OH} + \text{CH}_2=\text{CF}_2$. The recommended parameters were derived from a fit to the data from Baasandorj et al. [73] who found the rate constant to be pressure independent between 20 and 600 Torr indicating that the high pressure limit is achieved for the reaction of this fluorinated alkene. Howard [672] studied this reaction at lower pressures and found a smaller rate constant that increased with pressure between 0.7 Torr and 7 Torr. This dependence is consistent with the recommended high pressure limit from Baasandorj et al. [73]. (Table: 10-6, Note: 10-6, Evaluated: 10-6) [Back to Table](#)
- E33. $\text{OH} + \text{CF}_2=\text{CF}_2$. The recommended value for $k(298 \text{ K})$ is an average of the values determined in the studies of Acerboni et al. [6] (two relative rate determinations referenced to the rate constants for the

reactions of OH with propene and cyclohexane) and the absolute rate studies of Orkin et al. [1118], and Orkin et al. [1125]. The value for E/R is from a fit to the data of Orkin et al. [1125], with the value for A calculated to agree with the recommended value for k(298 K). As discussed in note E31 the recommended rate constant represents the high-pressure limit for this reaction. (Table: 02-25, Note: 10-6, Evaluated: 10-6) [Back to Table](#)

- E34. $\text{OH} + \text{CH}_2=\text{CHCH}_2\text{F}$. The recommended parameters are derived from a fit to the absolute rate data of Albaladejo et al. [19]. As discussed in note E31 the recommended rate constant represents the high pressure limit for this reaction. (Table: 10-6, Note: 10-6, Evaluated: 10-6) [Back to Table](#)
- E35. $\text{OH} + \text{CH}_2=\text{CHCF}_3$. The recommended value for k(298 K) is an average of the values from the absolute rate study by Orkin et al. [1118] and from the two relative studies by Andersen et al. [30] for which the results were recalculated using the current recommendation for the reference reactions of OH with C_2H_4 and C_2H_2 . The recommended value for E/R is from Orkin et al. [1118]. The A factor was calculated to agree with k(298 K). As discussed in note E31 the recommended rate constant represents the high pressure limit for this reaction. (Table: 10-6, Note: 10-6, Evaluated: 10-6) [Back to Table](#)
- E36. $\text{OH} + \text{CH}_2=\text{CFCF}_3$. The recommended parameters are derived from a combined fit at $T \leq 300$ K to the data of Papadimitriou et al. [1140] and Orkin et al. [1126], which supercedes the results of Orkin et al. [1118], which are in excellent agreement with the latter study but are of lower accuracy. The two relative rate determinations at 298 K by Nielsen et al. [1078] recalculated using the current recommendations for the reference reactions of OH with C_2H_4 and C_2H_2 lie within the 95% uncertainty assigned to k(298 K). Papadimitriou et al. [1140] found the rate constant to be pressure independent between 25 and 600 Torr and Orkin et al. [1126] found the rate constant to be pressure independent between 30 and 300 Torr indicating that the high pressure limit is achieved for this reaction. (Table: 10-6, Note: 10-6, Evaluated: 10-6) [Back to Table](#)
- E37. $\text{OH} + E\text{-CHF}=\text{CHCF}_3$. The recommended parameters are derived from a fit to the data of Orkin et al. [1126] at $T \leq 300$ K. Orkin et al. [1126] found the rate constant to be pressure independent between 30 and 200 Torr indicating that the high pressure limit is achieved for this reaction. The two relative rate determinations at 298 K by Sondergaard et al. [1343] recalculated using the current recommendations for the reference reactions of OH with C_2H_4 and C_2H_2 lie about 30% higher than the recommended value. (Table: 10-6, Note: 10-6, Evaluated: 10-6) [Back to Table](#)
- E38. $\text{OH} + E\text{-CHF}=\text{CFCF}_3$. The recommended value for k(298 K) is an average of the two relative rate determinations by Hurley et al. [693] recalculated using the current recommendation for the reaction of OH with the reference compounds (C_2H_4 and C_2H_2). The value for E/R is estimated from that for similar fluorinated propenes, with the A factor calculated to agree with k(298 K). As discussed in note E31 the recommended rate constant represents the high pressure limit for this reaction. (Table: 10-6, Note: 10-6, Evaluated: 10-6) [Back to Table](#)
- E39. $\text{OH} + Z\text{-CHF}=\text{CFCF}_3$. The recommended value for k(298 K) is from Papadimitriou et al. [1140] who found the rate constant to be pressure independent between 25 and 600 Torr indicating that the high pressure limit is achieved for this reaction. The two room temperature values from the relative rate studies by Hurley et al. [693] are in very good agreement with this recommendation. The recommended value for E/R is derived from a fit to the data of Papadimitriou et al. [1140] at $T \leq 300$ K. The A factor was calculated to agree with the value of k(298 K). As discussed in note E31 the recommended rate constant represents the high pressure limit for this reaction. (Table: 10-6, Note: 10-6, Evaluated: 10-6) [Back to Table](#)
- E40. $\text{OH} + \text{CF}_2=\text{CFCF}_3$. The recommended value for k(298 K) is an average of the values reported in the absolute rate constant investigations by McIlroy and Tully [988], Orkin et al. [1118], and Tokuhashi et al. [1451] (two studies). The recommended value for E/R is an average of the values for this parameter obtained from individual fits to the data these four studies at $T \leq 300$ K. The relative rate studies at room temperature (two measurements each by Mashino et al. [978] and by Acerboni et al. [5]) are internally inconsistent even after recalculating the original results using the current recommendations for the reference reactions, and lie systematically higher than the results of the absolute studies. However, the results of Mashino et al. [978] are encompassed by the 95% confidence limits of the current recommendation. The A factor was calculated to agree with the

value of $k(298\text{ K})$. As discussed in note E31 the recommended rate constant represents the high pressure limit for this reaction. (Table: 10-6, Note: 10-6, Evaluated: 10-6) [Back to Table](#)

- E41. $\text{OH} + \text{CH}_2=\text{CHCF}_2\text{CF}_3$. The recommended value for $k(298\text{ K})$ is an average of the two relative study results by Andersen et al. [30], which were recalculated using the current recommendation for the reference reactions of OH with C_2H_4 and C_2H_2 . The recommended value for E/R is estimated as being the same as that for $\text{CH}_2=\text{CHCF}_3$. Actually, Andersen et al. [30] measured the rate constants at $T = 296\text{ K}$ for OH reactions with $\text{CH}_2=\text{CHC}_x\text{F}_{2x+1}$ (for $x=1,2,4,6,8$) and the recommendation given here covers all of these compounds. As discussed in note E31 the recommended rate constant represents the high-pressure limit for this reaction. (Table: 10-6, Note: 10-6, Evaluated: 10-6) [Back to Table](#)
- E42. $\text{OH} + \text{CF}_3\text{OH}$. There are no measurements of the rate coefficient of this reaction. The recommendation is based on the recommended limit for the reverse reaction rate coefficient and an estimated equilibrium constant. The thermochemistry of CF_3O and CF_3OH are taken from *ab initio* calculations (Montgomery et al. [1027] and Schneider and Wallington [1276]) and laboratory measurements (Huey et al. [690]) to estimate $\Delta G^\circ_{298}(\text{OH} + \text{CF}_3\text{OH} \rightarrow \text{CF}_3\text{O} + \text{H}_2\text{O})$ to be about $(2\pm4)\text{ kcal mol}^{-1}$. In considering the large uncertainty in the free energy change, the estimated rate coefficient limit is based on the assumption that the reaction is approximately thermoneutral. (Table: 97-4, Note: 97-4) [Back to Table](#)
- E43. $\text{OH} + \text{CH}_2\text{FCH}_2\text{OH}$. The recommended parameters are from a combined fit to the absolute rate data of Rajakumar et al. [1198] and Orkin et al. [1123] with the former data corrected for an apparent error in the UV absorption cross section of $\text{CH}_2\text{FCH}_2\text{OH}$ (which was used to determine the reactant concentration). When this correction is made, the data from these two studies are indistinguishable. The room temperature rate constant determined in the relative rate study of Sellevag et al. [1292] is about 50% greater than that recommended. (Table: 10-6, Note: 10-6, Evaluated: 10-6) [Back to Table](#)
- E44. $\text{OH} + \text{CHF}_2\text{CH}_2\text{OH}$. The recommended value of $k(298\text{ K})$ is an average of the values reported in the absolute rate studies of Kovacs et al. [819] and Orkin et al. [1123]. The value of E/R is derived from a fit at $T \leq 300\text{ K}$ to the data of Orkin et al. [1123], which are the only temperature dependant data available. The room temperature rate constant determined in the relative rate study of Sellevag et al. [1292] is about 80% greater than that recommended. (Table: 10-6, Note: 10-6, Evaluated: 10-6) [Back to Table](#)
- E45. $\text{OH} + \text{CF}_3\text{CH}_2\text{OH}$. The recommended value for $k(298\text{ K})$ is an average of the values reported in the absolute rate studies of Wallington et al. [1546], Inoue et al. [715], Tokuhashi et al. [1449] (two independent studies), Kovacs et al. [819], and Orkin et al. [1123], and the relative rate study of Hurley et al. [694] (using C_2H_2 as the reference reactant). The value of $k(298\text{ K})$ reported by Sellevag et al. [1292] is significantly larger than that from all of the other studies and was not used in deriving the recommended value. The recommended value for E/R is an average of the values derived from fits to the data below 300 K of Tokuhashi et al. [1449] and Orkin et al. [1123]. The A factor was calculated to agree with the recommended value for $k(298\text{ K})$. (Table: 10-6, Note: 10-6, Evaluated: 10-6) [Back to Table](#)
- E46. $\text{OH} + \text{CF}_3\text{CF}_2\text{CH}_2\text{OH}$. The recommended parameters were derived from a combined fit to the data below 400 K from Tokuhashi et al. [1449] (two independent absolute studies) and the relative rate studies of Chen et al. [285] (recalculated based on the current recommendation for the rate constant for the $\text{OH} + \text{CH}_2\text{Cl}_2$ reference reaction) and Hurley et al. [694] (recalculated based on the current recommendation for the rate constant for the $\text{OH} + \text{C}_2\text{H}_2$ reaction). (Table: 10-6, Note: 10-6, Evaluated: 10-6) [Back to Table](#)
- E47. $\text{OH} + (\text{CF}_3)_2\text{CHOH}$. The recommended parameters were derived from a fit to the data (below 400 K) of Tokuhashi et al. [1449] (three independent absolute measurement studies). (Table: 10-6, Note: 10-6, Evaluated: 10-6) [Back to Table](#)
- E48. $\text{OH} + \text{CF}_3\text{CF}_2\text{CF}_2\text{CF}_2\text{CH}_2\text{OH}$. The recommended value of $k(298\text{ K})$ is from Hurley et al. [694], a relative rate study using C_2H_2 as the reference reactant. The recommended value for E/R is estimated

as being the same as that for the reaction of OH with $\text{CF}_3\text{CF}_2\text{CH}_2\text{OH}$. (Table: 10-6, Note: 10-6, Evaluated: 10-6) [Back to Table](#)

- E49. $\text{OH} + \text{CH}_3\text{OCHF}_2$ (HFE-152a). The recommended rate expression is derived from a fit to the data of Orkin et al. [1121] below 400 K. (Table: 02-25, Note: 02-25) [Back to Table](#)
- E50. $\text{OH} + \text{CH}_3\text{OCF}_3$ (HFE-143a). The recommended rate expression is derived from a combined fit to the data of Orkin et al. [1121], Hsu and DeMore [685] (two relative rate determinations which have been recalculated based on the current recommendations for the rate constants of the $\text{OH} + \text{CH}_3\text{CHF}_2$ and $\text{OH} + \text{CH}_2\text{F}_2$ reference reactions), and Chen et al. [286] (two relative rate determinations which have been recalculated based on the current recommendations for the rate constants of the $\text{OH} + \text{CH}_4$ and $\text{OH} + \text{CH}_3\text{CCl}_3$ reference reactions). The renormalization procedure for relative rate measurements referenced to the $\text{OH} + \text{CH}_3\text{CHF}_2$ reaction is discussed in the note for that reaction. The room temperature result of Zhang et al. [1688] was not used in the derivation since it is significantly higher than the values of the other studies and may be influenced by the presence of reactive impurities. (Table: 10-6, Note: 10-6, Evaluated: 10-6) [Back to Table](#)
- E51. $\text{OH} + \text{CHF}_2\text{OCHF}_2$ (HFE-134). The recommended values of $k(298\text{ K})$ and E/R were derived from a combined fit to the data of Hsu and DeMore [685] (a relative rate study whose results have been recalculated using the current recommendation for the rate constant of the $\text{OH} + \text{CH}_3\text{CCl}_3$ reference reaction), Orkin et al. [1127], and Wilson et al. [1619]. The more scattered measurements of Garland et al. [533] were not used in derivation of the preferred value. (Table: 02-25, Note: 02-25) [Back to Table](#)
- E52. $\text{OH} + \text{CHF}_2\text{OCF}_3$ (HFE-125). The recommended rate expression is based on results of the relative rate study of Hsu and DeMore [685] (recalculated using the rate constant for the CHF_3 reference reaction given in this evaluation). Additional measurements by Hsu and DeMore [685] relative to CHF_2CF_3 and CH_4 are encompassed well within the 2σ uncertainty limits, but were not used for assigning the recommended rate expression due to the large differences in reactivity between these two species and the target molecule. The room temperature result of Zhang et al. [1688] lies significantly higher than the recommended value, possibly due to the presence of reactive impurities in the sample. (Table: 02-25, Note: 02-25) [Back to Table](#)
- E53. $\text{OH} + \text{CH}_3\text{OCHF}_2\text{CF}_3$. The recommended parameters were derived from a combined fit to the data from two relative rate studies by Chen et al. [289], which were recalculated using the rate constants for the reactions of reference species (C_2H_6 and CH_3CHF_2) given in this evaluation. Following this recalculation the results from the two studies are in far better agreement than originally presented by the authors. (Table: 10-6, Note: 10-6, Evaluated: 10-6) [Back to Table](#)
- E54. $\text{OH} + \text{CH}_3\text{OCF}_2\text{CHF}_2$. The recommended parameters were derived from a fit to the data (below 400 K) of Tokuhashi et al. [1453] (two independent absolute measurement studies). A room temperature measurement by Heathfield et al. [624] is nearly an order of magnitude higher than recommended and may be affected by reactive impurities. (Table: 02-25, Note: 02-25) [Back to Table](#)
- E55. $\text{OH} + \text{CH}_3\text{OCF}_2\text{CF}_3$. The recommended parameters were derived from a fit to the data (below 400 K) of Tokuhashi et al. [1452] (two independent absolute measurement studies). The expression, as expected, is similar to those for the $\text{OH} + \text{CH}_3\text{OCF}_3$ and $\text{OH} + \text{CH}_3\text{OCF}_2\text{CF}_2\text{CF}_3$ reactions. (Table: 02-25, Note: 02-25) [Back to Table](#)
- E56. $\text{OH} + \text{CHF}_2\text{OCH}_2\text{CF}_3$ (HFE-245fa). The recommended value of $k(298\text{ K})$ is an average of the values reported in the absolute studies of Zhang et al. [1688] and Orkin et al. [1121] and in the relative rate study of Oyaro et al. [1136] (relative to the reactions of OH with CH_3CCl_3 and $\text{CHF}_2\text{CH}_2\text{F}$). The recommended value of E/R is derived from a fit to the data of Orkin et al. [1121] below 400 K. (Table: 10-6, Note: 10-6, Evaluated: 10-6) [Back to Table](#)
- E57. $\text{OH} + \text{CHF}_2\text{OCHF}_2\text{CF}_3$. The recommended value for $k(298\text{ K})$ is an average of the values obtained in the two relative rate studies of Oyaro et al. [1136] (relative to the reactions of OH with CH_3CCl_3 and $\text{CHF}_2\text{CH}_2\text{F}$) and in the absolute study of Langbein et al. [851]. The value of $f(298\text{ K})$ was chosen to encompass the value of $k(298\text{ K})$ recommended for $\text{CHF}_2\text{OCHF}_2$. The recommended value for E/R is estimated as being similar to that for $\text{CHF}_2\text{OCHF}_2$. (Table: 10-6, Note: 10-6, Evaluated: 10-6) [Back to Table](#)

- E58. $\text{OH} + \text{CHF}_2\text{OCF}_2\text{CHF}_2$. The recommended value for $k(298\text{ K})$ is an average of the relative rate determinations of Chen et al. [288] (2 studies) and Wilson et al. [1617] (2 studies), all of which were normalized to the current recommendations for the reference reactions of OH with $\text{CH}_3\text{OCF}_2\text{CF}_3$ and $\text{CH}_3\text{OCF}_2\text{CF}_2\text{CF}_3$ (Chen et al. [288]) and HFC-134a and HFC-143a (Wilson et al. [1617]). The recommended value for E/R is from a combined fit to the data of Chen et al. [288] and Wilson et al. [1617] after the data were normalized to the recommended value of $k(298\text{ K})$. (Table: 10-6, Note: 10-6, Evaluated: 10-6) [Back to Table](#)
- E59. $\text{OH} + \text{CF}_3\text{OCHFCF}_3$. The recommended value for $k(298\text{ K})$ is an average of the values reported in the relative rate studies of Takahashi et al. [1407] (two studies using C_2H_4 and C_2H_2 as the reference reactants) and Oyaro et al. [1136] (using HFC-143 as the reference) and in the two absolute studies of Tokuhashi et al. [1448]. The $k(298\text{ K})$ value reported by Li et al. [907] is approximately a factor of 5 greater than that recommended. The recommended value of E/R comes from a fit to the data of Tokuhashi et al. [1448] below 400 K. (Table: 10-6, Note: 10-6, Evaluated: 10-6) [Back to Table](#)
- E60. $\text{OH} + \text{CH}_3\text{OCF}_2\text{CF}_2\text{CF}_3$. The recommended value for $k(298\text{ K})$ is an average of the values reported by Tokuhashi et al. [1452] (two independent absolute measurement studies) and Nonomiya et al. [1097] (two relative rate determinations which have been recalculated based on the current recommendations for the rate constants of the $\text{OH} + \text{CH}_4$ and $\text{OH} + \text{CH}_3\text{Cl}$ reference reactions). The value for E/R was determined from a fit to the data (below 400 K) of Tokuhashi et al. and the A factor calculated to agree with the value for $k(298\text{ K})$. The expression, as expected, is similar to those for the $\text{OH} + \text{CH}_3\text{OCF}_3$ and $\text{OH} + \text{CH}_3\text{OCF}_2\text{CF}_3$ reactions. (Table: 02-25, Note: 02-25) [Back to Table](#)
- E61. $\text{OH} + \text{CH}_3\text{OCF}(\text{CF}_3)_2$. The recommended parameters were derived from a fit to the data (below 400 K) of Tokuhashi et al. [1452] (three independent absolute measurement studies). The recommended uncertainties were set to encompass the recommendation for the similar $\text{OH} + \text{CH}_3\text{OCF}_3$ and $\text{OH} + \text{CH}_3\text{OCF}_2\text{CF}_3$ reactions. (Table: 10-6, Note: 10-6, Evaluated: 10-6) [Back to Table](#)
- E62. $\text{OH} + \text{CH}_3\text{OC}_4\text{F}_9$. The recommendation for $k(298\text{ K})$ is based on the relative rate measurements by Wallington et al. [1560] using CH_3Cl as the reference reactant. Measurements in the same study using CH_4 as the reference reactant are in general agreement, but exhibit more scatter. The recommendation is consistent with ones for the similar compounds: CH_3OCF_3 and $\text{CH}_3\text{OC}_2\text{F}_5$, and $\text{CH}_3\text{OC}_3\text{F}_7$. A relative rate study by Cavalli et al. at 298 K [268] yielded a rate constant about 60% lower than recommended. The recommended value for E/R is estimated to be approximately equal to that for the reactions of OH with $\text{CH}_3\text{OC}_2\text{F}_5$ and $\text{CH}_3\text{OC}_3\text{F}_7$. (Table: 10-6, Note: 10-6, Evaluated: 10-6) [Back to Table](#)
- E63. $\text{OH} + \text{CHF}_2\text{OCH}_2\text{CF}_2\text{CHF}_2$. The recommended parameters were derived from a fit to the data (below 400 K) of Tokuhashi et al. [1453] (two independent absolute measurement studies). (Table: 02-25, Note: 02-25) [Back to Table](#)
- E64. $\text{OH} + \text{CHF}_2\text{OCH}_2\text{CF}_2\text{CF}_3$. The recommended parameters were derived from a fit to the data (below 400 K) of Tokuhashi et al. [1453] (two independent absolute measurement studies). (Table: 02-25, Note: 02-25) [Back to Table](#)
- E65. $\text{OH} + \text{CHF}_2\text{OCH}(\text{CF}_3)_2$. The recommended parameters are obtained from a combined fit to the data from two relative rate studies by Wilson et al. [1617] with each renormalized to the current recommendations for the reactions of OH with the reference compounds, HFC-134a and HFC-143a. (Table: 10-6, Note: 10-6, Evaluated: 10-6) [Back to Table](#)
- E66. $\text{OH} + \text{CH}_3\text{CH}_2\text{OCF}_2\text{CHF}_2$. The recommended parameters are from a combined fit to the data obtained by Tokuhashi et al. [1450] (3 absolute studies) below 400 K. A room temperature rate constant determined by Heathfield et al. [624] is about a factor of two greater than that recommended. (Table: 10-6, Note: 10-6, Evaluated: 10-6) [Back to Table](#)
- E67. $\text{OH} + \text{CF}_3\text{CH}_2\text{OCH}_2\text{CF}_3$. The recommended value for $k(298\text{ K})$ is an average of the rate constants measured in the absolute study of Orkin et al. [1127] and in the relative rate studies of Oyaro et al. [1135] and Wilson et al. [1617] (2 studies). The relative rate data were recalculated using the recommendations in this evaluation for the OH reactions with the reference compound (CHCl_3 for Oyaro et al. [1135] and HFC-152a and HFC-161 for Wilson et al. [1617]). The recommended value

for E/R is an average of the values for this parameter derived from fits to the Orkin et al. [1127] and Wilson et al. [1617] data. The A factor was calculated to agree with the recommended value for $k(298\text{ K})$. (Table: 10-6, Note: 10-6, Evaluated: 10-6) [Back to Table](#)

- E68. $\text{OH} + \text{CF}_3\text{CH}_2\text{OCF}_2\text{CHF}_2$. The recommended value for $k(298\text{ K})$ is an average of the rate constants measured in the absolute study of Tokuhashi et al (3 studies) [1453] and in the relative rate experiments of Chen et al. [290] (2 studies relative to CH_3CCl_3 and CHF_2Cl) and of Wilson et al. [1617] (2 studies relative to HFC-152a and HFC-32). All results of the relative rate studies were renormalized using the current recommendations for the reference reactions. The recommended value of E/R is from a combined fit to the data from all three groups following normalization of the data to the recommended value of $k(298\text{ K})$. The A factor was calculated to agree with the recommended value for $k(298\text{ K})$. The room temperature rate constant reported by Heathfield et al. [624] is about an order or magnitude greater than that from any of the other investigations and was not used to derive the recommendations given here. (Table: 10-6, Note: 10-6, Evaluated: 10-6) [Back to Table](#)
- E69. $\text{OH} + \text{CHF}_2\text{OCF}_2\text{OCHF}_2$. The recommended value for $k(298\text{ K})$ is from the relative rate study by Cavalli et al. [268] renormalized to the current recommendation for the reference reaction of $\text{OH} + \text{CH}_4$. The value for $k(298\text{ K})$ is identical to that for $\text{CHF}_2\text{OCHF}_2$, whose reactivity might be expected to be a bit higher. The value for E/R is estimated as being similar to that for the reaction of OH with $\text{CHF}_2\text{OCHF}_2$. The A factor has been calculated to agree with the value of $k(298\text{ K})$. (Table: 10-6, Note: 10-6, Evaluated: 10-6) [Back to Table](#)
- E70. $\text{OH} + \text{CHF}_2\text{OCF}_2\text{CF}_2\text{OCHF}_2$. The recommended value for $k(298\text{ K})$ is from the relative rate study by Cavalli et al. [268] renormalized to the current recommendation for the reference reaction of $\text{OH} + \text{CH}_4$. However, the value for $k(298\text{ K})$ is inexplicably a factor of two greater than that measured in the same study for $\text{CHF}_2\text{OCF}_2\text{OCHF}_2$, whose reactivity might be expected to be the same or even a bit higher. Hence the value of $f(298\text{ K})$ was selected accordingly. As with $\text{CHF}_2\text{OCF}_2\text{OCHF}_2$, the value for E/R is estimated as being similar to that for the reaction of OH with $\text{CHF}_2\text{OCHF}_2$. The A factor has been calculated to agree with the value of $k(298\text{ K})$. (Table: 10-6, Note: 10-6, Evaluated: 10-6) [Back to Table](#)
- E71. $\text{OH} + \text{CHF}_2\text{OCF}_2\text{CF}_2\text{OCF}_2\text{OCHF}_2$. The recommended value for $k(298\text{ K})$ is from the relative rate study by Cavalli et al. [268] renormalized to the current recommendation for the reference reaction of $\text{OH} + \text{CH}_4$. The value for $k(298\text{ K})$ is almost the same as that measured for $\text{CHF}_2\text{OCF}_2\text{CF}_2\text{OCHF}_2$ in the same study. For both compounds, the measured values for $k(298\text{ K})$ are inexplicably a factor of two greater than that measured in the same study for $\text{CHF}_2\text{OCF}_2\text{OCHF}_2$, whose reactivity might be expected to be the same or even a bit higher. Hence the value of $f(298\text{ K})$ was selected accordingly. As with $\text{CHF}_2\text{OCF}_2\text{OCHF}_2$ and $\text{CHF}_2\text{OCF}_2\text{CF}_2\text{OCHF}_2$ the value for E/R is estimated as being similar to that for the reaction of OH with $\text{CHF}_2\text{OCHF}_2$. The A factor has been calculated to agree with the value of $k(298\text{ K})$. (Table: 10-6, Note: 10-6, Evaluated: 10-6) [Back to Table](#)
- E72. $\text{F} + \text{O}_3$. The recommended value is based on results of the room temperature study of Bedzhanyan et al. [139] and the temperature-dependent study of Wagner et al. [1533]. The value appears to be quite reasonable in view of the well-known reactivity of atomic chlorine with O_3 . (Table: 94-26, Note: 94-26) [Back to Table](#)
- E73. $\text{F} + \text{H}_2$. The value of k at 298 K seems to be well established with the results reported by Zhitneva and Pshezhetskii [1691], Heidner et al. [625, 626], Wurzburg and Houston [1647], Dodonov et al. [444], Clyne et al. [327], Bozzelli [187], Igoshin et al. [709], Clyne and Hodgson [320] and Stevens et al. [1367] being in excellent agreement (range of k being $2.3\text{--}3.0 \times 10^{-11}\text{ cm}^3\text{ molecule}^{-1}\text{ s}^{-1}$). The preferred value at 298 K is taken to be the mean of the values reported in these references. Values of E/R range from 433–595 K (Heidner et al.; Wurzburg and Houston; Igoshin et al.; and Stevens et al.). The preferred value of E/R is derived from a fit to the data in these studies. The A-factor was chosen to fit the recommended room temperature value. (Table: 90-1, Note: 90-1) [Back to Table](#)
- E74. $\text{F} + \text{H}_2\text{O}$. The recommended temperature-independent value is based on results reported in the study by Stevens et al. [1367] over the temperature range 240–373 K using a discharge flow system with chemical conversion of fluorine atoms to deuterium atoms and detection of the latter by resonant

fluorescence. This value is in excellent agreement with the room temperature results of Frost et al. [528] and Walther and Wagner [1562]. The latter authors in a limited temperature-dependent study reported an E/R value of 400 K. Although these data have not been included in the derivation of the preferred value, with the exception of the one low temperature data point, they are encompassed within the indicated uncertainty limits. (Table: 90-1, Note: 90-1) [Back to Table](#)

- E75. $F + HNO_3$. The recommendation is based on results of the temperature-dependent study of Wine et al. [1633] and the room temperature results of Mellouki et al. [1000], Rahman et al. [1195] and Becker et al. [118]. The values at room temperature are in good agreement. The study of Wine et al. [1633] was over the temperature range 260–373 K. Below 320 K the data were fitted with the Arrhenius expression recommended here, whereas at higher temperatures a temperature-independent value was found, suggesting the occurrence of different mechanisms in the two temperature regimes. (Table: 90-1, Note: 90-1) [Back to Table](#)
- E76. $F + CH_4$. The recommended room temperature value is the mean of the results of Wagner et al. [1531], Clyne et al. [327], Kompa and Wanner [816], Foon and Reid [516], Fasano and Nogar [497], and Persky et al. [1161]. The temperature dependence is that reported by Persky et al. in a competitive study using the reaction $F + D_2$ as the reference reaction. These results are preferred over the temperature dependences reported in the earlier studies of Wagner et al. and Foon and Reid. (Table: 97-4, Note: 97-4) [Back to Table](#)
- E77. $FO + O_3$. The recommended upper limit is based on the results of Li et al. [905] in a study using a discharge flow-mass spectrometric technique. FO was produced in the reaction of F atoms with excess O_3 . No appreciable decay of FO, and only a small increase in FO_2 , was detected, allowing an upper limit to the rate constant of $10^{-14} \text{ cm}^3 \text{ molecule}^{-1} \text{ s}^{-1}$ to be derived. A two orders of magnitude higher upper limit was derived by Sehested et al. [1291]. A lower value of the upper limit was derived by Colussi and Grela [345] from a re-analysis of data on the quantum yields for ozone destruction in F_2/O_3 mixtures reported by Starrico et al. [1356]. The results of the recent, more direct, study of Li et al. [905] are preferred over the earlier results of Starrico et al. There are two possible pathways which are exothermic, resulting in the production of $F + 2O_2$ or $FO_2 + O_2$. (Table: 97-4, Note: 97-4) [Back to Table](#)
- E78. $FO + NO$. The recommended value is based on results of the temperature-dependent study of Bedzhanyan et al. [137] and the value reported by Ray and Watson [1221] for k at 298 K using the discharge flow-mass spectrometric technique. (Table: 94-26, Note: 94-26) [Back to Table](#)
- E79. $FO + FO$. The recommended value is based on the results of Bedzhanyan et al. [138] and Clyne and Watson [338]. Wagner et al. [1533], in a less direct study, report a higher value. The results of Bedzhanyan et al. indicate the predominant reaction channel is that to produce $2F + O_2$. (Table: 94-26, Note: 94-26) [Back to Table](#)
- E80. $FO_2 + O_3$. The recommended value is based on results of Sehested et al. [1291]. A higher upper limit has been reported by Li et al. [905]. (Table: 94-26, Note: 97-4) [Back to Table](#)
- E81. $FO_2 + NO$. The recommended values are based on results of Li et al. [905], the only temperature-dependent study. The room temperature value is nearly a factor of 2 less than the previous recommendation, which was based on the results of Sehested et al. [1291]. (Table: 97-4, Note: 97-4) [Back to Table](#)
- E82. $FO_2 + NO_2$. Recommended values are based on the results of Li et al. [905], the only temperature-dependent study. The room temperature value is a factor of 2.5 less than the previous recommendation, which was based on the results of Sehested et al. [1291]. This discrepancy might be attributable to a small NO impurity in the NO_2 sample used in the Sehested et al. study. (Table: 97-4, Note: 97-4) [Back to Table](#)
- E83. $FO_2 + CO$. The recommended value is based on results of Sehested et al. [1291], the only published study of this reaction. (Table: 94-26, Note: 94-26) [Back to Table](#)
- E84. $FO_2 + CH_4$. The recommended value is based on results of Li et al. [905]. This upper limit is a factor of 20 less than the previously recommended upper limit, which was based on the results of Sehested et al. [1291]. (Table: 97-4, Note: 97-4) [Back to Table](#)

- E85. $\text{CF}_3\text{O} + \text{O}_2$. The recommendation is based upon the results of Turnipseed et al. [1476] who reported $k(373 \text{ K}) \leq 4 \times 10^{-17} \text{ cm}^3 \text{ molecule}^{-1} \text{ s}^{-1}$. Assuming an E/R of 5000 K, which is equal to the reaction endothermicity, yields the recommended A and $k(298 \text{ K})$ limits. By comparison to other reactions involving abstraction by O_2 the A- factor is likely to be much smaller. (Table: 94-26, Note: 94-26) [Back to Table](#)
- E86. $\text{CF}_3\text{O} + \text{O}_3$. The recommendation is based on the average of room temperature measurements reported by Turnipseed et al. [1476], Wallington and Ball [1542], and Bourbon et al. [183]. Turnipseed et al. and Bourbon et al. made direct measurements using LIF detection of CF_3O with pulsed photolysis and flow tube reactors, respectively. Wallington and Ball used a competitive reaction scheme with IR absorption detection and $\text{CF}_3\text{O} + \text{CH}_4$ as the reference reaction. The recommended A factor is estimated by comparison to other CF_3O reactions, and the E/R is calculated to agree with the recommended $k(298 \text{ K})$. Upper limits reported by Maricq and Sente [962], Nielsen and Sehested [1081], and Wallington et al. [1553] are consistent with the $k(298 \text{ K})$ recommendation. Measurements reported by Fockenberg et al. [514] and Meller and Moortgat [996] gave rate coefficients about an order of magnitude less than the recommended value. Although the reason for this discrepancy is not known, both studies appear to have the possibility of significant secondary chemistry. The reaction products have not been observed. (Table: 97-4, Note: 97-4) [Back to Table](#)
- E87. $\text{CF}_3\text{O} + \text{H}_2\text{O}$. The recommendation is based upon the measurement $k(381 \text{ K}) \leq 2 \times 10^{-16} \text{ cm}^3 \text{ molecule}^{-1} \text{ s}^{-1}$ reported by Turnipseed et al. [1474]. The A factor is estimated and the E/R is calculated to fit $k(381 \text{ K})$. The limits $k = (0.2\text{--}40) \times 10^{-17} \text{ cm}^3 \text{ molecule}^{-1} \text{ s}^{-1}$ at $296 \pm 2 \text{ K}$ given by Wallington et al. [1554] are consistent with the recommendation. (Table: 94-26, Note: 94-26) [Back to Table](#)
- E88. $\text{CF}_3\text{O} + \text{NO}$. The recommendation is based upon the room temperature rate coefficients reported by Sehested and Nielsen [1289], Turnipseed et al. [1476], and Jensen et al. [737] which are in very good agreement. An earlier low value given by Bevilacqua et al. [150] is superseded by Jensen et al. The temperature-dependence is derived from measurements by Turnipseed (233–360 K) and Jensen et al. (231–393 K). Room temperature results from Bourbon et al. [184] and Bhatnagar and Carr [152] and a temperature dependence study by Dibble et al. [430] are in good agreement with the recommendation. The reaction products have been reported by Chen et al. [282], Bevilacqua et al. [150], Bhatnagar and Carr [152], and Dibble et al. [430] (Table: 94-26, Note: 97-4) [Back to Table](#)
- E89. $\text{CF}_3\text{O} + \text{NO}_2$. There are no published measurements of the rate coefficient for this reaction. The reaction products have been reported by Chen et al. [281] who used photolysis of CF_3NO to prepare CF_3O_2 and subsequently CF_3O in 700 Torr of air at $297 \pm 2 \text{ K}$. They considered two product channels: (a) CF_3ONO_2 obtained via three-body recombination and (b) $\text{CF}_2\text{O} + \text{FNO}_2$ obtained via fluorine transfer. Products from both channels were observed and found to be thermally stable in their reactor. They report $k_a/(k_a + k_b) \geq 90\%$ and $k_b/(k_a + k_b) \leq 10\%$, thus the formation of CF_3ONO_2 is the dominant channel at 700 torr and 297 K. (Table: 94-26, Note: 94-26) [Back to Table](#)
- E90. $\text{CF}_3\text{O} + \text{CO}$. The kinetics of this reaction were studied by Turnipseed et al. [1474], who used pulsed laser photolysis with pulsed laser-induced fluorescence detection and a flow tube reactor with chemical ionization detection to obtain data at temperatures from 233 to 332 K and at pressures from 0.8 to about 300 Torr in He and at about 300 Torr in SF_6 . The reaction was found to be predominantly a three-body recombination, presumably producing CF_3OCO as described in Table 2. The bimolecular reaction has at least two product channels: (a) $\text{CF}_2\text{O} + \text{CFO}$ and (b) $\text{CF}_3 + \text{CO}_2$. The recommended bimolecular rate coefficient limit is derived from the low pressure results of Turnipseed et al., where the reaction was in the fall-off region. Their low pressure data indicate that $k_b < 4 \times 10^{-16} \text{ cm}^3 \text{ molecule}^{-1} \text{ s}^{-1}$ at 298 K. The fate of the CF_3OCO adduct is uncertain, and it may lead to the regeneration of CF_3 or CF_3O radicals in the atmosphere. Wallington and Ball [1543] report a yield of $96 \pm 8\%$ CO_2 at one atmosphere and $296 \pm 2 \text{ K}$. (Table: 94-26, Note: 97-4) [Back to Table](#)
- E91. $\text{CF}_3\text{O} + \text{CH}_4$. The absolute rate coefficients reported by Saathoff and Zellner [1248], Barone et al. [101], Jensen et al. [737], Bourbon et al. [185], and Bednarek et al. [136] at room temperature are in

excellent agreement. Kelly et al. [772] used a relative method with FTIR detection to determine the ratio $k(\text{CF}_3\text{O} + \text{CH}_4)/k(\text{CF}_3\text{O} + \text{C}_2\text{H}_6) = R = 0.01 \pm 0.001$ at 298 ± 2 K. This does not agree with the ratio of our recommended values, which is 0.017. A relative rate measurement reported by Chen et al. [283] using FTIR methods also gives a low result for the rate coefficient. A relative rate measurement reported by Wallington and Ball [1543], $R = 0.0152 \pm 0.0023$ at 296 K, is in good agreement with the recommended rate coefficients. The temperature dependence is from the data of Barone et al. (247–360 K), Jensen et al. (231–385 K), and Bednarek et al. (235–401 K), who agree very well. Measurements at higher temperatures by Bourbon et al. (296–573 K) give a higher E/R (1606 K). The $k(298 \text{ K})$ is the average of the three absolute studies. The CF_3OH product was observed by Jensen et al. and Bevilacqua et al. [150]. (Table: 97-4, Note: 97-4) [Back to Table](#)

- E92. $\text{CF}_3\text{O} + \text{C}_2\text{H}_6$. The room temperature recommendation is based on results reported by Saathoff and Zellner [1248], Barone et al. [101], and Bourbon et al. [185]. These studies are in excellent agreement. Chen et al. [283] measured the rate coefficient relative to that for the $\text{CF}_3\text{O} + \text{NO}$ reaction in 700 Torr of air at 297 K. Their ratio is in good agreement with the values recommended in this evaluation. Kelly et al. [772] used a relative method with FTIR detection to determine the ratio $k(\text{CF}_3\text{O} + \text{CH}_4)/k(\text{CF}_3\text{O} + \text{C}_2\text{H}_6) = 0.01 \pm 0.001$ at 298 ± 2 K. This does not agree with the ratio of our recommended values, which is 0.017. A relative rate measurement reported by Wallington and Ball [1543], $R = 0.0152 \pm 0.0023$ at 296 K is in good agreement with the recommended rate coefficients. The temperature dependence is from the work of Barone et al., who studied the reaction over the temperature range from 233 to 360 K. Measurements by Bourbon et al. (295–573 K) gave a higher E/R (642 K). The products are inferred by analogy to other reactions of CF_3O with organic compounds. (Table: 97-4, Note: 97-4) [Back to Table](#)
- E93. $\text{CF}_3\text{O}_2 + \text{O}_3$. The recommended upper limit is given by the measurements reported by Ravishankara et al. [1212] who used chemical ionization detection of CF_3O_2 with a flow tube reactor. No measurable reaction was observed in their study. The less direct studies of Nielsen and Sehested [1081], Maricq and Szenté [962] and Turnipseed et al. [1476] report somewhat larger upper limits to the rate coefficient. An observable reaction was reported in an indirect measurement by Meller and Moortgat [996]. Their result for the $\text{CF}_3\text{O} + \text{O}_3$ reaction is not consistent with the value recommended above. Their study may have interference from unknown reactions. The products are assumed to be $\text{CF}_3\text{O} + 2\text{O}_2$. (Table: 94-26, Note: 94-26) [Back to Table](#)
- E94. $\text{CF}_3\text{O}_2 + \text{CO}$. The recommended upper limit is reported by Turnipseed et al. [1474] who used chemical ionization mass spectrometric detection of CF_3OO with a flow tube reactor at 296 K. This result is at odds with an earlier study by Czarnowski and Schumacher [378], who deduced a "fast reaction" when they observed the thermal decomposition of $\text{CF}_3\text{OOOCF}_3$ to accelerate in the presence of CO at 315–343 K. It is possible that the reaction of CF_3O with CO could account for their observations. (Table: 94-26, Note: 94-26) [Back to Table](#)
- E95. $\text{CF}_3\text{O}_2 + \text{NO}$. The recommendation is an average of the room temperature rate coefficients reported by Plumb and Ryan [1175], Dognon et al. [446], Peeters et al. [1154], Bevilacqua et al. [150], Sehested and Nielsen [1289], Turnipseed et al. [1476], Bourbon et al. [184], and Bhatnagar and Carr [152], all of whom are in excellent agreement. The temperature dependence is derived from the results of Dognon et al. Several studies have confirmed the identity of the products. (Table: 97-4, Note: 97-4) [Back to Table](#)
- F1. $\text{O} + \text{ClO}$. There have been six studies of this rate constant over an extended temperature range using a variety of techniques: Leu [899]; Margitan [959]; Schwab et al. [1281]; Ongstad and Birks [1116]; Nicovich et al. [1073] and Goldfarb et al. [564]. The recommended value is based on a least squares fit to the data reported in these studies and in the earlier studies of Zahniser and Kaufman [1669] and Ongstad and Birks [1115]. Values reported in the early studies of Bemand et al. [143] and Clyne and Nip [332] are significantly higher and were not used in deriving the recommended value. Leu and Yung [894] were unable to detect $\text{O}_2(^1\Delta)$ or $\text{O}_2(^1\Sigma)$ and set upper limits to the branching ratios for their production of 4.4×10^{-4} and 2.5×10^{-2} respectively. (Table: 10-6, Note: 10-6, Evaluated: 10-6) [Back to Table](#)
- F2. $\text{O} + \text{OCIO}$. The recommended value is based on results of the DF-RF study of Gleason et al. [561]. Over the temperature range from 400 K down to 240 K their data are well fitted by this Arrhenius

expression, but at lower temperatures down to 200 K their data show an abrupt change to a negative temperature dependence. At 200 K the value measured is a factor of 3 higher than that calculated from the Arrhenius expression. It appears that the earlier experiments of Bemand et al. [143], were complicated by secondary chemistry. The low temperature data of Gleason et al. qualitatively support the results of Colussi and Colussi et al. over an extended pressure range that demonstrate the importance of the termolecular reaction $O + OClO + M \rightarrow ClO_3 + M$ (see entry for this reaction in Table 2). Mauldin et al. [981] also observed product formation at low temperatures and higher pressures that is consistent with adduct formation. It should be noted that the termolecular rate constants derived by Gleason et al. on the basis of their low temperature data are not consistent with the termolecular rate constant expression recommended in this evaluation (factor of 3 difference). (Table: 10-6, Note: 10-6, Evaluated: 10-6) [Back to Table](#)

- F3. $O + Cl_2O$. Recommended value is based on the results of Stevens and Anderson [1366] and Miziolek and Molina [1022], which are in good agreement. The significantly lower values of Wecker et al. [1592] are not included, nor are earlier results by Basco and Dogra [108] and Freeman and Phillips [520] due to data analysis difficulties in both studies. (Table: 10-6, Note: 94-26, Evaluated: 10-6) [Back to Table](#)
- F4. $O + HCl$. The preferred value is based on the results of Brown and Smith [200], Wong and Belles [1640], Ravishankara et al. [1210], Hack et al. [597], Singleton and Cvetanovic [1318] and Mahmud et al. [954] near 300 K, but not on the results reported by Balakhnin et al. [79] which are substantially higher. A large uncertainty is attached to the temperature dependence below room temperature due to the limited number and range (no data below 290 K) of measurements. (Table: 10-6, Note: 10-6, Evaluated: 10-6) [Back to Table](#)
- F5. $O + HOCl$. Recommended value is based on results of Schindler et al. [1270]. In this study the rate constant was found to be practically independent of temperature in the range 213–298 K. Product analysis indicated that Cl atom abstraction is the predominant primary reaction channel, a conclusion that is supported by ab initio studies carried out by Xu and Lin [1651], Wang et al. [1570] and Schindler et al. (Table: 97-4, Note: 10-6, Evaluated: 10-6) [Back to Table](#)
- F6. $O + ClONO_2$. The recommended values are based on the results reported by Goldfarb et al. [565], Molina et al. [1025] and Kurylo [834]. The room temperature results of Tyndall et al. [1489] and Adler-Golden and Wiesenfeld [12] are in excellent agreement with the recommended value. The value reported by Ravishankara et al. [1205] at 245 K is a factor of 2 greater than those from the other studies, and this may possibly be attributed to (a) secondary kinetic complications, (b) the presence of NO_2 as a reactive impurity in the $ClONO_2$, or (c) formation of reactive photolytic products. Goldfarb et al. measured an essentially unit yield ($\pm 30\%$) of NO_2 from the reaction between the temperatures 248 K and 298 K. (Table: 10-6, Note: 10-6, Evaluated: 10-6) [Back to Table](#)
- F7. $O_3 + OClO$. The recommended value is based on results over the temperature range 262–296 K reported by Wongdontri-Stuper et al. [1641]. Within the indicated uncertainty limits it also encompasses the somewhat lower room temperature result of Birks et al. [163]. (Table: 90-1, Note: 90-1, Evaluated: 10-6) [Back to Table](#)
- F8. $O_3 + Cl_2O_2$. The recommended upper limit is taken from the study of DeMore and Tschuikow-Roux [422] measured at 195 K. (Table: 90-1, Note: 90-1, Evaluated: 10-6) [Back to Table](#)
- F9. $OH + Cl_2$. The recommended room temperature value is the average of the results reported by Bryukov et al. [208], Gilles et al. [553], Boodaghians et al. [177], Loewenstein and Anderson [930], Ravishankara et al. [1207], and Leu and Lin [890]. The temperature dependence is based on an error-weighted average of the Gilles et al. and Boodaghians et al. E/R values. Loewenstein and Anderson determined that the exclusive products are $Cl + HOCl$. (Table: 10-6, Note: 10-6, Evaluated: 10-6) [Back to Table](#)
- F10. $OH + ClO$. The reaction has two known product channels under atmospheric conditions: $OH + ClO \rightarrow Cl + HO_2$ and $OH + ClO \rightarrow HCl + O_2$. Most studies measure the rate coefficients for the overall reaction ($OH + ClO \rightarrow$ products) that is presumably the sum of the two channels. The recommendation for the $Cl + HO_2$ channel is obtained from the equilibrium constant for this channel

combined with the recommended value for the reverse reaction in entry F45. The difference between a critical assessment of the measurements of the overall reaction and the recommendation for the $\text{HCl} + \text{O}_2$ channel as discussed below is in reasonable accord.

The assessment of the overall reaction ($\text{OH} + \text{ClO} \rightarrow \text{products}$) is based on a fit to the 219–373 K data of Hills and Howard [650], the 208–298 K data of Lipson et al. [924], the 234–356 K data of Kegley-Owen et al. [771], the 298 K data of Poulet et al. [1184], measurements by Wang and Keyser (218–298 K) [1566], and measurements by Bedjanian et al. (230–360 K) [130]. Data reported in the studies of Burrows et al. [229], Ravishankara et al. [1207], and Leu and Lin [890] were not used in deriving the recommended value because ClO was not measured directly in these studies and the concentration of ClO was determined by an indirect method.

The minor reaction channel forming HCl poses significant experimental difficulties due to the complications associated with the measurement of the HCl reaction product. Early studies inferred the HCl branching ratio without measuring HCl. These included the 298 K measurements of the yield of the $\text{Cl} + \text{HO}_2$ channel by Leu and Lin [890] (>0.65); Burrows et al. [229] (0.85 ± 0.2) and Hills and Howard [650] (0.86 ± 0.14). Poulet et al. [1184] measured the $\text{Cl} + \text{HO}_2$ product yield to be 0.98 ± 0.12 using mass spectroscopy but their HCl sensitivity was marginal. These studies were not considered in the evaluation. Later studies of Lipson et al. using mass spectroscopy [924] and diode laser spectroscopy by Wang and Keyser [1567] improved the precision of the HCl product channel measurements. Lipson et al. [923] measured rate constants for the HCl channel over the temperature range 207–298 K and report a branching ratio of ($7 \pm 3\%$), while Wang and Keyser [1567] measured the HCl yield between 218–298 K, obtaining ($9.0 \pm 4.8\%$), independent of temperature. Their rate constant was computed from this yield and their overall rate constant [1566]. Measurements by Tyndall et al. [1488] and Bedjanian et al. [130] were also considered. (It was noted that although the values for this channel obtained by Lipson et al. by combining the values obtained in [924] and [923] and Bedjanian et al. [130] are in agreement, their values for the overall reaction differ by 40–70%.) The recommendation for the HCl channel is unchanged from JPL 06-2 and the error limits have been reduced. (Table: 09-31, Note: 09-31) [Back to Table](#)

- F11. $\text{OH} + \text{OCIO}$. The recommended value is that reported by Gierczak et al. [543] over the range 242 K – 392 K. An earlier study by Poulet et al. [1188] between 298 K and 473 K is in fair agreement with the recommendation. Differences between the studies may lie in the methods used to determine OCIO concentration. Gierczak et al. used in situ optical measurements of OCIO whereas Poulet et al. relied on measured flows of dilute mixtures. Product HOCl was detected in the Poulet et al. study by modulated molecular beam mass spectrometry. The branching ratio for the channel to produce $\text{HOCl} + \text{O}_2$ was determined to be close to unity, but experimental uncertainty would allow it to be as low as 0.80. (Table: 10-6, Note: 10-6, Evaluated: 10-6) [Back to Table](#)
- F12. $\text{OH} + \text{Cl}_2\text{O}$. The reaction has been studied as a function of temperature by Stevens and Anderson [1366] and Hansen et al. [613]. The results of these two studies are in excellent agreement at temperatures below 300 K. Hansen et al. suggest that data taken above 300 K by Stevens and Anderson was complicated by wall decomposition of Cl_2O . The recommended value of E/R is the average of the individual E/R's from the two studies for data below 300 K. The recommended value for $k(298 \text{ K})$ is an average of the results from Stevens and Anderson, Hansen et al, Ennis and Birks [486] and Leu and Lin [890]. (Table: 10-6, Note: 10-6, Evaluated: 10-6) [Back to Table](#)
- F13. $\text{OH} + \text{Cl}_2\text{O}_2$. The recommended value is based on results from the study of Hansen et al. [613] using a discharge flow technique coupled with direct detection of OH and Cl_2O_2 via resonance fluorescence and mass spectrometric techniques, respectively. Ab initio calculations by Hansen et al. support the finding of a negative temperature dependence. (Table: 10-6, Note: 10-6, Evaluated: 10-6) [Back to Table](#)
- F14. $\text{OH} + \text{HCl}$. The recommended value is based on a least squares fit to the data over the temperature range 204–300 K reported in the studies of Molina et al. [1026], Keyser [784], Ravishankara et al. [1218], Battin-Leclerc et al. [112] and Bryukov et al. [207]. In these studies particular attention was paid to the determination of the absolute concentration of HCl by UV and IR spectrophotometry. Earlier studies by Takacs and Glass [1402], Zahniser et al. [1670], Smith and Zellner [1338], Ravishankara et al. [1210], Hack et al. [597], Husain et al. [697], Cannon et al. [247], Husain et al.

[698], and Smith and Williams [1337] had reported somewhat lower room temperature values. The data of Sharkey and Smith [1297] over the temperature range 138–216 K, Battin-Leclerc et al. [112] below 240 K Bryukov et al over the temperature range 298 – 1015 K, depart from normal Arrhenius behavior. Quantum chemical and transition state calculations performed by Battin-Leclerc et al. [112], Bryukov et al. [207] and Steckler et al. [1357] generally support the existence of a weakly bound complex, however, a large tunneling effect is required to explain the low temperature data. Additional work at low temperature is needed to confirm the strong non-Arrhenius behavior. (Table:09-31, Note: 09-31) [Back to Table](#)

- F15. OH + HOCl. In the only reported study of this system Ennis and Birks [486] reported the value of this rate constant at room temperature to lie in the range $(1.7 - 9.5) \times 10^{-13} \text{ cm}^3 \text{ molecule}^{-1} \text{ s}^{-1}$. A temperature-dependent expression has been estimated by choosing a pre-exponential factor by analogy with the OH + H₂O₂ reaction and selecting the midpoint of the experimental range for the room temperature rate constant. Theoretical calculations by Wang et al. [1569], however, suggest that tunneling may play an important role at lower temperatures and give rise to a significant curvature in the Arrhenius curve. The large uncertainty factor is needed to encompass the entire range. (Table: 87-41, Note: 10-6, Evaluated: 10-6) [Back to Table](#)
- F16. OH + ClNO₂. The recommended value is based on results of the direct study of Ganske et al. [530, 531] using the discharge flow-resonance fluorescence technique. Mass spectrometric studies showed HOCl to be the major chlorine-containing product, with no evidence for a channel to produce HONO₂ + Cl. (Table: 94-26, Note: 94-26) [Back to Table](#)
- F17. OH + ClONO₂. The results reported by Zahniser et al. [1667] and Ravishankara et al. [1205] are in good agreement at ~245 K (within 25%), considering the difficulties associated with handling ClONO₂. The preferred value is that of Zahniser et al. Neither study reported any data on the reaction products. . (Table: 82-57, Note: 82-57, Evaluated: 10-6) [Back to Table](#)
- F18. OH + CH₃Cl. The recommended rate expression is derived from a combined fit (for T ≤ 400 K) to the data from the relative rate study by Hsu and DeMore [683] (recalculated based on the current recommendation for the rate constant for the OH + CH₃CHF₂ reference reaction, as described in the note for that reaction) and the absolute rate studies of Orkin et al. [1121] and Herndon et al. [636]. Data from the earlier studies of Howard and Evenson [674], Perry et al. [1158], Davis et al. [398], Paraskevopoulos et al. [1142], Taylor et al. [1424], and Jeong and Kaufman [742] are reasonably well encompassed within the 2σ uncertainty limits. The room temperature value from Taylor et al. [1424] is inconsistent with the higher temperature results in the same study and with the other investigations and lies outside of the 2σ band, as do the higher room temperature values of Cox et al. [357] and Brown et al. [198]. (Table: 02-25, Note: 02-25) [Back to Table](#)
- F19. OH + CH₂Cl₂. The recommended values for k(298 K) and E/R are averages of the values from the absolute rate studies of Villenave et al. [1520] and Herndon et al. [636] and the relative rate study of Hsu and DeMore [683] (two determinations which have been recalculated based on the current recommendations for the rate constants of the OH + CH₃CHF₂ and OH + CH₃CH₂F reference reactions). The renormalization procedure for relative rate measurements referenced to the OH + CH₃CHF₂ reaction is discussed in the note for that reaction. The rate constant determined relative to the rate constant of the OH + CH₃CH₂F was recalculated using a rate constant of the reference reaction obtained from the data of Schmoltner et al. [1275] and Kozlov et al. [821] above room temperature. The results of Cox et al. [357] and Davis et al. [398] support this recommendation. The results from Taylor et al. [1425], Jeong and Kaufman [742], Perry et al. [1158] and Howard and Evenson [674] lie considerably higher and were not used in deriving the recommended parameters. (Table: 02-25, Note: 02-25) [Back to Table](#)
- F20. OH + CHCl₃. The recommended value for k(298 K) is an average of the values from the relative rate study of Hsu and DeMore [683] (which has been recalculated based on the current recommendation for the rate constant of the OH + CH₃CHF₂ reference reaction, as described in the note for that reaction) and the absolute rate studies of Taylor et al. [1425] (which superseded Taylor et al. [1424]), Jeong and Kaufman [742], Davis et al. [398], and Howard and Evenson [674]. The recommended value of E/R is an average of values for this parameter derived in the first four of the above studies. (Table: 02-25, Note: 02-25) [Back to Table](#)

- F21. $\text{OH} + \text{CCl}_4$. The recommended upper limit at 298 K is based on the upper limit reported in the competitive study by Cox et al. [357]. The value given there has been increased by a factor of four to allow for uncertainties in the number of NO molecules oxidized. The recommendation is compatible with the less sensitive upper limits reported by Howard and Evenson [674] and Clyne and Holt [321]. None of these investigators reported any evidence for reaction between these species. The A-factor was estimated and a lower limit for E/R was derived. (Table: 90-1, Note: 90-1) [Back to Table](#)
- F22. $\text{OH} + \text{CH}_2\text{FCl}$ (HCFC-31). The recommended value for $k(298 \text{ K})$ is an average of the values from the relative rate study of DeMore [415] (which has been recalculated based on the current recommendation for the rate constant of the $\text{OH} + \text{CH}_2\text{Cl}_2$ reference reaction) and the absolute rate studies of Howard and Evenson [674], Paraskevopoulos et al. [1142], Watson et al. [1587], Handwerk and Zellner [611] and Jeong and Kaufman [742]. The recommended value for E/R is an average of the values for this parameter determined by DeMore, Watson et al., Handwerk and Zellner, and Jeong and Kaufman below 400 K. (Table: 02-25, Note: 02-25) [Back to Table](#)
- F23. $\text{OH} + \text{CHFCl}_2$ (HCFC-21). The recommended rate expression is derived from a combined fit to the data of Howard and Evenson [674], Perry et al. [1158], Watson et al. [1587], Chang and Kaufman [271], Paraskevopoulos et al. [1142], Jeong and Kaufman [742], and Fang et al. [492]. The rate constants reported by Clyne and Holt [322] are significantly higher than those from the other seven studies and were not used in deriving the recommended parameters. (Table: 02-25, Note: 02-25) [Back to Table](#)
- F24. $\text{OH} + \text{CHF}_2\text{Cl}$ (HCFC-22). Results for this compound show very good agreement among both absolute and relative rate constant measurements. The recommended rate expression is derived from a combined fit to the relative rate data of Hsu and DeMore [684] (which has been recalculated based on the current recommendation for the rate constant of the $\text{OH} + \text{CH}_4$ reference reaction), and the absolute rate studies of Orkin and Khamaganov [1119], Fang et al. [492], Atkinson et al. [59], Watson et al. [1587], Chang and Kaufman [271], Paraskevopoulos et al. [1142] and Jeong and Kaufman [742]. The more scattered results of Handwerk and Zellner [611] are in general agreement. The results from the studies of Howard and Evenson [674] and Clyne and Holt [322] are significantly different from those of the other studies and were not used in the derivation. (Table: 02-25, Note: 02-25) [Back to Table](#)
- F25. $\text{OH} + \text{CFCl}_3$ (CFC-11). The A-factor was estimated, and a lower limit for E/R was derived by using the upper limit for the rate constant reported by Chang and Kaufman [270] at about 480 K. This expression is compatible with the upper limits reported by Atkinson et al. [59], Howard and Evenson [674], Cox et al. [357] and Clyne and Holt [321]. None of the investigators reported any evidence for reaction. (Table: 02-25, Note: 02-25) [Back to Table](#)
- F26. $\text{OH} + \text{CF}_2\text{Cl}_2$ (CFC-12). The A-factor was estimated, and a lower limit for E/R was derived by using the upper limit for the rate constant reported by Chang and Kaufman [270] at about 480 K. This expression is compatible with the upper limits reported by Atkinson et al. [59], Howard and Evenson [674], Cox et al. [357], and Clyne and Holt [321]. None of the investigators reported any evidence for reaction. (Table: 02-25, Note: 02-25) [Back to Table](#)
- F27. $\text{OH} + \text{CH}_2\text{ClCH}_3$. The recommended value for $k(298 \text{ K})$ is an average of the values reported by Howard and Evenson [675], Paraskevopoulos et al. [1142], Kasner et al. [769], and Herndon et al. [636]. The recommended value for E/R is an average of the values for this parameter determined by Kasner et al. and Herndon et al. with the value for A calculated to agree with the recommended value for $k(298 \text{ K})$. Data from the study by Markert and Nielsen [967] were not used to derive the recommended parameters, as they are somewhat more scattered. (Table: 02-25, Note: 02-25) [Back to Table](#)
- F28. $\text{OH} + \text{CH}_3\text{CCl}_3$. The recommended value for $k(298 \text{ K})$ is an average of the values from the absolute rate studies of Talukdar et al. [1422] and Finlayson-Pitts et al. [506], and a relative rate study of DeMore [412] (recalculated based on the current recommendation for the rate constant of the $\text{OH} + \text{CH}_4$ reference reaction). The temperature dependence is a fit to the data between 243 K and 379 K of Talukdar et al. [1422]. These studies indicate both a lower $k(298 \text{ K})$ and E/R than was reported in earlier studies: Nelson et al. [1055], Jeong and Kaufman [741], and Kurylo et al. [837]. More recent

measurements by Jiang et al. [744] and Lancar et al. [849] yield rate constants that are slightly higher at 298 K than this recommendation. (Table: 06-2, Note: 06-2) [Back to Table](#)

- F29. $\text{OH} + \text{CH}_3\text{CFCl}_2$ (HCFC-141b). Both absolute and relative rate measurements are in excellent agreement for this compound, and the data are linear over a wide temperature range. The recommended rate expression is derived from a combined fit to the data of Huder and DeMore [689] (two relative rate determinations which have been recalculated based on the current recommendations for the rate constants for the reference reactions $\text{OH} + \text{CH}_4$ and $\text{OH} + \text{CH}_3\text{CCl}_3$), Lancar et al. [849], Zhang et al. [1682] (together with the data at 330 K and above from Liu et al. [928], Talukdar et al. [1415] above 253 K (two studies), and Mors et al. [1034]. The temperature-dependence data of Brown et al. [197] were not considered because the relatively large rate constants and Arrhenius curvature are suggestive of sample impurities. (Table: 02-25, Note: 02-25) [Back to Table](#)
- F30. $\text{OH} + \text{CH}_3\text{CF}_2\text{Cl}$ (HCFC-142b). The recommended value for $k(298 \text{ K})$ is an average of the values from Howard and Evenson [675], Cox et al. [357], Paraskevopoulos et al. [1142], Mors et al. [1034], Watson et al. [1587], Handwerk and Zellner [611], Liu et al. [928], Gierczak et al. [546], and Fang et al. [493]. The recommended value of E/R is an average of values for this parameter derived in the last five of these studies. The data from Brown et al. [197] and Clyne and Holt [322] were not used to derive the recommended parameters. The 270 K data of Zhang et al. [1682] are in reasonable agreement with the recommendation. (Table: 02-25, Note: 02-25) [Back to Table](#)
- F31. $\text{OH} + \text{CH}_2\text{ClCF}_2\text{Cl}$ (HCFC-132b). The recommended rate expression was derived from the data of Watson et al. [1589], which were corrected by these authors for the presence of alkene impurities. The data of Jeong et al. [740], indicating faster rate constants, may have been affected by such impurities; hence they were not included in deriving the recommendation. (Table: 02-25, Note: 02-25) [Back to Table](#)
- F32. $\text{OH} + \text{CH}_2\text{ClCF}_3$ (HCFC-133a). The recommended value of $k(298 \text{ K})$ is the average of the values of Howard and Evenson [675], Handwerk and Zellner [611], Fang et al. [491], and DeMore [416] (relative to the reaction of $\text{OH} + \text{CH}_3\text{CCl}_3$). The recommended temperature dependence is an average of that derived from a fit to the data of DeMore [416] and a combined fit to the data of Handwerk and Zellner [611] and Fang et al. [491] below 400 K. The data of Clyne and Holt [322] were not used in deriving the recommended parameters but (below 400 K) are encompassed within the 2σ uncertainty limits. (Table: 10-6, Note: 10-6, Evaluated: 10-6) [Back to Table](#)
- F33. $\text{OH} + \text{CHCl}_2\text{CF}_2\text{Cl}$ (HCFC-122). The recommended rate expression is derived from a combined fit to the data of Orkin and Khamaganov [1119] (below 400 K) and DeMore [415] (two determinations which have been recalculated based on the current recommendations for the rate constants of the $\text{OH} + \text{CH}_2\text{Cl}_2$ and $\text{OH} + \text{CHCl}_2\text{CF}_3$ reference reactions). (Table: 02-25, Note: 02-25) [Back to Table](#)
- F34. $\text{OH} + \text{CHFClCFCl}_2$ (HCFC-122a). The recommended rate expression was derived from the relative rate data of Hsu and DeMore [684] (recalculated based on the current recommendation for the rate constant for the $\text{OH} + \text{CH}_3\text{CHF}_2$ reference reaction, as discussed in the note for that reaction). (Table: 02-25, Note: 02-25) [Back to Table](#)
- F35. $\text{OH} + \text{CHCl}_2\text{CF}_3$ (HCFC-123). The recommended value of $k(298 \text{ K})$ is the average of the values from the absolute studies of Gierczak et al. [546] (two determinations) Liu et al. [928], and Yamada et al. [1654], and from the relative rate study by Hsu and DeMore [684] (recalculated based on the current recommendation for the rate constant for the $\text{OH} + \text{CH}_3\text{CHF}_2$ reference reaction, as discussed in the note for that reaction). The recommendation for the temperature dependence is derived from a fit to the data of these same five investigations. The temperature dependence data of Nielsen [1075], Watson et al. [1589], Clyne and Holt [322], and Brown et al. [197] and the room temperature data of Howard and Evenson [675] were not used in the derivations. (Table: 02-25, Note: 02-25) [Back to Table](#)
- F36. $\text{OH} + \text{CHFClCF}_2\text{Cl}$ (HCFC-123a). The recommended rate expression is based on the data of Orkin and Khamaganov [1119]. (Table: 02-25, Note: 02-25) [Back to Table](#)
- F37. $\text{OH} + \text{CHFClCF}_3$ (HCFC-124). The recommended value for $k(298 \text{ K})$ is an average of the values from the studies of Watson et al. [1589], Gierczak et al. [546] (2 studies), Yamada et al. [1654], and

Hsu and DeMore [684] (two relative rate determinations which have been recalculated based on the current recommendations for the rate constants of the OH + CH₄ and OH + CHF₂CHF₂ reference reactions). The room temperature rate constant of Howard and Evenson [675] is considerably higher than these other values and was not included in the average. The recommended temperature dependence is an average of the dependencies derived from these same studies (but using only data below 400 K from Gierczak et al. [546] and Yamada et al. [1654]). (Table: 02-25, Note: 02-25)

[Back to Table](#)

- F38. OH + CH₃CF₂CFCl₂ (HCFC-243cc). The recommended rate expression is derived from the temperature-dependence data of Nelson et al. [1051]. Although there is only a single study of this reaction, the uncertainties have been assigned to reflect our belief that the rate constant for this reaction should be less than that for OH + CH₃CF₂Cl. (Table: 02-25, Note: 02-25) [Back to Table](#)
- F39. OH + CHCl₂CF₃CF₂ (HCFC-225ca). The recommended value for k(298 K) is an average of the values from Nelson et al. [1051] and Zhang et al. [1683]. The recommendation for E/R is taken from Nelson et al. [1051]. The temperature-dependence data of Brown et al. [196] were not considered because the relatively large rate constants at and below room temperature and the Arrhenius curvature are suggestive of sample impurities. The temperature dependence results of Zhang et al. [1683] are in reasonable agreement with those of Nelson et al. [1051] over the temperature range of measurement overlap. However, the complete Zhang et al. [1683] data set yields a value for E/R much larger than currently recommended for the OH + CHCl₂CF₃ (HFC-123) reaction, for which the activation energy should be similar. (Table: 02-25, Note: 02-25) [Back to Table](#)
- F40. OH + CF₂ClCF₂CHFCI (HCFC-225cb). The recommended rate expression is derived from a combined fit to the temperature-dependence data of Nelson et al. [1051] and Zhang et al. [1683], which are in excellent agreement. (Table: 02-25, Note: 02-25) [Back to Table](#)
- F41. OH + CF₃CH₂CFCl₂. The recommended value for k(298 K) is from the relative rate study of Barry et al. [103]. The value for E/R is estimated as being slightly less than that for CF₃CH₂CF₃. (Table: 10-6, Note: 10-6, Evaluated: 10-6) [Back to Table](#)
- F42. OH + CH₂=CHCl. The recommended value for k(298 K) is an average of the values reported by Howard [672], Perry et al. [1157], Liu et al. [927] and Yamada et al. [1655]. The recommended value for E/R is an average of the values for this parameter derived from fits to the data of Perry et al., Liu et al. and Yamada et al. at temperatures below about 400 K. In the 400–500 K region the rate constant levels off before increasing at higher temperatures, suggesting the stronger importance of an abstraction mechanism at the higher temperatures. As discussed in note E31 the recommended rate constant represents the high pressure limit for this reaction. (Table: 02-25, Note: 10-6, Evaluated: 10-6) [Back to Table](#)
- F43. OH + CH₂=CCl₂. The recommended value for k(298 K) is an average of the values reported by Edney et al. [475], Tuazon et al. [1465], Abbatt and Anderson [1], Zhang et al. [1684], Canosa-Mas et al. [249], and Yamada et al. [1653]. The recommended value for E/R comes from a combined fit to the data of Abbatt and Anderson, Zhang et al., and Yamada et al. The data of Kirchner et al. [792] were not used in deriving the recommended parameters since they were obtained at very low pressure and the much stronger temperature dependence obtained may be indicative of a pressure dependence above room temperature. As discussed in note E31 the recommended rate constant represents the high pressure limit for this reaction. (Table: 02-25, Note: 10-6, Evaluated: 10-6) [Back to Table](#)
- F44. OH + CHCl=CCl₂. The recommended value for k(298 K) is the mean of the values reported by Howard [672], Chang and Kaufman [271], Kirchner et al. [792], Klopffer et al. [805], Edney et al. [475] and Tichenor et al. [1443]. The recommended value of E/R is an average of values for this parameter derived by Chang and Kaufman [271], Kirchner et al. [792], and Tichenor et al. [1443]. The value for k(298 K) derived from a relative rate study by Winer et al. [1636] is a factor of ~2 greater than the other values and is not considered in deriving the preferred value. An absolute study by Jiang et al. [745] yielding a significantly higher value for k(298 K) as well as a considerably stronger temperature dependence (E/R = –970 K) is assumed to be superseded by Tichenor et al.

[1443]. As discussed in note E31 the recommended rate constant represents the high pressure limit for this reaction. (Table: 02-25, Note: 10-6, Evaluated: 10-6) [Back to Table](#)

- F45. $\text{OH} + \text{CCl}_2=\text{CCl}_2$. The recommended value for $k(298\text{ K})$ is the mean of the values reported by Howard [672], Chang and Kaufman [271], and Kirchner et al. [792]. The room temperature value reported by Winer et al. [1636] is more than a factor of 10 greater and was not used in deriving the recommendation. The recommended value for E/R is an average of values for this parameter derived by Chang and Kaufman [271] and Kirchner et al. [792]. A study by Tichenor et al. [1444] yields a value for $k(298\text{ K})$ slightly lower than these other studies, but a temperature dependence less than half of that recommended. While these latest results were not used in deriving the recommendations, they are encompassed within the 95% confidence limits. As discussed in note E31 the recommended rate constant represents the high pressure limit for this reaction. (Table: 02-25, Note: 10-6, Evaluated: 10-6) [Back to Table](#)
- F46. $\text{OH} + \text{CHF}_2\text{OCHClCF}_3$. The recommended parameters are from a combined fit to the three absolute rate studies of Tokuhashi et al. [1450]. The values of k at 298 K determined in the discharge-flow experiments by Brown et al. [197] and Beach et al. [116] lie about 30% higher than recommended here. (Table: 10-6, Note: 10-6, Evaluated: 10-6) [Back to Table](#)
- F47. $\text{OH} + \text{CH}_3\text{OCl}$. The recommended rate expression is derived from a fit to the data of Crowley et al. [373], the only reported study of this reaction. (Table: 02-25, Note: 02-25) [Back to Table](#)
- F48. $\text{OH} + \text{CCl}_3\text{CHO}$. The recommended value for $k(298\text{ K})$ is an average of the values reported by Barry et al. [104] (using three independent techniques), Dobe et al. [437], Nelson et al. [1055], Ballestra-Garcia et al. [81], and Scollard et al. [1282]. The temperature dependence is derived from a fit to the data of Dobe et al. [437]. The A factor was then calculated to agree with the recommended value for $k(298\text{ K})$. (Table: 02-25, Note: 02-25) [Back to Table](#)
- F49. $\text{HO}_2 + \text{Cl}$. The recommendations for the two reaction channels are based upon the results of Hickson and Keyser [647], who measured both channels using the discharge flow-resonance fluorescence technique coupled with infrared diode laser spectroscopy, detecting HO , HO_2 , Cl and HCl , by Lee and Howard [876] who measured the total rate constant and the $\text{OH} + \text{ClO}$ channel, using a discharge flow system with laser magnetic resonance detection of HO_2 , OH , and ClO , and by Riffault et al. [1232] who measured the total rate constant and the $\text{OH} + \text{ClO}$ channel using the discharge flow mass spectrometric technique. The latter two studies suggest that the total rate constant is temperature independent with a value of $(4.2 \pm 0.7) \times 10^{-11}$ and $(4.4 \pm 0.6) \times 10^{-11} \text{ cm}^3 \text{ molecule}^{-1} \text{ s}^{-1}$ over the temperature range 250–420 K and 230–360 K respectively. The Hickson and Keyser study concludes that the HCl channel may be represented as $(1.4 \pm 0.3) \times 10^{-11} \exp[(269 \pm 58)/T]$ for temperatures from 256 to 296 K, while the OH channel is given by $(12.7 \pm 4.1) \times 10^{-11} \exp[-(801 \pm 94)/T]$ for temperatures of 226–336 K, the sum of which yields $4.3 \times 10^{-11} \text{ cm}^3 \text{ molecule}^{-1} \text{ s}^{-1}$ at 298 K with a small temperature dependence. These values for the total rate constant are in agreement with the results of indirect studies relative to $\text{Cl} + \text{H}_2\text{O}_2$ (Leu and DeMore [886], Poulet et al. [1186], Burrows et al. [224]) or to $\text{Cl} + \text{H}_2$ (Cox [351]). The contribution of the reaction channel producing $\text{OH} + \text{ClO}$ (22% at room temperature) is much higher than the upper limit reported by Burrows et al. (1% of total reaction). Cattell and Cox [267], using a molecular modulation-UV absorption technique over the pressure range 50–760 Torr, report results in good agreement with those of Lee and Howard both for the overall rate constant and for the relative contribution of the two reaction channels. A study by Dobis and Benson [443] reports a total rate constant in good agreement with this recommendation but a much lower contribution (5±3%) of the channel producing $\text{OH} + \text{ClO}$. The equilibrium constant for the channel producing $\text{ClO} + \text{OH}$ can be calculated with excellent accuracy. The recommended value for this channel comes from the combination of this equilibrium constant and the rate constant for the reverse reaction found in entry F10. (Table: 09-31, Note: 09-31) [Back to Table](#)
- F50. $\text{HO}_2 + \text{ClO}$. The recommended value is based on studies by Hickson et al. [648], Nickolaisen et al. [1064], Knight et al. [807], and Stimpfle et al. [1374] that studied the reaction as a function of temperature. Earlier room temperature studies by Reimann and Kaufman [1224]; Leck et al. [864], Burrows and Cox [225], and Cattell and Cox [267] are slightly lower than the current recommendation. The studies of Cattell and Cox and Nickolaisen et al. were performed over

extended pressure ranges and did not observe a pressure dependence. The most recent studies find the T-dependence to be characterized by linear Arrhenius behavior over the entire temperature range and do not support the finding of Stimpfle et al. of non-Arrhenius behavior. The recommended value for E/R is based on an average of individual E/R values for each of the four studies over their entire temperature ranges. The two most probable pairs of reaction products are, (1) HOCl + O₂ and (2) HCl + O₃. Finkbeiner et al. [505], using matrix isolation/ FTIR spectroscopy, studied product formation between 210 and 300 K at 700 Torr. HOCl was observed to be the dominant product (> 95% at all temperatures). Upper limits ranging from 0.3% to 2% have been determined for the channel (2) room temperature branching ratio by Leu [898], Leck et al., Knight et al., and Finkbeiner et al. Slightly larger branching ratio (<5%) upper limit values for k₂/k were determined at temperatures below 250 K by Finkbeiner et al. and Leck et al. However, no direct evidence of product channels other than channel (1) was found. Theoretical calculations are in generally good agreement on the structures and relative energetic of the intermediates in this reaction system (see the summary in Hickson et al.[648]). In particular, Xu et al. [1652] reported quantum chemistry and master equation calculations that are in reasonable agreement with the experiments. For atmospheric conditions, their calculations identified only two significant channels: the pressure-independent abstraction reaction to form HOCl + O₂ and pressure-dependent formation of HOOCl, which has thermal decomposition lifetimes ranging from hours to days under stratospheric conditions. At 250 K and 400 Torr of N₂, they calculate that the abstraction reaction constitutes ~60-70% of the total rate constant for ClO + HO₂, supporting the notion that a significant pressure-dependence exists. Further experimental studies on the formation, lifetime, and atmospheric fate of HOOCl are warranted. (Table: 09-31, Note: 10-6, Evaluated: 10-6) [Back to Table](#)

- F51. H₂O + ClONO₂. This recommendation is based on the upper limits to the homogeneous bimolecular rate constant reported by Atkinson et al. [65], and by Hatakeyama and Leu [621, 622]. Atkinson et al. observed by FTIR analysis the decay of ClONO₂ in the presence of H₂O in large-volume (2500 and 5800 liters) Teflon or Teflon-coated chambers. Their observed decay rate gives an upper limit to the homogeneous gas phase rate constant, and they conclude that the decay observed is due to heterogeneous processes. Hatakeyama and Leu, using a static photolysis system with FTIR analysis, derive a similar upper limit. Rowland et al. [1243] concluded that the decay they observed resulted from rapid heterogeneous processes. The homogeneous reaction is too slow to have any significant effect on atmospheric chemistry. (Table: 87-41, Note: 87-41, Evaluated: 10-6) [Back to Table](#)
- F52. NO + OCIO. The Arrhenius expression was estimated based on 298 K data reported by Bemand et al. [143]. Recent temperature data by Li et al. [909] is in good agreement with Bemand et al. at 298 K and displays a negative temperature dependence over the range 220 K – 367 K. However, the Li et al. data appears to be complicated by the secondary reaction of Cl with OCIO. (Table: 82-57, Note: 10-6, Evaluated: 10-6) [Back to Table](#)
- F53. NO + Cl₂O₂. The recommended upper limit is that determined by Ingham et al. [713] in a study using a DF-MS technique. (Table: 10-6, Note: 10-6, Evaluated: 10-6) [Back to Table](#)
- F54. NO₃ + HCl. The recommended upper limit is that reported by Mellouki et al. [1002] in a study using DF-EPR techniques. This upper limit shows that this reaction is of negligible importance in stratospheric chemistry. Somewhat lower upper limits have been reported by Cantrell et al. [254] and Canosa-Mas et al. [251]; the latter study also reports Arrhenius parameters at higher temperatures (333–473 K). (Table: 90-1, Note: 90-1, Evaluated: 10-6) [Back to Table](#)
- F55. HO₂NO₂ + HCl. This upper limit is based on results of static photolysis-FTIR experiments reported by Leu et al. [889]. (Table: 90-1, Note: 90-1, Evaluated: 10-6) [Back to Table](#)
- F56. Cl + O₃. The results reported for k(298 K) by Watson et al. [1588], Zahniser et al. [1671], Kurylo and Braun [838], Clyne and Nip [331], Nicovich et al. [1067], Seeley et al. [1285] and Beach et al. [117] are in good agreement, and have been used to determine the preferred value at this temperature. The values reported by Leu and DeMore [886] (due to the wide error limits) and Clyne and Watson [337] (the value is inexplicably high) are not considered. The six Arrhenius expressions are in fair agreement within the temperature range 205–300 K. In this temperature range, the rate constants at any particular temperature agree to within 30–40%. Although the values of the activation energy obtained by Watson et al. and Kurylo and Braun are in excellent agreement, the

value of k in the study of Kurylo and Braun is consistently (~17%) lower than that of Watson et al. This may suggest a systematic underestimate of the rate constant, as the values from the other three agree so well at 298 K. Two later studies (Nicovich et al. and Seeley et al.) obtained significantly smaller temperature dependences than those observed in the earlier studies. There is no reason to prefer any one set of data to any other; therefore, the preferred Arrhenius expression shown above was obtained by computing the mean of the six results between 205 and 298 K. DeMore [411] directly determined the ratio $k(\text{Cl} + \text{O}_3)/k(\text{Cl} + \text{CH}_4)$ at 197–217 K to be within 15% of that calculated from the absolute rate constant values recommended here.

Vanderzanden and Birks [1512] have interpreted their observation of oxygen atoms in this system as evidence for some production (0.1–0.5%) of $\text{O}_2(^1\Sigma)$ in this reaction. The possible production of singlet molecular oxygen in this reaction has also been discussed by DeMore [409], in connection with the Cl_2 photosensitized decomposition of ozone. However Choo and Leu [302] were unable to detect $\text{O}_2(^1\Sigma)$ or $\text{O}_2(^1\Delta)$ in the $\text{Cl} + \text{O}_3$ system and set upper limits to the branching ratios for their production of 5×10^{-4} and 2.5×10^{-2} , respectively. They suggested two possible mechanisms for the observed production of oxygen atoms, involving reactions of vibrationally excited ClO radicals with O_3 or with Cl atoms, respectively. Burkholder et al. [220], in a study of infrared line intensities of the ClO radical, present evidence in support of the second mechanism. In their experiments with excess Cl atoms, the vibrationally excited ClO radicals produced in the $\text{Cl} + \text{O}_3$ reaction can react with Cl atoms to give Cl_2 and oxygen atoms, which can then remove additional ClO radicals. These authors point out the possibility for systematic error from assuming a 1:1 stoichiometry for $[\text{Cl}]:[\text{O}_3]_0$ when using the $\text{Cl} + \text{O}_3$ reaction as a quantitative source of ClO radicals for kinetic and spectroscopic studies. (Table: 06-2, Note: 06-2) [Back to Table](#)

- F57. $\text{Cl} + \text{H}_2$. The recommended value for $k(298 \text{ K})$ is an average of the values measured by Westenberg and De Haas [1603], Lee et al. [867], Miller and Gordon [1021], and Kita and Stedman [795]. The value of $k(298 \text{ K})$ derived in the flash photolysis - resonance fluorescence study of Davis et al. [395] agrees with these studies but was probably overestimated by ~10% (the authors assumed that the fluorescence signal, I_f was proportional to $[\text{Cl}]^{0.9}$, whereas a linear relationship between I_f and $[\text{Cl}]$ probably held under their experimental conditions). Room temperature determinations by Kumaran et al. [829] (focused primarily on high temperature measurements) and Eberhard et al. [472] (focused on obtaining yields of HCl product in different vibrational levels) are both in reasonable agreement with the recommendation as are the results from the relative rate studies by Su et al. [1388] and by Rodebush and Klingelhofer [1239]. The value for E/R is derived from a fit to the data at temperatures below 300 K reported by Westenberg and De Haas [1603], Lee et al. [867], and Miller and Gordon [1021]. The value is in good agreement with that determined by Adusei and Fontijn [13], although these data lie systematically lower than the results from other studies. The Arrhenius A-factor was calculated from $k(298 \text{ K})$ and E/R . Extrapolation above room temperature using the recommended Arrhenius parameters is in reasonable agreement with the data of Benson et al. [145] and Kita and Stedman [795]. For a discussion of the large body of rate data at high temperatures, see the review by Baulch et al. [115]. Miller and Gordon [1021] and Kita and Stedman [795] also measured the rate of the reverse reaction, and found the ratio to be in good agreement with equilibrium constant data. (Table: 06-2, Note: 06-2) [Back to Table](#)
- F58. $\text{Cl} + \text{H}_2\text{O}_2$. The absolute rate coefficients determined at ~298 K by Watson et al. [1588], Leu and DeMore [886], Michael et al. [1019], Poulet et al. [1186] and Keyser [779] range in value from $(3.6\text{--}6.2) \times 10^{-13}$. The studies of Michael et al., Keyser, and Poulet et al. are presently considered to be the most reliable. The preferred value for the Arrhenius expression is taken to be that reported by Keyser. The A-factor reported by Michael et al. is considerably lower than that expected from theoretical considerations and may possibly be attributed to decomposition of H_2O_2 at temperatures above 300 K. The data of Michael et al. at and below 300 K are in good agreement with the Arrhenius expression reported by Keyser. Heneghan and Benson [632], using mass spectrometry, confirmed that this reaction proceeds only by the abstraction mechanism giving HCl and HO_2 as products. (Table: 02-25, Note: 02-25, Evaluated: 10-6) [Back to Table](#)
- F59. $\text{Cl} + \text{NO}_3$. The recommended value at room temperature is based on the discharge flow-EPR study of Mellouki et al. [1000] and the discharge flow-mass spectrometric study of Becker et al. [120]. The results of these direct absolute rate studies are preferred over results of the earlier relative rate

studies of Cox et al. [352], Burrows et al. [228], and Cox et al. [363], in all of which NO₃ was monitored in the photolysis of Cl₂-ClONO₂-N₂ mixtures. Complications in the chemistry of the earlier systems probably contributed to the spread in reported values. This radical-radical reaction is expected to have negligible temperature dependence, which is consistent with the results from the study of Cox et al. [363] in which the complications must have been temperature independent. (Table: 94-26, Note: 94-26, Evaluated: 10-6) [Back to Table](#)

- F60. Cl + N₂O. This rate coefficient has been determined in a study of the halogen-catalyzed decomposition of nitrous oxide at about 1000 K by Kaufman et al. [770]. The largest value reported was 10⁻¹⁷ cm³ molecule⁻¹ s⁻¹, with an activation energy of 34 kcal/mol. Extrapolation of these results to low temperature shows that this reaction cannot be of any significance in atmospheric chemistry. Kinetic isotope effects observed by Lesar et al. [880] are consistent with a reaction transition state where the chlorine atom is bonded to the oxygen atom of nitrous oxide with a planar trans arrangement of atoms. (Table: 87-41, Note: 10-6, Evaluated: 10-6) [Back to Table](#)
- F61. Cl + HNO₃. The recommended upper limit at room temperature is that reported in the study of Wine et al. [1633], in which long-path laser absorption spectroscopy was used to look for the appearance of NO₃ following the pulsed laser photolysis of Cl₂-HNO₃ mixtures with no evidence for NO₃ production observed. In the same study a less sensitive upper limit was derived from monitoring Cl atom decay by resonance fluorescence. A less sensitive upper limit was also found in the discharge flow-EPR study of Zagogianni et al. [1665]. Higher values obtained in earlier studies (Leu and DeMore [886], Kurylo et al. [844], and Clark et al. [311]) as well as the higher temperature results of Poulet et al. [1186] are not used. (Table: 90-1, Note: 90-1, Evaluated: 10-6) [Back to Table](#)
- F62. Cl + HO₂NO₂. The only study of this reaction is by Simonaitis and Leu [1313] using the low pressure discharge flow technique coupled with resonance fluorescence detection of Cl and mass spectrometric detection of HO₂NO₂ ion fragments. Consistent results were obtained monitoring either Cl or HO₂NO₂ decays and retrieved rate constants were less than 1 × 10⁻¹³ cm³ molecule⁻¹ s⁻¹ for all conditions. Impurities in the HO₂NO₂ sample (especially H₂O₂) complicated the measurements. A limited temperature study over the 298–399 K range suggests that E/R is in the range of 500 – 1500 K. Given the experimental difficulties, only an upper limit is recommended for the reaction rate. (Table: 02-25, Note: 02-25, Evaluated: 10-6) [Back to Table](#)
- F63. Cl + CH₄. The recommended value for k(298 K) is based on the values reported in the absolute rate constant studies of Manning and Kurylo [955], Whytock et al. [1606], Michael and Lee [1012], Lin et al. [920], Zahniser et al. [1666], Keyser [777], Baghal-Vayjooee et al. [76], Ravishankara and Wine [1213], Heneghan et al. [633], Dobis and Benson [441], Sawerysyn et al. [1265], Lazarou et al. [860], Beichert et al. [141], Seeley et al. [1285], Pilgrim et al. [1167], Mellouki et al. [997], Wang and Keyser [1565], and Bryukov et al. [209], all of which fall in the range (0.9 – 1.13) × 10⁻¹³ cm³ molecule⁻¹ s⁻¹. Other absolute studies by Davis et al. [395], Clyne and Walker [336], Poulet et al. [1185], Leu and DeMore [886], Watson et al. [1588], and Schlyer et al. [1271] give rate constant values slightly higher than those of the aforementioned studies. In some cases, this may be due to uncertainties in correcting the data for OH loss via reaction with trace levels of ethane and propane in the methane samples used. Nevertheless, these results were not used in deriving the recommended value for k(298 K). The values derived for k at 298 K from the competitive chlorination studies of Pritchard et al. [1189], Pritchard et al. [1190], Knox [809], Knox and Nelson [811], Lee and Rowland [865], and Lin et al. [920] are in the range (0.8 - 1.6) × 10⁻¹³ cm³ molecule⁻¹ s⁻¹ when the original data are referenced to the presently recommended rate constant values for the reference reactions of Cl with H₂ and C₂H₆. The recommended value k(298 K) = 1.0 × 10⁻¹³ cm³ molecule⁻¹ s⁻¹ is derived as an unweighted average of the rate constants from the thirteen preferred absolute studies and the most recent and comprehensive relative rate study of Lin et al. [920].

There have been nine absolute studies of the temperature dependence of k in which the measurements extend below 300 K (Watson et al. [1588], Manning and Kurylo [955], Whytock et al. [1606], Lin et al. [920], Zahniser et al. [1666], Keyser [777], Ravishankara and Wine [1213], Heneghan et al. [633], and Seeley et al. [1285]). In general, the agreement among most of these studies is quite good. However, systematic differences in activation energies are apparent when calculated using data obtained below 300 K versus data from above 300 K. Three resonance fluorescence studies have been performed over the temperature region between 200 and 500 K

(Whytock et al. [1606], Zahniser et al. [1666] and Keyser [777]), and in each case a non-linear Arrhenius behavior was observed. Ravishankara and Wine [1213] also noted nonlinear Arrhenius behavior over a more limited temperature range. This behavior tends to partially explain the variance in the values of E/R reported between those investigators who mainly studied this reaction below 300 K (Watson et al. [1588], Manning and Kurylo [955], and Seeley et al. [1285]) and those who only studied it above 300 K (Clyne and Walker [336], Poulet et al. [1185], and Lin et al. [920]). The agreement between all studies below 300 K is reasonably good, with values of E/R ranging from 1060 K to 1320 K. There have not been any absolute studies at stratospheric temperatures other than those that utilized the resonance fluorescence technique. Ravishankara and Wine [1213] have suggested that the results obtained using the discharge flow and competitive chlorination techniques may be in error at the lower temperatures (<240 K) due to a non-equilibration of the $^2P_{1/2}$ and $^2P_{3/2}$ states of atomic chlorine. They observed that at temperatures below 240 K the apparent bimolecular rate constant was dependent upon the chemical composition of the reaction mixture; i.e., if the mixture did not contain an efficient spin equilibrator, e.g., Ar or CCl₄, the bimolecular rate constant decreased at high CH₄ concentrations. The chemical composition in each of the flash photolysis studies contained an efficient spin equilibrator, whereas this was not the case in the discharge flow studies. However, the reactor walls in the discharge flow studies could have been expected to have acted as an efficient spin equilibrator. Consequently, until the hypothesis of Ravishankara and Wine is proven, it is assumed that the discharge flow and competitive chlorination results are reliable. A composite unweighted Arrhenius fit to all of the temperature dependent absolute studies with data in the temperature region ≤ 300 K (with the exception of the data of Watson et al. [1588], which appear to be systematically high due to reactive impurities) yields E/R = 1280 K and $k(298\text{ K}) = 1.0 \times 10^{-13} \text{ cm}^3 \text{ molecule}^{-1} \text{ s}^{-1}$. The Arrhenius A-factor was calculated from recommended $k(298\text{ K})$ and E/R. (Table: 06-2, Note: 06-2) [Back to Table](#)

- F64. Cl + CH₃D. The recommended value for $k(298\text{ K})$ is an average of the relative rate determinations by Saueressig et al. [1263] (two independent measurements) and by Tyler et al. [1484]. It agrees with the value determined by Wallington and Hurley [1550] after the latter is corrected as per a personal communication from the authors. The value for E/R is an average of the values determined by Saueressig et al. and Tyler et al. (Table: 06-2, Note: 06-2) [Back to Table](#)
- F65. Cl + H₂CO. The results from five of the six published studies (Michael et al. [1016], Anderson and Kurylo [32], Niki et al. [1086], Fasano and Nogar [496] and Poulet et al. [1181]) are in good agreement at ~ 298 K, but are $\sim 50\%$ greater than the value reported by Foon et al. [515]. The preferred value at 298 K was obtained by combining the absolute values reported by Michael et al., Anderson and Kurylo, and Fasano and Nogar, with the values obtained by combining the ratio of $k(\text{Cl} + \text{H}_2\text{CO})/k(\text{Cl} + \text{C}_2\text{H}_6)$ reported by Niki et al. (1.3 ± 0.1) and by Poulet et al. (1.16 ± 0.12) with the preferred value of $5.7 \times 10^{-11} \text{ cm}^3 \text{ molecule}^{-1} \text{ s}^{-1}$ for $k(\text{Cl} + \text{C}_2\text{H}_6)$ at 298 K. The preferred value of E/R was obtained from a least squares fit to all the data reported in Michael et al. and in Anderson and Kurylo. The A-factor was adjusted to agree with the preferred value at 298 K. (Table: 82-57, Note: 82-57) [Back to Table](#)
- F66. Cl + HC(O)OH. The room temperature kinetics of this reaction have been studied by Wallington et al. [1536] and Li et al. [903]. Wallington et al. used a relative rate technique at atmospheric pressure while Li et al. employed flash photolysis at a pressure of 10 Torr. The results of the two studies are in excellent agreement and have been averaged together to derive the recommended value. Reaction products have been investigated by Tyndall et al. [1501] at room temperature and 700 Torr pressure. They measured the CO₂ yield to be $96 \pm 5\%$ and suggested that the HOCO complex reacted with either O₂ or Cl₂ in their experiment to give the observed product. (Table: 02-25, Note: 02-25) [Back to Table](#)
- F67. Cl + CH₃O₂. The recommended value is based on results of Maricq et al. [965], Jungkamp et al. [755], and Daele and Poulet [380]. All three studies agree that this overall reaction is very fast. However, there is a discrepancy in the reported values of the branching ratios for the two pathways producing ClO + CH₃O (a) and HCl + CH₂O₂ (b). The branching ratio for the reaction channels producing HCl + CH₂O₂ (b) has been reported to be 50% by both Maricq et al. and Jungkamp et al., but has been reported to be 90% by Daele and Poulet. Because of this large discrepancy no branching ratios are recommended. (Table: 97-4, Note: 97-4) [Back to Table](#)

- F68. $\text{Cl} + \text{CH}_3\text{OH}$. This recommendation at 298 K is based on results of the absolute rate studies of Michael et al. [1017], Payne et al. [1152], Dobe et al. [438], Pagsberg et al. [1137] and Tyndall et al. [1492], and results obtained in the competitive chlorination studies of Wallington et al. [1561], Lightfoot et al. [912], Nelson et al. [1054], and Tyndall et al. The temperature independence of the rate constant was reported by Michael et al. in a direct study. This is consistent with the indirect results of Lightfoot et al. who deduced the rate coefficient for this reaction relative to that for methane as a function of temperature. This reaction can have two sets of products: $\text{CH}_2\text{OH} + \text{HCl}$, channel (a) and $\text{CH}_3\text{O} + \text{HCl}$, channel (b). Product analysis and isotopic substitution have established that the reaction proceeds via channel (a) rather than via channel (b). See Radford [1192], Radford et al. [1193], Meier et al. [994], and Payne et al. [1152]. This reaction has been used in the laboratory as a source of CH_2OH and as a source of HO_2 by the reaction of CH_2OH with O_2 . (Table: 02-25, Note: 02-25) [Back to Table](#)
- F69. $\text{Cl} + \text{CH}_3\text{OOH}$. The only study of this reaction was by Wallington et al. [1536], who measured the rate relative to $\text{Cl} + \text{C}_2\text{H}_6$ at 295 K and atmospheric pressure. (Table: 02-25, Note: 02-25) [Back to Table](#)
- F70. $\text{Cl} + \text{CH}_3\text{ONO}_2$. This reaction has been studied at 298 K by Nielsen et al [1082] using a relative rate technique. The reference compound was ethane. The recommended value is adjusted from that given by Nielsen et al. using the currently recommended value for $k(\text{Cl} + \text{C}_2\text{H}_6)$. The temperature dependence is estimated by assuming an A-factor equal to approximately 20 times that of $\text{OH} + \text{CH}_3\text{ONO}_2$. This is consistent with observed OH/Cl A-factor ratios for primary H-abstraction from alkanes. (Table: 02-25, Note: 02-25) [Back to Table](#)
- F71. $\text{Cl} + \text{C}_2\text{H}_6$. The recommended value for $k(298 \text{ K})$ is an average of the absolute rate coefficients reported in the studies of Manning and Kurylo [955], Lewis et al. [901], Dobis and Benson [442], Beichert et al. [141], Pilgrim et al. [1167], Tyndall et al. [1494], Hitsuda et al. [655], Bryukov et al. [210], and Hickson and Keyser [646], all of which fall in the range $(5.3 - 6.1) \times 10^{-11} \text{ cm}^3 \text{ molecule}^{-1} \text{ s}^{-1}$. The value derived by Ray et al. [1220] in a study whose primary focus was not the determination of the rate constant for the target reaction, lies in the same range. A somewhat higher value reported by Davis et al. [395], was probably overestimated by $\sim 10\%$ (the authors assumed that the fluorescence signal, I_f was proportional to $[\text{Cl}]^{0.9}$, whereas a linear relationship between I_f and $[\text{Cl}]$ probably held under their experimental conditions). The rate constant reported by Schlyer et al. [1271] lies significantly lower than those from all other absolute studies while the values from Mellouki et al. [997] and Kaiser et al. [760] lie slightly higher. Room temperature rate constants derived from the relative rate experiments of Pritchard et al. [1190], Knox and Nelson [811], Atkinson and Aschmann [48], Atkinson and Ashmann [49], Tschuikow-Roux et al. [1463], Wallington et al. [1561], Beichert et al. [141], Hooshiyar and Niki [665], and Lin et al. [920] exhibit considerably more scatter even when recalculated based on the same current recommendation for the rate constant of the reference reactions. Nevertheless, most are encompassed within the 95% uncertainty limits recommended for the value of $k(298 \text{ K})$. The relative rate results of Kelly et al. [773] and Lee and Rowland [865] are significantly lower than other room temperature measurements. The recommended value for E/R is taken from a combined fit to the data of Manning and Kurylo [955], Dobis and Benson [442], and Hickson and Keyser [646] after normalizing all three data sets to the recommended value of $k(298 \text{ K})$. The data from Lewis et al. [901] and Lin et al. [920] below 300 K are encompassed by the 95% uncertainty bands. The temperature dependent studies by Pilgrim et al. [1167] and Bryukov et al. did not extend below room temperature. An extrapolation of the recommended Arrhenius parameters and the 95% uncertainty bands above room temperature encompasses the data of Pilgrim et al. but not those of Bryukov et al., which are characterized by a much stronger temperature dependence. The Arrhenius A-factor was calculated from the recommended $k(298 \text{ K})$ and E/R. The new data obtained at very low temperatures (167 K – 48 K) in Laval nozzle experiments by Hickson et al. [645] strongly support the current recommendations (Table: 06-2, Note: 10-6, Evaluated: 10-6) [Back to Table](#)
- F72. $\text{Cl} + \text{C}_2\text{H}_5\text{O}_2$. The recommended value is based on results of Maricq et al. [965]. (Table: 94-26, Note: 94-26) [Back to Table](#)

- F73. $\text{Cl} + \text{CH}_3\text{CH}_2\text{OH}$. The rate coefficient for this reaction has been studied at 298 K by four groups using a relative rate technique: Nelson et al. [1054] (relative to $\text{Cl} + \text{cyclohexane}$), Wallington et al. [1561] (relative to $\text{Cl} + \text{C}_2\text{H}_6$), Edelbuttel-Einhaus et al. [473] (relative to $\text{Cl} + \text{C}_2\text{H}_6$), and Taatjes et al. [1400]. Nelson et al. measured this rate constant relative to $\text{Cl} + \text{cyclohexane}$ while the others used $\text{Cl} + \text{C}_2\text{H}_6$ as the reference reaction. Taatjes et al. also measured this rate coefficient by measuring the temporal profile of the HCl product. The agreement between these five measurements is quite good, yielding an average value that is recommended. The temperature dependence of this rate coefficient is based on the results of Taatjes et al., who studied this reaction above 298 K and found it to be essentially independent of temperature. We recommend the same independence of temperature at atmospheric temperatures.
- This reaction can have three sets of products: $\text{CH}_2\text{CH}_2\text{OH} + \text{HCl}$, channel (a); CH_3CHOH , channel (b); and $\text{CH}_3\text{CH}_2\text{O}$ channel (c). Taatjes et al. have deduced that channel (c) is negligible and that channel (a) is about 8% at 298 K. Therefore, the majority of reaction is expected to occur via channel (b). It is very unlikely that these branching ratios will change significantly at lower atmospheric temperatures. (Table: 02-25, Note: 02-25) [Back to Table](#)
- F74. $\text{Cl} + \text{CH}_3\text{C(O)OH}$. Koch and Moortgat [813] have studied this reaction at room temperature using the relative rate technique. Deuterium substitution of the methyl hydrogens decreased the observed rate by a factor of 3.75. In addition, CO and CO_2 reaction products were observed in a stoichiometric ratio of 1:1. These observations were interpreted in terms of methyl hydrogen abstraction from acetic acid to form the $\text{CH}_2\text{C(O)OH}$ radical followed by reaction with O_2 to form a peroxy radical. Thermal decomposition of the peroxy radical produces HCHO , CO_2 , and atomic H . In the laboratory system, the HCHO reacts with atomic chlorine to yield CO . (Table: 02-25, Note: 02-25) [Back to Table](#)
- F75. $\text{Cl} + \text{CH}_3\text{CN}$. The recommendation is based on the study by Tyndall et al. [1495]. The results of this study, using both relative and absolute methods and obtained over a wide range of experimental conditions are preferred over the results of earlier studies of Kurylo and Knable [840], Poulet et al. [1180], and Olbregts et al. [1113]. Product studies reported by Tyndall et al. [1495] show that reaction proceeds predominantly if not exclusively by hydrogen atom abstraction. (Table: 97-4, Note: 97-4) [Back to Table](#)
- F76. $\text{Cl} + \text{C}_2\text{H}_5\text{ONO}_2$. Wallington et al. [1549] and Nielsen et al. [1082] have measured the rate of this reaction at room temperature relative to atomic chlorine reactions with ethyl chloride and ethane, respectively. The two studies are in excellent agreement and the recommended value is based on an average of the two. The values given in Wallington et al. and Nielsen et al. were adjusted based on the currently accepted values of the reference rate constants. The temperature dependence is estimated by assuming an A-factor equal to approximately 20 times that of $\text{OH} + \text{CH}_3\text{ONO}_2$. This is consistent with observed OH/Cl A-factor ratios for primary H-abstraction from alkanes. (Table: 02-25, Note: 02-25) [Back to Table](#)
- F77. $\text{Cl} + \text{CH}_3\text{CO}_2\text{NO}_2$ (PAN). The recommended value is based on results of the relative rate study of Wallington et al. [1536]. In this study no reaction of PAN was observed in the presence of Cl atoms. These results are preferred over the results of the direct study of Tsalkani et al. [1462] using a discharge flow system with EPR detection of Cl atom decay (in which study the authors reported a rate constant of $(3.7 \pm 1.7) \times 10^{-13} \text{ cm}^3 \text{ molecule}^{-1} \text{ s}^{-1}$). In both studies the major impurity in the PAN samples would be the alkane solvent. The presence of 0.1% tridecane in the PAN sample used by Tsalkani et al. could account for the observed Cl atom decay; however, solvent impurities in the PAN sample would be of no consequence in the relative rate study of Wallington et al. (Table: 92-20, Note: 92-20) [Back to Table](#)
- F78. $\text{Cl} + \text{C}_3\text{H}_8$. The recommended value for $k(298 \text{ K})$ is the mean of results of the competitive chlorination studies of Pritchard et al. [1190], Knox and Nelson [811], Kelly et al. [773], Tschuikow-Roux et al. [1464], Atkinson and Aschmann [48], Wallington et al. [1561], Beichert et al. [141], Hooshiyar and Niki [665], Tyndall et al. [1494] (two determinations), and Sarzynski and Sztuba [1261], and the absolute rate studies of Lewis et al. [901], Beichert et al. [141], Pilgrim et al. [1167]), Mellouki [997], and Hitsuda et al. [655]. The recommended $E/R = 0$ is based on the data obtained between 300 K and 400 K in the most recent and comprehensive study of Sarzynski and

Sztuba. The new data obtained at very low temperatures (167 K – 48 K) in Laval nozzle experiments by Hickson et al. [645] strongly support the current recommendations.

The recommended $k(298\text{ K})$ values for both reaction channels are the means of the results from the competitive chlorination studies by Knox and Nelson [811], Kelly et al. [773], Tschuikow-Roux et al. [1464], Tyndall et al. [1494], and Sarzynski and Sztuba [1261]. The recommended E/R values are based on the data of Sarzynski and Sztuba obtained between 300 K and 400 K. The Arrhenius A-factors were calculated from the recommended $k(298\text{ K})$ and E/R. A sum of the recommended rate constant expressions for the two channels gives the same values as the rate constant expression recommended for the total reaction ($A = 1.45 \times 10^{-10}\text{ cm}^3\text{ molecule}^{-1}\text{ s}^{-1}$, $E/R = 0$, $k(298\text{ K}) = 1.4 \times 10^{-10}\text{ cm}^3\text{ molecule}^{-1}\text{ s}^{-1}$, $f(298\text{ K}) = 1.07$, $g = 20$). (Table: 06-2, Note: 10-6, Evaluated: 10-6) [Back to Table](#)

- F79. $\text{Cl} + \text{CH}_3\text{C}(\text{O})\text{CH}_3$. The rate coefficient for this reaction has only been reported at 298 K. Wallington et al. [1561] and Olsson et al. [1114] report values of 2.37×10^{-12} and $1.69 \times 10^{-12}\text{ cm}^3\text{ molecule}^{-1}\text{ s}^{-1}$ at 298 K measured via relative rate methods. The only direct measurement of this rate constant is by Notario et al. [1104] who report a value of $(3.06 \pm 0.38) \times 10^{-12}\text{ cm}^3\text{ molecule}^{-1}\text{ s}^{-1}$ at 298 K. Because of the reasons noted by Wallington et al. [1561], the value reported by Olsson et al. is suspect and is not considered here. The average of the results from Wallington et al. and Notario et al. is recommended for $k(298\text{ K})$. In the absence of temperature dependent measurements, based on analogy with other Cl atom reactions with halogenated hydrocarbons whose rate coefficients at 298 K are close to that for $\text{Cl} + \text{CH}_3\text{C}(\text{O})\text{CH}_3$, we recommend an E/R value of 1000 K with a g value of 500 K. Such a temperature dependence is consistent with this reaction proceeding via H atom abstraction. This E/R and $k(298\text{ K})$ lead to an A factor of $7.7 \times 10^{-11}\text{ cm}^3\text{ molecule}^{-1}\text{ s}^{-1}$. This A factor is the same as that for the reaction of Cl atom with ethane, which also contains six primary C–H bonds. End product studies clearly show that the products of this reaction are $\text{CH}_3\text{C}(\text{O})\text{CH}_2$ and HCl. (Table: 02-25, Note: 02-25) [Back to Table](#)
- F80. $\text{Cl} + \text{CH}_2=\text{C}(\text{CH}_3)\text{CH}=\text{CH}_2 \rightarrow \text{products}$. The recommended 298 K rate constant is an un-weighted average of room temperature results reported by Ragains & Finlayson-Pitts [1194], Notario et al. [1103], [494], Bedjanian et al. [126], Stutz et al. [1387], Finlayson-Pitts et al. [508], Canosa-Mas et al. [250], Suh & Zhang [1394], Albaladejo [20], and Orlando et al. [1129]. The recommended E/R is based on the single temperature dependence study by Bedjanian et al., which covered the range 233–320 K [126]. Although the atmospheric pressure relative rate studies of Ragains & Finlayson-Pitts, Fantechi et al., Finlayson-Pitts et al., and Canosa-Mas et al. suggest a 298 K rate constant that is nearly 20% faster than the recommended value, Bedjanian et al. report little or no pressure dependence over the range 0.25–3.0 Torr He. A recommended temperature-dependent yield for HCl is given by the expression $1.18 \exp(-595/T)$; the temperature dependence is that reported by Bedjanian et al. while the pre-exponential factor is adjusted to give a 298 K yield of 0.16, the average of values reported by Bedjanian et al., Ragains & Finlayson-Pitts, Fantechi et al., and Suh & Zhang. The four reported 298 K HCl yields are in excellent agreement even though they were obtained under very different conditions of pressure and bath gas, i.e., 1 Torr He [126], 10 Torr He [1394], 740 Torr Air [494], and 760 Torr N_2 [1194]. (Table: 10-6, Note: 10-6, Evaluated: 10-6) [Back to Table](#)
- F81. $\text{Cl} + \text{C}_2\text{H}_5\text{CO}_3\text{NO}_2$. Wallington et al. [1536] have measured this rate constant relative to $\text{Cl} + \text{CH}_3\text{Cl}$. The recommended value is adjusted from that given by Wallington et al. using the currently recommended value for the reference reaction rate constant. (Table: 02-25, Note: 02-25) [Back to Table](#)
- F82. $\text{Cl} + 1\text{-C}_3\text{H}_7\text{ONO}_2$. The recommended value of $k(298\text{ K})$ is based on the studies of Wallington et al. [1549] and Nielsen et al. [1082] who measured the rate constant at room temperature relative to atomic chlorine reactions with ethyl chloride and ethane, respectively. The two studies are in excellent agreement and the recommended value is based on an average of the two. (Table: 10-6, Note: 10-6) [Back to Table](#)
- F83. $\text{Cl} + 2\text{-C}_3\text{H}_7\text{ONO}_2$. The recommended value of $k(298\text{ K})$ is taken from Wallington et al. [1549], who studied the reaction at 295 K relative to $\text{Cl} + \text{C}_2\text{H}_5\text{Cl}$. (Table: 10-6, Note: 10-6) [Back to Table](#)

- F84. $\text{Cl} + \text{OCIO}$. The data of Toohey [1455] are in good agreement with the results of Bemand et al. [143] at room temperature, and the recommended value at room temperature is the mean of the values reported in these two studies. The slight negative temperature dependence reported by Toohey [1455] is accepted but with error limits that encompass the temperature independence reported in the earlier study. (Table: 90-1, Note: 90-1, Evaluated:10-6) [Back to Table](#)
- F85. $\text{Cl} + \text{ClOO}$. The recommended value is based on the results of studies by Mauldin et al. [982] and Baer et al. [75], in which ClOO was formed by the pulsed photolysis of Cl_2/O_2 mixtures and its overall loss rate was monitored by UV absorption. In both studies k was found to be independent of temperature. These results are preferred over the results of the earlier, indirect studies of Johnston et al. [747], Cox et al. [358], and Ashford et al. [43]. The earlier studies did show that the predominant reaction pathway is that yielding $\text{Cl}_2 + \text{O}_2$ as products. From the branching ratio data of Cox et al., Ashford et al., and Nicholas and Norrish [1062], it can be estimated that this reaction channel constitutes 95% of the overall reaction with ClO + ClO the products of the minor (5%) reaction channel. (Table: 92-20, Note: 92-20) [Back to Table](#)
- F86. $\text{Cl} + \text{Cl}_2\text{O}$. The preferred value was determined from results of the temperature-dependent study of Stevens and Anderson [1366] and the results of two independent absolute rate coefficient studies reported by Ray et al. [1220], which used the discharge flow-resonance fluorescence and discharge flow-mass spectrometric techniques. This value has been confirmed by Burrows and Cox [225], who determined the ratio $k(\text{Cl} + \text{Cl}_2\text{O})/k(\text{Cl} + \text{H}_2) = 6900$ in modulated photolysis experiments. The earlier value reported by Basco and Dogra [107] has been rejected. (Table: 94-26, Note: 94-26, Evaluated: 10-6) [Back to Table](#)
- F87. $\text{Cl} + \text{Cl}_2\text{O}_2$. The recommended value is that determined by Ingham et al. [713] in a study between 217 K and 298 K using a DF-MS/RF technique. The room temperature value reported by Cox and Hayman [364] in a study using a static photolysis technique with photodiode array UV spectroscopy is in excellent agreement with the recommended value. (Table: 10-6, Note: 10-6, Evaluated: 10-6) [Back to Table](#)
- F88. $\text{Cl} + \text{HOCl}$. This recommendation is based on results over the temperature range 243–365 K reported by Cook et al. [346] and the room temperature result of Kukui et al. [826]. The earlier work of Vogt and Schindler [1523] is thought to have been plagued by complexities with the F-atom titration procedure used for HOCl calibration. Ennis and Birks [485] and Kukui et al. reported that the major reaction channel gives the products $\text{Cl}_2 + \text{OH}$ with measured yields of $91 \pm 6\%$ and $96 \pm 5\%$, respectively. Theoretical calculations by Wang et al. [1568] lend support to the predominance of the $\text{Cl}_2 + \text{OH}$ channel at all temperatures below 300 K. (Table: 10-6, Note: 10-6, Evaluated: 10-6) [Back to Table](#)
- F89. $\text{Cl} + \text{ClNO}$. The discharge flow-resonance fluorescence study of Abbatt et al. [4] provides the first reliable data on the temperature dependence. The laser photolysis-LMR study of Chasovnikov et al. [275] provides rate data for each Cl atom spin state, and they attribute the low value reported by Nelson and Johnston [1053] in a laser flash photolysis-resonance fluorescence study to reaction of the $\text{Cl } ^2\text{P}_{1/2}$ state. Adsorption and decomposition of ClNO on the walls of their static system may account for the very low value of Grimley and Houston [585]. The results of Clyne and Cruse [317] in a discharge flow-resonance fluorescence study are significantly lower than all recent results. The recommended value at room temperature is the mean of the values reported by Abbatt et al. [4], Chasovnikov et al. [275], Nesbitt et al. [1060], and Kita and Stedman [795]. The room temperature result of Chesnokov [296] is in fair agreement with the recommended value. The recommended temperature dependence is from the study of Abbatt et al. [4]. (Table: 90-1, Note: 10-6, Evaluated: 10-6) [Back to Table](#)
- F90. $\text{Cl} + \text{ClONO}_2$. Recommended value is based on the results of Yokelson et al. [1659] and those of Margitan [958]. These results are in excellent agreement; the slightly higher values of Kurylo et al. [841] lie just outside the stated uncertainties. Yokelson et al. report that at 298 K, more than 95% of this reaction proceeds by the reaction channel giving $\text{Cl}_2 + \text{NO}_3$ as products. (Table: 10-6, Note: 10-6, Evaluated: 10-6) [Back to Table](#)
- F91. $\text{Cl} + \text{CH}_3\text{Cl}$. The recommended value for $k(298 \text{ K})$ is the mean of results of the absolute rate study of Manning and Kurylo [955] and the relative rate studies of Wallington et al. [1536], Beichert et al.

[141], and Orlando [1128] (two independent determinations). The recommended temperature dependence is derived from a fit to the data from Manning and Kurylo [955] and from the two relative rate studies of Orlando [1128]. The Arrhenius A-factor was calculated from $k(298\text{ K})$ and E/R . While the 298 K results reported by Clyne and Walker [336] are in good agreement, the value of the activation energy derived by these researchers is significantly higher than that recommended, similar to the situation encountered for the $\text{Cl} + \text{CH}_4$ reaction. Hence, it is assumed that the discharge flow-mass spectrometric studies of these authors were subject to a systematic error. Both the room temperature measurements and E/R obtained between 300 K and 400 K by Bryukov et al. [210], from a study primarily focused at higher temperatures, are in good agreement with the recommendations. The early relative rate studies by Pritchard et al. [1190], Goldfinger et al. [566], Knox [809], and Tschuikow-Roux et al. [1463], were not used to derive the recommended parameters since they were performed at temperatures above 298 K and, with the exception of Pritchard et al., yield somewhat higher values for E/R . (Table: 06-2, Note: 06-2) [Back to Table](#)

- F92. $\text{Cl} + \text{CH}_2\text{Cl}_2$. The recommended value for $k(298\text{ K})$ is an average of the values measured in the relative rate studies of Niki et al. [1088], Beichert et al. [141], Catoire et al. [265], and Orlando [1128] (two independent determinations), and in the absolute rate study of Bryukov et al. [210]. For this evaluation all of the relative rate measurements were recalculated based on the current recommendations for the rate constant of the reference reactions. The recommended value for E/R is taken from a fit to the data of Orlando and agrees with a fit to the data of Bryukov et al. (obtained at room temperature and above) up to 400 K. Above 400 K, these latter data increase more rapidly with temperature. The relative rate studies of Goldfinger et al. [566], Knox [810], Tschuikow-Roux et al. [1463] were performed at temperatures above 298 K and yield significantly higher values for E/R , with the exception of one of the Knox et al. determinations (relative to CH_4), which gives a value of E/R in good agreement with that recommended. The results of Clyne and Walker [336] are higher than those from any other study and were not used in deriving the recommended parameters. (Table: 06-2, Note: 06-2) [Back to Table](#)
- F93. $\text{Cl} + \text{CHCl}_3$. The recommended $k(298\text{ K})$ is an average of the values measured in the relative rate studies of Beichert et al. [141], Brahan et al. [190] (two independent determinations), Catoire et al. [265], and Orlando [1128] (two independent determinations). The recommended temperature dependence is derived from a fit to the two determinations by Orlando and agrees with a fit to the absolute rate data of Bryukov et al. [210] (obtained at room temperature and above) up to 400 K. Above 400 K, these latter data increase more rapidly with temperature. The room temperature value determined in the relative rate study by Yu and Wijnen [1660] is a factor of 50 greater than recommended and was not considered in the recommendation. The results of the absolute investigation of Clyne and Walker [336] are also higher and more scattered than those from most other studies and were not used, nor was the room temperature value derived from the study by Jeoung et al. [743], which is more than a factor of two lower than recommended. The relative rate study by Goldfinger et al. [566] performed near 500 K also resulted in values higher than those in more recent investigations. The relative rate study of Knox [810] yields a similar temperature dependence to that recommended but with rate constant values systematically lower than other studies. The absolute study by Talhaoui et al. [1412] yielded a 298 K rate constant somewhat lower than recommended and a temperature dependence somewhat higher. For this evaluation all of the relative rate measurements were recalculated based on the current recommendations for the rate constant of the reference reactions. The Arrhenius A-factor has been derived from the recommended parameters. (Table: 06-2, Note: 06-2) [Back to Table](#)
- F94. $\text{Cl} + \text{CH}_3\text{F}$ (HFC-41). The recommended value for $k(298\text{ K})$ is an average of the values from the absolute rate studies of Manning and Kurylo [955] and Hitsuda et al. [655] and the relative rate studies of Tschuikow-Roux et al. [1463], Tuazon et al. [1466], and Wallington et al. [1544]. The recommended value for E/R is based on the study of Tschuikow-Roux et al. conducted at room temperature and above. However, in formulating this recommendation, their reported value for the temperature dependence was reduced slightly (by approximately 100 K) to account for what appears to be a small systematic difference between the activation energies obtained in their similar investigations of the $\text{Cl} + \text{CH}_3\text{Cl}$ and $\text{Cl} + \text{CH}_3\text{Br}$ reactions above room temperature and the recommendations that are based on data at 300 K and below. The temperature dependence reported

by Manning and Kurylo is significantly lower, seemingly due to a shift in their data below 250 K. This lower value of E/R is not consistent with the recommended values of E/R for $\text{Cl} + \text{CH}_3\text{Cl}$ and $\text{Cl} + \text{CH}_3\text{Br}$ when compared with those for $\text{OH} + \text{CH}_3\text{F}$, $\text{OH} + \text{CH}_3\text{Cl}$, and $\text{OH} + \text{CH}_3\text{Br}$. Hence, it appears that the Manning and Kurylo data may have been influenced by some systematic error at the lower temperatures. (Table: 06-2, Note: 06-2) [Back to Table](#)

- F95. $\text{Cl} + \text{CH}_2\text{F}_2$ (HFC-32). The recommended value for $k(298\text{ K})$ is from the relative rate study of Nielsen et al. [1076], calculated using the rate constant for the reference reaction ($\text{Cl} + \text{CH}_4$) recommended in this evaluation. The room temperature value from the relative rate study of Tschuikow-Roux et al. [1464] is encompassed within the recommended 95% uncertainty limits. The temperature dependence is estimated from a comparison among the Cl and OH reactions with CH_2F_2 , CH_2Cl_2 , and CH_2FCl . The recommended value of E/R (identical to that for the $\text{OH} + \text{CH}_2\text{F}_2$ reaction) is slightly lower than that determined by Tschuikow-Roux et al. from data at room temperature and above. However, as discussed for other Cl + halomethane reactions, there appears to be a small systematic overestimation in the temperature dependencies determined by these authors. The A-factor has been calculated from the recommended parameters. (Table: 06-2, Note: 06-2) [Back to Table](#)
- F96. $\text{Cl} + \text{CF}_3\text{H}$ (HFC-23). The recommended upper limit for $k(298\text{ K})$ is based on results from the absolute rate study by Jourdain et al. [754] and from the relative rate study by Coomber and Whittle [347], which gives a room temperature value a factor of 50 smaller. (Table: 06-2, Note: 06-2) [Back to Table](#)
- F97. $\text{Cl} + \text{CH}_2\text{FCl}$ (HCFC-31). The recommended value for $k(298\text{ K})$ is an average of the room temperature results from the absolute rate study by Jourdain et al. [754] and the relative rate studies by Tuazon et al. [1466] and Wallington et al. [1555]. The temperature dependence is estimated from a comparison among the Cl and OH reactions with CH_2F_2 , CH_2Cl_2 , and CH_2FCl . The recommended value of E/R (essentially the same as that for the $\text{OH} + \text{CH}_2\text{FCl}$ reaction) is slightly lower than that determined by Tschuikow-Roux et al. [1463], recalculated based on the current recommendation for the rate constant of the reference reaction ($\text{Cl} + \text{CH}_4$). However, as discussed for other Cl + halomethane reactions, there appears to be a small systematic overestimation in the temperature dependencies determined by these authors. The A-factor has been calculated from the recommended parameters. (Table: 06-2, Note: 06-2) [Back to Table](#)
- F98. $\text{Cl} + \text{CHFCl}_2$ (HCFC-21). The recommended value for $k(298\text{ K})$ is the average of the results from the relative rate study of Tuazon et al. [1466] and the absolute rate study of Talhaoui et al. [1412]. These results are preferred over the earlier room temperature results of Glavas and Heicklen [559]. The room temperature value of Jourdain et al. [754] is approximately 50% higher than the recommendation. The recommended value for E/R was obtained from a fit to the data of Talhaoui et al. The A-factor has been calculated from the recommended $k(298\text{ K})$ and E/R. (Table: 06-2, Note: 06-2) [Back to Table](#)
- F99. $\text{Cl} + \text{CHF}_2\text{Cl}$ (HCFC-22). The recommended value for $k(298\text{ K})$ is the mean of the values derived in the relative rate study by Tuazon et al. [1466] and in the absolute rate studies of Jourdain et al. [754] and Talhaoui et al. [1412] (which is assumed to supercede the earlier study by Sawerysyn et al. [1266]). The temperature dependence is from Talhaoui et al. The A-factor from that study has been adjusted to fit the recommended room temperature value. (Table: 06-2, Note: 06-2) [Back to Table](#)
- F100. $\text{Cl} + \text{CH}_3\text{CCl}_3$. The recommended value for $k(298\text{ K})$ is an average of the results from the absolute rate study by Talhaoui et al. [1413] and the relative rate study by Platz et al. [1172]. The recommended value for E/R is derived from a fit to the data of Talhaoui et al. It is reasonably consistent with the value derived by Cillien et al. [306] in a relative rate study conducted over a very narrow temperature range above room temperature, but is somewhat smaller than the value derived in the relative rate study of Tschuikow-Roux et al. [1464]. (Table: 06-2, Note: 06-2) [Back to Table](#)
- F101. $\text{Cl} + \text{CH}_3\text{CH}_2\text{F}$ (HFC-161). The recommended values for both $k(298\text{ K})$ and E/R for each of the two reaction channels are averages of the individual values derived in the relative rate studies of Cadman et al. [239], Martens et al. [968], and Tschuikow-Roux et al. [1464], with each recalculated based on the current recommendation for the rate constant of the reference reaction. The value for $k(298\text{ K})$ of the total reaction obtained from a sum of the two channels is in excellent agreement with the value

obtained in the absolute rate study by Hitsuda et al. [655]. The parameters for the total reaction are: $A = 2.28 \times 10^{-11} \text{ cm}^3 \text{ molecule}^{-1} \text{ s}^{-1}$, $E/R = 370 \text{ K}$, $k(298 \text{ K}) = 6.6 \times 10^{-12} \text{ cm}^3 \text{ molecule}^{-1} \text{ s}^{-1}$, $f(298 \text{ K}) = 1.1$, $g = 100$. (Table: 06-2, Note: 06-2) [Back to Table](#)

- F102. $\text{Cl} + \text{CH}_3\text{CHF}_2$ (HFC-152a). The recommended values for both $k(298 \text{ K})$ and E/R for each of the two reaction channels are averages of the individual values derived in the relative rate studies of Cadman et al. [239], Martens et al. [968], and Yano and Tschuikow-Roux [1657], with each recalculated based on the current recommendation for the rate constant of the appropriate reference reaction. The value for $k(298 \text{ K})$ for the overall reaction obtained by summing the values from the two channels is in excellent agreement with results of the room temperature relative rate studies of Wallington and Hurley [1550], and Tuazon et al. [1466]. The parameters for the overall reaction ($\text{Cl} + \text{CH}_3\text{CHF}_2 \rightarrow \text{products}$) are: $A = 6.0 \times 10^{-12} \text{ cm}^3 \text{ molecule}^{-1} \text{ s}^{-1}$, $E/R = 960 \text{ K}$, $k(298 \text{ K}) = 2.4 \times 10^{-13} \text{ cm}^3 \text{ molecule}^{-1} \text{ s}^{-1}$, $f(298 \text{ K}) = 1.1$, $g = 100$. (Table: 06-2, Note: 06-2) [Back to Table](#)
- F103. $\text{Cl} + \text{CH}_2\text{FCH}_2\text{F}$ (HFC-152). The recommended value for $k(298 \text{ K})$ is an average of the values derived in the relative rate studies of Yano and Tschuikow-Roux [1657] and Wallington et al. [1555] (two determinations), after recalculating each one based on the current recommendation for the rate constant of the appropriate reference reaction. The recommended temperature dependence was determined from a fit to the data of Yano and Tschuikow-Roux, which were obtained at room temperature and above. The temperature dependence may exhibit curvature below room temperature, similar to that for $\text{OH} + \text{CH}_2\text{FCH}_2\text{F}$. Such curvature is most probably encompassed by the assigned uncertainty parameters. (Table: 06-2, Note: 06-2) [Back to Table](#)
- F104. $\text{Cl} + \text{CH}_3\text{CFCl}_2$ (HCFC-141b). The recommended value for $k(298 \text{ K})$ is an average of the values derived in the absolute rate studies of Talhaoui et al. [1413] by the discharge flow - mass spectrometric and the relative rate studies of Wallington and Hurley [1550] and Tuazon et al. [1466]. The room temperature results of Talhaoui et al. are assumed to supercede those of Sawerysyn et al. [1266]. The recommended E/R was obtained from a fit to the data of Talhaoui et al. The data of Warren and Ravishankara [1580] at room temperature agree with the recommendation. However, at higher temperatures the data exhibit considerable scatter apparently due to Cl atom regeneration from decomposition of the radical product ($\text{CH}_2\text{-CFCl}_2$). Hence, this study was not used in deriving the recommended parameters. (Table: 06-2, Note: 06-2) [Back to Table](#)
- F105. $\text{Cl} + \text{CH}_3\text{CF}_2\text{Cl}$ (HCFC-142b). The recommended value for $k(298 \text{ K})$ is an average of the results of the relative rate studies of Wallington and Hurley [1550] and Tuazon et al. [1466], and the absolute rate studies of Jourdain et al. [754] and Talhaoui et al. [1413]; the Talhaoui et al. study is assumed to supercede the earlier study by Sawerysyn et al. [1266]. The recommended temperature dependence is a fit to the data of Talhaoui et al. The A-factor from that study has been adjusted to fit the recommended room temperature value. (Table: 06-2, Note: 06-2) [Back to Table](#)
- F106. $\text{Cl} + \text{CH}_3\text{CF}_3$ (HFC-143a). The recommended values for $k(298 \text{ K})$ and E/R are based on results of the relative rate study of Tschuikow-Roux et al. [1464], recalculated based on the current recommendation for the rate constant of the reference reaction ($\text{Cl} + \text{CH}_4$). An upper limit for $k(298 \text{ K})$ more than two orders of magnitude larger than the recommended value was derived by Hitsuda et al. [655]. (Table: 06-2, Note: 06-2) [Back to Table](#)
- F107. $\text{Cl} + \text{CH}_2\text{FCHF}_2$ (HFC-143). The recommended values for $k(298 \text{ K})$ and E/R for each of the two reaction channels are based on results of the relative rate study of Tschuikow-Roux et al. [1464] recalculated based on the current recommendation for the rate constant of the reference reaction ($\text{Cl} + \text{CH}_4$). The recommended parameters for the total reaction are derived from the sum of the recommended rate expressions for the two reaction channels. The parameters for the total reaction are: $A = 1.57 \times 10^{-11} \text{ cm}^3 \text{ molecule}^{-1} \text{ s}^{-1}$, $E/R = 1720 \text{ K}$, $k(298 \text{ K}) = 4.9 \times 10^{-14}$, $f(298 \text{ K}) = 1.3$, $g = 200$. (Table: 06-2, Note: 06-2) [Back to Table](#)
- F108. $\text{Cl} + \text{CH}_2\text{ClCF}_3$ (HCFC-133a). The recommended value for $k(298 \text{ K})$ is an average of the results from the absolute rate study of Jourdain et al. [751] and the relative rate study of Mogelberg et al. [1023] (two determinations). The recommended value for E/R is a fit to the data of Jourdain et al. (Table: 06-2, Note: 06-2) [Back to Table](#)

- F109. $\text{Cl} + \text{CH}_2\text{FCF}_3$ (HFC-134a). The recommended value for $k(298\text{ K})$ is an average of the results from the relative rate studies of Wallington and Hurley [1550], Tuazon et al. [1466], and Kaiser [756], and from the absolute rate study of Louis et al. [935], which is assumed to supercede the earlier study by Sawerysyn et al. [1266]. The recommended value for E/R is an average of the values determined by Kaiser et al. and Louis et al. (Table: 06-2, Note: 06-2) [Back to Table](#)
- F110. $\text{Cl} + \text{CHF}_2\text{CHF}_2$ (HFC-134). The recommended value for $k(298\text{ K})$ is an average of the results from the relative rate studies of Nielsen et al. [1077] and Yano and Tschuikow-Roux [1657], each recalculated based on the current recommendation for the rate constant of the appropriate reference reaction. The recommended value of E/R is determined from a fit to the data of Yano and Tschuikow-Roux. (Table: 06-2, Note: 06-2) [Back to Table](#)
- F111. $\text{Cl} + \text{CHCl}_2\text{CF}_3$ (HCFC-123). The recommended value for $k(298\text{ K})$ is an average of the results from the absolute rate study of Warren and Ravishankara [1580] and the relative rate studies of Wallington and Hurley [1550] and Tuazon et al. [1466] each recalculated based on the current recommendation for the rate constant of the appropriate reference reaction. The recommended value of E/R is derived from a fit to the data of Warren and Ravishankara. (Table: 06-2, Note: 06-2) [Back to Table](#)
- F112. $\text{Cl} + \text{CHFClCF}_3$ (HCFC-124). The recommended value for $k(298\text{ K})$ is an average of the results from the absolute rate study by Warren and Ravishankara [1580] and the relative rate study by Tuazon et al. [1466]. The recommended value for E/R is based on a fit to the data of Warren and Ravishankara. (Table: 06-2, Note: 06-2) [Back to Table](#)
- F113. $\text{Cl} + \text{CHF}_2\text{CF}_3$ (HFC-125). The recommended value for $k(298\text{ K})$ is an average of the results from the relative rate studies of Tuazon et al. [1466], Sehested et al. [1288], and Edney and Driscoll [474], all conducted only at room temperature. The temperature dependence is estimated from a comparison among the Cl and OH reactions with CH_2FCF_3 , CHF_2CHF_2 , and CHF_2CF_3 . The relative rate study by Coomber and Whittle [347] conducted between 303 K and 399 K corresponds to a value for $k(298\text{ K})$ a factor of 2.5 greater than that recommended. However, the value for E/R derived by these authors is only slightly lower than that estimated. (Table: 06-2, Note: 06-2) [Back to Table](#)
- F114. $\text{ClO} + \text{O}_3$. There are two possible channels for this reaction: $\text{ClO} + \text{O}_3 \rightarrow \text{ClOO} + \text{O}_2$ (k_1); and $\text{ClO} + \text{O}_3 \rightarrow \text{OCIO} + \text{O}_2$ (k_2). The recommended upper limit for k_1 at 298 K is based on results of Stevens and Anderson [1365]. These authors also report that $k_1 = (4 \pm 2) \times 10^{-16} \text{ cm}^3 \text{ molecule}^{-1} \text{ s}^{-1}$ at 413 K. These data can be combined to derive the Arrhenius parameters $A = 2 \times 10^{-12} \text{ cm}^3 \text{ molecule}^{-1} \text{ s}^{-1}$ and $E/R > 3600\text{ K}$. The upper limit for k_2 is based on results reported by DeMore et al. [420] and Wongdontri-Stuper et al. [1641], the Arrhenius parameters for k_2 were estimated. (Table: 92-20, Note: 92-20, Evaluated: 10-6) [Back to Table](#)
- F115. $\text{ClO} + \text{H}_2$. The Arrhenius expression was estimated based on the $\sim 600\text{ K}$ data of Walker (reported in Clyne and Watson [337]). (Table: 82-57, Note: 82-57, Evaluated: 10-6) [Back to Table](#)
- F116. $\text{ClO} + \text{NO}$. The absolute rate coefficients determined in the four discharge flow-mass spectrometric studies (Clyne and Watson [337], Leu and DeMore [888], Ray and Watson [1221] and Clyne and MacRobert [323]) and the discharge flow laser magnetic resonance study of Lee et al. [877] are in excellent agreement at 298 K, and are averaged to yield the preferred value. The value reported by Zahniser and Kaufman [1669] from a competitive study is not used in the derivation of the preferred value as it is about 33% higher. The magnitudes of the temperature dependences reported by Leu and DeMore [888] and Lee et al. are in excellent agreement. Although the E/R value reported by Zahniser and Kaufman [1669] is in fair agreement with the other values, it is not considered as it is dependent upon the E/R value assumed for the $\text{Cl} + \text{O}_3$ reaction. The Arrhenius expression was derived from a least squares fit to the data reported by Clyne and Watson, Leu and DeMore, Ray and Watson, Clyne and MacRobert, and Lee et al. Theoretical rate calculations by Sayin and McKee [1267] give a reaction activation energy ($\sim 0.35\text{ kcal/mol}$) over the temperature range 200 K – 400 K that is supportive of the experimental values. (Table: 82-57, Note: 10-6, Evaluated: 10-6) [Back to Table](#)

- F117. $\text{ClO} + \text{NO}_3$. The recommended value is based on results reported by Cox et al. [352], Cox et al. [363], Biggs et al. [159], and Kukui et al. [824]. Biggs et al. report the rate constant to be independent of temperature, consistent with the results of Cox et al. [363]. This recent study of Kukui et al. supersedes the earlier study of Becker et al. [120] from the same laboratory, which had indicated the major products to be $\text{OCIO} + \text{NO}_2$. There is now agreement among all studies that the major reaction channel forms $\text{ClOO} + \text{NO}_2$ (see Biggs et al. [159], Cox et al. [363], and Kukui et al. [824]). From a study of the OCIO/NO_3 system Friedl et al. [525] conclude that at 220 K the formation of $\text{ClOO} + \text{NO}_2$ is favored. (Table: 82-57, Note: 82-57, Evaluated: 10-6X) [Back to Table](#)
- F118. $\text{ClO} + \text{N}_2\text{O}$. The Arrhenius expression was estimated based on the ~600 K data of Walker (reported in Clyne and Watson [337]). (Table: 82-57, Note: 82-57, Evaluated: 10-6) [Back to Table](#)
- F119. $\text{ClO} + \text{CO}$. The Arrhenius expression was estimated based on the ~600 K data of Walker (reported in Clyne and Watson [337]). (Table: 82-57, Note: 82-57, Evaluated: 10-6) [Back to Table](#)
- F120. $\text{ClO} + \text{CH}_4$. The Arrhenius expression was estimated based on the ~600 K data of Walker (reported in Clyne and Watson [337]). (Table: 82-57, Note: 82-57) [Back to Table](#)
- F121. $\text{ClO} + \text{H}_2\text{CO}$. Poulet et al. [1187] have reported an upper limit of $10^{-15} \text{ cm}^3 \text{ molecule}^{-1} \text{ s}^{-1}$ for k at 298 K using the discharge flow-EPR technique. (Table: 81-3, Note: 81-3) [Back to Table](#)
- F122. $\text{ClO} + \text{CH}_3\text{O}_2$. The recommended expressions for the overall rate constant is based on the results of Helleis et al. [629]. It is consistent with the room temperature measurements of Simon et al. [1308] and Kenner et al. [774]. The results of Kukui et al. [827] for the overall reaction are in agreement with the recommendation at room temperature, but these values show a slight negative temperature dependence in contrast with the slight positive temperature dependence recommended here. There is general agreement that the only important reaction channels are the two channels resulting in the production of $\text{ClOO} + \text{CH}_3\text{O}$ (a) and $\text{CH}_3\text{OCl} + \text{O}_2$ (b). However, there is severe disagreement on their relative importance; at room temperature reaction channel (a) is reported to be the major channel by Helleis et al. [629], Simon et al. [1308], Kukui et al. [827], and Helleis et al. [630], but it is reported to be the minor channel by Biggs et al. [157] and Daele and Poulet [380]. Because of this large discrepancy, no branching ratios are recommended. The branching ratio studies that go down to low temperatures (Helleis et al. [629], Kukui et al. [827], and Helleis et al. [630]) report that reaction channels (a) and (b) are both significant down to lower polar stratospheric temperatures. (Table: 97-4, Note: 97-4) [Back to Table](#)
- F123. $\text{ClO} + \text{ClO}$. There are three bimolecular channels for this reaction: $\text{ClO} + \text{ClO} \rightarrow \text{Cl}_2 + \text{O}_2$ (k_1); $\text{ClO} + \text{ClO} \rightarrow \text{ClOO} + \text{Cl}$ (k_2); and $\text{ClO} + \text{ClO} \rightarrow \text{OCIO} + \text{Cl}$ (k_3). The recommended values for the individual reaction channels are from the study of Nikolaisen et al. [1063]. This study, using a flash photolysis/long path ultraviolet absorption technique, is the most comprehensive study of this system, covering a wide range of temperature and pressure. These results are preferred over the results of earlier studies of the total bimolecular rate coefficient at low pressures by Clyne and Coxon [315], Clyne and White [341], and Clyne et al. [328], and those of other studies reported by Hayman et al. [623], Cox and Derwent [356], Simon et al. [1309], Horowitz et al. [668], and Horowitz et al. [669]. The room temperature branching ratios are $k_1:k_2:k_3 = 0.29:0.50:0.21$. The reaction exhibits both bimolecular and termolecular reaction channels (see entry in Table 2). The termolecular reaction dominates at pressures higher than about 10 Torr. The equilibrium constant for formation of the Cl_2O_2 dimer is given in Table 3. (Table: 94-26, Note: 97-4, Evaluated: 10-6) [Back to Table](#)
- F124. $\text{HCl} + \text{ClONO}_2$. Results of four studies of the kinetics of this system have been published, in which the following upper limits to the homogeneous bimolecular rate constant were reported: $10^{-19} \text{ cm}^3 \text{ molecule}^{-1} \text{ s}^{-1}$ by a static wall-less long-path UV absorption technique and a steady-state flow FTIR technique (Molina et al. [1024]); $5 \times 10^{-18} \text{ cm}^3 \text{ molecule}^{-1} \text{ s}^{-1}$ using a flow reactor with FTIR analysis (Friedl et al. [523]); $8.4 \times 10^{-21} \text{ cm}^3 \text{ molecule}^{-1} \text{ s}^{-1}$ using a static photolysis system with FTIR analysis (Hatakeyama and Leu [621] and Leu et al. [889]); and $1.5 \times 10^{-19} \text{ cm}^3 \text{ molecule}^{-1} \text{ s}^{-1}$ by FTIR analysis of the decay of ClONO_2 in the presence of HCl in large-volume (2500 and 5800 liters) Teflon or Teflon-coated chambers (Atkinson et al. [49]). Earlier, Birks et al. [163] had reported a higher upper limit. All studies found this reaction to be catalyzed by surfaces. The differences in the reported upper limits can be accounted for in terms of the very different reactor

characteristics and detection sensitivities of the various studies. The homogeneous reaction is too slow to have any significant effect on atmospheric chemistry. (Table: 87-41, Note: 87-41, Evaluated: 10-6) [Back to Table](#)

- F125. $\text{CH}_2\text{ClO} + \text{O}_2$. The CH_2ClO radical is reported to be resistant to unimolecular dissociation into $\text{Cl} + \text{CH}_2\text{O}$ products, according to chain reaction/product analysis studies by Sanhueza and Heicklen [1258] and Niki et al. [1088], and kinetics studies by Catoire et al. [264]. The recommendation is based on the work of Kaiser and Wallington [761] who studied the competition between reaction with O_2 and HCl elimination in a complex photochemical reaction system using FTIR detection of stable products. The recommendation is a factor of 5 higher than estimated using the empirical relationship given by Atkinson and Carter [58]. The fate of CH_2ClO in the atmosphere is reaction with O_2 . (Table: 94-26, Note: 94-26) [Back to Table](#)
- F126. $\text{CH}_2\text{ClO}_2 + \text{HO}_2$. The recommendation is based on the measurement reported by Catoire et al. [264], who used pulsed photolysis with UV absorption detection at 1 atm pressure and 251–588 K. (Table: 94-26, Note: 94-26) [Back to Table](#)
- F127. $\text{CH}_2\text{ClO}_2 + \text{NO}$. The recommendation is based on the value reported by Sehested et al. [1290], who used pulsed radiolysis and UV absorption detection of NO_2 to measure the rate coefficient. The temperature dependence is estimated by analogy to similar $\text{RO}_2 + \text{NO}$ reactions. (Table: 94-26, Note: 94-26) [Back to Table](#)
- F128. $\text{CCl}_3\text{O}_2 + \text{NO}$. The recommendation is based upon the measurements of Ryan and Plumb [1247] and Dognon et al. [446], who agree well at room temperature. The temperature dependence is derived from the data of Dognon et al., who covered the temperature range 228–413 K. The CCl_3O primary product of the reaction of CCl_3O_2 with NO decomposes rapidly to eliminate Cl , according to Lesclaux et al. [883]. (Table: 94-26, Note: 94-26) [Back to Table](#)
- F129. $\text{CCl}_2\text{FO}_2 + \text{NO}$. The recommendation is based on the measurements made by Dognon et al. [446] using pulsed photolysis with mass spectrometry detection at 1–10 Torr and 228–413 K. These results supersede the earlier study of Lesclaux and Caralp [881]. The CCl_2FO radical primary product of the $\text{CCl}_2\text{FO}_2 + \text{NO}$ reaction is reported by Lesclaux et al. [883] and Wu and Carr [1645] to rapidly decompose to eliminate Cl and to give the products indicated. (Table: 94-26, Note: 94-26) [Back to Table](#)
- F130. $\text{CClF}_2\text{O}_2 + \text{NO}$. The recommendation is based on the measurements made by Dognon et al. [446], who used pulsed photolysis with mass spectrometry detection at 1–10 Torr and 228–413 K, and Sehested et al. [1290], who used pulsed radiolysis with UV absorption detection of the NO_2 product at one atm and 298 K. Wu and Carr [1645] observed the CClF_2O radical primary product to rapidly dissociate to CF_2O and Cl . (Table: 94-26, Note: 94-26) [Back to Table](#)
- G1. $\text{O} + \text{BrO}$. The preferred value is based on the value reported by Thorn et al. [1436] using a dual laser flash photolysis/long path absorption/resonance fluorescence technique. Clyne et al. [330] reported a value approximately 40% lower. (Table: 97-4, Note: 97-4, Evaluated: 10-6) [Back to Table](#)
- G2. $\text{O} + \text{HBr}$. Results of the flash photolysis-resonance fluorescence study of Nava et al. [1044] for 221–455 K and the laser flash photolysis-resonance fluorescence study of Nicovich and Wine [1072] for 250–402 K provide the only data at stratospheric temperatures. Results reported include those of Singleton and Cvetanovic [1317] for 298–554 K by a phase-shift technique, and discharge flow results of Brown and Smith [200] for 267–430 K and Takacs and Glass [1404] at 298 K. The preferred value is based on the results of Nava et al., as well as those of Nicovich and Wine and those of Singleton and Cvetanovic over the same temperature range, since these results are less subject to complications due to secondary chemistry than are the results using discharge flow techniques. The uncertainty at 298 K has been set to encompass these latter results. (Table: 90-1, Note: 90-1, Evaluated: 10-6) [Back to Table](#)
- G3. $\text{O} + \text{HOBr}$. The recommended room temperature value is the mean of results of Monks et al. [1436] and Kukui et al. [825]. The temperature dependence is from Nesbitt et al. [1059]. The A-factor from that study has been adjusted to fit the recommended room temperature value. Kukui et al.

determined that the Br atom abstraction channel is the only pathway at room temperature. (Table: 97-4, Note: 97-4, Evaluated: 10-6) [Back to Table](#)

- G4. $O + BrONO_2$. The recommendation is based on the study of Soller et al. [1342] that employed the laser flash photolysis – resonance fluorescence technique and covered the temperature range 227 – 339 K. The recommended uncertainty parameters are larger than those reported by Soller et al. pending independent confirmation of their results. Burkholder [219] has coupled laser flash photolysis with detection of NO_3 by long path absorption spectroscopy to show that the NO_3 yield is >0.85 at 298 K. (Table: 06-2, Note: 06-2) [Back to Table](#)
- G5. $OH + Br_2$. The recommended room temperature value is the average of the values reported by, Poulet et al. [1182], Loewenstein and Anderson [930], Gilles et al. [553], and Bedjanian et al. [128]. The temperature dependence is from an average of the E/R values of Gilles et al. and Bedjanian et al. The results of Boodaghians et al. [177] were not considered. Loewenstein and Anderson determined that the exclusive products are $Br + HOBr$. (Table: 06-2, Note: 06-2) [Back to Table](#)
- G6. $OH + BrO$. The preferred value of $k(298\text{ K})$ is from an average of the results of Gilles et al. [554] and Bedjanian et al. [133]. The only temperature dependence study is from Bedjanian et al. The recommendation is based on their results. The likely products of this reaction are $Br + HO_2$. Bedjanian et al. attempted to measure the branching ratio for HBr formation but there were significant problems from secondary chemistry. An upper limit of 3% was reported for the HBr yield. (Table: 06-2, Note: 06-2) [Back to Table](#)
- G7. $OH + HBr$. The preferred value at room temperature is the average of the values reported by Ravishankara et al. [1214] using FP-RF, Jourdain et al. [753] using DF-EPR, Cannon et al. [247] using FP-LIF, Ravishankara et al. [1217] using LFP-RF and LFP-LIF, and Bedjanian et al. [131] using DF-MS. Values reported by Takacs and Glass [1403] and Husain et al. [697] as well as the preliminary value of Smith and Zellner [1338] are a factor of 2 lower and were not included in the derivation of the preferred value. The recommendation for the temperature dependence is derived from the data of Bedjanian et al. [131]. This study obtained a small negative temperature dependence which is in qualitative agreement with the Laval nozzle studies of Sims et al. [1314], Atkinson et al. [45], and Jaramillo et al. [725] over the 200-300 K temperature range. The data of Ravishankara et al. [1214] show no dependence on temperature over the range 249–416 K. (Table: 06-2, Note: 06-2) [Back to Table](#)
- G8. $OH + CH_3Br$. The recommended rate expression is derived from a combined fit to the data from the relative rate study of Hsu and DeMore [683] (recalculated based on the current recommendation for the rate constant for the $OH + CH_3CHF_2$ reference reaction, as discussed in the note for that reaction) and the absolute determinations by Chichinin et al. [297], Mellouki et al. [1006], and Zhang et al. [1687]. The results of these extensive studies are in excellent agreement and are preferred over the higher values reported in the earlier studies of Davis et al. [398] and Howard and Evenson [674]. (Table: 02-25, Note: 02-25) [Back to Table](#)
- G9. $OH + CH_2Br_2$. The recommended value for $k(298\text{ K})$ is an average of the values from the absolute studies of Mellouki et al. [1006] and Zhang et al. [1679] and from the relative rate measurements of DeMore [415] (recalculated based on the current recommendation for the rate constant for the $OH + CH_2Cl_2$ reference reaction) and Orlando et al. [1132] (recalculated based on the current recommendation for the rate constant for the $OH + CH_3C(O)CH_3$ reference reaction). The recommended value of E/R is from the study of Mellouki et al. [1006]. (Table: 02-25, Note: 02-25) [Back to Table](#)
- G10. $OH + CHBr_3$. The recommended rate expression is derived from a fit to the data from the relative rate study of DeMore [415] (recalculated based on the current recommendation for the rate constant for the $OH + CH_2Cl_2$ reference reaction). The results of Orkin et al. [1121] are higher by a factor of 2 but have the same temperature dependence. They are encompassed within the 2σ confidence limits. (Table: 02-25, Note: 02-25) [Back to Table](#)
- G11. $OH + CHF_2Br$. The recommended values for $k(298\text{ K})$ and E/R are derived from a fit to the data of Talukdar et al. [1414] (two studies), Orkin and Khamaganov [1120], and Hsu and DeMore [684] (a relative rate measurement recalculated using the current recommendation for the rate constant for the

- OH + CH₄ reference reaction). These data are preferred over the consistently higher results reported by Brown et al. [196]. (Table: 02-25, Note: 02-25) [Back to Table](#)
- G12. OH + CH₂ClBr. The recommended value for k(298 K) is an average of the values from two relative rate studies by DeMore [415] (recalculated based on the current recommendation for the rate constant for the OH + CH₂Cl₂ reference reaction) and Bilde et al. [161] (recalculated using the current recommendation for the rate constant for the OH + CH₂Br₂ reference reaction) and two absolute determinations by Orkin et al. [1122], all of which are in good agreement. The recommended E/R is obtained from a fit to the data of DeMore and Orkin et al. The A factor was then calculated. (Table: 02-25, Note: 02-25) [Back to Table](#)
- G13. OH + CF₂Br₂. The A-factor was estimated, and a lower limit for E/R was derived by using the upper limit for the rate constant at 298 K reported by Burkholder et al. [222] in a study using pulsed photolysis-LIF and DF-LMR techniques. (Table: 02-25, Note: 02-25) [Back to Table](#)
- G14. OH + CF₃Br. The A-factor was estimated and a lower limit for E/R was derived by using the upper limit for the rate constant at 460 K reported by Orkin and Khamaganov [1120]. These parameters were then used to calculate an upper limit for k(298 K). The upper limit for k(298 K) determined by Burkholder et al. [222] in a study using pulsed photolysis-LIF and DF-LMR techniques at room temperature is understandably higher. A less sensitive upper limit was also reported by Le Bras and Combourieu [861]. (Table: 02-25, Note: 02-25) [Back to Table](#)
- G15. OH + CF₂ClBr. The A-factor was estimated, and a lower limit for E/R was derived using the upper limit for the rate constant at 298 K reported by Burkholder et al. [222] in a study using pulsed photolysis-LIF and DF-LMR techniques. A less sensitive upper limit was reported by Clyne and Holt [321]. (Table: 02-25, Note: 02-25) [Back to Table](#)
- G16. OH + CH₂BrCH₃. The recommended values for k(298 K) and E/R are derived from a fit to the data (T ≤ 300 K) of Herndon et al. [636]. These data suggest a curvature of the Arrhenius plot similar to that found for the OH reaction with CH₃CH₂F. The data of Qiu et al. [1191] (which include earlier data reported by the same research group in Xing et al. [1650]) were not used because they were obtained mainly above room temperature and exhibit a very steep temperature dependence resulting in a value for E/R that is larger than the E/R value obtained from data at T > 298 K for the OH reaction with CH₃CH₂F. The k(300 K) value reported by Donaghy et al. [451] seems too low for this reaction when compared with the recommendation for presumably slower (and better studied) OH reaction with CH₃CH₂F. (Table: 02-25, Note: 02-25) [Back to Table](#)
- G17. OH + CH₂BrCF₃. The recommended values for k(298 K) and E/R are from a combined fit to the data of Nelson et al. [1048] and Orkin and Khamaganov [1120]. (Table: 02-25, Note: 02-25) [Back to Table](#)
- G18. OH + CHFBrCF₃. The recommended rate expression is derived from a combined fit to the data (below 400°K) of Orkin and Khamaganov [1120] and Brown et al. [196]. (Table: 02-25, Note: 02-25) [Back to Table](#)
- G19. OH + CHClBrCF₃. The recommended rate expression is derived from a fit to the data of Orkin and Khamaganov [1120] (for T ≤ 400 K). The room temperature value measured by Brown et al. [197] lies somewhat higher than this recommendation but is encompassed within the 2σ confidence limits. (Table: 02-25, Note: 02-25) [Back to Table](#)
- G20. OH + CHFClCF₂Br. The recommended rate expression is derived from a fit to the data from the relative rate study of DeMore [415] (recalculated based on the current recommendation for the rate constant for the OH + CH₃CCl₃ reference reaction). (Table: 02-25, Note: 02-25) [Back to Table](#)
- G21. OH + CF₂BrCF₂Br. The A-factor was estimated and a lower limit for E/R was derived by using the upper limit for the rate constant at 460 K reported by Orkin and Khamaganov [1120]. These parameters were then used to calculate an upper limit for k(298 K). The upper limit for k(298 K) determined by Burkholder et al. [222] in a study using pulsed photolysis-LIF and DF-LMR techniques at room temperature is understandably higher. (Table: 02-25, Note: 02-25) [Back to Table](#)

- G22. $\text{OH} + \text{CH}_2\text{BrCH}_2\text{CH}_3$. The recommended values for $k(298\text{ K})$ and E/R are derived from a fit to the data ($T \leq 300\text{ K}$) from Donaghy et al. [451] (using cyclopropane as the reference reactant), Teton et al. [1430], Nelson et al. [1049], Herndon et al. [636], Gilles et al. [552], and Kozlov et al. [821]. Significant curvature in the Arrhenius plot has been observed over the 480 K to 210 K temperature range, due to the three different hydrogen-abstraction reaction channels that occur. These channels have been quantified in the study of Gilles et al. In spite of the noticeable Arrhenius curvature, the data below 300 K can be well represented by a two-parameter Arrhenius fit. (Table: 10-6, Note: 10-6, Evaluated: 10-6) [Back to Table](#)
- G23. $\text{OH} + \text{CH}_3\text{CHBrCH}_3$. The recommendation for $k(298\text{ K})$ is an average of the values reported in the absolute rate studies of Herndon et al. [636], Kozlov et al. [821], and Bryukov et al. [211] and in the relative rate study of Donaghy et al. [451] (using cyclopropane as the reference reactant). The recommended value for E/R is an average of the parameters derived from a fit to the data ($T \leq 300\text{ K}$) of Herndon et al. [636] and Kozlov et al. [821], which are in excellent agreement. The A factor was then calculated. The absolute temperature dependent data of Teton et al. [1430] lie systematically higher than those from the three more recent studies. Significant curvature in the Arrhenius plot has been observed over the 480 K to 210 K temperature range, presumably due to the two different hydrogen-abstraction reaction channels that occur. In spite of the noticeable Arrhenius curvature, the data below 300 K can be well represented by a two-parameter Arrhenius fit. (Table: 10-6, Note: 10-6, Evaluated: 10-6) [Back to Table](#)
- G24. $\text{HO}_2 + \text{Br}$. The room temperature rate constant is obtained from an average of the results of Laverdet et al. [857], Toohey et al. [1457] and Bedjanian et al. [132]. The results of Posey et al. [1178] were not considered because of problems with the experimental method. The results of Poulet et al. [1183] were not considered because of complications associated with secondary reactions. The recommendation for the temperature dependence is based on the results of Bedjanian et al. [132]. (Table: 06-2, Note: 06-2) [Back to Table](#)
- G25. $\text{HO}_2 + \text{BrO}$. The recommendation is based on results of the temperature-dependent studies of Elrod et al. [481], Li et al. [906] and Bedjanian et al. [134]. It is assumed that the Bedjanian et al. results supercede those of Larichev et al. [854] since the same experimental technique was used, and the same research group was involved in both studies. The recommended room temperature value is the mean of the values reported in these studies, as well as those of Cronkhite et al. [371] and Bloss et al. [172]. The room temperature value of Bridier et al. [194], which was not obtained under pseudo-first-order decay conditions, was not included in derivation of the recommendation. Bedjanian et al. have determined an upper limit of 0.4% for production of HBr and O_3 at 298 K. From a study of the reverse reaction above room temperature, Mellouki et al. [1005] determined by extrapolation that the yield of $\text{HBr} + \text{O}_3$ is an insignificant fraction ($<0.01\%$) of the total reaction down to 200 K. (Table: 06-2, Note: 06-2) [Back to Table](#)
- G26. $\text{NO}_3 + \text{HBr}$. The recommendation is the upper limit reported by Mellouki et al. [1002] in a study using DF-EPR techniques. This upper limit shows that this reaction is of negligible importance in stratospheric chemistry. Canosa-Mas et al. [251] reported a value that is consistent, within experimental error, with the upper limit of Mellouki et al. (Table: 90-1, Note: 92-20, Evaluated: 10-6) [Back to Table](#)
- G27. $\text{Cl} + \text{CH}_3\text{Br}$. The recommended value for $k(298\text{ K})$ is an average of the results from the absolute rate studies of Gierczak et al. [545], Kambanis et al. [763] and Piety et al. [1166], and from the relative rate study of Orlando et al. [1132]. The recommended value for E/R is based on a combined fit to these same four studies restricted to temperatures of 300 K and below. Results of the relative rate study Tschuirow-Roux et al. [1463] were not used in derivation of the recommended values since they appear to be systematically higher than the results of the other investigations. The products of this reaction are expected to primarily be CH_2Br and HCl. The possible production of $\text{CH}_3\text{Cl} + \text{Br}$ is very small in the atmosphere [567]. (Table: 06-2, Note: 06-2) [Back to Table](#)
- G28. $\text{Cl} + \text{CH}_2\text{Br}_2$. The recommended value for $k(298\text{ K})$ is an average of the results from the absolute rate studies of Gierczak et al. [545] and Kambanis et al. [763] and from the three relative rate experiments of Orlando et al. [1132]. The recommended value for E/R is based on a combined fit to the data ($T < 300\text{ K}$) from these same studies after normalizing each one to the recommended value

for $k(298\text{ K})$. Results of the relative rate study of Tschuikow-Roux et al. [1463] were not used in derivation of the recommended parameters since they are significantly greater at 298 K and correspond to a temperature dependence substantially stronger than derived from the data of other investigations. (Table: 06-2, Note: 06-2) [Back to Table](#)

- G29. $\text{Cl} + \text{CHBr}_3$. The recommended parameters are based on the only reported study of this reaction by Kambanis et al. [763], who employed a very low pressure reactor and monitored reactants and products using mass spectrometry. (Table: 06-2, Note: 06-2) [Back to Table](#)
- G30. $\text{Cl} + \text{CH}_2\text{ClBr}$. The recommended value for $k(298\text{ K})$ is an average of two relative rate determinations by Bilde et al. [161] (recalculated based on the current recommendation for the rate constants of the reference). The temperature dependence is estimated from a comparison with the reactions of Cl with CH_2Cl_2 and CH_2Br_2 . The relative rate investigation by Tschuikow-Roux et al. [1463] gives a value for $k(298\text{ K})$ only slightly larger than recommended, but a temperature dependence that is significantly stronger and inconsistent with the that recommended for the $\text{Cl} + \text{CH}_2\text{Cl}_2$ and $\text{Cl} + \text{CH}_2\text{Br}_2$ reactions. (Table: 06-2, Note: 06-2) [Back to Table](#)
- G31. $\text{Br} + \text{O}_3$. The results reported for $k(298\text{ K})$ by Clyne and Watson [339], Leu and DeMore [887], Michael et al. [1013], Michael and Payne [1018], Toohey et al. [1458], Nicovich et al. [1067] and Ninomiya et al. [1096] are in excellent agreement. The preferred value at 298 K is derived by taking the mean of these seven values. There is less agreement among reported temperature dependences, with E/R values ranging from ~900 (Leu and DeMore and Toohey et al.) to ~600 (Michael et al. and Michael and Payne). The preferred value of E/R represents an average of the E/R's from the five studies carried out as a function of temperature (not including Clyne and Watson and Ninomiya et al. which were room temperature only). (Table: 09-31, Note: 09-31) [Back to Table](#)
- G32. $\text{Br} + \text{H}_2\text{O}_2$. The recommended upper limit of the rate constant at room temperature is based on results reported in the study by Toohey et al. [1457] using a discharge flow-resonance fluorescence/laser magnetic resonance technique. Their upper limit determined over the temperature range 298–378 K is consistent with less sensitive upper limits determined by Leu [897] and Posey et al. [1178] using the discharge flow-mass spectrometric technique. The much higher value reported by Heneghan and Benson [632] may result from the presence of excited Br atoms in the very low pressure reactor. The pre-exponential factor was chosen to be consistent with that for the $\text{Cl} + \text{H}_2\text{O}_2$ rate constant, and the E/R value was fit to the upper limit at 298 K. Mellouki et al. [1005] have measured the rate of the reverse reaction. (Table: 87-41, Note: 94-26, Evaluated: 10-6) [Back to Table](#)
- G33. $\text{Br} + \text{NO}_3$. The recommended value is that reported by Mellouki et al. [1002] in a study using DF-DPR techniques. (Table: 90-1, Note: 92-20, Evaluated: 10-6) [Back to Table](#)
- G34. $\text{Br} + \text{H}_2\text{CO}$. There have been two direct studies of this rate constant as a function of temperature: Nava et al. [1046], using the flash photolysis–resonance fluorescence technique, and Poulet et al. [1181], using the discharge flow-mass spectrometric technique. These results are in reasonably good agreement. The Arrhenius expression was derived from a least squares fit to the data reported in these two studies. The higher room temperature value of Le Bras et al. [862], using the discharge flow–EPR technique, has been shown to be in error due to secondary chemistry (Poulet et al.). The relative rate study of Ramacher et al. [1200] is in good agreement with the recommendation. (Table: 09-31, Note: 09-31) [Back to Table](#)
- G35. $\text{Br} + \text{CH}_2=\text{C}(\text{CH}_3)\text{CH}=\text{CH}_2 \rightarrow \text{products}$. A single relative rate study by Bierbach et al. [155], which employed air as the bath gas at a pressure of 1 bar, has been reported. The process studied by Bierbach et al. is not an elementary reaction. The overall rate constant for loss of isoprene via a multi-reaction sequence was measured relative to the overall rate constant for loss of 1,3-butadiene via a similar multi-reaction sequence. The multi-reaction sequence involves addition of Br to the di-alkenes to form (possibly several) bromo-alkyl radicals that react with O_2 in competition with decomposition back to Br + di-alkene reactants. A complicated dependence of the overall rate constant on temperature, pressure, and $[\text{O}_2]$ is likely, so the recommended rate constant of $7.4 \times 10^{-11} \text{ cm}^3 \text{ molecule}^{-1} \text{ s}^{-1}$ with $f(298\text{ K}) = 1.25$ should only be used at temperatures very close to 298

K and O₂ concentrations very close to those present in air at P ~ 1 bar. (Table: 10-6, Note: 10-6, Evaluated: 10-6) [Back to Table](#)

- G36. Br + OCIO. The recommended rate constant at room temperature is the mean of the values reported by Clyne and Watson [340] and Toohey [1455]. In the study of Clyne and Watson, correction for the effect of the rapid reverse reaction was required. The temperature dependence reported by Toohey [1455] is accepted but with increased error limits. (Table: 90-1, Note: 90-1, Evaluated: 10-6) [Back to Table](#)
- G37. Br + Cl₂O. The recommended value is based on results reported by Stevens and Anderson [1366] and by Sander and Friedl [1251], which are in good agreement. (Table: 94-26, Note: 94-26, Evaluated: 10-6) [Back to Table](#)
- G38. Br + Cl₂O₂. The recommended value is that determined in a study by Ingham et al. [713] between 223 K and 298 K using a DF-MS/RF technique. Ingham et al. found that BrCl was the only major Br-containing product from the reaction. (Table: 10-6, Note: 10-6, Evaluated: 10-6) [Back to Table](#)
- G39. BrO + O₃. The recommended upper limit value is based on the studies of Rattigan et al. [1202] and Rowley et al. [1244]. Both papers report a value of $\sim 2 \times 10^{-18} \text{ cm}^3 \text{ molecule}^{-1} \text{ s}^{-1}$ for the channel to produce OBrO + O₂. The recommended upper limit of $2 \times 10^{-17} \text{ cm}^3 \text{ molecule}^{-1} \text{ s}^{-1}$ is a factor of 2.5 less than the upper limit of 5×10^{-17} , derived by Mauldin et al. [983]. The pre-exponential factor was estimated, and E/R was calculated. (Table: 97-4, Note: 10-6, Evaluated: 10-6) [Back to Table](#)
- G40. BrO + NO. The results of three low pressure mass spectrometric studies (Clyne and Watson [339]; Ray and Watson [1221]; Leu [895]) and a high pressure UV absorption study (Watson et al. [1590]), which all used pseudo-first-order conditions, are in excellent agreement at 298 K and are thought to be much more reliable than an earlier low pressure UV absorption study (Clyne and Cruse [316]). The results of the two temperature-dependence studies are in good agreement and both show a small negative temperature dependence. The preferred Arrhenius expression was derived from a least squares fit to all the data reported in the four studies mentioned above. By combining the data reported by Watson et al. with those from the three mass spectrometric studies, it can be shown that this reaction does not exhibit any observable pressure dependence between 1 and 700 Torr total pressure. The temperature dependences of k for the analogous ClO and HO₂ reactions are also negative and are similar in magnitude. (Table: 82-57, Note: 82-57, Evaluated: 10-6) [Back to Table](#)
- G41. BrO + NO₃. The recommended value is the geometric mean of the lower and upper limits reported by Mellouki et al. [1002] in a study using DF-DPR techniques. These reported limits are encompassed within the indicated uncertainty limits. (Table: 90-1, Note: 92-20, Evaluated: 10-6) [Back to Table](#)
- G42. BrO + ClO. Friedl and Sander [524], using DF/MS techniques, measured the overall rate constant over the temperature range 220–400 K and also over this temperature range determined directly branching ratios for the reaction channels producing BrCl and OCIO. The same authors in a separate study using flash photolysis–ultraviolet absorption techniques (Sander and Friedl [1251]) determined the overall rate constant over the temperature range 220–400 K and pressure range 50–750 Torr and also determined at 220 K and 298 K the branching ratio for OCIO production. The results by these two independent techniques are in excellent agreement, with the overall rate constant showing a negative temperature dependence. Toohey and Anderson [1456], using DF/RF/LMR techniques, reported room temperature values of the overall rate constant and the branching ratio for OCIO production. They also found evidence for the direct production of BrCl in a vibrationally excited Π state. Poulet et al. [1179], using DF/MS techniques, reported room temperature values of the overall rate constant and branching ratios for OCIO and BrCl production. Overall room temperature rate constant values reported also include those from the DF/MS study of Clyne and Watson [340] and the very low value derived in the flash photolysis study of Basco and Dogra [106]. The recommended Arrhenius expressions for the individual reaction channels are taken from the study of Friedl and Sander [524] and Turnipseed et al. [1480]. These studies contain the most comprehensive sets of rate constant and branching ratio data. The overall rate constants reported in these two studies are in good agreement (20%) at room temperature and in excellent agreement at stratospheric temperatures. Both studies report that OCIO production by channel (1) accounts for 60% of the overall reaction at 200 K. Both studies report a BrCl yield by channel (3) of about 8%,

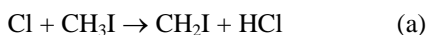
relatively independent of temperature. The recommended expressions are consistent with the body of data from all studies except those of Hills et al. [649] and Basco and Dogra [106]. (Table:09-31, Note: 09-31) [Back to Table](#)

- G43. $\text{BrO} + \text{BrO}$. Measurements of the overall rate constant can be divided into categories—those in which BrO was monitored by UV absorption and those in which BrO was monitored by mass spectrometry. Gilles et al. [556] have re-analyzed the results of the UV absorption studies and scaled the reported values of the rate constant to the UV absorption cross sections reported in their paper. When scaled in this manner, the room temperature rate constant values reported in the UV absorption studies (Sander and Watson [1254], Mauldin et al. [983], Bridier et al. [194], Rowley et al. [1244], Laszlo et al. [855], and Gilles et al.) come into very good agreement among themselves and also with results of the mass spectrometric studies of Clyne and Watson [339] and Lancar et al. [848]. This provides the basis for the recommended room temperature value. The temperature dependence is based on results of Sander and Watson, Turnipseed et al. [1479] and Gilles et al. The results of Harwood et al. [619] are in good agreement with the recommendation.

There are two possible bimolecular channels for this reaction: $\text{BrO} + \text{BrO} \rightarrow 2\text{Br} + \text{O}_2$ (k_1) and $\text{BrO} + \text{BrO} \rightarrow \text{Br}_2 + \text{O}_2$ (k_2). The partitioning of the total rate constant into its two components, k_1 and k_2 , has been measured at room temperature by Sander and Watson [1254], Turnipseed et al. [1479], and Lancar et al. [848], by Jaffe and Mainquist [721] from 258 to 333 K, by Cox et al. [367] from 278 to 348 K, and by Mauldin et al. [983] from 220 to 298 K. All are in agreement that $k_1/k = 0.85 \pm 0.03$ at 298 K. From the values of $k_1/k = 0.85$ at 298 K (all studies) and 0.68 at 220 K (Mauldin et al. and Cox et al. extrapolated), one can derive the temperature-dependent expression $k_1/k = 1.60 \exp(-190/T)$. From the recommended Arrhenius expression for the overall rate constant $k = k_1 + k_2$ and the expression for the branching ratio k_1/k , one can derive the following Arrhenius expressions for the individual reaction channels: $k_1 = 2.4 \times 10^{-12} \exp(40/T) \text{ cm}^3 \text{ molecule}^{-1} \text{ s}^{-1}$ and $k_2 = 2.8 \times 10^{-14} \exp(860/T) \text{ cm}^3 \text{ molecule}^{-1} \text{ s}^{-1}$. (Table: 97-4, Note: 97-4, Evaluated: 10-6) [Back to Table](#)

- G44. $\text{O}_3 + \text{OBrO}$. An upper limit has been determined by Li et al. [908] using DF/MS. (Table: 10-6, Note: 10-6, Evaluated: 10-6) [Back to Table](#)
- G45. $\text{NO} + \text{OBrO}$. The recommended value is that determined by Li et al. [908] using DF/MS to monitor the decay of OBrO in excess NO. A possible complication in these experiments exists from the secondary reaction of Br with OBrO. (Table: 10-6, Note: 10-6, Evaluated: 10-6) [Back to Table](#)
- G46. $\text{CH}_2\text{BrO}_2 + \text{NO}$. The recommendation is based on the 298 K measurement of Sehested et al. [1290], who used pulsed radiolysis with UV absorption detection of the NO_2 product formation rate. The temperature dependence is estimated based on analogy to similar $\text{RO}_2 + \text{NO}$ reactions. The CH_2BrO product has been shown to undergo rapid unimolecular decomposition to yield $\text{CH}_2\text{O} + \text{Br}$ by Chen et al. [280] and Orlando et al. [1131]. The domination of this channel over the reaction of CH_2BrO with O_2 is consistent with the fate of other alkoxy radicals (Chen et al. and Orlando et al.), but contradicts the earlier result of Nielson et al. [1079]. (Table: 94-26, Note: 97-4) [Back to Table](#)
- H1. $\text{O} + \text{I}_2$. Based on the room temperature data of Ray and Watson [1221] and Laszlo et al. [856]. The molecular beam study of Parrish and Herschbach [1146] suggests a zero activation energy, consistent with the near gas kinetic value of k at 298 K. (Table: 97-4, Note: 97-4) [Back to Table](#)
- H2. $\text{O} + \text{IO}$. Based on results of Laszlo et al. [856], the only reported study of this rate constant. This value was derived from modeling a system in which the concentrations of I_2 and IO were monitored simultaneously. This rate constant is a factor of 4 greater than the values for the corresponding reactions of O with ClO and BrO. (Table: 97-4, Note: 97-4) [Back to Table](#)
- H3. $\text{OH} + \text{I}_2$. Based on the data of Loewenstein and Anderson [931] and Jenkin et al. [731]. (Table: 94-26, Note: 94-26) [Back to Table](#)
- H4. $\text{OH} + \text{HI}$. Based on the data of Lancar et al. [850] and MacLeod et al. [948]. (Table: 94-26, Note: 94-26) [Back to Table](#)
- H5. $\text{OH} + \text{CH}_3\text{I}$. The recommended rate expression is derived from a fit to the data of Brown et al. [198], the only reported study of this reaction. (Table: 02-25, Note: 02-25) [Back to Table](#)

- H6. OH + CF₃I. The recommended rate expression is derived from a fit to the data of Gilles et al. [555]. The results from the studies by Garraway and Donovan [535] and Berry et al. [149] were not used in deriving the recommendation as the results were possibly influenced by reactant photolysis. The room temperature value from the discharge flow/resonance fluorescence study of Brown et al. [198] agrees within the 2σ limits. (Table: 02-25, Note: 02-25) [Back to Table](#)
- H7. HO₂ + I. Based on the data of Jenkin et al. [736], the only reported study of this reaction. (Table: 94-26, Note: 94-26) [Back to Table](#)
- H8. HO₂ + IO. The recommended value is the average of the values reported by Jenkin et al. [735] and Maguin et al. [952]. (Table: 94-26, Note: 94-26) [Back to Table](#)
- H9. NO₃ + HI. No recommendation is given, based on the potential for severe complications resulting from secondary chemistry in the only reported study of the reaction (Lancar et al. [850]). (Table: 94-26, Note: 94-26) [Back to Table](#)
- H10. Cl + CH₃I. This reaction, thought to be a simple H abstraction reaction, has been shown by Ayhens et al. [71] to be quite complex. At low temperatures, Cl atom reversibly adds to CH₃I to form CH₃ICl. Thus, there are at least two channels for this reaction,



The rate coefficient for channel (a) has been measured by Ayhens et al. above 364 K, Kambanis et al. [763] between 273 and 363 K, Bilde and Wallington [160] at 298 K, and Cotter et al. [349] at 298 K. The recommendation is based on these studies.

Under atmospheric conditions reaction (b) to form the adduct is about two orders of magnitude faster than reaction (a). However, the fate of the CH₃ICl adduct in the atmosphere is unclear. Its lifetime, based on the studies of Ayhens et al., can be as long as a few seconds at 200 K and a few hundred Torr pressure. Therefore, it is possible that it could react with O₂ or be photolyzed. At 298 K, in one atmosphere of O₂, it appears that the overall fate of the CH₃ICl is to decompose back to the reactants, based on the work of Bilde and Wallington [160]. Therefore, if O₂ were to react with CH₃ICl, this rate coefficient has to be less than about 10⁻¹⁷ cm³ molecule⁻¹ s⁻¹, using the rate coefficient for its decomposition measured by Ayhens et al. If the rate coefficient for CH₃ICl + O₂ were to remain approximately the same, i.e., 10⁻¹⁷ cm³ molecule⁻¹ s⁻¹, at lower temperatures, the possible loss of CH₃ICl via reaction with O₂ cannot be ignored. Further, the possible atmospheric photolysis of CH₃ICl may be important if it has a J-value greater than 0.1 s⁻¹.

There is a third possible product channel for this reaction to yield CH₃Cl + I (Goliff and Rowland [567]). Based on the results of Bilde and Wallington and Goliff and Rowland, we recommend that the rate coefficient for the Cl + CH₃I → CH₃Cl + I reaction to be less than 0.2k_a at 298 K. Since such a reaction is likely to have a significant barrier in the gas phase, even though it is exothermic by ~14 kcal mol⁻¹ at 298 K, the branching ratio for the production of CH₃Cl and I in the atmosphere will be likely less than that at 298 K. (Table: 02-25, Note: 02-25) [Back to Table](#)

- H11. I + O₃. Based on the room temperature data of Jenkin and Cox [732] and Sander [1250], and the temperature dependent data of Buben et al. [212] and Turnipseed et al. [1481]. (Table: 97-4, Note: 97-4) [Back to Table](#)
- H12. I + BrO. Based on results of Laszlo et al. [855], the only reported study of this rate constant. This value was derived from modeling the simultaneous decay of BrO and IO in a Br₂/I₂/N₂O system. (Table: 97-4, Note: 97-4) [Back to Table](#)
- H13. IO + NO. Based on the data of Ray and Watson [1221], Daykin and Wine [403], Buben et al. [213], and Turnipseed et al. [1481]. (Table: 94-26, Note: 94-26) [Back to Table](#)
- H14. IO + ClO. Based on results of Turnipseed et al. [1482], the only reported study of this reaction. These authors also reported the product yield for channel(s) yielding an I atom to be 0.8 ± 0.2. (Table: 97-4, Note: 97-4) [Back to Table](#)
- H15. IO + BrO. Based primarily on results of Laszlo et al. [855]. Gilles et al. [556] reported the following Arrhenius expression for non-iodine atom producing channels: 2.5 × 10⁻¹¹ exp(260/T)

$\text{cm}^3 \text{ molecule}^{-1} \text{ s}^{-1}$. They also reported a branching ratio of <0.35 for channels producing I atoms. From their data they could constrain the value of the overall rate constant to be: $6 \times 10^{-11} < k < 10 \times 10^{-11} \text{ cm}^3 \text{ molecule}^{-1} \text{ s}^{-1}$, the range of which is consistent with the results of Laszlo et al. (Table: 97-4, Note: 97-4) [Back to Table](#)

- H16. IO + IO. Changed from the previous recommendation, which was based on the results of Sander [1250]. In that study, over the temperature range 250–373 K, a negative temperature dependence was reported for the overall rate constant and for the absorption cross section at 427.2 nm. In the recent study of Harwood et al. [618], the overall rate constant and the absorption cross section were found to be independent of temperature from 253 to 320 K. The recommended room temperature value is the average of the values reported by Sander, Harwood et al., and Laszlo et al. [856]. The recommended temperature dependence is the average of the values reported by Sander and by Harwood et al., with an uncertainty sufficient to encompass the two reported values. The A-factor has been fitted to the recommended room temperature rate constant and the recommended temperature dependence. The overall rate constant for the decay of IO in the absence of ozone has been found to be independent of pressure by Sander, Laszlo et al., and Harwood et al. A comparison of the overall rate observed in excess ozone to that in the absence of ozone was interpreted by Sander and by Harwood et al. to imply that formation of the dimer I_2O_2 is the dominant reaction channel in the IO self-reaction. (Table: 97-4, Note: 97-4) [Back to Table](#)
- H17. INO + INO. Based on the data of Van den Bergh and Troe [1509]. (Table: 94-26, Note: 94-26) [Back to Table](#)
- H18. $\text{INO}_2 + \text{INO}_2$. Based on the data of Van den Bergh and Troe [1509]. (Table: 94-26, Note: 94-26) [Back to Table](#)
- I1. O + SH. This recommendation accepts the results of Cupitt and Glass [376]. The large uncertainty reflects the absence of any confirming investigation. (Table: 82-57, Note: 82-57) [Back to Table](#)
- I2. O + CS. The room temperature recommendation is an average of the rate constants determined by Slagle et al. [1330], Bida et al. [153], Lilenfeld and Richardson [916], and Hancock and Smith [610]. The temperature dependence is that of Lilenfeld and Richardson, with the A-factor adjusted to yield the recommended value of $k(298 \text{ K})$. (Table: 94-26, Note: 94-26) [Back to Table](#)
- I3. O + H_2S . This recommendation is derived from an un-weighted least-squares fit of the data of Singleton et al. [1320] and Whytock et al. [1607]. The results of Slagle et al. [1328] show very good agreement for E/R in the temperature region of overlap (300 – 500 K) but lie systematically higher at every temperature. The uncertainty factor at 298 K has been chosen to encompass the room temperature rate constant values of Slagle et al. [1328] and Hollinden et al. [663]. Other than the 263 K data point of Whytock et al. and the 281 K point of Slagle et al., the main body of rate constant data below 298 K comes from the study of Hollinden et al., which indicates a dramatic change in E/R in this temperature region. Thus, the parameter g was set to account for these observations. Such a non-linearity in the Arrhenius plot might indicate a change in the reaction mechanism from abstraction (as written) to addition. An addition channel (resulting in H atom displacement) has been proposed by Slagle et al. [1328], Singleton et al. [1320], and Singleton et al. [1322]. In the latter two studies, an upper limit of 20% was placed on the displacement channel. Direct observations of product HSO were made in the reactive scattering experiments of Clemo et al. [313] and Davidson et al. [388]. A threshold energy of 3.3 kcal/mole was observed (similar to the activation energy measured in earlier studies), suggesting the importance of this direct displacement channel. Addition products from this reaction have been seen in a matrix by Smardzewski and Lin [1333]. Further kinetic studies in the 200–300 K temperature range, as well as quantitative direct mechanistic information, could clarify these issues. However, this reaction is thought to be of limited importance in atmospheric chemistry. (Table: 82-57, Note: 82-57) [Back to Table](#)
- I4. O + OCS. The value of $k(298 \text{ K})$ is the average of the determinations by Westenberg and de Haas [1597], Klemm and Stief [804], Wei and Timmons [1593], Manning et al. [956], and Breckenridge and Miller [193]. The recommended value of E/R is the average value taken from the first three listed studies. Hsu et al. [682] report that this reaction proceeds exclusively by a stripping mechanism. The vibrational and rotational state distributions in the SO and CO products have been

reported by Chen et al. [292] and Nickolaisen et al. [1065] respectively. (Table: 06-2, Note: 06-2) [Back to Table](#)

15. $O + CS_2$. The value of $k(298\text{ K})$ is an average of the rate constants determined by Wei and Timmons [1593], Westenberg and de Haas [1597], Slagle et al. [1329], Callear and Smith [241], Callear and Hedges [240], Homann et al. [664], Borissenko et al. [179], and Graham and Gutman [571]. The E/R value is an average of the determinations by Wei and Timmons and Graham and Gutman. The g value has been set to encompass the temperature-dependent data of Westenberg and de Haas. The principal reaction products are thought to be $CS + SO$. However, Hsu et al. [682] report that 1.4% of the reaction at 298 K proceeds through a channel yielding $CO + S_2$ and calculate a rate constant for the overall process in agreement with that recommended. Graham and Gutman [571] have found that 9.6% of the reaction proceeds to yield $OCS + S$ at room temperature. Using time-resolved diode laser spectroscopy, Cooper and Hershberger [348] determined the branching ratios for the CO - and OCS -producing channels to be $(3.0 \pm 1.0)\%$ and $(8.5 \pm 1.0)\%$, respectively. (Table: 82-57, Note: 82-57) [Back to Table](#)
16. $O + CH_3SCH_3$. This recommendation is based on a fit of the data from Nip et al. [1098], Lee et al. [873], and Lee et al. [872]. Product studies by Cvetanovic et al. [377] indicate that the reaction proceeds almost entirely by addition followed by rapid fragmentation to the products as written. Pavanaja et al. [1151] examined the pressure and reactant ratio dependencies of $OH(A^2\Sigma^+)$ and $SO_2(^3B, ^1B)$ emissions in this reaction system. Their observations are consistent with initial product formation as written, followed by secondary generation of both OH and SO_2 . (Table: 94-26, Note: 97-4) [Back to Table](#)
17. $O + CH_3SSCH_3$. This recommendation averages the 298 K rate constants of Nip et al. [1098] and Borissenko et al. [179], which are in good agreement with each other, but are about a factor of 2 slower than the value reported by Lee et al. [869]. The recommendation for E/R has been obtained from an un-weighted Arrhenius fit that employs all available data, but scales the data of Lee et al. downward by a factor of 2.04 to bring their data into agreement with the other data at room temperature. Product studies by Cvetanovic et al. [377] indicate that the reaction proceeds mainly by addition followed by rapid fragmentation to the products as written. Pavanaja et al. [1151] examined the pressure and reactant ratio dependencies of $OH(A^2\Sigma^+)$ and $SO_2(^3B, ^1B)$ emissions in this reaction system. Their observations are consistent with initial product formation as written, followed by secondary generation of both OH and SO_2 . (Table: 06-2, Note: 06-2) [Back to Table](#)
18. $O + CH_3S(O)CH_3$. The recommended 298 K rate constant is the average of values reported from a laser flash photolysis – resonance fluorescence study by Pope et al. [1177], and from a discharge flow – mass spectrometry study by Riffault et al. [1234]. A rate constant reported by Barnes et al. [91] (with no details about how the rate constant was obtained) is somewhat faster than the recommendation, but in agreement to within the recommended uncertainty factor. The recommended value for E/R is from Pope et al. The recommended value for the parameter g is larger than the value reported by Pope et al. to reflect the fact that only a single temperature dependence study has been reported. In their study at one Torr total pressure, Riffault et al. found that the products $SO_2 + 2\text{ CH}_3$ are produced with near unit yield. (Table: 06-2, Note: 06-2) [Back to Table](#)
19. $O_3 + H_2S$. This upper limit was determined by Becker et al. [124] from measurements of the rates of SO_2 production and O_3 consumption. The heterogeneous reaction between H_2S and O_3 occurs more rapidly than the gas phase reaction in most laboratory systems. (Table: 92-20, Note: 92-20) [Back to Table](#)
110. $O_3 + CH_3SCH_3$. The recommendation is based on the study of Du et al. [460] which gives a more sensitive upper limit than an earlier study by Martinez and Herron [977]. Du et al. used cyclohexane to scavenge OH radicals and high levels of O_2 to scavenge oxygen atoms and convert more reactive carbon-centered radicals to less reactive peroxy radicals. Their reported rate constant is $(1.04 \pm 0.21) \times 10^{-19} \text{ cm}^3 \text{ molecule}^{-1} \text{ s}^{-1}$. Because of the potential for interference from wall reaction or reactions involving radicals generated via secondary chemistry, the recommendation is an upper limit equal to the rate constant reported by Du et al. plus twice its reported uncertainty. (Table: 10-6, Note: 10-6, Evaluated: 10-6) [Back to Table](#)

- I11. $\text{O}_3 + \text{SO}_2$. This recommendation is based on the limited data of Davis et al. [399] at 300 K and 360 K in a stopped flow investigation using mass spectrometric and UV spectroscopic detection. (Table: 85-37, Note: 85-37) [Back to Table](#)
- I12. $\text{O}_3 + \text{SO}_2\text{F}_2 \rightarrow \text{products}$. The recommended upper limit is based on the results of Dillon et al. [433] and Sulbaek-Andersen et al. [1395]. (Table: 10-6, Note: 10-6, Evaluated: 10-6) [Back to Table](#)
- I13. $\text{OH} + \text{H}_2\text{S}$. The values of $k(298 \text{ K})$ and E/R are derived from a composite un-weighted least-squares fit to the individual data points of Perry et al. [1159], Cox and Sheppard [366], Wine et al. [1623], Leu and Smith [893], Michael et al. [1014], Lin [918], Lin et al. [921], Wang and Lee [1572], Barnes et al. [87], Lafage et al. [846], and Wang et al. [1563]. The studies of Leu and Smith [893], Lin et al. [921], Lin [918], and Lafage et al. [846] show a slight parabolic temperature dependence of k with a minimum occurring near room temperature. However, with the error limits stated in this evaluation, all data are fit reasonably well by an Arrhenius expression. Lafage et al. and Michael et al. discuss the results in terms of a two-channel reaction scheme involving direct H atom abstraction and complex (adduct) formation. Lafage et al. analyzed their results above room temperature to yield an apparent $E/R = 400 \text{ K}$ for the abstraction channel, in good agreement with the E/R value determined above room temperature by Westenberg and de Haas [1599, 1600]. The results of these latter workers lie systematically higher (by about 70%), presumably due to secondary reactions. The room temperature value measured by Stuhl [1382] lies just outside the 2σ error limit set for $k(298 \text{ K})$. Theoretical work by Ellingson and Truhlar [480] supports the non-Arrhenius temperature dependence reported by some investigators (see above); they attribute the unusual temperature dependence to “a dynamical bottleneck at an energy below reactants, following an addition complex on the reaction path with a classical binding energy of 4.4 kcal/mol.” Butkovskaya and Setser [234] have observed infrared emission from vibrationally excited levels of the expected reaction product H_2O . (Table: 06-2, Note: 10-6) [Back to Table](#)
- I14. $\text{OH} + \text{OCS}$. The value of $k(298 \text{ K})$ is an average of the determinations by Wahner and Ravishankara [1534] and Cheng and Lee [293]. The room temperature rate constants from these studies are a factor of 3 higher than the earlier determination by Leu and Smith [891]. As discussed in the later studies, this difference may be due to an overcorrection of the Leu and Smith data to account for OH reaction with H_2S impurities and also to possible regeneration of OH. Nevertheless, the uncertainty factor at 298 K has been set to encompass the earlier study within 2σ . The work by Wahner and Ravishankara [1534] supersedes the study of Ravishankara et al. [1208], which minimized complications due to secondary and/or excited state reactions that presumably were interfering with the experiments of Atkinson et al. [61] and Kurylo [836]. The upper limit for $k(298 \text{ K})$ reported by Cox and Sheppard [366] is too insensitive to permit comparison with the more recent studies. The room temperature measurements of Wahner and Ravishankara demonstrate the lack of an effect of total pressure (or O_2 partial pressure) on the rate constant and are supported by the more limited pressure- and O_2 -dependent studies of Cheng and Lee. The recommendation for E/R is based on the study of Cheng and Lee who determined a value considerably lower than reported by Leu and Smith, although this difference may be due in part to the earlier mentioned overcorrection of the data by the latter authors.

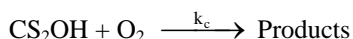
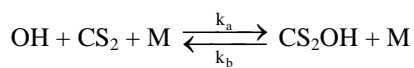
Product observations by Leu and Smith indicate that SH is a primary product of this reaction and tentatively confirm the suggestion of Kurylo and Laufer [842] that the predominant reaction pathway is to produce $\text{SH} + \text{CO}_2$ through a complex (adduct) mechanism similar to that observed for the $\text{OH} + \text{CS}_2$ reaction. However, the absence of an O_2 /pressure effect for $\text{OH} + \text{OCS}$ is in marked contrast with the strong dependence seen in studies of $\text{OH} + \text{CS}_2$ (see note for the latter reaction).

Experiments by Greenblatt and Howard [577] have shown that oxygen atom exchange in the reaction of ^{18}OH with OCS is relatively unimportant, leading to an upper limit of $10^{-15} \text{ cm}^3 \text{ molecule}^{-1} \text{ s}^{-1}$ being set on the rate constant of the exchange reaction. (Table 87-41, Note: 92-20) [Back to Table](#)

- I15. $\text{OH} + \text{CS}_2 \rightarrow \text{SH} + \text{OCS}$. There is a consensus of experimental evidence that this reaction proceeds very slowly as a direct bimolecular process. Wine et al. [1631] set an upper limit on $k(298 \text{ K})$ of $1.5 \times 10^{-15} \text{ cm}^3 \text{ molecule}^{-1} \text{ s}^{-1}$. A consistent upper limit is also reported by Iyer and Rowland [718] for the rate of direct production of OCS, suggesting that OCS and SH are primary products of the

bimolecular process. This mechanistic interpretation is further supported by the studies of Leu and Smith [892] and Biermann et al. [156], which set somewhat higher upper limits on $k(298\text{ K})$. The more rapid reaction rates measured by Atkinson et al. [61], Kurylo [836], and Cox and Sheppard [366] may be attributable to severe complications arising from excited state and secondary chemistry in their photolytic systems. The Cox and Sheppard study in particular may have been affected by the reaction of electronically excited CS_2 (produced via the 350 nm photolysis) with O_2 (in the 1-atm synthetic air mixture) as well as by the accelerating effect of O_2 on the $\text{OH} + \text{CS}_2$ reaction itself, which has been observed by other workers as summarized below. The possible importance of electronically excited CS_2 reactions in the tropospheric oxidation of CS_2 to OCS has been discussed by Wine et al. [1622]. (Table: 06-2, Note: 06-2) [Back to Table](#)

- I16. $\text{OH} + \text{CS}_2 \xrightarrow{\text{O}_2} \text{CS}_2\text{OH} \xrightarrow{\text{O}_2} \text{products}$. An accelerating effect of O_2 on the $\text{OH} + \text{CS}_2$ reaction rate has been observed by Jones et al. [750], Barnes et al. [95], and Hynes et al. [705], along with a near unity product yield for SO_2 and OCS . In the latter two studies the effective bimolecular rate constant was found to be a function of total pressure ($\text{O}_2 + \text{N}_2$), and exhibited an appreciably negative temperature dependence. These observations are consistent with the formation of a long-lived adduct as postulated by Kurylo [836] and Kurylo and Laufer [842] followed by its reaction with O_2 :



The effective second order rate constant for CS_2 or OH removal in the above reaction scheme can be expressed as

$$1/k_{\text{eff}} = (k_b/k_a k_c)(1/P_{\text{O}_2}) + (1/k_a)(1/P_{\text{M}})$$

where P_{O_2} is the partial pressure of O_2 and P_{M} equals $P_{\text{O}_2} + P_{\text{N}_2}$. The validity of this expression requires that k_a and k_b are invariant with the $P_{\text{O}_2}/P_{\text{N}_2}$ ratio. A $1/k$ vs $1/P_{\text{O}_2}$ plot of the data of Jones et al. [750] taken at atmospheric pressure exhibits marked curvature, suggesting a more complex mechanistic involvement of O_2 , whereas the data of Barnes et al. [95] and Hynes et al. [705] are more satisfactorily represented by this analytical expression. Nevertheless, while the qualitative features of the data from all three laboratories agree, there are some quantitative inconsistencies. First, under similar conditions of O_2 and N_2 pressures, the Barnes et al. rate constants lie approximately 60% higher than those of Jones et al. and up to a factor of 2 higher than those derived by Hynes et al. Secondly, two fits each of both the Barnes et al. and Hynes et al. data can be made: one at fixed P_{M} and varying P_{O_2} , and the other at fixed P_{O_2} and varying P_{M} (i.e., varying added N_2). Within each data set, rate constants calculated from both fits agree reasonably well for mole fractions of O_2 near 0.2 (equivalent to air) but disagree by more than a factor of 2 for measurements in a pure O_2 system. Finally, the temperature dependence (from 264–293 K) of the k_{eff} values from Barnes et al. varies systematically from an E/R of -1300 K for experiments in pure O_2 (at 700 Torr total pressure) to -2900 K for experiments in a 50 Torr O_2 plus 650 Torr N_2 mixture. An Arrhenius fit of the Hynes et al. data (from 251–348 K) recorded in synthetic air at 690 Torr yields an $E/R = -3300\text{ K}$, although the data show marked curvature over the temperature range of study. These observations suggest that k_a and k_b may not be independent of the identity of M . For this reason, we limit our recommendation to air mixtures (i.e., $P_{\text{O}_2}/P_{\text{N}_2} = 0.25$) at atmospheric pressure. Since most CS_2 is oxidized within the atmospheric boundary layer, such restriction does not limit the applicability of this recommendation in atmospheric modeling.

The present recommendation accepts the measurements of Hynes et al. [705], which appear to be the most sensitive of the three investigations. Thus, $k(298\text{ K})$ is derived from the Arrhenius fit of the data near room temperature.

$$k(298\text{ K}) = 1.2 \times 10^{-12} \text{ cm}^3 \text{ molecule}^{-1} \text{ s}^{-1}$$

To compute values of k below 298 K, we have accepted the analysis of Hynes et al.:

$$k(T) = \{1.25 \times 10^{-16} \exp(4550/T)\} / \{T + 1.81 \times 10^{-3} \exp(3400/T)\} \text{ cm}^3 \text{ molecule}^{-1} \text{ s}^{-1}.$$

This recommendation is only valid for one atmosphere pressure of air. It is interesting to note that measurements by Hynes et al. [705] at approximately 250 K and 700 Torr total pressure result in k_{eff} values that are independent of the amount of O_2 for partial pressures between 145 and 680 Torr. This suggests that the adduct is quite stable with respect to dissociation into the reactants ($\text{OH} + \text{CS}_2$) at this low temperature and that the effective rate constant for reactant removal approaches the elementary rate constant for adduct formation. (Table: 06-2, Note: 06-2) [Back to Table](#)

- I17. $\text{CS}_2\text{OH} + \text{O}_2$. Three groups have obtained kinetic information about this reaction by observing either the perturbation of $\text{OH}/\text{CS}_2\text{OH}$ equilibration kinetics upon addition of O_2 , or by modeling the dependence of the observed rate constant for OH loss on $[\text{O}_2]$. Hynes et al. [705], Murrells et al. [1037], and Diau and Lee [426] agree quite well on the value of k , with an average value of $2.8 \times 10^{-14} \text{ cm}^3 \text{ molecule}^{-1} \text{ s}^{-1}$ independent of temperature and pressure being recommended. Diau and Lee also report rate constants for the reactions of the adduct (CS_2OH) with NO and NO_2 to be 7.3×10^{-13} and $4.2 \times 10^{-11} \text{ cm}^3 \text{ molecule}^{-1} \text{ s}^{-1}$, respectively.

From a mechanistic viewpoint, the primary products of this reaction determine the products of CS_2 oxidation in air. Lovejoy et al. [938] have shown that the yields of HO_2 and SO_2 are equal and near unity. Further insight is provided by the mechanistic study of Stickel et al. [1368], who observe OCS and CO product yields of (0.83 ± 0.08) and (0.16 ± 0.03) , respectively. The results from this study are interpreted to imply that OCS and CO are formed either as primary products of the $\text{CS}_2\text{OH} + \text{O}_2$ reaction or as products of a secondary reaction between a primary product and O_2 . These same authors report an SO_2 yield of (1.15 ± 0.10) , with the results suggesting that only about 75% of the SO_2 is formed as a prompt product, with the remainder generated via a slow reaction of SO (generated as a prompt product of the $\text{CS}_2\text{OH} + \text{O}_2$ reaction) with O_2 . Insight into the specific reaction pathways can be gleaned from the study of Lovejoy et al. [937] in which the rate constant for the reaction of $\text{CS}_2\text{OD} + \text{O}_2$ was found to be the same as that for $\text{CS}_2\text{OH} + \text{O}_2$, indicating that simple H atom abstraction is not the likely process. Rather, HO_2 production most likely involves complex formation followed by HO_2 elimination. Lovejoy et al. [939] found that the ^{18}O atom in the ^{18}OH reactant is transferred predominantly $(90 \pm 20)\%$ to the SO_2 product. These findings are consistent with an S–O–bonded $\text{CS}_2\text{–OH}$ adduct and preservation of the S–O bond in the steps leading to SO_2 formation.

Theoretical studies by Zhang and Qin [1680] and by McKee and Wine [989] have provided further insight into the reaction mechanism. The initial step is, indeed, formation of SCS–OH followed by addition of O_2 to the carbon atom. A key subsequent step appears to be an O atom transfer to the sulfur bearing the hydroxyl group which leads directly to $\text{HOSO} + \text{OCS}$. The reaction $\text{HOSO} + \text{O}_2 \rightarrow \text{HO}_2 + \text{SO}_2$ is expected to occur rapidly under atmospheric conditions. One remaining problem is identification of the pathway for generation of CO , which is observed as a minor product. (Table: 06-2, Note: 06-2) [Back to Table](#)

- I18. $\text{OH} + \text{CH}_3\text{SH}$. This recommendation is based on a composite fit to the data of Atkinson et al. [60], Wine et al. [1623], Wine et al. [1632], and Hynes and Wine [702], which are in excellent agreement. The results from the relative rate study of Barnes et al. [87] are in agreement with this recommendation and indicate that the higher value of Cox and Sheppard [366] is due to complications resulting from the presence of O_2 and NO in their reaction system. MacLeod et al. [949, 950] and Lee and Tang [871] obtained rate constants at 298 K approximately 50% lower than recommended here. These authors also obtained lower values for the ethanethiol reaction in comparison with results from studies upon which the methanethiol recommendation is made. Wine et al. [1632] present evidence that this reaction proceeds via adduct formation to produce a species that is thermally stable over the temperature range and time scales of the kinetic measurements. Tyndall and Ravishankara [1497] have determined the yield of CH_3S (via laser-induced fluorescence) to be unity, indicating that any adduct must be short lived (less than 100 μs). Longer lifetimes would have led to anomalies in the OH decay kinetics used for the rate constant determinations. Butkovskaya and Setser [236], based on observations of IR emissions from the products of the reactions of OH and OD with CH_3SH and CH_3SD , conclude that H-abstraction from the methyl group occurs with a yield of $24 \pm 8\%$ for the OH reactions and $11 \pm 4\%$ for the OD reactions. Hynes and Wine [702] observed that the rate constant is independent of O_2 partial pressure. (Table: 06-2, Note: 06-2) [Back to Table](#)

- I19. $\text{OH} + \text{CH}_3\text{SCH}_3 \rightarrow \text{H}_2\text{O} + \text{CH}_2\text{SCH}_3$. The $\text{OH} + \text{CH}_3\text{SCH}_3$ reaction is complex, proceeding by both H-abstraction and reversible addition pathways. In the presence of atmospheric levels of O_2 , adduct reaction with O_2 makes the addition pathway partially irreversible. Only kinetic data obtained in the absence of O_2 and at low enough CH_3SCH_3 concentrations for the adduct to be a negligible reservoir for OH are considered in evaluation of the H-abstraction rate constant. This recommendation is based on the results of Hynes et al. [706], Wine et al. [1623], Hsu et al. [686], Abbatt et al. [3], Barone et al. [102], Turnipseed et al. [1477], Williams et al. [1613-1615], and Wang et al. [1563]. The earlier larger rate constant values of Atkinson et al. [61] and Kurylo [835] are presumably due to reactive impurities, while those of MacLeod et al. [950] were most likely overestimated because of heterogeneous reactions. Unlike other temperature dependence studies, the rate constants reported by Albu et al. [22] (at $T = 250\text{--}299\text{ K}$) suggest a significant negative activation energy, leading to suspicion of an interference from adduct reaction with impurity O_2 . Absolute determinations lower than those recommended were obtained by Martin et al. [971], Wallington et al. [1538], and Nielsen et al. [1084]. The reasons for these differences are not readily apparent. Confirmation that H-abstraction is the dominant pathway under the experimental conditions specified above comes from the studies of Stickel et al. [1370] and Turnipseed et al. [1477]. Stickel et al. used tunable diode laser spectroscopy to measure an HDO product yield of 0.84 ± 0.15 for the $\text{OD} + \text{CH}_3\text{SCH}_3$ reaction in 10-30 Torr N_2 , while Turnipseed et al. used laser induced fluorescence observations of CH_3S production from $\text{OH} + \text{CH}_3\text{SCH}_3$ to show that the branching ratio for the CH_3S elimination channel is <0.04 and the direct H-abstraction yield is 0.84 ± 0.26 . Further support for the dominance of the H-abstraction pathway comes from the work of Zhao et al. [1690], who obtained an upper limit yield of 0.07 for the methyl elimination channel in the $\text{OD} + \text{CH}_3\text{SCH}_3$ reaction. Barnes et al. [98, 99], Turnipseed et al., and Urbanski et al. [1503] report that the abstraction product CH_3SCH_2 is converted predominantly to CH_3S under atmospheric conditions. Barnes et al. [98] measure a 0.7% yield of OCS under low NO_x conditions, which they attribute to further oxidation of CH_3S . (Table: 10-6, Note: 10-6, Evaluated: 10-6) [Back to Table](#)
- I20. $\text{OH} + \text{CH}_3\text{SCH}_3 \rightarrow (\text{CH}_3)_2\text{SOH} \rightarrow \text{products}$. The $\text{OH} + \text{CH}_3\text{SCH}_3$ reaction is complex, proceeding by both direct H-abstraction and reversible addition pathways. A recommendation for the direct reaction is given separately in Table 1. The product of the reversible addition pathway reacts with O_2 creating an irreversible path as well. Mechanistically, this pathway is described by combining the rate constants k_f for the addition step, k_r for the reverse dissociation step, and k_{O_2} for the adduct reaction with O_2 . The equilibrium constant for the reversible addition process is $K_c = k_f/k_r$. Recommendations for K_c , k_f , and k_{O_2} are found in Tables 3, 2, and 1, respectively. Subtracting the temperature-dependent H-abstraction rate constant from the overall irreversible rate constant (which depends on T , P , and P_{O_2}) yields the rate constant for irreversible addition (k_{ia}), which can be expressed as

$$k_{\text{ia}} = K_c k_{\text{O}_2} [\text{O}_2] / \{1 + (K_c k_{\text{O}_2} [\text{O}_2] / k_f)\}.$$

Much of the kinetic data available for evaluating this reaction were obtained for $\text{OH} + \text{CD}_3\text{SCD}_3$. Although the methyl hydrogens are not directly involved in the reaction, the rate constants for OH addition reactions with CH_3SCH_3 and CD_3SCD_3 differ somewhat [1615] as they are in the low pressure limit where the value depends on the density of states, which are different for the two isotopomers. The recommended expression (units are $\text{cm}^3 \text{ molecule}^{-1} \text{ s}^{-1}$),

$$k_{\text{ia}}(T, [\text{O}_2], [\text{M}]) = 8.2 \times 10^{-39} [\text{O}_2] \exp(+5376/T) / \{1 + 1.05 \times 10^{-5} ([\text{O}_2] / [\text{M}]) \exp(+3644/T)\},$$

is based on the recommendations for K_c , k_f , and k_{O_2} given elsewhere in this evaluation. It reproduces the data of Hynes et al. [706], Williams et al. [1613-1615], and Albu et al. [22] quite well for both isotopomers and for all mole fractions of O_2 in N_2/O_2 mixtures; however, it should be used with caution at temperatures below 240 K (where no data are available) or above 310 K (where k_{ia} is very small). The 298 K relative rate study of Wang et al. [1563] suggests rate constants in air and pure O_2 at atmospheric pressure that are about a factor of two faster than those predicted by the above expression. Since the kinetic data of Hynes et al. and Williams et al. were obtained by

monitoring OH loss, the overall rate constant for removal of CH_3SCH_3 would be underestimated if the adduct + O_2 reaction generated OH + dimethylsulfone ($\text{CH}_3(\text{O})\text{S}(\text{O})\text{CH}_3$) with a significant yield; the available data cannot rule out a small but significant branching ratio for this channel. (Table: 10-6, Note: 10-6, Evaluated: 10-6) [Back to Table](#)

- I21. $(\text{CH}_3)_2\text{SOH} + \text{O}_2$. All available kinetic data for this reaction were obtained by measuring k_{obs} for the $\text{OH} + \text{CH}_3\text{SCH}_3$ reaction as a function of O_2 partial pressure ($k_{\text{obs}} \equiv$ the sum of the rate constants for H-abstraction and irreversible addition). Much of the available data were obtained for $\text{OH} + \text{CD}_3\text{SCD}_3$. Since the methyl hydrogens are not directly involved in the reaction, the rate constant is expected to be virtually the same for CH_3SCH_3 as for CD_3SCD_3 ; hence, data for both reactants are used in the evaluation. The recommendation is based on the data of Hynes et al. [701], Barone et al. [102], and Williams et al. [1614, 1615]. The Hynes et al. study supercedes an earlier report of a considerably faster rate constant [706]. Over the range of experimental conditions where data are available (222 – 267 K and 30 – 200 Torr), the rate constant appears to be independent of temperature and pressure. By monitoring the regeneration of OH in the presence of NO, Hynes et al. [700] and Turnipseed et al. [1477] have determined the yield for the $\text{HO}_2 + \text{CH}_3\text{S}(\text{O})\text{CH}_3$ (DMSO) channel to be ~0.5. A theoretical study by Ramirez-Anguila et al. [1201] suggests possible pathways for generating $\text{CH}_3\text{SOH} + \text{CH}_3\text{OO}/\text{CH}_2\text{OOH}$. (Table: 10-6, Note: 10-6, Evaluated: 10-6) [Back to Table](#)
- I22. $\text{OH} + \text{CH}_3\text{SCH}_2\text{Cl} \rightarrow \text{products}$. The recommendation is based on the low-pressure discharge flow resonance fluorescence study of Shallcross et al. [1296]. The uncertainty reflects the fact that only one study performed under a limited range of experimental conditions has been reported. Shallcross et al. suggest that the likely reaction pathway is H-abstraction under the low pressure conditions of their experiments. However, further experimental and/or theoretical research is needed before an addition-elimination pathway involving C–S bond cleavage can be ruled out. If H-abstraction dominates at low pressure, then under atmospheric conditions the rate constant could be significantly faster than reported by Shallcross et al. due to the occurrence of an irreversible addition channel at higher pressure and in the presence of O_2 . (Table: 10-6, Note: 10-6, Evaluated: 10-6) [Back to Table](#)
- I23. $\text{OH} + \text{CH}_3\text{SSCH}_3$. This recommendation is based on the temperature-dependent studies of Wine et al. [1623] and Abbatt et al. [3] and the room temperature relative rate study of Cox and Sheppard [366]. Domine and Ravishankara [449] have observed both CH_3S (via laser-induced fluorescence) and CH_3SOH (via photo-ionization mass spectrometry) as products of this reaction. At 298 K, the yield of CH_3S alone was quantified at approximately 30%. An FTIR product study of the photooxidation of dimethyl disulfide by Barnes et al. [97] presents evidence that oxidation of the CH_3SOH product is the principal source of the methane sulfonic acid observed. Butkovskaya and Setser [235] have observed that HDO and D_2O are produced from $\text{OD} + \text{CH}_3\text{SSCH}_3$ in the same proportion and with the same vibrational state distributions as the products observed by the same investigators in a similar study of the $\text{OD} + \text{CH}_3\text{SD}$ reaction [236], leading these authors to suggest that the major product channel for $\text{OD} + \text{CH}_3\text{SSCH}_3$ is $\text{CH}_3\text{SD} + \text{CH}_3\text{SO}$. (Table: 94-26, Note: 94-26) [Back to Table](#)
- I24. $\text{OH} + \text{CH}_3\text{S}(\text{O})\text{CH}_3$. The recommended 298 K rate constant is the average of the direct studies of Hynes and Wine [704], Urbanski et al. [1502], and Kukui et al. [822], which employed three different experimental approaches and are in excellent agreement. Competitive kinetics studies by Barnes et al. [91] and Falbe-Hanson et al. [490] report rate constants in 1 atm. of air about a factor of 1.5 slower than those obtained in the direct studies. The recommended value for E/R is based on the only study of the temperature dependence [704], where a significant negative activation energy was observed. The large uncertainty in E/R reflects the availability of very limited data (none below room temperature). The experimental studies of Urbanski et al., Kukui et al. and Arsene et al. [42], as well as the theoretical study of Wang and Zhang [1571], provide strong evidence that the dominant reaction channel is production of $\text{CH}_3 + \text{CH}_3\text{S}(\text{O})\text{OH}$ (MSIA, methanesulfinic acid). Arsene et al. attribute the failure to observe MSIA production in the chamber study of Sorensen et al. [1345] to loss via secondary gas phase and condensed phase oxidation before sampling. (Table: 06-2, Note: 06-2) [Back to Table](#)
- I25. $\text{OH} + \text{CH}_3\text{S}(\text{O})\text{OH}$. The recommendation is based on a turbulent flow reactor – chemical ionization mass spectrometry study by Kukui et al. [822], which was carried out with OH in excess over

CH₃S(O)OH at total pressures of 200–400 Torr N₂. The large uncertainty factor results from the facts that (1) only a single room temperature study is reported in the literature and (2) CH₃S(O)OH is a difficult species to study in the gas phase because of its low vapor pressure. Kukui et al. found that SO₂ was produced as a reaction product with near unit yield, suggesting that the dominant reaction channel (at least in the absence of O₂) is production of CH₃ + SO₂ + H₂O. Theoretical studies by Gonzalez-Garcia et al. [568] and Tian et al. [1442] provide strong evidence that the CH₃S(O)OH–OH adduct is too short-lived to react with O₂ under atmospheric conditions. (Table: 10-6, Note: 10-6, Evaluated: 10-6) [Back to Table](#)

- I26. OH + S. This recommendation is based on the study by Jourdain et al. [752]. Their measured value for $k(298\text{ K})$ compares favorably with the recommended value of $k(\text{O} + \text{OH})$ when one considers the slightly greater exothermicity of the present reaction. (Table: 82-57, Note: 82-57) [Back to Table](#)
- I27. OH + SO. The value recommended for $k(298\text{ K})$ is an average of the determinations by Fair and Thrush [488], Jourdain et al. [752], and Blitz et al. [171]. The result reported by Fair and Thrush was corrected using the present recommendation for the O + OH reaction. The recommended value for E/R is taken from the temperature dependent data of Blitz et al. over the range 295–453 K. Higher temperature data of Blitz et al. are not used because significant curvature in the Arrhenius plot is observed at $T > 500\text{ K}$. The recommended value for g is conservative because only one temperature dependence study has been reported. (Table: 06-2, Note: 06-2) [Back to Table](#)
- I28. OH + SO₂F₂ → products. The recommended upper limit is based on the relative rate experiments of Papadimitriou et al. [1139]. Less sensitive upper limits are reported by Dillon et al. [433] and Sulbaek-Andersen et al. [1395]. (Table: 10-6, Note: 10-6, Evaluated: 10-6) [Back to Table](#)
- I29. HO₂ + H₂S, HO₂ + CH₃SH, HO₂ + CH₃SCH₃. These upper limits are taken from the discharge flow laser magnetic resonance study of Mellouki and Ravishankara [1003]. The H₂S value disagrees with the rate constant reported by Bulatov et al. [218] by approximately three orders of magnitude. The reason for this difference is not readily apparent. However, the recommended upper limit is consistent with the values for CH₃SH and CH₃SCH₃, which respectively agree with upper limits from the work of Barnes et al. [87] and Niki (reported as a private communication in the Mellouki and Ravishankara paper). (Table: 94-26, Note: 94-26) [Back to Table](#)
- I30. HO₂ + SO₂. This upper limit is based on the atmospheric pressure study of Graham et al. [574]. A low pressure laser magnetic resonance study by Burrows et al. [224] places a somewhat higher upper limit on $k(298\text{ K})$ of $4 \times 10^{-17}\text{ cm}^3\text{ molecule}^{-1}\text{ s}^{-1}$ (determined relative to OH + H₂O₂). Their limit is based on the assumption that the products are OH and SO₃. The weight of evidence from both studies suggests an error in the earlier determination by Payne et al. [1153]. (Table: 82-57, Note: 82-57) [Back to Table](#)
- I31. NO₂ + SO₂. This recommendation is based on the study of Penzhorn and Canosa [1155] using second derivative UV spectroscopy. While these authors actually report a measured value for $k(298\text{ K})$, their observations of strong heterogeneous and water vapor catalyzed effects prompt us to accept their measurement as an upper limit. This value is approximately two orders of magnitude lower than that for a dark reaction observed by Jaffe and Klein [720], much of which may have been due to heterogeneous processes. Penzhorn and Canosa suggest that the products of this reaction are NO + SO₃. (Table: 85-37, Note: 85-37) [Back to Table](#)
- I32. NO₃ + H₂S. This recommendation accepts the upper limit set by Dlugokencky and Howard [435] based on experiments in which NO₃ loss was followed in the presence of large concentrations of H₂S. Less sensitive upper limits for the rate constant have been reported by Wallington et al. [1540] and Cantrell et al. [254]. (Table: 90-1, Note: 90-1) [Back to Table](#)
- I33. NO₃ + OCS. This upper limit is based on the relative rate data of MacLeod et al. [947]. (Table: 90-1, Note: 90-1) [Back to Table](#)
- I34. NO₃ + CS₂. This upper limit is based on the study of Burrows et al. [228]. A somewhat higher upper limit was derived in the relative rate study of MacLeod et al. [947]. (Table: 90-1, Note: 90-1) [Back to Table](#)
- I35. NO₃ + CH₃SH. The recommended values are derived from a composite fit to the data of Wallington et al. [1540], Rahman et al. [1195], and Dlugokencky and Howard [435]. The room temperature rate

constant derived in the relative rate experiments of MacLeod et al. [947] is in good agreement with the recommended value. The suite of investigations shows the rate constant to be pressure independent over the range 1–700 Torr. Dlugokencky and Howard place an upper limit of 5% on the production of NO₂ via this reaction at low pressure. Based on the product distribution observed in their investigation, Jensen et al. [739] propose a reaction mechanism initiated by abstraction of the hydrogen atom from the SH group, possibly after formation of an initial adduct as suggested by Wallington et al. and Dlugokencky and Howard. (Table: 90-1, Note: 94-26) [Back to Table](#)

- I36. NO₃ + CH₃SCH₃. The recommended value for k(298 K) is obtained by averaging the rate constants reported by Tyndall et al. [1486], Dlugokencky and Howard [435], and Daykin and Wine [404]. The recommended value of E/R is that reported by Dlugokencky and Howard. Tyndall et al. and Nakano et al. [1042] report data over rather narrow temperature ranges that are consistent with the Dlugokencky and Howard result. The relative rate study of Atkinson et al. [63] yields a rate constant at room temperature that is about a factor two lower than the recommended value. Wallington et al. [1541] [1540] also report rate constants that are somewhat lower than the recommended values; their results are suspect because their reaction mixtures contained F₂ in ten-fold excess over CH₃SCH₃, and it is now well-established that F₂ and CH₃SCH₃ react with each other rapidly [943, 944, 1478]. The results of Nakano et al. are suspect because of the likely presence of background NO₃ associated with the use of N₂O₅ + hv as the NO₃ source. The experimental data from all investigations demonstrate the pressure independence of the rate constant over the range 1–740 Torr. Jensen et al. [738] propose a mechanism that involves hydrogen abstraction as the first step to explain their observed product distribution. In a later study, Jensen et al. [739] measured a kinetic isotope effect for the rate constant for CH₃SCH₃ vs. that for CD₃SCD₃ of k_H/k_D = (3.8±0.6), in agreement with the kinetic isotope effect reported by Daykin and Wine; this provides further confirmation of the H-abstraction mechanism. Butkovskaya and Le Bras [232] utilized chemical titration of the primary radical produced from NO₃ + CH₃SCH₃ in a discharge flow mass spectrometry system to show that the reaction produces predominantly CH₃SCH₂ + HNO₃. An upper limit of 2% was placed on the reaction channel yielding CH₃ + CH₃SONO₂. (Table: 10-6, Note: 10-6, Evaluated: 10-6) [Back to Table](#)
- I37. NO₃ + CH₃SSCH₃. The recommended values were derived from a composite fit to the data of Wallington et al. [1540] and Dlugokencky and Howard [435]. The investigation by Atkinson et al. [54] indicates that the relative rate technique cannot be considered as yielding reliable rate data for this reaction due to chemical complexities. Thus, the much lower room temperature results from the study of MacLeod et al. [947] can be considered to be erroneous. Based on their observations of intermediate and end products, Jensen et al. [739] proposed a reaction mechanism in which the initial addition of NO₃ to one of the sulfur atoms results in formation of CH₃S + CH₃SO + NO₂. (Table: 90-1, Note: 94-26) [Back to Table](#)
- I38. NO₃ + CH₃S(O)CH₃. The recommendation is the geometric mean of the rate constants reported by Barnes et al. [91] and Falbe-Hansen et al. [490] from similar competitive kinetics studies; the reported rate constants and associated 2σ uncertainties in units of 10⁻¹³ cm³ molecule⁻¹ s⁻¹ are 1.7±0.6 (Barnes et al.) and 5.0±3.8 (Falbe-Hansen et al.). In both studies, the only observed sulfur-containing end-product was dimethylsulfone (CH₃(O)S(O)CH₃). Barnes et al. suggest that reaction proceeds via formation of an adduct that rapidly decomposes to NO₂ + CH₃(O)S(O)CH₃. (Table: 06-2, Note: 06-2) [Back to Table](#)
- I39. NO₃ + SO₂. This recommended upper limit for k(298 K) is based on the study by Daubendiek and Calvert [386]. Considerably higher upper limits have been derived by Burrows et al. [228], Wallington et al. [1540], Canosa-Mas et al. [248], and Dlugokencky and Howard [435]. (Table 87-41, Note: 90-1) [Back to Table](#)
- I40. N₂O₅ + CH₃SCH₃. This recommendation is based on the value estimated by Tyndall and Ravishankara [1498] from the study by Atkinson et al. [63]. (Table: 92-20, Note: 92-20) [Back to Table](#)
- I41. CH₃O₂ + SO₂. This recommendation accepts the results from the study of Sander and Watson [1255]. These authors conducted experiments using much lower CH₃O₂ concentrations than employed in the earlier investigations of Sanhueza et al. [1259] and Kan et al. [765], both of which

resulted in $k(298\text{ K})$ values approximately 100 times greater. A later report by Kan et al. [764] postulates that these differences are due to the reactive removal of the $\text{CH}_3\text{O}_2\text{SO}_2$ adduct at high CH_3O_2 concentrations prior to its reversible decomposition into CH_3O_2 and SO_2 . They suggest that such behavior of $\text{CH}_3\text{O}_2\text{SO}_2$ or its equilibrated adduct with O_2 ($\text{CH}_3\text{O}_2\text{SO}_2\text{O}_2$) would be expected in the studies yielding high k values, while decomposition of $\text{CH}_3\text{O}_2\text{SO}_2$ into reactants would dominate in the Sander and Watson experiments. It does not appear likely that such secondary reactions involving CH_3O_2 , NO , or other radical species would be rapid enough, if they occur under normal atmospheric conditions to compete with the adduct decomposition. This interpretation, however, does not explain the high rate constant derived by Cocks et al. [343] under conditions of low $[\text{CH}_3\text{O}_2]$. (Table: 81-3, Note: 81-3) [Back to Table](#)

- I42. $\text{F} + \text{CH}_3\text{SCH}_3$. This recommendation is based on the discharge flow mass spectrometric study by Butkovskaya et al. [233]. The uncertainty placed on this recommendation has been increased over that estimated by the authors to reflect the lack of confirming investigations. Titration of the primary organic radical products indicated that the reaction proceeds via two channels to produce $\text{HF} + \text{CH}_3\text{SCH}_2$ and $\text{CH}_3 + \text{CH}_3\text{SF}$ with a branching ratio of approximately 0.8/0.2 respectively. (Table: 97-4, Note: 97-4) [Back to Table](#)

- I43. $\text{Cl} + \text{H}_2\text{S}$. This recommendation is based on the study by Nicovich et al. [1070], who conducted an elaborate study with attention to sources of possible systematic error. The rate constant at 298 K is in good agreement with that determined by Nesbitt and Leone [1056], who refined the data of Braithwaite and Leone [191], but is significantly greater than the values reported by Clyne and Ono [334], Clyne et al. [325], Nava et al. [1045], and Chen et al. [284]. The small, but clearly observed, negative activation energy determined by Nicovich et al. contrasts with the lack of a temperature dependence observed by Nava et al. In fact, at the lowest temperature of overlap, the results from these two studies differ by 50%. Nevertheless, the Nicovich et al. study yields consistent results for both H_2S and CH_3SH as well as for D_2S and CD_3SD . In addition, Hossenlopp et al. [671] report a room temperature rate constant for $\text{Cl} + \text{D}_2\text{S}$ that is in excellent agreement with the value reported by Nicovich et al. While the reason for these differences remains to be determined, the full range of reported values is encompassed within the 2σ error limits recommended. Lu et al. [942] also measured a temperature-independent rate constant but report a value at 298 K that is about 40% greater than that of Nicovich et al. However, the presence of 4000 Torr of CF_3Cl bath gas in the Lu et al. study may suggest a slight pressure dependence of the reaction, although Nicovich et al. observed no pressure dependence for pressures ranging up to 600 Torr N_2 . A theoretical study by Wilson and Hirst [1616] suggests the dominance of an addition-elimination pathway with a small but significant fraction of reactive events occurring via a direct hydrogen abstraction mechanism. (Table: 06-2, Note: 06-2) [Back to Table](#)

- I44. $\text{Cl} + \text{SO}_2\text{F}_2 \rightarrow \text{products}$. The recommended upper limit is based on the relative rate experiments of Sulbaek-Andersen et al. [1395]. The recommendation is a factor of 3 higher than the upper limit reported by Sulbaek-Andersen et al. to account for a large uncertainty in the rate constant for the reference reaction they employed ($\text{Cl} + \text{CF}_3\text{CH}_3$). A less sensitive upper limit is reported by Papadimitriou et al. [1139]. (Table: 10-6, Note: 10-6, Evaluated: 10-6) [Back to Table](#)

- I45. $\text{Cl} + \text{OCS}$. This upper limit is based on the minimum detectable decrease in atomic chlorine measured by Eibling and Kaufman [478]. Based on the observation of product SCl , these authors set a lower limit on $k(298\text{ K})$ of $10^{-18}\text{ cm}^3\text{ molecule}^{-1}\text{ s}^{-1}$ for the $\text{SCl} + \text{CO}$ reaction channel. Considerably higher upper limits on $k(298\text{ K})$ were determined in the studies of Clyne et al. [325] and Nava et al. [1045]. (Table 83-62, Note: 87-41) [Back to Table](#)

- I46. $\text{CS}_2\text{Cl} + \text{O}_2$. This recommendation is based on the study of Nicovich et al. [1069] who employed a laser flash photolysis resonance fluorescence technique to observe the effect of added O_2 on the kinetics of the $\text{Cl} + \text{CS}_2 \leftrightarrow \text{CS}_2\text{Cl}$ equilibration reactions. Martin et al. [969] report competitive kinetics results which they interpret as suggesting a fast $\text{CS}_2\text{Cl} + \text{O}_2$ reaction, but Wallington et al. [1537] have suggested that secondary production of OH in the photochemical system employed by Martin et al. is responsible for the observed dependence of the CS_2 loss rate on $[\text{O}_2]$. (Table: 06-2, Note: 06-2) [Back to Table](#)

- I47. $\text{Cl} + \text{CH}_3\text{SH}$. This recommendation is based on the results of Nicovich et al. [1070], who used laser flash photolysis with resonance fluorescence detection to study the reactions of Cl with H_2S , D_2S , CH_3SH , and CD_3SD . The room temperature determination by Nesbitt and Leone [1056] is in good agreement with the recommended value. The $k(298\text{ K})$ value from the study of Mellouki et al. [999] is nearly a factor of 2 lower. However, the low sensitivity of EPR detection of Cl atoms did not permit these latter authors to conduct a precise determination of k under pseudo first-order conditions, and a more complex analysis of experiments conducted under second-order conditions was required. Nesbitt and Leone [1057] report that $2\pm 1\%$ of the reaction occurs via abstraction of an H atom from the CH_3 group. A theoretical study by Wilson and Hirst [1616] predicts a Cl–S adduct bond strength (298 K) of $13.6\text{ kcal mol}^{-1}$, but is unable to deduce the relative importance of addition-elimination vs. direct hydrogen abstraction pathways. (Table: 06-2, Note: 06-2) [Back to Table](#)
- I48. $\text{Cl} + \text{CH}_3\text{SCH}_3$. Stickel et al. [1369] have used laser flash photolysis resonance fluorescence to measure the rate constant between 240 and 421 K, over the pressure range 3–700 Torr. The rate constant is near collisional but increases with increasing pressure from a low pressure limit of 1.8×10^{-10} to a value of $3.3\times 10^{-10}\text{ cm}^3\text{ molecule}^{-1}\text{ s}^{-1}$ at 700 Torr. The yield of HCl at 297 K, measured by diode laser spectroscopy, decreased from near unity at low pressure to a value of approximately 0.5 at 203 Torr, suggesting that stabilization of a $(\text{CH}_3)_2\text{SCl}$ adduct becomes competitive with hydrogen atom abstraction with increasing pressure. These investigators also observed a negative temperature dependence for the reaction at low pressure. Butkovskaya et al. [233] conducted a discharge flow mass spectrometry study at 298 K, in which they determined that the reaction proceeds to form $\text{HCl} + \text{CH}_3\text{SCH}_2$ almost exclusively at 1 Torr total pressure. The sum of all other possible channels was estimated at less than 3%. Zhao et al. [1690] used laser photolysis coupled with CH_3 detection by time-resolved tunable diode laser absorption spectroscopy to determine an upper limit yield of 0.02 for CH_3 elimination at 298 K and pressures in the range 10–30 Torr. Langer et al. [852] coupled cw photolysis with gas chromatographic detection of products to show that the yield of CH_3Cl is $(1.34 \pm 0.07) \times 10^{-3}$. Theoretical studies by Wilson and Hirst [1616], Resende and De Almeida [1227] and Thompson et al. [1435] support the experimentally observed dominance of the H-abstraction pathway at low pressure. Diaz-de-Mera et al. [429] have employed a discharge flow – mass spectrometry technique to measure rate constants at pressures of 0.5 – 1.0 Torr He over the temperature range 259 – 364 K. The 298 K rate constant reported by Diaz-de-Mera et al. is nearly a factor of 3 slower than the low-temperature limit value reported by Stickel et al. Furthermore, Diaz-de-Mera et al. report a small positive activation energy whereas Stickel et al. report a small negative activation energy. The present recommendation for the H-abstraction pathway is based on an extrapolated low pressure limit rate constant obtained from the data of Stickel et al., with the uncertainty adjusted to encompass the result of Diaz-de-Mera et al. The data of Stickel et al. suggest that a high pressure limit is reached at $P \sim 150$ Torr. Urbanski and Wine [1504] have observed the UV-visible absorption spectrum of $(\text{CH}_3)_2\text{SCl}$ in 155 Torr O_2 and used absorbance rise-time data to derive a rate constant that agrees well with those measured by Stickel et al. at pressures of 150–750 Torr N_2 . Enami et al. [483] have observed the kinetics of adduct formation using cavity ring down spectroscopy, and derived rate constants over the temperature and pressure ranges 278–318 K and 20–300 Torr N_2 that also agree well with those reported by Stickel et al. Room temperature competitive kinetics measurements by Nielsen et al. [1083] at 740 Torr, Kinnison et al. [790] at 760 Torr, and Arsene et al. [41] at 750 Torr agree quite well with the results of Stickel et al., Urbanski and Wine, and Enami et al. Kinnison et al. and Arsene et al. report that the rate constant at atmospheric pressure is $\sim 20\%$ faster in synthetic air than in N_2 bath gas, suggesting that the $(\text{CH}_3)_2\text{SCl}$ adduct reacts with O_2 ; however, the results of Urbanski and Wine, and Enami et al. argue against the occurrence of such a reaction. Stickel et al. report that the high-pressure rate constant in N_2 is independent of temperature whereas Arsene et al. report large negative activation energies in both N_2 and synthetic air bath gases. The large negative activation energies reported by Arsene et al. seem unlikely to result from a two-channel elementary reaction (H-abstraction and addition); hence, the recommended E/R is that reported by Stickel et al. (Table: 10-6, Note: 10-6, Evaluated: 10-6) [Back to Table](#)
- I49. $(\text{CH}_3)_2\text{SCl} + \text{O}_2, \text{NO}, \text{NO}_2$. The recommendations are based on the study of Urbanski and Wine [1504] which combined laser flash photolytic production of $(\text{CH}_3)_2\text{SCl}$ with kinetic observations by time-resolved absorption spectroscopy. The recommended uncertainties for the NO and NO_2

reactions are larger than those reported by Urbanski and Wine pending independent confirmation of their results. As in the Urbanski and Wine study, Enami et al. [483] report no observable reaction between $(\text{CH}_3)_2\text{SCl}$ and O_2 . (Table: 06-02, Note: 06-02) [Back to Table](#)

150. $\text{Cl} + \text{CH}_3\text{S}(\text{O})\text{CH}_3 \rightarrow \text{CH}_3\text{S}(\text{O})\text{CH}_2 + \text{HCl}$. The recommended value of $k(298 \text{ K})$ for H-abstraction is based on the analysis of Nicovich et al. [1068], who corrected the low pressure discharge flow mass spectrometry studies of Martinez et al. [976] and Riffault et al. [1233] to account for the contribution of the addition reaction. The temperature dependence studies of Martinez et al. (273–335 K) and Nicovich et al. (438–571 K) suggest the possibility of curvature in the Arrhenius plot. The recommended $E/R (= 0)$ is appropriate for the 200–300 K temperature regime but not for higher temperatures. Vandresen and Resende [1513] report a theoretical rate coefficient of $1.2 \times 10^{-10} \text{ cm}^3 \text{ molecule}^{-1} \text{ s}^{-1}$, i.e., a factor of seven faster than the value suggested by experimental results. (Table: 10-6, Note: 10-6, Evaluated: 10-6) [Back to Table](#)
151. $\text{CH}_3(\text{Cl})\text{S}(\text{O})\text{CH}_3 + \text{O}_2, \text{NO}, \text{NO}_2$. The recommendations are based on the study of Kleissas et al. [801] which combined laser flash photolytic production of $\text{CH}_3(\text{Cl})\text{S}(\text{O})\text{CH}_3$ with kinetic observations by time-resolved absorption spectroscopy. The recommended uncertainties for the NO and NO_2 reactions are larger than those reported by Kleissas et al. pending independent confirmation of their results. (Table: 10-6, Note: 10-6, Evaluated: 10-6) [Back to Table](#)
152. $\text{Cl}_2 + \text{CH}_3\text{SCH}_3 \rightarrow \text{products}$. Dyke et al. [470] have employed a flow tube technique with reactant and product detection by photoelectron spectroscopy to obtain a rate constant of $(3.4 \pm 0.7) \times 10^{-14} \text{ cm}^3 \text{ molecule}^{-1} \text{ s}^{-1}$ at 294 K and 1.6–3.0 Torr helium bath gas (the reported uncertainty is 1σ , precision); this rate constant is consistent with an upper limit value of $8 \times 10^{-14} \text{ cm}^3 \text{ molecule}^{-1} \text{ s}^{-1}$ at 298 K in 1 Torr helium reported by Butkovskaya et al. [233]. Dyke et al. [469] have obtained the photoelectron spectrum of a reaction intermediate that they assign as $(\text{CH}_3)_2\text{S}-\text{Cl}_2$ (each Cl bound to S). A theoretical analysis suggests that the observed intermediate is stable by $26.3 \text{ kcal mol}^{-1}$ relative to reactants and dissociates over a $29.0 \text{ kcal mol}^{-1}$ barrier to the end products $\text{HCl} + \text{CH}_3\text{SCH}_2\text{Cl}$, both of which were observed by photoelectron spectroscopy [469]. Because it is not clear how Dyke et al. differentiated gas phase reaction of Cl_2 with CH_3SCH_3 from reaction on the flow tube walls in their investigation [470], the recommendation treats their result plus two standard deviations as an upper limit for the gas phase rate constant. (Table: 10-6, Note: 10-6, Evaluated: 10-6) [Back to Table](#)
153. $\text{ClO} + \text{OCS}; \text{ClO} + \text{SO}_2$. These recommendations are based on the discharge flow mass spectrometric data of Eibling and Kaufman [478]. The upper limit on $k(298 \text{ K})$ for $\text{ClO} + \text{OCS}$ was set from the minimum detectable decrease in ClO. No products were observed. The upper limit on $k(298 \text{ K})$ for $\text{ClO} + \text{SO}_2$ is based on the authors' estimate of their SO_3 detection limit. The upper limit for this same reaction based on the minimum detectable decrease in ClO was not used due to the potential problem of ClO reformation from the $\text{Cl} + \text{O}_3$ source reaction. (Table 83-62, Note: 83-62) [Back to Table](#)
154. $\text{ClO} + \text{CH}_3\text{SCH}_3$. The 298 K recommendation is the average of the values reported in discharge flow mass spectrometry studies by Barnes et al. [92] and Diaz-de-Mera et al. [429]. Barnes et al. prefer their more recent rate constant to one a factor of 4 higher that they determined using an earlier version of their apparatus. The recommendation for E/R is based on the temperature dependence observed by Diaz-de-Mera et al. over the range 259 – 335 K. The uncertainty factors reflect the fact that the two reported values for $k(298 \text{ K})$ differ by more than a factor of two and that the activation energy is defined by data from a single study over a moderately narrow temperature range. (Table: 06-2, Note: 06-2) [Back to Table](#)
155. $\text{ClO} + \text{CH}_3\text{S}(\text{O})\text{CH}_3$. The recommendation is based on the results of a low-pressure discharge flow mass spectrometry study by Riffault et al. [1233]. These investigators were also able to establish an even lower upper limit of $2 \times 10^{-15} \text{ cm}^3 \text{ molecule}^{-1} \text{ s}^{-1}$ for the channel that produces Cl atoms (Table: 06-2, Note: 06-2) [Back to Table](#)
156. $\text{ClO} + \text{SO}$. The value of $k(298 \text{ K})$ is an average of the determinations by Clyne and MacRobert [324] and Brunning and Stief [206]. The temperature independence is taken from the latter study with the A-factor recalculated to fit the $k(298 \text{ K})$ recommendation. (Table 87-41, Note: 87-41) [Back to Table](#)

- I57. $\text{Br} + \text{H}_2\text{S}$, $\text{Br} + \text{CH}_3\text{SH}$. These recommendations are based on the study by Nicovich et al. [1066] who measured both the forward and reverse reactions by time-resolved resonance fluorescence detection of Br atoms. The uncertainties placed on these recommendations have been increased over those estimated by the authors to reflect the absence of any confirming investigations. (Table: 94-26, Note: 94-26) [Back to Table](#)
- I58. $\text{Br} + \text{CH}_3\text{SCH}_3$. It is well-established based on studies by Wine et al. [1625], Ingham et al. [712], and Nakano et al. [1043] that, under atmospheric conditions, attack of Br on CH_3SCH_3 occurs predominantly by addition to the sulfur atom. Above 375 K, adduct decomposition is so rapid that the addition channel is effectively negligible. Jefferson et al. [729] report high temperature experiments where the individual hydrogen transfer reactions $\text{Br} + \text{CH}_3\text{SCH}_3 \rightarrow \text{CH}_3\text{SCH}_2 + \text{HBr}$ (forward reaction) and $\text{CH}_3\text{SCH}_2 + \text{HBr} \rightarrow \text{Br} + \text{CH}_3\text{SCH}_3$ (reverse reaction) were isolated in a laser flash photolysis resonance fluorescence system, and their kinetics were separately studied over the temperature range 386 – 604 K. These investigators determined Arrhenius expressions for the forward and reverse reactions to be $9.0 \times 10^{-11} \exp(-2386/T)$ and $8.6 \times 10^{-13} \exp(+836/T) \text{ cm}^3 \text{ molecule}^{-1} \text{ s}^{-1}$, respectively. Analysis of the equilibrium data also permitted determination of the heat of formation of CH_3SCH_2 (see Appendix 1). Extrapolation of the Jefferson et al. Arrhenius expression to 298 K gives a rate constant for the non-adduct-forming part of the $\text{Br} + \text{CH}_3\text{SCH}_3$ reaction (presumably direct hydrogen abstraction) of $3.0 \times 10^{-14} \text{ cm}^3 \text{ molecule}^{-1} \text{ s}^{-1}$. This estimated rate constant agrees quite well with the value of $(4.9 \pm 2.0) \times 10^{-14} \text{ cm}^3 \text{ molecule}^{-1} \text{ s}^{-1}$ obtained in a competitive kinetics study at atmospheric pressure in air by Ballesteros et al. [83], and is consistent with an upper limit of $1 \times 10^{-13} \text{ cm}^3 \text{ molecule}^{-1} \text{ s}^{-1}$ reported in a similar study by Maurer et al. [984]. Direct comparison of the Jefferson et al. and Ballesteros et al. kinetic data is warranted only if essentially all adduct formation is reversible in the Ballesteros et al. experiment, which is possible based on the apparent absence of an adduct + O_2 pathway [984], [1043], but is not yet well-established. The recommendation for the pressure-independent bimolecular reaction is based on extrapolation of the Arrhenius expression of Jefferson et al. to the atmospheric temperature regime. The large uncertainty reflects the need for a rather long extrapolation. (Table: 06-2, Note: 06-2) [Back to Table](#)
- I59. $\text{Br} + \text{CH}_3\text{S(O)CH}_3$. The recommendation is based on the results of a low-pressure discharge flow mass spectrometry study by Riffault et al. [1233]. These authors obtained an upper limit for the total rate constant of $1.5 \times 10^{-14} \text{ cm}^3 \text{ molecule}^{-1} \text{ s}^{-1}$, and also report channel-specific rate constants in units of $10^{-15} \text{ cm}^3 \text{ molecule}^{-1} \text{ s}^{-1}$ of 11 ± 3 for the H-abstraction channel and 1.2 ± 0.3 for the methyl elimination channel. A competitive kinetics study in 740 Torr air by Ballesteros et al. [83] reports a less sensitive upper limit rate constant of $6 \times 10^{-14} \text{ cm}^3 \text{ molecule}^{-1} \text{ s}^{-1}$. (Table: 06-2, Note: 06-2) [Back to Table](#)
- I60. $\text{BrO} + \text{CH}_3\text{SH} \rightarrow \text{products}$. The recommendation is based on the low-pressure discharge flow mass spectrometry study of Aranda et al. [36]. A significant negative activation energy of $-6.9 \pm 2.0 \text{ kJ/mol}$ was observed at $P = 1.0 \text{ Torr}$ He over the temperature range 259 – 333 K. At $T = 298 \text{ K}$, reported rate coefficients in units of $10^{-14} \text{ cm}^3 \text{ molecule}^{-1} \text{ s}^{-1}$ increase with increasing helium pressure from 2.7 ± 0.5 at $P = 0.5 \text{ Torr}$ to 4.9 ± 0.4 at $P = 3.0 \text{ Torr}$. HOBr was observed as a reaction product suggesting that an important reaction pathway is addition of BrO to CH_3SH followed by dissociation to $\text{HOBr} + \text{CH}_3\text{S}$ in competition with dissociation to reactants. Until kinetic data are reported at higher pressures, no recommendation of appropriate rate constants for atmospheric modeling is made. (Table: 10-6, Note: 10-6, Evaluated: 10-6) [Back to Table](#)
- I61. $\text{BrO} + \text{CH}_3\text{SCH}_3$. This recommendation is an average of results obtained in the discharge flow studies of Barnes et al. [92] and Bedjanian et al. [129], and the flash photolysis studies of Ingham et al. [712] and Nakano et al. [1043]. The flash photolysis studies were carried out at pressures of 60–200 Torr and give rate constants that are almost a factor of two greater than those obtained in the discharge flow studies at $P \sim 1 \text{ Torr}$. The error limits in the present evaluation are adjusted to include all available data. A new study to investigate the pressure dependence of the rate constant is needed. Both Bedjanian et al. and Ingham et al. have shown that DMSO ($\text{CH}_3\text{S(O)CH}_3$) is produced with near unit yield. Ballesteros et al. [83] report that the rate constants for $\text{BrO} + \text{CH}_3\text{SCH}_3$ and $\text{BrO} + \text{CD}_3\text{SCD}_3$ are identical, a result that is consistent with reaction proceeding via formation of a short-lived adduct that rapidly decomposes to $\text{Br} + \text{DMSO}$. (Table: 06-2, Note: 06-2) [Back to Table](#)

- I62. $\text{BrO} + \text{CH}_3\text{SSCH}_3$. The recommendation is based on a competitive kinetics study in 740 Torr air by Ballesteros et al. [83]. The large uncertainty factor results from the fact that the reported rate constant is measured relative to an assumed value of $3.2 \times 10^{-13} \text{ cm}^3 \text{ molecule}^{-1} \text{ s}^{-1}$ for the $\text{BrO} + \text{CH}_3\text{SCH}_3$ rate constant, which has an uncertain pressure dependence (see above), and from the fact that there is only a single study upon which to base a recommendation. (Table: 06-2, Note: 06-2) [Back to Table](#)
- I63. $\text{BrO} + \text{CH}_3\text{S(O)CH}_3$. The recommendation is based on a competitive kinetics study in 740 Torr air by Ballesteros et al. [83]. A low-pressure discharge flow mass spectrometry study by Riffault et al. [1233], gives an upper limit that is consistent with the recommendation. The large uncertainty factor results primarily from the fact that the reported rate constant is obtained from a series of competitive kinetics experiments that are referenced to an assumed value of $3.2 \times 10^{-13} \text{ cm}^3 \text{ molecule}^{-1} \text{ s}^{-1}$ for the $\text{BrO} + \text{CH}_3\text{SCH}_3$ rate constant, which has an uncertain pressure dependence (see above). (Table: 06-2, Note: 06-2) [Back to Table](#)
- I64. $\text{BrO} + \text{SO}$. This recommendation is based on the measurements of Brunning and Stief [205] performed under both excess BrO and excess SO conditions. The rate constant is supported by the lower limit assigned by Clyne and MacRobert [324] from measurements of SO_2 production. (Table 87-41, Note: 87-41) [Back to Table](#)
- I65. $\text{IO} + \text{CH}_3\text{SH}$. The value of $k(298 \text{ K})$ comes from the study by Maguin et al. [953] using discharge flow mass spectrometry. The investigators establish a branching ratio near unity for the production of HOI. The uncertainty factor reflects the absence of confirming investigations. (Table: 94-26, Note: 94-26) [Back to Table](#)
- I66. $\text{IO} + \text{CH}_3\text{SCH}_3$. This recommendation is based on the room temperature studies by Maguin et al. [953], Barnes et al. [92], and Knight et al. [808] using discharge flow mass spectrometry and the temperature-dependent studies of Gravestock et al. [575] and Dillon et al. [434]; the Gravestock et al. data at $T < 344 \text{ K}$ only are used in arriving at the recommendation. The studies of Maguin et al. and Barnes et al. supersede earlier, less direct measurements by the same groups [94, 970], which reported much greater rate constants. Nakano et al. [1041] have employed a laser flash photolysis cavity ring down spectroscopy technique to investigate the temperature and pressure dependence of the rate constant. These investigators report that the 298 K rate constant increases from 1 to $25 \times 10^{-14} \text{ cm}^3 \text{ molecule}^{-1} \text{ s}^{-1}$ as pressure increases from 5 to 100 Torr N_2 , then levels off at higher pressure. Nakano et al. also investigated the temperature dependence of the rate constant at $P = 100$ Torr and observed a very strong negative temperature dependence, i.e., $E/R = -2230 \pm 460$. The pressure dependence reported by Nakano et al. is in conflict with the results of Daykin and Wine [402], Gravestock et al., and Dillon et al., while the temperature dependence reported by Nakano et al. is in conflict with the results of Gravestock et al. and Dillon et al. (Table: 10-6, Note: 10-6, Evaluated: 10-6) [Back to Table](#)
- I67. $\text{S} + \text{O}_2$. This recommendation is based primarily on the study of Davis et al. [397]. Modest agreement at 298 K is found in the studies of Fair and Thrush [488], Fair et al. [489], Donovan and Little [455], and Clyne and Townsend [335]. The study by Clyne and Whitefield [342], which indicates a slightly negative E/R between 300 and 400 K, is encompassed by the assigned uncertainty limits. (Table: 82-57, Note: 82-57) [Back to Table](#)
- I68. $\text{S} + \text{O}_3$. This recommendation accepts the only available experimental data of Clyne and Townsend [335]. In this study the authors measure a value of the rate constant for $\text{S} + \text{O}_2$ in reasonable agreement with that recommended above. (Table: 82-57, Note: 82-57) [Back to Table](#)
- I69. $\text{SO} + \text{O}_2$. This recommendation is based on the low temperature measurements of Black et al. [168, 169] and Schurath and Goede [1278]. The room temperature rate constant reported by Black et al. supercedes an earlier value [169] as recommended by the authors. The recommended values for $k(T)$ lie significantly higher than an extrapolation of the higher temperature data of Homann et al. [664], but are consistent with the more recent high temperature study of Garland [532]. A room temperature upper limit on k set by Breckenridge and Miller [193] is consistent with the recommendation. (Table: 06-2, Note: 06-2) [Back to Table](#)

- I70. $\text{SO} + \text{O}_3$. The value of $k(298 \text{ K})$ is an average of the determinations by Halstead and Thrush [605], Robertshaw and Smith [1236], Schurath and Goede [1278] and Black et al. [168, 169]. The value of E/R is an average of the values reported by Halstead and Thrush, Schurath and Goede, and Black et al. [169], with the A-factor recalculated to fit the recommendation for $k(298 \text{ K})$. (Table: 06-2, Note: 06-2) [Back to Table](#)
- I71. $\text{SO} + \text{NO}_2$. The value of $k(298 \text{ K})$ is an average of the determinations by Clyne and MacRobert [323], Black et al. [168], and Brunning and Stief [206], which agree quite well with the rate constant calculated from the relative rate measurements of Clyne et al. [319]. The Arrhenius parameters are taken from Brunning and Stief. (Table: 82-57, Note: 82-57) [Back to Table](#)
- I72. $\text{SO} + \text{OCIO}$. This recommendation is based on the room temperature study by Clyne and MacRobert [324]. The uncertainty reflects the absence of any confirming investigation. (Table: 82-57, Note: 82-57) [Back to Table](#)
- I73. $\text{SO}_3 + 2 \text{H}_2\text{O}$. Several research groups have attempted to quantify the rate of sulfuric acid formation via this reaction in the gas phase. Reiner and Arnold [1225] placed an upper limit of $2.4 \times 10^{-15} \text{ cm}^3 \text{ molecule}^{-1} \text{ s}^{-1}$ on the rate constant, slightly lower than that determined by Wang et al. [1576]. The inability to cite the results as other than an upper limit is due to the difficulty in excluding all heterogeneous effects from the experiments. The higher rate constant reported earlier by Castleman et al. [263] may have resulted from an underestimation of the effects of such heterogeneous reactions. Subsequently, Reiner and Arnold [1226] sought to improve their rate constant determination by more detailed quantification of heterogeneous contributions. They derived a value of $1.2 \times 10^{-15} \text{ cm}^3 \text{ molecule}^{-1} \text{ s}^{-1}$, independent of pressure (from 31–260 mbar of synthetic air). Evidence was also obtained that H_2SO_4 was, indeed, the product of the reaction.

Kolb et al. [815] attempted to measure the gas phase rate constant using a turbulent flow reactor designed to minimize wall effects. Their results, when analyzed as representing a bimolecular reaction, support a rate constant in the range $(1 - 7) \times 10^{-15} \text{ cm}^3 \text{ molecule}^{-1} \text{ s}^{-1}$. However, a more detailed analysis of the data indicated that the gas phase reaction was second order in water vapor. The reaction rate was also observed to increase as the temperature was lowered from 333 K to 243 K. These observations, together with calculations by Morokuma and Mugurama [1030], led the latter authors to suggest that SO_3 consumption likely involved its reaction with the water dimer or the reaction $\text{SO}_3\text{--H}_2\text{O} + \text{H}_2\text{O}$, leading to the formation of sulfuric acid.

A laminar flow reactor study by Lovejoy et al. [936] over the temperature range 250 to 360 K also revealed SO_3 loss to be second order in water concentration and independent of pressure (from 20 to 80 Torr of N_2 at 300 K). These latter authors measured a strong negative temperature dependence for the rate constant and a significant kinetic isotope effect ($k_{\text{H}_2\text{O}} \approx 2k_{\text{D}_2\text{O}}$), leading them to describe the reaction as proceeding via the rapid association between SO_3 and H_2O followed by a slower reaction between the adduct and water to form sulfuric acid. Lovejoy et al.'s measurement of a $-13 \text{ kcal mol}^{-1}$ "activation" energy was viewed as energetically inconsistent with a $\text{SO}_3 + \text{water dimer}$ reaction mechanism since it would require a large negative activation energy for the $\text{SO}_3 + (\text{H}_2\text{O})_2$ step. Jayne et al. [728] have carried out a turbulent flow reactor study over the temperature range 283 to 370 K and the pressure range 100 to 760 Torr N_2 . Their results provide further support for a mechanism involving formation of an $\text{SO}_3\text{--H}_2\text{O}$ adduct that reacts with a second H_2O to form H_2SO_4 , and the rate constants they report agree quite well with those reported by Lovejoy et al. The recommended expression for first order loss of SO_3 ,

$$k^{\text{I}} = 8.5 \times 10^{-41} \exp(+6540/T) [\text{H}_2\text{O}]^2 \text{ s}^{-1} \quad ([\text{H}_2\text{O}] \text{ in molecules cm}^{-3})$$

is the best fit of the combined data of Lovejoy et al. and Jayne et al. to an Arrhenius form. (Table: 06-02, Note: 06-02) [Back to Table](#)

- I74. $\text{SO}_3 + \text{NO}_2$. This recommendation is based on the study of Penzhorn and Canosa [1155] using second derivative UV spectroscopy. These authors observe the production of a white aerosol, which they interpret to be the adduct NSO_5 . This claim is supported by ESCA spectra. (Table: 85-37, Note: 85-37) [Back to Table](#)
- I75. $\text{SH} + \text{O}_2$. This upper limit for $k(298 \text{ K})$ is based on the study by Stachnik and Molina [1354] utilizing experiments sensitive to the production of OH. Somewhat higher upper limits of $1.0 \times 10^{-}$

17 and $1.5 \times 10^{-17} \text{ cm}^3 \text{ molecule}^{-1} \text{ s}^{-1}$ were assigned by Friedl et al. [522] and Wang et al. [1574] respectively from the sensitivities for OH detection and SH decay respectively. An even higher upper limit by Black [165], based on the lack of SH decay, may have been complicated by SH regeneration. Much less sensitive upper limits have been calculated by Tiee et al. [1445], Nielsen [1074], and Cupitt and Glass [376]. Stachnik and Molina [1354] also report a somewhat higher upper limit ($< 1.0 \times 10^{-18} \text{ cm}^3 \text{ molecule}^{-1} \text{ s}^{-1}$) for the rate constant for the sum of the two $\text{SH} + \text{O}_2$ reaction channels (producing $\text{OH} + \text{SO}$ and $\text{H} + \text{SO}_2$). (Table: 85-37, Note: 85-37) [Back to Table](#)

- I76. $\text{SH} + \text{O}_3$. The value for $k(298 \text{ K})$ is an average of the determinations by Friedl et al. [522] (laser induced fluorescence detection of SH), Schonle et al. [1277] (mass spectrometric detection of reactant SH and product HSO) as revised by Schindler and Benter [1269], and Wang and Howard [1573] (laser magnetic resonance detection of SH). The temperature dependence is from Wang and Howard with the A-factor calculated to agree with the recommended value for $k(298 \text{ K})$. The recommendation for g reflects the fact that the temperature dependence comes from measurements above room temperature and, thus, extrapolation to lower temperatures may be subject to additional uncertainties. Wang and Howard report observing a minor reaction channel that produces $\text{H} + \text{SO} + \text{O}_2$. A theoretical study by Resende and Ornellas [1228] concludes that if reaction occurs on the ground state potential energy surface, the rate constant should be several orders of magnitude slower than the experimental value. (Table: 06-2, Note: 06-2) [Back to Table](#)
- I77. $\text{SH} + \text{H}_2\text{O}_2$. This recommended upper limit for $k(298 \text{ K})$ is based on the study of Friedl et al. [522]. Their value is calculated from the lack of SH decay (measured by laser induced fluorescence) and the lack of OH production (measured by resonance fluorescence). The three possible product channels are $\text{H}_2\text{S} + \text{HO}_2$, $\text{HSOH} + \text{OH}$, and $\text{HSO} + \text{H}_2\text{O}$. (Table: 85-37, Note: 85-37) [Back to Table](#)
- I78. $\text{SH} + \text{NO}_2$. This recommendation is based on the measurements of Wang et al. [1574] and Herndon and Ravishankara [637]. Wang et al. suggest that the lower values of $k(298 \text{ K})$ reported by Black [165], Friedl et al. [522], and Bulatov et al. [215] are due to SH regeneration from the H_2S source compound. Herndon and Ravishankara suggest that simultaneous detection of SH and SO may have corrupted earlier studies where laser induced fluorescence was employed as the detection technique [165] [522]. In the study by Stachnik and Molina [1354], attempts were made at minimizing SH regeneration, and the reported value of $k(298 \text{ K})$ was significantly greater than that from the earlier studies, but still 30% less than that measured by Wang et al., who used two independent SH source reactions. A slightly larger rate constant measured by Schonle et al. [1277], as revised by Schindler and Benter [1269], has not been recommended due to the somewhat more limited database for their determination. The reaction as written represents the most exothermic channel. In fact, HSO has been detected as a product by Leu and Smith [893], Bulatov et al. [215], Schonle et al. [1277], and Wang et al. The absence of a primary deuterium isotope effect, as observed by both Wang et al. and Herndon and Ravishankara, coupled with the large magnitude of the rate constant suggests that the (four-center intermediate) channels producing $\text{SO} + \text{HNO}$ and $\text{OH} + \text{SNO}$ are of minor importance. No evidence for a three-body combination reaction was found by either Black or Friedl et al. Based on a pressure independence of the rate constant between 30 and 300 Torr, Black set an upper limit of $7.0 \times 10^{-31} \text{ cm}^6 \text{ molecule}^{-2} \text{ s}^{-1}$ for the termolecular rate constant. Similarly, Stachnik and Molina [1354] observed no change in decay rate between 100 and 730 Torr with O_2 (although these O_2 experiments were designed primarily to limit SH regeneration). The recommendation given here is supported by the discharge flow laser induced fluorescence study of the $\text{SD} + \text{NO}_2$ reaction by Fenter and Anderson [499]. These investigators report a rate constant at 298 K of $6.8 \times 10^{-11} \text{ cm}^3 \text{ molecule}^{-1} \text{ s}^{-1}$, which compares favorably with the values of 7.3×10^{-11} and $6.6 \times 10^{-11} \text{ cm}^3 \text{ molecule}^{-1} \text{ s}^{-1}$ determined by Wang et al. and Herndon and Ravishankara, respectively, in studies of the same reaction. Fenter and Anderson also obtained an E/R value of -210 K , very similar to the -279 K value derived by Herndon and Ravishankara for the SD reaction and the values -240 K and -270 K derived by Wang et al. and Herndon and Ravishankara, respectively, for the SH reaction. (Table: 10-6, Note: 10-6, Evaluated: 10-6) [Back to Table](#)
- I79. $\text{SH} + \text{N}_2\text{O}$. The recommendation is the upper limit rate constant reported by Herndon et al. [635]. As discussed by Herndon et al., the much greater (four orders of magnitude) rate constant reported by Ravichandran et al. [1203] appears to result from mis-interpretation of the source of

electronically excited HSO, chemiluminescence from which was employed by Ravichandran et al. to follow the reaction kinetics. (Table: 06-02, Note: 06-02) [Back to Table](#)

180. $\text{SH} + \text{Cl}_2$. The recommended 298 K rate constant is based on the work of Nesbitt and Leone [1056], who studied the kinetics of the $\text{Cl} + \text{H}_2\text{S} \rightarrow \text{SH} + \text{HCl}$, $\text{SH} + \text{Cl}_2 \rightarrow \text{ClSH} + \text{Cl}$ chain reaction. Fenter and Anderson [498] employed a discharge flow laser induced fluorescence technique to study the $\text{SD} + \text{Cl}_2$ reaction over the temperature range 273–373 K. The 298 K rate constant reported by Fenter and Anderson is about 20% greater than the one reported by Nesbitt and Leone, which is consistent with the expected secondary kinetic isotope effect. The recommended value of E/R is taken from the work of Fenter and Anderson; the recommended value for the parameter g reflects the absence of confirming studies and uncertainty in the isotope effect on E/R. (Table: 06-2, Note: 06-2) [Back to Table](#)
181. $\text{SH} + \text{BrCl}$; $\text{SH} + \text{Br}_2$; $\text{SH} + \text{F}_2$. The recommendations for these reactions are derived from the data of Fenter and Anderson [498] for the SD radical. The uncertainties have been increased over those estimated by the investigators to reflect the absence of any confirming investigations and the influence of the secondary isotope effect. For the BrCl reaction, the channel producing ClSD + Br was found to be described by the rate expression $k = 2.3 \times 10^{-11} \exp(100/T) \text{ cm}^3 \text{ molecule}^{-1} \text{ s}^{-1}$. (Table: 92-20, Note: 06-2) [Back to Table](#)
182. $\text{HSO} + \text{O}_2$. This recommendation is based on the study by Lovejoy et al. [940], who employed laser magnetic resonance monitoring of HSO in a discharge flow system. The upper limit thus derived for k(298 K) is nearly two orders of magnitude smaller than measured by Bulatov et al. [217]. (Table: 87-41, Note: 87-41 (Table: 92-20, Note: 92-20)) [Back to Table](#)
183. $\text{HSO} + \text{O}_3$. This recommendation is based on the determinations by Friedl et al. [522] and Wang and Howard [1573]. In the first study, performed at higher O_3 concentrations, greater quantities of HSO were produced in the flow tube and SH approached a steady state due to its generation via $\text{HSO} + \text{O}_3$. The rate constant for this reaction was thus determined relative to $\text{SH} + \text{O}_3$ from measurements of the steady state SH concentration as a function of the initial SH concentration. In the second study, the rate constant and its branching ratio were measured at two temperatures. At room temperature, the overall rate constant is in excellent agreement with that of Friedl et al. More recently, Lee et al. [878] determined a room temperature rate constant of $4.7 \times 10^{-14} \text{ cm}^3 \text{ molecule}^{-1} \text{ s}^{-1}$ for the sum of all reaction channels not producing HS. This value is approximately 30% greater than that measured by Wang and Howard for the same channels. Lee et al. derive an Arrhenius activation energy of 1120 K for these channels from data between 273 and 423 K, in agreement with the more limited temperature-dependent data of Wang and Howard.
- The lack of an isotope effect when SD was employed in the Friedl et al. study suggests that the products of the $\text{HSO} + \text{O}_3$ reaction are $\text{SH} + 2\text{O}_2$ (analogous to those for $\text{HO}_2 + \text{O}_3$). However, Wang and Howard found that only 70% of the reaction leads to HS formation. In addition, their observations of HO_2 production in the presence of O_2 suggests the existence of a reaction channel producing $\text{HSO}_2 + \text{O}_2$ followed by $\text{HSO}_2 + \text{O}_2 \rightarrow \text{HO}_2 + \text{SO}_2$. At the present time, no recommendation is given for the product channels. Further mechanistic work is suggested, since it is important to understand whether this reaction in the atmosphere leads to HS regeneration or to oxidation of the sulfur. (Table: 92-20, Note: 94-26) [Back to Table](#)
184. $\text{HSO} + \text{NO}$; $\text{HSO} + \text{NO}_2$. The recommendations for these reactions are based on the study by Lovejoy et al. [940] in which laser magnetic resonance was used to monitor HSO in a discharge flow system. Their upper limit for the NO reaction is a factor of 25 smaller than the rate constant measured by Bulatov et al. [216] using intracavity laser absorption at pressures between 10 and 100 Torr. Since it is unlikely that this reaction rate undergoes a factor of 25 increase between 1 Torr (the pressure of the Lovejoy et al. work) and 10 Torr, the higher rate constant may be due to secondary chemistry associated with the HSO production methods employed.

The recommendation for the NO_2 reaction is a factor of 2 higher than the rate constant reported by Bulatov et al. [215]. Lovejoy et al. have attributed this difference to HSO regeneration under the experimental conditions used by Bulatov et al. [215]. The product assignment for this reaction is discussed in the note for the $\text{HSO}_2 + \text{O}_2$ reaction. (Table 87-41, Note: 87-41) [Back to Table](#)

- I85. $\text{HSO}_2 + \text{O}_2$. This recommendation is based on the rate of HO_2 formation measured by Lovejoy et al. [940] upon addition of O_2 to the $\text{HSO} + \text{NO}_2$ reaction system. While HSO_2 was not observed directly, a consideration of the mechanistic possibilities for $\text{HSO} + \text{NO}_2$, coupled with measurements of the HO_2 production rate at various O_2 pressures, led these authors to suggest that HSO_2 is both a major product of the $\text{HSO} + \text{NO}_2$ reaction and a precursor for HO_2 via reaction with O_2 . (Table: 87-41, Note: 87-41) [Back to Table](#)
- I86. $\text{HOSO}_2 + \text{O}_2$. This recommendation is based on the studies of Gleason et al. [562] and Gleason and Howard [560] in which the HOSO_2 reactant was monitored using a chemical ionization mass spectrometric technique. Gleason and Howard conducted their measurements over the 297–423 K temperature range in the only temperature dependence investigation. Thus, the parameter g has been increased from their quoted limits to account for the potential uncertainties in extrapolating their data to sub-ambient temperatures. The value of $k(298 \text{ K})$ derives further support from the studies of Margitan [960] and Martin et al. [972], both of whom used modeling fits of OH radical decays in the $\text{OH} + \text{SO}_2 + \text{M}$ reaction system in the presence of O_2 and NO. In this latter analysis, the HOSO_2 reacts with O_2 , yielding HO_2 , which subsequently regenerates OH through its reaction with NO. The infrared spectrum of HOSO_2 has been recorded in low temperature matrix isolation experiments by Hashimoto et al. [620] and Nagase et al. [1040]. Mass spectrometric detection of HOSO_2 in the gas phase has also been reported by Egsgaard et al. [476]. (Table: 06-2, Note: 06-2) [Back to Table](#)
- I87. $\text{CS} + \text{O}_2$. The recommendation given for $k(298 \text{ K})$ is based on the work of Black et al. [167] using laser induced fluorescence to monitor CS. This value agrees with the somewhat less precise determination by Richardson [1230] using OCS formation rates. The latter author presents evidence that this reaction channel dominates over the one producing $\text{SO} + \text{CO}$ by more than a factor of 10. Measurements by Richardson at 293 K and 495 K yield an E/R of 1860 K. However, use of this activation energy with the recommended value of $k(298 \text{ K})$ results in an unusually low Arrhenius A-factor of $1.5 \times 10^{-16} \text{ cm}^3 \text{ molecule}^{-1} \text{ s}^{-1}$. In view of this, no recommendation is given for the temperature dependence. (Table: 85-37, Note: 85-37) [Back to Table](#)
- I88. $\text{CS} + \text{O}_3$; $\text{CS} + \text{NO}_2$. The $k(298 \text{ K})$ recommendations for both reactions accept the results of Black et al. [167], who used laser-induced fluorescence to monitor the CS reactant in a room temperature experiment. The uncertainty factors reflect the absence of any confirming measurements. (Table: 85-37, Note: 85-37) [Back to Table](#)
- I89. $\text{CH}_3\text{S} + \text{O}_2$. This upper limit is based on the study by Tyndall and Ravishankara [1496]. Somewhat higher upper limits were derived in the earlier studies of Balla et al. [82] and Black and Jusinski [166]. (Table: 90-1, Note: 90-1) [Back to Table](#)
- I90. $\text{CH}_3\text{S} + \text{O}_3$. The recommendation for $k(298 \text{ K})$ is the average of room temperature rate constants reported by Tyndall and Ravishankara [1497], Domine et al. [450], Turnipseed et al. [1475], and Martinez et al. [975]. The recommendation for E/R is the average of values obtained from least squares fits of the temperature-dependent data of Turnipseed et al. and Martinez et al. using only rate constants at temperatures below 345 K. A failure to observe significant reaction in the study by Black and Jusinski [166] is interpreted as due to rapid regeneration of CH_3S in their system. Tyndall and Ravishankara [1497] corrected their measured 298 K rate constant downward by ~20% to account for CH_3S regeneration via the $\text{CH}_3\text{SO} + \text{O}_3$ reaction, but the magnitude of the correction is now highly uncertain in light of the results of Domine et al. and Turnipseed et al. Domine et al. measured the yield of CH_3SO to be 15%. (Table: 06-2, Note: 06-2) [Back to Table](#)
- I91. $\text{CH}_3\text{S} + \text{NO}$. The upper limit for the bimolecular reaction between CH_3S and NO is based on estimates by Balla et al. [82], who conducted a temperature dependence study of the termolecular reaction. (Table: 92-20, Note: 92-20) [Back to Table](#)
- I92. $\text{CH}_3\text{S} + \text{NO}_2$. The recommendation for $k(298 \text{ K})$ is the average of room temperature rate constants reported by Tyndall and Ravishankara [1496], Domine et al. [448], Turnipseed et al. [1475], Martinez et al. [975], and Chang et al. [273]. The recommendation for E/R is the average of values reported by Turnipseed et al., Martinez et al., and Chang et al. An earlier study by Balla et al. [82] appears to have been affected by secondary reactions resulting from high radical concentrations. Tyndall and Ravishankara determined the NO yield to be $(80 \pm 20)\%$. Together with the unity yield

of CH_3SO obtained by Domine et al., this implies that the primary reaction channel is as written. (Table: 06-2, Note: 06-2) [Back to Table](#)

- I93. $\text{CH}_2\text{SH} + \text{O}_2$. This recommendation is the average of the rate constant obtained by Rahman et al. [1196] in a fast flow mass spectrometry system and that from Anastasi et al. [27] using a pulse radiolysis – kinetic absorption apparatus. The value of Anastasi et al. is nearly twice that of Rahman et al. It is difficult at present to indicate a preference for the results of one study over the other, and the value of $f(298\text{ K})$ has been chosen to reflect this uncertainty. Since this is a fast bimolecular reaction, one would expect the products to be $\text{HO}_2 + \text{CH}_2\text{S}$, by analogy with the reaction between CH_2OH and O_2 . (Table: 94-26, Note: 94-26) [Back to Table](#)
- I94. $\text{CH}_2\text{SH} + \text{O}_3$. The value of $k(298\text{ K})$ comes from the study by Rahman et al. [1196] using fast flow mass spectrometry. The uncertainty factor reflects the absence of any confirming investigations. (Table: 94-26, Note: 94-26) [Back to Table](#)
- I95. $\text{CH}_2\text{SH} + \text{NO}$. The value of $k(298\text{ K})$ comes from the study by Anastasi et al. [27] using a pulse radiolysis kinetic absorption apparatus. The uncertainty factor reflects the absence of any confirming investigations. (Table: 94-26, Note: 94-26) [Back to Table](#)
- I96. $\text{CH}_2\text{SH} + \text{NO}_2$. This recommendation averages the rate constant obtained by Rahman et al. [1196] in a fast flow mass spectrometry system with that from Anastasi et al. [27], using a pulse radiolysis kinetic absorption apparatus. The value of Rahman et al. is nearly twice that of Anastasi et al. It is difficult to indicate a preference for the results of one study over the other, and the value of $f(298\text{ K})$ has been chosen to reflect this uncertainty. (Table: 94-26, Note: 94-26) [Back to Table](#)
- I97. $\text{CH}_3\text{SO} + \text{O}_3$. This recommendation is the average of values reported by Domine et al. [450] and Borissenko et al. [179]. It is supported by the study of Tyndall and Ravishankara [1497], in which the rate constant was derived from a complex analysis of the $\text{CH}_3\text{S} + \text{O}_3$ reaction system. Borissenko et al. measured the rate constant relative to the rate constant for the $\text{CH}_3\text{SO} + \text{NO}_2$ reaction; they report that the $\text{CH}_3\text{SO} + \text{NO}_2$ rate constant is greater by a factor of 47. Domine et al. place the direct yield of CH_2SO at approximately 10% and that of CH_3S at 13% at low pressure. Borissenko et al. report that the SO_2 yield is near unity in 100–600 Torr N_2 . (Table: 06-2, Note: 06-2) [Back to Table](#)
- I98. $\text{CH}_3\text{SO} + \text{NO}_2$. This recommendation is based on the direct measurements of Domine et al. [448]. The results are supported by somewhat less direct measurements of Tyndall and Ravishankara [1496], Mellouki et al. [998], and Kukui et al. [823]. The results of Kukui et al. suggest a small negative activation energy, but their data set is not extensive enough to warrant a recommendation for E/R without independent confirmation. Borissenko et al. [179] report that the SO_2 yield drops from ~0.4 in 100 Torr N_2 to ~0.25 in 660 Torr N_2 . (Table: 06-2, Note: 06-2) [Back to Table](#)
- I99. $\text{CH}_3\text{SOO} + \text{O}_3$, $\text{CH}_3\text{SOO} + \text{NO}$, $\text{CH}_3\text{SOO} + \text{NO}_2$. These recommendations are based on the experiments of Turnipseed et al. [1475] in which CH_3S was monitored by laser induced fluorescence in equilibrium with CH_3SOO . The upper limit for the O_3 reaction was determined from experiments at 227 K. The results for the NO and NO_2 reactions were independent of temperature over the ranges 227–256 K and 227–246 K, respectively. The uncertainties placed on these recommendations have been increased over those estimated by the authors to reflect the absence of any confirming investigations. (Table: 94-26, Note: 94-26) [Back to Table](#)
- I100. $\text{CH}_3\text{SO}_2 + \text{NO}_2$. This recommendation is based on the study by Ray et al. [1219] using a discharge flow reactor equipped with laser induced fluorescence and mass spectrometric detection. The CH_3SO_2 was produced by the sequential oxidation of CH_3S and CH_3SO by NO_2 and is to be differentiated from the weakly bound adduct, CH_3SOO , formed by the reaction of CH_3S with O_2 at low temperature (Turnipseed et al. [1475]). The uncertainty limit on the rate constant has been increased over that given by the authors to reflect the absence of any confirming investigation. However, some additional support for this recommendation does come from the study of the $\text{CH}_3\text{S} + \text{NO}_2$ reaction by Tyndall and Ravishankara [1496]. These authors observed fluorescence from a product species tentatively identified as CH_3SO_2 , produced by the reaction of CH_3SO with NO_2 . Computer simulation of the rise and fall of the fluorescence signal yielded an approximate rate constant value for the reaction $\text{CH}_3\text{SO}_2 + \text{NO}_2$ of $7.0 \times 10^{-12} \text{ cm}^3 \text{ molecule}^{-1} \text{ s}^{-1}$. However, an

unambiguous differentiation between the production and disappearance rate constants was not possible. (Table: 97-4, Note: 97-4) [Back to Table](#)

- I101. $\text{CH}_3\text{SCH}_2 + \text{NO}_3$. This recommendation is based on the experiments of Butkovskaya and Le Bras [232]. The uncertainty factor reflects the absence of any confirming investigation. (Table: 94-26, Note: 94-26) [Back to Table](#)
- I102. $\text{CH}_3\text{SCH}_2\text{O}_2 + \text{NO}$. The recommended 298 K rate constant is based on the experiments of Urbanski et al. [1503], which are less impacted by secondary chemistry complications than the experiments of Wallington et al. [1548] or Turnipseed et al. [1477]; the error limits are chosen to encompass the rate constants reported in all three studies. The E/R value is taken from Urbanski et al., who report the only available temperature dependence data. The recommended value for the parameter g is larger than reported by Urbanski et al. pending independent confirmation of their result. (Table: 06-2, Note: 06-2) [Back to Table](#)
- I103. $\text{CH}_3\text{SCH}_2\text{O}_2 + \text{CH}_3\text{SCH}_2\text{O}_2$. The recommended 298 K rate constant is the average of values reported by Wallington et al. [1548] using a pulse radiolysis UV absorption technique and Urbanski et al. [1503] using a laser flash photolysis tunable diode laser absorption technique. Urbanski et al. observed that the reaction produces formaldehyde with unit yield, suggesting that the dominant reaction pathway is $2 \text{CH}_3\text{SCH}_2\text{O}_2 \rightarrow 2 \text{CH}_3\text{SCH}_2\text{O} + \text{O}_2$ ($\text{CH}_3\text{SCH}_2\text{O}$ rapidly decomposes to $\text{CH}_3\text{S} + \text{H}_2\text{CO}$). (Table 06-02, Note 06-02) [Back to Table](#)
- I104. $\text{CH}_3\text{SS} + \text{O}_3$. This recommendation is based on the discharge flow photoionization mass spectrometry study by Domine et al. [450]. The uncertainty factor reflects the absence of any confirming investigations. The rate constant ratio for the reactions of CH_3SS with O_3 and NO_2 is consistent with the rate constant ratio for the corresponding CH_3S reactions. (Table: 92-20, Note: 92-20) [Back to Table](#)
- I105. $\text{CH}_3\text{SS} + \text{NO}_2$; $\text{CH}_3\text{SSO} + \text{NO}_2$. These recommendations are based on the discharge flow photoionization mass spectrometry study by Domine et al. [448]. The rate constant ratio for these two reactions agrees with that observed for other RS/RSO radicals with NO_2 . The assigned uncertainties reflect this agreement but acknowledge the absence of any confirming investigation. In the Domine et al. study, CH_3SSO was produced by reacting away all CH_3SS with high NO_2 concentrations. Thus, as expected, O atom transfer may be the primary channel in the CH_3SS reaction. (Table: 92-20, Note: 92-20) [Back to Table](#)
- J1. $\text{Na} + \text{O}_3$. The recommendation is based on the measurements of Ager et al. [16], Worsnop et al. [1642] as corrected in Worsnop et al. [1643], and Plane et al. [1170]. The data of Worsnop et al. supersede earlier work from that laboratory (Silver and Kolb [1305]). Measurements made by Husain et al. [696] at 500 K are somewhat lower, probably because they did not recognize that secondary chemistry, $\text{NaO} + \text{O}_3 \rightarrow \text{Na} + 2\text{O}_2$, interferes with the rate coefficient measurement. The temperature dependence is from results of Worsnop et al. [1643] (214–294 K) and Plane et al. [1170] (208–377K). Ager et al. [16] estimate that the $\text{NaO}_2 + \text{O}$ product channel is $\leq 5\%$. Evidence that the NaO product is in the $^2\Sigma^+$ excited electronic state was reported by Shi et al. [1299] and Wright et al. [1644]. (Table: 94-26, Note: 94-26) [Back to Table](#)
- J2. $\text{Na} + \text{N}_2\text{O}$. The recommendation incorporates the data of Husain and Marshall [695], Ager et al. [16], Plane and Rajasekhar [1171], and Worsnop et al. [1643]. Silver and Kolb [1305] measured a rate coefficient at 295 K that is lower and is superseded by Worsnop et al. [1643]. Helmer and Plane [631] report a measurement at 300 K in excellent agreement with the recommendation. Earlier, less direct studies are discussed by Ager et al. [16]. The NaO product does not react significantly with N_2O at room temperature [k (for $\text{Na} + \text{N}_2 + \text{O}_2$ products) $\leq 10^{-16}$ and k (for $\text{NaO}_2 + \text{N}_2$ products) $\leq 2 \times 10^{-15}$ (Ager et al.). Wright et al. [Wright, 1993 #1863] used UV photoelectron spectroscopy to determine the product NaO is formed predominantly in the excited $^2\Sigma^+$ state. (Table: 92-20, Note: 94-26) [Back to Table](#)
- J3. $\text{Na} + \text{Cl}_2$. Two measurements of the rate coefficient for this reaction are in excellent agreement: Silver [1301] and Talcott et al. [1411]. The recommended value is the average of these room temperature results. (Table 87-41, Note: 87-41) [Back to Table](#)

- J4. NaO + O. The recommendation is based on measurements by Plane and Husain [1169] and Griffin et al. [584]. The Na + O₃ reaction produces NaO predominately in the low lying A ²Σ⁺ state which can radiatively and collisionally decay slowly to the X ²Π ground state. The Plane and Husain [1169] experiment was configured so the predominant reactant was NaO X ²Π while the Griffin et al. [584] experiment was designed to maximize NaO A ²Σ⁺ concentrations. While the two states may not have identical reaction rate constants, their energy difference is small compared to reaction exothermicity and both states show reaction rate constants near the collisional limit. Since this reaction in the atmosphere will probably proceed through a mixture of the two lowest NaO electronic states and data are available at only one temperature for each state, the recommended rate constant is an average of the two measurements. Plane and Husain [1169] reported that ~0.01 of the Na product is in the 3²P excited state, while Griffin et al. [584] report a Na 3²P product branching ratio of 0.14±0.04. This difference is consistent with the orbital correlation predictions of products for reaction of each NaO state as presented by Herschbach et al. [642]. (Table: 06-2, Note: 06-2) [Back to Table](#)
- J5. NaO + O₃. This reaction was studied by Silver and Kolb [1305], Ager et al. [16], and Plane et al. [1170], who agree on the rate coefficient and branching ratio. This agreement may be fortuitous because Silver and Kolb used an indirect method and an analysis based on their rate coefficient for the Na + O₃ reaction, which is about 1/2 of the recommended value. Ager et al. employed a somewhat more direct measurement, but the study is complicated by a chain reaction mechanism in the Na/O₃ system. Plane et al. reported rate coefficient measurements for the NaO₂ + O₂ product channel over the temperature range 207–377 K using pulsed photolysis LIF methods. The recommendation for that channel is based on all three studies, and the recommendation for the Na + 2O₂ channel is based upon the results of Silver and Kolb and Ager et al. The latter reaction channel may also have a significant temperature dependence. (Table: 94-26, Note: 94-26) [Back to Table](#)
- J6. NaO + H₂. The recommendation is based on a measurement by Ager and Howard [15]. They also reported a significant Na + H₂O product channel and that a small fraction of the Na from this channel is in the 3²P excited state. (Table 87-41, Note: 87-41) [Back to Table](#)
- J7. NaO + H₂O. The recommendation is based on a room temperature measurement by Ager and Howard [15] and a temperature dependent measurement by Cox and Plane [368] with the more extensive temperature dependent data favored. (Table: 06-2, Note: 06-2) [Back to Table](#)
- J8. NaO + NO. The recommendation is based on an indirect measurement reported by Ager et al. [16]. (Table 87-41, Note: 87-41) [Back to Table](#)
- J9. NaO + HCl. There is only one indirect measurement of the rate coefficient for this reaction, that from the study by Silver et al. [1307]. They indicate that the products are NaCl and OH, although some NaOH and Cl production is not ruled out. (Table: 85-37, Note: 85-37) [Back to Table](#)
- J10. NaO₂ + O. The recommendation is based on a flow tube study at 300 K by Helmer and Plane [631]. (Table: 94-26, Note: 94-26) [Back to Table](#)
- J11. NaO₂ + NO. This reaction is endothermic. The upper limit recommended is from an experimental study by Ager et al. [16]. (Table 87-41, Note: 87-41) [Back to Table](#)
- J12. NaO₂ + HCl. The recommendation is based on a measurement reported by Silver and Kolb [1304]. They indicated that the products are NaCl + HO₂, but NaOOH + Cl may be possible products. (Table 87-41, Note: 87-41) [Back to Table](#)
- J13. NaOH + HCl. The recommendation is based on the study by Silver et al. [1307], which is the only published study of this reaction. (Table: 85-37, Note: 85-37) [Back to Table](#)
- J14. NaHCO₃ + H. The recommendation is based on measurements at 307 and 227 K by Cox et al. [369]. It is consistent with an upper limit reported by Ager and Howard [14]. (Table: 10-6, Note: 10-6, Evaluated: 10-6) [Back to Table](#)

1.4 References

1. Abbatt, J. P. D. and J. G. Anderson, 1991, *J. Phys. Chem. B*, **95**, 2382-2390.
2. Abbatt, J. P. D., K. L. Demerjian and J. G. Anderson, 1990, *J. Phys. Chem.*, **94**, 4566-4575.
3. Abbatt, J. P. D., F. F. Fentner and J. G. Anderson, 1992, *J. Phys. Chem.*, **96**, 1780-1785.
4. Abbatt, J. P. D., D. W. Toohey, F. F. Fenter, P. S. Stevens, W. H. Brune and J. G. Anderson, 1989, *J. Phys. Chem.*, **93**, 1022-1029.
5. Acerboni, G., J. A. Beukes, N. R. Jensen, J. Hjorth, G. Myhre, C. J. Nielsen and J. K. Sundet, 2001, *Atmos. Environ.*, **35**, 4113-4123.
6. Acerboni, G., N. R. Jensen, B. Rindone and J. Hjorth, 1999, *Chem. Phys. Lett.*, **309**, 364-368.
7. Adachi, H. and N. Basco, 1979, *Chem. Phys. Lett.*, **63**, 490-492.
8. Adachi, H., N. Basco and D. G. L. James, 1979, *Int. J. Chem. Kinet.*, **11**, 1211-1229.
9. Addison, M. C., J. P. Burrows, R. A. Cox and R. Patrick, 1980, *Chem. Phys. Lett.*, **73**, 283-287.
10. Addison, M. C., R. J. Donovan and J. Garraway, 1979, *J. Chem. Soc. Faraday Disc.*, **67**, 286-296.
11. Adeniji, S. A., J. A. Kerr and M. R. Williams, 1981, *Int. J. Chem. Kinet.*, **13**, 209-217.
12. Adler-Golden, S. M. and J. R. Wiesenfeld, 1981, *Chem. Phys. Lett.*, **82**, 281-284.
13. Adusei, G. Y. and A. Fontijn. "Experimental studies of Cl-atom reactions at high temperatures: $\text{Cl} + \text{H}_2 = \text{HCl} + \text{H}$ from 291 to 1283 K"; *Int. Symp. on Combust.*, 1994, 801-808.
14. Ager, J. W., III and C. J. Howard, 1987, *J. Geophys. Res.*, **92**, 6675-6678.
15. Ager, J. W., III and C. J. Howard, 1987, *J. Chem. Phys.*, **87**, 921-925.
16. Ager, J. W., III, C. L. Talcott and C. J. Howard, 1986, *J. Chem. Phys.*, **85**, 5584-5592.
17. Agrawalla, B. S., A. S. Manocha and D. W. Setser, 1981, *J. Phys. Chem.*, **85**, 2873-2877.
18. Aker, P. M., B. I. Niefer, J. J. Sloan and H. Heydtmann, 1987, *J. Chem. Phys.*, **87**, 203-209.
19. Albaladejo, J., B. Ballesteros, E. Jimenez, Y. Diaz de Mera and E. Martinez, 2003, *Atmos. Environ.*, **37**, 2919 - 2926.
20. Albaladejo, J., A. Notario, C. A. Cuevas, B. Ballesteros and E. Martinez, 2003, *J. Atmos. Chem.*, **45**, 35-50.
21. Albers, E. A., K. Hoyerhmann, H. G. Wagner and J. Wolfram, 1971, *Proceedings of the Combustion Institute*, **13**, 81-88.
22. Albu, M., I. Barnes, K. H. Becker, I. Patroescu-Klotz, R. Mocanu and T. Benter, 2006, *Phys. Chem. Chem. Phys.*, **8**, 728-736.
23. Aleksandrov, E. N., V. S. Arutyunov and S. N. Kozlov, 1981, *Kinetics and Catalysis*, **22**, 391-394.
24. Amimoto, S. T., A. P. Force, R. G. Gulotty, Jr. and J. R. Wiesenfeld, 1979, *J. Chem. Phys.*, **71**, 3640-3647.
25. Amimoto, S. T., A. P. Force and J. R. Wiesenfeld, 1978, *Chem. Phys. Lett.*, **60**, 40-43.
26. Amimoto, S. T. and J. R. Wiesenfeld, 1980, *J. Chem. Phys.*, **72**, 3899-3903.
27. Anastasi, C., M. Broomfield, O. J. Nielsen and P. Pagsberg, 1992, *J. Phys. Chem.*, **96**, 696-701.
28. Anastasi, C., M. J. Brown, D. B. Smith and D. J. Waddington. Joint French and Italian sections of the Combustion Institute, 1987, Amalfi, Italy,
29. Anastasi, C., D. J. Waddington and A. Woolley, 1983, *J. Chem. Soc. Faraday Trans.*, **79**, 505-516.
30. Andersen, M. P. S., O. J. Nielsen, A. Toft, T. Nakayama, Y. Matsumi, R. L. Waterland, R. C. Buck, M. D. Hurley and T. J. Wallington, 2005, *Journal of Photochemistry and Photobiology A*, **176**, 124-128.
31. Anderson, J. G. and F. Kaufman, 1973, *Chem. Phys. Lett.*, **19**, 483-486.
32. Anderson, P. C. and M. J. Kurylo, 1979, *J. Phys. Chem.*, **83**, 2055-2057.
33. Anderson, S. M., J. Morton, K. Mauersberger, Y. L. Yung and W. B. DeMore, 1992, *Chem. Phys. Lett.*, **189**, 581-585.
34. Andersson, B. Y., R. A. Cox and M. E. Jenkin, 1988, *International Journal of Chemical Kinetics*, **20**, 283-295.
35. Andresen, P., A. Jacobs, C. Kleinerhmanns and J. Wolfrum. In *19th Symp. (Intl.) Combustion*, 1982; pp 11.
36. Aranda, A., Y. Diaz de Mera, D. Rodríguez, S. Salgado and E. Martinez, 2002, *Chem. Phys. Lett.*, **357**, 471-476.
37. Ariel, M., K. C. Ward and D. L. Tolbert, 2009, *Cerebellum*, **8**, 463-476.
38. Arnold, I. and F. J. Comes, 1979, *Chem. Phys.*, **42**, 231-239.
39. Arnold, I. and F. J. Comes, 1980, *Chem. Phys.*, **47**, 125-130.

40. Arrington, C. A., W. Brennen, G. P. Glass, J. V. Michael and H. Niki, 1965, *J. Chem. Phys.*, **43**, 525-533.
41. Arsene, C., I. Barnes, K. H. Becker and T. Benter, 2005, *Int. J. Chem. Kinet.*, **37**, 66-73.
42. Arsene, C., I. Barnes, K. H. Becker, W. F. Schneider, T. J. Wallington, N. Mihalopoulos and J. V. Patroescu-Klotz, 2002, *Environ. Sci. Technol.*, **36**, 5155-5163.
43. Ashford, R. D., N. Basco and J. E. Hunt, 1978, *Int. J. Chem. Kinet.*, **10**, 1233-1244.
44. Atakan, B. A. Jacobs, M. Wahl, R. Weller and J. Wolfrum, 1989, *Chem. Phys. Lett.*, **155**, 609-613.
45. Atkinson, D. B., V. I. Jaramillo and M. A. Smith, 1997, *J. Phys. Chem A*, **101**, 3356-3359.
46. Atkinson, R. and S. M. Aschmann, 1984, *Int. J. Chem. Kinet.*, **16**, 259-268.
47. Atkinson, R. and S. M. Aschmann, 1984, *Int. J. Chem. Kinet.*, **16**, 1175-1186.
48. Atkinson, R. and S. M. Aschmann, 1985, *Int. J. Chem. Kinet.*, **17**, 33-41.
49. Atkinson, R. and S. M. Aschmann, 1987, *Int. J. Chem. Kinet.*, **19**, 1097-1105.
50. Atkinson, R. and S. M. Aschmann, 1989, *Int. J. Chem. Kinet.*, **21**, 1123-1129.
51. Atkinson, R., S. M. Aschmann, J. Arey and B. Shorees, 1992, *J. Geophys. Res.*, **97**, 6065-6073.
52. Atkinson, R., S. M. Aschmann, W. P. L. Carter and A. M. Winer, 1982, *International Journal of Chemical Kinetics*, **14**, 919-926.
53. Atkinson, R., S. M. Aschmann, D. R. Fitz, A. M. Winer and J. N. Pitts, Jr., 1982, *Int. J. Chem. Kinet.*, **14**, 13.
54. Atkinson, R., S. M. Aschmann and J. N. Pitts, Jr., 1988, *J. Geophys. Res.*, **93**, 7125-7126.
55. Atkinson, R., S. M. Aschmann and J. N. Pitts, Jr., 1988, *J. Phys. Chem.*, **92**, 3454-3457.
56. Atkinson, R., S. M. Aschmann, A. M. Winer and J. N. Pitts, Jr., 1984, *Environ. Sci. Technol.*, **18**, 370-375.
57. Atkinson, R., G. M. Breuer and J. N. Pitts Jr., 1976, *J. Geophys. Res.*, **81**, 5765-5770.
58. Atkinson, R. and W. P. L. Carter, 1991, *J. Atmos. Chem.*, **13**, 195-210.
59. Atkinson, R., D. A. Hansen and J. N. Pitts, Jr., 1975, *J. Chem. Phys.*, **63**, 1703-1706.
60. Atkinson, R., R. A. Perry and J. N. Pitts, Jr., 1977, *J. Chem. Phys.*, **66**, 1578-1581.
61. Atkinson, R., R. A. Perry and J. N. Pitts Jr., 1978, *Chem. Phys. Lett.*, **54**, 14-18.
62. Atkinson, R. and J. Pitts, J. N., 1978, *J. Chem. Phys.*, **68**, 3581-3590.
63. Atkinson, R., J. N. Pitts, Jr. and S. M. Aschmann, 1984, *J. Phys. Chem.*, **88**, 1584-1587.
64. Atkinson, R., C. N. Plum, W. P. L. Carter, A. M. Winer and J. N. Pitts, Jr., 1984, *J. Phys. Chem.*, **88**, 1210-1215.
65. Atkinson, R., R. C. Tuazon, H. Macleod, S. M. Aschmann and A. M. Winer, 1986, *Geophys. Res. Lett.*, **13**, 117-120.
66. Audley, G. J., D. L. Baulch and I. M. Campbell, 1981, *Int. J. Chem. Kinet.*, **77**, 2541.
67. Avery, H. E. and R. J. Cvetanovic, 1965, *J. Chem. Phys.*, **43**, 3727-3733.
68. Aviles, R. G., D. F. Muller and P. L. Houston, 1980, *Appl. Phys. Lett.*, **37**, 358-360.
69. Avramenko, L. I. and R. V. Kolesnikova, 1961, *Bull. Acad. Sci. USSR, Div. Chem. Sci.*, 545.
70. Avzianova, E. V. and P. A. Ariya, 2002, *Int. J. Chem. Kinet.*, **34**, 678-684.
71. Ayhens, Y. V., J. M. Nicovich, M. L. McKee and P. H. Wine, 1997, *J. Phys. Chem. A*, **101**, 9382-9390.
72. Azad, K. and J. M. Andino, 1999, *Int. J. Chem. Kinet.*, **31**, 810-818.
73. Baasandorj, M., S. Griffith, S. Dusanter and P. S. Stevens, 2009, *Journal of Physical Chemistry A*, **113**, 10495-10502.
74. Bacher, C., G. S. Tyndall and J. J. Orlando, 2001, *J. Atmos. Chem.*, **39**, 171-189.
75. Baer, S., H. Hippler, R. Rahn, M. Siefke, N. Seitzinger and J. Troe, 1991, *J. Chem. Phys.*, **95**, 6463-6470.
76. Baghal-Vayjooee, M. H., A. J. Colussi and S. W. Benson, 1978, *J. Am. Chem. Soc.*, **100**, 3214-3215.
77. Bahng, M.-K. and R. G. Macdonald, 2007, *J. Phys. Chem. A*, **111**, 3850-3861.
78. Bahta, A., R. Simonaitis and J. Heicklen, 1984, *Int. J. Chem. Kinet.*, **16**, 1227.
79. Balakhnin, V. P., V. I. Egorov and E. I. Intezarova, 1971, *Kinetics and Catalysis* **12**, 299.
80. Baldwin, A. C. and D. M. Golden, 1978, *Chem. Phys. Lett.*, **55**, 350.
81. Balestra-Garcia, C., G. Le Bras and H. MacLeod, 1992, *J. Phys. Chem.*, **96**, 3312-3316.
82. Balla, R. J., H. H. Nelson and J. R. McDonald, 1986, *Chem. Phys.*, **109**, 101-107.
83. Ballesteros, B., N. R. Jensen, and J. Hjorth, 2002, *J. Atmos. Chem.*, **43**, 135-150.

84. Balucani, N., L. Beneventi, P. Casavecchia, G. G. Volpi, E. J. Kruus and J. J. Sloan, 1994, *Can. J. Chem.*, **72**, 888-902.
85. Bardwell, M. W., A. Bacak, M. T. Raventos, C. J. Percival, G. Sanchez-Reyna and D. E. Shallcross, 2003, *Physical Chemistry Chemical Physics*, **5**, 2381-2385.
86. Barker, J. R., S. W. Benson and D. M. Golden, 1977, *Int. J. Chem. Kinet.*, **9**, 31.
87. Barnes, I., V. Bastian, K. H. Becker, E. H. Fink and W. Nelsen, 1986, *J. Atmos. Chem.*, **4**, 445-466.
88. Barnes, I., V. Bastian, K. H. Becker, E. H. Fink and F. Zabel, 1981, *Chem. Phys. Lett.*, **83**, 459-464.
89. Barnes, I., V. Bastian, K. H. Becker, E. H. Fink and F. Zabel, 1982, *Atmos. Environ.*, **16**, 545.
90. Barnes, I., V. Bastian, K. H. Becker, E. H. Fink and F. Zabel, 1986, *Chem. Phys. Lett.*, **123**, 28-32.
91. Barnes, I., V. Bastian, K. H. Becker and D. Martin. In *Biogenic Sulfur in the Environment*; ACS Symp. Ser. 1989; Vol. 393; pp 476-488.
92. Barnes, I., V. Bastian, K. H. Becker and R. D. Overath, 1991, *Int. J. Chem. Kinet.*, **23**, 579-591.
93. Barnes, I., V. Bastian, K. H. Becker and Z. Tong, 1990, *J. Phys. Chem.*, **94**, 2413-2419.
94. Barnes, I., K. H. Becker, P. Carlier and G. Mouvier, 1987, *Int. J. Chem. Kinet.*, **19**, 489-501.
95. Barnes, I., K. H. Becker, E. H. Fink, A. Reimer, F. Zabel and H. Niki, 1983, *Int. J. Chem. Kinet.*, **15**, 631-645.
96. Barnes, I., K. H. Becker, E. H. Fink, A. Reimer, F. Zabel and H. Niki, 1985, *Chem. Phys. Lett.*, **115**, 1.
97. Barnes, I., K. H. Becker and N. Mihalopoulos, 1994, *J. Atmos. Chem.*, **18**, 267-289.
98. Barnes, I., K. H. Becker and I. Patroescu, 1994, *Geophys. Res. Lett.*, **21**, 2389-2392.
99. Barnes, I., K. H. Becker and I. Patroescu, 1996, *Atmos. Environ.*, **30**, 1805-1814.
100. Barnett, A. J., G. Marston and R. P. Wayne, 1987, *J. Chem. Soc. Faraday Trans. 2*, **83**, 1453-1463.
101. Barone, S. B., A. A. Turnipseed and A. R. Ravishankara, 1994, *J. Phys. Chem.*, **98**, 4602-4608.
102. Barone, S. B., A. A. Turnipseed and A. R. Ravishankara, 1996, *J. Phys. Chem.*, **100**, 14694-14702.
103. Barry, J., G. Locke, D. Scollard, H. Sidebottom, J. Treacy, C. Clerbaux, R. Colin and J. Franklin, 1997, *Int. J. Chem. Kinet.*, **29**, 607-617.
104. Barry, J., D. J. Scollard, J. J. Treacy, H. W. Sidebottom, G. Le Bras, G. Poulet, S. Teton, A. Chichinin, C. E. Canosa-Mas, D. J. Kinnison, R. P. Wayne and O. J. Nielsen, 1994, *Chem. Phys. Lett.*, **221**, 353-358.
105. Barry, J., H. Sidebottom, J. Treacy and J. Franklin, 1995, *Int. J. Chem. Kinet.*, **27**, 27-36.
106. Basco, N. and S. K. Dogra, 1971, *Proc. Roy. Soc. A.*, **323**, 417-429.
107. Basco, N. and S. K. Dogra, 1971, *Proc. Roy. Soc. A.*, **323**, 401.
108. Basco, N. and S. K. Dogra, 1971, *Proc. Roy. Soc. A.*, **323**, 29-68.
109. Basco, N. and S. S. Parmar, 1985, *Int. J. Chem. Kinet.*, **17**, 891-900.
110. Batt, L., R. T. Milne and R. D. McCulloch, 1977, *Int. J. Chem. Kinet.*, **9**, 567-587.
111. Batt, L. and G. N. Robinson, 1979, *Int. J. Chem. Kinet.*, **11**, 1045.
112. Battin-Leclerc, F., I. K. Kim, R. K. Talukdar, R. W. Portmann, A. R. Ravishankara, R. Steckler and D. Brown, 1999, *J. Phys. Chem. A*, **103**, 3237-3244.
113. Bauer, D., J. N. Crowley and G. K. Moortgat, 1992, *Journal of Photochemistry and Photobiology A*, **A65**, 329-344.
114. Baulch, D. L., I. M. Campbell and S. M. Saunders, 1985, *J. Chem. Soc. Faraday Trans. 1*, **81**, 259-263.
115. Baulch, D. L., R. A. Cox, R. F. Hampson, Jr., J. A. Kerr, J. Troe and R. T. Watson, 1980, *J. Phys. Chem. Ref. Data*, **9**, 295-471.
116. Beach, S. D., K. M. Hickson, I. W. M. Smith and R. P. Tuckett, 2001, *Phys. Chem. Chem. Phys.*, **3**, 3064 - 3069.
117. Beach, S. D., I. W. M. Smith and R. P. Tuckett, 2001, *International Journal of Chemical Kinetics*, **34**, 104-109.
118. Becker, E., T. Benter, R. Kampf, R. N. Schindler and U. Wille, 1991, *Ber. Bunsenges. Phys. Chem.*, **95**, 1168-1173.
119. Becker, E., M. M. Rahman and R. N. Schindler, 1992, *Ber. Bunsenges. Phys. Chem.*, **96**, 776-783.
120. Becker, E., U. Wille, M. M. Rahman and R. H. Schindler, 1991, *Ber. Bunsenges. Phys. Chem.*, **95**, 1173-1179.

121. Becker, K. H., W. Groth and D. Kley, 1969, *Z. Naturforsch.*, **A24**, 1280.
122. Becker, K. H., W. Groth and U. Schurath, 1971, *Chem. Phys. Lett.*, **8**, 259-262.
123. Becker, K. H., W. Groth and U. Schurath, 1972, *Chemical Physics Letters*, **14**, 489-492.
124. Becker, K. H., M. A. Inocencio and U. Schurath, 1975, *Int. J. Chem. Kinet.*, **Symp. 1**, 205-220.
125. Becker, K. H. and K. Wirtz, 1989, *Journal of Atmospheric Chemistry*, **9**, 419-433.
126. Bedjanian, Y., G. Laverdet and G. Le Bras, 1998, *J. Phys. Chem. A*, **102**, 953-959.
127. Bedjanian, Y., G. Le Bras and G. Poulet, 1999, *Journal of Physical Chemistry*, **103**, 7017-7025.
128. Bedjanian, Y., G. Le Bras and G. Poulet, 1999, *International Journal of Chemical Kinetics*, **31**, 698-704.
129. Bedjanian, Y., G. Poulet and G. Le Bras, 1996, *Int. J. Chem. Kinet*, **28**, 383-389.
130. Bedjanian, Y., V. Riffault and G. Le Bras, 2001, *International Journal of Chemical Kinetics*, **33**, 587-599.
131. Bedjanian, Y., V. Riffault, G. Le Bras and G. Poulet, 1999, *J. Photochem. Photobiol. A*, **128**, 15-25.
132. Bedjanian, Y., V. Riffault, G. Le Bras and G. Poulet, 2001, *J. Phys. Chem A*, **105**, 573-578.
133. Bedjanian, Y., V. Riffault, G. Le Bras and G. Poulet, 2001, *J. Phys. Chem A*, **105**, 6154-6166.
134. Bedjanian, Y., V. Riffault and G. Poulet, 2001, *J. Phys. Chem A*, **105**, 3167-3175.
135. Bednarek, G., M. Breil, A. Hoffman, J. P. Kohlman, V. Mors and R. Zellner, 1996, *Ber. Bunsenges. Phys. Chem.*, **100**, 528-539.
136. Bednarek, G., J. P. Kohlmann, H. Saathoff and R. Zellner, 1995, *Zeitschrift fur Physikalische Chemie*, **188**, 1-15.
137. Bedzhanyan, Y. R., E. M. Markin and Y. M. Gershenzon, 1993, *Kinetics and Catalysis*, **34**, 1-3.
138. Bedzhanyan, Y. R., E. M. Markin and Y. M. Gershenzon, 1993, *Kinetics and Catalysis*, **33**, 601-606.
139. Bedzhanyan, Y. R., E. M. Markin and Y. M. Gershenzon, 1993, *Kinetics and Catalysis*, **33**, 594-601.
140. Bedzhanyan, Y. R., E. M. Markin, G. G. Politenkova and Y. M. Gershenzon, 1993, *Kinetics and Catalysis*, **33**, 797-801.
141. Beichert, P., L. Wingen, J. Lee, R. Vogt, M. J. Ezell, M. Ragains, R. Neavyn and B. J. Finlayson-Pitts, 1995, *J. Phys. Chem.*, **99**, 13156-13162.
142. Bemand, P. P. and M. A. A. Clyne, 1977, *J. Chem. Soc. Faraday Trans. 2*, **73**, 394.
143. Bemand, P. P., M. A. A. Clyne and R. T. Watson, 1973, *J. Chem. Soc. Faraday Trans. 1*, **69**, 1356-1374.
144. Bemand, P. P., M. A. A. Clyne and R. T. Watson, 1974, *J. Chem. Soc. Faraday Trans. 2*, **70**, 564-576.
145. Benson, S. W., F. R. Cruickshank and R. Shaw, 1969, *Int. J. Chem. Kinet.*, **1**, 29.
146. Benter, T. and R. N. Schindler, 1988, *Chem. Phys. Lett.*, **145**, 67-70.
147. Bera, R. K. and R. J. Hanrahan, 1988, *Radiation Physics and Chemistry*, **32**, 579-584.
148. Berndt, T. and O. Böge, 1997, *Int. J. Chem. Kinet.*, **29**, 755-765.
149. Berry, R., J. Yuan, A. Misra and P. Marshall, 1998, *J. Phys. Chem. A*, **102**, 5182-5188.
150. Bevilacqua, T. J., D. R. Hanson and C. J. Howard, 1993, *J. Phys. Chem.*, **97**, 3750-3757.
151. Bhaskaran, K. A., P. Frank and T. Just. In *12th International Shock Tube Symposium Jerusalem.*, 1979.
152. Bhatnagar, A. and R. W. Carr, 1994, *Chem. Phys. Lett.*, **231**, 454-459.
153. Bida, G. T., W. H. Breckenridge and W. S. Kolln, 1976, *J. Chem. Phys.*, **64**, 3296-3302.
154. Biedenkapp, D. and E. J. Bair, 1970, *J. Chem. Phys.*, **52**, 6119-6125.
155. Bierbach, A., I. Barnes and K. H. Becker, 1996, *Int. J. Chem. Kinet.*, **28**, 565-577.
156. Biermann, H. W., G. W. Harris and J. N. Pitts, Jr., 1982, *J. Phys. Chem.*, **86**, 2958-2964.
157. Biggs, P., C. E. Canosa-Mas, J.-M. Fracheboud, D. E. Shallcross and R. P. Wayne, 1995, *Geophys. Res. Lett.*, **22**, 1221-1224.
158. Biggs, P., C. E. Canosa-Mas, P. S. Monks, R. P. Wayne, T. Benter and R. N. Schindler, 1993, *Int. J. Chem. Kinet.*, **25**, 805-817.
159. Biggs, P., M. H. Harwood, A. D. Parr and R. P. Wayne, 1991, *J. Phys. Chem.*, **97**, 7746-7751.
160. Bilde, M. and T. J. Wallington, 1998, *J. Phys. Chem.*, **102**, 1550-1555.
161. Bilde, M., T. J. Wallington, G. Ferronato, J. J. Orlando, G. S. Tyndall, E. Estupinan and S. Haberkorn, 1998, *J. Phys. Chem. A*, **102**, 1976-1986.

162. Billington, A. P. and P. Borrell, 1986, J. Chem. Soc. Faraday Trans. 2, **82**, 963-970.
163. Birks, J. W., B. Shoemaker, T. J. Leck, R. A. Borders and L. J. Hart, 1977, J. Chem. Phys., **66**, 4591-4599.
164. Birks, J. W., B. Shoemaker, T. J. Leck and D. M. Hinton, 1976, J. Chem. Phys., **65**, 5181-5185.
165. Black, G., 1984, J. Chem. Phys., **80**, 1103-1107.
166. Black, G. and L. E. Jusinski, 1986, J. Chem. Soc. Faraday Trans. 2, **86**, 2143-2151.
167. Black, G., L. E. Jusinski and T. G. Slanger, 1983, Chem. Phys. Lett., **102**, 64-68.
168. Black, G., R. L. Sharpless and T. G. Slanger, 1982, Chem. Phys. Lett., **90**, 55-58.
169. Black, G., R. L. Sharpless and T. G. Slanger, 1982, Chem. Phys. Lett., **93**, 598-602.
170. Blitz, M. A., T. J. Dillon, D. E. Heard, M. J. Pilling and I. D. Trought, 2004, Phys. Chem. Chem. Phys., **6**, 2162-2171.
171. Blitz, M. A., K. W. McKee and M. J. Pilling, 2000, Proceedings of the Combustion Institute, **28**, 2491-2497.
172. Bloss, W. J., D. M. Rowley, R. A. Cox and R. L. Jones, 2002, Phys. Chem. Chem. Phys., **4**, 3639-3647.
173. Bohmer, E. and W. Hack, 1991, Ber. Bunsenges. Phys. Chem., **95**, 1688-1690.
174. Bohn, B. and C. Zetzsch, 1997, Journal of Physical Chemistry A, **101**, 1488-1493.
175. Bonard, A., V. Daele, J.-L. Delfau and C. Vovelle, 2002, J. Phys. Chem. A, **106**, 4348-4389.
176. Boodaghians, R. B., C. E. Canosa-Mas, P. J. Carpenter and R. P. Wayne, 1988, J. Chem. Soc. Faraday Trans. 2, **84**, 931-948.
177. Boodaghians, R. B., I. W. Hall and R. P. Wayne, 1987, J. Chem. Soc. Faraday Trans. 2, **83**, 529-538.
178. Borders, R. A. and J. W. Birks, 1982, J. Phys. Chem., **86**, 3295-3302.
179. Borissenko, D., A. Kukui, G. Laverdet and G. Le Bras, 2003, J. Phys. Chem. A, **107**, 1155-1161.
180. Borrell, P., P. Borrell and K. R. Grant, 1983, J. Chem. Phys., **78**, 748-756.
181. Borrell, P., P. M. Borrell and M. D. Pedley, 1977, Chem. Phys. Lett., **51**, 300-302.
182. Borrell, P. and D. S. Richards, 1989, Journal of the Chemical Society, Faraday Transactions 2: Molecular and Chemical Physics, **85**, 1401-1411.
183. Bourbon, C., M. Brioukov and P. Devolder, 1996, C.R. Acad. Sci. Paris **322**, 181-188.
184. Bourbon, C., M. Brioukov, B. Hanoune, J. P. Sawerysyn and P. Devolder, 1996, Chem. Phys. Lett., **254**, 203-212.
185. Bourbon, C., C. Fittschen, J. P. Sawerysyn and P. Devolder, 1995, J. Phys. Chem., **99**, 15102-15107.
186. Bourmada, N., C. Lafage and P. Devolder, 1987, Chem. Phys. Lett., **136**, 209-214.
187. Bozzelli, J. W. *Ph.D. Thesis*; Dept. of Chemistry, Princeton University, (Diss. Abstr. Int. B 34(2) 608), 1973.
188. Bozzelli, J. W. and A. M. Dean, 1990, J. Phys. Chem., **94**, 3313-3317.
189. Bradley, J. N., W. Hack, K. Hoyeremann and H. G. Wagner, 1973, J. Chem. Soc. Faraday Trans. 1, **69**, 1889.
190. Brahan, K. M., A. D. Hewitt, G. D. Boone and S. A. Hewitt, 1996, Int. J. Chem. Kinet., **28**, 397-404.
191. Braithwaite, M. and S. R. Leone, 1978, J. Chem. Phys., **69**, 839-845.
192. Braithwaite, M., E. A. Ogryzlo, J. A. Davidson and H. I. Schiff, 1976, J. Chem. Soc. Faraday Trans. II **72**, 2075-2081.
193. Breckenridge, W. H. and T. A. Miller, 1972, J. Chem. Phys., **56**, 465-474.
194. Bridier, I., B. Veyret and R. Lesclaux, 1993, Chem. Phys. Lett., **201**, 563-568.
195. Bridier, I., B. Veyret, R. Lesclaux and M. E. Jenkin, 1993, J. Chem. Soc. Faraday Trans., **89**, 2993-2997.
196. Brown, A. C., C. E. Canosa-Mas, A. D. Parr, K. Rothwell and R. P. Wayne, 1990, Nature, **347**, 541-543.
197. Brown, A. C., C. E. Canosa-Mas, A. D. Parr and R. P. Wayne, 1990, Atmos. Environ., **24A**, 2499-2511.
198. Brown, A. C., C. E. Canosa-Mas and R. P. Wayne, 1990, Atmos. Environ., **24A**, 361-367.
199. Brown, A. C. and B. A. Thrush, 1967, Trans. Faraday Soc., **63**, 630.
200. Brown, R. D. and I. W. M. Smith, 1975, Int. J. Chem. Kinet., **7**, 301.

201. Brown, S. S., J. B. Burkholder, R. K. Talukdar and A. R. Ravishankara, 2001, *Journal of Physical Chemistry A*, **105**, 1605-1614.
202. Brown, S. S., R. K. Talukdar and A. R. Ravishankara, 1999, *J. Phys. Chem. A*, **103**, 3031-3037.
203. Brune, W. H., J. J. Schwab and J. G. Anderson, 1983, *J. Phys. Chem.*, **87**, 4503-4514.
204. Brunning, J. and M. A. A. Clyne, 1984, *J. Chem. Soc. Faraday Trans 2*, **80**, 1001-1014.
205. Brunning, J. and L. J. Stief, 1986, *J. Chem. Phys.*, **85**, 2591-2594.
206. Brunning, J. and L. J. Stief, 1986, *J. Chem. Phys.*, **84**, 4371-4377.
207. Bryukov, M. G., B. Dellinger and V. D. Knyazev, 2006, *Journal of Physical Chemistry A*, **110**, 936-943.
208. Bryukov, M. G., V. D. Knyazev, S. M. Lomnicki, C. A. McFerrin and B. Dellinger, 2004, *Journal of Physical Chemistry A*, **108**, 10464-10472.
209. Bryukov, M. G., I. R. Slagle and V. D. Knyazev, 2002, *J. Phys. Chem. A*, **106**, 10532-10542.
210. Bryukov, M. G., I. R. Slagle and V. D. Knyazev, 2003, *J. Phys. Chem. A*, **107**, 6565-6573.
211. Bryukov, M. G., R. G. Vidrine and B. Dellinger, 2007, *J. Phys. Chem. A*, **111**, 6197 - 6203.
212. Buben, S. N., I. K. Larin, N. A. Messineva and E. M. Trofimova, 1990, *Khim. Fiz.*, **9**, 116-126.
213. Buben, S. N., I. K. Larin, N. A. Messineva and E. M. Trofimova, 1996, *Khim. Fiz.*, **15**, 116-125.
214. Bulatov, V. P., A. A. Buloyan, S. G. Cheskis, M. Z. Kozliner, O. M. Sarkisov and A. I. Trostin, 1980, *Chem. Phys. Lett.*, **74**, 288.
215. Bulatov, V. P., M. Z. Kozliner and O. M. Sarkisov, 1984, *Khim. Fiz.*, **3**, 1300-1305.
216. Bulatov, V. P., M. Z. Kozliner and O. M. Sarkisov, 1985, *Khim. Fiz.*, **4**, 1353-1357.
217. Bulatov, V. P., O. M. Sarkisov, M. Z. Kozliner and V. G. Ergorov, 1986, *Khim. Fiz.*, **5**, 1031-1036.
218. Bulatov, V. P., S. I. Vereschchuk, F. N. Dzegilenko, O. M. Sarkisov and V. N. Khabarov, 1990, *Khim. Fiz.*, **9**, 1214-1223.
219. Burkholder, J. B., 2000, *J. Phys. Chem. A*, **104**, 6733-6737.
220. Burkholder, J. B., P. D. Hammer, C. J. Howard and A. Goldman, 1989, *J. Geophys. Res.*, **94**, 2225-2234.
221. Burkholder, J. B., A. Mellouki, R. Talukdar and A. R. Ravishankara, 1994, *Int. J. Chem. Kinet.*, **24**, 711-725.
222. Burkholder, J. B., R. R. Wilson, T. Gierczak, R. Talukdar, S. A. McKeen, J. J. Orlando, G. L. Vaghjiani and A. R. Ravishankara, 1991, *J. Geophys. Res.*, **96**, 5025-5043.
223. Burks, T. L. and M. C. Lin, 1981, *Int. J. Chem. Kinet.*, **13**, 977-999.
224. Burrows, J. P., D. I. Cliff, G. W. Harris, B. A. Thrush and J. P. T. Wilkinson, 1979, *Proc. Roy. Soc. (London)*, **A368**, 463-481.
225. Burrows, J. P. and R. A. Cox, 1981, *J. Chem. Soc. Faraday Trans. 1*, **77**, 2465-2479.
226. Burrows, J. P., R. A. Cox and R. G. Derwent, 1981, *J. Photochem.*, **16**, 147-168.
227. Burrows, J. P., G. W. Harris and B. A. Thrush, 1977, *Nature*, **267**, 233-234.
228. Burrows, J. P., G. S. Tyndall and G. K. Moortgat, 1985, *J. Phys. Chem.*, **89**, 4848-4856.
229. Burrows, J. P., T. J. Wallington and R. P. Wayne, 1984, *J. Chem. Soc. Faraday Trans. 2*, **80**, 957-971.
230. Butkovskaya, N. I., A. Kukui and G. Le Bras, 2004, *J. Phys. Chem. A*, **108**, 1160 - 1168.
231. Butkovskaya, N. I., A. Kukui, N. Pouvesle and G. Le Bras, 2004, *J. Phys. Chem. A*, **108**, 7021-7026.
232. Butkovskaya, N. I. and G. Le Bras, 1994, *J. Phys. Chem.*, **98**, 2582-2591.
233. Butkovskaya, N. I., G. Poulet and G. Le Bras, 1995, *J. Phys. Chem.*, **99**, 4536-4543.
234. Butkovskaya, N. I. and D. W. Setser, 1998, *J. Phys. Chem. A*, **102**, 6395-6405.
235. Butkovskaya, N. I. and D. W. Setser, 1999, *Chem. Phys. Lett.*, **312**, 37-44.
236. Butkovskaya, N. I. and D. W. Setser, 1999, *J. Phys. Chem. A*, **103**, 6921-6929.
237. Cadle, R. D. and J. W. Powers, 1967, *J. Phys. Chem.*, **71**, 1702-1706.
238. Cadle, R. D. and C. Schadt, 1953, *J. Phys. Chem.*, **21**, 163.
239. Cadman, P., A. W. Kirk and A. F. Trotman-Dickenson, 1976, *J. Chem. Soc. Chem. Commun.*, **72**, 1027-1032.
240. Callear, A. B. and R. E. M. Hedges, 1970, *Trans. Faraday Soc.*, **66**, 605-614.
241. Callear, A. B. and I. W. M. Smith, 1967, *Nature*, **213**, 382-383.
242. Calvert, J. G. and J. N. Pitts. In *Photochemistry*; John Wiley & Sons, Inc.: New York, 1966; pp 377.

243. Cameron, M., V. Sivakumaran, T. J. Dillon and J. Crowley, 2002, *Phys. Chem. Chem. Phys.*, **4**, 3628-3638.
244. Campbell, I. M., D. F. McLaughlin and B. J. Handy, 1976, *Chem. Phys. Lett.*, **38**, 362-364.
245. Campuzano-Jost, P., M. B. Williams, L. D'Ottone and A. J. Hynes, 2000, *Geophys. Res. Lett.*, **27**, 693-696.
246. Campuzano-Jost, P., M. B. Williams, L. D'Ottone and A. J. Hynes, 2004, *J. Phys. Chem. A*, **108**, 1537-1551.
247. Cannon, B. D., J. S. Robertshaw, I. W. M. Smith and M. D. Williams, 1984, *Chem. Phys. Lett.*, **105**, 380-385.
248. Canosa-Mas, C., S. J. Smith, S. Toby and R. P. Wayne, 1988, *J. Chem. Soc. Faraday Trans. 2*, **84**, 247-262.
249. Canosa-Mas, C. E., R. J. Dillon, H. Sidebottom, K. C. Thompson and R. P. Wayne, 2001, *Phys. Chem. Chem. Phys.*, **3**, 542-550.
250. Canosa-Mas, C. E., H. R. Hutton-Squire, M. D. King, D. J. Stewart, K. C. Thompson and R. P. Wayne, 1999, *J. Atmos. Chem.*, **34**, 163-170.
251. Canosa-Mas, C. E., S. J. Smith, S. Toby and R. P. Wayne, 1989, *J. Chem. Soc. Faraday Trans. 2*, **85**, 709-725.
252. Cantrell, C. A., J. A. Davidson, K. L. Busarow and J. G. Calvert, 1986, *J. Geophys. Res.*, **91**, 5347-5353.
253. Cantrell, C. A., J. A. Davidson, A. H. McDaniel, R. E. Shetter and J. G. Calvert, 1988, *J. Chem. Phys.*, **88**, 4997-5006.
254. Cantrell, C. A., J. A. Davidson, R. E. Shetter, B. A. Anderson and J. G. Calvert, 1987, *J. Phys. Chem.*, **91**, 5858-5863.
255. Cantrell, C. A., R. E. Shetter and J. G. Calvert, 1994, *J. Geophys. Res.*, **99**, 3739-3743.
256. Cantrell, C. A., R. E. Shetter, A. H. McDaniel and J. G. Calvert, 1990, *J. Geophys. Res.*, **95**, 20531-20537.
257. Cantrell, C. A., R. E. Shetter, A. J. McDaniel, J. G. Calvert, J. A. Davidson, D. C. Lowe, S. C. Tyler, R. J. Cicerone and J. P. Greenberg, 1990, *J. Geophys. Res.*, **95**, 22455-22462.
258. Cantrell, C. A., W. R. Stockwell, L. G. Anderson, K. L. Busarow, D. Perner, A. Schmeltekopf, J. G. Calvert and H. S. Johnston, 1985, *J. Phys. Chem.*, **89**, 139-146.
259. Carl, S. A., 2005, *Phys. Chem. Chem. Phys.*, **7**, 4051-4053.
260. Carr, S., D. E. Heard and M. A. Blitz, 2009, *Science*, **324**.
261. Carr, S. A., M. T. Baeza-Romero, M. A. Blitz, B. J. S. Price and P. W. Seakins, 2008, *Int J. Chem. Kinet.*, **40**, 504-514.
262. Casavecchia, P., R. J. Buss, S. J. Sibener and Y. T. Lee, 1980, *J. Chem. Phys.*, **73**, 6351-6352.
263. Castleman, A. W., R. E. Davis, H. R. Munkelwitz, I. N. Tang and W. P. Wood, 1975, *Int. J. Chem. Kinet.*, **Symp. 1**, 629-640.
264. Catoire, V., R. Lesclaux, P. D. Lightfoot and M.-T. Rayez, 1994, *J. Phys. Chem.*, **98**, 2889-2898.
265. Catoire, V., R. Lesclaux, W. F. Schneider and T. J. Wallington, 1996, *J. Phys. Chem.*, **100**, 14356-14371.
266. Cattell, F. C., J. Cavanagh, R. A. Cox and M. E. Jenkin, 1986, *J. Chem. Soc. Faraday Trans. 2*, **82**, 1999-2018.
267. Cattell, F. C. and R. A. Cox, 1986, *J. Chem. Soc. Faraday Trans. 2*, **82**, 1413-1426.
268. Cavalli, F., M. Glasius, J. Hjorth, B. Rindone and N. R. Jensen, 1998, *Atmos. Environ.*, **32**, 3767 - 3773.
269. Chang, J. S. and J. R. Barker, 1979, *J. Phys. Chem.*, **83**, 3059.
270. Chang, J. S. and F. Kaufman, 1977, *Geophys. Res. Lett.*, **4**, 192-194.
271. Chang, J. S. and F. Kaufman, 1977, *J. Chem. Phys.*, **66**, 4989.
272. Chang, J. S., P. L. Trevor and J. R. Barker, 1981, *Int. J. Chem. Kinet.*, **13**, 1151-1161.
273. Chang, P.-F., T. T. Wang, S. W. Niann, Y.-L. Hwang and Y.-P. Lee, 2000, *J. Phys. Chem. A*, **104**, 5525-5529.
274. Chapman, C. J. and R. P. Wayne, 1974, *Int. J. Chem. Kinet.*, **6**, 617-630.
275. Chasovnikov, S. A., A. I. Chichinin and L. N. Krasnoperov, 1987, *Chem. Phys.*, **116**, 91-99.
276. Chatha, J. P. S., P. K. Arora, N. Raja, P. B. Kulkarni and K. G. Vohra, 1979, *Int. J. Chem. Kinet.*, **11**, 175-185.
277. Cheah, C. T. and M. A. A. Clyne, 1980, *J. Chem. Soc. Faraday Trans.*, **76**, 1543.

278. Cheema, S. A., K. A. Holbrook, G. A. Oldershaw and R. W. Walker, 2002, *Int. J. Chem. Kinet.*, **34**, 110-121.
279. Chen, H.-b., W. D. Thweatt, J. Wang, G. P. Glass and R. F. Curl, 2005, *J. Phys. Chem. A*, **109**, 2207-2216.
280. Chen, J., V. Catoire and H. Niki, 1995, *Chem. Phys. Lett.*, **245**, 519-528.
281. Chen, J., V. Young, T. Zhu and H. Niki, 1993, *J. Phys. Chem.*, **97**, 11696-11698.
282. Chen, J., T. Zhu and H. Niki, 1992, *J. Phys. Chem.*, **96**, 6115-6117.
283. Chen, J., T. Zhu, H. Niki and G. J. Mains, 1992, *Geophys. Res. Lett.*, **19**, 2215-2218.
284. Chen, K. S., S. S. Cheng and Y. P. Lee, 2003, *J. Chem. Phys.*, **119**, 4229-4236.
285. Chen, L., F. Fukuda, N. Takenaka, H. Bandow and Y. Maeda, 2000, *Int. J. Chem. Kinet.*, **25**, 73-78.
286. Chen, L., S. Kutsuna, K. Nohara, K. Takeuchi and T. Ibusuki, 2001, *J. Phys. Chem. A*, **105**, 10854-10859.
287. Chen, L., S. Kutsuna, K. Tokuhashi and A. Sekiya, 2003, *Int J. Chem. Kinet.*, **35**, 317-325.
288. Chen, L., S. Kutsuna, K. Tokuhashi and A. Sekiya, 2005, *Chem. Phys. Lett.*, **403**, 180 - 184.
289. Chen, L., S. Kutsuna, K. Tokuhashi and A. Sekiya, 2006, *J. Phys. Chem. A*, **110**, 12845-12851.
290. Chen, L., S. Kutsuna, K. Tokuhashi, A. Sekiya, K. Takeuchi and T. Ibusuki, 2003, *International Journal of Chemical Kinetics*, **35**, 239 - 245.
291. Chen, M. C. and H. A. Taylor, 1961, *J. Chem. Phys.*, **34**, 1344-1347.
292. Chen, X., F. Wu and B. R. Weiner, 1995, *Chem. Phys. Lett.*, **247**, 313-320.
293. Cheng, B.-M. and Y.-P. Lee, 1986, *Int. J. Chem. Kinet.*, **18**, 1303-1314.
294. Cheskis, S. G., A. A. Iogansen, O. M. Sarkisov and A. A. Titov, 1985, *Chem. Phys. Lett.*, **120**, 45-49.
295. Cheskis, S. G. and O. M. Sarkisov, 1979, *Chem. Phys. Lett.*, **62**, 72.
296. Chesnokov, E. N., 1991, *Khimicheskaya Fizika*, **10**, 204-212.
297. Chichinin, A., S. Teton, G. Le Bras and G. Poulet, 1994, *J. Atmos. Chem*, **18**, 239-245.
298. Chichinin, A. I., 1997, *J. Chem. Phys.*, **106**, 1057.
299. Chichinin, A. I., 2000, *Chem. Phys. Lett.*, **316**, 425-432.
300. Chiorboli, C., C. A. Bignozzi, A. Maldotti, P. F. Giardini, A. Rossi and V. Carassiti, 1983, *Int. J. Chem. Kinet.*, **15**, 579-586.
301. Choo, K. Y. and M.-T. Leu, 1985, *International Journal of Chemical Kinetics*, **17**, 1155-1167.
302. Choo, K. Y. and M. T. Leu, 1985, *J. Phys. Chem.*, **89**, 4832-4837.
303. Christensen, L. E., M. Okumura, J. C. Hansen, S. P. Sander and J. S. Francisco, 2006, *J. Phys. Chem. A*, **110**, 6948-6959.
304. Christensen, L. E., M. Okumura, S. P. Sander, R. J. Salawitch, G. C. Toon, B. Sen, J.-F. Blavier and K. W. Jucks, 2002, *Geophys. Res. Lett.*, **29**, 1029/2001GL014525.
305. Chuong, B. and P. S. Stevens, 2000, *J. Phys. Chem. A*, **104**, 5230-5237.
306. Cillien, C., P. Goldfinger, G. Huybrechts and G. Martens, 1967, *Trans. Faraday Soc.*, **63**, 1631-1635.
307. Clark, I. D., I. T. N. Jones and R. P. Wayne, 1970, *Proc. Roy. Soc. Lond. A.*, **317**, 407-416.
308. Clark, I. D. and R. P. Wayne, 1969, *Chem. Phys. Lett.*, **3**, 405-407.
309. Clark, I. D. and R. P. Wayne, 1969, *Proc. Roy. Soc. Lond. A.*, **314**, 111-127.
310. Clark, I. D. and R. P. Wayne, 1970, *Proc. Roy. Soc. London. A.*, **316**, 539-550.
311. Clark, R. H., D. Husain and J. Y. Jezequel, 1982, *J. Photochem.*, **18**, 39-46.
312. Clarke, J. S., J. H. Kroll, N. M. Donahue and J. G. Anderson, 1998, *J. Phys. Chem. A.*, **102**, 9847-9857.
313. Clemo, A. R., F. E. Davidson, G. L. Duncan and R. Grice, 1981, *Chem. Phys. Lett.*, **84**, 509-511.
314. Clough, P. N. and B. A. Thrush, 1967, *Trans. Faraday Soc.*, **63**, 915-925.
315. Clyne, M. A. A. and J. A. Coxon, 1968, *Proc. Roy. Soc. A*, **303**, 207-231.
316. Clyne, M. A. A. and H. W. Cruse, 1970, *Trans. Faraday Soc.*, **66**, 2227.
317. Clyne, M. A. A. and H. W. Cruse, 1972, *J. Chem. Soc. Faraday Trans. 2*, **68**, 1281.
318. Clyne, M. A. A. and S. Down, 1974, *J. Chem. Soc. Faraday Trans. 2*, **70**, 253-266.
319. Clyne, M. A. A., C. J. Halstead and B. A. Thrush, 1966, *Proc. Soc. London Ser. A.*, **295**, 355-362.
320. Clyne, M. A. A. and A. Hodgson, 1985, *J. Chem. Soc. Faraday Trans. 2*, **81**, 443-455.
321. Clyne, M. A. A. and P. M. Holt, 1979, *J. Chem. Soc. Faraday Trans. 2*, **75**, 569-581.
322. Clyne, M. A. A. and P. M. Holt, 1979, *J. Chem. Soc. Faraday Trans. 2*, **75**, 582-591.

323. Clyne, M. A. A. and A. J. MacRobert, 1980, *Int. J. Chem. Kinet.*, **12**, 79-96.
324. Clyne, M. A. A. and A. J. MacRobert, 1981, *Int. J. Chem. Kinet.*, **13**, 187-197.
325. Clyne, M. A. A., A. J. MacRobert, T. P. Murrells and L. J. Stief, 1984, *J. Chem. Soc. Faraday Trans. 2*, **80**, 877-886.
326. Clyne, M. A. A. and I. S. McDermid, 1975, *J. Chem. Soc. Faraday Trans. 1*, **71**, 2189.
327. Clyne, M. A. A., D. J. McKenney and R. F. Walker, 1973, *Can. J. Chem.*, **51**, 3596.
328. Clyne, M. A. A., D. J. McKenney and R. T. Watson, 1975, *Chem. Soc. Faraday Trans. 1*, **71**, 322-335.
329. Clyne, M. A. A. and P. Monkhouse, 1977, *J. Chem. Soc. Faraday Trans. 2*, **73**, 298-309.
330. Clyne, M. A. A., P. B. Monkhouse and L. W. Townsend, 1976, *Int. J. Chem. Kinet.*, **8**, 425.
331. Clyne, M. A. A. and W. S. Nip, 1976, *J. Chem. Soc. Faraday Trans. 2*, **72**, 838-847.
332. Clyne, M. A. A. and W. S. Nip, 1976, *J. Chem. Soc. Faraday Trans. 1*, **72**, 2211-2217.
333. Clyne, M. A. A. and Y. Ono, 1982, *Chem. Phys.*, **69**, 381-388.
334. Clyne, M. A. A. and Y. Ono, 1983, *Chem. Phys. Lett.*, **94**, 597-602.
335. Clyne, M. A. A. and L. W. Townsend, 1975, *Int. J. Chem. Kinet.*, **Symp. 1**, 73-84.
336. Clyne, M. A. A. and R. F. Walker, 1973, *J. Chem. Soc. Faraday Trans. 1*, **69**, 1547-1567.
337. Clyne, M. A. A. and R. T. Watson, 1974, *J. Chem. Soc. Faraday Trans. 1*, **70**, 2250-2259.
338. Clyne, M. A. A. and R. T. Watson, 1974, *J. Chem. Soc. Faraday Trans. 1*, **70**, 1109.
339. Clyne, M. A. A. and R. T. Watson, 1975, *J. Chem. Soc. Faraday Trans. 1*, **71**, 336.
340. Clyne, M. A. A. and R. T. Watson, 1977, *J. Chem. Soc. Faraday Trans. 1*, **73**, 1169-1187.
341. Clyne, M. A. A. and I. F. White, 1971, *Trans. Faraday Soc.*, **67**, 2068-2076.
342. Clyne, M. A. A. and P. D. Whitefield, 1979, *J. Chem. Soc. Faraday Trans. 2*, **75**, 1327-1340.
343. Cocks, A. T., R. P. Fernanado and I. S. Fletcher, 1986, *Atmos. Environ.*, **20**, 2359-2366.
344. Collins, R. J., D. Husain and R. J. Donovan, 1973, *J. Chem. Soc. Faraday Trans. 2*, **69**, 145-157.
345. Colussi, A. J. and M. A. Grela, 1994, *Chem. Phys. Lett.*, **229**, 134-138.
346. Cook, J. L., C. A. Ennis, T. J. Leck and J. W. Birks, 1981, *J. Chem. Phys.*, **74**, 545.
347. Coomber, J. W. and E. Whittle, 1966, *Trans. Faraday Soc.*, **62**, 2183-2190.
348. Cooper, W. F. and J. F. Hershberger, 1992, *J. Phys. Chem.*, **96**, 5405-5410.
349. Cotter, E. S. N., N. J. Booth, C. E. Canosa-Mas, D. J. Gray, D. E. Shallcross and R. P. Wayne, 2001, *Chem. Phys. Phys. Chem.*, **3**, 402-408.
350. Cox, J. W., H. H. Nelson and J. R. McDonald, 1985, *Chem. Phys.*, **96**, 175.
351. Cox, R. A., 1980, *Int. J. Chem. Kinet.*, **12**, 649.
352. Cox, R. A., R. A. Barton, E. Ljungstrum and D. W. Stocker, 1984, *Chem. Phys. Lett.*, **108**, 228-232.
353. Cox, R. A. and J. P. Burrows, 1979, *J. Phys. Chem.*, **83**, 2560-2568.
354. Cox, R. A., J. P. Burrows and T. J. Wallington, 1981, *Chem. Phys. Lett.*, **84**, 217-221.
355. Cox, R. A. and G. B. Coker, 1983, *J. Atmos. Chem.*, **1**, 53.
356. Cox, R. A. and R. G. Derwent, 1979, *Journal of the Chemical Society, Faraday Transactions 1: Physical Chemistry in Condensed Phases*, **75**, 1635-1647.
357. Cox, R. A., R. G. Derwent, A. E. J. Eggleton and J. E. Lovelock, 1976, *Atmos. Environ.*, **10**, 305.
358. Cox, R. A., R. G. Derwent, A. E. J. Eggleton and H. J. Read, 1979, *J. Chem. Soc. Faraday Trans. I*, **75**, 1648-1666.
359. Cox, R. A., R. G. Derwent and P. M. Holt, 1975, *Chemosphere*, **4**, 201.
360. Cox, R. A., R. G. Derwent and P. M. Holt, 1976, *J. Chem. Soc. Faraday Trans. 1*, **72**, 2031.
361. Cox, R. A., R. G. Derwent, S. V. Kearsey, L. Batt and K. G. Patrick, 1980, *J. Photochem.*, **13**, 149.
362. Cox, R. A., R. G. Derwent and M. R. Williams, 1980, *Environmental Science and Technology*, **14**, 57-61.
363. Cox, R. A., M. Fowles, D. Moulton and R. P. Wayne, 1987, *J. Phys. Chem.*, **91**, 3361-3365.
364. Cox, R. A. and G. D. Hayman, 1988, *Nature*, **332**, 796-800.
365. Cox, R. A. and S. A. Penkett, 1972, *J. Chem. Soc., Faraday Trans. 1*, **68**, 1735.
366. Cox, R. A. and D. Sheppard, 1980, *Nature*, **284**, 330-331.
367. Cox, R. A., D. W. Sheppard and M. P. Stevens, 1982, *J. Photochem.*, **19**, 189-207.
368. Cox, R. M. and J. M. C. Plane, 1999, *Phys. Chem. Chem. Phys.*, **1**, 4713-4720.
369. Cox, R. M., D. E. Self and J. M. C. Plane, 2001, *J. Geophys. Res.*, **106**, 1733-1739.
370. Crawford, M. A., T. J. Wallington, J. J. Szenté, M. M. Maricq and J. S. Francisco, 1999, *J. Phys. Chem. A*, **103**, 365-378.

371. Cronkhite, J. M., R. E. Stickel, J. M. Nicovich and P. H. Wine, 1998, *J. Phys. Chem A*, **102**, 6651-6658.
372. Cronkhite, J. M. and P. H. Wine, 1998, *Int. J. Chem. Kinet.*, **30**, 555-563.
373. Crowley, J. N., P. Campuzano-Jost and G. K. Moortgat, 1996, *J. Phys. Chem.*, **100**, 3601-3606.
374. Crowley, J. N. and S. A. Carl, 1997, *Journal of Physical Chemistry A*, **101**, 4178-4184.
375. Crunaire, S., J. Tarmoul, C. Fittschen, A. Tomas, B. Lemoine and P. Coddeville, 2006, *Appl. Phys. B*, **85**, 467-476.
376. Cupitt, L. T. and G. P. Glass, 1975, *Int. J. Chem. Kinet.*, **Symp. 1**, 39-50.
377. Cvetanovic, R. J., D. L. Singleton and R. S. Irwin, 1981, *J. Am. Chem. Soc.*, **103**, 3530-3539.
378. Czarnowski, J. and H. J. Schumacher, 1981, *Int. J. Chem. Kinet.*, **13**, 639-649.
379. D'Anna, B., O. Andresen, Z. Gefen, C. J. Nielsen, K. Brudnik and J. T. Jodkowski, 2001, *Phys. Chem. Chem. Phys.*, **3**, 3057-3063.
380. Daele, V. and G. Poulet, 1996, *J. Chim. Phys.*, **93**, 1081-1099.
381. Daele, V., A. Ray, I. Vassali, G. Poulet and G. Le Bras, 1995, *Int. J. Chem. Kinet.*, **27**, 1121-1133.
382. Dagaut, P., T. J. Wallington and M. J. Kurylo, 1988, *J. Phys. Chem.*, **92**, 3833-3836.
383. Dagaut, P., T. J. Wallington and M. J. Kurylo, 1988, *J. Phys. Chem.*, **92**, 3836-3839.
384. Dagaut, P., T. J. Wallington, R. Liu and M. J. Kurylo, 1988, *Int. J. Chem. Kinet.*, **20**, 331-338.
385. Daniels, F. and E. H. Johnston, 1921, *J. Am. Chem. Soc.*, **43**, 53.
386. Daubendiek, R. L. and J. G. Calvert, 1975, *Environ. Lett.*, **8**, 103-116.
387. Davenport, J. E., B. Ridley, H. I. Schiff and K. H. Welge, 1972, *J. Chem. Soc. Faraday Discussion*, **53**, 230-231.
388. Davidson, F. E., A. R. Clemo, G. L. Duncan, R. J. Browett, J. H. Hobson and R. Grice, 1982, *Molecular Physics*, **46**, 33-40.
389. Davidson, J. A., C. A. Cantrell, S. C. Tyler, R. E. Shetter, R. J. Cicerone and J. G. Calvert, 1987, *J. Geophys. Res.*, **92**, 2195-2199.
390. Davidson, J. A., C. J. Howard, H. I. Schiff and F. C. Fehsenfeld, 1979, *J. Chem. Phys.*, **70**, 1697-1704.
391. Davidson, J. A., K. E. Kear and E. W. Abrahamson, 1972/1973, *J. Photochem.*, **1**, 307-316.
392. Davidson, J. A., H. I. Schiff, T. J. Brown and C. J. Howard, 1978, *J. Chem. Phys.*, **69**, 4277-4279.
393. Davidson, J. A., H. I. Schiff, G. E. Streit, J. R. McAfee, A. L. Schmeltekopf and C. J. Howard, 1977, *J. Chem. Phys.*, **67**, 5021-5025.
394. Davies, P. B. and B. A. Thrush, 1968, *Trans. Far. Soc.*, **64**, 1836.
395. Davis, D. D., W. Braun and A. M. Bass, 1970, *Int. J. Chem. Kinet.*, **2**, 101.
396. Davis, D. D., J. T. Herron and R. E. Huie, 1973, *J. Chem. Phys.*, **58**, 530-535.
397. Davis, D. D., R. B. Klemm and M. Pilling, 1972, *Int. J. Chem. Kinet.*, **4**, 367-382.
398. Davis, D. D., G. Machado, B. Conaway, Y. Oh and R. T. Watson, 1976, *J. Chem. Phys.*, **65**, 1268.
399. Davis, D. D., J. Prusazcyk, M. Dwyer and P. Kim, 1974, *J. Phys. Chem.*, **78**, 1775-1779.
400. Davis, D. D., W. Wong and J. Lephardt, 1973, *Chem. Phys. Lett.*, **22**, 273-278.
401. Davis, D. D., W. Wong and R. Schiff, 1974, *J. Phys. Chem.*, **78**, 463-464.
402. Daykin, E. P. and P. H. Wine, 1990, *J. Geophys. Res.*, **95**, 18547-18553.
403. Daykin, E. P. and P. H. Wine, 1990, *J. Phys. Chem.*, **94**, 4528-4535.
404. Daykin, E. P. and P. H. Wine, 1990, *Int. J. Chem. Kinet.*, **22**, 1083-1094.
405. De Sousa, A. R., M. Touzeau and M. Petitdidier, 1985, *Chem. Phys. Lett.*, **121**, 423-428.
406. DeMore, W. B., 1969, *Int. J. Chem. Kinet.*, **1**, 209-220.
407. DeMore, W. B., 1971, *Int. J. Chem. Kinet.*, **3**, 161-173.
408. DeMore, W. B., 1979, *J. Phys. Chem.*, **83**, 1113-1118.
409. DeMore, W. B. 182nd National Meeting of the American Chemical Society, 1981, New York,
410. DeMore, W. B., 1982, *J. Phys. Chem*, **86**, 121-126.
411. DeMore, W. B., 1991, *J. Geophys. Res.*, **96**, 4995-5000.
412. DeMore, W. B., 1992, *Geophys. Res. Lett.*, **19**, 1367-1370.
413. DeMore, W. B., 1993, *Geophys. Res. Lett.*, **20**, 1359-1362.
414. DeMore, W. B., 1993, *J. Phys. Chem.*, **97**, 8564-8566.
415. DeMore, W. B., 1996, *J. Phys. Chem.*, **100**, 5813-5820.
416. DeMore, W. B., 2005, *J. Photochem. Photobiol. A Chem.*, **176**, 129 - 135.
417. DeMore, W. B. and K. D. Bayes, 1999, *J. Phys. Chem. A*, **103**, 2649-2654.
418. DeMore, W. B. and C. Dede, 1970, *J. Phys. Chem.*, **74**, 2621-2625.

419. DeMore, W. B. and C. L. Lin, 1973, *J. Org. Chem.*, **38**, 985-989.
420. DeMore, W. B., C. L. Lin and S. Jaffe. 12th Informal Conference on Photochemistry, 1976, 287-289.
421. DeMore, W. B. and E. Tschuikow-Roux, 1974, *J. Phys. Chem.*, **78**, 1447-1451.
422. DeMore, W. B. and E. Tschuikow-Roux, 1990, *J. Phys. Chem.*, **94**, 5856-5860.
423. DeMore, W. B. and E. W. Wilson Jr., 1999, *J. Phys. Chem. A*, **103**, 573-576.
424. Derwent, R. G. and B. A. Thrush, 1971, *Trans. Faraday Soc.*, **67**, 2036-2043.
425. Devolder, P., M. Carlier, J. F. Pauwels and L. R. Sochet, 1984, *Chem. Phys. Lett.*, **111**, 94-99.
426. Diau, E. W.-G. and Y.-P. Lee, 1991, *J. Phys. Chem.*, **95**, 7726-7732.
427. Diau, E. W.-G., T.-L. Tso and Y.-P. Lee, 1990, *J. Phys. Chem.*, **94**, 5261-5265.
428. Diau, E. W., T. Yu, M. A. G. Wagner and M. C. Lin, 1994, *J. Phys. Chem.*, **98**, 4034-4042.
429. Diaz-de-Mera, Y., A. Aranda, D. Rodriguez, R. López, B. Cabañas and E. Martinez, 2002, *J. Phys. Chem. A*, **106**, 8627-8633.
430. Dibble, T. S., M. M. Maricq, J. J. Szenté and J. S. Francisco, 1995, *J. Phys. Chem.*, **99**, 17394-17402.
431. Dillon, T. J., D. Hölscher, V. Sivakumaran, A. Horowitz and J. N. Crowley, 2005, *Phys. Chem. Chem. Phys.*, **7**, 349-355.
432. Dillon, T. J., A. Horowitz and J. N. Crowley, 2007, *Chemical Physics Letters*, **443**, 12-16.
433. Dillon, T. J., A. Horowitz and J. N. Crowley, 2008, *Atmos. Chem. Phys.*, **8**, 1547-1557.
434. Dillon, T. J., R. Karunanandan and J. N. Crowley, 2006, *Phys. Chem. Chem. Phys.*, **8**, 847-855.
435. Dlugokencky, E. J. and C. J. Howard, 1988, *J. Phys. Chem.*, **92**, 1188-1193.
436. Dlugokencky, E. J. and C. J. Howard, 1989, *J. Phys. Chem.*, **93**, 1091-1096.
437. Dobe, S., L. A. Khachatryan and T. Berces, 1989, *Ber. Bunsenges. Phys. Chem.*, **93**, 847-852.
438. Dobe, S., M. Otting, F. Temps, H. G. Wagner and H. Ziemer, 1993, *Ber. Bunsenges. Phys. Chem.*, **97**, 877-884.
439. Dobe, S., F. Temps, T. Bohland and H. G. Wagner, 1985, *Z. Naturforsch.*, **40a**, 1289-1298.
440. Dobe, S., T. Turanyi, A. A. Iogansen and T. Berces, 1992, *Int. J. Chem. Kinet.*, **24**, 191-198.
441. Dobis, O. and S. W. Benson, 1987, *Int. J. Chem. Kinet.*, **19**, 691-708.
442. Dobis, O. and S. W. Benson, 1991, *J. Am. Chem. Soc.*, **113**, 6377-6386.
443. Dobis, O. and S. W. Benson, 1993, *J. Am. Chem. Soc.*, **115**, 8798-8809.
444. Dodonov, A. F., G. K. Lavrovskaya, I. I. Morozov and V. L. Tal'rose, 1971, *Dokl. Akad. Nauk USSR*, 1971, Vol. 198, 622; *Dokl. Phys. Chem. (Engl. Trans.)*, **198**, 440-442.
445. Dodonov, A. F., V. V. Zelenov, A. S. Kukui and E. A. P. V. L. Tal'Rose, 1985, *Khim. Fiz.*, **4**, 1335-1343.
446. Dognon, A. M., F. Caralp and R. Lesclaux, 1985, *J. Chim. Phys. Phys.-Chim. Biol.*, **82**, 349-352.
447. Dolson, D. A., 1986, *J. Phys. Chem.*, **90**, 6714-6718.
448. Domine, F., T. P. Murrells and C. J. Howard, 1990, *J. Phys. Chem.*, **94**, 5839-5847.
449. Domine, F. and A. R. Ravishankara, 1992, *Int. J. Chem. Kinet.*, **24**, 943-951.
450. Domine, F., A. R. Ravishankara and C. J. Howard, 1992, *J. Phys. Chem.*, **96**, 2171-2178.
451. Donaghy, T., I. Shanahan, M. Hande and S. Fitzpatrick, 1993, *Int. J. Chem. Kinet.*, **25**, 273-284.
452. Donahue, N. M., J. G. Anderson and K. L. Demerjian, 1998, *J. Phys. Chem. A*, **102**, 3121-3126.
453. Donahue, N. M. and J. S. Clarke, 2004, *Int. J. Chem. Kinet.*, **36**, 259-272.
454. Donahue, N. M., J. H. Kroll, J. G. Anderson and K. L. Demerjian, 1998, *Geophys. Res. Lett.*, **25**, 59-62.
455. Donovan, R. J. and D. J. Little, 1972, *Chem. Phys. Lett.*, **13**, 488-490.
456. Dransfeld, P. and H. G. Wagner, 1987, *Z. Naturforsch.*, **42a**, 471-476.
457. Dreier, T. and J. Wolfrum. 20th International Symposium on Combustion, 1984, 695-702.
458. Dreyer, J. W., D. Perner and C. R. Roy, 1974, *J. Chem. Phys.*, **61**, 3164.
459. Droege, A. T. and F. P. Tully, 1986, *J. Phys. Chem.*, **90**, 1949-1954.
460. Du, L., Y. Xu, M. Ge, J. Long, L. Yao and W. Wang, 2007, *Chem. Phys. Lett.*, **436**, 36-40.
461. Dunlea, E. J. Thesis: Atmospheric reactions of electronically excited atomic and molecular oxygen, Ph. D., University of Colorado, Boulder, 2002.
462. Dunlea, E. J. and A. R. Ravishankara, 2004, *Phys. Chem. Chem. Phys.*, **6**, 2152-2161.
463. Dunlea, E. J. and A. R. Ravishankara, 2004, *Phys. Chem. Chem. Phys.*, **6**, 3333-3340.
464. Dunlea, E. J., A. R. Ravishankara, R. S. Strekowski, J. M. Nicovich and P. H. Wine, 2004, *Phys. Chem. Chem. Phys.*, **6**, 5484-5489.

465. Dunlea, E. J., R. K. Talukdar and A. R. Ravishankara, 2005, *J. Phys. Chem. A*, **109**, 3912-3920.
466. Dunlea, E. J., R. K. Talukdar and A. R. Ravishankara, 2010, *Zeitschrift fur Physikalische Chemie*, **224**, 989-1007.
467. Dunlop, J. R. and F. P. Tully, 1993, *J. Phys. Chem.*, **97**, 6457-6464.
468. Dunlop, J. R. and F. P. Tully, 1993, *J. Phys. Chem.*, **97**, 11148-11150.
469. Dyke, J. M., M. V. Ghosh, M. Goubet, E. P. F. Lee, G. Levita, K. Miqueu and D. E. Shallcross, 2006, *Chem. Phys.*, **324**, 85-95.
470. Dyke, J. M., M. V. Ghosh, D. J. Kinnison, G. Levita, A. Morris and D. E. Shallcross, 2005, *Phys. Chem. Chem. Phys.*, **7**, 866-873.
471. Eberhard, J. and C. J. Howard, 1996, *Int. J. Chem. Kinet.*, **28**, 731-740.
472. Eberhard, J., P.-S. Yeh and Y.-P. Lee, 1997, *J. Chem. Phys.*, **107**, 6499-6502.
473. Edelbuttel-Einhaus, J., K.-H. Hoyer mann, G. Rohde and J. Seeba, 1992, *Proceedings of the Combustion Institute*, **24**, 661-668.
474. Edney, E. O. and D. J. Driscoll, 1992, *Int. J. Chem. Kinet.*, **24**, 1067-1081.
475. Edney, E. O., T. E. Kleindienst and E. W. Corse, 1986, *Int. J. Chem. Kinet.*, **18**, 1355-1371.
476. Egsgaard, H., L. Carlson, H. Florencio, T. Drewello and H. Schwarz, 1988, *Chem. Phys. Lett.*, **148**, 537-540.
477. Ehhalt, D. H., J. A. Davidson, C. A. Cantrell, I. Friedman and S. Tyler, 1989, *J. Geophys. Res.*, **94**, 9831-9836.
478. Eibling, R. E. and M. Kaufman, 1983, *Atmos. Environ.*, **17**, 429-431.
479. Ellermann, T., O. J. Nielsen and H. Skov, 1992, *Chem. Phys. Lett.*, **200**, 224-229.
480. Ellingson, B. A. and D. G. Truhlar, 2007, *J. Am. Chem. Soc.*, **129**, 12765-12771.
481. Elrod, M. J., R. F. Meads, J. B. Lipson, J. V. Seeley and M. J. Molina, 1996, *J. Phys. Chem.*, **100**, 5808-5812.
482. Elrod, M. J., D. L. Ranschaert and N. J. Schneider, 2001, *Int. J. Chem. Kinet.*, **33**, 363-376.
483. Enami, S., Y. Nakano, S. Hashimoto, M. Kawasaki, S. Aloisio and J. S. Francisco, 2004, *J. Phys. Chem. A*, **108**, 7785-7789.
484. English, A. M., J. C. Hansen, J. J. Szente and M. M. Maricq, 2008, *J. Phys. Chem. A*, **112**, 9220-9228.
485. Ennis, C. A. and J. W. Birks, 1985, *J. Phys. Chem.*, **89**, 186-191.
486. Ennis, C. A. and J. W. Birks, 1988, *J. Phys. Chem.*, **93**, 1119-1126.
487. Estupiñán, E. G., J. M. Nicovich and P.H. Wine, 2001, *J. Phys. Chem. A*, **105**, 9697-9703.
488. Fair, R. W. and B. A. Thrush, 1969, *Trans. Faraday Soc.*, **65**, 1557-1570.
489. Fair, R. W., A. van Roodaelaar and O. P. Strausz, 1971, *Can. J. Chem.*, **49**, 1659-1664.
490. Falbe-Hansen, H., S. Sorensen, N. R. Jensen, T. Pedersen and J. Hjorth, 2000, *Atmos. Environ.*, **34**, 1543-1551.
491. Fang, T. D., P. H. Taylor and R. J. Berry, 1999, *J. Phys. Chem. A*, **103**, 2700 - 2704.
492. Fang, T. D., P. H. Taylor and B. Dellinger, 1996, *J. Phys. Chem.*, **100**, 4048-4054.
493. Fang, T. D., P. H. Taylor, B. Dellinger, C. J. Ehlers and R. J. Berry, 1997, *J. Phys. Chem. A*, **101**, 5758-5764.
494. Fantechi, G., N. R. Jensen, O. Saastad, J. Hjorth and J. Peeters, 1998, *J. Atmos. Chem.*, **31**, 247-267.
495. Farquharson, G. K. and R. H. Smith, 1980, *Aust. J. Chem.*, **33**, 1425-1435.
496. Fasano, D. M. and N. S. Nogar, 1981, *Int. J. Chem. Kinet.*, **13**, 325.
497. Fasano, D. M. and N. S. Nogar, 1982, *Chem. Phys. Lett.*, **92**, 411-414.
498. Fenter, F. F. and J. G. Anderson, 1991, *J. Phys. Chem.*, **95**, 3172-3180.
499. Fenter, F. F. and J. G. Anderson, 1994, *Int. J. Chem. Kinet.*, **26**, 801-812.
500. Fenter, F. F., V. Catoire, R. Lesclaux and P. D. Lightfoot, 1993, *J. Phys. Chem.*, **97**, 3530-3538.
501. Filseth, S. V., A. Zia and K. H. Welge, 1970, *J. Chem. Phys.*, **52**, 5502-5510.
502. Findlay, F. D., C. J. Fortin and D. R. Snelling, 1969, *Chem. Phys. Lett.*, **3**, 204-206.
503. Findlay, F. D. and D. R. Snelling, 1971, *J. Chem. Phys.*, **55**, 545-551.
504. Findlay, F. D. and D. R. Snelling, 1971, *J. Chem. Phys.*, **54**, 2750-2755.
505. Finkbeiner, M., J. N. Crowley, O. Horie, R. Muller, G. K. Moortgat and P. J. Crutzen, 1995, *J. Phys. Chem.*, **99**, 16264-16275.
506. Finlayson-Pitts, B. J., M. J. Ezell, T. M. Jayaweera, H. N. Berko and C. C. Lai, 1992, *Geophys. Res. Lett.*, **19**, 1371-1374.

507. Finlayson-Pitts, B. J., S. K. Hernandez and H. N. Berko, 1993, *J. Phys. Chem.*, **97**, 1172-1177.
508. Finlayson-Pitts, B. J., C. J. Keoshian, B. Buehler and A. A. Ezell, 1999, *Int. J. Chem. Kinet.*, **31**, 491-499.
509. Finlayson-Pitts, B. J. and T. E. Kleindienst, 1979, *J. Chem. Phys.*, **70**, 4804-4806.
510. Finlayson-Pitts, B. J., T. E. Kleindienst, J. J. Ezell and D. W. Toohey, 1981, *J. Chem. Phys.*, **74**, 4533-4543.
511. Fletcher, I. S. and D. Husain, 1976, *Can. J. Chem.*, **54**, 1765-1770.
512. Fletcher, I. S. and D. Husain, 1976, *J. Phys. Chem.*, **80**, 1837-1840.
513. Fletcher, I. S. and D. Husain, 1978, *J. Photochem.*, **8**, 355-361.
514. Fockenberg, C., H. Saathoff and R. Zellner, 1994, *Chem. Phys. Lett.*, **218**, 21-28.
515. Foon, R., G. Le Bras and J. Combourieu, 1979, *C.R. Acad. Sci. Paris, Series C* **288**, 241.
516. Foon, R. and G. P. Reid, 1971, *Trans. Faraday Soc.*, **67**, 3513.
517. Force, A. P. and J. R. Wiesenfeld, 1981, *J. Phys. Chem.*, **85**, 782-785.
518. Force, A. P. and J. R. Wiesenfeld, 1981, *J. Chem. Phys.*, **74**, 1718-1723.
519. Fraser, M. E. and L. G. Piper, 1989, *J. Phys. Chem.*, **93**, 1107-1111.
520. Freeman, C. G. and L. F. Phillips, 1968, *J. Phys. Chem.*, **72**, 3025.
521. Freudenstein, K. and D. Biedenkapp, 1976, *Ber. Bunsenges. Phys. Chem.*, **80**, 42-48.
522. Friedl, R. R., W. H. Brune and J. G. Anderson, 1985, *J. Phys. Chem.*, **89**, 5505-5510.
523. Friedl, R. R., J. H. Goble and S. P. Sander, 1986, *Geophys. Res. Lett.*, **13**, 1351-1354.
524. Friedl, R. R. and S. P. Sander, 1989, *J. Phys. Chem.*, **93**, 4756-4764.
525. Friedl, R. R., S. P. Sander and Y. L. Yung, 1992, *J. Phys. Chem.*, **96**, 7490-7493.
526. Fritz, B., K. Lorenz, W. Steinert and R. Zellner, 1984, *Oxidation Communications*, **6**, 363-370.
527. Frost, M. J. and I. W. M. Smith, 1990, *J. Chem. Soc. Faraday Trans.*, **86**, 1757-1762.
528. Frost, R. J., D. S. Green, M. K. Osborn and I. W. M. Smith, 1986, *Int. J. Chem. Kinet.*, **18**, 885-898.
529. Gaffney, J. S., R. Fajer, G. I. Senum and J. H. Lee, 1986, *Int. J. Chem. Kinet.*, **18**, 399-407.
530. Ganske, J. A., H. N. Berko, M. J. Ezell and B. J. Finlayson-Pitts, 1992, *J. Phys. Chem.*, **96**, 2568-2572.
531. Ganske, J. A., M. J. Ezell, H. N. Berko and B. J. Finlayson-Pitts, 1991, *Chem. Phys. Lett.*, **179**, 204-210.
532. Garland, N. L., 1998, *Chem. Phys. Lett.*, **290**, 385-390.
533. Garland, N. L., L. J. Medhurst and H. H. Nelson, 1993, *JOURNAL OF GEOPHYSICAL RESEARCH-ATMOSPHERES*, **98**, 23107-23111.
534. Garland, N. L. and H. H. Nelson, 1996, *Chem. Phys. Lett.*, **248**, 296-300.
535. Garraway, J. and R. J. Donovan, 1979, *J. Chem. Soc. Chem. Commun.*, 1108-1108.
536. Garvin, D. and H. P. Broida. 9th Symposium on Combustion, 1963, 678.
537. Gauthier, M. J. E. and D. R. Snelling, 1974, *Can. J. Chem.*, **52**, 4007-4015.
538. Gauthier, M. J. E. and D. R. Snelling, 1974, *J. Photochem.*, **4**, 27-50.
539. Geers-Muller, R. and F. Stuhl, 1987, *Chem. Phys. Lett.*, **135**, 263-268.
540. Gehring, M., K. Hoyer mann, H. Sahaeke and J. Wolfrum. 14th Int. Symposium on Combustion, 1973, 99.
541. Gericke, K.-H. and F. J. Comes, 1981, *Chem. Phys. Lett.*, **81**, 218-222.
542. Gierczak, T., J. B. Burkholder and A. R. Ravishankara, 1999, *J. Phys. Chem. A*, **103**, 877-883.
543. Gierczak, T., J. B. Burkholder and A. R. Ravishankara, 2006, *International Journal of Chemical Kinetics*, **38**, 234-241.
544. Gierczak, T., M. K. Gilles, S. Bauerle and A. R. Ravishankara, 2003, *Journal of Physical Chemistry A*, **107**, 5014-5020.
545. Gierczak, T., L. Goldfarb, D. Sueper and A. R. Ravishankara, 1994, *Int. J. Chem. Kinet.*, **26**, 719-728.
546. Gierczak, T., R. Talukdar, G. L. Vaghjiani, E. R. Lovejoy and A. R. Ravishankara, 1991, *J. Geophys. Res.*, **96**, 5001-5011.
547. Gierczak, T., R. K. Talukdar, J. B. Burkholder, R. W. Portmann, J. S. Daniel, S. Solomon and A. R. Ravishankara, 1996, *J. Geophys. Res.*, **101**, 12905-12911.
548. Gierczak, T., R. K. Talukdar and A. R. Ravishankara, 1997, *Journal of Physical Chemistry A*, **101**, 3125-3134.

549. Gierczak, T., S. Talukdar, S. Herndon, G. L. Vaghjiani and A. R. Ravishankara, 1997, *J. Phys. Chem. A*, **101**, 3125-3134.
550. Gill, K. G. and R. A. Hites, 2002, *J. Phys. Chem. A*, **106**, 2538-2544.
551. Gill, R. J., W. D. Johnson and G. H. Atkinson, 1981, *Chem. Phys.*, **58**, 29.
552. Gilles, M. K., J. B. Burkholder, T. Gierczak, P. Marshall and A. R. Ravishankara, 2002, *J. Phys. Chem. A*, **104**, 8945-8950.
553. Gilles, M. K., J. B. Burkholder and A. R. Ravishankara, 1999, *International Journal of Chemical Kinetics*, **31**, 417-424.
554. Gilles, M. K., D. C. McCabe, J. B. Burkholder and A. R. Ravishankara, 2001, *J. Phys. Chem. A*, **105**, 5849-5853.
555. Gilles, M. K., R. K. Talukdar and A. R. Ravishankara, 2000, *J. Phys. Chem. A*, **104**, 8945-8950.
556. Gilles, M. K., A. A. Turnipseed, J. B. Burkholder and A. R. Ravishankara, 1997, *J. Phys. Chem. A*, **101**, 5526-5534.
557. Gilpin, R., H. I. Schiff and K. H. Welge, 1971, *J. Chem. Phys.*, **55**, 1087-1093.
558. Glaschick-Schimpf, I., A. Leiss, P. B. Monkhouse, U. Schurath, K. H. Becker and E. H. Fink, 1979, *Chem. Phys. Lett.*, **67**, 318-323.
559. Glavas, S. and J. Heicklen, 1985, *J. Photochem.*, **31**, 21-28.
560. Gleason, J. F. and C. J. Howard, 1988, *J. Phys. Chem.*, **92**, 3414-3417.
561. Gleason, J. F., F. L. Nesbitt and L. J. Stief, 1994, *J. Phys. Chem.*, **98**, 126-131.
562. Gleason, J. F., A. Sinha and C. J. Howard, 1987, *J. Phys. Chem.*, **91**, 719-724.
563. Glinski, R. J. and J. W. Birks, 1985, *J. Phys. Chem.*, **89**, 3449-3453.
564. Goldfarb, L., J. B. Burkholder and A. R. Ravishankara, 2001, *J. Phys. Chem. A*, **105**, 5402-5409.
565. Goldfarb, L., M. H. Harwood, J. B. Burkholder and A. R. Ravishankara, 1998, *Journal of Physical Chemistry A*, **102**, 8556-8563.
566. Goldfinger, P., G. Huybrechts and G. Martens, 1961, *Trans. Faraday Soc.*, **57**, 2210-2219.
567. Goliff, W. S. and F. S. Rowland, 1997, *Geophys. Res. Lett.*, **23**, 3029-3032.
568. Gonzalez-Garcia, N., A. Gonzalez-Lafont and J. M. Lluch, 2007, *J. Phys. Chem. A*, **111**, 7825-7832.
569. Gordon, S., W. Mulac and P. Nangia, 1971, *J. Phys. Chem.*, **75**, 2087.
570. Gordon, S. and W. A. Mulac, 1975, *Int. J. Chem. Kinet.*, **Symp. 1**, 289-299.
571. Graham, R. A. and D. J. Gutman, 1977, *J. Phys. Chem.*, **81**, 207-209.
572. Graham, R. A. and H. S. Johnston, 1974, *J. Chem. Phys.*, **60**, 4628.
573. Graham, R. A. and H. S. Johnston, 1978, *J. Phys. Chem.*, **82**, 254-268.
574. Graham, R. A., A. M. Winer, R. Atkinson and J. N. Pitts, Jr., 1979, *J. Phys. Chem.*, **83**, 1563.
575. Gravestock, T., M. A. Blitz and D. E. Heard, 2005, *Phys. Chem. Chem. Phys.*, **7**, 2173-2181.
576. Green, R. G. and R. P. Wayne, 1976/77, *J. Photochem.*, **6**, 371-374.
577. Greenblatt, G. D. and C. J. Howard, 1989, *J. Phys. Chem.*, **93**, 1035-1042.
578. Greenblatt, G. D. and A. R. Ravishankara, 1990, *J. Geophys. Res.*, **95**, 3539-3547.
579. Greene, C. R. and R. Atkinson, 1992, *Int. J. Chem. Kinet.*, **24**, 803-811.
580. Greenhill, P. G. and B. V. O'Grady, 1986, *Aust. J. Chem.*, **39**, 1775-1787.
581. Greiner, N. R., 1967, *J. Chem. Phys.*, **46**, 3389-3392.
582. Greiner, N. R., 1969, *J. Chem. Phys.*, **51**, 5049-5051.
583. Greiner, N. R., 1970, *J. Chem. Phys.*, **53**, 1284-1285.
584. Griffin, J., D.R. Worsnop, R.C. Brown, C.E. Kolb and D.R. Herschbach, 2001, *J. Phys. Chem. A*, **105**, 1643-1648.
585. Grimley, A. J. and P. L. Houston, 1980, *J. Chem. Phys.*, **72**, 1471-1475.
586. Grimsrud, E. P., H. H. Westberg and R. A. Rasmussen, 1975, *International Journal of Chemical Kinetics*, **Symp 1**, 183-195.
587. Grosjean, D., E. L. Williams, II and E. Grosjean, 1993, *Environ. Sci. Technol.*, **27**, 830-840.
588. Grosjean, E. and D. Grosjean, 1996, *Int. J. Chem. Kinet.*, **28**, 911-918.
589. Grotheer, H. H., G. Riekert, U. Meier and T. Just, 1985, *Ber. Bunsenges. Phys. Chem.*, **89**, 187-191.
590. Grotheer, H. H., G. Riekert, D. Walter and T. Just, 1988, *J. Phys. Chem.*, **92**, 4028.
591. Gutbrod, R., E. Kraka, R. N. Schindler and D. Cremer, 1997, *J. Am. Chem. Soc.*, **119**, 7330-7342.
592. Gutbrod, R., S. Meyer, M. M. Rahman and R. N. Schindler, 1997, *International Journal of Chemical Kinetics*, **29**, 717-723.

593. Gutman, D., N. Sanders and J. E. Butler, 1982, *J. Phys. Chem.*, **86**, 66.
594. Hack, W., O. Horie and H. G. Wagner, 1981, *Ber. Bunsenges. Phys. Chem.*, **85**, 72.
595. Hack, W., O. Horie and H. G. Wagner, 1982, *J. Phys. Chem.*, **86**, 765.
596. Hack, W., K. Hoyer mann and H. G. Wagner, 1974, *Ber. Bunsenges. Phys. Chem.*, **78**, 386.
597. Hack, W., G. Mex and H. G. Wagner, 1977, *Ber. Bunsenges. Phys. Chem.*, **81**, 677-684.
598. Hack, W., A. W. Preuss, F. Temps and H. G. Wagner, 1979, *Ber. Bunsenges. Phys. Chem.*, **83**, 1275-1279.
599. Hack, W., A. W. Preuss, F. Temps, H. G. Wagner and K. Hoyer mann, 1980, *Int. J. Chem. Kinet.*, **12**, 851-860.
600. Hack, W., A. W. Preuss, H. G. Wagner and K. Hoyer mann, 1979, *Ber. Bunsenges. Phys. Chem.*, **83**, 212-217.
601. Hack, W., H. Schacke, M. Schroter and H. G. Wagner. 17th International Symposium on Combustion, 1979,
602. Hack, W., H. G. Wagner and K. Hoyer mann, 1978, *Ber. Bunsenges. Phys. Chem.*, **82**, 713-719.
603. Hagele, J., K. Lorenz, D. Rhasa and R. Zellner, 1983, *Ber. Bunsenges. Phys. Chem.*, **87**, 1023-1026.
604. Hall, I. W., R. P. Wayne, R. A. Cox, M. E. Jenkin and G. D. Hayman, 1988, *J. Phys. Chem.*, **92**, 5049-5054.
605. Halstead, C. J. and B. A. Thrush, 1966, *Proc. Roy. Soc. London*, **Ser. A 295**, 380-398
606. Hamilton, E. J., Jr., 1975, *J. Chem. Phys.*, **63**, 3682-3683.
607. Hamilton, E. J., Jr. and R.-R. Lii, 1977, *Int. J. Chem. Kinet.*, **9**, 875-885.
608. Hammer, P. D., E. J. Dlugokencky and C. J. Howard, 1986, *J. Phys. Chem.*, **90**, 2491-2496.
609. Hancock, G., W. Lange, M. Lenzi and K. H. Welge, 1975, *Chem. Phys. Lett.*, **33**, 168.
610. Hancock, G. and I. W. M. Smith, 1971, *Trans. Faraday Soc.*, **67**, 2586-2597.
611. Handwerk, V. and R. Zellner, 1978, *Ber. Bunsenges. Phys. Chem.*, **82**, 1161-1166.
612. Hansen, I., K. Hoinghaus, C. Zetzsch and F. Stuhl, 1976, *Chem. Phys. Lett.*, **42**, 370-372.
613. Hansen, J. C., R. R. Friedl and S. P. Sander, 2008, *Journal of Physical Chemistry A*, **112**, 9229-9237.
614. Harding, L. B. and A. F. Wagner, 1988, *Proceedings of the Combustion Institute*, **22**, 983-989.
615. Harris, G. W., T. E. Kleindienst and J. N. Pitts, Jr., 1981, *Chem. Phys. Lett.*, **80**, 479-483.
616. Harrison, J. A., A. R. Whyte and L. F. Phillips, 1986, *Chem. Phys. Lett.*, **129**, 346-352.
617. Hartmann, D., J. Karthäuser, J. P. Sawerysyn and R. Zellner, 1990, *Ber. Bunsenges. Phys. Chem.*, **94**, 639-645.
618. Harwood, M. H., J. B. Burkholder, M. Hunter, R. W. Fox and A. R. Ravishankara, 1997, *J. Phys. Chem. A*, **101**, 853-863.
619. Harwood, M. H., D. M. Rowley, R. A. Cox and R. L. Jones, 1998, *J. Phys. Chem A*, **102**, 1790-1802.
620. Hashimoto, S., G. Inoue and H. Akimoto, 1984, *Chem. Phys. Lett.*, **107**, 198-202.
621. Hatakeyama, S. and M. T. Leu, 1986, *Geophys. Res. Lett.*, **13**, 1343-1346.
622. Hatakeyama, S. and M. T. Leu, 1989, *J. Phys. Chem.*, **93**, 5784-5789.
623. Hayman, G. D., J. M. Davies and R. A. Cox, 1986, *Geophys. Res. Lett.*, **13**, 1347-1350.
624. Heathfield, A. E., C. Anastasi, P. Pagsberg and A. McCulloch, 1998, *Atmos. Environ.*, **32**, 711-717.
625. Heidner, R. F., J. F. Bott, C. E. Gardner and J. E. Melzer, 1979, *J. Chem. Phys.*, **70**, 4509.
626. Heidner, R. F., J. F. Bott, C. E. Gardner and J. E. Melzer, 1980, *J. Chem. Phys.*, **72**, 4815.
627. Heidner, R. F., III, D. Husain and J. R. Weisenfeld, 1973, *J. Chem. Soc. Faraday Trans. 2*, **69**, 927-938.
628. Heidner, R. F., III and D. Husain, 1973, *Int. J. Chem. Kinet.*, **5**, 819-831.
629. Helleis, F., J. N. Crowley and G. K. Moortgat, 1993, *J. Phys. Chem.*, **97**, 11464-11473.
630. Helleis, F., J. N. Crowley and G. K. Moortgat, 1994, *Geophys. Res. Lett.*, **21**, 1795-1798.
631. Helmer, M. and J. M. C. Plane, 1993, *J. Geophys. Res.*, **98**, 23207-23222.
632. Heneghan, S. P. and S. W. Benson, 1983, *Int. J. Chem. Kinet.*, **15**, 1311-1319.
633. Heneghan, S. P., P. A. Knoop and S. W. Benson, 1981, *Int. J. Chem. Kinet.*, **13**, 677-691.
634. Henon, E., S. Canneaux, F. Bohr and S. Dobe, 2003, *Phys. Chem. Chem. Phys.*, **5**, 333-341.
635. Herndon, S. C., K. D. Froyd, E. R. Lovejoy and A. R. Ravishankara, 1999, *J. Phys. Chem. A*, **103**, 6778-6785.

636. Herndon, S. C., Gierczak, R. K. Talukdar and A. R. Ravishankara, 2001, *Phys. Chem. Chem. Phys.*, **3**, 4529-4535.
637. Herndon, S. C. and A. R. Ravishankara, 2006, *J. Phys. Chem. A*, **110**, 106-113.
638. Herndon, S. C., P. W. Villalta, D. D. Nelson, J. T. Jayne and M. S. Zahniser, 2001, *J. Phys. Chem. A*, **105**, 1583-1591.
639. Herron, J. T., 1961, *J. Chem. Phys.*, **35**, 1138.
640. Herron, J. T. and R. E. Huie, 1974, *J. Phys. Chem.*, **78**, 2085
641. Herron, J. T. and R. D. Penzhorn, 1969, *J. Phys. Chem.*, **73**, 191.
642. Herschbach, D. R., C.E. Kolb, D.R. Worsnop and X. Shi, 1992, *Nature*, **356**, 414-416.
643. Hess, W. P. and F. P. Tully, 1988, *Chem. Phys. Lett.*, **152**, 183-189.
644. Hess, W. P. and F. P. Tully, 1989, *J. Phys. Chem.*, **93**, 1944-1947.
645. Hickson, K. M., A. Bergeat and M. Costes, 2010, *J. Chem. Phys.*
646. Hickson, K. M. and L. F. Keyser, 2004, *Journal of Physical Chemistry A*, **108**, 1150-1159.
647. Hickson, K. M. and L. F. Keyser, 2005, *Journal of Physical Chemistry A*, **109**, 6887-6900.
648. Hickson, K. M., L. F. Keyser and S. P. Sander, 2007, *J. Phys. Chem. A*, **111**, 8126-8138.
649. Hills, A. J., R. J. Cicerone, J. G. Calvert and J. W. Birks, 1988, *J. Phys. Chem.*, **92**, 1853-1858.
650. Hills, A. J. and C. J. Howard, 1984, *J. Chem. Phys.*, **81**, 4458-4465.
651. Hippler, H. and J. Troe, 1992, *Chem. Phys. Lett.*, **192**, 333-337.
652. Hippler, H., J. Troe and J. Willner, 1990, *J. Chem. Phys.*, **93**, 1755-1760.
653. Hislop, J. R. and R. P. Wayne, 1977, *J. Chem. Soc. Faraday Trans. 2*, **73**, 506-516.
654. Hites, R. A. and A. M. Turner, 2009, *Int. J. Chem. Kinet.*, **41**, 407-413.
655. Hitsuda, K., K. Takahashi, Y. Matsumi and T. J. Wallington, 2001, *J. Phys. Chem. A*, **105**, 5131-5136.
656. Hjorth, J., F. Cappellani, C. J. Nielsen and G. Restelli, 1989, *J. Phys. Chem.*, **93**, 5458-5461.
657. Hjorth, J., G. Ottobriani, F. Cappellani and G. Restelli, 1987, *J. Phys. Chem.*, **91**, 1565-1568.
658. Hjorth, J., G. Ottobriani and G. Restelli, 1986, *Int. J. Chem. Kinet.*, **18**, 819-828.
659. Hjorth, J., G. Ottobriani and G. Restelli, 1988, *J. Phys. Chem.*, **92**, 2669.
660. Hochanadel, C. J., J. A. Ghormley and P. J. Ogren, 1972, *J. Chem. Phys.*, **56**, 4426-4432.
661. Hochanadel, C. J., T. J. Sworski and P. J. Ogren, 1980, *J. Phys. Chem.*, **84**, 3274-3277.
662. Hohmann, J., G. Muller, G. Schonnenbeck and F. Stuhl, 1994, *Chem. Phys. Lett.*, **217**, 577.
663. Hollinden, G. A., M. J. Kurylo and R. B. Timmons, 1970, *J. Phys. Chem.*, **74**, 988-991.
664. Homann, K. H., G. Krome and H. G. Wagner, 1968, *Ber. Bunsenges. Phys. Chem.*, **72**, 998.
665. Hooshiyar, P. A. and H. Niki, 1995, *Int. J. Chem. Kinet.*, **27**, 1197-1206.
666. Horie, O. and G. K. Moortgat, 1992, *J. Chem. Soc. Faraday Trans.*, **88**, 3305-3312.
667. Horne, D. G. and R. G. W. Norrish, 1967, *Nature (London)*, **215**, 1373-1374.
668. Horowitz, A., D. Bauer, J. N. Crowley and G. K. Moortgat, 1993, *Geophys. Res. Lett.*, **20**, 1423-1426.
669. Horowitz, A., J. N. Crowley and G. K. Moortgat, 1994, *J. Phys. Chem.*, **98**, 11924-11930.
670. Horowitz, A., F. Su and J. G. Calvert, 1978, *Int. J. Chem. Kinet.*, **10**, 1099.
671. Hossenlopp, J. M., J. F. Hershberger and G. W. Flynn, 1990, *J. Phys. Chem.*, **94**, 1346-1351.
672. Howard, C. J., 1976, *J. Chem. Phys.*, **65**, 4771.
673. Howard, C. J., 1979, *J. Chem. Phys.*, **71**, 2352-2359.
674. Howard, C. J. and K. M. Evenson, 1976, *J. Chem. Phys.*, **64**, 197.
675. Howard, C. J. and K. M. Evenson, 1976, *J. Chem. Phys.*, **64**, 4303.
676. Howard, C. J. and K. M. Evenson, 1977, *Geophys. Res. Lett.*, **4**, 437-440.
677. Howard, C. J. and B. J. Finlayson-Pitts, 1980, *J. Chem. Phys.*, **72**, 3842-3843.
678. Howard, M. J. and I. W. M. Smith, 1981, *J. Chem. Soc. Faraday Trans. 2*, **77**, 997-1008.
679. Hoyer mann, K., H. G. Wagner and J. Wolfrum, 1967, *Z. Phys. Chem.*, **55**, 72.
680. Hoyer mann, K., H. G. Wagner and J. Wolfrum, 1969, *Z. Phys. Chem.*, **63**, 193.
681. Hsu, C.-C., A. M. Mebel and M. C. Lin, 1996, *J. Chem. Phys.*, **105**, 2346.
682. Hsu, D. S. Y., W. M. Shaub, T. L. Burks and M. C. Lin, 1979, *Chem Phys.*, **44**, 143-150.
683. Hsu, K. J. and W. B. DeMore, 1994, *Geophys. Res. Lett.*, **21**, 805-808.
684. Hsu, K. J. and W. B. DeMore, 1995, *J. Phys. Chem.*, **99**, 1235-1244.
685. Hsu, K. J. and W. B. DeMore, 1995, *J. Phys. Chem.*, **99**, 11141-11930.
686. Hsu, Y.-C., D.-S. Chen and Y.-P. Lee, 1987, *Int. J. Chem. Kinet.*, **19** 1073-1082.
687. Huang, Y.-w., T. J. Dransfield and J. G. Anderson, 2010, *J. Phys. Chem. A*, **114**, 11538-11544.

688. Huang, Y.-w., T. J. Dransfield, J. D. Miller, R. D. Rojas, X. G. Castillo and J. G. Anderson, 2009, *J. Phys. Chem. A*, **113**, 423-430.
689. Huder, K. J. and W. B. DeMore, 1993, *Geophys. Res. Lett.*, **20**, 1575-1577.
690. Huey, L. G., E. J. Dunlea and C. J. Howard, 1996, *J. Phys. Chem.*, **100**, 6504-6508.
691. Huie, R. E. and J. T. Herron, 1974, *Chem. Phys. Lett.*, **27**, 411.
692. Hunziker, H. E., H. Knepe and H. R. Wendt, 1981, *J. Photochem.*, **17**, 377.
693. Hurley, M. D., J. C. Ball and T. J. Wallington, 2007, *J. Phys. Chem. A*, **111**, 9789-9795.
694. Hurley, M. D., T. J. Wallington, M. P. S. Andersen, D. A. Ellis, J. W. Martin and S. A. Mabury, 2004, *J. Phys. Chem. A*, **108**, 1973.
695. Husain, D. and P. Marshall, 1985, *Combust. and Flame*, **60**, 81-87.
696. Husain, D., P. Marshall and J. M. C. Plane, 1985, *J. Chem. Soc. Chem. Comm.*, 1216-1218.
697. Husain, D., J. M. C. Plane and N. K. H. Slater, 1981, *J. Chem. Soc. Faraday Trans. 2*, **77**, 1949-1962.
698. Husain, D., J. M. C. Plane and C. C. Xiang, 1984, *J. Chem. Soc. Faraday Trans. 2*, **80**, 713-728.
699. Husain, D. and N. K. H. Slater, 1980, *J. Chem. Soc. Faraday Trans. 2*, **76**, 606-619.
700. Hynes, A. J., R. E. Stickel, A. J. Pounds, Z. Zhao, T. McKay, J. D. Bradshaw and P. H. Wine. *Dimethylsulfide: Oceans, Atmosphere, and Climate*; G. Restelli and G. Angletti, Eds.; Kluwer: Brussels, 1993; pp 211-221.
701. Hynes, A. J., R. B. Stocker, A. J. Pounds, T. McKay, J. D. Bradshaw, J. M. Nicovich and P. H. Wine, 1995, *J. Phys. Chem.*, **99**, 16967-16975.
702. Hynes, A. J. and P. H. Wine, 1987, *J. Phys. Chem.*, **91**, 3672-3676.
703. Hynes, A. J. and P. H. Wine, 1991, *J. Phys. Chem.*, **95**, 1232-1240.
704. Hynes, A. J. and P. H. Wine, 1996, *J. Atmos. Chem.*, **24**, 23-37.
705. Hynes, A. J., P. H. Wine and J. M. Nicovich, 1988, *J. Phys. Chem.*, **92**, 3846-3852.
706. Hynes, A. J., P. H. Wine and D. H. Semmes, 1986, *J. Phys. Chem.*, **90**, 4148-4156.
707. Iannuzzi, M. P., J. B. Jeffries and F. Kaufman, 1982, *Chem. Phys. Lett.*, **87**, 570-574.
708. Iannuzzi, M. P. and F. Kaufman, 1981, *J. Phys. Chem.*, **85**, 2163.
709. Igoshin, V. I., L. V. Kulakov and A. I. Nikitin, 1974, *Sov. J. Quant. Electron.*, **3**, 306.
710. Iida, Y., K. Obi and T. Imamura, 2002, *Chem. Lett.*, **31**, 792-793.
711. Imamura, T. and N. Washida, 1995, *Laser Chem.*, **16**, 43-51.
712. Ingham, T., D. Bauer, R. Sander, P. J. Crutzen and J. N. Crowley, 1999, *J. Phys. Chem. A*, **103**, 7199-7209.
713. Ingham, T., S. P. Sander and R. R. Friedl, 2005, *Faraday Discuss.*, **130**, 1-22.
714. Inoue, G. and H. Akimoto, 1981, *J. Chem. Phys.*, **84**, 425-433.
715. Inoue, G., K. Izumi and V. A. Lozovsky, 1993, presented at the Third International Conference on Chemical Kinetics, Gaithersburg, MD.
716. Ishikawa, Y., K. Sugawara and S. Sato *Abstracts of Papers*; ACS/CSJ Chemical Congress, 1979; Vol. 1.
717. Iwata, R., R. A. Ferrieri and A. P. Wolf, 1986, *J. Phys. Chem.*, **90**, 6722-6726.
718. Iyer, R. S. and F. S. Rowland, 1980, *Geophys. Res. Lett.*, **7**, 797-800.
719. Izod, T. P. J. and R. P. Wayne, 1968 *Proc. Roy. Soc. A*, **308**, 81-94.
720. Jaffe, S. and F. S. Klein, 1966, *Trans. Faraday Soc.*, **62**, 2150-2157.
721. Jaffe, S. and W. K. Mainquist, 1980, *J. Phys. Chem.*, **84**, 3277.
722. James, G. S. and G. P. Glass, 1970, *J. Chem. Phys.*, **50**, 2268.
723. Japar, S. M., C. H. Wu and H. Niki, 1974, *J. Phys. Chem.*, **78**, 2318.
724. Japar, S. M., C. H. Wu and H. Niki, 1976, *J. Phys. Chem.*, **80**, 2057.
725. Jaramillo, V. I., S. Gougeon, S. Le Picard, A. Canosa, M. Smith and B. Rowe, 2002, *Int. J. Chem. Kinet.*, **34**, 339-344.
726. Jayanty, R. K. M., R. Simonaitis and J. Heicklen, 1976, *J. Phys. Chem.*, **80**, 443.
727. Jayanty, R. K. M., R. Simonaitis and J. Heicklen, 1976, *J. Photochem.*, **5**, 217-224.
728. Jayne, J. T., U. Poschl, Y. Chen, D. Dai, L. T. Molina, D. R. Worsnop, C. E. Kolb and M. J. Molina, 1997, *J. Phys. Chem. A*, **101**, 10,000-10,011.
729. Jefferson, A., J. M. Nicovich and P. H. Wine, 1994, *J. Phys. Chem.*, **98**, 7128-7135.
730. Jemi-Alade, A. A. and B. A. Thrush, 1990, *J. Chem. Soc. Faraday Trans. 2*, **86**, 3355-3363.
731. Jenkin, M. E., K. C. Clemitshaw and R. A. Cox, 1984, *J. Chem. Soc. Faraday Trans. 2*, **80**, 1633-1641.

732. Jenkin, M. E. and R. A. Cox, 1985, *J. Phys. Chem.*, **89**, 192-199.
733. Jenkin, M. E. and R. A. Cox, 1987, *Chem. Phys. Lett.*, **137**, 548-552.
734. Jenkin, M. E., R. A. Cox, M. Emrich and G. K. Moortgat, 1993, *J. Chem. Soc. Faraday Trans.*, **89**, 2983-2991.
735. Jenkin, M. E., R. A. Cox and G. D. Hayman, 1991, *Chem. Phys. Lett.*, **177**, 272-278.
736. Jenkin, M. E., R. A. Cox, A. Mellouki, G. Le Bras and G. Poulet, 1990, *J. Phys. Chem.*, **94**, 2927-2934.
737. Jensen, N. R., D. R. Hanson and C. J. Howard, 1994, *J. Phys. Chem.*, **98**, 8574-8579.
738. Jensen, N. R., J. Hjorth, C. Lohse, H. Skov and G. Restelli, 1991, *Atmos. Environ.*, **24A**, 1897-1904.
739. Jensen, N. R., J. Hjorth, C. Lohse, H. Skov and G. Restelli, 1992, *J. Atmos. Chem.*, **14**, 95-108.
740. Jeong, K. M., K. J. Hsu, J. B. Jeffries and F. Kaufman, 1984, *J. Phys. Chem.*, **88**, 1222-1226.
741. Jeong, K. M. and F. Kaufman, 1979, *Geophys. Res. Lett.*, **6**, 757-759.
742. Jeong, K. M. and F. Kaufman, 1982, *J. Phys. Chem.*, **86**, 1808-1815.
743. Jeoung, S. C., K. Y. Choo and S. W. Benson, 1991, *J. Phys. Chem.*, **95**, 7282-7290.
744. Jiang, Z., P. H. Taylor and B. Dellinger, 1992, *J. Phys. Chem.*, **96**, 8961-8964.
745. Jiang, Z., P. H. Taylor and B. Dellinger, 1993, *J. Phys. Chem.*, **97**, 5050-5053.
746. Jimenez, E., M. K. Gilles and A. R. Ravishankara, 2003, *J. Photochem. Photobiol. A: Chem.*, **157**, 237-245.
747. Johnston, H. S., E. D. Morris, Jr. and J. Van den Bogaerde, 1969, *J. Am. Chem. Soc.*, **91**, 7712-7727.
748. Johnston, H. S. and Y.-S. Tao, 1951, *J. Am. Chem. Soc.*, **73**, 2948.
749. Jolly, G. S., D. J. McKenney, D. L. Singleton, G. Paraskevopoulos and A. R. Bossard, 1986, *J. Phys. Chem.*, **90**, 6557-6562.
750. Jones, B. M. R., J. P. Burrows, R. A. Cox and S. A. Penkett, 1982, *Chem. Phys. Lett.*, **88**, 372-376.
751. Jourdain, J. L., G. Le Bras and J. Combourieu, 1978, *J. Chim. Phys.*, **75**, 318-323.
752. Jourdain, J. L., G. Le Bras and J. Combourieu, 1979, *Int. J. Chem. Kinet.*, **11**, 569-577.
753. Jourdain, J. L., G. Le Bras and J. Combourieu, 1981, *Chem. Phys. Lett.*, **78**, 483.
754. Jourdain, J. L., G. Poulet, J. Barassin, G. Le Bras and J. Combourieu, 1977, *Pollut. Atmos.*, **75**, 256-259.
755. Jungkamp, T. P., A. Kukui and R. N. Schindler, 1995, *Ber. Bunsenges. Phys. Chem.*, **99**, 1057-1066.
756. Kaiser, E. W., 1993, *Int. J. Chem. Kinet.*, **25**, 667-680.
757. Kaiser, E. W. and S. M. Japar, 1977, *Chem. Phys. Lett.*, **52**, 121.
758. Kaiser, E. W. and S. M. Japar, 1978, *Chem. Phys. Lett.*, **54**, 265.
759. Kaiser, E. W., I. M. Lorkovic and T. J. Wallington, 1990, *J. Phys. Chem.*, **94**, 3352-3354.
760. Kaiser, E. W., L. Rimai, E. Schwab and E. C. Lim, 1992, *J. Phys. Chem.*, **96**, 303-306.
761. Kaiser, E. W. and T. J. Wallington, 1994, *J. Phys. Chem.*, **98**, 5679-5685.
762. Kakesu, M., H. Bandow, N. Takenaka, Y. Maeda and N. Washida, 1997, *International Journal of Chemical Kinetics*, **29**, 933-941.
763. Kambanis, K. G., Y. G. Lazarou and P. J. Papagiannakopoulos, 1997, *J. Phys. Chem.*, **101**, 8496-8502.
764. Kan, C. S., J. G. Calvert and J. H. Shaw, 1981, *J. Phys. Chem.*, **85**, 1126-1132.
765. Kan, C. S., R. D. McQuigg, M. R. Whitbeck and J. G. Calvert, 1979, *Int. J. Chem. Kinet.*, **11**, 921-933.
766. Kanno, N., K. Tonokura and M. Koshi, 2006, *Journal of Geophysical Research, D: Atmospheres*, **111**, D20312.
767. Kanno, N., K. Tonokura, A. Tezaki and M. Koshi, 2005, *J. Phys. Chem. A*, **109**, 3153-3158.
768. Karl, M., T. Brauers, H.-P. Dorn, F. Holland, M. Komenda, D. Poppe, F. Rohrer, L. Rupp, A. Schaub and A. Wahner, 2004, *Geophys. Res. Lett.*, **31**, L05117.
769. Kasner, J. H., P. H. Taylor and B. Dellinger, 1990, *J. Phys. Chem.*, **94**, 3250-3253.
770. Kaufman, F., N. J. Gerri and D. A. Pascale, 1956, *J. Chem. Phys.*, **24**, 32-34.
771. Kegley-Owen, C. S., M. K. Gilles, J. B. Burkholder and A. R. Ravishankara, 1999, *J. Phys. Chem. A*, **103**, 5040-5048.
772. Kelly, C., J. Treacy, H. W. Sidebottom and O. J. Nielsen, 1993, *Chem. Phys. Lett.*, **207**, 498-503.

773. Kelly, C. C., W. H. S. Yu and M. H. J. Wijnen, 1970, *Can. J. Chem.*, **48**, 603-606.
774. Kenner, R. D., K. R. Ryan and I. C. Plumb, 1993, *Geophys. Res. Lett.*, **20**, 1571-1574.
775. Kerr, J. A. and D. W. Sheppard, 1981, *Environ. Sci. and Technol.*, **15**, 960.
776. Kerr, J. A. and D. W. Stocker, 1986, *J. Atmos. Chem.*, **4**, 253-262.
777. Keyser, L. F., 1978, *J. Chem. Phys.*, **69**, 214-218.
778. Keyser, L. F., 1979, *J. Phys. Chem.*, **83**, 645-648.
779. Keyser, L. F., 1980, *J. Phys. Chem.*, **84**, 11-14.
780. Keyser, L. F., 1980, *J. Phys. Chem.*, **84**, 1659-1663.
781. Keyser, L. F., 1981, *J. Phys. Chem.*, **85**, 3667-3673.
782. Keyser, L. F., 1982, *J. Phys. Chem.*, **86**, 3439-3446.
783. Keyser, L. F., 1983, *J. Phys. Chem.*, **87**, 837-841.
784. Keyser, L. F., 1984, *J. Phys. Chem.*, **88**, 4750-4758.
785. Keyser, L. F., 1986, *J. Phys. Chem.*, **90**, 2994-3003.
786. Keyser, L. F., 1988, *J. Phys. Chem.*, **92**, 1193-1200.
787. Keyser, L. F., K. Y. Choo and M. T. Leu, 1985, *Int. J. Chem. Kinet.*, **17**, 1169-1185.
788. Khamaganov, V. G., V. X. Bui, S. A. Carl and J. Peeters, 2006, *J. Phys. Chem. A*, **110**, 12852-12859.
789. Khamaganov, V. G. and R. A. Hites, 2001, *J. Phys. Chem. A*, **105**, 815-822.
790. Kinnison, D. J., W. Mengon and J. A. Kerr, 1996, *J. Chem. Soc. Faraday Trans.*, **92**, 369-372.
791. Kircher, C. C. and S. P. Sander, 1984, *J. Phys. Chem.*, **88**, 2082-91.
792. Kirchner, K., D. Helf, P. Ott and S. Vogt, 1990, *Ber. Bunsenges. Phys. Chem.*, **94**, 77-83.
793. Kistiakowsky, G. B. and G. G. Volpi, 1957, *J. Chem. Phys.*, **27**, 1141-1149.
794. Kistiakowsky, G. B. and G. G. Volpi, 1958, *J. Chem. Phys.*, **28**, 665.
795. Kita, D. and D. H. Stedman, 1982, *J. Chem. Soc. Faraday Trans. 2*, **78**, 1249-1259.
796. Klais, O., P. C. Anderson, A. H. Laufer and M. J. Kurylo, 1979, *Chem. Phys. Lett.*, **66**, 598.
797. Klais, O., A. H. Laufer and M. J. Kurylo, 1980, *J. Chem. Phys.*, **73**, 2696-2699.
798. Klawatsch-Carrasco, N., J. F. Doussin and P. Carlier, 2004, *Int. J. Chem. Kinet.*, **36**, 152-156.
799. Kleindienst, T. E., G. W. Harris and J. N. Pitts, Jr., 1982, *Environ. Sci. Technol.*, **16**, 844-846.
800. Kleinermanns, K. and A. C. Luntz, 1981, *J. Phys. Chem.*, **85**, 1966.
801. Kleissas, K. M., J. M. Nicovich and P. H. Wine, 2007, *J. Photochem. Photobiol. A: Chem.*, **187**, 1-9.
802. Klemm, R. B., 1979, *J. Chem. Phys.*, **71**, 1987.
803. Klemm, R. B., E. G. Skolnik and J. V. Michael, 1980, *J. Chem. Phys.*, **72**, 1256.
804. Klemm, R. B. and L. J. Stief, 1974, *J. Chem. Phys.*, **61**, 4900-4906.
805. Klopffer, W., R. Frank, E. G. Kohl and F. Haag, 1986, *Chemiker-Zeitung*, **110**, 57-61.
806. Knickelbein, M. B., K. L. Marsh, O. E. Ulrich and G. E. Busch, 1987, *J. Chem. Phys.*, **87**, 2392-2393.
807. Knight, G. P., T. Beiderhase, F. Helleis, G. K. Moortgat and J. N. Crowley, 2000, *Journal of Physical Chemistry A*, **104**, 1674-1685.
808. Knight, G. P. and J. N. Crowley, 2001, *Phys. Chem. Chem. Phys.*, **3**, 393-401.
809. Knox, J. H., 1955, *Chemistry and Industry*, 1631-1632.
810. Knox, J. H., 1962, *Trans. Faraday Soc.*, **58**, 275.
811. Knox, J. H. and R. L. Nelson, 1959, *Trans. Far. Soc.*, **55**, 937-946.
812. Ko, T. and A. Fontijn, 1991, *J. Phys. Chem.*, **95**, 3984-3987.
813. Koch, S. and G. K. Moortgat, 1990, *Chem. Phys. Lett.*, **173**, 531-536.
814. Kohse-Höinghaus, K. and F. Stuhl, 1980, *J. Chem. Phys.*, **72**, 3720-3726.
815. Kolb, C. E., J. T. Jayne, D. R. Worsnop, M. J. Molina, R. F. Meads and A. A. Viggiano, 1994, *J. Am. Chem. Soc.*, **116**, 10314-10315.
816. Kompa, K. L. and J. Wanner, 1972, *Chem. Phys. Lett.*, **12**, 560.
817. Kono, M. and Y. Matsumi, 2001, *J. Phys. Chem.*, **105**, 65-69.
818. Koppe, S., T. Laurent, P. D. Naik, H.-R. Volpp, J. Wolfrum, T. Arusi-Parpar, I. Bar and S. Rosenwaks, 1993, *Chem. Phys. Lett.*, **214**, 546-552.
819. Kovacs, G., T. Szasz-Vadasz, V. C. Papadimitriou, S. Dobe, T. Berces and F. Marta, 2005, *React. Kinet. Catal. Lett.*, **87**, 129-138.
820. Kowalczyk, J., A. Jowko and M. Symanowicz, 1998, *J. Radioanal. Nucl. Chem.*, **232**, 75-78.
821. Kozlov, S. N., V. L. Orkin, R. E. Huie and M. J. Kurylo, 2003, *J. Phys. Chem. A*, **107**, 1333-1338.

822. Kukui, A., D. Borrisenko, G. Laverdet and G. Le Bras, 2003, *J. Phys. Chem. A*, **107**, 5732-5742.
823. Kukui, A., V. Bossoutrot, G. Laverdet and G. Le Bras, 2000, *J. Phys. Chem. A*, **104**, 935-946.
824. Kukui, A., T. P. W. Jungkamp and R. N. Schindler, 1994, *Ber. Bunsenges. Phys. Chem.*, **98**, 1619-1621.
825. Kukui, A., U. Kirchner, T. Benter and R. N. Schindler, 1996, *Ber. Bunsenges. Phys. Chem.*, **100**, 455-461.
826. Kukui, A., J. Roggenbuck and R. N. Schindler, 1997, *Ber. Bunsenges. Phys. Chem.*, **101**, 281-286.
827. Kukui, A. S., T. P. W. Jungkamp and R. N. Schindler, 1994, *Ber. Bunsenges. Phys. Chem.*, **98**, 1298-1302.
828. Kulcke, A., B. Blackman, W. B. Chapman, I. K. Kim and D. J. Nesbitt, 1998, *J. Phys. Chem. A*, **102**, 1965-1972.
829. Kumaran, S. S., K. P. Lim and J. V. Michael, 1994, *J. Chem. Phys.*, **101**, 9487-9498.
830. Kurasawa, H. and R. Lesclaux, 1979, *Chem. Phys. Lett.*, **66**, 602.
831. Kurasawa, H. and R. Lesclaux. 14th Informal Photochemistry Conference, 1980, Newport Beach, CA,
832. Kurasawa, H. and R. Lesclaux, 1980, *Chem. Phys. Lett.*, **72**, 437.
833. Kurylo, M. J., 1973, *Chem. Phys. Lett.*, **23**, 467-471.
834. Kurylo, M. J., 1977, *Chem. Phys. Lett.*, **49**, 467.
835. Kurylo, M. J., 1978, *Chem. Phys. Lett.*, **58**, 233-237.
836. Kurylo, M. J., 1978, *Chem. Phys. Lett.*, **58**, 238-242.
837. Kurylo, M. J., P. C. Anderson and O. Klais, 1979, *Geophys. Res. Lett.*, **6**, 760-762.
838. Kurylo, M. J. and W. Braun, 1976, *Chem. Phys. Lett.*, **37**, 232-235.
839. Kurylo, M. J., O. Klais and A. H. Laufer, 1981, *J. Phys. Chem.*, **85**, 3674-3678.
840. Kurylo, M. J. and G. L. Knable, 1984, *J. Phys. Chem.*, **88**, 3305-3308.
841. Kurylo, M. J., G. L. Knable and J. L. Murphy, 1983, *Chem. Phys. Lett.*, **95**, 9-12.
842. Kurylo, M. J. and A. H. Laufer, 1979, *J. Chem. Phys.*, **70**, 2032-2033.
843. Kurylo, M. J., J. L. Murphy, G. S. Haller and K. D. Cornett, 1982, *Int. J. Chem. Kinet*, **14**, 1149-1161.
844. Kurylo, M. J., J. L. Murphy and G. L. Knable, 1983, *Chem. Phys. Lett.*, **94**, 281-284.
845. Kurylo, M. J., P. A. Ouellette and A. H. Laufer, 1986, *J. Phys. Chem.*, **90**, 437-440.
846. Lafage, C., J.-F. Pauwels, M. Carlier and P. Devolder, 1987, *J. Chem. Soc. Faraday Trans. 2*, **83**, 731-739.
847. Lamb, J. J., L. T. Molina, C. A. Smith and M. J. Molina, 1983, *J. Phys. Chem.*, **87**, 4467-4470.
848. Lancar, I., G. Laverdet, G. Le Bras and G. Poulet, 1991, *Int. J. Chem. Kinet.*, **23**, 37-45.
849. Lancar, I., G. Le Bras and G. Poulet, 1993, *J. Chim. Physique*, **90**, 1897-1908.
850. Lancar, I., A. Mellouki and G. Poulet, 1991, *Chem. Phys. Lett.*, **177**, 554-558.
851. Langbein, T., H. Sonntag, D. Trapp, A. Hoffmann, W. Malms, E. P. Roth, V. Mors and R. Zellner, 1999, *BRITISH JOURNAL OF ANAESTHESIA*, **82**, 66-73.
852. Langer, S., B. T. McGovney, B. J. Finlayson-Pitts and R. M. Moore, 1996, *Geophys. Res. Lett.*, **23**, 1661-1664.
853. Langford, A. O. and C. B. Moore, 1984, *J. Chem. Phys.*, **80**, 4211-4221.
854. Larichev, M., F. Maguin, G. Le Bras and G. Poulet, 1995, *J. Phys. Chem.*, **99**, 15911-15918.
855. Laszlo, B., R. E. Huie, M. J. Kurylo and A. W. Miziolek, 1997, *J. Geophys. Res.*, **102**, 1523-1532.
856. Laszlo, B., M. J. Kurylo and R. E. Huie, 1995, *J. Phys. Chem.*, **99**, 11701-11707.
857. Laverdet, G., G. Le Bras, A. Mellouki and G. Poulet, 1990, *Chem. Phys. Lett.*, **172**, 430-434.
858. Lawton, S. A., S. E. Novick, H. P. Broida and A. V. Phelps, 1977, *J. Chem. Phys.*, **66**, 1381-1382.
859. Lawton, S. A. and A. V. Phelps, 1978, *J. Chem. Phys.*, **69**, 1055-1068.
860. Lazarou, Y. G., C. Michael and P. Papagiannakopoulos, 1992, *J. Phys. Chem.*, **96**, 1705-1708.
861. Le Bras, G. and J. Combourieu, 1978, *Int. J. Chem. Kinet.*, **10**, 1205-1213.
862. Le Bras, G., R. Foon and J. Combourieu, 1980, *Chem. Phys. Lett.*, **73**, 357-361.
863. Le Calve, S., D. Hitier, G. Le Bras and A. Mellouki, 1998, *J. Phys. Chem. A*, **102**, 4579-4584.
864. Leck, T. J., J. E. Cook and J. W. Birks, 1980, *J. Chem. Phys.*, **72**, 2364-2373.
865. Lee, F. S. C. and F. S. Rowland, 1977, *J. Phys. Chem.*, **81**, 86-87.
866. Lee, J. H., J. V. Michael, W. A. Payne, Jr. and L. J. Stief, 1978, *J. Chem. Phys.*, **69**, 350-353.
867. Lee, J. H., J. V. Michael, W. A. Payne, Jr. and L. J. Stief, 1977, *J. Chem. Soc. Faraday Trans. 1*, **73**, 1530-1536.

868. Lee, J. H., J. V. Michael, W. A. Payne, Jr. and L. J. Stief, 1978, *J. Chem. Phys.*, **69**, 3069-3076.
869. Lee, J. H. and I. N. Tang, 1980, *J. Chem. Phys.*, **72**, 5718-5720.
870. Lee, J. H. and I. N. Tang, 1982, *J. Chem. Phys.*, **77**, 4459-63.
871. Lee, J. H. and I. N. Tang, 1983, *J. Chem. Phys.*, **78**, 6646-6649.
872. Lee, J. H., I. N. Tang and R. B. Klemm, 1980, *J. Chem. Phys.*, **72**, 1793-1796.
873. Lee, J. H., R. B. Timmons and L. J. Stief, 1976, *J. Chem. Phys.*, **64**, 300-305.
874. Lee, L. C. and T. G. Slinger, 1978, *J. Chem. Phys.*, **69**, 4053-4060.
875. Lee, L. C. and T. G. Slinger, 1979, *Geophys. Res. Lett.*, **6**, 165-166.
876. Lee, Y.-P. and C. J. Howard, 1982, *J. Chem. Phys.*, **77**, 756-763.
877. Lee, Y.-P., R. M. Stimpfle, R. A. Perry, J. A. Mucha, K. M. Evenson, D. A. Jennings and C. J. Howard, 1982, *Int. J. Chem. Kinet.*, **14**, 711-732.
878. Lee, Y.-Y., Y.-P. Lee and N. S. Wang, 1994, *J. Chem. Phys.*, **100**, 387-392.
879. Leiss, A., U. Schurath, K. H. Becker and E. H. Fink, 1978, *J. Photochem.*, **8**, 211-214.
880. Lesar, A., M. Hodoscek and J. Senegacnik, 1996, *Journal of Chemical Physics*, **105**, 917-926.
881. Lesclaux, R. and F. Caralp, 1984, *Int. J. Chem. Kinet.*, **16**, 1117-1128.
882. Lesclaux, R. and M. Demissy, 1977, *Nouv. J. Chim.*, **1**, 443.
883. Lesclaux, R., A. M. Dognon and F. Caralp, 1987, *Journal of Photochemistry and Photobiology A*, **A41**, 1-11.
884. Lesclaux, R., P. V. Khe, P. Dezausier and J. C. Soullignac, 1975, *Chem. Phys. Lett.*, **35**, 493.
885. Leu, G.-H. and Y.-P. Lee, 1994, *J. Chin. Chem. Soc.*, **41**, 645-649.
886. Leu, M.-T. and W. B. DeMore, 1976, *Chem. Phys. Lett.*, **41**, 121-124.
887. Leu, M.-T. and W. B. DeMore, 1977, *Chem. Phys. Lett.*, **48**, 317-320.
888. Leu, M.-T. and W. B. DeMore, 1978, *J. Phys. Chem.*, **82**, 2049.
889. Leu, M.-T., S. Hatkeyama and K. J. Hsu, 1989, *J. Phys. Chem.*, **93**, 5778-5784.
890. Leu, M.-T. and C. L. Lin, 1979, *Geophys. Res. Lett.*, **6**, 425-428.
891. Leu, M.-T. and R. H. Smith, 1981, *J. Phys. Chem.*, **85**, 2570-2575.
892. Leu, M.-T. and R. H. Smith, 1982, *J. Phys. Chem.*, **86**, 958-961.
893. Leu, M.-T. and R. H. Smith, 1982, *J. Phys. Chem.*, **86**, 73-81.
894. Leu, M.-T. and Y. L. Yung, 1987, *Geophys. Res. Lett.*, **14**, 949-952.
895. Leu, M. T., 1979, *Chem. Phys. Lett.*, **61**, 275-279.
896. Leu, M. T., 1979, *J. Chem. Phys.*, **70**, 1662-1666.
897. Leu, M. T., 1980, *Chem. Phys. Lett.*, **69**, 37-39.
898. Leu, M. T., 1980, *Geophys. Res. Lett.*, **7**, 173-175.
899. Leu, M. T., 1984, *J. Phys. Chem.*, **88**, 1394-1398.
900. Lewin, A. G., D. Johnson, D. W. Price and G. Marston, 2001, *Phys. Chem. Chem. Phys.*, **3**, 1253-1261.
901. Lewis, R. S., S. P. Sander, S. Wagner and R. T. Watson, 1980, *J. Phys. Chem.*, **84**, 2009-2015.
902. Lewis, R. S. and R. T. Watson, 1980, *J. Phys. Chem.*, **84**, 3495-3503.
903. Li, Q., M. C. Osborne and I. W. M. Smith, 2000, *International Journal of Chemical Kinetics*, **32**, 85-91.
904. Li, S. P., J. Matthews and A. Sinha, 2008, *Science*, **319**, 1657-1660.
905. Li, Z., R. R. Friedl and S. P. Sander, 1995, *J. Phys. Chem.*, **99**, 13445-13451.
906. Li, Z., R. R. Friedl and S. P. Sander, 1997, *Journal of the Chemical Society, Faraday Transactions*, 2683-2691.
907. Li, Z., G.-R. Jeong, J. C. Hansen, D. A. Good and J. S. Francisco, 2000, *Chemical Physics Letters*, **320**, 70-76.
908. Li, Z. J., G. R. Jeong and E. Person, 2002, *International Journal of Chemical Kinetics*, **34**, 430-437.
909. Li, Z. J., R. D. Wuebbles and N. J. Pylawka, 2002, *Chemical Physics Letters*, **354**, 491-497.
910. Lightfoot, P. D., R. A. Cox, J. N. Crowley, M. Destriau, G. D. Hayman, M. E. Jenkin, G. K. Moortgat and F. Zabel, 1992, *Atmos. Environ.*, **26A**, 1805-1961.
911. Lightfoot, P. D., B. Veyret and R. Lesclaux, 1988, *Chem. Phys. Lett.*, **150**, 120-126.
912. Lightfoot, P. D., B. Veyret and R. Lesclaux, 1990, *J. Phys. Chem.*, **94**, 708-714.
913. Lii, R.-R., R. A. Gorse, Jr., M. C. Sauer, Jr. and S. Gordon, 1980, *J. Phys. Chem.*, **84**, 819-821.
914. Lii, R.-R., M. C. Sauer and S. Gordon, 1980, *J. Phys. Chem.*, **84**, 817-.
915. Lii, R.-R., M. C. Sauer, Jr. and S. Gordon, 1981, *J. Phys. Chem.*, **85**, 2833-2834.

916. Lilenfeld, H. V. and R. J. Richardson, 1977, *J. Chem. Phys.*, **67**, 3991-3997.
917. Lin, C.-L., D. A. Parkes and F. Kaufman, 1970, *J. Chem. Phys.*, **53**, 3896-3900.
918. Lin, C. L., 1982, *Int. J. Chem. Kinet.*, **14**, 593-598.
919. Lin, C. L. and W. B. DeMore, 1973, *J. Photochem.*, **2**, 161-164.
920. Lin, C. L., M. T. Leu and W. B. DeMore, 1978, *J. Phys. Chem.*, **82**, 1772-1777.
921. Lin, Y.-L., N.-S. Wang and Y.-P. Lee, 1985, *Int. J. Chem. Kinet.*, **17**, 1201-1214.
922. Lippmann, H. H., B. Jesser and U. Schurath, 1980, *Int. J. Chem. Kinet.*, **12**, 547-554.
923. Lipson, J. B., T. W. Beiderhase, L. T. Molina, M. J. Molina and M. Olzmann, 1999, *J. Phys. Chem. A*, **103**, 6540-6551.
924. Lipson, J. B., M. J. Elrod, T. W. Beiderhase, L. T. Molina and M. J. Molina, 1997, *J. Chem. Soc. Faraday Trans.*, **93**, 2665-2673.
925. Lissi, E. and J. Heicklen, 1972, *J. Photochem.*, **1**, 39-68.
926. Littlejohn, D. and H. S. Johnston, 1980, *EOS*, **61**, 966.
927. Liu, A., W. A. Mulac and C. D. Jonah, 1989, *J. Phys. Chem.*, **93**, 4092-4094.
928. Liu, R., R. E. Huie and M. J. Kurylo, 1990, *J. Phys. Chem.*, **94**, 3247-3249.
929. Lloyd, A. C., K. R. Darnall, A. M. Winer and J. N. Pitts Jr., 1976, *Chem. Phys. Lett.*, **42**, 205-208.
930. Loewenstein, L. M. and J. G. Anderson, 1984, *J. Phys. Chem.*, **88**, 6277-6286.
931. Loewenstein, L. M. and J. G. Anderson, 1985, *J. Phys. Chem.*, **89**, 5371-5379.
932. Lorenz, K., D. Rhasa, R. Zellner and B. Fritz, 1985, *Ber. Bunsenges. Phys. Chem.*, **89**, 341-342.
933. Lorenzen-Schmidt, H., R. Weller and O. Schrems, 1994, *Ber. Bunsenges. Phys. Chem.*, **98**, 1622-1629.
934. Louge, M. Y. and R. K. Hanson, 1984, Twentieth Symposium (International) on Combustion, 665-672.
935. Louis, F., A. Talhaoui, J.-P. Sawerysyn, M.-T. Rayez and J.-C. Rayez, 1997, *J. Phys. Chem. A*, **101**, 8503-8507.
936. Lovejoy, E. R., D. R. Hanson and L. G. Huey, 1996, *J. Phys. Chem.*, **100**, 19911-19916.
937. Lovejoy, E. R., K. S. Kroeger and A. R. Ravishankara, 1990, *Chem. Phys. Lett.*, **167**, 183-187.
938. Lovejoy, E. R., T. P. Murrells, A. R. Ravishankara and C. J. Howard, 1990, *J. Phys. Chem.*, **94**, 2386-2393.
939. Lovejoy, E. R., A. R. Ravishankara and C. J. Howard, 1994, *Int. J. Chem. Kinet.*, **26**, 551-560.
940. Lovejoy, E. R., N. S. Wang and C. J. Howard, 1987, *J. Phys. Chem.*, **91**, 5749-5755.
941. Lozovsky, V. A., M. A. Ioffe and O. M. Sarkisov, 1984, *Chem. Phys. Lett.*, **110**, 651-654.
942. Lu, E. C. C., R. S. Iyer and F. S. Rowland, 1986, *J. Phys. Chem.*, **90**, 1988-1990.
943. Lu, Y.-J., L. Lee, J.-W. Pan, H. A. Witek and J. J. Lin, 2007, *J. Chem. Phys.*, **127**, 101101.
944. Lu, Y.-J., L. Lee, J.-W. Pan, T. Xie, H. A. Witek and J. J. Lin, 2008, *J. Chem. Phys.*, **128**, 104317.
945. Mack, G. P. R. and B. Thrush, 1973, *J. Chem. Soc. Faraday Trans. 1*, **69**, 208.
946. Mack, G. P. R. and B. Thrush, 1974, *J. Chem. Soc. Faraday Trans. 1*, **70**, 173-186.
947. MacLeod, H., S. M. Aschmann, R. Atkinson, E. C. Tuazon, J. A. Sweetman, A. M. Winer and J. N. Pitts, Jr., 1986, *J. Geophys. Res.*, **91**, 5338-5346.
948. MacLeod, H., C. Balestra, J. L. Jourdain, G. Laverdet and G. Le Bras, 1990, *Int. J. Chem. Kinet.*, **22**, 1167-1176.
949. MacLeod, H., J. L. Jourdain, G. Poulet and G. Le Bras, 1984, *Atmos. Environ.*, **18**, 2621-2626.
950. MacLeod, H., G. Poulet and G. Le Bras, 1983, *J. Chim. Phys.*, **80**, 287-292.
951. Magneron, I., A. Mellouki and G. Le Bras, 2005, *Journal of Physical Chemistry A*, **109**, 4552-4561.
952. Maguin, F., G. Laverdet, G. Le Bras and G. Poulet, 1992, *J. Phys. Chem.*, **96**, 1775-1780.
953. Maguin, F., A. Mellouki, G. Laverdet, G. Poulet and G. Le Bras, 1991, *Int. J. Chem. Kinet.*, **23**, 237-245.
954. Mahmud, K., J. S. Kim and A. Fontijn, 1990, *Journal of Physical Chemistry*, **94**, 2994-2998.
955. Manning, R. and M. J. Kurylo, 1977, *J. Phys. Chem.*, **81**, 291-296.
956. Manning, R. G., W. Braun and M. J. Kurylo, 1976, *J. Chem. Phys.*, **65**, 2609-2615.
957. Manzanares, E. R., M. Suto, L. C. Lee and D. Coffey, 1986, *J. Chem. Phys.*, **85**, 5027-5034.
958. Margitan, J. J., 1983, *J. Phys. Chem.*, **87**, 674-679.
959. Margitan, J. J., 1984, *J. Phys. Chem.*, **88**, 3638-3643.
960. Margitan, J. J., 1984, *J. Phys. Chem.*, **88**, 3314-3318.

961. Margitan, J. J. and R. T. Watson, 1982, *J. Phys. Chem.*, **86**, 3819-3824.
962. Maricq, M. M. and J. J. Szente, 1993, *Chem. Phys. Lett.*, **213**, 449-456.
963. Maricq, M. M. and J. J. Szente, 1994, *J. Phys. Chem.*, **98**, 2078-2082.
964. Maricq, M. M. and J. J. Szente, 1996, *J. Phys. Chem.*, **100**, 12374.
965. Maricq, M. M., J. J. Szente, E. W. Kaiser and J. Shi, 1994, *J. Phys. Chem.*, **98**, 2083-2089.
966. Marinelli, W. J. and H. S. Johnston, 1982, *J. Chem. Phys.*, **77**, 1225-1234.
967. Markert, F. and O. J. Nielsen, 1992, *Chem. Phys. Lett.*, **194**, 123-127.
968. Martens, G. J., M. Godfroid, J. Delvaux and J. Verbeyst, 1976, *Int. J. Chem. Kinet.*, **8**, 153-158.
969. Martin, D., I. Barnes and K. H. Becker, 1987, *Chem. Phys. Lett.*, **140**, 195-199.
970. Martin, D., J. L. Jourdain, G. Laverdet and G. Le Bras, 1987, *Int. J. Chem. Kinet.*, **19**, 503-512.
971. Martin, D., J. L. Jourdain and G. Le Bras, 1985, *Int. J. Chem. Kinet.*, **17**, 1247-1261.
972. Martin, D., J. L. Jourdain and G. Le Bras, 1986, *J. Phys. Chem.*, **90**, 4143-4147.
973. Martin, J.-P. and G. Paraskevopoulos, 1983, *Can. J. Chem.*, **61**, 861-865.
974. Martin, L. R., R. B. Cohen and J. F. Schatz, 1976, *Chem. Phys. Lett.*, **41**, 394-396.
975. Martinez, E., A. Albaladejo, E. Jiminez, A. Notario and A. Aranda, 1999, **308**, 37-44.
976. Martinez, E., A. Aranda, Y. Diaz-de-Mera, D. Rodriguez, M. Reyes Lopez and J. Albaladejo, 2002, *Environ. Sci. Technol.*, **36**, 1226-1230.
977. Martinez, R. I. and J. T. Herron, 1978, *Int. J. Chem. Kinet.*, **10**, 433-452.
978. Mashino, M., Y. Ninomiya, M. Kawasaki, T. J. Wallington and M. D. Hurley, 2000, *J. Phys. Chem. A*, **104**, 7255-7260.
979. Matsumi, Y., S. Nomura, M. Kawasaki and T. Imamura, 1996, *J. Phys. Chem.*, **100**, 176-179.
980. Matsumi, Y., K. Tonokura, Y. Inagaki and M. Kawasaki, 1993, *J. Phys. Chem.*, **97**, 6816-6821.
981. Mauldin, R. L., J. B. Burkholder and A. R. Ravishankara, 1997, *International Journal of Chemical Kinetics*, **29**, 139-147.
982. Mauldin, R. L., III, J. B. Burkholder and A. R. Ravishankara, 1992, *J. Phys. Chem.*, **96**, 2582-2588.
983. Mauldin, R. L., III, A. Wahner and A. R. Ravishankara, 1993, *J. Phys. Chem.*, **97**, 7585-7596.
984. Maurer, T., I. Barnes, and K. H. Becker, 1999, *Int. J. Chem. Kinet.*, **31**, 883-893.
985. McCaulley, J. A., S. M. Anderson, J. B. Jeffries and F. Kaufman, 1985, *Chem Phys. Lett.*, **115**, 180.
986. McCrumb, J. L. and F. Kaufman, 1972, *J. Chem. Phys.*, **57**, 1270-1276.
987. McGivern, W. S., I. Suh, A. D. Clinkenbeard, R. Zhang and S. W. North, 2000, *J. Phys. Chem. A*, **104**, 6609-6616.
988. McIlroy, A. and F. P. Tully, 1993, *J. Phys. Chem.*, **97**, 610-614.
989. McKee, M. L. and P. H. Wine, 2001, *J. Am. Chem. Soc.*, **123**, 2344-2353.
990. McKenzie, A., M. F. R. Mulcahy and J. R. Steven, 1973, *J. Chem. Phys.*, **59**, 3244-3254.
991. McLaren, I. A., N. W. Morris and R. P. Wayne, 1981, *J. Photochem.*, **16**, 311-319.
992. McNeal, R. J. and G. R. Cook, 1967, *J. Chem. Phys.*, **47**, 5385-5389.
993. Medhurst, L. J., J. Fleming and H. H. Nelson, 1977, *Chem. Phys. Lett.*, **266**, 607-611.
994. Meier, U., H. H. Grotheer and T. Just, 1984, *Chem. Phys. Lett.*, **106**, 97-101.
995. Meier, U., H. H. Grotheer, G. Riekert and T. Just, 1985, *Chem. Phys. Lett.*, **115**, 221-225.
996. Meller, R. and G. K. Moortgat, 1995, *J. Photochem. Photobio. A: Chem.*, **86**, 15-25.
997. Mellouki, A., 1998, *J. Chim. Phys.*, **95**, 513-522.
998. Mellouki, A., J. L. Jourdain and G. Le Bras, 1988, *Chem. Phys. Lett.*, **148**, 231-236.
999. Mellouki, A., G. Laverdet, L. Jourdain and G. Poulet, 1989, *Int. J. Chem. Kinet.*, **21**, 1161-1172.
1000. Mellouki, A., G. Le Bras and G. Poulet, 1987, *J. Phys. Chem.*, **91**, 5760-5764.
1001. Mellouki, A., G. Le Bras and G. Poulet, 1988, *J. Phys. Chem.*, **92**, 2229-2234.
1002. Mellouki, A., G. Poulet, G. Le Bras, R. Singer, J. P. Burrows and G. K. Moortgat, 1989, *J. Phys. Chem.*, **93**, 8017-8021.
1003. Mellouki, A. and A. R. Ravishankara, 1994, *Int. J. Chem. Kinet.*, **26**, 355-365.
1004. Mellouki, A., R. K. Talukdar, A. M. R. P. Bopegedera and C. J. Howard, 1993, *Int. J. Chem. Kinet.*, **25**, 25-39.
1005. Mellouki, A., R. K. Talukdar and C. J. Howard, 1994, *J. Geophys. Res.*, **99**, 22949-22954.
1006. Mellouki, A., R. K. Talukdar, A.-M. Schmoltner, T. Gierczak, M. J. Mills, S. Soloman and A. R. Ravishankara, 1992, *Geophys. Res. Lett.*, **19**, 2059-2062.

1007. Mellouki, A., S. Teton, G. Laverdet, A. Quilgars and G. Le Bras, 1994, *Journal de Chimie Physique et de Physico-Chimie Biologique*, **91**, 473-487.
1008. Mellouki, A., S. Teton and G. Le Bras, 1995, *Geophys. Res. Lett.*, **22**, 389-392.
1009. Michael, J. V., J. E. Allen, Jr. and W. D. Brobst, 1981, *J. Phys. Chem.*, **85**, 4109-4117.
1010. Michael, J. V., D. G. Keil and R. B. Klemm, 1985, *J. Chem. Phys.*, **83**, 1630-1636.
1011. Michael, J. V., R. B. Klemm, W. D. Brobst, S. R. Bosco and D. F. Nava, 1985, *J. Phys. Chem.*, **89**, 3335-3337.
1012. Michael, J. V. and J. H. Lee, 1977, *Chem. Phys. Lett.*, **51**, 303-306.
1013. Michael, J. V., J. H. Lee, W. A. Payne and L. J. Stief, 1978, *J. Chem. Phys.*, **68**, 4093-4097.
1014. Michael, J. V., D. F. Nava, W. Brobst, R. P. Borkowski and L. J. Stief, 1982, *J. Phys. Chem.*, **86**, 81-84.
1015. Michael, J. V., D. F. Nava, W. A. Payne, J. H. Lee and L. J. Stief, 1979, *J. Phys. Chem.*, **83**, 2818.
1016. Michael, J. V., D. F. Nava, W. A. Payne and L. J. Stief, 1979, *J. Chem. Phys.*, **70**, 1147.
1017. Michael, J. V., D. F. Nava, W. A. Payne and L. J. Stief, 1979, *J. Chem. Phys.*, **70**, 3652.
1018. Michael, J. V. and W. A. Payne, 1979, *Int. J. Chem. Kinet.*, **11**, 799.
1019. Michael, J. V., D. A. Whytock, J. H. Lee, W. A. Payne and L. J. Stief, 1977, *J. Chem. Phys.*, **67**, 3533.
1020. Michelangeli, D. V., K.-Y. Choo and M. T. Leu, 1988, *Int. J. Chem. Kinet.*, **20**, 915-938.
1021. Miller, J. C. and R. J. Gordon, 1981, *J. Chem. Phys.*, **75**, 5305.
1022. Miziolek, A. W. and M. J. Molina, 1978, *J. Phys. Chem.*, **82**, 1769.
1023. Mogelberg, T. E., O. J. Nielsen, J. Sehested and T. J. Wallington, 1995, *J. Phys. Chem.*, **99**, 13437-13444.
1024. Molina, L. T., M. J. Molina, R. A. Stachnik and R. D. Tom, 1985, *J. Phys. Chem.*, **89**, 3779-3781.
1025. Molina, L. T., J. E. Spencer and M. J. Molina, 1977, *Chem. Phys. Lett.*, **45**, 158-162.
1026. Molina, M. J., L. T. Molina and C. A. Smith, 1984, *Int. J. Chem. Kinet.*, **16**, 1151-1160.
1027. Montgomery, J. A., H. H. Michels and J. S. Francisco, 1994, *Chem. Phys. Lett.*, **220**, 391-396.
1028. Moonen, P. C., J. N. Cape, R. L. Storeton-West and R. McColm, 1998, *J. Atmos. Chem.*, **29**, 299-314.
1029. Moortgat, G. K., B. Veyret and R. Lesclaux, 1989, *J. Phys. Chem.*, **93**, 2362-2368.
1030. Morokuma, K. and C. Muguruma, 1994, *J. Am. Chem. Soc.*, **116**, 10316-10317.
1031. Morris, E. D., Jr. and H. Niki, 1971, *J. Chem. Phys.*, **55**, 1991-1992.
1032. Morris, E. D. and H. Niki, 1974, *J. Phys. Chem.*, **78**, 1337-1338.
1033. Morris, E. D., D. H. Stedman and H. Niki, 1971, *J. Am. Chem. Soc.*, **93**, 3570.
1034. Mors, V., A. Hoffman, W. Malms and R. Zellner, 1996, *Ber. Bunsenges, Phys. Chem.*, **100**, 540-552.
1035. Muller, D. F. and P. L. Houston, 1981, *J. Phys. Chem.*, **85**, 3563-3565.
1036. Munk, J., P. Pagsberg, E. Ratajczak and A. Sillesen, 1986, *J. Phys. Chem.*, **90**, 2752-2757.
1037. Murrells, T. P., E. R. Lovejoy and A. R. Ravishankara, 1990, *J. Phys. Chem.*, **94**, 2381-2386.
1038. Myers, G. H. and R. J. O'Brien, Jr., 1970, *Ann. N.Y. Acad. Sci.*, **171**, 224-225.
1039. Nadochenko, V. A., O. M. Sarkisov and V. I. Vedenev, 1979, *Doklady Akademii Nauk SSSR*, **244**, 152.
1040. Nagase, S., S. Hashimoto and H. Akimoto, 1988, *J. Phys. Chem.*, **92**, 641-644.
1041. Nakano, Y., S. Enami, S. Nakamichi, S. Aloisio, S. Hashimoto and M. Kawasaki, 2003, *J. Phys. Chem.*, **107**, 6381-6387.
1042. Nakano, Y., T. Ishiwata, S. Aloisio and M. Kawasaki, 2006, *J. Phys. Chem. A*, **110**, 7401-7405.
1043. Nakano, Y., M. Goto, S. Hashimoto, M. Kawasaki, and T. J. Wallington, 2001, *J. Phys. Chem. A*, **105**, 11045-11050.
1044. Nava, D. F., S. R. Bosco and L. J. Stief, 1983, *J. Chem. Phys.*, **78**, 2443-2448.
1045. Nava, D. F., W. D. Brobst and L. J. Stief, 1985, *J. Phys. Chem.*, **89**, 4703-4707.
1046. Nava, D. F., J. V. Michael and L. J. Stief, 1981, *J. Phys. Chem.*, **85**, 1896-1899.
1047. Neeb, P. and G. K. Moorgat, 1999, *J. Phys. Chem. A*, **103**, 9003-9012.
1048. Nelson, D. D., Jr., M. S. Zahniser and C. E. Kolb, 1993, *Geophys. Res. Lett.*, **20**, 197-200.
1049. Nelson, D. D., Jr., J. C. Wormhoudt, M. S. Zahniser, C. E. Kolb, M. K. W. Ko and D. K. Weisenstein, 1997, *J. Phys. Chem. A*, **101**, 4987-4990.
1050. Nelson, D. D., Jr. and M. S. Zahniser, 1994, *J. Phys. Chem.*, **98**, 2101-2104.
1051. Nelson, D. D., Jr., M. S. Zahniser and C. E. Kolb, 1992, *J. Phys. Chem.*, **96**, 249-253.

1052. Nelson, D. D., M. S. Zahniser, C. E. Kolb and H. Magid, 1995, *J. Phys. Chem.*, **99**, 16301-16306.
1053. Nelson, H. H. and H. S. Johnston, 1981, *J. Phys. Chem.*, **85**, 3891-3896.
1054. Nelson, L., O. Rattigan, R. Neavyn, H. Sidebottom, J. Treacy and O. J. Nielsen, 1990, *Int. J. Chem. Kinet.*, **22**, 1111-1126.
1055. Nelson, L., I. Shanahan, H. W. Sidebottom, J. Treacy and O. J. Nielsen, 1990, *Int. J. Chem. Kinet.*, **22**, 577-590.
1056. Nesbitt, D. J. and S. R. Leone, 1980, *J. Chem. Phys.*, **72**, 1722-1732.
1057. Nesbitt, D. J. and S. R. Leone, 1981, *J. Chem. Phys.*, **75**, 4949-4959.
1058. Nesbitt, F. L., J. F. Gleason and L. J. Stief, 1999, *J. Phys. Chem. A*, **103**, 3038-3043.
1059. Nesbitt, F. L., P. S. Monks, W. A. Payne, L. J. Stief and R. Toumi, 1995, *Geophys. Res. Lett.*, **22**, 827-830.
1060. Nesbitt, F. L., D. F. Nava, W. A. Payne and L. J. Stief, 1987, *J. Phys. Chem.*, **91**, 5337-5340.
1061. Nesbitt, F. L., W. A. Payne and L. J. Stief, 1988, *J. Phys. Chem.*, **92**, 4030-4032.
1062. Nicholas, J. E. and R. G. W. Norrish, 1968, *Proc. Roy. Soc. A*, **307**, 391.
1063. Nickolaissen, S. L., R. R. Friedl and S. P. Sander, 1994, *J. Phys. Chem.*, **98**, 155-169.
1064. Nickolaissen, S. L., C. M. Roehl, L. K. Blakeley, R. R. Friedl, J. S. Francisco, R. F. Liu and S. P. Sander, 2000, *J. Phys. Chem. A*, **104**, 308-319.
1065. Nickolaissen, S. L., D. W. Veney and H. E. Cartland, 1994, *J. Chem. Phys.*, **100**, 4925-4931.
1066. Nicovich, J. M., K. D. Kreutter, C. A. van Dijk and P. H. Wine, 1992, *J. Phys. Chem.*, **96**, 2518-2528.
1067. Nicovich, J. M., K. D. Kreutter and P. H. Wine, 1990, *Int. J. Chem. Kinet.*, **22**, 399-414.
1068. Nicovich, J. M., S. Parthasarathy, F. D. Pope, A. T. Pegus, M. L. McKee and P. H. Wine, 2006, *J. Phys. Chem. A*, **110**, 6874-6885.
1069. Nicovich, J. M., C. J. Shackelford and P. H. Wine, 1990, *J. Phys. Chem.*, **94**, 2896-2903.
1070. Nicovich, J. M., S. Wang and P. H. Wine, 1995, *Int. J. Chem. Kinet.*, **27**, 359-368.
1071. Nicovich, J. M. and P. H. Wine, 1987, *J. Phys. Chem.*, **91**, 5118-5123.
1072. Nicovich, J. M. and P. H. Wine, 1990, *Int. J. Chem. Kinet.*, **22**, 379-397.
1073. Nicovich, J. M., P. H. Wine and A. R. Ravishankara, 1988, *J. Chem. Phys.*, **89**, 5670-5679.
1074. Nielsen, O. J. "Chemical Kinetics in the Gas Phase Pulse Radiolysis of Hydrogen Sulfide Systems," Riso-M-2216, Riso National Laboratory 1979
1075. Nielsen, O. J., 1991, *Chem. Phys. Lett.*, **187**, 286-290.
1076. Nielsen, O. J., T. Ellermann, E. Bartkiewicz, T. J. Wallington and M. D. Hurley, 1992, *Chem. Phys. Lett.*, **192**, 82-88.
1077. Nielsen, O. J., T. Ellermann, J. Sehested and T. J. Wallington, 1992, *J. Phys. Chem.*, **96**, 10875-10879.
1078. Nielsen, O. J., M. S. Javadi, M. P. S. Andersen, M. D. Hurley, T. J. Wallington and R. Singh, 2007, *Chem. Phys. Lett.*, **439**, 18-22.
1079. Nielsen, O. J., J. Munk, G. Locke and T. J. Wallington, 1991, *J. Phys. Chem.*, **95**, 8714-8719.
1080. Nielsen, O. J., J. Munk, P. Pagsberg and A. Sillesen, 1986, *Chem. Phys. Lett.*, **128**, 168-171.
1081. Nielsen, O. J. and J. Sehested, 1993, *Chem. Phys. Lett.*, **213**, 433-441.
1082. Nielsen, O. J., H. W. Sidebottom, M. Donlon and J. Treacy, 1991, *Chem. Phys. Lett.*, **178**, 163-170.
1083. Nielsen, O. J., H. W. Sidebottom, L. Nelson, O. Rattigan, J. J. Treacy and D. J. O'Farrell, 1990, *Int. J. Chem. Kinet.*, **22**, 603-612.
1084. Nielsen, O. J., H. W. Sidebottom, L. Nelson, J. J. Treacy and D. J. O'Farrell, 1989, *Int. J. Chem. Kinet.*, **21**, 1101-1112.
1085. Niki, H., E. E. Daby and B. Weinstock. In *Twelfth Symposium (International) on Combustion*; The Combustion Institute, 1969; pp 277.
1086. Niki, H., P. D. Maker, L. P. Breitenbach and C. M. Savage, 1978, *Chem. Phys. Lett.*, **57**, 596.
1087. Niki, H., P. D. Maker, C. M. Savage and L. P. Breitenbach, 1978, *J. Phys. Chem.*, **82**, 132.
1088. Niki, H., P. D. Maker, C. M. Savage and L. P. Breitenbach, 1980, *Int. J. Chem. Kinet.*, **12**, 1001-1012.
1089. Niki, H., P. D. Maker, C. M. Savage and L. P. Breitenbach, 1980, *Chem. Phys. Lett.*, **73**, 43-46.
1090. Niki, H., P. D. Maker, C. M. Savage and L. P. Breitenbach, 1981, *J. Phys. Chem.*, **85**, 877.
1091. Niki, H., P. D. Maker, C. M. Savage and L. P. Breitenbach, 1982, *J. Phys. Chem.*, **86**, 3825.
1092. Niki, H., P. D. Maker, C. M. Savage and L. P. Breitenbach, 1983, *J. Phys. Chem.*, **87**, 2190-2193.

1093. Niki, H., P. D. Maker, C. M. Savage and L. P. Breitenbach, 1984, *J. Phys. Chem.*, **88**, 2116-2119.
1094. Niki, H., P. D. Maker, C. M. Savage and L. P. Breitenbach, 1984, *J. Phys. Chem.*, **88**, 5342-5344.
1095. Niki, H., P. D. Maker, C. M. Savage and M. D. Hurley, 1987, *J. Phys. Chem.*, **91**, 2174-2178.
1096. Ninomiya, Y., S. Hashimoto, M. Kawasaki and T. J. Wallington, 2000, *International Journal of Chemical Kinetics*, **32**, 125-130.
1097. Ninomiya, Y., M. Kawasaki, A. Guschin, L. T. Molina, M. J. Molina and T. J. Wallington, 2000, *Environ. Sci. Technol.*, **34**, 2973-2978.
1098. Nip, W. S., D. L. Singleton and R. J. Cvetanovic, 1981, *J. Am. Chem. Soc.*, **103**, 3526-3530.
1099. Nip, W. S., D. L. Singleton, R. Overend and G. Paraskevopoulos, 1979, *J. Phys. Chem.*, **83**, 2440-2443.
1100. Nishida, S., K. Takahashi, Y. Matsumi, N. Taniguchi and S. Hayashida, 2004, *J. Phys. Chem. A*, **108**, 2451-2456.
1101. Nizkorodov, S. A., W. W. Harper, B. W. Blackmon and D. J. Nesbitt, 2000, *J. Phys. Chem. A*, **104**, 3964-3973.
1102. Nolte, J., J. Grussdorf, F. Temps and H. Wagner, 1993, *Zeitschrift fur Naturforschung A: Journal of Physical Sciences*, **48**, 1234-1238.
1103. Notario, A., G. Le Bras and A. Mellouki, 1997, *Chem. Phys. Lett.*, **281**, 421-425.
1104. Notario, A., A. Mellouki and G. Le Bras, 2000, *Int. J. Chem. Kinet.*, **32**, 62-66.
1105. Noxon, J. F., 1970, *J. Chem. Phys.*, **52**, 1852-1873.
1106. O'Brien, R. J., Jr. and G. H. Myers, 1970, *J. Chem. Phys.*, **53**, 3832-3835.
1107. Ogren, P. J., T. J. Sworski, C. J. Hochenadel and J. M. Cassel, 1982, *J. Phys. Chem.*, **86**, 238-242.
1108. Ogryzlo, E. A., R. Paltenghi and K. D. Bayes, 1981, *Int. J. Chem. Kinet.*, **13**, 667-675.
1109. Oh, S. and J. Andino, 2000, *Atmos. Environ.*, **34**, 2901-2908.
1110. Oh, S. and J. M. Andino, 2001, *Int. J. Chem. Kinet.*, **30**, 839-847.
1111. Ohmori, K., K. Yamasaki and H. Matsui, 1993, *Bull. Chem. Soc. Jpn.*, **66**, 51-56.
1112. Ohta, T., 1983, *J. Phys. Chem.*, **87**, 1209-1213.
1113. Olbregts, J., G. Brasseur and E. J. Arijs, 1984, *J. Photochem.*, **24**, 315-322.
1114. Olsson, B., M. Hallquist, E. Ljungstrom and J. Davidsson, 1997, *Int. J. Chem. Kinet.*, **29**, 195.
1115. Ongstad, A. P. and J. W. Birks, 1984, *J. Chem. Phys.*, **81**, 3922-3930.
1116. Ongstad, A. P. and J. W. Birks, 1986, *J. Chem. Phys.*, **85**, 3359-3368.
1117. Orkin, V. L., R. E. Huie and M. J. Kurylo, 1996, *J. Phys. Chem.*, **100**, 8907-8912.
1118. Orkin, V. L., R. E. Huie and M. J. Kurylo, 1997, *J. Phys. Chem. A*, **101**, 9118-9124.
1119. Orkin, V. L. and V. G. Khamaganov, 1993, *J. Atmos. Chem.*, **16**, 157-167.
1120. Orkin, V. L. and V. G. Khamaganov, 1993, *J. Atmos. Chem.*, **16**, 169-178.
1121. Orkin, V. L., V. G. Khamaganov, A. G. Guschin, R. E. Huie and M. J. Kurylo. *International Symposium on Gas Kinetics*, 1994, Dublin,
1122. Orkin, V. L., V. G. Khamaganov, A. G. Guschin, R. E. Huie and M. J. Kurylo, 1997, *J. Phys. Chem. A*, **101**, 174-178.
1123. Orkin, V. L., V. G. Khamaganov, L. E. Martynova and M. J. Kurylo, 2010, *J. Phys. Chem. A*.
1124. Orkin, V. L., S. N. Kozlov, G. A. Poskrebyshv, R. E. Huie and M. J. Kurylo, 2006, *J. Phys. Chem. A*, **110**, 6978-6985.
1125. Orkin, V. L., F. Louis, R. E. Huie and M. J. Kurylo, 2002, *J. Phys. Chem. A*, **106**, 10195-10199.
1126. Orkin, V. L., L. E. Martynova and A. N. Ilchev, 2010, *Journal of Physical Chemistry A*, **114**, 5967-5979.
1127. Orkin, V. L., E. Villenave, R. E. Huie and M. J. Kurylo, 1999, *Journal of Physical Chemistry A*, **103**, 9770-9779.
1128. Orlando, J. J., 1999, *Int. J. Chem. Kinet.*, **31**, 515-524.
1129. Orlando, J. J., G. S. Tyndall, E. C. Apel, D. D. Riemer and S. E. Paulson, 2003, *Int. J. Chem. Kinet.*, **35**, 334-353.
1130. Orlando, J. J., G. S. Tyndall, L. Vereecken and J. Peeters, 2000, *J. Phys. Chem. A*, **104**, 11578-11588.
1131. Orlando, J. J., G. S. Tyndall and T. J. Wallington, 1996, *J. Phys. Chem.*, **100**, 7026-7033.
1132. Orlando, J. J., G. S. Tyndall, T. J. Wallington and M. Dill, 1996, *Int. J. Chem. Kinet.*, **28**, 433-442.
1133. Overend, R. and G. Paraskevopoulos, 1978, *J. Phys. Chem.*, **82**, 1329-1333.
1134. Overend, R. P., G. Paraskevopoulos and R. J. Cvetanovic, 1975, *Canad. J. Chem.*, **53**, 3374-3382.
1135. Oyaro, N., S. R. Sellevag and C. J. Nielsen, 2004, *Environ. Sci. Technol.*, **38**, 5567 - 5576.

1136. Oyaro, N., S. R. Sellevag and C. J. Nielsen, 2005, J. Phys. Chem. A, **109**, 337-346.
1137. Pagsberg, P., J. Munk, A. Sillesen and C. Anastasi, 1988, Chem. Phys. Lett., **146**, 375-381.
1138. Pagsberg, P. B., J. Erikson and H. C. Christensen, 1979, J. Phys. Chem., **83**, 582.
1139. Papadimitriou, V. C., R. W. Portmann, D. W. Fahey, J. Muhle, R. F. Weiss and J. B. Burkholder, 2008, J. Phys. Chem. A, **112**, 12657-12666.
1140. Papadimitriou, V. C., R. K. Talukdar, R. W. Portmann, A. R. Ravishankara and J. B. Burkholder, 2008, Phys. Chem. Chem. Phys., **10**, 808 - 820.
1141. Papagni, C., J. Arey and R. Atkinson, 2000, Int. J. Chem. Kinet., **32**, 79-.
1142. Paraskevopoulos, G., D. L. Singleton and R. S. Irwin, 1981, J. Phys. Chem., **85**, 561.
1143. Park, C. R. and J. R. Wiesenfeld, 1991, Chem. Phys. Lett., **186**, 170-176.
1144. Park, J., C. G. Jongsma, R. Zhang and S. W. North, 2004, Journal of Physical Chemistry A, **108**, 10688-10697.
1145. Park, J. and M. C. Lin, 1996, J. Phys. Chem., **100**, 3317-3319.
1146. Parrish, D. D. and D. R. Herschbach, 1973, J. Am. Chem. Soc., **95**, 6133-6134.
1147. Pate, C. T., R. Atkinson and J. N. Pitts, Jr., 1976, J. Environ. Sci. Health, **A11**, 1.
1148. Patrick, R. and D. M. Golden, 1984, J. Phys. Chem., **88**, 491-495.
1149. Paulson, S. E., M. Chung, A. D. Sen and G. Orzechowska, 1998, J. Geophys. Res., **103**, 25533-25539.
1150. Paulson, S. E., J. J. Orlando, G. S. Tyndall and J. G. Calvert, 1995, Int. J. Chem. Kinet., **27**, 997-1008.
1151. Pavanaja, U. B., H. P. Upadhyaya, A. V. Sapre, K. V. S. R. Rao and J. P. Mittal, 1994, J. Chem. Soc. Faraday. Trans., **90**, 825-829.
1152. Payne, W. A., J. Brunning, M. B. Mitchell and L. J. Stief, 1988, Int. J. Chem. Kinet., **20**, 63-74.
1153. Payne, W. A., L. J. Stief and D. D. Davis, 1973, J. Am. Chem. Soc., **95**, 7614-7619.
1154. Peeters, J., J. Vertommen and I. Langhans, 1992, Ber. Bunsenges. Phys. Chem., **96**, 431-436.
1155. Penzhorn, R. D. and C. E. Canosa, 1983, Ber. Bunsenges. Phys. Chem., **87**, 648-654.
1156. Perri, M. J., A. L. Van Wyngarden, K. A. Boering, J. J. Lin and Y. T. Lee, 2003, J. Chem. Phys., **119**, 8213-8216.
1157. Perry, R. A., R. Atkinson and J. N. Pitts, 1977, J. Chem. Phys., **67**, 458-462.
1158. Perry, R. A., R. Atkinson and J. N. Pitts, Jr., 1976, J. Chem. Phys., **64**, 1618.
1159. Perry, R. A., R. Atkinson and J. N. Pitts, Jr., 1976, J. Chem. Phys., **64**, 3237-3239.
1160. Perry, R. A. and C. F. Melius. In *Twentieth Symposium (International) on Combustion*; The Combustion Institute, 1984; pp 639-646.
1161. Persky, A., 1996, J. Phys. Chem., **100**, 689-693.
1162. Petty, J. T., J. A. Harrison and C. B. Moore, 1993, J. Phys. Chem., **97**, 11194-11198.
1163. Phillips, L. F., 1978, Chem. Phys. Lett., **57**, 538-539.
1164. Phillips, L. F. and H. I. Schiff, 1962, J. Chem. Phys., **36**, 1509-1517.
1165. Picquet, B., S. Heroux, A. Chebbi, J. Doussin, R. Durand-Jolibois, A. Monod, H. Loirat and P. Carlier, 1998, Int. J. Chem. Kinet., **30**, 839.
1166. Piety, C. A., R. Solter, J. M. Nicovich, M. L. McKee and P. H. Wine, 1998, Chem. Phys., **231**, 155-169.
1167. Pilgrim, J. S., A. McIlroy and C. A. Taatjes, 1997, J. Phys. Chem. A, **101**, 1873-1880.
1168. Piper, L. G., G. E. Caledonia and J. P. Konnealy, 1981, J. Chem. Phys., **74**, 2888.
1169. Plane, J. M. C. and D. Husain, 1986, J. Chem. Soc. Faraday 2, **82**, 2047-2052.
1170. Plane, J. M. C., C.-F. Nien, M. R. Allen and M. Helmer, 1993, J. Phys. Chem., **97**, 4459-4467.
1171. Plane, J. M. C. and B. Rajasekhar, 1989, J. Phys. Chem., **93**, 3135-3140.
1172. Platz, J., O. J. Nielson, J. Sehested and T. J. Wallington, 1995, J. Phys. Chem., **99**, 6570-6579.
1173. Plum, C. N., E. Sanhueza, R. Atkinson, W. P. L. Carter and J. N. J. Pitts, 1983, Environ. Sci. Technol., **17**, 479-484.
1174. Plumb, I. C. and K. R. Ryan, 1982, Int. J. Chem. Kinet., **14**, 861-874.
1175. Plumb, I. C. and K. R. Ryan, 1982, Chem. Phys. Lett., **92**, 236-238.
1176. Plumb, I. C., K. R. Ryan, J. R. Steven and M. F. R. Mulcahy, 1982, Int. J. Chem. Kinet., **14**, 183.
1177. Pope, F. D., J. M. Nicovich and P. H. Wine, 2002, Int. J. Chem. Kinet., **34**, 156-161.
1178. Posey, J., J. Sherwell and M. Kaufman, 1981, Chem. Phys. Lett., **77**, 476-479.
1179. Poulet, G., I. T. Lancar, G. Laverdet and G. Le Bras, 1990, J. Phys. Chem., **94**, 278-284.
1180. Poulet, G., G. Laverdet, J. L. Jourdain and G. Le Bras, 1984, J. Phys. Chem., **88**, 6259-6263.

1181. Poulet, G., G. Laverdet and G. Le Bras, 1981, *J. Phys. Chem.*, **85**, 1892-1895.
1182. Poulet, G., G. Laverdet and G. Le Bras, 1983, *Chem. Phys. Lett.*, **94**, 129-132.
1183. Poulet, G., G. Laverdet and G. Le Bras, 1984, *J. Chem. Phys.*, **80**, 1922-1928.
1184. Poulet, G., G. Laverdet and G. Le Bras, 1986, *J. Phys. Chem.*, **90**, 159-165.
1185. Poulet, G., G. Le Bras and J. Combourieu, 1974, *J. Chim. Physique*, **71**, 101-106.
1186. Poulet, G., G. Le Bras and J. Combourieu, 1978, *J. Chem. Phys.*, **69**, 767-773.
1187. Poulet, G., G. Le Bras and J. Combourieu, 1980, *Geophys. Res. Lett.*, **7**, 413-414.
1188. Poulet, G., H. Zagogianni and G. Le Bras, 1986, *Int. J. Chem. Kinet.*, **18**, 847-859.
1189. Pritchard, H. O., J. B. Pyke and A. F. Trotman-Dickenson, 1954, *Journal of the American Chemical Society*, **76**, 1201-1202.
1190. Pritchard, H. O., J. B. Pyke and A. F. Trotman-Dickenson, 1955, *Journal of the American Chemical Society*, **77**, 2629-2633.
1191. Qiu, L. X., S.-H. Shi, S. B. Xing and X. G. Chen, 1992, *J. Phys. Chem.*, **96**, 685-689.
1192. Radford, H. E., 1980, *Chem. Phys. Lett.*, **71**, 195.
1193. Radford, H. E., K. M. Evenson and D. A. Jennings, 1981, *Chem. Phys. Lett.*, **78**, 589.
1194. Ragains, M. L. and B. J. Finlayson Pitts, 1997, *J. Phys. Chem. A*, **101**, 1509-1517.
1195. Rahman, M. M., E. Becker, T. Benter and R. N. Schindler, 1988, *Ber. Bunsenges. Phys. Chem.*, **92**, 91-100.
1196. Rahman, M. M., E. Becker, U. Wille and R. N. Schindler, 1992, *Ber. Bunsenges. Phys. Chem.*, **96**, 783-787.
1197. Raja, N., P. K. Arora and J. P. S. Chatha, 1986, *Int. J. Chem. Kinetics*, **18**, 505-512.
1198. Rajakumar, B., J. B. Burkholder, R. W. Portmann and A. R. Ravishankara, 2005, *Phys. Chem. Chem. Phys.*, **7**, 2498-2505.
1199. Rajakumar, B., R. W. Portmann, J. B. Burkholder and A. R. Ravishankara, 2006, *J. Phys. Chem. A*, **110**, 6724 - 6731.
1200. Ramacher, B., J. J. Orlando and G. S. Tyndall, 2000, *International Journal of Chemical Kinetics*, **32**, 460-465.
1201. Ramirez-Anguila, J. M., A. Gonzalez-Lafont and J. M. Lluch, 2009, *Theor. Chem. Acc.*, **123**, 93-103.
1202. Rattigan, O. V., R. A. Cox and R. L. Jones, 1995, *J. Chem. Soc. Faraday Soc. Trans.*, **91**, 4189-4197.
1203. Ravichandran, K., R. Williams and T. R. Fletcher, 1994, *Chem. Phys. Lett.*, **217**, 375-380.
1204. Ravishankara, A. R. and D. D. Davis, 1978, *J. Phys. Chem.*, **82**, 2852-2853.
1205. Ravishankara, A. R., D. D. Davis, G. Smith, G. Tesi and J. Spencer, 1977, *Geophys. Res. Lett.*, **4**, 7.
1206. Ravishankara, A. R., E. J. Dunlea, M. A. Blitz, T. J. Dillon, D. E. Heard, M. J. Pilling, R. S. Strekowski, J. M. Nicovich and P. H. Wine, 2002, *Geophys. Res. Lett.*, **29**, 35.
1207. Ravishankara, A. R., F. L. Eisele and P. H. Wine, 1983, *J. Chem. Phys.*, **78**, 1140-1144.
1208. Ravishankara, A. R., N. M. Kreutter, R. C. Shah and P. H. Wine, 1980, *Geophys. Res. Lett.*, **7**, 861-864.
1209. Ravishankara, A. R., J. M. Nicovich, R. L. Thompson and F. P. Tully, 1981, *J. Phys. Chem.*, **85**, 2498-2503.
1210. Ravishankara, A. R., G. Smith, R. T. Watson and D. D. Davis, 1977, *J. Phys. Chem.*, **81**, 2220-2225.
1211. Ravishankara, A. R., S. Solomon, A. A. Turnipseed and R. F. Warren, 1993, *Science*, **259**, 194-199.
1212. Ravishankara, A. R., A. A. Turnipseed, N. R. Jensen, S. Barone, M. Mills, C. J. Howard and S. Solomon, 1994, *Science*, **263**, 71-75.
1213. Ravishankara, A. R. and P. H. Wine, 1980, *J. Chem. Phys.*, **72**, 25-30.
1214. Ravishankara, A. R., P. H. Wine and A. O. Langford, 1979, *Chem. Phys. Lett.*, **63**, 479-484.
1215. Ravishankara, A. R., P. H. Wine and A. O. Langford, 1979, *J. Chem. Phys.*, **70**, 984-989.
1216. Ravishankara, A. R., P. H. Wine and J. M. Nicovich, 1983, *J. Chem. Phys.*, **78**, 6629-6639.
1217. Ravishankara, A. R., P. H. Wine and J. R. Wells, 1985, *J. Chem. Phys.*, **83**, 447-448.
1218. Ravishankara, A. R., P. H. Wine, J. R. Wells and R. L. Thompson, 1985, *Int. J. Chem. Kinet.*, **17**, 1281-1297.
1219. Ray, A., I. Vassalli, G. Laverdet and G. Le Bras, 1996, *J. Phys. Chem.*, **100**, 8895-8900.

1220. Ray, G. W., L. F. Keyser and R. T. Watson, 1980, J. Phys. Chem., **84**, 1674-1681.
1221. Ray, G. W. and R. T. Watson, 1981, J. Phys. Chem., **85**, 2955-2960.
1222. Ray, G. W. and R. T. Watson, 1981, J. Phys. Chem., **85**, 1673-1676.
1223. Reilly, J. D., J. H. Clark, C. B. Moore and G. C. Pimentel, 1978, J. Chem. Phys., **69**, 4381.
1224. Reimann, B. and F. Kaufman, 1978, J. Chem. Phys., **69**, 2925-2926.
1225. Reiner, T. and F. Arnold, 1993, Geophys. Res. Lett., **20**, 2659-2662.
1226. Reiner, T. and F. Arnold, 1994, J. Chem. Phys., **101**, 7399-7407.
1227. Resende, S. M. and W. B. D. Almeida, 1997, J. Phys. Chem. A, **101**, 9738-9744.
1228. Resende, S. M. and R. Ornellas, 2001, Chem. Phys. Lett., **349**, 123-130.
1229. Rhasa, D. In *Diplomarbeit* Univ. of Gottingen FRG, 1983.
1230. Richardson, R. J., 1975, J. Phys. Chem., **79**, 1153-1158.
1231. Rickard, A. R., D. Johnson, C. D. McGill and G. Marston, 1999, J. Phys. Chem. A, **103**, 7656-7664.
1232. Riffault, V., Y. Bedjanian and G. Le Bras, 2001, International Journal of Chemical Kinetics, **33**, 317-327.
1233. Riffault, V., Y. Bedjanian and G. Le Bras, 2003, Phys. Chem. Chem. Phys., **5**, 2828-2835.
1234. Riffault, V., Y. Bedjanian and G. Le Bras, 2003, J. Phys. Chem. A, **107**, 5404-5411.
1235. Riffault, V., T. Gierczak, J. B. Burkholder and A. R. Ravishankara, 2006, Phys. Chem. Chem. Phys., **8**, 1079 -1085.
1236. Robertshaw, J. S. and I. W. M. Smith, 1980, Int. J. Chem. Kinet. **12**, 729-739.
1237. Robertson, R. and G. P. Smith, 2006, J. Phys. Chem. A, **110**, 6673-6679.
1238. Robertson, R. G. and G. P. Smith, 2002, Chem. Phys. Lett., **358**, 157-162.
1239. Rodebush, W. H. and W. C. Klingelhoefer, Jr., 1933, J. Am. Chem. Soc., **55**, 130.
1240. Roehl, C. M., D. Bauer and G. K. Moortgat, 1996, J. Phys. Chem., **100**, 4038-4047.
1241. Roscoe, J. M., 1982, Int. J. Chem. Kinet., **14**, 471-478.
1242. Roth, P., R. Lohr and H. D. Hermanns, 1980, Ber. Bunsenges. Phys. Chem., **84**, 835-840.
1243. Rowland, F. S., H. Sato, H. Khwaja and S. M. Elliott, 1986, J. Phys. Chem., **90**, 1985 -1988.
1244. Rowley, D. M., M. H. Harwood, R. A. Freshwater and R. L. Jones, 1996, J. Phys. Chem., **100**, 3020-3029.
1245. Rozenshtein, V. B., Y. M. Gershenzon, S. O. Il'in and O. P. Kishkovitch, 1984, Chem. Phys. Lett., **112**, 473-478.
1246. Rust, F. and C. M. Stevens, 1980, Int. J. Chem. Kinet., **12**, 371-377.
1247. Ryan, K. R. and I. C. Plumb, 1984, Int. J. Chem. Kinet., **16**, 591-602.
1248. Saathoff, H. and R. Zellner, 1993, Chem. Phys. Lett., **206**, 349-354.
1249. Sander, S. P., 1984, J. Phys. Chem., **88**, 6018-6021.
1250. Sander, S. P., 1986, J. Phys. Chem., **90**, 2194-2199.
1251. Sander, S. P. and R. R. Friedl, 1989, J. Phys. Chem., **93**, 4764-4771.
1252. Sander, S. P. and C. C. Kircher, 1986, Chem. Phys. Lett., **126**, 149-152.
1253. Sander, S. P., M. Peterson, R. T. Watson and R. Patrick, 1982, J. Phys. Chem., **86**, 1236-1240.
1254. Sander, S. P. and R. T. Watson, 1981, J. Phys. Chem., **85**, 4000.
1255. Sander, S. P. and R. T. Watson, 1981, Chem. Phys. Lett., **77**, 473-475.
1256. Sanders, N. D., J. E. Butler and J. R. McDonald, 1980, J. Chem. Phys., **73**, 5381-5383.
1257. Sanders, N. D., J. E. Butler, L. R. Pasternack and J. R. McDonald, 1980, Chem. Phys., **48**, 203.
1258. Sanhueza, E. and J. Heicklen, 1975, J. Phys. Chem., **79**, 7-11.
1259. Sanhueza, E., R. Simonaitis and J. Heicklen, 1979, Int. J. Chem. Kinet., **11**, 907-914.
1260. Sarkisov, O. M., S. G. Cheskis and E. A. Sviridenkov, 1978, Bull. Acad. Sci. USSR Chem., **Ser. 27**, 2336.
1261. Sarzynski, D. and S. Sztuba, 2002, Int. J. Chem. Kinet., 34, No.12, 651-658 (2002), **34**, 651-658.
1262. Satyapal, S., J. Park, R. Bersohn and B. Katz, 1989, J. Chem. Phys., **91**, 6873-6879.
1263. Saueressig, G., P. Bergamaschi, J. N. Crowley, H. Fischer and G. W. Harris, 1996, Geophys. Res. Lett., **23**, 3619-3622.
1264. Saunders, S. M., K. J. Hughes, M. J. Pilling, D. L. Baulch and P. I. Smurthwaite. "Reactions of hydroxyl radicals with selected hydrocarbons of importance in atmospheric chemistry"; Optical Methods in Atmospheric Chemistry, 1992, Berlin, 88-89.
1265. Sawerysyn, J.-P., C. Lafage, B. Meriaux and A. Tighezza, 1987, J. Chim. Phys., **84**, 1187-1193.

1266. Sawerysyn, J. P., A. Talhaoui, B. Meriaux and P. Devolder, 1992, Chem. Phys. Lett., **198**, 197-199.
1267. Sayin, H. and M. L. McKee, 2005, Journal of Physical Chemistry A, **109**, 4736-4743.
1268. Schiffman, A., D. D. Nelson, M. S. Robinson and D. J. Nesbitt, 1991, J. Phys. Chem., **95**, 2629-2636.
1269. Schindler, R. N. and T. Benter, 1988, Ber. Bunsenges. Phys. Chem., **92**, 558.
1270. Schindler, R. N., J. Dethlefs and M. Schmidt, 1996, Ber. Bunsenges. Phys. Chem., **100**, 1242-1249.
1271. Schlyer, D. F., A. P. Wolf and P. P. Gaspar, 1978, J. Phys. Chem., **82**, 2633-2637.
1272. Schmidt, C. and H. I. Schiff, 1973, Chem. Phys. Lett., **23**, 339-342.
1273. Schmidt, V., G. Y. Zhu, K. H. Becker and E. H. Fink, 1985, Ber. Bunsenges. Phys. Chem., **89**, 321.
1274. Schmoltner, A.-M., P. M. Chu, R. J. Brudzynski and Y. T. Lee, 1989, J. Chem. Phys., **91**, 6926-6936.
1275. Schmoltner, A.-M., R. K. Talukdar, R. F. Warren, A. Mellouki, L. Goldfarb, T. Gierczak, S. A. McKeen and A. R. Ravishankara, 1993, J. Phys. Chem., **97**, 8976-8982.
1276. Schneider, W. F. and T. J. Wallington, 1994, J. Phys. Chem., **98**, 7448-7451.
1277. Schonle, G., M. M. Rahman and R. N. Schindler, 1987, Ber. Bunsenges. Phys. Chem., **91**, 66-75.
1278. Schurath, U. and H.-J. Goede, 1984, Physico-Chemical Behaviour of Atmospheric Pollutants, Proc. 3rd European Symposium, Varese, Italy, 227-239.
1279. Schurath, U., H. H. Lippmann and B. Jesser, 1981, Ber. Bunsenges. Phys. Chem., **85**, 807-813.
1280. Schwab, J. J., W. H. Brune and J. G. Anderson, 1989, J. Phys. Chem., **93**, 1030-1035.
1281. Schwab, J. J., D. W. Toohey, W. H. Brune and J. G. Anderson, 1984, J. Geophys. Res., **89**, 9581-9587.
1282. Scollard, D. J., J. J. Treacy, H. W. Sidebottom, C. Balestra-Garacia, G. Laverdet, G. Le Bras, H. MacLeod and S. Teton, 1993, J. Phys. Chem., **97**, 4683-4688.
1283. Sedlacek, A. J., D. R. Harding, J. Weston, R.E. , T. G. Kreutz and G. W. Flynn, 1989, J. Chem. Phys., **91**, 7550-7555.
1284. Seeley, J. V., J. T. Jayne and M. J. Molina, 1993, International Journal of Chemical Kinetics, **25**, 571-594.
1285. Seeley, J. V., J. T. Jayne and M. J. Molina, 1996, J. Phys. Chem., **100**, 4019-4025.
1286. Seeley, J. V., R. F. Meads, M. J. Elrod and M. J. Molina, 1996, J. Phys. Chem., **100**, 4026-4031.
1287. Sehested, J., L. K. Christensen, O. J. Nielsen, M. Bilde, T. J. Wallington, J. J. Schneider, J. J. Orlando and G. S. Tyndall, 1998, Int. J. Chem. Kinet., **30**, 475-489.
1288. Sehested, J., T. Ellermann, O. J. Nielsen, T. J. Wallington and M. D. Hurley, 1993, Int. J. Chem. Kinet., **25**, 701-717.
1289. Sehested, J. and O. J. Nielsen, 1993, Chem. Phys. Lett., **206**, 369-375.
1290. Sehested, J., O. J. Nielsen and T. J. Wallington, 1993, Chem. Phys. Lett., **213**, 457-464.
1291. Sehested, J., K. Sehested, O. J. Nielsen and T. J. Wallington, 1994, J. Phys. Chem., **98**, 6731-6739.
1292. Sellevag, S. R., C. J. Nielsen, O. A. Sovde, G. Myhre, J. K. Sundet, F. Stordal and I. S. Isaksen, 2004, Atmos. Environ., **38**, 6725-6735.
1293. Selzer, E. A. and K. D. Bayes, 1983, J. Phys. Chem., **87**, 392-394.
1294. Semmes, D. H., A. R. Ravishankara, C. A. Gump-Perkins and P. H. Wine, 1985, Int. J. Chem. Kinet., **17**, 303-313.
1295. Shallcross, D. E., P. Biggs, C. E. CanosaMas, K. C. Clemitshaw, M. G. Harrison, M. R. L. Alanon, J. A. Pyle, A. Vipond and R. P. Wayne, 1997, Journal of the Chemical Society, Faraday Transactions, **93**, 2807-2811.
1296. Shallcross, D. E., S. Vaughn, D. R. Trease, C. Canosa-Mas, M. V. Ghosh, J. M. Dyke and R. P. Wayne, 2006, Atmos. Environ., **40**, 6899-6904.
1297. Sharkey, P. and I. W. M. Smith, 1993, J. Chem. Soc. Faraday Trans., **89**, 631-638.
1298. Shi, J. and J. R. Barker, 1990, Int. J. Chem. Kinetics, **20**, 1283-1301.
1299. Shi, X., D. R. Herschbach, D. R. Worsnop and C. E. Kolb, 1993, J. Phys. Chem., **97**, 2113-2122.
1300. Shibuya, K., T. Ebatu, K. Obi and I. Tanaka, 1977, J. Phys. Chem., **81**, 2292.
1301. Silver, J. A., 1986, J. Chem. Phys., **84**, 4718-4720.
1302. Silver, J. A. and C. E. Kolb, 1980, Chem. Phys. Lett., **75**, 191.

1303. Silver, J. A. and C. E. Kolb, 1982, *J. Phys. Chem.*, **86**, 3240-3246.
1304. Silver, J. A. and C. E. Kolb, 1986, *J. Phys. Chem.*, **90**, 3267-3269.
1305. Silver, J. A. and C. E. Kolb, 1986, *J. Phys. Chem.*, **90**, 3263-3266.
1306. Silver, J. A. and C. E. Kolb, 1987, *J. Phys. Chem.*, **91**, 3713-3714.
1307. Silver, J. A., A. D. Stanton, M. S. Zahniser and C. E. Kolb, 1984, *J. Phys. Chem.*, **88**, 3123-3129.
1308. Simon, F. G., J. P. Burrows, W. Schneider, G. K. Moortgat and P. J. Crutzen, 1989, *J. Phys. Chem.*, **93**, 7807-7813.
1309. Simon, F. G., W. Schneider, G. K. Moortgat and J. P. Burrows, 1990, *Journal of Photochemistry and Photobiology*, **A55**, 1-23.
1310. Simonaitis, R. and J. Heicklen, 1973, *J. Phys. Chem.*, **77**, 1932-1935.
1311. Simonaitis, R. and J. Heicklen, 1975, *J. Phys. Chem.*, **79**, 298.
1312. Simonaitis, R. and J. Heicklen, 1982, *J. Phys. Chem.*, **86**, 3416-3418.
1313. Simonaitis, R. and M. T. Leu, 1985, *Int. J. Chem. Kinet.*, **17**, 293-301.
1314. Sims, I. R., I. W. M. Smith, D. C. Clary, P. Bocherel and B. R. Rowe, 1994, *J. Chem. Phys.*, **101**, 1748-1751.
1315. Singh, J. P. and D. W. Setser, 1985, *J. Phys. Chem.*, **89**, 5353-5358.
1316. Singh, S. and Z. Li, 2007, *J. Phys. Chem. A*, **111**, 11843-11851.
1317. Singleton, D. L. and R. J. Cvetanovic, 1978, *Can. J. Chem.*, **56**, 2934.
1318. Singleton, D. L. and R. J. Cvetanovic, 1981, *Int. J. Chem. Kinet.*, **13**, 945.
1319. Singleton, D. L., R. S. Irwin and R. J. Cvetanovic, 1977, *Can. J. Chem.*, **55**, 3321-3327.
1320. Singleton, D. L., R. S. Irwin, W. S. Nip and R. J. Cvetanovic, 1979, *J. Phys. Chem.*, **83**, 2195-2200.
1321. Singleton, D. L., G. Paraskevopoulos and R. S. Irwin, 1980, *J. Phys. Chem.*, **84**, 2339-2343.
1322. Singleton, D. L., G. Paraskevopoulos and R. S. Irwin, 1982, *J. Phys. Chem.*, **86**, 2605-2609.
1323. Singleton, D. L., G. Paraskevopoulos and R. S. Irwin, 1989, *J. Am. Chem. Soc.*, **111**, 5248-5251.
1324. Singleton, D. L., G. Paraskevopoulos, R. S. Irwin, G. S. Jolly and D. J. McKenney, 1988, *J. Am. Chem. Soc.*, **110**, 7786-7790.
1325. Sinha, A., E. R. Lovejoy and C. J. Howard, 1987, *J. Chem. Phys.*, **87**, 2122-2128.
1326. Sivakumaran, V. and J. N. Crowley, 2003, *Phys. Chem. Chem. Phys.*, **5**, 106-111.
1327. Sivakumaran, V., D. Holscher, T. J. Dillon and J. Crowley, 2003, *Phys. Chem. Chem. Phys.*, **5**, 4821.
1328. Slagle, I. R., F. Baiocchi and D. Gutman, 1978, *J. Phys. Chem.*, **82**, 1333-1336.
1329. Slagle, I. R., J. R. Gilbert and D. Gutman, 1974, *J. Chem. Phys.*, **61**, 704-709.
1330. Slagle, I. R., R. E. Graham, J. R. Gilbert and D. Gutman, 1975, *Chem. Phys. Lett.*, **32**, 184-186.
1331. Slinger, T. G. and G. Black, 1979, *J. Chem. Phys.*, **70**, 3434-3438.
1332. Slinger, T. G., B. J. Wood and G. Black, 1973, *Int. J. Chem. Kinet.*, **5**, 615-620.
1333. Smardzewski, R. R. and M. C. Lin, 1977, *J. Chem. Phys.*, **66**, 3197-3204.
1334. Smedt, F. D., X. V. Bui, T. L. Nguyen, J. Peeters and L. Vereecken, 2005, *J. Phys. Chem. A*, **109**, 2401-2409.
1335. Smith, C. A., L. T. Molina, J. J. Lamb and M. J. Molina, 1984, *Int. J. Chem. Kinet.*, **16**, 41-55.
1336. Smith, I. W. M. and D. W. A. Stewart, 1994, *Journal of the Chemical Society, Faraday Transactions*, **90**, 3221-3227.
1337. Smith, I. W. M. and M. D. Williams, 1986, *J. Chem. Soc. Faraday Trans. 2*, **82**, 1043-1055.
1338. Smith, I. W. M. and R. Zellner, 1974, *J. Chem. Soc. Faraday Trans. 2*, **70**, 1045-1056.
1339. Smith, I. W. M. and R. Zellner, 1975, *Int. J. Chem. Kinet.*, **Symp. 1**, 341.
1340. Smith, R. H., 1978, *Int. J. Chem. Kinet.*, **10**, 519.
1341. Snelling, D. R., 1974, *Can. J. Chem.*, **52**, 257-270.
1342. Soller, R., J. M. Nicovich and P. H. Wine, 2001, *J. Phys. Chem. A*, **105**, 1416-1422.
1343. Sondergaard, R., O. J. Nielsen, M. D. Hurley, T. J. Wallington and R. Singh, 2007, *Chem. Phys. Lett.*, **443**, 199-204.
1344. Sorensen, M., M. D. Hurley, T. J. Wallington, T. S. Dibble and O. J. Nielsen, 2002, *Atmos. Environ.*, **36**, 5947-5952.
1345. Sorensen, S., H. Falbe-Hansen, M. Mangoni, J. Hjorth and N. R. Jensen, 1996, *J. Atmos. Chem.*, **24**, 299-315.
1346. Sorokin, V. I., N. P. Gristan and A. I. Chichinin, 1998, *J. Chem. Phys.*, **108**, 8995-9003.

1347. Spangenberg, T., S. Kohler, B. Hansmann, U. Wachsmuth, B. Abel and M. A. Smith, 2004, J. Phys. Chem. A, **108**, 7527-7534.
1348. Sridharan, U. C., F. S. Klein and F. Kaufman, 1985, J. Chem. Phys., **82**, 592-593.
1349. Sridharan, U. C., L. X. Qiu and F. Kaufman, 1981, J. Phys. Chem., **85**, 3361-3363.
1350. Sridharan, U. C., L. X. Qiu and F. Kaufman, 1982, J. Phys. Chem., **86**, 4569-4574.
1351. Sridharan, U. C., L. X. Qiu and F. Kaufman, 1984, J. Phys. Chem., **88**, 1281-1282.
1352. Sridharan, U. C., B. Reimann and F. Kaufman, 1980, J. Chem. Phys., **73**, 1286-1293.
1353. Stabel, J. R., M. S. Johnson and S. Langer, 2005, Int. J. Chem. Kinet., **37**, 57-65.
1354. Stachnik, R. A. and M. J. Molina, 1987, J. Phys. Chem., **91**, 4603-4606.
1355. Stachnik, R. A., M. J. Molina and L. T. Molina, 1986, J. Phys. Chem., **90**, 2777-2780.
1356. Staricco, E. H., S. E. Sicre and H. J. Schumacher, 1962, Z. Phys. Chem. N.F., **31**, 385.
1357. Steckler, R., G. M. Thurman, J. D. Watts and R. J. Bartlett, 1997, Journal of Chemical Physics, **106**, 3926-3933.
1358. Stedman, D. H. and H. Niki, 1973, Environ. Lett., **4**, 303.
1359. Stedman, D. H. and H. Niki, 1973, J. Phys. Chem., **77**, 2604-2609.
1360. Stedman, D. H., C. H. Wu and H. Niki, 1973, J. Phys. Chem., **77**, 2511.
1361. Steer, R. P., R. A. Ackerman and J. N. Pitts, Jr., 1969, J. Chem. Phys., **51**, 843-844.
1362. Stephens, J. W., C. L. Morter, S. K. Farhat, G. P. Glass and R. F. Curl, 1993, J. Phys. Chem., **97**, 8944-8951.
1363. Stephens, R. D., 1984, J. Phys. Chem., **88**, 3308-3313.
1364. Stevens, P., D. L'Esperance, B. Chuong and G. Martin, 1999, Int. J. Chem. Kinet., **31**, 637-643.
1365. Stevens, P. S. and J. G. Anderson, 1990, Geophys. Res. Lett., **17**, 1287-1290.
1366. Stevens, P. S. and J. G. Anderson, 1992, J. Phys. Chem., **96**, 1708-1718.
1367. Stevens, P. S., W. H. Brune and J. G. Anderson, 1989, J. Phys. Chem., **93**, 4068-4079.
1368. Stickel, R. E., M. Chin, E. P. Daykin, A. J. Hynes, P. H. Wine and T. J. Wallington, 1993, J. Phys. Chem., **97**, 13653-13661.
1369. Stickel, R. E., J. M. Nicovich, S. Wang, Z. Zhao and P. H. Wine, 1992, J. Phys. Chem., **96**, 9875-9883.
1370. Stickel, R. E., Z. Zhao and P. H. Wine, 1993, Chem. Phys. Lett., **212**, 312-318.
1371. Stief, L. J., W. D. Brobst, D. F. Nava, R. P. Borkowski and J. V. Michael, 1982, J. Chem. Soc. Faraday Trans. 2, **78**, 1391-1401.
1372. Stief, L. J., D. F. Nava, W. A. Payne and J. V. Michael, 1980, J. Chem. Phys., **73**, 2254-2258.
1373. Stief, L. J., W. A. Payne, J. H. Lee and J. V. Michael, 1979, J. Chem. Phys., **70**, 5241-5243.
1374. Stimpfle, R., R. Perry and C. J. Howard, 1979, J. Chem. Phys., **71**, 5183-5190.
1375. Stone, D. and D. M. Rowley, 2005, Phys. Chem. Chem. Phys., **7**, 2156 - 2163.
1376. Streit, G. E., C. J. Howard, A. L. Schmeltekopf, J. A. Davidson and H. I. Schiff, 1976, J. Chem. Phys., **65**, 4761-4764.
1377. Streit, G. E., J. S. Wells, F. C. Fehsenfeld and C. J. Howard, 1979, J. Chem. Phys., **70**, 3439-3443.
1378. Strekowski, R. S., J. M. Nicovich and P. H. Wine, 2000, Chem. Phys. Lett., **330**, 354-360.
1379. Strekowski, R. S., J. M. Nicovich and P. H. Wine, 2001, International Journal of Chemical Kinetics, **33**, 262-270.
1380. Strekowski, R. S., J. M. Nicovich and P. H. Wine, 2004, Phys. Chem. Chem. Phys., **6**, 2145-2151.
1381. Stuhl, F., 1973, J. Chem. Phys., **59**, 635.
1382. Stuhl, F., 1974, Ber. Bunsenges. Phys. Chem., **78**, 230-232.
1383. Stuhl, F. and H. Niki, 1970, Chem. Phys. Lett., **7**, 473-474.
1384. Stuhl, F. and H. Niki, 1971, J. Chem. Phys., **55**, 3954-3957.
1385. Stuhl, F. and H. Niki, 1972, J. Chem. Phys., **57**, 3671-3677.
1386. Stuhl, F. and K. H. Welge, 1969, Can. J. Chem., **47**, 1870-1871.
1387. Stutz, J., M. J. Ezell, A. A. Ezell and B. J. Finlayson-Pitts, 1998, J. Phys. Chem. A, **102**, 8510-8519.
1388. Su, F., J. G. Calvert, C. R. Lindley, W. M. Uselman and J. H. Shaw, 1979, J. Phys. Chem., **83**, 912-920.
1389. Su, F., J. G. Calvert and J. H. Shaw, 1979, J. Phys. Chem., **83**, 3185-3191.
1390. Su, F., J. G. Calvert and J. H. Shaw, 1980, J. Phys. Chem., **84**, 239.
1391. Su, F., J. G. Calvert, J. H. Shaw, H. Niki, P. D. Maker, C. M. Savage and L. D. Breitenbach, 1979, Chem. Phys. Lett., **65**, 221-225.

1392. Sugawara, K., Y. Ishikawa and S. Sato, 1980, Bull. Chem. Soc. Japan, **53**, 3159.
1393. Suh, I., W. Lei and R. Zhang, 2001, J. Phys. Chem. A, **105**, 6471-6478.
1394. Suh, I. and R. Zhang, 2000, J. Phys. Chem. A, **104**, 6590-6596.
1395. Sulbaek-Andersen, M. P., D. R. Blake, F. S. Rowland, M. D. Hurley and T. J. Wallington, 2009, Env. Sci. Technol., **43**, 1067-1070.
1396. Sullivan, J. O. and P. Warneck, 1965, J. Phys. Chem., **69**, 1749.
1397. Sverdrup, G. M., C. W. Spicer and G. F. Ward, 1987, Int. J. Chem. Kinet., **19**, 191-205.
1398. Szekely, A., R. K. Hanson and C. Bowman. In *Twentieth Symposium (International) on Combustion*; The Combustion Institute, 1984; pp 647-654.
1399. Szilagyi, I., S. Dobe and T. Berces, 2000, Reaction Kinetics and Catalysis Letters, **70**, 319-324.
1400. Taatjes, C. A., L. K. Christensen, M. D. Hurley and T. J. Wallington, 1999, J. Phys. Chem. A, **103**, 9805.
1401. Tachibana, K. and A. V. Phelps, 1981, J. Chem. Phys., **75**, 3315-3320.
1402. Takacs, G. A. and G. P. Glass, 1973, J. Phys. Chem., **77**, 1948-1951.
1403. Takacs, G. A. and G. P. Glass, 1973, J. Phys. Chem., **77**, 1060.
1404. Takacs, G. A. and G. P. Glass, 1973, J. Phys. Chem., **77**, 1182.
1405. Takacs, G. A. and C. J. Howard, 1984, J. Phys. Chem. , **88**, 2110.
1406. Takacs, G. A. and C. J. Howard, 1986, J. Phys. Chem., **90**, 687-690.
1407. Takahashi, K., Y. Matsumi, T. J. Wallington and M. D. Hurley, 2002, J. Geophys. Res. Atmos., **107**.
1408. Takahashi, K., Y. Takeuchi and Y. Matsumi, 2005, Chemical Physics Letters, **410**, 196-200.
1409. Takahashi, K., R. Wada, Y. Matsumi and M. Kawasaki, 1996, J. Phys. Chem., **100**, 10145-10149.
1410. Taketani, F., T. Nakayama, K. Takahashi, Y. Matsumi, M. D. Hurley, T. J. Wallington, A. Toft and M. P. Andersen, 2005, J. Phys. Chem. A, **109**, 9061 - 9069.
1411. Talcott, C. L., J. W. Ager, III and C. J. Howard, 1986, J. Chem. Phys., **84**, 6161-6169.
1412. Talhaoui, A., B. Louis, B. Meriaux, P. Devolder and J. P. Sawerysyn, 1996, J. Phys. Chem., **100**, 2107-2113.
1413. Talhaoui, A., F. Louis, P. Devolder, B. Meriaux, J. P. Sawerysyn, M. T. Rayez and J. C. Rayez, 1996, J. Phys. Chem., **100**, 13531-13538.
1414. Talukdar, R., A. Mellouki, T. Gierczak, J. B. Burkholder, S. A. McKeen and A. R. Ravishankara, 1991, Science, **252**, 693-695.
1415. Talukdar, R., A. Mellouki, T. Gierczak, J. B. Burkholder, S. A. McKeen and A. R. Ravishankara, 1991, J. Phys. Chem., **95**, 5815-5821.
1416. Talukdar, R. K., J. B. Burkholder, A.-M. Schmoltner, J. M. Roberts, R. Wilson and A. R. Ravishankara, 1995, J. Geophys. Res., **100**, 14163-14173.
1417. Talukdar, R. K., E. J. Dunlea, S. S. Brown, J. S. Daniel and A. R. Ravishankara, 2002, Journal of Physical Chemistry A, **106**, 8461.
1418. Talukdar, R. K., T. Gierczak, L. Goldfarb, Y. Rudich, B. S. Madhava Rao and A. R. Ravishankara, 1996, J. Phys. Chem., **100**, 3037-3043.
1419. Talukdar, R. K., T. Gierczak, D. C. McCabe and A. R. Ravishankara, 2003, J. Phys. Chem. A, **107**, 5021-5032.
1420. Talukdar, R. K., S. C. Herndon, J. B. Burkholder, J. M. Roberts and A. R. Ravishankara, 1997, Journal of the Chemical Society, Faraday Transactions, **93**, 2787-2796.
1421. Talukdar, R. K., A. Mellouki, T. Gierczak, S. Barone, S.-Y. Chiang and A. R. Ravishankara, 1994, Int. J. Chem. Kinet., **26**, 973-990.
1422. Talukdar, R. K., A. Mellouki, A.-M. Schmoltner, T. Watson, S. Montzka and A. R. Ravishankara, 1992, Science, **257**, 227-230.
1423. Talukdar, R. K. and A. R. Ravishankara, 1996, Chem. Phys. Lett., **253**, 177-183.
1424. Taylor, P. H., J. A. D'Angelo, M. C. Martin, J. H. Kasner and B. Dellinger, 1989, Int. J. Chem. Kinet., **21**, 829-846.
1425. Taylor, P. H., Z. Jiang and B. Dellinger, 1993, Int. J. Chem. Kinet., **25**, 9-23.
1426. Taylor, P. H., M. S. Rahman, M. Arif, B. Dellinger and P. Marshall, 1996, Symp. Int. Combust. Proc., **26**, 497-504.
1427. Taylor, P. H., T. Yamada and P. Marshall, 2006, Int. J. Chem. Kinet., **38**, 489-495.
1428. Temps, F. and H. G. Wagner, 1982, Ber. Bunsenges. Phys. Chem., **86**, 119-125.
1429. Temps, F. and H. G. Wagner, 1984, Ber. Bunsenges Phys. Chem., **88**, 415.

1430. Teton, S., A. El-Boudali and A. Mellouki, 1996, *J. Chim. Phys.*, **93**, 274-282.
1431. Thevenet, R., A. Mellouki and G. LeBras, 2000, *Int. J. Chem. Kinet.*, **32**, 676-685.
1432. Thomas, J. W. and F. Kaufman, 1985, *J. Chem. Phys.*, **83**, 2900-2903.
1433. Thomas, R. G. O. and B. A. Thrush, 1975, *J. Chem. Soc. Faraday Trans. 2*, **71**, 664-667.
1434. Thompson, J. E. and A. R. Ravishankara, 1993, *Int. J. Chem. Kinet.*, **25**, 479-487.
1435. Thompson, K. C., C. E. Canosa-Mas and R. P. Wayne, 2002, *Phys. Chem. Chem. Phys.*, **4**, 4133-4139.
1436. Thorn, R. P., J. M. Conkhite, J. M. Nicovich and P. H. Wine, 1995, *J. Chem. Phys.*, **102**, 4131-4142.
1437. Thrush, B. A. and G. S. Tyndall, 1982, *J. Chem. Soc. Faraday 2*, **78**, 1469-1475.
1438. Thrush, B. A. and G. S. Tyndall, 1982, *Chem. Phys. Lett.*, **92**, 232-235.
1439. Thrush, B. A. and J. P. T. Wilkinson, 1979, *Chem. Phys. Lett.*, **66**, 441-443.
1440. Thrush, B. A. and J. P. T. Wilkinson, 1981, *Chem. Phys. Lett.*, **84**, 17-19.
1441. Thrush, B. A. and J. P. T. Wilkinson, 1981, *Chem. Phys. Lett.*, **81**, 1-3.
1442. Tian, Y., Z.-M. Tian, W.-M. Wei, T.-J. He, D.-M. Chen and F.-C. Liu, 2007, *Chem. Phys.*, **335**, 133-140.
1443. Tichenor, L. B., A. El-Sinawi, T. Yamada, P. H. Taylor, J. P. Peng, X. Hu and P. Marshall, 2001, *Chemosphere*, **42**, 571-577.
1444. Tichenor, L. B., J. L. Graham, T. Yamada, P. H. Taylor, J. P. Peng, X. H. Hu and P. Marshall, 2000, *Journal of Physical Chemistry A*, **104**, 1700-1707.
1445. Tiee, J. J., F. B. Wampler, R. C. Oldenborg and W. W. Rice, 1981, *Chem. Phys. Lett.*, **82**, 80-84.
1446. Timonen, R. S., E. Ratajczak and D. Gutman, 1988, *J. Phys. Chem.*, **92**, 651-655.
1447. Toby, F. S., S. Toby and H. E. O'Neal, 1976, *Int. J. Chem. Kinet.*, **8**, 25.
1448. Tokuhashi, K., L. Chen, S. Kutsuna, T. Uchimaru, M. Sugie and A. Sekiya, 2004, *J. Fluor. Chem.*, **125**, 1801 - 1807.
1449. Tokuhashi, K., H. Nagai, A. Takahashi, M. Kaise, S. Kondo, A. Sekiya, M. Takahashi, Y. Gotoh and A. Suga, 1999, *J. Phys. Chem. A*, **103**, 2664-2672.
1450. Tokuhashi, K., A. Takahashi, M. Kaise and S. Kondo, 1999, *J. Geophys. Res.*, **104**, 18681 - 18688.
1451. Tokuhashi, K., A. Takahashi, M. Kaise, S. Kondo, A. Sekiya and E. Fujimoto, 2000, *Chem. Phys. Lett.*, **325**, 189 - 195.
1452. Tokuhashi, K., A. Takahashi, M. Kaise, S. Kondo, A. Sekiya, S. Yamashita and H. Ito, 1999, *Int. J. Chem. Kinet.*, **31**, 846-853.
1453. Tokuhashi, K., A. Takahashi, M. Kaise, S. Kondo, A. Sekiya, S. Yamashita and H. Ito, 2000, *J. Phys. Chem., A*, **104**, 1165-1170.
1454. Tomas, A. E., E. Villenave and R. Lesclaux, 2001, *J. Phys. Chem. A*, **105**, 3505-3514.
1455. Toohey, D. W. Kinetic and Mechanistic Studies of Reactions of Bromine and Chlorine Species Important in the Earth's Stratosphere, Ph. D. Thesis, Harvard University, 1988.
1456. Toohey, D. W. and J. G. Anderson, 1988, *J. Phys. Chem.*, **92**, 1705-1708.
1457. Toohey, D. W., W. H. Brune and J. G. Anderson, 1987, *J. Phys. Chem.*, **91**, 1215-1222.
1458. Toohey, D. W., W. H. Brune and J. G. Anderson, 1988, *Int. J. Chem. Kinet.*, **20**, 131-144.
1459. Trainor, D. W. and C. W. von Rosenberg, Jr., 1974, *J. Chem. Phys.*, **61**, 1010-1015.
1460. Treacy, J., M. El-Hag, D. O'Farrell and H. Sidebottom, 1992, *Ber. Bunsenges. Phys. Chem.*, **96**, 422-427.
1461. Trevor, P. L., G. Black and J. R. Barker, 1982, *J. Phys. Chem.*, **86**, 1661.
1462. Tsalkani, N., A. Mellouki, G. Poulet, G. Toupance and G. Le Bras, 1988, *J. Atmos. Chem.*, **7**, 409-419.
1463. Tschuikow-Roux, E., F. Faraji, S. Paddison, J. Niedzielski and K. Miyokawa, 1988, *J. Phys. Chem.*, **92**, 1488-1495.
1464. Tschuikow-Roux, E., T. Yano and J. Niedzielski, 1985, *J. Chem. Phys.*, **82**, 65-74.
1465. Tuazon, E. C., R. Atkinson, S. M. Aschmann, M. A. Goodman and A. M. Winer, 1988, *Int. J. Chem. Kinet.*, **20**, 241-265.
1466. Tuazon, E. C., R. Atkinson and S. B. Corchnoy, 1992, *Int. J. Chem. Kinet.*, **24**, 639-648.
1467. Tuazon, E. C., R. Atkinson, C. N. Plum, A. M. Winer and J. N. Pitts, 1983, *Geophys. Res. Lett.*, **10**, 953-956.

1468. Tuazon, E. C., W. P. L. Carter, R. Atkinson and J. N. Pitts, Jr., 1983, *Int. J. Chem. Kinet.*, **15**, 619-629.
1469. Tuazon, E. C., E. Sanhueza, R. Atkinson, W. P. L. Carter, A. M. Winer and J. N. Pitts, Jr., 1984, *J. Phys. Chem.*, **88**, 3095-3098.
1470. Tully, F. P., 1983, *Chem. Phys. Lett.*, **96**, 148-153.
1471. Tully, F. P., A. T. Droege, M. L. Koszykowski and C. F. Melius, 1986, *J. Phys. Chem.*, **90**, 691-698.
1472. Tully, F. P. and A. R. Ravishankara, 1980, *J. Phys. Chem.*, **84**, 3126-3130.
1473. Tully, F. P., A. R. Ravishankara and K. Carr, 1983, *Inter. J. Chem. Kinet.*, **15**, 1111-1118.
1474. Turnipseed, A. A., S. B. Barone, N. R. Jensen, D. R. Hanson, C. J. Howard and A. R. Ravishankara, 1995, *J. Phys. Chem.*, **99**, 6000-6009.
1475. Turnipseed, A. A., S. B. Barone and A. R. Ravishankara, 1993, *J. Phys. Chem.*, **97**, 5926-5934.
1476. Turnipseed, A. A., S. B. Barone and A. R. Ravishankara, 1994, *J. Phys. Chem.*, **98**, 4594-4601.
1477. Turnipseed, A. A., S. B. Barone and A. R. Ravishankara, 1996, *J. Phys. Chem.*, **100**, 14703-14713.
1478. Turnipseed, A. A. and J. W. Birks, 1991, *J. Phys. Chem.*, **95**, 6569-6574.
1479. Turnipseed, A. A., J. W. Birks and J. G. Calvert, 1990, *J. Phys. Chem.*, **94**, 7477-7482.
1480. Turnipseed, A. A., J. W. Birks and J. G. Calvert, 1991, *J. Phys. Chem.*, **95**, 4356-4364.
1481. Turnipseed, A. A., M. K. Gilles, J. B. Burkholder and A. R. Ravishankara, 1995, *Chem. Phys. Lett.*, **242**, 427-434.
1482. Turnipseed, A. A., M. K. Gilles, J. B. Burkholder and A. R. Ravishankara, 1997, *J. Phys. Chem.*, **101**, 5517-5525.
1483. Turnipseed, A. A., G. L. Vaghjiani, T. Gierczak, J. E. Thompson and A. R. Ravishankara, 1991, *J. Chem. Phys.*, **95**, 3244-3251.
1484. Tyler, S. C., H. O. Ajie, A. L. Rice and R. J. Cicerone, 2000, *Geophys. Res. Letters*, **27**, 1715-1718.
1485. Tyndall, G. R. S., J. J. Orlando, T. J. Wallington, M. D. Hurley, M. Goto and M. Kawasaki, 2002, *Phys. Chem. Chem. Phys.*, **4**, 2189-2193.
1486. Tyndall, G. S., J. P. Burrows, W. Schneider and G. K. Moortgat, 1986, *Chem. Phys. Lett.*, **130**, 463-466.
1487. Tyndall, G. S., R. A. Cox, C. Granier, R. Lesclaux, G. K. Moortgat, M. J. Pilling, A. R. Ravishankara and T. J. Wallington, 2001, *J. Geophys. Res.*, **106**, 12157-12182.
1488. Tyndall, G. S., C. S. Kegley-Owen, G. S. Orlando and A. Fried, 2002, *J. Phys. Chem. A*, **106**, 1567-1575.
1489. Tyndall, G. S., C. S. KegleyOwen, J. J. Orlando and J. G. Calvert, 1997, *J. Chem. Soc. Faraday Trans.*, **93**, 2675-2682.
1490. Tyndall, G. S., J. J. Orlando and J. G. Calvert, 1995, *Environ. Sci. Technol.*, **29**, 202-206.
1491. Tyndall, G. S., J. J. Orlando, C. A. Cantrell, R. E. Shetter and J. G. Calvert, 1991, *J. Phys. Chem.*, **95**, 4381-4386.
1492. Tyndall, G. S., J. J. Orlando, C. S. Kegley-Owen, T. J. Wallington and M. D. Hurley, 1999, *Int. J. Chem. Kinet.*, **31**, 776-784.
1493. Tyndall, G. S., J. J. Orlando, K. E. Nickerson, C. A. Cantrell and J. G. Calvert, 1991, *J. Geophys. Res.*, **96**, 20761-20768.
1494. Tyndall, G. S., J. J. Orlando, T. J. Wallington, M. Dill and E. W. Kaiser, 1997, *Int. J. Chem. Kinet.*, **29**, 43-55.
1495. Tyndall, G. S., J. J. Orlando, T. J. Wallington, J. Sehested and O. J. Nielsen, 1996, *J. Phys. Chem.*, **100**, 660-668.
1496. Tyndall, G. S. and A. R. Ravishankara, 1989, *J. Phys. Chem.*, **93**, 2426-2435.
1497. Tyndall, G. S. and A. R. Ravishankara, 1989, *J. Phys. Chem.*, **93**, 4707-4710.
1498. Tyndall, G. S. and A. R. Ravishankara, 1991, *Int. J. Chem. Kinet.*, **23**, 483-527.
1499. Tyndall, G. S., T. A. Stafelbach, J. J. Orlando and J. G. Calvert, 1995, *Int. J. Chem. Kin.*, **27**, 1009-1020.
1500. Tyndall, G. S., T. J. Wallington and J. C. Ball, 1998, *J. Phys. Chem. A*, **102**, 2547-2554.
1501. Tyndall, G. S., T. J. Wallington and A. R. Potts, 1991, *Chemical Physics Letters*, **186**, 149-153.
1502. Urbanski, R. E. Stickel and P. H. Wine, 1998, *J. Phys. Chem. A*, **102**, 10522-10529.

1503. Urbanski, S. P., R. E. Stickel, Z. Zhao and P. H. Wine, 1997, *J. Chem. Soc. Faraday Trans.*, **93**, 2813 - 2819.
1504. Urbanski, S. P. and P. H. Wine, 1999, *J. Phys. Chem. A*, **103**, 10935-10944.
1505. Vaghjiani, G. L. and A. R. Ravishankara, 1989, *J. Phys. Chem.*, **93**, 1948.
1506. Vaghjiani, G. L. and A. R. Ravishankara, 1991, *Nature*, **350**, 406-409.
1507. Vaghjiani, G. L., A. R. Ravishankara and N. Cohen, 1989, *J. Phys. Chem.*, **93**, 7833-7837.
1508. Vakhnin, A. B., D. C. McCabe, A. R. Ravishankara and S. R. Leone, 2003, *J. Phys. Chem., A*, **107**, 10642-10647.
1509. Van den Bergh, H. and J. Troe, 1976, *J. Chem. Phys.*, **64**, 736-742.
1510. Vandenberg, S. and J. Peeters, 2003, *J. Photochem. Photobiol. A*, **157**, 269-274.
1511. Vandenberg, S., L. Vereecken and J. Peeters, 2002, *Phys. Chem. Chem. Phys.*, **4**, 461-466.
1512. Vanderzanden, J. W. and J. W. Birks, 1982, *Chem. Phys. Lett.*, **88**, 109-114.
1513. Vandresen, S. and S. M. Resende, 2004, *J. Phys. Chem. A*, **108**, 2284-2289.
1514. Vasvari, G., I. Szilagyi, A. Bencsura, S. Dobe, T. Berces, E. Heron, S. Canneaux and F. Bohr, 2001, *Phys. Chem. Chem. Phys.*, **3**, 551-555.
1515. Verhees, P. W. C. and E. H. Adema, 1985, *J. Atmos. Chem.*, **2**, 387.
1516. Veyret, B. and R. Lesclaux, 1981, *J. Phys. Chem.*, **85**, 1918.
1517. Veyret, B., R. Lesclaux, M.-T. Rayez, J.-C. Rayez, R. A. Cox and G. K. Moortgat, 1989, *J. Phys. Chem.*, **93**, 2368-2374.
1518. Veyret, B., J. C. Rayez and R. Lesclaux, 1982, *J. Phys. Chem.*, **86**, 3424-3430.
1519. Villenave, E. and R. Lesclaux, 1996, *J. Phys. Chem.*, **100**, 14372-14382.
1520. Villenave, E., V. L. Orkin, R. E. Huie and M. J. Kurylo, 1997, *J. Phys. Chem. A*, **101**, 8513-8517.
1521. Vimal, D. and P. S. Stevens, 2006, *J. Phys. Chem. A*, **110**, 11509-11516.
1522. Vinckier, C., M. Schaekers and J. Peeters, 1985, *J. Phys. Chem.*, **89**, 508-512.
1523. Vogt, R. and R. N. Schindler, 1993, *Ber. Bunsenges. Phys. Chem.*, **97**, 819-829.
1524. Vöhringer-Martinez, E., B. Hansmann, H. Hernandez, J. S. Francisco, J. Troe and B. Abel, 2007, *Science*, **315**, 497-501.
1525. Von Ellenrieder, G., E. Castellano and H. J. Schumacher, 1971, *Chem. Phys. Lett.*, **9**, 152-156.
1526. Vranckx, S., J. Peeters and S. Carl, 2008, *Phys. Chem. Chem. Phys.*, **10**, 5714 - 5722.
1527. Vranckx, S., J. Peeters and S. A. Carl, 2008, *Atmospheric Chemistry and Physics*, **8**, 6261-6272.
1528. Vranckx, S., J. Peeters and S. A. Carl, 2010, *Physical Chemistry Chemical Physics*, **12**, 9213-9221.
1529. Wagner, A. F., I. R. Slagle, D. Sarzynski and D. Gutman, 1990, *J. Phys. Chem.*, **94**, 1853-1864.
1530. Wagner, G. and R. Zellner, 1981, *Ber. Bunsenges. Phys. Chem.*, **85**, 1122-1128.
1531. Wagner, H. G., J. Warnatz and C. Zetzsch, 1971, *Anales Assoc. Quim. Argentina*, **59**, 169-177.
1532. Wagner, H. G., U. Welzbacher and R. Zellner, 1976, *Berichte der Bunsen-Gesellschaft Physical Chemistry Chemical Physics*, **80**, 1023-1027.
1533. Wagner, H. G., C. Zetzsch and J. Warnatz, 1972, *Ber. Bunsenges. Phys. Chem.*, **76**, 526.
1534. Wahner, A. and A. R. Ravishankara, 1987, *J. Geophys. Res.*, **92**, 2189-2194.
1535. Walch, S. P., 1993, *J. Chem. Phys.*, **99**, 5295-5300.
1536. Wallington, T. J., J. M. Andino, J. C. Ball and S. M. Japar, 1990, *J. Atmos. Chem.*, **10**, 301-313.
1537. Wallington, T. J., J. M. Andino, A. R. Potts and P. H. Wine, 1991, *Chem. Phys. Lett.*, **176**, 103-108.
1538. Wallington, T. J., R. Atkinson, E. C. Tuazon and S. M. Aschmann, 1986, *Int. J. Chem. Kinet.*, **18**, 837-846.
1539. Wallington, T. J., R. Atkinson and A. M. Winer, 1984, *Geophys. Res. Lett.*, **11**, 861-864.
1540. Wallington, T. J., R. Atkinson, A. M. Winer and J. N. Pitts, Jr., 1986, *J. Phys. Chem.*, **90**, 5393-5396.
1541. Wallington, T. J., R. Atkinson, A. M. Winer and J. N. Pitts Jr., 1986, *J. Phys. Chem.*, **90**, 4640-4644.
1542. Wallington, T. J. and J. C. Ball, 1995, *Chem. Phys. Lett.*, **234**, 187-194.
1543. Wallington, T. J. and J. C. Ball, 1995, *J. Phys. Chem.*, **99**, 3201-3205.
1544. Wallington, T. J., J. C. Ball, O. J. Nielsen and E. Bartkiewicz, 1992, *J. Phys. Chem.*, **96**, 1241-1246.
1545. Wallington, T. J., P. Dagaut and M. J. Kurylo, 1988, *Journal of Photochemistry and Photobiology A*, **42**, 173-185.

1546. Wallington, T. J., P. Dagaut and M. J. Kurylo, 1988, *J. Phys. Chem.*, **92**, 5024-5028.
1547. Wallington, T. J., P. Dagaut and M. J. Kurylo, 1992, *Chem. Rev.*, **92**, 667-710.
1548. Wallington, T. J., T. Ellermann and O. J. Nielsen, 1993, *J. Phys. Chem.*, **97**, 8442-8449.
1549. Wallington, T. J., M. M. Hinman, J. M. Andino, W. O. Siegl and S. M. Japar, 1990, *International Journal of Chemical Kinetics*, **22**, 665-671.
1550. Wallington, T. J. and M. D. Hurley, 1992, *Chem. Phys. Lett.*, **189**, 437-442.
1551. Wallington, T. J. and M. D. Hurley, 1993, *Environ. Sci. Technol.*, **27**, 1448-1452.
1552. Wallington, T. J., M. D. Hurley, O. J. Nielsen and M. P. S. Andersen, 2004, *J. Phys. Chem. A*, **108**, 11333 - 11338.
1553. Wallington, T. J., M. D. Hurley and W. F. Schneider, 1993, *Chem. Phys. Lett.*, **213**, 442-448.
1554. Wallington, T. J., M. D. Hurley, W. F. Schneider, J. Sehested and O. J. Nielsen, 1993, *J. Phys. Chem.*, **97**, 7606-7611.
1555. Wallington, T. J., M. D. Hurley, W. F. Schneider, J. Sehested and O. J. Nielsen, 1994, *Chem. Phys. Lett.*, **218**, 34-42.
1556. Wallington, T. J. and S. M. Japar, 1990, *Chem. Phys. Lett.*, **166**, 495-499.
1557. Wallington, T. J. and M. J. Kurylo, 1987, *Int. J. Chem. Kinet.*, **19**, 1015-1023.
1558. Wallington, T. J. and M. J. Kurylo, 1987, *J. Phys. Chem.*, **91**, 5050-5054.
1559. Wallington, T. J., D. M. Neuman and M. J. Kurylo, 1987, *Int. J. Chem. Kinet.*, **19**, 725-739.
1560. Wallington, T. J., W. F. Schneider, J. Sehested, M. Bilde, J. Platz, O. J. Nielsen, L. K. Christensen, M. J. Molina, L. T. Molina and P. W. Wooldridge, 1997, *J. Phys. Chem. A*, **101**, 8264 - 8274.
1561. Wallington, T. J., L. M. Skewes, W. O. Siegl, C. H. Wu and S. M. Japar, 1988, *Int. J. Chem. Kinet.*, **20**, 867-875.
1562. Walther, C.-D. and H. G. Wagner, 1983, *Ber. Bunsenges. Phys. Chem.*, **87**, 403-409.
1563. Wang, H.-T., Y.-J. Zhang and Y.-J. Mu, 2008, *Acta Phys.-Chim. Sin.*, **24**, 945-950.
1564. Wang, J. J., H. B. Chen, G. P. Glass and R. F. Curl, 2003, *J. Phys. Chem. A*, **107**, 10834-10844.
1565. Wang, J. J. and L. F. Keyser, 1999, *Journal of Physical Chemistry A*, **103**, 7460-7469.
1566. Wang, J. J. and L. F. Keyser, 2001, *J. Phys. Chem. A*, **105**, 10544-10552.
1567. Wang, J. J. and L. F. Keyser, 2001, *J. Phys. Chem. A*, **105**, 6479-6489.
1568. Wang, L., J. Y. Liu, Z. S. Li, X. R. Huang and C. C. Sun, 2003, *Journal of Physical Chemistry A*, **107**, 4921-4928.
1569. Wang, L., J. Y. Liu, Z. S. Li and C. C. Sun, 2004, *Journal of Computational Chemistry*, **25**, 558-564.
1570. Wang, L., J. Y. Liu, Z. S. Li and C. C. Sun, 2005, *Chemical Physics Letters*, **411**, 225-232.
1571. Wang, L. and J. Zhang, 2002, *Chem. Phys. Lett.*, **356**, 490-496.
1572. Wang, N.-S. and Y.-P. Lee, 1985, *Proc. Nat. Sci. Council(Taiwan)*, **9**, 87-94.
1573. Wang, N. S. and C. J. Howard, 1990, *J. Phys. Chem.*, **94**, 8787-8794.
1574. Wang, N. S., E. R. Lovejoy and C. J. Howard, 1987, *J. Phys. Chem.*, **91**, 5743-5749.
1575. Wang, W. C., M. Suto and L. C. Lee, 1984, *J. Chem. Phys.*, **81**, 3122-3126.
1576. Wang, X., Y. G. Jin, M. Suto and L. C. Lee, 1988, *J. Chem. Phys.*, **89**, 4853-4860.
1577. Wang, X., M. Suto and L. C. Lee, 1988, *Journal of Chemical Physics*, **88**, 896-899.
1578. Wantuck, P. J., R. C. Oldenberg, S. L. Baughcum and K. R. Winn, 1987, *J. Phys. Chem.*, **91**, 4653.
1579. Warren, R., T. Gierczak and A. R. Ravishankara, 1991, *Chem. Phys. Lett.*, **183**, 403-409.
1580. Warren, R. F. and A. R. Ravishankara, 1993, *Int. J. Chem. Kinet.*, **25**, 833-844.
1581. Washida, N., 1980, *J. Chem. Phys.*, **73**, 1665.
1582. Washida, N., H. Akimoto and M. Okuda, 1980, *J. Chem. Phys.*, **72**, 5781-5783.
1583. Washida, N., H. Akimoto and M. Okuda, 1980, *Bull. Chem. Soc. Japan*, **53**, 3496-3503.
1584. Washida, N. and K. D. Bayes, 1976, *Int. J. Chem. Kinet.*, **8**, 777.
1585. Washida, N., R. J. Martinez and K. D. Bayes, 1974, *Z. Naturforsch.*, **29A**, 251.
1586. Wategaonkar, S. J. and D. W. Setser, 1989, *J. Chem. Phys.*, **90**, 251-264.
1587. Watson, R. T., G. Machado, B. C. Conaway, S. Wagner and D. D. Davis, 1977, *J. Phys. Chem.*, **81**, 256.
1588. Watson, R. T., G. Machado, S. Fischer and D. D. Davis, 1976, *J. Chem. Phys.*, **65**, 2126-2138.
1589. Watson, R. T., A. R. Ravishankara, G. Machado, S. Wagner and D. D. Davis, 1979, *Int. J. Chem. Kinet.*, **11**, 187-197.

1590. Watson, R. T., S. P. Sander and Y. L. Yung, 1979, J. Phys. Chem., **83**, 2936.
1591. Wayne, R. P. and J. N. Pitts, Jr., 1969, J. Chem. Phys., **50**, 3644-3645.
1592. Wecker, D., R. Johanssen and R. N. Schindler, 1982, Ber. Bunsenges. Phys. Chem., **86**, 532-538.
1593. Wei, C. N. and R. B. Timmons, 1975, J. Chem. Phys., **62**, 3240-3245.
1594. Wennberg, P. O., J. G. Anderson and D. K. Weisenstein, 1994, J. Geophys. Res., **99**, 18839-18846.
1595. West, G. A., R. E. Weston, Jr. and G. W. Flynn, 1978, Chem. Phys. Lett., **56**, 429.
1596. Westenberg, A. A. and N. de Haas, 1969, J. Phys. Chem., **73**, 1181.
1597. Westenberg, A. A. and N. de Haas, 1969, J. Chem. Phys., **50**, 707-709.
1598. Westenberg, A. A. and N. de Haas, 1973, J. Chem. Phys., **58**, 4061-4065.
1599. Westenberg, A. A. and N. de Haas, 1973, J. Chem. Phys., **58**, 4066-4071.
1600. Westenberg, A. A. and N. de Haas, 1973, J. Chem. Phys., **59**, 6685-6686.
1601. Westenberg, A. A. and N. de Haas, 1977, J. Chem. Phys., **66**, 4900.
1602. Westenberg, A. A., N. de Haas and J. M. Roscoe, 1970, J. Phys. Chem., **74**, 3431.
1603. Westenberg, A. A. and N. DeHaas, 1968, J. Chem. Phys., **48**, 4405.
1604. Westenberg, A. A., J. M. Roscoe and N. de Haas, 1970, Chem. Phys. Lett., **7**, 597-599.
1605. Whyte, A. R. and L. F. Phillips, 1983, Chem. Phys. Lett., **102**, 451-454.
1606. Whytock, D. A., J. H. Lee, J. V. Michael, W. A. Payne and L. J. Stief, 1977, J. Chem. Phys., **66**, 2690-2695.
1607. Whytock, D. A., R. B. Timmons, J. H. Lee, J. V. Michael, W. A. Payne and L. J. Stief, 1976, J. Chem. Phys., **65**, 2052-2055.
1608. Wiebe, H. A. and J. Heicklen, 1973, J. Am. Chem. Soc., **95**, 1-7.
1609. Wildt, J., G. Bednarek, E. H. Fink and R. P. Wayne, 1988, Chem. Phys., **122**, 463-470.
1610. Wildt, J., E. H. Fink, P. Biggs and R. P. Wayne, 1989, Chem. Phys., **139**, 401-407.
1611. Wildt, J., E. H. Fink, P. Biggs, R. P. Wayne and A. F. Vilesov, 1992, Chem. Phys., **159**, 127-140.
1612. Wille, U., E. Becker, R. N. Schindler, I. T. Lancar, G. Poulet and G. LeBras, 1991, J. Atmos. Chem., **13**, 183-193.
1613. Williams, M. B., P. Campuzano-Jost, D. Bauer and A. J. Hynes, 2001, Chem. Phys. Lett., **344**, 61-67.
1614. Williams, M. B., P. Campuzano-Jost, B. M. Cossairt, A. J. Hynes and A. J. Pounds, 2007, J. Phys. Chem. A, **111**, 89-104.
1615. Williams, M. B., P. Campuzano-Jost, A. J. Hynes and A. J. Pounds, 2009, Journal of Physical Chemistry A, **113**, 6697-6709.
1616. Wilson, C. and D. M. Hirst, 1997, J. Chem. Soc. Faraday. Trans., **93**, 2831 - 2837.
1617. Wilson, E. W., W. A. Hamilton, H. R. Mount and W. B. DeMore, 2007, J. Phys. Chem. A, **111**, 1610 - 1617.
1618. Wilson, E. W., A. M. Jacoby, S. J. Kukta, L. E. Gilbert and W. B. DeMore, 2003, J. Phys. Chem. A, **107**, 9357 - 9361.
1619. Wilson, E. W., A. A. Sawyer and H. A. Sawyer, 2001, J. Phys. Chem. A, **105**, 1445-1448.
1620. Wilson, W. E., 1967, J. Chem. Phys., **46**, 2017-2018.
1621. Wine, P. H., R. J. Astalos and R. L. Mauldin, III, 1985, J. Phys. Chem., **89**, 2620-2624.
1622. Wine, P. H., W. L. Chameides and A. R. Ravishankara, 1981, Geophys. Res. Lett., **8**, 543-546.
1623. Wine, P. H., N. M. Kreutter, C. A. Gump and A. R. Ravishankara, 1981, J. Phys. Chem., **85**, 2660-2665.
1624. Wine, P. H., J. M. Nicovich and A. R. Ravishankara, 1985, J. Phys. Chem., **89**, 3914-3918.
1625. Wine, P. H., J. M. Nicovich, R. E. Stickel, Z. Zhao, C. J. Shackelford, K. D. Kreutter, E. P. Daykin and S. Wang. In *The Tropospheric Chemistry of Ozone in the Polar Regions*; Springer-Verlag: Berlin, 1993; Vol. I7; pp 385-395.
1626. Wine, P. H., J. M. Nicovich, R. J. Thompson and A. R. Ravishankara, 1983, J. Phys. Chem., **87**, 3948-3954.
1627. Wine, P. H. and A. R. Ravishankara, 1981, Chem. Phys. Lett., **77**, 103-109.
1628. Wine, P. H. and A. R. Ravishankara, 1982, Chem. Phys., **69**, 365-373.
1629. Wine, P. H. and A. R. Ravishankara, 1983, Chem. Phys. Lett., **96**, 129-132.
1630. Wine, P. H., D. H. Semmes and A. R. Ravishankara, 1981, J. Chem. Phys., **75**, 4390-4395.
1631. Wine, P. H., R. C. Shah and A. R. Ravishankara, 1980, J. Phys. Chem., **84**, 2499-2503.
1632. Wine, P. H., R. J. Thompson and D. H. Semmes, 1984, Int. J. Chem. Kinet., **16**, 1623-1636.

1633. Wine, P. H., J. R. Wells and J. M. Nicovich, 1988, J. Phys. Chem., **92**, 2223-2228.
1634. Wine, P. H., J. R. Wells and A. R. Ravishankara, 1986, J. Chem. Phys., **84**, 1349-1354.
1635. Winer, A. M., A. C. Lloyd, K. R. Darnall, R. Atkinson and J. N. Pitts, Jr., 1977, Chem. Phys. Lett., **51**, 221-226.
1636. Winer, A. M., A. C. Lloyd, K. R. Darnall and J. N. Pitts, Jr., 1976, J. Phys. Chem., **80**, 1635-1639.
1637. Winkler, I. C., R. A. Stachnik, J. I. Steinfeld and S. M. Miller, 1986, J. Chem. Phys., **85**, 890.
1638. Wolf, M., D. L. Yang and J. L. Durant, 1994, J. Photochem. Photobiol. A: Chem., **80**, 85-93.
1639. Wollenhaupt, M., S. A. Carl, A. Horowitz and J. N. Crowley, 2000, J. Phys. Chem., **A**, **104**, 2695-2705.
1640. Wong, E. L. and F. R. Belles; NASA TN D-6495 NASA Washington, D. C., 1971.
1641. Wongdontri-Stuper, W., R. K. M. Jayanty, R. Simonaitis and J. Heicklen, 1979, J. Photochem., **10**, 163.
1642. Worsnop, D. R., M. S. Zahniser and C. E. Kolb, 1991, J. Phys. Chem., **95**, 3960-3964.
1643. Worsnop, D. R., M. S. Zahniser and C. E. Kolb, 1992, J. Phys. Chem., **96**, 9088-9088.
1644. Wright, T. G., A. M. Ellis and J. M. Dyke, 1993, J. Chem. Phys., **98**, 2891-2907.
1645. Wu, F. and R. W. Carr, 1992, J. Phys. Chem., **96**, 1743-1748.
1646. Wu, H., Y. Mu, X. Xiang and G. Jiang, 2003, Int. J. Chem. Kinet., **35**, 81-87.
1647. Wurzburg, E. and P. L. Houston, 1980, J. Chem. Phys., **72**, 4811.
1648. Xia, W. S. and M. C. Lin, 2001, Journal of Chemical Physics, **114**, 4522-4532.
1649. Xiang, T., M. L. Torres and W. A. Guillory, 1985, J. Chem. Phys., **83**, 1623-1629.
1650. Xing, S. B., S.-H. Shi and L. X. Qiu, 1992, Int. J. Chem. Kinet., **24**, 1-10.
1651. Xu, Z. F. and M. C. Lin, 2009, Journal of Physical Chemistry A, **113**, 8811-8817.
1652. Xu, Z. F., R. S. Zhu and M. C. Lin, 2003, J. Phys. Chem. A, **107**, 3841-3850.
1653. Yamada, T., A. El-Sinawi, M. Siraj, P. H. Taylor, J. Peng, X. Hu and P. Marshall, 2001, J. Phys. Chem. A, **105**, 7588-7597.
1654. Yamada, T., T. D. Fang, P. H. Taylor and R. J. Berry, 2000, J. Phys. Chem. A, **104**, 5013-5022.
1655. Yamada, T., M. Siraj, P. H. Taylor, J. Peng, X. Hu and P. Marshall, 2001, J. Phys. Chem. A, **105**, 9436-9444.
1656. Yamada, T., P. H. Taylor, A. Goumri and P. Marshall, 2003, J. Chem. Phys., **119**, 10600-10606.
1657. Yano, T. and E. Tschuikow-Roux, 1986, J. Photochem., **32**, 25-37.
1658. Yetter, R. A., H. Rabitz, F. L. Dryer, R. G. Maki and R. B. Klemm, 1989, J. Chem. Phys., **91**, 4088-4097.
1659. Yokelson, R. J., J. B. Burkholder, L. Goldfarb, R. W. Fox, M. K. Gilles and A. R. Ravishankara, 1995, J. Phys. Chem., **99**, 13976-13983.
1660. Yu, W. H. S. and M. H. J. Wijnen, 1970, J. Chem. Phys., **52**, 2736-2739.
1661. Yujing, M. and A. Mellouki, 2001, Chem. Phys. Lett., **333**, 63-68.
1662. Zabarnick, S. and J. Heicklen, 1985, Int. J. Chem. Kinet., **17**, 455-476.
1663. Zabarnick, S., J. W. Fleming and M. C. Lin, 1988, Int. J. Chem. Kinet., **20**, 117-129.
1664. Zabel, F., K. A. Sahetchian and C. Chachaty, 1987, Chem. Phys. Lett., **134**, 433.
1665. Zagogianni, H., A. Mellouki and G. Poulet, 1987, C. R. Acad. Sci. Paris, **Series II** **304**, 573-578.
1666. Zahniser, M. S., B. M. Berquist and F. Kaufman, 1978, Int. J. Chem. Kinet., **10**, 15-29.
1667. Zahniser, M. S., J. Chang and F. Kaufman, 1977, J. Chem. Phys., **67**, 997-1003.
1668. Zahniser, M. S. and C. J. Howard, 1980, J. Chem. Phys., **73**, 1620-1626.
1669. Zahniser, M. S. and F. Kaufman, 1977, J. Chem. Phys., **66**, 3673-3681.
1670. Zahniser, M. S., F. Kaufman and J. G. Anderson, 1974, Chem. Phys. Lett., **27**, 507-510.
1671. Zahniser, M. S., F. Kaufman and J. G. Anderson, 1976, Chem. Phys. Lett., **37**, 226-231.
1672. Zellner, R., 1987, J. Chem. Phys., **84**, 403.
1673. Zellner, R., G. Bednarek, A. Hoffmann, J. P. Kohlmann, V. Mors and H. Saathoff, 1994, Ber. Bunsenges. Phys. Chem., **98**, 141-146.
1674. Zellner, R. and F. Ewig, 1988, J. Phys. Chem., **92**, 2971.
1675. Zellner, R. and W. Steinert, 1981, Chem. Phys. Lett., **81**, 568-572.
1676. Zellner, R., G. Wagner and B. Himme, 1980, J. Phys. Chem., **84**, 3196-3198.
1677. Zetzsch, C. "Rate constants for the reactions of OH with acetone and methylethylketone in the gas phase"; 7th International Symposium on Gas Kinetics, 1982, Goettingen, Germany,

1678. Zetzsch, C. and F. Stuhl. In *Proceedings of the 2nd European Symposium on the Physico-Chemical Behaviour of Atmospheric Pollutants*; D. Reidel Publishing Co.: Dordrecht, Holland, 1982; pp 129-137.
1679. Zhang, D. Q., J. X. Zhong and L. X. Qiu, 1997, *J. Atmos. Chem.*, **27**, 209-215.
1680. Zhang, L. and Q.-Z. Qin, 2000, *J. Mol. Structure (Theochem)*, **531**, 375-379.
1681. Zhang, R., I. Suh, W. Lei, A. D. Clinkenbeard and S. W. North, 2000, *J. Geophys. Res.*, **105**, 24627-24635.
1682. Zhang, Z., R. E. Huie and M. J. Kurylo, 1992, *J. Phys. Chem.*, **96**, 1533-1535.
1683. Zhang, Z., R. Liu, R. E. Huie and M. J. Kurylo, 1991, *Geophys. Res. Lett.*, **18**, 5-7.
1684. Zhang, Z., R. F. Liu, R. E. Huie and M. J. Kurylo, 1991, *J. Phys. Chem.*, **95**, 194-196.
1685. Zhang, Z., S. Padmaja, R. D. Saini, R. E. Huie and M. J. Kurylo, 1994, *J. Phys. Chem.*, **98**, 4312-4315.
1686. Zhang, Z., R. D. Saini, M. J. Kurylo and R. E. Huie, 1992, *Chem. Phys. Lett.*, **200**, 230-234.
1687. Zhang, Z., R. D. Saini, M. J. Kurylo and R. E. Huie, 1992, *Geophys. Res. Lett.*, **19**, 2413-2416.
1688. Zhang, Z., R. D. Saini, M. J. Kurylo and R. E. Huie, 1992, *J. Phys. Chem.*, **96**, 9301-9304.
1689. Zhao, Z., P. L. Laine, J. M. Nicovich and P. H. Wine, 2010, *Proc. Nat. Acad. Sci.*, **107**, 6610-6615.
1690. Zhao, Z., R. E. Stickel and P. H. Wine, 1996, *Chem. Phys. Lett.*, **251**, 59-66.
1691. Zhitneva, G. P. and S. Y. Pshezhetskii, 1978, *Kinetika i Kataliz*, **19**, 296.
1692. Zhu, L., R. K. Talukdar, J. B. Burkholder and A. R. Ravishankara, 2008, *Int. J. Chem. Kinet.*, **40**, 635-646.
1693. Zipf, E. C., 1980, *Nature (London)*, **287**, 523-525.

SECTION 2. TERMOLICULAR REACTIONS

Table of Contents

SECTION 2. TERMOLICULAR REACTIONS	2-1
2.1 Introduction	2-1
2.2 Low-Pressure-Limiting Rate Constant, $k_o^x(T)$	2-2
2.3 Temperature Dependence of Low-Pressure Limiting Rate Constants: T^n	2-2
2.4 High-Pressure-Limit Rate Constants, $k_\infty(T)$	2-3
2.5 Temperature Dependence of High-Pressure-Limiting Rate Constants: T^m	2-3
2.6 Uncertainty Estimates	2-3
2.7 Notes to Table 2	2-8
2.8 References	2-20

Tables

Table 2-1. Rate Constants for Termolecular Reactions	2-4
--	-----

2.1 Introduction

Rate constants for association reactions (Table 2) of the type $A + B \leftrightarrow [AB]^* \xrightarrow{M} AB$ can be pressure dependent. The low-pressure-limiting rate constants are given in the form:

$$k_o(T) = k_o^{300} \left(\frac{T}{300} \right)^{-n} \text{ cm}^6 \text{ molecule}^{-2} \text{ s}^{-1},$$

(where k_o^{300} has been adjusted for air as the third body). The limiting high-pressure rate constant is given in a similar form:

$$k_\infty(T) = k_\infty^{300} \left(\frac{T}{300} \right)^{-m} \text{ cm}^3 \text{ molecule}^{-1} \text{ s}^{-1}.$$

To obtain the effective second-order rate constant for a given condition of temperature and pressure (altitude), the following formula is used:

$$k_f([M], T) = \left(\frac{k_o(T)[M]}{1 + \frac{k_o(T)[M]}{k_\infty(T)}} \right) 0.6 \left\{ 1 + \left[\log_{10} \left(\frac{k_o(T)[M]}{k_\infty(T)} \right) \right]^2 \right\}^{-1}$$

The fixed value 0.6 that appears in this formula fits the data for all listed reactions adequately, although in principle this quantity may be different for each reaction, and also temperature dependent. There are rarely sufficient data to accommodate another parameter.

Some reactions that appear to be simple bimolecular processes proceed via bound intermediates. For example, the reaction between HO and CO to yield H + CO₂ takes place on a potential energy surface that contains the radical HOCO. The yield of H and CO₂ is diminished as the pressure rises. The loss of reactants is thus the sum of two processes, an association to yield HOCO and the chemical activation process yielding H and CO₂. The total rate constant for loss of reactants is fit by the equation above for the association added to the chemical activation rate constant which can be represented by a similar looking equation:

$$k_f^{ca}([M], T) = \left(\frac{k_o(T)}{1 + \frac{k_o(T)}{k_\infty(T)[M]}} \right) 0.6 \left\{ 1 + \left[\log_{10} \left(\frac{k_o(T)}{k_\infty(T)[M]} \right) \right]^2 \right\}^{-1}$$

Thus, a compilation of rate constants requires the stipulation of the four parameters, $k_o(300)$, n , $k_\infty(300)$, and m . These can be found in Table 2. The discussion that follows outlines the general methods we have used in establishing this table, and the notes to the table discuss specific data sources. Recent advances in theory have allowed direct calculation of rate constants for some reactions using RRKM/Master Equation methods.

When sufficient and precise data exist for a given reaction, we have fit the data to the four parameter expression above. We have used theory as a guide whenever possible.

2.2 Low-Pressure-Limiting Rate Constant, $k_o^x(T)$

Troe [358] has described a simple method for obtaining low-pressure-limiting rate constants. In essence this method depends on the definition:

$$k_o^x(T) \equiv \beta_x k_{o,sc}^x$$

Here sc signifies “strong” collisions, x denotes the bath gas, and β_x is an efficiency parameter ($0 < \beta_x < 1$), which provides a measure of energy transfer. The strong collision rate constant can be calculated with some accuracy from knowledge of molecular parameters available from experiment and more and more from theory.

The coefficient β_x is related to the average energy transferred in a collision with gas x , $\langle \Delta E \rangle_x$, via:

$$\frac{\beta_x}{(1 - \sqrt{\beta_x})} = \frac{\langle \Delta E \rangle_x}{F_E kT}$$

Notice that $\langle \Delta E \rangle$ is quite sensitive to β . F_E is the correction factor of the energy dependence of the density of states (a quantity of the order of 1.1 for most species of stratospheric interest).

For some of the reactions of possible stratospheric interest reviewed here, there exist data in the low-pressure limit (or very close thereto), and we have chosen to evaluate and unify this data by calculating $k_o^x(T)$ for the appropriate bath gas x and computing the value of β_x corresponding to the experimental value [358]. A compilation [293] gives details for many of the reactions considered here.

From the β_x values (most of which are for N_2 , i.e., β_{N_2}), we compute $\langle \Delta E \rangle_x$ according to the above equation. Values of $\langle \Delta E \rangle_{N_2}$ of approximately 0.3–1 kcal mole⁻¹ are generally expected. If multiple data exist, we average the values of $\langle \Delta E \rangle_{N_2}$ and recommend a rate constant corresponding to the β_{N_2} computed in the equation above.

Master equation calculations allow direct calculation of low pressure rate constants and of β_x .

Where no data exist we have sometimes estimated the low-pressure rate constant by taking $\beta_{N_2} = 0.3$ at $T = 300$ K, a value based on those cases where data exist.

2.3 Temperature Dependence of Low-Pressure Limiting Rate Constants: T^n

The value of n recommended here comes from measurements or, in some cases, a calculation of $\langle \Delta E \rangle_{N_2}$ from the data at 300 K, and a computation of β_{N_2} (200 K) assuming that $\langle \Delta E \rangle_{N_2}$ is independent of temperature in this range. This β_{N_2} (200 K) value is combined with the computed value of k_o^{sc} (200 K) to give the expected value of the actual rate constant at 200 K. This latter, in combination with the value at 300 K, yields the value of n .

This procedure can be directly compared with measured values of k_o (200 K) when those exist. Unfortunately, very few values at 200 K are available. There are often temperature-dependent studies, but some ambiguity exists when one attempts to extrapolate these down to 200 K. If data are to be extrapolated beyond the measured temperature range, a choice must be made as to the functional form of the temperature dependence.

There are two general ways of expressing the temperature dependence of rate constants. Either the Arrhenius expression

$$k_o(T) = A \exp(-E/RT)$$

or the form

$$k_o(T) = A' T^{-n}$$

is employed. Neither of these extrapolation techniques is soundly based, and since they often yield values that differ substantially, we have used the power law expression above as the basis of our recommendations.

2.4 High-Pressure-Limit Rate Constants, $k_\infty(T)$

High-pressure rate constants can often be obtained experimentally, but those for the relatively small species of atmospheric importance usually reach the high-pressure limit at inaccessibly high pressures. This leaves two sources of these numbers, the first being estimates based upon theory, and the second being extrapolation of fall-off data up to higher pressures.

Stratospheric conditions generally render reactions of interest much closer to the low-pressure limit and thus are fairly insensitive to the high-pressure value. This means that while the extrapolation is long, and the value of $k_\infty(T)$ is often not very accurate, a “reasonable guess” of $k_\infty(T)$ will then suffice. In a few cases we have declined to guess since the low-pressure limit is effective over the entire range of stratospheric conditions.

2.5 Temperature Dependence of High-Pressure-Limiting Rate Constants: T^m

There are very few data upon which to base a recommendation for values of m . Values in Table 2 are often estimated, based on models for the transition state of bond-association reactions and whatever data are available. In general the temperature dependence of these rate constants is expected to be small.

2.6 Uncertainty Estimates

For three-body reactions (Table 2) uncertainties are assigned using a procedure that is analogous to that employed for bimolecular reactions in Table 1. Values of $f(298\text{ K})$ are given for these rate constants at room temperature and assumed to be valid at all pressures. The additional uncertainty arising from the temperature extrapolation is expressed with a g -factor as in Table 1. Given that uncertainties for an expression with four parameters are expressed with only two parameters, a certain amount of arbitrariness is involved in their choice. In general we have tried to have the “two sigma” range incorporate most of the data.

Table 2-1. Rate Constants for Termolecular Reactions

Reaction	Low-Pressure Limit ^a $k_0(T) = k_0^{300} (T/300)^{-n}$		High-Pressure Limit ^b $k_\infty(T) = k_\infty^{300} (T/300)^{-m}$		f	g	Notes
	k_0^{300}	n	k_∞^{300}	m			
O_x Reactions							
$O + O_2 \xrightarrow{M} O_3$	(6.0) (-34)	2.4	–	–	1.1	50	<u>A1</u>
O(¹D) Reactions							
$O(^1D) + N_2 \xrightarrow{M} N_2O$	(2.8) (-36)	0.9	–	–	1.3	75	<u>A2</u>
HO_x Reactions							
$H + O_2 \xrightarrow{M} HO_2$	(4.4) (-32)	1.3	(7.5) (-11)	-0.2	1.3	50	<u>B1</u>
$OH + OH \xrightarrow{M} H_2O_2$	(6.9) (-31)	1.0	(2.6) (-11)	0	1.5	100	<u>B2</u>
NO_x Reactions							
$O + NO \xrightarrow{M} NO_2$	(9.0) (-32)	1.5	(3.0) (-11)	0.0	1.2	100	<u>C1</u>
$O + NO_2 \xrightarrow{M} NO_3$	(2.5) (-31)	1.8	(2.2) (-11)	0.7	1.3	100	<u>C2</u>
$OH + NO \xrightarrow{M} HONO$	(7.0) (-31)	2.6	(3.6) (-11)	0.1	1.2	50	<u>C3</u>
$OH + NO_2 \xrightarrow{M} HONO_2$	(1.8) (-30)	3.0	(2.8) (-11)	0	1.3	100	<u>C4</u>
$OH + NO_2 \xrightarrow{M} HOONO$	(9.1) (-32)	3.9	(4.2) (-11)	0.5	1.5	200	<u>C4</u>
$HO_2 + NO \xrightarrow{M} HONO_2$	See Note						<u>C5</u>
$HO_2 + NO_2 \xrightarrow{M} HO_2NO_2$	(2.0) (-31)	3.4	(2.9) (-12)	1.1	1.1	50	<u>C6</u>
$NO_2 + NO_3 \xrightarrow{M} N_2O_5$	(2.0) (-30)	4.4	(1.4) (-12)	0.7	1.2	100	<u>C7</u>
$NO_3 \xrightarrow{M} NO + O_2$	See Note						<u>C8</u>
Hydrocarbon Reactions							
$OH + CO \xrightarrow{M} HOCO$	(5.9) (-33)	1.4	(1.1) (-12)	-1.3	1.1	100	<u>D1</u>
$OH + CO \xrightarrow{M} H + CO_2$ [See Note]	(1.5) (-13)	-0.6	(2.1) (9)	-6.1			
$CH_3 + O_2 \xrightarrow{M} CH_3O_2$	(4.0) (-31)	3.6	(1.2) (-12)	-1.1	1.1	50	<u>D2</u>
$C_2H_5 + O_2 \xrightarrow{M} C_2H_5O_2$	(1.5) (-28)	3.0	(8.0) (-12)	0	1.2	50	<u>D3</u>
$OH + C_2H_2 \xrightarrow{M} HOCHCH$	(5.5) (-30)	0.0	(8.3) (-13)	-2	1.1	50	<u>D4</u>
$OH + C_2H_4 \xrightarrow{M} HOCH_2CH_2$	(1.0) (-28)	4.5	(7.5) (-12)	.85	1.2	50	<u>D5</u>

Reaction	Low-Pressure Limit ^a $k_0(T) = k_0^{300} (T/300)^{-n}$		High-Pressure Limit ^b $k_\infty(T) = k_\infty^{300} (T/300)^{-m}$		f	g	Notes
	k_0^{300}	n	k_∞^{300}	m			
$\text{CH}_3\text{O} + \text{NO} \xrightarrow{\text{M}} \text{CH}_3\text{ONO}$	(2.3) (-29)	2.8	(3.8) (-11)	0.6	1.3	100	<u>D6</u>
$\text{CH}_3\text{O} + \text{NO}_2 \xrightarrow{\text{M}} \text{CH}_3\text{ONO}_2$	(5.3) (-29)	4.4	(1.9) (-11)	1.8	1.1	0	<u>D7</u>
$\text{C}_2\text{H}_5\text{O} + \text{NO} \xrightarrow{\text{M}} \text{C}_2\text{H}_5\text{ONO}$	(2.8) (-27)	4.0	(5.0) (-11)	0.2	1.2	50	<u>D8</u>
$\text{C}_2\text{H}_5\text{O} + \text{NO}_2 \xrightarrow{\text{M}} \text{C}_2\text{H}_5\text{ONO}_2$	(2.0) (-27)	4.0	(2.8) (-11)	1.0	1.1	100	<u>D9</u>
$\text{CH}_3\text{O}_2 + \text{NO}_2 \xrightarrow{\text{M}} \text{CH}_3\text{O}_2\text{NO}_2$	(1.0) (-30)	4.8	(7.2) (-12)	2.1	1.5	100	<u>D10</u>
$\text{C}_2\text{H}_5\text{O}_2 + \text{NO}_2 \xrightarrow{\text{M}} \text{C}_2\text{H}_5\text{O}_2\text{NO}_2$	(1.2) (-29)	4.0	(9.0) (-12)	0.0	1.3	50	<u>D11</u>
$\text{CH}_3\text{C}(\text{O})\text{O}_2 + \text{NO}_2 \xrightarrow{\text{M}} \text{CH}_3\text{C}(\text{O})\text{O}_2\text{NO}_2$	(9.7) (-29)	5.6	(9.3) (-12)	1.5	1.2	50	<u>D12</u>
$\text{CH}_3\text{CH}_2\text{C}(\text{O})\text{O}_2 + \text{NO}_2 \xrightarrow{\text{M}} \text{CH}_3\text{CH}_2\text{C}(\text{O})\text{O}_2\text{NO}_2$	(9.0) (-28)	8.9	(7.7) (-12)	0.2	2.0	100	<u>D13</u>
$\text{CH}_3\text{C}(\text{O})\text{CH}_2 + \text{O}_2 \xrightarrow{\text{M}} \text{CH}_3\text{C}(\text{O})\text{CH}_2\text{O}_2$	(3) (-29)		(1.0) (-12)		1.3		<u>D14</u>
FO_x Reactions							
$\text{F} + \text{O}_2 \xrightarrow{\text{M}} \text{FO}_2$	(5.8) (-33)	1.7	(1) (-10)	0	1.3	100	<u>E1</u>
$\text{F} + \text{NO} \xrightarrow{\text{M}} \text{FNO}$	(1.2) (-31)	0.5	(2.8) (-10)	0	1.4	200	<u>E2</u>
$\text{F} + \text{NO}_2 \xrightarrow{\text{M}} \text{FNO}_2$	(1.5) (-30)	2.0	(1.0) (-11)	0.0	1.3	100	<u>E3</u>
$\text{FO} + \text{NO}_2 \xrightarrow{\text{M}} \text{FONO}_2$	(2.6) (-31)	1.3	(2.0) (-11)	1.5	3	200	<u>E4</u>
$\text{CF}_3 + \text{O}_2 \xrightarrow{\text{M}} \text{CF}_3\text{O}_2$	(3.0) (-29)	4.0	(3.0) (-12)	1.0	1.2	100	<u>E5</u>
$\text{CF}_3\text{O} + \text{NO}_2 \xrightarrow{\text{M}} \text{CF}_3\text{ONO}_2$	1.7 (-28)	6.9	1.1 (-11)	1	1.1	50	<u>E6</u>
$\text{CF}_3\text{O}_2 + \text{NO}_2 \xrightarrow{\text{M}} \text{CF}_3\text{O}_2\text{NO}_2$	(1.5) (-29)	2.2	(9.6) (-12)	1	1.1	50	<u>E7</u>
$\text{CF}_3\text{O} + \text{CO} \xrightarrow{\text{M}} \text{CF}_3\text{OCO}$	(2.5) (-31)	2	(6.8) (-14)	-1.2	1.2	500	<u>E8</u>
$\text{CF}_3\text{O} \xrightarrow{\text{M}} \text{CF}_2\text{O} + \text{F}$	See Note						<u>E9</u>
CIO_x Reactions							
$\text{Cl} + \text{O}_2 \xrightarrow{\text{M}} \text{ClOO}$	(2.2) (-33)	3.1	(1.8) (-10)	0	1.1	50	<u>F1</u>
$\text{Cl} + \text{NO} \xrightarrow{\text{M}} \text{ClNO}$	(7.6) (-32)	1.8	-	-	1.2	50	<u>F2</u>
$\text{Cl} + \text{NO}_2 \xrightarrow{\text{M}} \text{ClONO}$ $\xrightarrow{\text{M}} \text{ClONO}_2$	(1.3) (-30)	2	(1) (-10)	1	1.2	100	<u>F3</u>
	(1.8) (-31)	2	(1) (-10)	1	1.3	100	
$\text{Cl} + \text{CO} \xrightarrow{\text{M}} \text{ClCO}$	(1.3) (-33)	3.8	-	-	1.1	50	<u>F4</u>
$\text{Cl} + \text{C}_2\text{H}_2 \xrightarrow{\text{M}} \text{ClC}_2\text{H}_2$	(5.2) (-30)	2.4	(2.2) (-10)	0.7	1.1	50	<u>F5</u>

Reaction	Low-Pressure Limit ^a $k_0(T) = k_0^{300} (T/300)^{-n}$		High-Pressure Limit ^b $k_\infty(T) = k_\infty^{300} (T/300)^{-m}$		f	g	Notes
	k_0^{300}	n	k_∞^{300}	m			
$\text{Cl} + \text{C}_2\text{H}_4 \xrightarrow{\text{M}} \text{ClC}_2\text{H}_4$	(1.6) (-29)	3.3	(3.1) (-10)	1.0	1.5	50	<u>F6</u>
$\text{Cl} + \text{C}_2\text{Cl}_4 \xrightarrow{\text{M}} \text{C}_2\text{Cl}_5$	(1.4) (-28)	8.5	(4.0) (-11)	1.2	1.2	50	<u>F7</u>
$\text{ClO} + \text{NO}_2 \xrightarrow{\text{M}} \text{ClONO}_2$	(1.8) (-31)	3.4	(1.5) (-11)	1.9	1.3	50	<u>F8</u>
$\text{OCIO} + \text{NO}_3 \xrightarrow{\text{M}} \text{O}_2\text{ClONO}_2$	See Note						<u>F9</u>
$\text{ClO} + \text{ClO} \xrightarrow{\text{M}} \text{Cl}_2\text{O}_2$	(1.6) (-32)	4.5	(3.0) (-12)	2.0	1.15	0	<u>F10</u>
$\text{ClO} + \text{OCIO} \xrightarrow{\text{M}} \text{Cl}_2\text{O}_3$	(6.2) (-32)	4.7	(2.4) (-11)	0	1.1	25	<u>F11</u>
$\text{OCIO} + \text{O} \xrightarrow{\text{M}} \text{ClO}_3$	(2.9) (-31)	3.1	(8.3) (-12)	0	1.1	100	<u>F12</u>
$\text{CH}_2\text{Cl} + \text{O}_2 \xrightarrow{\text{M}} \text{CH}_2\text{ClO}_2$	(1.9) (-30)	3.2	(2.9) (-12)	1.2	1.1	125	<u>F13</u>
$\text{CHCl}_2 + \text{O}_2 \xrightarrow{\text{M}} \text{CHCl}_2\text{O}_2$	(1.3) (-30)	4.0	(2.8) (-12)	1.4	1.1	125	<u>F14</u>
$\text{CCl}_3 + \text{O}_2 \xrightarrow{\text{M}} \text{CCl}_3\text{O}_2$	(8) (-31)	6	(3.5) (-12)	1	1.2	50	<u>F15</u>
$\text{CFCl}_2 + \text{O}_2 \xrightarrow{\text{M}} \text{CFCl}_2\text{O}_2$	(5.0) (-30)	4.0	(6.0) (-12)	1.0	1.3	200	<u>F16</u>
$\text{CF}_2\text{Cl} + \text{O}_2 \xrightarrow{\text{M}} \text{CF}_2\text{ClO}_2$	(5.2) (-29)	5.6	(1.0) (-11)	0.8	2	300	<u>F17</u>
$\text{CCl}_3\text{O}_2 + \text{NO}_2 \xrightarrow{\text{M}} \text{CCl}_3\text{O}_2\text{NO}_2$	(2.9) (-29)	6.8	(1.3) (-11)	1	1.1	50	<u>F18</u>
$\text{CFCl}_2\text{O}_2 + \text{NO}_2 \xrightarrow{\text{M}} \text{CFCl}_2\text{O}_2\text{NO}_2$	(2.2) (-29)	5.8	(1.0) (-11)	1	1.1	50	<u>F19</u>
$\text{CF}_2\text{ClO}_2 + \text{NO}_2 \xrightarrow{\text{M}} \text{CF}_2\text{ClO}_2\text{NO}_2$	(1.1) (-29)	4.6	(1.7) (-11)	1.2	2	300	<u>F20</u>
BrO_x Reactions							
$\text{Br} + \text{NO}_2 \xrightarrow{\text{M}} \text{t-BrONO}$	(4.2) (-31)	2.4	(2.7) (-11)	0	1.1	50	<u>G1</u>
$\text{BrO} + \text{NO}_2 \xrightarrow{\text{M}} \text{BrONO}_2$	(5.2) (-31)	3.2	(6.9) (-12)	2.9	1.2	400	<u>G2</u>
IO_x Reactions							
$\text{I} + \text{NO} \xrightarrow{\text{M}} \text{INO}$	(1.8) (-32)	1.0	(1.7) (-11)	0	1.3	150	<u>H1</u>
$\text{I} + \text{NO}_2 \xrightarrow{\text{M}} \text{INO}_2$	(3.0) (-31)	1.0	(6.6) (-11)	0	1.2	300	<u>H2</u>
$\text{IO} + \text{NO}_2 \xrightarrow{\text{M}} \text{IONO}_2$	(7.5) (-31)	3.5	(7.6) (-12)	1.5	1.3	50	<u>H3</u>
SO_x Reactions							
$\text{HS} + \text{NO} \xrightarrow{\text{M}} \text{HSNO}$	(2.4) (-31)	2.5	(2.7) (-11)	0	1.2	100	<u>I1</u>
$\text{CH}_3\text{S} + \text{NO} \xrightarrow{\text{M}} \text{CH}_3\text{SNO}$	(3.2) (-29)	4.0	(3.5) (-11)	1.8	1.2	100	<u>I2</u>
$\text{O} + \text{SO}_2 \xrightarrow{\text{M}} \text{SO}_3$	(1.8) (-33)	-2	4.2 (-14)	-1.8	2	100	<u>I3</u>

Reaction	Low-Pressure Limit ^a $k_0(T) = k_0^{300} (T/300)^{-n}$		High-Pressure Limit ^b $k_\infty(T) = k_\infty^{300} (T/300)^{-m}$		f	g	Notes
	k_0^{300}	n	k_∞^{300}	m			
$\text{OH} + \text{SO}_2 \xrightarrow{\text{M}} \text{HOSO}_2$	(3.3) (-31)	4.3	(1.6) (-12)		1.1	100	<u>I4</u>
$\text{CH}_3\text{SCH}_2 + \text{O}_2 \xrightarrow{\text{M}} \text{CH}_3\text{SCH}_2\text{O}_2$	See Note						<u>I5</u>
$\text{SO}_3 + \text{NH}_3 \xrightarrow{\text{M}} \text{H}_3\text{NSO}_3$	(3.6) (-30)	6.1	(4.3) (-11)	0	1.2	200	<u>I6</u>
$\text{HO} + \text{CS}_2 \xrightarrow{\text{M}} \text{HO} \cdots \text{CS}_2$	(4.9) (-31)	3.5	(1.4) (-11)	1	1.5	100	<u>I7</u>
$\text{Cl} + \text{CS}_2 \xrightarrow{\text{M}} \text{Cl} \cdots \text{CS}_2$	(5.9) (-31)	3.6	(4.6) (-10)	0	1.1	50	<u>I8</u>
$\text{HO} + (\text{CH}_3)_2\text{S} \xrightarrow{\text{M}} \text{HO} \cdots (\text{CH}_3)_2\text{S}$	(2.9) (-31)	6.24			1.2		<u>I9</u>
$\text{Cl} + (\text{CH}_3)_2\text{S} \xrightarrow{\text{M}} \text{Cl} \cdots (\text{CH}_3)_2\text{S}$	(4) (-28)	7	(2) (-10)	1	1.1	50	<u>I10</u>
$\text{Br} + (\text{CH}_3)_2\text{S} \xrightarrow{\text{M}} \text{Br} \cdots (\text{CH}_3)_2\text{S}$	(3.7) (-29)	5.3	(1.5) (-10)	2	1.1	100	<u>I11</u>
Metal Reactions							
$\text{Na} + \text{O}_2 \xrightarrow{\text{M}} \text{NaO}_2$	(3.2) (-30)	1.4	(6.0) (-10)	0	1.3	200	<u>J1</u>
$\text{NaO} + \text{O}_2 \xrightarrow{\text{M}} \text{NaO}_3$	(3.5) (-30)	2.0	(5.7) (-10)	0	1.3	200	<u>J2</u>
$\text{NaO} + \text{CO}_2 \xrightarrow{\text{M}} \text{NaCO}_3$	(8.7) (-28)	2.0	(6.5) (-10)	0	1.3	200	<u>J3</u>
$\text{NaOH} + \text{CO}_2 \xrightarrow{\text{M}} \text{NaHCO}_3$	(1.3) (-28)	2.0	(6.8) (-10)	0	1.3	200	<u>J4</u>

Shaded areas indicate changes or additions since JPL 06-2.

The values quoted are suitable for air as the third body, M.

a Units are $\text{cm}^6 \text{molecule}^{-2} \text{s}^{-1}$.

b Units are $\text{cm}^3 \text{molecule}^{-1} \text{s}^{-1}$.

f(298 K) is the uncertainty factor at 298 K. To calculate the uncertainty at other temperatures, use the expression:

$$f(T) = f(298) \exp \left[g \left(\frac{1}{T} - \frac{1}{298} \right) \right]$$

Note that the exponent is absolute value

2.7 Notes to Table 2

JPL Publication numbers for the most recent revision of the table entry and note are given at the end of each note.

- A1. $O + O_2$. Low pressure limit and T dependence are an average of Klais et al. [201], Huie et al. [174] and Lin and Leu [228]. These studies in N_2 and Ar are in the temperature range ($200 < T/K < 268$). The result is in agreement with the study of Hippler et al. [163] and the extrapolated recommendation fits their lower pressure N_2 data down to 100 K. High pressure studies by Croce de Cobos and Troe [91] are in agreement with this recommendation. Rawlins et al. [308] estimate values in Ar between 80 and 150 K from nascent vibrational distributions that are a factor of two higher than the recommendation extrapolated to 80 K. The temperature dependence of the rate constant determined from the experimental data are in excellent agreement with the value of $n=2.36$ determined from the calculations of Patrick and Golden [293]. However there is some reason to believe that a radical-complex plays a role in this process. [165, 180, 234, 414] Kaye [195] has calculated isotope effects for this reaction, using methods similar to those discussed in the Introduction of this document (see Troe [358] and Patrick and Golden [293].) Isotope effects have been reported by Anderson et al. [9] and Gross and Billing [153]. Measurements of isotopic fractionation by Mauersberger and colleagues [397] and Thiemens and co-workers [323] reveal distinctly non-statistical effects. Various attempts at theoretical explanations exist [158], but the detailed knowledge of the potential energy surface required is unavailable. A summary of theoretical and experimental studies by Schinke et al. [326] goes into great detail on this subject as does a study by Gao and Marcus. [140]. (Table: 02-25, Note: 10-6, Evaluated 10-6) [Back to table](#)
- A2. $O(^1D) + N_2$. Recommended parameters (including f and g) from Estupiñán et al. [117] whose detection capabilities were more advanced than those employed in earlier studies. Kajimoto and Cvetanovic [193] report a value at 296K of $6.5 \times 10^{-37} \text{ cm}^6 \text{ s}^{-1}$. Maric and Burrows [237] extract $(8.8 \pm 3.3) \times 10^{-37} \text{ cm}^6 \text{ s}^{-1}$ from a study of the photolysis of synthetic air. Gaedtke et al. [139] report an approximate value of 10^{12} in molar units, which translates to 2.8×10^{-36} in molecular units. The rate constant is extremely low in this special system due to electronic curve crossing. (Table: 06-2, Note: 06-2) [Back to table](#)
- B1. $H + O_2$. Studies by Kurylo [208], Wong and Davis [399], Hsu et al. [173], Hsu et al. [172], Cobos et al. [77], Pirraglia et al. [299], Carleton et al. [66], Troe [359], Bates et al. [26], Michael et al. [248] and Fernandes et al. [123] have been considered. All are in good agreement. A theoretical study by Sellevåg et al. [331] improves the knowledge of the high pressure limit and verifies the low pressure limit. The parameters in [331] are the basis for the recommendation. Several studies, [26, 248] have pointed out the large effect of water vapor as the collider gas. Baulch et al. [27] have evaluated this reaction over the temperature range $298K < T/K < 1500$. *The value of m in JPL 06-02 should be negative!* (Table: 10-6, Note: 10-6, Evaluated: 10-6) [Back to table](#)
- B2. $OH + OH$. Recommended values are from fits of measurements by Zellner et al. [406] in N_2 , by Forster et al. [129] and Fulle et al. [137] in 1–150 bar He scaled to N_2 . A study by Fagerstrom et al. [118] in 85–1000 mbar SF_6 gives slightly different values. A pressure independent bimolecular channel to $H_2O + O$ with a rate 1.8×10^{-12} is observed (see Table 1). Zellner et al. used somewhat different values for this rate constant to make substantial corrections to their measured values. Changing to the accepted value will make large changes in the Zellner et al. values and it is unclear how to evaluate this. Trainor and von Rosenberg [357] report a value at 300 K that is lower than recommended by a factor of 2.7. A theoretical study by Sellevåg et al. [332] recommends values for He that are compatible with the recommendation. (Table: 02-25, Note: 10-6, Evaluated: 10-6) [Back to table](#)
- C1. $O + NO$. Low pressure limit and n from direct measurements of Schieferstein et al. [325] and their re-analysis of the data of Whytock et al. [391]. Error limits encompass other studies. High pressure limit and m from fitting the data of Hippler et al. [164], who report higher values for the high pressure limiting rate constant, to the format used in this compilation. Shock tube measurements by Yarwood et al. [402] in argon from 300–1300 K are consistent with the values in Table 2. (Table: 06-2, Note: 06-2) [Back to table](#)
- C2. $O + NO_2$. Values of rate constants and temperature dependences from a combination of the study by Burkholder and Ravishankara [53] and that of Hahn et al. [154]. At 300 K these studies almost overlap at the highest pressure of Burkholder and Ravishankara and the lowest pressure studied by Hahn et al. The former values are larger by a factor of 2.2 under these conditions. This recommendation is in reasonable agreement with the evaluation of Baulch et al. [29], which fits the Hahn et al. values very well. (Table: 02-25, Note: 02-25) [Back to table](#)
- C3. $OH + NO$. The low pressure limit rate constant has been reported by Anderson and Kaufman [7], Stuhl and Niki [352], Morley and Smith [256], Westenberg and de Haas [390], Anderson et al. [8], Howard and Evenson [171], Harris and Wayne [156], Atkinson et al. [17], Overend et al. [279], Anastasi and Smith [6], Burrows et al. [55]

and Atkinson and Smith [12]. The general agreement is good, and the recommended values of both the rate constant and the temperature dependence are weighted averages. Studies by Sharkey et al. [337] and Donahue et al. [110] in the transition regime between low and high pressure limits are in agreement and serve to reduce the uncertainty. These latter studies yield a value for the high pressure limiting rate constant in agreement with the results of Forster et al. [129], whose study reached pressures of 100 bar in He. The temperature dependence of the high pressure limiting rate constant is from the data of Anastasi and Smith [6] and Sharkey et al. (Both cis- and trans-HONO are expected to be formed.) Fulle et al. [138] report a high pressure limit in agreement with Forster et al. [129]. Pagsberg et al. [280] report low pressure values in SF₆ that are compatible (i.e. the ratio of collision efficiencies is about a factor of two.) with the recommendation. A study by Zabarnick [403] is noted. The error limits encompass the differences with the IUPAC [15] recommendation. (Table: 06-2, Note: 06-2) [Back to table](#)

- C4. OH + NO₂. This reaction has been the subject of detailed study. There are two product channels, one to HONO₂ (nitric acid) and the other to HOONO (pernitrous acid). (There are at least two conformers of HOONO, cis-cis and trans-perp, but they are thought to be equilibrated under atmospheric conditions.) Golden and Smith [149] concluded that there were two pathways and they offered parameters in the format of this recommendation that were given in the note in JPL 02-25 [318]. Experiments by Hippler and co-workers [129, 138] up to about 100 bar at 300 K and the finding of a double exponential decay of OH at 430 K and 100 bar implicate a second pathway [162]. Nizkorodov and Wennberg [269] report 5% HOONO at 253K and 20 Torr of an N₂/He buffer gas. Bean et al. [30] and Pollack et al. [302] report on the spectroscopy of the HOONO conformer. Golden et al. [148] have performed RRKM/master-equation calculations on an ab initio potential energy surface to yield the parameters recommended herein. The low pressure limit and the high pressure limiting rate constants and their temperature dependences are from a fit to the data of Hippler et al. [162], Anastasi and Smith [5], Wine et al. [394], Donahue et al. [110], Dransfield et al. [111], Brown et al. [48] and D'Ottone et al. [92]. (Brown et al. report that O₂ is about 30% less efficient than N₂ as a collider and suggest that air might therefore have a total efficiency of 0.94 relative to N₂) Data from Anderson et al. [8], Howard and Evenson [171], Burrows et al. [55], and Erler et al. [116] are in essential agreement. Data of Forster et al. [129] and Fulle et al. [138] are acknowledged to be about 30% too high [162]. Burkholder et al. [51] and Dransfield et al. [111] have searched for the isomer HOONO and have been unable to identify it. The description of the reaction between HO and NO₂, as consisting of two product channels, requires that the data obtained at lower than 300 K represent the sum of the two pathways. Thus the fate of HOONO has to be included in atmospheric models. If this fate involves rapid loss due to reaction or photolysis, the effect of the second pathway is the diminution of the HONO₂ forming rate constant. Evaluation of data, taking into account both pathways, indicates that the contribution of the HOONO forming reaction can be from 5 to 15% under atmospheric conditions. Mollner et al. [254] have measured the rate constant for the sum of both pathways at 298 K in N₂, O₂ and air from 50 to 900 Torr. They find the efficiency of air to be 94% that of N₂. They measured the branching ratio at 298 K in a mixture of N₂ and H₂ from 20 to 760 Torr. They suggest parameters at 298 K in the form used herein of: $k_0 = 1.51 \times 10^{-30}$ and $k_\infty = 1.84 \times 10^{-30}$ for the HONO₂ pathway and $k_0 = 6.2 \times 10^{-32}$ and $k_\infty = 8.1 \times 10^{-11}$ for the HOONO pathway. These are 15% lower than those in Table 2. The equilibrium constant is given in Table 3-1. (Table: 06-2, Note: 10-6, Evaluated 10-6) [Back to table](#)

- C5. HO₂ + NO. Butkovskaya et al. studied this reaction in a high pressure turbulent flow reactor coupled to a chemical ionization mass spectrometer [56-58]. Very small yields (<1%) of nitric acid were measured from 223 to 323 K and from 72 to 600 Torr of (mostly) N₂ and in the absence of water vapor. The yields were enhanced by the presence of water vapor [57, 58]. In systems not including water vapor, they summarized the yield of nitric acid relative to the yield of NO₂ (from HO₂ + NO → OH + NO₂) as follows:

$$\beta(T, P) = (530 \pm 10)/T(K) + (6.4 \pm 1.3) \times 10^{-4} P(\text{Torr}) - (1.73 \pm 0.07).$$

At low temperatures, β extrapolated below 100 Torr has a large non-zero intercept at zero pressure [56, 58], which is not expected for a gas phase reaction. In the presence of water vapor, the chemical ionization mass spectrometer signals are affected significantly [57] and the yield of nitric acid increases linearly with added water vapor [57, 58], reaching an enhancement factor of ~8 at [H₂O] = 4×10^{17} molecule cm⁻³ and 298 K [57]:

$$f_{\text{H}_2\text{O}} \approx (1 + 2 \times 10^{-17} [\text{H}_2\text{O}])$$

where the concentration of H₂O is expressed in molecules cm⁻³. If this effect is due to reaction of the hydrated HO₂ complex (i.e. HO₂•H₂O + NO → HNO₃ + H₂O), then the rate constant of the complex with NO is ~ 6×10^{-13} cm³ s⁻¹ at 298 K in the presence of 200 Torr of N₂ [57].

Ab initio electronic structure calculations support the possibility of gas phase HONO₂ formation, but satisfactory simulations using master equations have been elusive [22, 148, 409, 410]. The measured yields show a surprising intercept at zero pressure, which might be indicative of wall reactions. However, Butkovskaya et al.

have made great efforts to minimize wall reactions, and their analysis suggests that wall reactions should not be important [57, 58]. Until the results have been confirmed by other groups and are better understood, no recommendation can be made. These rate parameters are provided for the purposes of model evaluation only and do not constitute a recommendation by the Panel. (Table: 10-6, Note: 10-6, Evaluated 10-6) [Back to Table](#)

- C6. $\text{HO}_2 + \text{NO}_2$. Christensen et al. [72] report rate constants $219 < T/K < 298$ and $45 < P/\text{torr} < 200$. They show that methanol, present in most other studies confounds the results by forming bound complexes with HO_2 . They also suggest that some measurements yielded low rate constants as a result of perturbations to the $\text{NO}_2/\text{N}_2\text{O}_4$ equilibrium. The parameters recommended are those from this study incorporating the results of Kurylo and Ouellette [209, 210] and Sander and Peterson [320]. The recommended k_o (300 K) is consistent with Howard [170]. Other studies by Simonaitis and Heicklen [341] and Cox and Patrick [89] are in reasonable agreement with the recommendation, as is the value of Christensen et al. [73]. (Table: 06-2, Note: 06-2) [Back to table](#)
- C7. $\text{NO}_2 + \text{NO}_3$. Data with N_2 as the bath gas from Kircher et al. [199], Smith et al. [344], Burrows et al. [54], Wallington et al. [377] and Orlando et al. [276] ranging from 236 to 358 K were used to obtain k_o , k_∞ , n and m . Values from Croce de Cobos et al. [90] are excluded due to arguments given by Orlando et al. [276], who point out that a reanalysis of these data using better values for the rate constant for $\text{NO}_3 + \text{NO} \rightarrow 2\text{NO}_2$ yields a negative value for $\text{NO}_2 + \text{NO}_3 + \text{M}$. The study of Fowles et al. [131] is noted, but not used. Johnston et al. [183] have reviewed this reaction. Hahn et al. [154] have studied this reaction between 300 and 400 K at pressures from 30 to 900 bar. Their suggested parameterization yields values indistinguishable from those in this recommendation under most atmospheric conditions. (There are deviations of 30 to 50% at pressures less than a mbar and greater than 5 bar.)

A study of the reverse reaction has been carried out by Cantrell et al. [61]. These data are in excellent agreement with those obtained by Connell and Johnston [81] and Viggiano et al. [370]. The equilibrium constant recommended in Table 3 is the one given in Cantrell et al. [61], who computed it from the ratio of the rate constant of Orlando et al [276] and their rate constants for the reverse reaction. (Table: 02-25, Note: 02-25) [Back to table](#)

- C8. $\text{NO}_3 + \text{M}$. Johnston et al. [183] and Davidson et al. [98] have suggested significant thermal decomposition of NO_3 . This has been disputed by Russell et al. [313]. Davis et al. [100] claim that the barrier to thermal dissociation is $47.3 \text{ kcal mol}^{-1}$. This would seem to rule out such a process in the atmosphere. (Table: 94-26, Note: 94-26) [Back to table](#)
- D1. $\text{HO} + \text{CO}$. This recommendation takes into account the fact that the reaction proceeds via two channels, a chemical activation process directly to $\text{H} + \text{CO}_2$ and an association to yield HOCO . In the presence of O_2 , the HOCO intermediate is converted to $\text{HO}_2 + \text{CO}_2$ (DeMore [102], Miyoshi et al. [252]). Miyoshi et al. report a rate constant for the reaction of HOCO with O_2 of $\sim 1.5 \times 10^{-12} \text{ cm}^3 \text{ molecule}^{-1} \text{ s}^{-1}$ at 298 K). Therefore, for atmospheric purposes, the products can be taken to be HO_2 and CO_2 . The parameters are taken directly from Senosiain et al. [334] who performed master equation calculations on a theoretical surface. (The value of the exponent of k_o for the chemical activation pathway has a sign error in the reference. The values in Table 2 are correct.) Pressure and temperature dependence of data from McCabe et al. [244] and Hynes et al. [176] are well represented by these parameters. In contrast with the previous evaluation where the rate constant increased with pressure, in this evaluation, it is shown to increase with number density. This reaction has been studied often by many workers. In general the results are in keeping with the current recommendation. Values have been reported by Dreier and Wolfrum [112], Husain et al. [175], Ravishankara and Thompson [307], Paraskevopoulos and Irwin [287], Hofzumahaus and Stuhl [167]. The results of Jonah et al. [185] are too high and were not included. An increase in k with pressure has been observed by a large number of investigators (Overend and Paraskevopoulos [278], Perry et al. [296], Chan et al. [67], Biermann et al. [33], Cox et al. [86], Butler et al. [59], Paraskevop and Irwin [286, 287], DeMore [102], Hofzumahaus and Stuhl [167], Hynes et al. [176]), and McCabe et al., [244]. In addition, Niki et al. [268] have measured k relative to $\text{OH} + \text{C}_2\text{H}_4$ in one atmosphere of air by following CO_2 production using FTIR. Previous controversy regarding the effect of small amounts of O_2 (Biermann et al. [33]) has been resolved and is attributed to secondary reactions (DeMore [102], Hofzumahaus and Stuhl [167]). The results of Butler et al. [59] have to be re-evaluated in the light of refinements in the rate coefficient for the $\text{OH} + \text{H}_2\text{O}_2$ reaction. The corrected rate coefficient is in approximate agreement with the recommended value. Currently, there are no indications to suggest that the presence of O_2 has any effect on the rate coefficient other than as a third body. Beno et al. [32] observe an enhancement of k with water vapor, which is in conflict with the flash photolysis studies; e.g., Ravishankara and Thompson [307], Paraskevopoulos and Irwin [287], Hynes et al. [176], and McCabe et al. [244]. Water is not expected to significantly change the rate coefficient for the reaction in the atmosphere and it is not expected to alter the products of the reaction.

Important: To calculate rate constants for the reaction $\text{OH} + \text{CO} \rightarrow \text{HOCO}$, use the standard expression for termolecular reactions, $k_f([\text{M}], T)$, given in the Introduction (Section 2.1). The Arrhenius parameters for the reaction $\text{HOCO} + \text{O}_2 \rightarrow \text{HO}_2 + \text{CO}_2$ are given in Table 1-1. To calculate rate constants for the reaction $\text{OH} + \text{CO} \rightarrow \text{H} + \text{CO}_2$, use the expression for chemical activation reactions, $k_f^{\text{ca}}([\text{M}], T)$, given in the Introduction (Section 2.1). (Table: 06-2, Note: 10-6, Evaluation 06-2) [Back to table](#)

- D2. $\text{CH}_3 + \text{O}_2$. *The temperature dependence of the high pressure limit is positive. There has been a sign error in the last several versions of this recommendation!* Data from Kaiser [188] are fit to the NASA format. This ranges of this study were $3 < P/\text{torr} < 11000$ and $264 < T/\text{K} < 370$. The rate constant was measured relative to the reaction $\text{CH}_3 + \text{Cl}_2 \rightarrow \text{CH}_3\text{Cl} + \text{Cl}$. [$\text{k}/\text{cm}^3 \text{molecule}^{-1} \text{s}^{-1} = 1.61\text{E-}12 \exp(-530/RT)$] The recommended values are in good agreement with those from Selzer and Bayes [333]. These workers determined the rate constants as a function of pressure in N_2 , Ar, O_2 , and He. Plumb and Ryan [301] report a value in He which is consistent within error limits with the work of Selzer and Bayes. Pilling and Smith [298] have measured this process in Ar (32–490 Torr). Cobos et al. [76] have made measurements in Ar and N_2 from 0.25 to 150 atmospheres. They report parameters somewhat different than recommended here. The work of Laguna and Baughcum [211] seems to be in the fall-off region. Results of Pratt and Wood [304] in Ar are consistent with this recommendation, although the measurements are indirect. The suggested value accommodates the values of Keiffer et al., [196], who measured the process in Ar between 20 and 600 Torr and in the range $334 < T/\text{K} < 582$. Data of van den Bergh and Callear [369], Hochanadel et al. [166], Basco et al. [25], Washida and Bayes [389], Laufer and Bass [214], and Washida [388] are also considered. A theoretical study by Zhu et al. [411] is in reasonable agreement with the recommendation. A study by Fernandes et al. [122] at pressures from 2-1000 bar and temperatures between 300 and 700K presents a parameterization of the rate constant as a function of pressure and temperature which is in agreement with this recommendation at 300K. If their parameters are used at 200K the agreement is not as good, but is within the 95% uncertainty limit. (Table: 06-2, Note: 10-6, Evaluated: 10-6) [Back to table](#)
- D3. $\text{C}_2\text{H}_5 + \text{O}_2$. Kaiser et al. [191] extract from a relative rate study: $k_\infty = (9.2 \pm 0.9) \times 10^{-12} \text{ cm}^3 \text{ molecule}^{-1} \text{ s}^{-1}$ and $k_0 = (6.5 \pm 2.0) \times 10^{-29} \text{ cm}^6 \text{ molecule}^{-2} \text{ s}^{-1}$ in He at 298 K and pressures between 3 and 1500 Torr. k_∞ has been calculated by Wagner et al. [373], Miller and Klippenstein [250], and Sheng et al. [339] with $k_\infty(300\text{K}) = 8, 10$, and $4 \times 10^{-12} \text{ cm}^3 \text{ molecule}^{-1} \text{ s}^{-1}$, respectively. Although all cite some small temperature dependence, the values are stated to hold above 300K. The Kaiser et al. [191], extrapolation to the low-pressure limit is difficult due to the complex potential energy surface, but agrees with a Patrick and Golden-type calculation [293] using $\Delta H_0^0 = 32.4 \text{ kcal mol}^{-1}$. The recommended values use the calculated temperature dependence and a 2.5 times higher rate constant for air as the bath gas, in line with suggestions in Kaiser et al. [189]. (Table: 06-2, Note: 06-2) [Back to table](#)
- D4. $\text{OH} + \text{C}_2\text{H}_2$. The rate constant for this complex process has been examined by Smith et al. [345] in the temperature range from 228 to 1400 K, and in the pressure range 1 to 760 Torr. Their analysis, which is cast in similar terms to those used here, is the source of the rate constants and temperature dependences at both limits. The negative value of m reflects the fact that their analysis includes a 1.2 kcal/mol barrier for the addition of OH to C_2H_2 . The data analyzed include those of Pastrana and Carr [292], Perry et al. [296], Michael et al. [249], and Perry and Williamson [297]. Other data of Wilson and Westenberg [393], Breen and Glass [43], Smith and Zellner [348], and Davis et al. [99] were not included. Studies by Liu et al. [229] and Lai et al. [212] are in general agreement with the recommendation. Calculations of k_0 via the methods of Patrick and Golden [293] yield values compatible with those of Smith et al. [345]. A study by Sørensen et al. [349] at 298 K and pressures from 25 to 8000 torr of bath gas suggests $k_0/\text{cm}^6 \text{ molecule}^{-2} \text{ s}^{-1} = 2.92\text{E-}30$, $k_\infty/\text{cm}^3 \text{ molecule}^{-1} \text{ s}^{-1} = 9.69\text{E-}13$ and $F_c = 0.6$. No difference was found between air, N_2/O_2 mixtures or O_2 as the bath gas. These values yield rate constants as a function of pressure at 298K in agreement with this recommendation, so the recommended values are unchanged from JPL 02-25. Earlier, Fulle et al. [136] reported a high pressure limiting rate constant of $2\text{E-}12 \text{ cm}^3 \text{ molecule}^{-1} \text{ s}^{-1}$, which is the basis for the IUPAC [15] recommendation. A theoretical study by Senosiain et al. [335] is in essential agreement with this recommendation. (Table: 06-2, Note: 06-2) [Back to table](#)
- D5. $\text{OH} + \text{C}_2\text{H}_4$. A study by Vakhtin et al. [366] at 296K in N_2 between 2.85×10^{16} and $3.25 \times 10^{18} \text{ molecules cm}^{-3}$ and individual points 96K, $1.9 \times 10^{16} \text{ molecules cm}^{-3}$; 110K, $2.65 \times 10^{16} \text{ molecules cm}^{-3}$; and 165K and $3.5 \times 10^{16} \text{ molecules cm}^{-3}$, as well as data of Tully [363], Davis et al. [99], Howard [169], Greiner [151], Morris et al. [257], and Overend and Paraskevopoulos [277] in helium, Atkinson et al. [12] in argon, and Lloyd et al. [231] and Cox [83] and Klein et al. [202] in nitrogen/oxygen mixtures, have been considered in the evaluation. This well-studied reaction is considerably more complex than most others in this table. The parameters recommended here fit the same curve proposed by Klein et al. [202] at 298 K. Kuo and Lee [207] report very strong temperature dependence for the low-pressure limit ($n=4$). Calculations of the type in Patrick and Golden

[293] as described in Vakhtin et al. [366] yield $n = 4.2$, although they use a somewhat low value for energy transfer by nitrogen. The high-pressure limit temperature dependence has been determined by several workers. Zellner and Lorenz [407] report a value equivalent to $m = +0.8$ over the range ($296 < T/K < 524$) at about 1 atmosphere. A value of $m = +2.0$ fits the data ($540 < T/K < 670$) of Diau and Lee [105]. Cleary et al. [75] report values in N_2 at 295K. They also report values in He between 200 and 400K. They perform master equation calculations and report fitting parameters. Taylor et al. [354] report data at a single pressure and 69 and 86K. Their data are well-accommodated by this recommendation and by the parameters in [75]. A small change in the high-pressure limit fits all data slightly better. (Table: 10-6, Note: 10-6, Evaluated: 10-6) [Back to table](#)

- D6. $CH_3O + NO$. This reaction proceeds via a complex potential energy surface that includes both chemical activation and direct abstraction routes [65] to the disproportionation products CH_2O and HNO as well as the combination to form CH_3NO . The chemical activation process would have inverse pressure dependence and the direct abstraction would be pressure independent. The recommended values take into account the results of Frost and Smith [134] in Ar and CF_4 and of Caralp et al. [65] in He and Ar. In both of these references the disproportionation process is subtracted from total loss of CH_3O with a pressure independent, temperature dependent value. At 300K below one torr the disproportionation process dominates. Temperature dependences are from the higher temperature results. The low pressure rate constant is consistent with the measurements of McCaulley et al. [246] and Daële et al. [93] in helium. Studies by Ohmori et al. [272] and Dobé et al. [109] are in general agreement with respect to both the addition and bimolecular pathways. (See the note in Table 1-1 for the bimolecular pathway.) (Table: 06-2, Note: 06-2) [Back to table](#)
- D7. $CH_3O + NO_2$. The recommended values are from the work mostly in Ar of Wollenhaupt and Crowley [398]. Agreement is good with earlier work at 298 K from the study of Frost and Smith [133] in Ar (corrected by Frost and Smith [135] and that of Biggs et al [34] and Martinez et al. [242] in He. Low pressure results agree within a factor of two with the measurements of McCaulley et al. [245] in He. A minor bimolecular (chemical activation) pathway is also observed. (See Table 1-1.) (Table: 02-25, Note: 06-2) [Back to table](#)
- D8. $C_2H_5O + NO$. High-pressure data at 298 K in Ar from Frost and Smith [134] and in He between 286 and 388K at pressures from 30 to 500 torr, from Fitschen et al. [125]. Low-pressure measurements in He are from Daele et al. [94]. He experiments were scaled to N_2 by dividing by a factor of 2.5. Ar data were taken as equivalent to N_2 or air. The data were fit by subtracting an assumed pressure independent value of $1E-11$ from the measured rate constants to account for the route to form HNO and CH_3CHO . The low pressure value agrees with theory. The bimolecular channel with an estimated rate of about 10^{-11} needs to be verified by direct studies. The temperature dependence of the low pressure limit is estimated and that of the high pressure limit is taken from Fitschen et al. [125]. (The high pressure rate expression in Fitschen et al. seems to be in error.) (Table: 06-2, Note: 06-2) [Back to table](#)
- D9. $C_2H_5O + NO_2$. High-pressure rate constant at 298 K from Frost and Smith [133]. Other values estimated from similar reactions. (Table: 06-2, Note: JPL92-20) [Back to table](#)
- D10. $CH_3O_2 + NO_2$. Golden [143] has re-evaluated the data for this reaction. The recommended parameters are from a fit to Percival [295] and temperature- and pressure-dependent data in Sander and Watson [322] and Ravishankara et al. [305]. The temperature dependence of the high pressure rate constant is a little high, but results from the statistical fit to the data. The values recommended herein, were taken with the data in a study of the reverse reaction by Zabel et al. [404] to compute the value of the equilibrium constant in Table 3. Destriau and Troe [104] have fit the above data with k_∞ independent of temperature and $F_c = 0.36$. Bridier et al. [46] are in good agreement with this recommendation at one atmosphere and 298 K. (Table: 06-2, Note: 06-2) [Back to table](#)
- D11. $C_2H_5O_2 + NO_2$. The only experimental study is that of Elfers et al. [113] who measured the rate constant relative to the $C_2H_5O_2 + NO$ reaction between 10 and 1000 mbar. Elfers et al. used a value of $k = 8.9 \times 10^{-12} \text{ cm}^3 \text{ molecule}^{-1} \text{ s}^{-1}$ for the reference reaction. By comparison the recommended rate constant for the reference reaction from Table 1-1 of this evaluation is $1.1 \times 10^{-11} \text{ cm}^3 \text{ molecule}^{-1} \text{ s}^{-1}$ at 254 K. There are three data points. An evaluation of the Elfers et al. work by Destriau and Troe [104] cast the data in the format used in the IUPAC evaluation [16]. The parameters in Table 2 are adjusted to agree with the data corrected for the change in the reference reaction, using the simpler formula employed in this recommendation. (Table: 02-25, Note: 02-25) [Back to table](#)
- D12. $CH_3C(O)O_2 + NO_2$. The recommended parameters are from the data of Bridier et al. [45], who report in the format represented here, but using $F_c = 0.3$. Their values are: $k_0^{300} = (2.7 \pm 1.5) \times 10^{-28}$, $k_\infty^{300} = (12.1 \pm 2.0) \times 10^{-12}$, with $n = 7.1 \pm 1.7$ and $m = 0.9 \pm 0.15$. Studies of the decomposition of $CH_3C(O)O_2NO_2$ [PAN] by Roberts and Bertman [312], Grosjean et al. [152], and Orlando et al. [275] are in accord with those of Bridier et al. [45]. In the Roberts and Bertman [312] study it was shown that PAN decomposition yields only peroxyacetyl radical and NO_2 ; no methyl nitrate. Studies by Seefeld et al. [328] and Sehested et al. [330] of the relative rates of

CH₃C(O)O₂ with NO and NO₂ are confirmatory. A study by von Ahsen et al. [372] involving matrix isolation of the products of PAN decomposition, suggests a minor pathway due to O-O bond fission. (Table: 06-2, Note: 06-2) [Back to table](#)

- D13. CH₃CH₂C(O)O₂ + NO₂. This reaction, forming peroxypropionyl nitrate (PPN), has been studied in the reverse direction by Schurath and Wipprecht [327], Mineshos and Glavas [251], Grosjean et al. [152] and Kirchner et al. [200]. Group additivity considerations indicate that the equilibrium constant for both PAN and PPN will be the same (both sides of the equilibrium for PPN differ from those for PAN by the group C-(C)(CO)(H)₂.) Therefore, the recommended value for the association reaction is taken from the decomposition studies multiplied by the same equilibrium constant as for PAN. The resulting values are very similar to those for CH₃C(O)O₂ + NO₂ forming peroxyacetyl nitrate (PAN). Conservative error limits are estimated. (Table: 02-25, Note: 06-2) [Back to table](#)
- D14. CH₃C(O)CH₂ + O₂. Cox et al. [88] reported a value of $k = (1.5 \pm 0.3) \times 10^{-12} \text{ cm}^3 \text{ molecule}^{-1} \text{ s}^{-1}$ at 298 K and 1 atm of SF₆ in which a pulse radiolysis study was modeled. Studies in He at 298 K have been reported by Oguchi et al. [271], Imrik et al. [177], Kovacs et al. [205] and Hassouna et al. [157]. This data can be accommodated with $k_0 = 1.5 \times 10^{-29} \text{ cm}^3 \text{ molecule}^{-1} \text{ s}^{-1}$, $k_\infty = 1.0 \times 10^{-12} \text{ s}^{-1}$ with $f = 1.15$. To account for the difference between He and N₂, $k_0 = 3 \times 10^{-29}$, and $f = 1.3$ are estimated and recommended. Hassouna et al. report rate constants in the temperature range 291 to 400 K at 130 and 650 bar He showing a slight negative temperature dependence. They also report data at 10 bar He in the temperature range 459 to 520 K. These latter data exhibit biexponential decays from which the equilibrium constant is also extracted. (See Table 3.) (Table: 10-6, Note: 10-6, Evaluated: 10-6) [Back to table](#)
- E1. F + O₂. Values are taken from a study by Campuzano-Jost et al. [60], with experiments from 100 to 420 K at pressures of He, Ar and N₂ from 1 to 1000 bar. (They used $F_c = 0.54(T/300)^{-0.09}$, but the results are essentially the same with $F_c = 0.6$.) A study by Pagsberg et al. [284] reports k_0 in argon $= 4.38 \times 10^{-33} (T/300)^{-1.2}$. There is also good agreement with earlier values of Smith and Wrigley [346], Smith and Wrigley [347], Shamonina and Kotov [336], Arutyunov et al. [10], Wallington and Nielsen [383], Wallington et al. [382] and Ellerman et al. [114]. The values are slightly lower than the values of Chen et al. [70] and Chegodaev et al. [69]. Lyman and Holland [235] report a slightly lower value in Ar at 298 K. Campuzano-Jost et al. [60] and Pagsberg et al. [284], also determined the equilibrium constant and thus $\Delta H_{f,298}(\text{FO}_2) = 6.13 \pm 0.5 \text{ kcal mol}^{-1}$. See F + O₂ in Table 3-1. (Table: 06-2, Note: 06-2) [Back to table](#)
- E2. F + NO. A study by Pagsberg et al. [282], taking into account data from Zetzsch [408], Skolnik et al. [342], Kim et al. [198], Pagsberg et al. [283] and Wallington et al. [380], reports rate constants for this reaction in several bath gases. Re-evaluating the data and converting to the form used in this compilation yields the recommended parameters. (Table: 06-2, Note: 06-2) [Back to table](#)
- E3. F + NO₂. Fasano and Nogar [119] studied this reaction in N₂ at 300 K. Pagsberg et al. [281] studied the reaction in SF₆ and Zetzsch [408] studied it in He. The results from Fasano and Nogar [119] and Pagsberg et al. [281] were used to determine both the high and low pressure limits at 300 K. Treatment of the data for this system requires knowledge of the relative stabilities of FNO₂ and FONO. Patrick and Golden [293] assumed that the difference between these would be the same as between the ClNO₂ isomers. Theoretical work by Dixon and Christie [108], Lee and Rice [219] and Amos et al. [4] indicates that FNO₂ is 35–40 kcal mol⁻¹ more stable than FONO, and therefore the measured rate refers to FNO₂ formation. The value of $n = 2$ is from Patrick and Golden, but consistent with Pagsberg et al. [281] who made a few measurements at 341 K. The value of m is a rough estimate from similar reactions, but is also consistent with Pagsberg et al. [281]. (Table: 06-2, Note: 06-2) [Back to table](#)
- E4. FO + NO₂. Low pressure limit from strong collision calculation and $\beta = 0.33$. T dependence from resultant $\langle \Delta E \rangle = 0.523 \text{ kcal mol}^{-1}$, high-pressure limit and T dependence estimated. A theoretical study by Rayez and Destriau [309] indicates that the product is the single isomer FONO₂. Bedzhanyan et al. [31] report a value extracted from a complex mixture of bath gases. (Table: 06-2, Note: 94-26) [Back to table](#)
- E5. CF₃ + O₂. Caralp et al. [63] have measured the rate constant in N₂ between 1 and 10 Torr. This supersedes the value from Caralp and Lesclaux [62]. Kaiser et al. [192] have extended the pressure range to 580 Torr measuring the reaction relative to the reaction of CF₃ with Cl₂. Breheny et al. [44] report values at 295 K from 2–110 torr and they make a cogent argument for lowering the value of the rate constant used by Kaiser et al. for their reference reaction by about 50%. This has the effect of lowering the Kaiser values. Each study recommends different parameters, but the data are well represented by the currently recommended values. Data of Ryan and Plumb [315] are in general agreement. Forst and Caralp [127] have examined this reaction theoretically. (Table: 06-2, Note: 06-2) [Back to table](#)

- E6. $\text{CF}_3\text{O} + \text{NO}_2$. Fockenberg et al. [126] report values in nitrogen with $250 < T/\text{K} < 302$ and $7 < p/\text{mbar} < 107$. They report large error limits. Their values, including two sigma errors, using the previous format are: $k_0 = (3.1 \pm 3.0) \times 10^{-28}$; $n = (2.0 \pm 2.0)$; $k_\infty = (1.5 \pm 0.5) \times 10^{-28}$; $m = (2.8 \pm 2.0)$. These were used in JPL 02-25. Here the data has been fit forcing $m=1$, as values as large as $m=2.8$ are not justifiable. The reaction products agree with those reported by Chen et al. [71], who used photolysis of CF_3NO to prepare CF_3O_2 and subsequently CF_3O in 700 Torr of air at 297 ± 2 K. They considered two product channels: (a) CF_3ONO_2 obtained via three-body recombination and (b) $\text{CF}_2\text{O} + \text{FNO}_2$ obtained via fluorine transfer. Both products were observed and found to be thermally stable in their reactor. They report $k_a/(k_a+k_b) > 90\%$ and $k_b/(k_a+k_b) < 10\%$, thus the formation of CF_3ONO_2 is the dominant channel at 700 Torr and 297 K. (Table: 06-2, Note: 06-2) [Back to Table](#)
- E7. $\text{CF}_3\text{O}_2 + \text{NO}_2$. The data are from experiments in O_2 of Caralp et al. [64], who suggest a somewhat different fitting procedure than used here. A statistical best fit to the data yields a value of $m=5.7$, but the values recommended here fit the data just about as well. Destriau and Troe [104] use yet a different fitting procedure that does not represent the data quite as well as that recommended here. Reverse rate data are given by Köppenkaströf and Zabel [204]. (Table: 06-2, Note: 06-2) [Back to table](#)
- E8. $\text{CF}_3\text{O} + \text{CO}$. Values taken from Turnipseed et al. [364]. The numbers were obtained for Ar as the bath gas and are assumed to hold for N_2 as well. The temperature dependence of the high-pressure rate constant was determined over the range $233 < T/\text{K} < 332$ in SF_6 . No temperature dependence of the low-pressure-limiting rate constant was reported. The value in the table is an estimate. Wallington and Ball [378] report values in good agreement with Turnipseed et al. [364]. (Table: 06-2, Note: 06-2) [Back to table](#)
- E9. $\text{CF}_3\text{O} + \text{M}$. The activation energy for thermal decomposition of CF_3O to $\text{CF}_2\text{O} + \text{F}$ has been reported to be 31 kcal mol^{-1} by Kennedy and Levy [197]. Thermochemical data yield $\Delta H^\circ(298) = 23 \text{ kcal mol}^{-1}$. This implies an intrinsic barrier of about 8 kcal mol^{-1} to elimination of F from CF_3O . Electronic structure calculations by Li and Francisco [227] support this observation. Adopting the A-factor for unimolecular dissociation, $A = 3 \times 10^{14} \text{ s}^{-1}$ and $E = 31 \text{ kcal mol}^{-1}$ from Kennedy and Levy, k_∞ (298 K) is about $6 \times 10^{-9} \text{ s}^{-1}$. This corresponds to a lifetime of about 6 years; therefore, thermal decomposition of CF_3O is unimportant throughout the atmosphere. (Table: 94-26, Note: 94-26) [Back to table](#)
- F1. $\text{Cl} + \text{O}_2$. Nicovich et al. [263] measured the rate constant at $181 < T/\text{K} < 200$ and $15 < p/\text{torr} < 40$ in O_2 . They reported $k_0 = (9 \pm 3) \times 10^{-33} \text{ cm}^6 \text{ molecule}^{-2} \text{ s}^{-1}$ at $T = 187 \pm 6 \text{ K}$ in O_2 . The recommended low pressure limiting parameters are from fitting their data over the entire range and assuming the same value for N_2 as the bath gas. The value from the calculation at 300 K (i.e., $2.2 \times 10^{-33} \text{ cm}^6 \text{ molecules}^{-2} \text{ s}^{-1}$) compares with an older value of Nicholas and Norrish [261] of 1.7×10^{-33} in an $\text{N}_2 + \text{O}_2$ mixture. Baer et al. [19] report a value in O_2 of $k_0 = (1.6) \times 10^{-33} (T/300)^{-2.9} \text{ cm}^6 \text{ molecule}^{-2} \text{ s}^{-1}$ in good agreement with the value recommended here. They also report a value in N_2 of $k_0 = (1.4) \times 10^{-33} (T/300)^{-3.9} \text{ cm}^6 \text{ molecule}^{-2} \text{ s}^{-1}$. A theoretical study by Zhu and Lin [415] suggests $k_0 = (1.26) \times 10^{-16} T^{6.22} \exp(-943/T) \text{ cm}^6 \text{ molecule}^{-2} \text{ s}^{-1}$ in O_2 (2.0×10^{-33}) at 300K with $k_\infty = (1.8) \times 10^{-10} \text{ s}^{-1}$, which is adopted here. The Nicovich et al [263] data are so far from the high pressure limit, that the difference in values for the high pressure rate constant can't be evaluated easily. Baer et al [19] suggest $k_\infty = 2.7 \times 10^{-11} \text{ s}^{-1}$, but the data suggest a higher value. (Table: 06-2, Note: 06-2) [Back to table](#)
- F2. $\text{Cl} + \text{NO}$. Low-pressure limit and temperature dependence is from re-evaluation of data from Lee et al. [216]. Clark et al. [74] and Ashmore and Spencer [11] also have data in agreement with the recommendation. (Table: 06-2, Note: 06-2) [Back to table](#)
- F3. $\text{Cl} + \text{NO}_2$. Low-pressure limit at 300 K from Leu [225] and Ravishankara et al. [306]. The latter study extended the data to 200 Torr in He. A turbulent flow study by Seeley et al. [329] extended the results to 250 Torr of Ar and the high-pressure limit was chosen to fit these two studies after taking into account differences in collisional efficiencies of the bath gases. Leu [225] confirms the observation of Niki et al. [267] that both ClONO and ClNO_2 are formed, with the former dominating. This has been explained by Chang et al. [68], with detailed calculations in Patrick and Golden [293]. The temperature dependence is as predicted in Patrick and Golden [293] and is the same as Leu's results in He. Ravishankara et al. [306] report a few data points in N_2 that may suggest a somewhat higher temperature dependence. The temperature dependence of the high-pressure limit is estimated. The uncertainty limits are estimated. Master Equation/RRKM studies by Zhu and Lin [416] and by Golden [145], using potential energy surfaces computed by Lee [217], Zhu and Lin [416] and Sayin and McKee [324], report differences in their ability to fit the data. Zhu and Lin [416] claim to fit, while Golden [145] finds the calculations to underpredict the low pressure data. (Table: 10-6, Note: 10-6, Evaluated: 10-6) [Back to table](#)
- F4. $\text{Cl} + \text{CO}$. From Nicovich et al. [264], who measured the process in N_2 for $185 \leq T/\text{K} \leq 260$. Hewitt et al. [161] report a value at one atmosphere and 298 K with ^{13}CO in agreement with Nicovich et al. [264]. (Table: 06-2, Note: 06-2) [Back to table](#)

- F5. $\text{Cl} + \text{C}_2\text{H}_2$. The recommended values are a statistical fit to the work of Kaiser [187] in air. Kaiser and Wallington [186] extends the pressure range at 296K to 0.3–6000 Torr. The data are in reasonable agreement with earlier measurements of Brunning and Stief [49] and Wallington et al. [375], although the derived temperature dependence is less than obtained by Brunning and Stief [49]. These values are compatible with earlier studies of Poulet et al. [303], Atkinson and Aschmann [13], Lee and Rowland [215] and Wallington et al. [384]. Using FTIR, Zhu et al. [417] reported branching of 16% and 84% to the trans and cis adduct isomers, respectively, at 700 Torr N_2 and 295 K. (Table: 06-2, Note: 06-2) [Back to table](#)
- F6. $\text{Cl} + \text{C}_2\text{H}_4$. Values at 300 K are from a relative rate study by Wallington et al. [375]. A relative rate study by Kaiser and Wallington [186] extends the pressure range to 0.3–6000 Torr and is compatible with earlier studies. Temperature dependence of k_0 is taken from Kaiser and Wallington [190]. The temperature dependence of k_∞ is estimated. Values are in reasonable agreement with studies by Maricq et al. [238], Lee and Rowland [215], Iyer et al. [181], Atkinson and Aschmann [13], Atkinson and Aschmann [14] and Wallington et al. [385]. A study in He by Stutz et al. [353] is noted, as is a comment on it by Kaiser and Wallington [190]. Knyazev et al. [203] have done an extensive experimental and theoretical analysis. Their values agree with this recommendation. (Table: 97-4, Note: 02-25) [Back to table](#)
- F7. $\text{Cl} + \text{C}_2\text{Cl}_4$. Recommendation is from the flash-photolysis study of Nicovich et al. [265] done at 231–390 K in 3–700 Torr N_2 . A study by Thuner et al. [356] is in agreement. (Table: 97-4, Note: 02-25) [Back to table](#)
- F8. $\text{ClO} + \text{NO}_2$. The low-pressure-limit recommendation and uncertainties are based on temperature-dependent values from Zahniser et al. [405], Lee et al. [221], Birks et al. [37], Leu et al. [225], Wallington and Cox [379], Cox et al. [84] and Molina et al. [253]. All of these data were collected in N_2 bath gas, except for several points from Lee et al. [221] collected in O_2 . The high-pressure-limit recommendation is based on the RRKM calculations of Smith and Golden [149]. There are several pressure-dependent data sets in the literature, such as Percival et al. [294], Handwerk and Zellner [155], Dasch et al. [97] and Cox and Lewis [87]; however, they are too disparate to extract unambiguous values. These data are all reproduced within two-sigma error limits by the current recommendation. However, the value of $m = 1.9$ is somewhat large for a radical-radical process. If $m = 1$ is chosen the computed rate constant is lower by about 20% at 180K and pressures above 500 torr. Golden [147] has attempted to fit the data with a master equation analysis and finds that the usual energy transfer treatment at low pressures is insufficient to fit the data. (Table: 06-2, Note: 10-6, Evaluated: 10-6) [Back to table](#)
- F9. $\text{OCIO} + \text{NO}_3$. Friedl et al. [132], studied this system at $1 \leq P/\text{Torr} \leq 5$ for helium and $220 \leq T/\text{K} \leq 298$. They deduced values for the rate constant consistent with their data of $k_0 \approx 10^{-31}$ and $k_\infty \approx 10^{-11}$. They also suggest a value for the equilibrium constant: $\text{K}/\text{cm}^3 \text{ molecule}^{-1} = 1 \times 10^{-28} \exp(9300/T)$. Boyd et al. [42] raised the question of possible heterogeneous effects in this system. Parthiban et al. [291] in a theoretical study, support the finding of Friedl et al. [132] of the species O_2ClONO_2 , but suggest a very different equilibrium constant. (See Table 3-1). (Table: 94-26, Note: 06-2) [Back to table](#)
- F10. $\text{ClO} + \text{ClO}$. The recommendation is based on a fit to data from Sander et al. (195–247 K) [319] as quoted by Nickolaissen et al. (260–390 K) [262], Bloss et al. (183–245 K) [40], Trolier et al. (200–263 K) [361] and Boakes et al. [41]. The Trolier et al. data have been corrected for values at the zero pressure intercept as suggested in the Trolier et al. paper. With this adjustment all the data except the Boakes et al. values are in reasonable agreement. Boakes et al. [41] report higher values. They found a zero pressure intercept as well, but they suggest disregarding their data at less than 100 Torr and report preferred parameters of 2.79×10^{-32} ; 3.78; 3.44×10^{-12} ; 1.73. The Boakes et al [41] values are accommodated in this evaluation by the change in the values of the high pressure limiting rate constant compared with the evaluation in JPL 06-2 [317]. Error limits represent an attempt to include all the data within the 95% uncertainty. Golden [142] has performed RRKM and master equation calculations using the potential energy surface in Zhu and Lin [413] and concluded that while a channel to form ClOClO might exist, the best representation of the data remains that only a single channel exists. The value of $m = 2$ is somewhat high, but attempts to statistically model any and all of the data sets yield even higher values. The k_0 value for N_2 is not in accord with a simple theory as explained in Patrick and Golden [293] and in some detail in Golden [142]. It has been suggested [360] that the “radical-complex” mechanism may apply here, although a study by Liu and Barker [230] suggests otherwise. Ferracci and Rowley [124] report values at one atmosphere and temperature from 250 to 313 K in essential agreement with Boakes et al. [41]. Other previous rate constant measurements, such as those of Hayman et al. [159], Cox and Derwent [85], Basco and Hunt [24], Walker [374], and Johnston et al. [184], range from $(1-5) \times 10^{-32} \text{ cm}^6 \text{ molecule}^{-2} \text{ s}^{-1}$, with N_2 or O_2 as third bodies. The major dimerization product is chlorine peroxide (Birk et al. [36], DeMore and Tschuikow-Roux [103], Slanina and Uhlik [343], Stanton et al. [350] and Lee et al. [220]). (Table 09-31, Note:10-6, Evaluated: 10-6) [Back to table](#)

- F11. $\text{ClO} + \text{OCIO}$. Data are from Burkholder et al. [52], who measured the rate constant in N_2 at $200 \leq T/\text{K} \leq 260$ and densities from $(1.1\text{--}10.9) \times 10^{18} \text{ molecules cm}^{-3}$. They also measured the equilibrium constant. (See Table 3) Parr et al. [289] also report a value for the rate constant in reasonable agreement with the recommendation. Zhu and Lin [414] report an ab initio study of this system. Their parameters are somewhat different from those herein, but they fit the data equally well. Green et al. [150] report a value in He that is consistent with the values recommended herein. (Table: 06-2, Note: 06-2) [Back to table](#)
- F12. $\text{O} + \text{OCIO}$. The recommendation is based on data of Colussi et al. [80] and Colussi [79], who measured the pressure dependence between 248 and 312 K in Ar. They interpret the intercept of their k vs $[\text{M}]$ curves as a zero-pressure rate constant of $(1.6 \pm 0.4) \times 10^{-13} \text{ cm}^3 \text{ molecule}^{-1} \text{ s}^{-1}$ with a negative activation energy corresponding to a chemical activation channel producing $\text{ClO} + \text{O}_2$. A low pressure study by Gleason et al. [141], as well as a theoretical study by Zhu and Lin [412], suggests a direct abstraction with a positive activation energy. (Zhu and Lin [412] point out that sym-ClO_3 has a positive barrier for dissociation to $\text{ClO} + \text{O}_2$.) The recommended values are fit to the data after subtracting the abstraction channel. See Table 1-1. (Table: 06-2, Note: 06-2) [Back to table](#)
- F13. $\text{CH}_2\text{Cl} + \text{O}_2$. Measured by Fenter et al. [120] over the range $298 \leq T/\text{K} \leq 448$ and $1 \leq P/\text{Torr} \leq 760$ in nitrogen. Two different techniques were employed: laser photolysis/photoionization mass spectrometry in the range 1–10 Torr and laser photolysis/UV absorption for the range 20–760 Torr. A study by Bilde et al. [35] in N_2 relative to the reaction $\text{CH}_2\text{Cl} + \text{Cl}_2 \rightarrow \text{CH}_2\text{Cl}_2 + \text{Cl}$ is in excellent agreement. Error limits transposed to the current format. (Table: 06-2, Note: 06-2) [Back to table](#)
- F14. $\text{CHCl}_2 + \text{O}_2$. Measured by Fenter et al. [120] over the range $298 \leq T/\text{K} \leq 383$ and $1 \leq P/\text{Torr} \leq 760$ in nitrogen. Two different techniques were employed: laser photolysis/photoionization mass spectrometry in the range 1–10 Torr and laser photolysis/UV absorption for the range 20–760 Torr. A study by Nottingham et al. [270], in He, is in agreement. Error limits transposed to the current format. [Back to table](#)
- F15. $\text{CCl}_3 + \text{O}_2$. The recommendation incorporates studies by Fenter et al. [121], Danis et al. [96] and Luther et al. [234]. (Their data above 100 bar are affected by diffusion.) Experimental data of Ryan and Plumb [316] have been considered in the evaluation. A study by Nottingham et al. [270], in He, is in agreement. Forst and Caralp [127] have examined this reaction theoretically. A Patrick and Golden-type calculation using the thermochemistry of Russell et al. [314] yields $k_0^{300} = 1.5 \times 10^{-30}$, with $\beta = 0.3$. A value of $k_\infty^{300} = 5 \times 10^{-12}$ has been reported by Cooper et al. [82]. The value of the rate constants recommended here vary slightly from those of Luther et al., (who report $k_\infty^{300} = 5.2 \times 10^{-12}$; $m = 1.4$ and $k_0^{300} = 1.5 \times 10^{-30}$; $n = -6.3$; $F_c = 0.35 \times (T/300)^{-0.35}$ using the IUPAC formula) but yield an overall rate constant within their error limits. (Table: 06-2, Note: 06-2) [Back to table](#)
- F16. $\text{CFCl}_2 + \text{O}_2$. Values for both low- and high-pressure limits at 300 K are from Caralp and Lesclaux [62]. Forst and Caralp [127] have examined this reaction theoretically. Temperature dependences are rough estimates based on their calculations and similar reactions. (Table: 06-2, Note: 06-2) [Back to table](#)
- F17. $\text{CF}_2\text{Cl} + \text{O}_2$. The recommended $k_0(300)$ and $k_\infty(300)$ are from the experimental work reported by Codnia and Azcárate [78], and the recommended temperature exponents are the theoretical predictions of Forst and Caralp [127]. Codnia and Azcárate used CO_2 laser IR multiphoton dissociation of CF_2Cl_2 to prepare CF_2Cl radicals in the presence of O_2 (and N_2 buffer gas) at 300 K. Subsequent fast reactions produced vibrationally excited CF_2O^* , which they monitored by measuring its spontaneous IR fluorescence near 1928 cm^{-1} . They showed that the growth and decay rates of the IR fluorescence intensity are due to the reactions of CF_2Cl radicals with O_2 and to the rate of collisional deactivation of CF_2O^* . Analysis of the reaction rates between CF_2Cl and O_2 revealed the existence of both the pressure-dependent recombination reaction and a direct bimolecular step (previously proposed by other workers; Table 1) are important in the pressure range from 0 to 20 mbar of N_2 . Separate control of O_2 enabled them to obtain the rate constant for the direct reaction (Table 1), as well as $k_0(300)$ and $k_\infty(300)$ for the recombination. The latter values are in rough agreement with the theoretical predictions of Forst and Caralp [127], who predicted temperature exponents in approximate agreement with similar reactions. The estimated errors are relatively large because the reaction has been measured only once at 300 K and because the temperature dependence is based on theoretical predictions. (Table: 10-6, Note: 10-6; Evaluated 10-6) [Back to table](#)
- F18. $\text{CCl}_3\text{O}_2 + \text{NO}_2$. Statistical fit (constrained to $m=1$) to experiments in O_2 of Caralp et al. [64], who suggest a somewhat different fitting procedure, but the values recommended here fit the data as well. Destriau and Troe [104] use yet a different fitting procedure that does not represent the data quite as well as that recommended herein. Reverse rate data are given by Köppenkaströ and Zabel [204]. (Table: 06-2, Note: 06-2) [Back to table](#)
- F19. $\text{CFCl}_2\text{O}_2 + \text{NO}_2$. Statistical fit to experiments in O_2 of Caralp et al. [64] with constraint that $m=1$. Caralp et al. [64] suggest a different fitting procedure, but the values recommended here fit the data as well. Destriau and

Troe [104] use yet a different fitting procedure that does not represent the data quite as well as that recommended herein. Reverse rate data are given by Köppenkaströ and Zabel [204]. (Table: 06-2, Note: 06-2) [Back to table](#)

- F20. $\text{CF}_2\text{ClO}_2 + \text{NO}_2$. A study by Xiong and Carr [401] of the reverse reaction, combined with the equilibrium constant, which was computed from correcting the study by Wu and Carr [400] of the forward reaction in a bath gas consisting of 80% CF_2ClBr + 20% O_2 for N_2 bath gas. (The study by Wu and Carr [400] supersedes the earlier work of Moore and Carr [255].) Xiong and Carr [401] report their parameterization differently than in this recommendation, but the values herein reproduce their results to a few percent. Reverse rate data are also given by Köppenkaströ and Zabel [204] and in a theoretical study by Forst and Caralp [128]. (Table: 06-2, Note: 06-2) [Back to table](#)
- G1. $\text{Br} + \text{NO}_2$. The recommended values are from a study by Kreutter et al. [206]. They regarded the product as BrNO_2 . Their k_0 value in He agrees with the measurement of Mellouki et al. [247] at 300 K. Broske and Zabel [47] and Orlando and Burkholder [273] have shown that cis- BrONO is the major product in their studies. Orlando and Burkholder [273] suggest that isomerization to BrNO_2 is heterogeneous. Lee [218] calculated structure, frequencies and energetics for BrNO_2 , cis- BrONO and trans- BrONO . A Patrick-and-Golden-type calculation using the Lee [218] results yields k_0 (strong collision) $\approx 1.2, 2.5$ and 2.1 in units of $1 \times 10^{-31} \text{ cm}^6 \text{ molecule}^{-2} \text{ s}^{-1}$ for trans- BrONO , cis- BrONO and BrNO_2 , respectively. The sum, 5.9×10^{-31} , multiplied by a collision efficiency in N_2 of 0.3 is a factor of about 2.5 lower than the observed k_0 value. Also, the relative yield of BrNO_2 is somewhat too high since Orlando and Burkholder [273] measure $\text{BrONO} > 75\%$. Kreutter et al. [206] report an equilibrium constant, which, if cis- BrONO is assumed to be the product, suggests bond strengths for the BrONO compounds that are about 4 kcal mole^{-1} higher than the Lee [218] calculation. Computing k_0 with these new values yields $k_0 \approx 4.5$ and 6.4 in units of 1×10^{-31} for trans- BrONO and cis- BrONO respectively. When the sum of the rate constants for the three channels is multiplied by the collision efficiency (0.3), the result is $3.9\text{E-}31$ and the yield of BrONO is 85%. (Table: 06-2, Note: 06-2) [Back to table](#)
- G2. $\text{BrO} + \text{NO}_2$. Values from a study by Thorn et al. [355] that is in excellent agreement with Sander et al. [321] are recommended. Error limits are from a reanalysis of the data. Danis et al. [95] give slightly lower values for the low-pressure-limiting rate constant and a smaller temperature dependence as well. This latter study may be hampered by heterogeneous effects, but can be accommodated within the error limits recommended. A theoretical study by Rayez and Destriau [309] suggests that the bond-dissociation energy in BrONO_2 is 8.5 kcal mol^{-1} higher than in ClONO_2 , thus rationalizing the relative values of the low-pressure-limiting rate constants for these two processes. A more detailed theoretical study by Parthiban and Lee [290], as well as a study by Orlando and Tyndall [274], who measured BrONO_2 decomposition and thus an equilibrium constant, both determine only 1.6 kcal mol^{-1} for the above difference. A theoretical study by Zou et al. [418] agrees with the latter figure. A Patrick and Golden [293] type calculation, even with the stronger bond of Rayez and Destriau [309] yields a value for the low pressure limiting rate constant that is less than observed. Lessar et al. [223] calculate a potential energy surface for BrOONO . They find that the $\text{BrO} - \text{ONO}$ bond strength is of the order of 7 kcal mol^{-1} , which is too weak to have any effect on the overall rate of $\text{BrO} + \text{NO}_2$. *The temperature dependence of the high pressure rate constant seems large. The data can be fit quite well with $k_\infty = 8 \times 10^{-12} (T/300)^{-1}$.* Walsh and Golden [146, 386] have attempted to fit the data with a master equation analysis and find that the usual energy transfer treatment at low pressures is insufficient to fit the data. (Table: 06-2, Note: 10-6, Evaluated: 10-6) [Back to table](#)
- H1. $\text{I} + \text{NO}$. Evaluation taken from IUPAC [179]. The data are from van den Bergh et al. [367] and Basco and Hunt [23]. Error limits transposed to the current format. The heat of formation of INO is given as 120.0 ± 0.3 kJ/mole by Forte et al. [130]. (Table: 06-2, Note: 06-2) [Back to table](#)
- H2. $\text{I} + \text{NO}_2$. Evaluation taken from IUPAC [179]. The data are from van den Bergh et al. [367], Mellouki et al. [247], Buben et al. [50] and van den Bergh and Troe [368]. IUPAC uses $F_c = 0.63$, which is the same as the universal value adopted here of $F_c = 0.6$. (No evidence of possible isomers $[\text{INO}_2]$ or $[\text{IONO}]$ is reported.) Error limits transposed to the current format. Tucceri et al. [362] used laser flash photolysis coupled to resonance-fluorescence detection of I atoms to measure the rate coefficients for the reaction: $\text{I} + \text{NO}_2 + \text{M} \rightarrow \text{INO}_2 + \text{M}$. Rate coefficients at 298 K when combined with other datasets obtained at higher and lower pressures, were adequately described by a simplified Troe function with the parameters: $k_0(\text{He}, 330 \text{ K}) = 1.48 \times 10^{-31} \text{ cm}^6 \text{ molecule}^{-2} \text{ s}^{-1}$, $F_c(\text{He}) = 0.43$, and $k_\infty = 1.1 \times 10^{-10} \text{ cm}^3 \text{ molecule}^{-1} \text{ s}^{-1}$ for He as bath gas. In N_2 (or air) the following parameters were obtained $k_0(\text{N}_2, 300 \text{ K}) = 3.2 \times 10^{-31} \text{ cm}^6 \text{ molecule}^{-2} \text{ s}^{-1}$, $F_c(\text{N}_2) = 0.48$, with $k_\infty = 1.1 \times 10^{-10} \text{ cm}^3 \text{ molecule}^{-1} \text{ s}^{-1}$. These parameters essentially reproduce the values at 300 K from the parameters in the Table. (Table: 10-6, Note: 10-6, Evaluated 10-6) [Back to table](#)
- H3. $\text{IO} + \text{NO}_2$. Data from Daykin and Wine [101], Hölscher and Zellner [168], Allan and Plane [3], Jenkin and Cox [182] and Dillon et al. [107] are considered. Dillon et al. suggest that the value from Hölscher and Zellner

might be low at 298 K due to regeneration of IO, although their values at lower temperatures are in agreement with others. The recommendation takes this into consideration and accommodates the rest of the data. Two more studies at lower pressures are available, Larin et al. [213], and Maguin et al. [236]. These latter do not agree very well with the above five studies and have higher experimental errors. The recommended k_0 and k_∞ also agree with a theoretical study by Rayez and Destriau [309]. A computational study by Marshall [239] sets the bond dissociation energy as $DH_0(\text{IO-NO}_2) = 113.6 \pm 3.1 \text{ kJ mol}^{-1}$ and suggests $k_0 = (5.3\text{--}13.3) \times 10^{-31} \text{ cm}^6 \text{ molecule}^{-1} \text{ s}^{-1}$ for N_2 as the bath gas, while an ME/RRKM study by Golden [144] required $DH_0(\text{IO-NO}_2) \sim 150 \text{ kJ mol}^{-1}$ to fit the data. Papayannis and Kosmas [285] compute $DH_0(\text{IO-NO}_2) = 137.6$ or $131.7 \text{ kJ mol}^{-1}$, depending on spin orbit coupling corrections in IO. A computational study by Koltsoyannis and Plane [194] concludes that $DH_0(\text{IO-NO}_2) = 117.9 \text{ kJ mol}^{-1}$. (Table: 10-6, Note: 10-6, Evaluated: 10-6) [Back to table](#)

- I1. $\text{HS} + \text{NO}$. Data and analysis are from the work of Black et al. [38]. The temperature dependence of k_0 has been adjusted to give a better fit than in JPL 02-25. The temperature dependence of k_∞ has been estimated. (Table: 06-2, Note: 06-2) [Back to table](#)
- I2. $\text{CH}_3\text{S} + \text{NO}$. The recommended values are fit to the study by Balla et al. [20]. The temperature range was 295 to 453 K and pressures of N_2 from 1.5 to 300 torr. The change in the high pressure limiting rate coefficient and its temperature dependence reflect a better fit to the data. (Table: 06-2, Note: 06-2) [Back to table](#)
- I3. $\text{O} + \text{SO}_2$. Naidoo et al. [259] studied this spin forbidden reaction in Ar over the temperature range $290 < T/\text{K} < 840$ and pressure range $100 < P/\text{mbar} < 880$. They fit the data very well using the IUPAC [15] format with $k_0 = 9.5 \times 10^{-23} T^3 \exp(-2400/T) \text{ cm}^6 \text{ molecule}^{-2} \text{ s}^{-1}$, $k_\infty = 6.1 \times 10^{-13} \exp(-850/T) \text{ cm}^3 \text{ molecule}^{-1} \text{ s}^{-1}$ and $F_c = 0.558 \exp(-T/316) + 0.442 \exp(-T/7442)$. The recommended values transpose the rate constants to the form used in this evaluation and are used with the standard value of $F_c = 0.6$. These parameters don't fit the higher temperatures as well as the values derived by Naidoo et al. [259], missing the values at 840 K by about 50% and those at 699 K by about 20%. Values at 289, 399 and 581 K are fit quite well and are adequate for atmospheric conditions. Earlier values are reported by Atkinson and Pitts [18] and Müller et al. [258] (Table: 06-2, Note: 06-2) [Back to table](#)
- I4. $\text{OH} + \text{SO}_2$. Values of the rate constant as a function of pressure and temperature are from Blitz et al. [39]. They used a five parameter fit to the data, allowing F_c to be temperature dependent. The values of k_0 and k_∞ have been adjusted in the Table to accommodate $F_c = 0.6$. Blitz et al. [39] determined the high pressure limit from the reaction of $\text{OH}(v=1)$ with SO_2 . Their low pressure value was taken by re-evaluating the data of Wine et al. [396] in various bath gases at pressures up to 150 torr and temperatures between 260 K and 420 K, through the use of a master equation. The data of Paraskevopoulos et al. [288] in the same pressure range, is equally well fit. Lower pressure data from at 298 K from Leu [224] and Lee et al. [222] are well accommodated by the recommendation herein. Earlier data listed in Baulch et al. [29], Baulch et al. [28] and Atkinson et al. [15] are noted. Blitz et al. [39] have calculated the entropy and measured a third law heat of formation for HOSO_2 ($373 \pm 6 \text{ kJ/mol}$). See also Li and McKee [226]. (Table: 06-2, Note: 06-2) [Back to table](#)
- I5. $\text{CH}_3\text{SCH}_2 + \text{O}_2$. Wallington et al. [381] have employed a pulse radiolysis technique, obtaining $k = (5.7 \pm 0.4) \times 10^{-12} \text{ cm}^3 \text{ molecule}^{-1} \text{ s}^{-1}$ in 992 mbar of SF_6 at room temperature. A theoretical study by Resende and De Alemeida [310] yields a heat of formation of the product, $\text{CH}_3\text{SCH}_2\text{O}_2$, as $6.51 \text{ kcal mol}^{-1}$. (Table: 94-26, Note: 06-2) [Back to table](#)
- I6. $\text{SO}_3 + \text{NH}_3$. Recommendation is from Lovejoy [232]. This study covered 20–80 Torr from 280 – 340 K. An earlier study by Lovejoy and Hanson [233], who studied this reaction from 10–400 Torr N_2 at 295 K is in agreement. Lovejoy and Hanson [233] observed that any incipient adduct rapidly becomes sulfamic acid (H_3NSO_3) which clusters efficiently with itself and sulfuric acid. The observed sulfamic acid dimerization rate constant exceeds $5 \times 10^{-11} \text{ cm}^3 \text{ molecule}^{-1} \text{ s}^{-1}$. Measurements of Shen et al. [338] made at 1–2 Torr He are much higher than those of Lovejoy and Hanson [233] or Lovejoy [232]. Error limits have been adjusted to take into account the fact that the exponent of the temperature dependence of the low pressure rate constant is unusually large. Lovejoy [232] also reports an equilibrium constant and heat of formation of sulfamic acid of $-24 \pm 1 \text{ kcal mol}^{-1}$. (Table: 06-2, Note: 06-2) [Back to table](#)
- I7. $\text{HO} + \text{CS}_2$. The data are from Hynes et al. [reaction 38 in Table 3-1] and Murrells et al. [reaction 32 in Table 3-1]. The value $m = 1$ is constrained. The adduct reacts slowly with O_2 . (See Table 1-1.) (Table: 06-2, Note: 06-2) [Back to table](#)
- I8. $\text{Cl} + \text{CS}_2$. The data are from Nicovich et al. [266]. Wallington et al. [376] have also studied this system. The value $m = 0$ is constrained. Nicovich et al. [266] confirm that the reaction proceeds via reversible adduct formation as suggested by Martin et al. [241]. The much larger rate constant values determined by Martin et al. may possibly be attributed to reactive impurities in the CS_2 sample. Nicovich et al. set an upper limit on the rate

constant for the adduct (CS_2Cl) reacting with O_2 of $2.5 \times 10^{-16} \text{ cm}^3 \text{ molecule}^{-1} \text{ s}^{-1}$ at room temperature. Wang and Phillips [387] have performed a theoretical study of the adduct. (Table: 06-2, Note: 06-2) [Back to table](#)

- I9. $\text{OH} + \text{CH}_3\text{SCH}_3 \rightarrow (\text{CH}_3)_2\text{SOH} \rightarrow \text{products}$. The $\text{OH} + \text{CH}_3\text{SCH}_3$ reaction is complex, proceeding by both direct H-abstraction and reversible addition pathways. A recommendation for the direct reaction is discussed separately in Table 1. The product of the reversible addition pathway reacts with O_2 creating an irreversible path as well. Mechanistically, this pathway is described by combining the rate constants k_f for the addition step, k_r for the reverse dissociation step, and k_{O_2} for the adduct reaction with O_2 . This is discussed in detail in the notes for Table 1. The equilibrium constant for the reversible addition process is $K_c = k_f/k_r$. Recommendations for K_c , and k_{O_2} are found in Tables 3, and 1, respectively. The value for k_f recommended here is from Williams et al. [392]. The discussion in Table 1 points out that this value taken with K_c and k_{O_2} fits the extant data very well. (Table: 10-6; Note: 10-6; Evaluated: 10-6) [Back to table](#)
- I10. $\text{Cl} + (\text{CH}_3)_2\text{S}$. [See Table 1] If the HCl yield at 297K from Stickel et al. [351] is used as a measure of the abstraction reaction, the rate constant would be $1.64 \times 10^{-10} \text{ cm}^3 \text{ molecule}^{-1} \text{ s}^{-1}$. Using this value the complete data set from Stickel et al. [351] can be fit with the form used in Table 2 with the addition of a term for the abstraction in the form $k_{\text{abs}} = 1.64 \times 10^{-10} * (T/300)^a$. The value of “a” obtained in this manner is almost zero, so the data are fit with: $k_0 = 4 \times 10^{-28} (T/300)^{-7.0}$ and $k_{\infty} = 2 \times 10^{-10} (T/300)^{-1}$ along with the temperature independent value of k_{abs} . These parameters are recommended herein. Enami et al. [115] propose $k_0 = 2.2 \times 10^{-28}$ and $k_{\infty} = 2.2 \times 10^{-10}$ at 298K along with $k_{\text{abs}} = 1.8 \times 10^{-10}$. On the other hand, a study by Diaz-de-Mera et al. [106] performed in the temperature range $259 < T/\text{K} < 364$ and in helium at pressures of $0.5 < p/\text{torr} < 1$ reports a value $k_{\text{abs}} = (2.0 \pm 1.2) \times 10^{-10} \exp[-(332 \pm 173)/T]$, which yields $6.6 \times 10^{-11} \text{ cm}^3 \text{ molecule}^{-1} \text{ s}^{-1}$ at room temperature. Several studies, both experimental by Urbanski and Wine [365] and theoretical by Resende and De Almeida [311] make it clear that at higher pressures an adduct $\text{Cl-S}(\text{CH}_3)_2$ is formed and this adduct does not yield CH_3 radicals or the products of the abstraction pathway. (Table: 06-2, Note: 10-6, Evaluated 10-6) [Back to table](#)
- I11. $\text{Br} + (\text{CH}_3)_2\text{S}$. Wine et al. [395] data for the adduct formation in N_2 at $25 < P/\text{torr} < 600$ and $263 < T/\text{K} < 310$ can be evaluated in the NASA format. This leads to the values recommended. Studies by Ingham et al. [178] and Nakano et al. [260] are in agreement. Nakano et al. [260] is also in agreement with the value of the equilibrium constant. However, Maurer et al. [243] find a value at 300K and 1 bar total pressure of a mixture of 5% O_2 and 95% N_2 , only 2% as high as the value computed from the recommended parameters. This latter value is supported by Ballesteros et al. [21]. (Table: 06-2, Note: 06-2) [Back to table](#)
- J1. $\text{Na} + \text{O}_2$. A study by Plane and Rajasekhar [300] finds $k_0 = (2.9 \pm 0.7) \times 10^{-30} \text{ cm}^6 \text{ molecule}^{-2} \text{ s}^{-1}$ at 300 K with $n = 1.30 \pm .04$. They also estimate k_{∞} to be about $6 \times 10^{-10} \text{ cm}^3 \text{ molecule}^{-1} \text{ s}^{-1}$ with a small positive temperature dependence. Another study by Helmer and Plane [160] yields $k_0 = (3.1 \pm 0.2) \times 10^{-30} \text{ cm}^6 \text{ molecule}^{-2} \text{ s}^{-1}$ at 300 K with $n = 1.52 \pm 0.27$. The recommended values are taken from these studies. They are consistent with values measured by Marshall et al. [240] at 600 K and those measured by Vinckier et al. [371] at higher temperature. The k_0 value is about 60% higher than that of Silver et al. [340]. (Table: 06-2, Note: 06-2) [Back to table](#)
- J2. $\text{NaO} + \text{O}_2$. Ager and Howard [1] have measured the low- pressure limit at room temperature in several bath gases. Their value in N_2 is used in the recommendation. They performed a Troe calculation, as per Patrick and Golden [293], to obtain collision efficiency and temperature dependence. They obtained a high-pressure-limit rate constant by use of a simple model. The temperature dependence is estimated. (Table: 06-2, Note: 06-2) [Back to table](#)
- J3. $\text{NaO} + \text{CO}_2$. Ager and Howard [1] have measured the rate constant for this process in the “fall-off” regime. Their lowest pressures are very close to the low-pressure limit. The temperature dependence is an estimate. Ager and Howard calculate the high-pressure rate constant from a simple model. (Table: 06-2, Note: 06-2) [Back to table](#)
- J4. $\text{NaOH} + \text{CO}_2$. Ager and Howard [2] have measured the low-pressure-limiting rate constant. The temperature dependence is an estimate. Ager and Howard have calculated the high-pressure limit using a simple model. (Table: 06-2, Note: 06-2) [Back to table](#)

2.8 References

1. Ager, J. W., III and C. J. Howard, 1986, *Geophys. Res. Lett.*, **13**, 1395-1398.
2. Ager, J. W., III and C. J. Howard, 1987, *J. Chem. Phys.*, **87**, 921-925.
3. Allan, B. J., and J. M. C. Plane, 2002, *J. Phys. Chem. A*, **106**, 8634-8641.
4. Amos, R. D., C. W. Murray and N. C. Handy, 1993, *Chem. Phys. Lett.*, **202**, 489-494.
5. Anastasi, C. and I. W. M. Smith, 1976, *J. Chem. Soc. Faraday Trans. 2*, **72**, 1459-1468.
6. Anastasi, C. and I. W. M. Smith, 1978, *J. Chem. Soc. Faraday Trans. 2*, **74**, 1056.
7. Anderson, J. G. and F. Kaufman, 1972, *Chem. Phys. Lett.*, **16**, 375-379.
8. Anderson, J. G., J. J. Margitan and F. Kaufman, 1974, *J. Chem. Phys.*, **60**, 3310.
9. Anderson, S. M., D. Hulsebusch and Mauersberger, 1997, *J. Chem. Phys.*, **107**, 5385-5392.
10. Arutyunov, V. S., L. S. Popov and A. M. Chaikin, 1976, *Kinet. Katal.*, **17**, 286.
11. Ashmore, P. G. and M. S. Spencer, 1959, *Trans. Faraday Soc.*, **55**, 1868.
12. Atkinson, D. B. and M. A. Smith, 1994, *J. Phys. Chem.*, **98**, 5797-5800.
13. Atkinson, R. and S. M. Aschmann, 1985, *Int. J. Chem. Kinet.*, **17**, 33-41.
14. Atkinson, R. and S. M. Aschmann, 1987, *Int. J. Chem. Kinet.*, **19**, 1097-1105.
15. Atkinson, R., D. L. Baulch, R. A. Cox, J. N. Crowley, J. Hampson, R. F., R. G. Hynes, M. E. Jenkin, J. A. Kerr, M. J. Rossi and J. Troe. Web Version, 2004.
16. Atkinson, R., D. L. Baulch, R. A. Cox, J. Hampson, R. F., J. A. Kerr, M. J. Rossi and J. Troe, 1997, *J. Phys. Chem. Ref. Data*, **26**, 1329-1499.
17. Atkinson, R., D. A. Hansen and J. Pitts, J. N., 1975, *J. Chem. Phys.*, **62**, 3284-3288.
18. Atkinson, R. and J. N. Pitts Jr., 1978, *Int. J. Chem. Kinet.*, **10**, 1081.
19. Baer, S., H. Hippler, R. Rahn, M. Siefke, N. Seitzinger and J. Troe, 1991, *J. Chem. Phys.*, **95**, 6463-6470.
20. Balla, R. J., H. H. Nelson and J. R. McDonald, 1986, *Chem. Phys.*, **109**, 101-107.
21. Ballesteros, B., N. R. Jensen, and J. Hjorth, 2002, *J. Atmos. Chem.*, **43**, 135-150.
22. Barker, J. R., L. L. Lohr, R. M. Shroll and S. Reading, 2003, *J. Phys. Chem. A*, **107**, 7434-44.
23. Basco, N. and J. E. Hunt, 1978, *Int. J. Chem Kinet.*, **10**, 733-743.
24. Basco, N. and J. E. Hunt, 1979, *Int. J. Chem. Kinet.*, **11**, 649-664.
25. Basco, N., D. G. L. James and F. C. James, 1972, *Int. J. Chem. Kinet.*, **4**, 129.
26. Bates, R. W., D. M. Golden, R. K. Hanson and C. T. Bowman, 2001, *Phys. Chem. Chem. Phys.*, **3**, 2337-2342.
27. Baulch, D. L., C. T. Bowman, C. J. Cobos, R. A. Cox, T. Just, J. A. Kerr, M. J. Pilling, D. Stocker, J. Troe, W. Tsang, R. W. Walker and J. Warnatz, 2005, *J. Phys. Chem. Ref. Data* **34**, 757-.
28. Baulch, D. L., R. A. Cox, P. J. Crutzen, R. F. Hampson, Jr., J. A. Kerr, J. Troe and R. T. Watson, 1982, *J. Phys. Chem. Ref. Data*, **11**, 327-496.
29. Baulch, D. L., R. A. Cox, R. F. Hampson, Jr., J. A. Kerr, J. Troe and R. T. Watson, 1980, *J. Phys. Chem. Ref. Data*, **9**, 295-471.
30. Bean, B. D., A. K. Mollner, S. A. Nizkorodov, G. Nair, M. Okumura, S. P. Sander, K. A. Peterson and J. S. Francisco, 2003, *Journal of Physical Chemistry A*, **107**, 6974-6985.
31. Bedzhanyan, Y. R., E. M. Markin and Y. M. Gershenzon, 1993, *Kinetics and Catalysis*, **34**, 190-193.
32. Beno, M. F., C. D. Jonah and W. A. Mulac, 1985, *Int. J. Chem. Kinet.*, **17**, 1091-1101.
33. Biermann, H. W., C. Zetzsch and F. Stuhl, 1978, *Ber. Bunsenges Phys. Chem.*, **82**, 633.
34. Biggs, P., C. E. Canosa-Mas, J. M. Fracheboud, D. E. Shallcross, R. P. Wayne and F. Caralp, 1993, *J. Chem. Soc. Faraday Trans.*, **89**, 4163-4169.
35. Bilde, M., J. Sehested, O. J. Nielsen, T. J. Wallington, R. J. Meagher, M. E. McIntosh, C. A. Piety, J. M. Nicovich and P. H. Wine, 1997, *J. Phys. Chem. A*, **101**, 8035-8041.
36. Birk, M., R. R. Friedl, E. A. Cohen, H. M. Pickett and S. P. Sander, 1989, *J. Chem. Phys.*, **91**, 6588-6597.
37. Birks, J. W., B. Shoemaker, T. J. Leck, R. A. Borders and L. J. Hart, 1977, *J. Chem. Phys.*, **66**, 4591-4599.
38. Black, G., R. Patrick, L. E. Jusinski and T. G. Slanger, 1984, *J. Chem. Phys.*, **80**, 4065-4070.
39. Blitz, M. A., K. J. Hughes and M. J. Pilling, 2003, *J. Phys. Chem. A*, **101**, 1971-1978.
40. Bloss, W. J., S. L. Nikolaisen, R. J. Salawitch, R. R. Friedl and S. P. Sander, 2001, *J. Phys. Chem. A*, **105**, 11226-11239.
41. Boakes, G., W. H. H. Mok and D. M. Rowley, 2005, *Physical Chemistry Chemical Physics*, **7**, 4102-4113.
42. Boyd, A. A., G. Marston and R. P. Wayne, 1996, *J. Phys. Chem.*, **100**, 130-137.
43. Breen, J. E. and G. P. Glass, 1971, *Int. J. Chem. Kinet.*, **3**, 145.
44. Breheny, C., G. Hancock, and C. Morrell, 2001, *Zeitschrift für Physikal. Chemie*, **215**, 305-317.

45. Bridier, I., F. Caralp, H. Loirat, R. Lesclaux, B. Veyret, K. H. Becker, A. Reimer and F. Zabel, 1991, *J. Phys. Chem.*, **95**, 3594-3600.
46. Bridier, I., R. Lesclaux and B. Veyret, 1992, *Chem. Phys. Lett.*, **191**, 259-263.
47. Broske, R. and F. Zabel, 1998, *J. Phys. Chem. A*, **102**, 8626-8631.
48. Brown, S. S., R. K. Talukdar and A. R. Ravishankara, 1999, *Chem. Phys. Lett.*, **299**, 277-284.
49. Brunning, J. and L. J. Stief, 1985, *J. Chem. Phys.*, **83**, 1005-1009.
50. Buben, S. N., I. K. Larin, N. A. Messineva and E. M. Trofimova, 1990, *Kinetika i Kataliz*, **31**, 973.
51. Burkholder, J. B., P. D. Hammer and C. J. Howard, 1987, *J. Phys. Chem.*, **91**, 2136-2144.
52. Burkholder, J. B., R. L. Mauldin, R. J. Yokelson, S. Solomon and A. R. Ravishankara, 1993, *J. Phys. Chem.*, **97**, 7597-7605.
53. Burkholder, J. B. and A. R. Ravishankara, 2000, *J. Phys. Chem. A*, **104**, 6752-6757.
54. Burrows, J. P., G. S. Tyndall and G. K. Moortgat, 1985, *J. Phys. Chem.*, **89**, 4848-4856.
55. Burrows, J. P., T. J. Wallington and R. P. Wayne, 1983, *J. Chem. Soc. Faraday Trans. 2*, **79**, 111-122.
56. Butkovskaya, N., A. Kukui and G. Le Bras, 2007, *Journal of Physical Chemistry A*, **111**, 9047-9053.
57. Butkovskaya, N., M.-T. Rayez, J.-C. Rayez, A. Kukui and G. Le Bras, 2009, *Journal of Physical Chemistry A*, **113**, 11327-11342.
58. Butkovskaya, N. I., A. Kukui, N. Pouvesle and G. Le Bras, 2005, *J. Phys. Chem. A*, **109**, 6509-6520.
59. Butler, R., I. J. Solomon and A. Snelson, 1978, *Chem. Phys. Lett.*, **54**, 19.
60. Campuzano-Jost, P., A. E. Croce, H. Hippler, M. Siefke, and J. Troe, 1995, *J. Chem. Phys.*, **102**, 5317-5326.
61. Cantrell, C. A., R. E. Shetter, J. G. Calvert, G. S. Tyndall and J. J. Orlando, 1993, *J. Phys. Chem.*, **97**, 9141-9148.
62. Caralp, F. and R. Lesclaux, 1983, *Chem. Phys. Lett.*, **102**, 54-58.
63. Caralp, F., R. Lesclaux and A. M. Dognon, 1986, *Chem. Phys. Lett.*, **129**, 433-438.
64. Caralp, F., R. Lesclaux, M. T. Rayez, J.-C. Rayez and W. Forst, 1988, *J. Chem. Soc. Faraday Trans. 2*, **84**, 569-585.
65. Caralp, F., M.-T. Rayez, W. Forst, N. Gomez, B. Delcroix, D. Fitschen and P. Devolder, 1998, *J. Chem. Soc., Faraday Trans.*, **94**, 3321-3330.
66. Carleton, K. J., W. J. Kessler and W. J. Marinelli, 1993, *J. Phys. Chem.*, **97**, 6412-6417.
67. Chan, W. H., W. M. Uselman, J. G. Calvert and J. H. Shaw, 1977, *Chem. Phys. Lett.*, **45**, 240.
68. Chang, J. S., A. C. Baldwin and D. M. Golden, 1979, *Chem. Phys.*, **71**, 2021.
69. Chegodaev, P. P. and B. I. Tubikov, 1973, *Dokl. Akad. Nauk. SSSR*, **210**, 647-649.
70. Chen, H. L., D. W. Trainor, R. E. Center and W. T. Fyfe, 1977, *J. Chem. Phys.*, **66**, 5513.
71. Chen, J., V. Young, T. Zhu and H. Niki, 1993, *J. Phys. Chem.*, **97**, 11696-11698.
72. Christensen, L. E., M. Okumura, S. P. Sander, R. R. Friedl, C. E. Miller and J. J. Sloan, 2004, *J. Phys. Chem. A*, **108**, 80-91.
73. Christensen, L. E., M. Okumura, S. P. Sander, R. J. Salawitch, G. C. Toon, B. Sen, J.-F. Blavier and K. W. Jucks, 2002, *Geophys. Res. Lett.*, **29**, 1029/2001GL014525.
74. Clark, T. C., M. A. A. Clyne and D. H. Stedman, 1966, *Trans. Faraday Soc.*, **62**, 3354.
75. Cleary, P. A., M. T. B. Romero, M. A. Blitz, D. E. Heard, M. J. Pilling, P. W. Seakins and L. Wang, 2006, *Phys. Chem. Chem. Phys.*, **8**, 5633-5642.
76. Cobos, C. J., H. Hippler, K. Luther, A. R. Ravishankara and J. Troe, 1985, *J. Phys. Chem.*, **89**, 4332-4338.
77. Cobos, C. J., H. Hippler and J. Troe, 1985, *J. Phys. Chem.*, **89**, 342-349.
78. Codnia, J. and M. L. Azcarate, 2006, *Photochem. Photobio.*, **82**, 755-762.
79. Colussi, A. J., 1990, *J. Phys. Chem.*, **94**, 8922-8926.
80. Colussi, A. J., S. P. Sander and R. R. Friedl, 1992, *J. Phys. Chem.*, **96**, 4442-4445.
81. Connell, P. S. and H. S. Johnston, 1979, *Geophys. Res. Lett.*, **6**, 553-556.
82. Cooper, R., J. B. Cumming, S. Gordon and W. A. Mulac, 1980, *Radiat. Phys. Chem.*, **16**, 169.
83. Cox, R. A., 1975, *Int. J. Chem. Kinet. Symp.*, **1**, 379.
84. Cox, R. A., J. P. Burrows and G. B. Coker, 1984, *Int. J. Chem. Kinet.*, **16**, 445-67.
85. Cox, R. A. and R. G. Derwent, 1979, *Journal of the Chemical Society, Faraday Transactions 1: Physical Chemistry in Condensed Phases*, **75**, 1635-1647.
86. Cox, R. A., R. G. Derwent and P. M. Holt, 1976, *J. Chem. Soc. Faraday Trans. 1*, **72**, 2031.
87. Cox, R. A. and R. Lewis, 1979, *J. Chem. Soc. Faraday Trans. 1*, **75**, 2649-2661.
88. Cox, R. A., J. Munk, O. J. Nielsen, P. Pagsberg and E. Ratajczak, 1990, *Chem. Phys. Lett.*, **173**, 206-210.
89. Cox, R. A. and R. Patrick, 1979, *Int. J. Chem. Kinet.*, **11**, 635-648.
90. Croce de Cobos, A. E., H. Hippler and J. Troe, 1984, *J. Phys. Chem.*, **88**, 5083-5086.

91. Croce de Cobos, A. E. and J. Troe, 1984, *Int. J. Chem. Kinet.*, **16**, 1519-1530.
92. D'Ottone, L., P. Campuzano-Jost, D. Bauer and A. J. Hynes, 2001, *J. Phys. Chem. A*, **105**, 10538-10543.
93. Daele, V., G. Laverdet, G. Le Bras and G. Poulet, 1995, *J. Phys. Chem.*, **99**, 1470-1477.
94. Daele, V., A. Ray, I. Vassali, G. Poulet and G. Le Bras, 1995, *Int. J. Chem. Kinet.*, **27**, 1121-1133.
95. Danis, F., F. Caralp, J. Masanet and R. Lesclaux, 1990, *Chem. Phys. Lett.*, **167**, 450.
96. Danis, F., F. Caralp, M. Rayez and R. Lesclaux, 1991, *J. Phys. Chem.*, **95**, 7300-7307.
97. Dasch, W., K.-H. Sternberg and R. N. Schindler, 1981, *Ber. Bunsenges. Phys. Chem.*, **85**, 611-615.
98. Davidson, J. A., C. A. Cantrell, R. E. Shetter, A. H. McDaniel and J. G. Calvert, 1990, *J. Geophys. Res.*, **95**, 13963-13969.
99. Davis, D. D., S. Fischer, R. Schiff, R. T. Watson and W. Bollinger, 1975, *J. Chem. Phys.*, **63**, 1707.
100. Davis, H. F., B. Kim, H. S. Johnston and Y. T. Lee, 1993, *J. Phys. Chem.*, **97**, 2172-2180.
101. Daykin, E. P. and P. H. Wine, 1990, *J. Phys. Chem.*, **94**, 4528-4535.
102. DeMore, W. B., 1984, *Int. J. Chem. Kinet.*, **16**, 1187-1200.
103. DeMore, W. B. and E. Tschuikow-Roux, 1990, *J. Phys. Chem.*, **94**, 5856-5860.
104. Destriau, M. and J. Troe, 1990, *Int. J. Chem. Kinet.*, **22**, 915-934.
105. Diau, E. W.-G. and Y.-P. Lee, 1992, *J. Chem. Phys.*, **96**, 377-386.
106. Diaz-de-Mera, Y., A. Aranda, D. Rodriguez, R. López, B. Cabañas and E. Martinez, 2002, *J. Phys. Chem. A*, **106**, 8627-8633.
107. Dillon, T. J., M. A. Blitz and D. E. Heard, 2006, *J. Phys. Chem. A*, **110**, 6995-7002.
108. Dixon, D. A. and K. O. Christie, 1992, *J. Phys. Chem.*, **95**, 1018-1021.
109. Dobe, S., G. Lendvay, I. Szilagyi and T. Berces, 1994, *Int. J. Chem. Kinet.*, **26**, 887-901.
110. Donahue, N. M., M. K. Dubey, R. Mohrschladt, K. Demerjian and J. G. Anderson, 1997, *J. Geophys. Res.*, **102**, 6159-6168.
111. Dransfield, T. J., K. K. Perkins, N. M. Donahue, J. G. Anderson, M. M. Sprengnether and K. Demerjian, 1999, *Geophys. Res. Lett.*, **26**, 687-690.
112. Dreier, T. and J. Wolfrum, 1980, *Proceedings of the Combustion Institute*, **18**, 801-809.
113. Elfers, G., F. Zabel and K. H. Becker, 1990, *chem. Phys. Lett.*, **168**, 14-19.
114. Ellerman, T., J. Sehested, O. J. Nielson, P. Pagsberg and T. J. Wallington, 1994, *Chem. Phys. Lett.*, **218**, 287-294.
115. Enami, S., Y. Nakano, S. Hashimoto, M. Kawasaki, S. Aloisio and J. S. Francisco, 2004, *J. Phys. Chem. A*, **108**, 7785-7789.
116. Erler, K., D. Field, R. Zellner and I. W. M. Smith, 1977, *Ber. Bunsenges. Phys. Chem.*, **81**, 22.
117. Estupiñán, E. G., J. M. Nicovich, J. Li, D. M. Cunnold, and P. H. Wine, 2002, *J. Phys. Chem. A*, **106**, 5880-5890.
118. Fagerstrom, K., A. Lund, G. Mahmoud, J. T. Jodkowski and E. Ratajczak, 1994, *Chem. Phys. Lett.*, **224**, 43-50.
119. Fasano, D. M. and N. S. Nogar, 1983, *J. Chem. Phys.*, **78**, 6688-6694.
120. Fenter, F. F., P. D. Lightfoot, F. Caralp, R. Lesclaux, J. T. Niranen and D. Gutman, 1993, *J. Phys. Chem.*, **97**, 4695-4703.
121. Fenter, F. F., P. D. Lightfoot, J. T. Niranen and D. Gutman, 1993, *J. Phys. Chem.*, **97**, 5313-5320.
122. Fernandes, R. X., K. Luther and J. Troe, 2006, *Journal of Physical Chemistry A*, **110**, 4442-4449.
123. Fernandes, R. X., K. Luther, J. Troe and V. G. Ushakov, 2008, *Phys. Chem. Chem. Phys.*, **10**, 4313-4321.
124. Ferracci, V. and D. M. Rowley, 2010, *Phys. Chem. Chem. Phys.*, **12**, 11596-11608.
125. Fitschen, C., A. Frenzel, K. Imrik, and P. Devolder, 1999, *Int. J. Chem. Kinet.*, **31**, 860-866.
126. Fockenberg, C., H. Somnitz, G. Bednarek and R. Zellner, 1997, *Ber. Bunsenges. Phys. Chem.*, **101**, 1411-1420.
127. Forst, W., and F. Caralp, 1991, *J. Chem. Soc., Faraday Trans.*, **87**, 2307-2315.
128. Forst, W., and F. Caralp, 1992, *J. Phys. Chem.*, **96**, 6291-6298.
129. Forster, R., M. Frost, D. Fulle, H. F. Hamann, H. Hippler, Schlepegreli and J. Troe, 1995, *J. Chem. Phys.*, **103**, 2949-2958.
130. Forte, E., H. Hippler and H. van den Bergh, 1981, *Int. J. Chem. Kinet.*, **13**, 1227-1233.
131. Fowles, M., D. N. Mitchell, J. W. L. Morgan and R. P. Wayne, 1982, *J. Chem. Soc. Faraday Trans. 2*, **78**, 1239-1248.
132. Friedl, R. R., S. P. Sander and Y. L. Yung, 1992, *J. Phys. Chem.*, **96**, 7490-7493.
133. Frost, M. J. and I. W. M. Smith, 1990, *J. Chem. Soc. Farad. Trans.*, **86**, 1751-1756.
134. Frost, M. J. and I. W. M. Smith, 1990, *J. Chem. Soc. Faraday Trans.*, **86**, 1757-1762.
135. Frost, M. J. and I. W. M. Smith, 1993, *J. Chem. Soc. Faraday Trans.*, **89**, 4251.
136. Fulle, D., H. F. Hamann, H. Hippler and C. P. Jansch, 1997, *Ber. Bunsenges. Phys. Chem.*, **101**, 1433-1442.

137. Fulle, D., H. F. Hamann, H. Hippler and J. Troe, 1996, *J. Chem. Phys.*, **105**, 1001-1006.
138. Fulle, D. H., H. F. Hamann, H. Hippler and J. Troe, 1998, *J. Chem. Phys.*, **108**, 5391-5397.
139. Gaedtke, H. K., H. Hippler, K. Luther, and J. Troe, 1973, *Proceedings of the Combustion Institute*, **14**, 295-303.
140. Gao, Y. Q. and R. A. Marcus, 2007, *J. Chem. Phys.*, **127**, 244316.
141. Gleason, J. F., F. L. Nesbitt and L. J. Stief, 1994, *J. Phys. Chem.*, **98**, 126-131.
142. Golden, D. M., 2003, *Int. J. Chem. Kinet.*, **35**, 206-211.
143. Golden, D. M., 2005, *Int. J. Chem. Kinet.*, **37**, 625-632.
144. Golden, D. M., 2006, *J. Phys. Chem. A*, **110**, 2940-2943.
145. Golden, D. M., 2007, *J. Phys. Chem. A*, **111**, 6772-6780.
146. Golden, D. M., 2008, *Chem. Soc. Rev.*, **37**, 717-731.
147. Golden, D. M., 2009, *International Journal of Chemical Kinetics*, **41**, 573-581.
148. Golden, D. M., J. R. Barker, and L. L. Lohr, 2003, *J. Phys. Chem. A*, **107**, 11057-11071.
149. Golden, D. M. and G. P. Smith, 2000, *J. Phys. Chem. A*, **104**, 3991-3997.
150. Green, T. J., M. Islam, P. Guest, K. Hickson, C. E. Canosa-Mas, and R. P. Wayne, 2003, *Phys. Chem. Chem. Phys.*, **5**, 5409-5418.
151. Greiner, N. R., 1970, *J. Chem. Phys.*, **53**, 1284-1285.
152. Grosjean, D., E. Grosjean and E. L. Williams, 1994, *J. Air and Waste Manage. Assoc.*, **44**, 391-396.
153. Gross, A. and G. D. Billing, 1997, *Chem. Phys.*, **217**, 1-18.
154. Hahn, J., K. Luther and J. Troe, 2000, *Phys. Chem. Chem. Phys.*, **2**, 5098-5104.
155. Handwerk, V. and R. Zellner, 1984, *Ber. Bunsenges. Phys. Chem.*, **88**, 405.
156. Harris, G. W. and R. P. Wayne, 1975, *J. Chem. Soc. Faraday Trans. 1*, **71**, 610.
157. Hassouna, M., E. Delbos, P. Devolder, B. Viskolcz and C. Fittschen, 2006, *Journal of Physical Chemistry A*, **110**, 6667-6672.
158. Hathorn, B. C. and R. A. Marcus, 2000, *J. Chem. Phys.*, **113**, 9497-9509.
159. Hayman, G. D., J. M. Davies and R. A. Cox, 1986, *Geophys. Res. Lett.*, **13**, 1347-1350.
160. Helmer, M. and J. M. C. Plane, 1993, *J. Geophys. Res.*, **98**, 23207-23222.
161. Hewitt, A. D., K. M. Brahan, G. D. Boone, and S. A. Hewitt, 1996, *Int. J. Chem. Kinet.*, **28**, 763-771.
162. Hippler, H., S. Nasterlack and F. Striebel, 2002, *Phys. Chem. Chem. Phys.*, **4**, 2959-2964.
163. Hippler, H., R. Rahn and J. Troe, 1990, *J. Chem. Phys.*, **93**, 6560.
164. Hippler, H., M. Siefke, H. Stark and J. Troe, 1999, *Phys. Chem. Chem. Phys.*, **1**, 57-61.
165. Hippler, H., J. Troe and J. Willner, 1990, *J. Chem. Phys.*, **93**, 1755-1760.
166. Hochanadel, C. J., J. A. Ghormley, J. W. Boyle and P. J. Ogren, 1977, *J. Phys. Chem.*, **81**, 3-7.
167. Hofzumahaus, A. and F. Stuhl, 1984, *Ber. Bunsenges Phys. Chem.*, **88**, 557-561.
168. Hölscher, D. and R. Zellner, 2002, *Phys. Chem. Chem. Phys.*, **4**, 1839-1845.
169. Howard, C. J., 1976, *J. Chem. Phys.*, **65**, 4771.
170. Howard, C. J., 1977, *J. Chem. Phys.*, **67**, 5258.
171. Howard, C. J. and K. M. Evenson, 1974, *J. Chem. Phys.*, **61**, 1943.
172. Hsu, K. J., S. M. Anderson, J. L. Durant and F. Kaufman, 1989, *J. Phys. Chem.*, **93**, 1018.
173. Hsu, K. J., J. L. Durant and F. Kaufman, 1987, *J. Phys. Chem.*, **91**, 1895-1899.
174. Huie, R. E., J. T. Herron and D. D. Davis, 1972, *J. Phys. Chem.*, **76**, 2653-2658.
175. Husain, D., J. M. C. Plane and N. K. H. Slater, 1981, *J. Chem. Soc. Faraday Trans. 2*, **77**, 1949-1962.
176. Hynes, A. J., P. H. Wine and A. R. Ravishankara, 1986, *J. Geophys. Res.*, **91**, 815-820.
177. Imrik, K., E. Farkas, G. Vasvári, I. Szilágyi, D. Sarzyski, S. Dóbbé, T. Bérces and F. Márta, 2004, *Phys. Chem. Chem. Phys.*, **6**, 3958-3968.
178. Ingham, T., D. Bauer, R. Sander, P. J. Crutzen and J. N. Crowley, 1999, *J. Phys. Chem. A*, **103**, 7199-7209.
179. IUPAC, 1992, *J. Phys. Chem. Ref. Data*, **21**, 1125-1568.
180. Ivanov, A. V., Y. M. Gershenzon, F. Gratpanche, P. Devolder and J.-P. Saverysyn, 1996, *Ann. Geophys.*, **14**, 659-664.
181. Iyer, R. S., P. J. Rogers and F. S. Rowland, 1983, *J. Phys. Chem.*, **87**, 3799.
182. Jenkin, M. E. and R. A. Cox, 1985, *J. Phys. Chem.*, **89**, 192-199.
183. Johnston, H. S., C. A. Cantrell and J. G. Calvert, 1986, *J. Geophys. Res.*, **91**, 5159-5172.
184. Johnston, H. S., E. D. Morris, Jr. and J. Van den Bogaerde, 1969, *J. Am. Chem. Soc.*, **91**, 7712-7727.
185. Jonah, C. D., W. A. Mulac and P. Zeglinski, 1984, *J. Phys. Chem.*, **88**, 4100-4104.
186. Kaiser, E. W. and T. J. Wallington, 1996, *J. Phys. Chem.*, **100**, 4111-4119.
187. Kaiser, E. W., 1992, *Int. J. Chem. Kinet.*, **24**, 179-189.
188. Kaiser, E. W., 1993, *J. Phys. Chem.*, **97**, 11681-11688.
189. Kaiser, E. W., I. M. Lorkovic and T. J. Wallington, 1990, *J. Phys. Chem.*, **94**, 3352-3354.

190. Kaiser, E. W. and T. J. Wallington, 1998, *J. Phys. Chem. A*, **102**, 6054-6055.
191. Kaiser, E. W., T. J. Wallington and J. M. Andino, 1990, *Chem. Phys. Lett.*, **168**, 309.
192. Kaiser, E. W., T. J. Wallington and M. D. Hurley, 1995, *Int. J. Chem. Kinet.*, **27**, 205-218.
193. Kajimoto, O. and R. J. Cvetanovic, 1976, *J. Chem. Phys.*, **64**, 1005.
194. Kaltsoyannis, N. and J. M. C. Plane, 2008, *Phys. Chem. Chem. Phys.*, **10**, 1723-1733.
195. Kaye, J. A., 1986, *J. Geophys. Res.*, **91**, 7865-7874.
196. Keiffer, M., M. J. Pilling and M. J. C. Smith, 1987, *J. Phys. Chem.*, **91**, 6028-6034.
197. Kennedy, R. C. and J. B. Levy, 1972, *J. Phys. Chem.*, **76**, 3480-3488.
198. Kim, P., D. I. MacLean and W. G. Valence, 1980, *J. Phys. Chem.*, **84**, 1806.
199. Kircher, C. C., J. J. Margitan and S. P. Sander, 1984, *J. Phys. Chem.*, **88**, 4370-4375.
200. Kirchner, F., A. Mayer-Figge, F. Zabel and K. H. Becker, 1999, *Int. J. Chem. Kin.*, **31**, 127-144.
201. Klais, O., P. C. Anderson and M. J. Kurylo, 1980, *Int. J. Chem. Kinet.*, **12**, 469-490.
202. Klein, T., I. Barnes, K. H. Becker, E. H. Fink and F. Zabel, 1984, *J. Phys. Chem.*, **88**, 5020-5025.
203. Knyazev, V. D., I. J. Kalinovski and I. R. Slagle, 1999, *J. Phys. Chem. A*, **103**, 3216-3221.
204. Köppenkastrup, D. and F. Zabel, 1991, *Int. J. Chem. Kinet.*, **23**, 1-15.
205. Kovács, G., J. Zádor, E. Farkas, R. Nádasdi, I. Szilágyi, S. Dóbbé, T. Bérces, F. Márta and G. Lendvay, 2007, *Phys. Chem. Chem. Phys.*, **9**, 4142 - 4154.
206. Kreutter, K. D., J. M. Nicovich and P. H. Wine, 1991, *J. Phys. Chem.*, **95**, 4020.
207. Kuo, C. H. and Y.-P. Lee, 1991, *J. Phys. Chem.*, **95**, 1253.
208. Kurylo, M. J., 1972, *J. Phys. Chem.*, **76**, 3518.
209. Kurylo, M. J. and P. A. Ouellette, 1986, *J. Phys. Chem.*, **90**, 441-444.
210. Kurylo, M. J. and P. A. Ouellette, 1987, *J. Phys. Chem.*, **91**, 3365-3368.
211. Laguna, G. A. and S. L. Baughcum, 1982, *Chem. Phys. Lett.*, **88**, 568-71.
212. Lai, L.-H., Y.-C. Hsu and Y.-P. Lee, 1992, *J. Chem. Phys.*, **97**, 3092-3099.
213. Larin, I. K., D. V. Nevozhai, A. I. Spasskii, and E. M. Trofimova, 1998, *Kinetics and Catalysis*, **39**, 666-672.
214. Laufer, A. H. and A. M. Bass, 1975, *Int. J. Chem. Kinet.*, **7**, 639.
215. Lee, F. S. C. and F. S. Rowland, 1977, *J. Phys. Chem.*, **81**, 86-87.
216. Lee, J. H., J. V. Michael, W. A. Payne, Jr. and L. J. Stief, 1978, *J. Chem. Phys.*, **68**, 5410-5413.
217. Lee, T. J., 1994, *J. Phys. Chem.*, **98**, 111-115.
218. Lee, T. J., 1996, *J. Phys. Chem.*, **100**, 19847-19852.
219. Lee, T. J. and J. E. Rice, 1992, *J. Chem. Phys.*, **97**, 4223-4232.
220. Lee, T. J., C. M. Rohlfing and J. E. Rice, 1992, *J. Chem. Phys.*, **97**, 6593-6605.
221. Lee, Y.-P., R. M. Stimpfle, R. A. Perry, J. A. Mucha, K. M. Evenson, D. A. Jennings and C. J. Howard, 1982, *Int. J. Chem. Kinet.*, **14**, 711-732.
222. Lee, Y.-Y., W. C. Kao and Y.-P. Lee, 1990, *J. Phys. Chem.*, **94**, 4535.
223. Lesar, A., S. Prebil, M. Mühlhäuser and M. Hodošek, 2002, *Chem. Phys. Lett.*, **368**, 399-407.
224. Leu, M. T., 1982, *J. Phys. Chem.*, **86**, 4558.
225. Leu, M. T., 1984, *Int. J. Chem. Kinet.*, **16**, 1311-1320.
226. Li, W.-K., and M. L. McKee, 1997, *J. Phys. Chem. A*, **101**, 9778-9782.
227. Li, Z. and J. S. Francisco, 1989, *J. Am. Chem. Soc.*, **111**, 5660-5667.
228. Lin, C. L. and M. T. Leu, 1982, *Int. J. Chem. Kinet.*, **14**, 417.
229. Liu, A., W. A. Mulac and C. D. Jonah, 1988, *J. Phys. Chem.*, **92**, 5942-5945.
230. Liu, J. Y. and J. R. Barker, 2007, *Journal of Physical Chemistry A*, **111**, 8689-8698.
231. Lloyd, A. C., K. R. Darnall, A. M. Winer and J. N. Pitts, Jr., 1976, *J. Phys. Chem.*, **80**, 789.
232. Lovejoy, E. R., 1997, *J. Phys. Chem. A*, **101**, 4950-4953.
233. Lovejoy, E. R. and D. R. Hanson, 1996, *J. Phys. Chem.*, **100**, 4459-4465.
234. Luther, K., K. Oum and J. Troe, 2001, *J. Phys. Chem. A*, **105**, 5535-5541.
235. Lyman, J. and R. Holland, 1988, *J. Phys. Chem.*, **92**, 7232-7241.
236. Maguin, F., G. Laverdet, G. Le Bras and G. Poulet, 1992, *J. Phys. Chem.*, **96**, 1775-1780.
237. Maric, D. and J. P. Burrows, 1992, *J. Photochem. Photobiol. A: Chem.*, **66**, 291-312.
238. Maricq, M. M., J. J. Szente and E. W. Kaiser, 1993, *J. Phys. Chem.*, **97**, 7970-7977.
239. Marshall, P., 2008, *Advances in Quantum Chemistry*, 159-175.
240. Marshall, P., A. S. Narayan and A. Fontijn, 1990, *J. Phys. Chem.*, **94**, 2998.
241. Martin, D., J. L. Jourdain and G. Le Bras, 1985, *Int. J. Chem. Kinet.*, **17**, 1247-1261.
242. Martinez, E., J. Albaladejo, E. Jiménez, A. Notario, and Y. Diaz de Mera, 2000, *Chem. Phys. Lett.*, **329**, 191-.
243. Maurer, T., I. Barnes, and K. H. Becker, 1999, *Int. J. Chem. Kinet.*, **31**, 883-893.

244. McCabe, D. C., T. Gierczak, R. K. Talukdar and A. R. Ravishankara, 2001, *Geophys. Res. Lett.*, **28**, 3135-3138.
245. McCaulley, J. A., S. M. Anderson, J. B. Jeffries and F. Kaufman, 1985, *Chem Phys. Lett.*, **115**, 180.
246. McCaulley, J. A., A. M. Moyle, M. F. Golde, S. M. Anderson and F. Kaufman, 1990, *J. Chem Soc. Farad. Trans.*, **86**, 4001-4009.
247. Mellouki, A., G. Laverdet, J. L. Jourdain and G. Poulet, 1989, *Int. J. Chem. Kinet.*, **21**, 1161.
248. Michael, J. V., M.-C. Su, J. W. Sutherland, J. J. Carroll and A. F. Wagner, 2002, *J. Phys. Chem. A*, **106**, 5297-5313.
249. Michael, J. V., D. F. Nava, R. P. Borkowski, W. A. Payne and L. J. Stief, 1980, *J. Chem. Phys.*, **73**, 6108.
250. Miller, J. A., and S. J. Klippenstein, 2001, *Int. J. Chem. Kinet.*, **33**, 654-668.
251. Mineshos, G. and S. Glavas, 1991, *React. Kinet. Catal. Lett.*, **45**, 305-312.
252. Miyoshi, A., H. Matsui and N. Washida, 1994, *J. Chem. Phys.*, **100**, 3532-3539.
253. Molina, M. J., L. T. Molina and T. Ishiwata, 1980, *J. Phys. Chem.*, **84**, 3100-3104.
254. Mollner, A. K., S. Valluvadasan, L. Feng, M. K. Sprague, M. Okumura, D. B. Milligan, W. J. Bloss, S. P. Sander, P. T. Martien, R. A. Harley, A. B. McCoy and W. P. L. Carter, 2010, *Science*, **330**, 646-649.
255. Moore, S. B. and R. W. Carr, 1990, *J. Phys. Chem.*, **94**, 1393.
256. Morley, C. and I. W. M. Smith, 1972, *J. Chem. Soc. Faraday Trans.*, **68**, 1016.
257. Morris, E. D., D. H. Stedman and H. Niki, 1971, *J. Am. Chem. Soc.*, **93**, 3570.
258. Müller, M. A., R. A. Yetter, and F. L. Dryer, 2000, *Int. J. Chem. Kinet.*, **32**, 317-339.
259. Naidoo, J., A. Goumri, and P. Marshall, 2005, *Proceedings of the Combustion Institute*, **30**, 1219-1225.
260. Nakano, Y., M. Goto, S. Hashimoto, M. Kawasaki, and T. J. Wallington, 2001, *J. Phys. Chem. A*, **105**, 11045-11050.
261. Nicholas, J. E. and R. G. W. Norrish, 1968, *Proc. Roy. Soc. A*, **307**, 391.
262. Nickolaisen, S. L., R. R. Friedl and S. P. Sander, 1994, *J. Phys. Chem.*, **98**, 155-169.
263. Nicovich, J. M., K. D. Kreutter, C. J. Shackelford and P. H. Wine, 1991, *Chem. Phys. Lett.*, **179**, 367-373.
264. Nicovich, J. M., K. D. Kreutter and P. H. Wine, 1990, *J. Chem. Phys.*, **92**, 3539-3544.
265. Nicovich, J. M., L. Wang, M. L. McKee and P. H. Wine, 1996, *J. Phys. Chem.*, **100**, 680-688.
266. Nicovich, J. M. and P. H. Wine, 1990, *Int. J. Chem. Kinet.*, **22**, 379-397.
267. Niki, H., P. D. Maker, C. M. Savage and L. P. Breitenbach, 1978, *Chem. Phys. Lett.*, **59**, 78.
268. Niki, H., P. D. Maker, C. M. Savage and L. P. Breitenbach, 1984, *J. Phys. Chem.*, **88**, 2116-2119.
269. Nizkorodov, S. A. and P. O. Wennberg, 2002, *J. Phys. Chem. A*, **106**, 855-859.
270. Nottingham, W. C., R. N. Rudolph, K. P. Andrews, J. H. Moore and J. A. Tossell, 1994, *Int. J. Chem. Kinet.*, **26**, 749-756.
271. Oguchi, T., A. Miyoshi, M. Koshi, H. Matsui and N. Washida, 2000, *The Journal of Physical Chemistry A*, **105**, 378-382.
272. Ohmori, K., K. Yamasaki and H. Matsui, 1993, *Bull. Chem. Soc. Jpn.*, **66**, 51-56.
273. Orlando, J. J. and J. B. Burkholder, 2000, *J. Phys. Chem. A*, **104**, 2048-2053.
274. Orlando, J. J. and G. S. Tyndall, 1996, *J. Phys. Chem.*, **100**, 19398-19405.
275. Orlando, J. J., G. S. Tyndall and J. G. Calvert, 1992, *Atmos. Environ.*, **26A**, 3111-3118.
276. Orlando, J. J., G. S. Tyndall, C. A. Cantrell and J. G. Calvert, 1991, *J. Chem. Soc. Far. Trans.*, **87**, 2345-2349.
277. Overend, R. P. and G. Paraskevopoulos, 1977, *J. Chem. Phys.*, **67**, 674.
278. Overend, R. P. and G. Paraskevopoulos, 1977, *Chem. Phys. Lett.*, **49**, 109.
279. Overend, R. P., G. Paraskevopoulos and C. Black, 1976, *J. Chem. Phys.*, **64**, 4149.
280. Pagsberg, P., E. Bjergbakke, E. Ratajczak and A. Sillesen, 1997, *Chem. Phys. Lett.*, **272**, 383-390.
281. Pagsberg, P., A. Sillesen, J. T. Jodowski and E. Ratajczak, 1996, *Chem. Phys. Lett.*, **252**, 165-171.
282. Pagsberg, P., A. Sillesen, J. T. Jodowski and E. Ratajczak, 1996, *Chem. Phys. Lett.*, **249**, 358-364.
283. Pagsberg, P., B. Sztuba, E. Ratajczak and A. Sillesen, 1991, *Acta Chem. Scand.*, **45**, 329.
284. Pagsberg, P. B., E. Ratajczak, A. Sillesen and J. T. Jodowski, 1987, *Chem. Phys. Lett.*, **141**, 88-94.
285. Papayanis, D. K. and A. M. Kosmas, 2004, *Chem. Phys. Lett.*, **398**, 75-81.
286. Paraskevopoulos, G. and R. S. Irwin. XV Informal Conference on Photochemistry, 1982, Stanford, CA,
287. Paraskevopoulos, G. and R. S. Irwin, 1984, *J. Chem. Phys.*, **80**, 259-266.
288. Paraskevopoulos, G., D. L. Singleton and R. S. Irwin, 1983, *Chem. Phys. Lett.*, **100**, 83-87.
289. Parr, A. D., R. P. Wayne, G. D. Hayman, M. E. Jenkin and R. A. Cox, 1990, *Geophys. Res. Lett.*, **17**, 2357-2360.
290. Parthiban, P. and T. Lee, 1998, *J. Chem. Phys.*, **109**, 525-530.
291. Parthiban, S., T. J. Lee, S. Guha, and J. S. Francisco, 2003, *J. Amer. Chem. Soc.*, **125**, 10446-10458.
292. Pastrana, A. V. and R. W. Carr, Jr., 1974, *Int. J. Chem. Kinet.*, **6**, 587.

293. Patrick, R. and D. M. Golden, 1983, *Int. J. Chem. Kinet.*, **15**, 1189-1227.
294. Percival, C. J., G. D. Smith, L. T. Molina and M. J. Molina, 1997, *J. Phys. Chem. A*, **101**, 8830-8833.
295. Percival, D. T. R.-D., A. Bacak, A. Bardwell. In *International Gas Kinetics Symposium*; Bristol, UK, 2004.
296. Perry, R. A., R. Atkinson and J. N. Pitts, Jr., 1977, *J. Chem. Phys.*, **67**, 5577.
297. Perry, R. A. and D. Williamson, 1982, *Chem. Phys. Lett.*, **93**, 331-334.
298. Pilling, M. J. and M. J. C. Smith, 1985, *J. Phys. Chem.*, **89**, 4713-4720.
299. Pirraglia, A. N., J. V. Michael, J. W. Sutherland and R. B. Klemm, 1989, *J. Phys. Chem.*, **93**, 282-291.
300. Plane, J. M. C. and B. Rajasekhar, 1989, *J. Phys. Chem.*, **93**, 3135-3140.
301. Plumb, I. C. and K. R. Ryan, 1982, *Int. J. Chem. Kinet.*, **14**, 861-874.
302. Pollack, I. B., I. M. Konen, E. X. J. Li, and M. I. Lester, 2003, *J. Chem. Phys.*, **119**, 9981-9984.
303. Poulet, G., J. Barassin, G. Le Bras and J. Combourieu, 1973, *Bull. Soc. Chim. Fr.*, **1**, 1.
304. Pratt, G. L. and S. W. Wood, 1984, *J. Chem. Soc. Faraday Trans. 1*, **80**, 3419-3427.
305. Ravishankara, A. R., F. L. Eisele and P. H. Wine, 1980, *J. Chem. Phys.*, **73**, 3743.
306. Ravishankara, A. R., G. J. Smith and D. D. Davis, 1988, *Int. J. Chem. Kinet.*, **20**, 811-814.
307. Ravishankara, A. R. and R. L. Thompson, 1983, *Chem. Phys. Lett.*, **99**, 377.
308. Rawlins, W. T., G. E. Caledonia and R. A. Armstrong, 1987, *J. Chem. Phys.*, **87**, 5209-5213.
309. Rayez, M. T. and M. Destriau, 1993, *Chem. Phys. Lett.*, **206**, 278-284.
310. Resende, S. M. and W. B. D. Alemeida, 1999, *J. Phys. Chem. A*, **103**, 4191-4195.
311. Resende, S. M. and W. B. D. Almeida, 1997, *J. Phys. Chem. A*, **101**, 9738-9744.
312. Roberts, J. M. and S. B. Bertman, 1992, *Int. J. Chem. Kinet.*, **24**, 297-307.
313. Russell, A. G., G. R. Cass and J. H. Seinfeld, 1986, *Environ. Sci. Technol.*, **20**, 1167-1172.
314. Russell, J. J., J. A. Setula, D. Gutman, F. Danis, F. Caralp, P. D. Lightfoot, R. Lesclaux, C. F. Melius and S. M. Senkan, 1990, *J. Phys. Chem.*, **94**, 3277-3283.
315. Ryan, K. R. and I. C. Plumb, 1982, *J. Phys. Chem.*, **86**, 4678-4683.
316. Ryan, K. R. and I. C. Plumb, 1984, *Int. J. Chem. Kinet.*, **16**, 591-602.
317. Sander, S. P., B. J. Finlayson-Pitts, R. R. Friedl, D. M. Golden, R. E. Huie, H. Keller-Rudek, C. E. Kolb, M. J. Kurylo, M. J. Molina, G. K. Moortgat, V. L. Orkin, A. R. Ravishankara and P. H. Wine "Chemical Kinetics and Photochemical Data for Use in Atmospheric Studies, Evaluation Number 15," JPL Publication 06-2, Jet Propulsion Laboratory, Pasadena, 2006 <http://jpldataeval.jpl.nasa.gov>.
318. Sander, S. P., B. J. Finlayson-Pitts, R. R. Friedl, D. M. Golden, R. E. Huie, C. E. Kolb, M. J. Kurylo, M. J. Molina, G. K. Moortgat, V. L. Orkin and A. R. Ravishankara "Chemical Kinetics and Photochemical Data for Use in Atmospheric Studies, Evaluation Number 14," JPL Publication 02-25, Jet Propulsion Laboratory, Pasadena, 2002 <http://jpldataeval.jpl.nasa.gov>.
319. Sander, S. P., R. P. Friedl and Y. L. Yung, 1989, *Science*, **245**, 1095-1098.
320. Sander, S. P. and M. Peterson, 1984, *J. Phys. Chem.*, **88**, 1566-1571.
321. Sander, S. P., G. W. Ray and R. T. Watson, 1981, *J. Phys. Chem.*, **85**, 199.
322. Sander, S. P. and R. T. Watson, 1980, *J. Phys. Chem.*, **84**, 1664-1674.
323. Savarino, J. and M. Thieme, 1999, *J. Phys. Chem. A*, **103**, 9221-9229.
324. Sayin, H. and M. L. McKee, 2005, *Journal of Physical Chemistry A*, **109**, 4736-4743.
325. Schieferstein, M., K. Kohse-Höinghaus and F. Stuhl, 1983, *Ber. Bunsenges. Phys. Chem.*, **87**, 361-366.
326. Schinke, R., S. Y. Grebenshchikov, M. V. Ivanov and P. Fleurat-Lessard, 2006, *Ann. Rev. Phys. Chem.*, **57**, 625-661.
327. Schurath, U. and V. Wipprecht. 1st European Symposium on Physico-Chemical Behavior of Atmospheric Pollutants, 1979, Ispira, 157-166.
328. Seefeld, S., D. J. Kinnison and J. A. Kerr, 1997, *J. Phys. Chem. A*, **101**, 55-59.
329. Seeley, J. V., J. T. Jayne and M. J. Molina, 1996, *J. Phys. Chem.*, **100**, 4019-4025.
330. Sehested, J., L. K. Christensen, T. Mogelberg, O. J. Nielsen, T. J. Wallington, A. Guschin, J. J. Orlando and G. S. Tyndall, 1998, *J. Phys. Chem. A*, **102**, 1779-1789.
331. Sellevåg, S. R., Y. Georgievskii and J. A. Miller, 2008, *J. Phys. Chem. A*, **112**, 5085-5095.
332. Sellevåg, S. R., Y. Georgievskii and J. A. Miller, 2009, *J. Phys. Chem. A*, **113**, xxx-xxx.
333. Selzer, E. A. and K. D. Bayes, 1983, *J. Phys. Chem.*, **87**, 392-394.
334. Senosiain, J. P., C. B. Musgrave and D. M. Golden, 2003, *Int. J. Chem. Kinet.*, **35**, 464-474.
335. Senosiain, J. P., S. J. Klippenstein and J. A. Miller, 2005, *J. Phys. Chem. A*, **109**, 6045-6055.
336. Shamonina, N. F. and A. G. Kotov, 1979, *Kinet. i Kataliz.*, **20**, 233.
337. Sharkey, P., I. R. Sims, I. W. M. Smith, P. Bocherl and B. R. Rowe, 1994, *J. Chem. Soc. Far. Trans.*, **90**, 3609-3616.
338. Shen, G., M. Suto and L. C. Lee, 1990, *J. Geophys. Res.*, **95**, 13981-13984.

339. Sheng, C. Y., J. W. Bozzelli, A. M. Dean, and A. Y. Chang, 2002, *J. Phys. Chem. A*, **106**, 7276-7293.
340. Silver, J. A., M. S. Zahniser, A. C. Stanton and C. E. Kolb, 1984, *Proceedings of the Combustion Institute*, **20**, 605-612.
341. Simonaitis, R. and J. Heicklen, 1978, *Int. J. Chem. Kinet.*, **10**, 67-87.
342. Skolnik, E. D., M. G. Veysey, M. G. Ahmed and W. E. Jones, 1975, *Can. J. Chem.*, **53**, 3188.
343. Slanina, Z. and F. Uhlik, 1991, *Chem. Phys. Lett.*, **182**, 51-56.
344. Smith, C. A., A. R. Ravishankara and P. H. Wine, 1985, *J. Phys. Chem.*, **89**, 1423-1427.
345. Smith, G. P., P. W. Fairchild and D. R. Crosley, 1984, *J. Chem. Phys.*, **81**, 2667.
346. Smith, I. W. M. and D. J. Wrigley, 1980, *Chem. Phys. Lett.*, **70**, 481.
347. Smith, I. W. M. and D. J. Wrigley, 1981, *Chem. Phys.*, **63**, 321.
348. Smith, I. W. M. and R. Zellner, 1973, *J. Chem. Soc. Faraday Trans. 2*, **69**, 1617.
349. Sørensen, M., E. W. Kaiser, M. D. Hurley, T. J. Wallington and O. J. Nielsen, 2003, *Int. J. Chem. Kinet.*, **35**, 191-197.
350. Stanton, J. F., C. M. L. Rittby, R. J. Bartlett and D. W. Toohey, 1991, *J. Phys. Chem.*, **95**, 2107-2110.
351. Stickel, R. E., J. M. Nicovich, S. Wang, Z. Zhao and P. H. Wine, 1992, *J. Phys. Chem.*, **96**, 9875-9883.
352. Stuhl, F. and H. Niki, 1972, *J. Chem. Phys.*, **57**, 3677-3679.
353. Stutz, J., M. J. Ezell and B. J. Finlayson-Pitts, 1997, *J. Phys. Chem. A*, **101**, 9187-9190.
354. Taylor, S. E., A. Goddard, M. A. Blitz, P. A. Cleary and D. E. Heard, 2008, *Phys. Chem. Chem. Phys.*, **10**, 422-437.
355. Thorn, R. P., E. P. Daykin and P. H. Wine, 1993, *Int. J. Chem. Kinet.*, **25**, 521-537.
356. Thuner, L. P., I. Barnes, K. H. Becker, T. J. Wallington, L. K. Christensen, J. J. Orlando and B. Ramacher, 1999, *J. Phys. Chem. A*, **103**, 8657-8663.
357. Trainor, D. W. and C. W. von Rosenberg, Jr., 1974, *J. Chem. Phys.*, **61**, 1010-1015.
358. Troe, J., 1977, *J. Chem. Phys.*, **66**, 4745.
359. Troe, J., 2001, *Proc. Combust. inst.*, **28**, 1463-1469.
360. Troe, J., 2004, *Chem. Rev.*, **104**, 4565-4576.
361. Trolrier, M., R. L. Mauldin, III and A. R. Ravishankara, 1990, *J. Phys. Chem.*, **94**, 4896-4907.
362. Tucceri, M. E., T. J. Dillon and J. N. Crowley, 2005, *Phys. Chem. Chem. Phys.*, **10**, 1657-1663.
363. Tully, F. P., 1983, *Chem. Phys. Lett.*, **96**, 148-153.
364. Turnipseed, A. A., S. B. Barone, N. R. Jensen, D. R. Hanson, C. J. Howard and A. R. Ravishankara, 1995, *J. Phys. Chem.*, **99**, 6000-6009.
365. Urbanski, S. P. and P. H. Wine, 1999, *J. Phys. Chem. A*, **103**, 10935-10944.
366. Vakhtin, A. B., J. E. Murphy and S. R. Leone, 2003, *J. Phys. Chem. A*, **107**, 10055-10062.
367. Van den Bergh, H., N. Benoit-Guyot and J. Troe, 1977, *Int. J. Chem. Kinet.*, **9**, 223-234.
368. Van den Bergh, H. and J. Troe, 1976, *J. Chem. Phys.*, **64**, 736-742.
369. Van den Bergh, H. E. and A. B. Callear, 1971, *Trans. Faraday Soc.*, **67**, 2017.
370. Viggiano, A. A., J. A. Davidson, F. C. Fehsenfeld and E. E. Ferguson, 1981, *J. Chem. Phys.*, **74**, 6113-6125.
371. Vinckier, C., A. Dumoulin and S. DeJaegere, 1991, *J. Chem. Soc. Faraday Trans.*, **87**, 1075-1081.
372. von Ahsen, S., H. Wilner and J. S. Francisco, 2004, *J. Chem. Phys.*, **121**, 2048-2057.
373. Wagner, A. F., I. R. Slagle, D. Sarzynski and D. Gutman, 1990, *J. Phys. Chem.*, **94**, 1853-1864.
374. Walker, R. W., Ph.D. Thesis, Queen Mary College University of London, 1972.
375. Wallington, T. J., J. M. Andino, I. M. Lorkovic, E. W. Kaiser and G. Marston, 1990, *J. Phys. Chem.*, **94**, 3644-3648.
376. Wallington, T. J., J. M. Andino, A. R. Potts and P. H. Wine, 1991, *Chem. Phys. Lett.*, **176**, 103-108.
377. Wallington, T. J., R. Atkinson, A. M. Winer and J. N. Pitts, Jr., 1987, *Int. J. Chem. Kinet.*, **19**, 243-249.
378. Wallington, T. J. and J. C. Ball, 1995, *J. Phys. Chem.*, **99**, 3201-3205.
379. Wallington, T. J. and R. A. Cox, 1986, *J. Chem. Soc. Faraday Trans. 2*, **82**, 275-289.
380. Wallington, T. J., T. Ellerman, O. J. Nielsen and J. Sehested, 1994, *J. Phys. Chem.*, **98**, 2346.
381. Wallington, T. J., T. Ellermann and O. J. Nielsen, 1993, *J. Phys. Chem.*, **97**, 8442-8449.
382. Wallington, T. J., M. M. Mariq, T. Ellerman and O. J. Nielsen, 1992, *J. Phys. Chem.*, **96**, 982-986.
383. Wallington, T. J. and O. J. Nielsen, 1991, *Int. J. Chem. Kinet.*, **23**, 785-798.
384. Wallington, T. J., L. M. Skewes and W. O. Siegl, 1988, *J. Photochem. Photobiol. A*, **45**, 167.
385. Wallington, T. J., L. M. Skewes, W. O. Siegl, C. H. Wu and S. M. Japar, 1988, *Int. J. Chem. Kinet.*, **20**, 867-875.
386. Walsh, R. and D. M. Golden, 2008, *J. Phys. Chem. A*, **112**, 3891-3897.
387. Wang, D., and D. L. Phillips, 2002, *Chem. Phys. Lett.*, **362**, 205-209.
388. Washida, N., 1980, *J. Chem. Phys.*, **73**, 1665.

389. Washida, N. and K. D. Bayes, 1976, *Int. J. Chem. Kinet.*, **8**, 777
390. Westenberg, A. A. and N. de Haas, 1972, *J. Chem. Phys.*, **57**, 5375-5378.
391. Whytock, D. A., J. V. Michael and W. A. Payne, 1976, *Chem. Phys. Lett.*, **42**, 466-471.
392. Williams, M. B., P. Campuzano-Jost, A. J. Hynes and A. J. Pounds, 2009, *Journal of Physical Chemistry A*, **113**, 6697-6709.
393. Wilson, W. E. and A. A. Westenberg, 1967, *Proceedings of the Combustion Institute*, **11**, 1143.
394. Wine, P. H., N. M. Kreutter and A. R. Ravishankara, 1979, *J. Phys. Chem.*, **83**, 3191.
395. Wine, P. H., J. M. Nicovich, R. E. Stickel, Z. Zhao, C. J. Shackelford, K. D. Kreutter, E. P. Daykin and S. Wang. In *The Tropospheric Chemistry of Ozone in the Polar Regions*; Springer-Verlag: Berlin, 1993; Vol. I7; pp 385-395.
396. Wine, P. H., R. J. Thompson, A. R. Ravishankara, D. H. Semmes, C. A. Gump, A. Torabi and J. M. Nicovich, 1984, *J. Phys. Chem.*, **88**, 2095.
397. Wolf, S., M. Bitter, D. Krankowsky and K. Mauersberger, 2000, *J. Chem. Phys.*, **113**, 2684-2686.
398. Wollenhaupt, M. and J. N. Crowley, 2000, *J. Phys. Chem. A*, **104**, 6429-6438.
399. Wong, W. D. and D. Davis, 1974, *Int. J. Chem. Kinet.*, **6**, 401.
400. Wu, F. and R. W. Carr, 1991, *Int. J. Chem. Kinet.*, **23**, 701-715.
401. Xiong, J. Q. and R. W. Carr, 1994, *J. Phys. Chem.*, **98**, 9811-9822.
402. Yarwood, G., J. W. Sutherland, M. A. Wickramaarachchi and R. B. Klemm, 1991, *J. Phys. Chem.*, **95**, 8771-8775.
403. Zabarnick, S., 1993, *Chem Phys.*, **171**, 265-273.
404. Zabel, F., A. Reimer, K. H. Becker and E. H. Fink, 1989, *J. Phys. Chem.*, **93**, 5500-5507.
405. Zahniser, M. S., J. Chang and F. Kaufman, 1977, *J. Chem. Phys.*, **67**, 997-1003.
406. Zellner, R., F. Ewig, R. Paschke and G. Wagner, 1988, *J. Phys. Chem.*, **92**, 4184-4190.
407. Zellner, R. and K. Lorenz, 1984, *J. Phys. Chem.*, **88**, 984-989.
408. Zetzsch, C. *European Symposium on Combustion*, 1973, 35.
409. Zhang, J. and N. M. Donahue, 2006, *J. Phys. Chem. A*, **110**, 6898-6911.
410. Zhang, J. Y., T. Dransfield and N. M. Donahue, 2004, *Journal of Physical Chemistry A*, **108**, 9082-9095.
411. Zhu, R., C.-C. Hsu and M. C. Lin, 2001, *J. Chem. Phys.*, **115**, 195-203.
412. Zhu, R. S. and M. C. Lin, 2002, *J. Phys. Chem., A*, **106**, 8386-8390.
413. Zhu, R. S. and M. C. Lin, 2003, *Journal of Chemical Physics*, **118**, 4094-4106.
414. Zhu, R. S. and M. C. Lin, 2003, *J. Chem. Phys.*, **118**, 8645-8655.
415. Zhu, R. S. and M. C. Lin, 2003, *J. Chem. Phys.*, **119**, 2075-2082.
416. Zhu, R. S. and M. C. Lin, 2004, *Chemphyschem*, **5**, 1864-1870.
417. Zhu, T., G. Yarwood, J. Chen and H. Niki, 1994, *J. Phys. Chem.*, **98**, 5065-5067.
418. Zou, P., A. Derecskei-Kovacs and S. W. North, 2003, *J. Phys. Chem. A*, **107**, 888-896.

SECTION 3. EQUILIBRIUM CONSTANTS

Table of Contents

SECTION 3. EQUILIBRIUM CONSTANTS	3-1
3.1 Format	3-1
3.2 Definitions.....	3-1
3.3 Notes to Table 3	3-5
3.4 References.....	3-10

Tables

Table 3-1. Equilibrium Constants.....	3-3
---------------------------------------	-----

3.1 Format

Some of the three-body reactions in Table 2 form products that are thermally unstable at atmospheric temperatures. In such cases the thermal decomposition reaction may compete with other loss processes, such as photodissociation or radical attack. Table 3 lists the equilibrium constants, $K_{eq}(T)$, for several reactions which may fall into this category. The table has three column entries, the first two being the parameters A and B which can be used to express $K_{eq}(T)$:

$$K_{eq}(T)/\text{cm}^3 \text{ molecule}^{-1} = A \exp(B/T) \quad (200 < T < 300 \text{ K})$$

The third column entry in Table 3 is the calculated value of K_{eq} at 298 K.

The data sources for $K_{eq}(T)$ are described in the individual notes to Table 3.

3.2 Definitions

When values of the heats of formation and entropies of all species are known at the temperature T, we note that the equilibrium constant is given by the van't Hoff equation:

$$\log_{10} [K_{eq}(T) / \text{bar}^{-1}] = \frac{\Delta S_T^\circ}{2.303R} - \frac{\Delta H_T^\circ}{2.303RT}$$

$$\log_{10} [K_{eq}(T) / \text{cm}^3 \text{ molecule}^{-1}] = \frac{\Delta S_T^\circ}{2.303R} - \frac{\Delta H_T^\circ}{2.303RT} + \log_{10}(T) - 21.87$$

Where the superscript "o" refers to a standard state of one bar. When the entropy is known (or can be calculated from molecular properties) as a function of temperature, experimental values of $K_{eq}(T)$ can be used to extract a value for ΔH_0 and $K_{eq}(T)$ can be calculated over a wide temperature range (Third law method.). The parameters A and B can then be determined from a linear fit. In other cases the $K_{eq}(T)$ values were calculated directly from kinetic data for the forward and reverse reactions. When only thermochemical values at 298 K were available, they were treated as temperature independent and used to calculate the equilibrium constants between 200 and 300 K. The following equations were then used to calculate the parameters A and B:

$$B/K = 2.303 \left[\frac{(300 \times 200)}{(300 - 200)} \right] \log_{10} \left(\frac{K_{eq}^{200}}{K_{eq}^{300}} \right) = 1382 \log_{10} \left(\frac{K_{eq}^{200}}{K_{eq}^{300}} \right)$$

$$\log_{10}(A) = \log_{10}(K_{eq}^T) - \frac{B}{2.303T}$$

The relationships between the parameters A and B and the quantities $\Delta S^\circ(298 \text{ K})$ and $\Delta H^\circ(298 \text{ K})$ are:

$$A = \frac{eR'T}{N_{av}} \exp\left(\frac{\Delta S_{298K}^0}{R}\right) = 3.7 \times 10^{-22} T \exp\left(\frac{\Delta S_{298K}^0}{R}\right)$$

where $R' = 82.1 \text{ cm}^3 \text{ bar mole}^{-1} \text{K}^{-1}$, and $N_{av} = 6.02 \times 10^{23} \text{ molecule mole}^{-1}$ and

$$B/^{\circ}\text{K} = -\left[\frac{\Delta H_{298K}^0 + RT}{R}\right]$$

Table 3-1. Equilibrium Constants

Reaction	A/cm ³ molecule ⁻¹	B/°K	K _{eq} (298 K)	f(298 K) ^a	g	Note
HO + NO ₂ → HOONO	3.5×10 ⁻²⁷	10135	2.2×10 ⁻¹²	1.4	200	<u>1</u>
HO ₂ + NO ₂ → HO ₂ NO ₂	2.1×10 ⁻²⁷	10900	1.6×10 ⁻¹¹	1.3	100	<u>2</u>
HO ₂ + H ₂ O → HO ₂ •H ₂ O	2.4×10 ⁻²⁵	4350	5.2×10 ⁻¹⁹	2	200	<u>3</u>
HO ₂ + CH ₃ OH → HO ₂ •CH ₃ OH	1.1×10 ⁻²⁴	4093	1.0×10 ⁻¹⁸	1.2 (at 230 K)	100	<u>4</u>
NO + NO ₂ → N ₂ O ₃	3.3×10 ⁻²⁷	4667	2.1×10 ⁻²⁰	2	100	<u>5</u>
NO ₂ + NO ₂ → N ₂ O ₄	5.9×10 ⁻²⁹	6643	2.8×10 ⁻¹⁹	1.4	100	<u>6</u>
NO ₂ + NO ₃ → N ₂ O ₅	2.7×10 ⁻²⁷	11000	2.9×10 ⁻¹¹	1.2	100	<u>7</u>
CH ₃ O ₂ + NO ₂ → CH ₃ O ₂ NO ₂	9.5×10 ⁻²⁹	11234	2.2×10 ⁻¹²	1.3	500	<u>8</u>
CH ₃ C(O)O ₂ + NO ₂ → CH ₃ C(O)O ₂ NO ₂	9.0×10 ⁻²⁹	14000	2.3×10 ⁻⁸	1.2	200	<u>9</u>
CH ₃ CH ₂ C(O)O ₂ + NO ₂ → CH ₃ CH ₂ C(O)O ₂ NO ₂	9.0×10 ⁻²⁹	14000	2.3×10 ⁻⁸	10	800	<u>10</u>
CH ₃ C(O)CH ₂ + O ₂ → CH ₃ C(O)CH ₂ O ₂	6.3×10 ⁻²⁷	12200	3.8×10 ⁻⁹	1.5	0	<u>11</u>
F + O ₂ → FOO	4.5×10 ⁻²⁵	6118	3.7×10 ⁻¹⁶	1.5	300	<u>12</u>
Cl + O ₂ → ClOO	6.6×10 ⁻²⁵	2502	2.9×10 ⁻²¹	1.7	100	<u>13</u>
Cl + CO → ClCO	3.5×10 ⁻²⁵	3730	9.6×10 ⁻²⁰	1.2	200	<u>14</u>
ClO + O ₂ → ClO•O ₂	2.9×10 ⁻²⁶	<3700	<7.2×10 ⁻²¹			<u>15</u>
ClO + ClO → Cl ₂ O ₂	1.72×10 ⁻²⁷	8649	6.9×10 ⁻¹⁵	1.25	200	<u>16</u>
Cl + OClO → ClClO ₂	1.3×10 ⁻²⁶	12500	2.1×10 ⁻⁸	2	600	<u>17</u>
ClO + OClO → Cl ₂ O ₃	1.5×10 ⁻²⁷	7170	4.2×10 ⁻¹⁷	1.2	400	<u>18</u>
OCIO + NO ₃ → O ₂ ClONO ₂	6.6×10 ⁻²⁹	3971	4.0×10 ⁻²³	2.3	250	<u>19</u>
OH + CS ₂ → CS ₂ OH	4.5×10 ⁻²⁵	5140	1.4×10 ⁻¹⁷	1.4	300	<u>20</u>
CH ₃ S + O ₂ → CH ₃ SO ₂	1.8×10 ⁻²⁷	5545	2.2×10 ⁻¹⁹	1.4	300	<u>21</u>
Cl + CS ₂ → Cl---CS ₂	1.8×10 ⁻²⁵	4982	3.3×10 ⁻¹⁸	1.3	150	<u>22</u>
OH+(CH ₃) ₂ S→HO---(CH ₃) ₂ S	9.6×10 ⁻²⁷	5376	6.6×10 ⁻¹⁹	1.4	0	<u>23</u>
Br + (CH ₃) ₂ S→Br---(CH ₃) ₂ S	3.4×10 ⁻²⁵	3021	4.6×10 ⁻¹⁵	1.2	100	<u>24</u>

$K_{\text{eq}}/\text{cm}^3 \text{ molecule}^{-1} = A \exp (B/T)$ [$200 < T/K < 300$] – shaded areas indicate changes or additions since JPL06-2

- a $f(298 \text{ K})$ is the uncertainty factor at 298 K, and g is a measure of the uncertainty in the quantity B . To calculate the uncertainty at temperatures other than 298 K, use the expression:

$$f(T) = f(298 \text{ K}) \exp \left[g \left(\frac{1}{T} - \frac{1}{298} \right) \right]$$

3.3 Notes to Table 3

JPL Publication numbers for the most recent revision of the table entry, note and evaluation date are given at the end of each note.

1. $\text{HO} + \text{NO}_2 \rightarrow \text{HOONO}$. The tabulated value is for the cis,cis-HOONO product channel (see below for formation of the trans,perp-HOONO isomer, which is unlikely to be important in the atmosphere). Using the data from Hippler et al. [55], Golden et al. [45] [44] performed a third law analysis using structures and frequencies from an ab initio quantum calculation to extract the heat of formation of cis-cis HOONO ($\Delta H_f^\circ(0 \text{ K}) = -9.3 \text{ kJ mol}^{-1}$). The data covers $430 < T/\text{K} < 475$ with 30% uncertainties. Most vibrational frequencies recently have been identified using matrix isolation spectroscopy [115] and the moments of inertia have been measured by microwave spectroscopy [40]. High level CCSD(T) calculations and spectral simulation of overtone and action spectra have examined the torsion in considerable detail [73]. Mathews and Sinha [70] measured overtone action spectra and carried out an analysis that gave $D_0 = 83.3 \pm 2.1 \text{ kJ mol}^{-1}$. By using the observed frequencies (supplemented by the high level CCSD(T) calculations [115]), moments of inertia, and the potential energy and moment of inertia of the internal rotor [73], a new third law analysis using the data from Hippler et al. [55] gives the entropy for reaction that differs from the previous analysis by $-5.6 \text{ J K}^{-1} \text{ mol}^{-1}$ and a new estimate of $D_0 = 81.5 \pm 0.8 \text{ kJ mol}^{-1}$ and $\Delta H_f^\circ(0 \text{ K}) = -7.6 \text{ kJ mol}^{-1}$ ($\Delta H_f^\circ(298 \text{ K}) = -14.9 \text{ kJ mol}^{-1}$ and $S_f^\circ(298) = 279 \text{ J K}^{-1} \text{ mol}^{-1}$).

For formation of the trans,perp-HOONO product channel (which is of negligible atmospheric importance), the reaction is written $\text{HO} + \text{NO}_2 \rightarrow \text{trans,perp-HOONO}$. Konen et al. [64, 65] used infrared overtone action spectroscopy in a molecular beam apparatus to determine $D_0 = 67.8 \pm 0.4 \text{ kJ mol}^{-1}$. High level CCSD(T) calculations [64] supported by analysis [67] of the action spectra give vibrational frequencies and moments of inertia. These data are used to calculate $\Delta H_f^\circ(0 \text{ K}) = 6.1 \text{ kJ mol}^{-1}$ ($\Delta H_f^\circ(298 \text{ K}) = -0.5 \text{ kJ mol}^{-1}$ and $S_f^\circ(298) = 291 \text{ J K}^{-1} \text{ mol}^{-1}$). Using these parameters, the equilibrium constant is given by $K_{\text{eq}}(\text{trans,perp}) = 1.33 \times 10^{-26} \exp(8390/T)$ with uncertainty factors $f=1.4$ and $g=200$. (Table: 10-6, Note: 10-6, Evaluated: 10-6) [Back to table](#)

2. $\text{HO}_2 + \text{NO}_2$. The value was obtained by combining the expression from Table 2-1 for the rate constant of the reaction as written with that from an average of the expressions from Graham et al. [48] and Zabel [113] for the reverse reaction. Values for the entropy and heat of formation of pernitric acid may be extracted. These values are: $S(298 \text{ K}) = 71.7 \text{ cal mole}^{-1} \text{ K}^{-1}$ and $\Delta H_f^\circ(298 \text{ K}) = -12.9 \text{ kcal mole}^{-1}$. If the entropy is calculated from the frequencies and moments of inertia given by Chen and Hamilton [24], the value becomes 71.0 and the heat is -13.1 . The values in the Appendix to this report reflect these results. A study of the thermal decomposition of HO_2NO_2 by Gierczak et al. [41] combined with values for the association reaction are in agreement. (Table: JPL06, Note: JPL06) [Back to table](#)
3. $\text{HO}_2 + \text{H}_2\text{O}$. The influence of water vapor on the $\text{HO}_2 + \text{HO}_2$ bimolecular rate constant was first shown by Hamilton [50], who invoked formation of a $\text{HO}_2 \cdot \text{H}_2\text{O}$ complex with $\sim 38 \text{ kJ mol}^{-1}$ binding energy. Since then, several other groups have quantified the effect on the $\text{HO}_2 + \text{HO}_2$ reaction (see Table 1). Only two direct measurements of the equilibrium constant have been carried out. Aloisio et al. [1] used FTIR absorption spectroscopy around 1120 cm^{-1} to measure the depletion of gas phase HO_2 as it formed a complex with H_2O . They measured K_{eq} at 230 and 250 K, but only an upper limit at room temperature. Kanno et al. [61, 62] also monitored depletion of gas-phase HO_2 , but with high resolution FM spectroscopy of the HO_2 A-X transition near 7020 cm^{-1} with apparently higher sensitivity than in the FTIR measurement of Aloisio et al., since they could measure K_{eq} up to much higher temperatures ($250 \text{ K} \leq T \leq 350 \text{ K}$). The two studies are in rough agreement on parameter B, but differ on parameter A by a factor of 7. Kanno et al.'s results are in very good agreement with the Aloisio et al. ab initio calculations of parameter A. The indirect estimate of K_{eq} by Cox and Burrows [28] agrees better with Kanno et al., and the indirect estimate by Hamilton and Lii [51] is in better agreement with Aloisio et al. The current recommendation for K_{eq} is based on Kanno et al. [61, 62] because their technique had higher sensitivity and because they measured K_{eq} over a much wider temperature range. A 3rd Law analysis of the Kanno et al. experimental data was carried out using the harmonic frequencies calculated by Aloisio et al [1] and the microwave rotational constants from Suma et al. [102]. This gives $S_{298}^\circ(\text{HO}_2 \cdot \text{H}_2\text{O}) = 308.9 \text{ J K}^{-1} \text{ mol}^{-1}$ and $D_0 = 35.9 \pm 1.2 \text{ kJ mol}^{-1}$ (one sigma). Since the analysis is

based only on the Kanno experiments, we adopt an estimated 95% confidence limit of $\pm 3 \text{ kJ mol}^{-1}$. The results give $\Delta H_{f,0}(\text{HO}_2\cdot\text{H}_2\text{O}) = -259.6 \pm 3 \text{ kJ mol}^{-1}$ and $\Delta H_{f,298}(\text{HO}_2\cdot\text{H}_2\text{O}) = -268.0 \pm 3 \text{ kJ mol}^{-1}$. The values of f(298) and g were made large enough to include the data of Aloisio et al. [1]. (Table: 10-6, Note: 10-6, Evaluated: 10-6) **Back to table**

4. $\text{HO}_2 + \text{CH}_3\text{OH}$. The influence of CH_3OH on the $\text{HO}_2 + \text{HO}_2$ bimolecular rate constant was first shown by Andersson et al. [3], who invoked formation of a $\text{HO}_2\cdot\text{CH}_3\text{OH}$ complex with $\sim 25 \text{ kJ mol}^{-1}$ binding energy to explain their results. Since then, several other groups have quantified the effect on the $\text{HO}_2 + \text{HO}_2$ reaction (see Table 1). The only direct measurement of the equilibrium constant was carried out by Christensen et al. [25] from 231 to 261 K. Their measurements are the basis for this recommendation. They obtained $\Delta_r H^\circ(246\text{K}) = -37.4 \pm 4.8 \text{ kJ mol}^{-1}$ and $\Delta_r S^\circ(246\text{K}) = -100 \pm 19 \text{ J K}^{-1} \text{ mol}^{-1}$. Christensen et al. also measured the forward and reverse rate constants and performed ab initio calculations, which are in reasonable agreement with the measured thermochemistry. (Table: 10-6, Note: 10-6, Evaluated: 10-6) **Back to table**
5. $\text{NO} + \text{NO}_2$. The data are from JANAF [60] and Chao et al. [22]. This process is included because a measurement of the rate constant by Smith and Yarwood [100] and Markwalder et al. [69] shows that it is too slow to be an important process in most atmospheric and laboratory systems. (Table: 94-26, Note: 94-26) **Back to table**
6. $\text{NO}_2 + \text{NO}_2$. The data are from JANAF [60] and Vosper [108], Chao et al. [21] and Amoroso et al. [2]. Rate data for this process are reported by Brunning et al. [14], Borrell et al. [10] Gozel et al. [46] and Markwalder et al. [69]. A direct study by Harwood and Jones [52] at low temperatures is in agreement with the recommendation. Re-evaluation of the data suggests slightly different error limits than recommended in JPL 02-25. Estupiñán et al. [34], Wollenhaupt and Crowley [112] and Tuchler et al. [104] deduce values that are in essential agreement, within uncertainties, with the recommendation. (Table: 02-25, Note: 02-25) **Back to table**
7. $\text{NO}_2 + \text{NO}_3$. The recommendation is from Cantrell et al. [19]. They report rate constants for the decomposition reaction, which they combine with the rate constants of Orlando et al. [85] to obtain the equilibrium constant. Agreement is quite good with the data of Burrows et al. [16] and Cantrell et al. [18] and the room temperature data of Tuazon et al. [103] Perner et al. [88] and Hjorth et al. [56]. An evaluation by Pritchard [92] is also in excellent agreement with the recommendation. Pritchard [92] examined the data of Cantrell et al. [18], Burrows et al. [16], Graham and Johnston [47], Wangberg et al [109], Schott and Davidson [97], and the room temperature data of Tuazon et al. [103], Perner et al. [88] and Hjorth et al. [56]. He also included the values given by Smith et al. [99], and Kircher et al. [63], who combined data on the forward reaction, tabulated in Table 2-1, with decomposition data of by Connell and Johnston [27] and Viggiano et al. [106]. The Pritchard [92] result was used as the basis for the value in JPL 00-3, but some uncertainties in the entropies of NO_3 and N_2O_5 justify the reversion to the JPL 97-4 recommendations. In JPL 02-25, the values of the parameters were inadvertently left unchanged from those in JPL 00-3. The differences are very small. The one sigma error limits are better described with $f(298) = 1.2$. (Table: JPL06, Note: JPL06) **Back to table**
8. $\text{CH}_3\text{O}_2 + \text{NO}_2$. Zabel et al. [114] have measured $k(\text{dissociation})$ as a function of pressure ($10 < P/\text{torr} < 800$) and temperature ($253 < T/\text{K} < 272$). Bahta et al. [6] have measured $k(\text{dissociation})$ at 263 K. Using the values of $k(\text{recombination})$ suggested in this evaluation, (Table-2) Golden [43] has re-evaluated the equilibrium constant. Bridier et al. [12] measure an equilibrium constant in good agreement with this recommendation, reducing the uncertainty even further. (Table: JPL06, Note: JPL06) **Back to table**
9. $\text{CH}_3\text{C(O)O}_2 + \text{NO}_2$. The recommendation is derived from measurements of the rate constants in both directions by Bridier et al. [11]. These authors used the values of the rate constants at 298K and a calculated value of the entropy change to get a third law value of the equilibrium constant. Their value of the enthalpy is exactly reproduced in a theoretical study by Miller et al. [76]. A theoretical study by Wei et al.[93] is noted. (Table: JPL06, Note: JPL10, Evaluated JPL10) **Back to table**
10. $\text{CH}_3\text{CH}_2\text{C(O)O}_2 + \text{NO}_2$. Assumed to be the same as for PAN (Note 7). Both sides of the of the reaction differ from PAN by the group $\text{C}-(\text{C})(\text{CO})(\text{H})_2$. Error limits are estimated and expanded from those for PAN. (Table: 02-25, Note: 02-25) **Back to table**
11. $\text{CH}_3\text{C(O)CH}_2 + \text{O}_2$. Hassouna et al.[53] measured the rate constant and equilibrium constant for this reaction.

The temperature range for the equilibrium measurements was $459 < T/K < 520$. They extracted the entropy and enthalpy changes over this temperature range from a van't Hoff plot. (Second Law.) Values reported are $\Delta S = -143.0 \pm 4.0 \text{ J mol}^{-1} \text{ K}^{-1}$ and $\Delta H = -105.0 \pm 2.0 \text{ kJ mol}^{-1}$. The value in Table 3 is computed assuming that these thermochemical values are constant to 200K. They also performed quantum calculations which confirmed the enthalpy measurement. They suggest $\Delta H_{f,298}(\text{CH}_3\text{C}(\text{O})\text{CH}_2) = -32.9 \pm 2.0 \text{ kJ mol}^{-1}$. (Table: 10-6, Note: 10-6, Evaluated: 10-6) **[Back to table](#)**

12. $\text{F} + \text{O}_2$. Taken from Campuzano-Jost et al. [17]. There is good agreement with data from Pagsberg et al. [86]. This corresponds to a value for $\Delta H_{f,298}(\text{FO}_2) = 6.13 \pm 0.5 \text{ kcal mol}^{-1}$. There are several modern theoretical computations [31, 35, 38] of this value, ranging from 6 to 9 kcal mol^{-1} . Feller et al. [36] compute $5.8 \pm 0.3 \text{ kcal mol}^{-1}$. (Table: 10-6, Note: 10-6, Evaluated: 10-6) **[Back to table](#)**
13. $\text{Cl} + \text{O}_2$. Data are from Baer et al. [5], Nicovich et al. [82] and Mauldin et al. [72]. Zhu and Lin [118] have reported structure and frequency calculations and a heat of formation for ClOO. Using known thermochemistry for Cl and O_2 and entropy values for ClOO computed from Zhu and Lin, $\Delta H_{f,0}(\text{ClOO}) = 23.85 \pm 0.1 \text{ kcal mole}^{-1}$ is obtained by the third law method from the individual data points of the Nicovich et al. [82] data. The Baer et al. [5] paper reports only one value at each temperature and only graphically, but yields essentially the same value as Nicovich et al [82]. The third law value from Mauldin et al. [72] is less stable by 0.4 kcal mole^{-1} . Earlier values, both experimental and theoretical, of the structural parameters of ClOO are referenced in [118]. $S^\circ_{298}(\text{ClOO}) = 64.6 \text{ cal mole}^{-1} \text{ K}^{-1}$ and $\Delta H_{f,298}(\text{ClOO}) = 23.5 \pm 0.5 \text{ kcal mole}^{-1}$ are recommended. (Table: JPL06, Note: JPL06) **[Back to table](#)**
14. $\text{Cl} + \text{CO}$. From fitting the data of Nicovich et al. [83] who measured both k and K_{eq} between 185 and 260 K in N_2 . They report $\Delta H_{f,298}(\text{ClCO}) = -5.2 \pm 0.6 \text{ kcal mole}^{-1}$. (Table: JPL06, Note: JPL06) **[Back to table](#)**
15. $\text{ClO} + \text{O}_2$. DeMore [30] reports $K_{\text{eq}} < 4 \times 10^{-18} \text{ cm}^3 \text{ molecule}^{-1}$ at 197 K. His temperature dependence of the equilibrium constant is estimated using $S^\circ_{298}(\text{ClO} \cdot \text{O}_2) = 73 \text{ cal mol}^{-1} \text{ K}^{-1}$ and $\Delta H^\circ_{298} < 7.7 \text{ kcal mol}^{-1}$. A higher value of K_{eq} has been proposed by Prasad [90], but it requires $S^\circ(\text{ClO} \cdot \text{O}_2)$ to be about 83 $\text{cal mol}^{-1} \text{ K}^{-1}$, which seems unreasonably high. Carter and Andrews [20] found no experimental evidence for $\text{ClO} \cdot \text{O}_2$ in matrix experiments. Prasad and Lee [91] discuss these issues and question the validity of the upper limit reported by DeMore. (Table: 92-20, Note: 94-26) **[Back to table](#)**
16. $\text{ClO} + \text{ClO}$. The tabulated entry is for formation of the ClOOCi isomer (see below for formation of the ClOCiO isomer, which is unlikely to be important in the atmosphere). The values of the equilibrium constant and the thermochemical parameters are from a third-law calculation based on the data from Cox and Hayman [29] and Nickolaissen et al. [81]. The 95% error limits were chosen to incorporate all the data points in these two studies. The entropy of ClOOCi, the value of which is $72.0 \text{ cal mol}^{-1} \text{ K}^{-1}$ ($301.1 \text{ J mol}^{-1} \text{ K}^{-1}$) at 300 K, can be calculated from structures and frequencies calculated by Zhu and Lin [116] (symmetry number corrected by Golden [42] to account for optical isomers) or by treatment of the torsion as a hindered rotor [7], in which case the symmetry number correction is not required. The latter has been adopted here, but there is very little difference between the results. The heat of formation at 0 K is $\Delta H^\circ_{f,0} = 31.6 \pm 0.5 \text{ kcal mol}^{-1}$ ($132.4 \pm 2 \text{ kJ mol}^{-1}$) and at 300 K is $\Delta H^\circ_{f,300} = 30.8 \pm 0.5 \text{ kcal mol}^{-1}$ ($129.0 \pm 2 \text{ kJ mol}^{-1}$). A study of branching ratios of $\text{ClO} + \text{ClO}$ channels in $\text{Cl}_2/\text{O}_2/\text{O}_3$ mixtures by Horowitz et al. [57] also finds the equilibrium constant in O_2 at 285 K to be in agreement with the recommendation. Values at single temperatures are available from Ellermann et al. [33] and Boakes et al. [9], the former agreeing with this recommendation, while the latter is a bit outside the 95% confidence limit. Broske and Zabel [13] measured the reverse reaction at four temperatures between 245 and 260 K. They used the parameters for the forward reaction recommended in JPL 02-25 to suggest van't Hoff parameters of 5.09×10^{-26} and 7584. Van't Hoff parameters suggested by Plenge et al. [89], who measured $\Delta H_{f,0}(\text{ClOOCi}) = 134.0 \pm 2.80 \text{ kJ mol}^{-1}$ by photoionization mass spectrometry and computed the entropy change for the reaction, are 1.92×10^{-27} and 8430.

Ferracci and Rowley [37] report values of between 250 and 313 K. A third law analysis of their values in the manner mentioned above yields $K_{\text{eq}} = 1.76 \times 10^{-27} \exp(8766/T)$, which results in values higher than those given in Table 3 by factors of 1.5 to 2.

Several studies have derived values of K_{eq} using atmospheric measurements in the nighttime polar stratosphere under conditions where ClO and ClOOCi should be in equilibrium. These are summarized here but are not used in the derivation of the recommended equilibrium constants. Avallone and Toohey [4] used $K_{\text{eq}} = 1.99 \times 10^{-30} \times T \times \exp(8854/T)$ derived from *in situ* aircraft experiments. The Avallone and Toohey [4] expression yields values that are quite close to those from the recommended expression. Atmospheric

measurements from an airborne platform have also been used by von Hobe et al. [107] to deduce K_{eq} parameters of 3.61×10^{-27} and 8167, resulting in values which lie outside the 95% confidence limits. A reanalysis by Salawitch and Canty [95] of ER-2 data between 185 and 200 K, from Stimpfle et al. [101] results in an expression for K_{eq} which lies within the uncertainty bounds and is quite close to the Avallone and Toohey [4] expression. Santee et al. [96] report measurements in the Arctic and Antarctic night by satellite based instruments, which by constraining the value of A to that recommended herein, yields a value of $B = 8570 \pm 135$, and a K_{eq} lower by about a factor of 1.4 than recommended herein at stratospheric temperatures.

Formation of the ClOClO isomer: $\text{ClO} + \text{ClO} \rightarrow \text{ClOClO}$. Zhu and Lin [116] used the G2 composite method to calculate the bond dissociation energy $D_0(\text{ClO}-\text{ClO}) = 49.8 \text{ kJ mol}^{-1}$. Matus et al. [71] used the CCSD(T)/aug-cc-pV(5+d)/Z method extrapolated to the complete basis set limit and found that ClOClO is less strongly bound than ClOOCl by 33.9 kJ mol^{-1} (Matus et al. estimate their errors to be less than 1 kcal mol^{-1}). Combining this value from Matus et al. with $\Delta H_{f,0}(\text{ClOOCl}) = 132.4 \pm 3 \text{ kJ mol}^{-1}$ (see Note 14a) gives $\Delta H_{f,0} = 166.3 \text{ kJ/mol}$ ($\Delta H_{f,298} = 163.7 \text{ kJ/mol}$) for ClOClO. The vibrational frequencies and moments of inertia calculated by Matus et al. are in good agreement with those of Zhu and Lin [116]. The entropy of ClOClO was calculated using the harmonic frequencies from Matus et al. [71] and rotational constants from Chase [23], giving $S^\circ_{298}(\text{ClOClO}) = 312.3 \text{ J K}^{-1} \text{ mol}^{-1}$. Thermodynamic data for ClO radicals were taken from Chase [23]. The 1-sigma errors in $\Delta S_{r,298}$ and $\Delta H_{r,298}$ are estimated to be $6 \text{ J K}^{-1} \text{ mol}^{-1}$ and 5 kJ mol^{-1} , respectively. Using these parameters, the equilibrium constant is given by $K_{eq}(\text{ClOClO}) = 2.5 \times 10^{-26} \exp(4350/T)$ with uncertainty factors $f = 2$ and $g = 600$. (Table: 10-6, Note: 10-6, Evaluated: 10-6) **Back to table**

17. $\text{Cl} + \text{OCIO}$. Because of the high energy barriers calculated for other plausible pathways ($\text{ClO} + \text{ClO}$ or isomerization of ClOOCl and ClOClO), this pathway seems to be the most relevant for formation and dissociation of ClClO_2 (chloryl chloride). Zhu and Lin [116] found energy barriers of $>19 \text{ kcal mol}^{-1}$ separating ClClO_2 from ClOOCl and ClOClO; they did not identify any low energy paths from $\text{ClO} + \text{ClO}$. It is noteworthy that Bröske and Zabel [13] did not see any evidence for formation of ClClO_2 when they measured the gas phase thermolysis of ClOOCl, although they were able to measure ClClO_2 produced in wall reactions. Thus it seems unlikely that the gas phase isomerization reactions are fast enough to be significant. The recommended K_{eq} is based on the thermodynamic calculation. The vibrational frequencies and moments of inertia are known [77, 78], giving $S^\circ_{298}(\text{ClClO}_2) = 294.4 \text{ J K}^{-1} \text{ mol}^{-1}$. The heat of formation of ClClO_2 has not been measured, but it has been calculated many times (see Zhu and Lin [116] for a summary of calculations up to 2003). The CCSD(T) calculations by Lee et al. [66] with large ANO basis sets was formerly regarded as the best. Recently, Matus et al. [71] carried out even better calculations (i.e. CBS(Q5)) and concluded that $\Delta H_{f,0}(\text{ClClO}_2)$ is $3.5 \text{ kcal mol}^{-1}$ below that of ClOOCl. Matus et al. estimate their relative errors to be less than $\pm 1 \text{ kcal mol}^{-1}$. Coupled with the recommended value of $132.4 \pm 3 \text{ kJ/mol}$ for ClOOCl (see Note 14a), this gives $\Delta H_{f,0}(\text{ClClO}_2) = 117.8 \text{ kJ/mol}$ and $\Delta H_{f,298} = 113.7 \text{ kJ/mol}$. The 1-sigma errors in $\Delta S_{r,298}$ and $\Delta H_{r,298}$ are estimated to be $6 \text{ J K}^{-1} \text{ mol}^{-1}$ and 5 kJ mol^{-1} , respectively. (Table: 10-6, Note: 10-6, Evaluated: 10-6) **Back to table**
18. $\text{ClO} + \text{OCIO}$. Data are from Burkholder et al. [15], Hayman and Cox [54] and Green et al. [49]. The best van't Hoff fit to all the data yields the recommended parameters. The 95% error limits encompass all the data. A calculation of the entropy and heat capacity from the structure and frequencies of ClOCl(O)O reported by Zhu and Lin [117] allows a "3rd Law" fit that gives $K_{eq}/\text{cm}^{-1} \text{ molecule}^{-1} = 1.6 \times 10^{-27} \exp(7155/T)$ for $232 < T/K < 298$. By including the hindered rotor potential explicitly [7], a new "3rd Law" fit obtained by fitting the data of [15] and [54], including the lowest temperature point, gives the new recommendation: $S^\circ_{298}(\text{Cl}_2\text{O}_3) = 337.8 \text{ J K}^{-1} \text{ mol}^{-1}$ ($80.7 \text{ cal mol}^{-1} \text{ K}^{-1}$) and $\Delta H_{f,0}(\text{Cl}_2\text{O}_3) = 143.9 \text{ kJ mol}^{-1}$ ($34.4 \text{ kcal mol}^{-1}$) and $\Delta H_{f,298}(\text{Cl}_2\text{O}_3) = 138.9 \text{ kJ mol}^{-1}$ ($33.2 \text{ kcal mol}^{-1}$). This compares to calculated values of $\Delta H_{f,0}(\text{Cl}_2\text{O}_3) = 32.3 \text{ kcal mol}^{-1}$ from [117] and $32.9 \text{ kcal mol}^{-1}$ from [98]. Burkholder et al. [15] claim that treating the lowest vibration as a free internal rotation increases the entropy of ClOCl(O)O by almost $9 \text{ cal mol}^{-1} \text{ K}^{-1}$. This value, repeated by Green et al. [49], is not correct. Clark and Francisco [26], who calculated structure and frequencies, concluded that $S^\circ_{298}(\text{Cl}_2\text{O}_3) = 78.5 \text{ cal mol}^{-1} \text{ K}^{-1}$, based on harmonic frequencies. Li et al. [68] have also reported theoretical structure and frequencies in general agreement with [117] and [26], but energetics that are quite different. (Table: 10-6, Note: 10-6, Evaluated: 10-6) **Back to table**
19. $\text{OCIO} + \text{NO}_3$. Theoretical calculations of Parthiban et al. [87]. This value replaces the value in 02-25 that was deduced by Friedl et al. [39]. Uncertainties are based on $\pm 1 \text{ kcal mole}^{-1}$ uncertainty in calculated heat of formation. Values in JPL06-02 were for $\pm 2 \text{ kcal mol}^{-1}$ uncertainty. (Table: 10-6, Note: 10-6, Evaluated: 10-6)

Back to table

20. OH + CS₂. Fit to the data of Murrells et al. [79], Hynes et al. [58] and Diau and Lee [32] between 246 and 318 K. Re-analysis of errors led to lower value of g than in JPL-02-25. (Table: JPL06, Note: JPL06) **Back to table**
21. CH₃S + O₂. Turnipseed et al. [105] report the equilibrium constant for $216 \leq T/K \leq 258$. From a third law analysis using $\Delta S^\circ_{237} = -36.8 \pm 2.6$ eu, they obtain $\Delta H^\circ_{237} = -11.5 \pm 0.9$ kcal/mole. (Table: 94-26, Note: 94-26) **Back to table**
22. Cl + CS₂. Fit to the data of Nicovich et al. [84] between 193 and 258 K. (Table: 10-6, Note: 10-6, Evaluated 10-6) **Back to table**
23. OH + (CH₃)₂S → (CH₃)₂SOH. This recommendation is based on the results of Hynes et al. [59] and Barone et al.[8], who used deuterated dimethyl sulfide (DMS-d₆), and Williams et al. [110], who used both DMS-d₆ and non-deuterated DMS-d₀, in studies of the rate constants for the reaction and found clear evidence for adduct formation. In each case, K_{eq} was obtained by analyzing the rate constant data, which showed double-exponential decays. Hynes et al. [59] measured K_{eq} from 250-267 K and reported an adduct bond energy of 13.0 ± 3.3 kcal/mol from a van't Hoff (2nd Law) analysis and a bond energy of 10.1 ± 1.1 kcal/mol based on a 3rd Law analysis using the theoretical molecular parameters computed by McKee [74]. Barone et al. measured K_{eq} from 217-240 K and reported bond energies of 10.2 and 10.7 ± 2.5 kcal/mol from 2nd and 3rd Law calculations, respectively. Williams et al. analyzed only their K_{eq} data for OH + DMS-d₆ (240-245 K) and obtained bond strengths of 10.9 ± 1.0 kcal/mol from a 2nd Law analysis and 10.5 kcal/mol from a 3rd Law analysis based on their own MP2/6-31+G(2d,p) quantum chemical calculations (in good agreement with McKee [75]). The present recommendation was obtained from a 3rd Law analysis of the data for OH + DMS-d₆ from all three DMD-d₆ studies combined with the data for OH + DMS-d₀ from Williams et al. The 61 data points covered the temperature range from 217-261 K. The 3rd Law analysis used the theoretical molecular parameters for DMS and HODMS computed by Williams et al. [110] and the properties of the OH radical from the JANAF Tables [23] and Ruscic et al. [94] to obtain the dissociation energy (without zero point energies) $D_e = 55.5 \pm 1.3$ kJ/mol (2σ). When the zero point energy differences are taken into account, this gives dissociation energies $D_0(\text{HO-DMS-d}_6) = 43.2 \pm 1.3$ kJ/mol and $D_0(\text{HO-DMS-d}_0) = 43.0 \pm 1.3$ kJ/mol (2σ). (Table: 10-6, Note: 10-6, Evaluated: 10-6) **Back to table**
24. Br + CH₃SCH₃. Second Law fit to data of Wine et al. [111] and Nakano et al. [80]. This corresponds to a bond dissociation energy in the adduct of 13.84 kcal mole⁻¹. (Table: 06-02, Note: 06-02, Evaluated: 06-02) **Back to table**

3.4 References

1. Aloisio, S., J. S. Francisco and R. R. Friedl, 2000, *J. Phys. Chem. A*, **104**, 6597-6601.
2. Amoruso, A., L. Crescentini, G. Fiocco and M. Volpe, 1993, *J. Geophys. Res.*, **98**, 16857-16863.
3. Andersson, B. Y., R. A. Cox and M. E. Jenkin, 1988, *International Journal of Chemical Kinetics*, **20**, 283-295.
4. Avallone, L. M. and D. W. Toohey, 2001, *J. Geophys. Res. A*, **106**, 10411-10421.
5. Baer, S., H. Hippler, R. Rahn, M. Siefke, N. Seitzinger and J. Troe, 1991, *J. Chem. Phys.*, **95**, 6463-6470.
6. Bahta, A., R. Simonaitis and J. Heicklen, 1982, *J. Phys. Chem.*, **86**, 1849.
7. Barker, J. R., N. F. Ortiz, J. M. Preses, L. L. Lohr, A. Maranzana, P. J. Stimac, T. L. Nguyen and T. J. D. Kumar. MultiWell <http://aoss.engin.umich.edu/multiwell/>. University of Michigan. Ann Arbor, MI, 2011.
8. Barone, S. B., A. A. Turnipseed and A. R. Ravishankara, 1996, *J. Phys. Chem.*, **100**, 14694-14702.
9. Boakes, G., W. H. H. Mok and D. M. Rowley, 2005, *Physical Chemistry Chemical Physics*, **7**, 4102-4113.
10. Borrell, P., C. J. Cobos and K. Luther, 1988, *J. Phys. Chem.*, **92**, 4377-4384.
11. Bridier, I., F. Caralp, H. Loirat, R. Lesclaux, B. Veyret, K. H. Becker, A. Reimer and F. Zabel, 1991, *J. Phys. Chem.*, **95**, 3594-3600.
12. Bridier, I., R. Lesclaux and B. Veyret, 1992, *Chem. Phys. Lett.*, **191**, 259-263.
13. Broske, R. and F. Zabel, 2006, *Journal of Physical Chemistry A*, **110**, 3280-3288.
14. Brunning, J., M. J. Frost and I. W. M. Smith, 1988, *Int. J. Chem. Kinetics*, **20**, 957.
15. Burkholder, J. B., R. L. Mauldin, R. J. Yokelson, S. Solomon and A. R. Ravishankara, 1993, *J. Phys. Chem.*, **97**, 7597-7605.
16. Burrows, J. P., G. S. Tyndall and G. K. Moortgat, 1985, *Chem. Phys. Lett.*, **119**, 193-198.
17. Campuzano-Jost, P., A. E. Croce, H. Hippler, M. Siefke, and J. Troe, 1995, *J. Chem. Phys.*, **102**, 5317-5326.
18. Cantrell, C. A., J. A. Davidson, A. H. McDaniel, R. E. Shetter and J. G. Calvert, 1988, *J. Chem. Phys.*, **88**, 4997-5006.
19. Cantrell, C. A., R. E. Shetter, J. G. Calvert, G. S. Tyndall and J. J. Orlando, 1993, *J. Phys. Chem.*, **97**, 9141-9148.
20. Carter, R. O. and L. Andrews, 1981, *J. Phys. Chem.*, **85**, 2351.
21. Chao, J., R. C. Wilhoit and B. J. Zwolinski, 1974, *Thermochim. Acta*, **10**, 361-371.
22. Chao, J., R. C. Wilhoit and B. J. Zwolinski, 1974, *Thermochim. Acta*, **10**, 359-360.
23. Chase, M. W., 1998, *J. Phys. Chem. Ref. Data*, **Monograph 9**.
24. Chen, Z. and T. P. Hamilton, 1996, *J. Phys. Chem.*, **100**, 15731-15734.
25. Christensen, L. E., M. Okumura, J. C. Hansen, S. P. Sander and J. S. Francisco, 2006, *J. Phys. Chem. A*, **110**, 6948-6959.
26. Clark, J. and J. S. Francisco, 1997, *J. Phys. Chem. A*, **101**, 7145-7153.
27. Connell, P. S. and H. S. Johnston, 1979, *Geophys. Res. Lett.*, **6**, 553-556.
28. Cox, R. A. and J. P. Burrows, 1979, *J. Phys. Chem.*, **83**, 2560-2568.
29. Cox, R. A. and G. D. Hayman, 1988, *Nature*, **332**, 796-800.
30. DeMore, W. B., 1990, *Geophys. Res. Lett.*, **17**, 2353-2355.
31. Denis, P. A., and O. N. Ventura, 2004, *Chem. Phys. Lett.*, **385**, 292-297.
32. Diau, E. W.-G. and Y.-P. Lee, 1991, *J. Phys. Chem.*, **95**, 7726-7732.
33. Ellermann, T., K. Johnsson, A. Lund and P. Pagsberg, 1995, *Acta Chemica Scandinavica*, **49**, 28-35.
34. Estupiñán, E. G., J. M. Nicovich and P.H. Wine, 2001, *J. Phys. Chem. A*, **105**, 9697-9703.
35. Feller, D. and D. A. Dixon, 2003, *J. Phys. Chem. A*, **107**, 9641-9651.
36. Feller, D., K. A. Peterson and D. A. Dixon, 2008, *The Journal of Chemical Physics*, **129**, 204105-32.
37. Ferracci, V. and D. M. Rowley, 2010, *Phys. Chem. Chem. Phys.*, **12**, 11596-11608.
38. Francisco, J. S., Y. Zhao, W. A. Lester, Jr., and I. H. Williams, 1992, *J. Chem. Phys.*, **96**, 2861-2867.
39. Friedl, R. R., S. P. Sander and Y. L. Yung, 1992, *J. Phys. Chem.*, **96**, 7490-7493.
40. Fry, J., L. J. Matthews, J. R. Lane, A. Sinha, H. G. Kjaergaard and P. O. Wennberg, 2006, *J. Phys. Chem. A*, **110**, 7072-7079.
41. Gierczak, T., E. Jimenez, V. Riffault, J. B. Burkholder, and A. R. Ravishankara, 2005, *J. Phys. Chem. A*, **109**, 586-596.
42. Golden, D. M., 2003, *Int. J. Chem. Kinet.*, **35**, 206-211.
43. Golden, D. M., 2005, *Int. J. Chem. Kinet.*, **37**, 625-632.
44. Golden, D. M., J. R. Barker and L. L. Lohr, 2004, *J. Phys. Chem. A*, **108**, 8552.

45. Golden, D. M., J. R. Barker, and L. L. Lohr, 2003, *J. Phys. Chem. A*, **107**, 11057-11071.
46. Gozel, P., B. Calpani and H. van den Bergh, 1984, *Isrl. J. Chem.*, **24**, 210.
47. Graham, R. A. and H. S. Johnston, 1978, *J. Phys. Chem.*, **82**, 254-268.
48. Graham, R. A., A. M. Winer and J. N. Pitts, Jr., 1977, *Chem. Phys. Lett.*, **51**, 215.
49. Green, T. J., M. Islam, P. Guest, K. Hickson, C. E. Canosa-Mas, and R. P. Wayne, 2003, *Phys. Chem. Chem. Phys.*, **5**, 5409-5418.
50. Hamilton, E. J., Jr., 1975, *J. Chem. Phys.*, **63**, 3682-3683.
51. Hamilton, E. J., Jr. and R.-R. Lii, 1977, *Int. J. Chem. Kinet.*, **9**, 875-885.
52. Harwood, M. H. and R. L. Jones, 1994, *J. Geophys. Res.*, **99**, 22955-22964.
53. Hassouna, M., E. Delbos, P. Devolder, B. Viskolcz and C. Fittschen, 2006, *Journal of Physical Chemistry A*, **110**, 6667-6672.
54. Hayman, G. D. and R. A. Cox, 1989, *Chem. Phys. Lett.*, **155**, 1-7.
55. Hippler, H., S. Nasterlack and F. Striebel, 2002, *Phys. Chem. Chem. Phys.*, **4**, 2959-2964.
56. Hjorth, J., J. Nothholt and G. Restelli, 1992, *Int. J. Chem. Kinet.*, **24**, 51-65.
57. Horowitz, A., J. N. Crowley and G. K. Moortgat, 1994, *J. Phys. Chem.*, **98**, 11924-11930.
58. Hynes, A. J., P. H. Wine and J. M. Nicovich, 1988, *J. Phys. Chem.*, **92**, 3846-3852.
59. Hynes, A. J., P. H. Wine and D. H. Semmes, 1986, *J. Phys. Chem.*, **90**, 4148-4156.
60. *JANAF Thermochemical Tables*, Third ed.; National Bureau of Standards, 1985.
61. Kanno, N., K. Tonokura and M. Koshi, 2006, *Journal of Geophysical Research, D: Atmospheres*, **111**, D20312.
62. Kanno, N., K. Tonokura, A. Tezaki and M. Koshi, 2005, *J. Phys. Chem. A*, **109**, 3153-3158.
63. Kircher, C. C., J. J. Margitan and S. P. Sander, 1984, *J. Phys. Chem.*, **88**, 4370-4375.
64. Konen, I. M., E. X. J. Li, T. A. Stephenson and M. I. Lester, 2005, *Journal of Chemical Physics*, **123**, 204318.
65. Konen, I. M., L. B. Pollack, E. X. J. Li, M. I. Lester, M. E. Varner and J. F. Stanton, 2005, *Journal of Chemical Physics*, **122**, 094320.
66. Lee, T. J., C. M. Rohlfing and J. E. Rice, 1992, *J. Chem. Phys.*, **97**, 6593-6605.
67. Li, E. X., I. M. Konan, M. I. Lester and A. B. McCoy, 2006, *J. Phys. Chem. A*, **110**.
68. Li, Q., S. Lu, Y. Xie, P. V. R. Schleyer and H. F. Schaefer, III, 2003, *Int. J. Quantum Chem.*, **95**, 731-757.
69. Markwalder, B., P. Gozel and H. van den Bergh, 1992, *J. Chem. Phys.*, **97**, 5472-5479.
70. Matthews, J. and A. Sinha, 2005, *J. Chem. Phys.*, **122**, 104313.
71. Matus, M. H., M. T. Nguyen, D. A. Dixon, K. A. Peterson and J. S. Francisco, 2008, *The Journal of Physical Chemistry A*, **112**, 9623-9627.
72. Mauldin, R. L., III, J. B. Burkholder and A. R. Ravishankara, 1992, *J. Phys. Chem.*, **96**, 2582-2588.
73. McCoy, A. B., J. L. Fry, J. S. Francisco, A. K. Mollner and M. Okumura, 2005, *J. Chem. Phys.*, **122**, 104311/1-14.
74. McKee, M. L., 1993, *J. Phys. Chem*, **97**, 10971-10976.
75. McKee, M. L., 2003, *J. Phys. Chem. A*, **107**, 6819-6827.
76. Miller, C. E., J. I. Lynton, D. M. Keevil and J. S. Francisco, 1999, *J. Phys. Chem. A*, **103**, 11451-11459.
77. Müller, H. S. P. and H. Willner, 1992, *Ber. Bunsenges. Phys. Chem.*, **96**, 427-431.
78. Müller, H. S. P. and H. Willner, 1992, *Inorg. Chem.*, **31**, 2527-2534.
79. Murrells, T. P., E. R. Lovejoy and A. R. Ravishankara, 1990, *J. Phys. Chem.*, **94**, 2381-2386.
80. Nakano, Y., M. Goto, S. Hashimoto, M. Kawasaki, and T. J. Wallington, 2001, *J. Phys. Chem. A*, **105**, 11045-11050.
81. Nickolaisen, S. L., R. R. Friedl and S. P. Sander, 1994, *J. Phys. Chem.*, **98**, 155-169.
82. Nicovich, J. M., K. D. Kreutter, C. J. Shackelford and P. H. Wine, 1991, *Chem. Phys. Lett.*, **179**, 367-373.
83. Nicovich, J. M., K. D. Kreutter and P. H. Wine, 1990, *J. Chem. Phys.*, **92**, 3539-3544.
84. Nicovich, J. M. and P. H. Wine, 1990, *Int. J. Chem. Kinet.*, **22**, 379-397.
85. Orlando, J. J., G. S. Tyndall, C. A. Cantrell and J. G. Calvert, 1991, *J. Chem. Soc. Far. Trans.*, **87**, 2345-2349.
86. Pagsberg, P. B., E. Ratajczak, A. Sillesen and J. T. Jodkowski, 1987, *Chem. Phys. Lett.*, **141**, 88-94.
87. Parthiban, S., T. J. Lee, S. Guha, and J. S. Francisco, 2003, *J. Amer. Chem. Soc.*, **125**, 10446-10458.
88. Perner, D., A. Schmeltekopf, R. H. Winkler, H. S. Johnston, J. G. Calvert, C. A. Cantrell and W. R. Stockwell, 1985, *J. Geophys. Res.*, **90**, 3807-3812.
89. Plenge, J., S. Kühl, B. Vogel, R. Müller, F. Strohm, M. von Hobe, R. Flesch and E. Rühl, 2005, *J. Phys. Chem. A*, **109**, 6730-6734.
90. Prasad, S. S., 1980, *Nature*, **285**, 152.

91. Prasad, S. S. and T. J. Lee, 1994, *J. Geophys. Res.*, **99**, 8225-8230.
92. Pritchard, H. O., 1994, *Int. J. Chem. Kinet.*, **26**, 61-72.
93. Ruscic, B., J. E. Boggs, A. Burcat, A. G. Csaszar, J. Demaison, R. Janoschek, J. M. L. Martin, M. L. Morton, M. J. Rossi, J. F. Stanton, P. G. Szalay, P. R. Westmoreland, F. Zabel and T. Berces, 2005, *Journal of Physical and Chemical Reference Data*, **34**, 573-656.
94. Ruscic, B., R. E. Pinzon, M. L. Morton, N. K. Srinivasan, M.-C. Su, J. W. Sutherland and J. V. Michael, 2006, *J. Phys. Chem. A*, **110**, 6592-6601.
95. Salawitch, R. J. and T. Canty, 2009, Personal Communication.
96. Santee, M. L., S. P. Sander, N. J. Livesey and L. Froidevaux, 2010, *Proceedings of the National Academy of Sciences of the United States of America*, **107**, 6588-6593.
97. Schott, G. and N. Davidson, 1958, *J. Amer. Chem. Soc.*, **80**, 1841-1853.
98. Sicre, J. E. and C. J. Cobos, 2003, *Journal of Molecular Structure: Theochem*, **620**, 215-226.
99. Smith, C. A., A. R. Ravishankara and P. H. Wine, 1985, *J. Phys. Chem.*, **89**, 1423-1427.
100. Smith, I. W. M. and G. Yarwood, 1986, *Chem. Phys. Lett.*, **130**, 24-28.
101. Stimpfle, R. M., D. M. Wilmouth, R. J. Salawitch and J. G. Anderson, 2004, *Journal of Geophysical Research, D: Atmospheres*, **109**, D03301, doi:10.1029/2003JD003811.
102. Suma, K., Y. Sumiyoshi and Y. Endo, 2006, *Science*, **311**, 1278-1281.
103. Tuazon, E. C., E. Sanhueza, R. Atkinson, W. P. L. Carter, A. M. Winer and J. N. Pitts, Jr., 1984, *J. Phys. Chem.*, **88**, 3095-3098.
104. Tuchler, M. F., K. L. Schmidt, and M. Morgan, 2005, *Chem. Phys. Lett.*, **401**, 393-399.
105. Turnipseed, A. A., S. B. Baron and A. R. Ravishankara, 1992, *J. Phys. Chem.*, **96**, 7502-7505.
106. Viggiano, A. A., J. A. Davidson, F. C. Fehsenfeld and E. E. Ferguson, 1981, *J. Chem. Phys.*, **74**, 6113-6125.
107. von Hobe, M., J. U. Grooss, R. Muller, S. Hrechanyy, U. Winkler and F. Stroh, 2005, *Atmospheric Chemistry and Physics*, **5**, 693-702.
108. Vosper, A. J., 1970, *J. Chem. Soc. A*, **1970**, 625.
109. Wangberg, I., T. Etzkorn, I. Barnes, U. Platt and K. H. Becker, 1997, *J. Phys. Chem. A*, **101**, 9694-9698.
110. Williams, M. B., P. Campuzano-Jost, B. M. Cossairt, A. J. Hynes and A. J. Pounds, 2007, *J. Phys. Chem. A*, **111**, 89-104.
111. Wine, P. H., J. M. Nicovich, R. E. Stickel, Z. Zhao, C. J. Shackelford, K. D. Kreutter, E. P. Daykin and S. Wang. In *The Tropospheric Chemistry of Ozone in the Polar Regions*; Springer-Verlag: Berlin, 1993; Vol. I7; pp 385-395.
112. Wollenhaupt, M. and J. N. Crowley, 2000, *J. Phys. Chem. A*, **104**, 6429-6438.
113. Zabel, F., 1995, *Zeitschrift fur Physikalische Chemie*, **188**, 119-142.
114. Zabel, F., A. Reimer, K. H. Becker and E. H. Fink, 1989, *J. Phys. Chem.*, **93**, 5500-5507.
115. Zhang, X., M. R. Nimlos, G. B. Ellison, M. E. Varner and J. F. Stanton, 2006, *J. Chem. Phys.*, **124**, 084305/1-084305/7.
116. Zhu, R. S. and M. C. Lin, 2003, *Journal of Chemical Physics*, **118**, 4094-4106.
117. Zhu, R. S. and M. C. Lin, 2003, *J. Chem. Phys.*, **118**, 8645-8655.
118. Zhu, R. S. and M. C. Lin, 2003, *J. Chem. Phys.*, **119**, 2075-2082.

SECTION 4. PHOTOCHEMICAL DATA

Table of Contents

SECTION 4. PHOTOCHEMICAL DATA	4-1
4.1 Format and Error Estimates	4-6
4.2 Halocarbon Absorption Cross Sections and Quantum Yields.....	4-6
4.3 Web Access to Recommended Data in Text and Graphical Formats	4-6
4.4 References.....	4-11
4A O _x Photochemistry.....	4A-1
References for Section 4A.....	4A-13
4B HO _x Photochemistry.....	4B-1
References for Section 4B.....	4B-8
4C NO _x Photochemistry	4C-1
References for Section 4C.....	4C-24
4D Organic Photochemistry.....	4D-1
References for Section 4D.....	4D-50
4E FO _x Photochemistry.....	4E-1
References for Section 4E.....	4E-21
4F ClO _x Photochemistry.....	4F-1
References for Section 4F.....	4F-63
4G BrO _x Photochemistry.....	4G-1
References for Section 4G.....	4G-51
4H IO _x Photochemistry.....	4H-1
References for Section 4H.....	4H-32
4I SO _x Photochemistry.....	4I-1
References for Section 4I.....	4I-7
4J Metal Photochemistry.....	4J-1
References for Section 4J.....	4J-5

Tables

Table 4-1. Photochemical Reactions	4-7
Table 4-2. Combined Uncertainties for Cross Sections and Quantum Yields	4-10

Section A: O_x Photochemistry

Table 4A-1	Summary of O ₂ Absorption Cross Section Studies
Table 4A-2	Absorption Cross Sections of O ₂ between 205 and 245 nm
Table 4A-3	Summary of O ₃ Absorption Cross Section Studies
Table 4A-4	Absorption Cross Sections of O ₃ at 218 and 293-298 K
Table 4A-5	Parameters for the Calculation of O(¹ D) Quantum Yields

Section B: HO_x Photochemistry

Table 4B-1	Absorption Cross Sections of HO ₂ at 298 K
Table 4B-2	Summary of H ₂ O Vapor Absorption Cross Section Studies
Table 4B-3	Absorption Cross Sections of H ₂ O Vapor at 298 K
Table 4B-4	Summary of H ₂ O ₂ Absorption Cross Section Studies
Table 4B-5	Absorption Cross Sections of H ₂ O ₂ Vapor at 298 and 355 K
Table 4B-6	Mathematical Expression for Absorption Cross Sections of H ₂ O ₂ as a Function of Temperature

Section C: NO_x Photochemistry

Table 4C-1	Summary of NO ₂ Absorption Cross Section Studies
Table 4C-2	Absorption Cross Sections of NO ₂ at 220 and 294 K
Table 4C-3	Quantum Yields for NO ₂ Photolysis
Table 4C-4	Summary of NO ₃ Absorption Cross Section Studies
Table 4C-5	Absorption Cross Sections of NO ₃ at 298 K
Table 4C-6	Product Channel Quantum Yields in the Photolysis of NO ₃ at 298, 230, and 190 K
Table 4C-7	Summary of N ₂ O Cross Section Studies
Table 4C-8	Absorption Cross Sections of N ₂ O at 298 K

Table 4C-9	Mathematical Expression for the Absorption Cross Sections of N_2O as a Function of Temperature
Table 4C-10	Summary of N_2O_4 Absorption Cross Section Studies
Table 4C-11	Absorption Cross Sections of N_2O_4 at 220 K
Table 4C-12	Summary of N_2O_5 Absorption Cross Section Studies
Table 4C-13	Absorption cross sections at 300 K and temperature coefficients for N_2O_5
Table 4C-14	N_2O_5 Photolysis Quantum Yields
Table 4C-15	Summary of HONO Absorption Cross Section Studies
Table 4C-16	Absorption Cross Sections of HONO at 298 K
Table 4C-17	Absorption Cross Sections at 298 K and Temperature Coefficients for HNO_3
Table 4C-18	Absorption Cross Sections of HO_2NO_2 at 298 K
Table 4C-19	HO_2NO_2 Photolysis Quantum Yields
Table 4C-20	Photodissociation Band Strengths and Quantum Yields for Several Overtone and Combination Bands of HO_2NO_2

Section D: Organic Photochemistry

Table 4D-1	Summary of CH_2O Cross Section Studies
Table 4D-2	Absorption Cross Sections of CH_2O at 298 K and Temperature Coefficients Averaged over 1 nm Intervals
Table 4D-3	Absorption Cross Sections of CH_2O at 298 K and 223 K and Temperature Dependence Coefficients Averaged over Intervals Used in Atmospheric Models
Table 4D-4	CH_2O Photolysis Quantum Yields at 300 K and 1 atmosphere
Table 4D-5	Absorption Cross Sections of CH_3CHO at 298 K
Table 4D-6	CH_3CHO Photolysis Quantum Yields at 1 bar Total Pressure
Table 4D-7	Absorption Cross Sections of $\text{C}_2\text{H}_5\text{CHO}$ at 298 K
Table 4D-8	Absorption Cross Sections of CH_3O_2 , $\text{C}_2\text{H}_5\text{O}_2$, and $\text{CH}_3\text{C}(\text{O})\text{O}_2$ at 298 K
Table 4D-9	UV Absorption Cross Sections of CH_3CO at 298 K
Table 4D-10	Vis Absorption Cross Sections of CH_3CO at 298 K
Table 4D-11	Absorption Cross Sections of $\text{CH}_3\text{C}(\text{O})\text{CH}_2\text{O}_2$ at 298 K
Table 4D-12	Absorption Cross Sections of CH_3OOH at 298 K
Table 4D-13	Absorption Cross Sections of HOCH_2OOH at 298 K
Table 4D-14	Absorption Cross Sections of CH_3ONO at 298 K
Table 4D-15	Absorption Cross Sections of CH_3ONO_2 at 298 K
Table 4D-16	Absorption Cross Sections of $\text{CH}_3\text{O}_2\text{NO}_2$ at 298 K
Table 4D-17	Absorption Cross Sections of $\text{CH}_3\text{C}(\text{O})\text{O}_2\text{NO}_2$ at 298 K and Temperature Coefficients
Table 4D-18	Absorption Cross Sections of $\text{C}_2\text{H}_5\text{C}(\text{O})\text{O}_2\text{NO}_2$ at 296 K and Temperature Coefficients
Table 4D-19	Absorption Cross Sections of $\text{CH}_2=\text{CHCHO}$ at 298 K
Table 4D-20	Absorption Cross Sections of $\text{CH}_2=\text{C}(\text{CH}_3)\text{CHO}$ at 298 K
Table 4D-21	Absorption Cross Sections of $\text{CH}_3\text{C}(\text{O})\text{CH}=\text{CH}_2$ at 298 K
Table 4D-22	Absorption Cross Sections of HOCH_2CHO at 298 K
Table 4D-23	Absorption Cross Sections of $\text{CH}_3\text{C}(\text{O})\text{CH}_3$ at 298 K and Temperature Coefficients
Table 4D-24	Acetone Photolysis Quantum Yields
Table 4D-25	Absorption Cross Sections of $\text{CH}_3\text{C}(\text{O})\text{CH}_2\text{OH}$ at 298 K
Table 4D-26	Absorption Cross Sections of CHOCHO at 296 K
Table 4D-27	CHOCHO Photolysis Quantum Yields at 1 Atm and 298 K
Table 4D-28	Absorption Cross Sections of $\text{CH}_3\text{COC}(\text{O})\text{H}$ at 298 K
Table 4D-29	Absorption Cross Sections of $\text{HC}(\text{O})\text{OH}$ and $(\text{HC}(\text{O})\text{OH})_2$ at 302 K
Table 4D-30	Absorption Cross Sections of $\text{CH}_3\text{C}(\text{O})\text{OH}$ and $(\text{CH}_3\text{C}(\text{O})\text{OH})_2$ at 298 K
Table 4D-31	Absorption Cross Sections $\text{CH}_3\text{C}(\text{O})\text{OOH}$ at 298 K
Table 4D-32	Absorption Cross Sections of $\text{CH}_3\text{C}(\text{O})\text{C}(\text{O})\text{OH}$ at 298 K
Table 4D-33	Absorption Cross Sections of $\text{HC}(\text{O})\text{OCH}_3$ at 298 K
Table 4D-34	Absorption Cross Sections of $\text{HC}(\text{O})\text{OC}_2\text{H}_5$ at 297 K

Section E: FO_x Photochemistry

Table 4E-1	Absorption Cross Sections of FO_2 at 295 K
Table 4E-2	Absorption Cross Sections of F_2O at 273 K
Table 4E-3	Absorption Cross Sections of F_2O_2 at 193 – 273 K

Table 4E-4	Absorption Cross Sections of FNO at 298 K
Table 4E-5	Summary of CF ₄ Absorption Cross Section Studies
Table 4E-6	Absorption Cross Sections of COF ₂ at 298 K
Table 4E-7	Absorption Cross Sections of COHF at 298 K
Table 4E-8	Absorption Cross Sections of CF ₃ O ₂ at 295 K
Table 4E-9	Absorption Cross Sections of CF ₃ OOCF ₃ at 298 K
Table 4E-10	Absorption Cross Sections of CF ₃ O ₃ CF ₃ at 298 K
Table 4E-11	Absorption Cross Sections of CF ₃ CHO at 298 K
Table 4E-12	Absorption Cross Sections of CF ₃ C(O)F at 298 and 238 K
Table 4E-13	Absorption Cross Sections of CF ₃ C(O)Cl at 300 and 253 K
Table 4E-14	Absorption Cross Sections of CF ₃ OONO ₂ at 300 and 253 K
Table 4E-15	Absorption Cross Sections of CF ₃ (O)O ₂ NO ₂ at 298 K
Table 4E-16	Absorption Cross Sections of CF ₃ CH ₂ CHO at 298 K
Table 4E-17	Absorption Cross Sections of CF ₃ C(O)OH at 296 K
Table 4E-18	Absorption Cross Sections of CH ₃ C(O)F at 296 K
Table 4E-19	Absorption Cross Sections of CH ₂ =CHCF ₃ at 295 K
Table 4E-20	Absorption Cross Sections of CH ₂ =CFCF ₃ at 295 K
Table 4E-21	Absorption Cross Sections of CF ₂ =CF ₂ at 296 K
Table 4E-22	Absorption Cross Sections of CF ₂ =CFCF ₃ at 296 K

Section F: ClO_x Photochemistry

Table 4F-1	Absorption Cross Sections of Cl ₂ at 298 K
Table 4F-2	Absorption Cross Sections of ClO at 298 K
Table 4F-3	Absorption Cross Sections of ClO at the band heads of the v',v'' = 1,0 to 21,0 bands
Table 4F-4	Absorption Cross Sections of ClOO at 191 K
Table 4F-5	Summary OCIO Cross Section Studies
Table 4F-6	Absorption Cross Sections of OCIO at 204 K (averages over 1 nm intervals)
Table 4F-7	Absorption Cross Sections of OCIO at the a(21) to a(3) Band Peaks at Temperatures in the Range 213 – 293 K
Table 4F-8	Absorption Cross Sections of OCIO at the Band Peaks
Table 4F-9	Absorption Cross Sections of Cl ₂ O at 298 K
Table 4F-10	Summary of ClOOCl UV Absorption Spectrum Studies
Table 4F-11	Absorption Cross Sections of ClOOCl
Table 4F-12	Absorption Cross Sections of Cl ₂ O ₃ at 220 – 260 K
Table 4F-13	Absorption Cross Sections of Cl ₂ O ₄ at 298 K
Table 4F-14	Absorption Cross Sections of Cl ₂ O ₆ at 298 K
Table 4F-15	Absorption Cross Sections of Cl ₂ O ₇ at 298 K
Table 4F-16	Absorption Cross Sections of ClClO ₂ at 298 K
Table 4F-17	Absorption Cross Sections of HCl and DCl at 298 K
Table 4F-18	Absorption Cross Sections of HOCl at 298 K
Table 4F-19	Absorption Cross Sections of ClNO at 298 K
Table 4F-20	Absorption Cross Sections of ClNO ₂ at 298 K
Table 4F-21	Absorption Cross Sections of ClONO at 231 K
Table 4F-22	Absorption Cross Sections and Temperature Coefficients of ClONO ₂
Table 4F-23	Absorption Cross Sections of CCl ₄ at 295 K
Table 4F-24	Absorption Cross Sections of CH ₃ OCl at 295 K
Table 4F-25	Absorption Cross Sections of CHCl ₃ at 296 K
Table 4F-26	Absorption Cross Sections of CH ₂ Cl ₂ at 298 K
Table 4F-27	Absorption Cross Sections of CH ₃ Cl at 298 K
Table 4F-28	Absorption Cross Sections of CH ₃ CCl ₃ at 298 K
Table 4F-29	Absorption Cross Sections of CH ₃ CH ₂ Cl at 298 K
Table 4F-30	Absorption Cross Sections of CH ₃ CHClCH ₃ at 295 K
Table 4F-31	Absorption Cross Sections of COCl ₂ at 298 K
Table 4F-32	Absorption Cross Sections of COHCl at 298 K
Table 4F-33	Absorption Cross Sections of COFCl at 298 K
Table 4F-34	COFCl Photolysis Quantum Yields
Table 4F-35	Absorption Cross Sections of CFCI ₃ at 298 K
Table 4F-36	Absorption Cross Sections of CF ₂ Cl ₂ at 298 K
Table 4F-37	Absorption Cross Sections of CF ₃ Cl at 295 K
Table 4F-38	Absorption Cross Sections of CF ₂ ClCFCI ₂ at 298 K

Table 4F-39	Absorption Cross Sections of $\text{CF}_2\text{ClCF}_2\text{Cl}$ at 295 K
Table 4F-40	Absorption Cross Sections of $\text{CF}_3\text{CF}_2\text{Cl}$ at 298 K
Table 4F-41	Absorption Cross Sections of CHFCl_2 at 298 K
Table 4F-42	Absorption Cross Sections of CHF_2Cl at 298 K
Table 4F-43	Absorption Cross Sections of CH_2FCl at 298 K
Table 4F-44	Absorption Cross Sections of CF_3CHCl_2 at 295 K
Table 4F-45	Absorption Cross Sections of CF_3CHFCl at 295 K
Table 4F-46	Absorption Cross Sections of $\text{CF}_3\text{CH}_2\text{Cl}$ at 298 K
Table 4F-47	Absorption Cross Sections of CH_3CFCl_2 at 298 K
Table 4F-48	Absorption Cross Sections of $\text{CH}_3\text{CF}_2\text{Cl}$ at 298 K
Table 4F-49	Absorption Cross Sections of CH_2ClCHO at 298 K
Table 4F-50	Absorption Cross Sections of CHCl_2CHO at 298 K
Table 4F-51	Absorption Cross Sections of CF_2ClCHO at 298 K and Temperature Coefficients
Table 4F-52	Absorption Cross Sections of CFCl_2CHO at 298 K and Temperature Coefficients
Table 4F-53	Absorption Cross Sections of CCl_3CHO at 298 K and Temperature Coefficients
Table 4F-54	Absorption Cross Sections of $\text{CH}_3\text{C(O)Cl}$ at 298 K
Table 4F-55	Absorption Cross Sections of $\text{CH}_2\text{ClC(O)Cl}$ at 298 K
Table 4F-56	Absorption Cross Sections of $\text{CHCl}_2\text{C(O)Cl}$ at 298 K
Table 4F-57	Absorption Cross Sections of $\text{CCl}_3\text{C(O)Cl}$ at 295 K
Table 4F-58	Absorption Cross Sections of $\text{CF}_3\text{CF}_2\text{CHCl}_2$ (HCFC-225ca) at 298 K
Table 4F-59	Absorption Cross Sections of $\text{CF}_2\text{ClCF}_2\text{CFCl}$ (HCFC-225cb) at 298 K
Table 4F-60	Absorption Cross Sections of $\text{CH}_3\text{C(O)CH}_2\text{Cl}$ at 296 K

Section G: BrO_x Photochemistry

Table 4G-1	Summary of Br_2 Cross Section Studies
Table 4G-2	Absorption Cross Sections of Br_2 at 298 K
Table 4G-3	Summary of HBr UV Absorption Cross Section Studies
Table 4G-4	Absorption Cross Sections of HBr at 298 K
Table 4G-5	Summary of BrO Cross Section Studies
Table 4G-6	Absorption Cross Sections at the Vibrational Band Peaks in the $\text{A} \leftarrow \text{X}$ Spectrum of BrO (0.4 nm resolution)
Table 4G-7	Absorption Cross Sections of BrO at 298 K
Table 4G-8	Peak Absorption Cross Sections of OBrO at 298 K
Table 4G-9	Absorption Cross Sections of OBrO at 298 K
Table 4G-10	Absorption Cross Sections of Br_2O at 298 K
Table 4G-11	Absorption Cross Sections of HOBr at 298 K
Table 4G-12	Absorption Cross Sections of BrNO at 298 K
Table 4G-13	Absorption Cross Sections of BrONO at 253 K
Table 4G-14	Absorption Cross Sections of BrNO_2 at 298 K
Table 4G-15	Absorption Cross Sections of BrONO_2 at 296 K and Temperature Coefficients
Table 4G-16	BrONO_2 Photolysis Quantum Yields
Table 4G-17	Absorption Cross Sections of BrCl at 298 K
Table 4G-18	Absorption Cross Sections of BrOCl at 298 K
Table 4G-19	Absorption Cross Sections of CH_3Br at 296 K
Table 4G-20	Absorption Cross Sections of CH_2Br_2 at 298 K
Table 4G-21	Absorption Cross Sections of CHBr_3 at 296 K
Table 4G-22	Absorption Cross Sections of $\text{CH}_2\text{BrCH}_2\text{Br}$ at 295 K
Table 4G-23	Absorption Cross Sections of $\text{C}_2\text{H}_5\text{Br}$ at 295 K
Table 4G-24	Absorption Cross Sections of COBr_2 at 298 K
Table 4G-25	Absorption Cross Sections of COHBr at 298 K
Table 4G-26	Absorption Cross Sections of CH_2ClBr at 295 K
Table 4G-27	Absorption Cross Sections of CHClBr_2 at 296 K
Table 4G-28	Absorption Cross Sections of CHCl_2Br at 298 K
Table 4G-29	Absorption Cross Sections of CCl_3Br at 298 K
Table 4G-30	Absorption Cross Sections of CHF_2Br at 298 K
Table 4G-31	Absorption Cross Sections of CF_2Br_2 at 296 K
Table 4G-32	Absorption Cross Sections of CF_2ClBr at 298 K
Table 4G-33	Absorption Cross Sections of CF_3Br at 296 K

Table 4G-34	Absorption Cross Sections of $\text{CH}_2=\text{CHBr}$ at 295 K
Table 4G-35	Absorption Cross Sections of $\text{CHBr}=\text{CF}_2$ at 295 K
Table 4G-36	Absorption Cross Sections of $\text{CFBr}=\text{CF}_2$ at 295 K
Table 4G-37	Absorption Cross Sections of $\text{CH}_2=\text{CBrCF}_3$ at 295 K
Table 4G-38	Absorption Cross Sections of $\text{CF}_3\text{CH}_2\text{Br}$ at 295 K
Table 4G-39	Absorption Cross Sections of CF_3CHClBr at 298 K
Table 4G-40	Absorption Cross Sections of CF_3CHFBr at 295 K
Table 4G-41	Absorption Cross Sections of $\text{CF}_2\text{BrCF}_2\text{Br}$ at 296 K
Table 4G-42	Absorption Cross Sections of $\text{CF}_3\text{CF}_2\text{Br}$ at 298 K
Table 4G-43	Absorption Cross Sections of $\text{CH}_3\text{CH}_2\text{CH}_2\text{Br}$ and $\text{CH}_3\text{CHBrCH}_3$ at 295 K
Table 4G-44	Absorption Cross Sections of $\text{CH}_3\text{C}(\text{O})\text{CH}_2\text{Br}$ at 296 K

Section H: IO_x Photochemistry

Table 4H-1	Summary of I_2 Absorption Cross Sections Studies
Table 4H-2	Absorption Cross Sections of I_2 at 295 K
Table 4H-3	Cross Sections at the Maxima and Minima of I_2 at 295 K
Table 4H-4	Summary of IO Absorption Cross Section Studies
Table 4H-5	Absorption Cross Sections of IO at 298 K
Table 4H-6	Absorption Cross Sections of OIO at 295 K
Table 4H-7	Summary of HI Absorption Cross Sections Studies
Table 4H-8	Absorption Cross Sections of HI at 298 K
Table 4H-9	Absorption Cross Sections of HOI at 298 K
Table 4H-10	Absorption Cross Sections of ICl at 298 K
Table 4H-11	Absorption Cross Sections of IBr at 298 K
Table 4H-12	Absorption Cross Sections of INO at 298 K
Table 4H-13	Absorption Cross Sections of IONO at 298 K
Table 4H-14	Absorption Cross Sections of IONO_2 at 298 K
Table 4H-15	Absorption Cross Sections of CH_3I at 298 K and Temperature Coefficients
Table 4H-16	Absorption Cross Sections of CH_2I_2 at 298 K
Table 4H-17	Absorption Cross Sections of $\text{C}_2\text{H}_5\text{I}$ at 298 K and Temperature Coefficients
Table 4H-18	Absorption Cross Sections of CH_3CHI_2 at 298 K
Table 4H-19	Absorption Cross Sections of $\text{C}_3\text{H}_7\text{I}$ at 298 K and Temperature Coefficients
Table 4H-20	Absorption Cross Sections of $(\text{CH}_3)_3\text{CI}$ at 298 K
Table 4H-21	Summary of CF_3I Absorption Cross Section Studies
Table 4H-22	Absorption Cross Sections of CF_3I at 298 K
Table 4H-23	Summary of CF_3I Quantum Yield Studies
Table 4H-24	Absorption Cross Sections of CF_2I_2 at 294 K
Table 4H-25	Absorption Cross Sections of $\text{C}_2\text{F}_5\text{I}$ at 323 K
Table 4H-26	Absorption Cross Sections of $n\text{-C}_3\text{F}_7\text{I}$ at 298 K
Table 4H-27	Absorption Cross Sections of CH_2ICl at 298 K and Temperature Coefficients
Table 4H-28	Absorption Cross Sections of CH_2BrI at 298 K and Temperature Coefficients
Table 4H-29	Absorption Cross Sections of $\text{CF}_2\text{BrCF}_2\text{I}$ at 298 K

Section I: SO_x Photochemistry

Table 4I-1	Absorption Cross Sections of SO_3 at 298 K
Table 4I-2	Absorption Cross Sections of H_2S at 298 K
Table 4I-3	Absorption Cross Sections of CS_2 at 298 K
Table 4I-4	Absorption Cross Sections of OCS at 225 and 295 K
Table 4I-5	Absorption Cross Sections of SO_2F_2 at 298 K

Section J: Metal Photochemistry

Table 4J-1	Absorption Cross Sections of NaOH at 298 K
Table 4J-2	Absorption Cross Sections of NaCl at 300 K
Table 4J-3	Absorption Cross Sections of NaO at 200 and 300 K
Table 4J-4	Absorption Cross Sections of NaO_2 at 300 K
Table 4J-5	Absorption Cross Sections of NaO_3 at 300 K
Table 4J-6	Absorption Cross Sections of NaHCO_3 at 200 and 300 K

Figures

Figure 4A-1	$\text{O}(^1\text{D})$ quantum yields in the photolysis of O_3 at $\lambda > 305$ nm
Figure 4C-1	Absorption spectrum of NO_3
Figure 4F-1	Absorption spectrum of ClO
Figure 4F-2	Absorption spectrum of OCIO at 204 K

4.1 Format and Error Estimates

In Table 4-1 we present a list of photochemical reactions considered to be of stratospheric interest. The absorption cross sections of O₂ and O₃ largely determine the extent of penetration of solar radiation into the stratosphere and troposphere. Some comments and references to these cross sections are presented in the text, but only a sample of the data is listed here (See, for example, WMO Report No. 11 [1]; WMO Report No. 16 [10]). The photodissociation of NO in the O₂ Schumann-Runge band spectral range is another important process requiring special treatment and is not discussed in this evaluation (see, for example, Frederick and Hudson [4], Allen and Frederick [2], WMO Report No. 11 [1], and Minschwaner and Siskind [7]).

For some other species having highly structured spectra, such as CS₂ and SO₂, some comments are given in the text, but the photochemical data are not presented. The species CH₂O, NO₂, NO₃, ClO, BrO, and OCIO also have complicated spectra, but in view of their importance for atmospheric chemistry a sample of the data is presented in the evaluation; for more detailed information on their high-resolution spectra and temperature dependence, the reader is referred to the original literature.

Table 4-2 gives recommended reliability factors for some of the more important photochemical reactions. These factors represent the combined uncertainty in cross sections and quantum yields, taking into consideration the atmospherically important wavelength regions, and they refer to the total dissociation rate regardless of product identity. The exception is O(¹D) production from photolysis of O₃; the reliability factor applies to the quantum yield at the indicated wavelengths.

The error estimates are not rigorous numbers resulting from a detailed error propagation analysis of statistical manipulations of the different sets of literature values; they merely represent a consensus among the panel members as to the reliability of the data for atmospheric photodissociation calculations, taking into account the difficulty of the measurements, the agreement among the results reported by various groups, etc.

The absorption cross sections are defined by the following expression of Beer's Law:

$$I = I_0 \exp(-\sigma n l),$$

where I₀ and I are the incident and transmitted light intensity, respectively, σ is the absorption cross section in cm² molecule⁻¹, n is the concentration in molecule cm⁻³, and l is the pathlength in cm. The cross sections are room temperature values at the specific wavelengths listed in the table, and the expected photodissociation quantum yields are unity, unless otherwise stated.

4.2 Halocarbon Absorption Cross Sections and Quantum Yields

The primary process in the photodissociation of chlorinated hydrocarbons is well established: absorption of ultraviolet radiation in the lowest frequency band is interpreted as an n-σ* transition involving excitation to a repulsive electronic state (anti-bonding in C-Cl), which dissociates by breaking the carbon-chlorine bond (Majer and Simons [6]). As expected, chlorofluoromethanes, which are a particular type of chlorinated hydrocarbons, behave in this fashion (Sandorfy [8]). Hence, the quantum yield for photodissociation is expected to be unity for these compounds. There are several studies that show specifically that this is the case for CF₂Cl₂, CFCl₃, and CCl₄. These studies, which were reviewed in CODATA [3], also indicate that at shorter wavelengths, two halogen atoms can be released simultaneously in the primary process.

4.3 Web Access to Recommended Data in Text and Graphical Formats

The tables of recommended cross sections from this evaluation can be downloaded from the spectral atlas of the Max-Planck Institute for Chemistry at: <http://www.atmosphere.mpg.de/spectral-atlas-mainz>

Table 4-1. Photochemical Reactions

O_x Photochemistry			D29. HC(O)OCH ₃ + hv → products
A1.	O ₂ + hv → O + O	R	D30. HC(O)OC ₂ H ₅ + hv → products
A2.	O ₃ + hv → O ₂ + O	R	D31. HCN + hv → products
	O ₃ + hv → O ₂ + O(¹ D)		D32. CH ₃ CN + hv → products
HO_x Photochemistry			FO_x Photochemistry
B1.	HO ₂ + hv → products	R	E1. HF + hv → H + F
B2.	H ₂ O + hv → H + OH		E2. FO ₂ + hv → products
B3.	H ₂ O ₂ + hv → OH + OH		E3. F ₂ O + hv → products
NO_x Photochemistry			E4. F ₂ O ₂ + hv → products
C1.	NO ₂ + hv → NO + O		E5. FNO + hv → F+ NO
C2.	NO ₃ + hv → NO ₂ + O		E6. CF ₄ + hv → products
	NO ₃ + hv → NO + O ₂		E7. C ₂ F ₆ + hv → products
C3.	N ₂ O + hv → N ₂ + O(¹ D)		E8. c-C₄F₈ + hv → products
C4.	N ₂ O ₄ + hv → products		E9. C₅F₁₂ + hv → products
C5.	N ₂ O ₅ + hv → products		E10. C₆F₁₄ + hv → products
	NH ₃ + hv → NH ₂ + H (1)		E11 (CF₃)₂c-C₄F₆ + hv → products
C6.	HONO + hv → OH + NO		E12. CF ₂ O + hv → products
C7.	HNO ₃ + hv → OH + NO ₂	E13. COHF + hv → products	E14. CF₃O₂ + hv → products
C8.	HO ₂ NO ₂ + hv → products	E15. CF ₃ OH + hv → products	E16. CF ₃ OOCF ₃ + hv → products
Organic Photochemistry			E17. CF ₃ OCF ₃ + hv → products
	CO + hv → C + O (1)		E18. CF ₃ CHO + hv → products
	CO ₂ + hv → CO + O (1)		E19. CF ₃ C(O)F + hv → products
	CH ₄ + hv → products (2)		E20. CF ₃ C(O)Cl + hv → products
D1.	CH ₂ O + hv → products	R	E21. CF₃OONO₂ + hv → products
D2.	CH ₃ CHO + hv → products		E22. CF ₃ C(O)O ₂ NO ₂ + hv → products
D3.	C ₂ H ₅ CHO hv → products		E23. CF ₃ CH ₂ CHO + hv → products
D4.	CH ₃ O ₂ + hv → products		E24. CF ₃ C(O)OH + hv → products
D5.	C ₂ H ₅ O ₂ + hv → products		E25. CH ₃ C(O)F + hv → products
D6. CH₃CO + hv → products			E26. CH ₂ =CHCF ₃ + hv → products
D7.	CH ₃ C(O)O ₂ + hv → products		E27. CH ₂ =CFCF ₃ + hv → products
D8. CH₃C(O)CH₂O₂ + hv → products			E28. CF ₂ =CF ₂ + hv → products
D9.	CH ₃ OOH + hv → products	R	E29. CF ₂ =CFCF ₃ + hv → products
D10.	HOCH ₂ OOH + hv → products	R	ClO_x Photochemistry
D11. CH₃ONO + hv → products			F1. Cl ₂ + hv → Cl + Cl
D12. CH₃ONO₂ + hv → products			F2. ClO + hv → Cl + O
D13. CH₃O₂NO₂ + hv → products			F3. ClOO + hv → products
D14.	CH ₃ C(O)O ₂ NO ₂ + hv → products		F4. OClO + hv → O + ClO
D15.	C ₂ H ₅ C(O)O ₂ NO ₂ + hv → products		F5. ClO ₃ + hv → products
D16.	CH ₂ =CHCHO + hv → products		F6. Cl ₂ O + hv → products
D17.	CH ₂ C(CH ₃)CHO + hv → products		F7. ClOOCl + hv → products
D18.	CH ₃ C(O)CH=CH ₂ + hv → products		F8. ClClO ₂ + hv → products
D19.	HOCH ₂ CHO + hv → products	R	F9. Cl ₂ O ₃ + hv → products
D20.	CH ₃ C(O)CH ₃ + hv → products		F10. Cl ₂ O ₄ + hv → products
D21.	CH ₃ C(O)CH ₂ OH + hv → products	R	F11. Cl ₂ O ₆ + hv → products
D22.	CHOCHO + hv → products	R	F12. Cl ₂ O ₇ + hv → products
D23.	CH ₃ C(O)C(O)H + hv → products		F13. HCl + hv → H + Cl
D24.	HC(O)OH + hv → products		DCl + hv → products
	(HC(O)OH) ₂ + hv → products		F14. HOCl + hv → products
D25.	CH ₃ C(O)OH + hv → products		F15. ClNO + hv → Cl + NO
D26.	CH ₃ C(O)OOH + hv → products		F16. ClNO ₂ + hv → products
D27.	C ₂ H ₅ C(O)OH + hv → products		
D28.	CH ₃ C(O)C(O)OH + hv → products		

F17. $\text{ClONO} + h\nu \rightarrow \text{products}$
 F18. $\text{ClONO}_2 + h\nu \rightarrow \text{products}$
 F19. $\text{CCl}_4 + h\nu \rightarrow \text{products}$
 F20. $\text{CH}_3\text{OCl} + h\nu \rightarrow \text{products}$
 F21. $\text{CHCl}_3 + h\nu \rightarrow \text{products}$
 F22. $\text{CH}_2\text{Cl}_2 + h\nu \rightarrow \text{products}$
 F23. $\text{CH}_3\text{Cl} + h\nu \rightarrow \text{products}$
 F24. $\text{CH}_3\text{CCl}_3 + h\nu \rightarrow \text{products}$
 F25. $\text{CH}_3\text{CH}_2\text{Cl} + h\nu \rightarrow \text{products}$
 F26. $\text{CH}_3\text{CHClCH}_3 + h\nu \rightarrow \text{products}$
 F27. $\text{CH}_2\text{ClCH}_2\text{Cl} + h\nu \rightarrow \text{products}$
 F28. $\text{CH}_2\text{ClCH}_2\text{CH}_2\text{Cl} + h\nu \rightarrow \text{products}$
 F29. $\text{CH}_2\text{Cl}(\text{CH}_2)_2\text{CH}_2\text{Cl} + h\nu \rightarrow \text{products}$
 F30. $\text{CCl}_2\text{O} + h\nu \rightarrow \text{products}$
 F31. $\text{COHCl} + h\nu \rightarrow \text{products}$
 F32. $\text{CClFO} + h\nu \rightarrow \text{products}$
 F33. CFCl_3 (CFC-11) + $h\nu \rightarrow \text{products}$
 F34. CF_2Cl_2 (CFC-12) + $h\nu \rightarrow \text{products}$
 F35. CF_3Cl (CFC-13) + $h\nu \rightarrow \text{products}$
 F36. $\text{CF}_2\text{ClCFCl}_2$ (CFC-113) + $h\nu \rightarrow \text{products}$
 F37. $\text{CF}_2\text{ClCF}_2\text{Cl}$ (CFC-114) + $h\nu \rightarrow \text{products}$
 F38. $\text{CF}_3\text{CF}_2\text{Cl}$ (CFC-115) + $h\nu \rightarrow \text{products}$
 F39. CHFCl_2 (HCFC-21) + $h\nu \rightarrow \text{products}$
 F40. CHF_2Cl (HCFC-22) + $h\nu \rightarrow \text{products}$
 F41. CH_2FCl (HCFC-31) + $h\nu \rightarrow \text{products}$
 F42. CF_3CHCl_2 (HCFC-123) + $h\nu \rightarrow \text{products}$
 F43. CF_3CHFCl (HCFC-124) + $h\nu \rightarrow \text{products}$
 F44. $\text{CF}_3\text{CH}_2\text{Cl}$ (HCFC-133) + $h\nu \rightarrow \text{products}$
 F45. CH_3CFCl_2 (HCFC-141b) + $h\nu \rightarrow \text{products}$
 F46. $\text{CH}_3\text{CF}_2\text{Cl}$ (HCFC-142b) + $h\nu \rightarrow \text{products}$
 F47. $\text{CH}_2\text{ClCHO} + h\nu \rightarrow \text{products}$
 F48. $\text{CHCl}_2\text{CHO} + h\nu \rightarrow \text{products}$
 F49. $\text{CF}_2\text{ClCHO} + h\nu \rightarrow \text{products}$
 F50. $\text{CFCl}_2\text{CHO} + h\nu \rightarrow \text{products}$
 F51. $\text{CCl}_3\text{CHO} + h\nu \rightarrow \text{products}$
 F52. $\text{CH}_3\text{C}(\text{O})\text{Cl} + h\nu \rightarrow \text{products}$
 F53. $\text{CH}_2\text{ClC}(\text{O})\text{Cl} + h\nu \rightarrow \text{products}$
 F54. $\text{CHCl}_2\text{C}(\text{O})\text{Cl} + h\nu \rightarrow \text{products}$
 F55. $\text{CCl}_3\text{C}(\text{O})\text{Cl} + h\nu \rightarrow \text{products}$
 F56. $\text{CF}_3\text{CF}_2\text{CHCl}_2$ (HCFC-225ca) + $h\nu \rightarrow \text{products}$
 F57. $\text{CF}_2\text{ClCF}_2\text{CHFCl}$ (HCFC-225cb) + $h\nu \rightarrow \text{products}$
 F58. $\text{CH}_3\text{C}(\text{O})\text{CH}_2\text{Cl} + h\nu \rightarrow \text{products}$

BrO_x Photochemistry

G1. $\text{Br}_2 + h\nu \rightarrow \text{products}$
 G2. $\text{HBr} + h\nu \rightarrow \text{products}$
 G3. $\text{BrO} + h\nu \rightarrow \text{products}$
 G4. $\text{OBrO} + h\nu \rightarrow \text{products}$
 G5. $\text{Br}_2\text{O} + h\nu \rightarrow \text{products}$
 G6. $\text{HOBr} + h\nu \rightarrow \text{products}$
 G7. $\text{BrNO} + h\nu \rightarrow \text{products}$
 G8. $\text{BrONO} + h\nu \rightarrow \text{products}$
G9. $\text{BrNO}_2 + h\nu \rightarrow \text{products}$
 G10. $\text{BrONO}_2 + h\nu \rightarrow \text{products}$

G11. $\text{BrCl} + h\nu \rightarrow \text{Br} + \text{Cl}$
 G12. $\text{BrOCl} + h\nu \rightarrow \text{products}$
 G13. $\text{CH}_3\text{Br} + h\nu \rightarrow \text{products}$
 G14. $\text{CH}_2\text{Br}_2 + h\nu \rightarrow \text{Products}$
 G15. $\text{CHBr}_3 + h\nu \rightarrow \text{Products}$
 G16. $\text{CH}_2\text{BrCH}_2\text{Br} + h\nu \rightarrow \text{Products}$
 G17. $\text{C}_2\text{H}_5\text{Br} + h\nu \rightarrow \text{Products}$
 G18. $\text{COBr}_2 + h\nu \rightarrow \text{products}$
 G19. $\text{COHBr} + h\nu \rightarrow \text{products}$
 G20. CH_2ClBr (Halon-1011) + $h\nu \rightarrow \text{Products}$
 G21. CHClBr_2 (Halon-1012) + $h\nu \rightarrow \text{Products}$
 G22. CHCl_2Br (Halon-1021) + $h\nu \rightarrow \text{Products}$
 G23. CCl_3Br (Halon-1031) + $h\nu \rightarrow \text{Products}$
 G24. CHF_2Br (Halon-1201) + $h\nu \rightarrow \text{Products}$
 G25. CF_2Br_2 (Halon-1202) + $h\nu \rightarrow \text{Products}$
 G26. CF_2ClBr (Halon-1211) + $h\nu \rightarrow \text{Products}$
 G27. CF_3Br (Halon-1301) + $h\nu \rightarrow \text{Products}$
 G28. $\text{CH}_2=\text{CHBr} + h\nu \rightarrow \text{Products}$
 G29. $\text{CHBr}=\text{CF}_2 + h\nu \rightarrow \text{Products}$
 G30. $\text{CFBr}=\text{CF}_2 + h\nu \rightarrow \text{Products}$
 G31. $\text{CH}_2=\text{CBrCF}_3 + h\nu \rightarrow \text{Products}$
 G32. $\text{CF}_3\text{CH}_2\text{Br}$ (Halon-2301) + $h\nu \rightarrow \text{Products}$
 G33. CF_3CHClBr (Halon-2311) + $h\nu \rightarrow \text{Products}$
 G34. CF_3CHFBr (Halon-2401) + $h\nu \rightarrow \text{Products}$
 G35. $\text{CF}_2\text{BrCF}_2\text{Br}$ (Halon-2402) + $h\nu \rightarrow \text{Products}$
 G36. $\text{CF}_3\text{CF}_2\text{Br}$ (Halon-2501) + $h\nu \rightarrow \text{Products}$
 G37. $\text{CH}_3\text{CH}_2\text{CH}_2\text{Br} + h\nu \rightarrow \text{Products}$
 G38. $\text{CH}_3\text{CHBrCH}_3 + h\nu \rightarrow \text{Products}$
 G39. $\text{CH}_3\text{C}(\text{O})\text{CH}_2\text{Br} + h\nu \rightarrow \text{products}$

IO_x Photochemistry

H1. $\text{I}_2 + h\nu \rightarrow 2 \text{I}$
 H2. $\text{IO} + h\nu \rightarrow \text{I} + \text{O}(^3\text{P}), \text{O}(^1\text{D})$
 H3. $\text{OIO} + h\nu \rightarrow \text{products}$
 H4. $\text{HI} + h\nu \rightarrow \text{products}$
 H5. $\text{HOI} + h\nu \rightarrow \text{OH} + \text{I}$
 H6. $\text{ICl} + h\nu \rightarrow \text{I} + \text{Cl}$
 H7. $\text{IBr} + h\nu \rightarrow \text{I} + \text{Br}$
 H8. $\text{INO} + h\nu \rightarrow \text{I} + \text{NO}$
 H9. $\text{IONO} + h\nu \rightarrow \text{I} + \text{NO}_2$
 H10. $\text{IONO}_2 + h\nu \rightarrow \text{products}$
 H11. $\text{CH}_3\text{I} + h\nu \rightarrow \text{CH}_3 + \text{I}$
 H12. $\text{CH}_2\text{I}_2 + h\nu \rightarrow \text{CH}_2\text{I} + \text{I}$
 H13. $\text{C}_2\text{H}_5\text{I} + h\nu \rightarrow \text{C}_2\text{H}_5 + \text{I}$
 H14. $\text{CH}_3\text{CHI}_2 + h\nu \rightarrow \text{Products}$
 H15. $\text{CH}_3\text{CH}_2\text{CH}_2\text{I} + h\nu \rightarrow \text{Products}$
 H16. $\text{CH}_3\text{CHICH}_3 + h\nu \rightarrow \text{Products}$
 H17. $\text{n-C}_4\text{H}_9\text{I} + h\nu \rightarrow \text{C}_4\text{H}_9 + \text{I}$
 H18. $(\text{CH}_3)_2\text{CHCH}_2\text{I} + h\nu \rightarrow (\text{CH}_3)_2\text{CCH}_2 + \text{I}$
 H19. $(\text{CH}_3)_3\text{CI} + h\nu \rightarrow (\text{CH}_3)_3\text{C} + \text{I}$
 H20. $\text{n-C}_5\text{H}_{11}\text{I} + h\nu \rightarrow \text{C}_5\text{H}_{11} + \text{I}$
 H21. $\text{CF}_3\text{I} + h\nu \rightarrow \text{CF}_3 + \text{I}$
 H22. $\text{CF}_2\text{I}_2 + h\nu \rightarrow \text{products}$

R

H23. $\text{C}_2\text{F}_5\text{I} + \text{h}\nu \rightarrow \text{C}_2\text{F}_5 + \text{I}$
H24. $\text{n-C}_3\text{F}_7\text{I} + \text{h}\nu \rightarrow \text{C}_3\text{F}_7 + \text{I}$
H25. $\text{n-C}_4\text{F}_9\text{I} + \text{h}\nu \rightarrow \text{C}_4\text{F}_9 + \text{I}$
H26. $\text{n-C}_6\text{F}_{13}\text{I} + \text{h}\nu \rightarrow \text{C}_6\text{F}_{13} + \text{I}$
H27. $\text{CH}_2\text{ICl} + \text{h}\nu \rightarrow \text{CH}_2\text{Cl} + \text{I}$
H28. $\text{CH}_2\text{BrI} + \text{h}\nu \rightarrow \text{products}$
H29. $\text{CF}_2\text{BrCF}_2\text{I} + \text{h}\nu \rightarrow \text{products}$

SO_x Photochemistry

I1. $\text{SO}_2 + \text{h}\nu \rightarrow \text{SO} + \text{O}$
I2. $\text{SO}_3 + \text{h}\nu \rightarrow \text{SO}_2 + \text{O}$
I3. $\text{H}_2\text{S} + \text{h}\nu \rightarrow \text{HS} + \text{H}$
I4. $\text{H}_2\text{SO}_4 + \text{h}\nu \rightarrow \text{products}$
I5. $\text{CS}_2 + \text{h}\nu \rightarrow \text{CS} + \text{S}$ R

I6. $\text{OCS} + \text{h}\nu \rightarrow \text{CO} + \text{S}$ R
I7. $\text{SF}_6 + \text{h}\nu \rightarrow \text{products}$
I8. $\text{SF}_5\text{CF}_3 + \text{h}\nu \rightarrow \text{products}$
I9. $\text{SO}_2\text{F}_2 + \text{h}\nu \rightarrow \text{products}$

Metal Photochemistry

J1. $\text{NaOH} + \text{h}\nu \rightarrow \text{Na} + \text{OH}$ R
J2. $\text{NaCl} + \text{h}\nu \rightarrow \text{Na} + \text{Cl}$
J3. $\text{NaO} + \text{h}\nu \rightarrow \text{Na} + \text{O}$
J4. $\text{NaO}_2 + \text{h}\nu \rightarrow \text{NaO} + \text{O}$
J5. $\text{NaO}_3 + \text{h}\nu \rightarrow \text{NaO}_2 + \text{O}$
J6. $\text{NaHCO}_3 + \text{h}\nu \rightarrow \text{Na} + \text{HCO}_3$

-
- (1) Hudson and Kieffer [5].
 - (2) Turco [9].
 - (3) “R” indicates that the recommendation has been revised.
 - (4) **Bold indicates a new entry**
 - (5) Shading indicates that the note has been revised.

Table 4-2. Combined Uncertainties for Cross Sections and Quantum Yields

Species	Uncertainty	Notes
O ₂ (Schumann-Runge bands)	1.2	
O ₂ (Continua)	1.2	
O ₃ (Cross Sections Only)	1.1	
O ₃ → O(¹ D), $\lambda > 310$ nm	1.3	
O ₃ → O(¹ D), $290 < \lambda < 310$ nm	1.2	
H ₂ O ₂	1.3	
NO ₂	1.2	
NO ₃	1.5	
N ₂ O	1.2	
N ₂ O ₅	2.0	
HNO ₃	1.3	
HO ₂ NO ₂	2.0	
CH ₂ O	1.4	
CH ₃ OOH	1.5	
CH ₃ C(O)O ₂ NO ₂	1.3	$\lambda < 300$ nm
CH ₃ C(O)O ₂ NO ₂	2.0	$\lambda \geq 300$ nm
HCl	1.1	
HOCl	1.4	
ClOOCl	see note	
Cl ₂ O ₃	1.5	$\lambda < 300$ nm
Cl ₂ O ₃	3.0	$\lambda \geq 300$ nm
ClONO ₂	1.3	
CCl ₄	1.1	
CCl ₃ F	1.1	
CCl ₂ F ₂	1.1	
CH ₃ Cl	1.1	
CF ₂ O	2.0	
CF ₃ Br	1.3	
CF ₂ ClBr	2.0	
CF ₂ Br ₂	2.0	
C ₂ F ₄ Br ₂	2.0	
HOBr	2.0	$\lambda < 350$ nm
HOBr	10	$\lambda \geq 350$ nm
BrONO ₂	1.4	

4.4 References

1. *The Stratosphere 1981: Theory and Measurements*; National Aeronautics and Space Administration, 1982.
2. Allen, M. and J. E. Frederick, 1982, *J. Atmos. Sci.*, **39**, 2066-2075.
3. Baulch, D. L., R. A. Cox, P. J. Crutzen, R. F. Hampson, Jr., J. A. Kerr, J. Troe and R. T. Watson, 1982, *J. Phys. Chem. Ref. Data*, **11**, 327-496.
4. Frederick, J. E. and R. D. Hudson, 1979, *J. Atmos. Sci.*, **36**, 737-745.
5. Hudson, R. D. and L. J. Kieffer. Absorption Cross Sections of Stratospheric Molecules. In *The Natural Stratosphere of 1974*; CIAP, 1975; Vol. Monograph 1; pp (5-156)-(5-194).
6. Majer, J. R. and J. P. Simons. Photochemical Processes in Halogenated Compounds. In *Advances in Photochemistry*; Interscience, 1964; Vol. 2; pp 137-181.
7. Minschwaner, K. and D. E. Siskind, 1993, *J. Geophys. Res.*, **98**, 20401-20412.
8. Sandorfy, C., 1976, *Atmos. Environ.*, **10**, 343-351.
9. Turco, R. P., 1975, *Geophys. Surveys*, **2**, 153-192.
10. WMO *Atmospheric Ozone: 1985*; National Aeronautics and Space Administration: Geneva, Report No. 16, Chapter 7, 1986.

SECTION 4A. O_x PHOTOCHEMISTRY

A1.	$O_2 + h\nu \rightarrow O(^3P) + O(^3P)$	494 kJ mol ⁻¹	242.3 nm	(1)
	$\rightarrow O(^3P) + O(^1D)$	684 kJ mol ⁻¹	175 nm	(2)
	$\rightarrow O(^1D) + O(^1D)$	873 kJ mol ⁻¹	137 nm	(3)
	$\rightarrow O(^3P) + O(^1S)$	906 kJ mol ⁻¹	132 nm	(4)
	$\rightarrow O(^1D) + O(^1S)$	1088 kJ mol ⁻¹	110 nm	(5)

(Recommendation: 10-6, Note: 10-6, Evaluated: 10-6)

Absorption Cross Sections: The photodissociation of molecular oxygen in the stratosphere is due primarily to absorption of solar radiation in the 200 – 240 nm wavelength region, i.e., within the Herzberg continuum, which arises from the $A^3\Sigma_u^+ \leftarrow X^3\Sigma_g^-$ transition. Between 240 and 300 nm the absorption spectrum is also due to the electronic transition from the ground $X^3\Sigma_g^-$ state to excited electronic states $A^3\Sigma_u^+ \leftarrow X^3\Sigma_g^-$ (Herzberg I), $c^1\Sigma_u^- \leftarrow X^3\Sigma_g^-$ (Herzberg II), and $A'^3\Delta_u \leftarrow X^3\Sigma_g^-$ (Herzberg III). The 175 – 205 nm region, the O₂ Schumann-Runge ($B^3\Sigma_g^- \leftarrow X^3\Sigma_g^-$) band spectral range, is also very important, since solar radiation penetrates efficiently into the stratosphere at these wavelengths. The Schumann-Runge band system is composed of hundreds of rotational lines with widths on the order of 1 cm⁻¹. The peak absorption cross sections in the Schumann-Runge system span ~5 orders of magnitude between 175 and 205 nm.

Table 4A-1. Summary of O₂ Absorption Cross Section Studies

Study	Year	Molecule ^a	Wavelength (nm)	Resolution (nm)	Temperature (K)
Preston [128]	1940	O ₂	121.567	0.01	298
Clark [46]	1952	O ₂	8 – 103	0.01	295
Watanabe et al. [158]	1952	O ₂	121.57	0.085	298
Weissler and Lee [161]	1952	O ₂	30 – 131	0.01	295
Watanabe et al. [159]	1953	O ₂	105 – 190	0.085	298
Aboud et al. [1]	1955	O ₂	11 – 87	0.1	295
Lee [89]	1955	O ₂	20 – 110	0.01	295
Wainfan et al. [156]	1955	O ₂	47 – 99	0.5	295
Watanabe and Marmo [160]	1956	O ₂	85 – 110 140 – 146	0.01	298
Tanaka et al. [147]	1959	O ₂	140 – 149	0.01	298
Ditchburn and Young [56]	1962	O ₂	185 – 250	0.01	298
Cook and Metzger [49]	1964	O ₂	60 – 103	0.05	295
Cook et al. [48]	1964	O ₂	83 – 103	0.05	295
Metzger and Cook [105]	1964	O ₂	110 – 167	0.05	298
Huffman et al. [76]	1964	O ₂	60 – 164	0.05	295
Samson and Cairns [129]	1964	O ₂	30 – 104	0.01	298
Samson and Cairns [130]	1965	O ₂	20 – 54	0.01	298
Goldstein and Mastrup [64]	1966	O ₂	127 – 175	0.04	298
Blake et al. [25]	1966	O ₂	125 – 235	0.02	298
Hudson et al. [72]	1966	O ₂	159 – 195	0.0075	300, 600, 900
Matsunaga and Watanabe [101]	1967	O ₂	58 – 108	0.03	298
Ogawa [118]	1968	O ₂	121.6	0.009	298
Huffman [75]	1969	O ₂	30 – 122	Review ^b	295
Ackerman et al. [4]	1969	O ₂	176 – 191	0.001	300
Shardanand [132]	1969	O ₂	200 – 280	0.25	298
Ackerman et al. [3]	1970	O ₂	176 – 201	0.001	300
Ackerman [2]	1971	O ₂	116 – 244	Review ^b	298
Bennett et al. [23]	1971	O ₂	58.4	0.1	295
Hasson and Nichols [68]	1971	O ₂	192 – 243	0.07	298
Ogawa [119]	1971	O ₂	181 – 235	0.0075	298
Hudson and Mahle [73]	1972	O ₂	176 – 210	0.1	150, 200, 250, 300
Starr and Loewenstein [138]	1972	O ₂	58.4	0.07	298

Brolley et al. [36]	1973	O ₂	58.4	0.1	298
Ogawa and Ogawa [121]	1975	O ₂ O ₂ (a ¹ Δ _g) ^c	108 – 160 108 – 152	0.014	298
Bertrand et al. [24]	1975	O ₂	123.6, 147	0.1	298
Kockarts [85]	1976	O ₂	176 – 203	J-calc-SR ^d	160 – 300
Shardanand and Prasad Rao [133]	1977	O ₂	200 – 250	0.25	300
Cole and Dexter [47]	1978	O ₂	5 – 34	0.02	298
Brion et al. [29]	1979	O ₂	4 – 248 (e,e)	0.2	298
Frederick and Mentall [60]	1982	O ₂	176 – 243	0.12	200, 250, 300
Herman and Mentall [70]	1982	O ₂	187 – 225	0.12	not stated
Anderson and Hall [10]	1983	O ₂	191 – 207	0.012	
Gibson et al. [63]	1983	O ₂	140 – 174	0.01	295, 575
Lewis et al. [94]	1983	O ₂	121.4 – 121.9	0.01	84, 203, 288, 366
Yoshino et al. [176]	1983	O ₂	179.3 – 201.5	0.0013	300
Cheung et al. [42]	1984	O ₂	193.5 – 204	0.0013	299
Cheung et al. [43]	1984	O ₂	193.5 – 204	0.0013	300
Pirre et al. [126]	1984	O ₂	202 – 220	0.01	not stated
Johnston et al. [82]	1984	O ₂	205 – 225	0.2	206 – 327
Yoshino et al. [175]	1984	O ₂	175 – 205	SR Atlas ^e	300
Kley [84]	1984	O ₂	121.567	0.01	208 – 305
Cheung et al. [44]	1986	O ₂	195 – 241	0.0013	298
Anderson and Hall [11]	1986	O ₂	191 – 215	0.012	not stated
Jenouvrier et al. [80]	1986	O ₂	205 – 240	0.05	298
Jenouvrier et al. [81]	1986	O ₂	205 – 240	0.04	294
Lewis et al. [92]	1986	¹⁶ O ¹⁶ O	175 – 205	0.004	295
Lewis et al. [93]	1986	¹⁶ O ¹⁶ O	175 – 205	0.004	295
Nicolet and Kennes [113]	1986	O ₂	200 – 244	J-calc-HC ^f	298
Saxon and Slinger [131]	1986	O ₂	195 – 300	σ-calc-HC ^g	298
Yoshino et al. [173]	1987	O ₂	179 – 198	0.0013	79
Wang et al. [157]	1987	O ₂	130 – 160	0.01	295, 575
Yoshino et al. [164]	1988	O ₂	205 – 240	recommended	298
Yoshino et al. [171]	1988	¹⁸ O ¹⁸ O	183 – 196	0.0013	79
Murtagh [109]	1988	O ₂	175 – 206	J-cal-SR ^d	150 – 300
Pirre et al. [127]	1988	O ₂	200 – 217	0.01	not stated
Nicolet and Kennes [114]	1988	O ₂	202 – 242	J-calc-HC ^f	not stated
Cheung et al. [41]	1989	¹⁶ O ¹⁸ O	175 – 205	0.0013	78, 300
Yoshino et al. [172]	1989	¹⁶ O ¹⁸ O	180 – 196	0.0013	79
Nicolet and Kennes [115]	1989	O ₂	175 – 202	σ-cal-HC ^g	190 – 300
Cheung et al. [40]	1990	O ₂	179 – 202	0.0013	79, 295
Chiu et al. [45]	1990	¹⁸ O ¹⁸ O, ¹⁶ O ¹⁸ O	180 – 196	0.0013	79
Coquart et al. [50]	1990	O ₂	196 – 205	0.065	219
Greenblatt et al. [65]	1990	O ₂	330 – 1130	0.6	196, 296
Yoshino et al. [166]	1990	O ₂	184 – 204	0.0013	295
Yoshino et al. [165]	1992	O ₂	179 – 240	0.0013	300
Minschwaner et al. [106]	1992	O ₂	175 – 205	σ-calc-SR ^h	130 – 500
Minschwaner et al. [107]	1993	O ₂	175 – 205	σ-calc-SR ^h	205 – 300
Yoshino et al. [178]	1994	O ₂	240 – 270	0.06 cm ⁻¹	295
Huestis et al. [74]	1994	O ₂	243 – 258	0.25 cm ⁻¹	295
Yoshino et al. [168]	1995	O ₂	240 – 270	0.06 cm ⁻¹	295
Bao et al. [19]	1995	O ₂	248 – 249	0.4 cm ⁻¹	298
Oshima et al. [124]	1995	O ₂	230 – 280	0.2	310
Slinger et al. [136]	1996	O ₂	242.1 – 244.2	0.2 cm ⁻¹	298
Ahmed et al. [7]	1996	O ₂	130, 165	0.05	295, 373, 473, 573
Amoruso et al. [9]	1996	O ₂	208 – 240	0.001	280

Vattulainen et al. [151]	1997	O ₂	195 – 260	0.5	293, 873, 1073
Kanik et al. [83]	1997	O ₂	120, 149, 174	0.03	295, 373, 473, 573
Yoshino et al. [177]	1998	O ₂	240 – 270	0.06 cm ⁻¹	295
Yoshino et al. [169]	1999	O ₂	240 – 275	0.06 cm ⁻¹	295
Fally et al. [59]	2000	O ₂	240 – 294	2 cm ⁻¹	288
Yoshino et al. [170]	2000	O ₂	240 – 275	0.06 cm ⁻¹	295
Bogumil et al. [27]	2003	O ₂	234 – 440 650 – 800	0.24 0.48	203, 243, 293
Wu et al. [163]	2005	O ₂	83, 92, 108	0.0008	295, 535
Yoshino et al. [179]	2005	O ₂	130 – 173	0.066	78, 90, 295

^a Entries labeled “O₂” refer to molecular oxygen with natural isotopic abundance; studies of specific isotopes are labeled accordingly

^b Review: a status report on absorption cross section measurements

^c Refers to the low lying metastable state of O₂

^d J-calc-SR: a calculation of O₂ photodissociation coefficients in the Schumann-Runge bands

^e SR Atlas: a detailed compendium of line assignments of the Schumann-Runge bands

^f J-calc-HC: a calculation of O₂ photodissociation coefficients in the Herzberg Continuum

^g σ-calc-HC: a calculation of absorption cross sections in the Herzberg Continuum

^h σ-calc-SR: a calculation of absorption cross sections of the Schumann-Runge bands

Measurements of the absorption cross sections in the VUV have mainly been reported at low resolution during the period from 1952 to 1979 as listed in Table 4A-1. High resolution cross sections have been reported by Cole and Dexter [47], Brion et al. [29], Gibson et al. [63], Ahmed et al. [7], Wu et al. [163], and Yoshino et al. [179].

At Lyman-α (121.567 nm), absorption cross section measurements were reported (in cm² molecule⁻¹) by Preston [128] (1.17 x 10⁻²⁰), Watanabe et al. [158] (1.23 x 10⁻²⁰), Ogawa [118] (1.03 x 10⁻²⁰), Kley [84] (1.13 x 10⁻²⁰), and Lewis et al. [94] (9.1 x 10⁻²¹). The latter authors measured the temperature dependence in the range 84 – 366 K. A value of (1.1 ± 0.1) x 10⁻²⁰ cm² molecule⁻¹ is recommended. Kley [84] measured the pressure dependence of the Lyman-α cross section in the pressure range 20 – 880 Torr and in the temperature range 208 – 305 K. The cross sections were parameterized by the following equation: σ_{O₂} = (1.13 ± 0.09) x 10⁻²⁰ + (1.72 ± 0.21) x 10⁻²³ x P where P is the pressure in Torr.

In the Herzberg continuum (200 – 240 nm) Frederick and Mentall [60], Herman and Mentall [70], Anderson and Hall [10, 11], and Pirre et al. [126, 127] estimated O₂ absorption cross sections from balloon measurements of solar irradiance in the stratosphere. These authors found the cross sections in the 200 – 210 nm range to be ~35% smaller than the smallest of the older laboratory results, which are those of Ditchburn and Young [56], Hasson and Nichols [68], Ogawa [119], Shardanand [132], and Shardanand and Prasad Rao [133]. The more recent laboratory studies (Johnston et al. [82], Cheung et al. [42-44], and Jenouvrier et al. [80, 81]) confirm the lower values obtained from solar irradiance measurements. The recommended absorption cross section values between 205 and 240 nm are based on the data of Cheung et al. [44] and Jenouvrier et al. [81] and were evaluated by Yoshino et al. [164] as listed in Table 4A-2. The recommended values from 241-245 nm are from Fally et al. [59] (see below). Amoruso et al. [9] have also carried out cross section measurements in the wavelength range 208 – 240 nm of the Herzberg continuum; their values are ~15% lower than those reported by Yoshino et al. [164]. Coquart et al. [50] have reported Herzberg continuum absorption cross sections at 219 K in the wavelength region 196 – 205 nm of the S-R bands, in agreement with the determinations of Cheung et al. [43, 44] and Ogawa [119] and in line with the data of Yoshino et al. [164]. Calculations of the absorption continua in the range 195 – 300 nm were performed by Saxon and Slinger [131]. Cross sections at elevated temperatures (up to 1073 K) and pressures (up to 6 bar) were reported by Vattulainen et al. [151].

Table 4A-2. Absorption Cross Sections of O₂ between 205 and 245 nm

λ (nm)	$10^{24} \sigma$ (cm ²)	λ (nm)	$10^{24} \sigma$ (cm ²)
205	7.35	226	3.21
206	7.13	227	2.98
207	7.05	228	2.77
208	6.86	229	2.63
209	6.68	230	2.43
210	6.51	231	2.25
211	6.24	232	2.10
212	6.05	233	1.94
213	5.89	234	1.78
214	5.72	235	1.63
215	5.59	236	1.48
216	5.35	237	1.34
217	5.13	238	1.22
218	4.88	239	1.10
219	4.64	240	1.01
220	4.46	241	0.88
221	4.26	242	0.81
222	4.09	243	0.39
223	3.89	244	0.13
224	3.67	245	0.05
225	3.45		

Note:

205 – 240 nm: Yoshino et al. [164]

241 – 245 nm: Fally et al. [59]

The studies of the penetration of solar radiation in the atmosphere in the Schumann-Runge wavelength region were based originally on laboratory cross sections measured using insufficient spectral resolution. Yoshino et al. [176] reported high resolution O₂ cross section measurements and band oscillator strengths of the (1,0)-(12,0) S-R bands in the wavelength range 179 – 202 nm at 300 K, obtaining the first set of results that were not limited by the instrument lineshape. Additional studies at other temperatures, wavelengths, and isotopic compositions have been carried out by Yoshino et al. [166, 171-173, 175], Lewis et al. [92, 93], Cheung et al. [40, 41], and Chiu et al. [45]. More recently, Yoshino et al. [165] reported cross sections of the S-R bands in the window region between the rotational lines for wavelengths between 180 and 195 nm; these measurements supersede the their earlier values reported in Yoshino et al. [176].

Absorption cross sections of the S-R continuum (130 – 175 nm) at room temperature were measured by Watanabe et al. [159], Metzger and Cook [105], and Ogawa and Ogawa [121]. Measurements of the temperature dependence were reported by Gibson et al. [63], Hudson et al. [72], Wang et al. [157], Kanik et al. [83] and Yoshino et al. [179].

Minschwaner et al. [106] have fit temperature dependent (130<T<500 K) O₂ cross sections between 175 and 204 nm with polynomial expressions, providing an accurate model of the Schumann-Runge band cross sections that incorporates the most recent laboratory data. Detailed photodissociation rates for the Herzberg continuum $\lambda > 200$ nm were calculated by Nicolet and Kennes [113]. A parameterization in the Herzberg continuum was reported by Nicolet and Kennes [114].

For parameterizations of the O₂ absorption in the Schumann-Runge bands used in atmospheric modeling calculations see Kockarts [85] and the review in WMO Report No. 16 [162]. More recent work by Murtagh [109], Nicolet and Kennes, [115], and Minschwaner et al. [106] incorporates results of the later laboratory measurements into efficient schemes for computing broadband transmission and photolysis rates. Transmission values obtained by Murtagh [109] agree well with the WMO [162] recommendations, although the high resolution calculations of Minschwaner et al. [107] differ with the WMO values by as much as 10–20% at some wavelengths.

Absorption cross section measurements in the region 240 – 300 nm were performed by Fally et al. [59]. The different components of the spectrum, namely the discrete bands of the three Herzberg systems I, II, III (A, c, A' ← X), the Herzberg continuum, and the collision-induced Wulf bands were reported separately. The Herzberg continuum cross sections at 240 nm are in good agreement with the values reported by Yoshino et al. [164] and Jenouvrier et al. [81]. The absorption cross sections measured by Fally et al. [59] in the range 241 – 245 nm are entered in Table 4A-2. The absorption cross sections reported by Bogumil et al. [27] are roughly five times larger (at 241 nm) than those reported by Fally et al. [59]. High resolution studies were performed by Yoshino et al. [168, 177, 178], Huestis et al. [74], Bao et al. [19], and Slinger et al. [136] in the 242 to 248 nm range, where weak absorptions cross sections were reported for some vibrational bands in the Herzberg systems.

Photolysis Quantum yields and Product studies: The overall quantum yield for channel (1), $O(^3P) + O(^3P)$, is unity, $\Phi(1) = 1$, for $175 < \lambda < 242$ nm. Above the threshold for channel (2), $O(^3P) + O(^1D)$, at 175 nm, the formation of $O(^1D)$ is possible. Lee et al. [88] and Nee and Lee [111] determined the quantum yield of $O(^1D)$ to be unity, thus $\Phi(2) = 1$, in the wavelength range 139 – 175 nm. At 157 nm, both product channels (1) and (2) have been observed by Lin et al. [95], with a relative yield for channel (1) of 0.55 ± 0.05 . At wavelengths shorter than 139 nm Lee et al. [88] observed strong variations in $\Phi(O^1D)$, which was confirmed by Nee and Lee [111] (116 – 139 nm), Lee and Nee [90] (113 – 130 nm), and Lee and Nee [91] (105 – 113 nm). Lee et al. [88] reported $\Phi(O^1D) = \Phi(2) = 0.44 \pm 0.05$ at the Lyman- α line (121.567 nm). Lacoursière et al. [86] determined the $O(^1D)$ yield across the entire Lyman- α profile from 121.2 to 121.9 nm at a spectral resolution of 0.0012 nm, and found $\Phi(O^1D)$ to be strongly wavelength dependent in this window. $\Phi(O^1D)$ varied from 1.0 at 121.35 nm through a minimum of 0.48 near 121.62 nm. Strong temperature dependence was found by Lewis et al. [94] with a minimum yield of 0.28 near 121.62 nm at 84 K.

A2.	$O_3 + h\nu \rightarrow O(^3P) + O_2(X^3\Sigma_g^-)$	101 kJ mol ⁻¹	1180 nm	(1)
	$\rightarrow O(^3P) + O_2(a^1\Delta_g)$	195 kJ mol ⁻¹	612 nm	(2)
	$\rightarrow O(^3P) + O_2(b^1\Sigma_g^+)$	258 kJ mol ⁻¹	463 nm	(3)
	$\rightarrow O(^1D) + O_2(X^3\Sigma_g^-)$	291 kJ mol ⁻¹	411 nm	(4)
	$\rightarrow O(^1D) + O_2(a^1\Delta_g)$	386 kJ mol ⁻¹	310 nm	(5)
	$\rightarrow O(^1D) + O_2(b^1\Sigma_g^+)$	448 kJ mol ⁻¹	267 nm	(6)
	$\rightarrow 3 O(^3P)$	595 kJ mol ⁻¹	201 nm	(7)
	$\rightarrow O(^1S) + O_2(a^1\Delta_g)$	610 kJ mol ⁻¹	196 nm	(8)

(Recommendation: 10-6, Note: 10-6, Evaluated: 10-6)

Absorption Cross Sections. The O_3 absorption cross sections in the 200 – 790 nm region can be separated into four systems: the Hartley band (200 – 300 nm), the Huggins bands (300 – 370 nm), the Chappuis band (370 – 790 nm), and the Wulf bands extending towards longer wavelengths. The Hartley band is the strongest band and peaks around 255 nm. Although its overall shape is very smooth, there is residual vibrational structure in the region 250 – 260 nm. The Huggins band consists of a series of individual peaks and is marked with a drastic change of absorption cross sections (over more than five orders of magnitude) and strong temperature dependence. The Chappuis band is composed of a vibrational band progression superimposed on a continuous absorption in the visible region and is about a thousand times weaker than the Hartley band. The very weak near infrared part of the Chappuis band is clearly structured and corresponds to a different electronic transition (called the “Wulf bands”).

Photolysis of ozone in the Hartley system occurs predominantly via the two spin-allowed channels (1) and (5) (Ball et al. [18]) whereas channels (2), (3) and (4) are spin forbidden. Channels (2) and (4) have been identified from photolysis in the Huggins band (Silvente et al. [134] and Denzer et al. [55]).

For the three main bands in the 200 – 790 nm region, there have been many different measurements of the absorption spectrum and cross sections at various experimental (temperature and pressure) and instrumental conditions (resolution) during the last century as given in Table 4A-3. The available measurements can be organized into three groups: (A) measurements of absolute cross sections at single wavelengths (e.g. at the Hg resonance line at 253.65 nm), (B) measurements of absolute cross sections over broad spectral regions (typically covering a few hundred nm), and (C) measurements of relative O_3 absorption spectra over broad spectral regions that have been scaled to absolute spectra using results from other studies (Type A or B).

Table 4A-3. Summary of O₃ Absorption Cross Section Studies

Study	Year	Spectral Range (nm)	Type	Resolution (nm)	Temperature (K)
Ny and Choong [117]	1933	213 – 353	B	0.05	298
Vassy and Vassy [150]	1948	450 – 601	A	not stated	291, 231, 193, 168
Vigroux [152]	1953	230 – 793 245 – 345	B	0.05	291 181 – 393
Inn and Tanaka [77]	1953	200 – 750	B	0.5	290
Tanaka et al. [146]	1953	105 – 220	B	0.5	300
Ogawa and Cook [120]	1958	53 – 131	C	not stated	295
Inn and Tanaka [79]	1959	200 – 350 400 – 750	B	~0.05 0.5	273
Hearn [69]	1961	253.7 – 577.0	A	0.01-0.09	295
DeMore and Raper [54]	1964	210 – 300	B	0.2	77, 273
Vigroux [153]	1967	304 – 341	B	0.05	291
Griggs [66]	1968	200 – 360 450 – 850	B	0.1 0.5	303
Vigroux [154]	1969	230 – 270	B	0.1	291
Simons et al. [135]	1973	300 – 370	B	0.4	195, 300, 333
Astholtz et al. [15]	1982	210 – 320	B	3	300, 500, 720, 900
Davenport [53]	1982	253 – 370	B	not stated	206, 225, 271, 298
McPeters and Bass [104]	1982	300 – 310	C	0.02	229, 245, 295
Daumont et al. [52]	1983	310 – 350	B	0.012	223, 294
Brion et al. [32]	1983	310 – 350	B	0.012	223, 294
Brion et al. [33]	1984	310 – 350	B	0.012	223, 294
Freeman et al. [61]	1984	250 – 350	C*	0.002	195
Bass and Paur [21]	1985	230 – 350	C*	<0.025	200, 298
Paur and Bass [125]	1985	245 – 340	C*	<0.025	203, 218, 228, 243, 273, 298
Freeman et al. [62]	1985	281 – 335	A	0.003	195, 228, 293
Molina and Molina [108]	1986	185 – 350	B	0.07	226, 263, 298
Mauersberger et. al. [102]	1986	253.7	A	not stated	297.5
Mauersberger et. al. [103]	1987	253.7	A	not stated	297.5
Barnes and Mauersberger [20]	1987	237.7	A,C	not stated	195, 221, 237, 253, 273, 297, 318, 335, 351
Yoshino et al. [174]	1988	238.2 – 344.4	A, C*	0.13 – 0.003	195, 228, 295
Malicet et al. [96]	1989	253.36	A	not stated	229, 295
Cacciani et al. [39]	1989	339 – 355	B	0.012	220, 293
Amoruso et al. [8]	1990	590 – 610	B	0.05	230, 299
Daumont et al. [51]	1992	195 – 345	B*	0.01	295
Anderson and Mauersberger [13]	1992	543.5 – 632.8	A	not stated	295
Anderson et al. [12]	1993	750 – 975	A	not stated	295
Brion et al. [31];	1993	195 – 345 300 – 345	B*	0.01	218, 228, 243, 295, 273
Yoshino et al. [167]	1993	185 – 254	A, B	0.13 – 0.003	195, 228, 295
Burkholder and Talukdar [37]	1994	407 – 763	C*	0.2	220, 240, 260, 280, 298
Malicet et al. [97]	1995	195 – 345	C*	0.01	218, 228, 243, 273, 295,
Mason et al. [98]	1996	110 – 172	C*	0.05	298
Brion et al. [30]	1998	345 – 830 515 – 650	B*	0.01	295 218
Burrows et al. [38]	1999	231 – 794	B*	0.2 - 0.4	202, 221, 241, 273, 293
Voigt et al. [155]	2001	230 – 850	C*	5 cm ⁻¹	203, 223, 246, 280,

Study	Year	Spectral Range (nm)	Type	Resolution (nm)	Temperature (K)
					293
Bogumil et al. [26]	2001	230 – 2400	C*	0.17 – 1.44	203, 293
Bogumil et al. [28]	2003	230 – 1070	C*	0.2 – 0.4	203, 223, 243, 273, 293
Enami et al. [58]	2004	759 – 768	A	0.002	214-5, 245, 260, 273, 296-8
El Helou et al. [57]	2005	540 – 1080	A	4 cm ⁻¹	144, 150, 175, 222-5, 291-4

Earlier reviews on the measured absorption cross sections were presented by Inn and Tanaka [78], Ackermann [5], Hudson [71], Nicolet [112], Brion et al., [34], Steinfeld et al. [139], Bacis et al. [16], Matsumi and Kawasaki [100], and the WMO Report No. 16 [162], which was the basis for the JPL-97-4 evaluation. Orphal [122, 123] has recently critically reviewed the available laboratory measurements up to 2003, and the current JPL evaluation is partly based on that review. Relevant for that evaluation are the measurements of type B and C, particularly those studies whose data were digitally available (marked with an asterisk*). Unfortunately, the recommended data set for the JPL-97-4 evaluation of Molina and Molina [108] was not considered in his review.

In the Hartley and Huggins bands (about 240 – 325 nm) there is generally very good agreement (better than 2-3%) between the data measured at room temperature (293 – 300 K) by Bass and Paur [21] and Paur and Bass [125], Molina and Molina [108], Freeman et al. [61], Yoshino et al. [174], the Reims-team (Daumont et al. [51], Brion et al. [31], Malicet et al. [97] and Brion et al. [30]), Yoshino et al. [167], and the Bremen-team (Burrows et al. [38], Voigt et al. [155] and Bogumil et al. [28]). The older data by Ny and Choong [117], Inn and Tanaka [77] and Vigroux [152] are about 8% greater than the data of Molina and Molina [108]. The vibration structure between 240 and 270 nm was observed in most studies, except those of Inn and Tanaka [77], DeMore and Raper [54], Davenport [53], and Astholz et al. [15], who used lower resolution instruments.

At shorter wavelengths, measurements of absorption cross sections in the VUV region were performed by Tanaka et al. [146], Ogawa and Cook [120], and Mason et al. [98]. At the Lyman- α wavelength, 121.567 nm, an absorption cross section of 2.32×10^{-17} cm² molecule⁻¹ was cited in the review by Ackermann [5]. Ogawa and Cook [120] measured 2.28×10^{-17} cm² molecule⁻¹ whereas Mason et al. [98] reported 2.99×10^{-17} cm² molecule⁻¹. The latter more recent value is recommended and entered in Table 4A-4.

A comparison of the O₃ cross-sections at the Hg-line wavelength 253.7 nm was performed by Orphal [122, 123] involving 13 absolute measurements and provided a mean value of $(114.1 \pm 0.9) \times 10^{-19}$ cm² molecule⁻¹. The temperature dependence of the cross sections at 253.7 nm has been measured by Barnes and Mauersberger [20] between 195 and 351 K and by Malicet et al. [96] at 229 and 295 K. It has to be noted that the data of Bass and Paur [21] and Paur and Bass [125] are normalized to the absolute value 114.7×10^{-19} cm² molecule⁻¹ at 253.7 nm and 295 K measured by Hearn [69]. In the range 230 – 260 nm, the data of the Reims-team (Daumont-Brion-Malicet-Brion) are generally lower (up to 2.5%) than the data of Molina and Molina [108], Bass and Paur [21] and the Bremen-team (Burrows-Voigt-Bogumil). Furthermore, the data of Voigt et al. [155] show a strong baseline shift below 255 nm and in the range 310 – 320 nm; in addition, the spectra are very noisy in the Hartley band maximum. The data of Bogumil et al. [26] contain periodic artifacts on the order of 0.5–1.0% in the range 240 – 270 nm and a straylight feature around 305 nm on the order of 2%.

Below 225 nm the room temperature cross sections of Molina and Molina [108], DeMore and Raper [54], and the Reims-team (Daumont-Brion-Malicet) agree within 1-2%, but are 2-5% larger than the measurements of Yoshino et al. [167]. Other reported values measured by Ny and Choong [117], Inn and Tanaka [77], Astholz et al. [15], and Griggs [66] differ up to 15%.

In the Huggins bands (310 – 350 nm) the studies differ in spectral resolution, which is mostly relevant only to atmospheric remote sensing. At wavelengths larger than 310 nm the vibrational structure becomes pronounced. In the range 310 – 340 nm, the agreement between the different studies is rather good (about 2%) for the data of Bass and Paur [21], the Reims-team (Daumont-Brion-Malicet-Brion), and Burrows et al. [38], although important differences (up to 13%) due to wavelength shifts and spectral resolution are reported by Orphal [122, 123]. The data of Bass and Paur [21] and of the Reims-team (Daumont-Brion-Malicet-Brion) show wavelength shift of more than 0.02 nm. The data of Voigt et al. [155] and Bogumil et al. [28] contain systematic baseline drifts. Above 312 nm, the data of Molina and Molina [108], which are listed every 0.5 nm up to 350 nm, occasionally miss the maxima and minima of the peaks. The reported values by Cacciani et al. [39] are typically 5-8% lower than the values of Molina and Molina [108] in the range 339 – 355 nm.

The O₃ absorption cross sections in the 350 – 450 nm region between the Huggins and Chappuis bands are very small and the available measurements of absolute values scatter significantly. They have been measured by Brion et al. [30] and the Bremen team (Burrows-Voigt-Bogumil). At the minimum near 378 nm, the reported absolute cross sections at 298 K vary between 5×10^{-23} cm² molecule⁻¹ from Voigt et al. [155] and 5×10^{-24} cm² molecule⁻¹ from Brion et al. [30].

Absorption cross section measurements of the Chappuis band of O₃ in the wavelength range 450 – 750 nm have been reported by Burkholder and Talukdar [37], Brion et al. [30], the Bremen team (Burrows-Voigt-Bogumil), El Helou et al. [57], and at single wavelengths by Hearn [69], Anderson and Mauersberger [13], Anderson et al. [12], and Enami et al. [58]. At the peak of the Chappuis band near 602 nm, the values agree within a few percent, although the data of the Bremen-team (Burrows-Voigt-Bogumil) are consistently larger than those of Brion et al. [30] (by 2%) and Burkholder and Talukdar [37] (by 4%) (the latter data are scaled using the measurements of Anderson and Mauersberger [13]). Note that there are pronounced deviations of data from Burkholder and Talukdar [37] in the region 425 – 490 nm. The older values of Vassy and Vassy [150], Vigroux [152], Inn and Tanaka [77], Griggs [66], and Amoroso et al. [8] deviate up to 20%.

Absorption cross sections in the Wulf band region (wavelength >750 nm) have been reported by Anderson et al. [12], Burkholder and Talukdar [37], the Bremen-team (Burrows-Voigt-Bogumil), Enami et al. [58] and El Helou et al. [57]. The data measured at room temperature by the latter group are in excellent agreement (within 0.25 %) with those of Anderson et al. [12].

The temperature dependence of the O₃ cross sections has also been studied by several of the groups mentioned above and tabulated in Table 4A-3. In the critical review, Orphal [122, 123] calculated and compared the integrated cross sections for 5 temperatures in the range 203 – 295 K in the different spectral regions of the O₃ spectrum. At all temperatures the agreement of the integrated cross sections in the Hartley band is better than 2% and less good agreement in the Chappuis band (4%). In particular, the integrated cross sections of Burkholder and Talukdar [37] lie systematically below the other measurements by about 3% and the data of Burrows et al. [38] are always higher by 2%. In the Huggins bands and the blue tail of the Chappuis band the integrated cross sections scatter by several percent (up to 5%), indicating systematic differences between the available data. The Hartley band integrated cross sections remain constant in the temperature range 203 – 293 K within the experimental uncertainties. The integrated cross sections in the Huggins bands decrease by more than 30% between 298 K and 203 K and the differential cross sections of the bands increase significantly.

In the Hartley band most studies report a slight (0.9-1.6%) increase of the cross section below 260 nm between room temperature and low temperatures 202 – 298 K, while Yoshino et al. [167] concluded that the temperature effect is negligible. Above 260 nm the cross section decreases significantly at lower temperatures. This effect is due to the changing populations of the various vibrational and rotational quantum states of ozone and has been analyzed by Simons et al. [135]. The cross section values are not linearly proportional to the temperature; instead the effect is larger at the maxima than it is at the minima of the spectral features.

The absorption cross sections in the Huggins bands (310 – 350 nm) of O₃ decrease strongly with decreasing temperatures. Additionally, they depend on instrumental line shape and differences in wavelength calibration so that discrepancies up to 20% at the lowest temperatures are observed between the various studies. Comparison of the spectra obtained in the temperature range 220 – 229 K show good agreement (~3% at 325 nm, ~ 5% at 340 nm) with the data of Bass and Paur [21], Molina and Molina [108], the Brion team (Daumont-Brion-Malicet-Brion), and Burrows et al. [38]. The data of Voigt et al. [155] and Bogumil et al. [28] display sudden baseline jumps and are consistently lower than the other cited data sets. Voigt et al. [155] observed in the region 335 – 380 nm the presence of “hot bands”, which disappear with decreasing temperature, and “cold bands”, which become more pronounced at lower temperatures.

In the Chappuis band, the available cross sections agree in showing a very small increase (1%) with decreasing temperature in the wavelength range 550 – 560 nm. However there is strong disagreement in the relative temperature dependence of the cross sections in the wings (400 – 550 nm and 650 – 790 nm) of the Chappuis band. Burkholder and Talukdar [37] report a decrease from 4% at 520 nm to 40% at 420 nm between 298 and 220 K, while Burrows et al. [38] observe a decrease at 420 nm to 70% at 221 K, and Bogumil et al. [28] a decrease of 20% at 223 K. These discrepancies could be due to baseline problems in the different measurements. It was also noted by the Bremen-team (Burrows-Voigt-Bogumil) that in the wings the differential cross sections increase up to 10% between 298 and 203 K. In addition, the band structures between 400 and 500 nm shift toward shorter wavelengths with decreasing temperature. El Helou et al. [57] found the cross sections of the Wulf bands to be highly temperature dependent, increasing up to 91% upon reducing the temperature to 150 K.

Three different models have been proposed to reproduce the temperature dependence of the O₃ cross sections in the entire ultraviolet and visible regions within the experimental uncertainties. The first model was developed for the Hartley band by Adler-Golden [6] and uses an exponential function. The second model, developed by Bass and Paur [21], uses a quadratic polynomial to be applied in the Hartley and Huggins bands. The third model of Voigt et al. [155] uses a double exponential function. The accuracy of the models was checked by Orphal [122, 123], who concluded that the experimental data are better reproduced using a quadratic polynomial.

The pressure dependence of the O₃ absorption cross sections was investigated by Hearn [69] in the Hartley band and by Voigt et al. [155] in the entire spectral region 240 – 790 nm. Both groups did not find experimental or theoretical support for pressure dependence, although Voigt et al. [155] proposed that temperature variations of the cross sections around 400 nm might be due to the formation of a weakly bound O₂-O₃ complex.

The recommended absorption cross sections are listed in Table 4A-4, averaged over atmospheric intervals at 218 K and at room temperature (293 – 298 K). It has to be noted that cross sections are listed over 500 cm⁻¹ intervals in the region 185 – 300 nm, over 1 nm intervals in the region 300 – 321 nm, over 2 nm intervals in the region 321.5 – 326.5 nm, and over 5 nm intervals in the region 330 – 825 nm. The 218 K values measured by the Reims-team (Daumont-Brion-Malicet-Brion) are only listed for the range 196 – 340 nm. The room temperature data were selected for the range 185 – 233 nm from the data of Molina and Molina [108], for the range 323 – 310 nm from Burrows et al. [38], and for the range 310 – 825 nm from the Reims team (Daumont-Brion-Malicet-Brion).

Table 4A-4. Absorption Cross Sections of O₃ at 218 and 293-298 K

λ (nm)	$10^{20} \sigma \text{ (cm}^2\text{)}$ 218 K 293-298 K		λ (nm)	$10^{20} \sigma \text{ (cm}^2\text{)}$ 293-298 K
121.567 (Lyman α)		2990		
185.185 – 186.916		62.2	412.5 – 417.5	0.00295
186.916 – 188.679		57.6	417.5 – 422.5	0.00393
188.679 – 190.476		52.6	422.5 – 427.5	0.00656
190.476 – 192.308		47.7	427.5 – 432.5	0.00697
192.308 – 194.175		42.9	432.5 – 437.5	0.00882
194.175 – 196.078		38.5	437.5 – 442.5	0.0137
196.078 – 198.020	34.4	34.9	442.5 – 447.5	0.0165
198.020 – 200.000	32.0	32.4	447.5 – 452.5	0.0185
200.000 – 202.020	31.2	31.5	452.5 – 457.5	0.0218
202.020 – 204.082	32.4	32.6	457.5 – 462.5	0.0366
204.082 – 206.186	36.2	36.3	462.5 – 467.5	0.0367
206.186 – 208.333	43.2	43.3	467.5 – 472.5	0.0410
208.333 – 210.526	54.2	53.9	472.5 – 477.5	0.0481
210.526 – 212.766	69.6	69.3	477.5 – 482.5	0.0754
212.766 – 215.054	90.6	90.3	482.5 – 487.5	0.0813
215.054 – 217.391	119	118	487.5 – 492.5	0.0816
217.391 – 219.780	155	154	492.5 – 497.5	0.0908
219.780 – 222.222	201	199	497.5 – 502.5	0.121
222.222 – 224.719	256	255	502.5 – 507.5	0.160
224.719 – 227.273	323	322	507.5 – 512.5	0.158
227.273 – 229.885	403	401	512.5 – 517.5	0.166
229.885 – 232.558	492	490	517.5 – 522.5	0.183
232.558 – 235.294	589	590	522.5 – 527.5	0.219
235.294 – 238.095	692	693	527.5 – 532.5	0.267
238.095 – 240.964	799	802	532.5 – 537.5	0.287
240.964 – 243.902	905	908	537.5 – 542.5	0.295
243.902 – 246.914	995	1001	542.5 – 547.5	0.319
246.914 – 250.000	1074	1080	547.5 – 552.5	0.337
250.000 – 253.165	1116	1125	552.5 – 557.5	0.358
253.165 – 256.410	1136	1148	557.5 – 562.5	0.398
256.410 – 259.740	1105	1122	562.5 – 567.5	0.439

λ (nm)	$10^{20} \sigma \text{ (cm}^2\text{)}$		λ (nm)	$10^{20} \sigma \text{ (cm}^2\text{)}$ 293-298 K
	218 K	293-298 K		
259.740 – 263.158	1047	1064	567.5 – 572.5	0.467
263.158 – 266.667	952	968	572.5 – 577.5	0.481
266.667 – 270.270	823	840	577.5 – 582.5	0.464
270.270 – 273.973	681	698	582.5 – 587.5	0.446
273.973 – 277.778	531	547	587.5 – 592.5	0.447
277.778 – 281.690	391	406	592.5 – 597.5	0.476
281.690 – 285.714	271	282	597.5 – 602.5	0.513
285.714 – 289.855	175	184	602.5 – 607.5	0.514
289.855 – 294.118	105	113	607.5 – 612.5	0.478
294.118 – 298.507	59.4	65.1	612.5 – 617.5	0.438
298.507 – 299.5	40.7	45.2	617.5 – 622.5	0.406
299.5 – 300.5	35.1	39.2	622.5 – 627.5	0.382
300.5 – 301.5	30.5	34.3	627.5 – 632.5	0.356
301.5 – 302.5	26.9	30.3	632.5 – 637.5	0.327
302.5 – 303.5	22.9	26.2	637.5 – 642.5	0.297
303.5 – 304.5	20.6	23.4	642.5 – 647.5	0.271
304.5 – 305.5	17.3	20.1	647.5 – 652.5	0.251
305.5 – 306.5	15.6	17.9	652.5 – 657.5	0.231
306.5 – 307.5	13.3	15.5	657.5 – 662.5	0.210
307.5 – 308.5	11.5	13.5	662.5 – 667.5	0.190
308.5 – 309.5	10.4	12.2	667.5 – 672.5	0.170
309.5 – 310.5	8.50	10.2	672.5 – 677.5	0.151
310.5 – 311.5	7.76	9.24	677.5 – 682.5	0.137
311.5 – 312.5	6.53	7.95	682.5 – 687.5	0.126
312.5 – 313.5	5.62	6.91	687.5 – 692.5	0.113
313.5 – 314.5	5.05	6.25	692.5 – 697.5	0.0989
314.5 – 315.5	4.08	5.19	697.5 – 702.5	0.0868
315.5 – 316.5	3.82	4.77	702.5 – 707.5	0.0784
316.5 – 317.5	3.11	4.02	707.5 – 712.5	0.0731
317.5 – 318.5	2.94	3.72	712.5 – 717.5	0.0696
318.5 – 319.5	2.11	2.89	717.5 – 722.5	0.0622
319.5 – 320.5	2.41	2.99	722.5 – 727.5	0.0543
320.5 – 321.5	1.43	2.10	727.5 – 732.5	0.0478
321.5 – 323.5	1.57	2.05	732.5 – 737.5	0.0442
323.5 – 325.5	1.02	1.41	737.5 – 742.5	0.0432
325.5 – 327.5	0.658	1.01	742.5 – 747.5	0.0447
327.5 – 332.5	0.483	0.697	747.5 – 752.5	0.0425
332.5 – 337.5	0.204	0.320	752.5 – 757.5	0.0338
337.5 – 342.5	0.0797	0.146	757.5 – 762.5	0.0286
342.5 – 347.5		0.0779	762.5 – 767.5	0.0262
347.5 – 352.5		0.0306	767.5 – 772.5	0.0260
352.5 – 357.5		0.0136	772.5 – 777.5	0.0294
357.5 – 362.5		0.00694	777.5 – 782.5	0.0318
362.5 – 367.5		0.00305	782.5 – 787.5	0.0262
367.5 – 372.5		0.00130	787.5 – 792.5	0.0208
372.5 – 377.5		0.000850	792.5 – 797.5	0.0173
377.5 – 382.5		0.000572	797.5 – 802.5	0.0157
382.5 – 387.5		0.000542	802.5 – 807.5	0.0156
387.5 – 392.5		0.000668	807.5 – 812.5	0.0186
392.5 – 397.5		0.000956	812.5 – 817.5	0.0221
397.5 – 402.5		0.00115	817.5 – 822.5	0.0206
402.5 – 407.5		0.00158	822.5 – 827.5	0.0145
407.5 – 412.5		0.00258		

Note:

T = 218 K, 196.078 – 342.5 nm, Reims team (1992-1995) (Daumont et al. [51], Brion et al. [31], Malicet et al. [97])
T = 298 K, 185.185 – 232.558 nm, Molina and Molina [108]
T = 293 K, 232.558 – 309.5 nm, Burrows et al. [38]
T = 295 K, 309.5 – 827.5 nm, Reims team (1992-1998) (Daumont et al. [51], Brion et al., [31], Malicet et al. [97], Brion et al. [30])

Photolysis Quantum Yields and Product Studies. The recommendation for the O(¹D) quantum yield from ozone photolysis as a function of wavelength and temperature, based on the review of Matsumi et al. [99], is given by the expression (Eqn 4-1)

$$\Phi(\lambda, T) = \left(\frac{q_1}{q_1 + q_2} \right) \times A_1 \times \exp \left\{ - \left(\frac{X_1 - \lambda}{\omega_1} \right)^4 \right\} + \left(\frac{q_2}{q_1 + q_2} \right) \times A_2 \times \left(\frac{T}{300} \right)^2 \times \exp \left\{ - \left(\frac{X_2 - \lambda}{\omega_2} \right)^2 \right\} + A_3 \times \left(\frac{T}{300} \right)^{1.5} \times \exp \left\{ - \left(\frac{X_3 - \lambda}{\omega_3} \right)^2 \right\} + c \quad \text{Eqn 4-1}$$

where $q_i = \exp \left(- \frac{v_i}{RT} \right)$ and X_{1-3} , A_{1-3} , ω_{1-3} , v_{1-2} and c are best-fit parameters given in Table 4A-5, λ is in nm,

T is in K, and $R = 0.695 \text{ (cm}^{-1} \text{ K}^{-1})$. The parameter c is assumed to be temperature and wavelength independent. This expression is valid only for the wavelength range 306 – 328 nm and temperature range 200 – 320 K.

Table 4A-5. Parameters for the Calculation of O(¹D) Quantum Yields

Parameter	i = 1	i = 2	i = 3
X_i (nm)	304.225	314.957	310.737
ω_i (nm)	5.576	6.601	2.187
A_i	0.8036	8.9061	0.1192
$v_i \text{ (cm}^{-1})$	0	825.518	–
c	0.0765	–	–

At room temperature (298 K) the uncertainties of the quantum yield values calculated with the above expression are estimated to be $\pm 10 \%$ (1σ) for $\Phi(\lambda, 298 \text{ K}) \geq 0.4$, while the uncertainties are estimated to be ± 0.04 for $\Phi(\lambda, 298 \text{ K}) < 0.4$. At temperatures other than room temperature, the uncertainties are estimated to be $\pm 15 \%$ for $\Phi(\lambda, T) \geq 0.4$ and ± 0.06 for $\Phi(\lambda, T) < 0.4$.

In the wavelength range 329 – 340 nm the recommended value of $\Phi(\text{O}^1\text{D}) = 0.08 \pm 0.04$, independent of temperature. For $\lambda > 340$ nm, the quantum yield may be non-zero but no recommendation is made. For the wavelength range 220 – 305 nm, the recommended O(¹D) quantum yield is 0.90, independent of temperature, based on the study by Takahashi et al. [141] and the review by Matsumi and Kawasaki [100]. The quantum yield for O(¹D) formation in the range 193 – 225 nm was measured by Nishida et al. [116], who found that the O(¹D) yield decreased from 0.90 ± 0.12 (225 nm) to 0.48 ± 0.03 (193 nm). A simple expression in the wavelength range 193 – 225 nm was derived

$$\Phi^{\text{O}^1\text{D}}(\lambda) = 1.37 \times 10^{-2} \lambda - 2.16$$

The recommendation for the temperature and wavelength dependences of the quantum yield for O(¹D) production, $\Phi(\text{O}^1\text{D})$, is taken from the review of Matsumi et al. [99]. Matsumi et al. [99] derived the recommended values using the following procedure: the measured O(¹D) quantum yields at 298 K between 306 and 328 nm from eight studies (Talukdar et al. [145], Takahashi et al. [142], Ball et al. [17], Armerding et al. [14], Bauer et al. [22], which superseded the data of Silvente et al. [134] from the same group, Brock and Watson [35], Troler and Wiesenfeld [148], and Smith et al. [137] were normalized using $\Phi(\text{O}^1\text{D}) = 0.79$ at 308 nm. This value was derived from the studies listed in Table 1 of Matsumi et al. [99]. The renormalized data were averaged. The wavelength dependence quantum yield data at various temperatures reported by Talukdar et al. [144, 145], Takahashi et al. [142], Hancock and Hofzumahaus [67] (this includes all the data from the Oxford group), Bauer et al. [22] and Smith et al. [137] were normalized to the value at 308 nm given above. These normalized data were used to obtain the best fit parameters for Eqn. 4-1 for the wavelength range 306 – 328 nm and temperature range 200 – 320 K. Because of the large number of studies upon which

the 298 K evaluation is based, the averaged 298 K data were given a larger weight in the fitting procedure than the data at other temperatures. The recommended $O(^1D)$ quantum yields calculated from Eqn. 4-1 using the fitting parameters given in Table 4A-5 is shown in Figure 4-1 for 200, 253 and 298 K in the wavelength range 306 – 328 nm (solid lines), based on the review of Matsumi et al. [99].

Products and yields from O_3 photodissociation at 157.6 nm were measured by Taherian and Slanger [140]. The primary atomic oxygen yield was measured to be 1.90 ± 0.30 , of which 71% is $O(^3P)$ and 29% $O(^1D)$. Turnipseed et al. [149] measured the quantum yield for $O(^3P)$ and $O(^1D)$ formation from 193 nm photolysis to be 0.57 ± 0.14 and 0.46 ± 0.29 , respectively, and at 222 nm they observed a quantum yield of 0.13 ± 0.02 for $O(^3P)$ and 0.87 ± 0.04 for $O(^1D)$.

Lee et al. [87] reported an upper limit of $<0.1\%$ for the quantum yield for the formation of $O(^1S)$ via channel (8) in the 170 – 240 nm range. Takahashi et al. [143] measured the quantum yield of $O(^1S)$ formation to be $(2.5 \pm 1.1) \times 10^{-3}$ in the 193 nm photolysis of O_3 , while Nakayama et al. [110] reported $(1.4 \pm 0.4) \times 10^{-4}$ and $(5 \pm 3) \times 10^{-5}$ for the $O(^1S)$ formation at 215 and 220 nm, respectively.

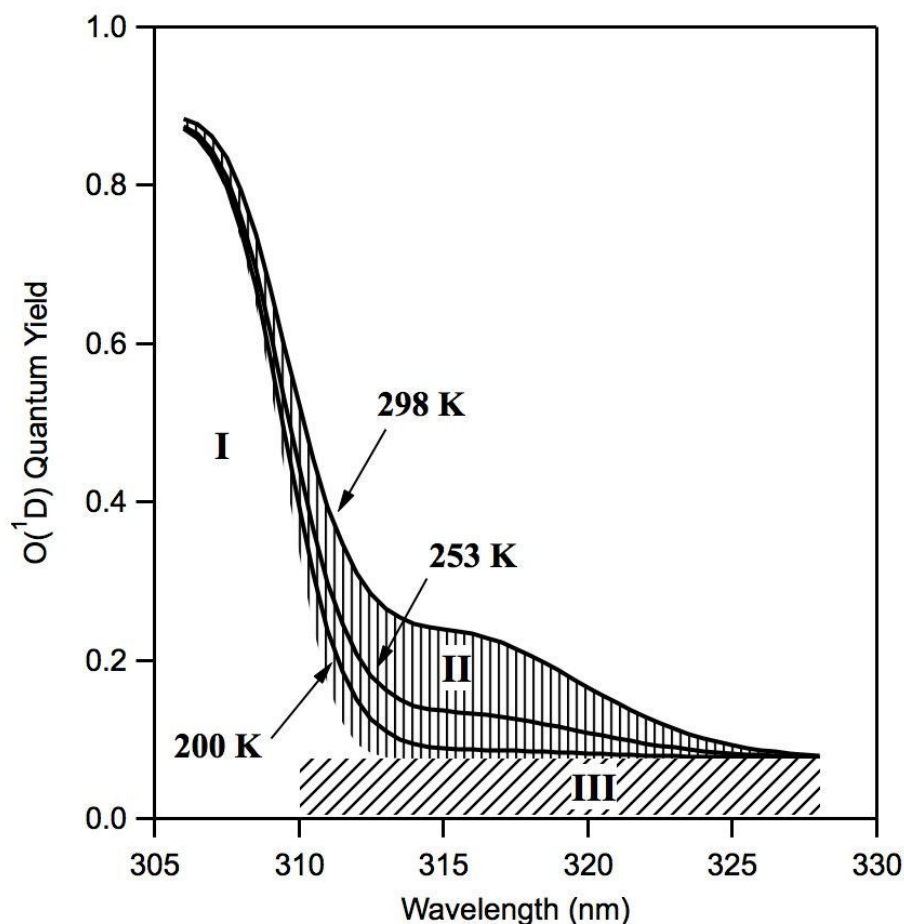


Figure 4A-1. Recommended $O(^1D)$ quantum yields calculated from Eqn. 4-1 using the fitting parameters given in Table 4A-5 for 200, 253 and 298 K in the wavelength range 306-328 nm (solid lines), based on Matsumi et al. [99]. Contributions from different photolysis channels are indicated: region I corresponds to $O(^1D)$ formed via channel (5), $O(^1D) + O_2(a^1\Delta_g)$, region II (vertical hatching) represents the contribution of the hot-band excitation process via channel (5), while region III (diagonal hatching) corresponds to the contribution of $O(^1D)$ via the spin-forbidden channel (4), $O(^1D) + O_2(X^3\Sigma_g^-)$.

References for Section 4A

1. Aboud, A. A., J. P. Curtis, R. Mercure and W. A. Rense, 1955, J. Opt. Soc. Am., 45, 767-768.
2. Ackerman, M. UV-solar radiation related to mesospheric processes. In *Mesospheric Models and Related Experiments*; G. Fiocco, Ed.; D. Reidel Publishing Company, Dordrecht, 1971; pp 149-159.
3. Ackerman, M., F. Biaumé and B. Kockarts, 1970, Planet. Space Sci., 18, 1639-1651.
4. Ackerman, M., F. Biaumé and M. Nicolet, 1969, Can. J. Chem., 47, 1834-1940.
5. Ackermann, M. In *Mesospheric Models and Related Experiments*; G. Fiocco, Ed., 1971; pp 149-159.
6. Adler-Golden, S. M., 1983, J. Quant. Spectrosc. Radiat. Transfer, 30, 175-185.
7. Ahmed, S. M., I. Kanik and R. Link, 1996, Chem. Phys. Lett., 259, 545-553.
8. Amoruso, A., M. Cacciani, A. di Sarra and G. Fiocco, 1990, J. Geophys. Res., 95, 20565.
9. Amoruso, A., L. Crescentini, M. Silvia Cola and G. Fiocco, 1996, J. Quant. Spectrosc. Radiat. Transfer, 56, 145-152.
10. Anderson, G. P. and L. A. Hall, 1983, J. Geophys. Res., 88, 6801-6806.
11. Anderson, G. P. and L. A. Hall, 1986, J. Geophys. Res., 91, 14509-14514.
12. Anderson, M., P. Hupalo and K. Mauersberger, 1993, Geophys. Res. Lett., 20, 1579-1582.
13. Anderson, S. M. and K. Mauersberger, 1992, Geophys. Res. Lett., 19, 933-936.
14. Armerding, W., F. J. Comes and B. Schulke, 1995, J. Phys. Chem., 99, 3137-3143.
15. Astholz, D. C., A. E. Croce and J. Troe, 1982, J. Phys. Chem., 86, 696-699.
16. Baci, A., J. Bouvier and J. M. Flaud, 1998, Spectrochimica Acta, Part A, 54, 17-34.
17. Ball, S. M., G. Hancock, S. E. Martin and J. C. Pinot de Moira, 1997, Chem. Phys. Lett., 264, 531-538.
18. Ball, S. M., G. Hancock and F. Winterbottom, 1995, Faraday Discuss., 100, 215.
19. Bao, Z.-C., W. O. Yu and J. R. Barker, 1995, J. Chem. Phys., 103, 6-13.
20. Barnes, J. and K. Mauersberger, 1987, J. Geophys. Res., 92, 14861-14864.
21. Bass, A. M. and R. J. Paur. In *Atmospheric Ozone*; C. S. Zerefos and A. Ghazi, Eds., 1985; pp 606-610.
22. Bauer, D., L. D'Ottone and A. J. Hynes, 2000, Phys. Chem. Chem. Phys., 2, 1421-1424.
23. Bennett, S. W., J. B. Tellinghuisen and L. F. Phillips, 1971, J. Phys. Chem., 75, 719-721.
24. Bertrand, C., G. J. Collin and H. Gagnon, 1975, J. Chim. Phys., 72, 719-723.
25. Blake, A. J., J. H. Carver and G. N. Haddad, 1966, J. Quant. Spectrosc. Radiat. Transfer, 6, 451-459.
26. Bogumil, K., J. Orphal, J. P. Burrows and J.-M. Flaud, 2001, Chem. Phys. Lett., 349, 241-248.
27. Bogumil, K., J. Orphal, T. Homann, S. Voigt, P. Spietz, O. C. Fleischmann, A. Vogel, M. Hartmann, H. Bovensmann, J. Frerick and J. P. Burrows, 2003, J. Photochem. Photobiol. A: Chem., 157, 167-184.
28. Bogumil, K., J. Orphal, T. Homann, S. Voigt, P. Spietz, O. C. Fleischmann, A. Vogel, M. Hartmann, H. Krominga, H. Bovensmann, J. Frerick and J. P. Burrows, 2003, J. Photochem. Photobiol. A: Chem., 157, 167-184.
29. Brion, C. E., K. H. Tan, M. J. v. d. Wiel and P. E. v. d. Leeuw, 1979, J. Electron Spectrosc. Relat. Phenom., 17, 101-119.
30. Brion, J., A. Chakir, J. Charbonnier, D. Daumont, C. Parisse and J. Malicet, 1998, J. Atmos. Chem., 30, 291-299.
31. Brion, J., A. Chakir, D. Daumont, J. Malicet and C. Parisse, 1993, Chem. Phys. Lett., 213, 610-612.
32. Brion, J., D. Daumont and J. Malicet, 1983, C. R. Acad. Sc. Paris, 297, 401-404.
33. Brion, J., D. Daumont and J. Malicet, 1984, J. Physique. Lett., 45, L57-L60.
34. Brion, J., D. Daumont, J. Malicet and P. Marché, 1985, J. Physique. Lett., 46, L105-L110.
35. Brock, J. C. and R. T. Watson, 1980, Chem. Phys., 46, 477-484.
36. Brolley, J. E., L. E. Porter, R. H. Sherman, J. K. Theobald and J. C. Fong, 1973, J. Geophys. Res., 78, 1627-1632.
37. Burkholder, J. B. and R. K. Talukdar, 1994, Geophys. Res. Lett., 21, 581-584.
38. Burrows, J. P., A. Richter, A. Dehn, B. Deters, S. Himmelmann, S. Voigt and J. Orphal, 1999, J. Quant. Spectrosc. Radiat. Transfer, 61, 509-517.
39. Cacciani, M., A. D. di Sarra, G. Fiocco and A. Amoruso, 1989, J. Geophys. Res., 94, 8485-8490.

40. Cheung, A. S. C., K. Yoshino, J. R. Esmond, S. S. L. Chiu, D. E. Freeman and W. H. Parkinson, 1990, J. Chem. Phys., 92, 842-849.
41. Cheung, A. S. C., K. Yoshino, D. E. Freeman, R. S. Friedman, A. Dalgarno and W. H. Parkinson, 1989, J. Mol. Spectrosc., 134, 362-389.
42. Cheung, A. S. C., K. Yoshino, W. H. Parkinson and D. E. Freeman, 1984, Geophys. Res. Lett., 11, 580-582.
43. Cheung, A. S. C., K. Yoshino, W. H. Parkinson and D. E. Freeman, 1984, Can. J. Phys., 62, 1752-1762.
44. Cheung, A. S. C., K. Yoshino, W. H. Parkinson, S. L. Guberman and D. E. Freeman, 1986, Planet. Space Sci., 34, 1007-1021.
45. Chiu, S. S. L., A. S. C. Cheung, K. Yoshino, J. R. Esmond, D. E. Freeman and W. H. Parkinson, 1990, J. Chem. Phys., 93, 5539-5543.
46. Clark, K. C., 1952, Phys. Rev., 87, 271-276.
47. Cole, B. E. and R. N. Dexter, 1978, J. Phys. B: Atom. Mol. Phys., 11, 1011-1023.
48. Cook, G. R., B. K. Ching and R. A. Becker, 1964, Discuss. Faraday Soc., 37, 149-158.
49. Cook, G. R. and P. H. Metzger, 1964, J. Chem. Phys., 41, 321-336.
50. Coquart, B., M. F. Merienne and A. Jenouvrier, 1990, Planet. Space Sci., 38, 287.
51. Daumont, D., J. Brion, J. Charbonnier and J. Malicet, 1992, J. Atmos. Chem., 15, 145-155.
52. Daumont, D., J. Brion and J. Malicet, 1983, Planet. Space Sci., 31, 1229-1234.
53. Davenport, J. E., 1982, National Technical Information Service, Report FAA-EE-80-44.
54. DeMore, W. B. and O. Raper, 1964, J. Phys. Chem., 68, 412-414.
55. Denzer, W., G. Hancock, J. C. Pinot de Moira and P. L. Tyley, 1988, Chem. Phys., 231, 109-119.
56. Ditchburn, R. W. and P. A. Young, 1962, J. Atmos. Terr. Phys., 24, 127-139.
57. El Helou, Z., S. Churassy, G. Wannous, R. Bacis and E. Boursey, 2005, J. Chem. Phys., 122, 244311 (1-9).
58. Enami, S., J. Ueda, Y. Nakano, S. Hashimoto and M. Kawasaki, 2004, J. Geophys. Res., 109, D05309.
59. Fally, S., A. C. Vandaele, M. Carleer, C. Hermans, A. Jenouvrier, M.-F. Mérieulle, B. Coquart and R. Colin, 2000, J. Mol. Spectrosc., 204, 10-20.
60. Frederick, J. E. and J. E. Mentall, 1982, Geophys. Res. Lett., 9, 461-464.
61. Freeman, D. E., K. Yoshino, J. R. Esmond and W. H. Parkinson, 1984, Planet. Space Sci., 32, 239-248.
62. Freeman, D. E., K. Yoshino, J. R. Esmond and W. H. Parkinson. In *Atmospheric Ozone*; C. S. Zerefos and A. Ghazi, Eds., 1985; pp 622-624.
63. Gibson, S. T., H. P. F. Gies, A. J. Blake, D. G. McCoy and P. J. Rogers, 1983, J. Quant. Spectrosc. Radiat. Transfer, 30, 385-393.
64. Goldstein, R. and F. N. Mastrup, 1966, J. Opt. Soc. Am., 56, 765-769.
65. Greenblatt, G. D., J. J. Orlando, J. B. Burkholder and A. R. Ravishankara, 1990, J. Geophys. Res., 95, 18577-18582.
66. Griggs, M., 1968, J. Phys. Chem., 49, 857-859.
67. Hancock, G. and A. Hofzumahaus "Experimental Study of the Altitude Dependence of the Tropospheric Ozone Photolysis Frequency, J(O(1D)) Between 0 and 12 km Height (ATOP)," ENV4-CT95-0158, EU R and D Programme Environment and Climate 1997
68. Hasson, V. and R. W. Nichols, 1971, J. Phys. B. Atom. Mol. Phys., 4, 1789-1797.
69. Hearn, A. G., 1961, Proc. Phys. Soc. London, 78, 932-940.
70. Herman, J. R. and J. E. Mentall, 1982, J. Geophys. Res., 87, 8967-8975.
71. Hudson, R. D., 1974, Canad. J. Chem., 52, 1465-1478.
72. Hudson, R. D., V. L. Carter and J. A. Stein, 1966, J. Geophys. Res., 71, 2295-2298.
73. Hudson, R. D. and S. H. Mahle, 1972, J. Geophys. Res., 77, 2902-2914.
74. Huestis, D. L., R. A. Copeland, K. Knutsen, T. G. Slanger, R. T. Jogma, M. G. H. Boogaarts and G. Meijer, 1994, Can. J. Phys., 1109-1121.
75. Huffman, R. E., 1969, Can. J. Chem., 47, 1823-1834.
76. Huffman, R. E., Y. Tanaka and H. E. Larrabee, 1964, Discuss. Faraday Soc., 37, 159-166.
77. Inn, E. C. Y. and Y. Tanaka, 1953, J. Opt. Soc. Am., 43, 870-873.

78. Inn, E. C. Y. and Y. Tanaka, 1958, *Adv. Chem. Ser.*, 21, 263-268.
79. Inn, E. C. Y. and Y. Tanaka, 1959, *Adv. Chem. Ser.*, 21, 263-268.
80. Jenouvrier, A., B. Coquart and M. F. Mérienne-Lafore, 1986, *Planet. Space Sci.*, 34, 253-254.
81. Jenouvrier, A., B. Coquart and M. F. Merienne, 1986, *J. Quant. Spectros. Radiat. Transfer* 36, 349-354.
82. Johnston, H. S., M. Paige and F. Yao, 1984, *J. Geophys. Res.*, 89, 11661-11665.
83. Kanik, I., L. Beegle, C. Noren, S. M. Ahmed and R. Link, 1997, *Chem. Phys. Lett.*, 279, 297-302.
84. Kley, D., 1984, *J. Atmos. Chem.*, 2, 203-210.
85. Kockarts, G., 1976, *Planet. Space Sci.*, 24, 589-604.
86. Lacoursière, J., S. A. Meyer, G. W. Faris, T. G. Slanger, B. R. Lewis and S. T. Gibson, 1999, *J. Chem. Phys.*, 110, 1949-1958.
87. Lee, L. C., G. Black, R. L. Sharpless and T. G. Slanger, 1980, *J. Chem. Phys.*, 73, 256-258.
88. Lee, L. C., T. G. Slanger, G. Black and Sharpless, 1977, *J. Chem. Phys.*, 67, 5602-5606.
89. Lee, P., 1955, *J. Opt. Soc. Am.*, 45, 703-709.
90. Lee, P. C. and J. B. Nee, 2000, *J. Chem. Phys.*, 112, 1763-1768.
91. Lee, P. C. and J. B. Nee, 2001, *J. Chem. Phys.*, 114, 792-797.
92. Lewis, B. R., L. Berzins and J. H. Carver, 1986, *J. Quant. Spectrosc. Radiat. Transfer*, 36, 209-232.
93. Lewis, B. R., L. Berzins, J. H. Carver and S. T. Gibson, 1986, *J. Quant. Spectrosc. Radiat. Transfer*, 36, 187-207.
94. Lewis, B. R., I. M. Vardavas and J. H. Carver, 1983, *J. Geophys. Res.*, 88, 4935-4940.
95. Lin, J. J., D. W. Huang, Y. T. Lee and X. Yang, 1998, *J. Chem. Phys.*, 109, 1758-1762.
96. Malicet, J., J. Brion and D. Daumont, 1989, *Chem. Phys. Lett.*, 158, 293-296.
97. Malicet, J., D. Daumont, J. Charbonnier, C. Parisse, A. Chakir and J. Brion, 1995, *J. Atm. Chem*, 21, 263-273.
98. Mason, N. J., J. M. Gingell, J. A. Davies, H. Zhao, I. C. Walker and M. R. F. Siggel, 1996, *J. Phys. B: Atom. Mol. Phys.*, 29, 3075-3089.
99. Matsumi, Y., F. J. Comes, G. Hancock, A. Hofzumahaus, A. J. Hynes, M. Kawasaki and A. R. Ravishankara, 2002, *J. Geophys. Res.*, 107, D3, 4024, doi: 10.1029/2001JD000510.
100. Matsumi, Y. and M. Kawasaki, 2003, *Chem. Rev.*, 103, 4767-4781.
101. Matsunaga, F. M. and K. Watanabe, 1967, *Sci. Light*, 16, 31-42.
102. Mauersberger, K., J. Barnes, D. Hanson and J. Morton, 1986, *Geophys. Res. Lett.*, 13, 671-673.
103. Mauersberger, K., D. Hanson, J. Barnes and J. Morton, 1987, *J. Geophys. Res.*, 92, 8480-8482.
104. McPeters, R. D. and A. M. Bass, 1982, *Geophys. Res. Lett.*, 9, 227-230.
105. Metzger, P. H. and G. R. Cook, 1964, *J. Quant. Spectrosc. Radiat. Transfer*, 4, 107-116.
106. Minschwaner, K., G. P. Anderson, L. A. Hall and K. Yoshino, 1992, *J. Geophys. Res.*, 97, 10103-10108.
107. Minschwaner, K., R. J. Salawitch and M. B. McElroy, 1993, *J. Geophys. Res.*, 98, 10543-10561.
108. Molina, L. T. and M. J. Molina, 1986, *J. Geophys. Res.*, 91, 14501-14508.
109. Murtagh, D. P., 1988, *Planet. Space Sci.*, 36, 819-828.
110. Nakayama, T., K. Takahashi, Y. Matsumi and H. Fujiwara, 2006, *J. Atmos. Chem.*, 53, 107-122.
111. Nee, J. B. and P. C. Lee, 1997, *J. Phys. Chem. A*, 101, 6653-6657.
112. Nicolet, M., 1981, *Planet. Space Sci.*, 29, 951-974.
113. Nicolet, M. and R. Kennes, 1986, *Planet. Space Sci.*, 34, 1043-1059.
114. Nicolet, M. and R. Kennes, 1988, *Planet. Space Sci.*, 36, 1069-1076.
115. Nicolet, M. and R. Kennes, 1989, *Planet. Space Sci.*, 37, 459-491.
116. Nishida, S., K. Takahashi, Y. Matsumi, N. Taniguchi and S. Hayashida, 2004, *J. Phys. Chem. A*, 108, 2451-2456.
117. Ny, T.-Z. and S.-P. Choong, 1933, *Chinese J. Phys.*, 1, 38-54.
118. Ogawa, M., 1968, *J. Geophys. Res.*, 73, 6759-6763.
119. Ogawa, M., 1971, *J. Chem. Phys.*, 54, 2550-2556.
120. Ogawa, M. and G. R. Cook, 1958, *J. Chem. Phys.*, 28, 173-174.

121. Ogawa, S. and M. Ogawa, 1975, *Can. J. Phys.*, 53, 1845-1852.
122. Orphal, J. "A Critical Review of the Absorption Cross-Sections of O₃ and NO₂ in the 240-790 nm Region, Part 1, Ozone," ESA Technical Note MO-TN-ESA-GO-0302, European Space Agency, ESA-ESTEC, Noordwijk, 2002
123. Orphal, J., 2003, *J. Photochem. Photobiol.*, A 157, 185-209.
124. Oshima, Y., Y. Okamoto and S. Koda, 1995, *J. Phys. Chem.*, 99, 11830-11833.
125. Paur, R. J. and A. M. Bass. In *Atmospheric Ozone*; C. S. Zerefos and A. Ghazi, Eds., 1985; pp 610-616.
126. Pirre, M., P. Rigaud and D. Huguenin, 1984, *Geophys. Res. Lett.*, 11, 1199-1202.
127. Pirre, M., P. Rigaud and D. Huguenin, 1988, *Annales Geophysicae*, 6, 535-540.
128. Preston, W. M., 1940, *Phys. Rev.*, 57, 887-894.
129. Samson, J. A. R. and R. B. Cairns, 1964, *J. Geophys. Res.*, 69, 4583-4590.
130. Samson, J. A. R. and R. B. Cairns, 1965, *J. Opt. Soc. Am.*, 45, 1035-1040.
131. Saxon, R. P. and T. G. Slanger, 1986, *J. Geophys. Res.*, 91, 9877-9879.
132. Shardanand, 1969, *Phys. Rev.*, 186, 5-9.
133. Shardanand and A. D. P. Rao, 1977, *J. Quant. Spectrosc. Radiat. Transfer*, 17, 433-439.
134. Silvente, E., R. C. Richter, M. Zheng, E. S. Saltzman and A. J. Hynes, 1997, *Chem. Phys. Lett.*, 264, 309-315.
135. Simons, J. W., R. J. Paur, H. A. Webster III and E. J. Blair, 1973, *J. Phys. Chem.*, 59, 1203-1208.
136. Slanger, T. G., D. L. Huestis, P. C. Cosby, N. Naus and G. Meijer, 1996, *J. Chem. Phys.*, 105, 9393-9402.
137. Smith, G. D., L. T. Molina and M. J. Molina, 2000, *J. Phys. Chem. A*, 104, 8916-8921.
138. Starr, W. L. and M. Loewenstein, 1972, *J. Geophys. Res.*, 77, 4790-4796.
139. Steinfeld, J. I., S. M. Adler-Golden and J. W. Gallagher, 1987, *J. Phys. Chem. Ref. Data*, 16, 911-951.
140. Taherian, M. R. and T. G. Slanger, 1985, *J. Chem. Phys.*, 83, 6246-6250.
141. Takahashi, K., S. Hayashi, Y. Matsumi, N. Taniguchi and S. Hayashida, 2002, *J. Geophys. Res.*, 107, 4440.
142. Takahashi, K., Y. Matsumi and M. Kawasaki, 1996, *J. Phys. Chem.*, 100, 4084-4089.
143. Takahashi, T., T. Nakayama and Y. Matsumi, 2003, *J. Phys. Chem. A*, 107, 9368-9373.
144. Talukdar, R. K., M. K. Gilles, F. Battin-Leclerc, A. R. Ravishankara, J.-M. Fracheboud, J. J. Orlando and G. S. Tyndall, 1997, *Geophys. Res. Lett.*, 24, 1091-1094.
145. Talukdar, R. K., C. A. Longfellow, M. K. Gilles and A. R. Ravishankara, 1998, *Geophys. Res. Lett.*, 25, 143-146.
146. Tanaka, Y., E. C. Y. Inn and K. Watanabe, 1953, *J. Chem. Phys.*, 21, 1651-1653.
147. Tanaka, Y., A. S. Jursa, F. J. LeBlanc and E. C. Y. Inn, 1959, *Planet. Space Sci.*, 1, 7-13.
148. Troler, M. and J. R. Wiesenfeld, 1988, *J. Geophys. Res.*, 93, 7119-7124.
149. Turnipseed, A. A., G. L. Vaghjani, T. Gierczak, J. E. Thompson and A. R. Ravishankara, 1991, *J. Chem. Phys.*, 95, 3244-3251.
150. Vassy, A. and E. Vassy, 1948, *J. Chem. Phys.*, 16, 1163-1164.
151. Vattulainen, J., L. Wallenius, J. Stenberg, R. Hernberg and V. Linna, 1997, *Appl. Spectrosc.*, 57, 1311-1315.
152. Vigroux, E., 1953, *Ann. Phys.*, 8, 709-762.
153. Vigroux, E., 1967, *C. R. Acad. Sc. Paris*, 264, 1290-1291.
154. Vigroux, E., 1969, *Ann. Geophys.*, 25, 169-172.
155. Voigt, S., J. Orphal, K. Bogumil and J. P. Burrows, 2001, *J. Photochem. Photobiol. A*, 143, 1-9.
156. Wainfan, N., W. C. Walker and G. L. Weissler, 1955, *Phys. Rev.*, 99, 542-549.
157. Wang, J., D. G. McCoy, A. J. Blake and L. Torop, 1987, *J. Quant. Spectrosc. Radiat. Transfer*, 38, 19-27.
158. Watanabe, K., E. C. Y. Inn and M. Zelikoff, 1952, *J. Chem. Phys.*, 20, 1969-1970.
159. Watanabe, K., E. C. Y. Inn and M. Zelikoff, 1953, *J. Chem. Phys.*, 21, 1026-1030.
160. Watanabe, K. and F. F. Marmo, 1956, *J. Chem. Phys.*, 25, 965-971.
161. Weissler, G. L. and P. Lee, 1952, *J. Opt. Soc. Am.*, 42, 200-203.

162. WMO *Atmospheric Ozone: 1985*; National Aeronautics and Space Administration: Geneva, Report No. 16, Chapter 7, 1986.
163. Wu, C. Y. R., D. L. Judge and T. Matsui, 2005, *J. Electron Spectrosc. Related Phenom.*, 144-147, 123-126.
164. Yoshino, K., A. S. C. Cheung, J. R. Esmond, W. H. Parkinson, D. E. Freeman, S. L. Guberman, A. Jenouvrier, B. Coquart and M. F. Merienne, 1988, *Planet. Space Sci.*, 36, 1469-1475.
165. Yoshino, K., J. R. Esmond, A. S.-C. Cheung, D. E. Freeman and W. H. Parkinson, 1992, *Planet. Space Sci.*, 40, 185-192.
166. Yoshino, K., J. R. Esmond, A. S. C. Cheung, D. E. Freeman and W. H. Parkinson, 1990, *J. Geophys. Res.*, 95, 11743.
167. Yoshino, K., J. R. Esmond, D. E. Freeman and W. H. Parkinson, 1993, *J. Geophys. Res.*, 98, 5205-5211.
168. Yoshino, K., J. R. Esmond, J. E. Murray, W. H. Parkinson, A. P. Thorne, R. C. M. Learner and G. Cox, 1995, *J. Chem. Phys.*, 103, 1243-1249.
169. Yoshino, K., J. R. Esmond, W. H. Parkinson, A. P. Thorne, R. C. M. Learner and G. Cox, 1999, *J. Chem. Phys.*, 111, 2960-2967.
170. Yoshino, K., J. R. Esmond, W. H. Parkinson, A. P. Thorne, R. C. M. Learner, G. Cox and A. S.-C. Cheung, 2000, *J. Chem. Phys.*, 112, 9791-9801.
171. Yoshino, K., D. E. Freeman, J. R. Esmond, R. S. Friedman and W. H. Parkinson, 1988, *Planet. Space Sci.*, 36, 1201-1210.
172. Yoshino, K., D. E. Freeman, J. R. Esmond, R. S. Friedman and W. H. Parkinson, 1989, *Planet. Space Sci.*, 37, 419-426.
173. Yoshino, K., D. E. Freeman, J. R. Esmond and W. H. Parkinson, 1987, *Planet. Space Sci.*, 35, 1067-1075.
174. Yoshino, K., D. E. Freeman, J. R. Esmond and W. H. Parkinson, 1988, *Planet. Space Sci.*, 36, 395-398.
175. Yoshino, K., D. E. Freeman and W. H. Parkinson, 1984, *J. Phys. Chem. Ref. Data*, 13, 207-227.
176. Yoshino, K., D. F. Freeman, J. R. Esmond and W. H. Parkinson, 1983, *Planet. Space Sci.*, 31, 339-353.
177. Yoshino, K., D. L. Huestis and R. W. Nicholls, 1998, *J. Quant. Spectrosc. Radiat. Transfer*, 60, 1091.
178. Yoshino, K., J. E. Murray, J. R. Esmond, Y. Sun, W. H. Parkinson, A. P. Thorne, R. C. M. Learner and G. Cox, 1994, *Can. J. Phys.*, 72, 1101-1108.
179. Yoshino, K., W. H. Parkinson, K. Ito and T. Matsui, 2005, *J. Mol. Spectrosc.*, 229, 238-243.

SECTION 4B. HO_x PHOTOCHEMISTRY



(Recommendation: 06-2; Note: 10-6; Evaluated: 10-6)

Absorption Cross Sections: UV absorption cross sections of HO₂ in the wavelength range 190 – 260 nm have been measured at room temperature by Paukert and Johnston [60], Hochanadel et al. [26], Cox and Burrows [13], McAdam et al. [48], Kurylo et al. [37], Moortgat et al. [53], Dagaut and Kurylo [16], Lightfoot and Jemi-Alade [44], who measured the cross sections at temperatures up to 777 K, Crowley et al. [15], Maricq and Szente [47], Roehl et al. [63], and Sander et al. [64]. The HO₂ absorption cross section studies have been evaluated in reviews by Lightfoot et al. [43], Wallington et al. [83], and Tyndall et al. [75]. Discrepancies in the shape of the HO₂ spectrum and its absolute cross sections, particularly around 200 nm, exist among the available studies. Tyndall et al. [75] recommend absolute HO₂ cross sections based on a comparison of absorption cross sections for HO₂, CH₃O₂ and C₂H₅O₂ at 240 nm obtained by Roehl et al., Lightfoot and Jemi-Alade, and Maricq and Szente combined with the measurements by Crowley et al. [15] at 240 nm. Tyndall et al. [75] used the expression

$$\sigma = \left(\frac{\sigma_{\text{med}}}{1 - \frac{b}{\nu}} \right) \exp \left\{ -a \left[\ln \frac{(\nu - b)}{(\nu_{\text{med}} - b)} \right]^2 \right\}$$

where $\sigma_{\text{med}} = 1.64 \times 10^{-18} \text{ cm}^2 \text{ molecule}^{-1}$, $a = 4.91$, $b = 30612 \text{ cm}^{-1}$ and $\nu_{\text{med}} = 50260 \text{ cm}^{-1}$ that reproduces the HO₂ spectrum over the wavelength range 190 – 250 nm. They recommend that the spectrum be treated as temperature independent over the range 200 – 300 K. The recommended HO₂ cross sections in Table 4B-1 are taken from the Tyndall et al. [75] review.

Photolysis Quantum Yield and Product Studies: Lee [40] detected O(¹D) as a primary photodissociation product of HO₂ at 193 and 248 nm with a quantum yield that is about 15 times larger at the longer wavelength. An absolute quantum yield for O(¹D) production has not been reported.

Table 4B-1. Absorption Cross Sections of HO₂ at 298 K

λ (nm)	$10^{20} \sigma$ (cm ²)
190	368
195	402
200	423
205	427
210	415
215	385
220	341
225	288
230	230
235	173
240	122
245	79.7
250	48.0
255	26.3
260	12.9



(Recommendation: 10-6, Note: 10-6, Evaluated: 10-6)

Absorption Cross Sections: The VUV absorption spectrum of water vapor can be divided up into four main regions: (i) a broad continuum at wavelengths 145 – 190 nm with a maximum around 165 nm and the cross sections falling off rapidly toward longer wavelengths; (ii) a second continuum centered around 128 nm, which shows some diffuse vibrational structure; (iii) between 124 – 100 nm the absorption spectrum is dominated by progressions of sharp structured rovibronic peaks associated with Rydberg transitions; (iv) below 100 nm the spectrum is also a continuum consisting of two diffuse bands with maxima near 90 and 65 nm. In the atmosphere water, vapor is photodissociated mainly by the solar Lyman- α line (121.567 nm). The absorption cross sections and the photochemistry of water vapor were reviewed by Hudson [30, 31], Hudson and Kiefer [32], Calvert and Pitts [5], and Okabe [58]. Table 4-B2 summarizes the studies performed since 1950.

Table 4B-2. Summary of H₂O Vapor Absorption Cross Section Studies

Study	Year	Molecule	Wavelength (nm)	Resolution (nm)	Temperature (K)
Wilkinson and Johnston [86]	1950	H ₂ O	143 – 186	0.1	303
Watanabe and Zelikoff [85]	1953	H ₂ O	106 – 185	0.1	298
Wainfan et al. [82]	1955	H ₂ O	47 – 100	1.0	298
Harrison et al. [25]	1959	H ₂ O	154 – 200	0.3	295
Thompson et al. [73]	1963	H ₂ O	150 – 200	0.3	295
Metzger and Cook [50]	1964	H ₂ O	58.4 – 99	0.1	295
Watanabe and Jursa [84]	1964	H ₂ O	85 – 111	0.1	295
Laufer and McNesby [38]	1965	H ₂ O, D ₂ O	120 – 185	0.1	298
Schürgers and Welge [67]	1968	H ₂ O	120 – 183	0.25	298
de Reilhac and Damany [17]	1970	H ₂ O, D ₂ O	11.1 – 41.7	0.1	298
Bennett et al. [2]	1971	H ₂ O	58.4	0.1	295
Katayama et al. [34]	1973	H ₂ O, D ₂ O	58 – 105	0.05	298
Branton and Brion [3]	1974	H ₂ O	12-113, 138, 177, 248	0.1	298
Gürtler et al. [24]	1977	H ₂ O, D ₂ O	60 – 125	0.003	298
Phillips et al. [61]	1977	H ₂ O, D ₂ O	18 – 79	0.1	298
Tan et al. [70]	1978	H ₂ O	21-124, 138, 155, 177, 207	0.1	298
DeMore [18]	1979	H ₂ O	184.9	0.1	298
Lee [39]	1980	H ₂ O	105 – 137	0.2	294
Nicolet [56]	1981	H ₂ O	121.6	Calc J	230
Lewis et al. [42]	1983	H ₂ O	121.4 – 121.9	0.005	235, 292, 367
Kley [35]	1984	H ₂ O	121.6	0.005	298
Camy-Peyret et al. [6]	1985	H ₂ O	396.0 – 606.1	0.0127 cm ⁻¹	300
Mandin et al. [46]	1986	H ₂ O	606.1 – 757.6	0.0127 cm ⁻¹	300
Lee and Suto [41]	1986	H ₂ O, D ₂ O	50 – 190	0.2	295
Chan et al. [8]	1993	H ₂ O	6.2 – 206.6	0.5	298
Yoshino et al. [87]	1996	H ₂ O	120 – 188	0.0070	295
Brownsword et al. [4]	1997	H ₂ O	121.6	0.002	300
Cantrell et al. [7]	1997	H ₂ O, D ₂ O	184 – 193	0.2	273 – 353
Hofzumahaus et al. [27]	1997	H ₂ O	184.9	0.1	298
Creasey et al. [14]	2000	H ₂ O	184.9	0.1	298
Chung et al. [11]	2001	H ₂ O, D ₂ O HDO	140 – 195	0.1	295, 275, 250
The Harvard-Smithsonian Center for Astrophysics [29]	2001	H ₂ O	107.2 – 108.0 111.2 – 111.8 123.3 – 124.5	0.0002 0.0002 0.0007	295, 80 295 295, 80
Vatsa and Volpp [81]	2001	H ₂ O	121.567	0.0006	300
Coheur et al. [12]	2002	H ₂ O	385 – 758	0.06 cm ⁻¹	291.3
Tanaka et al. [71]	2002	H ₂ ¹⁸ O	606.5 – 688.7	0.06 cm ⁻¹	298
Fally et al. [20]	2003	H ₂ O	384.6 – 769.2	0.06 cm ⁻¹	289 ± 2
Mérienne et al. [49]	2003	H ₂ O	769.2 – 1081.1	0.03 cm ⁻¹	292 ± 3
Parkinson and Yoshino [59]	2003	H ₂ O	181 – 199	0.0066	295
Cheng et al. [9]	2004	H ₂ O, D ₂ O HDO	125 – 145	0.01	300
Fillion et al. [22]	2004	H ₂ O, D ₂ O	99.9 – 113.9	0.01 cm ⁻¹	298
Tanaka et al. [72]	2004	H ₂ ¹⁸ O	584.1 – 688.7	0.06 cm ⁻¹	298
Aldener et al. [1]	2005	H ₂ O	870 – 955	0.01 cm ⁻¹	298
Mota et al. [55]	2005	H ₂ O	114.8 – 193.9	0.075	298
Kassi et al. [33]	2005	H ₂ O	747.5 – 751.2	0.06 cm ⁻¹	298

The cross sections in the VUV band in the range 6 to 110 nm measured by Katayama et al. [34], Gürtler et al. [24], Phillips et al. [61], Tan et al. [70], Lee and Suto [41], Chan et al. [8] are in good agreement, whereas the data of Wainfan et al. [82], Metzger and Cook [50], de Reilhac and Damany [17], Bennett et al. [2] and Branton and Brion [3] show substantial deviations.

In the strong structured region between 100 and 125 nm cross sections were measured at low resolution by Watanabe and Zelikoff [85], Watanabe and Jursa [84], Tan et al. [70], Lee [39], Lee and Suto [41], Chan et al. [8], and at high resolution by Gürtler et al. [24], Lewis et al. [42], The Harvard-Smithsonian Center for Astrophysics [29], Fillion et al. [22], and Mota et al. [55].

Absorption cross sections were reported at the Lyman- α wavelength, 121.567 nm, in units 10^{-17} cm² molecule⁻¹, to be 1.44 ± 0.04 by Watanabe and Zelikoff [85], 1.4 ± 0.3 by Nicolet [56], 1.5 ± 0.1 by Gürtler et al. [24], 1.55 ± 0.1 by Lewis et al. [42], 1.59 ± 0.1 by Kley [35], 1.42 ± 0.1 by Lee [39], 1.3 ± 0.05 by Chan et al. [8], 1.4 ± 0.03 by Yoshino et al. [87], 1.6 ± 0.1 by Brownsword et al. [4], and 1.6 ± 0.1 by Vatsa and Volpp [81]. An average value $(1.48 \pm 0.10) \times 10^{-17}$ cm² molecule⁻¹ for the absorption cross section at the Lyman- α wavelength 121.567 nm is recommended.

In the weak structured region between 125 and 140 nm, measurements at low resolution were reported by Watanabe and Zelikoff [85], Laufer and McNesby [38], Schürgers and Welge [67], Branton and Brion [3], Tan et al. [70], Lee [39], Lee and Suto [41], Chan et al. [8], and at high resolution by Yoshino et al. [87], Cheng et al. [9], and Mota et al. [55].

In the broad continuum at long wavelengths 145 – 190 nm, measurements at low resolution were performed by Wilkinson and Johnston [86], Watanabe and Zelikoff [85], Harrison et al. [25], Thompson et al. [73], Laufer and McNesby [38], Schürgers and Welge [67], Branton and Brion [3], Tan et al. [70], Lee and Suto [41], Chan et al. [8], and at high resolution by Yoshino et al. [87], Chung et al. [11] and Mota et al. [55].

In the tail of the absorption band in the wavelength range 185 – 200 nm measurements were reported by Cantrell et al. [7], Creasey et al. [14], Chung et al. [11], Parkinson and Yoshino [59] and Mota et al. [55]. At the 184.94 nm Hg line, absorption cross sections were measured, in units 10^{-20} cm² molecule⁻¹, to be 7.8 by DeMore [18], 7.14 ± 0.2 by Cantrell et al. [7], 7.22 ± 0.22 by Creasey et al. [14], 10.1 ± 0.1 by Yoshino et al. [87], 7.0 by Hofzumahaus et al. [27], and 7.3 (a value measured by J. Crowley, cited by Hofzumahaus et al. [27]). Based on the latter studies, the recommended value for the absorption cross section at 184.94 nm is $(7.1 \pm 0.2) \times 10^{-20}$ cm² molecule⁻¹ at 298 K.

High resolution spectra of water vapor and complete sets of line parameters have been measured in the visible region by Camy-Peyret et al. [6] (369 – 606 nm), Mandin et al. [46] (606 – 758 nm), Fally et al. [20] (385 – 769 nm), Coheur et al. [12] (385 – 769 nm), and for H₂¹⁸O by Tanaka et al. [72] (584 – 689 nm), and Tanaka et al. [71] (606 – 689 nm); in the near infrared by Mérienne et al. [49] (769 – 1081 nm), Aldener et al. [1] (926 – 952 nm), and Kassi et al. [33] (747 – 752 nm).

The recommended absorption cross sections listed in Table 4B-3 are taken from Yoshino et al. [87] for the range 121 – 182 nm, from Cantrell et al. [7] for the range 183 – 191 nm, and from the interpolated data of Parkinson and Yoshino [59] for the range 192 – 198 nm.

Photolysis Quantum Yield and Product Studies: Stief et al. [69] reported a relative quantum yield of process (2) $\Phi_2[\text{H} + \text{OH}(\text{X}^2\Pi)] = 0.89$ and process (3) $\Phi_3[\text{H}_2 + \text{O}(^1\text{D})] = 0.11$ for the wavelength interval 105 – 145 nm, and $\Phi_2[\text{H} + \text{OH}(\text{X}^2\Pi)] \geq 0.99$ and $\Phi_3[\text{H}_2 + \text{O}(^1\text{D})] \leq 0.01$ for the interval 145 – 185 nm. Lee [39] measured the quantum yield of the emission of $\text{OH}(\text{A}^2\Sigma^+) \rightarrow \text{OH}(\text{X}^2\Pi)$ produced in process (4), varying between 2 and 11 % in the wavelength range 105 – 135 nm. The quantum yields show a maximum of 11% at 130 nm, decreasing slowly with decreasing wavelengths. Ung [76] measured the relative quantum yields $\Phi_2[\text{H} + \text{OH}(\text{X}^2\Pi)] = 0.92$ and $\Phi_3[\text{H}_2 + \text{O}(^1\text{D})] = 0.08$ for the photolysis at 147 nm. At the Lyman- α wavelength 121.567 nm the quantum yield for H atoms, $\Phi_{\text{H}} = 1.02$ was determined by Slinger and Black [68]. They also measured the quantum yield for processes (2) + (4), $\Phi_2[\text{H} + \text{OH}(\text{X}^2\Pi)] + \Phi_4[\text{OH}(\text{A}^2\Sigma^+) + \text{H}] = 0.78$, for process (3) $\Phi_3[\text{O}(^1\text{D}) + \text{H}_2] = 0.10$ and for process (5) $\Phi_5[\text{O}(^3\text{P}) + \text{H} + \text{H}] = 0.12$. Chou et al. [10] photolysed HTO at 174 nm and estimated $\Phi_1 \leq 0.003$ for the formation of $\text{HT} + \text{O}(^3\text{P})$ and $\Phi_2 \sim 1$ for the processes leading to $\text{H} + \text{OT}$ and $\text{T} + \text{OH}$. Mordaunt et al. [54] determined the absolute branching for the photodissociation channels at 121.567 nm as $\Phi_2[\text{H} + \text{OH}(\text{X}^2\Pi)] = 0.64$, $\Phi_3[\text{O}(^1\text{D}) + \text{H}_2] = 0.11$, $\Phi_4[\text{OH}(\text{A}^2\Sigma^+) + \text{H}] = 0.14$, and $\Phi_5[\text{O}(^3\text{P}) + \text{H} + \text{H}] = 0.11$.

Table 4B-3. Absorption Cross Sections of H₂O Vapor at 298 K

λ (nm)	$10^{20} \sigma$ (cm ²)	λ (nm)	$10^{20} \sigma$ (cm ²)	λ (nm)	$10^{20} \sigma$ (cm ²)	λ (nm)	$10^{20} \sigma$ (cm ²)
121.0	624	133.0	494	151	141	176	284
121.5	1276	133.5	513	152	165	177	240
121.567	1480	134.0	424	153	197	178	193
122.0	1689	134.5	382	154	211	179	140
122.5	826	135.0	367	155	236	180	90.0
123.0	283	135.5	310	156	266	181	54.6
123.5	589	136.0	251	157	295	182	32.9
124.0	1332	136.5	257	158	327	183	16.9
124.5	663	137.0	204	159	354	184	12.1
125.0	619	137.5	195	160	385	185	6.78
125.5	693	138.0	177	161	413	186	4.39
126.0	706	138.5	129	162	434	187	2.71
126.5	768	139.0	126	163	456	188	1.77
127.0	800	139.5	125	164	480	199	1.08
127.5	780	140	100	165	499	190	0.672
128.0	854	141	82.3	166	509	191	0.464
128.5	820	142	64.1	167	510	192	0.30
129.0	777	143	57.1	168	508	193	0.21
129.5	819	144	56.4	169	502	194	0.16
130.0	718	145	58.0	170	492	195	0.13
130.5	733	146	65.8	171	470	196	0.11
131.0	699	147	75.2	172	435	197	0.10
131.5	601	148	84.9	173	394	198	0.09
132.0	667	149	101	174	353		
132.5	538	150	120	175	319		

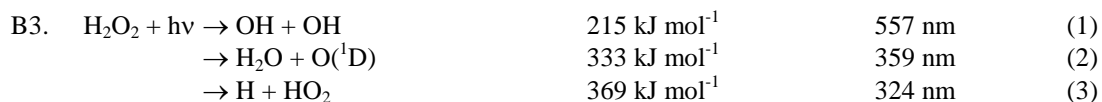
Note:

121.567 nm: Average value (see note)

121 – 182 nm: data integrated from Yoshino et al. [87]

183 – 191 nm: from Cantrell et al. [7]

192 – 198 nm: data interpolated from Parkinson and Yoshino [59]



(Recommendation: 90-1, Note: 10-6, Evaluated: 10-6)

Absorption Cross Sections: Absorption cross sections of hydrogen peroxide, H₂O₂, have been reported by a number of groups as summarized in Table 4B-4. The H₂O₂ spectrum is continuous and the absorption cross sections decrease monotonically from 180 nm toward longer wavelengths. The cross section data from the studies performed after 1972 are in reasonable agreement. Studies prior to 1977 are not considered for the recommendation. Nicovich and Wine [57] measured cross sections relative to the absolute values at 202.6 nm, $\sigma = 4.32 \times 10^{-19}$ cm², and 228.8 nm, $\sigma = 1.86 \times 10^{-19}$ cm², recommended in DeMore et al. [19]. Knight et al. [36] normalized their spectra to the spectra of Nicovich and Wine [57] between 250 nm and 280 nm. The spectra measured by Knight et al. [36] at $\lambda > 290$ nm are in excellent agreement with those reported by Nicovich and Wine [57] at all the temperatures studied. Vatsa and Volpp [81] measured the Lyman- α (121.567 nm) absorption cross section to be 9.8×10^{-18} cm² molecule⁻¹.

Table 4B-4. Summary of H₂O₂ Absorption Cross Section Studies

Study	Year	Wavelength Range (nm)	Temperature (K)
Urey et al. [77]	1929	215 – 275	298
Fergusson et al. [21]	1936	220 – 290	298
Holt et al. [28]	1948	155 – 220	298
Schumb et al. [66]	1955	200 – 400	298
Schürgers and Welge [67]	1968	125 – 200	298
Troe [74]	1969	220 – 290	300
Hochenadel et al. [26]	1972	185 – 260	298
Molina et al. [52]	1977	210 – 350	296
Lin et al. [45]	1978	195 – 350	296
Molina and Molina [51]	1981	190 – 350	298
Nicovich and Wine [57]	1988	193 – 350	296, 285-381
Vaghjiani and Ravishankara [78]	1989	210 – 345	297
Vatsa and Volpp [81]	2001	121.567	300
Knight et al. [36]	2002	250–350	273, 296 and 343

The recommended 298 K absorption cross section values in Table 4B-5 are the mean of the data from Lin et al. [45], Molina and Molina [51], Nicovich and Wine [57], and Vaghjiani and Ravishankara [78]. Molina and Molina [51] supersedes the results of Molina et al. [52].

The temperature dependence of the absorption spectrum has been measured by Nicovich and Wine [57] and Knight et al. [36]. The results of Nicovich and Wine and Knight et al. are in excellent agreement. Nicovich and Wine [57] parameterized the temperature dependence for wavelengths >260 nm as the sum of two temperature dependent components, σ_0 and σ_1 , using the expression given in Table 4B-6. In this parameterization σ_0 represents absorption from the ground vibrational state and σ_1 represents absorption from the O-O stretch vibrational level. For atmospheric model calculations the expression given in Table 4B-6 is recommended.

Table 4B-5. Absorption Cross Sections of H₂O₂ Vapor at 298 and 355 K

λ (nm)	$10^{20} \sigma$ (cm ²)		λ (nm)	$10^{20} \sigma$ (cm ²)	
	298 K	355 K		298 K	355 K
190	67.2	–	275	2.6	2.8
195	56.4	–	280	2.0	2.2
200	47.5	–	285	1.5	1.6
205	40.8	–	290	1.2	1.3
210	35.7	–	295	0.90	1.0
215	30.7	–	300	0.68	0.79
220	25.8	–	305	0.51	0.58
225	21.7	–	310	0.39	0.46
230	18.2	18.4	315	0.29	0.36
235	15.0	15.2	320	0.22	0.27
240	12.4	12.6	325	0.16	0.21
245	10.2	10.8	330	0.13	0.17
250	8.3	8.5	335	0.10	0.13
255	6.7	6.9	340	0.07	0.10
260	5.3	5.5	345	0.05	0.06
265	4.2	4.4	350	0.04	0.05
270	3.3	3.5			

Note:

190 – 350 nm: mean of the data from Lin et al. [45], Molina and Molina [51], Nicovich and Wine [57], and Vaghjiani and Ravishankara [78]

Table 4B-6. Mathematical Expression for Absorption Cross Sections of H₂O₂ as a Function of Temperature

$$10^{21} \sigma(\lambda, T) = \chi \sum_{n=0}^7 A_n \lambda^n + (1 - \chi) \sum_{n=0}^4 B_n \lambda^n$$

where T: temperature K; λ : nm; $\chi = (1 + \exp(-1265/T))^{-1}$

$A_0 = 6.4761 \times 10^4$	$B_0 = 6.8123 \times 10^3$
$A_1 = -9.2170972 \times 10^2$	$B_1 = -5.1351 \times 10^1$
$A_2 = 4.535649$	$B_2 = 1.1522 \times 10^{-1}$
$A_3 = -4.4589016 \times 10^{-3}$	$B_3 = -3.0493 \times 10^{-5}$
$A_4 = -4.035101 \times 10^{-5}$	$B_4 = -1.0924 \times 10^{-7}$
$A_5 = 1.6878206 \times 10^{-7}$	
$A_6 = -2.652014 \times 10^{-10}$	
$A_7 = 1.5534675 \times 10^{-13}$	

Range 260 – 350 nm; 200 – 400 K

Photolysis Quantum Yields and Product Studies. The photodissociation quantum yield is believed to be unity. At and above 248 nm, the major photodissociation process is that leading to OH, i.e., the quantum yield for OH production is 2 (Vaghjani and Ravishankara [79], Vaghjani et al. [80], Riffault et al. [62]). At 248 nm Vaghjani and Ravishankara [79] reported $\Phi(\text{OH}) = 2.09 \pm 0.36$, $\Phi(\text{O}) < 0.002$, and $\Phi(\text{H}) < 0.0002$. Schiffman et al. [65] reported a slightly lower value for $\Phi(\text{OH})$ at 248 nm of 1.58 ± 0.23 ; at 193 nm they obtained $\Phi(\text{OH}) = 1.22 \pm 0.13$. At 222 nm Vaghjani et al. [80] measured $\Phi(\text{OH}) = 2.02 \pm 0.35$, $\Phi(\text{O}) < 0.002$ and $\Phi(\text{H}) = 0.024 \pm 0.012$. At 193 nm they obtained $\Phi(\text{OH}) = 1.51 \pm 0.18$, $\Phi(\text{O}) < 0.02$ and $\Phi(\text{H}) = 0.16 \pm 0.04$. Riffault et al. [62] reported $\Phi(\text{OH})$ values of 1.93 ± 0.39 at 308 nm and 1.96 ± 0.50 at 320 nm. In addition, Gerlach-Meyer et al. [23] reported $\Phi(\text{H}) = 0.12 \pm 0.01$ and Schiffman et al. [65] report $\Phi(\text{OH}) = 1.22 \pm 0.13$ for 193 nm photolysis in reasonable agreement with Vaghjani et al. [80]. An OH quantum yield of 2 for $\lambda > 230$ nm is recommended. For 193 nm $\Phi(\text{OH}) = 1.7$ and $\Phi(\text{H}) = 0.15$ are recommended.

References for Section 4B

1. Aldener, M., S. S. Brown, H. Stark, J. S. Daniel and A. R. Ravishankara, 2005, *J. Mol. Spectrosc.*, 232, 223-230.
2. Bennett, S. W., J. B. Tellinghuisen and L. F. Phillips, 1971, *J. Phys. Chem.*, 75, 719-721.
3. Branton, G. R. and C. E. Brion, 1974, *J. Electron Spectrosc. Relat. Phenom.*, 3, 129-135.
4. Brownsword, R. A., M. Hillenkamp, T. Laurent, R. K. Vatsa, H.-R. Volpp and J. Wolfrum, 1997, *J. Chem. Phys.*, 106, 1359-1366.
5. Calvert, J. G. and J. N. Pitts. In *Photochemistry*; John Wiley & Sons, Inc.: New York, 1966; pp 230-231.
6. Camy-Peyret, C., J.-M. Flaud, J.-Y. Mandin, J.-P. Chevillard, J. Brault, D. A. Ramay, M. Vervloet and J. Chauville, 1985, *J. Mol. Spectrosc.*, 113, 208-228.
7. Cantrell, C. A., A. Zimmer and G. S. Tyndall, 1997, *Geophys. Res. Lett.*, 24, 2195-2198, 2687 (Erratum).
8. Chan, W. F., G. Cooper and C. E. Brion, 1993, *Chem. Phys.*, 178, 387-401.
9. Cheng, B.-M., C.-Y. Chung, M. Bahou, Y.-P. Lee, L. C. Lee, R. van Harreveld and M. C. van Hemert, 2004, *J. Chem. Phys.*, 120, 224-229.
10. Chou, C. C., J. G. Lo and F. S. Rowland, 1974, *J. Chem. Phys.*, 60, 1208-1210.
11. Chung, C.-Y., E. P. Chew, B.-M. Cheng, M. Bahou and Y.-P. Lee, 2001, *Nucl. Instr. Meth. Phys. Res. A*, 467-468, 1572-1576.
12. Coheur, P.-F., S. Fally, M. Carleer, C. Clerbaux, R. Colin, A. Jenouvrier, M.-F. Mérienne, C. Hermans and A. C. Vandaele, 2002, *J. Quant. Spectrosc. Radiat. Transfer*, 74, 493-510.
13. Cox, R. A. and J. P. Burrows, 1979, *J. Phys. Chem.*, 83, 2560-2568.
14. Creasey, D. J., D. E. Heard and J. D. Lee, 2000, *Geophys. Res. Lett.*, 27, 1651-1654.
15. Crowley, J. N., F. G. Simon, J. P. Burrows, G. K. Moortgat, M. E. Jenkin and R. A. Cox, 1991, *J. Photochem. and Photobiol. A: Chem.*, 60, 1-10.
16. Dagaut, P. and M. J. Kurylo, 1990, *J. Photochem. and Photobiol. A: Chem.*, 51, 133-140.
17. de Reilhac, L. and N. Damany, 1970, *Spectrochim. Acta*, 26A, 801-810.
18. DeMore, W. B., 1979, *J. Phys. Chem.*, 83, 1113-1118.
19. DeMore, W. B., D. M. Golden, R. F. Hampson, C. J. Howard, M. J. Kurylo, J. J. Margitan, M. J. Molina, A. R. Ravishankara and R. T. Watson "Chemical Kinetics and Photochemical Data for Use in Stratospheric Modeling, Evaluation Number 7," JPL Publication 85-37, Jet Propulsion Laboratory, California Institute of Technology, Pasadena CA, 1985
20. Fally, S., P.-F. Coheur, M. Carleer, C. Clerbaux, R. Colin, A. Jenouvrier, M.-F. Mérienne, C. Hermans and A. C. Vandaele, 2003, *J. Quant. Spectrosc. Radiat. Transfer*, 82, 119-131.
21. Fergusson, W. C., L. Slotin and W. G. Style, 1936, *Trans. Far. Soc.*, 32, 956-962.
22. Fillion, J.-H., J. Ruiz, X.-F. Yang, M. Castillejo, F. Rostas and J.-L. Lemaire, 2004, *J. Chem. Phys.*, 120, 6531-6541.
23. Gerlach-Meyer, U., E. Linnebach, K. Kleinermans and J. Wolfrum, 1987, *Chem. Phys. Lett.*, 133, 113-115.
24. Gürtler, P., V. Saile and E. E. Koch, 1977, *Chem. Phys. Lett.*, 51, 386-391.
25. Harrison, A. J., B. J. Cederholm and M. A. Terwilliger, 1959, *J. Chem. Phys.*, 30, 355-356.
26. Hochanadel, C. J., J. A. Ghormley and P. J. Ogren, 1972, *J. Chem. Phys.*, 56, 4426-4432.
27. Hofzumahaus, A., T. Brauers, U. Aschmutat, U. Brandenburger, H.-P. Dorn, M. Hausmann, M. Hessling, F. Holland, C. Plass-Dulmer, M. Sedlacek, M. Weber and D. H. Ehhalt, 1997, *Geophys. Res. Lett.*, 24, 3039-3040.
28. Holt, R. B., C. K. McLane and O. Oldenberg, 1948, *J. Chem. Phys.*, 16, 225-229.
29. <http://cfa-www.harvard.edu/amdata/ampdata/cfamols.html>. Harvard-Smithsonian Center for Astrophysics. 2009; Vol. Atomic and Molecular Physics Database.
30. Hudson, R. D., 1971, *Reviews of Geophysics and Space Physics*, 9, 305-399.
31. Hudson, R. D., 1974, *Canad. J. Chem.*, 52, 1465-1478.
32. Hudson, R. D. and L. J. Kieffer. Absorption Cross Sections of Stratospheric Molecules. In *The Natural Stratosphere of 1974*; CIAP, 1975; Vol. Monograph 1; pp (5-156)-(5-194).
33. Kass, S., P. Macko, O. Naumenko and A. Campargue, 2005, *Phys. Chem. Chem. Phys.*, 7, 2460-2467.
34. Katayama, D. H., R. E. Huffman and C. L. O'Bryan, 1973, *J. Chem. Phys.*, 59, 4309-4319.
35. Kley, D., 1984, *J. Atmos. Chem.*, 2, 203-210.
36. Knight, G. P., A. R. Ravishankara and J. B. Burkholder, 2002, *Phys. Chem. Chem. Phys.*, 4, 1432-1437.
37. Kurylo, M. J., T. J. Wallington and P. A. Ouellette, 1987, *J. Photochem.*, 39, 201-215.
38. Laufer, A. M. and J. R. McNesby, 1965, *Can. J. Chem.*, 43, 3487-3490.
39. Lee, L. C., 1980, *J. Chem. Phys.*, 72, 4334-4340.
40. Lee, L. C., 1982, *J. Chem. Phys.*, 76, 4909-4915.
41. Lee, L. C. and M. Suto, 1986, *Chem. Phys.*, 110, 161-169.

42. Lewis, B. R., I. M. Vardavas and J. H. Carver, 1983, *J. Geophys. Res.*, 88, 4935-4940.
43. Lightfoot, P. D., R. A. Cox, J. N. Crowley, M. Destriau, G. D. Hayman, M. E. Jenkin, G. K. Moortgat and F. Zabel, 1992, *Atmos. Environ.*, 26A, 1805-1961.
44. Lightfoot, P. D. and A. A. Jemi-Alade, 1991, *J. Photochem. and Photobiol. A: Chem.*, 59, 1-10.
45. Lin, C. L., N. K. Rohatgi and W. B. DeMore, 1978, *Geophys. Res. Lett.*, 5, 113-115.
46. Mandin, J.-Y., J.-P. Chevillard, C. Camy-Peyret, J.-M. Flaud and J. W. Brault, 1986, *J. Mol. Spectrosc.*, 116, 167-190.
47. Maricq, M. M. and J. J. Szente, 1994, *J. Phys. Chem.*, 98, 2078-2082.
48. McAdam, K., B. Veyret and R. Lesclaux, 1987, *Chem. Phys. Lett.*, 133, 39-44.
49. Mérienne, M.-F., A. Jenouvrier, C. Hermans, A. C. Vandaele, M. Carleer, C. Clerbaux, P.-F. Coheur, R. Colin, S. Fally and M. Bach, 2003, *J. Quant. Spectrosc. Radiat. Transfer*, 82, 99-117.
50. Metzger, P. H. and G. R. Cook, 1964, *J. Chem. Phys.*, 41, 642-648.
51. Molina, L. T. and M. J. Molina, 1981, *J. Photochem.*, 15, 97-108.
52. Molina, L. T., S. D. Schinke and M. J. Molina, 1977, *Geophys. Res. Lett.*, 4, 580-582.
53. Moortgat, G. K., B. Veyret and R. Lesclaux, 1989, *J. Phys. Chem.*, 93, 2362-2368.
54. Mordaunt, D. H., M. N. R. Ashfold and R. N. Dixon, 1994, *J. Chem. Phys.*, 100, 7360-7375.
55. Mota, R., R. Parafita, A. Giuliani, M.-J. Hubin-Franskin, J. M. C. Lourenço, G. Garcia, S. V. Hoffmann, M. J. Mason, P. A. Ribeiro, M. Raposo and P. Limão-Vieira, 2005, *Chem. Phys. Lett.*, 416, 152-159.
56. Nicolet, M., 1981, *J. Geophys. Res.*, 86, 5203-5208.
57. Nicovich, J. M. and P. H. Wine, 1988, *J. Geophys. Res.*, 93, 2417.
58. Okabe, H. In *Photochemistry of Small Molecules*; John Wiley and Sons Inc.: New York, 1978; pp 217.
59. Parkinson, W. H. and K. Yoshino, 2003, *Chem. Phys.*, 294, 31-35.
60. Paukert, T. T. and H. S. Johnston, 1972, *J. Chem. Phys.*, 56, 2824-2838.
61. Phillips, E., L. C. Lee and D. L. Judge, 1977, *J. Quant. Spectrosc. Radiat. Transfer*, 18, 309-313.
62. Riffault, V., T. Gierczak, J. B. Burkholder and A. R. Ravishankara, 2006, *Phys. Chem. Chem. Phys.*, 8, 1079 - 1085.
63. Roehl, C. M., D. Bauer and G. K. Moortgat, 1996, *J. Phys. Chem.*, 100, 4038-4047.
64. Sander, S. P., M. Peterson, R. T. Watson and R. Patrick, 1982, *J. Phys. Chem.*, 86, 1236-1240.
65. Schiffman, A., D. D. Nelson, Jr. and D. J. Nesbitt, 1993, *J. Chem. Phys.*, 98, 6935-6946.
66. Schumb, W. C., C. N. Satterfield and R. L. Wentworth; Reinhold Publishing Corporation: New York, 1955.
67. Schürgers, M. and K. H. Welge, 1968, *Z. Naturforsch.*, 23a, 1508-1510.
68. Slinger, T. G. and G. Black, 1982, *J. Chem. Phys.*, 77, 2432-2437.
69. Stief, L. J., W. A. Payne and R. B. Klemm, 1975, *J. Chem. Phys.*, 62, 4000-4008.
70. Tan, K. H., C. E. Brion, P. E. v. d. Leeuw and M. J. v. d. Wiel, 1978, *Chem. Phys.*, 29, 299-309.
71. Tanaka, M., J. W. Brault and J. Tennyson, 2002, *J. Molec. Spectrosc.*, 216, 77-80.
72. Tanaka, M., M. Snee, W. Ubachs and J. Tennyson, 2004, *J. Molec. Spectrosc.*, 226, 1-6.
73. Thompson, B. A., P. Harteck and R. R. Reeves Jr., 1963, *J. Geophys. Res.*, 68, 6431-6436.
74. Troe, J., 1969, *Ber. Bunsenges.*, 73, 946-952.
75. Tyndall, G. S., R. A. Cox, C. Granier, R. Lesclaux, G. K. Moortgat, M. J. Pilling, A. R. Ravishankara and T. J. Wallington, 2001, *J. Geophys. Res.*, 106, 12157-12182.
76. Ung, A. Y.-M., 1974, *Chem. Phys. Lett.*, 28, 603-607.
77. Urey, H. C., L. H. Dawsey and F. O. Rice, 1929, *J. Am. Chem. Soc.*, 51, 1371-1383.
78. Vaghjiani, G. L. and A. R. Ravishankara, 1989, *J. Geophys. Res.*, 94, 3487-3492.
79. Vaghjiani, G. L. and A. R. Ravishankara, 1990, *J. Chem. Phys.*, 92, 996-1003.
80. Vaghjiani, G. L., A. A. Turnipseed, R. F. Warren and A. R. Ravishankara, 1992, *J. Chem. Phys.*, 96, 5878.
81. Vatsa, R. K. and H.-R. Volpp, 2001, *Chem. Phys. Lett.*, 340, 289-295.
82. Wainfan, N., W. C. Walker and G. L. Weissler, 1955, *Phys. Rev.*, 99, 542-549.
83. Wallington, T. J., P. Dagaut and M. J. Kurylo, 1992, *Chem. Rev.*, 92, 667-710.
84. Watanabe, K. and A. S. Jursa, 1964, *J. Chem. Phys.*, 41, 1650-1653.
85. Watanabe, K. and M. Zelikoff, 1953, *J. Opt. Soc. Am.*, 43, 753-755.
86. Wilkinson, P. G. and H. L. Johnston, 1950, *J. Chem. Phys.*, 18, 190-193.
87. Yoshino, K., J. R. Esmond, W. H. Parkinson, K. Ito and T. Matsui, 1997, *Chem. Phys.*, 215, 429-430.

SECTION 4C. NO_x PHOTOCHEMISTRY



(Recommendation: 06-2, Note: 10-6, Evaluated: 10-6)

Absorption Cross Sections: The UV/vis absorption spectrum of nitrogen dioxide, NO₂, in the 200 – 800 nm region can be separated into two principal systems: the D-X band below 250 nm and the broad B-X and A-X bands between 300 and 800 nm with a maximum around 400 nm. The forbidden C-X transition also contributes to the visible spectrum. There is enormous spectral fine structure superimposed on the broad visible system. Due to the complexity of the electronic states of NO₂, it is impossible to predict its spectrum from molecular quantum theory within the accuracy of the experimental measurements. The absorption spectrum and cross sections of NO₂ have been extensively studied during the last century as summarized in Table 4C-1.

Table 4C-1. Summary of NO₂ Absorption Cross Section Studies

Study	Year	λ Range (nm)	Type	Resolution (nm)	Temperature (K)
Holmes and Daniels [57]	1934	265 – 436	B	1	298
Dixon [31]	1940	400 – 700	A	1.5 and 4.0	295
Hall and Blacet [48]	1952	240 – 500	A	0.2-0.5	298
Nakayama et al. [90]	1959	108 – 270	A	0.02	300
Jones and Bayes [69]	1973	297 – 579	B	0.2	300
Johnston and Graham [65]	1974	190 – 420	A	1.3	294
Bass et al. [4]	1976	185 – 410	B	0.015 – 0.04	235 and 298
Harker et al. [50]	1977	375 – 420	B	0.1	296
Hicks et al. [55]	1979	425 – 450 at single λ	B	0.04	235 and 298
Schneider et al. [123]	1987	200 – 700	A	0.04	298
Leroy et al. [75]	1987	427 – 450	B	0.04	235 and 298
Koffend et al. [74]	1987	391 – 414/ intervals	B	0.005	251 and 300
Calvert et al. [16]	1987	404.7	B	1.6	223, 273, 298, 325, 347, 370, 406, 496, 566
Davidson et al. [28]	1988	264 – 649	A	1.5 0.3 – 2.6 cm ⁻¹	233, 243, 253, 263, 273, 298, and up to 397
Corcoran et al. [22]	1992	450 – 650 470 – 616	A, B	0.075 0.008	295, 573, 673
Amoruso et al. [2]	1993	440 – 460	B	0.134	220 and 298
Harwood and Jones [52]	1994	313 – 568	A	0.54	213, 225, 233, 243, 253, 263, 273, 298
Mérierne et al. [84]	1995	300 – 500	A	0.01 – 0.015	293
Coquart et al. [21]	1995	400 – 500	B	0.01	220, 240, 293
Vandaele et al. [140]	1996	380 – 830	A	2.0 cm ⁻¹	294
Frost et al. [37]	1996	370 – 497	A	0.5 – 2.0 cm ⁻¹	220
Jenouvrier et al. [59]	1996	200 – 300	B	0.01	293
Mihalcea et al. [85]	1996	395, 670	B	0.001	296-774
Harder et al. [49]	1997	350 – 585 (294 K) 350 – 560 (low T)	A	0.15 cm ⁻¹	217, 230.2, 238.6, 293.8
Yoshino et al. [153]	1997	360 – 470	B	0.14 cm ⁻¹	298.5
Mérierne et al. [82]	1997	200 – 400	A	0.05	220
Vandaele et al. [141]	1998	238 – 1000	A	2.0 cm ⁻¹	220 and 294

Study	Year	λ Range (nm)	Type	Resolution (nm)	Temperature (K)
Burrows et al. [13]	1998	231 – 794	C	0.2 – 0.4	221, 241, 273, 293
Orphal et al. [98]	1998	667 – 1111	B	0.012 cm ⁻¹	298
Gierczak et al. [40]	1999	413.4	B	1	259, 298, 323, 348, 385
Voigt et al. [143]	2002	250 – 800	A	0.5 – 1.0 cm ⁻¹	223, 246, 260, 280, 293
Vandaele et al. [138]	2002	385 – 925	A	0.05 – 0.1 cm ⁻¹	220, 240, 294
Bogumil et al. [7]	2003	230 – 1070	C	0.2 – 0.4	203, 223, 243, 273, 293
Nizkorodov et al. [92]	2004	415 – 525	B	0.06 cm ⁻¹	215, 230, 250, 273, 298

The studies summarized in Table 4C-1 are organized into three measurement categories: *type A*, *absolute* cross section measurements over a broad spectral region (typically covering a few hundred nm); *type B*, *absolute* cross section measurements at specific wavelengths or over narrow spectral ranges; and *type C*, *relative* NO₂ absorption spectrum measurements over broad spectral region (typically a few hundred nm) that have been scaled to absolute cross section values using results from other studies.

In the earlier studies, the NO₂ ultraviolet-visible absorption cross section measurements were limited to lower spectral resolution. Since 1992, however, several sets of high resolution measurements, including temperature and pressure dependence studies, have been reported by several groups, which mainly aimed at improving the accuracy of atmospheric measurements, in particular, for the atmospheric remote sensing of NO₂. However, a number of laboratory measurements were also obtained at spectral resolutions that are limited by instrumental techniques.

The previous recommendations (JPL-97-04) [30] for the absorption cross sections of NO₂ were based on the work of Bass et al. [4], Schneider et al. [123] and Davidson et al. [28]. Although at room temperature the agreement between these three sets of measurements is good (within 5% between 305 and 345 nm and within 10% at the longer wavelengths), serious non-uniform wavelength calibration errors are apparent in the wavelength range 400 – 500 nm as described by Schneider et al. [123]. At shorter wavelengths and for temperatures below 298 K the agreement among these three sets of data is poor. A possible cause for the discrepancies is the presence of N₂O₄, which is the weakly bound NO₂ dimer present in equilibrium with the monomer. The ratio of the abundance of the two species is concentration and temperature dependent. Corrections were needed to account for the presence of N₂O₄ at wavelengths below 400 nm and especially near 200 nm where N₂O₄ absorbs strongly.

Kirmse et al. [72] analyzed the spectra reported between 1976 and 1995 and concatenated selected (and corrected) cross sections to create a “new standard” spectrum in the range 300 – 708 nm at a resolution of 0.05 nm, and another spectrum extending to 908 nm at a lower resolution of 1 nm. This high resolution “new standard” spectrum consisted of the Mérieu et al. (1995) [84] cross sections from 300 to 500 nm, the Corcoran et al. [22] cross sections from 500 to 600 nm, and the Schneider et al. [123] cross sections from 600 to 710 nm. A critical review and evaluation of the cross section studies has been recently performed by Orphal (2002) [96] and Orphal (2003) [99], covering most studies published since 1995. In his evaluation Orphal [96, 99] considered baseline problems, wavelength calibration and integrated cross sections (after convolution of high resolution cross sections of 0.1 nm or better). In addition, Vandaele et al. (2003) [139] derived temperature and pressure dependent parameters from high resolution spectral data obtained since 1995.

At room temperature (295 ± 3 K) there is excellent agreement (better than 2-3%) between the absolute cross sections over the wavelength range covered by the measurements of Mérieu et al. (1995) [84], Coquart et al. [21], Vandaele et al. (1996) [140], Jenouvrier et al. [59], Yoshino et al. [153], Mérieu et al. (1997) [82], Vandaele et al. (1998) [141], Bogumil et al. [7], and Nizkorodov et al. [92]. Many of these studies differ in spectral resolution, an issue relevant to atmospheric remote sensing applications. The cross sections of Harwood and Jones [52] are 6-8% below most of the other studies, while the data of Harder et al. [49] are slightly but systematically higher than the data of Vandaele et al. (1998) [141] (i.e. 2-5%) and show a systematic baseline drift of up to 10% at the lowest temperature.

The newest high pressure cross sections data of Vandaele et al. (2002) [138] and Vandaele et al. (2003) [139] are nearly 4% smaller than the Vandaele et al. (1996) [140] and Vandaele et al. (1998) [141] data. The cross

sections of Burrows et al. [13] are about 6-8% lower than most recent high resolution studies (Mérieu-95, Mérieu-97, Harder, Vandaele-96, Vandaele-98). The data of Voigt et al. [143] show several artificial peaks (probably Xenon lamp stray light) of a few percent and baseline shifts up to 10% (partly due to residual N₂O₄ absorption) at lower temperatures. The spectra of Bogumil et al. [7] were scaled to absolute values using the integrated cross section of Vandaele et al. (1998) [141].

The temperature effect on the NO₂ absorption cross sections has been studied by only a few research teams, as can be seen in Table 4C-1. The variation of the absorption consists mainly in an increase of the differential absorption cross sections with decreasing temperature. In his analysis of the temperature dependence of the cross sections in the 300 – 700 nm region, Orphal (2003) [97] observed a tilt in the baseline with decreasing temperature in the data of Davidson et al. [28], Burrows et al. [13], Bogumil et al. [7] but less pronounced in the data of Harwood and Jones [52], Harder et al. [49], and Vandaele et al. (2002) [138]. This is due to a change in the thermal population of the lower vibrational and rotational states causing large discrepancies in the relative change and the absolute magnitude of the absorption cross sections. The comparison of the high resolution absolute cross sections at temperatures below ambient reveals significant discrepancies in absolute magnitude of cross sections due to spectral resolution, baseline differences and possible wavelength calibration. For the temperatures 242 ± 2 and 220 ± 3 K, the overall agreement is within 15% in the region 350 – 500 nm, however outside this range the discrepancies are much larger. The integrated cross sections for the range 400 – 500 nm were calculated by Orphal (2003) [97] to be $(4.50 \pm 0.10) \times 10^{-17} \text{ cm}^2 \text{ molecule}^{-1} \text{ nm}$ and are independent of temperature, as recently shown by Nizkorodov et al. [92] for the temperature range 215 – 298 K.

Orphal (2003) [97] and Vandaele et al. (2003) [139] compared the spectra after degrading the high resolution spectra to a lower resolution. At 220 K the best agreement (within 1.6%) is obtained between the data of Coquart et al. [21], Mérieu et al. (1997) [82] and Vandaele et al. (1998) [141]. The data of Harder et al. [49] differ by 3.7% from the Vandaele et al. (1998) [141] data below 500 nm but seem to contain more noise at larger wavelengths. The data of Voigt et al. [143] show larger disagreement, different at every temperature set. At 223 K their data are 22% lower than the Vandaele et al. (1998) [141] values.

The temperature dependence of the NO₂ cross sections in the entire ultraviolet and visible regions can be reproduced within the experimental uncertainties using analytical expressions at least at low and moderate spectral resolutions (i.e. 0.05 nm and less). Linear functions were proposed by Davidson et al. [28], Kirmse et al. [72], and Vandaele et al. (2002) [138], a quadratic polynomial by Burrows et al. [13], and a double exponential function by Voigt et al. [143]. For the high resolution spectra Nizkorodov et al. [92] concluded that a linear temperature dependence is not valid, and a successful parameterization needs further work.

The NO₂ cross sections vary as a function of total pressure but these effects are only observed at high spectral resolution, i.e. better than 0.01 nm, as investigated by Harder et al. [49], Wennberg et al. [148], Vandaele et al. (1998) [141], Voigt et al. [143], Vandaele et al. (2002) [138], and Nizkorodov et al. [92], using NO₂/N₂ (or air) mixtures at total pressures up to 1 atm. Nizkorodov et al. [92] showed that a simple Lorentzian broadening model with linear dependence of the Lorentz width on pressure provides an adequate description of the pressure broadening effects in NO₂.

The current recommendation is based on the data of Vandaele et al. (1998) [141]. Table 4C-2 lists cross sections for 294 and 220 K averaged over atmospheric intervals.

Photolysis Quantum Yield and Product Studies: A number of studies of quantum yields of NO₂ photolysis for the atmospherically important 300 – 470 nm region have been reported: Jones and Bayes [69] for the wavelength range 295 – 445 nm and at 492 nm, 546 nm and 579 nm; Gaedtke and Troe [38] in the range 313 – 416 nm; Harker et al. [50] for the range 375 – 420 nm at 1 nm intervals; Davenport [27] for the range 390 – 420 nm at 223 and 300 K; Gardner et al. [39] for the range 334 – 404 nm at 298 K, and at 404 nm at 273 and 370 K; and Roehl et al. [117] in the range 388 – 411 nm at 248 and 298 K. In the range 360 – 398 nm the Φ_1 values show a wide scatter, with differences as much as 60%, especially due to the data of Harker et al. [50]. Although Gardner et al. [39] obtained values of Φ_1 between 0.89 ± 0.05 and 0.97 ± 0.06 in the range 379 – 397 nm, they made a critical assessment of the quantum yield data and recommended that Φ_1 is near unity at wavelengths up to and slightly beyond the dissociation limit of $\lambda_0 = 397.95 \text{ nm}$ (Jost et al., [70]) and then rapidly decreases to near zero at 424 nm. However Roehl et al. [117] determined $\Phi_1 = (0.93 \pm 0.10)$ in the range 388 – 398 nm at 298 K, and $\Phi_1 = (0.90 \pm 0.10)$ at 248 K. Troe [135] made a critical reanalysis of the quantum yield data of Gardner et al. [39] and Roehl et al. [117] below λ_0 and concluded that certain secondary reactions were not correctly accounted for, and recommended corrections for both data sets. The recommended quantum yield values in Table 4C-3 are based on the data of Roehl et al. [117] as corrected by Troe [135].

Table 4C-2. Absorption Cross Sections of NO₂ at 220 and 294 K

λ (nm)	$10^{20} \sigma(220 \text{ K})$ (cm ²)	$10^{20} \sigma(294 \text{ K})$ (cm ²)	λ (nm)	$10^{20} \sigma(220 \text{ K})$ (cm ²)	$10^{20} \sigma(294 \text{ K})$ (cm ²)
240.964 – 243.902	4.14	5.77	442.5 – 447.5	47.9	48.8
243.902 – 246.914	0.961	2.79	447.5 – 452.5	49.3	49.8
246.914 – 250.000	0.859	1.62	452.5 – 457.5	40.6	41.6
250.000 – 253.165	0.191	0.998	457.5 – 462.5	43.5	43.6
253.165 – 256.410	0.496	1.05	462.5 – 467.5	41.5	41.4
256.410 – 259.740	0.872	1.28	467.5 – 472.5	32.7	33.7
259.740 – 263.158	1.26	1.58	472.5 – 477.5	38.8	38.7
263.158 – 266.667	1.77	2.05	477.5 – 482.5	33.4	33.7
266.667 – 270.270	2.36	2.64	482.5 – 487.5	24.0	25.4
270.270 – 273.973	3.03	3.24	487.5 – 492.5	30.9	30.8
273.973 – 277.778	3.94	4.07	492.5 – 497.5	29.4	29.4
277.778 – 281.690	5.16	5.21	497.5 – 502.5	16.7	18.2
281.690 – 285.714	6.29	6.23	502.5 – 507.5	24.4	24.3
285.714 – 289.855	7.72	7.59	507.5 – 512.5	22.8	23.1
289.855 – 294.118	9.64	9.51	512.5 – 517.5	14.8	16.0
294.118 – 298.507	11.6	11.5	517.5 – 522.5	17.7	16.1
298.507 – 303.030	13.2	13.2	522.5 – 527.5	17.5	17.9
303.030 – 307.692	16.0	16.1	527.5 – 532.5	14.9	15.3
307.692 – 312.5	18.5	18.8	532.5 – 537.5	9.71	10.6
312.5 – 317.5	20.8	21.6	537.5 – 542.5	10.3	10.8
317.5 – 322.5	24.2	25.3	542.5 – 547.5	12.6	12.7
322.5 – 327.5	27.2	28.7	547.5 – 552.5	10.4	11.0
327.5 – 332.5	29.4	31.7	552.5 – 557.5	7.40	7.97
332.5 – 337.5	33.0	35.8	557.5 – 562.5	5.56	6.05
337.5 – 342.5	37.0	40.2	562.5 – 567.5	8.62	8.70
342.5 – 347.5	38.6	41.8	567.5 – 572.5	8.25	8.48
347.5 – 352.5	43.5	46.2	572.5 – 577.5	4.12	4.71
352.5 – 357.5	47.7	49.7	577.5 – 582.5	4.11	4.47
357.5 – 362.5	49.2	50.9	582.5 – 587.5	4.60	4.69
362.5 – 367.5	53.7	54.9	587.5 – 592.5	5.14	5.39
367.5 – 372.5	55.2	56.1	592.5 – 597.5	3.82	4.08
372.5 – 377.5	58.4	59.0	597.5 – 602.5	3.71	3.95
377.5 – 382.5	58.5	59.3	602.5 – 607.5	1.56	1.85
382.5 – 387.5	59.2	60.1	607.5 – 612.5	2.38	2.54
387.5 – 392.5	62.4	63.0	612.5 – 617.5	3.47	3.53
392.5 – 397.5	58.5	59.7	617.5 – 622.5	2.39	2.57
397.5 – 402.5	64.0	64.4	622.5 – 627.5	1.77	1.96
402.5 – 407.5	57.0	58.2	627.5 – 632.5	1.00	1.21
407.5 – 412.5	61.8	62.4	632.5 – 637.5	1.23	1.33
412.5 – 417.5	58.3	59.1	637.5 – 642.5	1.48	1.53
417.5 – 422.5	59.3	59.9	642.5 – 647.5	1.86	1.92
422.5 – 427.5	56.0	57.0	647.5 – 652.5	1.24	1.35
427.5 – 432.5	53.7	54.4	652.5 – 657.5	0.755	0.873
432.5 – 437.5	55.5	55.9	657.5 – 662.5	0.508	0.566
437.5 – 442.5	47.5	48.8			

Note:

Vandaele et al., 1998 [141]

Table 4C-3. Quantum Yields for NO₂ Photolysis

λ (nm)	$\Phi(298\text{ K})$	$\Phi(248\text{ K})$
300 – 398	1.00	1.00
399	0.95	0.94
400	0.88	0.86
401	0.75	0.69
402	0.62	0.56
403	0.53	0.44
404	0.44	0.34
405	0.37	0.28
406	0.30	0.22
407	0.26	0.18
408	0.22	0.14
409	0.18	0.12
410	0.15	0.10
411	0.13	0.08
412	0.11	0.07
413	0.09	0.06
414	0.08	0.04
415	0.06	0.03
416	0.05	0.02
417	0.04	0.02
418	0.03	0.02
419	0.02	0.01
420	0.02	0.01
422	0.01	0.01

Note:

Roehl et al. [117] as corrected by Troe [135]



(Recommendation: 06-2; Note: 10-6; Evaluated: 10-6)

Absorption Cross Sections: The vis absorption spectrum of the NO₃ radical contains ~20 diffuse bands between 400 and 700 nm, Figure 4C-1. The most intense features are the bands for the 0-0 and 1-0 transitions in the symmetric N-O stretching vibration in the excited state that are centered at 662 and 623 nm, respectively. The absorption cross section of the 0-0 band at 662 nm is of special interest, since it is commonly used to monitor NO₃ both in the laboratory and in the atmosphere.

The absorption cross sections of NO₃ have been the subject of many laboratory studies. The spectroscopy of NO₃ has been reviewed by Wayne et al. [147]. Although there is good agreement for the positions of the absorption features, the range in reported absolute cross sections is nearly a factor of two. The studies and reported cross sections values at the 662 nm peak are summarized in Table 4C-4.

Table 4C-4. Summary of NO₃ Absorption Cross Section Studies

	Study	Year	NO ₃ source Technique	T (K)	λ (nm)	Resolution (nm)	$\sigma(662\text{ nm})$ (10 ⁻¹⁷ cm ²)
1	Schott and Davidson [124]	1958	N ₂ O ₅ Shock pyrolysis	600, 650, 825, 1025	366 – 652	3.6	1.15 ± 0.4 ¹⁾
2	Johnston and Graham [65]	1974	N ₂ O ₅ + O ₃ Equilibrium constant calculation	295	450 – 680	0.7	0.347 (±50%) 1.48 ²⁾
3	Graham and Johnston [42]	1978	N ₂ O ₅ + O ₃ Modulated photolysis	298	400 – 704	0.83	1.708

	Study	Year	NO ₃ source Technique	T (K)	λ (nm)	Resolution (nm)	$\sigma(662 \text{ nm})$ (10 ⁻¹⁷ cm ²)
4	Mitchell et al. [86]	1980	NO ₂ + O ₃ Dual beam spectrometer	294 ± 4	498 – 671	0.05	1.21 ± 0.20
5	Marinelli et al. [80]	1982	NO ₂ + O ₃ Tunable dye laser abs.	296	654 – 671	0.05	1.90
6	Ravishankara and Wine [110]	1983	F + HNO ₃ Discharge flow, dye laser	298	565 – 673	0.05	1.78 ± 0.23
7	Cox et al. [23]	1984	Cl + ClONO ₂ Modulated photolysis, diode array spectrometer	296	662	0.4	1.63 ± 0.15
8	Burrows et al. [15]	1985	F + HNO ₃ , Cl + HNO ₃ Modulated photolysis	298	615 – 670	1	1.85 ± 0.56
9	Ravishankara and Mauldin [109]	1986	F + HNO ₃ Discharge flow, dye laser abs.	298	652.5- 672.5	0.05	1.90 ± 0.22
				240			2.31 ± 0.23
				220			2.71 ± 0.27
10	Sander [121]	1986	Cl + ClONO ₂ Flash photolysis, diode array spectrometer F + HNO ₃ Discharge flow	298	220 – 700	~0.4	2.28 ± 0.12 2.28 ± 0.34 ³⁾
				250			2.62 ± 0.13
				230			2.70 ± 0.14
				298			1.83 ± 0.27
11	Canosa-Mas et al. [17]	1987	F + HNO ₃ Discharge flow	296 ± 3	662	1.1	2.23 ± 0.35
12	Cantrell et al. [18]	1987	NO ₂ + O ₃ Fourier transform spectroscopy	348	662	0.22 (5 cm ⁻¹)	2.06 ± 0.27
				323			2.13 ± 0.22
				298			2.02 ± 0.20
				271			2.08 ± 0.18
				253			1.84 ± 0.43
				232			2.22 ± 0.33
				215			2.02 ± 0.24
				215-348			2.06 ± 0.32 (average)
13	Yokelson et al. [152]	1994	Cl + ClONO ₂ Flash photolysis, diode array spectrometer	298	440–720	~0.1	2.23 ± 0.09
				258			2.49 ± 0.13
				230			2.76 ± 0.13
				200			2.99 ± 0.14
14	Wängberg et al. [146]	1997	N ₂ O ₅ ↔ NO ₃ + NO ₃ Differential optical absorption spectroscopy	279.6- 294.2	603–682	0.42	scaled to 2.10 ⁴⁾
15	Orphal et al. [99]	2003	N ₂ O ₅ + O ₃ Fourier transform spectroscopy	294	465–794	0.6 cm ⁻¹ (0.026 nm at 662 nm)	2.18
16	Osthoff et al. [101]	2007	NO ₃ + NO ₃ ↔ N ₂ O ₅ Cavity ring-down spectroscopy	298	662.2 (vac)	0.5 cm ⁻¹	2.30 ± 0.19
				308			2.16 ± 0.18
				318			1.98 ± 0.17
				333			1.96 ± 0.16
				353			1.68 ± 0.13
				373			1.60 ± 0.13
				388			1.55 ± 0.12

¹⁾ Estimate for 300 K by Wayne et al. [147] from the data of Schott and Davidson [124].

²⁾ Improvement by Graham and Johnston [42] using their more actual kinetic data.

³⁾ The overall uncertainty (± 15%) includes the uncertainty of the absorbance measurement (± 5%) and the uncertainty of $\sigma(\text{ClONO}_2)$ (± 10%). The value for $\sigma(662 \text{ nm})$ obtained by the flash photolysis method is preferred by Sander [121] over that obtained by the discharge flow method.

⁴⁾ Recommendation by Wayne et al. [147].

The JPL-02 evaluation recommended a cross section value of $(2.00 \pm 0.25) \times 10^{-17} \text{ cm}^2 \text{ molecule}^{-1}$ at 662 nm derived from an average of the results from studies 5, 6, and 8-12 given in Table 4C-4. The recommendation by Wayne et al. [147] averaged the data of the more recent studies, studies 9-12, and resulted in a slightly higher value of $(2.10 \pm 0.20) \times 10^{-17} \text{ cm}^2 \text{ molecule}^{-1}$. Higher values for the absorption cross section at 662 nm were obtained in the more recent studies by Yokelson et al. [152] and Orphal et al. [99]. Here, the results from Sander [121] and Yokelson et al. [152] are averaged to derive a recommended cross section of $(2.25 \pm 0.15) \times 10^{-17} \text{ cm}^2 \text{ molecule}^{-1}$ at 662 nm. The recommended absorption cross sections at other wavelengths in Table 4C-5 are taken from Sander [121] after normalization to this value, which is actually only a reduction of 1.3% from the originally reported data.

The studies of the absorption spectrum temperature dependence indicate an increase of the 662 nm peak absorption cross section with decreasing temperature. At the 662 nm peak an increase by 42% between 298 and 220 K was reported by Ravishankara and Mauldin [109], by 17% between 298 and 230 K by Sander [121], and increases of 34% between 298 and 200 K and 24% between 298 and 230 K by Yokelson et al. [152], and a decrease of 48% between 298 and 388 K by Osthoff et al. [101]. Cantrell et al. [18] report a temperature independent cross section over the temperature range 210 – 348 K of $2.06 \times 10^{-17} \text{ cm}^2 \text{ molecule}^{-1}$ that is in disagreement with the findings from the other studies. Osthoff et al. [101] combined their data with the data from Yokelson et al. [152] and slightly modified the parameterization given by Yokelson et al. [152] for the peak cross section temperature dependence as

$$\sigma(662 \text{ nm}, T) = (4.582 \pm 0.096) - [(0.00796 \pm 0.0031) \times T] \times 10^{-17} \text{ cm}^2 \text{ molecule}^{-1}$$

for the range 220 – 388 K. Orphal et al. [99] interpreted the temperature dependence as resulting from changes in the ground vibrational state population of NO_3 (D_{3h} symmetry) and derived a formula for the cross section ratio as function of temperature

$$\sigma(T)/\sigma(298\text{K}) = [1 - \exp(-1096.4/T) - 2 \exp(-529.5/T)] / [1 - \exp(-1096.4/298.0) - 2 \exp(-529.5/298.0)]$$

where the values of 1096.4 K and 529.5 K are the vibrational energies of 762 cm^{-1} and 368 cm^{-1} divided by the Boltzmann constant. There is excellent agreement between the calculated temperature dependence using the Orphal model and the empirical relationships from Yokelson et al. [152] and Osthoff et al. [101].

Photolysis Quantum Yield and Product Studies: The quantum yields Φ_1 and Φ_2 have been measured by Graham and Johnston [42], and at higher spectral resolution by Magnotta and Johnston [78], who report the product of the cross section times the quantum yield in the 400 to 630 nm range. The total quantum yield value, $\Phi_1 + \Phi_2$, computed from the results of Magnotta and Johnston [78] and the cross sections of Graham and Johnston [42], is about 1.5 for $\lambda < 585 \text{ nm}$, based on the nearly constant yield of the major product $\text{O}(^3\text{P})$, and a quantum yield for the NO production Φ_1 near zero. Because systematic errors seem to exist in these data, in their review Wayne et al. [147] normalized Φ_2 quantum yields to unity at $\lambda < 585 \text{ nm}$. The quantum yield for the NO production Φ_1 increases from zero at 585 nm to a maximum of $\Phi_1 = 0.35$ at 595 nm, where $\Phi_2 = 0.65$. At longer wavelengths both quantum yields Φ_1 and Φ_2 decrease to zero at $\lambda = 640 \text{ nm}$. Orlando et al. [95] measured the $\text{O}(^3\text{P})$ and NO quantum yields in the photolysis of NO_3 between 570 and 635 nm. They qualitatively confirm the earlier measurements by Johnston and coworkers but provide more accurate data for both channels. The $\text{O}(^3\text{P})$ quantum yield was found to be unity in the wavelength range 570 – 585 nm and to decrease to 0.1 at 635 nm. They observed anomalously low $\text{O}(^3\text{P})$ yields in the region of the strong absorption band near 623 nm. The quantum yields for NO formation were < 0.10 at 580 nm and 0.20 ± 0.10 near 590 nm. The wavelength dependence of Φ_1 and Φ_2 are similar to those recommended in the review of Wayne et al. [147].

In a molecular beam study, Davis et al. [29] investigated the photodissociation processes of NO_3 over the wavelength range 532 – 662 nm and determined a sharp threshold for the dissociation of internally cold NO_3 into NO_2 and $\text{O}(^3\text{P})$ at 587 nm. At shorter wavelengths, e.g., 585 nm, the $\text{NO} + \text{O}_2$ yield dropped to < 0.05 . At excitation energies just below this threshold, i.e., $\lambda = 588 \text{ nm}$, a large quantum yield (0.70 ± 0.10) for a concerted three-center rearrangement was observed, resulting in $\text{NO} + \text{O}_2(^3\Sigma_g^-, ^1\Delta)$. The yield of this $\text{NO} + \text{O}_2$ process decreases at longer wavelengths to zero at 613 nm. At $\lambda > 588 \text{ nm}$ the $\text{O} + \text{NO}_2$ channel yield arises from vibrational excitation of the ground electronic state of NO_3 . These results imply that for thermally equilibrated NO_3 the branching ratios for dissociation of both channels (1) and (2) will strongly depend on temperature, especially near the threshold wavelength.

Johnston et al. [63] re-analyzed the available laboratory data relevant to NO_3 photolysis, including quantum yield data for NO and NO_2 formation, fluorescence, and threshold energies reported in the molecular beam study. Their model reproduces the wavelength dependent quantum yield values for $\Phi(\text{O} + \text{NO}_2)$, $\Phi(\text{NO} + \text{O}_2)$ and $\Phi(\text{fluorescence})$ at 190, 230, and 298 K. At 298 K the calculated $\Phi(\text{O} + \text{NO}_2)$ quantum yields agree reasonably well with those obtained by Orlando et al. [95], but shows a systematic offset in the wavelength

range 605 – 620 nm. The calculated $\Phi(\text{NO} + \text{O}_2)$ product yield agrees with those reported by Magnotta and Johnston [78] within the scatter of the experimental data.

The recommended quantum yields in Table 4C-6 over the wavelength range 685 – 640 nm at 190, 230, and 298 K are taken from Johnston et al. [63]. For $\lambda < 585$ nm, $\Phi(\text{O} + \text{NO}_2) = 1$, and $\Phi(\text{NO} + \text{O}_2) = 0$ and for $\lambda > 640$ nm $\Phi(\text{O} + \text{NO}_2)$ and $\Phi(\text{NO} + \text{O}_2)$ are zero. Photodissociation rates have been calculated by Johnston et al. [63] for overhead sun in the stratosphere to be

$$J(\text{NO} + \text{O}_2) = 0.0201 \text{ s}^{-1}$$

$$J(\text{NO}_2 + \text{O}) = 0.156 \text{ s}^{-1}$$

Table 4C-5. Absorption Cross Sections of NO_3 at 298 K

λ (nm)	$10^{20} \sigma$ (cm^2)	λ (nm)	$10^{20} \sigma$ (cm^2)	λ (nm)	$10^{20} \sigma$ (cm^2)	λ (nm)	$10^{20} \sigma$ (cm^2)	λ (nm)	$10^{20} \sigma$ (cm^2)
403	2	461	41	519	165	577	362	635	154
404	0	462	42	520	180	578	354	636	181
405	3	463	43	521	196	579	347	637	222
406	2	464	51	522	206	580	358	638	217
407	1	465	54	523	189	581	380	639	169
408	3	466	58	524	176	582	351	640	132
409	0	467	61	525	169	583	314	641	108
410	1	468	60	526	175	584	302	642	99
411	2	469	62	527	193	585	310	643	104
412	5	470	63	528	225	586	355	644	102
413	5	471	66	529	257	587	446	645	92
414	2	472	69	530	239	588	540	646	80
415	6	473	66	531	224	589	656	647	75
416	7	474	66	532	216	590	638	648	66
417	8	475	73	533	209	591	583	649	58
418	5	476	84	534	218	592	548	650	53
419	9	477	83	535	247	593	490	651	59
420	9	478	78	536	275	594	449	652	65
421	9	479	78	537	276	595	460	653	76
422	10	480	75	538	251	596	495	654	88
423	12	481	76	539	219	597	467	655	105
424	10	482	76	540	225	598	393	656	142
425	8	483	77	541	219	599	333	657	184
426	15	484	83	542	201	600	296	658	260
427	15	485	88	543	180	601	307	659	436
428	13	486	98	544	183	602	355	660	798
429	12	487	99	545	210	603	408	661	1551
430	18	488	102	546	260	604	468	662	2250
431	14	489	103	547	312	605	467	663	1869
432	16	490	111	548	320	606	355	664	1210
433	19	491	106	549	290	607	258	665	794
434	20	492	107	550	265	608	198	666	532
435	17	493	109	551	261	609	184	667	326
436	16	494	109	552	264	610	189	668	203
437	20	495	113	553	271	611	204	669	134
438	23	496	129	554	298	612	239	670	102
439	22	497	130	555	334	613	282	671	85
440	21	498	128	556	349	614	273	672	81
441	20	499	125	557	352	615	242	673	69
442	23	500	121	558	376	616	224	674	55
443	19	501	118	559	399	617	226	675	51
444	21	502	118	560	355	618	256	676	52
445	22	503	119	561	320	619	274	677	63
446	26	504	135	562	311	620	350	678	80

λ (nm)	$10^{20} \sigma$ (cm ²)	λ (nm)	$10^{20} \sigma$ (cm ²)	λ (nm)	$10^{20} \sigma$ (cm ²)	λ (nm)	$10^{20} \sigma$ (cm ²)	λ (nm)	$10^{20} \sigma$ (cm ²)
447	31	505	137	563	300	621	562	679	84
448	26	506	143	564	291	622	1090	680	74
449	30	507	137	565	292	623	1578	681	57
450	31	508	136	566	305	624	1291	682	42
451	33	509	145	567	301	625	898	683	33
452	36	510	162	568	305	626	783	684	28
453	34	511	186	569	310	627	806	685	19
454	38	512	189	570	299	628	789	686	17
455	38	513	172	571	296	629	748	687	13
456	38	514	169	572	294	630	724	688	13
457	42	515	170	573	298	631	518	689	13
458	39	516	167	574	306	632	350	690	11
459	45	517	160	575	330	633	233	691	8
460	42	518	154	576	350	634	176		

Note:

403 – 691 nm: data from Sander [121] normalized to $2.25 \times 10^{-17} \text{ cm}^2 \text{ molecule}^{-1}$ at 662 nm

**Table 4C-6. Product Channel Quantum Yields in the Photolysis of NO₃
at 298, 230, and 190 K**

λ (nm)	$10^3 \Phi(\text{NO} + \text{O}_2)$			$10^3 \Phi(\text{NO}_2 + \text{O}(^3\text{P}))$		
	298 K	230 K	190 K	298 K	230 K	190 K
585	0.0	0.0	0.0	983.0	996.0	999.0
586	15.2	26.4	37.9	967.0	970.0	961.0
587	39.1	66.7	94.4	943.0	930.0	905.0
588	97.1	161.0	221.0	885.0	836.0	779.0
589	128.0	209.0	283.0	854.0	788.0	716.0
590	190.0	300.0	397.0	793.0	696.0	602.0
591	220.0	343.0	448.0	763.0	653.0	551.0
592	249.0	383.0	495.0	734.0	614.0	505.0
593	303.0	455.0	575.0	680.0	542.0	424.0
594	328.0	487.0	610.0	654.0	510.0	390.0
595	359.0	517.0	630.0	608.0	453.0	332.0
596	357.0	501.0	598.0	587.0	429.0	307.0
597	318.0	430.0	493.0	567.0	406.0	285.0
598	323.0	421.0	468.0	531.0	367.0	249.0
599	314.0	396.0	429.0	509.0	345.0	229.0
600	291.0	346.0	355.0	472.0	307.0	196.0
601	296.0	338.0	335.0	438.0	275.0	170.0
602	291.0	322.0	310.0	415.0	254.0	153.0
603	283.0	294.0	267.0	371.0	215.0	123.0
604	280.0	282.0	249.0	351.0	198.0	111.0
605	264.0	253.0	213.0	323.0	176.0	94.4
606	271.0	251.0	205.0	296.0	155.0	80.0
607	268.0	243.0	194.0	280.0	143.0	71.9
608	250.0	217.0	167.0	259.0	128.0	62.1
609	248.0	208.0	155.0	238.0	113.0	53.0
610	236.0	193.0	140.0	226.0	105.0	48.1
611	205.0	159.0	111.0	210.0	94.7	42.2
612	200.0	150.0	101.0	193.0	84.0	36.2
613	190.0	138.0	90.6	181.0	77.3	32.6
614	166.0	114.0	71.2	166.0	68.4	28.0
615	166.0	110.0	66.1	147.0	58.3	22.9
616	160.0	102.0	59.7	137.0	52.7	20.2
617	141.0	85.5	47.5	124.0	46.5	17.3
618	143.0	83.5	44.8	108.0	38.6	13.8
619	139.0	78.4	40.9	99.3	34.6	12.1
620	131.0	71.5	36.0	89.7	30.3	10.2
621	127.0	66.0	32.0	76.9	24.8	8.03
622	122.0	61.9	29.2	70.4	22.1	6.99
623	117.0	57.6	26.5	64.3	19.7	6.07
624	106.0	49.6	21.9	55.2	16.2	4.8
625	98.5	44.5	19.0	48.7	13.8	3.94
626	92.3	40.6	16.8	44.2	12.2	3.39
627	84.8	36.0	14.5	39.3	10.5	2.83
628	73.9	29.9	11.5	33.9	8.67	2.26
629	69.9	27.4	10.2	29.4	7.23	1.81
630	64.9	24.7	9.01	26.4	6.29	1.53
631	57.8	21.3	7.52	23.6	5.45	1.29
632	50.8	17.8	6.02	19.5	4.29	0.969
633	46.6	15.9	5.23	17.7	3.8	0.838
634	42.6	14.2	4.54	16.1	3.36	0.724
635	37.3	12.0	3.73	14.6	2.97	0.624
636	32.3	9.86	2.93	11.9	2.3	0.462
637	29.4	8.7	2.52	10.7	2.02	0.396
638	26.6	7.66	2.16	9.57	1.77	0.338
639	23.5	6.53	1.78	8.56	1.54	0.288
640	20.3	5.38	1.41	7.15	1.24	0.224

Note:
Johnston et al. [63]

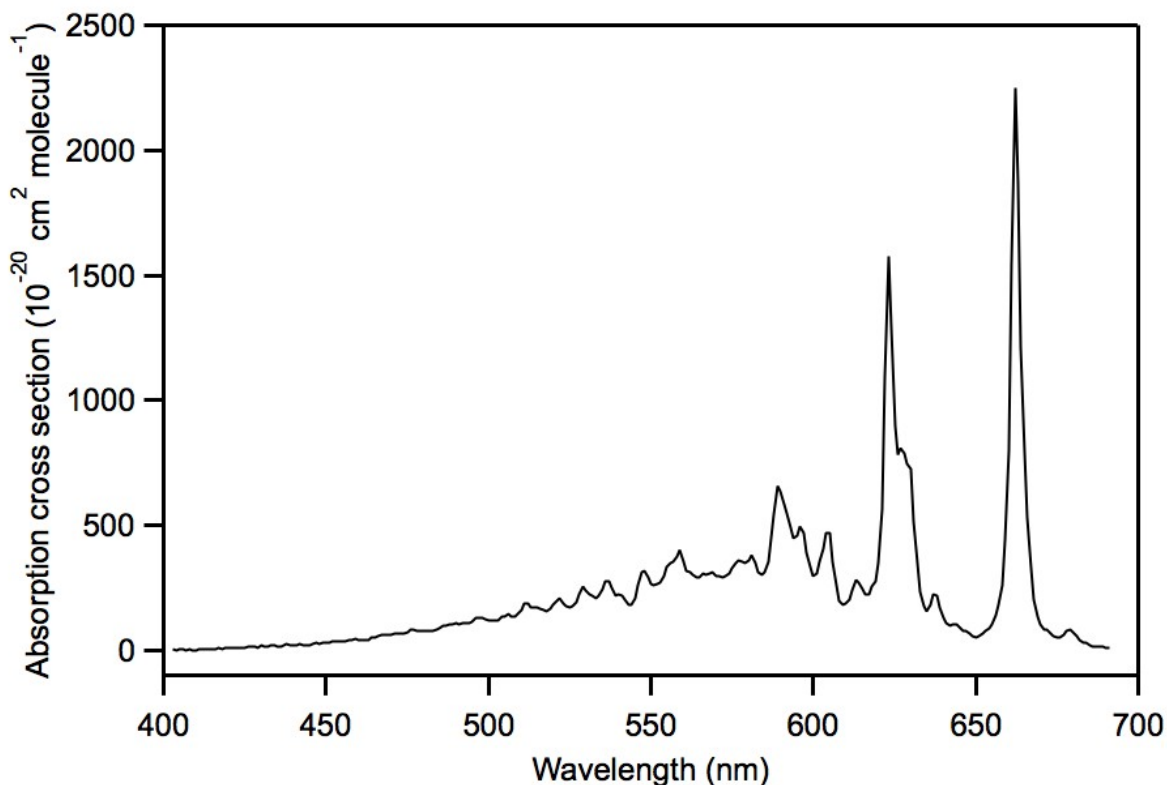
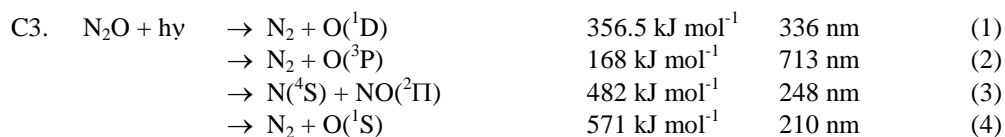


Figure 4C-1. Absorption Spectrum of NO₃



(Recommendation: 06-2; Note: 10-6; Evaluated: 10-6)

Absorption Cross Sections: The VUV/UV absorption spectrum of nitrous oxide, N₂O, has been measured in numerous studies covering the wavelength range 108 – 315 nm at temperatures between 194 and 302 K. A summary of the available spectroscopic studies is given in Table 4C-7.

Table 4C-7. Summary of N₂O Cross Section Studies

Study	Year	Temperature (K)	Wavelength range (nm)	Resolution (nm)
Romand and Mayence [118]	1949	291	139 – 231	–
Zelikoff et al. [157]	1953	298	108 – 210	0.085
Zelikoff and Aschenbrand [156]	1954	298	184.9	–
Thompson et al. [134]	1963	298	190 – 240	–
Bates and Hays [5]	1967	298	190 – 315	–
Johnston and Selwyn [66]	1975	298	210 – 300	–
Selwyn et al. [125]	1977	194, 225, 243, 263, 302	173 – 240	0.7, 0.075
Hitchcock et al. [56]	1980	298	16.8 – 155	0.5
Hubrich and Stuhl [58]	1980	208, 298	160 – 250	0.3
Selwyn and Johnston [126]	1981	150 – 500	172 – 197	0.003, 0.05, 0.07
Yoshino et al. [154]	1984	295 – 299	169.6 – 222.6	0.0006
Mérienne et al. [83]	1990	220, 240, 296	200 – 240	0.02
Chan et al. [20]	1994	298	6.1 – 168	0.5
Cantrell et al. [19]	1997	298, 353	184.9	<0.2

Study	Year	Temperature (K)	Wavelength range (nm)	Resolution (nm)
Creasey et al. [26]	2000	298	184.9	–
von Hessberg et al. [144]	2004	233, 283	180 – 218	0.7, 1.1

The N₂O spectrum has a broad absorption band between 160 and 260 nm with the peak near 182 nm ($\sigma_{\text{max}} = (1.24\text{--}1.47) \times 10^{-19} \text{ cm}^2 \text{ molecule}^{-1}$) and a stronger but weaker band between 137 and 160 nm with the maximum near 145 nm ($\sigma_{\text{max}} = (5\text{--}6) \times 10^{-18} \text{ cm}^2 \text{ molecule}^{-1}$). There is good agreement between the results from Selwyn et al. [125] and Hubrich and Stuhl [58]. The agreement over the entire 160 – 260 nm band is better than 15% and the difference at 182 nm is 5% with the data of Selwyn et al. [125] being greater. The results of Mérienne et al. [83] are in excellent agreement, better than 5%, with those of Selwyn et al. [125]. The results of Cantrell et al. [19] and Creasey et al. [26] at 184.9 nm are also in good agreement with the results of Selwyn et al. [125]. The high resolution absorption spectrum reported by Yoshino et al. [154] shows the diffuse vibrational structure around the maximum and their absolute cross sections are close to those reported by Hubrich and Stuhl [58]. At wavelengths >250 nm, there are large discrepancies between the results from Bates and Hayes [5] and Johnston and Selwyn [66]. The recommended cross sections listed in Table 4C-8 are based on the room temperature results at 160, 165, and 170 nm of Hubrich and Stuhl [58] and the room temperature data between 173 – 240 nm from Selwyn et al. [125]. The absorption cross section at Lyman- α (121.567 nm) is estimated from the spectra of Chan et al. [20] and Hitchcock et al. [56] to be $(2.5 \pm 0.5) \times 10^{-17} \text{ cm}^2 \text{ molecule}^{-1}$.

The temperature dependence of the N₂O absorption cross section in the atmospherically relevant wavelength region has been measured by Selwyn et al. [125], Hubrich and Stuhl [58], and Mérienne et al. [83]. The results from these studies are in excellent agreement with a decrease in absorption cross section with decreasing temperature. Selwyn et al. [125] parameterized their cross section data using the empirical expression given in Table 4C-9. Isotopomer specific cross sections for ¹⁴N¹⁴NO, ¹⁵N¹⁴NO, ¹⁴N¹⁵NO, ¹⁵N¹⁵NO over the wavelength range 181 – 218 nm have been reported by von Hessberg et al. [144] at 233 and 283 K. They observed a slight decrease of the absorption cross sections of ¹⁴N¹⁵NO and ¹⁵N¹⁵NO compared to those of ¹⁴N¹⁴NO and ¹⁵N¹⁴NO. They also observed a systematic decrease in absorption cross section with decreasing temperature.

Photolysis Quantum Yield and Product Studies: The quantum yield for photodissociation is unity in the range 140 – 230 nm and the photoproducts are almost exclusively N₂ and O(¹D) (Zelikoff and Aschenbrand [156], Greiner [46], Paraskevopoulos and Cvetanovic [103], Preston and Barr [105], Simonaitis et al. [127]). The yield of N(⁴S) and NO(²Π) is less than 1% (Greenblatt and Ravishankara [45]). Nishida et al. [91] reported the yield of O(³P) at 193 nm to be 0.005 ± 0.002 .

Several groups have investigated the isotopic fractionation of N₂O resulting from photolysis in the UV. Fractionation factors have been measured following photolysis at select wavelengths in the 193 – 213 nm range by Turatti et al. [136] (using high resolution FTIR spectroscopy), Röckmann et al. [113] (using a modified isotope ratio mass spectrometric technique), Rahn et al. [106] (utilizing isotope ratio mass spectrometry), and Zhang et al. [160] (using low resolution FTIR spectroscopy). Röckmann et al. [114] utilized a broadband photolysis source centered around 200 nm that simulated stratospheric actinic fluxes. The results are in reasonably good agreement and indicate that the fractionation factors increase with increasing wavelength between 193 and 213 nm. Furthermore, the fractionation factors show a clear dependence on the position of the ¹⁵N atom, in agreement with the theoretical zero point energy model of Yung and Miller [155]. However, the Yung and Miller calculations underestimate the laboratory results by about a factor of two. A more detailed Hermite propagation model used by Johnson et al., [61] achieves better agreement with experimental enrichment factors. Analysis of the isotopic composition of stratospheric air samples yields results that are in qualitative agreement with the laboratory results, confirming that photolysis is the predominant sink for N₂O [47, 114]. On the other hand, the fractionation factors measured in the atmospheric samples are smaller than those reported from the laboratory studies, indicating the influence of atmospheric diffusion and mixing (Röckmann et al. [114]).

Table 4C-8. Absorption Cross Sections of N₂O at 298 K

λ (nm)	$10^{20}\sigma$ (cm ²)	λ (nm)	$10^{20}\sigma$ (cm ²)	λ (nm)	$10^{20}\sigma$ (cm ²)	λ (nm)	$10^{20}\sigma$ (cm ²)
160	4.30	188	12.5	206	1.65	224	0.0375
165	5.61	189	11.7	207	1.38	225	0.0303
170	8.30	190	11.1	208	1.16	226	0.0239
173	11.3	191	10.4	209	0.980	227	0.0190
174	11.9	192	9.75	210	0.755	228	0.0151
175	12.6	193	8.95	211	0.619	229	0.0120
176	13.4	194	8.11	212	0.518	230	0.00955
177	14.0	195	7.57	213	0.421	231	0.00760
178	13.9	196	6.82	214	0.342	232	0.00605
179	14.4	197	6.10	215	0.276	233	0.00478
180	14.6	198	5.35	216	0.223	234	0.00360
181	14.6	199	4.70	217	0.179	235	0.00301
182	14.7	200	4.09	218	0.142	236	0.00240
183	14.6	201	3.58	219	0.115	237	0.00191
184	14.4	202	3.09	220	0.0922	238	0.00152
185	14.3	203	2.67	221	0.0739	239	0.00123
186	13.6	204	2.30	222	0.0588	240	0.00101
187	13.1	205	1.95	223	0.0474		

Note:

160 – 170 nm: Hubrich and Stuhl [58]

173 – 240 nm: Selwyn et al. [125]

Table 4C-9. Mathematical Expression for the Absorption Cross Sections of N₂O as a Function of Temperature

$$\ln(\sigma(\lambda, T)) = \sum_{n=0}^4 A_n \lambda^n + (T - 300) \exp\left(\sum_{n=0}^3 B_n \lambda^n\right)$$

where T \equiv temperature (K) and $\lambda \equiv$ wavelength (nm)

$$A_0 = 68.21023$$

$$B_0 = 123.4014$$

$$A_1 = -4.071805$$

$$B_1 = -2.116255$$

$$A_2 = 4.301146 \times 10^{-2}$$

$$B_2 = 1.111572 \times 10^{-2}$$

$$A_3 = -1.777846 \times 10^{-4}$$

$$B_3 = -1.881058 \times 10^{-5}$$

$$A_4 = 2.520672 \times 10^{-7}$$

Ranges of applicability: 173 nm < λ < 240 nm; 194 K < T < 302 K



(Recommendation: 06-2; Note: 10-6; Evaluated: 10-6)

Absorption Cross Sections: The UV/vis absorption spectrum of dinitrogen tetroxide, N₂O₄, has been derived from absorption measurements of NO₂-N₂O₄ mixtures. The available studies are summarized in Table 4C-10. The N₂O₄ absorption spectrum consists of a band between 300 and 400 nm with a maximum at ~340 nm, a second less pronounced maximum near ~265 nm, and a strong absorption at shorter wavelengths with a maximum near 190 nm. For the wavelength region 185 – 360 nm, there is good agreement for the shape of the absorption spectrum but there are discrepancies in the absolute absorption cross sections. In the region below 240 nm, there is good agreement between the absorption cross sections of Bass et al. [4] and Schneider et al. [123] whereas the values reported by Mérienne et al. [82] are lower by ~30%. In the region between

250 and 300 nm, the results of Vandaele et al. [141] are systematically lower than the results of Mérienne et al. [82] by ~15% whereas the results of Bass et al. [4] are higher by ~30%. In the region 300 – 380 nm, Harwood and Jones [52] reported a systematic study of the temperature dependence of the N₂O₄ absorption spectrum. The absorption cross sections near the peak at 340 nm show a weak dependence on temperature over the range 213 – 253 K. There is good agreement between the results of Hall and Blacet [48], the low-temperature data of Harwood and Jones [52], and the results of Vandaele et al [141] with the absorption cross sections at 340 nm agreeing to within 5%. Bass et al. [4] and Mérienne et al. [82] report cross section values at 340 nm that are 25% and 15% higher, respectively. The recommended cross section values in Table 4C-11 are averages over 2 nm intervals of the high resolution (0.01–0.03 nm) spectrum reported by Vandaele et al. [141] between 252 and 390 nm at 220 K.

Photolysis Quantum Yield and Product Studies: No studies available.

Table 4C-10. Summary of N₂O₄ Absorption Cross Section Studies

Study	Year	Temperature (K)	Wavelength (nm)	10 ²⁰ σ(340 nm) (cm ²)
Holmes and Daniels [57]	1934	273	265 – 405	~43
Hall and Blacet [48]*	1952	298	240 – 390	69
Nakayama et al. [90]	1959	300	197	–
Bass et al. [4]	1976	273	185 – 390	82.8
Schneider et al. [123]	1987	298	198 – 230	–
Harwood and Jones [52]	1994	213, 225 233, 243, 253, 273	320 – 405 320 – 430	64.2 66.5
Mérienne et al. [82]	1997	220	200 – 390	78.1
Vandaele et al. [141]	1998	220	250 – 455	68.1

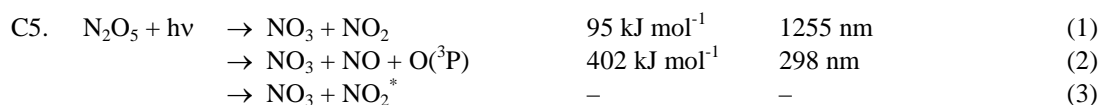
* (as given in Johnston and Graham [65])

Table 4C-11. Absorption Cross Sections of N₂O₄ at 220 K

λ (nm)	10 ²⁰ σ (cm ²)	λ (nm)	10 ²⁰ σ (cm ²)	λ (nm)	10 ²⁰ σ (cm ²)	λ (nm)	10 ²⁰ σ (cm ²)
252	64.8	288	27.5	324	47.5	360	26.8
254	65.1	290	25.0	326	51.9	362	22.5
256	64.7	292	22.9	328	55.9	364	18.7
258	64.8	294	21.0	330	59.7	366	15.4
260	64.3	296	19.5	332	63.0	368	12.5
262	63.2	298	18.5	334	65.7	370	10.0
264	61.8	300	17.9	336	67.3	372	8.13
266	60.0	302	18.0	338	68.1	374	6.50
268	57.9	304	18.5	340	68.1	376	5.33
270	55.2	306	19.3	342	66.8	378	4.24
272	52.3	308	20.8	344	64.4	380	3.52
274	49.3	310	22.9	346	61.3	382	2.93
276	46.2	312	25.3	348	57.3	384	2.47
278	43.0	314	28.3	350	52.5	386	2.16
280	39.7	316	31.9	352	47.3	388	1.89
282	36.4	318	35.3	354	42.1	390	1.78
284	33.3	320	39.1	356	36.9		
286	30.3	322	43.2	358	31.7		

Note:

Vandaele et al. [141]



(Recommendation: 06-2; Note: 10-6; Evaluated: 10-6)

Absorption Cross Sections: The UV/vis absorption spectrum of dinitrogen pentoxide, N₂O₅, exhibits an absorption maximum at 160 nm with continuously decreasing absorption cross sections toward longer wavelengths. The absorption cross sections of N₂O₅ have been measured in a number of studies that are summarized in Table 4C-12. The room temperature values from Yao et al. [151] and Harwood et al. [51, 53, 54] are in good agreement at wavelengths above 250 nm (within 10-20%). Below 250 nm, the cross sections reported by Yao et al. [151] that were recommended in the JPL-1997 evaluation are systematically higher than those reported by Harwood et al. [51] by up to a factor of ~2 at 208 nm. A possible explanation for this discrepancy proposed by Harwood et al. [51] was contributions to the measured absorption by HNO₃ impurities. Harwood et al. [51] used N₂O₅ samples containing less than a 1% HNO₃ impurity. This explanation was later confirmed by the measurements of Osborne et al. [100] who also used thoroughly purified N₂O₅ samples and reported absorption cross sections in agreement with those of Harwood et al. [51] at 210 – 240 nm but at a lower temperature.

The recommended absorption cross sections listed in Table 4C-13 are the mean of the data from Yao et al. [151] and Osborne [100] for 200 – 208 nm, the mean of the data from Yao et al. [151], Osborne et al. [100], and Harwood et al. [51] for 210 – 240 nm, the data of Harwood et al. [51] for 242 – 398 nm, and the data of Harwood et al. [53] for 400 – 420 nm.

The temperature dependence of the absorption spectrum was measured by Harwood et al. [51] and Yao et al. [151] and found to be significant for wavelengths >280 nm. The absorption cross sections decrease with decreasing temperature and the magnitude of the effect increases with increasing wavelength. Harwood et al. [53] parameterized the temperature dependence using the relationship

$$\log_{10}(\sigma) = A(\lambda) + 1000 \times B(\lambda)/T$$

which is valid over the temperature range 233 – 295 K. The A and B coefficients are given in Table 4C-13.

Table 4C-12. Summary of N₂O₅ Absorption Cross Section Studies

Study	Year	Temperature (K)	Wavelength (nm)
Holmes and Daniels [57]	1934	273	265, 280
Jones and Wulf [68]	1937	273	285 – 380
Johnston and Graham [65]	1974	298	210 – 290
Johnston et al. [62]	1974	298	200 – 360
Graham [41]	1975	298	205 – 310
Yao et al. [151]	1982	225, 243, 263, 277	290 – 380
Yao et al. [151]	1982	298-300	200 – 380
Harwood et al. [54]	1992	273, 295	280 – 380
Harwood et al. [53]	1993	233-295	240 – 420
Harwood et al. [51]	1998	295	208 – 398
Osborne et al. [100]	2000	195	152 – 240

Photolysis Quantum Yield and Product Studies: There are several studies of N₂O₅ primary photolysis products for wavelengths between 248 and 352.5 nm as summarized in Table 4C-14. The NO₃ radical is produced with unity quantum yield at wavelengths >300 nm. At shorter wavelengths the NO₃ quantum yield decreases to a value of ~0.71 at 248 nm and the O(³P) atom quantum increases. The study of Oh et al. [93] indicates that the primary photolysis products other than NO₃ are a wavelength dependent mixture of NO₂, NO₂* and NO + O, where NO₂* represents electronically excited NO₂ that is most likely the ²B₁ state. For atmospheric model calculations unit photolysis quantum yields of NO₃ and NO₂ are recommended for wavelengths >300 nm.

Table 4C-13. Absorption cross sections at 300 K and temperature coefficients for N₂O₅

λ (nm)	$10^{20} \sigma$ (cm ²)	A (cm ²)	B (cm ² K ⁻¹)	λ (nm)	$10^{20} \sigma$ (cm ²)	A (cm ²)	B (cm ² K ⁻¹)	λ (nm)	$10^{20} \sigma$ (cm ²)	A (cm ²)	B (cm ² K ⁻¹)
200	910			270	16.2	-18.42	-0.104	340	0.368	-18.77	-0.492
202	842			272	14.9			342	0.328		
204	771			274	13.7			344	0.293		
206	682			276	12.4			346	0.262		
208	585			278	11.4			348	0.234		
210	445			280	10.5	-18.59	-0.112	350	0.210	-18.71	-0.583
212	381			282	9.59			352	0.188		
214	322			284	8.74			354	0.167		
216	267			286	7.94			356	0.149		
218	220			288	7.20			358	0.133		
220	181			290	6.52	-18.72	-0.135	360	0.120	-18.31	-0.770
222	151			292	5.88			362	0.107		
224	129			294	5.29			364	0.0958		
226	113			296	4.75			366	0.0852		
228	98.4			298	4.26			368	0.0763		
230	88.2			300	3.81	-18.84	-0.170	370	0.0685	-18.14	-0.885
232	80.5			302	3.40			372	0.0613		
234	74.0			304	3.03			374	0.0545		
236	69.2			306	2.70			376	0.0484		
238	64.6			308	2.40			378	0.0431		
240	59.8			310	2.13	-18.90	-0.226	380	0.0383	-18.01	-0.992
242	53.1			312	1.90			382	0.0341		
244	49.3			314	1.68			384	0.0305		
246	45.6			316	1.49			386	0.0273		
248	41.9			318	1.33			388	0.0242		
250	38.6			320	1.18	-18.93	-0.294	390	0.0215	-18.42	-0.949
252	35.5			322	1.05			392	0.0193		
254	32.6			324	0.930			394	0.0172		
256	29.9			326	0.826			396	0.0150		
258	27.5			328	0.735			398	0.0134		
260	25.2	-18.27	-0.091	330	0.654	-18.87	-0.388	400	0.014	-18.59	-0.966
262	23.1			332	0.582			410	0.009	-18.13	-1.160
264	21.1			334	0.518			420	0.005		
266	19.4			336	0.462						
268	17.8			338	0.412						

Note:

Absorption cross sections:

200 – 208 nm: mean of the data from Yao et al. [151] and Osborne et al. [100]

210 – 240 nm: mean of the data from Yao et al. [151], Osborne et al. [100], and Harwood et al. [51]

242 – 398 nm: data from Harwood et al. [51]

400 – 420 nm: data from Harwood et al. [53]

Temperature coefficients:

Harwood et al. [53] (260 – 410 nm)

 $\log_{10}(\sigma) = A(\lambda) + 1000B(\lambda)/T$; valid over the range 233 – 295 K

Table 4C-14. N₂O₅ Photolysis Quantum Yields

Reference	Year	λ (nm)	$\Phi(\text{NO}_3)$	$\Phi(\text{O}^3\text{P})$
Swanson et al. [133]*	1984	248	0.73 ± 0.12	–
Ravishankara et al. [111]*	1986	248	0.77 ± 0.10	0.72 ± 0.09
Harwood et al. [51]	1998	248	0.64 ± 0.20	–
Burrows et al. [14]	1984	254	0.80	–
Ravishankara et al. [111]	1986	266	–	0.38 ± 0.08
Ravishankara et al. [111]	1986	287	–	0.21 ± 0.03
Ravishankara et al. [111]	1986	289	–	0.15 ± 0.03
Barker et al. [3]	1985	290	0.8 ± 0.2	< 0.1
Harwood et al. [51]	1998	308	0.96 ± 0.15	–
Swanson et al. [133]	1984	350	0.84 ± 0.09	–
Harwood et al. [51]	1998	352.5	1.03 ± 0.15	–

Note:

* The reported NO₃ quantum yields of (0.89 ± 0.15) by Swanson et al. [133] and (0.96 ± 0.13) by Ravishankara et al. [111] have been scaled using the currently recommended NO₃ absorption cross section at 662 nm.



(Recommendation: 06-2; Note: 10-6; Evaluated: 10-6)

Absorption Cross Sections: The UV absorption spectrum of nitrous acid, HONO, consists of a highly structured absorption band between 300 and 400 nm due to vibrational progressions in the $\text{A}^1\text{A}'' \leftarrow \text{X}^1\text{A}'$ transition, with a maximum intensity near 354 nm and a stronger continuous absorption band at shorter wavelengths with a maximum near 205 nm. A summary of the HONO room temperature absorption cross section studies for the near UV band is given in Table 4C-15.

Table 4C-15. Summary of HONO Absorption Cross Section Studies

Study	Year	Wavelength Range (nm)	Resolution (nm)	$10^{20} \sigma$ (354 nm) (cm ²)
Johnston and Graham [65]	1974	300 – 399	0.87	12.3
Cox and Derwent [24]	1976	200 – 394	< 0.1	56.0
Perner [119]	1977	310 – 388	0.6	55.2
Stockwell and Calvert [130]	1978	310 – 396	< 1	49.6
Platt et al. [104]	1980	336 – 376	0.8	47
Kenner et al. [71]	1986	184 – 274	0.38	–
Vasudev [142]	1990	310 – 393	–	(49.7)*
Bongartz et al. [9]	1991	300 – 400	0.1 ($\lambda < 375$ nm) 0.8 ($\lambda < 375$ nm)	64.2**
Bongartz et al. [8]	1994	300 – 400	0.1 ($\lambda < 375$ nm) 0.8 ($\lambda < 375$ nm)	54.9**
Febo et al. [35]	1996	50 – 380	1	49.7**
Pagsberg et al. [102]	1997	348 – 376	0.06	50.2
Brust et al. [11]	2000	323 – 394	0.5	38.9
Stutz et al. [131]	2000	291 – 404	0.061 ± 0.003	52.2
Wang and Zhang [145]	2000	352.2 354.2 357.0	< 0.1	48.9
Gratien et al. [44]	2009	300 – 400	0.18	–

Notes:

* Normalized to the spectrum of Stockwell and Calvert [130]

** Bongartz et al. [8] corrected their 1991 results by a factor of 0.855

There is good agreement among the various data sets for the peak positions and discrepancies in the peak

cross sections are generally a consequence of the differences in measurement spectral resolution. Stutz et al. [131] normalized the earlier cross section data to a resolution of 1 nm, which shows an agreement of better than 10% between their results and those of Bongartz et al. [8], Pagsberg et al. [102], and Vasudev [142]. The measurements of Stockwell and Calvert [130] are in reasonable agreement with the more recent studies. The cross sections from Cox and Derwent [24] are greater by ~26% (presumably due to uncorrected for NO₂ absorption) and those from Johnston and Graham [65] are less by 70% (presumably due to non-equilibrium of the NO/NO₂/H₂O mixture during the measurement) than the more recent studies. The source of the discrepancy with the measurements of Brust et al. [11] is unknown. Gratien et al. [44] performed simultaneous measurements of HONO absorption spectra in the IR and UV and confirmed that the UV cross sections of Bongartz et al. [8] and Stutz et al. [131] are consistent within 5% with independent infrared studies and that the UV cross sections of Brust et al. [11] are underestimated by ~22%.

The short wavelength absorption band was measured by Cox and Derwent [24] (200 – 300 nm, <0.1 nm resolution) and Kenner et al. [71] (184 – 274 nm, 0.38 nm resolution). The reported spectra are in quantitative agreement over the wavelength range 220 – 270 nm. The sharp peak at 215 nm reported by Cox and Derwent [24], however, was not observed by Kenner et al. [71], who give a number of arguments for the correctness of their results.

The recommended absorption cross sections in Table 4C-16 are a combination of data as follows: for the wavelength region 184 – 274 nm data was taken from Kenner et al. [71] as read from a figure in their paper, for the wavelength region 296 – 396 nm data was taken from Stutz et al. [131], for the wavelength regions 296 – 325 nm and 371 – 396 nm averages over 1 nm intervals of the Stutz et al. [131] high resolution spectrum are reported, and for the highly structured region 326 – 370 nm averages over 0.5 nm intervals were used.

Photolysis Quantum Yield and Product Studies: The photolysis quantum yield of HONO at wavelengths above the dissociation threshold are unity. The OH radical quantum yield at 365 ± 5 nm was determined by Cox and Derwent [24] to be (0.92 ± 0.16) . Wollenhaupt et al. [150] determined an upper limit of 0.01 for the quantum yield of H atom formation for photolysis at 351 nm. The OH(A) quantum yield from HONO laser photolysis at 193 nm was measured to be 1.8×10^{-5} by Kenner et al. [71]. The H + NO₂(X²A₁, A²B₂, B²B₁, C²A₂) product channels in the photodissociation of HONO at 193.3 nm were examined by Amaral et al. [1] and branching ratios of the NO₂ electronic states estimated to be X²A₁ : A²B₂ : B²B₁ : C²A₂ \approx 0.13 : 0.21 : 0.66, respectively.

Table 4C-16. Absorption Cross Sections of HONO at 298 K

λ (nm)	$10^{20} \sigma$ (cm ²)	λ (nm)	$10^{20} \sigma$ (cm ²)	λ (nm)	$10^{20} \sigma$ (cm ²)	λ (nm)	$10^{20} \sigma$ (cm ²)
184	85.0	296	0.326	335.5	6.55	360.0	6.87
186	95.0	297	0.565	336.0	5.33	360.5	6.32
188	106	298	0.517	336.5	4.36	361.0	6.05
190	124	299	0.429	337.0	4.23	361.5	5.95
192	143	300	0.617	337.5	5.13	362.0	5.98
194	162	301	0.690	338.0	9.38	362.5	6.35
196	179	302	0.579	338.5	16.52	363.0	7.39
198	196	303	0.925	339.0	14.32	363.5	9.22
200	210	304	1.04	339.5	9.96	364.0	11.49
202	219	305	1.57	340.0	7.79	364.5	12.71
204	223	306	1.29	340.5	8.51	365.0	12.82
205	224	307	0.916	341.0	16.13	365.5	13.19
206	223	308	1.45	341.5	31.52	366.0	14.84
208	220	309	2.01	342.0	29.40	366.5	18.43
210	213	310	1.51	342.5	18.47	367.0	25.08
212	204	311	2.07	343.0	11.43	367.5	35.18
214	193	312	2.42	343.5	8.29	368.0	43.56
216	179	313	2.25	344.0	7.59	368.5	41.37
218	164	314	3.35	344.5	8.18	369.0	31.45
220	150	315	2.54	345.0	8.77	369.5	21.72
222	135	316	1.61	345.5	9.10	370	15.05
224	121	317	3.21	346.0	9.64	370	9.49
226	108	318	4.49	346.5	8.87	372	7.96
228	94.5	319	3.19	347.0	7.80	373	6.30
230	84.5	320	4.66	347.5	7.06	374	4.59
232	74.0	321	5.96	348.0	6.63	375	3.55
234	66.0	322	4.05	348.5	6.26	376	3.36
236	58.0	323	4.56	349.0	6.00	377	3.66
238	50.0	324	5.89	349.5	6.47	378	4.33
240	43.0	325	4.05	350.0	9.06	379	5.66
242	37.0	326	2.65	350.5	14.95	380	7.21
244	32.0	326.5	3.55	351.0	16.94	381	9.13
246	27.5	327.0	6.44	351.5	14.07	382	12.44
248	23.5	327.5	10.26	352.0	12.42	383	17.03
250	20.0	328.0	9.22	352.5	12.81	384	19.47
252	17.0	328.5	6.38	353.0	16.34	385	16.09
254	14.5	329.0	5.20	353.5	28.49	386	10.52
256	12.3	329.5	6.12	354.0	48.73	387	6.59
258	10.3	330.0	9.92	354.5	44.34	388	4.30
260	8.6	330.5	15.06	355.0	27.64	389	2.81
262	7.3	331.0	14.32	355.5	16.40	390	1.71
264	6.2	331.5	9.88	356.0	11.13	391	0.992
266	5.3	332.0	6.94	356.5	9.35	392	0.731
268	4.3	332.5	6.00	357.0	9.45	393	0.597
270	3.7	333.0	6.31	357.5	10.08	394	0.528
272	3.0	333.5	7.11	358.0	9.84	395	0.403
274	2.5	334.0	8.35	358.5	9.02	396	0.237
		334.5	8.37	359.0	8.37		
		335.0	7.71	359.5	7.67		

Note:

184 – 274 nm: Kenner et al. [71]

296 – 325 nm: Stutz et al. [131] (average over 1 nm intervals)

326 – 370 nm: Stutz et al. [131] (average over 0.5 nm intervals)

C7.	$\text{HNO}_3 + h\nu \rightarrow \text{OH} + \text{NO}_2$	206 kJ mol^{-1}	581 nm	(1)
	$\rightarrow \text{HONO} + \text{O}(^3\text{P})$	305 kJ mol^{-1}	392 nm	(2)
	$\rightarrow \text{H} + \text{NO}_3$	427 kJ mol^{-1}	280 nm	(3)
	$\rightarrow \text{OH} + \text{NO}_2(^1\text{B}_2)$	–	–	(4)
	$\rightarrow \text{HONO} + \text{O}(^1\text{D})$	494 kJ mol^{-1}	242 nm	(5)
	$\rightarrow \text{HONO}(\text{a}^3\text{A}) + \text{O}(^3\text{P})$	–	–	(6)

(Recommendation: 06-2; Note: 10-6; Evaluated: 10-6)

Absorption Cross Sections: The UV absorption spectrum of nitric acid, HNO_3 , consists of a strong absorption band between 150 and 240 nm with the maximum near 183 nm and a second band near 270 nm that appears as a shoulder on the long wavelength wing of the strong band. The recommended absorption cross sections and their temperature dependence for the region 192 – 350 nm listed in Table 4C-17 are taken from the work of Burkholder et al. [12]. The temperature effect is very important for estimates of atmospheric photodissociation. The results of Burkholder et al. [12] agree well (within 10% above 200 nm) with those of Rattigan et al. [107, 108] at room temperature, whereas Rattigan et al. [107, 108] report significantly smaller cross section values at 239 K (15-30% smaller in the range 220 – 330 nm and ~50% smaller at 330 nm). The recommended room temperature absorption cross sections are in very good agreement with the data of Molina and Molina [87] (<15% difference up to 310 nm). The Burkholder et al. [12] data are also in good agreement with the values reported by Biauume [6] and Johnston and Graham [64], except at long wavelength. Okabe [94] reported cross sections in the 110 – 190 nm range that are 20–30% lower than those of Burkholder et al. [12], Biauume [6], and Johnston and Graham [64] in the region 185 – 190 nm. Suto and Lee [132] reported cross sections between 105 and 210 nm that are 10-20% higher than those of Burkholder et al. [12], Biauume [6], and Johnston and Graham [64] in the region 185 – 190 nm, but show excellent agreement with the results of Molina and Molina [87] above 185 nm and Burkholder et al. [12] above 189 nm.

Photolysis Quantum Yield and Product Studies: There have been a number of HNO_3 photolysis studies at wavelengths between 193 and 320 nm. On the basis of end-product analysis, Johnston et al. [62] reported a quantum yield of ~1 for the $\text{OH} + \text{NO}_2$ channel in the 200 – 315 nm range. Margitan and Watson [79] used atomic resonance fluorescence to determine the quantum yield for O atom production at 266 nm to be 0.03 and that for H atom production to be ≤ 0.002 . Jolly et al. [67] measured a quantum yield for OH production of 0.89 ± 0.08 at 222 nm. Turnipseed et al. [137] reported OH quantum yields of (0.95 ± 0.09) at 248, (0.90 ± 0.11) at 222 nm, and 0.33 ± 0.06 at 193 nm. Turnipseed et al. [137] also reported quantum yields for production of O atoms, $\text{O}(^3\text{P}) + \text{O}(^1\text{D})$, to be 0.031 ± 0.01 , 0.20 ± 0.03 and 0.81 ± 0.13 at 248, 222, and 193 nm, respectively. Both $\text{O}(^3\text{P})$ and $\text{O}(^1\text{D})$ atom formation was observed at 222 and 193 nm but only $\text{O}(^3\text{P})$ was detected at 248 nm. At 193 and 222 nm the $\text{O}(^1\text{D})$ yield was determined to be 40% of the total O atom yield, yielding $\Phi(\text{O}(^1\text{D})) = 0.28 \pm 0.07$ at 193 nm. Turnipseed et al. [137] reported upper limits for $\Phi(\text{H}(^2\text{S}))$ of ≤ 0.002 at 238 nm, ≤ 0.01 at 222 nm, and ≤ 0.012 at 193 nm. Riffault et al. [112] reported $\Phi(\text{OH})$ values of 0.88 ± 0.09 at 248 nm and 1.05 ± 0.29 at 308 nm. Schiffman et al. [122] reported $\Phi(\text{OH}) = 0.47 \pm 0.06$ at 193 nm, which is larger than the value reported by Turnipseed et al. [137]. At 248 nm they report $\Phi(\text{OH}) = 0.75 \pm 0.10$, which is a smaller value than reported in other studies.

Felder et al. [36] used molecular beam/photofragment translational spectroscopy and reported the yield for $(\text{OH} + \text{NO}_2)$ to be $\Phi(\text{OH}) = 0.6 \pm 0.1$ and for $(\text{O} + \text{HONO})$ to be $\Phi(\text{HONO}) = 0.4 \pm 0.1$ at 193 nm. Myers et al. [89] also used this technique to measure the primary processes in the photolysis at 193 nm from the different photofragment ions and found evidence for all channels except 4. They determined the branching ratio $(\text{OH} + \text{NO}_2)/(\text{O} + \text{HONO})$ to be 0.50 ± 0.05 , $\Phi(\text{OH}) = 0.33 \pm 0.04$ (in excellent agreement with the value obtained by Turnipseed et al. [137]). They also reported $\Phi(\text{O}(^3\text{P}) + \text{O}(^1\text{D})) = 0.67 \pm 0.04$, which is lower than the 0.81 ± 0.13 value reported by Turnipseed et al. [137] but the latter authors included the contribution of the secondary dissociation of NO_2 produced in channel (1). Their primary yield of $\text{O}(^1\text{D})$ formation of 0.54 ± 0.04 is much larger than the $\Phi(\text{O}(^1\text{D}))$ yield of 0.28 ± 0.07 measured by Turnipseed et al. [137] and this discrepancy remains unexplained. In a study using LIF and REMPI-TOF techniques, Li et al. [76] found evidence for the $(\text{O}(^3\text{P}) + \text{HONO})$ channel with a yield of ~0.06.

Band strengths for the OH stretch vibrational overtones of HNO_3 have been reported by Donaldson et al. [33], Zhang et al. [159] and Brown et al. [10]. Photodissociation of HNO_3 by excitation of the $3\nu_{\text{OH}}$ (~983 nm), $4\nu_{\text{OH}}$ (~755 nm) and $5\nu_{\text{OH}}$ (~618 nm) overtones is a possible source of atmospheric OH radicals. There is good agreement among the various studies. Band strengths (in units of $10^{-20} \text{ cm}^2 \text{ molecule}^{-1} \text{ cm}^{-1}$) of 2.63 for

$3\nu_{\text{OH}}$ and 0.237 for $4\nu_{\text{OH}}$ were reported by Donaldson et al. [33]. Zhang et al. [159] obtained band strengths of (2.9 ± 0.7) for $3\nu_{\text{OH}}$ and (0.28 ± 0.10) for $4\nu_{\text{OH}}$. Brown et al. [10] measured the band strengths for $4\nu_{\text{OH}}$ to be (0.225 ± 0.015) at 296 K and (0.223 ± 0.015) at 251 K and for $5\nu_{\text{OH}}$ to be (0.0257 ± 0.015) at 296 K and (0.0241 ± 0.035) at 251 K. Although the contribution to the overall atmospheric OH production rate from HNO_3 overtone photodissociation is small, it is larger than estimated by Donaldson et al. [32].

Table 4C-17. Absorption Cross Sections at 298 K and Temperature Coefficients for HNO_3

λ (nm)	$10^{20}\sigma$ (cm^2)	$10^3 B$ (K^{-1})	λ (nm)	$10^{20}\sigma$ (cm^2)	$10^3 B$ (K^{-1})	λ (nm)	$10^{20}\sigma$ (cm^2)	$10^3 B$ (K^{-1})
192	1225	0	246	2.06	1.61	300	0.263	3.10
194	1095	0	248	2.00	1.44	302	0.208	3.24
196	940	1.70	250	1.97	1.34	304	0.167	3.52
198	770	1.65	252	1.96	1.23	306	0.133	3.77
200	588	1.66	254	1.95	1.18	308	0.105	3.91
202	447	1.69	256	1.95	1.14	310	0.0814	4.23
204	328	1.74	258	1.93	1.12	312	0.0628	4.70
206	231	1.77	260	1.91	1.14	314	0.0468	5.15
208	156	1.85	262	1.87	1.14	316	0.0362	5.25
210	104	1.97	264	1.83	1.18	318	0.0271	5.74
212	67.5	2.08	266	1.77	1.22	320	0.0197	6.45
214	43.9	2.17	268	1.70	1.25	322	0.0154	6.70
216	29.2	2.17	270	1.62	1.45	324	0.0108	7.16
218	20.0	2.21	272	1.53	1.49	326	0.00820	7.55
220	14.9	2.15	274	1.44	1.56	328	0.00613	8.16
222	11.8	2.06	276	1.33	1.64	330	0.00431	9.75
224	9.61	1.96	278	1.23	1.69	332	0.00319	9.93
226	8.02	1.84	280	1.12	1.78	334	0.00243	9.60
228	6.82	1.78	282	1.01	1.87	336	0.00196	10.5
230	5.75	1.80	284	0.909	1.94	338	0.00142	10.8
232	4.87	1.86	286	0.807	2.04	340	0.00103	11.8
234	4.14	1.90	288	0.709	2.15	342	0.00086	11.8
236	3.36	1.97	290	0.615	2.27	344	0.00069	9.30
238	2.93	1.97	292	0.532	2.38	346	0.00050	12.1
240	2.58	1.97	294	0.453	2.52	348	0.00042	11.9
242	2.34	1.88	296	0.381	2.70	350	0.00042	9.30
244	2.16	1.75	298	0.316	2.92			

Note:

Absorption cross sections

192 – 350 nm: Burkholder et al. [12]

Temperature coefficients

Burkholder et al. [12]

$\sigma(\lambda, T) = \sigma(\lambda, 298 \text{ K}) \exp(B(\lambda)(T - 298))$, T in K

C8.	$\text{HO}_2\text{NO}_2 + \text{h}\nu$	$\rightarrow \text{HO}_2 + \text{NO}_2$	99 kJ mol^{-1}	1207 nm	(1)
		$\rightarrow \text{OH} + \text{NO}_3$	165 kJ mol^{-1}	726 nm	(2)
		$\rightarrow \text{O}(^3\text{P}) + \text{HNO}_3$	168 kJ mol^{-1}	713 nm	(3)
		$\rightarrow \text{H} + \text{NO}_2 + \text{O}_2$	305 kJ mol^{-1}	393 nm	(4)
		$\rightarrow \text{HO}_2 + \text{NO} + \text{O}(^3\text{P})$	353 kJ mol^{-1}	339 nm	(5)
		$\rightarrow \text{OH} + \text{NO}_2 + \text{O}$	373 kJ mol^{-1}	321 nm	(6)
		$\rightarrow \text{H} + \text{O}(^3\text{P}) + \text{NO}_3$	594 kJ mol^{-1}	201 nm	(7)
		$\rightarrow \text{HONO} + \text{O}_2(^1\Sigma)$	131 kJ mol^{-1}	911 nm	(8)
		$\rightarrow \text{HONO} + \text{O}_2(^1\Delta)$	69 kJ mol^{-1}	1744 nm	(9)

(Recommendation: 06-2; Note: 10-6; Evaluated: 10-6)

Absorption Cross Sections: The gas-phase UV absorption spectrum of peroxyntic acid, HO_2NO_2 , has been reported by Cox and Patrick [25] (195-265 nm; 284 K), Morel et al. [88] (200 – 290 nm; 298 K), Graham et al. [43] (190 – 330 nm; 269 K), Molina and Molina [87] (190 – 330 nm; 298 K), Singer et al. [128] (210 – 329 nm; 253, 273, and 298 K), and Knight et al. [73] (220 – 350 nm; 273, 296, 318, and 343 K). There is very good agreement (within 5%) between the results of Molina and Molina [87] and Singer et al. [128] over the range 210 – 290 nm but discrepancies of ~15-60% in the wavelength range critical for atmospheric photodissociation ($\lambda \geq 290$ nm). The cross section values from Cox and Patrick [25], Graham et al. [43] and Morel et al. [88] are systematically greater than those of Molina and Molina [87] at wavelengths >200 nm. Knight et al. [73] used the data of Molina and Molina [87] and Singer et al. [128] in the 250 – 270 nm region for normalization and yielded reliable data for the long wavelength region. The recommended room temperature absorption cross section data in Table 4C-18 are a combination of data from Molina and Molina [87] in the region 190 – 205 nm, the mean of the data from Molina and Molina [87] and Singer et al. [128] in the region 210 – 275 nm, and the data from Knight et al. [73] in the region 280 – 350 nm. The temperature dependence of the absorption spectrum was examined by Singer et al. [128], who found no temperature dependence between 253 and 298 K, and Knight et al. [73], who reported a systematic increase of the absorption cross sections with increasing temperature. Knight et al. [73] parameterized the temperature dependence using a two component model

$$\sigma(T, \lambda) = \sigma_0(\lambda)/Q + \sigma_1(\lambda) (1-1/Q)$$

where the partition function is given by $Q = 1 + \exp(-\Delta E/(0.69T))$ with $\Delta E = 988 \text{ cm}^{-1}$ (O-O stretching vibration) and T is in K.

Photolysis Quantum Yield and Product Studies: HO_2NO_2 photodissociates in the UV with a unit quantum yield. MacLeod et al. [77] measured the quantum yield of OH radicals at 248 nm as $\Phi(\text{OH}) = 0.34 \pm 0.16$ (the sum of channels 2 and 5), relative to the OH yield in the photolysis of H_2O_2 . Roehl et al. [115] determined the quantum yield of NO_2 in the photolysis at 248 nm (relative to the NO_2 yield in the photolysis of HNO_3) to be $\Phi(\text{NO}_2) = 0.56 \pm 0.17$ (the sum of channels 1,4 and 5). Jimenez et al. [60] measured the yield of OH and HO_2 (from channels 1 and 6) at 193 and 248 nm (relative to the photolysis of H_2O_2) and the yield of NO_3 (relative to the photolysis of ClONO_2) at 193, 248 and 308 nm over a pressure range of 10 to 84 Torr. Jimenez et al. [60] reported $\Phi_{193}(\text{OH}) = 0.21 \pm 0.12$, $\Phi_{248}(\text{OH}) = 0.085 \pm 0.08$, $\Phi_{193}(\text{HO}_2) = 0.56 \pm 0.02$, $\Phi_{248}(\text{HO}_2) = 0.89 \pm 0.26$, $\Phi_{193}(\text{NO}_3) = 0.35 \pm 0.03$, $\Phi_{248}(\text{NO}_3) = 0.08 \pm 0.03$ and $\Phi_{308}(\text{NO}_3) = 0.05 \pm 0.02$. Assuming that only channel (2) contributes to OH and NO_3 production, these results imply that at 248 nm the yields of OH and NO_3 are nearly identical, 0.08. This lower yield is in disagreement with the earlier 248 nm results of MacLeod et al. [77] and Roehl et al. [115]. The high HO_2 yield (0.89 ± 0.26) measured at 248 nm by Jimenez et al. [60] overlaps within the experimental uncertainties with the NO_2 yield (0.56 ± 0.17) of Roehl et al. [115], assuming that the HO_2 arises from channel (1). It cannot however not be excluded that the difference in NO_2 yields reflects the contribution of channel (6). The recommended quantum yields are given in Table 4C-19 where the values below 200 nm are taken from Jimenez et al. [60] and the values above 200 nm represent an average of the results from Jimenez et al., Roehl et al. and MacLeod et al. The estimated uncertainty in the recommended quantum yields is ± 0.2 .

The photodissociation of HO_2NO_2 via excitation of the OH stretch vibrational overtones $2\nu_1$, $3\nu_1$, and $4\nu_1$ in the near IR and visible is a possible atmospheric HO_x source [149] [120] [34]. The band strengths (in units of $10^{-20} \text{ cm}^2 \text{ molecule}^{-1} \text{ cm}^{-1}$) of (3.8 ± 0.11) for $3\nu_1$ and (0.30 ± 0.18) for $4\nu_1$ have been reported by Zhang et al. [158] and (3.3 ± 0.7) for $3\nu_1$ by Roehl et al. [116]. Stark et al. [129] report greater values for the $3\nu_1$ and $4\nu_1$ band strengths of (5.7 ± 1.1) and (0.49 ± 0.09) , respectively. Roehl et al. [116] also measured absolute integrated band strengths and photodissociation quantum yields for 3 dissociative bands in the infrared region: $2\nu_1 + \nu_3$ (8242 cm^{-1}), $2\nu_1$ (6900 cm^{-1}) and $\nu_1 + 2\nu_3$ (6252 cm^{-1}) as a function of temperature. Matthews et al. [81] photolysed HO_2NO_2 at 390 nm in its first OH-stretching overtone ($2\nu_1$) and reported a quantum yield of 0.30 at 298 K. The temperature dependent cross sections and dissociation quantum yields from Roehl et al. [116] are summarized in Table 4C-20.

Table 4C-18. Absorption Cross Sections of HO₂NO₂ at 298 K

λ (nm)	$10^{20} \sigma$ (cm ²)	λ (nm)	$10^{20} \sigma$ (cm ²)	λ (nm)	$10^{20} \sigma$ (cm ²)	λ (nm)	$10^{20} \sigma$ (cm ²)
190	1010	260	28.50	300	1.52	328	0.110
195	816	265	23.00	302	1.28	330	0.0926
200	563	270	18.05	304	1.05	332	0.0788
205	367	275	13.40	306	0.853	334	0.0650
210	239	280	9.29	308	0.702	336	0.0540
215	161	282	8.11	310	0.551	338	0.0456
220	117.5	284	6.93	312	0.465	340	0.0372
225	93.50	286	5.86	314	0.380	342	0.0320
230	79.20	288	4.91	316	0.313	344	0.0268
235	68.25	290	3.95	318	0.265	346	0.0228
240	58.10	292	3.37	320	0.216	348	0.0198
245	48.95	294	2.78	322	0.184	350	0.0168
250	41.25	296	2.30	324	0.152		
255	35.00	298	1.91	326	0.128		

Note:

190 – 205 nm: Molina and Molina [87]

210 – 275 nm: mean of the data from Molina and Molina [87] and Singer et al. [128]

280 – 350 nm: Knight et al. [73]

Table 4C-19. HO₂NO₂ Photolysis Quantum Yields

λ (nm)	Φ (OH)	Φ (NO ₃)	Φ (HO ₂)	Φ (NO ₂)
<200	0.3	0.3	0.7	0.7
>200	0.2	0.2	0.8	0.8

Table 4C-20. Photodissociation Band Strengths and Quantum Yields for Several Overtone and Combination Bands of HO₂NO₂

Band	Band center (cm ⁻¹)	$\int \sigma_{\text{diss}} \Phi_{\nu} d\nu$ cm ² molecule ⁻¹ cm ⁻¹	Quantum yield
4 ν_1	13105	3.0×10^{-21} (b)	1
3 ν_1	10090	3.3×10^{-20}	1
2 ν_1 + ν_3	8240	1.21×10^{-21}	0.76
2 ν_1	6900	$4.09 \times 10^{-18} \exp(-826.5/T)$ (195 K > T > 224 K)	0.14
ν_1 + 2 ν_3	6250	$1.87 \times 10^{-19} \exp(-1410.7/T)$ (195 K > T > 240 K)	0.02

Note:

a) Data from Roehl et al. [116]

b) Data from Zhang et al. [158]

References for Section 4C

1. Amaral, G., K. Xu and J. Zhang, 2001, *J. Phys. Chem., A*, **105**, 1465-1475.
2. Amoroso, A., L. Crescentini, G. Fiocco and M. Volpe, 1993, *J. Geophys. Res.*, **98**, 16857-16863.
3. Barker, J. R., L. Brouwer, R. Patrick, M. J. Rossi, P. L. Trevor and D. M. Golden, 1985, *Int. J. Chem. Kinet.*, **17**, 991-1006.
4. Bass, A. M., A. E. Ledford and A. H. Laufer, 1976, *J. Res. Natl. Bur. Stand.*, **80A**, 143-166.
5. Bates, D. R. and P. B. Hays, 1967, *Planet. Space Sci.*, **15**, 189-197.
6. Biaume, F., 1973, *J. Photochem.*, **2**, 139-149.
7. Bogumil, K., J. Orphal, T. Homann, S. Voigt, P. Spietz, O. C. Fleischmann, A. Vogel, M. Hartmann, H. Krominga, H. Bovensmann, J. Frerick and J. P. Burrows, 2003, *J. Photochem. Photobiol. A: Chem.*, **157**, 167-184.
8. Bongartz, A., J. Kames, U. Schurath, C. George, P. Mirabel and J. L. Ponche, 1994, *J. Atmos. Chem.*, **18**, 149-169.
9. Bongartz, A., J. Kames, F. Welter and U. Schurath, 1991, *J. Phys. Chem.*, **95**, 1076-1082.
10. Brown, S. S., R. W. Wilson and A. R. Ravishankara, 2000, *J. Phys. Chem., A*, **104**, 4963-4976.
11. Brust, A. S., K. H. Becker, J. Kleffmann and P. Wiesen, 2000, *Atmos. Environ.*, **34**, 13-19.
12. Burkholder, J. B., R. K. Talukdar, A. R. Ravishankara and S. Solomon, 1993, *J. Geophys. Res.*, **98**, 22937-22948.
13. Burrows, J. P., A. Dehn, B. Deters, S. Himmelmann, A. Richter, S. Voigt and J. Orphal, 1998, *J. Quant. Spectrosc. Radiat. Transfer*, **60**, 1025-1031.
14. Burrows, J. P., G. S. Tyndall and G. K. Moortgat, 16th Informal Conf. on Photochemistry, 1984, Boston,
15. Burrows, J. P., G. S. Tyndall and G. K. Moortgat, 1985, *J. Phys. Chem.*, **89**, 4848-4856.
16. Calvert, J. G., S. Madronich, E. P. Gardner, J. A. Davidson, C. A. Cantrell and R. E. Shetter, 1987, *J. Phys. Chem.*, **91**, 6339-6341.
17. Canosa-Mas, C. E., M. Fowles, P. J. Houghton and R. P. Wayne, 1987, *J. Chem. Soc. Faraday Trans. 2*, **83**, 1465-1474.
18. Cantrell, C. A., J. A. Davidson, R. E. Shetter, B. A. Anderson and J. G. Calvert, 1987, *J. Phys. Chem.*, **91**, 5858-5863.
19. Cantrell, C. A., A. Zimmer and G. S. Tyndall, 1997, *Geophys. Res. Lett.*, **24**, 2195-2198, 2687 (Erratum).
20. Chan, W. F., G. Cooper and C. E. Brion, 1994, *Chem. Phys.*, **180**, 77-88.
21. Coquart, B., A. Jenouvier and M. F. Merienne, 1995, *J. Atm. Chem*, **21**, 251-261.
22. Corcoran, T. C., E. J. Beiting and M. O. Mitchell, 1992, *J. Molecular Spectroscopy*, **154**, 119-128.
23. Cox, R. A., R. A. Barton, E. Ljungstrum and D. W. Stocker, 1984, *Chem. Phys. Lett.*, **108**, 228-232.
24. Cox, R. A. and R. G. Derwent, 1976, *J. Photochem.*, **52**, 23-34.
25. Cox, R. A. and R. Patrick, 1979, *Int. J. Chem. Kinet.*, **11**, 635-648.
26. Creasey, D. J., D. E. Heard and J. D. Lee, 2000, *Geophys. Res. Lett.*, **27**, 1651-1654.
27. Davenport, J. E. "Determination of NO₂ Photolysis Parameters for Stratospheric Modeling," FAA-EQ-78-14, Federal Aviation Administration, Washington, DC. 1978
28. Davidson, J. A., C. A. Cantrell, A. H. McDaniel, R. E. Shetter, S. Madronich and J. G. Calvert, 1988, *J. Geophys. Res.*, **93**, 7105-7112.
29. Davis, H. F., B. Kim, H. S. Johnston and Y. T. Lee, 1993, *J. Phys. Chem.*, **97**, 2172-2180.

30. DeMore, W. B., S. P. Sander, D. M. Golden, R. F. Hampson, M. J. Kurylo, C. J. Howard, A. R. Ravishankara, C. E. Kolb and M. J. Molina, 1997, JPL Publication 97-4, **Evaluation 12**.
31. Dixon, J. K., 1940, J. Chem. Phys., **8**, 157-160.
32. Donaldson, D. J., G. J. Frost, K. H. Rosenlof, A. F. Tuck and V. Vaida, 1997, Geophys. Res. Lett., **24**, 2651-2654.
33. Donaldson, J., J. J. Orlando, S. Amann, G. S. Tyndall, R. J. Proos, B. R. Henry and V. Vaida, 1998, J. Phys. Chem., **102**, 5171-5174.
34. Evans, J. T., M. P. Chipperfield, H. Oelhaf, M. Stowasser and G. Wetzell, 2003, Geophys. Res. Lett., **29**, 10.1029/2002GL016470, 27-21 - 27-24.
35. Febo, A., C. Perrino and I. Allegrini, 1996, Atmos. Environ., **30**, 3599-3609.
36. Felder, P., X. Yang and J. R. Huber, 1993, Chem. Phys. Lett., **215**, 221-227.
37. Frost, G. J., L. M. Goss and V. Vaida, 1996, J. Geophys. Res., **101**, 3869-3877.
38. Gaedtke, H. and J. Troe, 1975, Ber. Bunsenges. Phys. Chem., **79**, 184-191.
39. Gardner, E. P., P. D. Sperry and J. G. Calvert, 1987, J. Geophys. Res., **92**, 6642-6652.
40. Gierczak, T., J. B. Burkholder and A. R. Ravishankara, 1999, J. Phys. Chem. A, **103**, 877-883.
41. Graham, R. A. Photochemistry of NO₃ and the Kinetics of the N₂O₅-O₃ System, Ph. D. Thesis, University of California, Berkeley, CA, 1975.
42. Graham, R. A. and H. S. Johnston, 1978, J. Phys. Chem., **82**, 254-268.
43. Graham, R. A., A. M. Winer and J. N. Pitts, Jr., 1978, Geophys. Res. Lett., **5**, 909-911.
44. Gratien, A., M. Lefort, B. Picquet-Varrault, J. Orphal, J.-F. Doussin and J.-M. Flaud, 2009, J. Quant. Spectrosc. Radiat. Transfer, **110**, 256-263.
45. Greenblatt, G. D. and A. R. Ravishankara, 1990, J. Geophys. Res., **95**, 3539-3547.
46. Greiner, N. R., 1967, J. Chem. Phys., **47**, 4373-4377.
47. Griffith, D. W. T., G. C. Toon, B. Sen, J.-F. Blavier and R. A. Toth, 2000, Geophys. Res. Lett., **27**, 2485-2488.
48. Hall, J., T. C. and F. E. Blacet, 1952, J. Chem. Phys., **20**, 1745-1749.
49. Harder, J. W., J. W. Brault, P. V. Johnston and G. H. Mount, 1997, J. Geophys. Res., **D102**, 3681-3879.
50. Harker, A. B., W. Ho and J. J. Ratto, 1977, Chem. Phys. Lett., **50**, 394-397.
51. Harwood, M. H., J. B. Burkholder and A. R. Ravishankara, 1998, J. Phys. Chem. A, **102**, 1309-1317.
52. Harwood, M. H. and R. L. Jones, 1994, J. Geophys. Res., **99**, 22955-22964.
53. Harwood, M. H., R. L. Jones, R. A. Cox, E. Lutman and O. V. Rattigan, 1993, J. Photochem. Photobiol. A: Chem., **73**, 167-175.
54. Harwood, M. H., O. V. Rattigan, R. L. Jones and R. A. Cox, 1992, Proc. SPIE Int. Soc. Opt. Eng., **1715**, 113-124.
55. Hicks, E., B. Leroy, P. Rigaud, J.-L. Joudain and G. Le Bras, 1979, J. Chem. Phys., **76**, 693-698.
56. Hitchcock, V. C., E. Brion and M. J. van der Wiel, 1980, Chem. Phys., **45**, 461-478.
57. Holmes, H. H. and F. Daniels, 1934, J. Am. Chem. Soc., **56**, 630-637.
58. Hubrich, C. and F. Stuhl, 1980, J. Photochem., **12**, 93-107.
59. Jenouvrier, A., B. Coquart and M.-F. Mérieulle, 1996, J. Atmos. Chem., **25**, 21-32.
60. Jimenez, E., T. Gierczak, H. Stark, J. B. Burkholder and A. R. Ravishankara, 2005, Phys. Chem. Chem. Phys., **7**, 342-348.
61. Johnson, M. S., G. D. Billing, A. Gruodis and M. H. M. Janssen, 2001, J. Phys. Chem. A, **105**, 8672-8680.
62. Johnston, H. S., S. Chang and G. Whitten, 1974, J. Phys. Chem., **78**, 1-7.
63. Johnston, H. S., H. F. Davis and Y. T. Lee, 1996, J. Phys. Chem., **100**, 4713-4723.

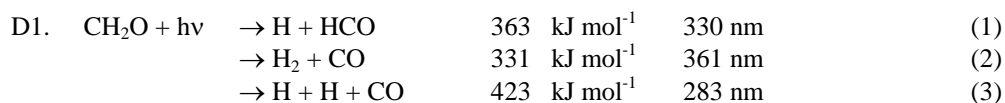
64. Johnston, H. S. and R. Graham, 1973, *J. Phys. Chem.*, **77**, 62-63.
65. Johnston, H. S. and R. Graham, 1974, *Canad. J. Chem.*, **52**, 1415-1423.
66. Johnston, H. S. and G. S. Selwyn, 1975, *Geophys. Res. Lett.*, **2**, 549-551.
67. Jolly, G. S., D. L. Singleton, D. J. McKenney and G. Paraskevopoulos, 1986, *J. Chem. Phys.*, **84**, 6662-6667.
68. Jones, E. L. and O. R. Wulf, 1937, *J. Chem. Phys.*, **5**, 873-877.
69. Jones, I. T. N. and K. Bayes, 1973, *J. Chem. Phys.*, **59**, 4836-4844.
70. Jost, R., J. Nygard, A. Pasinski and A. Delon, 1996, *J. Chem. Phys.*, **105**, 1287-1290.
71. Kenner, R. D., F. Rohrer and F. Stuhl, 1986, *J. Phys. Chem.*, **90**, 2635-2639.
72. Kirmse, B., A. Delon and R. Jost, 1997, *J. Geophys. Res.*, **D103**, 16089-16098.
73. Knight, G. P., A. R. Ravishankara and J. B. Burkholder, 2002, *Phys. Chem. Chem. Phys.*, **4**, 1432-1437.
74. Koffend, J. B., J. S. Holloway, M. A. Kwok and R. F. Heidner III, 1987, *J. Quant. Spectrosc. Radiat. Transfer*, **37**, 449-453.
75. Leroy, B., P. Rigaud and E. Hicks, 1987, *Ann. Geophys. A.*, **5**, 247-250.
76. Li, Q., R. T. Carter and J. R. Huber, 2001, *Chem. Phys. Lett.*, **334**, 39-46.
77. MacLeod, H., G. P. Smith and D. M. Golden, 1988, *J. Geophys. Res.*, **93**, 3813-3823.
78. Magnotta, F. and H. S. Johnston, 1980, *Geophys. Res. Lett.*, **7**, 769-772.
79. Margitan, J. J. and R. T. Watson, 1982, *J. Phys. Chem.*, **86**, 3819-3824.
80. Marinelli, W. J., D. M. Swanson and H. S. Johnston, 1982, *J. Chem. Phys.*, **76**, 2864-2870.
81. Matthews, J., R. Sharma and A. Sinha, 2004, *J. Phys. Chem. A*, **108**, 8134-8139.
82. Mérienne, M.-F., A. Jenouvrier, B. Coquart and J. P. Lux, 1997, *J. Atmos. Chem.*, **27**, 219-232.
83. Mérienne, M. F., B. Coquart and A. Jenouvrier, 1990, *Planet. Space Sci.*, **38**, 617-625.
84. Mérienne, M. F., A. Jenouvrier and B. Coquart, 1995, *J. Atm. Chem.*, **20**, 281-297.
85. Mihalcea, R. M., D. S. Baer and R. K. Hanson, 1996, *Appl. Optics*, **35**, 4059-4064.
86. Mitchell, D. N., R. P. Wayne, P. J. Allen, R. P. Harrison and R. J. Twin, 1980, *J. Chem. Soc. Faraday Trans. 2*, **76**, 785-793.
87. Molina, L. T. and M. J. Molina, 1981, *J. Photochem.*, **15**, 97-108.
88. Morel, O., R. Simonaitis and J. Heicklen, 1980, *Chem. Phys. Lett.*, **73**, 38-41.
89. Myers, T. L., N. R. Forde, B. Hu, D. C. Kitchen and L. J. Butler, 1997, *J. Chem. Phys.*, **81**, 5361-5373.
90. Nakayama, T., M. T. Kitamura and K. Watanabe, 1959, *J. Chem. Phys.*, **30**, 1180-1186.
91. Nishida, S., K. Takahashi, Y. Matsumi, N. Taniguchi and S. Hayashida, 2004, *J. Phys. Chem. A*, **108**, 2451-2456.
92. Nizkorodov, S. A., S. P. Sander and L. R. Brown, 2004, *Journal of Physical Chemistry A*, **108**, 4864-4872.
93. Oh, D., W. Sisk, A. Young and H. Johnston, 1986, *J. Chem. Phys.*, **85**, 7146-7158.
94. Okabe, H., 1980, *J. Chem. Phys.*, **72**, 6642-6650.
95. Orlando, J. J., G. S. Tyndall, G. K. Moortgat and J. G. Calvert, 1993, *J. Phys. Chem.*, **97**, 10996-11000.
96. Orphal, J. "A Critical Review of the Absorption Cross-Sections of O₃ and NO₂ in the 240-790 nm Region, Part 1, Ozone," ESA Technical Note MO-TN-ESA-GO-0302, European Space Agency, ESA-ESTEC, Noordwijk, 2002.
97. Orphal, J., 2003, *J. Photochem. Photobiol.*, **A 157**, 185-209.
98. Orphal, J., S. Dreher, S. Voigt, J. P. Burrows, R. Jost and A. Delon, 1998, *J. Chem. Phys.*, **109**, 10217-10221.
99. Orphal, J., C. E. Fellows and J.-M. Flaud, 2003, *J. Geophys. Res.*, **108 (D3)**, 4077.

100. Osbourne, B. A., G. Marston, L. Kaminski, N. C. Jones, J. M. Gingell, N. J. Mason, I. C. Walker, J. Delwiche and M.-J. Hubin-Franskin, 2000, *J. Quant. Spectrosc. Radiat. Transfer*, **64**, 67-74.
101. Osthoff, H. D., M. J. Pilling, A. R. Ravishankara and S. S. Brown, 2007, *Phys. Chem. Chem. Phys.*, **9**, 5785 - 5793.
102. Pagsberg, P., E. Bjergbakke, E. Ratajczak and A. Sillesen, 1997, *Chem. Phys. Lett.*, **272**, 383-390.
103. Paraskevopoulos, G. and R. J. Cvetanovic, 1969, *J. Am. Chem. Soc.*, **91**, 7572.
104. Platt, U., D. Perner, G. W. Harris, A. M. Winer and J. N. Pitts Jr., 1980, *Nature*, **285**, 312-314.
105. Preston, K. F. and R. F. Barr, 1971, *J. Chem. Phys.*, **54**, 3347-3348.
106. Rahn, T., H. Zhang, M. Wahlen and G. A. Blake, 1998, *Geophys. Res. Lett.*, **25**, 4489-4492.
107. Rattigan, O., E. Lutman, R. L. Jones and R. A. Cox, 1992, *Ber. Bunsenges. Phys. Chem.*, **96**, 399-404.
108. Rattigan, O., E. Lutman, R. L. Jones, R. A. Cox, K. Clemitshaw and J. Williams, 1992, *J. Photochem. Photobiol. A: Chem.*, **69**, 125-126.
109. Ravishankara, A. R. and R. L. Mauldin, 1986, *J. Geophys. Res.*, **91**, 8709-8712.
110. Ravishankara, A. R. and P. H. Wine, 1983, *Chem. Phys. Lett.*, **101**, 73-78.
111. Ravishankara, A. R., P. H. Wine, C. A. Smith, P. E. Barbone and A. Torabi, 1986, *J. Geophys. Res.*, **91**, 5355-5360.
112. Riffault, V., T. Gierczak, J. B. Burkholder and A. R. Ravishankara, 2006, *Phys. Chem. Chem. Phys.*, **8**, 1079 - 1085.
113. Röckmann, T. J., C. A. M. Brenninkmeijer, M. Wollenhaupt, J. N. Crowley and P. J. Crutzen, 2000, *Geophys. Res. Lett.*, **27**, 1399-1402.
114. Röckmann, T. J., J. Kaiser, C. A. M. Brenninkmeijer, J. N. Crowley, R. Borchers, W. A. Brand and P. J. Crutzen, 2001, *J. Geophys. Res.*, **106**, 10,403-10,410.
115. Roehl, C. M., T. L. Mazely, R. R. Friedl, Y. M. Li, J. S. Francisco and S. P. Sander, 2001, *J. Phys. Chem. A*, **105**, 1592-1598.
116. Roehl, C. M., S. A. Nizkorodov, H. Zhang, G. A. Blake and P. O. Wennberg, 2002, *J. Phys. Chem., A*, **106**, 3766-3772.
117. Roehl, C. M., J. J. Orlando, G. S. Tyndall, R. E. Shetter, G. J. Vasquez, C. A. Cantrell and J. G. Calvert, 1994, *J. Phys. Chem.*, **98**, 7837-7843.
118. Romand, J. and J. Mayence, 1949, *Compt. Rend. Acad. Sci. Paris*, **228**, 998-1000.
119. Röth, E. P., R. Ruhnke, G. Moortgat, R. Meller and W. Schneider "UV/VIS-Absorption Cross Sections and Quantum Yields for Use in Photochemistry and Atmospheric Modeling," Forschungszentrum Jülich Publication, Part 1 : Inorganic Substances (jül-3340), Part 2: Organic Substances (jül-3341), 1997
120. Salawitch, R. J., P. O. Wennberg, G. C. Toon, B. Sen and J.-F. Blavier, 2002, *Geophys. Res. Lett.*, **29**, 10.1029/2002GL015006, 9-1 - 9-4.
121. Sander, S. P., 1986, *J. Phys. Chem.*, **90**, 4135-4142.
122. Schiffman, A., D. D. Nelson, Jr. and D. J. Nesbitt, 1993, *J. Chem. Phys.*, **98**, 6935-6946.
123. Schneider, W., G. K. Moortgat, J. P. Burrows and G. Tyndall, 1987, *J. Photochem. Photobiol.*, **40**, 195-217.
124. Schott, G. and N. Davidson, 1958, *J. Amer. Chem. Soc.*, **80**, 1841-1853.
125. Selwyn, G., J. Podolske and H. S. Johnston, 1977, *Geophys. Res. Lett.*, **4**, 427-430.
126. Selwyn, G. S. and H. S. Johnston, 1981, *J. Chem. Phys.*, **74**, 3791-3803.
127. Simonaitis, R., R. I. Greenberg and J. Heicklen, 1972, *Int. J. Chem. Kinet.*, **4**, 497-512.
128. Singer, R. J., J. N. Crowley, J. P. Burrows, W. Schneider and G. K. Moortgat, 1989, *J. Photochem. Photobiol.*, **48**, 17-32.

129. Stark, H., S. S. Brown, J. B. Burkholder, M. Aldener, V. Riffault, T. Gierczak and A. R. Ravishankara, 2008, *J. Phys. Chem. A*, **112**, 9296-9303.
130. Stockwell, W. R. and J. G. Calvert, 1978, *J. Photochem.*, **8**, 193-203.
131. Stutz, J., E. S. Kim, U. Platt, P. Bruno, C. Perrino and A. Febo, 2000, *J. Geophys. Res.*, **105**, 14585-14592.
132. Suto, M. and L. C. Lee, 1984, *J. Chem. Phys.*, **81**, 1294-1297.
133. Swanson, D., B. Kan and H. S. Johnston, 1984, *J. Phys. Chem.*, **88**, 3115-3118.
134. Thompson, B. A., P. Harteck and J. Reeves, R. R., 1963, *J. Geophys. Res.*, **68**, 6431-6436.
135. Troe, J., 2000, *Z. Phys. Chem.*, **214**, 573-581.
136. Turatti, F., D. W. T. Griffith, S. R. Wilson, M. B. Esler, T. Rahn, H. Zhang and G. A. Blake, 2000, *Geophys. Res. Lett.*, **27**, 2489-2492.
137. Turnipseed, A. A., G. L. Vaghjiani, J. E. Thompson and A. R. Ravishankara, 1992, *J. Chem. Phys.*, **96**, 5887-5895.
138. Vandaele, A. C., C. Hermans, S. Fally, M. Carleer, R. Colin, M.-F. Mérienne, A. Jenouvrier and B. Coquart, 2002, *J. Geophys. Res.*, **D107**, 4384.
139. Vandaele, A. C., C. Hermans, S. Fally, M. Carleer and M.-F. Merienne, 2003, *J. Quant. Spectrosc. Radiat. Transfer*, **76**, 373-391.
140. Vandaele, A. C., C. Hermans, P. C. Simon, M. Van Roozendael, J. M. Guilmot, M. Carleer and R. Colin, 1966, *J. Atmos. Chem.*, **25**, 289-305.
141. Vandaele, A. C., D. Hermans, P. C. Simon, M. Carleer, R. Colin, S. Fally, M.-F. Merienne, A. Jenouvrier and B. Coquart, 1998, *J. Quant. Spectrosc. Radiat. Transfer*, **59**, 171-184.
142. Vasudev, R., 1990, *Geophys. Res. Lett.*, **17**, 2153-2155.
143. Voigt, S., J. Orphal and J. P. Burrows, 2002, *J. Photochem. Photobiol. A: Chem.*, **149**, 1-7.
144. von Hessberg, P., J. Kaiser, M. B. Enghoff, C. A. McLinden, S. L. Sorensen, T. Rockmann and M. S. Johnson, 2004, *Atmos. Chem. Phys.*, **4**, 1237-1253.
145. Wang, L. and J. Zhang, 2000, *Environ. Sci. Technol.*, **34**, 4221-4227.
146. Wangberg, I., T. Etzkorn, I. Barnes, U. Platt and K. H. Becker, 1997, *J. Phys. Chem. A*, **101**, 9694-9698.
147. Wayne, R. P., I. Barnes, J. P. Burrows, C. E. Canosa-Mas, J. Hjorth, G. Le Bras, G. K. Moortgat, D. Perner, G. Poulet, G. Restelli and H. Sidebottom, 1991, *Atmos. Environ.*, **25A**, 1-203.
148. Wennberg, P. O., J. W. Brault, T. F. Hanisco, R. J. Salawitch and G. H. Mount, 1997, *J. Geophys. Res.*, **D102**, 8887-8898.
149. Wennberg, P. O., R. J. Salawitch, D. J. Donaldson, T. F. Hanisco, E. J. Lanzendorf, K. K. Perkins, S. A. Lloyd, V. Vaida, R. S. Gao, E. J. Hints, R. C. Cohen, W. H. Swartz, T. L. Kusterer and D. E. Anderson, 1999, *Geophys. Res. Lett.*, **26**, 1373-1376.
150. Wollenhaupt, M., S. A. Carl, A. Horowitz and J. N. Crowley, 2000, *J. Phys. Chem., A*, **104**, 2695-2705.
151. Yao, F., I. Wilson and H. Johnston, 1982, *J. Phys. Chem.*, **86**, 3611-3615.
152. Yokelson, R. J., J. B. Burkholder, R. W. Fox, R. K. Talukdar and A. R. Ravishankara, 1994, *J. Phys. Chem.*, **98**, 13144-13150.
153. Yoshino, K., J. R. Esmond and W. H. Parkinson, 1997, *Chem. Phys.*, **221**, 169-174.
154. Yoshino, K., D. E. Freeman and W. H. Parkinson, 1984, *Planet. Space Sci.*, **32**, 1219-1222.
155. Yung, Y. L. and C. E. Miller, 1997, *Science*, **278**, 1778-1780.
156. Zelikoff, M. and L. M. Aschenbrand, 1954, *J. Chem. Phys.*, **22**, 1685-1687.
157. Zelikoff, M., K. Watanabe and E. C. Y. Inn, 1953, *J. Chem. Phys.*, **21**, 1643-1647.

158. Zhang, H., C. M. Roehl, S. P. Sander and P. O. Wennberg, 2000, J. Geophys. Res., **D 105**, 14593-14598.
159. Zhang, H., C. M. Roehl, S. P. Sander and P. O. Wennberg, 2000, J. Geophys. Res., **105**, 14593-14598.
160. Zhang, H., P. O. Wennberg, V. H. Wu and G. A. Blake, 2000, Geophys. Res. Lett., **27**, 2481-2484.

SECTION 4D. ORGANIC PHOTOCHEMISTRY



(Recommendation: 10-6, Note: 10-6, Evaluated: 10-6)

Absorption Cross Sections. The UV absorption spectrum of formaldehyde (CH_2O) displays a highly structured absorption band (the formally electric-dipole forbidden $S_1 \leftarrow S_0$ transition gives rise to the $\tilde{A}^1A_2 - X^1A_1$ band system, which becomes allowed through vibronic coupling) between 240 and 380 nm. The absorption spectrum of formaldehyde has been measured in many studies at temperatures between 222 and 353 K as summarized in Table 4D-1.

Table 4D-1. Summary of CH_2O Cross Section Studies

Study	Year	Temperature (K)	Wavelength range (nm)	Resolution (nm)	Medium
McMillan [36]	1966	348	202 – 374	1	air
McQuigg and Calvert [126]	1969	300	220 – 370	1	air
Calvert et al. [34]	1972	298	290 – 360	1	air
Bass et al. [16]	1980	223, 296	258 – 360	0.05	air
Moortgat et al. [138]	1980	285	215 – 370	0.5	air
Moortgat et al. [139]	1983	220 – 353	253 – 353	5	air
Cantrell et al. [40]	1990	223, 233, 243, 253, 263, 273, 283, 293, 296	300 – 385.8	1.0 cm^{-1} (~0.011)	vacuum
Rogers [168]	1990	296	235 – 365	0.01-0.04	vacuum
Meller and Moortgat [128]	2000	223, 298	224 – 373	~0.025	air
Chen and Zhu [44]	2003	293	290 – 330	0.0014	
Bogumil et al. [26]	2003	293	247 – 400	0.25	air
Pope et al. [159]	2005	263, 294	313 – 320	0.1 cm^{-1} (~0.001)	air/vacuum
Pope et al. [160]	2005	294	308 – 320	0.1 cm^{-1}	air/vacuum
Co et al. [48]	2005	220, 298	351 – 356	0.0003	vacuum
Smith et al. [178]	2006	245, 294	300 – 340	0.0035	air/vacuum
Gratien et al. [75]	2007	296	240 – 370	0.15	air
Gratien et al. [76]	2007	294	300 – 360	0.18	air
Gorrotxategi Carbajo et al. [74]	2008	245, 294	300 – 330	0.0035	air/vacuum

Meller and Moortgat [128] have reviewed the cross section studies prior to 2000 including descriptions of the techniques and experimental details of CH_2O generation and the absorption measurements as well as a comparison of the various results. The CH_2O absorption cross sections are a strong function of the measurement resolution that needs to be considered when comparing results from the various studies. Low resolution spectra were obtained by McMillan [36] and Moortgat et al. [138] whereas medium resolution measurements were reported by Bass et al. [16], Rogers [168], and Bogumil et al. [26]. The spectrum reported by Cantrell et al. [40] was measured with the highest resolution (0.011 nm) over the 300 – 358 nm region in the temperature range 223 – 293 K using Fourier transform spectroscopy. Meller and Moortgat [128] reported a high resolution spectrum (~0.025 nm) over the entire UV absorption band (224 – 373 nm) at 298 and 223 K using diode array spectroscopy. In general, the agreement between the medium and higher resolution data is good, although the cross section data of Bass et al. [16] and Rogers [168] are systematically lower than the Meller and Moortgat [128] data. The spectrum reported by Bogumil et al. [26] that was obtained using the SCIAMACHY pre-flight satellite instrument agrees with the data of Meller and Moortgat

[128]. The low resolution absorption cross sections reported by Chen and Zhu [43, 44] and Chen et al. [45] in the 280 – 330 nm region deviate substantially, up to 50%, from those reported by Meller and Moortgat [128].

A high resolution CH₂O spectrum, near the Doppler broadening limit of 0.07 cm⁻¹, was measured by Pope et al. [159, 160] in the range 308 – 320 nm using tunable UV laser absorption spectroscopy at 263 and 294 K. In a later study from the same laboratory, Smith et al. [178] extended the high resolution measurements (0.35 cm⁻¹) from 300 to 340 nm at 294 and 245 K. The high resolution CH₂O spectrum measured by Pope et al. [159, 160] is in excellent agreement with the spectral features reported by Cantrell et al. [40] and Meller and Moortgat [128] after convolution with the lower resolution instrument functions. Rotationally resolved absorption cross sections in the narrow spectral region 351 – 356 nm were measured by Co et al. [48] using Fourier Transform spectroscopy with an apodized resolution of 0.027 cm⁻¹. They observed a strong pressure dependence of the rotational lines over the pressure range 75 to 400 Torr and determined a pressure broadening coefficient in dry air of 1.8 x 10⁻⁴ cm⁻¹ Torr⁻¹ for several isolated lines in the 2₀4₁ band.

Gratien et al. [75, 76] measured UV (resolution 0.15 nm) and IR absorption cross sections simultaneously and compared the Integrated Band Intensities (IBI) of the main vibronic bands with previously published UV and IR data. The IBIs measured by Gratien et al. [76] in the region 300 – 360 nm compare well (within ~7%) with the IBI data derived from Meller and Moortgat [128] but are ~20% lower than the IBIs calculated from the Cantrell et al. [40] and Rogers [168] data. Gratien et al. [76] attribute the difference to the IR band strength given in the HITRAN database, which is based on the data from Cantrell et al. [40]. In a second study, Gratien et al. [75] compared the IBIs of 9 different band sections in the 300 to 360 nm region with more recent studies. In general, the IBI data of Gratien et al. [75] are in excellent agreement (within 2 %) with the high resolution results of Smith et al. [178]. It was also shown that the IBI data for 8 band sections measured by Smith et al. [178] are 2 to 14 % larger than the data of Meller and Moortgat [128]. The IBIs for the bands studied by Pope et al. [159, 160] (313.5 – 316.5 and 316.5 – 319.7 nm) are 4 and 13% larger, respectively, than the data of Meller and Moortgat [128]. On the other hand the IBI for the 351.7 – 355.5 nm band studied by Co et al. [48] is 12% larger than the values of Cantrell et al. [40] and Rogers [168] but in excellent agreement with those of Meller and Moortgat [128] and Gratien et al. [75]. In general, the consistency between the absorption cross section data of Smith et al. [178], Gratien et al. [75], and Pope et al. [159, 160] in the range 300 to 360 nm demonstrate that the previously recommended absorption cross sections cited in JPL06-2 as reported by Meller and Moortgat [128] are slightly too low by about 7-10%. However, since the data of Meller and Moortgat [128] encompass the range 225 – 375 nm, it is preferred to maintain the previous recommendation. Cross sections averaged over 1 nm intervals are listed in Table 4D-2 and over intervals used in atmospheric modeling in Table 4D-3.

The temperature dependence of the CH₂O absorption cross sections has been studied by Bass et al. [16], Moortgat et al. [138], Cantrell et al. [40], Meller and Moortgat [128], Pope et al. [159, 160], Co et al. [48] and Smith et al. [178] (see Table 4D-1). Temperature effects are the strongest at the maximum of the absorption bands where the lower temperatures result in larger absorptions. This effect is reversed in the wings of the absorption bands where higher temperatures result in a higher absorption. A linear parameterization of the absorption cross section temperature dependence between 223 and 323 K was derived by Meller and Moortgat [128]

$$\sigma(\lambda, T) = \sigma(\lambda, 298 \text{ K}) + \Gamma(\lambda) \times (T - 298)$$

Values of $\Gamma(\lambda)$ averaged over 1 nm intervals and intervals used in atmospheric modeling are listed in Table 4D-2 and Table 4D-3, respectively.

VUV absorption cross sections for the wavelength region 60 – 185 nm have been obtained by Gentieu and Mentall [69], Mentall et al. [131], and Glicker and Stief [73] using optical methods and by Cooper et al. [49] for the region 6 – 261 nm using (e, e) dipole spectroscopy.

Photolysis Quantum Yields and Product Studies: The quantum yield studies by McQuigg et al. [126] and Calvert et al. [34] established that over the wavelength range 290 – 360 nm the radical yield increases with decreasing wavelength. More precise wavelength dependent quantum yield studies using monochromatic light sources were performed by Lewis et al. [104], Marling [119], Horowitz and Calvert [84], Clark et al. [47], Moortgat et al. [140] and Tang et al. [188]. Moortgat and Warneck [142] and Moortgat et al. [138, 139] measured the yields of CO and H₂ in air (giving $\Phi_1(\text{H} + \text{HCO}) + \Phi_2(\text{H}_2 + \text{CO})$ and $\Phi_2(\text{H}_2 + \text{CO})$) as a function of wavelength (253 – 353 nm) and pressure (380 – 800 Torr) at 300 K and 220 K. These studies showed that the yield of CO was essential unity between 290 and 330 nm at all pressures with no systematic temperature dependence. For $\lambda > 330$ nm, both temperature and pressure have a significant effect on $\Phi_2(\text{H}_2 + \text{CO})$ but a negligible effect on $\Phi_1(\text{H} + \text{HCO})$. At $\lambda < 290$ nm the total CO yield was found to decrease to a value of 0.76 at 240 nm.

Smith et al. [179] measured relative quantum yields at 50 mbar for the production of the radical products H and HCO using NO-chemical amplification and subsequent detection of NO₂ with chemical ionization mass spectrometry. These authors measured the quantum yields in the range 269 to 339 nm with sufficient resolution (± 0.62 nm) to observe structure in the wavelength dependence, that was previously unreported, that is believed to provide evidence for a competition among the various dissociation pathways. The measured $\Phi_1(\text{H} + \text{HCO})$ yields were normalized to a value of 0.753 at 303.75 nm based on the JPL 97-4 recommendation [54] and agree with the previous determinations reported by Horowitz and Calvert [84] and Moortgat et al. [139]. However at $\lambda > 320$ nm the $\Phi_1(\text{H} + \text{HCO})$ yields reported by Smith et al. [179] are larger than the values recommended by DeMore et al. [54] resulting in a larger ($\sim 8\%$) overall rate of radical production.

Pope et al. [159, 160] and Gorrotxategi Carbajo et al. [74] used cavity ring-down spectroscopy to measure HCO radical absorption coefficients and CH₂O absorption cross sections from which absolute HCO quantum yields were calculated. The absolute HCO radical signal was calibrated against the HCO radical produced from the $\text{Cl} + \text{HCHO} \rightarrow \text{HCO} + \text{Cl}_2$ reaction following the photolysis of Cl₂/CH₂O/N₂ mixtures. In the 303 – 309 nm range $\Phi_{\text{HCO}} \sim 0.6 \pm 0.1$ was obtained which is 25% lower than the JPL 06-2 recommendation and the data reported by Smith et al. [179]. In the wavelength range 314 – 330 nm the Φ_{HCO} values (0.06 to 0.11) agree within the quoted uncertainties with the JPL 06-2 recommendation.

The experimental technique used by Gorrotxategi Carbajo et al. [74] measured the product of the high resolution absolute absorption cross section (identical as measured by Smith et al. [178]) and the absolute HCO quantum yield, $\Phi_{\text{HCO}}(\lambda)\sigma_{\text{CH}_2\text{O}}(\lambda)$, in the interval 302.6 – 331.0 nm with a wavelength resolution 0.005 nm. It is important to note that a separate calculation of the product $\Phi_{\text{HCO}}\sigma_{\text{CH}_2\text{O}}$ using single data of Φ_{HCO} and $\sigma_{\text{CH}_2\text{O}}$ at a given wavelength result in much lower $\Phi_{\text{HCO}}\sigma_{\text{CH}_2\text{O}}$ values (up to a factor 2) than obtained by the direct combined technique.

Troe [191] used theoretical calculations to evaluate the quantum yields for the molecular and radical photolysis processes at $\lambda > 310$ nm. An analytical representation was provided that enables extrapolation into temperature and pressure ranges that are not easily accessible experimentally.

The recommended quantum yields are listed in Table 4D-4 and are based on a polynomial fit over the wavelength range 250 – 338 nm of the data for $\Phi_1(\text{H} + \text{HCO})$ from Lewis et al. [104], Marling [119], Horowitz and Calvert [84], Clark et al. [47], Tang et al. [188], Moortgat et al. [139], Smith et al. [179], Pope et al. [159, 160], and Gorrotxategi Carbajo et al. [74].

$$\Phi_1(\text{H} + \text{HCO}) = a_0 + a_1\lambda + a_2\lambda^2 + a_3\lambda^3 + a_4\lambda^4$$

where

$$\begin{aligned} a_0 &= 557.95835182 \\ a_1 &= -7.31994058026 \\ a_2 &= 0.03553521598 \\ a_3 &= -7.54849718 \times 10^{-5} \\ a_4 &= 5.91001021 \times 10^{-8} \end{aligned}$$

$\Phi_2(\text{H}_2 + \text{CO})$ was optimized using the quantum data for CO from Moortgat et al. [139] and the relation $\Phi_2(\text{H}_2 + \text{CO}) = \Phi_{\text{tot}} - \Phi_1(\text{H} + \text{HCO})$. The pressure and temperature dependence of $\Phi_2(\text{H}_2 + \text{CO})$ is based on the algorithm cited in Calvert et al. [33] and is limited to wavelengths > 330 nm. The pressure dependence of $\Phi_2(\text{H}_2 + \text{CO})$ is represented in Stern-Volmer form

$$\Phi_2(\text{H}_2 + \text{CO}) = \left[\frac{1}{\frac{1}{(1 - \Phi_1(\lambda))} + \alpha(\lambda, T) \times P} \right]^{-1}$$

where $\alpha(\lambda, T)$ is the quenching coefficient whose values at 300 K can be estimated directly from Φ_1 and Φ_2

$$\alpha(\lambda, 300 \text{ K}) = \left[\frac{1}{\Phi_2(\lambda, 300 \text{ K})} - \frac{1}{(1 - \Phi_1(\lambda))} \right]^{-1}$$

where the quantum yields at standard pressure (1 atmosphere) and 300 K are given in Table 4D-4.

At temperatures between 220 and 300 K the quenching coefficient $\alpha(\lambda, T)$ can be calculated using

$$\alpha(\lambda, T) = \alpha(\lambda, 300 \text{ K}) \times \left\{ 1 + 0.05 \times (\lambda - 329) \times \left[\frac{(300 - T)}{80} \right] \right\}$$

The formulae given above for the pressure and temperature dependence of the quantum yields are recommended.

**Table 4D-2. Absorption Cross Sections of CH₂O at 298 K and Temperature Coefficients
Averaged over 1 nm Intervals**

λ (nm)	$10^{20} \sigma$ (cm ²)	$10^{24} \Gamma(\lambda)$ (cm ² ·K ⁻¹)	λ (nm)	$10^{20} \sigma$ (cm ²)	$10^{24} \Gamma(\lambda)$ (cm ² ·K ⁻¹)	λ (nm)	$10^{20} \sigma$ (cm ²)	$10^{24} \Gamma(\lambda)$ (cm ² ·K ⁻¹)
226	0.0179	—	276	2.59	-2.040	326	6.87	-5.640
227	0.0169	—	277	1.57	1.933	327	4.37	5.440
228	0.0177	—	278	1.03	1.427	328	1.22	5.067
229	0.0190	—	279	2.45	-2.547	329	3.12	-3.347
230	0.0205	—	280	2.34	-0.680	330	3.86	-2.173
231	0.0330	—	281	1.56	0.560	331	1.41	3.907
232	0.0335	—	282	0.972	0.809	332	0.346	1.792
233	0.0262	—	283	0.720	0.005	333	0.214	0.429
234	0.0325	—	284	4.27	-8.720	334	0.159	-0.228
235	0.0363	—	285	4.05	-1.800	335	0.0966	-0.005
236	0.0539	—	286	2.09	1.587	336	0.126	0.325
237	0.0771	—	287	1.15	0.760	337	0.383	0.329
238	0.0569	—	288	3.17	-4.707	338	1.92	1.600
239	0.0682	—	289	3.22	-1.213	339	5.50	-6.587
240	0.0782	—	290	1.17	1.707	340	3.15	5.520
241	0.0775	—	291	1.84	-1.160	341	0.978	5.863
242	0.123	—	292	0.796	1.155	342	0.504	1.216
243	0.159	—	293	3.11	-4.907	343	1.92	-2.987
244	0.109	—	294	7.15	-10.213	344	1.27	0.187
245	0.131	—	295	4.06	3.827	345	0.436	2.765
246	0.163	—	296	2.48	2.120	346	0.119	0.541
247	0.151	—	297	1.36	1.387	347	0.0441	-0.281
248	0.234	—	298	4.22	-4.933	348	0.0757	-0.664
249	0.318	—	299	3.17	1.480	349	0.0378	-0.560
250	0.257	0.203	300	0.963	4.267	350	0.0360	-0.728
251	0.204	0.177	301	1.63	-2.573	351	0.0894	-0.121
252	0.337	-0.072	302	0.852	-2.325	352	0.731	0.368
253	0.289	0.101	303	3.02	-3.600	353	2.28	-5.320
254	0.342	0.137	304	7.23	-4.827	354	1.65	0.600
255	0.450	0.272	305	4.74	4.173	355	0.696	2.456
256	0.629	0.169	306	4.29	0.320	356	0.148	-0.388
257	0.443	0.880	307	1.78	3.187	357	0.0344	—
258	0.307	0.681	308	1.38	0.333	358	0.0186	—
259	0.618	0.084	309	3.26	-3.867	359	0.0111	—
260	0.604	0.447	310	1.74	2.360	360	0.0087	—
261	0.660	0.093	311	0.461	0.075	361	0.0100	—
262	0.602	0.635	312	1.19	-1.227	362	0.0211	—
263	1.08	-0.813	313	0.902	-1.439	363	0.0141	—
264	0.947	0.580	314	5.65	0.720	364	0.0094	—
265	0.530	1.004	315	5.56	2.587	365	0.0088	—
266	0.538	0.431	316	2.54	4.760	366	0.0085	—
267	1.36	-0.880	317	5.79	-2.467	367	0.0091	—
268	1.24	-0.120	318	3.15	3.307	368	0.0143	—
269	0.990	1.116	319	0.975	2.532	369	0.0297	—
270	0.960	0.748	320	1.19	0.240	370	0.0636	—
271	1.94	-1.307	321	1.60	-2.187	371	0.0572	—
272	1.43	1.000	322	0.721	0.149	372	0.0197	—
273	0.810	1.228	323	0.327	0.389	373	0.0113	—
274	0.657	0.871	324	0.861	-0.456	374	0.0091	—
275	2.15	-2.733	325	1.54	2.213	375	0.0087	—

Note:

Meller and Moortgat [128]

$\sigma(\lambda, T) = \sigma(\lambda, 298 \text{ K}) + \Gamma(\lambda)(T - 298)$ for the temperature range 223 – 323 K

Table 4D-3. Absorption Cross Sections of CH₂O at 298 K and 223 K and Temperature Dependence Coefficients Averaged over Intervals Used in Atmospheric Models

λ (nm)	λ range (nm)	$10^{20} \sigma(298 \text{ K})$ (cm ²)	$10^{20} \sigma(223 \text{ K})$ (cm ²)	$10^{24} \Gamma(\lambda)$ (cm ² K ⁻¹)
226.0	224.7 – 227.3	0.0166	—	—
228.6	227.3 – 229.9	0.0181	—	—
231.2	229.9 – 232.6	0.0303	—	—
233.9	232.6 – 235.3	0.0313	—	—
236.7	235.3 – 238.1	0.0625	—	—
239.5	238.2 – 241.0	0.0704	—	—
242.4	241.0 – 243.9	0.126	—	—
245.4	243.9 – 246.9	0.139	—	—
248.5	246.9 – 250.0	0.254	—	—
251.6	250.0 – 253.2	0.270	0.265	0.720
254.8	253.2 – 256.4	0.449	0.435	1.77
258.1	256.4 – 259.7	0.478	0.438	5.35
261.4	259.7 – 263.2	0.698	0.687	1.45
264.9	263.2 – 266.7	0.736	0.698	5.00
268.5	266.7 – 270.3	1.13	1.110	2.80
272.1	270.3 – 274.0	1.30	1.270	3.87
275.9	274.0 – 277.8	1.84	1.890	-5.73
279.7	277.8 – 281.7	1.86	1.890	-3.60
283.7	281.7 – 285.7	2.55	2.720	-22.3
287.7	285.7 – 289.9	2.33	2.380	-7.47
292.0	289.9 – 294.1	2.66	2.930	-34.9
296.3	294.1 – 298.5	3.28	3.230	5.73
300.8	298.5 – 303.0	1.60	1.580	2.80
305.4	303.0 – 307.7	4.42	4.430	-1.73
310.1	307.7 – 312.5	1.63	1.670	-5.47
315	312.5 – 317.5	4.09	4.030	8.40
320	317.5 – 322.5	1.53	1.470	8.13
325	322.5 – 327.5	2.79	2.760	3.87
330	327.5 – 332.5	1.99	1.910	10.5
335	332.5 – 337.5	0.196	0.183	1.71
340	337.5 – 342.5	2.390	2.280	15.2
345	342.5 – 347.5	0.758	0.755	0.480
350	347.5 – 352.5	0.194	0.220	-3.40
355	352.5 – 357.5	0.961	—	—
360	357.5 – 362.5	0.0139	—	—
365	362.5 – 367.5	0.0100	—	—
370	367.5 – 372.5	0.0369	—	—

Note:

Absorption cross sections and temperature coefficients: Meller and Moortgat [128]

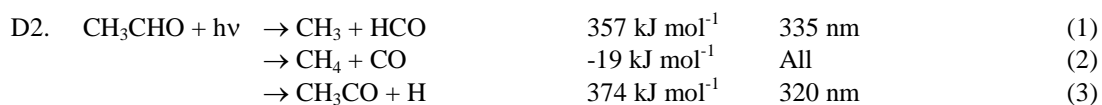
$\sigma(\lambda, T) = \sigma(\lambda, 298 \text{ K}) + \Gamma(\lambda)(T - 298)$ for the temperature range 223 – 323 K

Table 4D-4. CH₂O Photolysis Quantum Yields at 300 K and 1 atmosphere

λ (nm)	Φ (H + HCO)	Φ (H ₂ + CO)	λ (nm)	Φ (H + HCO)	Φ (H ₂ + CO)	λ (nm)	Φ (H + HCO)	Φ (H ₂ + CO)
250	0.310	0.490	288	0.669	0.291	326	0.463	0.537
251	0.308	0.492	289	0.680	0.284	327	0.435	0.565
252	0.307	0.493	290	0.690	0.278	328	0.406	0.594
253	0.306	0.494	291	0.700	0.272	329	0.375	0.625
254	0.305	0.495	292	0.710	0.266	330	0.343	0.657
255	0.304	0.496	293	0.718	0.262	331	0.310	0.690
256	0.304	0.496	294	0.726	0.259	332	0.276	0.714
257	0.303	0.497	295	0.734	0.256	333	0.240	0.730
258	0.303	0.497	296	0.740	0.254	334	0.203	0.737
259	0.304	0.496	297	0.746	0.252	335	0.165	0.735
260	0.307	0.493	298	0.751	0.249	336	0.126	0.724
261	0.312	0.490	299	0.755	0.245	337	0.085	0.705
262	0.318	0.487	300	0.758	0.242	338	0.043	0.687
263	0.325	0.485	301	0.761	0.239	339	0.0	0.665
264	0.333	0.482	302	0.762	0.238	340	—	0.645
265	0.343	0.477	303	0.762	0.238	341	—	0.620
266	0.354	0.471	304	0.762	0.238	342	—	0.590
267	0.365	0.465	305	0.760	0.240	343	—	0.560
268	0.377	0.458	306	0.758	0.242	344	—	0.530
269	0.390	0.450	307	0.754	0.246	345	—	0.505
270	0.404	0.441	308	0.749	0.251	346	—	0.480
271	0.418	0.432	309	0.744	0.256	347	—	0.450
272	0.433	0.422	310	0.737	0.263	348	—	0.425
273	0.448	0.412	311	0.729	0.271	349	—	0.400
274	0.464	0.401	312	0.720	0.280	350	—	0.375
275	0.479	0.391	313	0.709	0.291	351	—	0.350
276	0.495	0.380	314	0.698	0.302	352	—	0.320
277	0.512	0.371	315	0.685	0.315	353	—	0.285
278	0.528	0.362	316	0.671	0.329	354	—	0.250
279	0.544	0.356	317	0.656	0.344	355	—	0.220
280	0.560	0.347	318	0.639	0.361	356	—	0.190
281	0.576	0.337	319	0.622	0.378	357	—	0.160
282	0.591	0.329	320	0.603	0.397	358	—	0.130
283	0.606	0.321	321	0.583	0.417	359	—	0.09
284	0.620	0.313	322	0.561	0.439	360	—	0.04
285	0.633	0.307	323	0.539	0.461	361	—	0.0
286	0.645	0.302	324	0.515	0.485	—	—	—
287	0.657	0.296	325	0.489	0.511	—	—	—

Note:

The recommended quantum yields are based on a fit of the data for $\Phi(\text{H} + \text{HCO})$ from Lewis et al. [104], Marling [119], Horowitz and Calvert [84], Clark et al. [47], Tang et al. [188], Moortgat et al. [139], Smith et al. [179], Pope et al. [159, 160], and Gorrotxategi Carbajo et al. [74], and for $\Phi(\text{H}_2 + \text{CO})$ from Moortgat et al. [139]; see text for details.



(Recommendation: 06-2, Note: 10-6, Evaluated: 10-6)

Absorption Cross Sections: The UV absorption spectrum of acetaldehyde, CH₃CHO, has been measured at room temperature by McMillan [36] (200 – 345 nm), Meyrahn et al. [133] (221 – 345 nm), Schneider and

Moortgat [169] (197 – 362 nm), Libuda et al. [105, 107] (235 – 360 nm), Martinez et al. [120] (202 – 365 nm), Limão-Vieira et al. [110] (240 – 350 nm), and Weaver et al. [203] (290 – 355 nm). The spectrum at wavelengths >200 nm consists of an absorption band with a peak at 290 nm and diffuse vibrational structure (~12 maxima or shoulders) at wavelengths >260 nm. The agreement between the various cross section studies is very good, mostly 5% or better, except for the results from Meyrahn et al. [133], which are lower by ~10% in the structured region around the absorption maximum. The recommended cross sections in Table 4D-5 are based on the data of Libuda et al. [105, 107] (1 nm averages of 0.6 nm resolution data) and Martinez et al. [120] (4 nm averages of 0.5 nm resolution data at 202 – 278 nm and 1 nm averages at 280 – 360 nm), for which the agreement is within 5% between 255 and 325 nm.

Spectrum measurements in the VUV have been reported by Lake and Harrison [101] (150 – 180 nm), Lucazeau and Sandorfy [111] (118 – 189 nm), Brint et al. [30] (120 – 180 nm), and Limão-Vieira et al. [110] (113 – 200 nm).

Photolysis Quantum Yield and Product Studies: The photodissociation quantum yield of CH₃CHO and the product quantum yields are wavelength and pressure dependent. Quantum yield measurements have been reported by Calvert and Pitts [36] and Weaver et al. [203] at isolated wavelengths between 290 and 332 nm. Quantum yields of CO, CH₄ and CO₂ were determined in the photolysis of trace concentrations of CH₃CHO in air and N₂ in the spectral range 250 – 330 nm at 1 atmospheric pressure by Meyrahn et al. [133], which allowed the determination of ($\Phi_1 + \Phi_2$), Φ_2 , and Φ_3 . The product quantum yield pressure dependence was also investigated by Meyrahn [132] at 270, 303.4 and 313 nm. Horowitz et al. [86] and Horowitz and Calvert [85] measured the quantum yields of CO, CH₄ and H₂ formation at 290, 300, 313, 320 and 332 nm in the presence of various pressures of O₂ and CO₂ from which Φ_1 and Φ_2 were derived. There is evidence from the studies of Meyrahn et al. [132, 133] and Horowitz et al. [86] that some CO₂ is formed from secondary reactions of the CH₃CO radical that is produced in channel (3). The quantum yield for channel 3 was estimated to be 0.025 at 300 nm and to decrease to zero at 320 nm. Both Meyrahn et al. [132, 133] and Horowitz et al. [85, 86] observed a pressure dependence of the product yields, from which Stern-Volmer quenching coefficients were derived. These data were summarized by Calvert et al. [33].

The quantum yield recommendation given in Table 4D-6 for room temperature and atmospheric pressure are based on the evaluation by Atkinson and Lloyd [11] and the measurements by Horowitz and Calvert [85], Meyrahn et al. [133] and Meyrahn [132].

Table 4D-5. Absorption Cross Sections of CH₃CHO at 298 K

λ (nm)	$10^{20} \sigma$ (cm ²)	λ (nm)	$10^{20} \sigma$ (cm ²)	λ (nm)	$10^{20} \sigma$ (cm ²)	λ (nm)	$10^{20} \sigma$ (cm ²)
202	0.056	286	4.41	312	2.52	338	0.212
206	0.053	287	4.56	313	2.47	339	0.206
210	0.049	288	4.69	314	2.38	340	0.135
214	0.048	289	4.74	315	2.20	341	0.0664
218	0.052	290	4.86	316	2.07	342	0.0416
222	0.065	291	4.75	317	2.08	343	0.0305
226	0.096	292	4.66	318	1.98	344	0.0267
230	0.151	293	4.51	319	1.84	345	0.0210
234	0.241	294	4.31	320	1.70	346	0.0199
238	0.375	295	4.26	321	1.48	347	0.0149
242	0.639	296	4.24	322	1.38	348	0.0159
246	0.887	297	4.37	323	1.23	349	0.0664
250	1.18	298	4.41	324	1.06	350	0.00774
254	1.57	299	4.26	325	1.15	351	0.00695
258	2.03	300	4.15	326	1.09	352	0.00497
262	2.45	301	3.97	327	0.808	353	0.00552
266	3.06	302	3.87	328	0.715	354	0.00436
270	3.38	303	3.70	329	0.741	355	0.00500
274	4.03	304	3.46	330	0.699	356	0.00518
278	4.15	305	3.43	331	0.560	357	0.00345
280	4.48	306	3.41	332	0.496	358	0.00428
281	4.65	307	3.36	333	0.420	359	0.00207
282	4.66	308	3.31	334	0.333	360	0.00275
283	4.70	309	3.11	335	0.350		
284	4.58	310	2.92	336	0.227		
285	4.46	311	2.73	337	0.219		

Note:

202 – 238 nm: Martinez et al. [120]

240 – 360 nm: mean of data from Martinez et al. [120] and Libuda et al. [105, 107]

Table 4D-6. CH₃CHO Photolysis Quantum Yields at 1 bar Total Pressure

λ (nm)	Φ_1 (CH ₃ + HCO)	Φ_2 CH ₄ + CO	λ (nm)	Φ_1 (CH ₃ + HCO)
256	0.29	0.48	296	0.47
258	0.30	0.47	298	0.45
260	0.31	0.45	300	0.43
262	0.32	0.43	302	0.40
264	0.34	0.40	304	0.38
266	0.36	0.37	306	0.35
268	0.38	0.33	308	0.31
270	0.41	0.29	310	0.28
272	0.44	0.25	312	0.24
274	0.48	0.20	314	0.19
276	0.53	0.16	316	0.15
278	0.56	0.09	318	0.12
280	0.58	0.06	320	0.10
282	0.59	0.04	322	0.07
284	0.59	0.03	324	0.05
286	0.58	0.02	326	0.03
288	0.56	0.01	328	0.02
290	0.54	0.01	330	0.01
292	0.52	0.005	332	0
294	0.50	0		

D3.	$\text{C}_2\text{H}_5\text{CHO} + h\nu \rightarrow \text{C}_2\text{H}_5 + \text{HCO}$	351 kJ mol ⁻¹	341 nm	(1)
	$\rightarrow \text{C}_2\text{H}_6 + \text{CO}$	-8 kJ mol ⁻¹	All	(2)
	$\rightarrow \text{C}_2\text{H}_4 + \text{HCHO}$	129 kJ mol ⁻¹	926 nm	(3)
	$\rightarrow \text{CH}_3 + \text{CH}_2\text{CHO}$	343 kJ mol ⁻¹	349 nm	(4)

(Recommendation: 06-2, Note: 10-6, Evaluated: 10-6)

Absorption Cross Sections: The UV absorption spectrum of propionaldehyde ($\text{C}_2\text{H}_5\text{CHO}$, propanal) has been measured at room temperature by Lucazeau and Sandorfy [111] (118 – 190 nm), McMillan [36] (220 – 342 nm), and Martinez et al. [120] (262 – 365 nm). Absorption cross sections have also been reported for isolated wavelengths by Blacet and Crane [21] (187 – 313 nm), Heicklen et al. [80] (293-325 nm), and Chen and Zhu [43] (280 – 330 nm). The spectrum at wavelengths >200 nm consists of an absorption band with structured features (~9 maxima or shoulders) at wavelengths >260 nm and maximum absorption at 285 and 293 nm. The agreement between the results from Martinez et al. [120] and McMillan [36] is excellent, i.e., $\leq 5\%$, between 238 and 322 nm. At shorter (longer) wavelengths the differences increase to ~30% (~50%). The data points reported by Heicklen et al. [80] fit well to these studies although the value reported at 293 nm is 20% smaller. The cross sections reported at 5 nm intervals by Chen and Zhu [43] agree to within 10% with those reported by Martinez et al. [120], except the data at 285 and 330 nm which are 20% and 30% larger. The recommended absorption cross sections listed in Table 4D-7 are taken from Martinez et al. [120] and are 4 nm averages of the 0.5 nm resolution data in the region 202 – 278 nm and 1 nm averages in the region 280 – 360 nm.

Photolysis Quantum Yield and Product Studies: Quantum yield measurements have been performed by Heicklen et al. [80] and Chen and Zhu [43]. Heicklen et al. [80] measured the quantum yield of HO_2 and $\text{C}_2\text{H}_5\text{O}_2$ radicals (in air bath gas) using laser photolysis at 294, 302, 312 and 325 nm combined with UV absorption to determine Φ_1 . Quantum yields of CO and C_2H_6 were obtained in steady-state photolysis (at 254, 312 and 334 nm) experiments in O_2 where $\Phi_1 = \Phi(\text{CO}) - \Phi(\text{C}_2\text{H}_6)$ and $\Phi_2 = \Phi(\text{C}_2\text{H}_6)$. A Stern-Volmer pressure dependence of the quantum yields was observed at all wavelengths, i.e., lower quantum yields at higher pressures. At atmospheric pressure, values of $\Phi_1 = 0.22, 0.89, 0.85, 0.50, 0.26$ and 0.15 were derived at 254, 294, 302, 313, 325 and 334 nm, respectively. Heicklen et al. [80] reported $\Phi_2 = 0.33$ for 254 nm photolysis and $\Phi_2 = 0$ at longer wavelengths. The contribution of other primary processes (Φ_3 and Φ_4) was found to increase at wavelengths <265 nm from earlier studies as cited in Calvert and Pitts [36].

Chen and Zhu [43] measured the quantum yield of HCO radicals (Φ_1) over the wavelength range 280 – 330 nm using time-resolved cavity ring-down spectroscopy with detection of HCO at 613.8 nm. The reported HCO yields are 0.85 ± 0.06 at 280 nm, 1.01 ± 0.07 at 285 nm, 0.95 ± 0.06 at 290 nm, 0.98 ± 0.06 at 295 nm, 0.92 ± 0.06 at 300 nm, 0.95 ± 0.08 at 305 nm, 0.98 ± 0.11 at 310 nm, 0.91 ± 0.05 at 315 nm, 1.08 ± 0.07 at 320 nm, 1.07 ± 0.14 at 325 nm, and 0.84 ± 0.08 at 330 nm. These values are quoted for zero-pressure but no pressure dependence to the HCO quantum yield at any wavelength was observed for pressures over the range 10 – 400 Torr N_2 .

The quantum yield studies by Heicklen et al. [80] and Chen and Zhu [43] are only in agreement in the narrow wavelength range 290 – 305 nm. At $\lambda > 305$ nm, the data of Chen and Zhu do not show the decrease of Φ_1 reported by Heicklen et al [80]. Because of the discrepancies between these data sets no quantum yield recommendation is given.

Table 4D-7. Absorption Cross Sections of C₂H₅CHO at 298 K

λ (nm)	$10^{20} \sigma$ (cm ²)	λ (nm)	$10^{20} \sigma$ (cm ²)	λ (nm)	$10^{20} \sigma$ (cm ²)	λ (nm)	$10^{20} \sigma$ (cm ²)
202	0.049	285	5.86	310	3.60	335	0.325
206	0.049	286	5.82	311	3.53	336	0.280
210	0.057	287	5.72	312	3.50	337	0.230
214	0.069	288	5.59	313	3.32	338	0.185
218	0.080	289	5.52	314	3.06	339	0.166
222	0.091	290	5.56	315	2.77	340	0.155
226	0.115	291	5.68	316	2.43	341	0.119
230	0.163	292	5.81	317	2.18	342	0.076
234	0.257	293	5.88	318	2.00	343	0.045
238	0.407	294	5.80	319	1.86	344	0.031
242	0.622	295	5.57	320	1.83	345	0.025
246	0.909	296	5.37	321	1.78	346	0.019
250	1.29	297	5.16	322	1.66	347	0.016
254	1.75	298	5.02	323	1.58	348	0.014
258	2.25	299	5.02	324	1.49	349	0.013
262	2.88	300	5.04	325	1.30	350	0.010
266	3.43	301	5.09	326	1.13	351	0.008
270	4.12	302	5.07	327	0.996	352	0.007
274	4.59	303	4.94	328	0.828	353	0.005
278	5.17	304	4.69	329	0.685	354	0.004
280	5.16	305	4.32	330	0.575	355	0.002
281	5.21	306	4.04	331	0.494	356	0.001
282	5.35	307	3.81	332	0.466	357	0.001
283	5.57	308	3.65	333	0.430		
284	5.78	309	3.62	334	0.373		

Note:

202 – 357 nm: Martinez et al. [120]

D4. CH₃O₂ + hν → Products

(Recommendation: 06-2, Note: 10-6, Evaluated: 10-6)

Absorption Cross Sections: The UV absorption cross sections of the methylperoxy radical, CH₃O₂, in the 195 – 310 nm region have been measured at room temperature by Parkes et al. [155], Hochanadel et al. [83], Parkes [153], Anastasi et al. [8], Kan et al. [93], Cox and Tyndall [51, 52] at 250 nm only; Adachi et al. [3], Sander and Watson [171] at 250 nm only, Pilling and Smith [157] at 254 nm only, Kurylo et al. [99], McAdam et al. [124], Jenkin et al. [91], Wallington et al. [199], Moortgat et al. [141], Dagaut and Kurylo [53], Simon et al. [174], Jenkin and Cox [90], Lightfoot and Jemi-Alade [109] who measured the cross sections up to 777 K, Maricq and Wallington [118], Wallington et al. [201], Roehl et al. [166], Fahr et al. [60] and Nielsen et al. [148]. The absorption cross sections have been evaluated in earlier reviews by Lightfoot et al. [108] and Wallington et al. [200], who noted significant discrepancies in both the shapes of the spectra and the absolute magnitude of the cross section values. The ultraviolet absorption spectra have recently been reevaluated by Tyndall et al. [192], who fit the absorption spectra to a semi-logarithmic Gaussian distribution function suggested by Lightfoot et al. [108] and Maric et al. [115]

$$\sigma = \sigma_{\max} \exp \left[-a \left(\ln \left(\frac{\lambda_{\max}}{\lambda} \right) \right)^2 \right]$$

Screening of the data suggested that most spectra published before 1987 did not constrain the shape of the spectrum very well as indicated by the large relative uncertainty of the width parameter *a*. The shape was determined by averaging the individual fitting parameters from McAdam et al. [124], Moortgat et al. [141], Simon et al. [174], Lightfoot and Jemi-Alade [109], Jenkin and Cox [90] and Maricq and Wallington [118], which were judged to be most reliable by Tyndall et al. [192]. Absolute cross sections were based on relative measurements of absorption cross sections of CH₃O₂ and C₂H₅O₂ at 240 nm taken under identical conditions (Wallington et al. [200], Maricq and Wallington [118], Fenter et al. [63] and Roehl et al. [166]), combined

with independent calibrations by Dagaut and Kurylo [53], Simon et al. [174] and Lightfoot and Jemi-Alade [109]. The fit parameters are: $\sigma_{\max} = 4.26 \times 10^{-18} \text{ cm}^2 \text{ molecule}^{-1}$; $a = 44.4$; $\lambda_{\max} = 237.3 \text{ nm}$. Table 4D-8 lists the recommended cross sections, which are taken from the review by Tyndall et al. [192]. The shape of the UV spectrum measured by Nielsen et al. [148] is in excellent agreement with the recommendation of Tyndall et al. [192].

Photolysis Quantum Yield and Product Studies: Photolysis of CH_3O_2 in the stratosphere and troposphere is slow and can be neglected, but the UV absorption cross sections are important in laboratory studies of reaction kinetics.

Table 4D-8. Absorption Cross Sections of CH_3O_2 , $\text{C}_2\text{H}_5\text{O}_2$, and $\text{CH}_3\text{C(O)O}_2$ at 298 K

λ (nm)	$10^{20} \sigma \text{ (cm}^2\text{)}$		
	CH_3O_2	$\text{C}_2\text{H}_5\text{O}_2$	$\text{CH}_3\text{C(O)O}_2$
195.0			389
200.0			564
205.0	165		665
210.0	219	195	656
215.0	276	257	564
220.0	330	319	451
225.0	376	374	366
230.0	408	418	326
235.0	424	444	319
240.0	424	452	326
245.0	407	440	330
250.0	378	412	322
255.0	339	372	300
260.0	294	324	268
265.0	248	273	229
270.0	203	222	187
275.0	162	176	147
280.0	126	136	111
285.0	96.1	102	81.2
290.0	71.5	74.6	57.3
295.0	52.0	53.3	
300.0		37.3	

D5. $\text{C}_2\text{H}_5\text{O}_2 + h\nu \rightarrow \text{Products}$

(Recommendation: 06-2, Note: 10-6, Evaluated: 10-6)

Absorption Cross Sections: The absorption cross sections of the ethylperoxy radical, $\text{C}_2\text{H}_5\text{O}_2$, in the 200 – 310-nm region have been measured at room temperature by Adachi et al. [2], Cattell et al. [41], Wallington et al. [200], Bauer et al. [17], Maricq and Wallington [118], Fenter et al. [63], Munk et al. [144], and Nielsen et al. [2002] and as a function of temperature by Anastasi et al. [9], Fenter et al. [63], and Fauvet et al. [61]. The absorption cross sections have been evaluated in earlier reviews by Lightfoot et al. [108] and Wallington et al. [200], who noted significant discrepancies in the both the shapes of the spectra and the absolute magnitude of the cross section values. The ultraviolet absorption spectra have recently been reevaluated by Tyndall et al. [192], who fit the absorption spectra to a semi-logarithmic Gaussian distribution function suggested by Lightfoot et al. [108] and Maric et al. [115]

$$\sigma = \sigma_{\max} \exp \left[-a \left(\ln \left(\frac{\lambda_{\max}}{\lambda} \right) \right)^2 \right]$$

The shape was determined by averaging the individual fitting parameters from Wallington et al. [200], Bauer et al. [17], Maricq and Wallington [118], and Fenter et al. [63], which were judged to be most reliable by Tyndall et al. [192]. Absolute cross sections were based on relative measurements of absorption cross sections of CH_3O_2 and $\text{C}_2\text{H}_5\text{O}_2$ at 240 nm taken under identical conditions (Wallington et al. [200], Maricq and Wallington [118], Fenter et al. [63], Roehl et al. [166]) and Nielsen et al. [148] combined with independent calibrations. The fitting parameters are $\sigma_{\max} = 4.52 \times 10^{-18} \text{ cm}^2 \text{ molecule}^{-1}$, $a = 49.0$, $\lambda_{\max} =$

239.4 nm. Table 4D-8 lists the recommended cross sections, which are taken from the review by Tyndall et al.

Photolysis Quantum Yield and Product Studies: Photolysis of C₂H₅O₂ in the stratosphere and troposphere is slow and can be neglected, but important in laboratory studies of reaction kinetics.

D6. CH₃CO + hν → Products

(Recommendation: 10-6, Note: 10-6, Evaluated: 10-6)

Absorption Cross Sections. The UV absorption spectrum of the acetyl radical, CH₃CO, has been measured by Adachi et al. [1, 4], Parkes [154], Anastasi and Maw [7], Basco and Parmar [14], Maricq and Szenté [117] and Cameron et al. [39]. The spectrum has a very broad band in the range 190 – 270 nm with maximum near 215 nm. The shapes and magnitudes of the reported spectra differ substantially in the different studies. Adachi et al. [1, 4] and Basco and Parmar [14] report a peak cross section of 3.75 × 10⁻¹⁷ cm² molecule⁻¹ whereas Maricq and Szenté [117] report a value of 1.07 × 10⁻¹⁷ cm² molecule⁻¹ at 216 nm and Ansatasi and Maw [7] a value of 0.7 × 10⁻¹⁷ cm² molecule⁻¹ at 223 nm. Cameron et al. [39] measured a cross section of (1.4 ± 0.2) × 10⁻¹⁷ cm² molecule⁻¹ at 220 nm. Cameron et al. [39] also measured the spectrum using diode array spectroscopy in the range 190 – 247 nm; the shape of the spectrum being in reasonable agreement with the spectrum measured by Maricq and Szenté [117]. The spectrum by Cameron et al. [39] is given by the equation

$$\sigma(\lambda) = a_1 \exp[-a_2 (\ln(a_3/\lambda))^2]$$

where $a_1 = 1.549 \times 10^{-17}$ $a_2 = 129.19$ $a_3 = 213.985$

The visible absorption spectrum of CH₃CO was measured by Rajakumar et al. [162] in the wavelength range 490 – 660 nm using cavity ring-down spectroscopy. The spectrum has a broad continuous band with a broad peak at 535 nm. The spectrum obtained with the H₂O₂ photolysis source (in the presence of CH₃CHO) was used as a reference and fit with an empirical polynomial expression

$$\sigma(\lambda) = A + B\lambda + C\lambda^2 + D\lambda^3 + E\lambda^4$$

yielding the parameters (σ in units of cm² molecule⁻¹, λ in nm)

$$\begin{array}{ll} A = -6.6124 \times 10^{-17} & D = 1.02141 \times 10^{-24} \\ B = 4.1946 \times 10^{-19} & E = -3.93411 \times 10^{-28} \\ C = -9.865 \times 10^{-22} & \end{array}$$

The recommended UV absorption cross sections in Table 4D-9 were calculated using the equation from Cameron et al. [39]. The recommended cross sections in the visible region in Table 4D-10 were calculated using the polynomial expression from Rajakumar et al. [162].

Table 4D-9. UV Absorption Cross Sections of CH₃CO at 298 K

λ (nm)	$10^{20} \sigma$ (cm ²)	λ (nm)	$10^{20} \sigma$ (cm ²)	λ (nm)	$10^{20} \sigma$ (cm ²)
190	250	210	1480	230	790
192	339	212	1530	232	666
194	447	214	1550	234	551
196	572	216	1530	236	449
198	711	218	1480	238	359
200	859	220	1400	240	283
202	1010	222	1300	242	219
204	1150	224	1180	244	167
206	1290	226	1050	246	126
208	1400	228	921	248	93.1

Note:

using expression from Cameron et al. [39]

Table 4D-10. Vis Absorption Cross Sections of CH₃CO at 298 K

λ (nm)	$10^{20} \sigma$ (cm ²)	λ (nm)	$10^{20} \sigma$ (cm ²)	λ (nm)	$10^{20} \sigma$ (cm ²)
500	7.41	555	10.22	610	4.65
505	8.36	560	9.87	615	4.05
510	9.31	565	9.38	620	3.57
515	9.96	570	8.96	625	3.11
520	10.45	575	8.44	630	2.96
525	10.78	580	7.90	635	2.30
530	10.97	585	7.34	640	1.95
535	11.03	590	6.78	645	1.64
540	10.97	595	6.21	650	1.36
545	10.82	600	5.65	655	1.11
550	10.58	605	5.10	660	0.94

Note:

using expression from Rajakumar et al. [162]

D7. CH₃C(O)O₂ + hν → Products

(Recommendation: 06-2, Note: 10-6, Evaluated: 10-6)

Absorption Cross Sections: The UV absorption spectrum of the acetylperoxy radical, CH₃C(O)O₂, is continuous with two absorption bands in the 185 – 300 nm region. The band centered at 245 nm is overlapped by a stronger band that peaks near 207 nm. Absorption cross sections have been measured at room temperature by Addison et al. [5], Basco and Parmer [14], Moortgat et al. [141], Maricq and Szenté [116], and Roehl et al. [166]. The absorption cross sections have been evaluated in reviews by Lightfoot et al. [108], Wallington et al. [200], and Tyndall et al. [192] and significant discrepancies in the both the shapes of the spectra and the absolute magnitude of the cross section values have been noted. Tyndall et al. [192] fit the absorption spectrum reasonably well to the sum of two Gaussian shaped absorption bands

$$\sigma = \sigma_{\max 1} \exp^{-a_1 \left[\ln \left(\frac{\lambda_{\max 1}}{\lambda} \right) \right]^2} + \sigma_{\max 2} \exp^{-a_2 \left[\ln \left(\frac{\lambda_{\max 2}}{\lambda} \right) \right]^2}$$

The optimized fit parameters were determined by averaging the fit parameters from Maricq and Szenté [116] and Roehl et al. [166], which were judged to be the most reliable. It should be noted that the data from Maricq and Szenté were adjusted for their overcorrection for the contribution of CH₃O₂. Absolute cross sections were based on relative measurements to the absorption cross sections of C₂H₅O₂ at 240 nm. The fitting parameters are

$$\sigma_{\max 1} = 6.29 \times 10^{-18} \text{ cm}^2 \text{ molecule}^{-1} \quad \sigma_{\max 2} = 3.26 \times 10^{-18} \text{ cm}^2 \text{ molecule}^{-1}$$

$$\lambda_{\max 1} = 206.0 \text{ nm} \quad \lambda_{\max 2} = 246.1 \text{ nm}$$

$$a_1 = 168.0 \quad a_2 = 64.2.$$

The recommended absorption cross sections in Table 4D-8 are taken from the review by Tyndall et al. [192].

Photolysis Quantum Yield and Product Studies: Photolysis of $\text{CH}_3\text{C}(\text{O})\text{O}_2$ in the stratosphere and troposphere is slow and can be neglected.

D8. $\text{CH}_3\text{C}(\text{O})\text{CH}_2\text{O}_2 + h\nu \rightarrow \text{Products}$

(Recommendation: 10-6, Note: 10-6, Evaluated: 10-6)

Absorption Cross Sections: The UV absorption spectrum of the acetonylperoxy radical, $\text{CH}_3\text{C}(\text{O})\text{CH}_2\text{O}_2$, has been measured at room temperature by Cox et al. [50], Bridier et al. [29] and Nielsen et al. [148]. The spectra from Cox et al. [50] and Nielsen et al. [148] are in good agreement but differ significantly from the spectrum reported by Bridier et al. [29]. The spectrum reported by Cox et al. [50] and Nielsen et al. [148] exhibit two absorption features in the 200 – 340 nm region; a strong band at wavelengths <260 nm and a fairly weak band centered at 300 nm. Nielsen et al. [148] determined the cross section of the acetonylperoxy radical at 240 nm to be $(2.03 \pm 0.22) \times 10^{-18} \text{ cm}^2 \text{ molecule}^{-1}$ relative to the well-established absorption cross section of CH_3O_2 . The cross sections of Cox et al. [50], renormalized to the absolute value at 240 nm of Nielsen et al. [148], are recommended and listed in Table 4D-11.

Photolysis Quantum Yields and Product Studies: No product studies are available.

Table 4D-11. Absorption Cross Sections of $\text{CH}_3\text{C}(\text{O})\text{CH}_2\text{O}_2$ at 298 K

λ (nm)	$10^{20} \sigma$ (cm^2)	λ (nm)	$10^{20} \sigma$ (cm^2)
225	313	290	111
230	254	300	112
235	228	310	110
240	203	320	104
245	186	330	92
250	157	340	71
255	135	350	51
260	111	360	33
270	101	370	17
280	106	380	7

Note:

Cox et al. [50], normalized to the 240 nm cross section from Nielsen et al. [148]



(Recommendation: 10-6, Note: 10-6, Evaluated: 10-6)

Absorption Cross Sections: The absorption spectrum of CH_3OOH (methylhydroperoxide) was measured at room temperature by Cox and Tyndall [51] (210 – 280 nm), Nozière et al. [149] (220 – 250 nm), Molina and Arguello [135] (210 – 350 nm), Vaghjiani and Ravishankara [193] (210 – 365 nm), Blitz et al. [22] (210 – 355 nm), Matthews et al. [121] (365 – 405 nm) and Roehl et al. [167] (305 – 365 nm).

Vaghjiani and Ravishankara [193] measured the cross sections of CH_3OOH by monitoring the CH_3OOH concentration via trapping and titration. These results are recommended and are listed in Table 4D-12. The earlier results of Molina and Arguello [135] are consistently 40% higher than the values shown in Table 4D-12. This difference is believed to be due to difficulty in trapping CH_3OOH and measuring its concentration. The results of Blitz et al. [22] are consistently 30% smaller than the data of Vaghjiani and Ravishankara [193] in the range 225 – 325 nm but are unreliable above 325 nm due to baseline problems during their measurements. The absorption cross sections of Roehl et al. [167] determined using action spectroscopy are

8-21 % greater than those measured by Vaghjiani and Ravishankara [193]. Similar absorption measurements were performed by Matthews et al. [121] in the weak tail of the absorption band up to 405 nm. Their cross sections were normalized to the value of Vaghjiani and Ravishankara [193] at 355 nm and are included in the recommendation in Table 4D-12.

Matthews et al. [121] also measured the absorption of the $5\nu_{\text{OH}}$ overtone band near 620 nm as $(3.6 \pm 0.4) \times 10^{-24} \text{ cm}^2 \text{ molecule}^{-1}$.

Photolysis Quantum Yields and Product Studies: CH_3OOH dissociates upon light absorption to give CH_3O with unit quantum yield, $\Phi_1 = 1.00 \pm 0.18$ (Vaghjiani and Ravishankara [194]). These authors also observed some production of H (quantum yield of 0.038 ± 0.007) and O atoms (quantum yield < 0.007) at shorter wavelengths (i.e., 193 nm).

Thelen et al. [190] report unit quantum yields for OH production at 248 and 193 nm that are in agreement with the results of Vaghjiani and Ravishankara [193]. Quantum yields for OH and CH_3O were also measured by Blitz et al. [22] in the wavelength range 223 – 355 nm. These authors have shown that the quantum yield for both OH and CH_3O production is unity across this range of wavelengths.

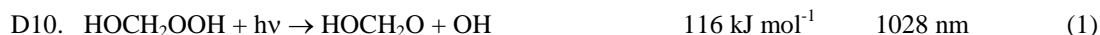
Table 4D-12. Absorption Cross Sections of CH_3OOH at 298 K

λ (nm)	$10^{20} \sigma$ (cm^2)	λ (nm)	$10^{20} \sigma$ (cm^2)
210	31.2	310	0.239
215	20.9	315	0.182
220	15.4	320	0.137
225	12.2	325	0.105
230	9.62	330	0.079
235	7.61	335	0.061
240	6.05	340	0.047
245	4.88	345	0.035
250	3.98	350	0.027
255	3.23	355	0.021
260	2.56	360	0.016
265	2.11	365	0.012
270	1.70	370	0.0075
275	1.39	375	0.0052
280	1.09	380	0.0040
285	0.863	385	0.0025
290	0.691	390	0.0014
295	0.551	395	0.0010
300	0.413	400	0.0006
305	0.313	405	0.0003

Note:

210 – 365 nm: data of Vaghjiani and Ravishankara [194]

370 – 405, 620 nm: data of Matthews et al. [121]



(Recommendation: 10-2, Note: 10-6, Evaluated: 10-6)

Absorption Cross Sections: The UV absorption spectrum of hydroxymethyl hydroperoxide, HOCH_2OOH , was measured at 298 K by Bauerle and Moortgat [18] in the range 205 – 360 nm, using a combination of diode array and FTIR spectroscopy. The absorption cross sections were also determined via action spectroscopy of the OH product by Roehl et al. [167] in the range 310 – 360 nm. The cross sections measured by Roehl et al. [167] were normalized to the value of Bauerle and Moortgat [18] at 320 nm. Their values are in reasonable agreement (within 20 %) between 310 and 340 nm but remain lower than those of Bauerle and Moortgat [18] at longer wavelengths (e.g. 33 % at 350 nm). The recommended cross sections listed in Table 4D-13 are taken from Bauerle and Moortgat [18] in the range 205 – 305 nm, and from the average of the values of Bauerle and Moortgat [18] and Roehl et al. [167] for the region 310 – 380 nm.

Photolysis Quantum Yields and Product Studies: The photolysis process is assumed to occur with unity quantum yield Φ_1 at wavelengths larger than 290 nm, in analogy with CH_3OOH . Overtone photodissociation spectrum and quantum yields were obtained in the OH-stretching region from the $4\nu_{\text{OH}}$ and $5\nu_{\text{OH}}$ transitions (centered near 750/738 and 617/604 nm, respectively) by Fry et al. [66]. Overtone photodissociation is not expected to be significant under atmospheric conditions.

Table 4D-13. Absorption Cross Sections of HOCH_2OOH at 298 K

λ (nm)	$10^{20} \sigma$ (cm^2)	λ (nm)	$10^{20} \sigma$ (cm^2)
205	26.9	285	0.75
210	22.6	290	0.63
215	18.7	295	0.51
220	15.5	300	0.40
225	12.5	305	0.29
230	10.1	310	0.23
235	7.89	315	0.18
240	5.98	320	0.13
245	4.68	325	0.098
250	3.78	330	0.072
255	2.88	335	0.056
260	2.31	340	0.042
265	1.81	345	0.032
270	1.48	350	0.025
275	1.21	355	0.019
280	0.93	360	0.014

Note:

205 – 305 nm: Bauerle and Moortgat [18]

310 – 380 nm: average of data from Bauerle and Moortgat [18] and Roehl et al. [167]



(Recommendation: 10-6, Note: 10-6, Evaluated: 10-6)

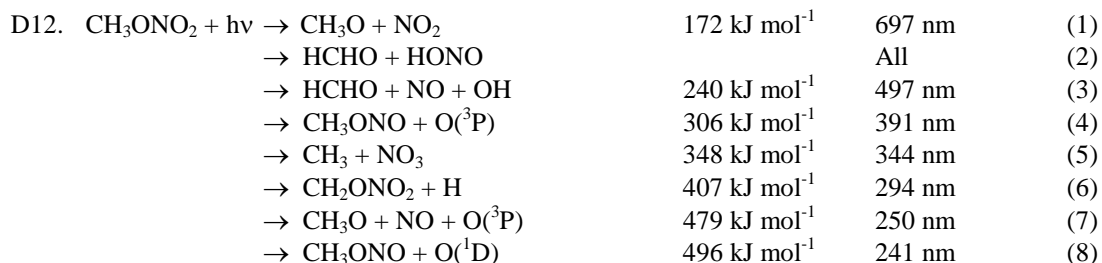
Absorption Cross Sections. The UV/vis absorption spectrum of methylnitrite (CH_3ONO) extends over the wavelength range between 190 and 440 nm and has a strong continuous band in the UV (190 – 300 nm) with maximum near 214 nm. A sharply banded region exists in the near UV-Visible region (300 – 440 nm) with nine absorption peaks, the strongest at ~339 nm. The spectrum has been measured at room temperature by McMillan [38], Taylor et al. [189], and Maricq and Wallington [118] while single wavelength absorption measurements have been reported by Napier and Norrish [147] at 215 and 339 nm at 298 K and by Wiebe and Heicklen [204] at 366 nm for temperatures in the range 298 – 423 K. Good agreement exists among these studies for the shape of the UV part of the spectrum. However, a slight wavelength shift is apparent (up to 4 nm) in the peak absorptions measured by Taylor et al. [189] and McMillan [38]. Taylor et al. [189] reported the cross section at the short wavelength band maximum near 215 nm to be $(4.59 \pm 0.58) \times 10^{-18}$ compared to 4.97×10^{-18} by Napier and Norrish [147], 4.2×10^{-18} by McMillan [38] and $4.47 \times 10^{-18} \text{ cm}^2 \text{ molecule}^{-1}$ by Maricq and Wallington [118]. A cross section of $(3.24 \pm 0.16) \times 10^{-19}$ measured by Taylor et al. [189] at $339 \pm 1 \text{ nm}$ is in accord with the values of 3.4×10^{-19} and $3.1 \times 10^{-19} \text{ cm}^2 \text{ molecule}^{-1}$ reported by Napier and Norrish [147] and McMillan [38], respectively. The spectrum measured by Taylor et al. [189] is recommended and listed in Table 4D-14.

Photolysis Quantum Yields and Product Studies: The quantum yield for the dissociation in the banded region (300 – 400 nm) was measured by Wiebe et al. [205] to be $\Phi_1 = 0.76$ at 366 nm.

Table 4D-14. Absorption Cross Sections of CH₃ONO at 298 K

λ (nm)	$10^{20} \sigma$ (cm ²)	λ (nm)	$10^{20} \sigma$ (cm ²)	λ (nm)	$10^{20} \sigma$ (cm ²)
190	180	306	6.2	362	15
195	240	310	9.0	364	17.2
200	300	312	8.0	366	17.4
205	370	314	7.0	368	12.4
210	430	316	10.5	370	12.4
215	455	318	14	372	12.0
220	440	320	10	374	10.0
225	390	322	8.0	376	8.0
230	340	324	10	378	6.0
235	280	326	13	380	5.05
240	230	328	18	382	5.1
245	180	330	23	384	5.4
250	140	332	13	386	5.6
255	105	334	10.2	388	5.2
260	80	339	32.4	390	4.3
265	57	342	19	395	1.4
270	41	345	13	400	0.5
275	29	348	18	405	0.2
280	20	350	29	410	0.1
285	13.5	352	31.5	415	0.045
290	10.0	354	24	420	0.022
295	8.0	356	19	425	0.011
300	6.9	358	15	430	0.006
302	7.1	360	14	440	0.0015

Note:
Taylor et al. [189]



(Recommendation: 10-6, Note: 10-6, Evaluated: 10-6)

Absorption Cross Sections: The UV absorption spectrum of methylnitrate (CH₃ONO₂) displays a strong continuous band in the region (190 – 250 nm) and a weaker band in the range (250 – 345 nm). The spectrum was measured at room temperature by McMillan [38] (201 – 323 nm), Maria et al. [114] (235 – 305 nm), Taylor et al. [189] (190 – 330 nm), Roberts and Fajer [165] (270 – 330 nm), Libuda and Zabel [106] (235 – 345 nm) and over a range of temperatures by Rattigan et al. [164] (220 – 335 nm) over the range 233 – 294 K and Talukdar et al. [186] (236 – 334 nm) over the range 240 – 360 K. Good agreement exists at wavelengths <240 nm between the absorption cross sections measured by Taylor et al. [189] and Rattigan et al. [164]. In the wavelength range 240 – 340 nm there is good agreement between the measurements of Roberts and Fajer [165], Libuda and Zabel [106], Rattigan et al. [164] and Talukdar et al. [186]. The values of Taylor et al. [189] are consistently larger at λ > 270 nm. Between 235 and 280 nm the absorption cross sections measured by Talukdar et al. [186] are nearly independent of temperature but for λ > 290 nm the cross sections decrease with decreasing temperature. At 330 nm the cross sections decrease by almost a factor of two between 298 and 240 K. Talukdar et al. [186] parameterized the absorption cross section temperature dependence using the expression

$$\sigma(\lambda, T) = \sigma(\lambda, 298 \text{ K}) \times \exp [B(\lambda) (T - 298)]$$

The absorption cross sections measured at 298 K by Taylor et al. [189] are recommended between 190 and 235 nm and those of Talukdar et al. [186] in the range 236 – 344 nm, Table 4D-15. The temperature dependence from Talukdar et al. [186] is recommended and the $B(\lambda)$ coefficients listed in Table 4D-15.

Photolysis Quantum Yields and Product Studies: The photodissociation quantum yield for CH_3ONO_2 to produce NO_2 and CH_3O was measured by Talukdar et al. [186] to be $\Phi_1 = 0.91 \pm 0.20$ at 248 nm. Upper limits for the other channels were determined experimentally to be $\Phi_2 < 0.05$, $\Phi_3 < 0.005$, $\Phi_{4+8} < 0.1$ and $\Phi_5 < 0.015 \pm 0.01$. It is expected that the quantum yield Φ_1 is unity at wavelengths >248 nm. Oxygen atoms were measured with quantum yield of 0.65 ± 0.15 at 193 nm and <0.01 at 248 and 308 nm. Yang et al. [209] studied the photodissociation of jet-cooled CH_3ONO_2 at 193 and 248 nm and found channel (1) to be the principal photolysis product channel with relative yields of 0.7 and 1 at 193 and 248 nm, respectively. They also reported an $\text{O}(^1\text{D})$ yield of 0.3 at 193 nm.

Table 4D-15. Absorption Cross Sections of CH_3ONO_2 at 298 K

λ (nm)	$10^{20} \sigma$ (cm^2)	$10^3 B$	λ (nm)	$10^{20} \sigma$ (cm^2)	$10^3 B$	λ (nm)	$10^{20} \sigma$ (cm^2)	$10^3 B$
190	1800	–	260	3.07	2.81	304	0.241	5.43
195	1500	–	262	2.96	2.84	306	0.194	5.67
200	1180	–	264	2.84	2.89	308	0.154	6.00
205	700	–	266	2.72	2.94	310	0.121	6.27
210	360	–	268	2.57	3.01	312	0.0940	6.68
215	145	–	270	2.42	3.08	314	0.0723	7.13
220	70	–	272	2.27	3.15	316	0.0548	7.54
225	33	–	274	2.10	3.24	318	0.0412	8.00
230	18	–	276	1.94	3.32	320	0.0304	8.88
235	10	–	278	1.77	3.40	322	0.0228	9.32
236	8.27	3.35	280	1.61	3.51	324	0.0164	10.3
238	6.77	3.44	282	1.45	3.61	326	0.01187	10.7
240	5.66	3.49	284	1.29	3.72	328	0.00868	11.5
242	4.88	3.45	286	1.14	3.84	330	0.00618	13.8
244	4.34	3.36	288	1.00	3.96	332	0.00447	15.5
246	3.97	3.24	290	0.871	4.08	334	0.00311	16.1
248	3.72	3.10	292	0.754	4.21	336	0.00216	–
250	3.56	2.97	294	0.642	4.38	338	0.00161	–
252	3.44	2.88	296	0.519	4.56	340	0.00116	–
254	3.34	2.82	298	0.435	4.72	342	0.000812	–
256	3.25	2.79	300	0.364	4.91	344	0.000468	–
258	3.16	2.80	302	0.298	5.14			

Note:

190 – 235 nm: Taylor et al. [189]

236 – 344 nm: Talukdar et al. [186]

$B(\lambda)$ are the temperature coefficients in the expression $\sigma(\lambda, T) = \sigma(\lambda, 298 \text{ K}) \times \exp [B(\lambda) (T - 298)]$, after Talukdar et al. [186]



(Recommendation: 10-6, Note: 10-6, Evaluated: 10-6)

Absorption Cross Sections: The UV absorption spectrum of $\text{CH}_3\text{O}_2\text{NO}_2$ (methylperoxynitrate) has been measured by Cox and Tyndall [51] (200 – 310 nm) at 275 K, Morel et al. [143] (200 – 290 nm) at 296 K, Sander and Watson [170] (240 – 280 nm) at 298 K, and Bridier et al. [28] (200 – 280 nm) at 298 K. The spectrum has a strong absorption band below 225 nm and a moderate band at longer wavelengths. The reported cross sections are in reasonable agreement in the range 230 – 250 nm but scatter in the cross section data exists at both shorter and longer wavelengths. The recommended cross sections listed in Table 4D-16 are a smoothed average of the data from the four studies.

Table 4D-17. Absorption Cross Sections of CH₃C(O)O₂NO₂ at 298 K and Temperature Coefficients

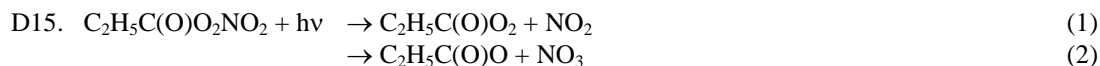
λ (nm)	$10^{20} \sigma$ (cm ²)	$10^3 B$ (K ⁻¹)	λ (nm)	$10^{20} \sigma$ (cm ²)	$10^3 B$ (K ⁻¹)	λ (nm)	$10^{20} \sigma$ (cm ²)	$10^3 B$ (K ⁻¹)
196	429	2.02	248	14.6	3.64	300	0.189	8.44
198	398	1.73	250	12.9	3.76	302	0.152	8.61
200	361	1.36	252	11.4	3.87	304	0.125	8.76
202	325	1.07	254	10.0	3.98	306	0.0998	8.87
204	292	0.86	256	8.86	4.10	308	0.0816	9.01
206	261	0.75	258	7.80	4.23	310	0.0666	9.13
208	226	0.71	260	6.85	4.38	312	0.0538	9.30
210	196	0.75	262	6.01	4.53	314	0.0462	9.46
212	168	0.84	264	5.23	4.68	316	0.0363	9.57
214	143	0.97	266	4.54	4.82	318	0.0300	9.75
216	122	1.12	268	3.94	4.97	320	0.0252	10.0
218	104	1.29	270	3.37	5.14	322	0.0199	10.2
220	89.7	1.47	272	2.87	5.34	324	0.0166	10.4
222	77.7	1.64	274	2.45	5.55	326	0.0140	10.6
224	67.6	1.81	276	2.07	5.76	328	0.0117	10.7
226	59.3	1.98	278	1.74	5.98	330	0.0106	10.9
228	52.0	2.14	280	1.46	6.20	332	0.00857	11.2
230	45.8	2.30	282	1.21	6.43	334	0.0072*	11.5
232	40.4	2.46	284	1.01	6.67	336	0.0061*	11.7
234	35.5	2.63	286	0.810	6.90	338	0.0050*	11.9
236	31.4	2.80	288	0.648	7.15	340	0.0042*	12.2
238	27.9	2.96	290	0.537	7.39	342	0.0035*	12.4
240	24.4	3.11	292	0.447	7.63	344	0.0029*	12.5
242	21.5	3.25	294	0.369	7.86	346	0.0024*	
244	18.8	3.39	296	0.297	8.08	348	0.0020*	
246	16.6	3.52	298	0.245	8.27	350	0.0016*	

Note:

Absorption cross sections σ : 196-350 nm, Talukdar et al. [187].

Temperature coefficients B: 250-298 K, Talukdar et al. [187] ($\ln \sigma(\lambda, T) = \ln \sigma(\lambda, 298 \text{ K}) + B(T-298)$)

* Data between 334 and 350 nm were smoothed.



(Recommendation: 06-2, Note: 10-6, Evaluated: 10-6)

Absorption Cross Sections: The absorption cross sections of C₂H₅C(O)O₂NO₂ (peroxypropionyl nitrate, PPN) have been measured at room temperature by Senum et al. [173] (200 – 300 nm) and at 253, 273, and 296 K by Harwood et al. [78] (210 – 340 nm). The absorption spectrum shows monotonically decreasing absorption cross sections with increasing wavelength over the range 200 – 340 nm. The absorption cross sections reported by Harwood et al. [78] are larger than those reported by Senum et al. [173] over the common wavelength range by ~10% at 210 nm up to ~30% at 300 nm. A wavelength dependent systematic decrease of the absorption cross sections with decreasing temperature was reported by Harwood et al. [78]. The temperature dependence was parameterized to the empirical expression

$$\ln \sigma(\lambda, T) = \ln \sigma(\lambda, 296 \text{ K}) + B(\lambda)(T - 296)$$

The recommended absorption cross sections and temperature coefficients in Table 4D-18 are taken from Harwood et al. [78].

Photolysis Quantum Yield and Product Studies: Quantum yields for the production of NO₃ in the photolysis of C₂H₅C(O)O₂NO₂ at 248 and 308 nm were measured by Harwood et al. [78] to be $\Phi_2(248 \text{ nm}) = 0.22 \pm 0.04$ and $\Phi_2(308 \text{ nm}) = 0.39 \pm 0.04$.

Table 4D-18. Absorption Cross Sections of C₂H₅C(O)O₂NO₂ at 296 K and Temperature Coefficients

λ (nm)	$10^{20} \sigma$ (cm ²)	$10^3 B$ (K ⁻¹)	λ (nm)	$10^{20} \sigma$ (cm ²)	$10^3 B$ (K ⁻¹)	λ (nm)	$10^{20} \sigma$ (cm ²)	$10^3 B$ (K ⁻¹)
210	174	1.22	254	9.27	3.25	298	0.325	10.3
212	154	1.20	256	8.23	3.47	300	0.273	10.8
214	135	1.19	258	7.28	3.69	302	0.228	11.2
216	115	1.20	260	6.44	3.92	304	0.192	11.7
218	99.9	1.21	262	5.66	4.17	306	0.162	12.2
220	86.1	1.24	264	4.96	4.42	308	0.136	12.6
222	74.7	1.27	266	4.35	4.69	310	0.114	13.2
224	64.8	1.32	268	3.80	4.96	312	0.0962	13.6
226	56.9	1.37	270	3.31	5.25	314	0.0835	14.2
228	49.6	1.44	272	2.87	5.54	316	0.0689	14.7
230	43.6	1.52	274	2.48	5.85	318	0.0571	15.2
232	38.3	1.60	276	2.14	6.17	320	0.0491	15.8
234	33.6	1.70	278	1.84	6.49	322	0.0443	16.3
236	29.5	1.81	280	1.57	6.83	324	0.0354	16.9
238	25.8	1.93	282	1.33	7.18	326	0.0282	17.5
2400	22.6	2.06	284	1.12	7.54	328	0.0242	18.1
242	19.8	2.20	286	0.940	7.91	330	0.0206	18.7
244	17.4	2.35	288	0.790	8.29	332	0.0174	19.3
246	15.3	2.51	290	0.662	8.68	334	0.0146	19.9
248	13.5	2.68	292	0.551	9.08	336	0.0107	20.5
250	11.9	2.86	294	0.462	9.49	338	0.0090	21.2
252	10.5	3.05	296	0.389	9.91	340	0.0066	21.8

Note:

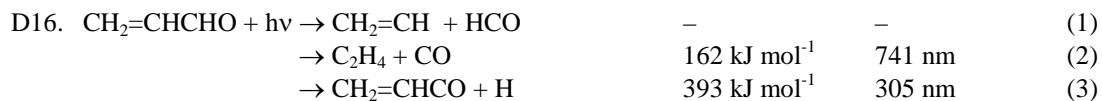
Absorption cross sections

210 – 340 nm: Harwood et al. [78]

Temperature coefficients

253 – 296 K: Harwood et al. [78]

$$\ln \sigma(\lambda, T) = \ln \sigma(\lambda, 298 \text{ K}) + B(\lambda)(T - 298)$$



(Recommendation: 06-2, Note: 10-6, Evaluated: 10-6)

Absorption Cross Sections: The VUV/UV/vis absorption spectrum of acrolein (CH₂=CHCHO, propenal) has been measured at room temperature by Gardner et al. [67] (227 – 380 nm), Magneron et al. [113] (192 – 431 nm), and Lee et al. [103]. The UV spectrum displays a broad absorption band between 250 and 400 nm, which is structured at wavelengths above 360 nm. The results of both studies agree to within 10% between 298 and 370 nm (with a few exceptions at 352, 360, 362 and 368 nm). Below 298 nm the differences increase up to ~40% with decreasing wavelength, above 368 nm the differences increase with increasing wavelength up to ~100%. The recommended absorption cross sections in Table 4D-19 are the 2 nm averages from the high resolution data of Magneron et al. [113].

Photolysis Quantum Yield and Product Studies: The photodecomposition of CH₂=CHCHO was studied by Gardner et al. [67] at 313 and 334 nm over the pressure range 26 – 760 Torr air. They found photolysis at high pressures to be very inefficient at both wavelengths but the photolysis quantum yield to increase at low pressure. At 313 nm the quantum yield for photodissociation Φ_d of acrolein was 0.0065 at 1 atm and 0.081 at 26 Torr. The pressure dependence was described by

$$1/(\Phi_d - 0.004) = 0.086 + 1.613 \times 10^{-17} [\text{M}]$$

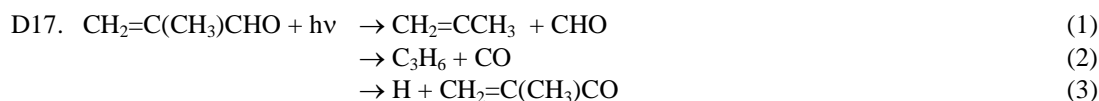
for concentrations (M) between 8×10^{17} and 2.6×10^{19} molecule cm^{-3} . The major products observed were CO and C_2H_4 . Magneron et al. [113] used broadband photolysis (275 – 380 nm) of dilute mixtures of acrolein in air to study $\text{CH}_2=\text{CHCHO}$ photodissociation but did not observe any products using long-path FTIR spectroscopy. An effective quantum yield for photolysis $\Phi_{\text{eff}} \leq 0.005$ nm was measured by Magneron et al. [113] in an outdoor smog chamber.

Table 4D-19. Absorption Cross Sections of $\text{CH}_2=\text{CHCHO}$ at 298 K

λ (nm)	$10^{20} \sigma$ (cm^2)	λ (nm)	$10^{20} \sigma$ (cm^2)	λ (nm)	$10^{20} \sigma$ (cm^2)	λ (nm)	$10^{20} \sigma$ (cm^2)
282	0.84	310	3.59	338	5.46	366	3.74
284	0.97	312	3.92	340	5.31	368	3.82
286	1.08	314	4.15	342	5.10	370	2.17
288	1.23	316	4.21	344	5.12	372	1.58
290	1.46	318	4.47	346	5.30	374	1.14
292	1.62	320	4.65	348	5.17	376	1.14
294	1.80	322	5.08	350	5.94	378	1.24
296	1.97	324	5.17	352	5.79	380	1.10
298	2.18	326	5.34	354	4.18	382	0.84
300	2.47	328	5.20	356	3.63	384	0.79
302	2.70	330	5.31	358	3.28	386	1.18
304	2.85	332	5.44	360	3.92	388	0.49
306	3.09	334	5.80	362	3.72	390	0.25
308	3.29	336	6.24	364	2.86		

Note:

282 – 390 nm: Magneron et al. [113]



(Recommendation: 06-2, Note: 10-6, Evaluated: 10-6)

Absorption Cross Sections: The VUV/UV absorption spectrum of methacrolein (2-methylpropenal, MACR), $\text{CH}_2=\text{C}(\text{CH}_3)\text{CHO}$, has been measured using diode array spectroscopy at room temperature by Meller (237 – 391 nm) (see Röth et al. [169]), Raber and Moortgat [161] (331 nm), Gierczak et al. [71] (214, 250 – 395 nm), and Lee et al. [103]. The spectrum exhibits a broad absorption band between 250 and 390 nm with vibrational structure above 310 nm. A detailed vibrational-electronic analysis was reported by Birge et al. [20]. The reported spectra are in very good agreement in the region 261-351 nm where the agreement is between ~1 and 10%. At shorter wavelengths, <260 nm, the differences increase to nearly 100% at 250 nm and the cross sections from Gierczak et al. [71] are consistently greater than those of Meller [169] and Raber and Moortgat [161]. The cross sections at the peaks in the structured region reported by Meller [169] and Raber and Moortgat [161] are consistently higher than those measured by Gierczak et al. [71] presumably due to the higher resolution used. At the band maximum, Raber and Moortgat [161] reported $\sigma(330.7 \text{ nm}) = 7.64 \times 10^{-20} \text{ cm}^2 \text{ molecule}^{-1}$ and Gierczak et al. [71] reported $\sigma(331 \text{ nm}) = 7.2 \times 10^{-20} \text{ cm}^2 \text{ molecule}^{-1}$. Gierczak et al. [71] also reported $\sigma(213.86 \text{ nm}) = (2.21 \pm 0.11) \times 10^{-17} \text{ cm}^2 \text{ molecule}^{-1}$ (Zn lamp source). The 1 nm averages of the results from Gierczak et al. [71] and Meller [169] are generally (with a few exceptions) within 20% of each other for wavelengths up to 376 nm. Above 380 nm, the results of Gierczak et al. [71] are larger with increasing wavelength by up to nearly 80% than the results of Meller [169]. A wavelength shift of ~1 nm toward longer wavelengths can be observed above 340 nm in the absorption spectrum of Gierczak et al. [71] when compared to the spectrum reported by Meller [169]. The recommended absorption cross sections listed in Table 4D-20 are from Gierczak et al. [71].

Photolysis Quantum Yield and Product Studies: The photodissociation quantum yield for $\text{CH}_2=\text{C}(\text{CH}_3)\text{CHO}$ at atmospherically relevant wavelengths is low. Quantum yields of $\text{CH}_2=\text{C}(\text{CH}_3)\text{CHO}$ were measured by Raber and Moortgat [161] using broad band photolysis in the wavelength range 275-380 nm, and determination of the stable products (CO, CO_2 , HCHO, C_2H_4 , C_3H_6 , C_2H_2) by FTIR spectroscopy. An upper limit of 0.05 was reported at 760 Torr. Gierczak et al. [71] used GC and GC-MS detection of photolysis end-

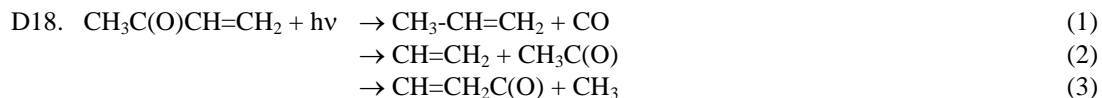
products to determined $\text{CH}_2=\text{C}(\text{CH}_3)\text{CHO}$ quantum yields at 308 nm of 0.008 ± 0.001 and 0.005 ± 0.001 at 25 and 650 Torr total pressure, respectively. At 351 nm they reported quantum yields of 0.005 ± 0.002 and 0.003 ± 0.001 at 25 and 650 Torr, respectively. A value of $\Phi < 0.01$ is recommended for wavelengths >308 nm.

Table 4D-20. Absorption Cross Sections of CH₂=C(CH₃)CHO at 298 K

λ (nm)	$10^{20} \sigma$ (cm ²)	λ (nm)	$10^{20} \sigma$ (cm ²)	λ (nm)	$10^{20} \sigma$ (cm ²)	λ (nm)	$10^{20} \sigma$ (cm ²)
250	0.207	287	1.67	324	6.58	361	4.28
251	0.194	288	1.79	325	6.74	362	3.61
252	0.187	289	1.90	326	6.73	363	2.86
253	0.180	290	2.03	327	6.68	364	2.68
254	0.179	291	2.16	328	6.83	365	2.33
255	0.177	292	2.28	329	7.07	366	1.92
256	0.180	293	2.39	330	7.15	367	1.62
257	0.180	294	2.52	331	7.16	368	1.40
258	0.186	295	2.68	332	7.03	369	1.31
259	0.193	296	2.85	333	6.69	370	1.42
260	0.201	297	2.99	334	6.41	371	1.67
261	0.211	298	3.13	335	6.08	372	1.53
262	0.224	299	3.26	336	5.97	373	1.43
263	0.241	300	3.44	337	6.25	374	1.08
264	0.263	301	3.61	338	6.38	375	0.977
265	0.283	302	3.76	339	6.37	376	1.00
266	0.305	303	3.91	340	6.24	377	1.07
267	0.333	304	4.04	341	6.02	378	1.35
268	0.363	305	4.19	342	5.98	379	2.18
269	0.398	306	4.40	343	6.58	380	1.30
270	0.436	307	4.58	344	6.79	381	0.984
271	0.479	308	4.71	345	6.53	382	0.555
272	0.520	309	4.81	346	6.11	383	0.456
273	0.567	310	4.92	347	5.63	384	0.364
274	0.616	311	5.13	348	5.22	385	0.331
275	0.673	312	5.35	349	4.55	386	0.246
276	0.732	313	5.50	350	4.16	387	0.205
277	0.793	314	5.61	351	3.85	388	0.181
278	0.863	315	5.70	352	3.89	389	0.161
279	0.936	316	5.87	353	4.35	390	0.147
280	1.01	317	6.04	354	4.31	391	0.156
281	1.09	318	6.19	355	4.14	392	0.159
282	1.18	319	6.28	356	3.62	393	0.153
283	1.26	320	6.27	357	3.53	394	0.149
284	1.35	321	6.18	358	3.46	395	0.123
285	1.45	322	6.21	359	3.81		
286	1.56	323	6.34	360	5.05		

Note:

250 – 395 nm: Gierczak et al. [71]



(Recommendation: 06-2, Note: 10-6, Evaluated: 10-6)

Absorption Cross Sections: The UV absorption spectrum of methyl vinyl ketone (MVK), CH₃C(O)CH=CH₂, has been measured at room temperature by Schneider and Moortgat (240 – 398 nm) (see Röth et al. [169]), Raber and Moortgat [161] (235 – 400 nm), Fahr et al. [59] (160 – 260 nm), and Gierczak et al. [71] (216.86 nm and 250 – 395 nm). The absorption band peaking at ~330 nm displays some weak vibrational band structure, which is superimposed on a continuum envelope. A detailed vibrational-electronic analysis was reported by Birge et al. [20]. The cross sections from Schneider and Moortgat are somewhat smaller around

the band maximum at 334 nm (agreement within ~10% between 290 and 365 nm), and larger by up to 50% and smaller by up to ~60% in the short- and long-wavelength tails, respectively, than the results of Gierczak et al. [71]. Gierczak et al. [71] reported $\sigma(213.86 \text{ nm}) = (6.6 \pm 0.04) \times 10^{-17} \text{ cm}^2 \text{ molecule}^{-1}$ (Zn lamp source). They also measured the spectrum at reduced temperatures (range 250 – 298 K), and observed a small increase in the peak cross section of <2% at 250 K. Fahr et al. [59] reported $\sigma(193 \text{ nm}) = (3.2 \pm 0.2) \times 10^{-17} \text{ cm}^2 \text{ molecule}^{-1}$. The recommended absorption cross sections in Table 4D-21 are taken from Gierczak et al. [71].

Photolysis Quantum Yield and Product Studies: Product quantum yields were measured by Raber and Moortgat [161] using broadband photolysis in the range 275 – 380 nm combined with FTIR monitoring of the stable photolysis products (major CO, C₃H₆ and HCHO; minor CO₂, HCOOH, CH₃OH, CH₃COOH). They report a pressure dependent quantum yield with $\Phi = 0.05$ at 760 Torr and $\Phi = 0.12$ at 54 Torr. Fahr et al. [59] used laser photolysis at 193.3 nm and measured the direct formation of CH₃ radicals at 216.4 nm and final products. They report a quantum yield close to unity for the formation of CH₃ and CH=CH₂ radicals. Gierczak et al. [71] measured quantum yields for photolysis at 308, 337 and 351 nm by monitoring the disappearance of MVK. They reported $\Phi = 0.16$ at 25 Torr and $\Phi = 0.04$ at 760 Torr at 308 nm, $\Phi = 0.04$ at 25 Torr and $\Phi = 0.01$ at 760 Torr at 337 nm; and $\Phi = 0.01$ independent of pressure at 351 nm. The quantum yield data were fit to the empirical Stern-Volmer type expression

$$\Phi(\lambda, P) = \exp[-0.055 (\lambda - 308)] / (5.5 + 9.2 \times 10^{-19} [M])$$

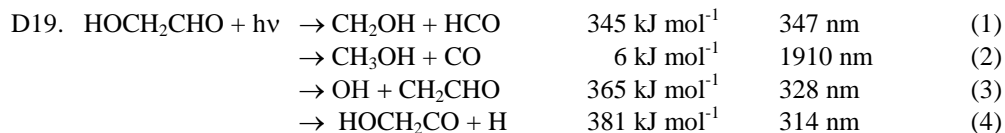
where λ is in nm and $[M]$ in molecule cm⁻³. This parameterization is recommended.

Table 4D-21. Absorption Cross Sections of CH₃C(O)CH=CH₂ at 298 K

λ (nm)	$10^{20} \sigma$ (cm ²)	λ (nm)	$10^{20} \sigma$ (cm ²)	λ (nm)	$10^{20} \sigma$ (cm ²)	λ (nm)	$10^{20} \sigma$ (cm ²)
250	0.241	287	2.03	324	6.88	361	3.60
251	0.241	288	2.15	325	6.95	362	3.49
252	0.224	289	2.29	326	7.02	363	3.36
253	0.241	290	2.43	327	7.09	364	3.29
254	0.241	291	2.55	328	7.16	365	3.03
255	0.258	292	2.67	329	7.23	366	2.77
256	0.275	293	2.81	330	7.28	367	2.50
257	0.275	294	2.93	331	7.30	368	2.20
258	0.293	295	3.08	332	7.26	369	2.01
259	0.310	296	3.24	333	7.18	370	1.88
260	0.327	297	3.39	334	7.04	371	1.74
261	0.361	298	3.56	335	6.94	372	1.58
262	0.379	299	3.70	336	6.85	373	1.48
263	0.396	300	3.87	337	6.70	374	1.39
264	0.430	301	4.05	338	6.56	375	1.31
265	0.465	302	4.20	339	6.47	376	1.26
266	0.499	303	4.35	340	6.44	377	1.24
267	0.534	304	4.51	341	6.42	378	1.21
268	0.568	305	4.66	342	6.35	379	1.21
269	0.620	306	4.82	343	6.35	380	1.05
270	0.654	307	4.96	344	6.30	381	0.981
271	0.706	308	5.13	345	6.23	382	0.912
272	0.757	309	5.30	346	6.14	383	0.878
273	0.809	310	5.44	347	6.08	384	0.929
274	0.878	311	5.58	348	5.77	385	0.757
275	0.929	312	5.73	349	5.47	386	0.637
276	0.998	313	5.87	350	5.20	387	0.534
277	1.08	314	6.02	351	4.94	388	0.448
278	1.15	315	6.14	352	4.72	389	0.396
279	1.24	316	6.28	353	4.53	390	0.344
280	1.33	317	6.42	354	4.32	391	0.310
281	1.41	318	6.54	355	4.15	392	0.293
282	1.50	319	6.63	356	4.03	393	0.275
283	1.60	320	6.70	357	3.94	394	0.241
284	1.70	321	6.76	358	3.89	395	0.207
285	1.81	322	6.83	359	3.89		
286	1.91	323	6.85	360	3.68		

Note:

250 – 395 nm: Gierczak et al. [71]



(Recommendation: 10-6, Note: 10-6, Evaluated: 10-6)

Absorption Cross Sections: The absorption cross sections of HOCH₂CHO (glycolaldehyde, hydroxyacetaldehyde) have been measured at room temperature by Bacher et al. [13] (205 – 335 nm), Magneron et al. [112] (210 – 330 nm), and Karunanandan et al. [94] (210 – 335 nm). The spectrum consists of a strong absorption below 220 nm and a weaker absorption band centered near 280 nm with evidence of

vibrational progressions. The measurements performed by Magneron et al. [112] were done at two different laboratories and are nearly identical but reveal significant differences compared to the spectrum measured by Bacher et al. [13], being about 20% at the maximum. The spectrum measured by Karunanandan et al. [94] is in excellent agreement with Magneron et al. [112] at the maximum near 282 nm and at longer wavelengths. At shorter wavelengths the cross sections are consistently larger than those measured by Magneron et al. [112]: 15 % at 250 nm, 40% at 230 nm and 85% at the minimum near 226 nm. At 184.9 nm the cross section was measured as $(3.85 \pm 0.2) \times 10^{-18} \text{ cm}^2 \text{ molecule}^{-1}$. The average of the cross sections of Magneron et al. [112] and Karunanandan et al. [94] are recommended and listed in Table 4D-22.

Photolysis Quantum Yields and Product Studies: The broad band photolysis ($285 \pm 25 \text{ nm}$) of glycolaldehyde in air performed by Bacher et al. [13] revealed an overall quantum yield $\Phi > 0.5$, relative to the quantum yield ($\Phi = 0.3$) of removal of acetone. Product studies by FTIR suggests that channel (1) is the major photolysis channel (65-80%), while channel (2) accounts to 15-20%, and channel (3) contributes up to 15%. The formation of channel (4) was suggested to produce HOCH_2CO as a source for OH radicals, whose presence was indirectly invoked due the formation of glyoxal. Magneron et al. [112] also photolysed glycolaldehyde (broadband lamps 275 – 380 nm) and measured products by FTIR (CO , CO_2 , HCHO and CH_3OH). They observed direct evidence for OH production via channel (3) using OH scavenger and OH tracer species and performed additional photolysis experiments where glycolaldehyde was used an OH source to measure rate constants for OH with a series of dienes. The contribution of channel (2) was estimated to be 10% and that of channels (1) + (2) to be 90%. No evidence was found for channel (4). Karunanandan et al. [94] measured a quantum yield of OH formation at 248 nm of $\Phi_3 = (7.0 \pm 1.5) \times 10^{-2}$. On the basis of the combined product studies the following quantum yields are recommended: $\Phi_1 = 0.83$, $\Phi_2 = 0.10$ and $\Phi_3 = 0.07$ in the range 248 – 328 nm.

Table 4D-22. Absorption Cross Sections of HOCH_2CHO at 298 K

λ (nm)	$10^{20} \sigma$ (cm^2)	λ (nm)	$10^{20} \sigma$ (cm^2)	λ (nm)	$10^{20} \sigma$ (cm^2)	λ (nm)	$10^{20} \sigma$ (cm^2)
208	20.6	240	1.39	272	6.74	304	2.65
210	13.1	242	1.63	274	6.98	306	2.26
212	8.15	244	1.77	276	6.98	308	1.88
214	4.93	246	2.25	278	6.93	310	1.57
216	2.94	248	2.57	280	6.91	312	1.28
218	1.72	250	2.94	282	6.92	314	0.94
220	1.00	252	3.37	284	6.60	316	0.70
222	0.64	254	3.76	286	6.38	318	0.53
224	0.45	256	4.15	288	6.09	320	0.40
226	0.39	258	4.61	290	5.88	322	0.31
228	0.42	260	5.03	292	5.43	324	0.21
230	0.53	262	5.33	294	4.87	326	0.14
232	0.63	264	5.68	296	4.50	328	0.10
234	0.79	266	6.10	298	4.10	330	0.07
236	0.97	268	6.35	300	3.74	332	0.04
238	1.15	270	6.49	302	3.19		

Note:

208 – 332 nm, average of Magneron et al. [112] and Karunanandan et al. [94]



(Recommendation: 06-2, Note: 10-6; Evaluated: 10-6)

Absorption Cross Sections: The absorption spectrum of acetone, $\text{CH}_3\text{C}(\text{O})\text{CH}_3$, has been measured at room temperature by Lake and Harrison [101] (159 – 203 nm), Calvert[37](200 – 300 nm), Meyrahn et al. [132, 134] (220 – 368 nm), Schneider and Moortgat (196 – 366 nm) (see Röth et al. [169]), Hynes et al. [89] (253.7 nm and 260 – 360 nm), Martinez et al. [120] (202 – 335 nm), Gierczak et al. [70] (215 – 349 nm), Wollenhaupt et al. [207] (220 – 346 nm) and Yujing and Mellouki [210] (240 – 350 nm). Absorption cross sections have also been determined at isolated wavelengths by Braun et al. [27] (193 nm, also for

CD₃C(O)CD₃), Seki and Okabe [172] (193 nm), Krasnoperov and Mehta [98] (216.51 nm), and Gierczak et al. [72] (184.9 nm, also for CD₃C(O)CD₃).

The spectrum below 200 nm is highly structured in the wavelength regions 160 – 170 nm and 180 – 195 nm. A broad absorption band was observed between 210 and 340 nm for which higher resolution measurements give evidence for band maxima at ~273 and ~278 nm. The reported absorption cross sections are in excellent agreement with the range of deviations being $\leq 8\%$ in the 240 – 320 nm region. The absorption cross section at the spectrum maximum range between 5.2×10^{-20} and 4.8×10^{-20} cm² molecule⁻¹. In the tails of the absorption band, the various data sets become more divergent with decreasing wavelength with differences of up to ~50% at 220 nm and with increasing wavelength up to more than 100% at 340 nm. The data measured by Meyrahn et al. [132, 134] are systematically higher at wavelengths >320 nm than the other studies. The absorption cross sections from Martinez et al. [120], Gierczak et al. [70], Wollenhaupt et al. [207] and Yujing and Mellouki [210] agree to within 2.5% in the region of the absorption maximum and to within 50% in the short and long wavelength tails of the band.

The absorption spectrum temperature dependence has been studied by Hynes et al. [89] (300 – 340 nm) over the range 261 – 362 K, Gierczak et al. [70] (215 – 349 nm) over the range 235 – 298 K, and Gierczak et al. [72] (184.9 nm, also for CD₃C(O)CD₃) over the range 222 – 296 K. The absorption spectrum has modest temperature dependence at wavelengths >270 nm with the cross sections decreasing with decreasing temperature. At shorter wavelengths the spectrum is essentially independent of temperature, the cross section changes by < 5% between 298 and 235 K. Gierczak et al. [70] parameterized the temperature dependent cross sections using the expression

$$\sigma(\lambda, T) = \sigma(\lambda, 298 \text{ K})[1 + c_1(\lambda)T + c_2(\lambda)T^2]$$

that was later superseded by Burkholder [31] using the expression

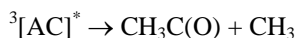
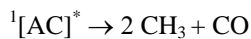
$$\sigma(\lambda, T) = \sigma(\lambda, 298 \text{ K})[1 + A(\lambda)T + B_2(\lambda)T^2 + C(\lambda)T^3]$$

The recommended absorption cross sections at 298 K in Table 4D-23 are taken from Gierczak et al. [70] and the temperature coefficients A, B, and C derived by Burkholder [31].

The absorption cross section of CH₃C(O)CH₃ at 184.9 nm was observed to decrease very slightly with decreasing temperature between 296 and 222 K leading to an average value of $(2.98 \pm 0.10) \times 10^{-18}$ cm² molecule⁻¹, whereas that of CD₃C(O)CD₃ increased noticeably from 3.91×10^{-18} cm² molecule⁻¹ (average of six results) at 295 K to 4.61×10^{-18} cm² molecule⁻¹ at 232 K, as reported by Gierczak et al. [72].

Photolysis Quantum Yield and Product Studies: The UV photodissociation of acetone is wavelength, pressure, and temperature dependent. Since JPL 06-2 there has been a number of acetone photodissociation laboratory studies published [Khamaganov et al. [95] (248 and 266 nm), Khamaganov et al. [96] (248 nm and 266 nm), Nádasdia et al. [145] (248 nm and 308 nm), Rajakumar et al. [163] (248 nm), Somnitz et al. [180, 181] (248 nm)]. The focus of these studies has been on the determination of the pressure and temperature dependence of the acetone loss and product (CH₃, CH₃CO, CO, and CO₂) photolysis quantum yields as described further below.

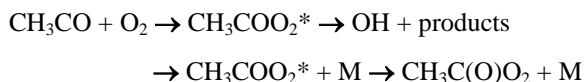
Gardner et al. [68] measured acetone loss (Φ_{AC}) and formation of the products CO₂, CO, CH₃OH and H₂CO following the photolysis of dilute acetone-air mixtures at four wavelengths in the range 279 – 313 nm as a function of pressure (25 – 745 Torr) and temperature (271-301 K). At pressures >300 Torr, they observed a near constant quantum yield, $\Phi_{AC} \approx \Phi_{CO_2} = \Phi_1 = 0.077$, for photolysis wavelengths in the range 279-313 nm with a slight increase at lower pressures. Meyrahn et al. [132, 134] measured the quantum yields of CO and CO₂ in the photolysis of dilute mixtures of acetone in air at nine wavelengths over the range 250-330 nm. At 1 atm, Φ_{CO_2} decreased from 1.59 at 250 nm to 0.11 at 310 nm and increased to 0.27 at 330 nm. Φ_{CO} decreased from 0.45 at 250 nm to 0.02 at 310 nm and increased to 0.09 at 330 nm. A CO₂ quantum yield larger than unity was explained to result from secondary reactions. Meyrahn et al. [132, 134] measured the quantum yield of peroxyacetyl nitrate, Φ_{PAN} , (which is assumed to be a direct measure of Φ_1) in the photolysis of acetone /air/NO₂ mixtures to decrease from ~0.78 in the region 250 – 260 nm to 0.03 at 330 nm. Meyrahn et al. [132, 134] observed Φ_{CO_2} to increase at lower pressures (Stern-Volmer mechanism) at 330 nm. Emrich and Warneck [57, 58] also determined Φ_{PAN} following the photolysis of acetone /air/NO₂ mixtures at six wavelengths between 280 and 330 nm at total pressures in the range 10 – 760 Torr. At 760 Torr, Φ_{PAN} decreased from a value of 1.00 at 280 nm to 0.06 at 320 nm and increased to 0.13 at 330 nm. A Stern-Volmer type pressure dependence was observed at all wavelengths. The results were explained in terms of the rate of photodissociation from the excited singlet ¹[AC]* state of acetone and the competing intersystem crossing to the triplet ³[AC]*, both relative to that of collisional quenching, as a function of energy above the dissociation threshold. It was proposed that



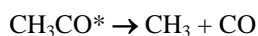
Gierczak et al. [70] determined Φ_{AC} and Φ_{CO_2} in the laser photolysis of acetone at nine wavelengths in the range 248–337 nm as a function of pressure (25 – 760 Torr, syn. air) and temperature (195 – 298 K). For photolysis wavelengths >270 nm, Φ followed a Stern-Volmer type pressure dependence and the zero-pressure quantum yield was found to increase with decreasing wavelength to a value of unity near 290 nm. Gierczak et al. [70] observed a temperature dependence to the 308 nm quantum yield except for the lowest temperature included in their study, 195 K, and choose to report a temperature independent quantum yield. The studies of Blitz et al. [24, 25] and Nádasdia et al. [145] have since reported temperature dependent quantum yields at 308 nm. The results from these studies are in good agreement. The Gierczak et al. [70] results are also in reasonable agreement. The Gierczak et al. [70] results at 298 K are nearly identical to those of Emrich and Warneck [57]. Gierczak et al. [70] and Warneck [202] have reported parameterizations for the quantum yields for the photodissociation of acetone dependence on wavelength and pressure.

Aloisio and Francisco [6] measured the quantum yield of acetone photodissociation at 248 and 308 nm in the presence and absence of water vapor. The apparent acetone quantum yield decreased from unity to 0.73 ± 0.07 for 248 nm photolysis and from 0.28 ± 0.07 to 0.06 ± 0.04 for 308 nm photolysis with the addition of 9 Torr of H_2O . Nádasdia et al. [145] performed a similar quantum yield study (with and without H_2O) at 298 K and a total pressure of 133 mbar. They studied the effect for the same photolysis wavelengths and report quantum yields for the loss of acetone to be independent of H_2O vapor to within their measurement accuracy; 0.945 ± 0.222 (without H_2O) and 1.021 ± 0.124 (with 12 mbar H_2O) at 248 nm and two sets of measurements at 308 nm using different acetone and H_2O concentrations, 0.342 ± 0.028 (without H_2O) and 0.319 ± 0.018 (with 12 mbar H_2O) and 0.308 ± 0.024 (without) and 0.320 ± 0.024 (with 4 mbar H_2O). There is no explanation for the apparent discrepancy between these studies.

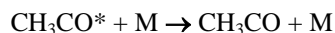
Blitz et al. [24, 25] reported the pressure and temperature (218 – 295 K) dependent quantum yields of acetone for photolysis wavelengths between 279 and 327.5 nm. Blitz et al. [24, 25] used a spectroscopic technique to indirectly detect the formation of the CH_3CO radical that is based on the detection of the OH radical formed in the reaction



The time-resolved studies of Blitz et al. [24, 25] are more direct and sensitive than earlier studies. They observed “classical” Stern-Volmer behavior at $\lambda < 302$ nm, but at $\lambda > 302$ nm an extended form of the Stern-Volmer expression was necessary to fit their data for pressures below 15 Torr; reflecting the dissociation and quenching from both $^1[\text{AC}]^*$ and $^3[\text{AC}]^*$ excited states as described in Blitz et al. [23]. On the basis of the low pressure quantum yield results at wavelengths >300 nm, Blitz et al. [24, 25] determined that $\Phi_{\text{CH}_3\text{CO}} = 0.65$ and $\Phi_{\text{CO}} = 0.35$ at 248 nm from measurements made relative to this reference photolysis wavelength. Their analysis assumes that the acetone quantum yield in the low pressure limit is unity in the long wavelength photolysis, the acetone quantum yield at 248 nm is unity, and that the CH_3CO quantum yield at 248 nm is independent of pressure. It has been established that the acetone quantum yield at 248 nm is unity and independent of temperature and pressure [Gierczak et al. [70], Khamaganov et al. [96], Aloisio and Francisco [6], Nádasdia et al. [145], and Somnitz et al. [181]]. Khamaganov et al. [96] also report that the acetone quantum yield is only weakly pressure dependent (60 – 760 Torr) at 266 nm. There is strong evidence now that the CH_3CO , CH_3 , and CO quantum yields at 248 nm are, however, pressure dependent. For photolysis at 248 nm there is sufficient energy for the nascent energetically excited CH_3CO radical to dissociate via a non-concerted step



or be collisionally quenched



Khamaganov et al. [95] (5 – 1500 Torr), Somnitz et al. [180, 181] (20 – 900 mbar), and Rajakumar et al. [163] (60 – 670 Torr) reported pressure dependent quantum yields for CH_3 , CO and CO_2 , and CH_3CO , respectively, over the range of pressures indicated in parenthesis. The results from these studies are in reasonable agreement and report low pressure quantum yields of $\Phi(\text{CH}_3) = 1.42 \pm 0.15$ (Khamaganov et al. [95]), $\Phi(\text{CO}) = 0.51$ (Sommritz et al. [181]), and $\Phi(\text{CH}_3\text{CO}) = 0.535 \pm 0.09$ (Rajakumar et al. [163]). Somnitz et al. [180, 181] have modeled the dissociation process using RRKM theory with a time-dependent master equation approach. The impact of a pressure dependence for the CH_3CO quantum yield at 248 nm on the interpretation of the Blitz et al. quantum yield data at longer wavelengths is at present unclear.

At $\lambda < 310$ nm and 1 atm, there was very good agreement with the data of Gierczak et al. [70] and Emrich and Warneck [57]; however at $\lambda > 310$ nm, the measured quantum yields were significantly smaller. The temperature dependence of Φ_{TOTAL} is quite striking at the longer wavelengths: the ratio of the quantum yields at 295 and 218 K reported by Blitz et al. [24, 25] are $\Phi_{\text{TOTAL}}(295 \text{ K}) / \Phi_{\text{TOTAL}}(218 \text{ K}) \approx 4$ and ≈ 20 at 310 nm and 322.5 nm, respectively.

A major difference in the study of Blitz et al. [24, 25] from several of the earlier studies is that the OH radicals are detected before undergoing secondary reactions, so that the OH yields represent the CH_3CO radicals produced. The quantum yields reported from the Gierczak et al. [70] and Emrich and Warneck [57] studies were based upon the removal of $\text{CH}_3\text{C(O)CH}_3$, which may be affected by the additional loss of acetone due to the $\text{OH} + \text{acetone}$ reaction where OH radicals are produced in the reaction of CH_3CO with O_2 . However, the OH yield in the $\text{CH}_3\text{CO} + \text{O}_2$ reaction is a strong function of pressure and measurements made at pressures > 50 Torr are expected to have negligible errors.

The quantum yield data of Blitz et al. [24, 25] are recommended. The optimized parameterization of the quantum yields for the wavelength range 279 – 327.5 nm, temperature range 218 – 295 K and pressure range 0 – 1000 mbar is as follows:

$$\Phi_{\text{TOTAL}}(\lambda, [\text{M}], T) = \Phi_{\text{CH}_3\text{CO}}(\lambda, [\text{M}], T) + \Phi_{\text{CO}}(\lambda, T); \quad \text{all } \lambda$$

For $\lambda = 279\text{-}327.5$ nm

$$\Phi_{\text{CO}}(\lambda, T) = 1 / (1 + A_0)$$

$$\begin{aligned} \text{where } A_0 &= [a_0 / (1 - a_0)] \exp[b_0 \{\lambda - 248\}] \\ a_0 &= (0.350 \pm 0.003) (T/295)^{(-1.28 \pm 0.03)} \\ b_0 &= (0.068 \pm 0.002) (T/295)^{(-2.65 \pm 0.20)} \end{aligned}$$

For $\lambda = 279\text{-}302$ nm

$$\Phi_{\text{CH}_3\text{CO}}(\lambda, [\text{M}], T) = \{1 - \Phi_{\text{CO}}(\lambda, T)\} / \{1 + A_1[\text{M}]\}$$

$$\begin{aligned} \text{where } A_1 &= a_1 \exp[-b_1 \{(10^7/\lambda) - 33113\}] \\ a_1 &= (1.600 \pm 0.032) \times 10^{-19} (T/295)^{(-2.38 \pm 0.08)} \\ b_1 &= (0.55 \pm 0.02) \times 10^{-3} (T/295)^{(-3.19 \pm 0.13)} \end{aligned}$$

For $\lambda = 302\text{-}327.5$ nm,

$$\Phi_{\text{CH}_3\text{CO}}(\lambda, [\text{M}], T) = \{(1 + A_4[\text{M}] + A_3) / [(1 + A_2[\text{M}] + A_3)(1 + A_4[\text{M}])]\} \{1 - \Phi_{\text{CO}}(\lambda, T)\}$$

$$\begin{aligned} \text{where } A_2 &= a_2 \exp[-b_2 \{(10^7/\lambda) - 30488\}] \\ a_2 &= (1.62 \pm 0.06) \times 10^{-17} (T/295)^{(-10.03 \pm 0.20)} \\ b_2 &= (1.79 \pm 0.02) \times 10^{-3} (T/295)^{(-1.364 \pm 0.036)} \\ A_3 &= a_3 \exp[-b_3 \{(10^7/\lambda) - c_3\}^2] \\ a_3 &= (26.29 \pm 0.88) (T/295)^{(-6.59 \pm 0.23)} \\ b_3 &= (5.72 \pm 0.20) \times 10^{-7} (T/295)^{(-2.93 \pm 0.09)} \\ c_3 &= (30006 \pm 41) (T/295)^{(-0.064 \pm 0.004)} \\ A_4 &= a_4 \exp[-b_4 \{(10^7/\lambda) - 30488\}] \\ a_4 &= (1.67 \pm 0.14) \times 10^{-15} (T/295)^{(-7.25 \pm 0.54)} \\ b_4 &= (2.08 \pm 0.02) \times 10^{-3} (T/295)^{(-1.16 \pm 0.15)} \end{aligned}$$

where $[\text{M}]$ is in molecule cm^{-3} , λ in nm and T in K. The equations given above have been used to calculate the quantum yields given in Table 4D-24.

It is well established that acetone photolysis at wavelengths > 300 nm has a strong dependence on pressure and temperature but there remains some uncertainty in the absolute quantum yield values in this wavelength region. The effect of the temperature dependent quantum yields of acetone on the chemistry of the upper troposphere has been modeled by Arnold et al. [10] and shown to be significant. Additional quantum yield studies are desired at atmospherically relevant photolysis wavelengths, > 290 nm, as a function of pressure and temperature to reduce uncertainties in model calculations.

Table 4D-23. Absorption Cross Sections of CH₃C(O)CH₃ at 298 K and Temperature Coefficients

λ (nm)	$10^{20} \sigma$ (cm ²)	$10^3 A$ (K ⁻¹)	$10^5 B$ (K ⁻²)	$10^8 C$ (K ⁻³)	λ (nm)	$10^{20} \sigma$ (cm ²)	$10^3 A$ (K ⁻¹)	$10^5 B$ (K ⁻²)	$10^8 C$ (K ⁻³)
215	0.167	-10.46	8.346	-16.43	283	4.71	1.137	-1.350	3.272
216	0.180	-9.192	7.357	-14.51	284	4.62	0.8530	-1.158	2.943
217	0.196	-6.233	5.039	-10.01	285	4.54	0.6518	-1.023	2.714
218	0.212	-3.190	2.651	-5.359	286	4.44	0.4907	-0.9154	2.531
219	0.228	-1.002	0.9314	-2.003	287	4.36	0.3190	-0.7992	2.332
220	0.246	0.4104	-0.1807	0.1679	288	4.28	0.1109	-0.6586	2.092
221	0.270	1.567	-1.090	1.936	289	4.15	-0.1230	-0.5036	1.833
222	0.294	2.962	-2.183	4.058	290	4.06	-0.3698	-0.3426	1.568
223	0.318	4.839	-3.651	6.909	291	3.95	-0.6430	-0.1615	1.265
224	0.346	6.940	-5.293	10.09	292	3.82	-0.9625	0.05796	0.8847
225	0.380	8.598	-6.588	12.60	293	3.71	-1.316	0.306	0.4472
226	0.419	9.380	-7.200	13.79	294	3.57	-1.650	0.535	0.0477
227	0.456	9.551	-7.336	14.06	295	3.42	-1.905	0.699	-0.2168
228	0.492	9.705	-7.462	14.31	296	3.26	-2.084	0.796	-0.3430
229	0.535	10.08	-7.761	14.89	297	3.11	-2.234	0.867	-0.4086
230	0.584	10.41	-8.023	15.41	298	2.98	-2.391	0.942	-0.4824
231	0.637	10.39	-8.002	15.36	299	2.82	-2.590	1.055	-0.6387
232	0.693	10.01	-7.707	14.79	300	2.67	-2.915	1.277	-1.020
233	0.750	9.534	-7.332	14.06	301	2.58	-3.421	1.649	-1.709
234	0.815	9.138	-7.022	13.46	302	2.45	-4.008	2.091	-2.543
235	0.885	8.851	-6.799	13.02	303	2.30	-4.508	2.465	-3.248
236	0.956	8.638	-6.634	12.70	304	2.18	-4.858	2.715	-3.699
237	1.03	8.471	-6.504	12.45	305	2.05	-5.120	2.880	-3.959
238	1.11	8.318	-6.385	12.22	306	1.89	-5.433	3.062	-4.219
239	1.21	8.125	-6.235	11.93	307	1.75	-6.010	3.429	-4.805
240	1.30	7.861	-6.031	11.53	308	1.61	-6.986	4.096	-5.954
241	1.40	7.554	-5.793	11.07	309	1.49	-8.135	4.899	-7.370
242	1.50	7.268	-5.571	10.64	310	1.36	-8.897	5.415	-8.255
243	1.60	7.035	-5.390	10.29	311	1.24	-8.923	5.378	-8.097
244	1.72	6.838	-5.237	9.994	312	1.14	-8.494	5.001	-7.305
245	1.83	6.649	-5.093	9.718	313	1.06	-8.228	4.754	-6.772
246	1.95	6.472	-4.960	9.464	314	0.944	-8.445	4.881	-6.959
247	2.07	6.326	-4.850	9.256	315	0.837	-8.966	5.240	-7.592
248	2.20	6.210	-4.763	9.091	316	0.760	-9.409	5.528	-8.076
249	2.33	6.099	-4.680	8.936	317	0.684	-9.584	5.588	-8.085
250	2.47	5.972	-4.587	8.763	318	0.598	-9.736	5.596	-7.946
251	2.60	5.832	-4.486	8.576	319	0.523	-10.39	5.958	-8.433
252	2.74	5.697	-4.389	8.399	320	0.455	-11.80	6.869	-9.933
253	2.87	5.581	-4.306	8.249	321	0.411	-13.48	7.962	-11.75
254	3.01	5.483	-4.235	8.120	322	0.348	-14.59	8.600	-12.67
255	3.15	5.385	-4.164	7.989	323	0.294	-14.98	8.670	-12.47
256	3.30	5.261	-4.075	7.825	324	0.248	-15.39	8.743	-12.27
257	3.44	5.101	-3.961	7.620	325	0.210	-16.28	9.187	-12.77
258	3.57	4.932	-3.843	7.410	326	0.174	-17.09	9.588	-13.21
259	3.69	4.802	-3.756	7.262	327	0.141	-17.21	9.471	-12.68
260	3.81	4.746	-3.723	7.215	328	0.113	-16.92	9.048	-11.58
261	3.94	4.744	-3.730	7.239	329	0.0913	-16.66	8.672	-10.62
262	4.07	4.734	-3.729	7.246	330	0.0740	-15.94	7.979	-9.099
263	4.20	4.651	-3.674	7.155	331	0.0586	-13.93	6.340	-5.829
264	4.32	4.482	-3.559	6.956	332	0.0465	-10.93	3.969	-1.214
265	4.41	4.271	-3.416	6.712	333	0.0375	-8.186	1.847	2.840

λ (nm)	$10^{20} \sigma$ (cm ²)	$10^3 A$ (K ⁻¹)	$10^5 B$ (K ⁻²)	$10^8 C$ (K ⁻³)	λ (nm)	$10^{20} \sigma$ (cm ²)	$10^3 A$ (K ⁻¹)	$10^5 B$ (K ⁻²)	$10^8 C$ (K ⁻³)
266	4.49	4.087	-3.296	6.513	334	0.0311	-6.530	0.6289	5.067
267	4.56	3.983	-3.234	6.420	335	0.0248	-5.692	0.1022	5.880
268	4.64	3.969	-3.235	6.440	336	0.0199	-4.656	-0.5382	6.860
269	4.72	4.009	-3.273	6.524	337	0.0162	-2.090	-2.355	10.09
270	4.79	4.025	-3.294	6.577	338	0.0135	3.113	-6.237	17.33
271	4.87	3.935	-3.240	6.494	339	0.0113	11.01	-12.26	28.77
272	4.91	3.704	-3.085	6.231	340	0.00912	20.02	-19.22	42.15
273	4.94	3.378	-2.861	5.845	341	0.00729	27.20	-24.83	53.03
274	4.94	3.061	-2.645	5.473	342	0.00583	29.63	-26.80	56.96
275	4.94	2.854	-2.508	5.243	343	0.00494	25.97	-24.04	51.78
276	4.93	2.790	-2.474	5.201	344	0.00365	16.35	-16.63	37.55
277	4.92	2.816	-2.505	5.276	345	0.00301	3.774	-6.858	18.72
278	4.94	2.820	-2.518	5.316	346	0.00235	-2.414	-1.987	9.304
279	4.92	2.692	-2.433	5.175	347	0.00158	7.880	-9.888	24.53
280	4.91	2.389	-2.222	4.803	348	0.00111	29.52	-26.61	56.78
281	4.86	1.963	-1.922	4.272	349	0.00107	41.03	-35.51	73.95
282	4.79	1.517	-1.612	3.726					

Note:

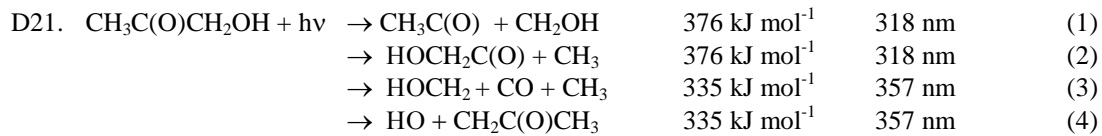
215 – 349 nm, Gierczak et al. [70], parameterization of the temperature dependence revised by Burkholder (2005) [31], $\sigma(T, \lambda) = \sigma(298 \text{ K}, \lambda) (1 + A T + B T^2 + C T^3)$ for $T = 235 - 298 \text{ K}$

Table 4D-24. Acetone Photolysis Quantum Yields

λ (nm)	$\Phi(218\text{ K})$	$\Phi(248\text{ K})$	$\Phi(273\text{ K})$	$\Phi(295\text{ K})$
279	0.680	0.579	0.571	0.617
280	0.663	0.558	0.551	0.597
281	0.644	0.536	0.530	0.578
282	0.621	0.513	0.509	0.559
283	0.594	0.489	0.489	0.540
284	0.565	0.465	0.468	0.521
285	0.534	0.441	0.448	0.502
286	0.500	0.417	0.427	0.483
287	0.465	0.393	0.407	0.464
288	0.430	0.369	0.388	0.446
289	0.394	0.345	0.368	0.428
290	0.359	0.322	0.350	0.411
291	0.324	0.300	0.331	0.394
292	0.291	0.279	0.314	0.377
293	0.260	0.258	0.297	0.361
294	0.231	0.239	0.280	0.345
295	0.205	0.221	0.264	0.330
296	0.180	0.203	0.249	0.315
297	0.158	0.187	0.235	0.301
298	0.138	0.172	0.221	0.287
299	0.121	0.158	0.208	0.274
300	0.105	0.144	0.195	0.261
301	0.0915	0.132	0.183	0.249
302	0.0794	0.121	0.125	0.237
303	0.0735	0.101	0.105	0.213
304	0.0557	0.0810	0.0873	0.184
305	0.0421	0.0646	0.0728	0.159
306	0.0317	0.0514	0.0608	0.137
307	0.0239	0.0409	0.0508	0.119
308	0.0180	0.0325	0.0426	0.103
309	0.0135	0.0258	0.0358	0.0887
310	0.0101	0.0205	0.0301	0.0769
311	0.00762	0.0164	0.0255	0.0669
312	0.00574	0.0131	0.0216	0.0584
313	0.00433	0.0105	0.0184	0.0511
314	0.00328	0.00842	0.0158	0.0449
315	0.00249	0.00679	0.0136	0.0396
316	0.00190	0.00550	0.0117	0.0350
317	0.00145	0.00447	0.0101	0.0311
318	0.00111	0.00365	0.00882	0.0278
319	0.000858	0.00299	0.00771	0.0248
320	0.000664	0.00246	0.00676	0.0223
321	0.000515	0.00204	0.00595	0.0201
322	0.000400	0.00169	0.00526	0.0181
323	0.000312	0.00141	0.00466	0.0164
324	0.000244	0.00117	0.00414	0.0149
325	0.000191	0.000983	0.00369	0.0135
326	0.000149	0.000826	0.00329	0.0124
327	0.000117	0.000696	0.00295	0.0113

Note:

Blitz et al. [24, 25], calculated using the expression given in the text



(Recommendation: 10-6, Note: 10-6, Evaluated: 10-6)

Absorption Cross Sections: The absorption cross sections of $\text{CH}_3\text{C}(\text{O})\text{CH}_2\text{OH}$ (hydroxyacetone, acetol) have been measured by Meller and Crowley [127] at 296 K in the range 207 – 333 nm; by Orlando et al. [152] at 298 K over the range 235 – 340 nm; and by Butkovskaya et al. [32] at 294 K over the range 240 – 350 nm using a static method, and at 328 K over the range 250 – 350 nm using a dynamic method. Dillon et al. [55] measured the cross section at 184.9 nm and 358 K to be $(5.4 \pm 0.1) \times 10^{-18} \text{ cm}^2 \text{ molecule}^{-1}$ whereas Baasandorj et al. [12] reported a value of $(5.43 \pm 0.08) \times 10^{-18} \text{ cm}^2 \text{ molecule}^{-1}$ at 298 K. The spectrum shows an absorption band with the maximum near 266 nm. The shape of the measured spectra are in excellent agreement except for the spectrum obtained by Butkovskaya et al. [32] using the dynamic method. The maxima cross sections reported by Butkovskaya et al. [32] are 15% and 24% lower for the static and dynamic methods, respectively, than the values obtained by Orlando et al. [152]; the maximum reported by Meller and Crowley [127] is 11% lower than that of Orlando et al. [152]. Large discrepancies between the measured spectra exist at $\lambda > 310 \text{ nm}$.

In Table 4D-25 are listed the averages over 1 nm intervals of the cross sections of Orlando et al. [152] and Butkovskaya et al. [32] (static) in the wavelength range 240 – 310 nm; at 311 – 336 nm, only those of Orlando et al. [152].

Photolysis Quantum Yield and Product Studies: Quantum yields for removal of hydroxyacetone were estimated by Orlando et al. [152] to be 0.65 ± 0.25 for the photolysis in the 240 – 420 nm band. They also suggested that $0.3 \pm 0.2 < \Phi_1 + \Phi_2 < 0.6$ for wavelengths larger than 290 nm. Products detected were CO , CO_2 , CH_2O , CH_3COOH , $\text{CH}_3\text{COO}_2\text{H}$, HCOOH and CH_3OH . These authors concluded that at most 50% of the photolysis occurred via channel (1). Direct observation of OH radicals, presumably arising from channel (4), was made by Chowdhury et al. [46] at 148 nm. Photolysis of hydroxyacetone at 193 nm was performed by Chowdhury et al. [46] and appears to occur by process (2) with the initial formation of HOCH_2CO yielding OH and ketene.

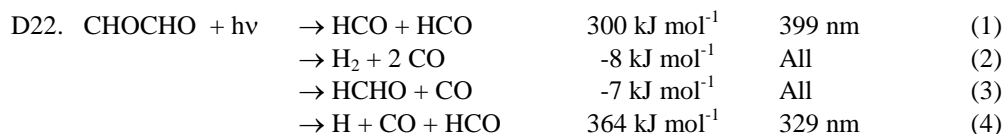
Table 4D-25. Absorption Cross Sections of CH₃C(O)CH₂OH at 298 K

λ (nm)	$10^{20} \sigma$ (cm ²)	λ (nm)	$10^{20} \sigma$ (cm ²)	λ (nm)	$10^{20} \sigma$ (cm ²)	λ (nm)	$10^{20} \sigma$ (cm ²)
240	2.43	264	6.06	288	3.03	312	0.219
241	2.60	265	6.07	289	2.80	313	0.192
242	2.78	266	6.09	290	2.58	314	0.177
243	2.97	267	6.09	291	2.37	315	0.157
244	3.15	268	6.07	292	2.18	316	0.142
245	3.34	269	6.04	293	2.00	317	0.133
246	3.54	270	5.98	294	1.82	318	0.117
247	3.73	271	5.90	295	1.65	319	0.104
248	3.91	272	5.82	296	1.49	320	0.095
249	4.11	273	5.72	297	1.34	321	0.087
250	4.29	274	5.61	298	1.19	322	0.078
251	4.50	275	5.49	299	1.07	323	0.072
252	4.67	276	5.37	300	0.955	324	0.067
253	4.83	277	5.22	301	0.874	325	0.063
254	4.98	278	5.05	302	0.772	326	0.056
255	5.14	279	4.87	303	0.682	327	0.053
256	5.31	280	4.68	304	0.603	328	0.051
257	5.46	281	4.48	305	0.535	329	0.047
258	5.59	282	4.28	306	0.477	330	0.044
259	5.69	283	4.09	307	0.424	331	0.041
260	5.79	284	3.89	308	0.377	332	0.038
261	5.87	285	3.69	309	0.333	333	0.036
262	5.96	286	3.48	310	0.291	334	0.034
263	6.02	287	3.26	311	0.249	335	0.032

Note:

240 – 310 nm: average of Orlando et al. [152], Butkovskaya et al. (static) [32]

311 – 335 nm: Orlando et al. [152] (at $\lambda > 326$ nm smoothed)



(Recommendation: 10-6, Note: 10-6, Evaluated: 10-6)

Absorption Cross Sections: The UV/vis absorption spectrum of glyoxal, CHOCHO, has been measured in a number of studies. The spectrum has two absorption bands in the wavelength region >220 nm; a weak band with evidence of diffuse vibrational structure in the 220 – 350 nm region and a stronger and highly structured band at wavelengths >360 nm with a maximum near 455 nm. The absorption cross sections, particularly in the visible absorption band, are dependent on the resolution used in the spectrum measurement and comparison of results from the various studies need to take this into consideration. The absorption spectrum of glyoxal has been reported at room temperature by Plum et al. [158] (230 – 460 nm), Langford and Moore [102] (308 nm), Zhu et al. [213] (193, 248, 308, and 351 nm), Chen and Zhu [44] (290 – 420 nm, in 10 nm intervals), Orlando and Tyndall [150] (210 – 450 nm, 0.6 nm resolution), Horowitz et al. [87] (210 – 480 nm, 0.25 nm resolution), Zhu and Johnston [212] (436 – 442 nm), and Volkamer et al. [198] (250 – 526 nm). Orlando and Tyndall [150] and Horowitz et al. [87] reported absorption spectra obtained using diode array spectroscopy and their spectra are in very good agreement, i.e., to better than 10% between 240 and 440 nm. The absorption cross sections from Chen and Zhu [44] are in reasonable agreement with these studies with differences in the 10 to 50% range depending on the wavelength. However, the absorption cross sections reported by Zhu et al. [213] at 248, 308, and 351 nm agree very well with the data of Horowitz et al. [87] and Orlando and Tyndall [150]. A strong absorption feature at wavelengths <200 nm indicated by the 193 nm measurement of Zhu et al. [213] ($\sigma = 4.8 \times 10^{-19}$ cm² molecule⁻¹) was also reported by Orlando and Tyndall

[150]. The cross section data from Plum et al. [158] are systematically less, by roughly 10 to 25%, than reported in the more recent studies with larger differences apparent in the region of the absorption minimum near 350 nm and at the shorter wavelengths.

Volkamer et al. [198] reported the highest available resolution absorption spectra of glyoxal to date which were obtained using Fourier transform spectroscopy at 1 cm⁻¹ (250 – 526 nm) and 0.06 cm⁻¹ (368 – 526 nm) resolution. The high resolution spectrum has more pronounced differential vibrational fine structure in the visible absorption band leading to higher absorption cross sections than reported in the lower resolution studies. The absorption cross sections reported by Volkamer et al. [198] are systematically 10% greater than reported by Horowitz et al. [87] and Orlando and Tyndall [150] (where comparison is possible). The differences in the absorption cross sections are most apparent in the short wavelength band. The UV spectrum reported by Volkamer et al. [198] is consistent with IR spectral parameters which were obtained by simultaneous recording of UV and IR spectra using the same glyoxal sample fillings of the absorption cell. Zhu and Johnston [212] report an absorption cross section at the absorption maximum near 440.7 nm (440.1 nm in the Volkamer et al. spectrum) of 4.6 x 10⁻¹⁹ cm² molecule⁻¹ obtained at high resolution using cavity ring-down spectroscopy. Their cross section value is in poor agreement with the high resolution data of Volkamer et al. [198] which is a factor of two greater. The recommended room temperature absorption cross sections in Table 4D-26 are averages over 1 nm intervals of the high resolution spectrum from Volkamer et al. [198] and are appropriate for use in atmospheric photolysis rate calculations. Studies requiring higher resolution data should consult the original literature.

Photolysis Quantum Yield and Product Studies: The photodissociation of CHOCHO as well as the photolysis product channel yields are wavelength and pressure dependent. Calvert and Pitts [37] have summarized the CHOCHO quantum yield data prior to 1966. On the basis of the work by Calvert and Layne [35] and Parmenter [156] it was established that the HCHO + CO photolysis channel (3) was the dominant photolysis channel with yields between 0.84 and 0.6 over the wavelength range 254 to 435 nm. There was little experimental evidence for the HCO + HCO radical channel (1) occurring and it was incorrectly concluded to be negligible. Plum et al. [158] has since reported the effective quantum yield for CHOCHO photolysis at wavelengths >290 nm to be 0.029, based on measured photolysis rates in an environmental chamber relative to NO₂ where J_{CHOCHO}/J_{NO₂} was found to be 0.008 ± 0.005. An effective atmospheric photolysis rate was measured using solar radiation in the EUPHORE outdoor chamber to be J_{obs} = 1.04 ± 0.10 × 10⁻⁴ s⁻¹, corresponding to an effective quantum yield for glyoxal loss of 0.035 ± 0.007 [136, 137] in reasonable agreement with the value reported by Plum et al. [158].

Langford and Moore [102] measured HCO produced in the photolysis of glyoxal in 1000 Torr N₂ at 305 nm by direct HCO resonance absorption and deduced a total HCO yield of 0.8 ± 0.4 at 305 nm. Using cavity ring-down spectroscopy, Zhu et al. [213] reported HCO quantum yields of 1.5 (Φ₁ ≈ 0.75) for photolysis at 351 nm, 0.69 at 308 nm, 0.52 at 248 nm and 0.42 at 193 nm. In a later study Chen and Zhu [44] reported zero pressure HCO yields, Φ₀(λ), at 10 nm intervals, to increase from 0.50 ± 0.01 at 290 nm to a maximum of 2.01 ± 0.08 at 390 nm and to decrease to 0.74 ± 0.08 at 400 nm, 0.56 ± 0.04 at 410 nm, and 0.48 ± 0.03 at 420 nm. HCO quantum yields were found to be independent of the N₂ buffer gas pressure (10-400 Torr) for photolysis in the 290-370 nm region. In the wavelength region 380-420 nm the HCO quantum yield decreased with increasing pressure. They reported HCO quantum yields at 760 Torr N₂ to be 0.49 at 380 nm, 0.54 nm at 390 nm, 0.32 at 400 nm, 0.22 at 410 nm and 0.14 at 420 nm. Feierabend et al. [62] measured quantum yields for the production of HCO at 85 discrete wavelengths in the wavelength range 290-420 nm at pressures between 50 and 550 Torr (N₂) at 298 K using pulsed laser photolysis combined with cavity ring-down spectroscopy detection of HCO. Φ₀(λ) varied smoothly with wavelength with a maximum value of ~1.8 in the range 300 – 385 nm with values decreasing to near 0 at 420 nm and 0.4 at 290 nm. The high precision of the measurements enabled the pressure dependence of the HCO quantum yield to be determined at each wavelength using the Stern-Volmer relationship

$$\frac{1}{\Phi(\lambda, P)} = \frac{1}{\Phi_0(\lambda)} + \frac{k_q}{k_d}(\lambda) [N_2]$$

where k_q is the collisional quenching rate coefficient and k_d is the rate coefficient for the dissociation of glyoxal. The wavelength dependence of the rate coefficient ratio was fit to the expression

$$k_q/k_d(\lambda) = 2.3 \times 10^{-20} + 1.5 \times 10^{-19} \exp(-0.4 \Delta E) \quad (\text{cm}^3 \text{ molecule}^{-1})$$

where $\Delta E = ((28571/\lambda) - 72.5)$ (kcal mol⁻¹), λ is the photolysis wavelength (nm), and 72.5 kcal mol⁻¹ is the threshold for glyoxal photodissociation (there is a small barrier to dissociation on the triplet surface). The Φ₀(λ) values from the Feierabend et al. [62] work are in good agreement with the values reported by Chen and Zhu [44].

Tadić et al. [185] photolysed glyoxal with broadband fluorescent lamps, which selectively overlapped with the two absorption bands, and measured the CO, HCHO and HCOOH end products. Using 275-380 nm irradiation, the quantum yield for glyoxal loss was found to be $\Phi_T = 0.97 \pm 0.05$ and independent of pressure. The absolute quantum yields obtained for 390 – 470 nm radiation, covering the visible absorption band, were found to be pressure dependent with values ranging from $\Phi_T = 0.12$ at 100 Torr to $\Phi_T = 0.04$ at 700 Torr and was described by the Stern-Volmer expression

$$\frac{1}{\Phi_T} = 6.80 + [251.8 \times 10^{-4} P(\text{Torr})]$$

The direct HCO quantum yield measurements of Feierabend et al. [62] and Chen and Zhu [44] combined with the end product yield results of Tadić et al. [185] indicate that dissociation into 2 HCO radicals is the most important pathway under atmospheric conditions. On the basis of their HCO quantum yield data, Feierabend et al. reported a set of revised wavelength dependent quantum yields for channels (1), (2) and (3) from those of Tadić et al. [185], which were recommended in JPL 06-2. The revised quantum yields are recommended and given in Table 4D-27. Although glyoxal has a very low effective quantum yield, photolysis remains an important removal path in the atmosphere.

Table 4D-26. Absorption Cross Sections of CHOCHO at 296 K

λ (nm)	$10^{20} \sigma$ (cm ²)	λ (nm)	$10^{20} \sigma$ (cm ²)	λ (nm)	$10^{20} \sigma$ (cm ²)	λ (nm)	$10^{20} \sigma$ (cm ²)	λ (nm)	$10^{20} \sigma$ (cm ²)
250	1.73	306	3.22	362	0.706	418	7.87	474	0.108
251	1.52	307	3.20	363	0.639	419	9.13	475	0.159
252	1.48	308	3.15	364	0.680	420	5.60	476	0.155
253	1.55	309	3.12	365	0.665	421	7.19	477	0.181
254	1.60	310	3.10	366	0.743	422	6.99	478	0.255
255	1.67	311	3.22	367	0.860	423	13.0	479	0.142
256	1.62	312	3.34	368	1.01	424	8.24	480	0.074
257	1.81	313	3.39	369	1.06	425	10.4	481	0.070
258	1.82	314	3.23	370	1.14	426	16.4	482	0.065
259	1.85	315	2.80	371	1.18	427	16.1	483	0.053
260	1.83	316	2.65	372	1.14	428	21.4	484	0.071
261	1.96	317	2.46	373	1.21	429	6.50	485	0.050
262	2.03	318	2.21	374	1.35	430	7.03	486	0.041
263	2.14	319	1.93	375	1.33	431	6.52	487	0.056
264	2.18	320	1.85	376	1.38	432	6.08	488	0.070
265	2.26	321	1.89	377	1.47	433	5.66	489	0.042
266	2.33	322	1.77	378	1.61	434	6.81	490	0.045
267	2.37	323	1.72	379	1.53	435	7.66	491	0.041
268	2.36	324	1.68	380	1.93	436	13.2	492	0.039
269	2.48	325	1.60	381	2.46	437	9.19	493	0.040
270	2.51	326	1.61	382	2.02	438	13.8	494	0.041
271	2.61	327	1.70	383	2.07	439	12.1	495	0.042
272	2.72	328	1.94	384	1.94	440	25.9	496	0.045
273	2.81	329	1.86	385	1.89	441	13.1	497	0.033
274	2.92	330	1.69	386	1.83	442	9.01	498	0.035
275	3.00	331	1.13	387	2.29	443	11.1	499	0.032
276	3.06	332	1.05	388	3.00	444	13.5	500	0.033
277	3.09	333	0.966	389	3.21	445	15.1	501	0.038
278	3.08	334	0.919	390	3.48	446	7.82	502	0.031
279	3.09	335	0.737	391	3.92	447	3.73	503	0.042
280	3.13	336	0.630	392	3.80	448	4.14	504	0.034
281	3.22	337	0.589	393	2.85	449	5.53	505	0.035
282	3.32	338	0.647	394	3.15	450	8.68	506	0.046
283	3.45	339	0.585	395	3.86	451	13.8	507	0.042
284	3.57	340	0.553	396	3.68	452	15.9	508	0.037
285	3.67	341	0.563	397	3.36	453	30.4	509	0.030

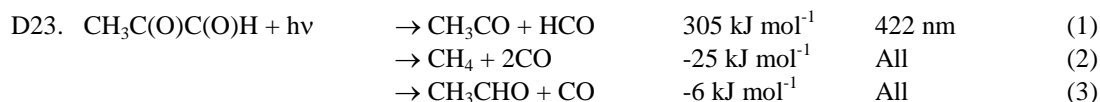
286	3.80	342	0.510	398	4.32	454	26.9	510	0.023
287	3.79	343	0.499	399	4.35	455	52.0	511	0.023
288	3.81	344	0.649	400	3.87	456	15.7	512	0.030
289	3.80	345	0.624	401	4.46	457	2.66	513	0.023
290	3.73	346	0.733	402	5.84	458	2.20	514	0.030
291	3.64	347	0.631	403	7.16	459	0.902	515	0.053
292	3.65	348	0.604	404	6.24	460	1.20	516	0.035
293	3.68	349	0.415	405	4.49	461	0.883	517	0.051
294	3.73	350	0.391	406	4.48	462	0.588	518	0.102
295	3.81	351	0.395	407	4.07	463	0.322	519	0.065
296	3.82	352	0.423	408	3.44	464	0.339	520	0.100
297	3.92	353	0.415	409	4.01	465	0.330	521	0.169
298	4.07	354	0.403	410	5.66	466	0.416	522	0.037
299	4.12	355	0.422	411	7.22	467	0.522	523	0.011
300	4.04	356	0.443	412	7.41	468	0.149	524	0.007
301	3.91	357	0.431	413	10.8	469	0.091	525	0.004
302	3.78	358	0.471	414	10.1	470	0.076	526	0.000
303	3.57	359	0.503	415	10.2	471	0.086		
304	3.35	360	0.546	416	6.07	472	0.092		
305	3.24	361	0.627	417	6.83	473	0.110		

Note:

Volkamer et al. [198], rounded to three significant figures

Table 4D-27. CHOCHO Photolysis Quantum Yields at 1 Atm and 298 K

λ (nm)	Φ Total	Φ_1 (HCO + HCO)	Φ_2 (H ₂ + 2CO)	Φ_3 (H ₂ CO + CO)
225	1	0.156	0.645	0.199
230	1	0.156	0.625	0.219
235	1	0.156	0.599	0.245
240	1	0.156	0.575	0.269
245	1	0.156	0.553	0.291
250	1	0.156	0.530	0.314
255	1	0.156	0.510	0.334
260	1	0.156	0.492	0.352
265	1	0.156	0.475	0.369
270	1	0.156	0.457	0.387
275	1	0.156	0.440	0.404
280	1	0.156	0.424	0.420
285	1	0.156	0.414	0.430
290	1	0.156	0.404	0.440
295	1	0.167	0.382	0.451
300	1	0.183	0.360	0.457
305	1	0.208	0.332	0.460
310	1	0.242	0.300	0.458
315	1	0.282	0.266	0.452
320	1	0.322	0.245	0.433
325	1	0.358	0.234	0.408
330	1	0.396	0.225	0.379
335	0.95	0.403	0.210	0.337
340	0.879	0.410	0.190	0.279
345	0.782	0.408	0.170	0.204
350	0.691	0.397	0.144	0.150
355	0.54	0.379	0.053	0.108
360	0.429	0.357	0	0.072
365	0.369	0.329	0	0.040
370	0.316	0.294	0	0.022
375	0.267	0.253	0	0.014
380	0.219	0.208	0	0.011
385	0.172	0.164	0	0.008
390	0.132	0.125	0	0.007
395	0.098	0.093	0	0.005
400	0.072	0.068	0	0.004
405	0.052	0.049	0	0.003
410	0.037	0.035	0	0.002
415	0.024	0.023	0	0.001
420	0	0	0	0



(Recommendation: 06-2, Note: 10-6, Evaluated: 10-6)

Absorption Cross Sections: The UV/vis absorption spectrum of methylglyoxal (MGLY), $\text{CH}_3\text{C}(\text{O})\text{C}(\text{O})\text{H}$, has been measured at room temperature by Plum et al. [158] (230 – 470 nm), Meller et al. [129] (218 – 494 nm), Chen et al. [42] (290 – 440 nm), and Staffelbach et al. [182] (205 – 474 nm). The absorption spectrum exhibits two absorption bands, a slightly structured band between 225 and 335 nm and a stronger band between 335 and 475 nm, which is highly structured in the region above 410 nm. A steep increase of the

absorption cross sections was observed at shorter wavelengths going from 225 to 200 nm by Staffebach et al. [182].

The room temperature values of Meller et al. [129] and Staffebach et al. [182] are in good agreement at wavelengths >230 nm. In the weaker absorption band the data of Meller et al. [129] are greater by up to 10-15%. In the strong absorption band up to 400 nm, the data of Staffebach et al. [182] are greater by up to ~10% than the data of Meller et al. [129], and at higher wavelengths the peak values reported by Meller et al. [129] are higher (due to the higher resolution used in their study) than those measured by Staffebach et al. [182]. The data points of Chen et al. [42] determined at 10 nm intervals fit well to the absorption curves of Meller et al. [129] and Staffebach et al. [182] except at 380 and 400 nm where the differences are ~20%. The cross sections reported by Plum et al. [158] are approximately only the half of the cross sections reported Meller et al. [129] and Staffebach et al. [182]. The recommended absorption cross sections in Table 4D-28 are from the data of Staffebach et al. [182] in the region 200 – 218 nm, the mean of the values from Meller et al. [129] and Staffebach et al. [182] in the region 219 – 235 nm, and averages over 1 nm intervals of the data from Meller et al. [129] in the region 236 – 493 nm.

The temperature dependence of the absorption spectrum is relatively weak with changes on the order of 10% observed in the spectrum measured by Staffebach et al. [182] between 298 and 248 K. The largest changes occur in the structured region between 410 and 450 nm where the fine structure becomes more pronounced at lower temperatures.

Photolysis Quantum Yield and Product Studies: Quantum yields have been measured in several studies. Kyle and Orchard [100] reported products formed in the photolysis of methylglyoxal at 387 K and 436 nm. Staffebach et al. [182] reported a determination of products after photolysis of dilute mixtures of methylglyoxal in air using a Xe arc equipped with different band pass filters to isolate several regions of the spectrum. The observed products (CO, CO₂, HCHO, CH₃COOH, CH₃COOOH, CH₃OH and HCOOH,) led to the conclusion that only channel (1) is important in the photolysis range 240 – 480 nm. Quantum yields were derived by modeling the products formed using a number of secondary radical reactions. At 760 Torr, the Φ_1 yields were: 0.005 for the wavelength region 410 – 418 nm, 0.055 for 355 – 480 nm, 0.07 for 280-240 nm and 0.14 for 240 – 420 nm. Raber and Moortgat [161] irradiated methylglyoxal in air at different total pressures using two types of broadband lamps and determined the products (CO, CO₂, HCHO, CH₃OOH, CH₃OH, HCOOH, CH₃CHO, CH₃COOH, CH₃COOOH and CH₃COCOOH). The quantum yield derived by modeling the products of the photolysis in the 275-380 nm region varied from 0.94 ± 0.04 at 54 Torr to 0.64 ± 0.03 at 760 Torr, and in the 390 – 470 nm region from 0.41 ± 0.04 to 0.23 ± 0.02 .

Koch and Moortgat [97] determined the quantum yields of CO, HCHO and CH₃CHO formation at 298 K as a function of wavelength (260 – 440 nm) and pressure of synthetic air (30 – 900 Torr) using “broad” monochromatic light, with an optical resolution of 8.5 nm. For photolysis in the 260 – 320 nm band, the overall quantum yield was found to be unity, independent of wavelength and pressure. The analysis of the data gave evidence that channel (1) is the predominant photolysis path. In the 380 – 440 nm band the quantum yield of CO showed a Stern-Volmer pressure dependence and the quantum yield of H₂CO increased with increasing methylglyoxal pressure, which was attributed to the reaction of excited methylglyoxal with ground state methylglyoxal.

The quantum yield of channel (1) over the wavelength range 250-500 nm was expressed as

$$\begin{aligned} 1/\Phi_1(\lambda) &= 1/\Phi_0(\lambda) + P(\text{Torr}) / k(\lambda) \\ \text{where } \Phi_0(\lambda) &= 1 \text{ for } \lambda < 380 \text{ nm} \\ \Phi_0(\lambda) &= (8.15 \pm 0.7) \cdot 10^{-9} [\exp(7131 \pm 267) / \lambda] \quad \text{for } \lambda > 380 \text{ nm} \\ k(\lambda) &= (7.34 \pm 0.1) \cdot 10^{-9} [\exp(8793 \pm 300) / \lambda] \end{aligned}$$

Chen et al. [42] used a tunable dye laser to photolysed methylglyoxal at 10 nm intervals over the range 290 – 440 nm combined with detection of the primary HCO radical photolysis product using cavity ring-down spectroscopy. The HCO quantum yield was calibrated against HCO produced in the photolysis of HCHO or Cl₂/HCHO mixtures. They report the HCO quantum yield to be unity in the wavelength range 320-360 nm, 0.82 ± 0.06 at 290 nm, and to decrease at wavelengths >370 nm to a value of 0.17 ± 0.02 at 440 nm. The HCO quantum yields were reported to be independent of pressure between 290 and 370 nm for the pressure range 10-400 Torr N₂ but to have a Stern-Volmer pressure dependence at wavelengths ≥380 nm given by

$$\begin{aligned} 1/\Phi_1(\lambda) &= 1/\Phi_0(\lambda) + k_Q(\lambda) P(\text{Torr}) \\ \text{where } \Phi_0(\lambda) &= (3.63 \pm 0.32) \cdot 10^{-7} [\exp(5693 \pm 533) / \lambda] \\ \text{and } k_Q(\lambda) &= (1.93 \pm 0.24) \times 10^4 [\exp(-(5639 \pm 497) / \lambda)] \end{aligned}$$

The zero pressure quantum yields, $\Phi_0(\lambda)$, are in good agreement for wavelengths ≤ 420 nm. However, the quantum yields at 760 Torr from the Chen et al. [42] and Koch and Moortgat [97] expressions deviate by a

factor 4 for wavelengths ≥ 420 nm. The data from the more direct study by Chen et al. [42] are recommended. Additional measurements are needed to establish the quantum yields in the long wavelength tail of the spectrum at atmospheric relevant pressures.

Table 4D-28. Absorption Cross Sections of $\text{CH}_3\text{COC(O)H}$ at 298 K

λ (nm)	$10^{20} \sigma$ (cm^2)	λ (nm)	$10^{20} \sigma$ (cm^2)	λ (nm)	$10^{20} \sigma$ (cm^2)	λ (nm)	$10^{20} \sigma$ (cm^2)	λ (nm)	$10^{20} \sigma$ (cm^2)
200	33.8	259	3.25	318	1.82	377	2.10	436	11.1
201	30.6	260	3.29	319	1.68	378	2.18	437	10.0
202	27.0	261	3.33	320	1.50	379	2.30	438	10.6
203	23.0	262	3.36	321	1.34	380	2.42	439	11.0
204	18.6	263	3.42	322	1.22	381	2.54	440	9.94
205	15.3	264	3.49	323	1.14	382	2.70	441	10.4
206	12.1	265	3.59	324	1.01	383	2.88	442	10.2
207	10.0	266	3.73	325	0.924	384	3.03	443	10.2
208	8.52	267	3.87	326	0.848	385	3.20	444	11.2
209	7.43	268	4.02	327	0.774	386	3.39	445	9.62
210	6.34	269	4.13	328	0.716	387	3.61	446	8.91
211	5.58	270	4.20	329	0.672	388	3.71	447	9.84
212	4.73	271	4.22	330	0.647	389	3.88	448	9.19
213	4.16	272	4.23	331	0.620	390	4.03	449	10.1
214	3.57	273	4.27	332	0.608	391	4.22	450	8.68
215	3.08	274	4.31	333	0.525	392	4.31	451	6.35
216	2.65	275	4.37	334	0.531	393	4.47	452	6.33
217	2.33	276	4.49	335	0.495	394	4.57	453	6.08
218	2.10	277	4.64	336	0.455	395	4.67	454	4.47
219	1.46	278	4.77	337	0.407	396	4.87	455	3.69
220	1.45	279	4.87	338	0.362	397	5.08	456	3.09
221	1.44	280	4.92	339	0.346	398	5.26	457	2.47
222	1.43	281	4.93	340	0.322	399	5.46	458	1.81
223	1.44	282	4.90	341	0.300	400	5.62	459	1.28
224	1.43	283	4.83	342	0.289	401	5.90	460	0.914
225	1.44	284	4.76	343	0.288	402	6.07	461	0.795
226	1.46	285	4.70	344	0.289	403	6.36	462	0.643
227	1.48	286	4.66	345	0.295	404	6.55	463	0.480
228	1.51	287	4.65	346	0.308	405	6.92	464	0.332
229	1.53	288	4.73	347	0.325	406	7.20	465	0.268
230	1.60	289	4.84	348	0.339	407	7.59	466	0.228
231	1.61	290	4.92	349	0.362	408	7.95	467	0.188
232	1.65	291	4.90	350	0.385	409	8.12	468	0.160
233	1.67	292	4.81	351	0.424	410	8.52	469	0.133
234	1.75	293	4.70	352	0.463	411	8.64	470	0.108
235	1.83	294	4.57	353	0.492	412	9.07	471	0.0998
236	1.86	295	4.37	354	0.523	413	9.38	472	0.0897
237	1.93	296	4.17	355	0.556	414	9.62	473	0.0776
238	1.96	297	4.00	356	0.597	415	9.69	474	0.0680
239	2.00	298	3.88	357	0.635	416	9.72	475	0.0627
240	2.07	299	3.76	358	0.676	417	10.0	476	0.0561
241	2.14	300	3.69	359	0.720	418	10.1	477	0.0515
242	2.19	301	3.70	360	0.765	419	10.1	478	0.0483
243	2.23	302	3.74	361	0.816	420	10.2	479	0.0462
244	2.27	303	3.74	362	0.872	421	10.3	480	0.0392
245	2.30	304	3.62	363	0.933	422	10.5	481	0.0366
246	2.33	305	3.38	364	1.00	423	10.5	482	0.0315
247	2.38	306	3.15	365	1.08	424	10.2	483	0.0278
248	2.46	307	2.92	366	1.15	425	10.3	484	0.0271
249	2.57	308	2.71	367	1.23	426	10.0	485	0.0243

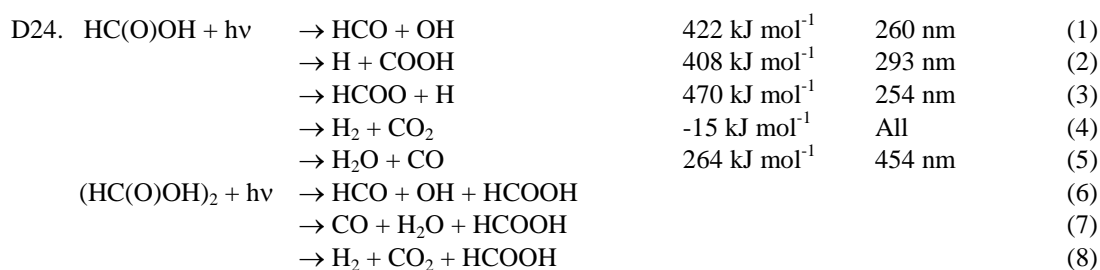
λ (nm)	$10^{20} \sigma$ (cm ²)	λ (nm)	$10^{20} \sigma$ (cm ²)	λ (nm)	$10^{20} \sigma$ (cm ²)	λ (nm)	$10^{20} \sigma$ (cm ²)	λ (nm)	$10^{20} \sigma$ (cm ²)
250	2.64	309	2.52	368	1.31	427	9.84	486	0.0217
251	2.68	310	2.34	369	1.40	428	10.0	487	0.0186
252	2.71	311	2.18	370	1.47	429	9.94	488	0.0181
253	2.73	312	2.06	371	1.55	430	10.4	489	0.0170
254	2.76	313	1.97	372	1.64	431	10.5	490	0.0174
255	2.82	314	1.90	373	1.73	432	9.79	491	0.0162
256	2.93	315	1.86	374	1.81	433	10.6	492	0.0161
257	3.06	316	1.86	375	1.90	434	10.5	493	0.0138
258	3.17	317	1.87	376	2.02	435	10.8		

Note:

200 – 218 nm: Staffebach et al. [182]

219 – 235 nm: mean of data from Meller et al. [129] and Staffebach et al. [182]

219 – 493 nm: Meller et al. [129]



(Recommendation: 06-2, Note: 10-6, Evaluated: 10-6)

Absorption Cross Sections: The UV absorption spectrum of formic acid, HC(O)OH, and formic acid dimer, (HC(O)OH)₂, have been measured near 300 K for a range of sample pressures by McMillan [36] (200 – 249 nm; 35.2, 16.4, and 2.45 Torr), Singleton et al. [175] (195 – 250 nm; 29 pressures between 0.5 and 22 Torr), Singleton et al. [177], and Nagakura et al. [146] (154 – 191 nm). Jolly et al. [92] also reported cross sections at 222 nm in connection with their quantum yield measurements. Singleton et al. [177] also measured spectra at 356.2 K. The absorption spectrum of the dimer has a broad maximum near 205 nm and a monotonic decrease in intensity with increasing wavelength. The absorption maximum of the monomer is shifted to longer wavelengths, peak near 215 nm, with about one third the peak cross section of the dimer. The decrease in cross sections with increasing wavelength is more rapid for the dimer than for the monomer, resulting in monomer cross sections being greater at 250 nm by approximately a factor 10. The absorption spectra reported by McMillan [36] were derived assuming monomers only in spite of undefined amounts of monomer and dimer contributions. The reported spectra lie between those reported by Singleton et al. [175] for the monomer and the dimer. The recommended absorption cross sections in Table 4D-29 are taken from Singleton et al [175] measured with a resolution of 1 nm.

Photolysis Quantum Yield and Product Studies: In the pre-1966 studies considered in Calvert and Pitts [36] yields of final products CO, CO₂, H₂, H₂O and suggested molecular elimination channels 4 and 5. However, in these experiments it would be difficult to distinguish between primary photolytic products and products formed by subsequent secondary free-radical reactions. Jolly et al. [92] determined the quantum yield of OH formation at 222 nm for the monomer to be 1.05 ± 0.14 and essentially zero for the dimer. In a follow-up study Singleton et al. [177] re-determined the OH quantum yields at 222 nm to be 0.704 ± 0.048 at 298 K and 0.771 ± 0.030 at 356.2 K for the monomer, and 0.153 ± 0.028 at 298 K for the dimer (the OH yield for the dimer at elevated temperatures was assumed to be zero). Photodissociation into the other radical channels 2 and 3 is minor and has been discussed by He and Fang [79]. Photodissociation quantum yields for the dimer were determined at 222 nm by Singleton et al. [176] to be $\Phi_{6,D} = 0.15$, $\Phi_{7,D} = 0.81$ and $\Phi_{8,D} = 0.04$.

Table 4D-29. Absorption Cross Sections of HC(O)OH and (HC(O)OH)₂ at 302 K

λ (nm)	$10^{20} \sigma$ (cm ²)		λ (nm)	$10^{20} \sigma$ (cm ²)	
	monomer	dimer		monomer	dimer
195	9.18	27.4	223	11.9	17.0
196	9.96	29.1	224	11.3	15.5
197	9.57	30.8	225	10.9	14.1
198	10.0	32.2	226	9.87	12.7
199	10.7	33.3	227	10.4	11.3
200	10.7	34.6	228	9.24	10.1
201	11.5	35.4	229	9.15	8.87
202	11.9	36.2	230	8.12	7.78
203	12.5	36.7	231	7.18	6.77
204	12.5	37.3	232	7.07	5.87
205	13.8	37.4	233	6.44	5.01
206	13.6	37.4	234	6.68	4.26
207	13.7	37.2	235	5.24	3.58
208	13.6	36.9	236	5.40	2.95
209	14.1	36.2	237	4.10	2.46
210	14.4	35.5	238	4.32	2.03
211	14.2	34.6	239	3.58	1.63
212	13.6	33.6	240	3.79	1.31
213	14.3	32.4	241	2.79	1.02
214	14.9	31.0	242	2.83	0.795
215	15.0	29.4	243	1.98	0.659
216	13.7	28.1	244	2.10	0.490
217	13.6	26.7	245	1.73	0.337
218	13.4	25.1	246	1.79	0.267
219	13.5	23.4	247	1.18	0.190
220	12.9	21.8	248	1.23	0.134
221	11.6	20.2	249	0.855	0.093
222	12.4	18.6	250	0.861	0.072

Note:

199 – 250 nm: Singleton et al. [175]

D25. CH ₃ C(O)OH + hv	→ CH ₄ + CO ₂	-35 kJ mol ⁻¹	All	(1)
	→ CH ₃ + COOH	391 kJ mol ⁻¹	306 nm	(2)
	→ CH ₃ CO + OH	459 kJ mol ⁻¹	260 nm	(3)
	→ CH ₃ COO + H	462 kJ mol ⁻¹	259 nm	(4)

(Recommendation: 06-2, Note: 10-6, Evaluated: 10-6)

Absorption Cross Sections: The UV absorption spectrum of acetic acid, CH₃C(O)OH, and the acetic acid dimer, (CH₃C(O)OH)₂, have been measured for a range of sample pressures at 300 K by McMillan [36] (200 – 241 nm; 12.9, 11.0, 8.3, and 3.6 Torr), at 283, 303 and 338 K by Hintze et al. [82] (195 – 220 nm), and at 270, 298, 325, and 345 K by Orlando and Tyndall [151] (210-245 nm; 0.12 – 3.6 Torr). Singleton et al. [177] also reported cross sections at 222 nm in connection with quantum yield measurements at 298 and 356.2 K. The monomer spectrum reported by Orlando and Tyndall [151] and Hintze et al. [82] has a broad maximum near 207 nm and a monotonic decrease in intensity with increasing wavelength. The absorption maximum for the dimer appears at shorter wavelength, below 205 nm, and is twice as intense as that of the monomer. The decrease in cross sections with increasing wavelength is more rapid for the dimer than for the monomer resulting in the monomer cross section being greater at 240 nm by a factor 6. Hinze et al. [82] determined the absorption cross section at the maximum for the monomer at 206.1 nm and 297 K to be $(1.27 \pm 0.10) \times 10^{-19}$ cm² molecule⁻¹ and for the dimer and at 208.1 nm to be $(2.44 \pm 0.08) \times 10^{-19}$ cm² molecule⁻¹. The absorption spectra reported by Calvert and Pitts [36] were derived assuming monomers only in spite of undefined amounts of monomer and dimer. The absorption spectrum for the greatest pressure is close to the dimer

spectrum reported by Orlando and Tyndall [151]. The recommended absorption cross sections in Table 4D-30 are taken from Orlando and Tyndall [151] (measured at 0.6 nm resolution).

Photolysis Quantum Yield and Product Studies: Early photolysis studies reported yields of the end products CO, CO₂, CH₄, and C₂H₆ (Calvert and Pitts [36]) and proposed molecular elimination (1) and radical reactions (2) to (4) originating from the monomer. Hunnicutt et al. [88] photolysed acetic acid at 218 nm and used photofragment laser fluorescence to determine channel (2) to be the dominant photochemical path. Singleton et al. [177] determined the OH quantum yield at 222 nm to be 0.546 ± 0.097 at 298 K and 0.692 ± 0.024 at 356.2 K for the monomer and 0.038 ± 0.026 at 298 K for the dimer (a dimer quantum yield of zero was assumed at elevated temperatures).

Table 4D-30. Absorption Cross Sections of CH₃C(O)OH and (CH₃C(O)OH)₂ at 298 K

λ (nm)	$10^{20} \sigma$ (cm ²)		λ (nm)	$10^{20} \sigma$ (cm ²)	
	monomer	dimer		monomer	dimer
210	15.1	23.4	228	6.00	3.60
212	14.7	20.9	230	5.09	2.45
214	13.5	18.4	232	4.20	1.71
216	12.5	15.8	234	3.44	1.11
218	11.7	13.2	236	2.71	0.65
220	10.5	10.9	238	2.11	0.45
222	9.33	8.54	240	1.64	0.27
224	8.19	6.68	242	1.19	
226	7.17	4.95	244	0.89	

Note:

210 – 244 nm: Orlando and Tyndall [151]

D26. CH₃C(O)OOH + hν → Products

(Recommendation: 06-2, Note: 10-6, Evaluated: 10-6)

Absorption Cross Sections: The UV absorption spectrum of peracetic acid, CH₃C(O)OOH, has been measured at 248 and 298 K by Orlando and Tyndall [151] (205 – 340 nm). The absorption cross sections decrease in a monotonic pseudo-exponential fashion with increasing wavelength. The spectrum recorded at 248 K shows an apparently faster fall-off with increasing wavelength than that recorded at room temperature. The recommended absorption cross sections in Table 4D-31 are taken from Orlando and Tyndall (measured at 0.6 nm resolution).

Photolysis Quantum Yield and Product Studies: No studies available.

Table 4D-31. Absorption Cross Sections CH₃C(O)OOH at 298 K

λ (nm)	$10^{20} \sigma$ (cm ²)	λ (nm)	$10^{20} \sigma$ (cm ²)	λ (nm)	$10^{20} \sigma$ (cm ²)	λ (nm)	$10^{20} \sigma$ (cm ²)
210	38.1	244	4.31	278	0.574	312	0.045
212	33.1	246	3.82	280	0.506	314	0.044
214	29.5	248	3.41	282	0.444	316	0.040
216	25.4	250	3.05	284	0.386	318	0.035
218	21.7	252	2.71	286	0.334	320	0.025
220	18.9	254	2.42	288	0.297	322	0.020
222	16.0	256	2.16	290	0.256	324	0.020
224	13.9	258	1.93	292	0.226	326	0.017
226	12.0	260	1.71	294	0.193	328	0.014
228	10.5	262	1.53	296	0.170	330	0.009
230	9.10	264	1.35	298	0.141	332	0.011
232	8.01	266	1.21	300	0.123	334	0.011
234	7.03	268	1.06	302	0.107	336	0.009
236	6.31	270	0.945	304	0.094	338	0.009
238	5.61	272	0.835	306	0.078	340	0.006

240	5.03	274	0.742	308	0.069		
242	4.83	276	0.651	310	0.062		

Note:

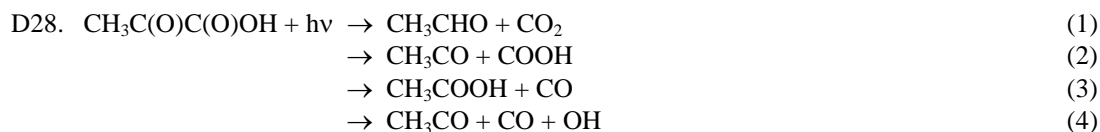
Orlando and Tyndall [151], 310 – 340 nm linear interpolation of $\ln(\sigma)$

D27. $\text{C}_2\text{H}_5\text{C}(\text{O})\text{OH} + h\nu \rightarrow \text{Products}$

(Recommendation: 06-2, Note: 10-6, Evaluated: 10-6)

Absorption Cross Sections: The absorption spectrum of propionic acid, $\text{C}_2\text{H}_5\text{C}(\text{O})\text{OH}$, and the propionic acid dimer, $(\text{C}_2\text{H}_5\text{C}(\text{O})\text{OH})_2$, have been measured by Hinze et al. [82] (195 – 220 nm) at 283, 303 and 338 K and Vicente et al. [197] (115 – 257 nm) at 313 K. The spectrum has a strong absorption band in the region 115 – 192 nm and a weaker band in the region 192 – 248 nm with a broad maximum near 207 nm. Hinze et al. [82] determined the absorption cross section for the monomer at 206.1 nm and 297 K to be $(1.52 \pm 0.16) \times 10^{-19} \text{ cm}^2 \text{ molecule}^{-1}$. The dimer cross section at 208.1 nm was determined to be $(3.24 \pm 0.22) \times 10^{-19} \text{ cm}^2 \text{ molecule}^{-1}$. Absorption cross sections have also been measured at 298 and 356.2 K and 222 nm by Singleton et al. [177]. The absorption cross sections are $12.2 \times 10^{-20} \text{ cm}^2 \text{ molecule}^{-1}$ at 298 K and $10.6 \times 10^{-20} \text{ cm}^2 \text{ molecule}^{-1}$ at 356.2 K for the monomer. The absorption cross sections are $10.6 \times 10^{-20} \text{ cm}^2 \text{ molecule}^{-1}$ at 298 K and $25.6 \times 10^{-20} \text{ cm}^2 \text{ molecule}^{-1}$ at 356.2 K for the dimer (obtained by an extrapolation procedure).

Photolysis Quantum Yield and Product Studies: Quantum yields for the formation of OH radicals at 222 nm have been measured by Singleton et al. [177] to be 0.148 ± 0.090 and 0.341 ± 0.014 for the monomer at 297.6 and 375.0 K, respectively, and 0.018 ± 0.06 at 297.6 K for the dimer (a dimer quantum yield of zero was assumed at elevated temperatures).



(Recommendation: 06-2, Note: 10-6, Evaluated: 10-6)

Absorption Cross Sections: The UV absorption spectrum of pyruvic acid, $\text{CH}_3\text{C}(\text{O})\text{C}(\text{O})\text{OH}$, has been measured at room temperature by Horowitz et al. [87] (250 – 410 nm, 0.25 nm resolution) and Mellouki and Mu [130] (290 – 380 nm). An absorption spectrum of pyruvic acid has also been reported by Yamamoto and Back [208] (250 – 400 nm) at 358 K. The continuous absorption band between 275 – 400 nm peaks near 350 nm and contains significant diffuse vibrational band structure. Absolute cross sections for the relative spectrum reported by Yamamoto and Back [208] were given in Horowitz et al. [87] following normalization of the spectrum at 350 nm to $3.82 \times 10^{-20} \text{ cm}^2 \text{ molecule}^{-1}$. The general shapes of the reported spectra are qualitatively similar although the spectrum reported by Yamamoto and Back [208] is red shifted and the cross sections at wavelengths <300 nm are considerably greater. The difference in cross section may in part be ascribed to the effect of temperature on the spectrum. The cross sections measured by Mellouki and Mu [130] are systematically greater than those obtained by Horowitz et al. [87]. The difference reaches a factor of two for wavelengths <295 nm and is ~20-30% between 305 and 370 nm. These discrepancies are most likely due to the difficulties in handling the pyruvic acid sample and determining its concentration. The recommended absorption cross sections in Table 4D-32 are 1 nm averages from Horowitz et al. [87] in the range 252 – 285 nm, the mean of the data from Horowitz et al. [87] and Mellouki and Mu [130] (both 1 nm averages) in the range 290 – 380 nm, and the data from Horowitz et al. [87] in the range 385 – 399 nm.

Photolysis Quantum Yield and Product Studies: Moortgat [136] reported an effective quantum yield for pyruvic acid under atmospheric conditions from a study in an outdoor photoreactor to be 0.43 ± 0.07 . Vesley and Leermakers [196] reported quantum yields of CO_2 of 1.02 ± 0.06 and of CH_3CHO of 0.6 for photolysis at 366 nm. Yamamoto and Back [208] measured quantum yields of CO_2 of 0.9 ± 0.1 and CH_3CHO of 0.45 at 366 nm and 340 K. The CH_3CHO yields obtained for 320 and 345 nm photolysis were more variable. Berges and Warneck [19] measured the quantum yields of CH_3CHO , CO_2 and CH_3COOH at 350 nm to be 0.48 ± 0.01 , 1.27 ± 0.18 and 0.14, respectively. In the presence of NO_2 , the quantum yield of CH_3CHO was reduced to 0.30 ± 0.04 and PAN was formed with a quantum yield of 0.15 ± 0.02 . Berges and Warneck [19] established $\Phi_1 = 0.48 \pm 0.01$ and $\Phi_2 = 0.39 \pm 0.10$. Mellouki and Mu [130] used a laser flash photolysis system at 355 nm and observed the formation of OH originating via channel (4) with a quantum yield of $\Phi_4 = 0.05 \pm 0.03$. The analysis of the products CH_3CHO , CO , CH_3COOH by Winterhalter et al. [206] are consistent with the data of Berges and Warneck [19] and lead to a quantum yield of channel (3) $\Phi_3 = 0.08 \pm$

0.03. For the photolysis of pyruvic acid at 366 nm the following quantum yields are recommended $\Phi_1 = 0.48 \pm 0.01$, $\Phi_2 = 0.39 \pm 0.10$, $\Phi_3 = 0.08 \pm 0.03$ and $\Phi_4 = 0.05 \pm 0.03$.

Table 4D-32. Absorption Cross Sections of $\text{CH}_3\text{C}(\text{O})\text{C}(\text{O})\text{OH}$ at 298 K

λ (nm)	$10^{20} \sigma$ (cm^2)	λ (nm)	$10^{20} \sigma$ (cm^2)	λ (nm)	$10^{20} \sigma$ (cm^2)	λ (nm)	$10^{20} \sigma$ (cm^2)	λ (nm)	$10^{20} \sigma$ (cm^2)
252	1.54	280	0.118	312	1.34	340	3.93	368	3.16
253	1.55	281	0.101	313	1.42	341	3.94	369	3.52
254	1.61	282	0.093	314	1.49	342	4.19	370	3.26
255	1.56	283	0.098	315	1.57	343	4.24	371	2.87
256	1.52	284	0.104	316	1.69	344	4.17	372	2.04
257	1.41	285	0.113	317	1.83	345	4.26	373	1.76
258	1.25	290	0.302	318	1.94	346	4.46	374	1.68
259	1.07	291	0.323	319	2.05	347	4.58	375	1.22
260	0.908	292	0.370	320	2.17	348	4.73	376	1.09
261	0.801	293	0.409	321	2.31	349	4.92	377	0.950
262	0.737	294	0.439	322	2.41	350	4.98	378	0.842
263	0.718	295	0.470	323	2.50	351	4.79	379	0.688
264	0.718	296	0.491	324	2.54	352	4.63	380	0.521
265	0.700	297	0.519	325	2.60	353	4.54	385	0.097
266	0.651	298	0.548	326	2.72	354	4.47	386	0.084
267	0.566	299	0.594	327	2.78	355	4.13	387	0.077
268	0.470	300	0.639	328	2.84	356	3.89	388	0.066
269	0.367	301	0.678	329	2.98	357	3.66	389	0.056
270	0.278	302	0.724	330	3.15	358	3.41	390	0.047
271	0.224	303	0.775	331	3.35	359	3.22	391	0.034
272	0.195	304	0.822	332	3.66	360	3.44	392	0.031
273	0.185	305	0.898	333	3.87	361	3.59	393	0.026
274	0.182	306	0.977	334	3.91	362	3.37	394	0.015
275	0.188	307	1.04	335	3.96	363	3.01	395	0.011
276	0.189	308	1.13	336	4.02	364	2.85	396	0.006
277	0.180	309	1.21	337	4.02	365	2.86	397	0.002
278	0.164	310	1.22	338	3.99	366	2.80	398	0.002
279	0.139	311	1.27	339	3.956	367	2.88	399	<0.001

Note:

252 – 285 nm: Horowitz et al. [87]

290 – 380 nm: mean of the data from Horowitz et al. [87] and Mellouki and Mu [130]

385 – 399 nm: Horowitz et al. [87]

D29. $\text{HC}(\text{O})\text{OCH}_3 + h\nu \rightarrow \text{Products}$

(Recommendation: 06-2, Note: 10-6, Evaluated: 10-6)

Absorption Cross Sections: The UV absorption spectrum of methyl formate, $\text{HC}(\text{O})\text{OCH}_3$, has been measured at room temperature by McMillan [36] (201 – 260 nm) and Vésine and Mellouki [195] (211 – 260 nm). The spectrum consists of a continuous absorption band with a maximum near 215 nm and weak diffuse structure. There is very good agreement, better than 10%, of the results from these studies. The recommended cross sections in Table 4D-33 are taken from McMillan [36] for the region 202 – 210 nm (read from a figure) and Vésine and Mellouki [195] for the region 211 – 260 nm. The Vésine and Mellouki [195] data given here are averages of their high resolution (0.04 nm) spectrum over 1 and 2 nm intervals in the ranges 211 – 230 and 230 – 260 nm, respectively.

Photolysis Quantum Yield and Product Studies: No photolysis studies are available.

Table 4D-33. Absorption Cross Sections of HC(O)OCH₃ at 298 K

λ (nm)	$10^{20} \sigma$ (cm ²)	λ (nm)	$10^{20} \sigma$ (cm ²)	λ (nm)	$10^{20} \sigma$ (cm ²)	λ (nm)	$10^{20} \sigma$ (cm ²)
202	16.2	213	20.3	224	16.8	240	3.56
203	17.0	214	21.2	225	15.7	242	2.65
204	17.9	215	21.1	226	14.0	244	1.65
205	18.2	216	20.3	227	12.5	246	1.24
206	18.7	217	19.3	228	12.4	248	0.770
207	18.9	218	19.7	229	12.3	250	0.480
208	19.1	219	20.0	230	11.3	252	0.301
209	19.5	220	19.2	232	8.36	254	0.162
210	20.4	221	17.9	234	7.48	256	0.0717
211	20.4	222	16.7	236	6.11	258	0.0455
212	20.1	223	16.6	238	4.15	260	0.0281

Note:

202 – 210 nm: McMillan (personal communication to Calvert [36])

211 – 260 nm: Vésine and Mellouki [195] (averages over 1 and 2 nm intervals)

D30. HC(O)OC₂H₅ + hν → Products

(Recommendation: 06-2, Note: 10-6, Evaluated: 10-6)

Absorption Cross Sections: The UV absorption spectrum of ethyl formate, HC(O)OC₂H₅, has been measured at room temperature by McMillan [36] (201 – 260 nm) and Vésine and Mellouki [195] (211 – 260 nm). The spectrum exhibits a structured absorption band with the maximum near 215 nm. The two data sets agree within ~15% with the data of Vésine and Mellouki [195] being systematically smaller. An explanation for the discrepancy could not be found by Vésine and Mellouki [195]. The recommended absorption cross sections in Table 4D-34 are the high resolution (0.04 nm) data of Vésine and Mellouki [195] averaged over 1 and 2 nm intervals in the ranges 211 – 230 and 230 – 260 nm, respectively.

Photolysis Quantum Yield and Product Studies: No photolysis studies are available.

Table 4D-34. Absorption Cross Sections of HC(O)OC₂H₅ at 297 K

λ (nm)	$10^{20} \sigma$ (cm ²)	λ (nm)	$10^{20} \sigma$ (cm ²)	λ (nm)	$10^{20} \sigma$ (cm ²)	λ (nm)	$10^{20} \sigma$ (cm ²)
211	18.6	220	17.8	229	11.2	246	1.47
212	18.6	221	17.1	230	11.0	248	1.04
213	18.3	222	15.9	232	9.03	250	0.665
214	18.5	223	15.1	234	7.21	252	0.405
215	19.0	224	15.0	236	6.50	254	0.251
216	18.9	225	14.9	238	4.96	256	0.119
217	18.1	226	14.0	240	3.67	258	0.0611
218	17.5	227	12.6	242	3.00	260	0.0391
219	17.6	228	11.5	244	2.18		

Note:

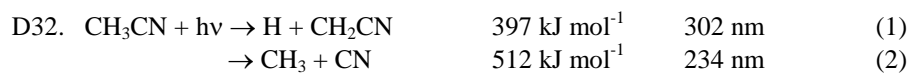
211 – 260 nm: Vésine and Mellouki [195], averaged over 1 and 2 nm intervals

D31. HCN + hν → H + CN 526 kJ mol⁻¹ 228 nm (1)

(Recommendation: 82-57, Note: 10-6, Evaluated: 10-6)

Absorption Cross Sections: Herzberg and Innes [81] have studied the spectroscopy of hydrogen cyanide, HCN, that starts absorbing weakly at $\lambda < 190$ nm.

Photolysis Quantum Yield and Product Studies: The solar photodissociation rate for HCN is rather small, even in the upper stratosphere. Estimates of the HCN atmospheric photolysis rate require additional studies of the absorption cross sections and quantum yields in the 200 nm region.



(Recommendation: 82-57, Note: 10-6, Evaluated: 10-6)

Absorption Cross Sections: Acetonitrile (CH_3CN , methyl cyanide) absorbs weakly at wavelengths $>180 \text{ nm}$ with absorption cross sections $<10^{-20} \text{ cm}^2 \text{ molecule}^{-1}$. Suto and Lee [184] (114 – 178 nm), Zetzsch [211] (155 – 185 nm), and Eden et al. [56] (113 – 320 nm) have reported cross section data.

Photolysis Quantum Yield and Product Studies: McElcheran et al. [125] studied the photodissociation of CH_3CN at 184.9 nm. Solar photodissociation is unimportant compared to reaction with OH radicals.

References for Section 4D

1. Adachi, H., N. Basco and D. G. L. James, 1978, Chem. Phys. Lett., 59, 502-505.
2. Adachi, H., N. Basco and D. G. L. James, 1979, Int. J. Chem. Kinet., 11, 1211-1229.
3. Adachi, H., N. Basco and D. G. L. James, 1980, Int. J. Chem. Kinet., 12, 949-977.
4. Adachi, H., N. Basco and D. G. L. James, 1981, Int. J. Chem. Kinet., 13, 1251-1276.
5. Addison, M. C., J. P. Burrows, R. A. Cox and R. Patrick, 1980, Chem. Phys. Lett., 73, 283-287.
6. Aloisio, S. and J. S. Francisco, 2000, Chem. Phys. Lett., 329, 179-184.
7. Anastasi, C. and P. R. Maw, 1982, J. Chem. Soc. Faraday Trans. 1, 78, 2423-2433.
8. Anastasi, C., I. W. M. Smith and D. A. Parkes, 1978, J. Chem. Soc. Faraday Trans. 1, 74, 1693-1701.
9. Anastasi, C., D. J. Waddington and A. Woolley, 1983, J. Chem. Soc. Faraday Trans., 79, 505-516.
10. Arnold, S. R., M. P. Chipperfield, M. A. Blitz, D. E. Heard and M. J. Pilling, 2004, Geophys. Res. Lett., L07110, doi:10.1029/2003GL019099.
11. Atkinson, R. and A. C. Lloyd, 1984, J. Phys. Chem. Ref. Data, 13, 315-444.
12. Baasandorj, M., S. Griffith, S. Dusanter and P. S. Stevens, 2009, Journal of Physical Chemistry A, 113, 10495-10502.
13. Bacher, C., G. S. Tyndall and J. J. Orlando, 2001, J. Atmos. Chem., 39, 171-189.
14. Basco, N. and S. S. Parmar, 1985, Int. J. Chem. Kinet., 17, 891-900.
15. Basco, N. and S. S. Parmar, 1987, Int. J. Chem. Kinet., 19, 115-128.
16. Bass, A. M., L. C. Glasgow, C. Miller, J. P. Jesson and S. L. Filken, 1980, Planet. Space Sci., 28, 675-679.
17. Bauer, D., J. N. Crowley and G. K. Moortgat, 1992, J. Photochem. and Photobiol., A65, 3530-3538.
18. Bauerle, S. and G. K. Moortgat, 1999, Chem. Phys. Lett., 309, 43-48.
19. Berges, M. G. M. and P. Warneck, 1992, Ber. Bunsenges. Phys. Chem., 96, 413-416.
20. Birge, R. R., W. C. Pringle and P. A. Leermakers, 1971, J. Am. Chem. Soc., 93, 6715-6726.
21. Blacet, F. E. and R. A. Crane, 1954, J. Am. Chem. Soc., 76, 5337-5340.
22. Blitz, M. A., D. E. Heard and M. J. Pilling, 2005, J. Photochem. Photobiol. A: Chem., 176, 107-113.
23. Blitz, M. A., D. E. Heard and M. J. Pilling, 2006, J. Phys. Chem. A, 110, 6742-6756.
24. Blitz, M. A., D. E. Heard, M. J. Pilling, S. R. Arnold and M. P. Chipperfield, 2004, Geophys. Res. Lett., 31, L09104, doi:10.1029/2004GL020182 (correction).
25. Blitz, M. A., D. E. Heard, M. J. Pilling, S. R. Arnold and M. P. Chipperfield, 2004, Geophys. Res. Lett., 31, L06111, doi:10.1029/2003GL018793.
26. Bogumil, K., J. Orphal, T. Homann, S. Voigt, P. Spietz, O. C. Fleischmann, A. Vogel, M. Hartmann, H. Krominga, H. Bovensmann, J. Frerick and J. P. Burrows, 2003, J. Photochem. Photobiol. A: Chem., 157, 167-184.
27. Braun, W., R. Klein, A. Fahr, H. Okabe and A. Mele, 1990, Chem. Phys. Lett., 166, 397-403.
28. Bridier, I., R. Lesclaux and B. Veyret, 1992, Chem. Phys. Lett., 191, 259-263.
29. Bridier, I., B. Veyret, R. Lesclaux and M. E. Jenkin, 1993, J. Chem. Soc. Faraday Trans., 89, 2993-2997.
30. Brint, P., L. O'Toole, C. A. Mayhew and W. Dussa, 1990, J. Chem. Soc. Faraday Trans., 86, 3349-3354.
31. Burkholder, J. B., 2005, personal communication to the NASA JPL Panel.
32. Butkovskaya, N. I., N. Pouvesle, A. Kukui, Y. Mu and G. L. Bras, 2006, J. Phys. Chem. A, 110, 6833-6843.
33. Calvert, J. G., R. Atkinson, J. A. Kerr, S. Madronich, G. K. Moortgat, T. J. Wallington and Y. G. *The mechanisms of atmospheric oxidation of the alkenes*; Oxford University Press: New York - Oxford, 2000.
34. Calvert, J. G., J. A. Kerr, K. L. Demerjian and R. D. McQuigg, 1972, Science, 175, 751-752.
35. Calvert, J. G. and G. S. Layne, 1953, J. Am. Chem. Soc., 75, 856-859.
36. Calvert, J. G. and J. N. Pitts Jr. In *Photochemistry*; John Wiley & Sons, Inc.: New York, 1966; pp 368.
37. Calvert, J. G. and J. N. Pitts Jr.; John Wiley & Sons, Inc.: New York, 1966.
38. Calvert, J. G. and J. N. Pitts Jr. *Photochemistry*; John Wiley and Sons: New York, 1966.
39. Cameron, M., V. Sivakumaran, T. J. Dillon and J. Crowley, 2002, Phys. Chem. Chem. Phys., 4, 3628-3638.
40. Cantrell, C. A., J. A. Davidson, A. H. McDaniel, R. E. Shetter and J. G. Calvert, 1990, J. Phys. Chem., 94, 3902-3908.
41. Cattell, F. C., J. Cavanagh, R. A. Cox and M. E. Jenkin, 1986, J. Chem. Soc. Faraday Trans. 2, 82, 1999-2018.
42. Chen, Y., W. Wang and L. Zhu, 2000, J. Phys. Chem. A, 104, 11126-11131.
43. Chen, Y. and L. Zhu, 2001, J. Phys. Chem. A, 105, 9689-9696.
44. Chen, Y. and L. Zhu, 2003, J. Chem. Phys. A, 107, 4643-4651.
45. Chen, Y., L. Zhu and J. S. Francisco, 2002, J. Chem. Phys. A, 106, 7755-7763.
46. Chowdhury, P. K., H. P. Upadhyaya, P. D. Naik and J. P. Mittal, 2002, Chem. Phys. Lett., 351, 201-207.
47. Clark, J. H., C. B. Moore and N. S. Nogar, 1978, J. Chem. Phys., 68, 1264-1271.
48. Co, D., T. F. Hanisco, J. G. Anderson and F. N. Keutsch, 2005, J. Phys. Chem. A, 109, 10675-10682.

49. Cooper, G., J. E. Anderson and C. E. Brion, 1996, *Chem. Phys.*, 209, 61-77.
50. Cox, R. A., J. Munk, O. J. Nielsen, P. Pagsberg and P. Ratajczak, 1990, *Chem. Phys. Lett.*, 173, 206-210.
51. Cox, R. A. and G. Tyndall, 1979, *Chem. Phys. Lett.*, 65, 357-360.
52. Cox, R. A. and G. S. Tyndall, 1980, *J. Chem. Soc. Faraday Trans. 2*, 76, 153-163.
53. Dagaut, P. and M. J. Kurylo, 1990, *J. Photochem. and Photobiol. A:Chem.*, 51, 133-140.
54. DeMore, W. B., S. P. Sander, D. M. Golden, R. F. Hampson, M. J. Kurylo, C. J. Howard, A. R. Ravishankara, C. E. Kolb and M. J. Molina "Chemical Kinetics and Photochemical Data for Use in Stratospheric Modeling, Evaluation Number 12," JPL Publication 97-4, Jet Propulsion Laboratory, California Institute of Technology, Pasadena, CA, 1997 <http://jpldataeval.jpl.nasa.gov>.
55. Dillon, T. J., A. Horowitz, D. Hölscher, J. N. Crowley, L. Vereecken and J. Peeters, 2008, *Phys. Chem. Chem. Phys.*, 8, 236-246.
56. Eden, S., P. Limão-Vieira, P. Kendall, N. J. Mason, S. V. Hoffmann and S. M. Spyrou, 2003, *Eur. Phys. J., D* 26, 201-210.
57. Emrich, M. and P. Warneck, 2000, *J. Phys. Chem. A*, 104, 9436-9442.
58. Emrich, M. and P. Warneck, 2005, *J. Phys. Chem. A*, 109, 1752.
59. Fahr, A., W. Braun and A. H. Laufer, 1993, *J. Phys. Chem.*, 97, 1502 - 1506.
60. Fahr, A., A. H. Laufer, M. Kraus and R. Osman, 1997, *J. Phys. Chem A*, 101, 4879-4886.
61. Fauvet, S., J. P. Ganne, J. Brion, D. Daumont, J. Malicet and A. Chakir, 1997, *J. Chim. Phys.*, 94, 484-502.
62. Feierabend, K. J., J. E. Flad, S. S. Brown and J. B. Burkholder, 2009, *J. Phys. Chem. A*, 113, 7784-7794.
63. Fenter, F. F., V. Catoire, R. Lesclaux and P. D. Lightfoot, 1993, *J. Phys. Chem.*, 97, 3530-3538.
64. Flowers, B. A., M. E. Angerhofer, W. R. Simpson, T. Nakayama and Y. Matsumi, 2005, *J. Phys. Chem. A*, 109, 2252-2558.
65. Flowers, B. A., J. F. Stanton and W. R. Simpson, 2007, *J. Phys. Chem. A*, 111, 11602-11607.
66. Fry, J., L. J. Matthews, J. R. Lane, A. Sinha, H. G. Kjaergaard and P. O. Wennberg, 2006, *J. Phys. Chem. A*, 110, 7072-7079.
67. Gardner, E. P., P. D. Sperry and J. G. Calvert, 1987, *J. Phys. Chem.*, 91, 1922-1930.
68. Gardner, E. P., R. D. Wijayarathne and J. G. Calvert, 1984, *J. Phys. Chem.*, 88, 5069-5076.
69. Gentieu, E. P. and J. E. Mentall, 1970, *Science*, 169, 681-683.
70. Gierczak, T., J. B. Burkholder, S. Bauerle and A. R. Ravishankara, 1998, *Chem. Phys.*, 231, 229-244.
71. Gierczak, T., J. B. Burkholder, R. K. Talukdar, A. Mellouki, S. B. Barone and A. R. Ravishankara, 1997, *J. Photochem. Photobiol. A: Chem.*, 110, 1-10.
72. Gierczak, T., M. K. Gilles, S. Bauerle and A. R. Ravishankara, 2003, *J. Phys. Chem. A*, 107, 5014-5020.
73. Glicker, S. and L. J. Stief, 1971, *J. Chem. Phys.*, 54, 2852-2857.
74. Gorrotxategi Carbajo, P., S. C. Smith, A.-L. Holloway, C. A. Smith, F. D. Pope, D. E. Shallcross and A. J. Orr-Ewing, 2008, *J. Phys. Chem. A*, 112, 12437-12448.
75. Gratien, A., E. Nilsson, J.-F. Doussin, M. S. Johnson, C. J. Nielsen, Y. Stenström and B. Picquet-Varrault, 2007, *J. Phys. Chem. A*, 111, 11506-11513.
76. Gratien, A., B. Picquet-Varrault, J. Orphal, E. Perraudin and J.-F. Doussin, 2007, *J. Geophys. Res.*, 112, D053005.
77. Harwood, M. H., J. B. Burkholder and A. R. Ravishankara, 1998, *J. Phys. Chem. A*, 102, 1309-1317.
78. Harwood, M. H., J. M. Roberts, G. J. Frost, A. R. Ravishankara and J. B. Burkholder, 2003, *J. Phys. Chem. A*, 107, 1148-1154.
79. He, H.-Y. and W.-H. Fang, 2003, *J. Am. Chem. Soc.*, 125, 16139-16147.
80. Heicklen, J., J. Desai, A. Bahta, C. Harper and R. Simonaitis, 1986, *J. Photochem.*, 34, 117-135.
81. Herzberg, G. and K. K. Innes, 1957, *Can. J. Phys.*, 35, 842-879.
82. Hintze, P. E., S. Aloisio and V. Vaida, 2001, *Chem. Phys. Lett.*, 343, 159-165.
83. Hochanadel, C. J., J. A. Ghormley, J. W. Boyle and P. J. Ogren, 1977, *J. Phys. Chem.*, 81, 3-7.
84. Horowitz, A. and J. G. Calvert, 1978, *Int. J. Chem. Kinet.*, 10, 805-819.
85. Horowitz, A. and J. G. Calvert, 1982, *J. Phys. Chem.*, 86, 3105-3114.
86. Horowitz, A., C. J. Kershner and J. G. Calvert, 1982, *J. Phys. Chem.*, 86, 3094-3104.
87. Horowitz, A., R. Meller and G. K. Moortgat, 2001, *J. Photochem. Photobiol. A: Chem.*, 146, 19-27.
88. Hunnicutt, S. S., L. D. Waits and J. A. Guest, 1989, *J. Phys. Chem.*, 93, 5188-5195.
89. Hynes, A. J., E. A. Kenyon, A. J. Pounds and P. H. Wine, 1992, *Spectrochim. Acta*, 48A, 1235-1242.
90. Jenkin, M. E. and R. A. Cox, 1991, *J. Phys. Chem.*, 95, 3229-3237.
91. Jenkin, M. E., R. A. Cox, G. Hayman and L. J. Whyte, 1988, *J. Chem. Soc. Faraday Trans. 2*, 84, 913-930.
92. Jolly, G. S., D. L. Singleton and G. Paraskevopoulos, 1987, *J. Phys. Chem.*, 91, 3463-3465.
93. Kan, C. S., R. D. McQuigg, M. R. Whitbeck and J. G. Calvert, 1979, *Int. J. Chem. Kinet.*, 11, 921-933.
94. Karunanandan, R., D. Hölscher, T. J. Dillon, A. Horowitz, J. N. Crowley, L. Vereecken and J. Peeters, 2007, *J. Phys. Chem. A*, 111, 897-908.

95. Khamaganov, V., R. Karunanandan, A. Rodriguez and J. N. Crowley, 2007, *Phys. Chem. Chem. Phys.*, 9, 4098 - 4113.
96. Khamaganov, V. G., R. Karunanandan, A. Horowitz, T. J. Dillon and J. N. Crowley, 2009, *Phys. Chem. Chem. Phys.*, 11, 6173 - 6181.
97. Koch, S. and G. K. Moortgat, 1998, *J. Phys. Chem. A*, 102, 9142-9153.
98. Krasnoperov, L. N. and K. Mehta, 1999, *J. Phys. Chem. A*, 103, 8008-8020.
99. Kurylo, M. J., T. J. Wallington and P. A. Ouellette, 1987, *J. Photochem.*, 39, 201-215.
100. Kyle, E. and S. W. Orchard, 1977, *J. Photochem.*, 7, 305-317.
101. Lake, J. S. and A. J. Harrison, 1959, *J. Chem. Phys.*, 30, 361-362.
102. Langford, A. O. and C. B. Moore, 1984, *J. Chem. Phys.*, 80, 4211-4221.
103. Lee, A. M. D., J. D. Coe, S. Ullrich, M.-L. Ho, S.-J. Lee, B.-M. Cheng, M. Z. Zgierski, I.-C. Chen, T. J. Martinez and A. Stolow, 2007, *J. Phys. Chem. A*, 111, 11948-11960.
104. Lewis, R. S., K. Y. Tang and E. K. C. Lee, 1976, *J. Chem. Phys.*, 65, 2910-2911.
105. Libuda, H. G. *Spektroskopische und kinetische Untersuchungen an halogenierten Carbonylverbindungen von atmosphärischem Interesse*, PhD-Thesis, University of Wuppertal, Germany, 1992.
106. Libuda, H. G. and F. Zabel, 1995, *Ber. Bunsenges. Phys. Chem.*, 99, 1205-1213.
107. Libuda, H. G., F. Zabel and K. H. Becker. "UV spectra of some organic chlorine and bromine compounds of atmospheric interest"; *Kinetics and Mechanisms for the Reactions of Halogenated Organic Compounds in the Troposphere. STEP-HALOCSIDE/AFEAS WORKSHOP*, 1991, Dublin, Ireland, 126-131.
108. Lightfoot, P. D., R. A. Cox, J. N. Crowley, M. Destriau, G. D. Hayman, M. E. Jenkin, G. K. Moortgat and F. Zabel, 1992, *Atmos. Environ.*, 26A, 1805-1961.
109. Lightfoot, P. D. and A. A. Jemi-Alade, 1991, *J. Photochem. and Photobiol. A: Chem.*, 59, 1-10.
110. Limão-Vieira, P., S. Eden, N. J. Mason and S. V. Hoffmann, 2003, *Chem. Phys. Lett.*, 376, 737-747.
111. Lucazeau, G. and C. Sandorfy, 1970, *J. Mol. Spectrosc.*, 35, 214-231.
112. Magneron, I., A. Mellouki, G. Le Bras, G. K. Moortgat, A. Horowitz and K. Wirtz, 2005, *J. Phys. Chem. A*, 109, 4552-4561.
113. Magneron, I., R. Thévenet, A. Mellouki, G. Le Bras, G. K. Moortgat and K. Wirtz, 2002, *J. Phys. Chem. A*, 106, 2526-2537.
114. Maria, H. J., J. R. McDonald and S. R. McGlynn, 1973, *J. Am. Chem. Soc.*, 95, 1050-1056.
115. Maric, D., J. N. Crowley and J. P. Burrows, 1997, *J. Phys. Chem.*, 101, 2561-2567.
116. Maricq, M. M. and J. J. Szente, 1996, *J. Phys. Chem.*, 100, 4507-4513.
117. Maricq, M. M. and J. J. Szente, 1996, *Chem. Phys. Lett.*, 253, 333-339.
118. Maricq, M. M. and T. J. Wallington, 1992, *J. Phys. Chem.*, 96, 982-986.
119. Marling, L., 1977, *J. Chem. Phys.*, 66, 4200-4225.
120. Martinez, R. D., A. A. Buitrago, N. W. Howell, C. H. Hearn and J. A. Joens, 1992, *Atmos. Environ.*, 26A, 785-792.
121. Matthews, J., A. Sinha and J. S. Francisco, 2005, *Proc. Natl. Acad. Sci.*, 102, 7449-7452.
122. Mazely, T. L., R. R. Friedl and S. P. Sander, 1995, *J. Phys. Chem.*, 99, 8162-8169.
123. Mazely, T. L., R. R. Friedl and S. P. Sander, 1997, *J. Phys. Chem.*, 101, 7090-7097.
124. McAdam, K., B. Veyret and R. Lesclaux, 1987, *Chem. Phys. Lett.*, 133, 39-44.
125. McElcheran, D. E., M. H. J. Wijnen and E. W. R. Steacie, 1958, *Can. J. Chem.*, 36, 321-339.
126. McQuigg, R. D. and J. G. Calvert, 1969, *J. Am. Chem. Soc.*, 91, 1590-1599.
127. Meller, R. and J. N. Crowley, 1998, *Personal Communication*.
128. Meller, R. and G. K. Moortgat, 2000, *J. Geophys. Res. D*, 105, 7089-7101.
129. Meller, R., W. Raber, J. N. Crowley, M. E. Jenkin and G. K. Moortgat, 1991, *J. Photochem. Photobiol.*, 62, 163-171.
130. Mellouki, A. and Y. Mu, 2003, *J. Photochem. Photobiol. A: Chem.*, 157, 295-300.
131. Mentall, J. E., E. P. Gentieu, M. Krauss and D. Neumann, 1971, *J. Chem. Phys.*, 55, 5471-5479.
132. Meyrahn, H. *Bildungswege und Analytik des Peroxyacetylnitrats (PAN) in der Atmosphäre*, PhD-Thesis, Johann-Gutenberg-Universität, 1984.
133. Meyrahn, H., G. K. Moortgat and P. Warneck, 1981, *J. Photochem.*, 17, 138.
134. Meyrahn, H., J. Pauly, W. Schneider and P. Warneck, 1986, *J. Atmos. Chem.*, 4, 277-291.
135. Molina, M. J. and G. Arguello, 1979, *Geophys. Res. Lett.*, 6, 953-955.
136. Moortgat, G. K., 2001, *Pure Appl. Chem.*, 73, 487-490.
137. Moortgat, G. K. "RADICAL: Evaluation of Radical Sources in Atmospheric Chemistry through Chamber and Laboratory Studies," ENVA-CT97-0419, EUR 20254 EN, 2002
138. Moortgat, G. K., W. Klippel, K. H. Möbus, W. Seiler and P. Warneck FAA-EE-80-47, Federal Aviation Administration, Washington, DC 1980
139. Moortgat, G. K., W. Seiler and P. Warneck, 1983, *J. Chem. Phys.*, 78, 1185-1190.
140. Moortgat, G. K., F. Slemr, W. Seiler and P. Warneck, 1978, *Chem. Phys. Lett.*, 54, 444-447.

141. Moortgat, G. K., B. Veyret and R. Lesclaux, 1989, J. Phys. Chem., 93, 2362-2368.
142. Moortgat, G. K. and P. Warneck, 1979, J. Chem. Phys., 70, 3639-3651.
143. Morel, O., R. Simonaitis and J. Heicklen, 1980, Chem. Phys. Lett., 73, 38-41.
144. Munk, J., P. Pagsberg, E. Ratajczak and A. Sillesen, 1986, J. Phys. Chem., 90, 2752-2757.
145. Nádasdia, R., G. Kovácsa, I. Szilágyia, A. Demetera and S. Dóbbé, 2007, Chem. Phys. Lett., 440, 31-35.
146. Nagakura, S., K. Kaya and H. Tsubomura, 1964, J. Mol. Spectrosc., 13, 1-8.
147. Napier, I. M. and R. G. W. Norrish, 1967, Proc. Roy. Soc. London A, 299, 317-336.
148. Nielsen, O. J., M. S. Johnson, T. J. Wallington, L. K. Christensen and J. Platz, 2002, Int. J. Chem. Kinet., 34, 283-291.
149. Nozière, B., R. Lesclaux, M. D. Hurley, M. A. Dearth and T. J. Wallington, 1994, J. Phys. Chem., 98, 2864-2873.
150. Orlando, J. J. and G. S. Tyndall, 2001, Int. J. Chem. Kinet., 33, 149-156.
151. Orlando, J. J. and G. S. Tyndall, 2003, J. Photochem. Photobiol. A: Photochem., 157, 161-166.
152. Orlando, J. J., G. S. Tyndall, J.-M. Fracheboud, E. G. Estupiñan, S. Haberkorn and A. Zimmer, 1999, Atmos. Environ., 33, 1621-1629.
153. Parkes, D. A., 1977, Int. J. Chem. Kinet., 9, 451-469.
154. Parkes, D. A., 1981, Chem. Phys. Lett., 77, 527-532.
155. Parkes, D. A., D. M. Paul, C. P. Quinn and R. C. Robson, 1973, Chem. Phys. Lett., 23, 425-429.
156. Parmenter, C. S., 1964, J. Chem. Phys., 41, 658-665.
157. Pilling, M. J. and M. J. C. Smith, 1985, J. Phys. Chem., 89, 4713-4720.
158. Plum, C. N., E. Sanhueza, R. Atkinson, W. P. L. Carter and J. N. J. Pitts, 1983, Environ. Sci. Technol., 17, 479-484.
159. Pope, F. D., C. A. Smith, N. M. R. Ashfold and A. J. Orr-Ewing, 2005, Phys. Chem. Chem. Phys., 7, 79-84.
160. Pope, F. D., C. A. Smith, P. R. Davis, D. E. Shallcross, M. N. R. Ashfold and A. J. Orr-Ewing, 2005, J. Chem. Soc., Faraday Disc, 130, 59-73.
161. Raber, W. H. and G. K. Moortgat. Photooxidation of selected carbonyl compounds in air: methyl ethyl ketone, methyl vinyl ketone, methacrolein, and methylglyoxal. In *Progress and Problems in Atmospheric Chemistry*; J. Barker, Ed.; World Scientific Publ. Co.: Singapore, 1996; pp 318-373.
162. Rajakumar, B., J. E. Flad, T. Gierczak, A. R. Ravishankara and J. B. Burkholder, 2007, J. Phys. Chem. A, 111, 8950-8958.
163. Rajakumar, B., T. Gierczak, J. E. Flad, A. R. Ravishankara and J. B. Burkholder, 2008, J. Photochem. Photobiol. A Chem., 199, 336-344.
164. Rattigan, O., R. L. Lutman, R. L. Jones and R. A. Cox, 1992, J. Photochem. Photobiol. A: Chem., 66, 313-326.
165. Roberts, J. M. and R. W. Fajer, 1989, Environ. Sci. Technol., 23, 945-951.
166. Roehl, C. M., D. Bauer and G. K. Moortgat, 1996, J. Phys. Chem., 100, 4038-4047.
167. Roehl, C. M., Z. Marka, J. L. Fry and P. O. Wennberg, 2007, Atmos. Chem. Phys., 7, 713-720.
168. Rogers, J. D., 1990, J. Phys. Chem., 94, 4011-4015.
169. Röth, E. P., R. Ruhnke, G. Moortgat, R. Meller and W. Schneider "UV/VIS-Absorption Cross Sections and Quantum Yields for Use in Photochemistry and Atmospheric Modeling," Forschungszentrum Jülich Publication, Part 1 : Inorganic Substances (jül-3340), Part 2: Organic Substances (jül-3341), 1997
170. Sander, S. P. and R. T. Watson, 1980, J. Phys. Chem., 84, 1664-1674.
171. Sander, S. P. and R. T. Watson, 1981, J. Phys. Chem., 85, 2960-2964.
172. Seki, K. and H. Okabe, 1992, J. Phys. Chem., 96, 3345-3349.
173. Senum, G. I., Y.-N. Lee and J. S. Gaffney, 1984, J. Phys. Chem., 88, 1269-1270.
174. Simon, F.-G., W. Schneider and G. K. Moortgat, 1990, Int. J. Chem. Kinet., 22, 791-813.
175. Singleton, D. L., G. Paraskevopoulos and R. S. Irwin, 1987, J. Photochem., 37, 209-216.
176. Singleton, D. L., G. Paraskevopoulos and R. S. Irwin, 1989, Res. Chem. Intermediates, 12, 1-12.
177. Singleton, D. L., G. Paraskevopoulos and R. S. Irwin, 1990, J. Phys. Chem., 94, 695-699.
178. Smith, C. A., F. D. Pope, B. Cronin, C. B. Parkes and A. J. Orr-Ewing, 2006, J. Phys. Chem. A, 110, 11645-11653.
179. Smith, G. D., L. T. Molina and M. J. Molina, 2002, J. Phys. Chem. A, 106, 1233-1240.
180. Somnitz, H., M. Fida, T. Ufer and R. Zellner, 2005, Phys. Chem. Chem. Phys., 7, 3342 - 3352, DOI: 10.1039/b506738c.
181. Somnitz, H., T. Ufer and R. Zellner, 2009, Phys. Chem. Chem. Phys., 11, 8522-8531.
182. Staffelbach, T. A., J. J. Orlando, G. S. Tyndall and J. G. Calvert, 1995, J. Geophys. Res., 100, 14189-14198.
183. Stephens, E. R., 1969, Adv. Environ. Sci. Technol., 1, 119-146.
184. Suto, M. and L. C. Lee, 1985, J. Geophys. Res., 90, 13037-13040.
185. Tadic, J., G. K. Moortgat and K. Wirtz, 2005, J. Photochem. Photobiol. A: Chem., 177, 116-124.

186. Talukdar, R. K., J. B. Burkholder, M. Hunter, M. K. Gilles, J. M. Roberts and A. R. Ravishankara, 1997, J. Chem. Soc. Faraday Trans., 93, 2797-2805.
187. Talukdar, R. K., J. B. Burkholder, A.-M. Schmoltner, J. M. Roberts, R. Wilson and A. R. Ravishankara, 1995, J. Geophys. Res., 100, 14163-14173.
188. Tang, K. Y., P. W. Fairchild and E. K. C. Lee, 1979, J. Phys. Chem., 83, 569-573.
189. Taylor, W. D., T. D. Allston, M. J. Moscato, G. B. Fazekas, R. Koslowski and G. A. Takacs, 1980, Int. J. Chem. Kinet., 12, 231-240.
190. Thelen, M.-A., P. Felder and J. R. Huber, 1993, Chem. Phys. Lett., 213, 275-281.
191. Troe, J., 2007, J. Phys. Chem. A, 111, 3868-3874.
192. Tyndall, G. S., R. A. Cox, C. Granier, R. Lesclaux, G. K. Moortgat, M. J. Pilling, A. R. Ravishankara and T. J. Wallington, 2001, J. Geophys. Res., 106, 12157-12182.
193. Vaghjiani, G. L. and A. R. Ravishankara, 1989, J. Geophys. Res., 94, 3487-3492.
194. Vaghjiani, G. L. and A. R. Ravishankara, 1990, J. Chem. Phys., 92, 996-1003.
195. Vésine, E. and A. Mellouki, 1997, J. Chim. Phys. Physico-Chim. Biol., 94, 1634-1641.
196. Vesley, G. F. and P. A. Leermakers, 1964, J. Phys. Chem., 68, 2364-2366.
197. Vicente, A., R. Antunes, D. Almeida, I. J. A. Franco, S. V. Hoffmann, N. J. Mason, S. Eden, D. Dufort, S. Canneaux, J. Delwiche, M.-J. Hubin-Franskin and P. Limão-Vieira, 2009, Phys. Chem. Chem. Phys., 11, 5729 - 5741.
198. Volkamer, R., P. Spietz, J. P. Burrows and U. Platt, 2005, J. Photochem. Photobiol. A: Chem., 172, 35-36.
199. Wallington, T. J., P. Dagaut and M. J. Kurylo, 1988, Journal of Photochemistry and Photobiology A, 42, 173-185.
200. Wallington, T. J., P. Dagaut and M. J. Kurylo, 1992, Chem. Rev., 92, 667-710.
201. Wallington, T. J., M. M. Mariq, T. Ellerman and O. J. Nielsen, 1992, J. Phys. Chem., 96, 982-986.
202. Warneck, P., 2001, Atmos. Environ., 35, 5773-5777.
203. Weaver, J., J. Meagher and J. Heicklen, 1976, J. Photochem., 6, 111-126.
204. Wiebe, H. A. and J. Heicklen, 1973, J. Am. Chem. Soc., 95, 1-7.
205. Wiebe, H. A., A. Villa, T. M. Hellman and J. Heicklen, 1973, J. Am. Chem. Soc., 95, 7-13.
206. Winterhalter, R., N. R. Jensen, I. Magneron, K. Wirtz, A. Mellouki, Y. Mu, J. Tadic, A. Horowitz, G. K. Moortgat and J. Hjorth. "Proceedings of the EUROTRAC-2 Symposium 2000", 2001, Springer, Berlin.
207. Wollenhaupt, M., S. A. Carl, A. Horowitz and J. N. Crowley, 2000, J. Phys. Chem., A, 104, 2695-2705.
208. Yamamoto, S. and R. A. Back, 1985, Can. J. Chem., 63, 549-554.
209. Yang, X., P. Felder and J. R. Huber, 1993, J. Phys. Chem., 97, 10903-10910.
210. Yujing, M. and A. Mellouki, 2000, J. Photochem. Photobiol. A: Chem., 134, 31-36.
211. Zetzsch, C. In *Proceedings of the International Ozone Symposium 1988*; R. Bojkov and P. Fabian, Eds.; Deepak: Hampton, VA, 1989.
212. Zhu, L. and G. Johnston, 1995, J. Phys. Chem., 99, 15114-15119.
213. Zhu, L., D. Kellis and C.-F. Ding, 1996, Chem. Phys. Lett., 257, 487-491.

SECTION 4E. FO_x PHOTOCHEMISTRY



(Recommendation: 06-2, Note: 10-6, Evaluated: 10-6)

Absorption Cross Sections: The UV absorption spectrum of hydrogen fluoride, HF, has been measured at 289.5, 326, 373, and 438 K by Safary et al. [60] and Safary [59] (153 – 182 nm) and at room temperature by Nee et al. [44] (107 – 145 nm), Carnovale et al. [7] (8 – 155 nm), and Hitchcock et al. [23] (30 – 200 nm). HF does not absorb significantly at wavelengths >180 nm.

Photolysis Quantum Yield and Product Studies: Photodissociation should be an unimportant loss process in the stratosphere.



(Recommendation: 06-2, Note: 10-6, Evaluated: 10-6)

Absorption Cross Sections: The gas-phase UV absorption spectrum of the fluoroperoxy radical, FO₂, has been measured at room temperature by Pagsberg et al. [50] (206 – 250 nm), Maricq and Szente [35], (186 – 276 nm), Ellermann et al. [17] (215 – 254 nm), and at 215 nm by Lyman and Holland [33]. In earlier studies, Chegodaev and Tupikov [8] and Matchuk et al. [37] reported spectra of FO₂ in liquid argon at 87 K. The results from Maricq and Szente [35], Ellermann et al. [17], and Lyman and Holland [33] are in excellent agreement. The cross sections reported by Pagsberg et al. [50] are larger by factors of 1.4 to 1.8 between 206 and 245 nm and a factor of 3 at 250 nm. The recommended absorption cross sections in Table 4E-1 are taken from Maricq and Szente [35].

Photolysis Quantum Yield and Product Studies: No photolysis studies are available.

Table 4E-1. Absorption Cross Sections of FO₂ at 295 K

λ (nm)	$10^{20} \sigma$ (cm ²)	λ (nm)	$10^{20} \sigma$ (cm ²)	λ (nm)	$10^{20} \sigma$ (cm ²)
185.9	950	214.2	1150	242.5	139
188.5	1050	216.8	1050	245.1	112
191.1	1130	219.4	933	247.6	82
193.6	1180	221.9	796	250.2	60
196.2	1200	224.5	677	252.8	51
198.8	1260	227.1	558	255.3	43
201.4	1310	229.6	451	257.9	36
203.9	1330	232.2	368	260.5	32
206.5	1350	234.8	289	263.1	26
209.1	1300	237.4	233	265.6	20
211.6	1240	239.9	173		

Note:

185.9 – 265.6 nm: Maricq and Szente [35]



(Recommendation: 06-2, Note: 10-6, Evaluated: 10-6)

Absorption Cross Sections: The UV absorption spectrum of difluorine monoxide, F₂O, has been measured at 273 K over the wavelength range 210 – 546 nm by Glissmann and Schuhmacher [20]. Their absorption cross section data are recommended and are listed in Table 4E-2.

Photolysis Quantum Yield and Product Studies: No studies are available.

Table 4E-2. Absorption Cross Sections of F₂O at 273 K

λ (nm)	$10^{20} \sigma$ (cm ²)	λ (nm)	$10^{20} \sigma$ (cm ²)	λ (nm)	$10^{20} \sigma$ (cm ²)	λ (nm)	$10^{20} \sigma$ (cm ²)
210.2	4.88	239.9	0.65	296.7	0.12	404.0	0.020
211.4	3.39	244.7	0.50	302.7	0.12	421.0	0.023
213.7	3.06	248.2	0.37	313.1	0.11	428.0	0.021
216.5	2.73	253.7	0.27	334.0	0.087	435.8	0.018
218.1	2.60	257.6	0.21	350.0	0.072	445.0	0.017
221.0	2.21	265.5	0.15	365.0	0.064	458.0	0.015
223.6	1.95	270.0	0.13	378.0	0.055	471.5	0.012
225.3	1.76	275.9	0.12	380.0	0.044	491.6	0.0091
229.5	1.30	280.6	0.12	387.0	0.033	513.5	0.0052
234.5	1.14	289.3	0.12	395.0	0.023	546.0	0.0052
237.8	0.78	292.5	0.12	399.0	0.020		

Note:

210 – 546 nm: Glissmamm and Schuhmacher [20]



(Recommendation: 06-2, Note: 10-6, Evaluated: 10-6)

Absorption Cross Sections: The gas-phase UV/vis absorption spectrum of dioxygen difluoride, F_2O_2 , has been measured at 193 K by Chegodaev and Tupikov [8] (197 – 260 nm), at 195 K by Matchuk et al. [37] (350 – 600 nm), at 273 K by Brodersen et al. [5] (220 – 522.5 nm), and at 298 K by Lyman and Holland [33] (215 nm). A measurement of F_2O_2 in liquid freon at 77 K has been reported by Kirshenbaum and Streng [26] (200 – 480 nm). The absorption spectrum shows decreasing absorption cross sections with increasing wavelength and evidence for several transitions that appear as shoulders in the spectrum. An absorption feature near 405 nm reported by Brodersen et al. [5] does not appear in the spectra reported by Matchuk et al. [37] and Kirshenbaum and Streng [26]. Although measured at significantly different temperatures the data from Brodersen et al. [5] and Chegodaev and Tupikov [8] in the wavelength range 220 – 250 nm agree within 10-15%. In the 250 – 360 nm region, the absorption spectrum reported by Brodersen et al. [5] agrees well with the absorption spectra reported by Chegodaev and Tupikov [8] and Matchuk et al. [37]. The recommended absorption cross sections in Table 4E-3 are from Chegodaev and Tupikov [8] in the region 200 – 250 nm, Brodersen et al. [5] in the region 260 – 360 nm, and Matchuk et al. [37] for the 370 – 600 nm region.

Photolysis Quantum Yield and Product Studies: No studies are available.

Table 4E-3. Absorption Cross Sections of F₂O₂ at 193 – 273 K

λ (nm)	$10^{20} \sigma$ (cm ²)	λ (nm)	$10^{20} \sigma$ (cm ²)	λ (nm)	$10^{20} \sigma$ (cm ²)
200	700	340	10.9	480	0.34
210	325	350	7.54	490	0.27
220	208	360	5.90	500	0.24
230	145	370	5.15	510	0.22
240	107	380	4.50	520	0.20
250	87.9	390	3.77	530	0.19
260	98.2	400	3.06	540	0.17
270	86.7	410	2.46	550	0.15
280	72.5	420	1.97	560	0.13
290	60.6	430	1.57	570	0.11
300	44.7	440	1.25	580	0.09
310	32.4	450	0.96	590	0.07
320	22.3	460	0.69	600	0.04
330	15.4	470	0.47		

Note:

200 – 250 nm: Chegodaev and Tupikov [8] (193 K)

260 – 360 nm: Brodersen et al. [5] (273 K)

370 – 600 nm: Matchuk et al. [37] (195 K)



(Recommendation: 06-2, Note: 10-6, Evaluated: 10-6)

Absorption Cross Sections: The UV absorption spectrum of nitrosyl fluoride, FNO, has been measured at room temperature by Burley et al. [6] (180 – 350 nm) and Pagsberg et al. [49] (310.5 nm). Johnston and Bertin [25] report a cross section at 195 K and 310.5 nm. The FNO spectrum has two similar strength bands centered at 180 nm and 310 nm. The 310 nm band has significant vibronic structure at wavelengths >250 nm. The agreement between the single wavelength measurement of Pagsberg et al. [49] and the Burley et al. [6] spectrum is good. The recommended absorption cross sections in Table 4E-4 are at 2 nm intervals for the continuous region of the spectrum ($\lambda < 260$ nm) and at 1 nm intervals in the structured region ($\lambda > 260$ nm).

Photolysis Quantum Yield and Product Studies: The quantum yield for decomposition is expected to be unity (Brandon et al. [4], Reid et al. [56]).

Table 4E-4. Absorption Cross Sections of FNO at 298 K

λ (nm)	$10^{20} \sigma$ (cm ²)	λ (nm)	$10^{20} \sigma$ (cm ²)	λ (nm)	$10^{20} \sigma$ (cm ²)	λ (nm)	$10^{20} \sigma$ (cm ²)
180	52.4	246	1.65	286	5.17	319	21.4
182	51.7	248	1.41	287	5.78	320	15.2
184	50.7	250	1.54	288	10.4	321	35.6
186	49.4	252	1.25	289	16.6	322	40.2
188	47.5	254	1.23	290	17.0	323	25.5
190	45.1	256	1.36	291	11.3	324	17.8
192	42.7	258	1.58	292	11.9	325	14.3
194	40.0	260	1.30	293	18.1	326	12.1
196	37.3	261	1.45	294	7.11	327	9.40
198	33.8	262	1.64	295	6.75	328	9.39
200	30.5	263	1.85	296	9.15	329	12.4
202	27.7	264	2.03	297	14.1	330	12.9
204	24.8	265	2.67	298	22.0	331	11.3
206	22.2	266	1.96	299	23.1	332	13.0
208	19.9	267	1.99	300	15.6	333	18.9
210	17.6	268	2.10	301	23.1	334	19.3
212	15.8	269	2.66	302	25.4	335	16.1
214	13.9	270	2.81	303	10.4	336	13.1
216	12.3	271	3.06	304	8.85	337	10.8
218	10.7	272	4.47	305	10.4	338	8.96
220	9.35	273	4.30	306	11.8	339	7.13
222	8.32	274	3.97	307	15.6	340	5.65
224	7.22	275	3.77	308	32.2	341	4.61
226	6.30	276	4.24	309	21.8	342	3.81
228	5.44	277	4.44	310	15.5	343	3.17
230	4.68	278	3.41	311	54.2	344	2.68
232	4.10	279	5.03	312	31.6	345	2.30
234	3.52	280	8.26	313	16.0	346	1.96
236	3.09	281	10.1	314	12.3	347	1.72
238	2.76	282	7.58	315	11.7	348	1.48
240	2.25	283	6.59	316	11.0	349	1.30
242	2.08	284	7.26	317	13.0	350	1.18
244	1.74	285	7.45	318	25.5		

Note:

180 – 350 nm: Burley et al. [6]



(Recommendation: 90-1, Note: 10-6, Evaluated: 10-6)

Absorption Cross Sections: The VUV spectrum of carbon tetrafluoride, CF_4 , consists of a strong absorption band between 6 and 120 nm with several broad features assigned to a Rydberg series with maxima near 54, 68, 78, 90 and 99 nm. The spectrum also has discrete vibrational structure in the region 56 to 63 nm. The absolute absorption cross sections have been studied extensively in the VUV by a number of groups as summarized in Table 4E-5. Good agreement exist in the wavelength range 6-100 nm between the data of Cook and Ching, Rebbert and Ausloos, Lee et al., Cole and Dexter, Lee et al., Au et al., Chim et al. and Hatherly and Flaxman.

The absorption cross section at Lyman- α (121.57 nm) was reported to be $(5.73 \pm 0.97) \times 10^{-21} \text{ cm}^2 \text{ molecule}^{-1}$ by Inn [24], $<1 \times 10^{-20} \text{ cm}^2 \text{ molecule}^{-1}$ by Lee et al. [29], and $8 \times 10^{-22} \text{ cm}^2 \text{ molecule}^{-1}$ by Ravishankara et al. [54]. An average value of $(5.5 \pm 4.6) \times 10^{-21} \text{ cm}^2 \text{ molecule}^{-1}$ is recommended for the cross section at Lyman- α .

Photolysis Quantum Yield and Product Studies: No studies are available. CF_4 does not absorb at wavelengths $>120 \text{ nm}$ and therefore it is not expected to photodissociate until it reaches the mesosphere.

Table 4E-5. Summary of CF₄ Absorption Cross Section Studies

Reference	Year	Wavelength Range (nm)	Temperature (K)
Rebbert and Ausloos [55]	1971	73.6 – 74.4	298
Sauvageau et al. [61]	1973	60 – 120	298
Lee et al. [28]	1977	17.5 – 77.0	295
Cole and Dexter [12]	1978	4.6, 10.0	298
Inn [24]	1980	121.57 (Lyman- α)	297
Lee et al. [29]	1986	50 – 130	298
Zhang et al. [66]	1989	6.2-103.2	298
Ravishankara et al. [54]	1993	121.57 (Lyman- α)	298
Au et al. [1]	1997	6.2 – 124	298
Cook and Ching [13]	2003	61 – 100	295
Hatherly and Flaxman [22]	2003	58.4 and 73.6 – 74.6	298
Chim et al. [10]	2003	30.7 – 129.5	298

E7. C₂F₆ + h ν → Products

(Recommendation: 10-6, Note: 10-6, Evaluated: 10-6)

Absorption Cross Sections: The VUV absorption spectrum of hexafluoroethane, C₂F₆, consists of a strong absorption band between 6 and 120 nm with several broad features and maxima near 58, 68, 79, 87 and 93 nm. Absolute absorption cross sections have been reported by Sauvageau et al. [61] (60 – 120 nm), Lee et al. [28] (17.5 – 77.0 nm), and Cole and Dexter [12] (6.5 and 10.0 nm). The cross section data from Sauvageau et al. over the range 60 to 75 nm are much smaller than those of Lee et al.

The absorption cross section at Lyman- α (121.57 nm) was determined by Ravishankara et al. [54] to be $(9.87 \pm 0.35) \times 10^{-21} \text{ cm}^2 \text{ molecule}^{-1}$.

Photolysis Quantum Yield and Product Studies: No studies are available. C₂F₆ does not absorb significantly at wavelengths >120 nm and therefore it is not expected to photodissociate until it reaches the mesosphere.

E8. c-C₄F₈ + h ν → Products

(Recommendation: 10-6, Note: 10-6, Evaluated: 10-6)

Absorption Cross Sections: The spectrum of perfluorocyclobutane, c-C₄F₈, consists of a strong absorption band in the VUV with a maximum at 117 nm and shows further weak absorption bands at 137 and 174 nm up to about 200 nm. The absolute photoabsorption cross sections have been measured at high resolution in the VUV by Limão-Vieira et al. [31] in the range 117 – 200 nm. They estimated a stratospheric photolysis lifetime of ~400 years at 20 km decreasing to a few days at 40-50 km.

The absorption cross section at Lyman- α (121.57 nm) was determined by Limão-Vieira et al. [31] to be $7.98 \times 10^{-18} \text{ cm}^2 \text{ molecule}^{-1}$ whereas Ravishankara et al. [54] reported a value of $(8.76 \pm 0.49) \times 10^{-18} \text{ cm}^2 \text{ molecule}^{-1}$.

Photolysis Quantum Yield and Product Studies: There are no product yield studies currently available.

E9. C₅F₁₂ + h ν → Products

(Recommendation: 10-6, Note: 10-6, Evaluated: 10-6)

Absorption Cross Sections: No absorption spectrum of perfluoropentane, C₅F₁₂, is known. However, an absorption cross section at Lyman- α (121.57 nm) was determined by Ravishankara et al. [54] to be $(5.32 \pm 0.30) \times 10^{-18} \text{ cm}^2 \text{ molecule}^{-1}$.

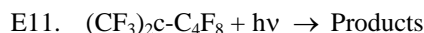
Photolysis Quantum Yield and Product Studies: There are no product yield studies currently available.

E10. C₆F₁₄ + h ν → Products

(Recommendation: 10-6, Note: 10-6, Evaluated: 10-6)

Absorption Cross Sections. No absorption spectrum of C₆F₁₄, perfluorohexane, is known. However, an absorption cross section at Lyman- α (121.57 nm) was determined by Ravishankara et al. [54] to be $(9.82 \pm 0.53) \times 10^{-18} \text{ cm}^2 \text{ molecule}^{-1}$.

Photolysis Quantum Yield and Product Studies: There are no product yield studies currently available.



(Recommendation: 10-6, Note: 10-6, Evaluated: 10-6)

Absorption Cross Sections: No absorption spectrum of perfluoro 1,2-dimethyl-cyclobutane, $(\text{CF}_3)_2\text{C}-\text{C}_4\text{F}_8$, is known. However, an absorption cross section at Lyman- α (121.57 nm) was determined by Ravishankara et al. [54] to be $(1.22 \pm 0.07) \times 10^{-17} \text{ cm}^2 \text{ molecule}^{-1}$. The large cross section implies a local lifetime of only a few days in the mesosphere.

Photolysis Quantum Yield and Product Studies: There are no product yield studies currently available.



(Recommendation: 06-2, Note: 10-6, Evaluated: 10-6)

Absorption Cross Sections: The UV absorption spectrum of carbonyl difluoride (difluorophosgene), COF_2 , has been measured at room temperature by Chou et al. [11] (185 – 226 nm), Molina and Molina [42] (186 – 224 nm), and Nölle et al. [46] (199 – 232 nm). The high resolution spectrum reported by Nölle et al. [46] is highly structured. The cross section data from Nölle et al. [46] are somewhat larger than those from Molina and Molina [42] with differences in the averaged values over 500 cm^{-1} intervals ranging between 1.5 and 22%. The cross section data of Chou et al. [11] are in good agreement with the data from Molina and Molina [42] in the region 186 – 197 nm. At longer wavelengths the cross sections from these studies diverge with the Chou et al. results being larger, ~200% near 225 nm. The recommended absorption cross sections in Table 4E-6 are the 500 cm^{-1} averages of the data from Molina and Molina [42] in the range 186 – 199 nm and the data from Nölle et al. [46] at longer wavelengths.

Photolysis Quantum Yield and Product Studies: The photodissociation of COF_2 has been studied by Nölle et al. [47] at 193, 210, and 220 nm and Molina and Molina [42] at 206 nm. Nölle et al. [47] determined the $\text{COF} + \text{F}$ quantum yields by combining FTIR detection of products with excimer laser photolysis at 193 nm and Hg lamp photolysis at 210 and 220 nm. The “apparent” quantum yields for COF_2 were 0.47 ± 0.03 , 0.57 ± 0.05 , and 0.11 ± 0.02 at 193, 210 and 220 nm, respectively. In the case of the laser photolysis at 193 nm, where high concentrations of COF are formed, the self-reaction of the COF photodissociation product regenerates COF_2 via $\text{COF} + \text{COF} \rightarrow \text{COF}_2 + \text{CO}$. Assuming that all COF radicals react quantitatively in this way the actual quantum yield at 193 nm is 0.94 ± 0.06 . The quantum yields at 210 and 220 nm obtained using the Hg lamp photolysis generated much lower COF radical concentrations and are reported as the actual quantum yields. Molina and Molina [42] report a quantum yield of 0.26 at 206 nm that is considerably lower than reported by Nölle et al. [47].

Table 4E-6. Absorption Cross Sections of COF_2 at 298 K

λ (nm)	$10^{20} \sigma$ (cm^2)	λ (nm)	$10^{20} \sigma$ (cm^2)	λ (nm)	$10^{20} \sigma$ (cm^2)
186.0	5.5	199.0	1.6	213.9	0.188
187.8	4.8	201.0	1.32	216.2	0.120
189.6	4.2	203.1	0.987	218.6	0.077
191.4	3.7	205.1	0.754	221.0	0.046
193.2	3.1	207.3	0.508	223.5	0.032
195.1	2.6	209.4	0.392	226.0	0.021
197.0	2.1	211.6	0.272	228.6	0.015

Note:

186 – 199 nm: Molina and Molina [42]

201 – 229 nm: Nölle et al. [46]



(Recommendation: 06-2, Note: 10-6, Evaluated: 10-6)

Absorption Cross Sections: The UV absorption spectrum of formyl fluoride, COHF, has been measured at room temperature by Giddings and Innes [19] (195 – 255 nm), Meller (194 – 267 nm) (see Röth et al. [58]), and Rattigan et al. [52] (220 – 267 nm). The high-resolution measurements show the long-wavelength wing of a highly structured absorption band. The absorption cross sections reported by Giddings and Innes [19] are larger by nearly a factor two than the high resolution (0.016 nm) data reported by Meller using diode array spectrometry. The cross sections measured by Rattigan et al. [52] at a resolution of 1.2 nm lie between the Giddings and Innes [19] and Meller data sets in the range 220 – 230 nm and closer to the data of Giddings and Innes [19] at 230 – 245 nm. Rattigan et al. [52] found the absorption cross sections to be independent of temperature over the range 233 – 318 K. The recommended absorption cross sections in Table 4E-7 are averages over 1 nm intervals of the high resolution data from Meller.

Photolysis Quantum Yield and Product Studies: No studies are available.

Table 4E-7. Absorption Cross Sections of COHF at 298 K

λ (nm)	$10^{20} \sigma$ (cm ²)	λ (nm)	$10^{20} \sigma$ (cm ²)	λ (nm)	$10^{20} \sigma$ (cm ²)	λ (nm)	$10^{20} \sigma$ (cm ²)
200	8.28	217	7.38	234	2.98	251	0.151
201	9.75	218	7.97	235	2.04	252	0.241
202	8.30	219	6.28	236	2.28	253	0.213
203	7.55	220	6.85	237	1.24	254	0.071
204	8.52	221	5.70	238	1.71	255	0.123
205	10.15	222	6.07	239	1.75	256	0.0674
206	8.28	223	6.58	240	1.55	257	0.0520
207	7.41	224	4.94	241	0.967	258	0.0382
208	8.44	225	5.33	242	1.19	259	0.0446
209	9.55	226	4.00	243	0.575	260	0.0427
210	7.76	227	4.65	244	0.765	261	0.0232
211	7.36	228	4.43	245	0.675	262	0.0153
212	7.92	229	4.61	246	0.719	263	0.0156
213	8.56	230	3.57	247	0.412	264	0.0170
214	9.22	231	2.55	248	0.484	265	0.0126
215	7.67	232	3.16	249	0.279	266	0.0118
216	6.51	233	3.09	250	0.210		

Note:

200 – 266 nm: Meller (see Röth et al. [58])

E14. CF₃O₂ + hν → Products

(Recommendation: 10-6, Note: 10-6, Evaluated: 10-6)

Absorption Cross Sections: The UV absorption cross sections of the trifluoromethylperoxy radical, CF₃O₂, have been measured at room temperature by Maricq and Szenté [35] (186 – 276 nm) and Nielsen et al. [45] (215 – 270 nm). The absorption spectrum displays a broad absorption band with a maximum at 210 nm. The cross sections reported by Nielsen et al. [45] are in good agreement with those measured by Maricq and Szenté [35] in the range 240 – 270 nm but are consistently smaller at shorter wavelengths (by 20 % at 215 nm). The recommended absorption cross sections listed in Table 4E-8 are taken from Maricq and Szenté [35].

Photolysis Quantum Yield and Product Studies: No photolysis studies are available.

Table 4E-8 Absorption Cross Sections of CF₃O₂ at 295 K

λ (nm)	$10^{20} \sigma$ (cm ²)	λ (nm)	$10^{20} \sigma$ (cm ²)	λ (nm)	$10^{20} \sigma$ (cm ²)
191.1	293	221.9	354	252.8	46
193.6	305	224.5	324	255.3	37*
196.2	334	227.1	292	257.9	31
198.8	363	229.6	257	260.5	25*
201.4	388	232.2	222	263.1	21
203.9	407	234.8	192	265.6	17
206.5	426	237.4	156	268.2	15
209.1	429	239.9	131	270.8	13
211.6	430	242.5	107	273.3	10
214.2	419	245.1	89	275.9	8
216.8	404	247.6	68		
219.4	383	250.2	54		

Note:

Maricq and Szente [35], *smoothed value



(Recommendation: 97-4, Note: 10-6, Evaluated: 10-6)

Absorption Cross Sections: An upper limit of 10^{-21} cm² molecule⁻¹ has been determined experimentally by Molina and Molina [43] for the absorption cross sections of trifluoromethanol, CF₃OH, over the wavelength range 185 – 300 nm. This upper limit is consistent with estimates based on similarities between CF₃OH and CH₃OH, as well as with quantum chemistry calculations reported by Schneider et al. [62].

Photolysis Quantum Yield and Product Studies: No studies are available.



(Recommendation: 06-2, Note: 10-6, Evaluated: 10-6)

Absorption Cross Sections. The UV absorption spectrum of hexafluorodimethyl peroxide, CF_3OOCF_3 , has been measured at room temperature over the wavelength range 200 – 263 nm by Meller and Moortgat [40]. The continuous spectrum shows part of a broad absorption band with monotonically increasing cross sections with decreasing wavelength. The recommended absorption cross sections in Table 4E-9 are averaged values over 1 nm intervals of the medium resolution (0.2 nm) spectrum from Meller and Moortgat [40].

Photolysis Quantum Yield and Product Studies: No studies are available.

Table 4E-9. Absorption Cross Sections of CF₃OOCF₃ at 298 K

λ (nm)	$10^{20} \sigma$ (cm ²)	λ (nm)	$10^{20} \sigma$ (cm ²)	λ (nm)	$10^{20} \sigma$ (cm ²)	λ (nm)	$10^{20} \sigma$ (cm ²)
200	3.61	216	1.25	232	0.501	248	0.204
201	3.37	217	1.18	233	0.462	249	0.195
202	3.13	218	1.10	234	0.433	250	0.183
203	2.92	219	1.04	235	0.408	251	0.174
204	2.73	220	0.983	236	0.380	252	0.166
205	2.53	221	0.926	237	0.361	253	0.157
206	2.35	222	0.869	238	0.339	254	0.147
207	2.20	223	0.822	239	0.323	255	0.138
208	2.06	224	0.778	240	0.303	256	0.132
209	1.94	225	0.737	241	0.288	257	0.125
210	1.80	226	0.693	242	0.274	258	0.119
211	1.69	227	0.654	243	0.263	259	0.112
212	1.61	228	0.614	244	0.246	260	0.107
213	1.51	229	0.584	245	0.240	261	0.101
214	1.42	230	0.555	246	0.227	262	0.096
215	1.33	231	0.525	247	0.214	263	0.091

Note:

200 – 263 nm: Meller and Moortgat [40]

- E17. CF₃O₃CF₃ + hν → Products (1)
(Recommendation: 06-2, Note: 10-6, Evaluated: 10-6)

Absorption Cross Sections: The UV absorption spectrum of hexafluorodimethyl trioxide, CF₃O₃CF₃, has been measured at room temperature and 200 – 312 nm by Meller and Moortgat [40]. The spectrum shows part of a broad absorption band with monotonically decreasing cross sections with increasing wavelength. The recommended absorption cross sections in Table 4E-10 are from Meller and Moortgat [40] (0.2 nm resolution) averaged over 1 nm intervals.

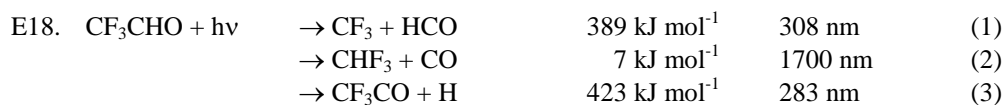
Photolysis Quantum Yield and Product Studies: No studies are available.

Table 4E-10. Absorption Cross Sections of CF₃O₃CF₃ at 298 K

λ (nm)	$10^{20} \sigma$ (cm ²)	λ (nm)	$10^{20} \sigma$ (cm ²)	λ (nm)	$10^{20} \sigma$ (cm ²)	λ (nm)	$10^{20} \sigma$ (cm ²)
200	46.9	229	20.3	258	4.26	287	0.565
201	45.5	230	19.5	259	3.99	288	0.526
202	44.2	231	18.8	260	3.73	289	0.491
203	42.8	232	18.0	261	3.51	290	0.458
204	41.4	233	17.2	262	3.28	291	0.427
205	40.2	234	16.5	263	3.07	292	0.400
206	39.0	235	15.7	264	2.86	293	0.373
207	37.9	236	15.0	265	2.67	294	0.347
208	37.0	237	14.3	266	2.50	295	0.325
209	36.1	238	13.7	267	2.33	296	0.302
210	35.2	239	13.0	268	2.17	297	0.281
211	34.4	240	12.3	269	2.03	298	0.262
212	33.6	241	11.7	270	1.89	299	0.244
213	32.8	242	11.1	271	1.76	300	0.228
214	32.1	243	10.5	272	1.64	301	0.213
215	31.3	244	10.0	273	1.53	302	0.197
216	30.5	245	9.46	274	1.43	303	0.185
217	29.8	246	8.95	275	1.33	304	0.174
218	29.0	247	8.45	276	1.24	305	0.164
219	28.2	248	7.95	277	1.15	306	0.154
220	27.4	249	7.48	278	1.07	307	0.143
221	26.7	250	7.04	279	0.999	308	0.133
222	25.9	251	6.64	280	0.929	309	0.122
223	25.1	252	6.25	281	0.860	310	0.112
224	24.3	253	5.87	282	0.800	311	0.106
225	23.5	254	5.52	283	0.748	312	0.096
226	22.7	255	5.18	284	0.699		
227	21.9	256	4.86	285	0.653		
228	21.1	257	4.56	286	0.608		

Note:

200 – 312 nm: Meller and Moortgat [40]



(Recommendation: 06-2, Note: 10-6, Evaluated: 10-6)

Absorption Cross Sections: The UV absorption spectrum of trifluoroacetaldehyde, CF₃CHO, has been measured at room temperature by Lucazeau and Sandorfy [32] (118 – 182 and 250-357 nm), Meller et al. [39] (229-364 nm), Francisco and Williams [18] (230 – 400 nm), Sellevåg et al. [63] (200 – 400 nm), Hashikawa et al. [21] (200 – 500 nm), and Chiappero et al. [9] (230 – 360 nm). The absorption spectrum exhibits an absorption band between 227 and 360 nm with a maximum at 301 nm and weak diffuse structure at wavelengths >250 nm. The absorption cross sections reported by Francisco and Williams [18], Meller et al. [39], Sellevåg et al. [63], Hashikawa et al. [21] and Chiappero et al. [9] are in good agreement, generally within 10% or better, in the wavelength region 245 – 354 nm. There are larger discrepancies in the cross section data in the long and short wavelength wings of the absorption band. In these regions, the cross sections from Sellevåg et al. [63] are smaller than those from Francisco and Williams [18] and larger than those from Meller et al. [39]. The data of Lucazeau and Sandorfy [32], which are reported in graphical form, are appreciably smaller than those reported in the other studies. The recommended absorption cross sections in Table 4E-11 are taken from Sellevåg et al. [63].

The temperature dependence of the absorption spectrum was examined by Chiappero et al. [9] (230 – 360 nm) between 249 and 297 K. No discernible variation of the absorption spectrum with temperature was observed. Borkowski and Ausloos [3] (313 and 334 nm) reported absorption cross sections at 329 K in good agreement with the other studies.

Photolysis Quantum Yield and Product Studies: The photolysis quantum yield for CF₃CHO and the product branching ratios are wavelength dependent. Sellevåg et al. [63] determined the effective atmospheric photolysis quantum yield for CF₃CHO using an outdoor photoreactor to be <0.02. Dodd and Watson-Smith [14] determined the products following photolysis at 313 nm to be $\Phi_1 = 0.12$ and $\Phi_2 = 0.021$. Pearce and Whytock [51] reported $\Phi_2 = 0$ for 313 nm photolysis. Richer et al. [57] studied the products formed following 254 nm photolysis and reported product yields of CHF₃ (14%), CF₂O (80%), CO (65%), CO₂ (45%) and $\Phi_2 = 0.14$. At 366 nm, Richer et al. [57] observed only a small degree of dissociation after >6 hours of photolysis. Chiappero et al. [9] reported photolysis quantum yields of $\Phi_1 = 0.41 \pm 0.07$ and $\Phi_2 = 0.38 \pm 0.07$ at 254 nm and $\Phi_1 = 0.17 \pm 0.03$ and $\Phi_2 \sim 0$ at 308 nm. Quantum yields of $\Phi_1 = 0.15 \pm 0.03$ and $\Phi_2 < 0.02$ are recommended at 313 nm.

Table 4E-11. Absorption Cross Sections of CF₃CHO at 298 K

λ (nm)	$10^{20} \sigma$ (cm ²)	λ (nm)	$10^{20} \sigma$ (cm ²)	λ (nm)	$10^{20} \sigma$ (cm ²)	λ (nm)	$10^{20} \sigma$ (cm ²)
210	0.197	248	0.311	286	2.63	324	2.06
211	0.192	249	0.339	287	2.67	325	1.90
212	0.179	250	0.369	288	2.73	326	1.72
213	0.172	251	0.400	289	2.79	327	1.64
214	0.159	252	0.433	290	2.86	328	1.62
215	0.152	253	0.472	291	2.92	329	1.55
216	0.140	254	0.511	292	2.94	330	1.44
217	0.132	255	0.548	293	3.00	331	1.35
218	0.121	256	0.591	294	3.05	332	1.26
219	0.113	257	0.638	295	3.06	333	1.18
220	0.105	258	0.686	296	3.08	334	1.13
221	0.098	259	0.737	297	3.08	335	1.06
222	0.090	260	0.789	298	3.10	336	1.01
223	0.084	261	0.840	299	3.14	337	0.993
224	0.080	262	0.896	300	3.17	338	0.891
225	0.076	263	0.954	301	3.20	339	0.730
226	0.074	264	1.02	302	3.15	340	0.622
227	0.073	265	1.09	303	3.12	341	0.585
228	0.075	266	1.15	304	3.15	342	0.569
229	0.075	267	1.22	305	3.13	343	0.531
230	0.078	268	1.29	306	3.07	344	0.471
231	0.081	269	1.35	307	3.03	345	0.425
232	0.086	270	1.42	308	2.97	346	0.385
233	0.091	271	1.50	309	2.95	347	0.337
234	0.097	272	1.58	310	2.92	348	0.310
235	0.104	273	1.66	311	2.92	349	0.286
236	0.112	274	1.74	312	2.91	350	0.246
237	0.121	275	1.82	313	2.78	351	0.235
238	0.131	276	1.89	314	2.67	352	0.232
239	0.142	277	1.96	315	2.65	353	0.162
240	0.155	278	2.03	316	2.62	354	0.096
241	0.169	279	2.11	317	2.52	355	0.071
242	0.184	280	2.19	318	2.42	356	0.058
243	0.201	281	2.28	319	2.33	357	0.050
244	0.220	282	2.35	320	2.25	358	0.044
245	0.240	283	2.42	321	2.19	359	0.042
246	0.262	284	2.50	322	2.13	360	0.038
247	0.285	285	2.57	323	2.08		

Note: 210 – 360 nm, Sellevåg et al. [63]



(Recommendation: 06-2, Note: 10-6, Evaluated: 10-6)

Absorption Cross Sections: The UV absorption spectrum of trifluoroacetyl fluoride, $\text{CF}_3\text{C}(\text{O})\text{F}$, has been measured at room temperature by Meller et al. [38] (200 – 281 nm), Rattigan et al. [53] (200 – 295 nm), and Malanca et al. [34] (200 – 340 nm). The cross sections from Meller et al. [38] and Malanca et al. [34] are in good agreement in the spectral region 200 – 260 nm. The position of the absorption maximum near 213 nm reported by Rattigan et al. [53] is shifted by ~3 nm to longer wavelengths as compared to that reported by Meller et al. [38] and Malanca et al. [34]. The cross sections from these studies differ by 20 to 30 % at wavelengths >260 nm.

The temperature dependence of the absorption spectrum has been reported by Rattigan et al. [53] (233 – 293 K) and Malanca et al. [34] (238 – 300 K). For wavelengths >210 nm, the absorption cross section decreases with decreasing temperature. The recommended absorption cross sections in Table 4E-12 are taken from Malanca et al. [34] in the region 200 – 260 nm at 300 and 238 K. In the region 265 – 280 nm, the data of Meller [38] are recommended at 297 K and those of Rattigan et al. [53] at 238 K.

Photolysis Quantum Yield and Product Studies: Bierbrauer et al. [2] measured the quantum yield of disappearance of $\text{CF}_3\text{C}(\text{O})\text{F}$ at 240 and 254 nm to be $\Phi_1 + \Phi_2 = 1.02 \pm 0.05$. It is assumed that this applies over the wavelength region 200 – 300 nm.

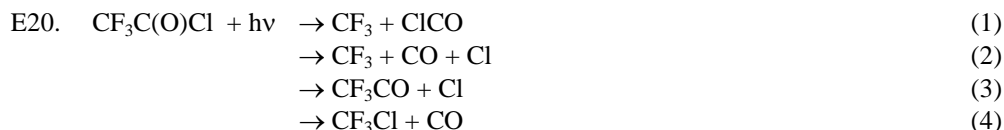
Table 4E-12. Absorption Cross Sections of $\text{CF}_3\text{C}(\text{O})\text{F}$ at 298 and 238 K

λ (nm)	$10^{20} \sigma$ (cm ²) 297 K	$10^{20} \sigma$ (cm ²) 238 K	λ (nm)	$10^{20} \sigma$ (cm ²) 297 K	$10^{20} \sigma$ (cm ²) 238 K
200	10.90	10.93	245	2.13	2.04
205	12.89	12.89	250	1.09	1.03
210	13.94	13.90	255	0.47	0.43
215	13.83	13.74	260	0.167	0.156
220	12.60	12.48	265	0.055	0.047
225	12.57	10.42	270	0.013	0.010
230	8.15	7.99	275	0.004	0.003
235	5.75	5.61	280	0.001	0.001
240	3.69	3.57			

Note:

200 – 260 nm, 297 and 238 K: Malanca et al. [34]

265 – 280 nm, 297 K: Meller et al. [38]; 238 K: Rattigan et al. [53]



(Recommendation: 06-2, Note: 10-6, Evaluated: 10-6)

Absorption Cross Sections: The UV absorption spectrum of trifluoroacetyl chloride, $\text{CF}_3\text{C}(\text{O})\text{Cl}$, has been measured at room temperature by Maricq and Szente [36] (190 – 342 nm), Rattigan et al. [53] (220 – 330 nm), Meller and Moortgat [41] (200 – 329 nm), and Malanca et al. [34] (200 – 325 nm). An absorption band was observed between 215 and 330 nm with the maximum around 255 nm and a strong increase of the absorption cross sections between 215 and 190 nm. The cross section data from Rattigan et al. [53], Meller and Moortgat [41] and Malanca et al. [34] are in excellent agreement for wavelengths >240 nm. The agreement among these studies is better than 5% between 240 and 315 nm. The cross section data of Meller and Moortgat [41] are larger than the data of Rattigan et al. [53] and Malanca et al. [34] by ~65% near the absorption minimum at 215 nm. Maricq and Szente [36] report a very noisy spectrum with an absorption maximum of $(4.6 \pm 0.7) \times 10^{-20} \text{ cm}^2 \text{ molecule}^{-1}$ at ~255 nm compared to $6.8 \times 10^{-20} \text{ cm}^2 \text{ molecule}^{-1}$ by Rattigan et al. [53] and Malanca et al. [34] and $6.7 \times 10^{-20} \text{ cm}^2 \text{ molecule}^{-1}$ by Meller and Moortgat [41].

The temperature dependence of the absorption spectrum has been measured by Rattigan et al. [53] (233, 253 and 296 K), Meller and Moortgat [41] (223, 248, 273 and 298 K), and Malanca et al. [34] (253 and 300 K). These studies show a decrease of the absorption cross sections with decreasing temperature from room temperature in the wavelength regions below ~215 nm and above 255 nm. For the region between 215 and 255 nm, a very slight decrease in absorption cross section with decreasing temperature was observed by Rattigan et al. [53] and Malanca et al. [34]. In this wavelength region, Meller and Moortgat [41] report nearly constant values for temperatures between 223 and 298 K and even a slight increase of the cross sections between 248 and 223 K. The recommended absorption cross sections in Table 4E-13 are taken from Malanca et al. [34].

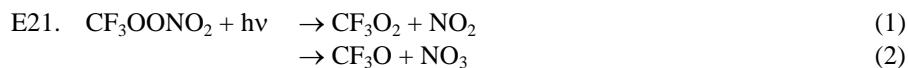
Photolysis Quantum Yield and Product Studies: Maricq and Szenté [36] photolysed CF₃C(O)Cl at 193 and 248 nm in O₂/N₂/C₂H₆ mixtures and measured the formation of the products CF₃O₂, HCl and CO. They report $\Phi_2 + \Phi_3 = 1.01 \pm 0.11$ at 193 nm and $\Phi_2 + \Phi_3 = 0.92 \pm 0.08$ at 248 nm where channel 2 was determined to be the major dissociation pathway at both wavelengths. Meller and Moortgat [41] [36] photolysed CF₃C(O)Cl at 254 nm in N₂ and air/C₂H₆ mixtures over the pressure range 100 – 760 Torr and measured the formation of the stable products CF₃Cl, C₂F₆, Cl₂ and CO. They report the quantum yield for the disappearance of CF₃C(O)Cl to be $\Phi_1 + \Phi_2 = 0.95 \pm 0.05$. Weibel et al. [65] photolysed CF₃C(O)Cl at 254 and 280 nm in N₂ and air/C₂H₆ mixtures in the pressure range 100 – 600 Torr and measured the formation of the products CF₃Cl, C₂F₆ and CO. A quantum yield for the decomposition of CF₃C(O)Cl = $\Phi[\text{CF}_3\text{Cl} + 2\text{C}_2\text{F}_6] = 0.98 \pm 0.13$, $\Phi_1 + \Phi_2 = 0.95 \pm 0.05$ was obtained. The quantum yields measured by Meller and Moortgat [41] and Weibel et al. [65] were independent of total pressure. There are no quantum yield data in the atmospherically important wavelength range >290 nm.

Table 4E-13. Absorption Cross Sections of CF₃C(O)Cl at 300 and 253 K

λ (nm)	$10^{20} \sigma$ (cm ²) 300 K	$10^{20} \sigma$ (cm ²) 253 K	λ (nm)	$10^{20} \sigma$ (cm ²) 300 K	$10^{20} \sigma$ (cm ²) 253 K
200	36.8	34.0	265	5.90	5.69
205	13.3	11.4	270	5.10	4.80
210	3.46	2.55	275	4.00	3.79
215	1.07	0.83	280	3.12	2.80
220	1.17	1.08	285	2.16	2.00
225	1.96	1.88	290	1.38	1.21
230	2.93	2.76	295	0.80	0.72
235	4.02	3.96	300	0.42	0.36
240	5.09	4.94	305	0.197	0.164
245	5.99	5.91	310	0.079	0.066
250	6.57	6.42	315	0.027	0.016
255	6.79	6.57	320	0.008	0.006
260	6.53	6.31	325	0.002	0.001

Note:

200 – 325 nm: Malanca et al. [34]



(Recommendation: 10-6, Note: 10-6, Evaluated: 10-6)

Absorption Cross Sections: The UV absorption cross sections of the trifluoro methyl peroxyxynitrate, CF₃OONO₂, have been measured at room temperature by Kopitzky et al. [27] (185 – 340 nm) and over the temperature range 233 – 300 K by Malanca et al. [34] (200 – 340 nm). The UV absorption spectrum consists of a strong absorption band with a broad maximum near 260 nm with continuously decreasing absorption cross sections at longer wavelengths. The absorption spectra measured at room temperature in these studies are in good agreement. The absorption cross sections at wavelengths 260 – 340 nm measured by Malanca et al. [34] increase significantly with increasing temperature. The temperature dependence was parameterized using the expression

$$\log_{10}(\sigma) = B \times T + \log_{10} \sigma_0$$

where σ and σ_0 are the cross sections in $\text{cm}^2 \text{ molecule}^{-1}$ at temperatures T and 0 K, respectively. The parameters $\sigma(0 \text{ K})$ and B at selected wavelengths are as follows:

λ (nm)	$10^3 B$ (K^{-1})	$10^{20} \sigma_0(0 \text{ K})$ ($\text{cm}^2 \text{ molecule}^{-1}$)
290	6.8	1.2×10^{-2}
295	8.3	2.9×10^{-3}
300	10.5	4.4×10^{-4}
305	12	8.4×10^{-5}
310	14	1.9×10^{-6}
315	16.4	2.9×10^{-6}
320	18	6.0×10^{-7}
325	22	3.7×10^{-8}
330	26	1.3×10^{-9}

Note that B increases with wavelength as a consequence of the larger temperature dependence at longer wavelengths

The recommended absorption cross sections listed in Table 4E-14 for 300 K were obtained by averaging the room temperature data from Malanca et al. [34] and Kopitzky et al. [27] and for 253 K the data is from Malanca et al. [34].

Photolysis Quantum Yield and Product Studies: No photolysis studies are available.

Table 4E-14. Absorption Cross Sections of CF_3OONO_2 at 300 and 253 K

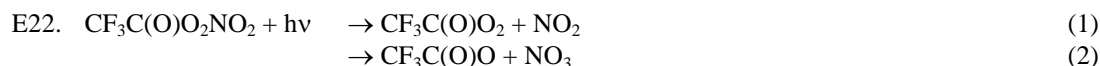
λ (nm)	$10^{20} \sigma$ (cm^2) 300 K	$10^{20} \sigma$ (cm^2) 253 K	λ (nm)	$10^{20} \sigma$ (cm^2) 300 K	$10^{20} \sigma$ (cm^2) 253 K
185	430	-	265	8.35	6.8
190	370	-	270	5.8	4.6
195	290	-	275	4.0	3.0
200	220	220	280	2.7	1.8
205	150	150	285	1.8	1.1
210	103	110	290	1.15	0.7
215	75.5	78	295	0.80	0.4
220	56	56	300	0.52	0.2
225	46.5	46	305	0.39	0.14
230	39	38	310	0.25	0.09
235	33.5	32	315	0.18	0.05
240	28.5	27	320	0.12	0.03
245	23	21	325	0.08	0.02
250	18.5	17	330	0.07	0.01
255	14.5	12.8	335	0.05	0.007
260	11.3	9.5	340	0.02	0.004

Note:

185 – 195 nm, 300 K: Kopitzky et al. [27]

200 – 325 nm, 300 K: Average of Malanca et al. [34] and Kopitzky et al. [27]

200 – 325 nm, 253 K: Malanca et al. [34]



(Recommendation: 06-2, Note: 10-6, Evaluated: 10-6)

Absorption Cross Sections: The UV absorption spectrum of trifluoroperoxyacetyl nitrate (FPAN), $\text{CF}_3\text{C(O)O}_2\text{NO}_2$, has been measured at room temperature over the wavelength range 227 – 305 nm by Libuda and Zabel [30]. Over this wavelength range the $\text{CF}_3\text{C(O)O}_2\text{NO}_2$ spectrum is ~5 nm red shifted from the $\text{CH}_3\text{C(O)O}_2\text{NO}_2$ spectrum. The recommended absorption cross sections in Table 4E-15 are averages over 5 nm intervals of the medium resolution (0.6 nm) data reported by Libuda and Zabel [30]. The estimated

uncertainties in the cross sections as reported by Libuda and Zabel [30] are ~10% at wavelengths <290 nm and 15 to 45% in the region 295 – 305 nm.

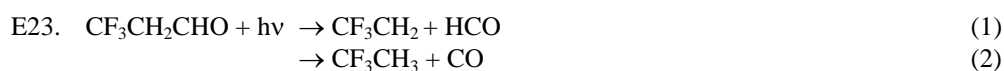
Photolysis Quantum Yield and Product Studies: No studies are available.

Table 4E-15. Absorption Cross Sections of CF₃(O)O₂NO₂ at 298 K

λ (nm)	$10^{20} \sigma$ (cm ²)	λ (nm)	$10^{20} \sigma$ (cm ²)	λ (nm)	$10^{20} \sigma$ (cm ²)
230	70.0	260	11.8	290	0.87
240	44.9	270	5.46	300	0.33
245	32.5	275	3.56	305	0.20
250	23.9	280	2.21		
255	17.0	285	1.40		

Note:

230 – 305 nm: Libuda and Zabel [30]



(Recommendation: 06-2, Note: 10-6, Evaluated: 10-6)

Absorption Cross Sections: The UV absorption spectrum of 3,3,3-trifluoropropionaldehyde, CF₃CH₂CHO, has been measured at room temperature by Sellevåg et al. [63] (200 – 400 nm) and Chiappero et al. [9] (230 – 355 nm). The spectrum exhibits a slightly structured absorption band between 270 and 343 nm. The reported spectra are in good agreement. The cross sections from Sellevåg et al. [63] are ~6 % larger than the values reported by Chiappero et al. [9] between 240 and 340 nm. The data reported for the wavelength region above 340 nm are in poor agreement. Chiappero et al. [9] measured the temperature dependence of the absorption spectrum over the range 249 – 297 K. No discernible variation of cross section with temperature was observed. The recommended absorption cross sections in Table 4E-16 are taken from Sellevåg et al. [63].

Photolysis Quantum Yield and Product Studies: Sellevåg et al. [63] reported the effective atmospheric photolysis quantum yield for CF₃CH₂CHO using an outdoor photoreactor to be < 0.02. The quantum yield for channels 1 and 2 were determined by Chiappero et al. [9] to be $\Phi_1 = 0.38 \pm 0.09$ and $\Phi_2 = 0.36 \pm 0.07$ for 254 nm photolysis and $\Phi_1 = 0.04 \pm 0.01$ and $\Phi_2 \sim 0$ at 308 nm.

Table 4E-16. Absorption Cross Sections of CF₃CH₂CHO at 298 K

λ (nm)	$10^{20} \sigma$ (cm ²)	λ (nm)	$10^{20} \sigma$ (cm ²)	λ (nm)	$10^{20} \sigma$ (cm ²)	λ (nm)	$10^{20} \sigma$ (cm ²)
200	0.939	236	0.309	272	2.43	308	3.04
201	0.825	237	0.324	273	2.58	309	3.07
202	0.732	238	0.344	274	2.72	310	3.13
203	0.668	239	0.362	275	2.83	311	3.15
204	0.611	240	0.377	276	2.89	312	3.04
205	0.542	241	0.395	277	2.92	313	2.83
206	0.483	242	0.422	278	2.94	314	2.56
207	0.432	243	0.443	279	2.98	315	2.30
208	0.397	244	0.474	280	3.07	316	2.11
209	0.367	245	0.513	281	3.22	317	1.97
210	0.334	246	0.552	282	3.37	318	1.93
211	0.311	247	0.593	283	3.49	319	1.93
212	0.309	248	0.629	284	3.55	320	1.92
213	0.298	249	0.671	285	3.54	321	1.95
214	0.285	250	0.728	286	3.53	322	1.97
215	0.273	251	0.788	287	3.51	323	1.93
216	0.267	252	0.842	288	3.51	324	1.79
217	0.266	253	0.904	289	3.59	325	1.59
218	0.263	254	0.963	290	3.69	326	1.32
219	0.263	255	1.01	291	3.80	327	1.09
220	0.270	256	1.08	292	3.85	328	0.938

Table 4E-17. Absorption Cross Sections of CF₃C(O)OH at 296 K

λ (nm)	$10^{20} \sigma$ (cm ²)	λ (nm)	$10^{20} \sigma$ (cm ²)
200	5.20	245	1.69
205	6.48	250	0.870
210	7.23	255	0.390
215	7.59	260	0.155
220	7.76	265	0.050
225	7.21	270	0.013
230	6.03	275	0.006
235	4.46		
240	2.89		

Note:

200 – 275 nm: Rattigan et al. [53]



(Recommendation: 06-2, Note: 10-6, Evaluated: 10-6)

Absorption Cross Sections: The UV absorption spectrum of acetyl fluoride, CH₃C(O)F, has been measured at room temperature over the wavelength range 200 – 310 nm by Rattigan et al. [53] using diode array spectroscopy. The spectrum shows two absorption bands with a maximum cross section near 206 nm and a shoulder near 260 nm. The recommended absorption cross sections in Table 4E-18 are averages over 5 nm intervals of the spectrum recorded at a resolution of 1.2 nm by Rattigan et al. [53].

Photolysis Quantum Yield and Product Studies: No studies are available.

Table 4E-18. Absorption Cross Sections of CH₃C(O)F at 296 K

λ (nm)	$10^{20} \sigma$ (cm ²)	λ (nm)	$10^{20} \sigma$ (cm ²)	λ (nm)	$10^{20} \sigma$ (cm ²)	λ (nm)	$10^{20} \sigma$ (cm ²)
200	11.3	230	3.83	260	0.158	290	0.008
205	12.2	235	2.19	265	0.120	295	0.004
210	12.0	240	1.14	270	0.090	300	0.002
215	10.5	245	0.566	275	0.056	305	0.001
220	8.35	250	0.311	280	0.029		
225	5.97	255	0.206	285	0.016		

Note:

200 – 305 nm : Rattigan et al. [53]

E26. $\text{CH}_2=\text{CHCF}_3 + h\nu \rightarrow \text{Products}$

(Recommendation: 06-2, Note: 10-6, Evaluated: 10-6)

Absorption Cross Sections: The VUV/UV absorption spectrum of 3,3,3-trifluoro-1-propene, $\text{CH}_2=\text{CHCF}_3$, has been measured at room temperature over the wavelength range 164 – 205 nm by Orkin et al. [48]. The recommended absorption cross sections in Table 4E-19 are from Orkin et al. [48].

Photolysis Quantum Yield and Product Studies: No studies are available.

Table 4E-19. Absorption Cross Sections of $\text{CH}_2=\text{CHCF}_3$ at 295 K

λ (nm)	$10^{20} \sigma$ (cm^2)	λ (nm)	$10^{20} \sigma$ (cm^2)	λ (nm)	$10^{20} \sigma$ (cm^2)
164	3569	178	168	192	0.681
165	3377	179	114	193	0.453
166	3146	180	77.7	194	0.298
167	2874	181	53.9	195	0.204
168	2538	182	36.5	196	0.131
169	2184	183	25.0	197	0.0872
170	1814	184	16.8	198	0.0581
171	1481	185	11.3	199	0.0404
172	1165	186	7.74	200	0.0278
173	899	187	5.22	201	0.0185
174	660	188	3.49	202	0.0129
175	475	189	2.32	203	0.00945
176	340	190	1.52	204	0.00669
177	240	191	1.02	205	0.00456

Note:

164 – 205 nm: Orkin et al. [48]

E27. $\text{CH}_2=\text{CF}_2\text{CF}_3 + h\nu \rightarrow \text{Products}$

(Recommendation: 06-2, Note: 10-6, Evaluated: 10-6)

Absorption Cross Sections: The VUV/UV absorption spectrum of 1,1,1,2-tetrafluoropropene, $\text{CH}_2=\text{CF}_2\text{CF}_3$, has been measured at room temperature over the wavelength range 164 – 186 nm by Orkin et al. [48]. The recommended absorption cross sections in Table 4E-20 are taken from Orkin et al. [48].

Photolysis Quantum Yield and Product Studies: No studies are available.

Table 4E-20. Absorption Cross Sections of $\text{CH}_2=\text{CF}_2\text{CF}_3$ at 295 K

λ (nm)	$10^{20} \sigma$ (cm^2)	λ (nm)	$10^{20} \sigma$ (cm^2)
164	3773	176	1130
165	3732	177	840
166	3730	178	600
167	3695	179	408
168	3594	180	273
169	3418	181	185
170	3176	182	124
171	2877	183	82.4
172	2535	184	55.5
173	2178	185	38.1
174	1802	186	26.2
175	1445		

Note: 164 – 186 nm: Orkin et al. [48]

E28. $\text{CF}_2=\text{CF}_2 + h\nu \rightarrow \text{Products}$

(Recommendation: 06-2, Note: 10-6, Evaluated: 10-6)

Absorption Cross Sections: The VUV/UV absorption spectrum of tetrafluoroethylene, $\text{CF}_2=\text{CF}_2$, has been measured at room temperature by Sharpe et al. [64] (185-209 nm), Orkin et al. [48] (164 – 220 nm), and Eden et al. [16] (115 – 320 nm). The spectrum shows a structured absorption band with five maxima between 170 and 220 nm (maximum near 189 nm). The spectra from Orkin et al. [48] and Eden et al. [16] agree to within 10% in the range 164 – 182 nm, 20% in the range 182 – 200 nm, and 10% in the range 203 – 205 nm. Above 200 nm, the absorption cross sections decrease monotonically toward longer wavelengths. The spectrum reported by Eden et al. [16] deviates from that of Orkin et al. [48] at wavelengths >200 nm but their spectrum is very noisy in this region. The absorption spectrum reported by Sharpe et al. [64] is systematically shifted by 1 to 2 nm to shorter wavelengths from the Orkin et al. [48] spectrum. The recommended absorption cross sections in Table 4E-21 are the mean of the data from Orkin et al. [48] and Eden et al. [16] for the region 164 – 205 nm and the data from Orkin et al. [48] in the region 206 – 220 nm.

Photolysis Quantum Yield and Product Studies: No studies are available.

Table 4E-21. Absorption Cross Sections of $\text{CF}_2=\text{CF}_2$ at 296 K

λ (nm)	$10^{20} \sigma$ (cm^2)	λ (nm)	$10^{20} \sigma$ (cm^2)	λ (nm)	$10^{20} \sigma$ (cm^2)	λ (nm)	$10^{20} \sigma$ (cm^2)
164	335	179	341	194	423	209	0.429
165	324	180	362	195	387	210	0.257
166	300	181	432	196	263	211	0.162
167	272	182	521	197	169	212	0.0998
168	243	183	559	198	108	213	0.0633
169	227	184	485	199	64.0	214	0.0392
170	238	185	442	200	39.9	215	0.0249
171	268	186	491	201	23.8	216	0.0160
172	286	187	596	202	14.5	217	0.0105
173	281	188	682	203	8.74	218	0.00668
174	289	189	671	204	5.73	219	0.00443
175	327	190	507	205	3.23	220	0.00288
176	372	191	417	206	1.99		
177	390	192	399	207	1.17		
178	376	193	410	208	0.713		

Note:

164 – 205 nm: mean of the data from Orkin et al. [48] and Eden et al. [16]

206 – 220 nm: data from Orkin et al. [48]

E29. $\text{CF}_2=\text{CFCF}_3 + h\nu \rightarrow \text{Products}$

(Recommendation: 06-2, Note: 10-6, Evaluated: 10-6)

Absorption Cross Sections: The VUV/UV absorption spectrum of hexafluoropropene, $\text{CF}_2=\text{CFCF}_3$, has been measured at room temperature by Sharpe et al. [64] (185 – 209 nm), Orkin et al. [48] (164 – 222 nm), and Eden et al. [15] (115 – 330 nm). The spectrum has overlapping absorption bands between 140 and 220 nm with maxima at 155 and 158.5 nm ($\sigma \approx 3 \times 10^{-17} \text{ cm}^2 \text{ molecule}^{-1}$), 166 and 180 nm. In the wavelength region 164 – 200 nm, the cross sections from Orkin et al. [48] and Eden et al. [15] agree to within 15%. In the region 185-200 nm, the cross sections from Orkin et al. [48], Eden et al. [15], and Sharpe et al. [64] agree to within 25%. Above 200 nm, the absorption cross sections decrease monotonically toward longer wavelengths. The spectrum reported by Eden et al. [15] deviates from that Orkin et al. [48] at wavelengths >200 nm but their spectrum is very noisy in this region. The recommended absorption cross sections in Table 4E-22 are the mean of the data from Orkin et al. [48] and Eden et al. [15] for the region 164 – 199 nm and the data from Orkin et al. [48] in the region 200 – 222 nm.

Photolysis Quantum Yield and Product Studies: No studies are available.

Table 4E-22. Absorption Cross Sections of CF₂=CFCF₃ at 296 K

λ (nm)	$10^{20} \sigma$ (cm ²)	λ (nm)	$10^{20} \sigma$ (cm ²)	λ (nm)	$10^{20} \sigma$ (cm ²)	λ (nm)	$10^{20} \sigma$ (cm ²)
164	2290	179	929	194	97.8	209	0.585
165	2210	180	912	195	73.3	210	0.396
166	2130	181	880	196	54.7	211	0.269
167	2040	182	835	197	40.4	212	0.184
168	1920	183	779	198	29.7	213	0.125
169	1760	184	708	199	22.3	214	0.0838
170	1570	185	629	200	16.2	215	0.0564
171	1380	186	550	201	11.6	216	0.0381
172	1210	187	472	202	8.17	217	0.0261
173	1080	188	391	203	5.70	218	0.0177
174	995	189	321	204	3.95	219	0.0119
175	946	190	259	205	2.70	220	0.00795
176	930	191	207	206	1.85	221	0.00533
177	928	192	163	207	1.28	222	0.00354
178	931	193	127	208	0.866		

Note:

164 – 199 nm: mean of the data of Orkin et al. [48] and Eden et al. [15]

200 – 222 nm: data of Orkin et al. [48]

References for Section 4E

1. Au, J. W., G. R. Burton and C. E. Brion, 1997, *Chem. Phys.*, 221, 151-168.
2. Bierbrauer, K. L., M. S. Chiappero, F. E. Malanca and G. A. Arguello, 1999, *J. Photochem. Photobiol. A: Chem.*, 122, 73-78.
3. Borkowski, R. P. and P. Ausloos, 1962, *J. Am. Chem. Soc.*, 84, 4044-4048.
4. Brandon, J. T., S. A. Reid, D. C. Robie and H. Reisler, 1992, *J. Chem. Phys.*, 97, 5246-5249.
5. Brodersen, P. H., P. Frisch and H.-J. Schumacher, 1937, *Z. Phys. Chem. B*, 37, 25-29.
6. Burley, J. D., C. E. Miller and H. S. Johnston, 1993, *J. Molec. Spec.*, 158, 377-391.
7. Carnovale, F., R. Tseng and C. E. Brion, 1981, *J. Phys. B: Atom. Mol. Phys.*, 14, 4771-4785.
8. Chegodaev, P. P. and B. I. Tubikov, 1973, *Dokl. Akad. Nauk. SSSR*, 210, 647-649.
9. Chiappero, M. S., F. E. Malanca, G. A. Arguello, S. T. Wooldridge, M. D. Hurley, J. C. Ball, T. J. Wallington, R. L. Waterland and R. C. Buck, 2006, *J. Phys. Chem. A*, 110, 11944-11953.
10. Chim, R. Y. L., R. A. Kennedy and R. P. Tuckett, 2003, *Chem. Phys. Lett.*, 367, 697-703.
11. Chou, C. C., G. Crescentini, H. Vera-Ruiz, W. S. Smith and F. S. Rowland. "Stratospheric Photochemistry of CF₂O, CClFO, and CCl₂O"; 173rd American Chemical Society Meeting, 1977, New Orleans, LA,
12. Cole, B. E. and R. N. Dexter, 1978, *J. Quant. Spectrosc. Radiat. Transfer*, 19, 303-309.
13. Cook, G. R. and B. K. Ching, 1965, *J. Chem. Phys.*, 43, 1794-1797.
14. Dodd, R. E. and J. Watson-Smith, 1957, *J. Chem. Soc.*, 1465-1473.
15. Eden, S., P. Limão-Vieira, S. V. Hoffmann and N. J. Mason, 2003, *Chem. Phys. Lett.*, 379, 170-176.
16. Eden, S., P. Limão-Vieira, P. A. Kendall, N. J. Mason, J. Delwich, M.-J. Hubin-Franskin, T. Tanaka, M. Kitajima, H. Tanaka, H. Cho and S. V. Hoffmann, 2004, *Chem. Phys.*, 297, 257-269.
17. Ellerman, T., J. Sehested, O. J. Nielson, P. Pagsberg and T. J. Wallington, 1994, *Chem. Phys. Lett.*, 218, 287-294.
18. Francisco, J. S. and I. H. Williams, 1992, *Mol. Phys.*, 76, 1433-1441.
19. Giddings, L. E., Jr. and K. K. Innes, 1961, *J. Mol. Spectrosc.*, 6, 528-549.
20. Glissmann, A. and H.-J. Schumacher, 1934, *Z. Phys. Chem. B*, 24, 328-334.
21. Hashikawa, Y., M. Kawasaki, R. L. Waterland, M. D. Hurley, J. C. Ball, T. J. Wallington, M. P. S. Andersen and O. J. Nielsen, 2004, *J. Fluorine Chemistry*, 125, 1925-1932.
22. Hatherly, P. A. and A. J. Flaxman, 2003, *Chem. Phys. Lett.*, 380, 512-515.
23. Hitchcock, A. P., G. R. J. Williams, C. E. Brion and P. W. Langhoff, 1984, *Chem. Phys.*, 88, 65-80.
24. Inn, E. C. Y., 1980, *J. Geophys. Res.*, 85, 7493-7494.
25. Johnston, H. S. and H. J. Bertin, Jr., 1959, *J. Mol. Spectrosc.*, 3, 683-696.
26. Kirshenbaum, A. D. and A. G. Streng, 1961, *J. Chem. Phys.*, 35, 1440-1442.
27. Kopitzky, R., H. Willner, H.-G. Mack, A. Pfeiffer and H. Oberhammer, 1998, *Inorg. Chem.*, 37, 6208-6213.
28. Lee, L. C., E. Philips and D. L. Judge, 1977, *J. Chem. Phys.*, 67, 1237-1246.
29. Lee, L. C., X. Wang and M. Suto, 1986, *J. Chem. Phys.*, 85, 6294-6300.
30. Libuda, H. G. and F. Zabel, 1995, *Ber. Bunsenges. Phys. Chem.*, 99, 1205-1213.
31. Limão-Vieira, P., E. Vasekova, A. Giuliani, J. M. C. Lourenço, P. M. Santos, D. Dufлот, S. V. Hoffmann, N. J. Mason, J. Delwiche and M.-J. Hubin-Franskin, 2007, *Phys. Rev.*, A 76, 032509-032509.
32. Lucazeau, G. and C. Sandorfy, 1970, *J. Mol. Spectrosc.*, 35, 214-231.
33. Lyman, J. and R. Holland, 1988, *J. Phys. Chem.*, 92, 7232-7241.
34. Malanca, F. E., M. S. Chiapero, G. A. Arguello and T. J. Wallington, 2005, *Atmos. Environ.*, 39, 5051-5057.
35. Maricq, M. M. and J. J. Szente, 1992, *J. Phys. Chem.*, 96, 4925-4930.
36. Maricq, M. M. and J. J. Szente, 1995, *J. Phys. Chem.*, 99, 4554-4557.
37. Matchuk, N. M., V. I. Tupikov, A. I. Malkova and S. Y. Pshezhetskii, 1976, *Opt. Spektrosk. (Opt. Spectrosc.)*, 40, 14-18 (17-19).
38. Meller, R., 1999, personal communication to NASA Data Panel.
39. Meller, R., D. Boglu and G. K. Moortgat. "UV spectra of several halogenated carbonyl compounds and FTIR studies of the degradation of CF₃COCl, HCFC-123 and HFC-143a"; Kinetics and Mechanisms for the Reactions of Halogenated Organic Compounds in the Troposphere. STEP-HALOCSIDE/AFEAS WORKSHOP, 1991, Dublin, Ireland, 14-16 May, 1991, 110-115.
40. Meller, R. and G. K. Moortgat, 1995, *J. Photochem. Photobiol. A: Chem.*, 86, 15-25.
41. Meller, R. and G. K. Moortgat, 1997, *J. Photochem. Photobiol. A: Chem.*, 108, 105-116.
42. Molina, L. T. and M. J. Molina. "Chemistry of fluorine in the stratosphere"; 182nd American Chemical Society National Meeting, 1982, New York,
43. Molina, L. T. and M. J. Molina, 1996, *Geophys. Res. Lett.*, 23, 563-565.
44. Nee, J. B., M. Suto and L. C. Lee, 1985, *J. Phys. B: Atom. Mol. Phys.*, 18, L293-L294.

45. Nielsen, O. J., T. Ellermann, J. Sehested, E. Bartkiewicz, T. J. Wallington and M. D. Hurley, 1992, *Int. J. Chem. Kinet.*, 24, 1009-1021.
46. Nölle, A., H. Heydtmann, R. Meller, W. Schneider and G. K. Moortgat, 1992, *Geophys. Res. Lett.*, 19, 281-284.
47. Nölle, A., C. Krumscheid and H. Heydtmann, 1999, *Chem. Phys. Lett.*, 299, 561-565.
48. Orkin, V. L., R. E. Huie and M. J. Kurylo, 1997, *J. Phys. Chem. A*, 101, 9118-9124.
49. Pagsberg, P., A. Sillesen, J. T. Jodowski and E. Ratajczak, 1996, *Chem. Phys. Lett.*, 249, 358-364.
50. Pagsberg, P. B., E. Ratajczak, A. Sillesen and J. T. Jodkowski, 1987, *Chem. Phys. Lett.*, 141, 88-94.
51. Pearce, C. and D. A. Whytock, 1971, *J. Chem. Soc., Chem. Commun.*, 1464-1466.
52. Rattigan, O. V., D. M. Rowley, O. Wild, R. L. Jones and R. A. Cox, 1994, *J. Chem. Soc. Faraday Trans.*, 90, 1819-1829.
53. Rattigan, O. V., O. Wild, R. L. Jones and R. A. Cox, 1993, *J. Photochem. Photobiol. A: Chem.*, 73, 1-9.
54. Ravishankara, A. R., S. Solomon, A. A. Turnipseed and R. F. Warren, 1993, *Science*, 259, 194-199.
55. Rebbert, R. E. and P. Ausloos, 1971, *J. Res. Natl. Bur. Stand., A* 75, 481-485.
56. Reid, S. A., J. T. Brandon and H. Reisler, 1993, *J. Phys. Chem.*, 97, 540-543.
57. Richer, H. R., J. R. Sodeau and I. Barnes, 1993, STEP-HALOCSIDE/AFEAS Workshop, Dublin, 23-25 March, 180-188.
58. Röth, E. P., R. Ruhnke, G. Moortgat, R. Meller and W. Schneider "UV/VIS-Absorption Cross Sections and Quantum Yields for Use in Photochemistry and Atmospheric Modeling," Forschungszentrum Jülich Publication, Part 1 : Inorganic Substances (jül-3340), Part 2: Organic Substances (jül-3341), 1997
59. Safary, E., 1954, *Ann. Phys. (Paris)*, 9, 203-254.
60. Safary, E., J. Romand and B. Vodar, 1951, *J. Chem. Phys.*, 19, 379-380.
61. Sauvageau, P., J. Doucet, R. Gilbert and C. Sandorfy, 1974, *J. Chem. Phys.*, 61, 391-395.
62. Schneider, W. F., T. J. Wallington, K. Minschwaner and E. A. Stahlberg, 1995, *Environ. Sci. Technol.*, 29, 247-250.
63. Sellevåg, S. R., T. Kelly, H. Sidebottom and C. J. Nielsen, 2004, *Phys. Chem. Chem. Phys.*, 6, 1243-1252.
64. Sharpe, S., B. Hartnett, H. S. Sethi and D. S. Sethi, 1987, *J. Photochem.*, 38, 1-13.
65. Weibel, D. E., G. A. Argüello, E. R. d. Staricco and E. H. Staricco, 1995, *J. Photochem. Photobiol. A: Chem.*, 86, 27-31.
66. Zhang, W., G. Cooper, T. Ibuki and C. E. Brion, 1989, *Chem. Phys.*, 137, 391-405.

SECTION 4F. ClO_x PHOTOCHEMISTRY



(Recommendation: 06-2, Note: 10-6, Evaluated: 10-6)

Absorption Cross Sections: The recommended absorption cross sections are taken from the work of Maric et al. [137], who studied the absorption spectrum in the range 200 – 550 nm using a spectral resolution of 0.2 nm at 298 K. These authors also measured banded features in the range 476 – 496 nm at 0.04 nm resolution. The absorption cross sections can be calculated in the range 250 – 550 nm at various temperatures with the expression derived from their study and previous investigations, given at the bottom of Table 4F-1. For convenience, some room temperature values are also listed in the table. Ganske et al. [69] have also measured the cross sections at room temperature and the agreement with the recommended values is excellent. These two sets of data also agree well with the earlier recommendation, which was based on the work of Seery and Britton [217], which is in turn in good agreement with the results reported by Gibson and Bayliss [70], Fergusson et al. [63], and Burkholder and Bair [23]. At wavelengths >250 nm, the absorption cross sections measured at room temperature by Hubinger and Nee [96] are in excellent agreement with the values of Maric et al. [137]. However, in the range 200 – 250 nm the cross sections deviate considerably between both groups. Room temperature cross sections have also been obtained by Roxlo and Mandl [207] for the range 170 – 214 nm. The low resolution absorption cross sections reported by Chen and Zhu [37, 38] and Chen et al. [39] for the 300 – 420 nm region at 5 and 10 nm intervals and measured for the calibration of quantum yield measurements of some carbonyl compounds deviate up to ~30% from those reported by Maric et al. [137].

Photolysis Quantum Yield and Product Studies: The estimated atmospheric photodissociation rate is only weakly affected by the temperature dependence of the spectrum. Chinin [41] measured an upper limit of 5% for the branching ratio for excited atomic Cl*(²P_{1/2}) at 351 nm in agreement with earlier studies by Bush et al. [30] at 347.1 nm and Park et al. [184] at 308 and 340 – 355 nm, who determined an upper limit for Cl* formation of 0.01.

Table 4F-1. Absorption Cross Sections of Cl₂ at 298 K

λ (nm)	10 ²⁰ σ (cm ²)	λ (nm)	10 ²⁰ σ (cm ²)	λ (nm)	10 ²⁰ σ (cm ²)
260	0.198	360	13.22	460	0.258
270	0.824	370	8.41	470	0.162
280	2.58	380	5.00	480	0.0957
290	6.22	390	2.94	490	0.0534
300	11.92	400	1.84	500	0.0283
310	18.50	410	1.28	510	0.0142
320	23.71	420	0.956	520	0.00681
330	25.55	430	0.732	530	0.00313
340	23.51	440	0.546	540	0.00137
350	18.77	450	0.387	550	0.00058

$$\sigma = 10^{-20} \alpha^{0.5} \left\{ 27.3 \exp \left(-99.0 \alpha \left(\ln \left(\frac{329.5}{\lambda} \right) \right)^2 \right) + 0.932 \exp \left(-91.5 \alpha \left(\ln \left(\frac{406.5}{\lambda} \right) \right)^2 \right) \right\}$$

where $\alpha = \tanh(402.7/T)$; λ in nm, 250 < λ < 550 nm, and T in K; 300 K > T > 195 K.



(Recommendation: 06-2, Note: 10-6, Evaluated: 10-6)

Absorption Cross Sections: The UV absorption spectrum of chlorine monoxide, ClO, shown in Figure 4-1, is partly composed of a continuum absorption band from 210 nm to the maximum near 265 nm, and a

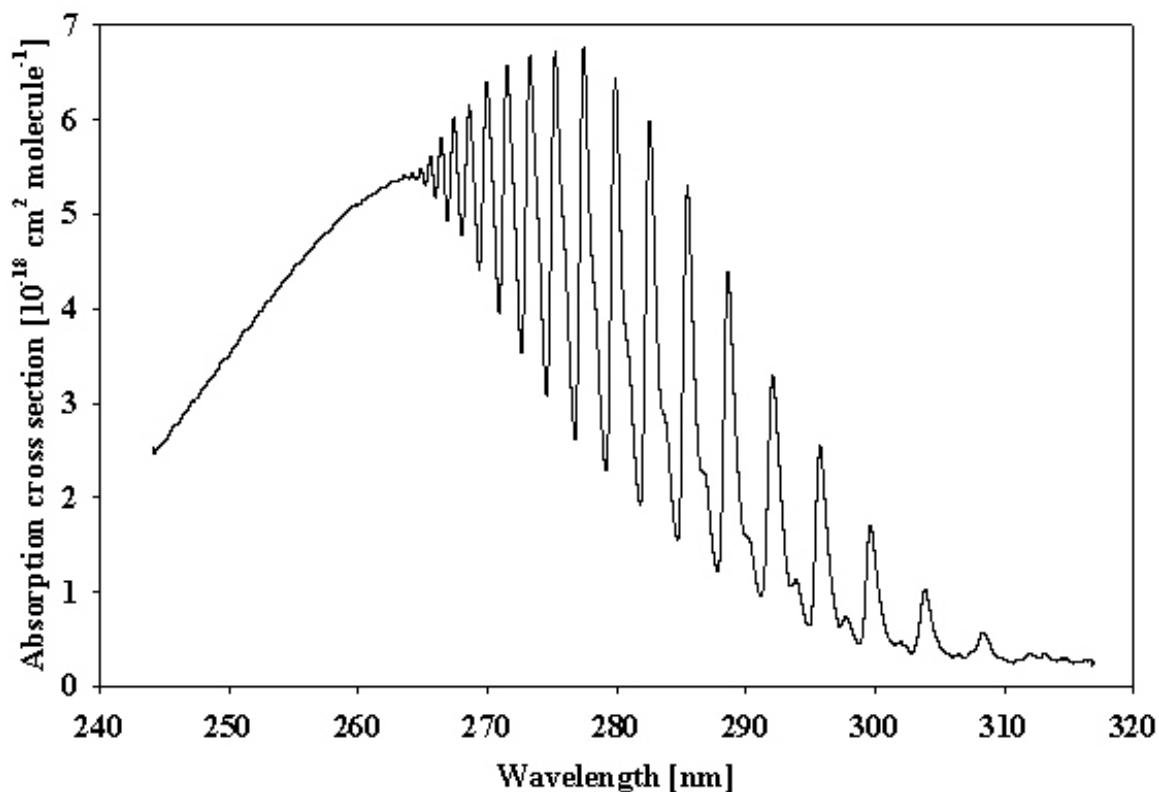
characterized banded structure of a strong $A^2\Pi_{3/2} \leftarrow X^2\Pi_{3/2}$ transition, superposing a weak $A^2\Pi_{1/2} \leftarrow X^2\Pi_{1/2}$ system between 265 nm and 315 nm. Watson [244] has reviewed the cross section measurements prior to 1977. The more recent measurements yield results in reasonable agreement with the earlier studies by Mandelman and Nicholls [134] (250 – 310 nm), Wine et al. [249] (near 283 nm), Rigaud et al. [199] (272 – 324 nm), Jourdain et al. [113] (272 – 320 nm), Barton et al. [7] (274 – 306 nm) at 315 K, Lang et al. [121] (253.7 and 257.7 nm), Sander and Friedl [212] (275.2 nm) at 220, 298, and 400 K, Trolrier et al. [231] (270 – 310 nm) over the temperature range 200 – 263 K, and Simon et al. [218] (240 – 310 nm). The peak cross section at the maximum of the continuum (near 265 nm) is $5.2 \times 10^{-18} \text{ cm}^2 \text{ molecule}^{-1}$, based on the average of the results from Jourdain et al., Sander and Friedl, Trolrier et al., Simon et al., and Johnston et al. [112]. At 257.7 nm an average value of $(4.86 \pm 0.04) \times 10^{-18} \text{ cm}^2 \text{ molecule}^{-1}$ was calculated from the data of the Mandelman and Nicholls, Lang et al., Sander and Friedl, Trolrier et al., and Simon et al. studies. It should be noted that the cross sections in the structured region of the spectrum are extremely dependent on instrument resolution. Figure 4F-1 shows a spectrum of ClO based on the data of Sander and Friedl. The recommended absorption cross sections listed in Table 4F-2 are averages over 1 nm intervals of the continuous and banded regions of the spectrum measured at a resolution of 0.3 nm by Sander and Friedl. In Table 4F-3 the absorption cross sections for the bandheads of the $v', v'' = 1, 0$ to 21, 0 transitions measured at various spectral resolutions are compared.

The cross sections of the continuum are independent of temperature (Trolrier et al. [231]), while the structured part is extremely temperature dependent. The bands sharpen and increase in intensity with decreasing temperature. Sander and Friedl [212] measured the temperature dependence at the peak of the 12-0 sub-band in the range 220 – 400 K. Clyne and Coxon [46] determined the following relationship for the 11-0 sub-band relative to the 294 K value for the temperature range 294 – 240 K

$$\sigma_{294} / \sigma_T = 1 + 0.0036 (T - 294)$$

Maric and Burrows [136] performed an analysis of the ClO spectrum and developed an analytical approach that allows the calculation of the UV absorption spectrum as a function of temperature and spectral resolution.

Photolysis Quantum Yield and Product Studies: The calculations of Coxon et al. [50] and Langhoff et al. [122] indicate that photodecomposition of ClO accounts for at most 2 to 3% of the total destruction rate of ClO in the stratosphere, which occurs predominantly by reaction with oxygen atoms and nitric oxide. The photodissociation of thermal ClO radicals in the wavelength range $237 < \lambda < 270 \text{ nm}$ was studied by Schmidt et al. [214] using REMPI. Cl ($^2P_{3/2,1/2}$) and O(1D) were formed with unity quantum yield. The threshold wavelength for O(1D) production was determined to be 263.4 nm.



4F-2

Figure 4F-1. Absorption Spectrum of ClO

Table 4F-2. Absorption Cross Sections of ClO at 298 K

λ (nm)	$10^{20} \sigma$ (cm ²)	λ (nm)	$10^{20} \sigma$ (cm ²)	λ (nm)	$10^{20} \sigma$ (cm ²)	λ (nm)	$10^{20} \sigma$ (cm ²)
245	260	263	536	281	329	299	74.8
246	279	264	540	282	311	300	133
247	297	265	541	283	445	301	56.6
248	315	266	549	284	245	302	45.2
249	333	267	546	285	292	303	44.9
250	352	268	529	286	362	304	87.8
251	371	269	529	287	200	305	45.5
252	388	270	575	288	197	306	33.2
253	407	271	489	289	337	307	33.1
254	425	272	532	290	165	308	47.7
255	442	273	515	291	111	309	41.9
256	457	274	470	292	270	310	28.7
257	473	275	507	293	161	311	27.3
258	486	276	456	294	102	312	33.1
259	500	277	418	295	94.5	313	32.5
260	511	278	501	296	206	314	28.9
261	520	279	283	297	83.1	315	27.8
262	529	280	538	298	65.1	316	26.8

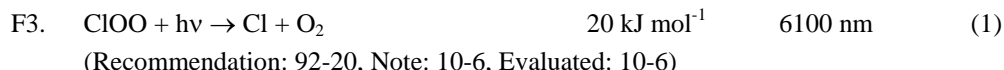
Note:

Sander and Friedl [212]: Averages over 1 nm intervals of the continuous and banded spectrum measured at 0.3 nm resolution.

Table 4F-3. Absorption Cross Sections of ClO at the band heads of the $v',v'' = 1,0$ to 21,0 bands

Band	λ (nm)	$10^{20} \sigma$ (cm ²)	λ (nm)	$10^{20} \sigma$ (cm ²)	λ (nm)	$10^{20} \sigma$ (cm ²)	λ (nm)	$10^{20} \sigma$ (cm ²)	λ (nm)	$10^{20} \sigma$ (cm ²)
v',v''	Troler et al. res. 0.6 nm		Sander, Friedl res. 0.3(0.18) nm		Simon et al. res. 0.3(0.03) nm		Mandelman res. 0.22 nm		Jourdain et al. res. 0.015 nm	
1,0			312.1	35					312.5	26
2,0	307.7	22	308.3	58	307.9	39	307.8	47	307.9	67
3,0	303.4	64	303.9	103	303.5	86	303.4	104	303.5	133
4,0	299.4	128	299.6	171	299.0	163	299.3	207	299.3	236
5,0	295.4	202	295.7	253	295.4	255	295.4	315	295.4	326
6,0	292.1	286	292.1	330	292.0	338 (400)	292.0	382	291.8	395
7,0	288.7	365	288.6	438	288.4	448 (502)	288.4	516	288.4	504
8,0	286.0	455	285.5	530	285.2	542	285.2	627	285.2	594
9,0	282.6	508	282.6	598	282.3	608	282.2	667	282.2	641
10,0	280.1	555	279.9	645	279.8	655	279.6	688	279.6	686
11,0	277.7	571	277.4	668	277.2	679	277.2	680	277.2	727
12,0	275.5	587	275.3	671 (836)	275.1	681	275.0	634	275.1	733
13,0	273.6	576	273.3	668					272.9	711
14,0	271.8	571	271.5	656						
15,0	269.9	556	270.0	640						
16,0	268.7	545	268.6	615						
17,0			267.4	603						
18,0			266.5	579						

19,0			265.6	562						
20,0			264.9	549						
21,0			264.2	543						



Absorption Cross Sections: Johnston et al. [112] measured the absorption spectrum of the ClOO radical (chlorine superoxide) using a molecular modulation technique and determined absorption cross sections using a complex kinetic scheme interpretation. More recently, Mauldin et al. [146] (220 – 280 nm, 191 K) and Baer et al. [3] (240 – 300 nm, 300 K) have reported cross section measurements. These two studies are in reasonable agreement with cross section values that are more than twice the earlier Johnston et al. [112] values. The recommended cross sections in Table 4F-4 are taken from Mauldin et al. [146].

Photolysis Quantum Yield and Product Studies: No studies are available but the photolysis quantum yield is assumed to be unity over the entire UV absorption band.

Table 4F-4. Absorption Cross Sections of ClOO at 191 K

λ (nm)	$10^{20} \sigma$ (cm ²)	λ (nm)	$10^{20} \sigma$ (cm ²)
220	611	252	2630
222	670	254	2370
224	747	256	2120
226	951	258	1890
228	1100	260	1610
230	1400	262	1370
232	1650	264	1120
234	1960	266	905
236	2240	268	725
238	2520	270	596
240	2730	272	435
242	2910	274	344
244	2960	276	282
246	2980	278	210
248	2950	280	200
250	2800		

Note:
Mauldin et al. [146]



(Recommendation: 06-2, Note: 10-6, Evaluated: 10-6)

Absorption Cross Sections: The UV/vis absorption spectrum of chlorine dioxide, OCIO, is characterized by a series of well developed progressions of bands extending from ~280 to 480 nm corresponding to the $\text{A}(^2\text{A}_2)$ (i,j,k) $\leftarrow \text{X}(^2\text{B}_1)$ (0,0,0) vibronic transitions. The spectroscopy of this molecule has been studied extensively and the quantum yield for photodissociation appears to be unity throughout the above wavelength range. See for example, the review by Watson [244]. Birks et al. [12] have estimated an atmospheric photodissociation half-life of OCIO of a few seconds. The measurement of absorption spectra at temperatures between 200 and 378 K has been the subject of many studies as summarized in Table 4F-5.

Table 4F-5. Summary OCIO Cross Section Studies

Study	Year	Type	Temperature (K)	Wavelength Range (nm)	Resolution (nm)
Martin and Gareis [141]	1956		298	263 – 414	Not given
Knauth et al. [116]	1979	A	333	270 – 440	0.3 – 1
Wahner et al. [243]	1987	A	204, 296, 378	242 – 477	0.25
Hubinger and Nee [95]	1994	R	298	240 – 477	Not given
Frost et al. [66]	1996	R	200	390 – 454	0.0015 – 0.0021
Marston et al. [140]	1998	R	298	275 – 400	0.05
Kromminga et al. [119]	2003	A	213, 233, 253	312.5 – 440.5	0.01 – 0.02
Bogumil et al. [16]	2003	R	293	290 – 460	0.25

Type:

A: Absolute cross section determination

R: Relative cross section determination

Absorption cross sections at 10 nm intervals for the region 270 – 440 nm and at 333 K have been reported by Knauth et al. [116], and for the 351.5 nm maximum at room temperature by Clyne and Coxon [46] and Basco and Dogra [46]. The absorption cross sections of Wahner et al. [243] obtained at a resolution of 0.25 nm, and at 204, 296, and 378 K have been used by Hubinger and Nee [95], Frost et al. [66] and Marston et al. [140] for the calibration of their relative spectra. The values at the peaks of the main vibrational bands $a(0)$ to $a(26)$ (i.e., $A(^2A_2)$ $(i,0,0) \leftarrow X(^2B_1)$ $(0,0,0)$, $i = 0$ to 26) reported by Wahner et al. [243] have been selected as recommended absorption cross sections of OCIO in preceding JPL evaluations. More recently, Kromminga et al. [119] reported high and medium resolution absorption spectra at five temperatures between 213 and 293 K obtained using Fourier transform spectroscopy, which has the advantage of accurate wavelength calibration. There is a clear wavelength shift (~ 0.2 – 0.5 nm) between the spectra of Kromminga et al. [119] and Wahner et al. [243] that cannot be explained by the shift between measurements in air and in vacuum. The absorption cross sections for the band peaks $a(3)$ to $a(26)$ reported by Kromminga et al. [119] are smaller by 5–10% than those reported by Wahner et al. [243]. A decrease of the temperature causes a sharpening of the vibrational bands and an increase of the peak cross sections as observed between 293 and 213 K by Kromminga et al. [119] and between 378 and 200 K by Wahner et al. [243].

The recommended absorption cross sections of OCIO in Table 4F-6 are averages over 1 nm intervals of the spectrum measured by Wahner et al. [243] (0.25 nm resolution). In Table 4F-7 are listed the $a(16)$ to $a(3)$ band peaks at 213, 233, 253, 273, and 293 K recorded in the medium resolution (0.2 – 0.4 nm) spectra by Kromminga et al. [119]. The values for the $a(17)$ to $a(23)$ bands at 293 K are the results of Bogumil et al. [16], who have measured the OCIO spectrum at medium resolution (0.24 – 0.44 nm) with the SCIAMACHY pre-flight satellite instrument and have scaled the absorption cross sections to those measured by Kromminga et al. [119]. In addition, the peak cross sections determined by Wahner et al. [243] are listed in Table 4F-8. Figure 4F-2 shows the spectrum of OCIO at 204 K based on the data of Wahner et al. [243].

VUV absorption cross sections have been measured by Basco and Morse [9], (148 – 183 nm), Flesch et al. [65] (50 – 207 nm), Hubinger and Nee [95] (127 – 183 nm), and Marston et al. [140] (115 – 191 nm).

Photolysis Quantum Yield and Product Studies: The photochemistry of OCIO is extremely complex, with several electronic excited states involved in the photodissociation dynamics. Several channels have been observed at wavelengths important in the stratosphere, including $O + ClO$, $Cl + O_2$ and isomerization to CIOO. Colussi [47] measured $\Phi(Cl)$ to be <0.01 , and $\Phi(Cl) = 1$ (within experimental error) for photolysis at 308 nm. Vaida et al. [234] and Ruhl et al. [208] reported Cl atom production at 362 nm and Bishenden et al. [13, 14] measured $\Phi(Cl)$ to be 0.15 ± 0.10 around the same wavelength. In contrast, Lawrence et al. [123] report $\Phi(Cl)$ in the 359 – 368 nm region to be $<5 \times 10^{-4}$. This conclusion is supported by photofragment studies of Davis and Lee [55] between 350 and 475 nm, who report $\Phi(Cl) < 0.2\%$ in the wavelength range 350 – 370 nm, rising to a maximum of $3.9 \pm 0.8\%$ near 404 nm. In a later study, Davis and Lee [54] report a substantial yield of $O_2(^1\Delta_g)$ and show that the branching ratio between $O + ClO$ and $Cl + O_2$ depends on the OCIO(A^2A_2) excited state vibrational mode. Delmdahl et al. [56] measured the yield of nascent Cl atoms to be below 3.6% in the photolysis in the 365 – 450 nm range. At $\lambda < 365$ nm, there was a sharp increase of the Cl yield, which was attributed to the photolysis of vibrationally excited ClO ($v \geq 4$).

The recommendation is to use a quantum yield value of unity for the production of $O(^3P)$ atoms in the range 270 – 480 nm. An upper limit for the Cl yield can be set at 0.04 for the wavelength range 365 – 450 nm.

While accurate absorption cross section values are valuable for atmospheric measurements of OCIO abundance, the identity of the photodissociation products is only of minor importance in the context of atmospheric processes.

Table 4F-6. Absorption Cross Sections of OCIO at 204 K (averages over 1 nm intervals)

λ (nm)	$10^{20} \sigma$ (cm ²)	λ (nm)	$10^{20} \sigma$ (cm ²)	λ (nm)	$10^{20} \sigma$ (cm ²)	λ (nm)	$10^{20} \sigma$ (cm ²)
247	35.6	304	96.1	361	477	418	107
248	34.4	305	276	362	173	419	75.1
249	33.7	306	328	363	179	420	81.4
250	34.6	307	190	364	207	421	323
251	34.3	308	116	365	361	422	151
252	34.6	309	85.4	366	403	423	50.0
253	34.1	310	168	367	625	424	23.8
254	34.9	311	511	368	919	425	23.3
255	34.3	312	338	369	903	426	14.5
256	34.8	313	174	370	268	427	43.8
257	34.8	314	107	371	107	428	99.5
258	35.1	315	94.2	372	180	429	46.9
259	35.0	316	239	373	170	430	44.3
260	35.8	317	686	374	364	431	23.3
261	36.5	318	360	375	376	432	47.0
262	37.5	319	176	376	554	433	173
263	38.2	320	114	377	718	434	69.6
264	38.0	321	125	378	881	435	24.6
265	38.8	322	279	379	278	436	11.2
266	39.9	323	873	380	92.4	437	7.68
267	40.4	324	443	381	135	438	9.09
268	42.3	325	192	382	148	439	5.13
269	44.6	326	121	383	266	440	12.5
270	44.3	327	147	384	298	441	47.8
271	45.7	328	221	385	440	442	23.2
272	49.9	329	838	386	345	443	14.7
273	49.1	330	782	387	762	444	7.59
274	48.1	331	285	388	591	445	3.96
275	54.8	332	155	389	173	446	46.8
276	58.3	333	147	390	71.4	447	55.2
277	52.5	334	208	391	123	448	18.4
278	54.3	335	355	392	109	449	7.17
279	67.4	336	1090	393	203	450	6.96
280	67.2	337	782	394	270	451	4.50
281	58.3	338	266	395	285	452	1.66
282	65.4	339	155	396	275	453	3.57
283	82.4	340	167	397	370	454	0.907
284	77.6	341	250	398	653	455	13.3
285	67.2	342	414	399	225	456	9.70
286	77.7	343	925	400	70.1	457	4.76
287	100	344	1090	401	45.6	458	4.25
288	93.7	345	388	402	96.9	459	3.98
289	79.4	346	176	403	56.3	460	1.84
290	90.5	347	161	404	196	461	17.1
291	127	348	258	405	194	462	17.9
292	116	349	320	406	185	463	11.8
293	90.9	350	581	407	160	464	10.0
294	94.1	351	1100	408	158	465	4.01
295	147	352	993	409	493	466	1.40
296	172	353	330	410	210	467	2.53

λ (nm)	$10^{20} \sigma$ (cm ²)	λ (nm)	$10^{20} \sigma$ (cm ²)	λ (nm)	$10^{20} \sigma$ (cm ²)	λ (nm)	$10^{20} \sigma$ (cm ²)
297	122	354	164	411	71.6	468	10.1
298	92.0	355	190	412	34.0	469	15.0
299	106	356	276	413	46.8	470	7.69
300	226	357	343	414	44.6	471	6.14
301	222	358	597	415	30.0	472	3.18
302	143	359	830	416	164		
303	94.3	360	1210	417	100		

Note:

Wahner et al. [243]

Table 4F-7. Absorption Cross Sections of OCIO at the a(21) to a(3) Band Peaks at Temperatures in the Range 213 – 293 K

Band peak	λ (nm)	$10^{20} \sigma$ (cm ²)	λ (nm)	$10^{20} \sigma$ (cm ²)	λ (nm)	$10^{20} \sigma$ (cm ²)	λ (nm)	$10^{20} \sigma$ (cm ²)	λ (nm)	$10^{20} \sigma$ (cm ²)
	T = 213 K		T = 233 K		T = 253 K		T = 273 K		T = 293 K	
a(21)									292.05	79.32
a(20)									295.79	107.60
a(19)									300.96	171.03
a(18)									306.12	273.85
a(17)									311.58	391.16
a(16)									316.86	528.84
a(15)	322.96	846.62	322.96	812.45	323.02	786.75	323.02	756.88	323.02	707.16
a(14)	329.49	1054.25	329.49	1011.91	329.55	984.42	329.55	945.36	329.55	892.88
a(13)	336.41	1224.61	336.41	1181.30	336.41	1148.79	336.48	1098.73	336.48	1044.48
a(12)	343.77	1313.77	343.77	1269.99	343.77	1243.47	343.77	1189.35	343.77	1134.36
a(11)	351.53	1328.23	351.53	1289.25	351.53	1265.01	351.53	1212.13	351.53	1164.23
a(10)	359.73	1280.34	359.73	1243.39	359.73	1220.29	359.73	1171.14	359.73	1127.62
a(9)	368.39	1187.04	368.39	1153.33	368.39	1128.23	368.39	1083.63	368.47	1045.41
a(8)	377.56	1048.31	377.56	1019.56	377.56	992.21	377.56	951.69	377.65	916.95
a(7)	387.29	869.95	387.29	849.00	387.29	818.37	387.29	783.53	387.38	750.49
a(6)	397.90	696.60	397.99	683.65	397.90	661.61	397.99	643.31	397.99	619.46
a(5)	408.82	523.40	408.82	518.32	408.82	488.85	408.92	473.08	408.92	452.82
a(4)	420.56	350.83	420.45	350.30	420.45	319.18	420.45	317.13	420.45	301.27
a(3)	432.88	220.71	432.99	197.98	432.99	174.81	432.99	194.21	432.99	189.51

Note:

292 – 317 nm: Bogumil et al. [16]

323 – 433 nm: Kromminga et al. [119]

Table 4F-8. Absorption Cross Sections of OCIO at the Band Peaks

λ (nm)	$10^{20} \sigma \text{ (cm}^2\text{)}$		
	204 K	296 K	378 K
475.53		13	
461.15	17	17	16
446.41	94	69	57
432.81	220	166	134
420.58	393	304	250
408.83	578	479	378
397.76	821	670	547
387.37	1046	844	698
377.44	1212	992	808
368.30	1365	1136	920
359.73	1454	1219	984
351.30	1531	1275	989
343.44	1507	1230	938
336.08	1441	1139	864
329.22	1243	974	746
322.78	1009	791	628
317.21	771	618	516
311.53	542	435	390
305.99	393	312	291
300.87	256	219	216
296.42	190	160	167
291.77	138	114	130
287.80	105	86	105
283.51	089	72	90
279.64	073	60	79
275.74	059	46	
272.93	053	33	

Note:
Wahner et al. [243]

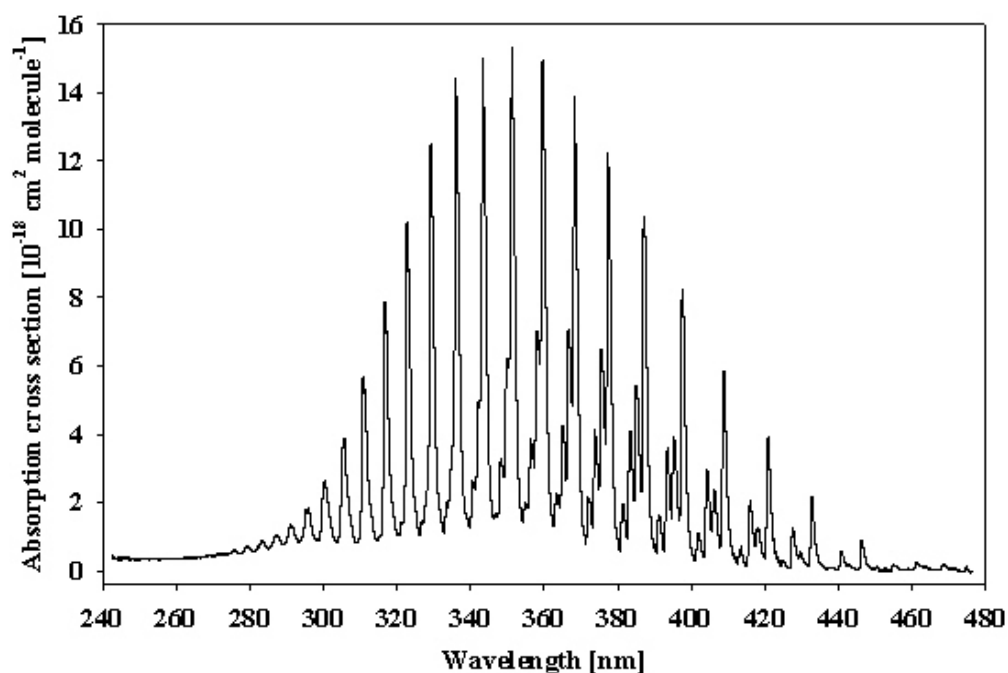


Figure 4F-2. Absorption Spectrum of OCIO at 204 K

F5. $\text{ClO}_3 + h\nu \rightarrow \text{Products}$

(Recommendation: 06-2, Note: 10-6, Evaluated: 10-6)

Absorption Cross Sections: The JPL-83 to JPL-90 recommendations for the absorption cross sections of the ClO_3 radical were based on the work of Goodeve and Richardson [79]. Lopez and Sicre [132] have, however, since shown that the spectrum reported by Goodeve and Richardson is most likely that of Cl_2O_6 . Thermochemical estimates by Colussi et al. [48] further corroborate this assignment.

Grothe and Willner [86], [87] have reported the UV and IR spectra of ClO_3 trapped in a neon matrix following thermal decomposition of Cl_2O_4 or FOClO_3 . By monitoring the amount of ClO formed as a photolysis product of ClO_3 , they determined the absorption cross sections in the range 250 – 500 nm. The spectrum has a highly structured absorption band around 320 nm ($\sigma \approx 3 \times 10^{-18} \text{ cm}^2 \text{ molecule}^{-1}$) and a second band around 425 nm ($\sigma \approx 2.5 \times 10^{-18} \text{ cm}^2 \text{ molecule}^{-1}$) as depicted in the review article of Wayne et al. [245]. A broad absorption spectrum between 280 and 450 nm peaking at $\approx 300 \text{ nm}$ ($\sigma \approx 1.8 \times 10^{-17} \text{ cm}^2 \text{ molecule}^{-1}$) was recorded for ClO_3 formed by radiolysis of aqueous solutions of chlorate ions. No recommendation is given for the absorption cross sections of ClO_3 in the gas phase.

Photolysis Quantum Yield and Product Studies: No studies are available.

F6.	$\text{Cl}_2\text{O} + h\nu$	$\rightarrow \text{Cl} + \text{ClO}$	142 kJ mol^{-1}	844 nm	(1)
		$\rightarrow \text{Cl}_2 + \text{O}(^3\text{P})$	168 kJ mol^{-1}	712 nm	(2)
		$\rightarrow \text{Cl}_2 + \text{O}(^1\text{D})$	356 kJ mol^{-1}	335 nm	(3)
		$\rightarrow \text{O} + 2\text{Cl}$	411 kJ mol^{-1}	291 nm	(4)

(Recommendation: 06-2, Note: 10-6, Evaluated: 10-6)

Absorption Cross Sections: The UV/vis absorption spectrum of dichlorine monoxide, Cl_2O , has been measured at room temperature by Goodeve and Wallace [80] (230 – 620 nm), Finkelnburg et al. [64] (220 – 650 nm), Martin and Gareis [141] (234 – 331 nm), Lin [128] (180 – 640 nm), Molina and Molina [157] (200 – 450 nm), Simon et al. [218] (236 – 320 nm), and Smith et al. [222] (190 – 399 nm). The earlier data reported by Goodeve and Wallace [80], Finkelnburg et al. [64], and Martin and Gareis [141] deviate substantially from the more recent results and are not considered further in this evaluation. Johnsson et al. [111] (210 – 350 nm) measured the absorption spectrum in Ar matrices and reported a gas-phase absorption cross section at 260 nm. Measurements at 298 and 333 K have been carried out by Knauth et al. [116] (200 – 500 nm). The spectrum exhibits three absorption bands in the UV/vis region. An asymmetrical band between ~ 220 – 380 nm with the maximum near 255 nm and a shoulder near 290 nm, and two weak bands at ~ 380 – 500 nm and ~ 500 – 650 nm with maxima near 420 nm and 550 nm, respectively. The absorption cross sections measured by Lin et al. [128], Molina and Molina [157], Knauth et al. [116], and Smith et al. [222] are in very good agreement, i.e., within 10%, for the UV absorption band between 200 and $\sim 350 \text{ nm}$. The values reported by Molina and Molina [157] and Knauth et al. [116] are somewhat larger than those reported by Lin [128], which are larger than those reported by Smith et al. [222]. The discrepancies between the various data sets are larger in the region of the absorption minimum. The spectrum measured by Simon et al. [218] has been normalized to the data of Lin [128].

The recommended absorption cross sections listed in Table 4F-9 are based on the data from Lin [128], Molina and Molina [157], Knauth et al. [116], and Smith et al. [222] in the region 200 – 350 nm, the mean of the data from Lin [128], Molina and Molina [157], and Knauth et al. [116] in the region 360 – 450 nm, the mean of the data from Lin [128] and Knauth et al. [116] in the region 460 – 500 nm, and the data from Lin [128] in the region 510 – 640 nm.

VUV absorption cross sections have been measured by Nee [170] (150 – 200 nm) and Motte-Tollet et al. [165] (128 – 190 nm).

Photolysis Quantum Yield and Product Studies: Sander and Friedl [212] have measured the quantum yield for production of O atoms to be 0.25 ± 0.05 , using a broadband photolysis source extending from 180 nm to beyond 400 nm. The main photolysis products are Cl and ClO. Using a molecular beam technique, Nelson et al. [172] found $\text{Cl} + \text{ClO}$ to be the only primary photodissociation channel at 308 nm, a major channel at 248 nm, and a minor channel at 193 nm. At 248 nm a fraction of the photoproduct ClO underwent spontaneous photodissociation. These authors find evidence that the dissociation to three atoms $2\text{Cl} + \text{O}$ takes place at 193 nm and that some $\text{O}(^1\text{D})$ atoms are generated as well. Nickolaisen et al. [175] reported that broadband photolysis at wavelengths $>300 \text{ nm}$ results in pressure-dependent ClO quantum yields, which was explained by the rapid intersystem crossing between two metastable states. These states undergo competitive dissociation to $\text{ClO} + \text{Cl}$ and collisional relaxation to the ground state. Furthermore, these authors detected a

transient absorption spectrum, which was assigned to a long-lived metastable triplet state of Cl₂O. However, Moore et al. [162] estimated the lifetime of the metastable excited state to be much shorter. Chichinin [41] and Tanaka et al. [227] found evidence of ground state (²P_{3/2}) and spin-orbit excited (²P_{1/2}) atomic chlorine photoproducts. The implication is that the photodecomposition quantum yield is less than unity at atmospherically relevant wavelengths in spite of the continuous nature of the absorption spectrum.

Table 4F-9. Absorption Cross Sections of Cl₂O at 298 K

λ (nm)	10 ²⁰ σ (cm ²)	λ (nm)	10 ²⁰ σ (cm ²)	λ (nm)	10 ²⁰ σ (cm ²)
200	67.7	350	1.84	500	0.218
210	22.4	360	0.893	510	0.210
220	8.42	370	0.493	520	0.214
230	26.5	380	0.446	530	0.237
240	101	390	0.575	540	0.256
250	184	400	0.829	550	0.256
260	186	410	1.08	560	0.222
270	144	420	1.25	570	0.203
280	121	430	1.23	580	0.176
290	98.9	440	1.10	590	0.149
300	68.1	450	0.848	600	0.122
310	38.6	460	0.625	610	0.0956
320	18.7	470	0.446	620	0.0688
330	8.59	480	0.313	630	0.0344
340	3.90	490	0.247	640	0.0153

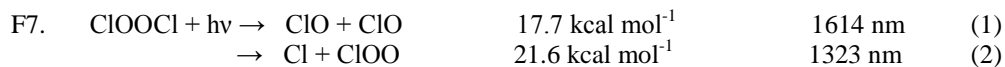
Note:

200 – 350 nm: mean of the data from Lin [128], Molina and Molina [157], Knauth et al. [116], and Smith et al. [222]

360 – 450 nm: mean of the data from Lin [128], Molina and Molina [157], and Knauth et al. [116]

460 – 500 nm: mean of the data from Lin [128] and Knauth et al. [116]

510 – 640 nm: data from Lin [128]



(Recommendation: 10-6, Note: 10-6, Evaluated: 10-6)

Absorption Cross Sections: The gas-phase UV absorption spectrum of ClOOC is continuous with a maximum near 245 nm, a minimum near 218 nm, and a weak diffuse shoulder in the wavelength region 280 – 300 nm. There are a number of studies that have reported UV absorption data for ClOOC over a range of wavelengths or at specific wavelengths. Table 4F-10 summarizes the currently available studies. The ClOOC UV absorption spectra reported by Basco and Hunt [8] and Molina and Molina [159] have been shown to contain systematic errors and are not considered further in this evaluation. In laboratory studies, ClOOC has been produced in the gas-phase at low temperature as a product of the termolecular ClO radical self-reaction, $\text{ClO} + \text{ClO} + \text{M}$. Studies, to date, indicate that only one stable isomer of Cl₂O₂ is produced in the ClO self-reaction and that this species is dichlorine peroxide, ClOOC, rather than ClOCIO or ClClO₂. Using sub-millimeter wave spectroscopy, Birk et al. [11] have further established the structure of the reaction product to be ClOOC. This is in general agreement with the quantum mechanical calculations of McGrath et al. [147, 148], Jensen and Odersheide [109], and Stanton et al. [224] although the recent theoretical study by Matus et al. [145] found the ClClO₂ isomer to be more stable than ClOOC by 3.1 kcal mol⁻¹ at 298 K.

Table 4F-10. Summary of ClOOCl UV Absorption Spectrum Studies

Study	Year	Temperature (K)	λ (nm)	$10^{20} \sigma(\lambda)$ (cm ²)
Cox and Hayman [49]	1988	200 – 300	220 – 360	640 ± 60*
Permien et al. [185]	1988	235	211 – 290	— ^{\$}
Burkholder et al. [26]	1990	205 – 250	212 – 410	650 +80/-50*
DeMore and Tschuikow-Roux [57]	1990	206	190 – 400	680 ± 80*
Vogt and Schindler [240]	1990	230	204 – 350	— ^{\$}
Huder and DeMore [99]	1995	195	200 – 310	— ^{\$,@}
Bloss et al. [15]	2001	183 – 245	210	294 ± 86
McKeachie et al. [149]	2004	223	235 – 400	— ^{\$}
Pope et al. [188]	2008	193	226 – 355	— ^{\$}
von Hobe et al. [242]	2009	10	220 – 400	— ^{\$.#}
Chen et al. [36]	2009	200	308	49 ^{&}
		250	308	50.9
		200	351	11.2
		250	351	12.6
Lien et al. [126]	2009	160	248.4	890 ^{&}
		200	248.4	885
		260	248.4	873
Wilmouth et al. [248]	2009	240 ± 10	248	660 ± 100 ^{&&}
			308	39.3 ± 4.9
			352	8.6 ± 1.2
Papanastasiou et al. [183]	2009	200 - 228	200 - 420	760 +80/-50*
Jin et al. [110]	2010	200	330	23.1 ^{&}
		250	330	24.7

* Absorption cross section values at the peak of the spectrum, ~245 nm. Cross section data also given over the reported range of wavelengths. ^{\$} Reported ClOOCl absorption spectrum without absolute cross section determination. [#] Solid-phase ClOOCl absorption spectrum measured in a Ne matrix. [@] ClOOCl absorption spectrum at wavelengths reported at >310 obtained using a log-linear extrapolation. [&] ClOOCl cross section obtained assuming a unit photolysis quantum yield. ^{&&} Product of absorption cross section and Cl-atom-producing channel: $\sigma \times \phi_{\text{Cl}}$.

Cox and Hayman [49], Burkholder et al. [26], DeMore and Tschuikow-Roux [57], Bloss et al. [15], and Papanastasiou et al. [183] report absolute ClOOCl cross section, $\sigma(\lambda)$, values over a substantial range of wavelengths. The studies of Permien et al. [185], Vogt and Schindler [240], Huder and DeMore [99], McKeachie et al. [149], and Pope et al. [188] report absorption spectra normalized to 245 nm. von Hobe et al. [242] report a solid-phase ClOOCl UV absorption spectrum measured in a Ne matrix at ~10 K with reported cross sections obtained by normalization using the 245 nm cross section recommended in JPL 06-2 [211] for the gas-phase spectrum.

Discrepancies in the wavelength dependence of the ClOOCl absorption spectrum at wavelengths >300 nm, the region that is most critical for atmospheric photolysis rate calculations, exist and most likely originate from uncertainties in corrections for spectral interferences by reactant precursors (O₃, Cl₂O, and Cl₂) and impurities (OCIO, Cl₂, and Cl₂O₃) formed in the ClOOCl source chemistry. Near the peak, the reported spectra are in reasonable agreement. The studies of Cox and Hayman, Burkholder et al., DeMore and Tschuikow-Roux, Vogt and Schindler, and McKeachie et al. show systematic deviations that are possibly consistent with spectral interference due to minor absorption by Cl₂O and, in the cases of Cox and Hayman, Burkholder et al., and McKeachie et al., possibly Cl₂O₃. At λ >300 nm, the ClOOCl spectrum is weaker and more sensitive to spectral interferences from impurities, in particular Cl₂. The studies of Burkholder et al. and DeMore and Tschuikow-Roux are the only pre-2007 gas-phase studies that report cross section data at λ > 360 nm. Pope et al. developed a method to isolate bulk samples of ClOOCl in which ClOOCl is produced in the gas-phase and condensed at low temperatures. Pope et al. measured gas-phase UV spectra that are due

mostly to Cl_2 and ClOOCl absorption following the warming of the condensate. The spectra were analyzed using a Gaussian fitting procedure and they report a ClOOCl absorption spectrum that decreases rapidly at $\lambda > 320$ nm with a cross section at 350 nm that is a factor of 6 lower than recommended in JPL-2006. The von Hobe et al. matrix study used the Pope et al. method to prepare their ClOOCl samples and Raman spectroscopy to evaluate the spectral contribution from Cl_2 impurities. They report a ClOOCl spectrum with significant absorption at wavelengths out to 400 nm. von Hobe et al. suggest that Pope et al. mistakenly attributed a long-wavelength ClOOCl spectral feature to Cl_2 impurity.

The recent study of Papanastasiou et al. [183], which is in generally good agreement with the earlier studies, was carried out using diode array spectroscopy and laser photolysis to generate ClO radicals. The spectral analysis utilized reaction stoichiometry and three observed isosbestic points to account for chemical species, including Cl_2 , which appear to represent an interference to a greater or lesser degree in all pre-2009 studies. The isosbestic point observed at 408.5 nm shows that ClOOCl absorbs measurably at wavelengths longer than 350 nm.

Lower limits to the absolute cross sections have been measured recently at specific wavelengths by a new experimental method involving pulsed laser photolysis of ClOOCl in a molecular beam combined with mass spectrometric detection to determine $\sigma(\lambda)\Phi(\lambda)$, where $\Phi(\lambda)$ is the ClOOCl photolysis quantum yield (see Chen et al. [36]). This new method is not sensitive to spectral interference from Cl_2 . It yields the lower-limit for the ClOOCl cross sections, assuming $\Phi(\lambda) = 1$, which is thought to be a very good assumption. Measurements by Chen et al. [36], Lien et al. [126], and Jin et al. [110] are slightly higher than, but in good agreement with, the data of Papanastasiou et al. [183]. Measurements over limited temperature ranges indicate that the cross sections are only weakly dependent on temperature.

Wilmouth et al. [248] used flow-tube and atomic resonance fluorescence techniques to measure Cl -atom production when ClOOCl is photolyzed at 248, 308, and 352 nm. By scaling their signals to the known Cl -atom yield in the photolysis of Cl_2 or the literature cross section at the peak of the ClOOCl absorption spectrum, they obtained the product of the ClOOCl absorption cross section and the quantum yield for the Cl -atom production channel, $\sigma(\lambda)\phi_{\text{Cl}}(\lambda)$, at the three wavelengths. It is noteworthy that the Cl_2 concentration was monitored in situ using fluorescence excited by the resonance lamp, and appropriate corrections to the Cl -atom yields were made. By assuming $\phi_{\text{Cl}}(\lambda) = 1$, they obtain the lower limit to the absorption cross section. Analyzed in this way, their lower limit cross sections at the three wavelengths are a little lower than the cross sections reported by Papanastasiou et al. [183], although the agreement is better when quantum yields (see below) are considered.

The recommended ClOOCl absorption cross sections are based on the measurements of Papanastasiou et al. [183] (which were corrected on the basis of the isosbestic analysis), Wilmouth et al. [247] (which were corrected on the basis of in situ monitoring of Cl_2), and Chen et al. [36], Lien et al. [126], and Jin et al. [110] (which are not susceptible to interfering species). The data of Papanastasiou et al. [183] and Wilmouth et al. [248] tend to be a little higher than the previous measurements, but somewhat lower than the measurements of Chen et al. [36], Lien et al. [126], and Jin et al. [110]. Bloss et al. [15] measured a value for $\sigma(210 \text{ nm})$ in a pulsed photolysis $\text{ClO} + \text{ClO} + \text{M}$ kinetics study over the temperature range 183 – 245 K that is similar to the current recommendation. The recommended values (taken from Papanastasiou et al. [183]) for the temperature range 190 – 250 K are listed in Table 4F-11. Data at $\lambda > 420$ nm can be estimated from the formula $\sigma(\lambda) = 9.5 \times 10^{-16} \times \exp(-0.0281 \times \lambda)$, where λ is in nm and σ is in units of $\text{cm}^2 \text{ molecule}^{-1}$.

Cross-Section Uncertainties: Over the wavelength range 200 – 300 nm, we estimate the uncertainty in $\sigma(\lambda)$ to be $\pm 35\%$. The estimated uncertainty increases towards longer wavelengths and the upper and lower limits for cross section $\sigma(\lambda > 300 \text{ nm})$ are given by: $\sigma(\lambda)^+ = 1.35 \times \sigma(\lambda) \times \exp[-(\lambda - 300) / 200]$ and $\sigma(\lambda)^- = 1 / (1.35 \times \sigma(\lambda) \times \exp[-(\lambda - 300) / 100])$. The estimated error limits cover a range that includes the values reported by Burkholder et al. (upper limit) and the measured values ($\lambda \leq 310$) of Huder and DeMore (lower limit). Further studies of the peak cross section as well as the spectrum at $\lambda > 300$ nm would be desirable in order to reduce uncertainties in the calculated atmospheric photolysis rate of ClOOCl .

Photolysis Quantum Yields and Product Studies: Molina et al. [160] reported a quantum yield, Φ , of approximately unity (1.03 ± 0.12) for the $\text{Cl} + \text{ClOO}$ pathway from a flash photolysis study at 308 nm, in which the yield of Cl atoms was measured using time-resolved atomic resonance fluorescence. These results are in agreement with the steady-state photolysis study of Cox and Hayman [49]. Plenge et al. [187] measured the primary products from ClOOCl photolysis at 250 and 308 nm using photoionization mass spectrometry. At both wavelengths $2\text{Cl} + \text{O}_2$ was observed as the exclusive product channel corresponding to a primary Cl quantum yield near unity at 250 nm ($\Phi_{\text{Cl}} \geq 0.98$) and at 308 nm ($\Phi_{\text{Cl}} \geq 0.90$). At both photolysis wavelengths the pathway leading to ClO was not observed corresponding to $\Phi_{\text{ClO}} \leq 0.02$ at 250 nm and $\Phi_{\text{ClO}} \leq 0.10$ at 308

nm.

In a molecular beam/flash-photolysis study Moore et al. [163] used photofragment translational spectroscopy to measure the relative Cl:CIO product yields from which they derived branching ratios for both photolysis channels $\text{ClOO} + \text{Cl}$ and $\text{ClO} + \text{ClO}$. At 248 nm, they obtained 0.88 ± 0.07 and 0.12 ± 0.07 respectively, and at 308 nm, 0.90 ± 0.1 and 0.10 ± 0.01 . In a very recent study, Huang et al. [94] also used photofragment translational spectroscopy to re-measure the branching ratios reported by Moore et al. The new results confirm and extend those of Moore et al. Huang et al. identified three product channels: (a) $2 \text{Cl} + \text{O}_2$, (b) 2ClO , and (c) $\text{ClO} + \text{Cl} + \text{O}$. The branching ratios among these product channels are 0.82, 0.08, and 0.10 at 248.4 nm, and 0.81, 0.19, and 0.00 at 308.4 nm. These results suggest that the branching ratio of channel-a is only weakly dependent on λ and that of channel-c arises from fragmentation of highly excited ClO radicals; at longer wavelengths, there is not enough available energy to break the bond.

Recommendations: Quantum yield of channel-a $\Phi_a = 0.8 (\pm 0.1)$ at all λ ; $\Phi_b + \Phi_c = 0.2 (\pm 0.1)$ at all λ ; $\Phi_c = 0.0 (\pm 0.1)$ at $\lambda > 300$ nm. Additional determinations of photolysis quantum yields and product branching ratios at wavelengths longer than 300 nm would be desirable.

Theoretical Studies: Toniolo et al. [229], Peterson and Francisco [186], and Matus et al. [145] report theoretical calculations for the electronic transitions of the ClOOCl UV absorption spectrum that include transitions to excited singlet and triplet states. Peterson and Francisco report that the strongest triplet transition is dissociative to $\text{Cl} + \text{ClOO}$, centered near 385 nm, and is three orders of magnitude weaker than the strongest singlet transition at shorter wavelengths. Kalekin and Morokuma [115] studied the ClOOCl photodissociation dynamics and predict the synchronous and sequential formation of $2 \text{Cl} + \text{O}_2$ at 308 nm, and three possible fragmentation routes at 248 nm: $2 \text{Cl} + \text{O}_2$, $\text{Cl} + \text{O}(^3\text{P}) + \text{ClO}$, and $2 \text{Cl} + 2\text{O}(^3\text{P})$. Similar theoretical calculations performed by Toniolo et al. [228] for excitation at 264, 325 and 406 nm found that $2 \text{Cl} + \text{O}_2$ was produced at all wavelengths with only a small yield of 2ClO at the shortest wavelength.

Table 4F-11. Absorption Cross Sections of ClOOCl

λ (nm)	$10^{20} \sigma$ (cm^2)	λ (nm)	$10^{20} \sigma$ (cm^2)	λ (nm)	$10^{20} \sigma$ (cm^2)	λ (nm)	$10^{20} \sigma$ (cm^2)
200	423	256	549	312	38.2	368	5.23
202	395	258	495	314	35.3	370	4.77
204	362	260	445	316	32.8	372	4.35
206	331	262	400	318	30.4	374	3.95
208	303	264	360	320	28.2	376	3.60
210	277	266	325	322	26.3	378	3.27
212	255	268	294	324	24.7	380	2.97
214	238	270	268	326	23.2	382	2.70
216	228	272	246	328	21.9	384	2.45
218	225	274	225	330	20.7	386	2.24
220	232	276	206	332	19.5	388	2.04
222	249	278	189	334	18.4	390	1.87
224	277	280	173	336	17.3	392	1.71
226	316	282	158	338	16.3	394	1.58
228	366	284	144	340	15.4	396	1.47
230	424	286	131	342	14.5	398	1.36
232	488	288	119	344	13.6	400	1.26
234	555	290	108	346	12.7	402	1.18
236	618	292	98.2	348	11.9	404	1.11
238	674	294	88.9	350	11.1	406	1.05
240	719	296	80.5	352	10.3	408	0.988
242	747	298	72.9	354	9.55	410	0.933
244	758	300	66.1	356	8.82	412	0.878
246	753	302	59.9	358	8.10	414	0.831
248	732	304	54.4	360	7.43	416	0.778

λ (nm)	$10^{20} \sigma$ (cm ²)	λ (nm)	$10^{20} \sigma$ (cm ²)	λ (nm)	$10^{20} \sigma$ (cm ²)	λ (nm)	$10^{20} \sigma$ (cm ²)
250	697	306	49.7	362	6.81	418	0.738
252	651	308	45.4	364	6.24	420	0.712
254	601	310	41.6	366	5.72	>420	(see Note)

Note: Recommendation based on Papanastasiou et al. [183] For wavelengths from >420 nm, use the extrapolation formula $\sigma(\lambda) = 9.5 \times 10^{-16} \times \exp(-0.0281 \times \lambda)$, where λ is in nm and σ is in units of cm² molecule⁻¹.

F8. Cl₂O₃ + hv → Products

(Recommendation: 06-2, Note: 10-6, Evaluated: 10-6)

Absorption Cross Sections: The UV absorption spectrum of Cl₂O₃ (dichlorine trioxide, chlorine sesquioxide, chlorine chlorate) has been measured by Lipscomb et al. [129] (257.7 nm) at 293 K, Hayman and Cox [90] (220 – 335 nm) at 233 K, Burkholder et al. [25] (220 – 320 nm) in the range 200 – 260 K, Harwood et al. [89] (220 – 330 nm) at 223 K, and Green et al. [85] (201 – 320 nm) at 298 K. The spectrum has a strong band centered near 265 nm and evidence for another band at shorter wavelengths. Overall, the agreement among the various studies in terms of the absolute absorption cross sections and the wavelength dependence of the spectrum is poor. Hayman and Cox [89] report the largest peak absorption cross section and Green et al. [85] report the lowest, ~30% lower. The spectra from Green et al. [85] and Burkholder et al. [25] are in reasonable agreement and have significantly lower cross sections in the long wavelength region than reported by Harwood et al. [89] and Hayman and Cox [321]. The recommended absorption cross sections in Table 4F-12 were obtained by averaging the cross section data from Hayman and Cox [90], Burkholder et al. [25], Harwood et al. [89], and Green et al. [85].

Photolysis Quantum Yield and Product Studies: No studies are available but absorption in the UV is expected to lead to unit photodissociation.

Table 4F-12. Absorption Cross Sections of Cl₂O₃ at 220 – 260 K

λ (nm)	$10^{20} \sigma$ (cm ²)	λ (nm)	$10^{20} \sigma$ (cm ²)	λ (nm)	$10^{20} \sigma$ (cm ²)
220	1145	255	1443	290	763
225	1113	260	1596	295	566
230	1060	265	1661	300	417
235	1028	270	1614	305	294
240	1044	275	1464	310	212
245	1127	280	1239	315	159
250	1271	285	995	320	132

Note:

220 – 320 nm: mean of the data from Hayman and Cox [90], Burkholder et al. [25], Harwood et al. [89], and Green et al. [85]

F9. Cl₂O₄ + hv → Products

(Recommendation: 06-2, Note: 10-6, Evaluated: 10-6)

Absorption Cross Sections: The UV absorption spectrum of Cl₂O₄ (dichlorine tetraoxide, chlorine perchlorate) has been measured at room temperature by Lopez and Sicre [131] (200 – 310 nm) and Green et al. [84] (200 – 350 nm). The absorption spectrum has a weak band between 303 and 350 nm with a maximum at 327 nm, a stronger band between 212 and 303 nm with a maximum at 233 nm, and a further increase in cross section below 212 nm. The absorption cross sections reported by Lopez and Sicre [131] and Green et al. [84], who applied a similar method of preparing Cl₂O₄, are in good agreement in the region ~215 – 250 nm. Discrepancies in the cross section data are apparent below 215 nm, where the values of Lopez and Sicre [131] are larger by as much as a factor ~1.7 at 200 nm and at wavelengths >260 nm. The recommended absorption cross sections in Table 4F-13 are from Green et al. [84] which is thought to be the more accurate measurement.

Photolysis Quantum Yield and Product Studies: No studies are available.

Table 4F-13. Absorption Cross Sections of Cl₂O₄ at 298 K

λ (nm)	$10^{20} \sigma$ (cm ²)	λ (nm)	$10^{20} \sigma$ (cm ²)	λ (nm)	$10^{20} \sigma$ (cm ²)	λ (nm)	$10^{20} \sigma$ (cm ²)
200	96.81	238	84.94	276	9.95	314	1.35
202	87.88	240	80.97	278	8.38	316	1.49
204	77.84	242	76.05	280	6.98	318	1.62
206	73.24	244	70.95	282	5.76	320	1.74
208	67.51	246	65.17	284	4.70	322	1.83
210	64.62	248	59.53	286	3.79	324	1.91
212	61.79	250	53.84	288	3.03	326	1.96
214	61.74	252	48.55	290	2.40	328	1.98
216	63.46	254	43.30	292	1.89	330	1.96
218	66.58	256	38.52	294	1.50	332	1.92
220	70.82	258	34.33	296	1.21	334	1.85
222	74.95	260	30.28	298	1.01	336	1.75
224	79.70	262	26.63	300	0.88	338	1.63
226	83.84	264	23.55	302	0.83	340	1.50
228	87.21	266	20.58	304	0.83	342	1.36
230	89.19	268	17.97	306	0.88	344	1.23
232	90.06	270	15.81	308	0.97	346	1.11
234	89.67	272	13.62	310	1.08	348	1.02
236	87.86	274	11.77	312	1.21	350	0.98

Note:

200 – 350 nm: Green et al. [84]

F10. Cl₂O₆ + hν → Products

(Recommendation: 06-2, Note: 10-6, Evaluated: 10-6)

Absorption Cross Sections: The UV/vis absorption spectrum of chlorine hexoxide, Cl₂O₆, has been measured at room temperature by Lopez and Sicre [132] (200 – 386 nm), Jansen et al. [108] (268 nm), and Green et al. [84] (200 – 450 nm). The spectrum reported by Goodeve and Richardson [79] and attributed to ClO₃ was shown by Lopez and Sicre [132] to most likely be that of Cl₂O₆. The cross sections measured by Lopez and Sicre [132] are several times larger than those reported by Goodeve and Richardson [79] but the shape of the spectrum is similar. There is excellent agreement between the data of Lopez and Sicre [132] and Green et al. [84] at wavelengths between 210 and 310 nm. At 200 nm the data from Green et al. [84] are smaller by ~10% than those of Lopez and Sicre [132]. At longer wavelengths the Green et al. [84] cross section data are larger with the difference increasing with increasing wavelength up to a factor ~3 at 380 nm. The recommended absorption cross sections in Table 4F-14 are taken from Green et al. [84].

Photolysis Quantum Yield and Product Studies: No studies are available

Table 4F-14. Absorption Cross Sections of Cl₂O₆ at 298 K

λ (nm)	$10^{20} \sigma$ (cm ²)	λ (nm)	$10^{20} \sigma$ (cm ²)	λ (nm)	$10^{20} \sigma$ (cm ²)	λ (nm)	$10^{20} \sigma$ (cm ²)
200	1104	248	1085	296	1173	344	195
202	1135	250	1111	298	1115	346	180
204	1161	252	1142	300	1056	348	167
206	1208	254	1177	302	997	350	153
208	1233	256	1217	304	939	352	141
210	1254	258	1256	306	880	354	130
212	1261	260	1297	308	822	356	121
214	1266	262	1337	310	767	358	111
216	1260	264	1375	312	714	360	103
218	1245	266	1410	314	664	362	96
220	1230	268	1440	316	615	364	89
222	1207	270	1466	318	569	366	81
224	1182	272	1485	320	526	368	75
226	1156	274	1496	322	485	370	71
228	1132	276	1500	324	447	372	66
230	1108	278	1497	326	412	374	61
232	1086	280	1488	328	380	376	57
234	1066	282	1469	330	350	378	52
236	1052	284	1444	332	322	380	49
238	1042	286	1411	334	296	382	46
240	1039	288	1373	336	271	384	43
242	1041	290	1329	338	251	386	40
244	1049	292	1281	340	231	388	37
246	1065	294	1229	342	212	390	36

Note:

200 – 390 nm: Green et al. [84]

F11. Cl₂O₇ + h ν → Products

(Recommendation: 06-2, Note: 10-6, Evaluated: 10-6)

Absorption Cross Sections: The UV absorption spectrum of chlorine heptoxide, Cl₂O₇, has been measured at room temperature by Goodeve and Windsor [81] (222 – 302 nm) and Lin [128] (180 – 310 nm). Although both studies report a spectrum with monotonically decreasing absorption cross sections with increasing wavelength, there is poor agreement between the two data sets. The cross sections reported by Goodeve and Windsor [81] are larger at wavelengths <290 nm than those reported by Lin [128] with a difference of a factor of 4 at 225 nm. At wavelengths >290 nm, the cross sections reported by Goodeve and Windsor [81] are smaller than those of Lin [128]. The recommended absorption cross sections in Table 4F-15 are taken from Lin [128].

Photolysis Quantum Yield and Product Studies: No studies are available.

Table 4F-15. Absorption Cross Sections of Cl₂O₇ at 298 K

λ (nm)	$10^{20} \sigma$ (cm ²)	λ (nm)	$10^{20} \sigma$ (cm ²)	λ (nm)	$10^{20} \sigma$ (cm ²)
180	1188	225	79.7	270	3.77
185	908.5	230	61.0	275	2.57
190	674.7	235	45.6	280	1.70
195	475.3	240	34.6	285	1.20
200	322	245	24.7	290	0.705
205	231	250	17.5	295	0.521
210	169	255	12.0	300	0.368
215	132	260	7.74	305	0.203
220	102	265	5.37	310	0.104

Note:

F12. $\text{ClClO}_2 + h\nu \rightarrow \text{Products}$

(Recommendation: 06-2, Note: 10-6, Evaluated: 10-6)

Absorption Cross Sections: The UV absorption spectrum of chloryl chloride, ClClO_2 , has been measured in the gas-phase at room temperature and in a noble gas matrix at low temperature by Müller and Willner [166] (220 – 390 nm). In another study from the same group, Jacobs et al. [106] (180 and 390 nm) re-investigated the spectrum. The spectrum has two overlapping absorption bands with maxima at 226 nm ($\sigma = 1.38 \times 10^{-17} \text{ cm}^2 \text{ molecule}^{-1}$) and 296 nm ($\sigma = 1.51 \times 10^{-17} \text{ cm}^2 \text{ molecule}^{-1}$). The recommended absorption cross sections in Table 4F-16 are taken from Müller and Willner [166].

Photolysis Quantum Yield and Product Studies: Photolysis of matrix isolated ClClO_2 suggest it absorbs in the visible between 500 and 800 nm with cross sections estimated to be $<10^{-20} \text{ cm}^2 \text{ molecule}^{-1}$.

Table 4F-16. Absorption Cross Sections of ClClO_2 at 298 K

λ (nm)	$10^{20} \sigma$ (cm^2)	λ (nm)	$10^{20} \sigma$ (cm^2)	λ (nm)	$10^{20} \sigma$ (cm^2)	λ (nm)	$10^{20} \sigma$ (cm^2)
220	920	265	550	310	1120	355	50
225	1160	270	660	315	870	360	40
230	1270	275	830	320	630	365	40
235	1210	280	1050	325	430	370	30
240	1060	285	1260	330	280	375	30
245	880	290	1430	335	190	380	20
250	720	295	1500	340	120	385	20
255	590	300	1470	345	80	390	20
260	530	305	1330	350	60		

Note:

220 – 390 nm: Müller and Willner [166]



(Recommendation: 06-2, Note: 10-6, Evaluated: 10-6)

Absorption Cross Sections: The VUV/UV absorption spectrum of hydrogen chloride, HCl, has been measured at room temperature by Romand and Vodar [204] (139 – 207 nm), Romand [203] (139 – 207 nm), Myer and Samson [167] (140 – 200 nm), Inn [105] (140 – 220 nm), Roxlo and Mandl [207] (170 – 215 nm), Nee et al. [171] (132 – 185 nm), Bahou et al. [4] (120 – 230 nm), Cheng et al. [40] (120 – 230 nm), Vatsa and Volpp [238] (121.6 nm), Mo et al. [155] (193 nm), and Hanf et al. [88] (135 nm). Bahou et al. [4] (120 – 230 nm) and Cheng et al. [40] (120 – 230 nm) have also measured the absorption spectrum of DCl. VUV absorption cross sections have been obtained by dipole (e,e) spectroscopy in the region 8-40 eV (155 – 31 nm) by Daviel et al. [53]. The absorption spectrum has a broad absorption band between 135 and 230 nm, corresponding to the $\text{A } ^1\Pi \leftarrow \text{X } ^1\Sigma^+$ transition, with the maximum at ~154 nm for HCl and ~156 nm for DCl. There is good agreement among the recent data of Bahou et al. [4] and Cheng et al. [40] with the data from Nee et al. [171] and Inn [105]. The cross sections of Bahou et al. [4] and Cheng et al. [40] are in general larger than those of Nee et al. [171] by <10% in the region 132 – 170 nm and by <25% at wavelengths >170 nm. In addition, the cross sections of Bahou et al. [4] and Cheng et al. [40] are slightly smaller, by <10%, than those of Inn [105] except for the region >210 nm. The absorption spectrum of Inn [105] has shoulders near 147.5 nm and 160 nm around the maximum at ~155 nm. This is in contrast to the results of Bahou et al. [4] and Cheng et al. [40] (0.1 nm resolution) and those of Nee et al. [171] (0.05 nm resolution). The recommended absorption cross sections for HCl and DCl in Table 4F-17 are averages over 2.5 nm and 5 nm intervals of the data from Bahou et al. [4].

Photolysis Quantum Yield and Product Studies: Photodissociation of HCl was studied by Matsumi et al. [142-144, 230] and the branching fraction $\text{Cl} (^2\text{P}_{1/2}) / (\text{Cl} (^2\text{P}_{1/2}) + \text{Cl} (^2\text{P}_{3/2}))$ determined to be 0.33 ± 0.05 at 193 nm and $0.45\text{-}0.47 (\pm 0.04)$ at 157 nm. Lambert et al. [120] measured branching fractions between 0.47 and 0.33 for eight wavelengths between 193 and 235 nm for HCl. Zhang et al. [252] obtained 0.41 ± 0.01 at

193.3 nm. Regan et al. [198] obtained values between 0.42 and 0.48 for 5 wavelengths in the range 201 – 210 nm, and Regan et al. [197] report values between 0.41 to 0.53 for selected ro-vibrational states at 235 nm. The results from Lambert et al. [120], Zhang et al. [252], Regan et al. [197] [198], and Liyanage et al. [130] are in good agreement with the calculations of Alexander et al. [2].

Table 4F-17. Absorption Cross Sections of HCl and DCl at 298 K

λ (nm)	$10^{20} \sigma$ (cm ²)		λ (nm)	$10^{20} \sigma$ (cm ²)	
	HCl	DCI		HCl	DCI
135.0	123	45.5	175.0	106	87.1
137.5	152	75.9	177.5	79.6	58.9
140.0	205	120	180.0	58.9	38.5
142.5	238	184	182.5	42.3	23.9
145.0	279	248	185.0	29.4	14.5
147.5	311	308	187.5	20.3	8.80
150.0	334	364	190.0	13.8	4.93
152.5	342	393	195.0	5.96	1.67
155.0	343	415	200.0	2.39	0.485
157.5	327	407	205.0	0.903	0.136
160.0	306	367	210.0	0.310	0.040
162.5	273	321	215.0	0.101	0.011
165.0	240	267	220.0	0.030	0.0027
167.5	199	211	225.0	0.010	
170.0	163	166	230.0	0.0034	
172.5	136	119			

Note:

135 – 230 nm: Bahou et al. [4]



(Recommendation: 06-2, Note: 10-6, Evaluated: 10-6)

Absorption Cross Sections: The UV/vis absorption spectrum of hypochlorous acid, HOCl, has an intensive singlet-singlet absorption in the near-UV with a maximum near 240 nm due mostly to the $2\ ^1A' \leftarrow 1\ ^1A'$ transition and a weaker band arising from the $1\ ^1A'' \leftarrow 1\ ^1A'$ transition that appears as a shoulder near 300 nm. The absorption cross sections of HOCl vapor have been reported by several groups. Molina and Molina [157] and Knauth et al. [116] produced HOCl using equilibrium mixtures with Cl_2O and H_2O . Mishalanie et al. [154] and Permien et al. [185] used a dynamic source to generate the HOCl vapor. The cross section values reported by Molina and Molina [157], Mishalanie et al. [154], and Permien et al. [185] are in reasonable agreement between 250 and 330 nm. In this wavelength range, the cross section values reported by Knauth et al. [116] are significantly smaller, e.g., a factor of 4 at 280 nm. At wavelengths >340 nm, the cross sections from Mishalanie et al. are significantly smaller than those obtained by the other three groups with a difference of an order of magnitude at 365 nm.

Burkholder [22] (200–380 nm) measured the HOCl absorption spectrum following photolysis of equilibrium mixtures of Cl_2O - H_2O -HOCl. The HOCl spectrum obtained has two absorption maxima with peaks at 242 and 304 nm in excellent agreement with the work of Knauth et al. [116]. The agreement with the spectra reported by Molina and Molina [157], Mishalanie et al. [154], and Permien et al. [185] is poor. The discrepancies can most likely be attributed to the methods and uncertainties associated with correcting measured absorption spectra for the presence of Cl_2 and Cl_2O . In the study by Burkholder [22], several control experiments were carried out in order to check the internal consistency of the data. Barnes et al. [6] examined the near UV HOCl spectrum by monitoring the OH fragments resulting from photodissociation and observed a weak band centered at 387 nm that extends to 480 nm. This transition arises from a weak singlet-triplet transition (Minaev [152]). The recommended cross sections in Table 4F-18 are calculated from an analytical expression provided by Barnes et al. [6] that was based on the cross section values from Burkholder [22] and Barnes et al. [6]. The HOCl spectrum reported by Jungkamp et al. [114] is in excellent

agreement with this recommendation for wavelengths <350 nm but deviates significantly at longer wavelengths.

Photolysis Quantum Yield and Product Studies: Molina et al. [161] observed production of OH radicals in the laser photolysis of HOCl around 310 nm. Butler and Phillips [31] found no evidence for O atom production following HOCl photolysis at 308 nm and reported an upper limit for the primary quantum yield for the HCl + O channel of ~0.02. Vogt and Schindler [241] used broadband photolysis in the 290 – 390 nm wavelength range and report $\Phi(\text{OH})$ to be >0.95. Schindler et al. [213] measured $\Phi(\text{Cl})$ to be 1.00 ± 0.05 at 308 nm. These authors also determined the probability, P, for production of $\text{Cl}^*(^2\text{P}_{1/2})$ relative to $\text{Cl} (^2\text{P}_{3/2})$ to be 0.035 ± 0.02 at 308 nm, and 0.35 ± 0.02 at 235 nm. These values are in agreement with the value of 0.30 ± 0.07 at 236 nm reported by Bell et al. [10]. Fujiwara and Ishiwata [67] determined the relative yield of $\text{OH}(^2\Pi_{3/2}) / \text{OH}(^2\Pi_{1/2})$ to be 2.0 at 266 nm and 1.5 at 355 nm. A unit quantum yield for the OH + Cl channel is recommended.

Table 4F-18. Absorption Cross Sections of HOCl at 298 K

λ (nm)	$10^{20} \sigma$ (cm ²)	λ (nm)	$10^{20} \sigma$ (cm ²)	λ (nm)	$10^{20} \sigma$ (cm ²)
200	7.18	274	5.26	348	1.55
202	6.39	276	4.94	350	1.43
204	5.81	278	4.74	352	1.33
206	5.46	280	4.64	354	1.24
208	5.37	282	4.62	356	1.17
210	5.54	284	4.68	358	1.11
212	5.98	286	4.79	360	1.06
214	6.68	288	4.95	362	1.02
216	7.63	290	5.13	364	0.985
218	8.81	292	5.33	366	0.951
220	10.2	294	5.52	368	0.919
222	11.6	296	5.71	370	0.888
224	13.2	298	5.86	372	0.855
226	14.7	300	5.99	374	0.822
228	16.2	302	6.08	376	0.786
230	17.5	304	6.12	378	0.748
232	18.7	306	6.12	380	0.708
234	19.6	308	6.07	382	0.667
236	20.2	310	5.97	384	0.624
238	20.5	312	5.84	386	0.580
240	20.6	314	5.66	388	0.535
242	20.3	316	5.45	390	0.491
244	19.8	318	5.21	392	0.447
246	19.0	320	4.95	394	0.405
248	18.1	322	4.67	396	0.364
250	17.0	324	4.38	398	0.325
252	15.8	326	4.09	400	0.288
254	14.6	328	3.79	402	0.254
256	13.3	330	3.50	404	0.222
258	12.1	332	3.21	406	0.194
260	10.9	334	2.94	406	0.168
262	9.73	336	2.68	410	0.144
264	8.68	338	2.44	412	0.124
266	7.75	340	2.22	414	0.105
268	6.94	342	2.02	416	0.089
270	6.25	344	1.84	418	0.075
272	5.69	346	1.69	420	0.063

Note:
Barnes et al. [6] (calculated using analytical expression)



(Recommendation: 02-25, Note: 10-6, Evaluated: 10-6)

Absorption Cross Sections: Nitrosyl chloride, ClNO, has a continuous UV/vis absorption spectrum extending beyond 650 nm. There is good agreement between the work of Martin and Gareis [141] (240 – 420 nm), Ballash and Armstrong [5] (185 – 540 nm), Illies and Takacs [104] (190 – 400 nm), and Tyndall et al. [233] (190 – 350 nm) except around 230 nm where the values of Ballash and Armstrong are larger by almost a factor of two. Roehl et al. [202] (350 – 650 nm) measured ClNO absorption cross sections at several temperatures between 223 and 343 K. Their room temperature results agree to within 15% with those of Martin and Gareis [141], Ballash and Armstrong [5], and Tyndall et al. [233]. The recommended absorption cross sections in Table 4F-19 are taken from the work of Tyndall et al. [233] between 190 and 350 nm and from Roehl et al. [202] beyond 350 nm.

Photolysis Quantum Yield and Product Studies: The quantum yield for the primary photolytic process has been reviewed by Calvert and Pitts [32]. The quantum yield is unity over the entire visible and near-ultraviolet bands. Chichinin [41] found evidence of ground state ($^2\text{P}_{3/2}$) and excited ($^2\text{P}_{1/2}$) atomic chlorine products and measured a relative quantum yield $\text{Cl}(^2\text{P}_{1/2}) / (\text{Cl}(^2\text{P}_{1/2}) + \text{Cl}(^2\text{P}_{3/2}))$ to be 0.88 ± 0.12 at 248 nm and 0.90 ± 0.10 at 351 nm. Felder and Morley [61] obtained 0.80 at 248 nm and Skorokhodov et al. [221] obtained 0.48 ± 0.03 at 212 nm, 0.30 at 235 nm., and 0.52 ± 0.03 at 248 nm.

Table 4F-19. Absorption Cross Sections of ClNO at 298 K

λ (nm)	$10^{20} \sigma$ (cm ²)	λ (nm)	$10^{20} \sigma$ (cm ²)	λ (nm)	$10^{20} \sigma$ (cm ²)	λ (nm)	$10^{20} \sigma$ (cm ²)
190	4320	246	45.2	302	10.3	370	11.0
192	5340	248	37.7	304	10.5	375	9.95
194	6150	250	31.7	306	10.8	380	8.86
196	6480	252	27.4	308	11.1	385	7.82
198	6310	254	23.7	310	11.5	390	6.86
200	5860	256	21.3	312	11.9	395	5.97
202	5250	258	19.0	314	12.2	400	5.13
204	4540	260	17.5	316	12.5	405	4.40
206	3840	262	16.5	318	13.0	410	3.83
208	3210	264	15.3	320	13.4	415	3.38
210	2630	266	14.4	322	13.6	420	2.89
212	2180	268	13.6	324	14.0	425	2.45
214	1760	270	12.9	326	14.3	430	2.21
216	1400	272	12.3	328	14.6	435	2.20
218	1110	274	11.8	330	14.7	440	2.20
220	896	276	11.3	332	14.9	445	2.07
222	707	278	10.7	334	15.1	450	1.87
224	552	280	10.6	336	15.3	455	1.79
226	436	282	10.2	338	15.3	460	1.95
228	339	284	9.99	340	15.2	465	2.25
230	266	286	9.84	342	15.3	470	2.50
232	212	288	9.71	344	15.1	475	2.61
234	164	290	9.64	346	15.1	480	2.53
236	120	292	9.63	348	14.9	485	2.33
238	101	294	9.69	350	14.2	490	2.07
240	82.5	296	9.71	355	13.6	495	1.78
242	67.2	298	9.89	360	12.9	500	1.50
244	55.2	300	10.0	365	12.0		

Note:

190 – 350 nm: Tyndall et al. [233]

350 – 500 nm: Roehl et al. [202]

Table 4F-21. Absorption Cross Sections of ClONO at 231 K

λ (nm)	$10^{20} \sigma$ (cm ²)	λ (nm)	$10^{20} \sigma$ (cm ²)
235	215.0	320	80.3
240	176.0	325	75.4
245	137.0	330	58.7
250	106.0	335	57.7
255	65.0	340	43.7
260	64.6	345	35.7
265	69.3	350	26.9
270	90.3	355	22.9
275	110.0	360	16.1
280	132.0	365	11.3
285	144.0	370	9.0
290	144.0	375	6.9
295	142.0	380	4.1
300	129.0	385	3.3
305	114.0	390	2.2
310	105.0	395	1.5
315	98.1	400	0.6

Note:

Molina and Molina [156]



(Recommendation: 06-2, Note: 10-6, Evaluated: 10-6)

Absorption Cross Sections: The recommended cross sections of chlorine nitrate, ClONO_2 , are taken from the work of Burkholder et al. [27]. The cross section values are listed in Table 4F-22 together with the parameters needed to compute their temperature dependence. These values are in good agreement with those reported by Molina and Molina [158], which provided the basis for earlier recommendations and which supersedes the work of Rowland et al. [206].

Photolysis Quantum Yield and Product Studies: Several groups have investigated the identity of the primary photolytic fragments. Smith et al. [223] report O + ClONO as the most likely products, using end-product analysis and steady-state photolysis. The results of Chang et al. [35], who employed the very low-pressure photolysis (VLPPh) technique, indicate that the products are Cl + NO₃, with a quantum yield of 1.0 ± 0.2 . Adler-Golden and Wiesenfeld [1], using a flash photolysis atomic absorption technique, find O atoms to be the predominant photolysis product and report a quantum yield for Cl atom production of less than 4%. Marinelli and Johnston [139] report a quantum yield for NO₃ production at 249 nm between 0.45 and 0.85, with a most likely value of 0.55; they monitored NO₃ by tunable dye laser absorption at 662 nm. Margitan [135] used atomic resonance fluorescence detection of O and Cl atoms and found the quantum yield at 266 nm and at 355 nm to be 0.9 ± 0.1 for Cl atom production and ~ 0.1 for O atom production, with no discernible difference at the two wavelengths. These results were confirmed by Knauth and Schindler [117], who used end-product analysis to infer the quantum yields from photolysis studies at 265 and 313 nm. Burrows et al. [28] report also Cl and NO₃ as the photolysis products at 254 nm, with a quantum yield of unity within experimental error, and an O atom quantum yield of 0.24. In contrast, Nikolaisen et al. [176] using broadband photolysis found that at $\lambda > 200$ nm the relative branching ratios are 0.61 ± 0.20 for the channel ClO + NO₂ and 0.39 ± 0.20 for the channel Cl + NO₃; in the $\lambda > 300$ nm region the quantum yields are found to be 0.44 ± 0.08 for production of ClO and NO₂ and 0.56 ± 0.08 for production of Cl and NO₃. Minton et al. [153], Nelson et al. [173], and Moore et al. [164] made the first direct measurements of ClO and obtained comparable yields for the Cl + NO₃ and the ClO + NO₂ channels, using a molecular beam technique: at 193, they obtained respectively 0.64 ± 0.08 and 0.36 ± 0.08 , at 248 nm 0.54 ± 0.08 and 0.46 ± 0.08 , and at 308 nm 0.67 ± 0.06 and 0.33 ± 0.06 . These authors found no evidence for the O + ClONO channel and placed an

upper limit for this channel of 0.04. Tyndall et al. [232] observed quantum yields of 0.80 ± 0.08 and 0.28 ± 0.12 for Cl and ClO at 308 nm using resonance fluorescence detection methods and reported a $O(^3P)$ yield of ≤ 0.05 . Ravishankara [192], Goldfarb et al. [78] and Yokelson et al. [251] have studied the photodissociation of ClONO₂ at 193, 222, 248 and 308 nm using atomic resonance fluorescence and time resolved absorption methods. They found that Cl and ClO are the two major dissociation products at 222, 248 and 308 nm, whereas at 193 nm, the quantum yield of O atoms was larger than the yield of ClO. At 193, 222, 248 and 308 nm, the yield of Cl was 0.53 ± 0.10 , 0.46 ± 0.10 , 0.41 ± 0.13 and 0.64 ± 0.20 , respectively; the O atom yield 0.73 ± 0.08 , 0.17 ± 0.08 , <0.10 and <0.05 ; and the ClO yield 0.29 ± 0.20 , 0.64 ± 0.20 , 0.39 ± 0.19 and 0.37 ± 0.19 . The NO₃ yield was determined by Yokelson et al. [251] to be 0.93 ± 0.24 at 352.5 nm, 0.67 ± 0.09 at 308 nm, 0.60 ± 0.09 at 248 nm, and 0.18 ± 0.04 at 193 nm. In addition, they measured the Cl atom yield as 0.73 ± 0.14 at 308 nm, 0.60 ± 0.12 at 248 nm and 0.45 ± 0.08 at 193 nm, and the O atom yield as <0.4 at 248 nm and <0.9 at 193 nm. Zou et al. [253] determined absolute quantum yields for the Cl and ClO channels at 235 nm to be 0.42 ± 0.1 and 0.58 ± 0.1 , respectively, using molecular beam techniques and TOFMS/REMPI. The recommended quantum yield values for production of Cl + NO₃ (Φ_1) and ClO + NO₂ (Φ_2) are given at the bottom of Table 4F-22 and are based on the work of Nelson et al. [173], Moore et al. [164], Nickolaissen et al. [176], and Goldfarb et al. [78] and Yokelson et al. [251]. For wavelengths shorter than 308 nm the value of Φ_1 is 0.6 and Φ_2 is 0.4. For longer wavelengths Φ_1 increases linearly to 0.9 at 350 nm with the corresponding decrease in Φ_2 to 0.1. There is no evidence for production of O + ClONO in the more recent work; the production of O atoms reported in some of the earlier studies may have resulted from the decomposition of excited NO₃. Zou et al. [253] determined the quantum yield of spontaneous decomposition of NO₃ into NO₂ + O to be 0.20 and into NO + O₂ to be 0.006.

Work by Nickolaissen et al. [176] indicates that the photodissociation quantum yield is less than unity at wavelengths longer than ~330 nm because of the formation of a long-lived intermediate that may be quenched under atmospheric conditions (a situation analogous to that of Cl₂O).

Table 4F-22. Absorption Cross Sections and Temperature Coefficients of ClONO₂

$$\sigma(\lambda, T) = \sigma(\lambda, 296) (1 + A1 (T - 296) + A2 (T - 296)^2); T \text{ in K}$$

λ (nm)	$10^{20}\sigma(\lambda, 296)$ (cm ²)	A1* (K ⁻¹)	A2* (K ⁻¹)	λ (nm)	$10^{20}\sigma(\lambda, 296)$ (cm ²)	A1* (K ⁻¹)	A2* (K ⁻¹)
196	310	9.90 (-5)	-8.38 (-6)	316	1.07	5.07 (-3)	1.56 (-5)
198	294	6.72 (-5)	-8.03 (-6)	318	0.947	5.24 (-3)	1.69 (-5)
200	282	-5.34 (-6)	-7.64 (-6)	320	0.831	5.40 (-3)	1.84 (-5)
202	277	-1.19 (-4)	-7.45 (-6)	322	0.731	5.55 (-3)	2.00 (-5)
204	280	-2.60 (-4)	-7.50 (-6)	324	0.647	5.68 (-3)	2.18 (-5)
206	288	-4.12 (-4)	-7.73 (-6)	326	0.578	5.80 (-3)	2.36 (-5)
208	300	-5.62 (-4)	-8.05 (-6)	328	0.518	5.88 (-3)	2.54 (-5)
210	314	-6.96 (-4)	-8.41 (-6)	330	0.466	5.92 (-3)	2.70 (-5)
212	329	-8.04 (-4)	-8.75 (-6)	332	0.420	5.92 (-3)	2.84 (-5)
214	339	-8.74 (-4)	-9.04 (-6)	334	0.382	5.88 (-3)	2.96 (-5)
216	345	-9.03 (-4)	-9.24 (-6)	336	0.351	5.80 (-3)	3.05 (-5)
218	341	-8.86 (-4)	-9.35 (-6)	338	0.326	5.68 (-3)	3.10 (-5)
220	332	-8.28 (-4)	-9.38 (-6)	340	0.302	5.51 (-3)	3.11 (-5)
222	314	-7.31 (-4)	-9.34 (-6)	342	0.282	5.32 (-3)	3.08 (-5)
224	291	-6.04 (-4)	-9.24 (-6)	344	0.264	5.07 (-3)	2.96 (-5)
226	264	-4.53 (-4)	-9.06 (-6)	346	0.252	4.76 (-3)	2.74 (-5)
228	235	-2.88 (-4)	-8.77 (-6)	348	0.243	4.39 (-3)	2.42 (-5)
230	208	-1.13 (-4)	-8.33 (-6)	350	0.229	4.02 (-3)	2.07 (-5)
232	182	6.18 (-5)	-7.74 (-6)	352	0.218	3.68 (-3)	1.76 (-5)
234	158	2.27 (-4)	-7.10 (-6)	354	0.212	3.40 (-3)	1.50 (-5)
236	138	3.72 (-4)	-6.52 (-6)	356	0.205	3.15 (-3)	1.27 (-5)
238	120	4.91 (-4)	-6.14 (-6)	358	0.203	2.92 (-3)	1.06 (-5)
240	105	5.86 (-4)	-5.98 (-6)	360	0.200	2.70 (-3)	8.59 (-6)
242	91.9	6.64 (-4)	-6.04 (-6)	362	0.190	2.47 (-3)	6.38 (-6)
244	81.2	7.33 (-4)	-6.27 (-6)	364	0.184	2.22 (-3)	3.66 (-6)
246	71.6	8.03 (-4)	-6.51 (-6)	366	0.175	1.93 (-3)	2.42 (-7)
248	62.4	8.85 (-4)	-6.59 (-6)	368	0.166	1.62 (-3)	-3.62 (-6)
250	56.0	9.84 (-4)	-6.40 (-6)	370	0.159	1.33 (-3)	-7.40 (-6)

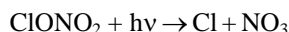
λ (nm)	$10^{20}\sigma(\lambda, 296)$ (cm ²)	A1* (K ⁻¹)	A2* (K ⁻¹)	λ (nm)	$10^{20}\sigma(\lambda, 296)$ (cm ²)	A1* (K ⁻¹)	A2* (K ⁻¹)
252	50.2	1.10 (-3)	-5.93 (-6)	372	0.151	1.07 (-3)	-1.07 (-5)
254	45.3	1.22 (-3)	-5.33 (-6)	374	0.144	8.60 (-4)	-1.33 (-5)
256	41.0	1.33 (-3)	-4.73 (-6)	376	0.138	6.73 (-4)	-1.54 (-5)
258	37.2	1.44 (-3)	-4.22 (-6)	378	0.129	5.01 (-4)	-1.74 (-5)
260	33.8	1.53 (-3)	-3.79 (-6)	380	0.121	3.53 (-4)	-1.91 (-5)
262	30.6	1.62 (-3)	-3.37 (-6)	382	0.115	2.54 (-4)	-2.05 (-5)
264	27.8	1.70 (-3)	-2.94 (-6)	384	0.108	2.25 (-4)	-2.11 (-5)
266	25.2	1.78 (-3)	-2.48 (-6)	386	0.103	2.62 (-4)	-2.11 (-5)
268	22.7	1.86 (-3)	-2.00 (-6)	388	0.0970	3.33 (-4)	-2.08 (-5)
270	20.5	1.94 (-3)	-1.50 (-6)	390	0.0909	4.10 (-4)	-2.05 (-5)
272	18.5	2.02 (-3)	-1.01 (-6)	392	0.0849	5.04 (-4)	-2.02 (-5)
274	16.6	2.11 (-3)	-4.84 (-7)	394	0.0780	6.62 (-4)	-1.94 (-5)
276	14.9	2.20 (-3)**	9.02 (-8)	396	0.0740	8.95 (-4)	-1.79 (-5)
278	13.3	2.29 (-3)	6.72 (-7)	398	0.0710	1.14 (-3)	-1.61 (-5)
280	11.9	2.38 (-3)	1.21 (-6)	400	0.0638	1.38 (-3)	-1.42 (-5)
282	10.5	2.47 (-3)	1.72 (-6)	402	0.0599	1.63 (-3)	-1.20 (-5)
284	9.35	2.56 (-3)	2.21 (-6)	404	0.0568	1.96 (-3)	-8.97 (-6)
286	8.26	2.66 (-3)	2.68 (-6)	406	0.0513	2.36 (-3)	-5.15 (-6)
288	7.24	2.75 (-3)	3.09 (-6)	408	0.0481	2.84 (-3)	-6.64 (-7)
290	6.41	2.84 (-3)	3.41 (-6)	410	0.0444	3.38 (-3)	4.47 (-6)
292	5.50	2.95 (-3)	3.74 (-6)	412	0.0413	3.96 (-3)	1.00 (-5)
294	4.67	3.08 (-3)	4.27 (-6)	414	0.0373	4.56 (-3)	1.60 (-5)
296	4.09	3.25 (-3)	5.13 (-6)	416	0.0356	5.22 (-3)	2.28 (-5)
298	3.57	3.45 (-3)	6.23 (-6)	418	0.0317	5.96 (-3)	3.07 (-5)
300	3.13	3.64 (-3)	7.36 (-6)	420	0.0316	6.70 (-3)	3.87 (-5)
302	2.74	3.83 (-3)	8.38 (-6)	422	0.0275	7.30 (-3)	4.58 (-5)
304	2.39	4.01 (-3)	9.30 (-6)	424	0.0242	7.82 (-3)	5.22 (-5)
306	2.09	4.18 (-3)	1.02 (-5)	426	0.0222	8.41 (-3)	5.95 (-5)
308	1.83	4.36 (-3)	1.11 (-5)	428	0.0207	9.11 (-3)	6.79 (-5)
310	1.60	4.53 (-3)	1.20 (-5)	430	0.0189	9.72 (-3)	7.52 (-5)
312	1.40	4.71 (-3)	1.30 (-5)	432	0.0188	9.96 (-3)	7.81 (-5)
314	1.22	4.89 (-3)	1.42 (-5)				

Notes:

*) (-n) means $\times 10^{-n}$.

**) Value corrected for an obvious misprint.

Quantum yields:



$$\Phi_1 = 0.6$$

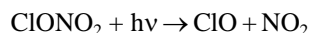
$$(\lambda < 308 \text{ nm})$$

$$\Phi_1 = 7.143 \times 10^{-3} \lambda \text{ (nm)} - 1.60$$

$$(308 \text{ nm} < \lambda < 364 \text{ nm})$$

$$\Phi_1 = 1.0$$

$$(\lambda > 364 \text{ nm})$$



$$\Phi_2 = 1 - \Phi_1$$



(Recommendation: 06-2, Note: 10-6, Evaluated: 10-6)

Absorption Cross Sections: The VUV/UV absorption spectrum of carbon tetrachloride, CCl_4 , has been measured extensively at room temperature by Russell et al. [209] (110 – 200 nm), Causley and Russell [34] (110 – 200 nm), Gordus and Bernstein [82] (204 – 250 nm), Rowland and Molina [205] (186 – 226 nm), Roxlo and Mandl [207] (170 – 230 nm), Hubrich and Stuhl [97] (160 – 275 nm), Ibuki et al. [101] (105 – 210

nm), Hanf et al. [88] (135 and 195 nm), Currie et al. [52] (250 nm), Vanlaethem-Meurée et al. [235] (190 – 252 nm), Simon et al. [219] (174 – 250 nm), and Prahlad and Kumar [189] (186 – 240 nm). The room temperature data agree to within 10% between 190 and 235 nm and to within 20% and 40% at 240 and 250 nm (except the value at 250 nm reported by Currie et al [52] that is significantly lower). The absorption spectrum of Prahlad and Kumar [189] has irregular structure over the entire wavelength range presumably due to the experimental precision of the measurements. In the range 180 – 186 nm, the cross section values reported by Hubrich and Stuhl [97] are higher by up to 25% than those reported by Simon et al. [219], and the value at 186 nm reported by Prahlad and Kumar [189] is lower by 18% than the value of Simon et al. [219]. At the maximum near 176 nm Hubrich and Stuhl [97] and Simon et al. [219] report an absorption cross section of $1.01 \times 10^{-17} \text{ cm}^2$. The peak cross section reported by Roxlo and Mandl [207] is lower, $\sim 7 \times 10^{-18} \text{ cm}^2$. Rebbert and Ausloos [194] derived a cross section at 313 nm of $\leq 3.7 \times 10^{-26} \text{ cm}^2$ from the $\text{C}_2\text{H}_5\text{Cl}$ yield in the photolysis of $\text{CCl}_4\text{-C}_2\text{H}_6$ mixtures. Absorption cross sections obtained using synchrotron radiation as a tunable light source have been reported by Ho [93] (4.9 – 200 nm) and Seccombe et al. [216] (50 – 200 nm). Burton et al. [29] has measured cross sections for the region 6.4 – 225 nm using dipole (e,e) spectroscopy. The recommended room temperature absorption cross sections in Table 4F-23 are the mean of the values reported by Hubrich and Stuhl [97] and Simon et al. [219] in the region 174 – 192 nm, from Simon et al. [219] in the region 194 – 250 nm, and from Hubrich and Stuhl [97] in the region 255 – 275 nm.

The temperature dependence of the absorption spectrum has been measured by Currie et al. [52] (250 nm) over the range 297 – 477 K, Vanlaethem-Meurée et al. [235] (190 – 252 nm) at 279 and 296 K, Simon et al. [219] (174 – 250 nm) over the range 225 – 295 K, and Prahlad and Kumar [189] (186 – 240 nm) over the range 220 – 300 K. The spectrum has a significant temperature dependence at wavelengths $> 205 \text{ nm}$ where the cross sections decrease with decreasing temperature. Simon et al. [219] parameterized the cross section temperature dependence using an empirical polynomial expansion

$$\log_{10} \sigma(\lambda, T) = \sum A_n \lambda^n + (T - 273) \times \sum B_n \lambda^n$$

and reported calculated cross section values for $T = 210, 230, 250, 270$, and 295 K . The parameters A_n and B_n , valid for the temperature range $210 - 300 \text{ K}$ and wavelength range $194 - 250 \text{ nm}$, given below are recommended for use in model calculations.

$$\begin{array}{ll} A_0 = -37.104 & B_0 = 1.0739 \\ A_1 = -5.8218 \times 10^{-1} & B_1 = -1.6275 \times 10^{-2} \\ A_2 = 9.9974 \times 10^{-3} & B_2 = 8.8141 \times 10^{-5} \\ A_3 = -4.6765 \times 10^{-5} & B_3 = -1.9811 \times 10^{-7} \\ A_4 = 6.8501 \times 10^{-8} & B_4 = 1.5022 \times 10^{-10} \end{array}$$

Photolysis Quantum Yield and Product Studies: Quantum yields ≥ 0.9 and ~ 0.75 for the photodissociative processes $\text{CCl}_4 + h\nu \rightarrow \text{CCl}_3 + \text{Cl}$ at 213.9 nm and $\text{CCl}_4 + h\nu \rightarrow \text{CCl}_2 + 2\text{Cl}$ at 163.3 nm , respectively, were derived from the gas-phase photolysis of CCl_4 in the presence of HCl , HBr , and C_2H_6 by Rebbert and Ausloos [194]. Clark and Husain [45] report a quantum yield for $\text{Cl}^*(^2\text{P}_{1/2})$ atom formation in the broadband photolysis of CCl_4 to be 0.78 ± 0.27 . Hanf et al. [88] reported Cl atom quantum yields in the photolysis of CCl_4 to be $\Phi(\text{Cl}) = 1.1 \pm 0.05$ and $\Phi(\text{Cl}^*) = 0.4 \pm 0.02$ (thus $\Phi(\text{Cl} + \text{Cl}^*) = 1.5 \pm 0.1$) at 193 nm and $\Phi(\text{Cl}) = 1.5 \pm 0.07$ and $\Phi(\text{Cl}^*) = 0.4 \pm 0.02$ (thus $\Phi(\text{Cl} + \text{Cl}^*) = 1.9 \pm 0.1$) at 135 nm . A quantum yield of unity with $\Phi(\text{Cl}) = 1$ is recommended.

Table 4F-23. Absorption Cross Sections of CCl_4 at 295 K

λ (nm)	$10^{20} \sigma$ (cm^2)	λ (nm)	$10^{20} \sigma$ (cm^2)	λ (nm)	$10^{20} \sigma$ (cm^2)
174	956	204	61.0	234	2.20
176	1010	206	57.0	236	1.60
178	982.5	208	52.5	238	1.16
180	806	210	46.9	240	0.830
182	647	212	41.0	242	0.590
184	478.5	214	34.5	244	0.413
186	338.5	216	27.8	246	0.290
188	227	218	22.1	248	0.210
190	145.5	220	17.5	250	0.148
192	99.6	222	13.6	255	0.0661
194	76.7	224	10.2	260	0.0253
196	69.5	226	7.60	265	0.0126

λ (nm)	$10^{20} \sigma$ (cm ²)	λ (nm)	$10^{20} \sigma$ (cm ²)	λ (nm)	$10^{20} \sigma$ (cm ²)
198	68.0	228	5.65	270	0.00610
200	66.0	230	4.28	275	0.00239
202	63.8	232	3.04		

Notes:

174 – 192 nm: mean of data from Hubrich and Stuhl [97] and Simon et al. [219]

194 – 250 nm: Simon et al. [219]

255 – 275 nm: Hubrich and Stuhl [97]



(Recommendation: 06-2, Note: 10-6, Evaluated: 10-6)

Absorption Cross Sections: The UV/vis absorption spectrum of methyl hypochlorite, CH_3OCl , has been measured by Crowley et al. [51] (400 – 460 nm) and Jungkamp et al. [114] (230 – 400 nm). The spectrum has overlapping absorption bands with maxima at 230 and 310 nm. The agreement between the two data sets is good at wavelengths longer than 250 nm. At the maximum near 230 nm the cross sections from Jungkamp et al. [114] are about 15% smaller. The recommended cross sections in Table 4F-24 are the mean of the values reported by these two groups.

Photolysis Quantum Yield and Product Studies: Schindler et al. [213] measured the quantum yield for the product channel $\text{Cl} + \text{CH}_3\text{O}$ to be 0.95 ± 0.05 at 308 nm. They also determined an upper limit of <0.01 for HCl formation at 248 nm and the ratio $\text{Cl}^*(^2\text{P}_{1/2})/\text{Cl}(^2\text{P}_{3/2})$ following photolysis at 235 and 238 nm to be 1.45 ± 0.05 . Krisch et al. [118] used photofragment translational spectroscopy to confirm that photodissociation of CH_3OCl at 248 nm resulted in only the cleavage of the O-Cl bond and the formation of Cl and CH_3O .

Table 4F-24. Absorption Cross Sections of CH_3OCl at 295 K

λ (nm)	$10^{20} \sigma$ (cm ²)	λ (nm)	$10^{20} \sigma$ (cm ²)	λ (nm)	$10^{20} \sigma$ (cm ²)
230	14.9	290	1.32	350	0.662
232	15.4	292	1.34	352	0.611
234	15.7	294	1.35	354	0.574
236	15.9	296	1.37	356	0.529
238	15.8	298	1.40	358	0.482
240	15.5	300	1.43	360	0.445
242	14.9	302	1.45	362	0.411
244	14.2	304	1.47	364	0.389
246	13.2	306	1.48	366	0.356
248	12.2	308	1.49	368	0.331
250	11.1	310	1.49	370	0.298
252	9.96	312	1.48	372	0.273
254	8.86	314	1.47	374	0.246
256	7.77	316	1.46	376	0.225
258	6.80	318	1.43	378	0.209
260	5.87	320	1.41	380	0.202
262	5.05	322	1.37	382	0.186
264	4.31	324	1.33	384	0.17
266	3.69	326	1.30	386	0.16
268	3.16	328	1.24	388	0.15
270	2.71	330	1.20	390	0.13
272	2.35	332	1.14	392	0.14
274	2.06	334	1.09	394	0.13
276	1.83	336	1.04		
278	1.64	338	0.980		

λ (nm)	$10^{20} \sigma$ (cm ²)	λ (nm)	$10^{20} \sigma$ (cm ²)	λ (nm)	$10^{20} \sigma$ (cm ²)
280	1.53	340	0.918		
282	1.42	342	0.875		
284	1.37	344	0.822		
286	1.33	346	0.760		
288	1.32	348	0.709		

Note:

230 – 394 nm: Mean of the data from Crowley et al. [51] and Jungkamp et al. [114]



(Recommendation: 02-25, Note: 10-6, Evaluated: 10-6)

Absorption Cross Sections: The VUV/UV absorption spectrum of CHCl_3 (trichloromethane, chloroform) has been measured at room temperature by Lucazeau and Sandorfy [133] (113 – 182 nm), Brownsword et al. [19] (Lyman- α , 121.6 nm), Russell et al. [209] (110 – 200 nm), Gordus and Bernstein [82] (222.7 nm), Hubrich and Stuhl [97] (160 – 255 nm), Vanlaethem-Meurée et al. [235] (190 – 230 nm), and Simon et al. [219] (174 – 240 nm). The room temperature cross sections from Vanlaethem-Meurée et al. [235] and Simon et al. [219] are nearly identical in the wavelength region 190 – 210 nm. Differences of ~15% exist at longer wavelengths. The data of Hubrich and Stuhl [97] and Simon et al. [219] agree to within 10% between 180 and 234 nm. Differences of ~25% exist in the long wavelength tail with the values of Hubrich and Stuhl [97] being larger. In the region of the absorption maximum at ~176 nm, the spread in the reported cross section values is the largest. Simon et al. [219] report $\sigma(176 \text{ nm}) = \sim 5 \times 10^{-18} \text{ cm}^2$ compared to $3.7 \times 10^{-18} \text{ cm}^2$ reported by Hubrich and Stuhl [97] and $< 2 \times 10^{-18} \text{ cm}^2$ by Lucazeau and Sandorfy [133]. The recommended absorption cross sections in Table 4F-25 are only for wavelengths >180 nm and are the mean of the values reported by Hubrich and Stuhl [97] and Simon et al. [219] for the wavelength range 180 – 240 nm. For the wavelength range 242 – 256 nm the recommended cross sections (in italics) are obtained by extrapolation, $\log \sigma(\lambda) = -1.2277 - 0.0844 \lambda$.

The temperature dependence of the absorption spectrum has been measured by Vanlaethem-Meurée et al. [235] (190 – 230 nm) at 279 and 296 K and Simon et al. [219] (174 – 240 nm) over the range 225 – 295 K. The temperature dependence is significant for wavelengths >194 nm where the cross sections decrease with decreasing temperature. Simon et al. [219] parameterized the cross section temperature dependence using an empirical polynomial expansion

$$\log_{10} \sigma(\lambda, T) = \sum A_n \lambda^n + (T - 273) \times \sum B_n \lambda^n$$

and reported calculated cross sections for $T = 210, 230, 250, 270$, and 295 K . The parameters A_n and B_n , valid for the temperature range 210 – 300 K and wavelength range 190 – 240, given below are recommended for use in model calculations.

$$\begin{array}{ll} A_0 = 269.80 & B_0 = 3.7973 \\ A_1 = -6.0908 & B_1 = -7.0913 \times 10^{-2} \\ A_2 = 4.7830 \times 10^{-2} & B_2 = 4.9397 \times 10^{-4} \\ A_3 = -1.6427 \times 10^{-4} & B_3 = -1.5226 \times 10^{-6} \\ A_4 = 2.0682 \times 10^{-7} & B_4 = 1.7555 \times 10^{-9} \end{array}$$

Photolysis Quantum Yield and Product Studies: Quantum yields for H atom formation have been measured by Brownsword et al. [19], [18] to be 0.23 ± 0.03 and 0.13 at 121.6 and 157.6 nm, respectively. H atom formation was not detected in the photolysis at 193.3 nm.

Table 4F-25. Absorption Cross Sections of CHCl₃ at 296 K

λ (nm)	$10^{20} \sigma$ (cm ²)	λ (nm)	$10^{20} \sigma$ (cm ²)	λ (nm)	$10^{20} \sigma$ (cm ²)
180	372	206	20.7	232	0.158
182	317	208	15.1	234	0.107
184	248	210	10.7	236	0.0730
186	186	212	7.48	238	0.0503
188	144	214	5.24	240	0.0347
190	113	216	3.60	242	0.0223
192	89.9	218	2.48	244	0.0151
194	76.1	220	1.69	246	0.01023
196	64.2	222	1.13	248	0.00694
198	53.0	224	0.750	250	0.00470
200	42.6	226	0.503	252	0.00319
202	34.4	228	0.342	254	0.00216
204	27.2	230	0.234	256	0.00147

Note:

180 – 240 nm: mean of data from Hubrich and Stuhl [97] and Simon et al. [219]

242 – 256 nm: extrapolation, $\log \sigma(\lambda) = -1.2277 - 0.0844 \lambda$



(Recommendation: 02-25, Note: 10-6, Evaluated: 10-6)

Absorption Cross Sections: The VUV/UV absorption spectrum of dichloromethane, CH₂Cl₂, has been measured at room temperature by Russell et al. [209] (110 – 200 nm), Brownsword et al. [19] (Lyman- α , 121.6 nm), Gordus and Bernstein [82] (213 nm), Hubrich and Stuhl [97] (160 – 255 nm), Vanlaethem-Meurée et al. [235] (176 – 216 nm), and Simon et al. [219] (176 – 220 nm). The room temperature data of Vanlaethem-Meurée et al. [235] and Simon et al. [219] are nearly identical. The cross sections of Hubrich and Stuhl [97] are as much as 12% greater than those of Simon et al. [219] in the 176 – 206 nm wavelength range. Differences of ~50% exist in the 185 – 220 nm range. The recommended absorption cross sections in Table 4F-26 are the mean of the values reported by Hubrich and Stuhl [97] and Simon et al. [219] for the wavelength range 176 – 220 nm. For wavelengths >220 nm the recommended cross sections (in italics) are obtained by extrapolation, $\log \sigma(\lambda) = -2.1337 - 0.08439 \lambda$. The measured cross section values in this wavelength range from Hubrich and Stuhl [97] are smaller by ~7% for wavelengths <230 nm and larger ~50% between 235 and 255 nm than the extrapolated values.

The temperature dependence of the absorption spectrum has been measured by Vanlaethem-Meurée et al. [235] (176 – 216 nm) at 279 and 296 K and Simon et al. [219] (176 – 220 nm) over the range 225 – 295 K. The temperature dependence is significant for wavelengths >190 nm where the cross sections decrease with decreasing temperature. Simon et al. [219] parameterized the cross section temperature dependence using an empirical polynomial expansion

$$\log_{10} \sigma(\lambda, T) = \sum A_n \lambda^n + (T - 273) \times \sum B_n \lambda^n$$

and reported calculated cross sections for T = 210, 230, 250, 270, and 295 K. The parameters A_n and B_n, valid for the temperature range 210 – 300 K and wavelength range 176 – 220 nm, given below are recommended for use in model calculations.

$$\begin{array}{ll} A_0 = -1431.8 & B_0 = -3.1171 \\ A_1 = 27.395 & B_1 = 6.7874 \times 10^{-2} \\ A_2 = -1.9807 \times 10^{-1} & B_2 = -5.5000 \times 10^{-4} \\ A_3 = 6.3468 \times 10^{-4} & B_3 = 1.9649 \times 10^{-6} \\ A_4 = -7.6298 \times 10^{-7} & B_4 = -2.6101 \times 10^{-9} \end{array}$$

Photolysis Quantum Yield and Product Studies: Quantum yields for H atom formation have been measured by Brownsword et al. [19], [18] to be 0.28 ± 0.03 , 0.23, and 0.002 ± 0.001 at 121.6, 157.6, and 193.3 nm, respectively.

Table 4F-26. Absorption Cross Sections of CH₂Cl₂ at 298 K

λ (nm)	$10^{20} \sigma$ (cm ²)	λ (nm)	$10^{20} \sigma$ (cm ²)	λ (nm)	$10^{20} \sigma$ (cm ²)
176	186	204	4.41	232	<i>0.0194</i>
178	182	206	3.07	234	<i>0.0132</i>
180	173	208	2.13	236	<i>0.00892</i>
182	156	210	1.45	238	<i>0.00605</i>
184	135	212	0.978	240	<i>0.00410</i>
186	110	214	0.651	242	<i>0.00278</i>
188	84.2	216	0.435	244	<i>0.00188</i>
190	61.0	218	0.291	246	<i>0.00128</i>
192	43.9	220	0.190	248	<i>0.000866</i>
194	30.5	222	<i>0.135</i>	250	<i>0.000587</i>
196	20.6	224	<i>0.0918</i>	252	<i>0.000398</i>
198	14.1	226	<i>0.0623</i>	254	<i>0.000270</i>
200	9.48	228	<i>0.0422</i>	256	<i>0.000183</i>
202	6.40	230	<i>0.0286</i>		

Note:

176 – 220 nm: mean of values from Hubrich and Stuhl [97] and Simon et al. [219]

222 – 256 nm: extrapolation, $\log \sigma(\lambda) = -2.1337 - 0.08439 \lambda$



(Recommendation: 06-2, Note: 10-6, Evaluated: 10-6)

Absorption Cross Sections: The VUV/UV absorption spectrum of CH₃Cl (chloromethane, methyl chloride) has been measured at room temperature by Russell et al. [209] (110 – 200 nm), Brownsword et al. [19] (Lyman- α , 121.6 nm), Felps et al. [62] (171.2 nm), Robbins [200] (174 – 220 nm), Hubrich et al. [98] (158 – 235 nm), Vanlaethem-Meurée et al. [235] (186 – 216 nm), Simon et al. [219] (174 – 216 nm). The room temperature data generally agree within 10% over the wavelength range 174 – 216 nm and the data of Vanlaethem-Meurée et al. [235] and Simon et al. [219] are nearly identical. The cross section at 171 nm from Felps et al. [18] is ~15% less than that of Hubrich et al. [98]. The recommended absorption cross sections in Table 4F-27 are the mean of the values reported by Robbins [200], Hubrich et al. [98], and Simon et al. [219] in the range 174 – 184 nm, the mean of the values reported by Robbins [200], Hubrich et al. [98], Vanlaethem-Meurée et al. [235], and Simon et al. [219] in the range 186 – 216 nm, and the mean of the values reported by Robbins [200] and Hubrich et al. [98] in the range 218 – 220 nm. For the wavelength range 222 – 236 nm the recommended values (in italics) were obtained from a log-linear fit to the Hubrich et al. [98] data in the range 200 – 235-nm, $\log \sigma(\lambda) = -0.24164 - 0.09743 \lambda$.

The temperature dependence of the absorption spectrum has been measured by Hubrich et al. [98] (158 – 235 nm) at 208 and 298 K, Vanlaethem-Meurée et al. [235] (186 – 216 nm) at 255, 279, and 296 K, and Simon et al. [219] (174 – 216 nm) over the range 225 – 295 K. The temperature dependence of the absorption cross sections is significant at wavelengths above 194 nm where the cross sections decrease with decreasing temperature. There is very good agreement in the values reported by Vanlaethem-Meurée et al. [235] and Simon et al. [219]. Simon et al. [219] parameterized the cross section temperature dependence using an empirical polynomial expansion

$$\log_{10} \sigma(\lambda, T) = \sum A_n \lambda^n + (T - 273) \times \sum B_n \lambda^n$$

and reported calculated cross sections for T = 210, 230, 250, 270, and 295 K. The parameters A_n and B_n, valid for the temperature range 210 – 300 K and wavelength range 176 – 216 nm, given below are recommended for use in model calculations.

$$\begin{aligned}
A_0 &= -299.80 & B_0 &= -7.1727 \\
A_1 &= 5.1047 & B_1 &= 1.4837 \times 10^{-1} \\
A_2 &= -3.3630 \times 10^{-2} & B_2 &= -1.1463 \times 10^{-3} \\
A_3 &= 9.5805 \times 10^{-5} & B_3 &= 3.9188 \times 10^{-6} \\
A_4 &= -1.0135 \times 10^{-7} & B_4 &= -4.9994 \times 10^{-9}
\end{aligned}$$

Photolysis Quantum Yield and Product Studies: Quantum yields for H atom formation have been measured by Brownsword et al. [19], [18] to be 0.53 ± 0.05 , 0.29, 0.012 ± 0.006 at 121.6, 157.6, and 193.3 nm, respectively.

Table 4F-27. Absorption Cross Sections of CH₃Cl at 298 K

λ (nm)	$10^{20} \sigma$ (cm ²)	λ (nm)	$10^{20} \sigma$ (cm ²)	λ (nm)	$10^{20} \sigma$ (cm ²)
174	110	196	3.96	218	0.0345
176	93.9	198	2.68	220	0.0220
178	78.2	200	1.77	222	<i>0.0135</i>
180	63.6	202	1.13	224	<i>0.00859</i>
182	46.5	204	0.731	226	<i>0.00549</i>
184	35.0	206	0.482	228	<i>0.00350</i>
186	25.8	208	0.313	230	<i>0.00224</i>
188	18.4	210	0.200	232	<i>0.00143</i>
190	12.8	212	0.127	234	<i>0.00091</i>
192	8.84	214	0.0860	236	<i>0.00058</i>
194	5.83	216	0.0534		

Note:

174 – 184 nm: mean of data from Robbins [200], Hubrich et al. [98], and Simon et al. [219]

186 – 216 nm: mean of data from Robbins [200], Hubrich et al. [98], Vanlaethem-Meurée et al [235] and Simon et al. [219]

218 – 220 nm: mean of data from Robbins [200] and Hubrich et al. [98]

222 – 236 nm: fit to data from Hubrich et al. [98], $\log \sigma(\lambda) = -0.24164 - 0.09743 \lambda$

F24. CH₃CCl₃ + hν → Products

(Recommendation: 02-25, Note: 10-6, Evaluated: 10-6)

Absorption Cross Sections: The VUV/UV absorption spectrum of CH₃CCl₃ (1,1,1-trichloroethane, methylchloroform) has been measured at room temperature by Salomon et al. [210] (147 nm), Hubrich and Stuhl [97] (160 – 255 nm), Vanlaethem-Meurée et al. [237] (182 – 240 nm), and Nayak et al. [169] (160 – 240 nm). Hubrich and Stuhl [97] corrected their measured spectrum between 170 and 190 nm for the presence of a 1,4-dioxane stabilizer, corrections were <10.7%. Nayak et al. [169] also measured the absorption cross sections in the liquid-phase over the range 235 – 260 nm and used a wavelength shift procedure to derive the gas-phase cross section data in this wavelength range. The agreement of the room temperature data is within 20% in the region 165 – 205 nm. Between 210 and 240 nm, the data of Vanlaethem-Meurée et al. [237] and Nayak et al. [169] agree to within 15%, whereas the data from Hubrich and Stuhl [97] are 100–150% greater. The recommended absorption cross sections in Table 4F-28 are the mean of the values reported by Hubrich and Stuhl [97] and Nayak et al. [169] in the range 170 – 180 nm, the mean of the values reported by Vanlaethem-Meurée et al. [237], Hubrich and Stuhl [97], and Nayak et al. [169] in the range 185 – 205 nm, and the mean of the values reported by Vanlaethem-Meurée et al. [237] and Nayak et al. [169] in the range 210 – 240 nm. For wavelengths >240 nm, the recommended values (in italics) were obtained by extrapolation of the Nayak et al. [169] data in the range 210 – 240 nm, $\log \sigma(\lambda) = -1.59792 - 0.08066 \lambda$. The values measured by Hubrich and Stuhl [97] in this wavelength range are greater by ~140% at 250 nm and less by ~80% at 255 nm than the recommended values.

The temperature dependence of the absorption spectrum has been measured by Vanlaethem-Meurée et al. [237] (182 – 240 nm) over the range 220 – 295 K and Nayak et al. [169] (160 – 240 nm) over the range 223 – 333 K. The temperature dependence of the absorption cross sections is significant at wavelengths >210 nm where the cross sections decrease with decreasing temperature. The studies of Nayak et al. [169] and

Vanlaethem-Meurée et al. [237] are in good agreement. Vanlaethem-Meurée et al. [237] parameterized the cross section temperature dependence using an empirical polynomial expansion

$$\log_{10} \sigma(\lambda, T) = \sum A_n \lambda^n + (T - 273) \times \sum B_n \lambda^n$$

and reported calculated cross sections for T = 210, 230, 250, 270, and 295 K. The parameters A_n and B_n , valid for the temperature range 210 – 300 K and wavelength range 182 – 240 nm, reported by Gillotay and Simon [75] and given below are recommended for use in model calculations.

$$\begin{array}{ll} A_0 = 341.085191 & B_0 = -1.660090 \\ A_1 = -7.273362 & B_1 = 3.079969 \times 10^{-2} \\ A_2 = 5.498387 \times 10^{-2} & B_2 = -2.106719 \times 10^{-4} \\ A_3 = -1.827552 \times 10^{-4} & B_3 = 6.264984 \times 10^{-7} \\ A_4 = 2.238640 \times 10^{-7} & B_4 = -6.781342 \times 10^{-10} \end{array}$$

Photolysis Quantum Yield and Product Studies: No studies are available.

Table 4F-28. Absorption Cross Sections of CH₃CCl₃ at 298 K

λ (nm)	$10^{20} \sigma$ (cm ²)	λ (nm)	$10^{20} \sigma$ (cm ²)	λ (nm)	$10^{20} \sigma$ (cm ²)
170	406	200	92.1	230	0.717
175	424	205	52.0	235	0.276
180	404	210	25.5	240	0.111
185	301	215	10.9	245	0.0437
190	212	220	4.47	250	0.0173
195	147	225	1.82	255	0.00682

Note:

170 – 180 nm: mean of Hubrich and Stuhl [97] and Nayak et al. [169]

185 – 205 nm: mean of Vanlaethem-Meurée et al. [237], Hubrich and Stuhl [97] and Nayak et al. [169]

210 – 240 nm: mean of Vanlaethem-Meurée et al. [237] and Nayak et al. [169]

245 – 255 nm: extrapolation, $\log \sigma(\lambda) = -1.59792 - 0.08066 \lambda$

F25. $\text{CH}_3\text{CH}_2\text{Cl} + h\nu \rightarrow \text{Products}$

(Recommendation: 02-25, Note: 10-6, Evaluated: 10-6)

Absorption Cross Sections: The room temperature VUV/UV absorption spectrum of $\text{CH}_3\text{CH}_2\text{Cl}$ (chloroethane, ethyl chloride) has been measured by Ichimura et al. [102] (147 nm) and Hubrich and Stuhl [97] (160 – 240 nm). The recommended absorption cross sections in Table 4F-29 are taken from Hubrich and Stuhl [97].

Photolysis Quantum Yield and Product Studies: No studies are available.

Table 4F-29. Absorption Cross Sections of $\text{CH}_3\text{CH}_2\text{Cl}$ at 298 K

λ (nm)	$10^{20} \sigma$ (cm^2)	λ (nm)	$10^{20} \sigma$ (cm^2)	λ (nm)	$10^{20} \sigma$ (cm^2)
160	189.0	190	6.85	220	0.0127
165	110.0	195	2.56	225	0.00463
170	70.5	200	1.17	230	0.00117
175	44.4	205	0.375	235	0.000395
180	30.4	210	0.147	240	0.000156
185	13.6	215	0.0433		

Note:

160 – 240 nm: Hubrich and Stuhl [97]

F26. $\text{CH}_3\text{CHClCH}_3 + h\nu \rightarrow \text{Products}$

(Recommendation: 02-25, Note: 10-6, Evaluated: 10-6)

Absorption Cross Sections: The VUV/UV absorption spectrum of 2-chloropropane, $\text{CH}_3\text{CHClCH}_3$, has been measured by Gillotay and Simon [72]. The Gillotay and Simon [72] results are reported (erroneously) as $\text{CH}_3\text{CH}_2\text{ClCH}_3$, which presumably should be $\text{CH}_3\text{CHClCH}_3$. The recommended data are listed in Table 4F-30.

Photolysis Quantum Yield and Product Studies: No studies are available.

Table 4F-30. Absorption Cross Sections of $\text{CH}_3\text{CHClCH}_3$ at 295 K

λ (nm)	$10^{20} \sigma$ (cm^2)	λ (nm)	$10^{20} \sigma$ (cm^2)	λ (nm)	$10^{20} \sigma$ (cm^2)
170	31.7	192	4.67	214	0.0965
172	27.0	194	3.49	216	0.0652
174	24.3	196	2.58	218	0.0444
176	22.1	198	1.88	220	0.0308
178	20.3	200	1.34	222	0.0212
180	18.0	202	0.954	224	0.0144
182	15.0	204	0.671	226	0.0107
184	12.2	206	0.463	228	0.00752
186	9.99	208	0.311	230	0.00580
188	7.93	210	0.214		
190	6.06	212	0.144		

Note:

170 – 230 nm: Gillotay and Simon [72]

F27. $\text{CH}_2\text{ClCH}_2\text{Cl} + h\nu \rightarrow \text{Products}$

(Recommendation: 02-25, Note: 10-6, Evaluated: 10-6)

Absorption Cross Sections: The VUV/UV absorption spectrum of 1,2-dichloroethane, $\text{CH}_2\text{ClCH}_2\text{Cl}$, has been measured by Russell et al. [209] (116 – 192 nm) and Yano and Tschuikow-Roux [250] (147 nm). No recommendation is given.

Photolysis Quantum Yield and Product Studies: No studies are available.

F28. $\text{CH}_2\text{ClCH}_2\text{CH}_2\text{Cl} + h\nu \rightarrow \text{Products}$

(Recommendation: 02-25, Note: 10-6, Evaluated: 10-6)

Absorption Cross Sections: The VUV/UV absorption spectrum of 1,3-dichloropropane, $\text{CH}_2\text{ClCH}_2\text{CH}_2\text{Cl}$, has been measured by Russell et al. [209] (116 – 192 nm). No recommendation is given.

Photolysis Quantum Yield and Product Studies: No studies are available.

F29. $\text{CH}_2\text{Cl}(\text{CH}_2)_2\text{CH}_2\text{Cl} + h\nu \rightarrow \text{Products}$

(Recommendation: 02-25, Note: 10-6, Evaluated: 10-6)

Absorption Cross Sections: The VUV/UV absorption spectrum of 1,4-dichlorobutane, $\text{CH}_2\text{Cl}(\text{CH}_2)_2\text{CH}_2\text{Cl}$, has been measured by Russell et al. [209] (129 – 188 nm). No recommendation is given.

Photolysis Quantum Yield and Product Studies: No studies are available.

F30.	$\text{COCl}_2 + h\nu$	$\rightarrow \text{CO} + \text{Cl}_2$	110 kJ mol^{-1}	1084 nm	(1)
		$\rightarrow \text{ClCO} + \text{Cl}$	318 kJ mol^{-1}	377 nm	(2)
		$\rightarrow \text{CO} + 2\text{Cl}$	353 kJ mol^{-1}	339 nm	(3)
		$\rightarrow \text{CCl}_2 + \text{O}$	700 kJ mol^{-1}	171 nm	(4)

(Recommendation: 94-26, Note: 10-6, Evaluated: 10-6)

Absorption Cross Sections: The UV absorption spectrum of COCl_2 (carbonyl dichloride, phosgene) has been measured at room temperature by Chou et al. [42] (185 – 226 nm), Okabe [179] (240 – 280 nm), Meller et al. [150] (200 – 315 nm), Jäger et al. [107] (172 – 220 nm), Okabe [180, 181] (147 and 254 nm), Glicker and Okabe [77] (147 and 254 nm), and Gillotay et al. [76] (166 – 308 nm). The spectrum shows a weak absorption band between 215 and 310 nm with the maximum at ~235 nm and a strong absorption band below 200 nm with the maximum at ~174 nm. The room temperature values reported in the various studies are in very good agreement, generally within 10%. An exception is in the region of the absorption minimum around 200 nm where the values of Jäger et al. [107] are lower than those of Gillotay et al. [76] by as much as 20%. In this region the values of Chou et al. [42] and Meller et al. [150] are between those of Gillotay et al. [76] and Jäger et al. [107].

The recommended absorption cross sections in Table 4F-31 as averages over the 500 cm^{-1} intervals used for atmospheric modeling are the values of Gillotay et al. [76] in the region 168.10 – 173.15 nm, the mean of the values from Gillotay et al. [76] and Jäger et al. [107] in the region 174.65 – 182.65 nm, the mean of the values from Chou et al. [42], Gillotay et al. [76], and Jäger et al. [107] in the region 184.35 – 199.00 nm, the mean of the values of Chou et al. [42], Gillotay et al. [76], Meller et al. [150], and Jäger et al. [107] in the region 201.01 – 218.59 nm, the mean of the values from Chou et al. [42], Gillotay et al. [76], and Meller et al. [150] in the region 221.00 – 226.00 nm, and the mean of the values from Gillotay et al. [76] and Meller et al. [150] in the region 228.58 – 305.36 nm.

The temperature dependence of the absorption spectrum has been measured by Gillotay et al. [76] (166 – 308 nm) over the range 210 – 295 K. The temperature dependence is significant only in the region <175 nm and >250 nm. The strong absorption band is shifted slightly to shorter wavelengths with decreasing temperature and a peak cross section increase of ~20% between 295 and 210 K. In the long wavelength region the absorption cross sections decrease with decreasing temperature with a decrease of ~80% at 305 nm between 295 and 210 K.

Photolysis Quantum Yield and Product Studies: Phosgene is a useful actinometer in the region 200 – 280 nm. The photodissociation processes $\text{COCl}_2 + h\nu \rightarrow \text{COCl} + \text{Cl}$ with subsequent decay of the COCl radical, $\text{COCl} \rightarrow \text{CO} + \text{Cl}$, produces CO with unity quantum yield (see Okabe, [179], Wijnen, [246], Heicklen [91], Calvert and Pitts [32]).

Table 4F-31. Absorption Cross Sections of COCl₂ at 298 K

λ (nm)	$10^{20} \sigma$ (cm ²)	λ (nm)	$10^{20} \sigma$ (cm ²)	λ (nm)	$10^{20} \sigma$ (cm ²)	λ (nm)	$10^{20} \sigma$ (cm ²)
168.10	301	193.25	68.8	223.47	12.6	264.92	2.68
170.95	433	195.15	52.1	226.00	13.0	268.50	1.85
173.15	493	197.05	40.6	228.58	13.2	272.12	1.17
174.65	509	199.00	31.7	231.23	13.4	275.88	0.689
176.20	475	201.01	25.7	233.93	13.5	279.74	0.370
177.80	427	203.05	20.7	236.69	13.0	283.70	0.182
179.40	369	205.14	17.2	239.53	12.4	287.78	0.0771
181.00	313	207.26	14.7	242.43	11.5	291.99	0.0298
182.65	261	209.43	13.0	245.41	10.4	296.32	0.0104
184.35	210	211.65	11.9	248.45	9.07	300.77	0.00323
186.05	178	213.89	11.4	251.59	7.75	305.36	0.00096
187.80	137	216.20	11.3	254.79	6.32		
189.60	112	218.59	11.5	258.08	5.02		
191.40	88.9	221.00	12.2	261.45	3.77		

Note:

168.10 – 173.15 nm: Gillotay et al. [76]

174.65 – 182.65 nm: mean of Gillotay et al. [76] and Jäger et al. [107]

184.35 – 199.00 nm: mean of Chou et al. [42], Gillotay et al. [76], and Jäger et al. [107]

201.01 – 218.59 nm: mean of Chou et al. [42], Gillotay et al. [76], Meller et al. [150], and Jäger et al. [107]

221.00 – 226.00 nm: mean of Chou et al. [42], Gillotay et al. [76], and Meller et al. [150]

228.58 – 305.36 nm: mean of Gillotay et al. [76] and Meller et al. [150]

F31. COHCl + hν → Products

(Recommendation: 06-2, Note: 10-6, Evaluated: 10-6)

Absorption Cross Sections: The UV absorption spectrum of formyl chloride, COHCl, has been measured at room temperature by Libuda et al. [125] (239 – 307 nm). The absorption spectrum has a highly structured absorption band with a maximum near 260 nm. The recommended cross sections in Table 4F-32 are the averages over 1 nm intervals of the data from Libuda et al. [125] (0.7 nm resolution).

Photolysis Quantum Yield and Product Studies: No studies are available.

Table 4F-32. Absorption Cross Sections of COHCl at 298 K

λ (nm)	$10^{20} \sigma$ (cm ²)	λ (nm)	$10^{20} \sigma$ (cm ²)	λ (nm)	$10^{20} \sigma$ (cm ²)	λ (nm)	$10^{20} \sigma$ (cm ²)
240	2.76	257	3.92	274	3.53	291	0.624
241	3.36	258	5.03	275	2.30	292	0.605
242	3.41	259	4.45	276	3.28	293	0.342
243	3.32	260	5.46	277	2.38	294	0.431
244	3.03	261	5.09	278	2.09	295	0.303
245	3.53	262	4.66	279	1.89	296	0.275
246	4.01	263	4.54	280	2.22	297	0.184
247	4.64	264	4.03	281	1.06	298	0.165
248	4.44	265	3.83	282	1.98	299	0.178
249	4.27	266	4.72	283	1.36	300	0.0562
250	3.92	267	3.76	284	1.15	301	0.0912
251	4.38	268	4.83	285	1.51	302	0.0805
252	4.57	269	3.79	286	1.00	303	0.0319
253	4.98	270	3.34	287	0.784	304	0.0587
254	5.20	271	3.72	288	0.748	305	0.0275
255	4.59	272	2.68	289	0.880	306	0.0157
256	5.07	273	2.74	290	0.371	307	0.0131

Note: Libuda [125]



(Recommendation: 94-26, Note: 10-6, Evaluated: 10-6)

Absorption Cross Sections: The UV absorption spectrum of COFCl (carbonyl chlorofluoride, fluorochlorophosgene) has been measured at room temperature by Chou et al. [42] (186 – 226 nm), Hermann et al. [92] (186 – 226 nm), and Nölle et al. [177] [178] (200 – 262 nm). The spectrum has monotonically decreasing absorptions cross sections with increasing wavelength with a shoulder in the spectrum around 200 nm. The room temperature data are in good agreement in the common wavelength range with differences $\leq 6\%$. The recommended absorption cross sections in Table 4F-33 are the averages over the 500 cm^{-1} intervals used for atmospheric modeling of the data from Chou et al. [42] and Hermann et al. [92] in the region 186 – 199 nm, the mean of the data from Chou et al. [42], Hermann et al. [92] and Nölle et al. [177] [178] at 201 and 203.1 nm, and the data from Nölle et al. [177] [178] at wavelengths $>205 \text{ nm}$.

The temperature dependence of the absorption spectrum was measured by Nölle et al. [177] [178] (200 – 262 nm) at 223, 248, 273, and 298 K. The cross sections decrease with decreasing temperature at wavelengths $>210 \text{ nm}$ with the magnitude of the difference increasing with increasing wavelength. At wavelengths $<210 \text{ nm}$ the cross sections increase with decreasing temperature with the difference in going from 298 to 223 K is $\sim 18\%$ at 201 nm.

Photolysis Quantum Yield and Product Studies: Photolysis quantum yields of COFCl have been measured by Hermann et al. [92] and Nölle et al. [178]. The results are summarized in Table 4F-34. The relative distribution of the CO and COF₂ products was shown by Hermann et al. [92] to depend on the total pressure over the range 10 to 900 mbar. The apparent quantum yields were taken as the quantum yields for the decomposition into COF + Cl and CO + F + Cl since the parent molecule cannot be reformed (as in the case of COF₂) and COCl is known to be unstable.

Table 4F-33. Absorption Cross Sections of COFCl at 298 K

λ (nm)	$10^{20} \sigma$ (cm^2)	λ (nm)	$10^{20} \sigma$ (cm^2)	λ (nm)	$10^{20} \sigma$ (cm^2)	λ (nm)	$10^{20} \sigma$ (cm^2)
186.0	15.6	201.0	12.2	218.6	5.79	239.5	0.459
187.8	14.0	203.1	11.9	221.0	4.77	242.4	0.292
189.6	13.4	205.1	11.5	223.5	3.81	245.4	0.178
191.4	12.9	207.3	10.8	226.0	2.93	248.5	0.103
193.2	12.7	209.4	9.91	228.6	2.19	251.6	0.0635
195.1	12.5	211.6	8.96	231.2	1.57	254.8	0.0409
197.0	12.4	213.9	7.90	233.9	1.09	258.1	0.0279
199.0	12.3	216.2	6.84	236.7	0.724	261.4	0.0214

Note:

186.0 – 199.0 nm: Chou et al. [42] and Hermann et al. [92]

201.0 and 203.1 nm: mean of the data from Chou et al. [42], Hermann et al. [92] and Nölle et al. [178]

205.1 – 261.4 nm: Nölle et al. [178]

Table 4F-34. COFCl Photolysis Quantum Yields

Reference	Year	Photolysis Wavelength (nm)	Φ
Hermann et al. [92]	1994	193	0.98 ± 0.09
Nölle et al. [178]	1991	210	0.85 ± 0.25
		210*	0.90 ± 0.05
		222.5	0.77 ± 0.33
		230	0.71 ± 0.30
		248	0.52 ± 0.14

* Hg lamp photolysis source

F33. CFCI₃ (CFC-11) + hν → Products

(Recommendation: 02-25, Note: 10-6, Evaluated: 10-6)

Absorption Cross Sections: The VUV/UV absorption spectrum of fluorotrichloromethane (CFC-11), CFCI₃, has been measured at room temperature by Gilbert et al. [71] (60 – 145 nm), Doucet et al. [58] (120 – 200 nm), Gordus and Bernstein [82] (225 nm), Rowland and Molina [205] (186 – 226 nm), Robbins and Stolarski [201] (174 – 226 nm), Greene and Wayne [83] (186 – 209 nm), Chou et al. [44] (185 – 226 nm), Hubrich et al. [98] (158 – 260 nm) and Hubrich and Stuhl [97] (158 – 260 nm), Vanlaethem-Meurée et al. [236] (190 – 220 nm), Simon et al. [219] (174 – 230 nm), and Mérienne et al. [151] (200 – 238 nm). Absorption cross sections in the region 148 – 225 nm have also been derived from electron energy loss measurements by Huebner et al. [100], which are up to 30% higher than the values obtained by optical measurements. The room temperature data for wavelengths >180 nm are in good agreement, generally within 10–15%. The recommended absorption cross sections in Table 4F-35 are the values from Simon et al. [219] in the region 174 – 198 nm, the mean of the values reported by Simon et al. [219] and Mérienne et al. [151] in the region 200 – 230 nm, and the data from Hubrich and Stuhl [97] in the region 235 – 260 nm.

The temperature dependence of the absorption spectrum was measured by Chou et al. [44] (185 – 226 nm) over the range 213 – 296 K, Hubrich et al. [98] (158 – 260 nm) and Hubrich and Stuhl [97] (158 – 260 nm) at 208 and 298 K, Vanlaethem-Meurée et al. [236] (190 – 220 nm) at 255, 279, and 296 K, Simon et al. [219] (174 – 230 nm) over the range 225 – 295 K, and Mérienne et al. [151] (200 – 238 nm) at 220, 240, and 296 K. The temperature dependence is significant at wavelengths above 185 nm where the cross sections decrease with decreasing temperature. Simon et al. [219] parameterized their cross section temperature dependence using an empirical polynomial expansion

$$\log_{10} \sigma(\lambda, T) = \sum A_n \lambda^n + (T - 273) \times \sum B_n \lambda^n$$

and reported calculated cross sections for T = 210, 230, 250, 270, and 295 K. The parameters A_n and B_n, valid for the temperature range 210 – 300 K and wavelength range 174 – 230 nm, given below are recommended for use in model calculations.

A ₀ = -84.611	B ₀ = -5.7912
A ₁ = 7.9551 × 10 ⁻¹	B ₁ = 1.1689 × 10 ⁻¹
A ₂ = -2.0550 × 10 ⁻³	B ₂ = -8.8069 × 10 ⁻⁴
A ₃ = -4.4812 × 10 ⁻⁶	B ₃ = 2.9335 × 10 ⁻⁶
A ₄ = 1.5838 × 10 ⁻⁸	B ₄ = -3.6421 × 10 ⁻⁹

Mérienne et al. [151] used a similar polynomial expansion to fit their data

$$\ln \sigma(\lambda, T) = \sum a_n (\lambda - 200)^n + (T - 296) \times \sum b_n (\lambda - 200)^n,$$

valid for the temperature range 220 – 296 K and wavelength range 200 – 238 nm. The reported a_n and b_n parameters are give here.

a ₀ = -41.925548	b ₀ = 3.58977 × 10 ⁻⁴
a ₁ = -1.142857 × 10 ⁻¹	b ₁ = 3.02973 × 10 ⁻⁴
a ₂ = -3.12034 × 10 ⁻³	b ₂ = -1.13 × 10 ⁻⁸
a ₃ = 3.6699 × 10 ⁻⁵	

Photolysis Quantum Yield and Product Studies: Clark and Husain [45] reported a quantum yield for Cl*(²P_{1/2}) atom formation in the broadband photolysis of CFCI₃ of 0.79 ± 0.27.

Table 4F-35. Absorption Cross Sections of CFCl₃ at 298 K

λ (nm)	$10^{20} \sigma$ (cm ²)	λ (nm)	$10^{20} \sigma$ (cm ²)	λ (nm)	$10^{20} \sigma$ (cm ²)
174	313.0	198	78.0	222	1.72
176	324.0	200	63.2	224	1.17
178	323.5	202	49.1	226	0.790
180	314.0	204	37.3	228	0.532
182	296.0	206	28.1	230	0.354
184	272.0	208	20.4	235	0.132
186	243.0	210	15.1	240	0.0470
188	213.0	212	10.7	245	0.0174
190	179.0	214	7.54	250	0.0066
192	154.0	216	5.25	255	0.0029
194	124.3	218	3.65	260	0.0015
196	99.1	220	2.51		

Note:

174 – 198 nm: Simon et al. [219]

200 – 230 nm: mean of Simon et al. [219] and Mérienne et al. [151]

235 – 260 nm: Hubrich and Stuhl [97]

F34. CF₂Cl₂ (CFC-12) + hν → Products

(Recommendation: 06-2, Note: 10-6, Evaluated: 10-6)

Absorption Cross Sections: The VUV/UV absorption spectrum of difluorodichloromethane (CFC-12), CF₂Cl₂, has been measured at room temperature by Gordus and Bernstein [82] (210 nm), Rowland and Molina [205] (186 – 216 nm), Robbins and Stolarski [201] (174 – 216 nm), Greene and Wayne [83] (186 – 206 nm), Rebbert and Ausloos [195] (213.9 nm), Chou et al. [44] (184 – 221 nm), Hubrich et al. [98] (159 – 240 nm), Vanlaethem-Meurée et al. [236] (190 – 216 nm), Simon et al. [219] (174 – 230 nm), and Mérienne et al. [151] (200 – 231 nm). The room temperature data are in good agreement, generally within 10–15%, except for data from Green and Wayne [83] at wavelengths >195 nm and the data from Rowland and Molina [205] near 210 nm. Absorption cross sections have also been derived from electron energy loss measurements by Huebner et al. [100] (148 – 218 nm), which agree to within 10% with the data obtained by optical measurements around the absorption maximum but are larger than the optical cross section data at wavelengths >196 nm by as much as 100%. The recommended absorption cross sections in Table 4F-36 are values from Hubrich et al. [98] in the region 170 – 172 nm, the mean of the values reported by Hubrich et al. [98] and Simon et al. [219] in the region 174 – 178 nm, the values from Simon et al. [219] in the region 180 – 198 nm, mean of the values reported by Simon et al. [219] and Mérienne et al. [151] in the region 200 – 226 nm, and the data of Mérienne et al. [151] in the region 228 – 230 nm. For the range 232 – 240 nm the recommended values (in italics) were obtained from a log-linear fit and extrapolation of the Mérienne et al. [151] data, $\log \sigma(\lambda) = 2.1448 - 0.1061 \lambda$. The measured cross section values from Hubrich et al. [98] over this wavelength range are lower by ~40% at 240 nm than the extrapolated values.

High resolution absorption cross section measurements have been carried out by Seccombe et al. [215] (50 – 150 nm) and Limao-Vieira et al. [127] (113 – 225 nm) using a synchrotron radiation light source. The results of Limao-Vieira et al. [127] for the absorption band at 170 – 204 nm are in very good agreement with the recommendation in Table 4F-36. These cross section measurements significantly improve upon the earlier data from Gilbert et al. [71] (60 – 135 nm) and Doucet et al. [58] (120 – 200 nm).

The temperature dependence of the absorption spectrum has been measured by Rebbert and Ausloos [195] (213.9 nm) over the range 234 – 442 K, Chou et al. [44] (184 – 221 nm) at 212, 252, and 296 K, Hubrich et al. [98] (159 – 240 nm) at 208 and 298 K, Vanlaethem-Meurée et al. [236] (190 – 216 nm) at 255, 279, and 296 K, Simon et al. [219] (174 – 230 nm) at 225–295 K, and Mérienne et al. [151] (200 – 231 nm) at 220, 240, and 296 K.

The temperature dependence is significant at wavelengths above 186 nm where the cross sections decrease with decreasing temperature. Mérienne et al. [151] parameterized the cross section temperature dependence using an empirical polynomial expansion

$$\ln \sigma(\lambda, T) = \sum a_n (\lambda - 200)^n + (T - 296) \times \sum b_n (\lambda - 200)^n$$

that is valid for the temperature range 220 – 296 K and wavelength range 200 – 231 nm. The a_n and b_n parameters given below are recommended for use in model calculations.

$$\begin{aligned} a_0 &= -43.8954569 & b_0 &= 4.8438 \times 10^{-3} \\ a_1 &= -2.403597 \times 10^{-1} & b_1 &= 4.96145 \times 10^{-4} \\ a_2 &= -4.2619 \times 10^{-4} & b_2 &= -5.6953 \times 10^{-6} \\ a_3 &= 9.8743 \times 10^{-6} \end{aligned}$$

Simon et al. [219] also parameterized the cross section temperature dependence of their data. However, the parameters reported by Simon et al. [219] contain typographical error(s) that were reproduced in JPL02-25. The correct parameters are unknown and therefore not given here.

Photolysis Quantum Yield and Product Studies: Clark and Husain [45] report the quantum yield for $\text{Cl}^*(^2\text{P}_{1/2})$ atom formation in the broad band photolysis of CF_2Cl_2 to be 0.75 ± 0.26 .

Table 4F-36. Absorption Cross Sections of CF_2Cl_2 at 298 K

λ (nm)	$10^{20} \sigma$ (cm^2)	λ (nm)	$10^{20} \sigma$ (cm^2)	λ (nm)	$10^{20} \sigma$ (cm^2)
170	124.0	194	31.5	218	0.103
172	151.0	196	21.1	220	0.0624
174	168.0	198	13.9	222	0.0381
176	185.5	200	8.71	224	0.0233
178	189.5	202	5.42	226	0.0140
180	179.0	204	3.37	228	0.0090
182	160.0	206	2.06	230	0.0057
184	134.0	208	1.26	232	0.0034
186	107.0	210	0.762	234	0.0021
188	82.8	212	0.458	236	0.0013
190	63.2	214	0.274	238	0.0008
192	45.50	216	0.163	240	0.0005

Note:

170 – 172 nm: Hubrich et al. [98]

174 – 178 nm: the mean of data from Hubrich et al. [98] and Simon et al. [219]

180 – 198 nm: Simon et al. [219]

200 – 230 nm: mean of data from Simon et al. [219] and Mérienne et al. [151]

232 – 240 nm: extrapolation of data from Mérienne et al. [151] data., $\log \sigma(\lambda) = 2.1448 - 0.1061 \lambda$

F35. CF_3Cl (CFC-13) + $h\nu \rightarrow$ Products

(Recommendation: 02-25, Note: 10-6, Evaluated: 10-6)

Absorption Cross Sections: The VUV/UV absorption spectrum of trifluorochloromethane (CFC-13), CF_3Cl , has been measured at room temperature by Chou et al. [43] (184 – 203 nm), Vanlaethem-Meurée et al. [236] (172 – 200 nm), Hubrich and Stuhl [97] (160 – 220 nm), Simon et al. [219] (172 – 200 nm). The cross section values from Vanlaethem-Meurée et al. [236] and Simon et al. [219] are identical. The cross section data from Hubrich and Stuhl [97] deviate from the Vanlaethem-Meurée et al. [236] and Simon et al. [219] values by $\pm 25\%$ and the data from Chou et al. [43] is systematically greater by 15–30% in the region 185 – 200 nm. The recommended absorption cross sections Table 4F-37 are taken from Simon et al. [219] for the range 172 – 200 nm. The recommended cross sections in the range 202 – 220 nm were obtained by a log-linear extrapolation of the Simon et al. [219] data, $\log \sigma(\lambda) = -5.048 - 0.0834 \lambda$.

The absorption spectrum has been measured in the far UV by Gilbert et al. [71] (65 – 130 nm), and Doucet et al. [58] (120 – 160 nm), and Ravishankara et al. [193] (Lyman- α , 121.6 nm).

The temperature dependence of the absorption spectrum was measured by Vanlaethem-Meurée et al. [236] (172 – 200 nm) at 255, 279, and 296 K, Hubrich and Stuhl [97] (160 – 220 nm) at 208 and 298 K, and Simon et al. [219] (172 – 200 nm) over the range 225 – 295 K. Vanlaethem-Meurée et al. [236] and Simon et al. [219] reported no measurable temperature dependence. Hubrich and Stuhl [97] report a decrease of the absorption cross sections at 208 K, 4% at 160 nm increasing to 74% at 205 nm. Simon et al. [219] parameterized the cross section wavelength dependence and the temperature dependence using an empirical polynomial expansion

$$\log_{10} \sigma(\lambda, T) = \sum A_n \lambda^n + (T - 273) \times \sum B_n \lambda^n \text{ (with all } B_n = 0)$$

and reported calculated values at 295 K. The A_n parameters, which are valid for the temperature range 210 – 300 K and wavelength range 172 – 200 nm, given below are recommended for model calculations.

$$\begin{aligned} A_0 &= -1.55.88 & A_1 &= 2.0993, \\ A_2 &= -1.0486 \times 10^{-2} & A_3 &= 1.6718 \times 10^{-5} \end{aligned}$$

Photolysis Quantum Yield and Product Studies: Clark and Husain [45] report a quantum yield for $\text{Cl}^*(^2\text{P}_{1/2})$ atom formation in the broad band photolysis of CF_3Cl to be 0.86 ± 0.29 .

Table 4F-37. Absorption Cross Sections of CF_3Cl at 295 K

λ (nm)	$10^{20} \sigma$ (cm^2)	λ (nm)	$10^{20} \sigma$ (cm^2)	λ (nm)	$10^{20} \sigma$ (cm^2)
172	1.100	190	0.128	206	<i>0.00595</i>
174	0.970	192	0.0900	208	<i>0.00406</i>
176	0.825	194	0.0610	210	<i>0.00276</i>
178	0.681	196	0.0410	212	<i>0.00188</i>
180	0.542	198	0.0280	214	<i>0.00128</i>
182	0.425	200	0.0190	216	<i>0.000872</i>
184	0.326	200	0.0189	218	<i>0.000594</i>
186	0.244	202	<i>0.0128</i>	220	<i>0.000405</i>
188	0.175	204	<i>0.00874</i>		

Note:

172 – 200 nm: Simon et al. [219]

202 – 220 nm: extrapolation of Simon et al. [219] data

F36. $\text{CF}_2\text{ClCFCl}_2$ (CFC-113) + $h\nu \rightarrow$ Products

(Recommendation: 06-2, Note: 10-6, Evaluated: 10-6)

Absorption Cross Sections: The UV absorption spectrum of 1,1,2-trifluoro-1,2,2-trichloroethane (CFC-113), $\text{CF}_2\text{ClCFCl}_2$, has been measured at room temperature by Chou et al. [43] (184 – 224 nm), Hubrich and Stuhl [97] (160 – 250 nm), and Simon et al. [220] (184 – 230 nm). The cross section values agree to within ~10% except in the region near 190 nm where the values of Hubrich and Stuhl [97] are smaller by as much as 20%. The preferred absorption cross sections in Table 4F-38 are the values from Hubrich and Stuhl [97] in the region 175 – 180 nm, the value at 184 nm was interpolated between those of Hubrich and Stuhl [97] at 180 nm and Simon et al. [220] at 186 nm, and the values from Simon et al. [220] in the region 186 – 230 nm. The recommended absorption cross sections for wavelengths >230 nm (in italics) were obtained from a log-linear extrapolation of the Simon et al. [220] data, $\log \sigma(\lambda) = -0.9860 - 0.0894 \lambda$. The values measured by Hubrich and Stuhl [97] in the region >230 nm are greater than the extrapolated values by ~20–80%.

The absorption spectrum in the far UV has been measured by Doucet et al. [59] (110 – 200 nm).

The temperature dependence of the absorption spectrum has been measured by Hubrich and Stuhl [97] (160 – 250 nm) at 208 and 298 K and Simon et al. [220] (184 – 230 nm) over the range 225 – 295 K. The temperature dependence is significant at wavelengths >194 nm and <170 nm where the cross sections decrease with decreasing temperature. Simon et al. [220] parameterized the temperature dependence of the cross sections using an empirical polynomial expansion

$$\log_{10} \sigma(\lambda, T) = \sum A_n \lambda^n + (T - 273) \times \sum B_n \lambda^n$$

and reported calculated values for $T = 210, 230, 250, 270$, and 295 K. The A_n and B_n parameters, valid over the temperature range 210 – 300 K and wavelength range 182 – 230 nm, given below are recommended for model calculations.

$$\begin{aligned} A_0 &= -1087.9 & B_0 &= 12.493 \\ A_1 &= 20.004 & B_1 &= -2.3937 \times 10^{-1} \\ A_2 &= -1.3920 \times 10^{-1} & B_2 &= 1.7142 \times 10^{-3} \\ A_3 &= 4.2828 \times 10^{-4} & B_3 &= -5.4393 \times 10^{-6} \\ A_4 &= -4.9384 \times 10^{-7} & B_4 &= 6.4548 \times 10^{-9} \end{aligned}$$

Photolysis Quantum Yield and Product Studies: No studies are available.

Table 4F-38. Absorption Cross Sections of CF₂ClCFCl₂ at 298 K

λ (nm)	$10^{20} \sigma$ (cm ²)	λ (nm)	$10^{20} \sigma$ (cm ²)	λ (nm)	$10^{20} \sigma$ (cm ²)
175	192	204	5.80	228	0.0410
180	155	206	4.00	230	0.0270
184	123	208	2.65	232	0.0188
186	104	210	1.80	234	0.0124
188	83.5	212	1.15	236	0.00824
190	64.5	214	0.760	238	0.00546
192	48.8	216	0.505	240	0.00361
194	36.0	218	0.318	242	0.00239
196	26.0	220	0.220	244	0.00159
198	18.3	222	0.145	246	0.00105
200	12.5	224	0.0950	248	0.000696
202	8.60	226	0.0630	250	0.000461

Note:

175 – 180 nm: Hubrich and Stuhl [97]

184 nm: interpolation of Hubrich and Stuhl [97] and Simon et al. [220] data

186 – 230 nm: Simon et al. [220]

232 – 250 nm: extrapolation of Simon et al. [220] data, $\log \sigma(\lambda) = -0.9860 - 0.0894 \lambda$

F37. CF₂ClCF₂Cl (CFC-114) + hν → Products

(Recommendation: 02-25, Note: 10-6, Evaluated: 10-6)

Absorption Cross Sections: The VUV/UV absorption spectrum of 1,1,2,2-tetrafluoro-1,2-dichloroethane (CFC-114), CF₂ClCF₂Cl, has been measured at room temperature by Chou et al. [43] (184 – 219 nm), Hubrich and Stuhl [97] (160 – 235 nm), and Simon et al. [220] (182 – 220 nm). The room temperature values of Simon et al. [220] and Chou et al. [43] agree to within 5% except at 185 and 195 nm. The cross section values from Hubrich and Stuhl [97] are systematically greater than those from Simon et al. [220]. The recommended absorption cross sections in Table 4F-39 are the values from Simon et al. [220] in the region 172 – 220 nm. The recommended cross sections for wavelengths >220 nm (in italics) were obtained from a log-linear extrapolation of the Simon et al. [220] data, $\log \sigma(\lambda) = -1.8233 - 0.00913 \lambda$. The values measured by Hubrich et al. [97] are greater by ~40% than the extrapolated values.

The absorption spectrum in the far UV has been measured by Ravishankara et al. [193] (Lyman-α, 121.6 nm) and Doucet et al. [59] (110 – 190 nm).

The temperature dependence of the absorption spectrum has been measured by Hubrich and Stuhl [97] (160 – 235 nm) at 208 and 298 K and Simon et al. [220] (182 – 220 nm) in the range 225 – 295 K. Simon et al. [220] report decreasing cross sections with decreasing temperature for wavelengths >190 nm. Hubrich and Stuhl [97] report a small decrease of the cross sections (generally <10%) for wavelengths in the range 160 – 210 nm. Simon et al. [220] parameterized the temperature dependence of the cross sections using an empirical polynomial expansion

$$\log_{10} \sigma(\lambda, T) = \sum A_n \lambda^n + (T - 273) \times \sum B_n \lambda^n$$

and reported calculated values for T = 210, 230, 250, 270, and 295 K. The A_n and B_n parameters, valid for the temperature range 210 – 300 K and wavelength range 172 – 220 nm, are given below and recommended for use in model calculations.

$$\begin{array}{ll} A_0 = -160.50 & B_0 = -1.5296 \\ A_1 = 2.4807 & B_1 = 3.5248 \times 10^{-2} \\ A_2 = -1.5202 \times 10^{-2} & B_2 = -2.9951 \times 10^{-4} \\ A_3 = 3.8412 \times 10^{-5} & B_3 = 1.1129 \times 10^{-6} \\ A_4 = -3.4373 \times 10^{-8} & B_4 = -1.5259 \times 10^{-9} \end{array}$$

Photolysis Quantum Yield and Product Studies: No studies are available.

Table 4F-39. Absorption Cross Sections of CF₂ClCF₂Cl at 295 K

λ (nm)	$10^{20} \sigma$ (cm ²)	λ (nm)	$10^{20} \sigma$ (cm ²)	λ (nm)	$10^{20} \sigma$ (cm ²)
172	69.0	194	2.56	216	0.0290
174	55.0	196	1.75	218	0.0190
176	43.0	198	1.20	220	0.0122
178	34.0	200	0.800	222	0.00809
180	26.2	202	0.540	224	0.00531
182	19.8	204	0.370	226	0.00349
184	15.0	206	0.245	228	0.00229
186	11.0	208	0.160	230	0.00151
188	7.80	210	0.104	232	0.00099
190	5.35	212	0.0680	234	0.00065
192	3.70	214	0.0440	235	0.00053

Note:

172 – 220 nm: Simon et al. [220]

222 – 235 nm: extrapolation of Simon et al. [220] data, $\log \sigma(\lambda) = -1.8233 - 0.00913 \lambda$

F38. CF₃CF₂Cl (CFC-115) + hν → Products

(Recommendation: 06-2, Note: 10-6, Evaluated: 10-6)

Absorption Cross Sections: The VUV/UV absorption spectrum of pentafluorochloroethane, CF₃CF₂Cl, has been measured at room temperature by Chou et al. [43] (184 – 207 nm), Hubrich and Stuhl [97] (160 – 230 nm), and Simon et al. [220] (172 – 204 nm). The room temperature cross section data of Simon et al. [220] and Hubrich and Stuhl [97] agree to within ~20% with the Hubrich and Stuhl [97] values being systematically greater over the range 172 – 204 nm. The data of Chou et al. [43] are greater than those of Simon et al. [220] by as much as 50%. The recommended absorption cross sections in Table 4F-40 are the mean of the values reported by Hubrich and Stuhl [97] and Simon et al. [220] in the region 172 – 204 nm. The recommended values for wavelengths >204 nm are the mean of the values measured by Hubrich and Stuhl [97] and those obtained by extrapolating the Simon et al. [220] data, $\log \sigma(\lambda) = -6.2191 - 0.0756 \lambda$, where the extrapolated values are greater than the values measured by Hubrich and Stuhl [97].

The absorption spectrum has been measured in the far UV by Ravishankara et al. [193] (Lyman-α, 121.6 nm) and Doucet et al. [59] (120 – 175 nm).

The temperature dependence of the absorption spectrum has been measured by Hubrich and Stuhl [97] (160 – 230 nm) at 208 and 298 K and Simon et al. [220] (172 – 204 nm) over the range 225 – 295 K. No measurable temperature dependence was reported in these studies. Simon et al. [220] parameterized the absorption cross sections using an empirical polynomial expansion

$$\log_{10} \sigma(\lambda, T) = \sum A_n \lambda^n + (T - 273) \times \sum B_n \lambda^n \text{ (with all } B_n = 0)$$

and reported calculated values for T = 295 K. The parameters A_n parameters, valid for the temperature range 210 – 300 K and wavelength range 172 – 204 nm, are given below and recommended for use in model calculations.

$$\begin{array}{ll} A_0 = 5.8281 & A_1 = -2.990 \times 10^{-1} \\ A_2 = 1.3525 \times 10^{-3} & A_3 = -2.6851 \times 10^{-6} \end{array}$$

Photolysis Quantum Yield and Product Studies: No studies are available.

Table 4F-40. Absorption Cross Sections of CF₃CF₂Cl at 298 K

λ (nm)	$10^{20} \sigma$ (cm ²)	λ (nm)	$10^{20} \sigma$ (cm ²)	λ (nm)	$10^{20} \sigma$ (cm ²)
172	5.50	188	0.403	204	0.0218
174	4.13	190	0.287	205	<i>0.0187</i>
176	3.08	192	0.203	210	<i>0.00700</i>
178	2.25	194	0.143	215	<i>0.00273</i>
180	1.58	196	0.0985	220	<i>0.00107</i>
182	1.13	198	0.0685	225	<i>0.00046</i>
184	0.790	200	0.0474	230	<i>0.00018</i>
186	0.563	202	0.0325		

Note:

172 – 204 nm: mean of Hubrich and Stuhl [97] and Simon et al. [220]

205 – 230 nm: mean of Hubrich and Stuhl [97] and extrapolated Simon et al. [220] data,

$\log \sigma(\lambda) = -6.2191 - 0.0756 \lambda$

F39. CHFC1₂ (HCFC-21) + hν → Products

(Recommendation: 02-25, Note: 10-6, Evaluated: 10-6)

Absorption Cross Sections: The UV absorption spectrum of fluorodichloromethane (HCFC-21), CHFC1₂, has been measured at room temperature by Gordus and Bernstein [82] (208 nm), Robbins and Stolarski [201] (174 – 222 nm), Green and Wayne [83] (184 – 205 nm), Rebbert et al. [196] (213.9 nm), Hubrich et al. [98] (158 – 235 nm), and Simon et al. [219] (174 – 222 nm). The absorption cross section data from these groups are in good agreement, generally to within 15%, except those from Green and Wayne [83] which deviate significantly. The data from Hubrich et al. [98] also contains irregular values around 205 and 220 nm where the agreement is only ~40%. The recommended absorption cross sections in Table 4F-41 are the values of Simon et al. [219] in the region 174 – 222 nm. The recommended values for wavelengths >222 nm (in italics) were obtained from a log-linear extrapolation of the Simon et al. [219] data, $\log \sigma(\lambda) = 0.9806 - 0.1014 \lambda$. The values measured by Hubrich et al. [98] deviate from the extrapolated values significantly.

Measurements in the far UV at 60 – 120 nm have been reported by Gilbert et al. [71], measurements at 120 – 200 nm by Doucet et al. [58], and a measurement at 147 nm by Rebbert et al. [196].

The temperature dependence of the absorption spectrum has been measured by Hubrich et al. [98] (158 – 235 nm) at 208 and 298 K and Simon et al. [219] (174 – 222 nm) over the range 225 – 295 K. The temperature dependence is significant at wavelengths >190 nm where the cross sections decrease with decreasing temperature. Simon et al. [219] parameterized the temperature dependence of the cross sections using an empirical polynomial expansion

$$\log_{10} \sigma(\lambda, T) = \sum A_n \lambda^n + (T - 273) \times \sum B_n \lambda^n$$

and reported calculated values for T = 210, 230, 250, 270, and 295 K. The A_n and B_n parameters, valid for the temperature range 210 – 300 K and wavelength range 174 – 222 nm, given below are recommended for use in model calculations.

$$\begin{array}{ll} A_0 = -514.56 & B_0 = -3.0577 \\ A_1 = 8.7940 & B_1 = 6.6539 \times 10^{-2} \\ A_2 = -5.6840 \times 10^{-2} & B_2 = -5.3964 \times 10^{-4} \\ A_3 = 1.5894 \times 10^{-4} & B_3 = 1.9322 \times 10^{-6} \\ A_4 = 1.6345 \times 10^{-7} & \end{array}$$

Photolysis Quantum Yield and Product Studies: No studies are available.

Table 4F-41. Absorption Cross Sections of CHFCl₂ at 298 K

λ (nm)	$10^{20} \sigma$ (cm ²)	λ (nm)	$10^{20} \sigma$ (cm ²)	λ (nm)	$10^{20} \sigma$ (cm ²)
174	166.0	198	8.10	222	0.0319
176	164.5	200	5.24	224	<i>0.0195</i>
178	155.0	202	3.35	225	<i>0.0154</i>
180	138.0	204	2.12	226	<i>0.0122</i>
182	116.0	206	1.34	228	<i>0.00766</i>
184	92.4	208	0.836	230	<i>0.00480</i>
186	71.5	210	0.522	232	<i>0.00301</i>
188	53.2	212	0.325	234	<i>0.00189</i>
190	38.4	214	0.203	235	<i>0.00150</i>
192	26.9	216	0.127	236	<i>0.00119</i>
194	18.4	218	0.0797		
196	12.3	220	0.0503		

Note:

174 – 222 nm: Simon et al. [219]

224 – 236 nm: extrapolation of Simon et al. [219] data, $\log \sigma(\lambda) = 0.9806 - 0.1014 \lambda$

F40. CHF₂Cl (HCFC-22) + hν → Products

(Recommendation: 02-25, Note: 10-6, Evaluated: 10-6)

Absorption Cross Sections: The UV absorption spectrum of difluorochloromethane (HCFC-22), CHF₂Cl, has been measured at room temperature by Robbins and Stolarski [201] (174 – 202 nm), Green and Wayne [83] (181 – 194 nm), Hubrich et al. [98] (158 – 220 nm), and Simon et al. [219] (174 – 204 nm). The results of Robbins and Stolarski [201], Hubrich et al. [98], and Simon et al. [219] are in agreement, generally to within 15–20%. However, the data from Green and Wayne [83] deviate significantly. The recommended absorption cross sections in Table 4F-42 are the values from Hubrich et al. [98] in the region 170 – 172 nm and the values from Simon et al. [219] in the region 174 – 204 nm. The recommended absorption cross sections for wavelengths >204 nm (in italics) were obtained from a log-linear extrapolation of the Simon et al. [219] data, $\log \sigma(\lambda) = -4.1001 - 0.0870 \lambda$. The measured values of Hubrich et al. [98] deviate from the extrapolated values by as much as 20%.

The absorption spectrum has been measured in the far UV by Gilbert et al. [71] (60 – 160 nm) and Doucet et al. [58] (120 – 200 nm).

The temperature dependence of the absorption spectrum has been measured by Hubrich et al. [98] (158 – 220 nm) at 208 and 298 K and Simon et al. [219] (174 – 204 nm) over the range 225 – 295 K. A weak temperature dependence was observed for wavelengths >190 nm where the cross sections decrease with decreasing temperature. Simon et al. [219] parameterized the cross sections temperature dependence using an empirical polynomial expansion

$$\log_{10} \sigma(\lambda, T) = \sum A_n \lambda^n + (T - 273) \times \sum B_n \lambda^n$$

and reported calculated cross section values for T = 210, 230, 250, 270, and 295 K. The A_n and B_n parameters, valid for the temperature range 210 – 300 K and wavelength range 174 – 204 nm, given below are recommended for use in model calculations.

$$\begin{array}{ll} A_0 = -106.029 & B_0 = -1.3399 \times 10^{-1} \\ A_1 = 1.5038 & B_1 = 2.7405 \times 10^{-3} \\ A_2 = -8.2476 \times 10^{-3} & B_2 = -1.8028 \times 10^{-5} \\ A_3 = 1.4206 \times 10^{-5} & B_3 = 3.8504 \times 10^{-8} \end{array}$$

Photolysis Quantum Yield and Product Studies: No studies are available.

Table 4F-42. Absorption Cross Sections of CHF₂Cl at 298 K

λ (nm)	$10^{20} \sigma$ (cm ²)	λ (nm)	$10^{20} \sigma$ (cm ²)	λ (nm)	$10^{20} \sigma$ (cm ²)
170	12.9	188	0.372	206	0.00842
172	9.79	190	0.245	208	0.00636
174	5.72	192	0.156	210	0.00426
176	4.04	194	0.103	212	0.00285
178	2.76	196	0.072	214	0.00191
180	1.91	198	0.048	216	0.00128
182	1.28	200	0.032	218	0.00086
184	0.842	202	0.0220	220	0.00057
186	0.576	204	0.0142		

Note:

170 – 172 nm: Hubrich et al. [98]

174 – 204 nm: Simon et al. [219]

206 – 220 nm: extrapolation of Simon et al. [219] data, $\log \sigma(\lambda) = -4.1001 - 0.0870 \lambda$

F41. CH₂FCI (HCFC–31) + hν → Products

(Recommendation: 02-25, Note: 10-6, Evaluated: 10-6)

Absorption Cross Sections: The absorption spectrum of fluorochloromethane (HCFC-31), CH₂FCI, has been measured at 208 and 298 K over the wavelength range 160 – 230 nm by Hubrich and Stuhl [97]. The recommended room temperature cross section from this study are listed in Table 4F-43.

The absorption spectrum has been measured in the far UV by Gilbert et al. [71] (60 – 120 nm) and Doucet et al. [58] (120 – 200 nm). The cross section values reported by Doucet et al. are significantly greater than those of Hubrich and Stuhl [97] for the common wavelength region.

Photolysis Quantum Yield and Product Studies: No studies are available.

Table 4F-43. Absorption Cross Sections of CH₂FCI at 298 K

λ (nm)	$10^{20} \sigma$ (cm ²)	λ (nm)	$10^{20} \sigma$ (cm ²)	λ (nm)	$10^{20} \sigma$ (cm ²)
160	47.9	185	4.20	210	0.0188
165	55.9	190	1.95	215	0.00560
170	43.0	195	0.544	220	0.00215
175	23.3	200	0.209	225	0.00049
180	12.5	205	0.069	230	0.00026

Note:

160 – 230 nm: Hubrich and Stuhl [97]

F42. CF₃CHCl₂ (HCFC–123) + hν → Products

(Recommendation: 06-2, Note: 10-6, Evaluated: 10-6)

Absorption Cross Sections: The absorption spectrum of 1,1,1-trifluoro-2,2-dichloroethane (HCFC-123), CF₃CHCl₂, has been measured at room temperature by Green and Wayne [83] (185 – 204 nm), Gillotay and Simon [74] (170 – 250 nm), Orlando et al. [182] (190 – 230 nm), and Nayak et al. [168] (160 – 230 nm). The absorption cross sections are within 25% of each other in the region below 220 nm with the exception of the Green and Wayne [83] data that is significantly lower at wavelengths <200 nm. The recommended absorption cross sections in Table 4F-44 are the mean of the values reported by Gillotay and Simon [74] and Nayak et al. [168] in the region 170 – 188 nm and the mean of the values reported by Gillotay and Simon [74], Orlando et al. [182], and Nayak et al. [168] in the region 190 – 230 nm. The recommended cross

sections for wavelengths >230 nm (in italics) were obtained using a log-linear extrapolation of the Orlando et al. [182] data, $\log \sigma(\lambda) = -3.1097 - 0.0794 \lambda$.

The temperature dependence of the absorption spectrum has been reported by Gillotay and Simon [74] (170 – 250 nm) at 225 – 295 K, Orlando et al. [182] (190 – 230 nm) over the range 203 – 295 K, and Nayak et al. [168] (160 – 230 nm) over the range 223 – 333 K. These studies report a decrease of the absorption cross sections with decreasing temperature at wavelengths >178 nm and <170 nm. Between 170 – 180 nm, an increase in the cross section with decreasing temperature was reported by Gillotay and Simon [74] and Nayak et al. [168]. An irregular temperature dependence was reported by Orlando et al. [182] for the range 210 – 230 nm where the absorption spectra show wiggles.

Various empirical functional forms have been proposed to parameterize the temperature dependence of the absorption cross sections. Gillotay and Simon [74] parameterized the cross sections and the temperature dependence using the polynomial expansion

$$\log_{10} \sigma(\lambda, T) = \sum A_n \lambda^n + (T - 273) \times \sum B_n \lambda^n$$

and report calculated cross section values for T = 210, 230, 250, 270, and 295 K. The A_n and B_n parameters, valid for the temperature range 210 – 300 K and wavelength range 182 – 250 nm, are given below.

$$\begin{aligned} A_0 &= -513.996354 & B_0 &= 1.757133 \\ A_1 &= 9.089141 & B_1 &= -3.499205 \times 10^{-2} \\ A_2 &= -6.136794 \times 10^{-2} & B_2 &= 2.593563 \times 10^{-4} \\ A_3 &= 1.814826 \times 10^{-4} & B_3 &= -8.489357 \times 10^{-7} \\ A_4 &= -1.999514 \times 10^{-7} & B_4 &= 1.037756 \times 10^{-9}. \end{aligned}$$

Nayak et al. [168] used a sixth-order polynomial of the form

$$\log_{10} (\sigma_T) = \sum C_n (\lambda - 170)^n$$

for the temperatures measured in their study for the wavelength range 160 – 230 nm. The C_n parameters listed below.

	223 K	273 K	295 K	333 K
C_0	-17.6732	-17.6773	-17.6792	-17.6722
C_1	1.70233×10^{-2}	1.3636×10^{-2}	1.19392×10^{-2}	9.07941×10^{-3}
C_2	-7.39366×10^{-4}	-4.98553×10^{-4}	-3.71661×10^{-4}	-1.29566×10^{-4}
C_3	-1.83761×10^{-4}	-1.70566×10^{-4}	-1.61218×10^{-4}	-1.56667×10^{-4}
C_4	7.80778×10^{-6}	6.73373×10^{-6}	6.03101×10^{-6}	5.56409×10^{-6}
C_5	-1.29836×10^{-7}	-1.02726×10^{-7}	-8.76762×10^{-8}	-7.77379×10^{-8}
C_6	8.05415×10^{-10}	5.66688×10^{-10}	4.61745×10^{-10}	3.93859×10^{-10}

Orlando et al. [182] used the expression

$$\ln \sigma(\lambda, T) = \sum (\sum a_{ij} (T - 245.4)^{j-1}) (\lambda - 206.214)^{i-1}, \quad i = 1-4, j = 1-3$$

that is valid for the temperature range 203 – 295 K and wavelength range 190 – 230 nm. The coefficients are given below.

$$\begin{aligned} a_{11} &= -4.500 \times 10^1 & a_{12} &= 3.529 \times 10^{-3} & a_{13} &= -4.181 \times 10^{-8} \\ a_{21} &= -1.985 \times 10^{-1} & a_{22} &= 6.826 \times 10^{-5} & a_{23} &= 1.555 \times 10^{-6} \\ a_{31} &= -2.802 \times 10^{-4} & a_{32} &= -1.018 \times 10^{-5} & a_{33} &= 4.037 \times 10^{-8} \\ a_{41} &= 6.312 \times 10^{-5} & a_{42} &= -3.055 \times 10^{-7} & a_{43} &= -2.473 \times 10^{-9} \end{aligned}$$

Photolysis Quantum Yield and Product Studies: No studies are available.

Table 4F-44. Absorption Cross Sections of CF₃CHCl₂ at 295 K

λ (nm)	$10^{20} \sigma$ (cm ²)	λ (nm)	$10^{20} \sigma$ (cm ²)	λ (nm)	$10^{20} \sigma$ (cm ²)
170	192	198	17.1	226	0.0880
172	207	200	11.9	228	0.0599
174	214	202	8.24	230	0.0451
176	213	204	5.70	232	0.0295
178	202	206	3.89	234	0.0205
180	184	208	2.67	236	0.0142
182	161	210	1.82	238	0.0098
184	135	212	1.23	240	0.0068
186	109	214	0.838	242	0.0047
188	85.5	216	0.573	244	0.0033
190	62.2	218	0.384	246	0.0023
192	46.4	220	0.266	248	0.0016
194	33.9	222	0.180	250	0.0011
196	24.2	224	0.124		

Notes:

170 – 188 nm: mean of the values from Gillotay and Simon [74] and Nayak et al. [168]

190 – 230 nm: mean of the values from Gillotay and Simon [74], Orlando et al. [182], and Nayak et al. [168]

232 – 250 nm: extrapolation of Orlando et al. [182] data, $\log \sigma(\lambda) = -3.1097 - 0.0794 \lambda$

F43. CF₃CHFCI (HCFC-124) + hν → Products

(Recommendation: 06-2, Note: 10-6, Evaluated: 10-6)

Absorption Cross Sections: The absorption spectrum of 1,1,1,2-tetrafluoro-2-chloroethane (HCFC-124), CF₃CHFCI, has been measured by Orlando et al. [182] (190 – 230 nm) over the range 203 – 295 K and Gillotay and Simon [73] (170 – 230 nm) over the range 210 – 295 K. The absorption cross sections from these studies agree to better than 10% between 190 and 220 nm. At wavelengths >220 nm the values of Orlando et al. [182] are greater than those of Gillotay and Simon [73] by as much as 133%. The recommended room temperature cross sections in Table 4F-45 are the values of Gillotay and Simon [73] in the region 170 – 188 nm and 222 – 230 nm and the mean of the values reported by Gillotay and Simon [73] and Orlando et al. [182] in the region 190 – 220 nm.

The absorption cross sections decrease with decreasing temperature. An irregular temperature behavior was reported by Orlando et al. [182] for the range 215 – 230 nm where the absorption spectra show wiggles. Gillotay and Simon [73] parameterized the cross sections and the temperature dependence using an empirical polynomial expansion

$$\log_{10} \sigma(\lambda, T) = \sum A_n \lambda^n + (T - 273) \times \sum B_n \lambda^n$$

and reported calculated cross section values for T = 210, 230, 250, 270, and 295 K. The A_n and B_n parameters, valid for the temperature range 210 – 300 K and wavelength range 170 – 230 nm, are given below.

$$\begin{aligned} A_0 &= -101.230250 & B_0 &= -5.795712 \times 10^{-2} \\ A_1 &= 1.333519 & B_1 &= 1.053901 \times 10^{-3} \\ A_2 &= -6.888672 \times 10^{-3} & B_2 &= -6.530379 \times 10^{-6} \\ A_3 &= 1.114172 \times 10^{-5} & B_3 &= 1.382056 \times 10^{-8} \end{aligned}$$

Orlando et al. [182] report a parameterization using the expression

$$\ln \sigma(\lambda, T) = \sum (\sum a_{ij} (T-251.7)^{j-1}) (\lambda - 206.214)^{i-1}, \quad i = 1-4, j = 1-3$$

for the temperature range 203 – 295 K and wavelength range 190 – 230 nm. The reported coefficients are given below.

$$\begin{array}{lll}
a_{11} = -4.967 \times 10^1 & a_{12} = 6.562 \times 10^{-3} & a_{13} = 1.735 \times 10^{-5} \\
a_{21} = -2.025 \times 10^{-1} & a_{22} = 2.788 \times 10^{-4} & a_{23} = -3.974 \times 10^{-6} \\
a_{31} = 6.839 \times 10^{-4} & a_{32} = 5.523 \times 10^{-6} & a_{33} = -3.092 \times 10^{-7} \\
a_{41} = 1.275 \times 10^{-4} & a_{42} = -2.959 \times 10^{-7} & a_{43} = -1.182 \times 10^{-8}
\end{array}$$

Photolysis Quantum Yield and Product Studies: No studies are available.

Table 4F-45. Absorption Cross Sections of CF₃CHFCl at 295 K

λ (nm)	$10^{20} \sigma$ (cm ²)	λ (nm)	$10^{20} \sigma$ (cm ²)	λ (nm)	$10^{20} \sigma$ (cm ²)
170	13.6	192	0.548	214	0.00859
172	11.1	194	0.387	216	0.00610
174	8.85	196	0.267	218	0.00431
176	6.93	198	0.185	220	0.00312
178	5.33	200	0.128	222	0.00214
180	4.03	202	0.0868	224	0.00153
182	3.00	204	0.0594	226	0.00111
184	2.20	206	0.0401	228	0.00082
186	1.60	208	0.0269	230	0.00061
188	1.14	210	0.0186		
190	0.772	212	0.0126		

Notes:

170 – 188 nm: Gillotay and Simon [73]

190 – 220 nm: mean of the values from Gillotay and Simon [73] and Orlando et al. [182]

222 – 230 nm: Gillotay and Simon [73]

F44. CF₃CH₂Cl (HCFC–133) + hν → Products

(Recommendation: 02-25, Note: 10-6, Evaluated: 10-6)

Absorption Cross Sections: The absorption spectrum of 1,1,1-trifluoro-2-chloroethane (HCFC–133), CF₃CH₂Cl, has been measured at room temperature by Ichimura et al. [103] (147 nm, $\sigma = 1.35 \times 10^{-17}$ cm²), and Green and Wayne [83] (186 – 203 nm), and at 208 and 298 K by Hubrich and Stuhl [97] (160 – 245 nm). The agreement in the absorption cross sections for wavelengths >180 nm is poor. The recommended absorption cross sections in Table 4F-46 are taken from Hubrich and Stuhl [97].

Photolysis Quantum Yield and Product Studies: No studies are available.

Table 4F-46. Absorption Cross Sections of CF₃CH₂Cl at 298 K

λ (nm)	$10^{20} \sigma$ (cm ²)	λ (nm)	$10^{20} \sigma$ (cm ²)	λ (nm)	$10^{20} \sigma$ (cm ²)
160	59.4	190	6.20	220	0.0887
165	64.6	195	2.95	225	0.0226
170	56.4	200	1.14	230	0.0147
175	37.3	205	0.598	235	0.00404
180	22.8	210	0.328	240	0.00181
185	11.6	215	0.169	245	0.00054

Note:

160 – 245 nm: Hubrich and Stuhl [97]

F45. CH₃CFCl₂ (HCFC–141b) + hν → Products

(Recommendation: 06-2, Note: 10-6, Evaluated: 10-6)

Absorption Cross Sections: The UV absorption spectrum of 1,1,1-fluorodichloroethane (HCFC-141b), CH_3CFCl_2 , has been measured over the temperature range 210 – 295 K by Gillotay and Simon [74] (170 – 240 nm), over the temperature range 203 – 295 K by Talukdar et al. [225] (190 – 230 nm), and at room temperature by Fahr et al. [60] (190 – 240 nm). Fahr et al. [60] also measured the absorption spectrum in the liquid-phase and used a wavelength-shift procedure to derive cross sections for the gas-phase. The agreement between the cross section values reported by Gillotay and Simon [74] and Fahr et al. [60] for the 190 – 240 nm region is good (1–10% up to 236 nm). The agreement of the results from Talukdar et al. [225] are not as good. Their absorption cross sections are smaller at wavelengths <210 nm by as much as ~20% and are greater at wavelengths >210 nm by as much as 70%. The recommended absorption cross sections in Table 4F-47 are the values of Gillotay and Simon [74] in the region 170 – 188 nm and the mean of the values reported by Gillotay and Simon [74] and Fahr et al. [60] in the region 190 – 240 nm.

A decrease of the absorption cross sections with decreasing temperature for wavelengths >188 nm and <172 nm was reported by Gillotay and Simon [74]. An increase in the cross sections with decreasing temperature was observed between 172 and 188 nm. Gillotay and Simon [74] parameterized the cross sections and the temperature dependence of the absorption cross sections using an empirical polynomial expansion

$$\log_{10} \sigma(\lambda, T) = \sum A_n \lambda^n + (T - 273) \times \sum B_n \lambda^n.$$

and report calculated cross section values for T = 210, 230, 250, 270, and 295 K. The parameters, valid for the temperature range 210 – 300 K and wavelength range 172–240 nm, are given below and recommended for use in model calculations.

$$\begin{array}{ll} A_0 = -682.913042 & B_0 = 4.074747 \\ A_1 = 12.122290 & B_1 = -8.053899 \times 10^{-2} \\ A_2 = -8.187699 \times 10^{-2} & B_2 = 5.946552 \times 10^{-4} \\ A_3 = 2.437244 \times 10^{-4} & B_3 = -1.945048 \times 10^{-6} \\ A_4 = -2.719103 \times 10^{-7} & B_4 = 2.380143 \times 10^{-9} \end{array}$$

Photolysis Quantum Yield and Product Studies: No studies are available.

Table 4F-47. Absorption Cross Sections of CH_3CFCl_2 at 298 K

λ (nm)	$10^{20} \sigma$ (cm^2)	λ (nm)	$10^{20} \sigma$ (cm^2)	λ (nm)	$10^{20} \sigma$ (cm^2)
170	143.1	194	47.2	218	0.382
172	145.1	196	34.1	220	0.248
174	154.2	198	24.0	222	0.161
176	162.9	200	16.6	224	0.105
178	172.6	202	11.3	226	0.0680
180	172.3	204	7.56	228	0.0444
182	162.9	206	5.02	230	0.0290
184	146.4	208	3.30	232	0.0189
186	125.7	210	2.16	234	0.0123
188	103.6	212	1.40	236	0.00801
190	83.0	214	0.909	238	0.00518
192	63.6	216	0.589	240	0.00334

Note:

170 – 188 nm: Gillotay and Simon [74]

190 – 240 nm: mean of data from Gillotay and Simon [74] and Fahr et al. [60]

- F46. $\text{CH}_3\text{CF}_2\text{Cl}$ (HCFC-142b) + $h\nu \rightarrow \text{CH}_3\text{CF}_2 + \text{Cl}$ 355 kJ mol⁻¹ 337 nm (1)
(Recommendation: 06-2, Note: 10-6, Evaluated: 10-6)

Absorption Cross Sections: The absorption spectrum of 1,1,1-difluorochloroethane (HCFC-142b), $\text{CH}_3\text{CF}_2\text{Cl}$, has been measured at room temperature by Doucet et al. [59] (120 – 180 nm), Green and Wayne [83] (184 – 210 nm), Hubrich and Stuhl [97] (160 – 230 nm), Gillotay and Simon [74] (170 – 230 nm), Orlando et al. [182] (190 – 230 nm), and Nayak et al. [168] (160 – 210 nm). For wavelengths <200 nm, the cross sections reported by Hubrich and Stuhl [97] and Nayak et al. [168] agree to within 15% while those by Gillotay and Simon [74] and Orlando et al. [182] are systematically smaller by as much as 30%. Over the

wavelength range 200 – 215 nm, the values of Gillotay and Simon [74], Orlando et al. [182], and Nayak et al. [168] agree to within 15%. For wavelengths >215 nm, the absorption spectrum reported by Orlando et al. [182] has wiggles and deviations of up to 100% from the data of Gillotay and Simon [74]. The values reported by Hubrich and Stuhl [97] in the range 205 – 230 nm have increasingly larger deviations from the values reported by Gillotay and Simon [74] with increasing wavelength. The results of Green and Wayne [83] are very significantly different from all the other data sets and are not considered in the recommendation. The recommended room temperature absorption cross sections in Table 4F-48 are the mean of the values reported by Hubrich and Stuhl [97], Gillotay and Simon [74], and Nayak et al. [168] in the region 175 – 185 nm, the mean of the values reported by Gillotay and Simon [74], Orlando et al. [182], and Nayak et al. [168] in the region 190 – 210 nm, and the values reported by Gillotay and Simon [74] in the region 212 – 230 nm.

The temperature dependence of the absorption spectrum has been measured by Hubrich and Stuhl [97] (160 – 230 nm) at 298 and 208 K, Gillotay and Simon [74] (170–230 nm) over the range 210 – 295 K, Orlando et al. [182] (190 – 230 nm) over the range 203 – 295 K, and Nayak et al. [168] (160 – 210 nm) over the range at 223 – 333 K. A decrease of the absorption cross sections with decreasing temperature was observed by Gillotay and Simon [74] and Nayak et al. [168] over the wavelength range 160 – 230 nm and by Orlando et al. [182] between 190 and 200 nm. An irregular temperature behavior was reported by Orlando et al. [182] for the range 215 – 230 nm where the absorption spectrum at various temperatures cross. The absorption cross sections and temperature dependence have been parameterized using several different empirical functional forms. Gillotay and Simon [74] used the polynomial expansion

$$\log_{10} \sigma(\lambda, T) = \sum A_n \lambda^n + (T - 273) \times \sum B_n \lambda^n$$

and reported calculated cross section values for T = 210, 230, 250, 270, and 295 K. The A_n and B_n parameters, valid for the temperature range 210 – 300 K and wavelength range 172 – 230 nm, are given below.

$A_0 = -328.092008$	$B_0 = 4.289533 \times 10^{-1}$
$A_1 = 6.342799$	$B_1 = -9.042817 \times 10^{-3}$
$A_2 = -4.810362 \times 10^{-2}$	$B_2 = 7.018009 \times 10^{-5}$
$A_3 = 1.611991 \times 10^{-4}$	$B_3 = -2.389065 \times 10^{-7}$
$A_4 = -2.042613 \times 10^{-7}$	$B_4 = 3.039799 \times 10^{-10}$

Nayak et al. [168] used the expression

$$\log_{10} (\sigma_T) = \sum C_n (\lambda - 160)^n$$

and reported coefficients for 223, 233, 253, 273, 295, 313, and 333 K and the wavelength range 160 – 210 nm. The reported C_n parameters are given below.

	223 K	273 K	295 K	333 K
C_0	-18.2361	-18.2441	-18.2406	-18.1777
C_1	-1.26669×10^{-2}	-7.37889×10^{-3}	-6.48269×10^{-3}	-2.39647×10^{-2}
C_2	-2.32945×10^{-3}	-2.66537×10^{-3}	-2.80923×10^{-3}	-7.23910×10^{-4}
C_3	2.81933×10^{-5}	4.19193×10^{-5}	5.01979×10^{-5}	-1.08049×10^{-5}
C_4	-1.37963×10^{-7}	-2.88472×10^{-7}	-3.96860×10^{-7}	1.37618×10^{-7}

Orlando et al. [182] used the expression

$$\ln \sigma(\lambda, T) = \sum (\sum a_{ij} (T-245.4)^{j-1}) (\lambda - 206.214)^{i-1}, \quad i = 1-4, j = 1-3$$

for the temperature range 203 – 295 K and wavelength range 190 – 230 nm. The coefficients are given below.

$a_{11} = -4.973 \times 10^1$	$a_{12} = 9.077 \times 10^{-3}$	$a_{13} = -4.651 \times 10^{-5}$
$a_{21} = -2.175 \times 10^{-1}$	$a_{22} = 4.712 \times 10^{-4}$	$a_{23} = -1.005 \times 10^{-5}$
$a_{31} = 4.133 \times 10^{-4}$	$a_{32} = -6.432 \times 10^{-5}$	$a_{33} = 1.141 \times 10^{-6}$
$a_{41} = 7.145 \times 10^{-5}$	$a_{42} = -5.396 \times 10^{-6}$	$a_{43} = 1.187 \times 10^{-7}$

Photolysis Quantum Yield and Product Studies: Quantum yields for Cl ($^2P_{3/2}$) and Cl* ($^2P_{1/2}$) atom formation in the photolysis of $\text{CH}_3\text{CF}_2\text{Cl}$ at 193.3 nm have been measured by Brownsword et al. [21] to be $\Phi(\text{Cl} + \text{Cl}^*) = 0.90 \pm 0.17$ with $\Phi(\text{Cl}) = 0.65 \pm 0.12$ and $\Phi(\text{Cl}^*) = 0.25 \pm 0.05$. Brownsword et al. [20] reported the quantum yields for H atom formation in the photolysis at 121.6 and 193.3 nm to be 0.53 ± 0.12 and 0.06 ± 0.02 , respectively.

Table 4F-48. Absorption Cross Sections of CH₃CF₂Cl at 298 K

λ (nm)	$10^{20} \sigma$ (cm ²)	λ (nm)	$10^{20} \sigma$ (cm ²)	λ (nm)	$10^{20} \sigma$ (cm ²)
170	27.1	200	0.145	218	0.00243
175	14.0	202	0.0949	220	0.00145
180	6.38	204	0.0622	222	0.000845
185	2.73	206	0.0399	224	0.000484
190	1.02	208	0.0256	226	0.000271
192	0.706	210	0.0161	228	0.000148
194	0.482	212	0.0105	230	0.0000783
196	0.324	214	0.00652		
198	0.218	216	0.00401		

Note:

170 – 185 nm: mean of data from Gillotay and Simon [74], Hubrich and Stuhl [97], and Nayak et al. [168]

190 – 210 nm: mean of data from Gillotay and Simon [74], Orlando et al. [182], and Nayak et al. [168]

212 – 230 nm: Gillotay and Simon [74]

F47. CH₂ClCHO + hν → Products

(Recommendation: 06-2, Note: 10-6, Evaluated: 10-6)

Absorption Cross Sections: The UV absorption spectrum of chloroacetaldehyde, CH₂ClCHO, has been measured at room temperature by Lucazeau and Sandorfy [133] (118 – 182 nm) and Libuda [124] (235 – 360 nm). The absorption band centered at ~290 nm has prominent diffuse band structure at wavelengths >280 nm. The recommended absorption cross sections in Table 4F-49 are the average absorption cross sections over 1 nm intervals of the spectrum reported by Libuda [124] (0.6 nm resolution).

Photolysis Quantum Yield and Product Studies: No studies are available.

Table 4F-49. Absorption Cross Sections of CH₂ClCHO at 298 K

λ (nm)	$10^{20} \sigma$ (cm ²)	λ (nm)	$10^{20} \sigma$ (cm ²)	λ (nm)	$10^{20} \sigma$ (cm ²)	λ (nm)	$10^{20} \sigma$ (cm ²)
240	0.952	270	2.46	300	5.57	330	1.64
241	0.887	271	2.65	301	5.10	331	1.52
242	0.885	272	2.85	302	4.92	332	1.68
243	0.881	273	2.98	303	5.01	333	1.42
244	0.845	274	3.04	304	5.30	334	1.36
245	0.814	275	3.13	305	5.27	335	1.06
246	0.815	276	3.29	306	5.48	336	0.747
247	0.841	277	3.38	307	5.34	337	0.622
248	0.857	278	3.57	308	5.44	338	0.502
249	0.864	279	3.82	309	5.37	339	0.411
250	0.875	280	3.99	310	5.03	340	0.340
251	0.884	281	4.23	311	4.61	341	0.281
252	0.926	282	4.09	312	3.92	342	0.247
253	0.959	283	4.15	313	3.71	343	0.213
254	0.977	284	4.31	314	3.73	344	0.190
255	1.01	285	4.55	315	3.96	345	0.159
256	1.08	286	4.64	316	3.85	346	0.136
257	1.18	287	4.80	317	4.16	347	0.0977
258	1.23	288	4.99	318	3.84	348	0.0791
259	1.28	289	5.03	319	3.78	349	0.0623
260	1.33	290	5.20	320	3.84	350	0.0545
261	1.42	291	4.95	321	3.43	351	0.0558
262	1.53	292	4.94	322	3.26	352	0.0603
263	1.68	293	5.14	323	2.49	353	0.0633
264	1.84	294	5.48	324	2.11	354	0.0565
265	1.91	295	5.47	325	1.92	355	0.0377
266	1.98	296	5.64	326	1.87	356	0.0239
267	2.08	297	5.56	327	1.87	357	0.0123
268	2.23	298	5.75	328	1.70		
269	2.33	299	5.63	329	1.92		

Note:

Libuda et al. [124]

F48. CHCl₂CHO + hν → Products

(Recommendation: 06-2, Note: 10-6, Evaluated: 10-6)

Absorption Cross Sections: The UV absorption spectrum of dichloroacetaldehyde, CHCl₂CHO, has been measured at room temperature by Lucazeau and Sandorfy [133] (118 – 182 nm) and Libuda [124] (253 – 360 nm) who report an absorption band with weak structure around the maximum at ~300 nm. The recommended absorption cross sections in Table 4F-50 are averages over 1 nm intervals of the spectrum reported by Libuda [124] (0.6 nm resolution).

Photolysis Quantum Yield and Product Studies: No studies are available.

Table 4F-50. Absorption Cross Sections of CHCl₂CHO at 298 K

λ (nm)	$10^{20} \sigma$ (cm ²)	λ (nm)	$10^{20} \sigma$ (cm ²)	λ (nm)	$10^{20} \sigma$ (cm ²)	λ (nm)	$10^{20} \sigma$ (cm ²)
256	0.0462	281	3.66	306	5.76	331	1.47
257	0.0787	282	3.85	307	5.70	332	1.34
258	0.167	283	4.02	308	5.49	333	1.22
259	0.221	284	4.23	309	5.36	334	1.21
260	0.247	285	4.43	310	5.25	335	1.05
261	0.313	286	4.63	311	4.99	336	0.859
262	0.445	287	4.88	312	4.58	337	0.720
263	0.596	288	4.96	313	4.40	338	0.594
264	0.705	289	5.17	314	4.26	339	0.495
265	0.785	290	5.32	315	4.11	340	0.418
266	0.914	291	5.38	316	3.98	341	0.362
267	1.09	292	5.51	317	3.85	342	0.315
268	1.30	293	5.68	318	3.73	343	0.259
269	1.49	294	5.85	319	3.51	344	0.209
270	1.67	295	5.88	320	3.30	345	0.182
271	1.77	296	6.06	321	3.18	346	0.155
272	1.91	297	5.97	322	3.00	347	0.134
273	2.08	298	6.04	323	2.73	348	0.117
274	2.28	299	6.02	324	2.48	349	0.102
275	2.57	300	6.14	325	2.27	350	0.0844
276	2.74	301	5.94	326	2.14	351	0.0707
277	3.01	302	5.97	327	1.99	352	0.0697
278	3.14	303	5.93	328	1.80	353	0.0638
279	3.26	304	5.90	329	1.67		
280	3.48	305	5.77	330	1.58		

Note:

Libuda et al. [124]

F49. CF₂ClCHO + hν → Products

(Recommendation: 06-2, Note: 10-6, Evaluated: 10-6)

Absorption Cross Sections: The UV absorption spectrum of difluorochloroacetaldehyde, CF₂ClCHO, has been measured at room temperature by Libuda [124] (235 – 355 nm) and Rattigan et al. [190] (235 – 370 nm). The spectrum displays an absorption band over the wavelength range of the measurements with a maximum at 300 nm. The room temperature cross section data are in good agreement, within 3-10% around the peak, with the data from Rattigan et al. [190] being systematic greater than those of Libuda [124]. At wavelengths away from the peak the data from Rattigan et al. [190] are also greater by 25% at 340 nm and 15 to 300% between 265 and 235 nm.

Rattigan et al. [190] also reported the temperature dependence of the absorption spectrum over the range 245 – 298 K. The cross sections increase near the peak and decrease in the long wavelength wing with decreasing temperature. Rattigan et al. [190] fit the measured temperature dependence with the empirical expression

$$\ln \sigma(\lambda, T) = \ln \sigma(\lambda, 298 \text{ K}) + B(\lambda)(T - 298)$$

The recommended room temperature absorption cross sections in Table 4F-51 are the mean values of the data from Libuda [124] (using 1 nm averages of spectra recorded with 0.6 nm resolution) and Rattigan et al. [190] (5 nm averages of spectra recorded with 0.6 nm resolution) in the region 235 – 350 nm and the data from Rattigan et al. [190] in the region 355 – 370 nm. The temperature coefficients are taken from Rattigan et al. [190].

Photolysis Quantum Yield and Product Studies: No studies are available.

Table 4F-51. Absorption Cross Sections of CF₂ClCHO at 298 K and Temperature Coefficients

λ (nm)	$10^{20} \sigma$ (cm ²)	$10^4 B$ (K ⁻¹)	λ (nm)	$10^{20} \sigma$ (cm ²)	$10^4 B$ (K ⁻¹)	λ (nm)	$10^{20} \sigma$ (cm ²)	$10^4 B$ (K ⁻¹)
235	0.120	-29.0	285	11.8	-10.2	335	4.64	-2.83
240	0.295	-17.9	290	13.7	-10.6	340	2.66	-2.84
245	0.584	-13.5	295	15.2	-9.54	345	1.46	14.0
250	1.07	-11.8	300	16.0	-10.4	350	0.670	37.3
255	1.78	-10.7	305	15.6	-7.09	355	0.148	68.1
260	2.78	-10.5	310	15.2	-9.73	360	0.036	75.8
265	4.09	-10.4	315	13.0	-8.32	365	0.012	52.9
270	5.75	-10.5	320	11.4	-7.71	370	0.003	63.1
275	7.67	-9.96	325	9.07	-5.02			
280	9.79	-10.6	330	6.38	-3.03			

Note:

Absorption cross-sections:

235 – 350 nm: mean of data from Libuda [124] and Rattigan et al. [190]

355 – 370 nm: Rattigan et al. [190]

Temperature coefficients:

Rattigan et al. [190]

$\ln \sigma(\lambda, T) = \ln \sigma(\lambda, 298 \text{ K}) + B(\lambda)(T - 298)$ for the temperature range 245 – 298 K

F50. CFC1₂CHO + hv → Products

(Recommendation: 06-2, Note: 10-6, Evaluated: 10-6)

Absorption Cross Sections: The UV absorption spectrum of fluorodichloroacetaldehyde, CFC1₂CHO, has been measured at room temperature by Libuda [124] (235 – 355 nm) and Rattigan et al. [190] (235 – 370 nm). Over this wavelength range there is an absorption band with a maximum near 296 nm. The cross section data from Libuda [124] are greater by 10-30% than the data from Rattigan et al. [190] over the entire absorption band (except for a few points in the wings).

Rattigan et al. [190] also reported the temperature dependence of the absorption spectrum over the temperature range 253 – 298 K. The cross sections increase near the peak and decrease in the long wavelength wing with decreasing temperature. Rattigan et al. [190] fit the measured temperature dependence with the empirical expression

$$\ln \sigma(\lambda, T) = \ln \sigma(\lambda, 298 \text{ K}) + B(\lambda)(T - 298)$$

The recommended room temperature absorption cross sections in Table 4F-52 are the mean values of the data from Libuda [124] (using 1 nm averages of spectra recorded with 0.6 nm resolution) and Rattigan et al. [190] (5 nm averages of spectra recorded with 0.6 nm resolution) in the region 235 – 355 nm and the data from Rattigan et al. [190] in the region 355 – 370 nm. The temperature coefficients are taken from Rattigan et al. [190].

Photolysis Quantum Yield and Product Studies: No studies are available.

Table 4F-52. Absorption Cross Sections of CFCl₂CHO at 298 K and Temperature Coefficients

λ (nm)	$10^{20} \sigma$ (cm ²)	$10^4 B$ (K-1)	λ (nm)	$10^{20} \sigma$ (cm ²)	$10^4 B$ (K-1)	λ (nm)	$10^{20} \sigma$ (cm ²)	$10^4 B$ (K-1)
235	0.305	136.0	285	14.1	-7.82	335	2.50	24.60
240	0.599	87.0	290	15.3	-6.89	340	1.20	36.50
245	1.22	30.6	295	16.1	-6.41	345	0.616	58.10
250	1.91	6.41	300	15.7	-4.50	350	0.245	84.90
255	2.89	1.24	305	14.9	-2.93	355	0.067	92.80
260	4.21	-6.12	310	13.0	1.73	360	0.017	93.20
265	5.89	-7.55	315	10.9	2.70	365	0.007	103.2
270	7.84	-8.11	320	8.66	6.97	370	0.002	138.3
275	9.95	-8.28	325	5.97	12.2			
280	12.1	-8.04	330	4.11	15.6			

Note:

Absorption cross-sections:

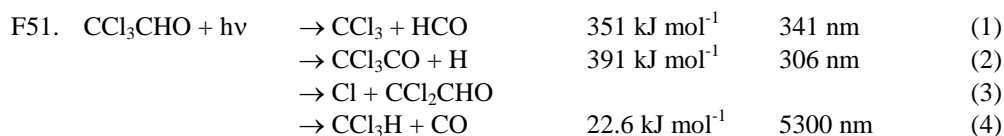
235 – 355 nm: mean of data from Libuda [124] and Rattigan et al. [190]

360 – 370 nm: Rattigan et al. [190]

Temperature coefficients:

Rattigan et al. [190]

$\ln \sigma(\lambda, T) = \ln \sigma(\lambda, 298 \text{ K}) + B(\lambda)(T - 298)$ for the temperature range 253 – 298 K



(Recommendation: 06-2, Note: 10-6, Evaluated: 10-6)

Absorption Cross Sections: The absorption spectrum of trichloroacetaldehyde (chloral), CCl_3CHO , has been measured at room temperature by Lucazeau and Sandorfy [133] (118 – 182 and 250 – 357 nm), Libuda [124] (235 – 350 nm), Rattigan et al. [191], [190] (200 – 360 nm), Gillotay et al. [76] (166 – 348 nm), and Talukdar et al. [226] (200 – 360 nm). Overlapping absorption bands were observed with a maximum near 290 nm and a strong band peaking below 180 nm. Except for the data of Lucazeau and Sandorfy [133], the results for the 290 nm absorption band are in reasonable agreement with a 20% range in cross section values at 290 nm. Gillotay et al. [76] report the largest cross section values and Libuda [124] the smallest. The data sets from Rattigan et al. [190] and Talukdar et al. [226] agree to better than 10% around the absorption maximum. At longer wavelengths, the data sets from Rattigan et al. [190] and Talukdar et al. [226] are nearly identical. The cross sections from Gillotay et al [76] are appreciably higher at the longer wavelengths and there is no explanation for this discrepancy. The temperature dependence of the absorption spectrum has been measured by Rattigan et al. [191], [190] (243 – 296 K), Gillotay et al. [76] (210 – 295 K), and Talukdar et al. [226] (240 – 360 K). These studies are in agreement and found that the absorption cross sections decrease with decreasing temperature below ~260 nm and above ~290 nm. Rattigan et al. [190] and Talukdar et al. [226] parameterized the temperature dependence using the empirical expression

$$\ln \sigma(\lambda, T) = \ln \sigma(\lambda, 298 \text{ K}) + B(\lambda)(T - 298)$$

The recommended absorption cross sections and $B(\lambda)$ temperature coefficients in Table 4F-53 are taken from Talukdar et al. [226].

Photolysis Quantum Yield and Product Studies: Quantum yields for the production of H, O(³P), and Cl atoms in the photolysis of CCl_3CHO at 193, 248, and 308 nm have been measured by Talukdar et al. [226]. The yields of H and O atoms were found to be small or below the detection limit, $\Phi(\text{O}(\text{}^3\text{P})) < 0.02$ and < 0.01 at 248 and 308 nm, respectively, and $\Phi(\text{H}) = 0.04 \pm 0.005$, < 0.01 , and < 0.002 at 193, 248, and 308 nm, respectively. Cl atoms were found to be the primary photolysis product at 308 nm photolysis with $\Phi(\text{Cl}) = 1.3 \pm 0.3$.

Table 4F-53. Absorption Cross Sections of CCl₃CHO at 298 K and Temperature Coefficients

λ (nm)	$10^{20} \sigma$ (cm ²)	$10^4 B$ (K ⁻¹)	λ (nm)	$10^{20} \sigma$ (cm ²)	$10^4 B$ (K ⁻¹)	λ (nm)	$10^{20} \sigma$ (cm ²)	$10^4 B$ (K ⁻¹)
200	187	22.0	250	2.18	3.73	300	9.25	3.07
202	153	23.9	252	2.54	1.50	302	8.77	3.60
204	122	27.2	254	2.92	0.324	304	8.17	4.37
206	95.7	30.6	256	3.36	-0.569	306	7.50	5.25
208	73.8	34.1	258	3.84	-0.877	308	6.86	6.10
210	56.3	37.5	260	4.35	-1.23	310	6.18	6.91
212	42.6	40.9	262	4.90	-1.65	312	5.58	7.90
214	31.8	44.0	264	5.48	-1.62	314	4.98	9.30
216	23.8	47.2	266	6.07	-1.50	316	4.33	11.2
218	17.1	50.2	268	6.68	-1.41	318	3.68	13.2
220	13.1	52.9	270	7.28	-1.22	320	3.09	15.1
222	9.75	55.6	272	7.88	-1.07	322	2.51	16.7
224	7.24	57.6	274	8.46	-0.931	324	2.09	18.5
226	5.39	59.0	276	8.99	-0.584	326	1.76	21.1
228	4.06	60.4	278	9.49	-0.412	328	1.43	25.0
230	3.07	60.5	280	9.94	-0.481	330	1.12	30.3
232	2.39	59.5	282	10.3	-0.235	332	0.849	36.6
234	1.90	55.9	284	10.6	0.242	334	0.590	43.3
236	1.62	49.2	286	10.8	0.475	336	0.373	49.8
238	1.43	41.6	288	10.9	0.750	338	0.261	55.6
240	1.39	33.0	290	10.9	1.09	340	0.188	60.2
242	1.41	24.0	292	10.8	1.51	342	0.136	65.0
244	1.53	16.4	294	10.6	1.96	344	0.100	69.0
246	1.66	10.4	296	10.3	2.38			
248	1.91	6.50	298	9.92	2.71			

Note:

Absorption cross-sections (σ):

Talukdar et al. [226]

Temperature coefficients (B):

Talukdar et al. [226]

$$\ln \sigma(\lambda, T) = \ln \sigma(\lambda, 298 \text{ K}) + B(\lambda)(T - 298) \quad (240 - 360 \text{ K range})$$

F52. CH₃C(O)Cl + hν → Products

(Recommendation: 06-2, Note: 10-6, Evaluated: 10-6)

Absorption Cross Sections: The UV absorption spectrum of acetyl chloride, CH₃C(O)Cl, has been measured at room temperature by Libuda [124] (233 – 300 nm) and Maricq [138] (190 – 341 nm). In this wavelength range the spectrum has two overlapping continuous absorption bands, one centered near 240 nm and a stronger band peaking below 190 nm. Both studies report a peak cross section for the 240 nm band of $\sim 1.16 \times 10^{-19} \text{ cm}^2 \text{ molecule}^{-1}$. However, the wavelength dependence of the 240 nm band is significantly different in the two studies. Libuda [124] report a narrower band with a peak shifted to longer wavelength compared to that of Maricq [138]. At wavelengths >280 nm the cross section data reported by Maricq [138] is very noisy making any comparisons difficult. The recommended absorption cross sections in Table 4F-54 are 1 nm averages of data from Maricq [138] (0.5 nm resolution) for the region 191 – 292 nm and 1 nm averages of the data from Libuda [124] (0.6 nm resolution) for the region 293 – 302 nm.

Photolysis Quantum Yield and Product Studies: No studies are available.

Table 4F-54. Absorption Cross Sections of CH₃C(O)Cl at 298 K

λ (nm)	$10^{20} \sigma$ (cm ²)	λ (nm)	$10^{20} \sigma$ (cm ²)	λ (nm)	$10^{20} \sigma$ (cm ²)	λ (nm)	$10^{20} \sigma$ (cm ²)
191	34.7	219	5.95	247	11.0	275	1.98
192	26.3	220	6.28	248	10.9	276	1.90
193	23.6	221	6.57	249	10.6	277	1.67
194	20.5	222	6.93	250	10.4	278	1.42
195	17.1	223	7.15	251	10.1	279	1.24
196	14.1	224	7.53	252	9.76	280	1.12
197	11.4	225	7.99	253	9.51	281	0.959
198	9.08	226	8.23	254	9.17	282	0.781
199	7.53	227	8.59	255	8.77	283	0.653
200	6.37	228	8.98	256	8.36	284	0.479
201	5.17	229	9.27	257	8.03	285	0.391
202	4.34	230	9.61	258	7.67	286	0.389
203	3.83	231	9.93	259	7.27	287	0.327
204	3.54	232	10.1	260	6.86	288	0.307
205	3.45	233	10.3	261	6.55	289	0.267
206	3.28	234	10.5	262	6.20	290	0.213
207	3.12	235	10.7	263	5.79	291	0.200
208	3.16	236	10.9	264	5.40	292	0.173
209	3.35	237	11.2	265	5.11	293	0.129
210	3.48	238	11.3	266	4.76	294	0.103
211	3.72	239	11.3	267	4.39	295	0.0846
212	3.89	240	11.4	268	4.03	296	0.0716
213	4.06	241	11.5	269	3.70	297	0.0599
214	4.40	242	11.5	270	3.36	298	0.0500
215	4.68	243	11.4	271	3.06	299	0.0404
216	4.88	244	11.3	272	2.77	300	0.0336
217	5.14	245	11.2	273	2.49	301	0.0298
218	5.54	246	11.1	274	2.19	302	0.0265

Note:

191 – 292 nm: Maricq [138]

293 – 302 nm: Libuda [124]

F53. CH₂ClC(O)Cl + hν → Products

(Recommendation: 06-2, Note: 10-6, Evaluated: 10-6)

Absorption Cross Sections: The UV absorption spectrum of chloroacetyl chloride, CH₂ClC(O)Cl, has been measured at room temperature and 234 – 342 nm by Libuda [124]. The spectrum has an absorption band with the maximum around 248 nm. Above 315 nm the data shows a somewhat irregular behavior and is considered unreliable. Therefore, the recommended absorption cross sections in Table 4F-55 are the 1 nm averages of the data from Libuda's [124] (0.6 nm resolution) excluding this region.

Photolysis Quantum Yield and Product Studies: No studies are available.

Table 4F-55. Absorption Cross Sections of CH₂ClC(O)Cl at 298 K

λ (nm)	$10^{20} \sigma$ (cm ²)	λ (nm)	$10^{20} \sigma$ (cm ²)	λ (nm)	$10^{20} \sigma$ (cm ²)	λ (nm)	$10^{20} \sigma$ (cm ²)
235	9.50	256	11.2	277	4.00	298	0.409
236	10.0	257	11.0	278	3.71	299	0.353
237	10.4	258	10.7	279	3.41	300	0.300
238	11.0	259	10.4	280	3.15	301	0.248
239	11.5	260	10.0	281	2.89	302	0.199
240	11.8	261	9.67	282	2.65	303	0.170
241	12.0	262	9.32	283	2.43	304	0.157
242	12.3	263	8.94	284	2.21	305	0.131
243	12.5	264	8.55	285	2.03	306	0.113
244	12.7	265	8.16	286	1.85	307	0.0909
245	12.7	266	7.80	287	1.67	308	0.0809
246	12.7	267	7.41	288	1.50	309	0.0657
247	12.7	268	7.06	289	1.33	310	0.0547
248	12.8	269	6.72	290	1.17	311	0.0522
249	12.7	270	6.30	291	1.04	312	0.0419
250	12.5	271	5.90	292	0.918	313	0.0380
251	12.4	272	5.53	293	0.814	314	0.0311
252	12.3	273	5.23	294	0.717	315	0.0286
253	12.1	274	4.93	295	0.628	316	0.0214
254	11.8	275	4.61	296	0.546		
255	11.5	276	4.33	297	0.473		

Note:

Libuda [124]

F54. CHCl₂C(O)Cl + hν → Products

(Recommendation: 06-2, Note: 10-6, Evaluated: 10-6)

Absorption Cross Sections: The UV absorption spectrum of dichloroacetyl chloride, CHCl₂C(O)Cl, has been measured at room temperature by Libuda [124] (235 – 338 nm) and Villenave et al. [239] (200 – 300 nm). An absorption band with the maximum around 258 nm was observed in that wavelength region. The reported cross sections are in very good agreement between 242 and 300 nm with the Villenave et al. [239] cross sections being systematically smaller by 1-10%. At shorter wavelengths the absorption cross sections reported by Libuda [124] are smaller by up to ~25% at 235 nm. Villenave et al. [239] observed a minimum near 232 nm and increasing cross sections between 230 and 220 nm. At the longer wavelengths the absorption spectrum reported by Libuda [124] is irregular at wavelengths >316 nm. The recommended absorption cross sections in Table 4F-56 are from Villenave et al. [239].

Photolysis Quantum Yield and Product Studies: No studies are available.

Table 4F-56. Absorption Cross Sections of $\text{CHCl}_2\text{C(O)Cl}$ at 298 K

λ (nm)	$10^{20} \sigma$ (cm^2)
220	21.7
230	13.2
240	15.7
250	20.0
256	20.9
260	20.8
270	17.1
280	10.5
290	4.7
300	1.4

Note:
Villenave et al. [239]

F55. $\text{CCl}_3\text{C(O)Cl} + h\nu \rightarrow \text{Products}$

(Recommendation: 06-2, Note: 10-6, Evaluated: 10-6)

Absorption Cross Sections: The UV absorption spectrum of trichloroacetyl chloride, $\text{CCl}_3\text{C(O)Cl}$, has been measured at room temperature by Libuda [124] (235 – 342 nm), Villenave et al. [239] (220 – 290 nm), and Gillotay et al. [76] (166 – 338 nm). The absorption spectrum has two overlapping bands with a peak near 256 nm and a stronger band at shorter wavelengths with a peak at ~176 nm. The spectra reported by Gillotay et al. [76] and Villenave et al. [239] are in good agreement. Although the absolute absorption cross sections are similar the absorption spectrum reported by Libuda [124] has a significantly different wavelength dependence than reported in the other studies. Although the cross section data from Villenave et al. [239] and Gillotay et al. [76] are in good agreement, the recommended absorption cross sections in Table 4F-57 are from Gillotay et al. [76] (0.015 nm resolution) and are averages over the 500 cm^{-1} and 5 nm intervals generally used in stratospheric photodissociation calculations.

The temperature dependence of the absorption spectrum has been measured by Gillotay et al. [76] over the temperature range 210 – 295 K. They report an increase in absorption cross section with increasing temperature at all wavelengths.

Photolysis Quantum Yield and Product Studies: No studies are available.

Table 4F-57. Absorption Cross Sections of CCl₃C(O)Cl at 295 K

λ (nm)	$10^{20} \sigma$ (cm ²)	λ (nm)	$10^{20} \sigma$ (cm ²)	λ (nm)	$10^{20} \sigma$ (cm ²)
166.7 – 169.5	671	204.1 – 206.2	231	256.4 – 259.7	22.6
169.5 – 172.4	699	206.2 – 208.3	194	259.7 – 263.2	22.3
172.4 – 173.9	712	208.3 – 210.5	160	263.2 – 266.7	21.1
173.9 – 175.4	716	210.5 – 212.8	129	266.7 – 270.3	19.1
175.4 – 177.0	717	212.8 – 215.0	102	270.3 – 274.0	16.6
177.0 – 178.6	714	215.0 – 217.4	78.9	274.0 – 277.8	13.7
178.6 – 180.2	706	217.4 – 219.8	59.5	277.8 – 281.7	10.7
180.2 – 181.8	694	219.8 – 222.2	44.0	281.7 – 285.7	8.14
181.8 – 183.5	677	222.2 – 224.7	31.8	285.7 – 289.9	5.86
183.5 – 185.2	655	224.7 – 227.3	25.8	289.9 – 294.1	4.03
185.2 – 186.9	630	227.3 – 229.9	21.9	294.1 – 298.5	2.67
186.9 – 188.7	599	229.9 – 232.6	19.5	298.5 – 303.0	1.68
188.7 – 190.5	567	232.6 – 235.3	18.3	303.0 – 307.7	0.921
190.5 – 192.3	528	235.3 – 238.1	17.9	307.7 – 312.5	0.605
192.3 – 194.2	487	238.1 – 241.0	18.1	312.5 – 317.5	0.339
194.2 – 196.1	445	241.0 – 243.9	18.7	317.5 – 322.5	0.188
196.1 – 198.0	402	243.9 – 246.9	19.7	322.5 – 327.5	0.104
198.0 – 200.0	358	246.9 – 250.0	20.9	327.5 – 332.5	0.0578
200.0 – 202.0	314	250.0 – 253.2	21.8	332.5 – 337.5	0.0326
202.0 – 204.1	272	253.2 – 256.4	22.3		

Note:

Gillotay et al. [76]

F56. CF₃CF₂CHCl₂ (HCFC–225ca) + hv → Products

(Recommendation: 02-25, Note: 10-6, Evaluated: 10-6)

Absorption Cross Sections: The UV absorption spectrum of 1,1,1,2,2-pentafluoro-3,3-dichloropropane (HCFC–225ca), CF₃CF₂CHCl₂, has been measured in the gas and liquid phase at 298 K by Braun et al. [17] (160 – 250 nm). The recommended absorption cross sections in Table 4F-58 are taken from this work. Braun et al. [17] give an expression that can be used to calculate the gas-phase absorption cross sections over the wavelength range 170 – 270 nm

$$\log_{10} \varepsilon = \sum a_n (\lambda - 160)^n$$

$$a_0 = 1.425 \quad a_1 = 4.542 \times 10^{-2}$$

$$a_2 = -2.036 \times 10^{-3} \quad a_3 = 1.042 \times 10^{-5}$$

where the absorption coefficients ε are in units of (atm, 298 K)⁻¹ cm⁻¹ ($\sigma = 4.06 \times 10^{-20} \varepsilon$).

Photolysis Quantum Yield and Product Studies: No studies are available.

Table 4F-58. Absorption Cross Sections of CF₃CF₂CHCl₂ (HCFC-225ca) at 298 K

λ (nm)	$10^{20} \sigma$ (cm ²)	λ (nm)	$10^{20} \sigma$ (cm ²)
160	268.7	202	11.58
162	236.8	204	8.185
164	207.6	206	5.802
166	189.0	208	4.084
168	181.4	210	2.903
170	182.7	212	2.042
172	182.8	214	1.429
174	189.0	216	1.05
176	190.9	218	0.727
178	187.9	220	0.463
180	177.5	222	0.308
182	161.1	224	0.209
184	140.3	226	0.145
186	118.3	228	0.0987
188	96.51	230	0.0653
190	74.30	232	0.0434
192	57.08	234	0.0299
194	42.83	236	0.0193
196	31.75	238	0.0134
198	23.22	239	0.0119
200	16.24		

Note:
Braun et al. [17]

F57. CF₂ClCF₂CHFCI (HCFC-225cb) + hν → Products

(Recommendation: 02-25, Note: 10-6, Evaluated: 10-6)

Absorption Cross Sections: The UV absorption spectrum of 1,1,2,2,3-pentafluoro-1,3-dichloropropane (HCFC-225cb), CF₂ClCF₂CHFCI, has been measured in the gas and liquid phase at 298 K by Braun et al. [17] (160 – 250 nm). The recommended absorption cross sections in Table 4F-59 are taken from this work. Braun et al. [17] give an expression that can be used to calculate the gas-phase absorption cross sections over the wavelength range 165 – 250 nm

$$\log_{10} \varepsilon = \sum a_n (\lambda - 160)^n$$

$$a_0 = 1.677 \quad a_1 = -2.175 \times 10^{-2}$$

$$a_2 = -1.484 \times 10^{-3} \quad a_3 = 1.147 \times 10^{-5}$$

where the absorption coefficients ε are in units of (atm, 298 K)⁻¹ cm⁻¹ ($\sigma = 4.06 \times 10^{-20} \varepsilon$).

Photolysis Quantum Yield and Product Studies: No studies are available.

Table 4F-59. Absorption Cross Sections of CF₂ClCF₂CFCl (HCFC-225cb) at 298 K

λ (nm)	$10^{20} \sigma$ (cm ²)	λ (nm)	$10^{20} \sigma$ (cm ²)
160	187.9	186	7.308
162	173.3	188	5.075
164	154.8	190	3.492
166	135.1	192	2.412
168	113.2	194	1.661
170	91.35	196	1.165
172	70.68	198	0.873
174	54.73	200	0.633
176	40.68	202	0.479
178	30.04	204	0.369
180	21.11	206	0.291
182	14.90	208	0.254
184	10.47	210	0.250

Note:
Braun et al. [17]

F58. CH₃C(O)CH₂Cl + hν → Products

(Recommendation: 06-2, Note: 10-6, Evaluated: 10-6)

Absorption Cross Sections: The UV absorption cross sections of chloroacetone, CH₃C(O)CH₂Cl, have been measured over the temperature range 243 – 296 K between 210 and 370 nm by Burkholder et al. [24] using diode array spectroscopy (~0.6 nm resolution). The spectrum has two absorption bands, a strong band with the maximum at ~224 nm (3.35×10^{-19} cm² molecule⁻¹ at room temperature) and a weaker broader band with the maximum at ~292 nm (1.02×10^{-19} cm² molecule⁻¹). A systematic decrease in the absorption cross section with decreasing temperature was observed at wavelengths >290 nm. A temperature dependence of the absorption cross sections was also reported for the short wavelength absorption band. The reported values at 253 K are larger than those at 273 K below ~240 nm and even larger than those at 296 K below ~230 nm. The recommended absorption cross sections in Table 4F-60 are taken from Burkholder et al. [24].

Photolysis Quantum Yield and Product Studies: Photodissociation quantum yields were measured by Burkholder et al. [24] to be 0.5 ± 0.08 at 308 nm and 351 nm. At both wavelengths, the yields of CO and CO₂ were 0.50 and ~0.25, respectively. The yield of HCOOH and HCl were reported to be 0.25 and 0.5, respectively, at both photolysis wavelengths.

Table 4F-60. Absorption Cross Sections of CH₃C(O)CH₂Cl at 296 K

λ (nm)	$10^{20} \sigma$ (cm ²)	λ (nm)	$10^{20} \sigma$ (cm ²)	λ (nm)	$10^{20} \sigma$ (cm ²)	λ (nm)	$10^{20} \sigma$ (cm ²)
210	22.0	248	3.36	286	9.89	324	2.58
211	23.0	249	3.11	287	9.98	325	2.37
212	24.3	250	2.96	288	10.00	326	2.16
213	25.5	251	2.90	289	10.10	327	1.95
214	26.4	252	2.92	290	10.20	328	1.73
215	27.5	253	3.00	291	10.20	329	1.52
216	28.9	254	3.10	292	10.20	330	1.33
217	30.1	255	3.24	293	10.20	331	1.14
218	30.9	256	3.39	294	10.10	332	0.979
219	31.7	257	3.56	295	10.00	333	0.832
220	32.4	258	3.75	296	9.89	334	0.707
221	32.8	259	3.97	297	9.77	335	0.598
222	33.2	260	4.19	298	9.66	336	0.506
223	33.5	261	4.40	299	9.54	337	0.427
224	33.5	262	4.63	300	9.41	338	0.361
225	33.0	263	4.86	301	9.25	339	0.302
226	32.3	264	5.12	302	9.04	340	0.2520
227	31.8	265	5.38	303	8.80	341	0.212
228	31.3	266	5.65	304	8.53	342	0.176
229	30.3	267	5.89	305	8.24	343	0.145
230	28.9	268	6.14	306	7.94	344	0.120
231	27.3	269	6.39	307	7.63	345	0.103
232	25.7	270	6.65	308	7.34	346	0.0887
233	24.0	271	6.93	309	7.06	347	0.0757
234	22.2	272	7.20	310	6.77	348	0.0642
235	20.3	273	7.47	311	6.50	349	0.0547
236	18.4	274	7.71	312	6.22	350	0.0458
237	16.5	275	7.94	313	5.93	351	0.0411
238	14.6	276	8.16	314	5.61	352	0.0328
239	12.7	277	8.37	315	5.28	353	0.0319
240	11.0	278	8.59	316	4.92	354	0.0220
241	9.50	279	8.82	317	4.57	355	0.0193
242	8.15	280	9.03	318	4.22	356	0.0138
243	6.93	281	9.23	319	3.89	357	0.0134
244	5.85	282	9.41	320	3.58	358	0.00917
245	4.95	283	9.56	321	3.30	359	0.0155
246	4.26	284	9.69	322	3.04	360	0.0128
247	3.74	285	9.80	323	2.80		

Note:

Burkholder et al. [24]

References for Section 4F

1. Adler-Golden, S. M. and J. R. Wiesenfeld, 1981, Chem. Phys. Lett., 82, 281-284.
2. Alexander, M. H., B. Pouilly and T. Duhoo, 1993, J. Chem. Phys., 99, 1752-1764.
3. Baer, S., H. Hippler, R. Rahn, M. Siefke, N. Seitzinger and J. Troe, 1991, J. Chem. Phys., 95, 6463-6470.
4. Bahou, M., C.-Y. Chung, Y.-P. Lee, B. M. Cheng, Y. L. Yung and L. C. Lee, 2001, Astrophys. J., 559, L179-L182.
5. Ballash, N. M. and D. A. Armstrong, 1974, Spectrochim Acta, 30A, 941-944.
6. Barnes, R. J., A. Sinha and H. A. Michelsen, 1998, J. Phys. Chem. A, 102, 8855-8859.
7. Barton, S. A., J. A. Coxon and U. K. Roychowdhury, 1984, Can. J. Phys., 62, 473-486.
8. Basco, N. and J. E. Hunt, 1979, Int. J. Chem. Kinet., 11, 649-664.
9. Basco, N. and R. D. Morse, 1974, Proc. Roy. Soc. London, A 336, 495-505.
10. Bell, A. J., S. A. Boggis, J. M. Dyke, J. R. Frey, R. Richter, N. Shaw and M. Tabrizchi, 1994, J. Chem. Soc. Faraday Trans., 90, 17-21.
11. Birk, M., R. R. Friedl, E. A. Cohen, H. M. Pickett and S. P. Sander, 1989, J. Chem. Phys., 91, 6588-6597.
12. Birks, J. W., B. Shoemaker, T. J. Leck, R. A. Borders and L. J. Hart, 1977, J. Chem. Phys., 66, 4591-4599.
13. Bishenden, E., J. Haddock and D. J. Donaldson, 1991, J. Phys. Chem., 95, 2113-2115.
14. Bishenden, E., J. Haddock and D. J. Donaldson, 1992, J. Phys. Chem., 96, 6513.
15. Bloss, W. J., S. L. Nikolaisen, R. J. Salawitch, R. R. Friedl and S. P. Sander, 2001, J. Phys. Chem. A, 105, 11226-11239.
16. Bogumil, K., J. Orphal, T. Homann, S. Voigt, P. Spietz, O. C. Fleischmann, A. Vogel, M. Hartmann, H. Krominga, H. Bovensmann, J. Frerick and J. P. Burrows, 2003, J. Photochem. Photobiol. A.: Chem., 157, 167-184.
17. Braun, M., A. Fahr, R. Klein, M. J. Kurylo and R. E. Huie, 1991, J. Geophys. Res., 96, 13009-13015.
18. Brownsword, R. A., M. Hillenkamp, T. Laurent, R. K. Vatsa, H.-R. Volpp and J. Wolfrum, 1997, J. Phys. Chem. A, 101, 5222-5227.
19. Brownsword, R. A., M. Hillenkamp, T. Laurent, R. K. Vatsa, H.-R. Volpp and J. Wolfrum, 1997, J. Chem. Phys., 106, 1359-1366.
20. Brownsword, R. A., M. Hillenkamp, T. Laurent, J. Wolfrum, H.-R. Volpp, R. K. Vatsa and H.-S. Yoo, 1997, J. Chem. Phys., 107, 779-785.
21. Brownsword, R. A., P. Schmiechen, H.-R. Volpp, H. P. Upadhyaya, Y. J. Jung and K.-H. Jung, 1999, J. Chem. Phys., 110, 11823-11829.
22. Burkholder, J. B., 1993, J. Geophys. Res., 98, 2963-2974.
23. Burkholder, J. B. and E. J. Bair, 1983, J. Phys. Chem., 87, 1859-1863.
24. Burkholder, J. B., M. K. Gilles, T. Gierczak and A. R. Ravishankara, 2002, Geophys. Res. Lett., 29, 1822, doi:10.1029/2002GL014712.
25. Burkholder, J. B., R. L. Mauldin, R. J. Yokelson, S. Solomon and A. R. Ravishankara, 1993, J. Phys. Chem., 97, 7597-7605.
26. Burkholder, J. B., J. J. Orlando and C. J. Howard, 1990, J. Phys. Chem., 94, 687-695.
27. Burkholder, J. B., R. K. Talukdar and A. R. Ravishankara, 1994, Geophys. Res. Lett., 21, 585-588.
28. Burrows, J. P., G. S. Tyndall and G. K. Moortgat, 1988, J. Phys. Chem., 92, 4340-4348.
29. Burton, G. R., W. F. Chan, G. Cooper and C. E. Brion, 1994, Chem. Phys., 181, 147-172.
30. Bush, G. E., R. T. Mahoney, R. I. Morse and K. R. Wilson, 1969, J. Chem. Phys., 51, 449-450.
31. Butler, P. J. D. and L. F. Phillips, 1983, J. Phys. Chem., 87, 183-184.
32. Calvert, J. G. and J. N. Pitts. In *Photochemistry*; John Wiley & Sons, Inc.: New York, 1966; pp 230-231.
33. Carter, R. T., A. Hallou and R. J. Huber, 1999, Chem. Phys. Lett., 310, 166-172.
34. Causley, G. C. and B. R. Russell, 1977, J. Electron Spectrosc. Relat. Phenom., 11, 383-397.
35. Chang, J. S., J. R. Barker, J. E. Davenport and D. M. Golden, 1979, Chem. Phys. Lett., 60, 385-390.
36. Chen, H.-Y., C-Y Lien, W-Y Lin, Y.T. Lee, and J.J. Lin, 2009, Science, 324, 781-784.
37. Chen, Y. and L. Zhu, 2001, J. Phys. Chem. A, 105, 9689-9696.

38. Chen, Y. and L. Zhu, 2003, J. Chem. Phys. A., 107, 4643-4651.
39. Chen, Y., L. Zhu and J. S. Francisco, 2002, J. Chem. Phys. A, 106, 7755-7763.
40. Cheng, B. M., C.-Y. Chung, M. Bahou, Y.-P. Lee and L. C. Lee, 2002, J. Chem. Phys., 117, 4293-4298.
41. Chichinin, A. I., 1993, Chem. Phys. Lett., 209, 459-463.
42. Chou, C. C., G. Crescentini, H. Vera-Ruiz, W. S. Smith and F. S. Rowland. "Stratospheric Photochemistry of CF₂O, CClFO, and CCl₂O"; 173rd American Chemical Society Meeting, 1977, New Orleans, LA,
43. Chou, C. C., R. J. Milstein, W. S. Smith, H. Vera-Ruiz, M. J. Molina and F. S. Rowland, 1978, J. Phys. Chem., 82, 1-7.
44. Chou, C. C., W. S. Smith, H. V. Ruiz, K. Moe, G. Crescentini, M. J. Molina and F. S. Rowland, 1977, J. Phys. Chem., 81, 286-290.
45. Clark, R. H. and D. Husain, 1984, J. Photochem., 24, 103-115.
46. Clyne, M. A. A. and J. A. Coxon, 1968, Proc. Roy. Soc. A, 303, 207-231.
47. Colussi, A. J., 1990, J. Phys. Chem., 94, 8922-8926.
48. Colussi, A. J., S. P. Sander and R. R. Friedl, 1992, J. Phys. Chem., 96, 4442-4445.
49. Cox, R. A. and G. D. Hayman, 1988, Nature, 332, 796-800.
50. Coxon, J. A., W. E. Jones and D. A. Ramsey. 12th International Symposium on Free Radicals, 1976, Laguna Beach, California,
51. Crowley, J. N., R. Helleis, R. Muller, G. K. Moortgat, P. J. Crutzen and J. J. Orlando, 1994, J. Geophys. Res., 99, 20683-20688.
52. Currie, J., J. H. Sidebottom and J. Tedder, 1974, Int. J. Chem. Kinet., 6, 481-492.
53. Daviel, S., Y. Iida, F. Carnovale and C. E. Brion, 1984, Chem. Phys., 83, 319-406.
54. Davis, F. H. and Y. T. Lee, 1996, J. Chem. Phys., 105, 8142-8163.
55. Davis, H. F. and Y. T. Lee, 1992, J. Phys. Chem., 96, 5681-5684.
56. Delmdahl, R. F., S. Ulrich and K.-H. Gericke, 1998, J. Phys. Chem. A., 102, 7680-7685.
57. DeMore, W. B. and E. Tschuikow-Roux, 1990, J. Phys. Chem., 94, 5856-5860.
58. Doucet, J., P. Sauvageau and C. Sandorfy, 1973, J. Chem. Phys., 58, 3708-3716.
59. Doucet, J., P. Sauvageau and C. Sandorfy, 1975, J. Chem. Phys., 62, 355-359.
60. Fahr, A., W. Braun and M. J. Kurylo, 1993, J. Geophys. Res., 98, 20467-20472.
61. Felder, P. and G. P. Morley, 1994, Chem. Phys., 185, 145-151.
62. Felps, W. S., K. Rupnik and S. P. McGlynn, 1991, J. Phys. Chem., 95, 639-656.
63. Fergusson, W. C., L. Slotin and W. G. Style, 1936, Trans. Far. Soc., 32, 956-962.
64. Finkelnburg, W., H.-J. Schumacher and G. Stieger, 1931, Z. Phys. Chem., B15, 127-156.
65. Flesch, R., E. Rühl, K. Hottmann and H. Baumgärtel, 1993, J. Phys. Chem., 97, 837-844.
66. Frost, G. J., L. M. Goss and V. Vaida, 1996, J. Geophys. Res., 101, 3879-3884.
67. Fujiwara, H. and T. Ishiwata, 1998, J. Phys. Chem., 102, 3856-3859.
68. Furlan, A., M. A. Haeberli and R. J. Huber, 2000, J. Phys. Chem. A, 104, 10392-10397.
69. Ganske, J. A., H. N. Berko and B. J. Finlayson-Pitts, 1992, J. Geophys. Res., 97, 7651-7656.
70. Gibson, G. E. and N. S. Bayliss, 1933, Phys. Rev., 44, 188-192.
71. Gilbert, R., P. Sauvageau and C. Sandorfy, 1974, J. Chem. Phys., 60, 4820-4824.
72. Gillotay, D. and P. C. Simon, 1990, Aeronomica Acta A, A356, 1-173.
73. Gillotay, D. and P. C. Simon, 1991, J. Atmos. Chem., 13, 289-299.
74. Gillotay, D. and P. C. Simon, 1991, J. Atmos. Chem., 12, 269-285.
75. Gillotay, D., P. C. Simon and L. Dierickx, 1988, Aeronomica Acta, A335, 1-25.
76. Gillotay, D., P. C. Simon and L. Dierickx, 1993, Aeronomica Acta, A368, 1-15.
77. Glicker, S. and H. Okabe, 1987, J. Phys. Chem., 91, 437-440.
78. Goldfarb, L., A.-M. Schmoltner, M. K. Gilles, J. Burkholder and A. R. Ravishankara, 1997, J. Phys. Chem. A., 101, 6658-6666.
79. Goodeve, C. F. and F. D. Richardson, 1937, Trans. Faraday Soc., 33, 453-457.
80. Goodeve, C. F. and J. I. Wallace, 1930, Trans. Faraday Soc., 26, 254-260.

81. Goodeve, C. F. and B. A. M. Windsor, 1936, *Trans. Faraday Soc.*, 32, 1518-1519.
82. Gordus, A. A. and R. B. Bernstein, 1954, *J. Chem. Phys.*, 22, 790-795.
83. Green, R. G. and R. P. Wayne, 1976/77, *J. Photochem.*, 6, 375-377.
84. Green, T. J., M. Islam, C. Canosa-Mas, G. Marston and R. P. Wayne, 2004, *J. Photochem. Photobiol. A: Chem.*, 162, 353-370.
85. Green, T. J., M. Islam, P. Guest, K. Hickson, C. E. Canosa-Mas, and R. P. Wayne, 2003, *Phys. Chem. Chem. Phys.*, 5, 5409-5418.
86. Grothe, H. and H. Willner, 1994, *Angew. Chem.*, 106, 1581-1584.
87. Grothe, H. and H. Willner, 1995, personal communication to Wayne et al. (1995).
88. Hanf, A., A. Laüter and H.-R. Volpp, 2003, *Chem. Phys. Lett.*, 368, 445-451.
89. Harwood, M. H., D. M. Rowley, R. A. Freshwater, R. A. Cox and R. L. Jones, 1995, *J. Chem. Soc. Faraday Trans*, 91, 3027-3032.
90. Hayman, G. D. and R. A. Cox, 1989, *Chem. Phys. Lett.*, 155, 1-7.
91. Heicklen, J., 1965, *J. Am. Chem. Soc.*, 87, 445-453.
92. Hermann, M., A. Nölle and H. Heydtmann, 1994, *Chem. Phys. Lett.*, 226, 559-562.
93. Ho, G. H., 1998, *Chem. Phys.*, 226, 101-111.
94. Huang, W.-T., A. F. Chen, I.-C. Chen, C.-H. Tsai and J. J.-M. Lin, 2011, *Physical Chemistry Chemical Physics*, doi: 10.1039/c0cp02453h.
95. Hubinger, S. and J. B. Nee, 1994, *Chem. Phys.*, 181, 247-257.
96. Hubinger, S. and J. B. Nee, 1995, *J. Photochem. Photobiol.*, 86, 1-7.
97. Hubrich, C. and F. Stuhl, 1980, *J. Photochem.*, 12, 93-107.
98. Hubrich, C., C. Zetzsch and F. Stuhl, 1977, *Ber. Bunsenges. Phys. Chem.*, 81, 437-442.
99. Huder, K. J. and W. B. DeMore, 1995, *J. Phys. Chem.*, 99, 3905-3908.
100. Huebner, R. H., J. Bushnell, D. L., R. J. Celotta, S. R. Mielczarek and C. E. Kuyatt, 1975, *Nature*, 257, 376-378.
101. Ibuki, T., N. Takahashi, A. Hiraya and K. Shobatake, 1986, *J. Chem. Phys.*, 85, 5717-5722.
102. Ichimura, T., A. W. Kirk, G. Kramer and E. Tschuikow-Roux, 1976/1977, *J. Photochem.*, 6, 77-90.
103. Ichimura, T., A. W. Kirk and E. Tschuikow-Roux, 1977, *J. Phys. Chem.*, 81, 1153-1156.
104. Illies, A. J. and G. A. Takacs, 1976, *J. Photochem.*, 6, 35-42.
105. Inn, E. C. Y., 1975, *J. Atmos. Sci.*, 32, 2375-2377.
106. Jacobs, J., M. Kronberg, H. S. P. Müller and H. Willner, 1994, *J. Am. Chem. Soc.*, 116, 1106-1114.
107. Jäger, M., H. Heydtmann and C. Zetzsch, 1996, *Chem. Phys. Lett.*, 263, 817-821.
108. Jansen, M., G. Schatte, K. M. Tobias and H. Willner, 1988, *Inorg. Chem.*, 27, 1703-1706.
109. Jensen, F. and J. Oddershede, 1990, *J. Phys. Chem.*, 94, 2235-2237.
110. Jin, B., I.-C. Chen, W.-T. Huang, C.-Y. Lien, N. Guchhait and J. J. Lin, 2010, *Journal of Physical Chemistry A*, 114, 4791-4797.
111. Johnsson, K., A. Engdahl and B. Nelander, 1995, *J. Phys. Chem.*, 99, 3965-3968.
112. Johnston, H. S., E. D. Morris, Jr. and J. Van den Bogaerde, 1969, *J. Am. Chem. Soc.*, 91, 7712-7727.
113. Jourdain, J. L., G. Le Bras, G. Poulet, J. Combourieu, P. Rigaud and B. LeRoy, 1978, *Chem. Phys. Lett.*, 57, 109-112.
114. Jungkamp, T. P. W., U. Kirchner, M. Schmidt and R. N. Schindler, 1995, *J. Photochem. Photobiol. A: Chemistry*, 99, 1-6.
115. Kalekin, A. L. and K. Morokuma, 2000, *J. Chem. Phys.*, 113, 5750-5762.
116. Knauth, H. D., H. Alberti and H. Clausen, 1979, *J. Phys. Chem.*, 83, 1604-1612.
117. Knauth, H. D. and R. N. Schindler, 1983, *Z. Naturforsch.*, 38a, 893-895.
118. Krisch, M. J., L. R. McCunn, K. Takematsu, L. J. Butler, F. R. Blase and J. Shu, 2004, *J. Phys. Chem., A*, 108, 1650-1656.
119. Kromminga, J., J. Orphal, P. Spietz, S. Voigt and J. P. Burrows, 2003, *J. Photochem. Photobiol. A: Chem.*, 157, 149-160.
120. Lambert, H. M., P. J. Dagdigian and M. H. Alexander, 1998, *J. Chem. Phys.*, 108, 4460-4466.

121. Lang, V. I., S. P. Sander and R. R. Friedl, 1988, *J. Mol. Spectrosc.*, 132, 89-103.
122. Langhoff, S. R., L. Jaffe and J. O. Arnold, 1977, *J. Quant. Spectrosc. Radiat. Transfer*, 18, 227-235.
123. Lawrence, W. G., K. C. Clemitshaw and V. A. Apkarian, 1990, *J. Geophys. Res.*, 95, 18591-18595.
124. Libuda, H. G. *Spektroskopische und kinetische Untersuchungen an halogenierten Carbonylverbindungen von atmosphärischem Interesse*, PhD-Thesis, University of Wuppertal, Germany, 1992.
125. Libuda, H. G., F. Zabel, E. H. Fink and K. H. Becker, 1990, *J. Phys. Chem.*, 94, 5860-5865.
126. Lien, C.-Y., W.-Y. Lin, H.-Y. Chen, W.-T. Huang, B. Jin, I.-C. Chen and J. J. Lin, 2009, *Journal of Chemical Physics*, 131, 174301-1 -174301-6.
127. Limao-Vieira, P., S. Eden, P. A. Kendall, N. J. Mason and S. V. Hoffmann, 2002, *Chem. Phys. Lett.*, 364, 535-541.
128. Lin, C. L., 1976, *J. Chem. Eng. Data*, 21, 411-413.
129. Lipscomb, F. J., R. G. W. Norrish and B. A. Thrush, 1956, *Proc. Roy. Soc. London, A* 233, 455-464.
130. Liyanage, R., Y.-A. Yang, S. Hashimoto, R. J. Gordon and R. W. Field, 1995, *J. Chem. Phys.*, 103, 6811-6814.
131. Lopez, M. I. and J. E. Sicre, 1988, *J. Phys. Chem.*, 92, 563-564.
132. Lopez, M. I. and J. E. Sicre, 1990, *J. Phys. Chem.*, 94, 3860-3863.
133. Lucazeau, G. and C. Sandorfy, 1970, *J. Mol. Spectrosc.*, 35, 214-231.
134. Mandelman, M. and R. W. Nicholls, 1977, *J. Quant. Spectrosc. Radiat. Trans.*, 17, 483-491.
135. Margitan, J. J., 1983, *J. Phys. Chem.*, 87, 674-679.
136. Maric, D. and J. P. Burrows, 1999, *J. Quant. Spectrosc. Radiat. Transfer*, 62, 345-369.
137. Maric, D., J. P. Burrows, R. Meller and G. K. Moortgat, 1993, *J. Photochem. Photobiol. A Chem.*, 70, 205-214.
138. Maricq, M. M., 1999, personal communication to JPL subcommittee.
139. Marinelli, W. J. and H. S. Johnston, 1982, *Chem. Phys. Lett.*, 93, 127-132.
140. Marston, G., I. C. Walker, N. J. Mason, J. M. Gingell, H. Zhao, K. L. Brown, F. Motte-Tollet, J. Delwiche and M. R. F. Siggel, 1998, *J. Phys. B: Atom. Mol. Phys.*, 31, 3387-3405.
141. Martin, H. and R. Gareis, 1956, *Z. Elektrochemie*, 60, 959-964.
142. Matsumi, Y., P. K. Das and M. Kawasaki, 1990, *J. Chem. Phys.*, 92, 1696-1701.
143. Matsumi, Y., P. K. Das and M. Kawasaki, 1992, *J. Chem. Phys.*, 97, 5261.
144. Matsumi, Y., K. Tonokura, M. Kawasaki and T. Ibuki, 1990, *J. Chem. Phys.*, 93, 7981-7985.
145. Matus, M. H., M. T. Nguyen, D. A. Dixon, K. A. Peterson and J. S. Francisco, 2008, *The Journal of Physical Chemistry A*, 112, 9623-9627.
146. Mauldin, R. L., III, J. B. Burkholder and A. R. Ravishankara, 1992, *J. Phys. Chem.*, 96, 2582-2588.
147. McGrath, M. P., K. C. Clemitshaw, F. S. Rowland and W. J. Hehre, 1988, *Geophys. Res. Lett.*, 15, 883-886.
148. McGrath, M. P., K. C. Clemitshaw, F. S. Rowland and W. J. Hehre, 1990, *J. Phys. Chem.*, 94, 6126-6132.
149. McKeachie, J. R., M. F. Appel, U. Kirchner, R. N. Schindler and T. Benter, 2004, *The Journal of Physical Chemistry B*, 108, 16786-16797.
150. Meller, R., D. Boglu and G. K. Moortgat. "UV spectra of several halogenated carbonyl compounds and FTIR studies of the degradation of CF₃COCl, HCFC-123 and HFC-143a"; *Kinetics and Mechanisms for the Reactions of Halogenated Organic Compounds in the Troposphere. STEP-HALOCSIDE/AFEAS WORKSHOP*, 1991, Dublin, Ireland, 14-16 May, 1991, 110-115.
151. Mérienne, M. F., B. Coquart and A. Jenouvrier, 1990, *Planet. Space Sci.*, 38, 617-625.
152. Minaev, B. F., 1999, *J. Phys. Chem. A*, 103, 7294-7309.
153. Minton, T. K., C. M. Nelson, T. A. Moore and M. Okumura, 1992, *Science*, 258, 1342-1345.
154. Mishalanie, E. A., J. C. Rutkowski, R. S. Hutte and J. W. Birks, 1986, *J. Phys. Chem.*, 90, 5578-5584.
155. Mo, Y., K. Tonokura, Y. Matsumi, M. Kawasaki, T. Sato, T. Arikawa, P. T. A. Reilly, Y. Xie, Y. Yang, Y. Huang and R. J. Gordon, 1992, *J. Chem. Phys.*, 97, 4815-4826.
156. Molina, L. T. and M. J. Molina, 1977, *Geophys. Res. Lett.*, 4, 83-86.
157. Molina, L. T. and M. J. Molina, 1978, *J. Phys. Chem.*, 82, 2410-2414.

158. Molina, L. T. and M. J. Molina, 1979, J. Photochem., 11, 139-144.
159. Molina, L. T. and M. J. Molina, 1987, J. Phys. Chem., 91 433-436.
160. Molina, M. J., A. J. Colussi, L. T. Molina, R. N. Schindler and T. L. Tso, 1990, Chem. Phys. Lett., 173, 310-315.
161. Molina, M. J., T. Ishiwata and L. T. Molina, 1980, J. Phys. Chem., 84, 821-826.
162. Moore, T. A., M. Okumura and T. K. Minton, 1997, J. Phys. Chem., 1-7, 3337-3338.
163. Moore, T. A., M. Okumura, J. W. Seale and T. K. Minton, 1999, J. Phys. Chem. A, 103, 1692-1695.
164. Moore, T. A., M. Okumura, M. Tagawa and T. K. Minton, 1995, Faraday Discuss, 100, 295-307.
165. Motte-Tollet, F., M.-P. Ska, G. M. Marston, I. C. Walker, M. R. F. Siggel, J. M. Gingell, L. Kaminski, K. L. Brown and N. J. Mason, 1997, Chem. Phys. Lett., 275, 298-306.
166. Müller, H. S. P. and H. Willner, 1992, Ber. Bunsenges. Phys. Chem., 96, 427-431.
167. Myer, J. A. and J. A. R. Samson, 1970, J. Chem. Phys., 52, 266-271.
168. Nayak, A. K., T. J. Buckley, M. J. Kurylo and A. Fahr, 1996, J. Geophys. Res., 101, 9055-9062.
169. Nayak, A. K., M. J. Kurylo and A. Fahr, 1995, J. Geophys. Res, 100, 11185-11189.
170. Nee, J. B., 1991, J. Quant. Spectrosc. Radiat. Transfer, 46, 55-58.
171. Nee, J. B., M. Suto and L. C. Lee, 1986, J. Chem. Phys., 85, 719-724.
172. Nelson, C. M., T. A. Moore and M. Okumura, 1994, J. Chem. Phys., 100, 8055-8064.
173. Nelson, C. M., T. A. Moore, M. Okumura and T. K. Minton, 1996, Chem. Phys, 2248, 287-307.
174. Nelson, H. H. and H. S. Johnston, 1981, J. Phys. Chem., 85, 3891-3896.
175. Nickolaisen, S. L., C. E. Miller, S. P. Sander, M. R. Hand, I. H. Williams and J. S. Francisco, 1996, J. Chem. Phys., 104, 2857-2868.
176. Nickolaisen, S. L., S. P. Sander and R. R. Friedl, 1996, J. Phys. Chem., 100, 10165-10178.
177. Nölle, A., H. Heydtmann, R. Meller and G. K. Moortgat, 1993, Geophys. Res. Lett., 20, 707-710.
178. Nölle, A., C. Krumscheid and H. Heydtmann, 1999, Chem. Phys. Lett., 299, 561-565.
179. Okabe, H., 1977, J. Chem. Phys., 66, 2058-2062.
180. Okabe, H., 1981, J. Chem. Phys., 75, 2772-2778.
181. Okabe, H., 1983, J. Chem. Phys., 78, 1312-1317.
182. Orlando, J. J., J. B. Burkholder, S. A. McKeen and A. R. Ravishankara, 1991, J. Geophys. Res., 96, 5013-5023.
183. Papanastasiou, D. K., V.C. Papadimitriou, D.W. Fahey, and J.B. Burkholder, 2009, J. Phys. Chem. A, 113, 13711-13726.
184. Park, J., Y. Lee and G. W. Flynn, 1991, Chem. Phys. Lett., 186, 441-449.
185. Permien, T., R. Vogt and R. N. Schindler. Mechanisms of Gas Phase-Liquid Phase Chemical Transformations. In *Air Pollution Report #17*; R. A. Cox, Ed.; Environmental Research Program of the CEC: Brussels, 1988.
186. Peterson, K. A. and J. S. Francisco, 2004, J. Chem. Phys., 121, 2611-2616.
187. Plenge, J., R. Flesch, S. Köhl, B. Vogel, R. Müller, F. Strohm and E. Rühl, 2004, J. Phys. Chem. A, 108, 4859-4863.
188. Pope, F. D., J. C. Hansen, K. D. Bayes, R. R. Friedl and S. P. Sander, 2007, J. Phys. Chem. A, 111, 4322-4332.
189. Prahlad, V. and V. Kumar, 1995, J. Quant. Spectrosc. Radiat. Transfer, 54, 945-955.
190. Rattigan, O. V., O. Wild and R. A. Cox, 1998, J. Photochem. Photobiol. A: Chem., 112, 1-7.
191. Rattigan, O. V., O. Wild, R. L. Jones and R. A. Cox, 1993, J. Photochem. Photobiol. A: Chem., 73, 1-9.
192. Ravishankara, A. R., 1995, Faraday Discuss, 100, 335-336.
193. Ravishankara, A. R., S. Solomon, A. A. Turnipseed and R. F. Warren, 1993, Science, 259, 194-199.
194. Rebbert, R. E. and P. Ausloos, 1976/1977, J. Photochem., 6, 265-276.
195. Rebbert, R. E. and P. J. Ausloos, 1975, J. Photochem., 4, 419-434.
196. Rebbert, R. E., S. G. Lias and P. Ausloos, 1978, J. Photochem., 8, 17-27.
197. Regan, P. M., D. Ascenzi, A. Brown, G. G. Balint-Kurti and A. J. Orr-Ewing, 2000, J. Chem. Phys., 112, 10259-10268.

198. Regan, P. M., S. R. Langford, D. Ascenzi, P. A. Cook, A. J. Orr-Ewing and M. N. R. Ashfold, 1999, *Phys. Chem. Chem. Phys.*, 1, 3247-3251.
199. Rigaud, P., B. Leroy, G. Le Bras, G. Poulet, J. L. Jourdain and J. Combourieu, 1977, *Chem. Phys. Lett.*, 46, 161-163.
200. Robbins, D. E., 1976, *Geophys. Res. Lett.*, 3, 213-216. See also Erratum, *GRL*, 1976, Vol. 3, p. 757.
201. Robbins, D. E. and R. S. Stolarski, 1976, *Geophys. Res. Lett.*, 3, 603-606.
202. Roehl, C. M., J. J. Orlando and J. G. Calvert, 1992, *J. Photochem. Photobiol. A: Chem.*, 69, 1-5.
203. Romand, J., 1949, *Ann. Phys. (Paris)*, 4, 529-590.
204. Romand, J. and B. Vodar, 1948, *Compt. Rend. Acad. Sci. Paris*, 226, 238-240.
205. Rowland, F. S. and M. J. Molina, 1975, *Rev. Geophys. Space Phys.*, 13, 1-35.
206. Rowland, F. S., J. E. Spencer and M. J. Molina, 1976, *J. Phys. Chem.*, 80, 2711-2713.
207. Roxlo, C. and A. Mandl, 1980, *J. Appl. Phys.*, 51, 2969-2972.
208. Ruhl, E., A. Jefferson and V. Vaida, 1990, *J. Phys. Chem.*, 94, 2990-2994.
209. Russell, B. R., L. O. Edwards and J. W. Raymond, 1973, *J. Am. Chem. Soc.*, 95, 2129-2133.
210. Salomon, D., A. W. Kirk and E. Tschuikow-Roux, 1977, *J. Photochem.*, 7, 345-353.
211. Sander, S. P., B. J. Finlayson-Pitts, R. R. Friedl, D. M. Golden, R. E. Huie, H. Keller-Rudek, C. E. Kolb, M. J. Kurylo, M. J. Molina, G. K. Moortgat, V. L. Orkin, A. R. Ravishankara and P. H. Wine "Chemical Kinetics and Photochemical Data for Use in Atmospheric Studies, Evaluation Number 15," JPL Publication 06-2, Jet Propulsion Laboratory, Pasadena, 2006 <http://jpldataeval.jpl.nasa.gov>.
212. Sander, S. P. and R. R. Friedl, 1989, *J. Phys. Chem.*, 93, 4764-4771.
213. Schindler, R., M. Liesner, S. Schmidt, U. Kirschner and T. Benter, 1997, *J. Photochem. Photobiol. A: Chem.*, 107, 9-19.
214. Schmidt, S., T. Benter and R. N. Schindler, 1998, *Chem. Phys. Lett.*, 282, 292-298.
215. Seccombe, D. P., R. Y. L. Chim, R. P. Tuckett, H. W. Jochims and H. Baumgaertel, 2001, *J. Chem. Phys.*, 114, 4058-4073.
216. Seccombe, D. P., R. P. Tuckett, H. Baumgärtel and H. W. Jochims, 1999, *Phys. Chem. Chem. Phys.*, 1, 773-782.
217. Seery, D. J. and D. Britton, 1964, *J. Phys. Chem.*, 68, 2263-2266.
218. Simon, F. G., W. Schneider, G. K. Moortgat and J. P. Burrows, 1990, *Journal of Photochemistry and Photobiology*, A55, 1-23.
219. Simon, P. C., D. Gillotay, N. Vanlaethem-Meurée and J. Wisenberg, 1988, *J. Atmos. Chem.*, 7, 107-135.
220. Simon, P. C., D. Gillotay, N. Vanlaethem-Meurée and J. Wisenberg, 1988, *Annales Geophysicae*, 6, 239-248.
221. Skorokhodov, V., Y. Sato, K. Suto, Y. Matsumi and M. Kawasaki, 1996, *J. Phys. Chem.*, 100, 12321-12328.
222. Smith, F.-G., F. M. G. Tablas, L. T. Molina and M. J. Molina, 2001, *J. Phys. Chem. A*, 105, 8658-8664.
223. Smith, W. S., C. C. Chou and F. S. Rowland, 1977, *Geophys. Res. Lett.*, 4, 517-519.
224. Stanton, J. F., C. M. L. Rittby, R. J. Bartlett and D. W. Toohey, 1991, *J. Phys. Chem.*, 95, 2107-2110.
225. Talukdar, R., A. Mellouki, T. Gierczak, J. B. Burkholder, S. A. McKeen and A. R. Ravishankara, 1991, *J. Phys. Chem.*, 95, 5815-5821.
226. Talukdar, R. K., A. Mellouki, J. B. Burkholder, M. K. Gilles, G. Le Bras and A. R. Ravishankara, 2001, *J. Phys. Chem. A*, 105, 5188-5196.
227. Tanaka, Y., M. Kawasaki, Y. Matsumi, H. Fujiwara, T. Ishiwata, L. J. Rogers, R. N. Dixon and M. N. R. Ashfold, 1998, *J. Chem. Phys.*, 109, 1315-1325.
228. Toniolo, A., G. Granucci, S. Inglese and M. Persico, 2001, *Phys. Chem. Chem. Phys.*, 3, 4266-4279.
229. Toniolo, A., M. Persico and D. Pitea, 2000, *J. Phys. Chem. A*, 104, 7278-7283.
230. Tonokura, K., Y. Matsumi, M. Kawasaki, S. Tasaki and R. Bersohn, 1992, *J. Chem. Phys.*, 97, 8210-8215.
231. Troler, M., R. L. Mauldin, III and A. R. Ravishankara, 1990, *J. Phys. Chem.*, 94, 4896-4907.
232. Tyndall, G. S., C. S. KegleyOwen, J. J. Orlando and J. G. Calvert, 1997, *J. Chem. Soc. Faraday Trans.*, 93, 2675-2682.

233. Tyndall, G. S., K. M. Stedman, W. Schneider, J. P. Burrows and G. K. Moortgat, 1987, *J. Photochem.*, 36, 133-139.
234. Vaida, V., S. Solomon, E. C. Richards, E. Ruhl and A. Jefferson, 1989, *Nature*, 342, 405-408.
235. Vanlaethem-Meurée, N., J. Wisenberg and P. C. Simon, 1978, *Bull. Acad. Roy. Belgique Cl. Sci.*, 64, 31.
236. Vanlaethem-Meurée, N., J. Wisenberg and P. C. Simon, 1978, *Bull. Acad. Roy. Belgique Cl. Sci.*, 64, 42.
237. Vanlaethem-Meurée, N., J. Wisenberg and P. C. Simon, 1979, *Geophys. Res. Lett.*, 6, 451-454.
238. Vatsa, R. K. and H.-R. Volpp, 2001, *Chem. Phys. Lett.*, 340, 289-295.
239. Villenave, E., I. Morozov and R. Lesclaux, 2000, *J. Phys. Chem. A*, 104, 9933-9940.
240. Vogt, R. and R. N. Schindler. *Air Pollution Report* 34, 1990; pp 167-171.
241. Vogt, R. and R. N. Schindler, 1992, *J. Photochem. Photobiol. A: Chem.*, 66, 133-140.
242. von Hobe, M., F. Stroh, H. Beckers, T. Benter and H. Willner, 2009, *Phys. Chem. Chem. Phys.*, 11, 1571-1580.
243. Wahner, A., G. S. Tyndall and A. R. Ravishankara, 1987, *J. Phys. Chem.*, 91, 2734-2738.
244. Watson, R. T., 1977, *J. Phys. Chem. Ref. Data*, 6, 871-917.
245. Wayne, R. P., G. Poulet, P. Biggs, J. P. Burrows, R. A. Cox, P. J. Crutzen, G. D. Hayman, M. E. Jenkin, G. Le Bras, G. K. Moortgat, U. Platt and R. N. Schindler, 1995, *Atmos. Environ.*, 29, 2675-2881.
246. Wijnen, M. H., 1961, *J. Am. Chem. Soc.*, 83, 3014-3017.
247. Wilmouth, D. M., T. Hanisco, R. M. Stimpfle and J. G. Anderson, 2009, *Journal of Physical Chemistry A*, 14099-14108.
248. Wilmouth, D. M., T. F. Hanisco, N. M. Donahue and J. G. Anderson, 1999, *J. Phys. Chem A*, 103, 8935-8945.
249. Wine, P. H., A. R. Ravishankara, D. L. Philen, D. D. Davis and R. T. Watson, 1977, *Chem. Phys. Lett.*, 50, 101-106.
250. Yano, T. and E. Tschuikow-Roux, 1980, *J. Phys. Chem.*, 84, 3372-3377.
251. Yokelson, R. J., J. Burkholder, R. W. Fox and A. R. Ravishankara, 1997, *J. Phys. Chem. A*, 101, 6667-6678.
252. Zhang, J., M. Dulligan and C. Wittig, 1997, *J. Chem. Phys.*, 107, 1403-1405.
253. Zou, P., J. Park, B. A. Schmitz, T. Nguyen and S. W. North, 2002, *J. Phys. Chem. A*, 106, 1004-1010.

SECTION 4G. BrO_x PHOTOCHEMISTRY



(Recommendation: 06-2, Note: 10-6, Evaluated: 10-6)

Absorption Cross Sections: The UV/vis absorption spectrum of bromine, Br₂, has been extensively studied as summarized in Table 4G-1.

Table 4G-1. Summary of Br₂ Cross Section Studies

Study	Year	Temperature (K)	Wavelength Range (nm)
Ribaud [91]	1919	289, 593, 893	356 – 608
Gray and Style [41]	1930	294	240 – 579
Acton et al. [1]	1936	293, 400, 531, 657, 767, 906	327.4 – 571.7
Seery and Britton [101]	1964	298	320 – 590
MacMillan [18]	1966	298	200 – 599
Passchier et al. [83]	1967	298, 348, 423, 298, 573, 648, 713	200 – 750
Wen and Noyes [119]	1972	303	220 – 290
Hemenway et al. [44]	1979	296	556 – 616.3
Roxlo and Mandl [96]	1980	298	170 – 230
Röth et al. [94]	1991	294	315.2 – 512.4 504.0 – 552.6
Hubinger and Nee [47]	1995	295	190 – 600
Tellinghuisen [111]	2008	295	190 – 300

The Br₂ spectrum exhibits an absorption band between 190 and 300 nm with a maximum near 223 nm and another stronger band between 300 and 600 nm, which is composed of three overlapping bands with the maxima at ~412, 480, and 549 nm. The reported absorption cross sections are in very good agreement in the region of the UV-visible absorption band. Discrepancies are observed at wavelengths >550 nm, where the data of McMillan [18] and Hemenway et al. [44] are as much as 60% and 100% lower, respectively, than the values measured in the other studies. Large discrepancies arise in the region of the absorption minimum between 230 and 340 nm due to a pressure dependent component of the Br₂ vapor, possibly a Br₂-Br₂ dimer. A detailed discussion of the available absorption data for Br₂ and an evaluation is given by Maric et al. [67]. Maric et al. fit the most reliable data, those of Passchier et al. [83] and Wen and Noyes [119], to a four-band semi-logarithmic distribution function and derived an expression that enables the calculation of the Br₂ absorption spectrum over the wavelength region 200 – 650 nm

$$\begin{aligned} \sigma(298 \text{ K}) = & 1.06 \times 10^{-20} \times \exp\{-52.3[\ln(223.3/\lambda)]^2\} \\ & + 6.19 \times 10^{-19} \times \exp\{-108.5[\ln(411.9/\lambda)]^2\} \\ & + 3.39 \times 10^{-19} \times \exp\{-106.8[\ln(480.2/\lambda)]^2\} \\ & + 3.78 \times 10^{-20} \times \exp\{-112.0[\ln(549.3/\lambda)]^2\} \end{aligned}$$

where λ is in nm and σ is in cm² molecule⁻¹. The recommended absorption cross sections calculated using this expression are listed in Table 4G-2. The results of Maric et al. [67] have been confirmed in general in a subsequent study by Hubinger and Nee [47], who reported absorption cross sections for the wavelength range 190 – 600 nm. The Hubinger and Nee cross sections values that are below 10⁻²¹ cm² molecule⁻¹, i.e., between 260 and 340 nm, differ from the parameterized data of Maric et al. [67] and can only be considered as upper limits.

The temperature dependence of the absorption spectrum has been measured by Acton et al. [1] (293 – 906 K) and Passchier et al. [83] (298 – 713 K). These studies report a decrease of the cross sections around the absorption maximum between ~380 and ~500 nm and an increase in the short and long wavelength tails with increasing temperature.

Photolysis Quantum Yield and Product Studies: Photodissociation of Br₂ leads to the formation of Br atoms in the ground Br(²P_{3/2}) and excited Br*(²P_{1/2}) states. A few studies have been performed to establish the relative quantum yields of (Br + Br) and (Br + Br*) at various photolysis wavelengths. Petersen and Smith [85] found the yield of Br* atoms to increase from 0.4 to 0.89 from 444 to 510 nm and decrease at longer

wavelengths to a value of ~ 0.4 at 530 nm. Lindeman and Wiesenfeld [63] observed the relative quantum yield ($\text{Br} + \text{Br}^*$) to increase from 0.07 at 434 nm to 0.64 at 482 nm and then to decrease to 0.57 at 511 nm. Haugen et al. [43] determined the relative quantum yield ($\text{Br} + \text{Br}^*$) to increase from 0.44 at 445 nm to 0.87 at 500 nm followed by a decrease to 0.40 at 530 nm. Cooper et al. [20] measured the relative ($\text{Br} + \text{Br}^*$) yield to be zero in the range 360 to 430 nm and to increase at longer wavelengths to 0.79 at 580 nm; at 260 nm they observed ($\text{Br} + \text{Br}^*$) to be dominant. Jee et al. [52, 53] measured the relative yield of the photodissociation channel into ($\text{Br} + \text{Br}^*$) at 234 nm to be unity and at 265 nm to be 0.96. Zaraga et al. [123] calculated the zero pressure predissociation quantum yield from high resolution spectroscopic studies in the banded region ($\text{B } ^3\Pi(0_u^+)$ state) overlapping a continuum at 588 nm to be near unity.

Table 4G-2. Absorption Cross Sections of Br_2 at 298 K

λ (nm)	$10^{20} \sigma$ (cm^2)	λ (nm)	$10^{20} \sigma$ (cm^2)	λ (nm)	$10^{20} \sigma$ (cm^2)	λ (nm)	$10^{20} \sigma$ (cm^2)
200	0.562	315	0.0274	430	60.1	545	10.1
205	0.723	320	0.0626	435	57.1	550	8.68
210	0.870	325	0.141	440	54.0	555	7.47
215	0.983	330	0.300	445	51.2	560	6.43
220	1.05	335	0.602	450	48.8	565	5.54
225	1.06	340	1.14	455	46.8	570	4.77
230	1.01	345	2.05	460	45.2	575	4.09
235	0.925	350	3.49	465	44.0	580	3.50
240	0.808	355	5.63	470	42.8	585	2.98
245	0.676	360	8.66	475	41.6	590	2.52
250	0.544	365	12.7	480	40.3	595	2.11
255	0.422	370	17.8	485	38.6	600	1.76
260	0.316	375	23.9	490	36.6	605	1.45
265	0.229	380	30.7	495	34.3	610	1.19
270	0.161	385	37.9	500	31.8	615	0.958
275	0.110	390	45.1	505	29.0	620	0.767
280	0.0728	395	51.8	510	26.2	625	0.607
285	0.0472	400	57.4	515	23.4	630	0.475
290	0.0299	405	61.6	520	20.6	635	0.368
295	0.0187	410	64.2	525	18.0	640	0.282
300	0.0122	415	65.1	530	15.7	645	0.214
305	0.0100	420	64.5	535	13.6	650	0.161
310	0.0135	425	62.8	540	11.7		

Note:

Calculated using the expression given by Maric et al. [67]



(Recommendation: 06-2, Note: 10-6, Evaluated: 10-6)

Absorption Cross Sections: The UV absorption spectrum of hydrogen bromide, HBr, at wavelengths >180 nm consists of a continuous band with a maximum near 178 nm and monotonically decreasing absorption cross sections that have been measured out to 270 nm. At shorter wavelengths the spectrum shows a large number of strong sharp bands that extend to 105 nm.

The room temperature absorption cross sections of HBr have been measured in a number of studies as outlined in Table 4G-3. The absorption cross sections near the maximum of the absorption band reported by Nee et al. [75] and Huebert and Martin [48] are in good agreement, 2.4×10^{-18} and $2.7 \times 10^{-18} \text{ cm}^2 \text{ molecule}^{-1}$, respectively. The values reported by Romand [93] and Roxlo and Mandl [96] are substantially lower, 2×10^{-18} and $1.4 \times 10^{-18} \text{ cm}^2 \text{ molecule}^{-1}$, respectively. The cross section at 193 nm reported by Vaghjani [114] and Barone et al. [3] are consistent with the absorption spectra reported by Nee et al. [75] and Huebert and Martin [48]. The cross sections at 184.9 nm measured by Ravishankara et al. [89] and Barone et al. [3] fall between those reported by Nee et al. [75] and Huebert and Martin [48]. The 184.9 nm cross section measured by Okabe [76] lies between those of Goodeve and Taylor [38] and Romand [93]. The recommended values in Table 4G-4 were derived as follows: the spectra of Goodeve and Taylor [38], Romand [93], Huebert and

Martin [48], and Nee et al. [75] have been normalized to $2.21 \times 10^{-18} \text{ cm}^2 \text{ molecule}^{-1}$ at 184.9 nm, which is the mean of the values reported by Okabe [76], Ravishankara et al. [89], and Barone et al. [3]; the normalized spectra have been averaged, the recommended cross sections for the range 152 – 168 nm are those of Romand [93] and Nee et al. [75], for the range 170 – 180 nm those of Romand [93], Huebert and Martin [48], and Nee et al. [75], and for the range 182 – 230 nm those of Goodeve and Taylor [38], Romand [93], Huebert and Martin [48], and Nee et al. [75].

Table 4G-3. Summary of HBr UV Absorption Cross Section Studies

Study	Year	Temperature (K)	Wavelength Range (nm)
Goodeve and Taylor [38]	1935	298	182 – 286
Romand [93]	1949	298	139 – 228
Huebert and Martin [48]	1968	297	170 – 230
Bridges and White [9]	1973	298	214
Okabe [76]	1977	296	240 – 270
Ravishankara et al. [89]	1979	298	184.9
Roxlo and Mandl [96]	1980	298	170 – 230
Okabe [77]	1983	296	184.9
Brion et al. [10]	1985	298	30 – 177
Nee et al. [75]	1986	298	105 – 238
Vaghjiani [114]	1993	296	193
Barone et al. [3]	1994	298	184.9, 193.0

Photolysis Quantum Yield and Product Studies: The branching fraction for the formation of excited $\text{Br}^*(^2\text{P}_{3/2})$ atoms was determined by Regan et al. [90] in the wavelength range 201 – 253 nm to vary between 0.15 and 0.23. Baumfalk et al. [5] obtained a value for the branching fraction for Br^* of 0.20 ± 0.03 at 243 nm and a value of 0.18 ± 0.03 at 193 nm.

Table 4G-4. Absorption Cross Sections of HBr at 298 K

λ (nm)	$10^{20} \sigma$ (cm^2)	λ (nm)	$10^{20} \sigma$ (cm^2)	λ (nm)	$10^{20} \sigma$ (cm^2)	λ (nm)	$10^{20} \sigma$ (cm^2)
152	139	172	233	192	181	212	54.8
154	124	174	240	194	168	214	45.7
156	138	176	244	196	154	216	38.8
158	148	178	244	198	140	218	33.0
160	161	180	242	200	125	220	28.0
162	176	182	233	202	111	222	22.9
164	189	184	225	204	98.1	224	18.2
166	201	186	217	206	85.5	226	14.4
168	211	188	206	208	74.7	228	11.7
170	225	190	194	210	64.4	230	9.32

Note:

Normalization of the data from Goodeve and Taylor [38], Romand [93], Huebert and Martin [48], and Nee et al. [75] to $2.21 \times 10^{-18} \text{ cm}^2 \text{ molecule}^{-1}$ at 184.9 nm and averaging:

152 – 168 nm: mean of Romand [93] and Nee et al. [75] data

170 – 180 nm: mean of Romand [93], Huebert and Martin [48] and Nee et al. [75] data

182 – 230 nm: mean of Goodeve and Taylor [38], Romand [93], Huebert and Martin [48] and Nee et al. [75] data



(Recommendation: 06-2, Note: 10-6, Evaluated: 10-6)

Absorption Cross Sections: The BrO radical has a banded UV absorption spectrum in the 290 – 380 nm range, which is attributed to the $\text{A } ^2\Pi_{3/2} \leftarrow \text{X } ^2\Pi_{3/2}$ transition. The spectrum measured by Wahner et al. [117]

is shown in Figure 4G-1 and laboratory measurements are summarized in Table 4G-5. The absorption spectrum has been measured and cross sections determined for single absorption peaks, the strongest, the (7, 0) peak at 338.5 nm and the (11, 0) and (12, 0) peaks at 320.8 nm and 317.3 nm.

Table 4G-5. Summary of BrO Cross Section Studies

Study	Year	Temperature (K)	Wavelength Range (nm)	Resolution (nm)
Clyne and Cruse [19]	1970	293	338.3	0.15
Basco and Dogra [4]	1971	298	320.8, 338.3	not given
Cox et al. [21]	1982	298	296 – 370	0.22
Wahner et al. [117]	1988	228, 243, 298	312 – 380	0.4
Sander and Friedl [97]	1989	220, 298	338.5	0.06 – 1.25
Orlando et al. [82]	1991	298	338.5	0.4
Laszlo et al [59]	1997	295	338.5	0.6
Gilles et al. [31]	1997	204, 222, 237, 252, 273, 298, 329, 369	338.5	0.5
Wheeler et al. [120]	1998	298	338, 317	4 cm ⁻¹
Wilmouth et al. [121]	1999	298	317 – 388	1.0 cm ⁻¹
Wilmouth et al. [121]	1999	228, 298	286 – 386	10 cm ⁻¹
Fleischmann et al. [29]	2003	203, 223, 243, 273, 298	300 – 385	4 cm ⁻¹

The cross sections are both temperature and resolution dependent, i.e., the peaks of the vibrational bands become greater and sharper with decreasing temperature and at higher resolution. Wilmouth et al. [121] used their absorption spectrum, recorded at 10 cm⁻¹ resolution, in a combined analysis of the results from Cox et al. [21], Wahner et al. [117], Orlando et al. [82], Laszlo et al. [59], and Gilles et al. [31] at a common resolution of 0.40 nm (details of this procedure are described in Wilmouth et al. [121]). The absorption cross sections for the peaks of the vibrational bands of the A ← X transition at 298 ± 2 and 228 ± 2 K obtained by this analysis are listed in Table 4G-6. Averages of the absorption cross sections over 0.5 nm intervals of the spectrum reported by Wilmouth et al. [121] are listed in Table 4G-7.

Absorption cross sections for the rotational peaks of the (7,0) and (12,0) bands were measured at high resolution (1.0 cm⁻¹) by Wilmouth et al. [121] to be $\sigma = 2.17 \times 10^{-17}$ cm² molecule⁻¹ for the peak of the (7,0) band and $\sigma = 1.38 \times 10^{-17}$ cm² molecule⁻¹ for the peak of the (12,0) band.

The (7,0) absorption maximum (338 nm) temperature dependence was measured by Gilles et al. [31] over the range 204 – 388 K at a resolution of 0.5 nm and given by the expression.

$$\sigma(T)_{338 \text{ nm}} = 3.29 - (5.58 \times 10^{-3}) \times T, \text{ in units of } 10^{-17} \text{ cm}^2 \text{ molecule}^{-1}$$

Photolysis Quantum Yield and Product Studies: Transitions in the A ← X system are expected to be dissociative.

Table 4G-6. Absorption Cross Sections at the Vibrational Band Peaks in the A ← X Spectrum of BrO (0.4 nm resolution)

v', v''	λ, nm	10 ²⁰ σ, cm ² molecule ⁻¹	
		298 ± 2 K	228 ± 2 K
26, 0	286.46	107	88.3
25, 0	287.38	132	133
24, 0	288.45	145	175
23, 0	289.83	188	208
22, 0	291.40	188	267
21, 0	292.99	242	284
20, 0	294.88	295	348
19, 0	296.97	356	441
18, 0	299.30	447	541
17, 0	301.81	523	636
16, 0	304.54	601	728
15, 0	307.46	679	819
14, 0	310.54	772	932
13, 0	313.81	904	1090
12, 0	317.29	1190	1480
11, 0	321.20	1360	1670
10, 0	325.37	1260	1510
9, 0	329.56	1210	1430
8, 0	333.89	1250	1510
7, 0	338.69	1580	1970
6, 0	344.04	923	1060
5, 0	349.09	715	828
4, 0	355.02	723	864
3, 0	360.64	267	287
4, 1	364.32	126	95.4
2, 0	367.94	128	129
1, 0	374.69	74.5	77.3
2, 1	381.27	27.5	27.4
0, 0	286.46	22.5	–
1, 1	287.38	9.86	–

Note:

Wilmouth et al. [121], analysis of spectra from Wilmouth et al. [121], Cox et al. [21], Wahner et al. [117], Orlando et al. [82], Laszlo et al. [59], Gilles et al. [31] at a common resolution of 0.40 nm.

Table 4G-7. Absorption Cross Sections of BrO at 298 K

λ (nm)	$10^{20} \sigma$ (cm ²)	λ (nm)	$10^{20} \sigma$ (cm ²)	λ (nm)	$10^{20} \sigma$ (cm ²)	λ (nm)	$10^{20} \sigma$ (cm ²)
286.5	104.8	311.5	453.1	336.5	258.7	361.5	226.6
287.0	106.5	312.0	294.8	337.0	222.1	362.0	182.9
287.5	128.8	312.5	203.7	337.5	202.0	362.5	145.2
288.0	95.04	313.0	197.3	338.0	201.8	363.0	119.9
288.5	147.7	313.5	723.9	338.5	1287.0	363.5	103.7
289.0	109.8	314.0	901.3	339.0	1296.0	364.0	113.3
289.5	126.4	314.5	650.8	339.5	734.4	364.5	122.2
290.0	183.8	315.0	443.2	340.0	444.8	365.0	99.15
290.5	133.1	315.5	310.9	340.5	303.1	365.5	87.15
291.0	133.5	316.0	231.7	341.0	243.1	366.0	86.23
291.5	188.6	316.5	173.7	341.5	217.5	366.5	91.26
292.0	157.2	317.0	721.1	342.0	235.0	367.0	105.0
292.5	128.3	317.5	1136.0	342.5	291.6	367.5	123.4
293.0	248.2	318.0	730.7	343.0	423.8	368.0	130.5
293.5	192.5	318.5	482.3	343.5	711.9	368.5	119.5
294.0	140.4	319.0	344.6	344.0	967.8	369.0	100.9
294.5	161.5	319.5	275.1	344.5	814.4	369.5	86.11
295.0	294.4	320.0	251.4	345.0	542.1	370.0	74.79
295.5	216.1	320.5	293.7	345.5	345.0	370.5	64.46
296.0	163.9	321.0	1138.0	346.0	225.9	371.0	53.91
296.5	152.9	321.5	1155.0	346.5	160.3	371.5	46.47
297.0	361.1	322.0	676.9	347.0	146.4	372.0	39.44
297.5	276.5	322.5	419.6	347.5	162.2	372.5	35.13
298.0	193.5	323.0	300.6	348.0	257.8	373.0	34.13
298.5	156.4	323.5	261.7	348.5	529.5	373.5	35.68
299.0	284.0	324.0	288.2	349.0	747.7	374.0	48.08
299.5	421.1	324.5	433.6	349.5	667.4	374.5	74.97
300.0	275.3	325.0	982.6	350.0	499.2	375.0	70.53
300.5	193.5	325.5	1283.0	350.5	363.4	375.5	51.46
301.0	180.1	326.0	837.6	351.0	272.4	376.0	35.44
301.5	350.9	326.5	494.8	351.5	215.3	376.5	30.47
302.0	502.3	327.0	312.0	352.0	181.9	377.0	27.46
302.5	318.4	327.5	231.1	352.5	165.9	377.5	25.66
303.0	217.4	328.0	223.5	353.0	162.8	378.0	25.61
303.5	195.9	328.5	343.1	353.5	163.2	378.5	21.82
304.0	274.0	329.0	789.1	354.0	179.5	379.0	18.60
304.5	609.6	329.5	1261.0	354.5	309.3	379.5	14.96
305.0	466.2	330.0	1058.0	355.0	789.4	380.0	12.28
305.5	298.4	330.5	706.2	355.5	498.6	380.5	13.03
306.0	221.1	331.0	453.4	356.0	276.2	381.0	19.55
306.5	209.7	331.5	295.9	356.5	166.2	381.5	20.93
307.0	407.2	332.0	203.1	357.0	119.9	382.0	16.76
307.5	703.1	332.5	164.7	357.5	111.1	382.5	9.049
308.0	518.3	333.0	259.8	358.0	115.3	383.0	3.059
308.5	343.6	333.5	952.8	358.5	123.6	383.5	4.924
309.0	227.6	334.0	1294.0	359.0	143.6	384.0	3.892
309.5	193.6	334.5	963.3	359.5	182.7	384.5	6.695
310.0	395.5	335.0	652.3	360.0	236.4	385.0	10.93
310.5	798.9	335.5	457.5	360.5	272.3		
311.0	659.2	336.0	338.8	361.0	264.4		

Note:

Wilmouth et al. [121], averages over 0.5 nm intervals

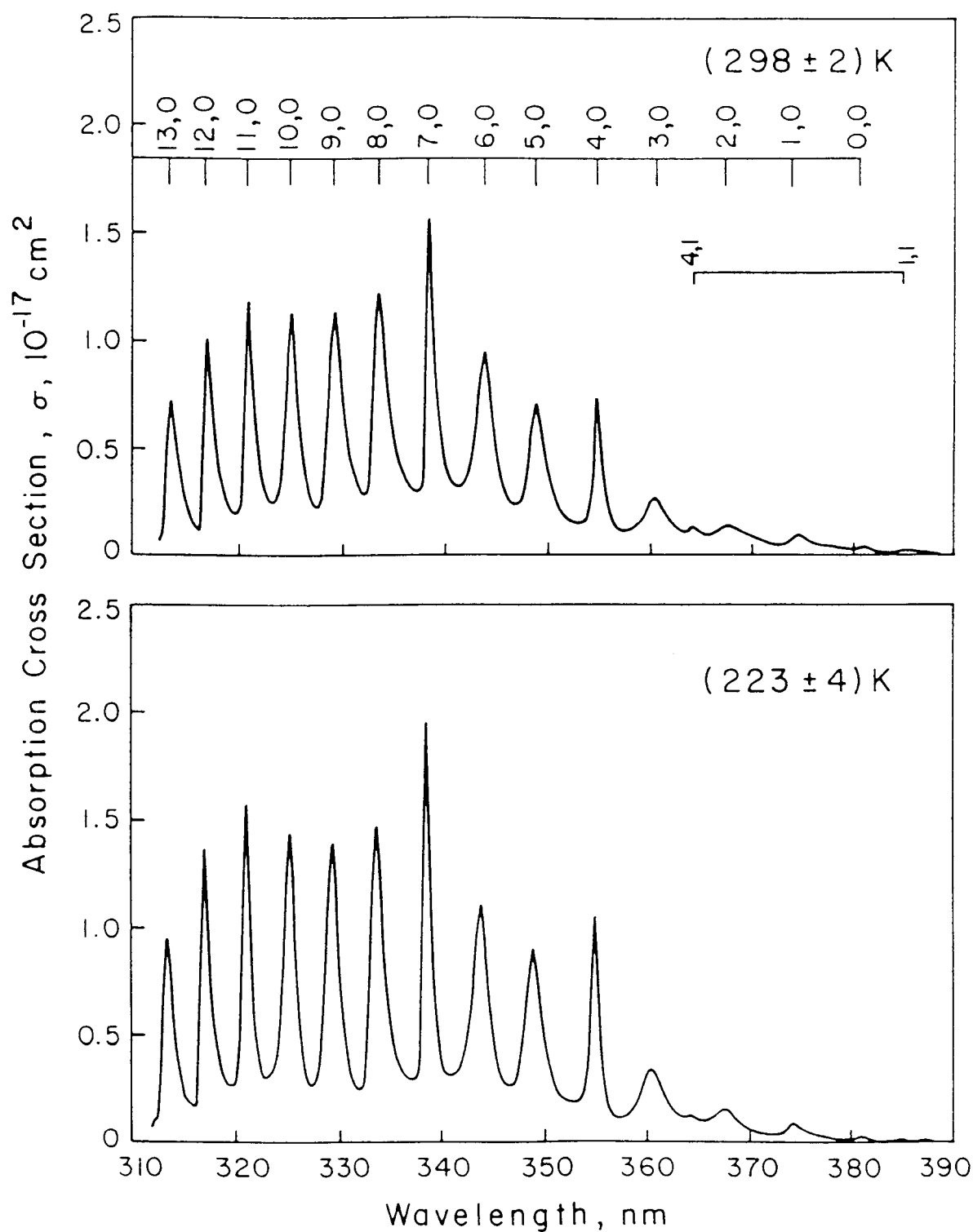


Figure 4G-1. Absorption Spectrum of BrO



(Recommendation: 06-2, Note: 10-6, Evaluated: 10-6)

Absorption Cross Sections: The visible absorption spectrum of bromine dioxide, OBrO, has been measured in the 400 – 600 nm region at room temperature by Rowley et al. [95], and Knight et al. [56] and at ~250 K

by Miller et al. [69] and at 273, 298, and 338 K by Rattigan et al. [87]. The OBrO spectrum measured by Knight et al. is shown in Figure 4G-2. The spectrum has a highly structured absorption band consisting of a progression of doublets with a maximum intensity near 500 nm and a progression of less intense bands between the doublets. The spectrum was assigned to the $C^2A_2 \leftarrow X^2B_1$ electronic transition by Miller et al. [69] who combined *ab initio* calculations of the lowest doublet electronic states of OBrO with Franck-Condon simulations. Knight et al. [56] reported absorption cross section data. The peak positions and cross sections for the vibrational progressions $(n,0,0) \leftarrow (0,0,0)$ and $(n,1,0) \leftarrow (0,0,0)$ in Table 4G-8 are taken from Knight et al. [56]. Table 4-141 gives the absorption cross section averages over 1 nm intervals of the spectrum reported by Knight et al. [56] (0.66 nm resolution).

Photolysis Quantum Yield and Product Studies: No quantum yields are available but theoretical calculations by Vetter et al. [116] indicate that photodissociation occurs via the $BrO + O(^3P)$ channel because of a large transition dipole moment for the $C^2A_2 \leftarrow X^2B_1$ transition. Photodissociation into $Br + O_2$ occurs via the 1^2B_2 state and is less probable and therefore less important.

Table 4G-8. Peak Absorption Cross Sections of OBrO at 298 K

n	$(n,0,0) \leftarrow (0,0,0)$ λ (nm)	$10^{20} \sigma$ (cm ²)	$(n,1,0) \leftarrow (0,0,0)$ λ (nm)	$10^{20} \sigma$ (cm ²)
0	630.4	—	622.0	—
1	606.1	—	598.4	—
2	583.8	—	576.8	—
3	563.4	1080	556.8	1350
4	544.4	1450	538.5	1740
5	527.1	1640	521.6	1910
6	510.7	1770	505.5	1960
7	495.5	1720	490.7	1760
8	481.2	1670	476.9	1510
9	468.2	1440	464.1	1260
10	455.8	1210	452.2	960
11	444.4	1020	440.8	720
12	433.7	790	430.4	490
13	423.5	570	420.6	310
14	414.1	400	411.0	220
15	405.1	260	402.3	130

Note:

Knight et al. [56]

Table 4G-9. Absorption Cross Sections of OBrO at 298 K

λ (nm)	$10^{20} \sigma$ (cm ²)	λ (nm)	$10^{20} \sigma$ (cm ²)	λ (nm)	$10^{20} \sigma$ (cm ²)	λ (nm)	$10^{20} \sigma$ (cm ²)
401	66.7	443	363	485	301	527	1530
402	112	444	834	486	463	528	1100
403	116	445	777	487	368	529	584
404	153	446	452	488	298	530	326
405	243	447	292	489	425	531	218
406	180	448	254	490	868	532	347
407	131	449	214	491	1580	533	547
408	113	450	180	492	993	534	361
409	105	451	323	493	641	535	344
410	128	452	854	494	583	536	539
411	201	453	672	495	1160	537	434
412	171	454	394	496	1430	538	1200
413	239	455	633	497	826	539	1500
414	380	456	1110	498	458	540	888
415	260	457	729	499	291	541	546
416	180	458	426	500	405	542	442
417	156	459	292	501	512	543	312
418	133	460	314	502	336	544	991
419	147	461	262	503	419	545	1230
420	269	462	213	504	483	546	716
421	274	463	399	505	1230	547	395
422	229	464	1100	506	1650	548	252
423	479	465	868	507	962	549	161
424	481	466	506	508	651	550	302
425	287	467	562	509	556	551	476
426	207	468	1230	510	1030	552	300
427	175	469	1020	511	1570	553	255
428	149	470	568	512	953	554	461
429	194	471	341	513	506	555	349
430	422	472	298	514	307	556	532
431	382	473	362	515	282	557	1250
432	274	474	239	516	532	558	870
433	577	475	286	517	433	559	472
434	661	476	563	518	303	560	350
435	392	477	1390	519	529	561	267
436	251	478	990	520	504	562	204
437	208	479	567	521	1390	563	791
438	179	480	577	522	1610	564	885
439	166	481	1260	523	921	565	504
440	363	482	1310	524	622	566	275
441	651	483	745	525	516	567	170
442	425	484	403	526	654	568	107

Note:

Knight et al. [56], data averages over 1 nm intervals

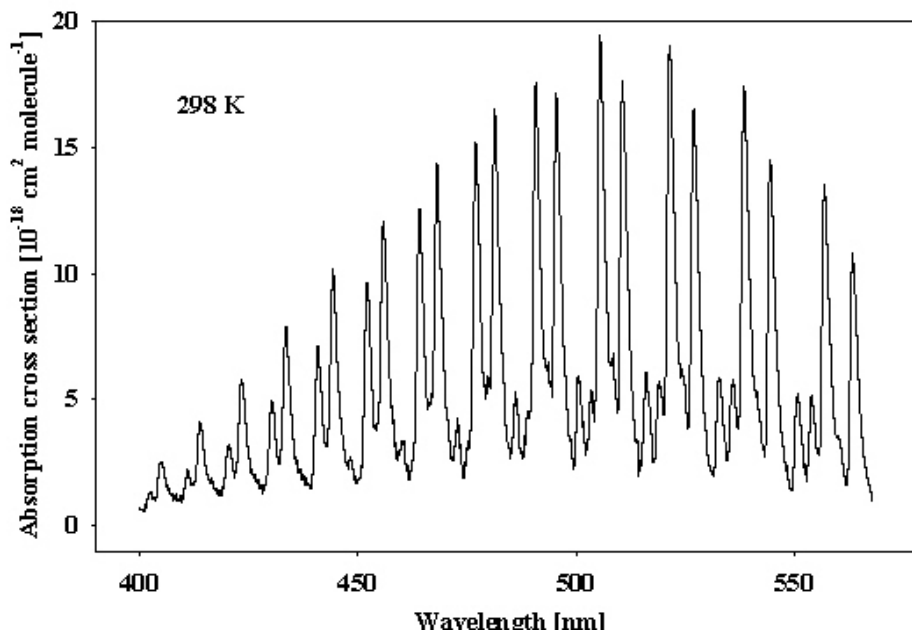


Figure 4G-2. Absorption spectrum of OBrO

G5.	Br ₂ O + hv	→ Br + BrO	128 kJ mol ⁻¹	938 nm	(1)
		→ Br ₂ + O	173 kJ mol ⁻¹	693 nm	(1)
		→ Br + Br + O	366 kJ mol ⁻¹	327 nm	(1)

(Recommendation: 06-2, Note: 10-6, Evaluated: 10-6)

Absorption Cross Sections: The UV absorption spectrum of dibromine monoxide, Br₂O, has been measured at room temperature by Orlando and Burkholder [81] (196 – 432 nm), Rattigan et al. [88] (240 – 515 nm), and Deters et al. [23] (208 – 444 nm). The spectrum exhibits a strong narrow band at wavelengths <220 nm with a maximum at 200 nm, a weaker and broader band extending from 250 nm to about 460 nm with a maximum at 313 nm and a shoulder near 350 nm, and two weak bands at 460 – 580 nm and 580 – 750 nm with maxima at ~520 nm and ~665 nm. There is good agreement between the various data sets in the wavelength region <380 nm where the data of Orlando and Burkholder [81] and Deters et al. [23] are nearly identical and those of Rattigan et al. [88] are smaller by ~10% below 250 nm and above 290 nm and smaller by up to ~25% in the region of the absorption minimum near 270 nm. Large discrepancies exist between the data sets at wavelengths >380 nm. The absorption cross sections reported by Orlando and Burkholder [81] and Deters et al. [23] decrease at longer wavelengths to values $\leq 1 \times 10^{-20}$ cm² molecule⁻¹ whereas the values reported by Rattigan et al. [88] show a decrease between 400 and 470 nm and evidence for another absorption band at longer wavelengths. The cutoff at 440 nm of the absorption spectrum reported by Orlando and Burkholder [81] is a result of the assumption that the absorbance of Br₂O is zero at wavelengths >440 nm. The correction procedure used by Rattigan et al. [88] taking the vibrational structure of the Br₂ spectrum into account resulted in appreciable absorption for Br₂O at wavelengths above 440 nm. The recommended cross sections in Table 4G-10 are the data from Orlando and Burkholder [81] at 196 and 200 nm, the mean of the data from Orlando and Burkholder [81] and Deters et al. [23] for the region 210 – 230 nm, and the mean of the data from Orlando and Burkholder [81], Deters et al. [23], and Rattigan et al. [88] for the region 240 – 400 nm. No recommendation is given for wavelengths >400 nm.

Photolysis Quantum Yield and Product Studies: By analogy to Cl₂O the predominate photodissociation channel is expected to be Br + BrO. Burkholder [11] measured the BrO yield at 308 nm to be near unity.

Table 4G-10. Absorption Cross Sections of Br₂O at 298 K

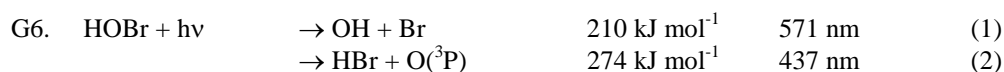
λ (nm)	$10^{20} \sigma$ (cm ²)	λ (nm)	$10^{20} \sigma$ (cm ²)
196	1740	300	167
200	2000	310	220
210	1050	320	212
220	288	330	192
230	140	340	188
240	85.8	350	186
250	45.4	360	162
260	24.6	370	132
270	18.8	380	99.0
280	33.5	390	74.8
290	85.5	400	54.0

Note:

196, 200 nm: Orlando and Burkholder [81]

210 – 230 nm: mean of data from Orlando and Burkholder [81] and Deters et al. [23]

240 – 400 nm: mean of data from Orlando and Burkholder [81], Deters et al. [23] and Rattigan et al. [88]



(Recommendation: 06-2, Note: 10-6, Evaluated: 10-6)

Absorption Cross Sections: The UV absorption spectrum of hypobromous acid, HOBr, has been measured by Orlando and Burkholder [81], Deters et al. [23], Benter et al. [7], Rattigan et al. [88], and Ingham et al. [51]. Orlando and Burkholder [81], Deters et al. [23], and Benter et al. [7] observe two absorption bands with maxima near 284 and 351 nm. The spectra agree reasonably well in shape with a sharp decrease in cross section at wavelengths greater than 400 nm. In contrast, the cross sections reported by Rattigan et al. [88] and Ingham et al. [51] are roughly 50% greater between 300 and 400 nm. In addition, the spectrum reported by Rattigan et al. [88] has a pronounced long wavelength tail extending to 520 nm. Ingham et al. [51] report a similar spectrum to Rattigan et al. but with a more prominent absorption band at long wavelength with a maximum at 457 nm. These two studies are consistent with the observations of Barnes et al. [2], who showed that laser photolysis of HOBr between 440 – 600 nm gives rise to OH photofragments. The presence of a weak band beyond 400 nm is attributable to the presence of a forbidden transition from the ground electronic to a triplet state as predicted by the *ab initio* calculations of Francisco et al. [30] and Minaev [70]. The differences in the spectral shapes are probably attributable to impurities such as Br₂O and Br₂, and/or the use of different Br₂O cross sections. However, the presence of impurities alone cannot explain the large difference in cross sections at the peak of the absorption bands.

The recommended absorption cross sections in Table 4G-11 are based on the study by Ingham et al. [51]. These authors generated HOBr in situ by laser photolytic production of OH in the presence of Br₂, and determined the HOBr spectrum using a gated diode camera shortly after the pulse, circumventing the problem associated with the presence of the strong absorbing impurity Br₂O, which was present in previous studies. The calibration of the absorption cross sections was made relative to the cross sections of Br₂. No recommendation is given for wavelengths <250 nm where the data are uncertain.

The data presented in Table 4G-11 are computed with the following expression taken from Ingham et al. [51], which is based on a combination of three Gaussian functions, one for each absorption band

$$\sigma(\lambda) = 24.77 \exp \left\{ -109.80 \left[\ln \left(\frac{284.01}{\lambda} \right) \right]^2 \right\} + 12.22 \exp \left\{ -93.63 \left[\ln \left(\frac{350.57}{\lambda} \right) \right]^2 \right\} \\ + 2.283 \exp \left\{ -242.40 \left[\ln \left(\frac{457.38}{\lambda} \right) \right]^2 \right\}$$

where $\sigma(\lambda)$ is in units of $10^{-20} \text{ cm}^2 \text{ molecule}^{-1}$.

Photolysis Quantum Yield and Product Studies: Benter et al. [7] measured quantum yields for HOBr photolysis at 261 and 363 nm (near the band peaks). The observed quantum yield for Br formation at 363 nm

was greater than 0.95 and a unity quantum yield into the product channel OH + Br is recommended. The O + HBr channel was not observed. The laser photofragment study of Barnes et al. [2] claimed that OH was the major photolysis product at wavelengths >400 nm. Lock et al. [64] found that at 490 and 510 nm OH and Br photofragments are in their respective vibrational and spin-orbit ground states.

Table 4G-11. Absorption Cross Sections of HOBr at 298 K

λ (nm)	$10^{20} \sigma$ (cm ²)	λ (nm)	$10^{20} \sigma$ (cm ²)	λ (nm)	$10^{20} \sigma$ (cm ²)
250	4.15	355	12.1	460	2.28
255	6.19	360	11.5	465	2.14
260	10.5	365	10.5	470	1.91
265	14.6	370	9.32	475	1.62
270	18.7	375	7.99	480	1.30
275	22.1	380	6.65	485	0.993
280	24.3	385	5.38	490	0.723
285	25.0	390	4.22	495	0.502
290	24.0	395	3.23	500	0.333
295	21.9	400	2.43	505	0.212
300	19.1	405	1.80	510	0.129
305	16.2	410	1.36	515	0.076
310	13.6	415	1.08	520	0.042
315	11.8	420	0.967	525	0.023
320	10.8	425	0.998	530	0.012
325	10.5	430	1.15	535	0.0059
330	10.8	435	1.40	540	0.0029
335	11.3	440	1.68	545	0.0013
340	11.9	445	1.96	550	0.0006
345	12.3	450	2.18		
350	12.4	455	2.29		

Note:

Ingham et al. [51], calculated using the expression given in the text



(Recommendation: 06-2, Note: 10-6, Evaluated: 10-6)

Absorption Cross Sections: The absorption spectrum of nitrosyl bromide, BrNO, has been measured at room temperature by Eden et al. [27] (275 – 550 nm), Houel and Van den Bergh [46] (200 – 800 nm), Uthman et al. [113] (189 – 300 nm), Hippler et al. [45] (266 nm) and Maloney and Palmer [65] (270 nm). The spectrum exhibits four absorption bands between 200 and 800 nm, a strong band between 190 and 290 nm with the maximum at ~213 nm, a weaker band between 290 and 600 nm with the maximum at 338 nm and a shoulder near 420 nm, and a still weaker band between 600 and 800 nm with the maximum at 708 nm. The absorption cross sections from these studies are in good agreement (after correction of an error in Maloney and Palmer [65]). The recommended absorption cross sections in Table 4G-12 are from Uthman et al. [113] for the region 189 – 300 nm and the peak cross sections at 338, 416, and 708 nm reported by Houel and Van den Bergh [46].

Photolysis Quantum Yield and Product Studies: No studies are available.

Table 4G-12. Absorption Cross Sections of BrNO at 298 K

λ (nm)	$10^{20} \sigma$ (cm ²)	λ (nm)	$10^{20} \sigma$ (cm ²)
189	18.3	224	4740
193	39.0	230	2990
194	46.2	235	1920
197	166	240	1090
200	566	250	360
201	861	260	117
203	1690	270	40.1
205.5	2950	280	19.5
207	4340	290	16.8
210	6470	300	18.0
211	6910	338	31.0
213	7270	416	20.1
216	7060	708	2.94
220	6070		

Note:

189 – 300 nm: Uthman et al. [113]

338, 416, 708 nm: Houel and Van den Bergh [46]

G8. BrONO + $h\nu$ → Products

(Recommendation: 06-2, Note: 10-6, Evaluated: 10-6)

Absorption Cross Sections: The UV absorption spectrum of bromine nitrite, *cis*-BrONO, has been measured in the temperature range 228 – 296 K by Burkholder and Orlando [14] (200 – 365 nm). The spectrum exhibits a strong absorption band between 200 and 270 nm with a maximum at 228 nm and a broader and weaker band between 270 and 364 nm with a maximum at 316 nm. The relative shape of the BrONO spectrum was temperature independent within the uncertainties of the measurements. The results from Burkholder and Orlando [14] are recommended and listed in Table 4G-13.

Photolysis Quantum Yield and Product Studies: No studies are available.

Table 4G-13. Absorption Cross Sections of BrONO at 253 K

λ (nm)	$10^{20} \sigma$ (cm ²)	λ (nm)	$10^{20} \sigma$ (cm ²)	λ (nm)	$10^{20} \sigma$ (cm ²)	λ (nm)	$10^{20} \sigma$ (cm ²)
200	0	242	1070	284	247	326	400
202	116	244	874	286	262	328	394
204	221	246	720	288	277	330	387
206	358	248	602	290	293	332	382
208	496	250	514	292	310	334	375
210	687	252	446	294	331	336	364
212	822	254	391	296	350	338	350
214	107	256	345	298	366	340	332
216	128	258	306	300	377	342	308
218	161	260	273	302	386	344	284
220	194	262	244	304	393	346	263
222	224	264	221	306	400	348	248
224	252	266	205	308	407	350	233
226	263	268	196	310	413	352	214
228	271	270	192	312	415	354	195
230	262	272	191	314	413	356	176
232	239	274	194	316	409	358	157
234	217	276	200	318	406	360	138
236	186	278	211	320	406	362	123
238	155	280	223	322	406	364	117
240	124	282	235	324	405		

Note:

Burkholder and Orlando [14]



(Table: 10-6, Note: 10-6, Evaluated: 10-6)

Absorption Cross Sections: Scheffler et al. [98] measured the room temperature absorption spectrum of nitryl bromide, BrNO₂, over the wavelength range 185 – 530 nm. The spectrum consists of several overlapping electronic transitions with a strong band in the actinic region. The recommended absorption cross sections in Table 4G-14 are taken from Scheffler et al. [98] between 185 and 430 nm while values at $\lambda > 430$ nm are obtained from a log-linear fit of the data reported by Scheffler et al. Under sunlit conditions, UV photolysis is expected to be a significant atmospheric loss process for BrNO₂.

Photolysis Quantum Yield and Product Studies: No quantum yield or product studies are currently available. By analogy with ClNO₂, the most likely photolysis products are expected to be Br + NO₂.

Table 4G-14. Absorption Cross Sections of BrNO₂ at 298 K

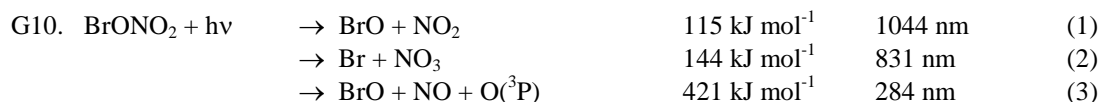
λ (nm)	$10^{20} \sigma$ (cm ²)	λ (nm)	$10^{20} \sigma$ (cm ²)	λ (nm)	$10^{20} \sigma$ (cm ²)
185	2048	310	11	435	8.03
190	3601	315	11	440	7.19
195	5013	320	10	445	6.44
200	5386	325	12	450	5.77
205	4499	330	13	455	5.17
210	2521	335	14	460	4.63
215	1170	340	16	465	4.15
220	554	345	15	470	3.71
225	373	350	16	475	3.33
230	343	355	16	480	2.98
235	362	360	18	485	2.67
240	387	365	19	490	2.39
245	390	370	17	495	2.14
250	363	375	18	500	1.917
255	310	380	17	505	1.72
260	251	385	17	510	1.54
265	197	390	16	515	1.38
270	154	395	15	520	1.23
275	116	400	14	525	1.10
280	88	405	14	530	0.99
285	63	410	13	540	0.79
290	44	415	12	550	0.64
295	30	420	11	560	0.51
300	20	425	10	570	0.41
305	15	430	9	580	0.33

Note:

185 – 430 nm: Scheffler et al. [98]

435 – 530 nm: log-linear fit to data reported in Scheffler et al. [98]

540 – 580 nm: log-linear extrapolation



(Recommendation: 06-2, Note: 10-6, Evaluated: 10-6)

Absorption Cross Sections: The UV/vis absorption spectrum of bromine nitrate, BrONO₂, has been measured at room temperature by Spencer and Rowland [104] (186 – 390 nm), Burkholder et al. [15] (200 – 500 nm), and Deters et al. [24] (210 – 500 nm). The absorption cross sections reported by Burkholder et al. [15] and Deters et al. [24] are nearly identical over the range of spectral overlap. The results of Spencer and Rowland [104] agree to within 10% with those of Burkholder et al. [15] and Deters et al. [24] except for the region between 315 and 350 nm where the Spencer data are higher by 10 to 20%.

The absorption spectrum temperature dependence has been measured by Burkholder et al. [15] (200 – 500 nm) at 220, 250, and 298 K and Deters et al. [24] (210 – 500 nm) at 230 and 298 K. The temperature dependence of the absorption cross sections is in general weak. Burkholder et al. [15] observed decreasing cross sections with decreasing temperature between 200 and 215 nm and between 230 and 500 nm and a slight increase between 215 and 230 nm. The reported ratio $\sigma(220 \text{ K})/\sigma(298 \text{ K})$ has values of ~0.8 to 1.03 between 200 and 235 nm, a minimum of 0.90 at 260 nm, nearly constant values of ~0.95 between 290 and 370 nm, a minimum of ~0.87 at 430 nm, two maxima of ~0.98 around 445 nm, and decreases to ~0.5 at 500 nm. The measurements of Deters et al. [24] show a similar behavior of $\sigma(230 \text{ K})/\sigma(298 \text{ K})$ vs. λ with all values below 1, i.e., a decrease of the cross sections with decreasing temperature is observed over the entire

spectrum. Burkholder et al. [15] parameterized the cross section temperature dependence using the expression

$$\sigma(\lambda, T) = \sigma(\lambda, 296 \text{ K}) [1 + A_1(\lambda)(T - 296) + A_2(\lambda)(T - 296)^2]$$

The recommended absorption cross sections and temperature coefficients in Table 4G-15 are taken from Burkholder et al. [15].

Photolysis Quantum Yield and Product Studies: Photodissociation quantum yields have been measured for photolysis wavelengths between 248 and 355 nm as summarized in Table 4G-16. The quantum yields for NO₃ production were measured by Harwood et al. [42] to be $\Phi(\text{NO}_3) = 0.28 \pm 0.09$ at 248 nm, 1.01 ± 0.35 at 305 nm and 0.92 ± 0.43 at 352.5 nm. The quantum yields for BrO and Br were also estimated at 248 nm to be $\Phi(\text{BrO}) \approx 0.5$ and $\Phi(\text{Br}) \approx 0.5$. Soller et al. [103] investigated the production of Br, O(³P) and BrO from the photolysis of BrONO₂ in the wavelength range 248 – 355 nm. The quantum yield for the Br atom are 0.35 ± 0.08 , 0.65 ± 0.14 , $>0.62 \pm 0.11$, and 0.77 ± 0.19 at 248, 266, 308 and 355 nm, respectively. The values for the O(³P) atom quantum yields are 0.66 ± 0.15 , 0.18 ± 0.04 , $<0.13 \pm 0.03$, and <0.02 at 248, 266, 308 and 355 nm, respectively. The measured quantum yields for BrO are 0.37 ± 0.12 at 266 nm and 0.23 ± 0.08 at 355 nm. The recommendation for wavelengths >300 nm is for a total quantum yield Φ_{BrONO_2} of unity with $\Phi_{\text{Br}+\text{NO}_3} = 0.85$ and $\Phi_{\text{BrO}+\text{NO}_2} = 0.15$. There is no recommendation given for wavelengths <300 nm.

Table 4G-15. Absorption Cross Sections of BrONO₂ at 296 K and Temperature Coefficients

λ (nm)	$10^{20} \sigma$ (cm ²)	$10^3 A_1$ (K ⁻¹)	$10^6 A_2$ (K ⁻²)	λ (nm)	$10^{20} \sigma$ (cm ²)	$10^3 A_1$ (K ⁻¹)	$10^6 A_2$ (K ⁻²)	λ (nm)	$10^{20} \sigma$ (cm ²)	$10^3 A_1$ (K ⁻¹)	$10^6 A_2$ (K ⁻²)
200	680	0.852	-26.0	302	17.5	0.781	0.784	404	2.04	1.91	3.64
202	616	0.608	-26.1	304	16.6	0.870	1.88	406	1.95	1.86	2.63
204	552	0.308	-26.2	306	15.8	0.872	1.62	408	1.88	1.78	1.52
206	488	0.138	-23.7	308	15.0	0.772	-0.229	410	1.81	1.70	0.316
208	425	0.158	-17.5	310	14.2	0.660	-2.28	412	1.75	1.59	-0.981
210	361	0.184	-9.09	312	13.5	0.652	-1.95	414	1.69	1.49	-2.37
212	334	0.401	-2.61	314	12.8	0.643	-1.58	416	1.63	1.40	-2.60
214	307	0.657	5.03	316	12.1	0.652	-1.42	418	1.56	1.35	-1.54
216	286	0.882	11.2	318	11.6	0.684	-1.48	420	1.50	1.29	-0.381
218	272	1.05	15.3	320	11.0	0.719	-1.56	422	1.45	1.00	-2.34
220	258	1.24	19.7	322	10.5	0.719	-1.06	424	1.40	0.694	-4.43
222	247	1.19	19.7	324	10.1	0.720	-0.508	426	1.36	0.599	-4.31
224	236	1.12	19.6	326	9.64	0.743	0.087	428	1.33	0.734	-1.78
226	226	1.14	20.3	328	9.29	0.791	0.722	430	1.30	0.877	0.880
228	215	1.26	21.8	330	8.94	0.843	1.41	432	1.26	0.747	0.484
230	205	1.40	23.4	332	8.65	0.825	1.33	434	1.22	0.609	0.0625
232	193	1.40	23.1	334	8.36	0.806	1.25	436	1.18	0.519	0.0968
234	180	1.41	22.8	336	8.10	0.800	1.30	438	1.15	0.484	0.632
236	167	1.47	22.8	338	7.87	0.809	1.49	440	1.11	0.447	1.20
238	153	1.59	23.4	340	7.64	0.818	1.70	442	1.08	0.384	-0.388
240	139	1.73	24.0	342	7.45	0.898	2.52	444	1.05	0.318	-2.06
242	126	1.65	20.9	344	7.26	0.982	3.38	446	1.02	0.335	-1.82
244	113	1.56	17.2	346	7.07	0.991	3.48	448	0.974	0.446	0.568
246	101	1.62	15.5	348	6.86	0.918	2.75	450	0.930	0.567	3.18
248	90.0	1.88	16.8	350	6.66	0.842	1.98	452	0.892	0.739	4.40
250	79.5	2.22	18.5	352	6.48	0.942	2.83	454	0.853	0.926	5.74
252	71.7	2.24	17.4	354	6.30	1.05	3.74	456	0.816	1.09	6.94
254	64.0	2.27	16.0	356	6.11	1.08	4.10	458	0.779	1.23	8.00
256	57.5	2.30	14.9	358	5.90	1.03	3.87	460	0.743	1.39	9.16
258	52.3	2.32	14.6	360	5.69	0.969	3.62	462	0.707	1.32	5.99
260	47.1	2.36	14.1	362	5.48	1.02	4.08	464	0.670	1.24	2.46
262	43.8	2.38	14.4	364	5.27	1.08	4.57	466	0.635	1.39	1.87
264	40.5	2.40	14.7	366	5.07	1.13	5.16	468	0.600	1.83	4.74
266	37.9	2.38	14.6	368	4.86	1.18	5.87	470	0.566	2.32	7.95
268	35.8	2.31	14.0	370	4.66	1.24	6.63	472	0.524	2.72	10.9
270	33.8	2.22	13.4	372	4.46	1.29	6.93	474	0.482	3.18	14.4
272	32.5	2.19	13.6	374	4.26	1.35	7.25	476	0.447	3.75	17.9
274	31.2	2.16	13.8	376	4.07	1.44	7.74	478	0.418	4.45	21.4
276	30.0	2.10	13.7	378	3.88	1.54	8.41	480	0.390	5.24	25.4
278	28.9	2.01	13.2	380	3.69	1.66	9.15	482	0.344	5.92	36.6
280	27.9	1.91	12.7	382	3.51	1.60	8.15	484	0.298	6.80	51.2
282	27.0	1.85	12.5	384	3.32	1.54	7.04	486	0.269	7.91	61.2
284	26.1	1.78	12.3	386	3.16	1.62	7.02	488	0.256	9.11	63.1
286	25.1	1.66	11.2	388	3.02	1.85	8.28	490	0.243	10.4	65.2
288	24.2	1.46	9.01	390	2.88	2.11	9.67	492	0.231	11.7	70.6
290	23.2	1.24	6.66	392	2.74	2.16	9.74	494	0.220	13.2	76.5
292	22.2	1.01	4.11	394	2.60	2.22	9.83	496	0.198	14.5	85.0
294	21.2	0.758	1.31	396	2.47	2.21	9.05	498	0.167	16.0	98.6
296	20.2	0.636	-0.188	398	2.36	2.10	7.28	500	0.135	18.2	119
298	19.3	0.666	-0.197	400	2.25	1.98	5.34				
300	18.4	0.699	-0.207	402	2.15	1.95	4.53				

Note:

Burkholder et al. [15], $\sigma(\lambda, T) = \sigma(\lambda, 296 \text{ K}) [1 + A_1 (T - 296) + A_2 (T - 296)^2]$

Table 4G-16. BrONO₂ Photolysis Quantum Yields

Wavelength (nm)	$\Phi(\text{NO}_3)$	$\Phi(\text{Br})$	$\Phi(\text{BrO})$	$\Phi(\text{O}(^3\text{P}))$
248	0.28 ± 0.09^a	$\approx 0.5^a$ 0.35 ± 0.08^b	$\approx 0.5^a$	0.66 ± 0.15^b
266	—	0.65 ± 0.14^b	0.37 ± 0.12^b	0.18 ± 0.04^b
305	1.01 ± 0.35^a	—	—	—
308	—	$>0.62 \pm 0.11^b$	—	$<0.13 \pm 0.03^b$
352.5	0.92 ± 0.43^a	—	—	—
355	—	0.77 ± 0.19^b	0.23 ± 0.08^b	$<0.02^b$

Note:

^aHarwood et al. [42]

^bSoller et al. [103]



(Recommendation: 06-2, Note: 10-6, Evaluated: 10-6)

Absorption Cross Sections: The UV absorption spectrum of bromine chloride, BrCl, has been measured at room temperature by Gray and Style [41] (240 – 313 nm and 546 nm), Jost [54] (486 – 548 nm), Seery and Britton [101] (220 – 510 nm), Maric et al. [67] (200 – 600 nm), Hubinger and Nee [47] (190 – 560 nm), and Tellinghuisen [110] (200 – 600 nm). The spectrum exhibits an absorption band between 190 and 290 nm with a maximum at 230 nm ($\sigma \approx (6.0\text{--}7.2) \times 10^{-20} \text{ cm}^2 \text{ molecule}^{-1}$) and a stronger band between 290 and 600 nm with the maximum at 375 nm ($\sigma \approx (3.9\text{--}4.1) \times 10^{-19} \text{ cm}^2 \text{ molecule}^{-1}$) and a shoulder near 470 nm. There is good agreement between the cross section results of the studies except for the values at 289 and 297 nm reported by Gray and Style [41] which are smaller by a factor of ~2.5 than the rest of the results. The agreement is within 20% for the short wavelength band around 230 nm between the results of Seery and Britton [101], Maric et al. [67], and Hubinger and Nee [47], where Seery and Britton [101] report the highest and Hubinger and Nee [47] the lowest values. There is very good agreement, to within ~5-15%, for the stronger band around 375 nm where Seery and Britton [101] and Tellinghuisen [110] report the highest and Hubinger and Nee [47] the lowest cross sections. The discrepancies are larger, up to 50%, in the region of the absorption minimum around 290 nm where Seery and Britton [101] and Hubinger and Nee [47] report the highest cross sections and Tellinghuisen [110] the lowest. Excellent agreement is observed in the long wavelength tail above 450 nm between the data of Maric et al. [67] and Tellinghuisen [110] whereas those from Hubinger and Nee [47] are 50% or more larger and those from Jost [54] are lower by ~20–40%. Maric et al. [67] fit their 0.2 nm resolution data to a three-band semi-logarithmic Gaussian distribution function and derived an expression

$$\begin{aligned} \sigma(298 \text{ K}) = & 6.52 \times 10^{-20} \times \exp\{-54.1 [\ln(227.6/\lambda)]^2\} \\ & + 3.86 \times 10^{-19} \times \exp\{-97.6 [\ln(372.5/\lambda)]^2\} \\ & + 9.99 \times 10^{-20} \times \exp\{-66.9 [\ln(442.4/\lambda)]^2\} \end{aligned}$$

where λ is in nm and σ is in $\text{cm}^2 \text{ molecule}^{-1}$ that allows the calculation of a BrCl absorption spectrum for the wavelength region 200 – 600 nm. The recommended absorption cross sections calculated using this expression are listed in Table 4G-17.

The temperature dependence of the BrCl absorption spectrum has not been measured. A semi-empirical expression based on the theory of Sulzer and Wieland [105], which describes the temperature and wavelength dependence of an absorption spectrum, was derived by Maric et al. [67] to be

$$\begin{aligned} \sigma(T, \lambda) = & 7.34 \times 10^{-20} \times \tanh^{0.5} \times \exp\{-68.6 \times \tanh \times [\ln(227.6/\lambda)]^2\} \\ & + 4.35 \times 10^{-19} \times \tanh^{0.5} \times \exp\{-123.6 \times \tanh \times [\ln(372.5/\lambda)]^2\} \\ & + 1.12 \times 10^{-19} \times \tanh^{0.5} \times \exp\{-84.8 \times \tanh \times [\ln(442.4/\lambda)]^2\} \end{aligned}$$

where λ is the wavelength in vacuum (200 – 600 nm), $\tanh = \tanh(hc\omega_e/2KT) = \tanh(318.8/T)$ (with $\omega_e = 443.1 \text{ cm}^{-1}$), and T the temperature (195 – 300 K).

Photolysis Quantum Yield and Product Studies: No quantum yield data are available but is expected that BrCl photodissociates with unity quantum yield.

Table 4G-17. Absorption Cross Sections of BrCl at 298 K

λ (nm)	$10^{20} \sigma$ (cm ²)	λ (nm)	$10^{20} \sigma$ (cm ²)	λ (nm)	$10^{20} \sigma$ (cm ²)	λ (nm)	$10^{20} \sigma$ (cm ²)
200	2.64	305	0.845	410	22.51	515	2.13
205	3.61	310	1.47	415	19.95	520	1.74
210	4.59	315	2.51	420	17.80	525	1.41
215	5.47	320	4.08	425	16.04	530	1.13
220	6.13	325	6.30	430	14.63	535	0.892
225	6.47	330	9.25	435	13.49	540	0.700
230	6.48	335	12.92	440	12.55	545	0.544
235	6.17	340	17.21	445	11.73	550	0.419
240	5.60	345	21.90	450	10.98	555	0.320
245	4.86	350	26.68	455	10.25	560	0.243
250	4.05	355	31.18	460	9.52	565	0.182
255	3.24	360	35.03	465	8.78	570	0.136
260	2.50	365	37.91	470	8.02	575	0.101
265	1.86	370	39.61	475	7.24	580	0.0739
270	1.35	375	40.04	480	6.47	585	0.0539
275	0.945	380	39.26	485	5.72	590	0.0390
280	0.653	385	37.45	490	4.99	595	0.0281
285	0.458	390	34.87	495	4.31	600	0.0200
290	0.357	395	31.82	500	3.68		
295	0.360	400	28.59	505	3.10		
300	0.504	405	25.43	510	2.59		

Note:

Maric et al. [67], calculated using the expression given in the text

G12. BrOCl + hv → Products

(Recommendation: 06-2, Note: 10-6, Evaluated: 10-6)

Absorption Cross Sections: Absorption spectrum of bromochloromonoxy, BrOCl, has been measured at room temperature over the wavelength range 230 – 390 nm by Burkholder et al. [13]. Their results are recommended and given in Table 4G-18.

Photolysis Quantum Yield and Product Studies: No studies are available.

Table 4G-18. Absorption Cross Sections of BrOCl at 298 K

λ (nm)	$10^{20} \sigma$ (cm ²)	λ (nm)	$10^{20} \sigma$ (cm ²)	λ (nm)	$10^{20} \sigma$ (cm ²)	λ (nm)	$10^{20} \sigma$ (cm ²)
230	16.8	272	200	314	55.8	338	46.7
232	15.4	274	199	316	56.6	358	22.5
234	15.2	276	191	318	57.2	360	20.2
236	15.5	278	179	320	57.4	362	18.1
238	16.6	280	165	322	57.3	364	16.1
240	18.6	282	149	324	56.9	366	14.2
242	21.7	284	132	326	56.1	368	12.3
244	26.1	286	115	328	55.1	370	10.6
246	31.6	288	100	330	53.8	372	8.66
248	39.1	290	87.2	332	52.3	374	7.34
250	48.1	292	76.3	334	50.6	376	6.12
252	59.9	294	67.9	336	48.7	378	5.01
254	73.8	296	61.6	340	44.5	380	4.00
256	89.4	298	57.0	342	42.3	382	3.10
258	107	300	54.0	344	39.9	384	2.30
260	126	302	52.4	346	37.3	386	1.62
262	145	304	52.1	348	34.7	388	1.03
264	163	306	52.3	350	32.4	390	0.55
266	179	308	53.0	352	29.8		
268	192	310	53.9	354	27.2		
270	198	312	54.7	356	24.8		

Note:

Burkholder et al. [13]



(Recommendation: 02-25, Note: 10-6, Evaluated: 10-6)

Absorption Cross Sections: The UV absorption spectrum of methyl bromide, CH₃Br, has been measured at room temperature by Davidson [22] (205 – 270 nm), Gordus and Bernstein [39] (204 – 260 nm), Robbins [92] (174 – 270 nm), Uthman et al. [113] (200 – 260 nm), Molina et al. [72] (190 – 290 nm), Felps et al. [28] (201.6 nm), Man et al. [66] (180 – 264 nm), and over the temperature range 210 – 295 K by Gillotay and Simon [33] (180 – 280 nm). At wavelengths >180 nm and <270 nm, the room temperature values of Gordus and Bernstein [39], Robbins [92], Uthman et al. [113], Molina et al. [72], Gillotay and Simon [33], and the values of Davidson [22] at wavelengths >210 nm are in very good agreement, to within 10% and within 2% at the absorption maximum ~201 nm. The value from Felps et al. [28] at 202 nm is lower by ~10% than the other studies. The cross section data of Man et al. [66], reported graphically, are lower by 20–30% over the entire band in comparison with the other data sets. The recommended absorption cross sections in Table 4G-19 are the values from Robbins [92] for the range 174 – 178 nm, the mean of the values reported by Gillotay and Simon [33] and Robbins [92] for the range 180 – 188 nm, the mean of the values reported by Gillotay and Simon [33], Uthman et al. [113], and Robbins [92] for the range 190 – 198 nm, the mean of the values reported by Gillotay and Simon [33], Molina et al. [72], Uthman et al. [113], and Robbins [92] for the range 200 – 260 nm, the mean of the values reported by Gillotay and Simon [33], Molina et al. [72], and Robbins [92] for the range 262 – 268 nm; the mean of the values reported by Gillotay and Simon [33] and Molina et al. [72] for the range 270 – 280 nm, and the data from Molina et al. [72] for the range 285 – 290 nm.

Gillotay and Simon [33] report a slight temperature dependence in the absorption cross sections for wavelengths >220 nm where the values decrease with decreasing temperature. Gillotay and Simon [33] parameterized the cross sections and the temperature dependence using an empirical polynomial expansion

$$\log_{10} \sigma(\lambda, T) = \sum A_n \lambda^n + (T - 273) \times \sum B_n \lambda^n$$

and reported calculated values for T = 210, 230, 250, 270, and 295 K. The A_n and B_n parameters, which are valid for the temperature range 210 – 300 K and wavelength range 200 – 280 nm are given below.

$$\begin{array}{ll} A_0 = 46.520 & B_0 = 9.3408 \times 10^{-1} \\ A_1 = -1.4580 & B_1 = -1.6887 \times 10^{-2} \\ A_2 = 1.1469 \times 10^{-2} & B_2 = 1.1487 \times 10^{-4} \\ A_3 = -3.7627 \times 10^{-5} & B_3 = -3.4881 \times 10^{-7} \\ A_4 = 4.3264 \times 10^{-8} & B_4 = 3.9945 \times 10^{-10} \end{array}$$

Photolysis Quantum Yield and Product Studies: Quantum yields for Br and H atom formation in the photodissociation of CH_3Br were measured at 298 K by Talukdar et al. [109]. The quantum yields for Br atom formation were found to be close to unity, $\Phi(\text{Br}) = 1.05 \pm 0.11$, 1.10 ± 0.20 , and 1.01 ± 0.16 at 193, 222, and 248 nm, respectively. The quantum yield for H atom formation in the photolysis at 193 nm was measured to be $\Phi(\text{H}) = 0.002 \pm 0.001$, whereas H atoms could not be detected in the photolysis at 222 and 248 nm. Broadband flash photolysis of CH_3Br produced $\text{Br}^*(^2\text{P}_{1/2})$ atoms with a quantum yield $\Phi(\text{Br}^*) = 0.15 \pm 0.12$ as reported by Ebenstein et al. [26].

Table 4G-19. Absorption Cross Sections of CH_3Br at 296 K

λ (nm)	$10^{20}\sigma$ (cm^2)	λ (nm)	$10^{20}\sigma$ (cm^2)	λ (nm)	$10^{20}\sigma$ (cm^2)
174	533	212	59.9	250	0.921
176	1010	214	54.2	252	0.683
178	1280	216	47.9	254	0.484
180	44.6	218	42.3	256	0.340
182	19.8	220	36.6	258	0.240
184	21.0	222	31.1	260	0.162
186	27.8	224	26.6	262	0.115
188	35.2	226	22.2	264	0.0795
190	44.2	228	18.1	266	0.0551
192	53.8	230	14.7	268	0.0356
194	62.6	232	11.9	270	0.0246
196	69.7	234	9.41	272	0.0172
198	76.1	236	7.38	274	0.0114
200	79.0	238	5.73	276	0.00808
202	79.2	240	4.32	278	0.00553
204	78.0	242	3.27	280	0.00382
206	75.2	244	2.37	285	0.00110
208	70.4	246	1.81	290	0.00030
210	65.5	248	1.31		

Note:

174 – 178 nm: Robbins [92]

180 – 188 nm: mean of data from Gillotay and Simon [33] and Robbins [92]

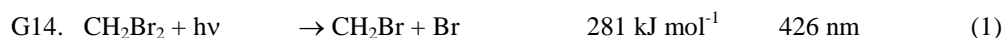
190 – 198 nm: mean of data from Gillotay and Simon [33], Uthman et al. [113], and Robbins [92]

200 – 260 nm: mean of data from Gillotay and Simon [33], Molina et al. [72], Uthman et al. [113] and Robbins [92],

262 – 268 nm: mean of data from Gillotay and Simon [33], Molina et al. [72], and Robbins [92]

270 – 280 nm: mean of Gillotay and Simon [33] and Molina et al. [72]

285 – 290 nm: Molina et al. [72]



(Recommendation: 06-2, Note: 10-6, Evaluated: 10-6)

Absorption Cross Sections: The UV absorption spectrum of dibromomethane, CH_2Br_2 , has been measured at room temperature by Molina et al. [72] (200 – 300 nm), Gillotay et al. [36], [35] (174 – 290 nm), and Mössinger et al. [74] (215 – 300 nm). The absorption cross sections are in good agreement in the range 200 – 255 nm, to within 10%, and at 275 nm there within 30%. The recommended absorption cross sections in

Table 4G-20 are the values from Gillotay et al. [36], [35] in the region 174 – 198 nm, the mean of the values reported by Molina et al. [72] and Gillotay et al. [36], [35] for the range 200 – 215 nm, the mean of the values reported by the three groups for the range 220 – 290 nm, and values from Mössinger et al. [74] for the range 295 – 300 nm.

The absorption spectrum temperature dependence has been measured by Gillotay et al. [36], [35] (174 – 290 nm) over the temperature range 210 – 295 K and Mössinger et al. [74] (215 – 300 nm) over the range 250 – 348 K. The absorption cross sections decrease at wavelength > ~235 nm and increase between 235 and 207 nm with decreasing temperature. At shorter wavelengths, Gillotay et al. [35, 36] report a slight increase in the cross sections in the range 175 – 189 nm and a slight decrease around the maximum near 200 nm. Gillotay et al. [35, 36] parameterized the cross sections and the temperature dependence using an empirical polynomial expansion

$$\log_{10} \sigma(\lambda, T) = \sum A_n \lambda^n + (T - 273) \times \sum B_n \lambda^n$$

and report calculated values for T = 210, 230, 250, 270, and 295 K. The A_n and B_n parameters, which are valid for the wavelength range 210 – 290 nm and temperature range 210 – 300 K are given below.

$$\begin{array}{ll} A_0 = -70.211776 & B_0 = 2.899280 \\ A_1 = 1.940326 \times 10^{-1} & B_1 = -4.327724 \times 10^{-2} \\ A_2 = 2.726152 \times 10^{-3} & B_2 = 2.391599 \times 10^{-4} \\ A_3 = -1.695472 \times 10^{-5} & B_3 = -5.807506 \times 10^{-7} \\ A_4 = 2.500066 \times 10^{-8} & B_4 = 5.244883 \times 10^{-10} \end{array}$$

Mössinger et al. [74] parameterized their cross section data using the expression

$$\ln \sigma(\lambda, T) = \ln \sigma(\lambda, 298 \text{ K}) + B(\lambda) (T - 298)$$

for the ranges 215 – 300 nm and 250 – 348 K. The parameterizations given by Gillotay et al. [35, 36] and Mössinger et al. [74] yield cross sections that agree at 250 K to within 5% in the range 215 – 265 nm and to within 10% in the range 270 – 285 nm. The $B(\lambda)$ coefficients from Mössinger et al. [74] are given in Table 4G-20 and recommended for use in model calculations.

Photolysis Quantum Yield and Product Studies: There are no quantum yield measurements but it is expected that photolysis will rupture the C-Br bond with unity quantum yield.

Table 4G-20. Absorption Cross Sections of CH₂Br₂ at 298 K

λ (nm)	$10^{20} \sigma$ (cm ²)	λ (nm)	$10^{20} \sigma$ (cm ²)	$10^3 B$ (K ⁻¹)	λ (nm)	$10^{20} \sigma$ (cm ²)	$10^3 B$ (K ⁻¹)
174	1170.9	198	226.0		255	14.10	3.91
176	662.4	200	225.6		260	6.607	5.16
178	377.2	205	215.3		265	3.037	6.33
180	241.0	210	234.5		270	1.347	7.75
182	178.4	215	263.2	-2.02	275	0.590	8.74
184	154.4	220	272.0	-1.79	280	0.255	11.6
186	153.5	225	247.4	-1.50	285	0.114	13.8
188	166.1	230	195.8	-0.96	290	0.0499	15.3
190	187.0	235	138.9	-0.04	295	0.0210	16.5
192	209.3	240	88.60	0.71	300	0.0090	21.9
194	222.5	245	51.90	1.80			
196	228.3	250	28.03	2.70			

Note:

Absorption cross sections (σ):

174 – 198 nm: Gillotay et al. [36], [35]

200 – 210 nm: mean of data from Molina et al. [72] and Gillotay et al. [36], [35]

215 – 290 nm: mean of data from Molina et al [72], Gillotay et al. [36], [35], and Mössinger et al. [74]

295 – 300 nm: Mössinger et al. [74]

Temperature dependence (B):

Mössinger et al. [74]



(Recommendation: 06-2, Note: 10-6, Evaluated: 10-6)

Absorption Cross Sections: The UV absorption spectrum of tribromomethane (bromoform), CHBr_3 , has been measured over the temperature range 240 – 295 K by Gillotay et al. [32] (170 – 310 nm) and over the range 256 – 296 K by Moortgat et al. [73] (286 – 362 nm). The agreement in the cross sections in the overlapping wavelength region is excellent. The recommended cross sections in Table 4G-21 are the values from Gillotay et al. [32] for the range 170 – 284 nm, the mean of the values reported by Gillotay et al. [32] and Moortgat et al. [73] for the range 286 – 310 nm; and the values of Moortgat et al. [73] for the range 286 – 362 nm.

The absorption cross sections increase around the three absorption maxima in the ranges 178 – 189 nm, 194 – 208 nm, and 208 – 234 nm, and decrease at wavelengths <179 nm, over the range 189 – 194 nm, and >235 nm with decreasing temperature. Gillotay et al. [32] parameterized the cross sections and the temperature dependence using an empirical polynomial expansion

$$\log_{10}(\sigma(\lambda, T)) = \sum A_n \lambda^n + (T - 273) \times \sum B_n \lambda^n$$

and report calculated values for $T = 210, 230, 250, 270$, and 295 K . The A_n and B_n parameters, which are valid for the wavelength range 240 – 310 nm and temperature range 210 – 300 K are given below.

$A_0 = -110.2782$	$B_0 = -1.5312 \times 10^{-1}$
$A_1 = 1.0281$	$B_1 = 1.6109 \times 10^{-3}$
$A_2 = -3.6626 \times 10^{-3}$	$B_2 = -5.8075 \times 10^{-6}$
$A_3 = 4.1226 \times 10^{-6}$	$B_3 = 7.2893 \times 10^{-9}$

Moortgat et al. [73] parameterized their data using the expression

$$\sigma(\lambda, T) = \exp \{ (0.06183 - 0.000241 \lambda) (273 - T) - (2.376 + 0.14757 \lambda) \}$$

which is valid for the wavelength range 290 – 340 nm and temperature range 210 – 300 K.

At wavelengths >290 nm, the CHBr_3 cross sections are relatively small. The presence of impurities as well as optical artifacts arising from adsorption of CHBr_3 on the cell windows complicated the measurements.

Photolysis Quantum Yield and Product Studies: The quantum yield for the formation of Br atoms were determined by Bayes et al. [6] between 266 and 324 nm. In the wavelength range 303 – 306 nm, the Br atom quantum yield is unity within experimental error. At longer wavelengths, the quantum yields decreases to 0.76 at 324 nm. Bayes et al. [6], however, claim that the lower than unity quantum yield is due to systematic and random errors and/or incorrect absorption cross sections. Support for a unity quantum yield at $\lambda > 300 \text{ nm}$ comes from theoretical calculations by Peterson and Francisco [86]. At 266 nm, the Br atom quantum yield is 0.76 ± 0.03 , indicating that another photodissociation channel becomes important. Xu et al. [122] measured atomic Br and molecular Br_2 by TOF mass spectrometry from bromoform photolysis at 234 and 267 nm and report evidence for the formation of $\text{CHBr} + \text{Br}_2$. Xu et al. [122] report $\Phi(\text{Br}) = 0.74$ and $\Phi(\text{Br}_2) = 0.26$ for 234 nm photolysis and $\Phi(\text{Br}) = 0.84$ and $\Phi(\text{Br}_2) = 0.16$ for 267 nm photolysis. A Br atom quantum yield of unity for wavelengths >300 nm is recommended.

Table 4G-21. Absorption Cross Sections of CHBr_3 at 296 K

λ (nm)	$10^{20} \sigma$ (cm^2)	λ (nm)	$10^{20} \sigma$ (cm^2)	λ (nm)	$10^{20} \sigma$ (cm^2)
170	1603.8	236	323.9	302	0.534
172	1173.2	238	294.7	304	0.397
174	969.6	240	272.8	306	0.297
176	872.0	242	253.3	308	0.222
178	857.6	244	233.7	310	0.165
180	831.3	246	214.4	312	0.127
182	770.3	248	193.9	314	0.0952
184	683.3	250	174.1	316	0.0712
186	570.4	252	157.7	318	0.0529
188	470.8	254	136.1	320	0.0390
190	399.1	256	116.4	322	0.0289
192	360.2	258	98.6	324	0.0215
194	351.3	260	82.8	326	0.0162
196	366.1	262	68.9	328	0.0121
198	393.6	264	56.9	330	0.00916
200	416.4	266	46.7	332	0.00690
202	433.6	268	38.0	334	0.00525
204	440.6	270	30.8	336	0.00396
206	445.0	272	24.8	338	0.00307
208	451.4	274	19.8	340	0.00240
210	468.5	276	15.8	342	0.00176
212	493.4	278	12.5	344	0.00135
214	524.2	280	9.88	346	0.00102
216	553.5	282	7.77	348	0.00080
218	573.9	284	6.10	350	0.00064
220	582.6	286	4.79	352	0.00054
222	578.0	288	3.74	354	0.00046
224	557.8	290	2.89	356	0.00032
226	527.2	292	2.20	358	0.00024
228	486.8	294	1.69	360	0.00017
230	441.2	296	1.28	362	0.00013
232	397.4	298	0.956		
234	361.8	300	0.719		

Note:

170 – 284 nm: Gillotay et al. [32]

286 – 310 nm: mean of data from Gillotay et al. [32] and Moortgat et al. [73]

312 – 362 nm: Moortgat et al. [73]

G16. $\text{CH}_2\text{BrCH}_2\text{Br} + h\nu \rightarrow \text{Products}$

(Recommendation: 02-25, Note: 10-6, Evaluated: 10-6)

Absorption Cross Sections: The absorption spectrum of 1,2-dibromoethane, $\text{CH}_2\text{BrCH}_2\text{Br}$, has been measured at room temperature over the wavelength range 190 – 270 nm by Uthman et al. [113]. Their data is recommended and listed in Table 4G-22.

Photolysis Quantum Yield and Product Studies: No studies are available.

Table 4G-22. Absorption Cross Sections of CH₂BrCH₂Br at 295 K

λ (nm)	$10^{20} \sigma$ (cm ²)	λ (nm)	$10^{20} \sigma$ (cm ²)	λ (nm)	$10^{20} \sigma$ (cm ²)
190	230	218	170	246	9.3
192	250	220	150	248	7.1
194	270	222	130	250	5.9
196	290	224	110	252	4.4
198	300	226	89	254	4.0
200	310	228	75	256	2.8
202	310	230	62	258	2.1
204	300	232	50	260	1.9
206	290	234	41	262	1.7
208	280	236	32	264	1.4
210	260	238	26	266	1.1
212	230	240	20	268	0.9
214	210	242	16	270	0.7
216	190	244	11		

Note:

190 – 270 nm: Uthman et al. [113]

G17. C₂H₅Br + hν → Products

(Recommendation: 02-25, Note: 10-6, Evaluated: 10-6)

Absorption Cross Sections: The absorption spectrum of bromoethane, C₂H₅Br, has been measured at 295 K over the wavelength range 200 – 260 nm by Zhang et al. [124]. In this wavelength range the spectrum shows part of an absorption band with a maximum cross section of $\sim 6 \times 10^{-19}$ cm² at ~ 200 nm. The recommended absorption cross sections in Table 4G-23 are estimated from a figure in Zhang et al. [124].

Photolysis Quantum Yield and Product Studies: No studies are available.

Table 4G-23. Absorption Cross Sections of C₂H₅Br at 295 K

λ (nm)	$10^{20} \sigma$ (cm ²)	λ (nm)	$10^{20} \sigma$ (cm ²)	λ (nm)	$10^{20} \sigma$ (cm ²)
200	61	225	24	250	1.1
205	60	230	15	255	0.5
210	54	235	8.3	260	0.2
215	45	240	4.3		
220	34	245	2.3		

Note:

Zhang et al. [124], values read from logarithmic plot

G18. COBr₂ + hν → Products

(Recommendation: 06-2, Note: 10-6, Evaluated: 10-6)

Absorption Cross Sections: The absorption spectrum of carbonyl dibromide (dibromophosgene), COBr₂, has been measured at room temperature over the wavelength range 235 – 353 nm by Libuda et al. [62] and Libuda [61]. The spectrum exhibits monotonically decreasing absorption cross sections with increasing wavelength over this range. The recommended absorption cross sections in Table 4G-24 are the averages over 1 nm intervals of the 0.6 nm resolution.

Photolysis Quantum Yield and Product Studies: No studies are available.

Table 4G-24. Absorption Cross Sections of COBr₂ at 298 K

λ (nm)	$10^{20} \sigma$ (cm ²)	λ (nm)	$10^{20} \sigma$ (cm ²)	λ (nm)	$10^{20} \sigma$ (cm ²)	λ (nm)	$10^{20} \sigma$ (cm ²)
240	58.3	263	20.9	286	4.50	309	0.301
241	56.5	264	19.9	287	4.13	310	0.260
242	55.3	265	18.8	288	3.73	311	0.230
243	54.1	266	17.9	289	3.38	312	0.204
244	52.3	267	17.0	290	3.09	313	0.178
245	50.6	268	16.1	291	2.81	314	0.159
246	48.8	269	15.2	292	2.58	315	0.143
247	47.1	270	14.4	293	2.32	316	0.127
248	45.2	271	13.6	294	2.07	317	0.114
249	43.2	272	12.8	295	1.82	318	0.0995
250	41.3	273	12.0	296	1.62	319	0.0892
251	39.5	274	11.4	297	1.42	320	0.0789
252	37.7	275	10.7	298	1.26	321	0.0694
253	35.7	276	9.98	299	1.11	322	0.0633
254	33.7	277	9.24	300	0.971	323	0.0578
255	32.0	278	8.56	301	0.858	324	0.0528
256	30.4	279	7.99	302	0.750	325	0.0499
257	28.9	280	7.44	303	0.661	326	0.0449
258	27.4	281	6.91	304	0.578	327	0.0397
259	26.0	282	6.35	305	0.501	328	0.0336
260	24.5	283	5.81	306	0.437	329	0.0296
261	23.3	284	5.34	307	0.386	330	0.0264
262	22.1	285	4.92	308	0.331	331	0.0229

Note:

Libuda et al. [62] and Libuda [61]

G19. COHBr + hv → Products

(Recommendation: 06-2, Note: 10-6, Evaluated: 10-6)

Absorption Cross Sections: The absorption spectrum of formyl bromide, COHBr, has been measured at room temperature over the wavelength range 240 – 340 nm by Libuda et al. [62] and Libuda [61]. The absorption spectrum exhibits a highly structured absorption band with a maximum near 268 nm. The recommended absorption cross sections in Table 4G-25 are averages over 1 nm intervals of the 0.6 nm resolution data.

Photolysis Quantum Yield and Product Studies: No studies are available.

Table 4G-25. Absorption Cross Sections of COHBr at 298 K

λ (nm)	$10^{20} \sigma$ (cm ²)	λ (nm)	$10^{20} \sigma$ (cm ²)	λ (nm)	$10^{20} \sigma$ (cm ²)	λ (nm)	$10^{20} \sigma$ (cm ²)
240	18.7	262	32.4	284	21.7	306	2.77
241	20.1	263	29.9	285	20.1	307	2.43
242	19.4	264	31.1	286	19.1	308	2.12
243	19.8	265	29.9	287	17.5	309	1.90
244	19.1	266	32.5	288	17.3	310	1.65
245	20.0	267	31.6	289	14.9	311	1.51
246	22.6	268	33.8	290	15.5	312	1.34
247	22.6	269	30.9	291	12.7	313	1.13
248	23.6	270	31.9	292	13.3	314	1.01
249	22.5	271	30.9	293	11.1	315	0.801
250	22.3	272	29.6	294	10.8	316	0.687
251	24.0	273	31.4	295	9.79	317	0.613
252	25.0	274	29.3	296	9.08	318	0.611
253	27.1	275	31.5	297	8.03	319	0.576
254	26.9	276	28.5	298	7.35	320	0.522
255	27.5	277	29.1	299	5.97	321	0.476
256	27.5	278	26.8	300	5.86	322	0.424
257	26.9	279	25.6	301	5.25	323	0.363
258	28.8	280	25.1	302	4.47	324	0.308
259	28.9	281	23.2	303	4.38		
260	31.9	282	23.8	304	3.53		
261	30.1	283	22.0	305	3.18		

Note:

Libuda [62]

G20. CH₂ClBr (Halon-1011) + hν → Products

(Recommendation: 02-25, Note: 10-6, Evaluated: 10-6)

Absorption Cross Sections: The UV absorption spectrum of chlorobromomethane (Halon-1011), CH₂ClBr, has been measured at room temperature by Cadman and Simons [17] (210 – 260 nm) and Orkin et al. [79] (187 – 290 nm). The cross section data from Cadman and Simons [17], reported in graphical form, are up to 20% less than the data from Orkin et al. [79]. The recommended absorption cross sections in Table 4G-26 are taken from Orkin et al. [79].

Photolysis Quantum Yield and Product Studies: Quantum yields for Br (²P_{3/2}) and Br* (²P_{1/2}) atom formation in the photolysis of CH₂ClBr at 193 and 242 nm and 248, 261.5, and 266.7 nm have been measured by Zou et al. [125] and McGivern et al. [68], respectively. The reported values are given here.

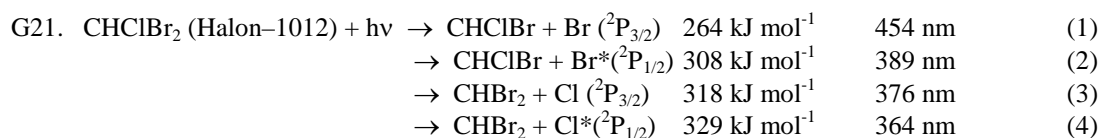
	193 nm	234 nm	248.5 nm	261.5 nm	266.7 nm
$\Phi(\text{Br } (^2\text{P}_{3/2}))$	0.82 ± 0.10	0.80 ± 0.10	0.86 ± 0.10	0.84 ± 0.10	0.91 ± 0.10
$\Phi(\text{Br}^* (^2\text{P}_{1/2}))$	0.18 ± 0.10	0.20 ± 0.10	0.14 ± 0.10	0.16 ± 0.10	0.09 ± 0.10

Table 4G-26. Absorption Cross Sections of CH₂ClBr at 295 K

λ (nm)	$10^{20} \sigma$ (cm ²)	λ (nm)	$10^{20} \sigma$ (cm ²)	λ (nm)	$10^{20} \sigma$ (cm ²)
187	151.1	222	57.4	258	1.45
188	126.4	224	50.5	260	1.09
190	104.6	226	44.1	262	0.807
192	100.5	228	38.2	264	0.596
194	104.7	230	32.8	266	0.440
196	111.8	232	28.0	268	0.322
198	119.4	234	23.6	270	0.235
200	124.7	236	19.7	272	0.170
202	127.1	238	16.3	274	0.123
204	126.3	240	13.4	276	0.089
206	122.5	242	10.8	278	0.064
208	116.3	244	8.73	280	0.046
210	108.4	246	6.94	282	0.033
212	99.6	248	5.46	284	0.024
214	90.5	250	4.24	286	0.0178
216	81.5	252	3.29	288	0.0129
218	72.9	254	2.52	290	0.0098
220	64.8	256	1.92		

Note:

Orkin et al. [79]



(Recommendation: 06-2, Note: 10-6, Evaluated: 10-6)

Absorption Cross Sections: The UV absorption spectrum of chlorodibromomethane (Halon-1012), CHClBr₂, has been measured at room temperature by Ibuki et al. [49] (106 – 200 nm) and Taketani et al. [106] (193.3 nm) and at 240, 261, and 296 K by Bilde et al. [8] (200 – 310 nm). Two absorption bands are apparent at wavelengths >200 nm with maxima near 206 nm and 240 nm. The cross sections at 240 K are approximately 10% greater than those at room temperature. In the long wavelength tail of the spectrum, the cross sections decrease with decreasing temperature, the room temperature cross section at 270 nm being ~15% greater than at 240 K. The recommended absorption cross sections in Table 4G-27 are from Bilde et al. [8] (reported at 1 nm intervals). Taketani et al. [106] reported a value of 304×10^{20} cm² molecule⁻¹ at 193.3 nm.

Photolysis Quantum Yield and Product Studies: Quantum yields for dissociation have been reported by Tzeng et al. [112] (193 and 248 nm), McGivern et al. [68] (248 – 268 nm), Zou et al. [125] (193 – 242 nm), Lee et al. [60] (234 nm), and Taketani et al. [106] (193.3 nm). In the range 248 – 262 nm, CHClBr₂ undergoes C-Br bond rupture exclusively, whereas in the range 193 – 242 nm it dissociates predominantly via C-Br bond rupture, with a minor contribution from C-Cl bond rupture. The relative quantum yield for ground state Br(²P_{3/2}) varies from 0.80 to 0.90 for photolysis in the range 193 to 267 nm.

Table 4G-27. Absorption Cross Sections of CHClBr_2 at 296 K

λ (nm)	$10^{20} \sigma$ (cm^2)	λ (nm)	$10^{20} \sigma$ (cm^2)	λ (nm)	$10^{20} \sigma$ (cm^2)
200	274.6	230	141.4	272	9.415
201	282.8	232	136.4	274	7.552
202	293.9	234	131.4	276	5.950
203	306.7	236	126.8	278	4.687
204	314.2	238	122.2	280	3.691
205	320.6	240	116.0	282	2.884
206	324.9	242	109.2	284	2.261
207	323.7	244	101.2	286	1.734
208	322.9	246	92.70	288	1.331
209	324.6	248	83.52	290	1.016
210	317.8	250	74.04	292	0.7907
211	306.2	252	64.83	294	0.6116
212	297.4	254	55.95	296	0.4583
214	279.4	256	47.67	298	0.3489
216	261.7	258	39.92	300	0.2692
218	234.9	260	33.35	302	0.2076
220	215.1	262	27.50	304	0.1588
222	199.1	264	22.50	306	0.1208
224	184.5	266	18.28	308	0.0945
226	165.3	268	14.78	310	0.0742
228	151.7	270	11.82		

Note:
Bilde et al. [8]

G22. CHCl_2Br (Halon-1021) + $h\nu \rightarrow$ Products

(Recommendation: 02-25, Note: 10-6, Evaluated: 10-6)

Absorption Cross Sections: The absorption spectrum of dichlorobromomethane (Halon-1021), CHCl_2Br , has been measured at room temperature by Ibuki [49] (106 – 200 nm), Cadman and Simons [17] (201 – 270 nm), Bilde et al. [8] (200 – 320 nm). Cadman and Simons [17], who reported their spectrum in graphical form, agree to within 15% with the room temperature cross section from Bilde et al. [8], however, the absorption maximum is shifted to lower wavelengths. The recommended absorption cross sections in Table 4G-28 are taken from Bilde et al. [8].

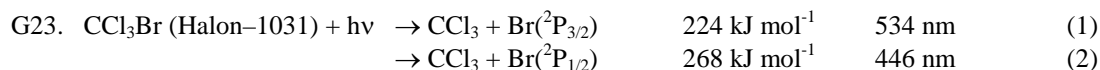
Bilde et al. [8] (200 – 320 nm) reported absorption spectrum measurements at 253, 273 and 298 K. A decrease of the absorption cross sections with decreasing temperature was observed over the entire spectrum. The cross section at 220 nm is ~6% lower at 253 K than at room temperature. A stronger temperature dependence was observed at longer wavelengths, the room temperature cross section at 320 nm being about four times larger than at 253 K.

Photolysis Quantum Yield and Product Studies: No studies are available.

Table 4G-28. Absorption Cross Sections of CHCl₃Br at 298 K

λ (nm)	$10^{20} \sigma$ (cm ²)	λ (nm)	$10^{20} \sigma$ (cm ²)	λ (nm)	$10^{20} \sigma$ (cm ²)
200	115.0	230	58.1	276	1.63
202	93.8	232	54.6	278	1.32
204	81.1	234	50.0	280	1.07
206	73.6	236	45.8	282	0.865
208	69.0	238	41.6	284	0.694
209	69.8	240	37.3	286	0.573
210	68.8	242	33.0	288	0.454
211	67.4	244	29.3	290	0.384
212	68.4	246	25.8	292	0.317
213	70.0	248	22.2	294	0.265
214	70.1	250	19.2	296	0.217
215	70.2	252	16.5	298	0.176
216	71.1	254	13.6	300	0.146
217	71.0	256	11.5	302	0.118
218	70.7	258	9.75	304	0.0962
219	71.3	260	8.19	306	0.0761
220	71.6	262	6.82	308	0.0617
221	70.6	264	5.61	310	0.0496
222	69.3	266	4.68	312	0.0395
223	68.7	268	3.74	314	0.0317
224	68.2	270	3.01	316	0.0259
226	65.2	272	2.48	318	0.0210
228	62.2	274	2.02	320	0.0171

Note:
Bilde et al. [8]



(Recommendation: 02-25, Note: 10-6, Evaluated: 10-6)

Absorption Cross Sections: The UV absorption spectrum of trichlorobromomethane (Halon-1031), CCl_3Br , has been measured at room temperature by Cadman and Simons [17] (207 – 305 nm), Sidebottom et al. [102] (365 nm), Roxlo and Mandl [96] (170 – 230 nm), Ibuki et al. [50] (105 – 198 nm), and Seccombe et al. [100] (50 – 200 nm). The absorption spectrum has a strong absorption band between 170 and 220 nm with the maximum near 185 nm and $\sigma \approx (1.1\text{--}1.4) \times 10^{-17} \text{ cm}^2 \text{ molecule}^{-1}$ with a shoulder in the range 220 – 305 nm. The recommended absorption cross sections in Table 4G-29 for the wavelength region 235 – 305 nm have been read at 5 nm intervals from a figure in the paper of Cadman and Simons [17] and the value for 365 nm was reported Sidebottom et al. [102].

Photolysis Quantum Yield and Product Studies: Product quantum yields were studied at 365 nm by Sidebottom et al. [102]. They report evidence that $\text{Br} + \text{CCl}_3$ are the primary products and the yields are pressure and temperature dependent. Quantum yields for $\text{Br}^*(^2\text{P}_{1/2})$ atom formation in the photolysis at 234 and 265 nm were reported to be 0.31 ± 0.01 and 0.68 ± 0.02 , respectively, by Jung et al. [55].

Table 4G-29. Absorption Cross Sections of CCl₃Br at 298 K

λ (nm)	$10^{20} \sigma$ (cm ²)	λ (nm)	$10^{20} \sigma$ (cm ²)
235	50	275	11
240	50	280	7.2
245	49	285	5.0
250	48	290	3.3
255	46	295	2.2
260	42	300	1.4
265	34	305	1.0
270	19	365	0.0077

Note:

235 – 305 nm: Cadman and Simons [17]

365 nm: Sidebottom et al. [102]

G24. CHF₂Br (Halon-1201) + hν → Products

(Recommendation: 02-25, Note: 10-6, Evaluated: 10-6)

Absorption Cross Sections: The UV absorption spectrum of difluorobromomethane (Halon-1201), CHF₂Br, has been measured at room temperature by Davidson [22] (207 – 255 nm), Talukdar et al. [107] (190 – 280 nm), Gillotay et al. [36] (166 – 267 nm), and Orkin and Kasimovskaya [78] (190 – 280 nm). Gillotay et al. [36] carried out measurements at 210 – 295 K over the wavelength range 166 – 267 nm and report smoothed calculated cross sections for T = 210, 230, 250, 270, and 295 K. The results of Davidson [22], Orkin and Kasimovskaya [78], and Gillotay et al. [36] are in excellent agreement at wavelengths <240 nm. The values from Gillotay et al. [36] are increasingly smaller (by up to about 40% at 260 nm) and those of Davidson [22] are smaller (by up to about 30% at 250 nm) than the values reported by Orkin and Kasimovskaya [78]. The results of Talukdar et al. [107], who report a spectrum in graphical form with extrapolated values out to 360 nm, appear to be in agreement with the results of Orkin and Kasimovskaya [78]. The recommended absorption cross sections in Table 4G-30 are the values from Gillotay et al. [36] at the centers of the 500 cm⁻¹ intervals between 168 and 188 nm and the values from Orkin and Kasimovskaya [78] in the region 190 – 280 nm.

An increase in the absorption cross sections around the absorption peak (168 – 215 nm) and a decrease at wavelengths >215 nm with decreasing temperature (295 – 210 K) was reported by Gillotay et al. [36].

Photolysis Quantum Yield and Product Studies: No studies are available.

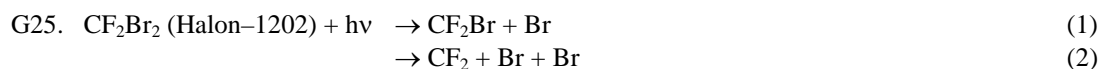
Table 4G-30. Absorption Cross Sections of CHF₂Br at 298 K

λ (nm)	$10^{20} \sigma$ (cm ²)	λ (nm)	$10^{20} \sigma$ (cm ²)	λ (nm)	$10^{20} \sigma$ (cm ²)
168.10	3.97	206	23.2	246	0.299
170.95	8.21	208	21.2	248	0.220
173.15	12.5	210	19.0	250	0.161
174.65	15.6	212	16.8	252	0.117
176.20	18.8	214	14.6	254	0.0849
177.80	21.9	216	12.6	256	0.0615
179.40	24.5	218	10.6	258	0.0444
181.00	26.6	220	8.85	260	0.0319
182.65	28.3	222	7.25	262	0.0230
184.35	29.6	224	5.88	264	0.0166
186.05	30.6	226	4.71	266	0.0121
187.80	31.4	228	3.73	268	0.0087
190	32.5	230	2.91	270	0.0063
192	32.4	232	2.24	272	0.0046
194	31.8	234	1.71	274	0.0034
196	31.0	236	1.30	276	0.0024
198	29.9	238	0.982	278	0.0018
200	28.6	240	0.735	280	0.0012
202	27.0	242	0.547		
204	25.2	244	0.405		

Note:

168 – 188 nm: Gillotay et al. [36]

190 – 280 nm: Orkin and Kasimovskaya [78]



(Recommendation: 06-2, Note: 10-6, Evaluated: 10-6)

Absorption Cross Sections: The UV absorption spectrum of difluorodibromomethane (Halon-1202), CF_2Br_2 , has been measured at room temperature by Davidson [22] (215 – 290 nm), Walton [118] (200 – 310 nm), Molina et al. [72] (190 – 340 nm), Orkin and Kasimovskaya [78] (190 – 320 nm), Gillotay and Simon [34] (170 – 304 nm), and Burkholder et al. [16] (190 – 320 nm). The room temperature cross section data, except those of Walton [118], are in good agreement, better than 10%, over the wavelength range 190 – 300 nm. At the absorption maximum near 226 nm, the data of Davidson [22] and Molina et al. [72] are the highest and lowest, respectively. At wavelengths >300 nm, the values from Orkin and Kasimovskaya [78] and Burkholder et al. [16] agree to within 15%, whereas those of Molina et al. [72] are larger with the difference increasing with increasing wavelength, up to $\sim 200\%$ at 320 nm (and larger by up to $\sim 660\%$ than the extrapolated values at 340 nm, see below). The recommended absorption cross sections in Table 4G-31 are the values from Gillotay and Simon [34] in the region 170 – 188 nm, the mean of the values reported by Gillotay and Simon [34], Orkin and Kasimovskaya [78], and Burkholder et al. [16] for the wavelength range 190 – 304 nm, and the mean of the values reported by Orkin and Kasimovskaya [78], and Burkholder et al. [16] for the range 306 – 320 nm. The recommendation for wavelengths in the range 322 – 340 nm was obtained from an extrapolation of the mean of the values from Orkin and Kasimovskaya [78] and Burkholder et al. [16], $\log \sigma(\lambda) = 1.85109 - 0.07755 \lambda$. Note that the cross section values measured by Molina et al. [72] are greater than the extrapolated values by $\sim 660\%$ at 340 nm.

The absorption spectrum in the far UV has been measured Doucet et al. [25] (60 – 220 nm) and Seccombe et al. [99] (55 – 175 nm).

The absorption spectrum temperature dependence was measured by Gillotay and Simon [34] (170 – 304 nm) over the range 210 – 295 K and Burkholder et al. [16] (190 – 320 nm) over the range. The absorption cross sections increase near the absorption peaks near 190 and 225 nm and decrease at wavelengths >240 nm and <177 nm with decreasing temperature. Gillotay and Simon [34] observed a systematic temperature behavior with an increase in the peak cross section at ~225 nm of $\sim 9 \times 10^{-20} \text{ cm}^2 \text{ molecule}^{-1}$ per 20 K decrease in

temperature. Burkholder et al. [16] observed a less pronounced temperature behavior below 250 K with the peak cross section at 210 K being 5% lower than that observed by Gillotay and Simon [34] (the cross sections at room temperature are nearly identical). Different empirical parameterizations for the temperature dependence of the absorption cross section were proposed. Gillotay and Simon [34] used a polynomial expansion

$$\log_{10} \sigma(\lambda, T) = \sum A_n \lambda^n + (T - 273) \times \sum B_n \lambda^n$$

and report calculated values for $T = 210, 230, 250, 270$, and 295 K. The A_n and B_n parameters, which are valid for the wavelength range $222 - 304$ nm and temperature range $210 - 300$ K are as follows.

$$\begin{array}{ll} A_0 = -206.2 & B_0 = 1.0460 \times 10^{-1} \\ A_1 = 2.3726 & B_1 = -1.4124 \times 10^{-3} \\ A_2 = -1.0527 \times 10^{-2} & B_2 = 6.9015 \times 10^{-6} \\ A_3 = 1.9239 \times 10^{-5} & B_3 = -1.5164 \times 10^{-8} \\ A_4 = -1.2242 \times 10^{-8} & B_4 = 1.3990 \times 10^{-11} \end{array}$$

Burkholder et al. [16] used the expression

$$\ln \sigma(\lambda, T) = (\sum A_i (\lambda - 268.7998)^i) (1 + (296 - T) \sum B_i (\lambda - 268.7998)^i)$$

and reported the following A_i and B_i parameters for the wavelength range $235 - 260$ nm and temperature range $210 - 296$ K.

$$\begin{array}{ll} A_0 = -44.42756 & B_0 = 1.481886 \times 10^{-4} \\ A_1 = -1.464955 \times 10^{-1} & B_1 = 6.77182 \times 10^{-6} \\ A_2 = -5.692188 \times 10^{-4} & B_2 = 1.154347 \times 10^{-7} \\ A_3 = 1.155366 \times 10^{-5} & B_3 = -2.77145 \times 10^{-11} \\ A_4 = -1.399502 \times 10^{-7} & B_4 = -6.619515 \times 10^{-11} \end{array}$$

Burkholder et al. [16] also report a parameterization for cross sections extrapolated out to 400 nm

$$\ln \sigma(\lambda, T) = (\sum A_i (\lambda - 301.0104)^i) (1 + (296 - T) \sum B_i (\lambda - 301.0104)^i)$$

with the following parameters.

$$\begin{array}{ll} A_0 = -49.50456 & B_0 = 3.616315 \times 10^{-4} \\ A_1 = -1.633525 \times 10^{-1} & B_1 = 5.534952 \times 10^{-6} \\ A_2 = 5.170758 \times 10^{-6} & B_2 = -1.997903 \times 10^{-8} \\ A_3 = 4.332654 \times 10^{-6} & B_3 = -9.234512 \times 10^{-11} \\ A_4 = -3.899051 \times 10^{-8} & B_4 = 1.776346 \times 10^{-12} \end{array}$$

Note: In the Burkholder et al. [16] paper, the parameterization equation is written in terms of $\log_{10}(\sigma(\lambda, T))$ but the correct expression should be given in terms of $\ln(\sigma(\lambda, T))$, as given here.

Photolysis Quantum Yield and Product Studies: The quantum yield for formation of CF_2O and Br_2 in the photolysis of CF_2Br_2 at 206, 248, and 302 nm in the presence of O_2 has been measured to be unity, independent of pressure, by Molina and Molina [71]. This is in contrast to an earlier report by Walton [118] that the quantum yield at 265 nm decreases from unity when the system pressure is raised to 50 Torr of CO_2 . Quantum yields for Br atom formation of $\Phi(\text{Br}) = 1.96 \pm 0.27$, 1.63 ± 0.19 , and 1.01 ± 0.15 , in the photodissociation of CF_2Br_2 at 193, 222, and 248 nm, respectively, were reported by Talukdar et al. [109]. A quantum yield for CF_2 formation, $\Phi(\text{CF}_2) = 1.15 \pm 0.30$, in the 193 nm photolysis was reported by Talukdar et al. [108]. The transient CF_2Br radical was detected by molecular beam [58] and spectroscopic studies [40, 115] during photolysis at 248 nm and confirm that the C-Br bond is broken.

Table 4G-31. Absorption Cross Sections of CF₂Br₂ at 296 K

λ (nm)	$10^{20} \sigma$ (cm ²)	λ (nm)	$10^{20} \sigma$ (cm ²)	λ (nm)	$10^{20} \sigma$ (cm ²)
170	124.5	228	253.4	286	0.336
172	78.1	230	244.7	288	0.245
174	55.3	232	230.2	290	0.178
176	49.5	234	211.9	292	0.128
178	60.3	236	191.6	294	0.0926
180	75.0	238	169.3	296	0.0672
182	86.6	240	147.3	298	0.0487
184	100.9	242	125.8	300	0.0352
186	111.8	244	106.0	302	0.0253
188	118.0	246	87.8	304	0.0183
190	115.9	248	72.0	306	0.0130
192	110.3	250	58.3	308	0.00919
194	101.6	252	46.5	310	0.00650
196	91.4	254	36.8	312	0.00456
198	82.1	256	28.9	314	0.00319
200	74.9	258	22.4	316	0.00222
202	71.7	260	17.3	318	0.00157
204	73.4	262	13.1	320	0.00105
206	80.7	264	9.90	322	0.000759
208	93.0	266	7.47	324	0.000531
210	110.0	268	5.59	326	0.000371
212	131.0	270	4.17	328	0.000260
214	154.9	272	3.08	330	0.000182
216	180.4	274	2.27	332	0.000127
218	204.7	276	1.66	334	0.000089
220	226.0	278	1.21	336	0.000062
222	244.2	280	0.888	338	0.000044
224	253.3	282	0.647	340	0.000030
226	256.8	284	0.470		

Note:

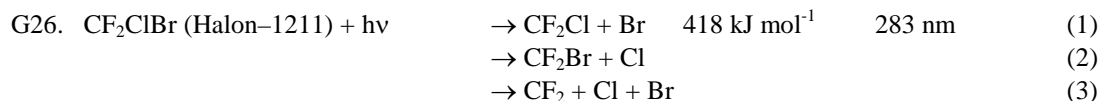
170 – 188 nm: Gillotay and Simon [34]

190 – 304 nm: mean of data from Gillotay and Simon [34], Orkin and Kasimovskaya [78], and Burkholder et al. [16]

306 – 320 nm: mean of data from Orkin and Kasimovskaya [78] and Burkholder et al. [16]

322 – 340 nm: extrapolation of mean of data from Orkin and Kasimovskaya [78] and Burkholder et al.

[16] , $\log \sigma(\lambda) = 1.85109 - 0.07755 \lambda$



(Recommendation: 06-2, Note: 10-6, Evaluated: 10-6)

Absorption Cross Sections: The UV absorption spectrum of difluorochlorobromomethane (Halon-1211), CF_2ClBr , has been measured at room temperature by Giolando et al. [37] (191 – 307 nm), Molina et al. [72] (190 – 330 nm), Orkin and Kasimovskaya [78] (190 – 304 nm), Gillotay and Simon [34] (170 – 302 nm), and Burkholder et al. [16] (190 – 320 nm). The agreement between the room temperature cross section data of Orkin and Kasimovskaya [78], Gillotay and Simon [34], and Burkholder et al. [16] is very good, within 10% over the range 190 – 240 nm and within 3% in the maximum near 205 nm. The data from Gillotay and Simon [34] near the absorption maximum differs from the other observations by ~10%. Molina et al. [72] reported values in the range 190 – 240 nm that are lower by 10–20% than the other data. The few data points of Giolando et al. [37] agree well with the absorption spectra reported by Orkin and Kasimovskaya [78], Gillotay and Simon [34], and Burkholder et al. [16]. The differences between the various data sets increase at

the longer wavelengths. The recommended absorption cross sections in Table 4G-32 are the values of Gillotay and Simon [34] in the region 170 – 188 nm, the mean of the values reported by Molina et al. [72], Gillotay and Simon [34], Burkholder et al. [16] and Orkin and Kasimovskaya [78] in the region 190 – 302 nm, the mean of the values reported by Molina et al. [72], Burkholder et al. [16], and Orkin and Kasimovskaya [78] in the region 304 nm, and the mean of the values reported by Molina et al. [72] and Burkholder et al. [16] in the region 306 – 320 nm.

The absorption spectrum has been measured in the far UV by Doucet et al. [25] (60 – 220 nm).

The temperature dependence of the absorption spectrum has been measured by Gillotay and Simon [34] (170 – 302 nm) over the range at 210 – 295 K and Burkholder et al. [16] (190 – 320 nm) over the range 210 – 296 K. The absorption cross sections increase near the peak, 204 – 206 nm, and decrease at wavelengths >233 nm and <180 nm with decreasing temperature. Gillotay and Simon [34] observed a systematic temperature dependence with an increase in the peak cross section by $\sim 5 \times 10^{-20} \text{ cm}^2 \text{ molecule}^{-1}$ per 20 K decrease in temperature. Burkholder et al. [16] reported a less pronounced temperature dependence with the peak cross section at 210 K being 15% less than reported Gillotay and Simon [34] (the cross sections at room temperature are within 4%). Different empirical parameterizations for the temperature dependence of the absorption cross section have been used. Gillotay and Simon [34] used a polynomial expansion

$$\log_{10} \sigma(\lambda, T) = \sum A_n \lambda^n + (T - 273) \times \sum B_n \lambda^n$$

and report calculated cross sections for T = 210, 230, 250, 270, and 295 K. The A_n and B_n parameters, which are valid for the wavelength range 200 – 302 nm and temperature range 210 – 300 K, are given below.

$$\begin{array}{ll} A_0 = -134.80 & B_0 = 3.3070 \times 10^{-1} \\ A_1 = 1.7084 & B_1 = -5.0957 \times 10^{-3} \\ A_2 = -9.1540 \times 10^{-3} & B_2 = 2.9361 \times 10^{-5} \\ A_3 = 2.1644 \times 10^{-5} & B_3 = -7.6198 \times 10^{-8} \\ A_4 = -1.9863 \times 10^{-8} & B_4 = 7.6825 \times 10^{-11} \end{array}$$

Burkholder et al. [16] parameterized their data using the expression

$$\ln \sigma(\lambda, T) = (\sum A_i (\lambda - 259.8989)^i) (1 + (296 - T) \sum B_i (\lambda - 259.8989)^i)$$

and report the following A_i and B_i parameters valid for the wavelength range 220–260 nm and temperature range 210 – 296 K.

$$\begin{array}{ll} A_0 = -45.4087 & B_0 = 1.528905 \times 10^{-4} \\ A_1 = -1.304811 \times 10^{-1} & B_1 = 6.024833 \times 10^{-6} \\ A_2 = -6.995443 \times 10^{-4} & B_2 = 1.030995 \times 10^{-7} \\ A_3 = 6.159709 \times 10^{-6} & B_3 = -6.387931 \times 10^{-11} \\ A_4 = -9.384074 \times 10^{-9} & B_4 = -3.718503 \times 10^{-11} \end{array}$$

Burkholder et al. [16] also report a parameterization for cross sections extrapolated to 400 nm

$$\ln \sigma(\lambda, T) = (\sum A_i (\lambda - 292.2083)^i) (1 + (296 - T) \sum B_i (\lambda - 292.2083)^i)$$

with the following parameters.

$$\begin{array}{ll} A_0 = -50.15428 & B_0 = 3.778659 \times 10^{-4} \\ A_1 = -1.547025 \times 10^{-1} & B_1 = 6.338322 \times 10^{-6} \\ A_2 = -9.551083 \times 10^{-5} & B_2 = -1.294407 \times 10^{-8} \\ A_3 = 4.076334 \times 10^{-6} & B_3 = -2.430137 \times 10^{-10} \\ A_4 = -2.747685 \times 10^{-8} & B_4 = 2.234599 \times 10^{-12} \end{array}$$

Note: Errors in the Burkholder et al. [16] paper are corrected here.

Photolysis Quantum Yield and Product Studies: Quantum yields for Cl and Br atom formation in the photodissociation of CF_2ClBr at 193, 222, and 248 nm, $\Phi(\text{Cl}) = 1.03 \pm 0.14$, 0.27 ± 0.04 , and 0.18 ± 0.03 , $\Phi(\text{Br}) = 1.04 \pm 0.13$, 0.86 ± 0.11 , and 0.75 ± 0.13 , respectively, and a quantum yield for CF_2 formation in the 193 nm photolysis, $\Phi(\text{CF}_2) = 0.91 \pm 0.30$, were reported by Talukdar et al. [108].

Table 4G-32. Absorption Cross Sections of CF₂ClBr at 298 K

λ (nm)	$10^{20} \sigma$ (cm ²)	λ (nm)	$10^{20} \sigma$ (cm ²)	λ (nm)	$10^{20} \sigma$ (cm ²)
170	323.0	222	68.3	274	0.250
172	234.2	224	60.4	276	0.184
174	176.0	226	52.7	278	0.135
176	120.9	228	45.7	280	0.0991
178	84.7	230	39.2	282	0.0724
180	58.1	232	33.8	284	0.0527
182	41.9	234	28.8	286	0.0385
184	35.0	236	24.4	288	0.0282
186	34.1	238	20.4	290	0.0205
188	38.9	240	16.9	292	0.0148
190	46.1	242	13.9	294	0.0106
192	57.0	244	11.4	296	0.00764
194	69.1	246	9.28	298	0.00544
196	81.4	248	7.50	300	0.00391
198	93.5	250	5.99	302	0.00279
200	106.0	252	4.76	304	0.00207
202	113.3	254	3.76	306	0.00161
204	117.4	256	2.94	308	0.00113
206	118.7	258	2.29	310	0.000803
208	117.7	260	1.76	312	0.000569
210	114.2	262	1.36	314	0.000403
212	108.5	264	1.03	316	0.000288
214	101.5	266	0.784	318	0.000213
216	93.6	268	0.593	320	0.000159
218	85.3	270	0.447		
220	76.8	272	0.336		

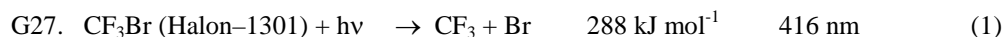
Note:

170 – 188 nm: Gillotay and Simon [34]

190 – 302 nm: mean of values from Molina et al. [72], Gillotay and Simon [34], Burkholder et al. [16], and Orkin and Kasimovskaya [78]

304 nm: mean of values from Molina et al. [72], Burkholder et al. [16], and Orkin and Kasimovskaya [78]

306 – 320 nm: mean of values from Molina et al. [72] and Burkholder et al. [16]



(Recommendation: 06-2, Note: 10-6, Evaluated: 10-6)

Absorption Cross Sections: The UV absorption spectrum of trifluorobromomethane (Halon-1301), CF₃Br, has been measured at room temperature by Davidson [22] (207 – 255 nm), Roxlo and Mandl [96] (170 – 230 nm), Pence et al. [84] (180 – 400 nm), Molina et al. [72] (190 – 300 nm), Orkin and Kasimovskaya [78] (190 – 270 nm), Gillotay and Simon [34] (168 – 280 nm), and Burkholder et al. [16] (190 – 285 nm). The agreement between the room temperature data is in general good in the region between 190 and 230 nm, 10% or better. The exceptions are the data of Davidson [22] below 210 nm and the data set from Roxlo and Mandl [96]. Pence et al. [84] report a spectrum graphically and an absorption cross section at 193 nm that is significantly less than the rest of the data at 193 nm. For wavelengths >250 nm, Burkholder et al. [16] and Orkin and Kasimovskaya [78] report values greater by up to ~ 35% at 270 nm than reported by Molina et al. [72] and Gillotay and Simon [34]. The recommended absorption cross sections in Table 4G-33 are the values from Gillotay and Simon [34] in the region 168 – 188 nm, the mean of the values reported by Molina et al. [72], Gillotay and Simon [34], Burkholder et al. [16], and Orkin and Kasimovskaya [78] in the region 190 – 270 nm, the mean of the values reported by Molina et al. [72], Gillotay and Simon [34], and Burkholder et al. [16] in the region 272 – 280 nm, and the values of Molina et al. [72] in the region 295 – 300 nm.

The absorption spectrum has been measured in the far UV by Doucet et al. [25] (60 – 220 nm).

The temperature dependence of the absorption spectrum has been measured by Gillotay and Simon [34] (168 – 280 nm) over the range 210 – 295 K and Burkholder et al. [16] (190 – 285 nm) over the range 210 – 296 K. The absorption cross sections increase between 174 and 216 nm and decrease at wavelengths >218 nm and <174 nm with decreasing temperature. Gillotay and Simon [34] observed a systematic temperature behavior with an increase of the peak cross section by $\sim 0.6 \times 10^{-20} \text{ cm}^2 \text{ molecule}^{-1}$ per 20 K decrease in temperature. Burkholder et al. [16] reported a less pronounced temperature dependence with the peak cross section at 210 K being $\sim 25\%$ lower than reported by Gillotay and Simon [34] (the cross sections at room temperature are within 6%). Different parameterizations for the temperature dependence of the absorption cross section have been proposed. Gillotay and Simon [34] give the polynomial expansion

$$\log_{10} \sigma(\lambda, T) = \sum A_n \lambda^n + (T - 273) \times \sum B_n \lambda^n$$

and report calculated values for $T = 210, 230, 250, 270,$ and 295 K . The A_n and B_n parameters, which are valid for the wavelength range 178 – 280 nm and temperature range 210 – 300 K are as follows.

$A_0 = 62.563$	$B_0 = -9.1755 \times 10^{-1}$
$A_1 = -2.0068$	$B_1 = 1.8575 \times 10^{-2}$
$A_2 = 1.6592 \times 10^{-2}$	$B_2 = -1.3857 \times 10^{-4}$
$A_3 = -5.6465 \times 10^{-5}$	$B_3 = 4.5066 \times 10^{-7}$
$A_4 = 6.7459 \times 10^{-8}$	$B_4 = -5.3803 \times 10^{-10}$

Burkholder et al. [16] parameterized their data using the expression

$$\ln \sigma(\lambda, T) = (\sum A_i (\lambda - 242.2466)^i) (1 + (296 - T) \sum B_i (\lambda - 242.266)^i)$$

and report the following A_i and B_i parameters valid for the wavelength range 214 – 285 nm and temperature range 210 – 296 K.

$A_0 = -46.70542$	$B_0 = 1.694026 \times 10^{-4}$
$A_1 = -1.55047 \times 10^{-1}$	$B_1 = 8.723247 \times 10^{-6}$
$A_2 = -1.020187 \times 10^{-3}$	$B_2 = 5.953165 \times 10^{-9}$
$A_3 = 2.246169 \times 10^{-5}$	$B_3 = -3.872168 \times 10^{-9}$
$A_4 = -1.300982 \times 10^{-7}$	$B_4 = -1.803325 \times 10^{-11}$

Note: In the Burkholder et al. [16] paper, the parameterization equation is written in terms of $\log_{10} \sigma(\lambda, T)$ but the correct expression should be given in terms of $\ln \sigma(\lambda, T)$, as given here.

Photolysis Quantum Yield and Product Studies: Talukdar et al. [109] reported quantum yields for Br ($\text{Br}(^2\text{P}_{3/2}) + \text{Br}^*(^2\text{P}_{1/2})$) atom formation in the photodissociation of CF_3Br at 193 and 222 nm to be 1.12 ± 0.16 and 0.92 ± 0.15 , respectively. A quantum yield for $\text{Br}^*(^2\text{P}_{1/2})$ atom formation at 193 nm was reported by Pence et al. [84] to be 0.56 ± 0.05 .

Table 4G-33. Absorption Cross Sections of CF₃Br at 296 K

λ (nm)	$10^{20} \sigma$ (cm ²)	λ (nm)	$10^{20} \sigma$ (cm ²)	λ (nm)	$10^{20} \sigma$ (cm ²)
168	0.517	210	12.1	252	0.107
170	0.696	212	11.4	254	0.0743
172	0.928	214	10.6	256	0.0516
174	1.22	216	9.71	258	0.0357
176	1.60	218	8.65	260	0.0248
178	2.05	220	7.56	262	0.0171
180	2.61	222	6.50	264	0.0118
182	3.26	224	5.47	266	0.00827
184	4.02	226	4.52	268	0.00580
186	4.88	228	3.69	270	0.00399
188	5.82	230	2.91	272	0.00271
190	6.56	232	2.32	274	0.00188
192	7.58	234	1.80	276	0.00129
194	8.63	236	1.39	278	0.00092
196	9.61	238	1.04	280	0.00064
198	10.5	240	0.766	285	0.00022
200	11.3	242	0.563	290	0.00008
202	11.9	244	0.414	295	0.00003
204	12.4	246	0.296	300	0.00001
206	12.5	248	0.212		
208	12.4	250	0.149		

Note:

170 – 188 nm: Gillotay and Simon [34]

190 – 270 nm: mean of Molina et al. [72], Gillotay and Simon [34], Burkholder et al. [16] and Orkin and Kasimovskaya [78]

272 – 280 nm: mean of Molina et al. [72] and Burkholder et al. [16]

285 – 300 nm: Molina et al. [72]

G28. $\text{CH}_2=\text{CHBr} + h\nu \rightarrow \text{Products}$

(Recommendation: 06-2, Note: 10-6, Evaluated: 10-6)

Absorption Cross Sections: The absorption spectrum of bromoethene (vinyl bromide), $\text{CH}_2=\text{CHBr}$, has been measured at room temperature over the wavelength range 164 – 254 nm by Orkin et al. [80]. The spectrum has a very strong absorption band with the maximum at 192 nm, characteristic of the $\text{CH}_2=\text{CBr}$ - group, and the absorption band of the $\text{CH}_2=\text{CH}$ - group around 170 nm. The recommended absorption cross sections in Table 4G-34 are taken from Orkin et al. [80] (reported in 0.5 nm increments).

Photolysis Quantum Yield and Product Studies: No studies are available.

Table 4G-34. Absorption Cross Sections of $\text{CH}_2=\text{CHBr}$ at 295 K

λ (nm)	$10^{20} \sigma$ (cm^2)	λ (nm)	$10^{20} \sigma$ (cm^2)	λ (nm)	$10^{20} \sigma$ (cm^2)
184	1970	208	306	232	18.2
186	2320	210	266	234	12.6
188	2710	212	232	236	8.47
190	3000	214	198	238	5.70
192	3160	216	166	240	3.69
194	2950	218	136	242	2.43
196	2470	220	109	244	1.58
198	1800	222	85.9	246	1.03
200	996	224	65.3	248	0.683
202	605	226	49.1	250	0.454
204	440	228	35.7	252	0.315
206	359	230	25.5	254	0.225

Note:

Orkin et al. [80]

G29. $\text{CHBr}=\text{CF}_2 + h\nu \rightarrow \text{Products}$

(Recommendation: 06-2, Note: 10-6, Evaluated: 10-6)

Absorption Cross Sections: The absorption spectrum of 1-bromo-2,2-difluoroethene, $\text{CHBr}=\text{CF}_2$, has been measured at room temperature over the wavelength range 164 – 266 nm by Orkin et al. [80]. The spectrum has strong absorption bands between 164 and 190 nm, a weaker and less pronounced band between 190 and 210 nm (maximum 194 nm), and a still weaker band above 210 nm with the maximum near 220 nm. The recommended absorption cross sections in Table 4G-35 are taken from Orkin et al. [80] (reported in 0.5 nm increments).

Photolysis Quantum Yield and Product Studies: No studies are available.

Table 4G-35. Absorption Cross Sections of $\text{CHBr}=\text{CF}_2$ at 295 K

λ (nm)	$10^{20} \sigma$ (cm^2)	λ (nm)	$10^{20} \sigma$ (cm^2)	λ (nm)	$10^{20} \sigma$ (cm^2)	λ (nm)	$10^{20} \sigma$ (cm^2)
184	2160	206	87.6	228	74.0	250	8.81
186	1020	208	70.1	230	68.2	252	6.51
188	670	210	63.4	232	61.3	254	4.75
190	635	212	63.5	234	53.7	256	3.49
192	671	214	66.7	236	45.9	258	2.54
194	703	216	71.1	238	38.8	260	1.86
196	610	218	75.8	240	31.7	262	1.37
198	471	220	79.3	242	25.5	264	1.04
200	306	222	80.7	244	20.1	266	0.796
202	193	224	80.6	246	15.4		
204	124	226	78.4	248	11.7		

Note:
Orkin et al. [80]

G30. $\text{CFBr=CF}_2 + h\nu \rightarrow \text{Products}$

(Recommendation: 06-2, Note: 10-6, Evaluated: 10-6)

Absorption Cross Sections: The absorption spectrum of trifluorobromoethene, CFBr=CF_2 , has been measured at room temperature over the wavelength range 164 – 274 nm by Orkin et al. [80]. The spectrum has strong absorption bands between 164 and 188 nm, a weaker and less pronounced band between 188 and 213 nm (maximum 194.5 nm), and a still weaker band above 213 nm with the maximum near 229 nm. The recommended absorption cross sections in Table 4G-36 are taken from Orkin et al. [80] (reported in 0.5 nm increments).

Photolysis Quantum Yield and Product Studies: No studies are available.

Table 4G-36. Absorption Cross Sections of CFBr=CF_2 at 295 K

λ (nm)	$10^{20} \sigma$ (cm^2)	λ (nm)	$10^{20} \sigma$ (cm^2)	λ (nm)	$10^{20} \sigma$ (cm^2)	λ (nm)	$10^{20} \sigma$ (cm^2)
184	456	208	56.1	232	58.1	256	6.87
186	367	210	39.5	234	54.7	258	5.15
188	350	212	34.1	236	50.4	260	3.77
190	373	214	34.5	238	45.1	262	2.78
192	415	216	37.7	240	39.5	264	2.04
194	439	218	42.2	242	33.9	266	1.49
196	434	220	47.2	244	28.5	268	1.09
198	412	222	52.1	246	23.5	270	0.812
200	354	224	56.2	248	19.2	272	0.613
202	263	226	59.0	250	15.2	274	0.469
204	167	228	60.4	252	11.8		
206	95.1	230	60.0	254	9.03		

Note:
Orkin et al. [80]

G31. $\text{CH}_2=\text{CBrCF}_3 + h\nu \rightarrow \text{Products}$

(Recommendation: 06-2, Note: 10-6, Evaluated: 10-6)

Absorption Cross Sections: The absorption spectrum of 2-bromo-3,3,3-trifluoro-1-propene, $\text{CH}_2=\text{CBrCF}_3$, has been measured at room temperature over the wavelength range 164 – 254 nm by Orkin et al. [80]. The spectrum has a very strong absorption band at wavelengths >174 nm with a maximum at 194 nm, characteristic of a $\text{CH}_2=\text{CBr-}$ group. The recommended absorption cross sections in Table 4G-37 are taken from Orkin et al. [80] (reported in 0.5 nm increments).

Photolysis Quantum Yield and Product Studies: No studies are available.

Table 4G-37. Absorption Cross Sections of $\text{CH}_2=\text{CBrCF}_3$ at 295 K

λ (nm)	$10^{20} \sigma$ (cm^2)	λ (nm)	$10^{20} \sigma$ (cm^2)	λ (nm)	$10^{20} \sigma$ (cm^2)	λ (nm)	$10^{20} \sigma$ (cm^2)
184	1370	202	1520	220	126	238	6.97
186	1700	204	1080	222	97.3	240	4.77
188	2040	206	774	224	73.1	242	3.26
190	2350	208	581	226	54.9	244	2.22
192	2590	210	440	228	40.1	246	1.50
194	2700	212	338	230	28.8	248	1.02
196	2620	214	263	232	20.5	250	0.705

198	2370	216	208	234	14.4	252	0.496
200	1980	218	162	236	10.2		

Note:

Orkin et al. [80]

G32. $\text{CF}_3\text{CH}_2\text{Br}$ (Halon-2301) + $h\nu \rightarrow$ Products

(Recommendation: 02-25, Note: 10-6, Evaluated: 10-6)

Absorption Cross Sections: The absorption spectrum of 1,1,1-trifluoro-2-bromoethane (Halon-2301), $\text{CF}_3\text{CH}_2\text{Br}$, has been measured at 295 K over the wavelength range 190 – 294 nm by Orkin and Kasimovskaya [78]. The recommended absorption cross sections in Table 4G-38 are taken from this study.

Photolysis Quantum Yield and Product Studies: No studies are available.

Table 4G-38. Absorption Cross Sections of $\text{CF}_3\text{CH}_2\text{Br}$ at 295 K

λ (nm)	$10^{20} \sigma$ (cm^2)	λ (nm)	$10^{20} \sigma$ (cm^2)	λ (nm)	$10^{20} \sigma$ (cm^2)
190	45.4	226	16.6	262	0.190
192	49.5	228	14.1	264	0.137
194	52.5	230	11.9	266	0.0983
196	54.4	232	9.85	268	0.0705
198	55.1	234	8.10	270	0.0504
200	54.7	236	6.58	272	0.0361
202	53.3	238	5.28	274	0.0258
204	51.2	240	4.20	276	0.0184
206	48.6	242	3.31	278	0.0132
208	45.7	244	2.58	280	0.0096
210	42.5	246	2.01	282	0.0069
212	39.1	248	1.53	284	0.0048
214	35.7	250	1.16	286	0.0034
216	32.2	252	0.876	288	0.0025
218	28.8	254	0.653	290	0.0018
220	25.5	256	0.484	292	0.0013
222	22.3	258	0.357	294	0.0011
224	19.4	260	0.261		

Note:

190 – 294 nm: Orkin and Kasimovskaya [78]

G33. CF_3CHClBr (Halon-2311) + $h\nu \rightarrow \text{CF}_3\text{CHCl} + \text{Br}$ (1)



(Recommendation: 06-2, Note: 10-6, Evaluated: 10-6)

Absorption Cross Sections: The absorption spectrum of 1,1,1-trifluoro-2,2-chlorobromoethane (Halon-2311), CF_3CHClBr , has been measured at room temperature by Orkin and Kasimovskaya [78] (190 – 310 nm), Gillotay et al. [35, 36] (170 – 290 nm), Bilde et al. [8] (200 – 310 nm), and Taketani et al. [106] (193.3 nm). The room temperature cross sections values are in good agreement, to within 5–15%, at wavelengths <280 nm. In this region Gillotay et al. [35, 36] report the lowest cross section values and Orkin and Kasimovskaya the greatest values. At wavelengths >280 nm, the data from Bilde et al. are greater than those of Orkin and Kasimovskaya with the difference increasing with increasing wavelength, 100% at 310 nm. The recommended absorption cross sections in Table 4G-39 are the values from Gillotay et al. [36] in the region 170 – 188 nm, the mean of the values reported by Gillotay et al. [36] and Orkin and Kasimovskaya in the region 190 – 198 nm, the mean of the values reported by the three groups in the region 200 – 290 nm, and the mean of the values reported by Orkin and Kasimovskaya and Bilde et al. in the region 292 – 310 nm.

The absorption spectrum temperature dependence has been measured by Gillotay et al. [36] (170 – 290 nm) over the range 210 – 295 K and Bilde et al. [8] (200 – 310 nm) over the range 223 – 298 K. Gillotay et al. [36] report an increase of the absorption cross sections between 192 and 238 nm with decreasing temperature and the opposite effect at wavelengths >238 nm and <192 nm. The increase at ~202 nm is $\sim 2.4 \times 10^{-20} \text{ cm}^2 \text{ molecule}^{-1}$ per 20 K decrease in temperature, i.e., an increase of ~10% between 295 and 210 K. Bilde et al. observed a less pronounced temperature behavior in the absorption band and a decrease of the absorption cross sections with decreasing temperature at wavelengths above 214 nm.

Gillotay and Simon [36] parameterized the cross sections and the temperature dependence using an empirical polynomial expansion

$$\log_{10} \sigma(\lambda, T) = \sum A_n \lambda^n + (T - 273) \times \sum B_n \lambda^n$$

and report calculated values for T = 210, 230, 250, 270, and 295 K. The A_n and B_n parameters, which are valid for the wavelength range 190 – 290 nm and temperature range 210 – 300 K, are given below and recommended for use in model calculations.

$$\begin{array}{ll} A_0 = -127.157358 & B_0 = -7.959828 \times 10^{-2} \\ A_1 = 1.635435 & B_1 = 1.978026 \times 10^{-3} \\ A_2 = -9.002683 \times 10^{-3} & B_2 = -1.627866 \times 10^{-5} \\ A_3 = 2.190678 \times 10^{-5} & B_3 = 5.480744 \times 10^{-8} \\ A_4 = -2.062651 \times 10^{-8} & B_4 = -6.480935 \times 10^{-11} \end{array}$$

Photolysis Quantum Yield and Product Studies: Taketani et al. [106] reported the total yield of Cl atoms to be 0.28 ± 0.02 in the photodissociation of CF_3CHClBr at 193.3 nm. Assuming a unit quantum yield for photodissociation this implies that the rupture of the C-Br bond should be dominant photodissociation channel.

Table 4G-39. Absorption Cross Sections of CF_3CHClBr at 298 K

λ (nm)	$10^{20} \sigma$ (cm^2)	λ (nm)	$10^{20} \sigma$ (cm^2)	λ (nm)	$10^{20} \sigma$ (cm^2)
170	702.6	218	78.7	266	0.980
172	614.6	220	71.0	268	0.765
174	496.8	222	63.3	270	0.575
176	379.8	224	56.3	272	0.444
178	281.1	226	49.5	274	0.339
180	206.1	228	43.3	276	0.258
182	153.3	230	37.3	278	0.196
184	118.4	232	32.2	280	0.149
186	97.1	234	27.6	282	0.111
188	86.6	236	23.6	284	0.0818
190	93.4	238	20.0	286	0.0606
192	99.8	240	16.8	288	0.0448
194	107.1	242	14.0	290	0.0331
196	114.3	244	11.7	292	0.0263
198	119.7	246	9.51	294	0.0198
200	121.5	248	7.79	296	0.0147
202	123.0	250	6.38	298	0.0109
204	122.3	252	5.15	300	0.00808
206	119.7	254	4.13	302	0.00583
208	115.1	256	3.31	304	0.00450
210	109.0	258	2.63	306	0.00313
212	102.0	260	2.06	308	0.00235
214	94.6	262	1.61	310	0.00180
216	86.7	264	1.26		

Note:

170 – 188 nm: Gillotay et al. [35, 36]

190 – 198 nm: mean of values from Gillotay et al. [35, 36] and Orkin and Kasimovskaya [78]

200 – 290 nm: mean of values from Gillotay et al. [35, 36], Orkin and Kasimovskaya [78], and Bilde et al. [8]
292 – 310 nm: mean of values from Orkin and Kasimovskaya [78] and Bilde et al. [8]

G34. CF_3CHFBr (Halon-2401) + $h\nu \rightarrow \text{Products}$

(Recommendation: 02-25, Note: 10-6, Evaluated: 10-6)

Absorption Cross Sections: The absorption spectrum of 1,1,1,2-tetrafluoro-2-bromoethane (Halon-2401), CF_3CHFBr , has been measured at 295 K over the wavelength range 190 – 280 nm by Orkin and Kasimovskaya [78]. Their results are recommended and given in Table 4G-40.

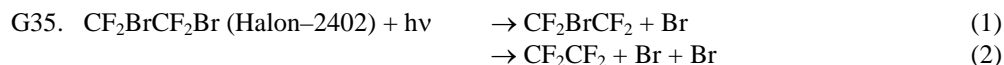
Photolysis Quantum Yield and Product Studies: No studies are available.

Table 4G-40. Absorption Cross Sections of CF_3CHFBr at 295 K

λ (nm)	$10^{20} \sigma$ (cm^2)	λ (nm)	$10^{20} \sigma$ (cm^2)	λ (nm)	$10^{20} \sigma$ (cm^2)
190	24.9	222	11.0	254	0.226
192	26.1	224	9.38	256	0.166
194	27.0	226	7.91	258	0.121
196	27.5	228	6.58	260	0.0873
198	27.7	230	5.42	262	0.0628
200	27.4	232	4.42	264	0.0450
202	26.9	234	3.53	266	0.0325
204	26.0	236	2.79	268	0.0235
206	24.8	238	2.19	270	0.0171
208	23.4	240	1.69	272	0.0124
210	21.9	242	1.30	274	0.0093
212	20.2	244	0.991	276	0.0069
214	18.3	246	0.736	278	0.0053
216	16.5	248	0.556	280	0.0040
218	14.6	250	0.416		
220	12.8	252	0.308		

Note:

Orkin and Kasimovskaya [78]



(Recommendation: 06-2, Note: 10-6, Evaluated: 10-6)

Absorption Cross Sections: The absorption cross sections of 1,1,2,2-tetrafluoro-1,2-dibromoethane (Halon-2402), $\text{CF}_2\text{BrCF}_2\text{Br}$, has been measured at room temperature by Molina et al. [72] (195 – 320 nm), Orkin and Kasimovskaya [78] (190 – 300 nm), Gillotay et al. [36] (170 – 280 nm), and Burkholder et al. [16] (190 – 320 nm). The room temperature absorption cross sections are in good agreement in the region 180 – 240 nm, generally to within 10%. The agreement at the absorption maximum near 200 nm is to within 5% and in the long wavelength tail out to 310 nm it is to within 15%. The recommended absorption cross sections in Table 4G-41 are the values from Gillotay et al. [36] in the region 170 – 186 nm, the mean of the values reported by Molina et al. [72], Gillotay et al. [36], Burkholder et al. [16], and Orkin and Kasimovskaya [78] in the region 196 – 280 nm, the mean of the values reported by Molina et al. [72], Burkholder et al. [16], and Orkin and Kasimovskaya [78] in the region 282 – 300 nm; and the mean of the values reported by Molina et al. [72] and Burkholder et al. [16] in the region 302 – 320 nm. In the region 186 and 196 nm a smoothed absorption spectrum was used to estimate values at 188, 190, 192, and 194 nm.

The temperature dependence of the absorption spectrum has been measured by Gillotay et al. [36] (170 – 280 nm) over the range 210 – 295 K and Burkholder et al. [16] (190 – 320 nm) over the range 210 – 296 K. The agreement of the results from these two studies is poor. A regular but weak decrease of the absorption cross sections at 194 – 280 nm with decreasing temperature and the reverse effect below 194 nm was observed by Gillotay et al. [36]. The decrease in the absorption maximum was $\sim 1.0 \times 10^{-20} \text{ cm}^2 \text{ molecule}^{-1}$ per 20 K temperature decrease, i.e., a decrease of $\sim 4\%$ between 295 and 210 K. Burkholder et al. [16] observed a strong increase in the peak absorption with decreasing temperature of $\sim 20\%$ over the temperature range

studied and the opposite behavior at wavelengths >230 nm. Gillotay and Simon [36] parameterized the cross section temperature dependence using an empirical polynomial expansion

$$\log_{10} \sigma(\lambda, T) = \sum A_n \lambda^n + (T - 273) \times \sum B_n \lambda^n$$

and report calculated values for T = 210, 230, 250, 270, and 295 K. The A_n and B_n parameters, which are valid for the wavelength range 190 – 290 nm and temperature range 210 – 300 K are given below.

$A_0 = 34.026000$	$B_0 = 4.010664 \times 10^{-1}$
$A_1 = -1.152616$	$B_1 = -8.358968 \times 10^{-3}$
$A_2 = 8.959798 \times 10^{-3}$	$B_2 = 6.415741 \times 10^{-5}$
$A_3 = -2.9089 \times 10^{-5}$	$B_3 = -2.157554 \times 10^{-7}$
$A_4 = 3.307212 \times 10^{-8}$	$B_4 = 2.691871 \times 10^{-10}$

Burkholder et al. [16] parameterized the temperature dependence using the empirical expression

$$\ln \sigma(\lambda, T) = (\sum A_i (\lambda - 242.4015)^i) (1 + (296 - T) \sum B_i (\lambda - 242.4015)^i)$$

and report the following A_i and B_i parameters for the wavelength range 190 – 320 nm and temperature range 210 – 296 K.

$A_0 = -43.69218$	$B_0 = 3.301341 \times 10^{-5}$
$A_1 = -1.124704 \times 10^{-1}$	$B_1 = 4.695917 \times 10^{-6}$
$A_2 = -1.213301 \times 10^{-3}$	$B_2 = 6.128629 \times 10^{-8}$
$A_3 = 5.275007 \times 10^{-6}$	$B_3 = -5.443107 \times 10^{-10}$
$A_4 = 6.936195 \times 10^{-8}$	$B_4 = -1.035596 \times 10^{-11}$

Note: In the original Burkholder et al. [16] paper, the parameterization equation is written in terms of $\log_{10}\sigma(\lambda, T)$ but the correct expression should be given in terms of $\ln\sigma(\lambda, T)$, as given here. No recommendation for the temperature dependence is given.

Photolysis Quantum Yield and Product Studies: Zou et al. [126] report quantum yields for Br atom formation in the photodissociation of $\text{CF}_2\text{BrCF}_2\text{Br}$ at 193, 233, and 266 nm to be 1.9 ± 0.1 , 1.9 ± 0.1 , and 1.4 ± 0.1 , respectively. These results indicate bond breaking of both C–Br bonds for photolysis at 193 and 233 nm and at an appreciable fraction at 266 nm.

Table 4G-41. Absorption Cross Sections of CF₂BrCF₂Br at 296 K

λ (nm)	$10^{20} \sigma$ (cm ²)	λ (nm)	$10^{20} \sigma$ (cm ²)	λ (nm)	$10^{20} \sigma$ (cm ²)
170	50.9	222	59.6	274	0.112
172	56.4	224	52.6	276	0.0813
174	62.3	226	45.9	278	0.0592
176	68.5	228	39.7	280	0.0428
178	75.1	230	33.9	282	0.0300
180	81.8	232	28.8	284	0.0216
182	88.6	234	24.1	286	0.0152
184	95.3	236	19.9	288	0.0109
186	101.8	238	16.4	290	0.00784
188	107.0	240	13.2	292	0.00569
190	112.0	242	10.6	294	0.00410
192	116.5	244	8.45	296	0.00301
194	120.0	246	6.68	298	0.00219
196	122.3	248	5.25	300	0.00161
198	123.7	250	4.03	302	0.00124
200	124.3	252	3.12	304	0.00094
202	123.6	254	2.37	306	0.00071
204	120.3	256	1.78	308	0.00054
206	115.9	258	1.34	310	0.00042
208	110.4	260	0.973	312	0.00033
210	104.2	262	0.718	314	0.00026
212	97.4	264	0.529	316	0.00020
214	90.1	266	0.390	318	0.00016
216	82.4	268	0.287	320	0.00014
218	74.8	270	0.211		
220	67.0	272	0.154		

Notes:

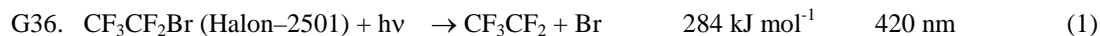
170 – 186 nm: Gillotay et al. [36]

188 – 194 nm: values estimated by smoothing the absorption curve

196 – 280 nm: mean of data from Molina et al. [72], Gillotay et al. [36], Burkholder et al. [16], and Orkin and Kasimovskaya [78]

282 – 300 nm: mean of data from Molina et al. [72], Burkholder et al. [16], and Orkin and Kasimovskaya [78]

302 – 320 nm: mean of data from Molina et al. [72] and Burkholder et al. [16]



(Recommendation: 02-25, Note: 10-6, Evaluated: 10-6)

Absorption Cross Sections: The UV absorption spectrum of pentafluorobromoethane (Halon-2501), CF₃CF₂Br, has been measured at room temperature by Molina et al. [72] (190 – 300 nm), Zhang et al. [124] (200 – 250 nm), and Pence et al. [84] (180 – 400 nm, 193 nm). The absorption cross sections from Zhang et al. [124], reported graphically, are ~30% greater than the results from Molina et al. [72]. Pence et al. [84] report a spectrum graphically over the range 180 – 400 nm and a 193 nm cross section that is ~40% less than reported by Molina et al. [72]. The recommended absorption cross sections in Table 4G-42 are taken from Molina et al. [72].

Photolysis Quantum Yield and Product Studies: Ebenstein et al. [26] used broadband flash photolysis of CF₃CF₂Br and reported a quantum yield of Br* to be 0.48 ± 0.02. A quantum yield for Br*(²P_{1/2}) atom formation at 193 nm, Φ(Br*) = 0.16 ± 0.08, was reported by Pence et al. [84].

Table 4G-42. Absorption Cross Sections of CF₃CF₂Br at 298 K

λ (nm)	$10^{20} \sigma$ (cm ²)	λ (nm)	$10^{20} \sigma$ (cm ²)	λ (nm)	$10^{20} \sigma$ (cm ²)
190	18.1	230	3.83	270	0.0112
195	18.4	235	2.22	275	0.00505
200	18.1	240	1.20	280	0.00218
205	16.9	245	0.620	285	0.00100
210	14.8	250	0.305	290	0.00045
215	12.0	255	0.135	295	0.00020
220	8.94	260	0.0590	300	0.00009
225	6.13	265	0.0260		

Note:

190 – 300 nm: Molina et al. [72]

G37. CH₃CH₂CH₂Br + hν → Products

(Recommendation: 06-2, Note: 10-6, Evaluated: 10-6)

Absorption Cross Sections: The absorption spectrum of 1-bromopropane (n-propyl bromide), CH₃CH₂CH₂Br, has been measured at room temperature by Kozlov et al. [57] (164 – 270 nm). The spectra has an absorption band above 180 nm with maxima at ~201 nm and structured features <180 nm characteristic of the C-Br band absorptions in bromoalkanes. The recommended absorption cross sections in Table 4G-43 are taken from Kozlov et al. [57].

Photolysis Quantum Yield and Product Studies: No studies are available.

Table 4G-43. Absorption Cross Sections of CH₃CH₂CH₂Br and CH₃CHBrCH₃ at 295 K

λ (nm)	$10^{20} \sigma$ (cm ²)		λ (nm)	$10^{20} \sigma$ (cm ²)	
	CH ₃ CH ₂ CH ₂ Br	CH ₃ CHBrCH ₃		CH ₃ CH ₂ CH ₂ Br	CH ₃ CHBrCH ₃
180	108.5	220.2	206	68.8	43.5
182	29.9	36.5	208	65.2	44.2
184	29.5	18.2	210	61.0	44.2
186	35.6	17.6	212	56.5	43.6
188	42.7	19.4	214	51.5	42.2
190	49.8	22.1	216	46.6	40.1
192	56.5	24.8	218	41.4	37.4
194	62.5	28.0	220	35.8	34.1
196	67.0	31.3	222	30.8	30.7
198	70.2	34.3	224	26.0	27.1
200	71.8	37.3	226	21.8	23.6
202	72.6	39.9	228	17.8	20.2
204	71.2	42.0	230	14.4	16.8

Note:

Kozlov et al. [57]

G38. CH₃CHBrCH₃ + hν → Products

(Recommendation: 06-2, Note: 10-6, Evaluated: 10-6)

Absorption Cross Sections: The absorption spectrum of 2-bromopropane (isopropyl bromide), CH₃CHBrCH₃, has been measured at room temperature by Kozlov et al. [57] (164 – 270 nm). The spectra has an absorption band above 180 nm with maxima at ~209 nm and structured features <180 nm

characteristic of the C-Br band absorptions in bromoalkanes. The recommended absorption cross sections in Table 4G-44 are taken from Kozlov et al. [57].

Photolysis Quantum Yield and Product Studies: No studies are available.

G39. $\text{CH}_3\text{C}(\text{O})\text{CH}_2\text{Br} + h\nu \rightarrow \text{Products}$

(Recommendation: 06-2, Note: 10-6, Evaluated: 10-6)

Absorption Cross Sections: The absorption spectrum of bromoacetone, $\text{CH}_3\text{C}(\text{O})\text{CH}_2\text{Br}$, has been measured by Burkholder et al. [12] (210-370 nm) over the temperature range 238 – 296 K using a diode array spectrometer (0.6 nm resolution). The spectrum has overlapping absorption bands with a maximum at 299 nm ($\sigma = 1.15 \times 10^{-19} \text{ cm}^2 \text{ molecule}^{-1}$ at room temperature) and increasing absorption cross sections below 255 nm to a second stronger band peaking below 210 nm. The recommended absorption cross sections in Table 4G-45 are taken from Burkholder et al. [12]. A slight, but not systematic, decrease of the absorption cross sections with decreasing temperature was observed around the absorption minimum at 255 nm and in the long wavelength wings of both absorption bands.

Photolysis Quantum Yield and Product Studies: The photodissociation quantum yield was measured by Burkholder et al. [12] to be 1.6 ± 0.25 at 308 nm and 1.0 ± 0.15 at 351 nm. At both wavelengths, the yields of CO and CO_2 were unity and ~0.5, respectively, whereas the yield of $\text{HC}(\text{O})\text{OH}$ was measured to be 0.15 and that of HBr to be ~0.15.

Table 4G-44. Absorption Cross Sections of CH₃C(O)CH₂Br at 296 K

λ (nm)	$10^{20} \sigma$ (cm ²)	λ (nm)	$10^{20} \sigma$ (cm ²)	λ (nm)	$10^{20} \sigma$ (cm ²)	λ (nm)	$10^{20} \sigma$ (cm ²)
210	59.2	248	6.40	286	9.78	324	5.55
211	58.0	249	6.07	287	9.98	325	5.20
212	57.5	250	5.77	288	10.2	326	4.87
213	56.2	251	5.49	289	10.4	327	4.55
214	53.2	252	5.25	290	10.6	328	4.24
215	50.7	253	5.14	291	10.8	329	3.94
216	48.4	254	4.98	292	11.0	330	3.64
217	46.2	255	4.88	293	11.1	331	3.35
218	43.9	256	4.76	294	11.2	332	3.06
219	41.8	257	4.68	295	11.3	333	2.77
220	39.7	258	4.62	296	11.4	334	2.51
221	37.5	259	4.66	297	11.4	335	2.26
222	35.6	260	4.70	298	11.5	336	2.02
223	33.9	261	4.76	299	11.5	337	1.80
224	32.0	262	4.72	300	11.5	338	1.60
225	30.1	263	4.79	301	11.4	339	1.41
226	28.5	264	4.91	302	11.4	340	1.24
227	26.8	265	5.01	303	11.3	341	1.09
228	25.2	266	5.12	304	11.2	342	0.955
229	23.7	267	5.39	305	11.1	343	0.831
230	22.1	268	5.44	306	11.1	344	0.724
231	20.7	269	5.57	307	10.9	345	0.627
232	19.4	270	5.77	308	10.7	346	0.545
233	18.1	271	6.03	309	10.4	347	0.473
234	16.9	272	6.25	310	10.2	348	0.408
235	15.7	273	6.48	311	9.89	349	0.351
236	14.7	274	6.68	312	9.62	350	0.303
237	13.6	275	6.90	313	9.36	351	0.259
238	12.6	276	7.16	314	9.10	352	0.223
239	11.7	277	7.45	315	8.82	353	0.190
240	10.9	278	7.74	316	8.52	354	0.164
241	10.2	279	8.00	317	8.19	355	0.140
242	9.47	280	8.25	318	7.83	356	0.120
243	8.80	281	8.50	319	7.45	357	0.108
244	8.18	282	8.75	320	7.06	358	0.0952
245	7.68	283	9.04	321	6.66	359	0.0838
246	7.22	284	9.29	322	6.28	360	0.0784
247	6.79	285	9.58	323	5.89		

Note:

Burkholder et al. [12]

References for Section 4G

1. Acton, A. P., R. G. Aickin and N. S. Bayliss, 1936, *J. Chem. Phys.*, 4, 474-479.
2. Barnes, R. J., M. Lock, J. Coleman and A. Sinha, 1996, *J. Phys. Chem.*, 100, 453-457.
3. Barone, S. B., A. A. Turnipseed, T. Gierczak and A. R. Ravishankara, 1994, *J. Phys. Chem.*, 98, 11969-11977.
4. Basco, N. and S. K. Dogra, 1971, *Proc. Roy. Soc. A.*, 323, 417-429.
5. Baumfalk, R., U. Buck, C. Frischkorn, N. H. Nahler and L. Hüwel, 1999, *J. Chem. Phys.*, 111, 2595-2605.
6. Bayes, K. D., D. W. Toohey, R. R. Friedl and S. P. Sander, 2003, *J. Geophys. Res.*, 108, 4095, doi:10.29/2002JD002877.
7. Benter, T., C. Feldmann, U. Kirchner, M. Schmidt, S. Schmidt and R. N. Schindler, 1995, *Ber. Bunsenges. Phys. Chem.*, 99, 1144-1147.
8. Bilde, M., T. J. Wallington, G. Ferronato, J. J. Orlando, G. S. Tyndall, E. Estupinan and S. Haberkorn, 1998, *J. Phys. Chem. A*, 102, 1976-1986.
9. Bridges, L. and J. M. White, 1973, *J. Phys. Chem.*, 77, 295-298.
10. Brion, C. E., Y. Iida, F. Carnovale and J. P. Thomson, 1985, *Chem. Phys.*, 98, 327-339.
11. Burkholder, J. B., 1998, *Int. J. Chem. Kinet.*, 30, 571-576.
12. Burkholder, J. B., M. K. Gilles, T. Gierczak and A. R. Ravishankara, 2002, *Geophys. Res. Lett.*, 29, 1822, doi:10.1029/2002GL014712.
13. Burkholder, J. B., G. P. Knight and J. J. Orlando, 2000, *J. Photochem. Photobiol. A: Chem.*, 134, 133-137.
14. Burkholder, J. B. and J. J. Orlando, 2000, *Chem. Phys. Lett.*, 317, 603-608.
15. Burkholder, J. B., A. R. Ravishankara and S. Solomon, 1995, *J. Geophys. Res.*, 100, 16793-16800.
16. Burkholder, J. B., R. R. Wilson, T. Gierczak, R. Talukdar, S. A. McKeen, J. J. Orlando, G. L. Vaghjiani and A. R. Ravishankara, 1991, *J. Geophys. Res.*, 96, 5025-5043.
17. Cadman, P. and J. P. Simons, 1966, *Trans. Faraday Soc.*, 62, 631-641.
18. Calvert, J. G. and J. N. Pitts Jr. New York, 1966.
19. Clyne, M. A. A. and H. W. Cruse, 1970, *Trans. Faraday Soc.*, 66, 2214-2226.
20. Cooper, M. J., E. Wrede, A. J. Orr-Ewing and M. N. R. Ashfold, 1998, *J. Chem. Soc. Faraday Trans.*, 94, 2901-2907.
21. Cox, R. A., D. W. Sheppard and M. P. Stevens, 1982, *J. Photochem.*, 19, 189-207.
22. Davidson, N., 1951, *J. Am. Chem. Soc.*, 73, 467-468.
23. Deters, B., J. P. Burrows, S. Himmelmann and C. Blindauer, 1996, *Ann. Geophysicae*, 14, 468-475.
24. Deters, B., J. P. Burrows and J. Orphal, 1998, *J. Geophys. Res.*, 103, 3563-3570.
25. Doucet, J., J. R. Gilbert, P. Sauvageau and C. Sandorfy, 1975, *J. Chem. Phys.*, 62, 366-369.
26. Ebenstein, W. L., J. R. Wiesenfeld and G. L. Wolk, 1978, *Chem. Phys. Lett.*, 53, 185-189.
27. Eden, C., H. Feilchenfeld and S. Manor, 1969, *Anal. Chem.*, 41, 1150-1151.
28. Felps, W. S., K. Rupnik and S. P. McGlynn, 1991, *J. Phys. Chem.*, 95, 639-656.
29. Fleischmann, O. C., J. P. Burrows and J. Orphal, 2003, *Photochem. Photobiol. A: Chem.*, 157, 127-136.
30. Francisco, J. S., M. R. Hand and I. H. Williams, 1996, *J. Phys. Chem.*, 100, 9250-9253.
31. Gilles, M. K., A. A. Turnipseed, J. B. Burkholder and A. R. Ravishankara, 1997, *J. Phys. Chem. A*, 101, 5526-5534.
32. Gillotay, D., A. Jenouvrier, B. Coquart, M. F. Mérienne and P. C. Simon, 1989, *Planet. Space Sci.*, 37, 1127-1140.
33. Gillotay, D. and P. C. Simon, 1988, *Annales Geophysicae*, 6, 211-215.
34. Gillotay, D. and P. C. Simon, 1989, *J. Atmos. Chem.*, 8, 41-62.
35. Gillotay, D. and P. C. Simon, 1990, *Aeronomica Acta A*, A356, 1-173.
36. Gillotay, D., P. C. Simon and L. Dierickx, 1988, *Aeronomica Acta*, A335, 1-25.
37. Giolando, D. M., G. B. Fazekas, W. D. Taylor and G. A. Takacs, 1980, *J. Photochem.*, 14, 335-339.
38. Goodeve, C. F. and A. W. C. Taylor, 1935, *Proc. Roy. Soc. London, A* 152, 221-230.
39. Gordus, A. A. and R. B. Bernstein, 1954, *J. Chem. Phys.*, 22, 790-795.
40. Gosnell, R. R., A. J. Taylor and J. L. Lyman, 1991, *J. Chem. Phys.*, 94, 5949-5953.
41. Gray, L. T. M. and D. W. G. Style, 1930, *Proc. Roy. Soc. London, A* 126, 603-612.
42. Harwood, M. H., J. B. Burkholder and A. R. Ravishankara, 1998, *J. Phys. Chem. A*, 102, 1309-1317.
43. Haugen, H. K., E. Weitz and S. R. Leone, 1985, *J. Chem. Phys.*, 83, 3402-3412.
44. Hemenway, C. P., T. G. Lindeman and J. R. Wiesenfeld, 1979, *J. Chem. Phys.*, 70, 3560-3561.
45. Hippler, H., S. Luu, H. Teitelbaum and J. Troe, 1978, *Int. J. Chem. Kinet.*, 10, 155-169.
46. Houel, N. and H. Van den Bergh, 1977, *Int. J. Chem. Kinet.*, 9, 867-874.
47. Hubinger, S. and J. B. Nee, 1995, *J. Photochem. and Photobiol. A: Chem.*, 86, 1-7.
48. Huebert, B. J. and R. M. Martin, 1968, *J. Phys. Chem.*, 72, 3046-3048.
49. Ibuki, T., 1992, *J. Chem. Phys.*, 96, 8793-8798.

50. Ibuki, T., N. Takahashi, A. Hiraya and K. Shobatake, 1986, J. Chem. Phys., 85, 5717-5722.
51. Ingham, T., D. Bauer, J. Landgraf and J. N. Crowley, 1998, J. Phys. Chem. A, 102, 3293-3298.
52. Jee, Y.-J., Y.-S. Jung and K.-H. Jung, 2001, J. Chem. Phys., 115, 9739-9746.
53. Jee, Y.-J., M. S. Park, Y. S. Kim, Y.-S. Jung and K.-H. Jung, 1998, Chem. Phys. Lett., 287, 701-708.
54. Jost, W., 1931, Z. Phys. Chem. A, 153, 143-152.
55. Jung, Y.-J., M. S. Park, Y. S. Kim, K.-H. Jung and H.-R. Volpp, 1999, J. Chem. Phys., 111, 4005-4012.
56. Knight, G. P., A. R. Ravishankara and J. B. Burkholder, 2000, J. Phys. Chem. A, 104, 11121-11125.
57. Kozlov, S. N., V. L. Orkin, R. E. Huie and M. J. Kurylo, 2003, J. Phys. Chem. A, 107, 1333-1338.
58. Krajnovich, D., Z. Zhang, L. Butler and Y. T. Lee, 1984, J. Chem. Phys., 88, 4561-4566.
59. Laszlo, B., R. E. Huie, M. J. Kurylo and A. W. Miziolek, 1997, J. Geophys. Res., 102, 1523-1532.
60. Lee, S.-H., Y.-J. Jung and K.-H. Jung, 2000, Chem. Phys., 260, 143-150.
61. Libuda, H. G. Spektroskopische und kinetische Untersuchungen an halogenierten Carbonylverbindungen von atmosphärischem Interesse, PhD-Thesis, University of Wuppertal, Germany, 1992.
62. Libuda, H. G., F. Zabel and K. H. Becker. "UV spectra of some organic chlorine and bromine compounds of atmospheric interest"; Kinetics and Mechanisms for the Reactions of Halogenated Organic Compounds in the Troposphere. STEP-HALOCIDE/AFEAS WORKSHOP, 1991, Dublin, Ireland, 126-131.
63. Lindeman, T. G. and J. R. Wiesenfeld, 1979, J. Chem. Phys., 70, 2882-2888.
64. Lock, M., R. J. Barmes and A. Sinha, 1996, J. Phys. Chem., 100, 7972-7980.
65. Maloney, K. K. and H. B. Palmer, 1973, Int. J. Chem. Kinet., 5, 1023-1037.
66. Man, S.-Q., W. M. Kwok, D. L. Phillips and A. E. Johnson, 1996, J. Chem. Phys., 105, 5842-5857.
67. Maric, D., J. P. Burrows and G. K. Moortgat, 1994, J. Photochem. Photobiol A: Chem., 83, 179-192.
68. McGivern, W. S., R. Li, P. Zou and S. W. North, 1999, J. Chem. Phys., 111, 5771-5779.
69. Miller, C. E., S. L. Nickolaisen, J. S. Francisco and S. P. Sander, 1997, J. Chem. Phys., 107, 2300-2307.
70. Minaev, B. F., 1999, J. Phys. Chem. A, 103, 7294-7309.
71. Molina, L. T. and M. J. Molina, 1983, J. Phys. Chem., 87, 1306-1308.
72. Molina, L. T., M. J. Molina and F. S. Rowland, 1982, J. Phys. Chem., 86, 2672-2676.
73. Moortgat, G. K., R. Meller and W. Schneider. Temperature dependence (256-296K) of the absorption cross-sections of bromoform in the wavelength range 285-360 nm. In *The Tropospheric Chemistry of Ozone in the Polar Regions*; H. Niki and K. H. Becker, Eds.; Springer-Verlag: Berlin, 1993; pp 359-369.
74. Mossinger, J. C., D. E. Shallcross and R. A. Cox, 1998, J. Chem. Soc. Faraday Trans., 94, 1391-1396.
75. Nee, J. B., M. Suto and L. C. Lee, 1986, J. Chem. Phys., 85, 4919-4924.
76. Okabe, H., 1977, J. Chem. Phys., 66, 2058-2062.
77. Okabe, H., 1983, J. Chem. Phys., 78, 1312-1317.
78. Orkin, V. L. and E. E. Kasimovskaya, 1995, J. Atm. Chem, 21, 1-11.
79. Orkin, V. L., V. G. Khamaganov, A. G. Guschin, R. E. Huie and M. J. Kurylo, 1997, J. Phys. Chem. A, 101, 174-178.
80. Orkin, V. L., F. Louis, R. E. Huie and M. J. Kurylo, 2002, J. Phys. Chem. A, 106, 10195-10199.
81. Orlando, J. J. and J. B. Burkholder, 1995, J. Phys. Chem., 99, 1143-1150.
82. Orlando, J. J., J. B. Burkholder, A. M. R. P. Bopegedera and C. J. Howard, 1991, J. Mol. Spectrosc., 145, 278-289.
83. Passchier, A. A., J. D. Christian and N. W. Gregory, 1967, J. Phys. Chem., 71, 937-942.
84. Pence, W., S. Baughum and S. Leone, 1981, J. Phys. Chem., 85, 3844-3851.
85. Petersen, A. B. and I. W. M. Smith, 1978, Chem. Phys., 30, 407-413.
86. Peterson, K. A. and J. S. Francisco, 2002, J. Chem. Phys., 117, 6103-6107.
87. Rattigan, O. V., R. L. Jones and R. A. Cox, 1994, Chem. Phys. Lett., 230, 121-126.
88. Rattigan, O. V., D. J. Lary, R. L. Jones and R. A. Cox, 1996, J. Geophys. Res., 101, 23021-23033.
89. Ravishankara, A. R., P. H. Wine and A. O. Langford, 1979, Chem. Phys. Lett., 63, 479-484.
90. Regan, P. M., S. R. Langford, A. J. Orr-Ewing and M. N. R. Ashfold, 1999, J. Chem. Phys., 110, 281-288.
91. Ribaud, M. G., 1919, Ann. Phys., 12, 107-226.
92. Robbins, D. E., 1976, Geophys. Res. Lett., 3, 213-216. See also Erratum, GRL, 1976, Vol. 3, p. 757.
93. Romand, J., 1949, Ann. Phys. (Paris), 4, 529-590.
94. Röth, E. P., R. Ruhnke, G. Moortgat, R. Meller and W. Schneider "UV/VIS-Absorption Cross Sections and Quantum Yields for Use in Photochemistry and Atmospheric Modeling," Forschungszentrum Jülich Publication, Part 1 : Inorganic Substances (jül-3340), Part 2: Organic Substances (jül-3341), 1997
95. Rowley, D. M., M. H. Harwood, R. A. Freshwater and R. L. Jones, 1996, J. Phys. Chem., 100, 3020-3029.
96. Roxlo, C. and A. Mandl, 1980, J. Appl. Phys., 51, 2969-2972.
97. Sander, S. P. and R. R. Friedl, 1989, J. Phys. Chem., 93, 4764-4771.
98. Scheffler, D., H. Grothe, H. Willner, A. Frenzel and C. Zetzsch, 1997, Inorg. Chem., 36, 335 - 38.
99. Seccombe, D. P., R. Y. L. Chim, R. P. Tuckett, H. W. Jochims and H. Baumgaertel, 2001, J. Chem. Phys., 114, 4058-4073.

100. Seccombe, D. P., R. P. Tuckett, H. Baumgärtel and H. W. Jochims, 1999, *Phys. Chem. Chem. Phys.*, 1, 773-782.
101. Seery, D. J. and D. Britton, 1964, *J. Phys. Chem.*, 68, 2263-2266.
102. Sidebottom, H. W., J. M. Tedder and J. C. Walton, 1969, *Trans. Faraday Soc.*, 65, 755-762.
103. Soller, R., J. M. Nicovich and P. H. Wine, 2002, *J. Phys. Chem. A*, 106, 8378-8385.
104. Spencer, J. E. and F. S. Rowland, 1978, *J. Phys. Chem.*, 82, 7-10.
105. Sulzer, P. and K. Wieland, 1952, *Helv. Phys. Acta*, 25, 653-676.
106. Taketani, F., K. Takahashi and Y. Matsumi, 2005, *J. Phys. Chem. A*, 109, 2855-2860.
107. Talukdar, R., A. Mellouki, T. Gierczak, J. B. Burkholder, S. A. McKeen and A. R. Ravishankara, 1991, *Science*, 252, 693-695.
108. Talukdar, R. K., M. Hunter, R. F. Warren, J. B. Burkholder and A. R. Ravishankara, 1996, *Chem. Phys. Lett.*, 262, 669-674.
109. Talukdar, R. K., G. L. Vashjani and A. R. Ravishankara, 1992, *J. Chem. Phys.*, 96, 8194-8201.
110. Tellinghuisen, J., 2003, *J. Phys. Chem. A*, 107, 753-775.
111. Tellinghuisen, J., 2008, *J. Phys. Chem. A*, 112, 5902-5907.
112. Tzeng, W. B., Y. R. Lee and S. M. Lin, 1994, *Chem. Phys. Lett.*, 227, 467-471.
113. Uthman, A. P., P. J. Demlein, T. D. Allston, M. C. Withiam, M. J. McClements and G. A. Takacs, 1978, *J. Phys. Chem.*, 82, 2252-2257.
114. Vaghjiani, G., 1993, *J. Chem. Phys.*, 99, 5936-5943.
115. Vatsa, R. K., A. Kumar, P. D. Naik, K. V. S. Rama Rao and J. P. Mittal, 1993, *Chem. Phys. Lett.*, 207, 75-80.
116. Vetter, R., T. Ritschel and L. Zulicke, 2003, *J. Phys. Chem., A*, 107, 1405-1412.
117. Wahner, A., A. R. Ravishankara, S. P. Sander and R. R. Friedl, 1988, *Chem. Phys. Lett.*, 152, 507-512.
118. Walton, J. C., 1972, *J. Chem. Soc. Farad. Trans.*, 68, 1559-1565.
119. Wen, W. Y. and R. M. Noyes, 1972, *J. Phys. Chem.*, 76, 1017-1018.
120. Wheeler, M. D., S. M. Newman, T. Ishiwata, M. Kawasaki and A. J. Orr-Ewing, 1998, *Chem. Phys. Lett.*, 285, 346-351.
121. Wilmouth, D. M., T. F. Hanisco, N. M. Donahue and J. G. Anderson, 1999, *J. Phys. Chem A*, 103, 8935-8945.
122. Xu, D., J. S. Francisco, J. Huang and W. M. Jackson, 2002, *J. Chem. Phys.*, 117, 2578-2585.
123. Zaraga, F., N. S. Nogar and C. B. Moore, 1976, *J. Mol. Spectrosc.*, 63, 564-571.
124. Zhang, L., W. Fuss and K. L. Kompa, 1990, *Chem. Phys.*, 144, 289-297.
125. Zou, P., W. S. McGivern and S. W. North, 2000, *Phys. Chem. Chem. Phys.*, 2, 3785-3790.
126. Zou, P., W. S. McGivern, O. Sokhabi, A. G. Suits and S. W. North, 2000, *J. Chem. Phys.*, 113, 7149-7157.

SECTION 4H. IO_x PHOTOCHEMISTRY



(Recommendation: 06-2, Note: 10-6, Evaluated: 10-6)

Absorption Cross Sections: The UV/vis absorption spectrum of molecular iodine, I₂, between 180 and 750 nm consists of several overlapping electronic transitions. The spectrum has a strong absorption band below 210 nm that peaks at ~181 nm and contains some diffuse band structure. Between 210 and 380 nm the spectrum is continuous with decreasing absorption cross sections toward longer wavelength and a minimum cross section of $\sim 1 \times 10^{-20}$ cm² molecule⁻¹ at 380 nm. The visible region of the spectrum shows a strong broad band between 400 and 650 nm that is continuous below 500 nm but shows pronounced rovibrational structure between 500 and 630 nm. The structure is due to the transition from the X¹Σ ground state to the bound B³Π upper state. There is also a weaker underlying continuum in the structured region with a maximum near 533 nm that is due to a transition to a ¹Π repulsive state. At wavelengths >650 nm there is evidence for another weak absorption band. There have been numerous studies of the I₂ absorption spectrum as summarized in Table 4H-1.

Table 4H-1. Summary of I₂ Absorption Cross Sections Studies

Study	Year	Temperature (K)	Wavelength (nm)	10 ²⁰ σ(500 nm) (cm ²)
Vogt and Koenigsberger [113]	1923	321 – 673	400 – 600	–
Rabinowitch and Wood [84]	1936	298	440 – 650	~291
Kortüm and Friedheim [60]	1947	353	450 – 580	~160 ± 30
Kortüm and Friedheim [60]	1947	613	230 – 600	~170 ± 30
Sulzer and Wieland [104]	1952	423 – 1323	360 – 740	*
Mathieson and Rees [70]	1956	393	600 – 850	–
McMillan [21]	1966	348	400 – 650	218
Myer and Samson [73]	1970	298	105 – 220	–
Tellinghuisen [105]	1973	298	420 – 800	219
Roxlo and Mandl [90]	1980	298	170 – 230	–
Bauer et al. [10]	1998	298	436 and 500	225 ± 9
Saiz-Lopez et al. [91]	2004	298	182 – 750	229 ± 27
Spietz [100]	2005	298	428 – 588	–
Spietz et al. [102]	2006	298	500	219 ± 2

Note:

Uncertainties as reported

* Cross section values at 488 nm are in the range (176 – 113) × 10⁻²⁰ cm² molecule⁻¹ over the temperature range 423 – 1323

The most recent cross section data sets from Tellinghuisen [105], Saiz-Lopez et al. [91], and Spietz et al. [100, 102] are the primary focus of this evaluation. Tellinghuisen [105] reported room temperature cross sections obtained with a continuum light source at moderate resolution (~2.5 nm). Saiz-Lopez et al. [91] used a Fourier transform spectrometer to record spectra at a resolution of 4 cm⁻¹ (0.1 nm at 500 nm). Spietz [100, 102] used a grating/CCD spectrometer with a resolution of 0.25 nm. The reported spectra show the largest differences in the structured and long wavelength regions of the spectrum. A direct comparison of cross section data in the structured region is, however, difficult due to the differences in measurement resolution. Saiz-Lopez et al. [91] examined the cross section dependence on absolute I₂ concentration and bath gas pressure. Their final cross section data were obtained at high bath gas pressure and high resolution. The cross section data sets agree in the structured region to within ~15% when averages over 5 nm intervals are compared. There are significant discrepancies between the Tellinghuisen [105] and Saiz-Lopez et al. [91] spectra at wavelengths > ~600 nm with differences increasing from 35% at 600 nm to factors of ~2 and ~20 at 710 and 740 nm, respectively. The cross sections reported by Bauer et al. [10] at 436 and 500 nm, (1.41 ± 0.05) × 10⁻¹⁸ and (2.25 ± 0.09) × 10⁻¹⁸ cm² molecule⁻¹, respectively, are in agreement with the Saiz-Lopez et al. [91] values.

The recommended absorption cross sections listed in Table 4H-2 are averages over 5 nm intervals of the data reported by Saiz-Lopez et al. [91] and are appropriate of atmospheric photolysis rate calculations. Higher resolution cross section data should be obtained from the original studies. Table 4H-3 lists the absorption cross sections at the maxima and minima in the banded region reported by Saiz-Lopez et al. [91].

Photolysis Quantum Yield and Product Studies: Photodissociation quantum yields for I₂ in the structured region of the spectrum were measured by Brewer and Tellinghuisen [16] using atomic fluorescence under conditions of steady-state irradiation of I₂ at 12 wavelengths in the region 501 – 624 nm. The quantum yields were determined relative to the purely dissociative continuum at 492 nm where a unity quantum yield is assumed. The quantum yields were found to be wavelength dependent with values ranging from 0.9 to 0.33.

Table 4H-2. Absorption Cross Sections of I₂ at 295 K

λ (nm)	$10^{20} \sigma$ (cm ²)	λ (nm)	$10^{20} \sigma$ (cm ²)	λ (nm)	$10^{20} \sigma$ (cm ²)	λ (nm)	$10^{20} \sigma$ (cm ²)
185	1853	315	15.1	445	25.8	575	96.6
190	2012	320	12.2	450	33.3	580	92.7
195	1226	325	10.5	455	44.0	585	74.1
200	732	330	7.79	460	57.1	590	65.8
205	519	335	6.18	465	72.2	595	59.4
210	418	340	4.71	470	89.7	600	47.4
215	352	345	4.08	475	109	605	43.3
220	302	350	2.58	480	131	610	40.8
225	290	355	1.94	485	155	615	34.4
230	225	360	1.24	490	179	620	30.5
235	197	365	1.02	495	204	625	28.2
240	169	370	0.659	500	228	630	28.0
245	147	375	0.823	505	254	635	22.6
250	128	380	1.14	510	277	640	23.6
255	110	385	1.01	515	297	645	22.8
260	97.1	390	0.925	520	309	650	21.6
265	84.2	395	1.11	525	319	655	20.7
270	72.9	400	2.93	530	326	660	19.0
275	63.1	405	3.89	535	320	665	17.3
280	54.4	410	4.43	540	306	670	17.7
285	45.9	415	5.44	545	281	675	15.9
290	38.9	420	5.96	550	265	680	14.9
295	32.4	425	8.32	555	237	685	13.9
300	27.4	430	13.5	560	191	690	12.8
305	23.1	435	15.7	565	155	695	10.9
310	18.1	440	20.3	570	130	700	10.3

Note:

185 – 700 nm: Saiz-Lopez et al. [91]

Table 4H-3. Cross Sections at the Maxima and Minima of I₂ at 295 K

λ (nm) Maximum	$10^{20} \sigma$ (cm ²)	λ (nm) minimum	$10^{20} \sigma$ (cm ²)	λ (nm) maximum	$10^{20} \sigma$ (cm ²)	λ (nm) minimum	$10^{20} \sigma$ (cm ²)
500.6	232.5	500.7	231.5	543.6	406.7	545.1	225.3
500.8	233.9	501.0	231.0	545.4	240.5	545.6	219.9
501.1	235.9	501.2	233.7	545.8	371.9	547.4	231.3
501.4	236.6	501.6	234.8	547.6	246.7	548.1	208.0
501.8	239.6	501.9	236.3	548.4	372.2	549.7	226.5
502.1	240.5	502.4	238.8	550.0	251.7	550.6	197.1
502.6	246.5	502.8	240.6	550.8	347.6	552.1	220.6
503.0	247.8	503.3	240.6	552.4	256.8	553.2	187.0
503.5	252.3	503.8	241.0	553.5	321.4	554.6	211.2
504.0	254.4	504.4	243.7	554.8	257.7	555.8	176.3
504.5	255.6	504.9	245.1	556.2	299.4	557.1	200.3
505.2	263.2	505.6	252.0	557.5	254.2	558.6	161.2
505.8	268.7	506.2	252.7	559.0	263.9	559.8	186.1
506.5	271.6	507.0	252.3	560.1	250.0	561.5	126.8
507.2	275.4	507.7	253.7	561.9	203.1	562.7	153.9
507.9	281.7	508.5	254.6	562.9	216.0	564.5	103.7
508.7	284.4	509.3	255.0	564.9	175.0	565.4	143.7
509.6	291.1	510.3	262.8	565.8	208.0	567.5	96.9
510.5	301.6	511.2	264.1	568.1	142.9	568.4	115.4
511.5	308.1	512.2	266.0	568.7	203.5	569.5	131.4
512.5	309.9	513.3	263.0	569.9	139.8	570.7	70.3
513.6	323.1	514.4	266.1	571.0	127.5	571.4	113.9
514.7	325.9	515.6	266.4	571.7	147.2	573.9	76.1
515.9	334.3	516.8	265.0	574.9	131.8	577.3	68.8
517.1	345.9	518.1	269.2	578.1	122.6	580.7	62.7
518.3	353.6	519.4	266.0	581.4	109.7	584.3	51.8
519.8	356.6	520.9	267.1	585.1	105.4	587.8	48.6
521.1	371.0	522.3	267.3	588.7	95.9	591.7	42.4
522.7	379.3	523.9	259.8	592.1	85.7	595.4	42.8
524.2	384.5	525.4	261.4	596.0	80.5	599.1	34.3
525.8	393.7	527.2	252.8	599.6	76.0	603.0	31.6
527.4	398.8	528.9	258.7	603.5	64.3	606.8	28.8
529.2	407.8	530.8	252.2	607.6	53.8	610.8	30.3
531.0	415.9	532.7	242.1	611.8	49.1	614.6	26.4
533.0	423.8	534.7	242.8	615.5	42.5	618.8	26.7
534.9	416.4	536.7	232.6	620.0	37.4	622.2	22.3
537.0	414.8	538.8	224.4	623.6	35.8	627.0	23.1
539.1	409.3	541.0	216.5	628.2	31.8	629.8	24.0
541.4	406.1	543.0	218.5				

Note:

Saiz-Lopez et al [91]



(Recommendation: 06-2, Note: 10-6, Evaluated: 10-6)

Absorption Cross Sections: The A ²Π_{3/2} ← X ²Π_{3/2} electronic transition for iodine monoxide, IO, yields a UV/vis absorption spectrum between 338 and 488 nm. The A –X band consists of a continuous absorption band with a maximum near 400 nm with a broad progression of vibrational bands superimposed on the continuum at wavelengths >400 nm. The pronounced vibrational band structure has been assigned to

progressions in v' , $7-0 \leftarrow 0$ and $3-1 \leftarrow 1$. Of particular interest (e.g. for the study of the reaction kinetics of IO) is the peak absorption cross section of the strongest vibrational band (4,0) at 427.2 nm. A summary of the available studies (which utilized photolysis of N_2O/I_2 , N_2O/CF_3I , and O_3/I_2 mixtures to produce IO) and the corresponding (4,0) peak cross sections at room temperature is given in Table 4H-4.

Table 4H-4. Summary of IO Absorption Cross Section Studies

Study	Year	Temperature (K)	Wavelength Range (nm)	Resolution (nm)	$\sigma(427.2 \text{ nm})$ 10^{-17} cm^2
Cox and Coker [26]	1983	303	415 – 470	0.27	$3.1^{+2.0}_{-1.5}$
Jenkin and Cox [48]	1985	303	426.9	0.27	2.2 ± 0.5
Sander [92]	1986	250, 273, 298, 317, 341, 373	427.2	0.17	3.1 ± 0.3
Stickel et al. [103]	1988	300	420 – 455 444.8 – 446.4	0.3 0.025	3.1 ± 0.6
Laszlo et al. [65]	1995	295	340 – 447	0.3	2.8 ± 0.5
Harwood et al [43]	1997	203, 220, 250, 338 – 488		0.14	$3.6 \pm 0.5^*$
		253, 275, 298, 323, 353, 373		0.44	3.0 ± 0.4
Atkinson et al. [4]	1999	295	444.48 – 447.83 454.98 – 457.88	0.0013	–
			445.04, 455.17	0.7	
Bloss et al. [15]	2001	220, 250, 273, 295, 325	342 – 455	1.13	1.9 ± 0.17
Dillon et al. [27]	2005	298	427.08, 427.2	0.08	3.55 ± 0.35
Gómez Martín et al. [41]	2005	298	427.7, 449.3, 484.9	0.12	3.5 ± 0.3
Spietz et al. [101]	2005	298	320.26 – 480.09	1.3	3.2

* Average value between 203 and 373 K (see text)

The shape of the 298 K spectra reported by Laszlo et al., Harwood et al. and Bloss et al. are similar but with notable differences in the magnitude of the vibrational features due to the dependence on the resolution of the measurement. The absorption cross sections reported by Harwood et al. with a resolution of 0.44 nm and scaled to 0.83 of the value obtained for the (4,0) peak cross section at higher resolution, 0.14 nm, are generally (with exceptions in the region 350 – 415 nm) higher than those reported by Laszlo et al. (0.3 nm resolution) and Bloss et al. (1.13 nm resolution). The Bloss et al. cross section data are the lowest throughout the spectral region 340 – 465 nm. The Bloss et al. cross section data are lower than the values reported by Harwood et al. by a factor of ~1.5 in the continuous region of the spectrum and at the peaks of the vibrational bands and up to factor of 5 at the minima between the vibrational bands. Bloss et al. attributed the differences in the spectra to an underlying absorption due to the absorbing species I_2O_2 that is considered to be a product of the IO self-reaction. The absorption spectrum of I_2O_2 is currently not known.

The absorption spectrum reported by Laszlo et al. is higher by a factor of ~1.2 – 1.5 in the wavelength region 350 – 370 nm and at the maxima in the 395 – 405-nm region than the values reported by Harwood et al. However, the spectra are similar in the region of the (6,0) to (4,0) maxima. The absorption cross section measured by Atkinson et al. at high resolution (0.0013 nm) for the (2,0) peak is higher by a factor of ~5 than that reported by Harwood et al. whereas the cross sections reported by Atkinson et al. and Harwood et al. for the (1,0) maximum are nearly the same.

The recommended cross sections in Table 4H-5 were obtained as follows: (1) the spectra of Harwood et al. and Laszlo et al. were degraded to the resolution of the spectrum of Bloss et al. (1.13 nm), (2) the degraded spectra of Harwood et al. were normalized to the (4,0) peak value of Bloss et al., (3) the mean of the degraded and normalized spectra of Harwood et al. and Laszlo et al. and that of Bloss et al. were calculated and averaged over 1 nm intervals. The studies of Dillon et al. [27], Gómez Martín et al. [41], and Spietz et al. [101] are noted but not considered in the present evaluation.

The temperature dependence of the absorption cross section of the (4,0) peak has been studied by Sander (250 – 373 K), Harwood et al. (203 – 373 K), and Bloss et al. (220 – 325 K). The results from these studies are significantly different. Sander report a significant increase in $\sigma(427 \text{ nm})$ from a value of $(2.1 \pm 0.1) \times 10^{-17} \text{ cm}^2 \text{ molecule}^{-1}$ at 373 K to $(5.3 \pm 0.5) \times 10^{-17} \text{ cm}^2 \text{ molecule}^{-1}$ at 250 K. Bloss et al. report a smaller increase in the absorption cross sections with the ratio $\sigma(T)/\sigma(295 \text{ K})$ being 0.85 and 1.23 at 325 K and 220 K, respectively. Harwood et al. used several pulsed laser photolysis sources of IO ($\text{N}_2\text{O}/\text{CF}_3\text{I}$, O_3/I_2 , and $\text{N}_2\text{O}/\text{I}_2$) in their experiments and reported absorption cross sections between $(3.1 \pm 0.4) \times 10^{-17}$ and $(3.9 \pm 0.1) \times 10^{-17} \text{ cm}^2 \text{ molecule}^{-1}$ independent of temperature (203 – 373 K) and report an average value of $(3.6 \pm 0.5) \times 10^{-17} \text{ cm}^2 \text{ molecule}^{-1}$.

Photolysis Quantum Yield and Product Studies: The quantum yield for $\text{O}(^3\text{P})$ formation following photolysis of IO at 355 nm was measured relative to NO_2 photolysis at the same wavelength to be 0.91 ($^{+0.19}_{-0.26}$) by Ingham et al. [47]. The lifetime of the $\text{A } ^2\Pi_{3/2}$ was measured to be $< 20 \text{ ns}$ by Turnipseed et al. [108], which indicates that electronic collisional quenching does not compete with the dissociation into $\text{O}(^3\text{P}) + \text{I}$. This is consistent with the results of Ingham et al.

Table 4H-5. Absorption Cross Sections of IO at 298 K

λ (nm)	$10^{20} \sigma$ (cm^2)	λ (nm)	$10^{20} \sigma$ (cm^2)	λ (nm)	$10^{20} \sigma$ (cm^2)	λ (nm)	$10^{20} \sigma$ (cm^2)
339	81.2	373	381	407	606	441	219
340	118	374	413	408	578	442	168
341	100	375	422	409	643	443	183
342	107	376	402	410	813	444	195
343	89	377	413	411	1010	445	957
344	96.2	378	435	412	976	446	805
345	86.2	379	463	413	786	447	392
346	126	380	504	414	589	448	214
347	112	381	548	415	568	449	269
348	108	382	472	416	414	450	156
349	142	383	435	417	460	451	96.9
350	160	384	523	418	734	452	102
351	154	385	560	419	1380	453	87.3
352	165	386	591	420	1200	454	100
353	163	387	603	421	681	455	457
354	181	388	580	422	365	456	441
355	185	389	598	423	253	457	213
356	194	390	622	424	204	458	132
357	207	391	620	425	205	459	183
358	223	392	617	426	302	460	123
359	230	393	642	427	2050	461	82.3
360	242	394	684	428	1370	462	51.9
361	247	395	694	429	543	463	53.6
362	242	396	709	430	309	464	38.2
363	241	397	701	431	208	465	43.4
364	268	398	654	432	173	466	118
365	273	399	671	433	166	467	134
366	291	400	671	434	177	468	67.2
367	313	401	700	435	653	469	24.2
368	326	402	765	436	1880	470	125
369	343	403	859	437	807	471	76.4
370	346	404	864	438	381		
371	339	405	787	439	249		
372	360	406	667	440	256		

Note:

339 – 471 nm: see text



(Recommendation: 06-2, Note: 10-6, Evaluated: 10-6)

Absorption Cross Sections: A qualitative absorption spectrum of iodine dioxide, OIO, was first reported by Himmelmann et al. [45] at 298 K over the wavelength range 476 – 667 nm. The absorption spectrum is highly structured due to transitions in $\text{A } (^2\text{A}_2) (\text{i,j,k}) \leftarrow \text{X } (^2\text{B}_1) (0,0,0)$ band with vibrational progressions in the upper state of the symmetric I-O stretch ($\text{i} = 0\text{--}9$) and O-I-O bend ($\text{j} = 0, 1, 2$). A first assessment indicated that the absorption cross section at 549.1 nm (in air, 0.3 nm resolution) to be $>2.5 \times 10^{-17} \text{ cm}^2 \text{ molecule}^{-1}$. Absorption cross sections have been measured at room temperature by Cox et al. [25] (400 – 600 nm) and Bloss et al. [15] (514 – 573 nm) at a resolution of 1.13 nm, Spietz et al. [101] (392 – 660 nm) and Gómez Martín et al. [41] at a resolution of 1.3 nm who report a cross section of $(1.3 \pm 0.3) \times 10^{-17} \text{ cm}^2 \text{ molecule}^{-1}$ at 549.1 nm, and at high resolution ($<0.006 \text{ nm}$) using cavity ring-down spectroscopy by Ashworth et al. [3] and Joseph et al. [51] (558 – 578 nm). Joseph et al. [51] report a cross section of $(1.5 \pm 0.18) \times 10^{-17} \text{ cm}^2 \text{ molecule}^{-1}$ at 567.93 nm.

The peak cross sections at 562 and 568 nm obtained at high resolution are higher by a factor ~ 1.7 than those reported for a resolution of 1.13 nm. The recommended cross sections listed in Table 4H-6 were obtained by averaging the data reported by Bloss et al. [15] over 1 nm intervals (reported at intervals of 0.22 nm). The estimated uncertainty in the absolute absorption cross sections is a factor of 3.

Photolysis Quantum Yield and Product Studies: Ingham et al. [47] studied the photodissociation of OIO at 532 nm. $\text{O}(^3\text{P})$ atom formation was not detected and an upper limit for the O atom quantum yield of <0.012 was reported (based on an OIO absorption cross section of $2.4 \times 10^{-17} \text{ cm}^2 \text{ molecule}^{-1}$ at 532 nm). Subsequently, Ashworth et al. [3] inferred that OIO predissociates to $\text{I} + \text{O}_2$ via the upper $^2\text{B}_2$ state. Ingham et al. [47] detected $\text{I}(^2\text{P}_j)$ atoms at high photolysis laser fluence, presumably in a sequential two-photon process, and an upper limit for the I atom quantum yield of <0.15 was reported. Joseph et al. [51] report the photolysis quantum yield of OIO at 562 nm to be <0.10 . Tucceri et al. [107] used pulsed laser photolysis combined with transient absorption spectroscopy/resonance fluorescence detection techniques and reported I atom quantum yields of <0.05 in the wavelength range 560 – 580 nm and <0.24 at 532 nm. A study by Gómez Martín et al. [40] contradicts the results from Joseph et al. [51], Ingham et al. [47], and Tucceri et al. [107]. Gómez Martín et al. [40] used a tunable pulsed laser photolysis source combined with cavity ring-down spectroscopy detection of OIO and atomic resonance fluorescence detection of I atoms. They report an I atom quantum yield of (1.07 ± 0.15) over the wavelength range 480 – 650 nm. In an additional study from the same group, Gómez Martín et al. [39] report the IO quantum yield to be unity at wavelengths $<480 \text{ nm}$. No quantum yield recommendation is given.

Table 4H-6. Absorption Cross Sections of OIO at 295 K

λ (nm)	$10^{20} \sigma$ (cm^2)	λ (nm)	$10^{20} \sigma$ (cm^2)	λ (nm)	$10^{20} \sigma$ (cm^2)	λ (nm)	$10^{20} \sigma$ (cm^2)
516	833	531	989	546	582	561	476
517	696	532	1012	547	513	562	769
518	565	533	779	548	665	563	709
519	599	534	636	549	1030	564	524
520	719	535	519	550	842	565	442
521	626	536	643	551	575	566	384
522	573	537	709	552	429	567	613
523	517	538	640	553	377	568	937
524	496	539	548	554	609	569	699
525	534	540	470	555	661	570	475
526	754	541	451	556	604	571	322
527	840	542	494	557	474	572	224
528	697	543	715	558	393		
529	626	544	817	559	373		
530	651	545	676	560	350		

Note:

516 – 572 nm: Bloss et al. [15]



(Recommendation: 06-2, Note: 10-6, Evaluated: 10-6)

Table 4H-7. Summary of HI Absorption Cross Sections Studies

Study	Year	Temperature (K)	Wavelength (nm)	10 ²⁰ σ(222 nm) (cm ²)
Goodeve and Taylor [42]	1936	298	200 – 368	69
Romand [88]	1949	298	149 – 159, 164 – 175, 178 – 244	62
Huebert and Martin [46]	1968	195 296	180 – 200 180 – 300	– 81
Ogilvie [75]	1971	298	192 – 313	84
Roxlo and Mandl [90]	1980	298	170 – 230	62
Bridges and White [18]	1973	298	254	–
Rebberet et al. [86]	1973	298	147	–
Campuzano-Jost and Crowley [22]	1999	298	198 – 341	81

Absorption Cross Sections: The UV absorption spectrum of hydrogen iodide, HI, at wavelengths >180 nm has a continuous absorption band with a maximum near 222 nm. At wavelengths <180 nm the spectrum shows strong diffuse band structure. The available studies are summarized in Table 4H-7. For wavelengths >180 nm there is good agreement between the room temperature absorption cross sections reported by Campuzano-Jost and Crowley [22], Ogilvie [75], and Huebert and Martin [46]. The data reported by Huebert and Martin [46] and Campuzano-Jost and Crowley [22] are nearly identical around the absorption maximum and out to ~275 nm. The cross sections reported by Ogilvie [75] are slightly greater. At wavelengths >280 nm, the absorption spectra from these three studies diverge somewhat with the cross sections reported by Huebert and Martin [46] being greater and those of Ogilvie [75] being smaller than the cross sections reported by Campuzano-Jost and Crowley [22]. The recommended cross sections listed in Table 4H-8 are average values over 1 nm intervals of the high resolution (0.08 nm) data from Campuzano-Jost and Crowley [22].

Photolysis Quantum Yield and Product Studies: Martin and Willard [68] measured the quantum yield for H and I atoms in the photolysis of HI at 184.9 and 253.7 nm to be near unity. A quantum yield for the loss of HI of unity is recommended for wavelengths >180 nm. Brewer et al. [17] reported the relative quantum yield for the formation of I*(²P_{1/2}) to be 0.47 ± 0.03 at 248 nm. Using broadband flash photolysis Donohue and Wiesenfeld [28] obtained an I*(²P_{1/2}) yield of 0.10 ± 0.05. Langford et al. [64] measured the branching ratio I*(²P_{1/2})/I(²P_{3/2}) in a detailed study at 24 different wavelengths in the range 200 – 303 nm. They reported a wavelength dependence of the ratio with a value of 0.2 near 208 nm, a maximum value of 1.7 near 252 nm, and a value of 0.1 at 303 nm. These authors review several similar earlier studies and should be consulted for more detailed information.

Table 4H-8. Absorption Cross Sections of HI at 298 K

λ (nm)	$10^{20} \sigma$ (cm ²)	λ (nm)	$10^{20} \sigma$ (cm ²)	λ (nm)	$10^{20} \sigma$ (cm ²)	λ (nm)	$10^{20} \sigma$ (cm ²)
199	59.7	235	71.9	271	16.1	307	1.29
200	61.1	236	70.6	272	15.1	308	1.19
201	62.4	237	69.2	273	14.2	309	1.10
202	63.7	238	67.6	274	13.3	310	1.01
203	65.0	239	66.2	275	12.5	311	0.929
204	66.4	240	64.6	276	11.7	312	0.852
205	67.7	241	62.9	277	10.9	313	0.781
206	69.0	242	61.3	278	10.2	314	0.715
207	70.3	243	59.6	279	9.57	315	0.653
208	71.5	244	57.9	280	8.94	316	0.596
209	72.7	245	56.1	281	8.36	317	0.544
210	73.8	246	54.2	282	7.81	318	0.495
211	74.8	247	52.5	283	7.30	319	0.450
212	75.9	248	50.7	284	6.82	320	0.409
213	76.9	249	48.8	285	6.37	321	0.371
214	77.7	250	47.0	286	5.94	322	0.336
215	78.4	251	45.2	287	5.55	323	0.303
216	79.1	252	43.5	288	5.18	324	0.274
217	79.7	253	41.7	289	4.83	325	0.247
218	80.2	254	39.9	290	4.51	326	0.223
219	80.5	255	38.2	291	4.21	327	0.200
220	80.8	256	36.5	292	3.92	328	0.180
221	80.9	257	34.8	293	3.66	329	0.162
222	81.0	258	33.2	294	3.41	330	0.145
223	80.9	259	31.6	295	3.18	331	0.130
224	80.7	260	30.0	296	2.96	332	0.116
225	80.4	261	28.5	297	2.76	333	0.104
226	80.0	262	27.1	298	2.57	334	0.0928
227	79.5	263	25.7	299	2.40	335	0.0828
228	78.9	264	24.3	300	2.23	336	0.0740
229	78.2	265	23.0	301	2.07	337	0.0660
230	77.4	266	21.7	302	1.92	338	0.0591
231	76.5	267	20.5	303	1.77	339	0.0528
232	75.5	268	19.4	304	1.64	340	0.0470
233	74.4	269	18.3	305	1.52		
234	73.2	270	17.2	306	1.40		

Note:

199 – 340 nm: Campuzano-Jost and Crowley [22]



(Recommendation: 06-2, Note: 10-6, Evaluated: 10-6)

Absorption Cross Sections: The absorption spectrum of hypiodous acid, HOI, has been measured at room temperature by Bauer et al. [10] (280 – 500 nm) and Rowley et al. [89] (280 – 450 nm). In these studies HOI was produced by reacting OH, which was generated by pulsed laser photolysis, with I₂. Absorption cross sections were determined assuming iodine mass balance and the measured loss of I₂. Two absorption bands of comparable intensity were observed, one between 280 and ~375 nm with a maximum near 340 nm and the other between ~375 and 500 nm with a maximum near 408 nm. The spectra of Bauer et al. [10] and Rowley et al. [89] are in reasonable agreement with slight differences in the wavelength of the absorption maxima, 2 – 3 nm, and absolute cross sections, less than ~15% difference. The recommended cross sections listed in Table 4H-9 are the mean of the values reported by Rowley et al. [89] and Bauer et al. [10].

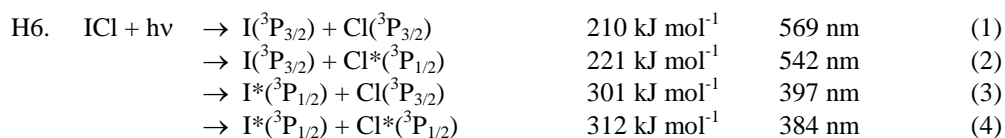
Photolysis Quantum Yield and Product Studies: The OH quantum yield in the photolysis of HOI at 355 nm was measured by Bauer et al. to be close to unity.

Table 4H-9. Absorption Cross Sections of HOI at 298 K

λ (nm)	$10^{20} \sigma$ (cm ²)	λ (nm)	$10^{20} \sigma$ (cm ²)	λ (nm)	$10^{20} \sigma$ (cm ²)	λ (nm)	$10^{20} \sigma$ (cm ²)
280	0.077	332	36.1	384	20.8	436	11.9
282	0.121	334	37.6	386	22.1	438	10.6
284	0.186	336	38.5	388	23.4	440	9.30
286	0.281	338	39.1	390	24.8	442	8.10
288	0.417	340	39.2	392	26.1	444	7.03
290	0.608	342	38.9	394	27.3	446	6.05
292	0.867	344	38.2	396	28.4	448	5.17
294	1.22	346	37.1	398	29.4	450	4.40
296	1.68	348	35.6	400	30.1	452	3.72
298	2.27	350	33.9	402	30.6	454	3.13
300	3.02	352	32.0	404	30.9	456	2.61
302	3.95	354	30.1	406	30.9	458	2.17
304	5.09	356	28.0	408	30.7	460	1.79
306	6.44	358	26.0	410	30.2	462	1.47
308	8.03	360	24.1	412	29.5	464	1.20
310	9.85	362	22.4	414	28.5	466	0.973
312	11.9	364	20.8	416	27.4	468	0.785
314	14.2	366	19.5	418	26.1	470	0.632
316	16.6	368	18.5	420	24.7	472	0.505
318	19.2	370	17.8	422	23.1	474	0.402
320	21.9	372	17.4	424	21.5	476	0.318
322	24.6	374	17.3	426	19.9	478	0.250
324	27.3	376	17.5	428	18.2	480	0.196
326	29.9	378	18.0	430	16.6		
328	32.2	380	18.8	432	15.0		
330	34.3	382	19.7	434	13.4		

Note:

280 – 480 nm: mean of the data from Bauer et al. [10] and Rowley et al. [89]



(Recommendation: 10-6, Note: 10-6, Evaluated: 10-6)

Absorption Cross Sections: The absorption spectrum of iodine chloride, ICl, has been measured at room temperature by Gibson and Ramsperger [38] (380 – 570 nm), Seery and Britton [96] (220 – 600 nm), Binder [14] (216.5 – 310 nm), and Jenkin et al. [49] (210 – 690 nm). Spectra measurements at elevated temperatures have been reported by Binder [14] (293, 387, 489, and 685 K). The spectrum shows two absorption bands of nearly equal height, one between 220 and 350 nm with the maximum at ~244 nm and one between 350 and 600 nm with the maximum near 470 nm. The latter band is asymmetric due to the overlap of the $\text{B } ^3\Pi_{0+} \leftarrow \text{X } ^1\Sigma_{0+}$, $^1\Pi \leftarrow \text{X } ^1\Sigma_{0+}$, and $\text{A } ^3\Pi_i \leftarrow \text{X } ^1\Sigma_{0+}$ transitions as discussed by Seery and Britton [96] and Mashnin et al. [69]. The experimental data of Seery and Britton [96] and Jenkin et al. [49] are in excellent agreement in the region of the visible absorption band but are appreciably higher (by ~35% at the maximum) than the earlier data from Gibson and Ramsperger [38]. The cross section at the 242 nm maximum reported by Jenkin et al. [49] is greater by ~14% than those observed by Gibson and Ramsperger [38] and Seery and Britton [96]. The larger absorption cross sections reported by Seery and Britton [96] over the wavelength range 290 – 360 nm are most likely due to Cl₂ impurities as argued by Jenkin et al. [49] who subtracted Cl₂ contributions in their spectral analysis. Jenkin et al. [49] report their absorption spectrum in graphical form along with cross

section values of $5.00 \times 10^{-19} \text{ cm}^2 \text{ molecule}^{-1}$ and $4.20 \times 10^{-19} \text{ cm}^2 \text{ molecule}^{-1}$ at 244 nm and 467 nm, respectively. The recommended cross sections in Table 4H-10 use these values combined with the absorption cross sections read from a figure given in Jenkin et al. [49].

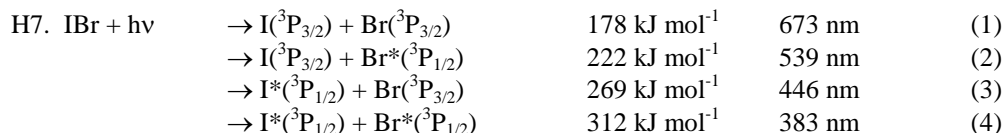
Binder [14] report a decrease in the 244 nm peak absorption cross section with increasing temperature from $4.40 \times 10^{-19} \text{ cm}^2 \text{ molecule}^{-1}$ at 293 K to $3.53 \times 10^{-19} \text{ cm}^2 \text{ molecule}^{-1}$ at 685 K.

Photolysis Quantum Yield and Product Studies: The ratio of the Cl atom spin-state quantum yields, $\Phi(\text{Cl}^*)/(\Phi(\text{Cl}^*) + \Phi(\text{Cl}))$, have been reported by several groups. Mashnin et al. [69] showed that for wavelengths in the range 437 – 532 nm the ratio varied between 0.41 ± 0.02 and 0.79 ± 0.02 . The ratio has been reported by Ni and Flynn [74] to be 0.17 ± 0.04 at 237 nm, 0.67 ± 0.05 at 248 nm by Chichinin [23], and 0.55 ± 0.05 at 530 nm by Chichinin et al. [24]. Tonokura et al. [106] reported $\Phi(\text{I} + \text{Cl})$, $\Phi(\text{I} + \text{Cl}^*)$ and $\Phi(\text{I}^* + \text{Cl})$ to be 0.2, 0.4 and 0.4, respectively, for the wavelength range 235 – 248 nm. The ratio of I^* to I , I^*/I , has been reported by Tonokura et al. [106] to be 0.71 ± 0.27 and Jung et al. [53] to be $\text{I}^*/\text{I} = 0.43$ at 304 nm.

Table 4H-10. Absorption Cross Sections of ICl at 298 K

λ (nm)	$10^{20} \sigma$ (cm^2)	λ (nm)	$10^{20} \sigma$ (cm^2)	λ (nm)	$10^{20} \sigma$ (cm^2)
210	7.4	340	<1	470	41.8
220	21.3	350	<1	480	40.0
230	40.0	360	2.3	490	35.4
240	49.0	370	4.6	500	29.0
244	50.0	380	8.74	510	21.1
250	47.8	390	13.8	520	15.6
260	36.8	400	19.0	530	11.0
270	24.4	410	25.0	540	7.3
280	12.9	420	28.5	550	5.5
290	6.4	430	32.0	560	4.2
300	3.2	440	35.4	570	3.4
310	<1	450	38.8	580	2.9
320	<1	460	41.7	590	2.1
330	<1	467	42.0	600	1.9

Note:
Jenkin et al. [49]



(Recommendation: 06-2, Note: 10-6, Evaluated: 10-6)

Absorption Cross Sections: The absorption spectrum of iodine bromide, IBr, has been measured at room temperature by Seery and Britton [96] over the wavelength range 220 – 600 nm. The spectrum consists of two absorption bands, a weak band between 220 and 350 nm with the maximum at ~270 nm and a stronger band between 350 and 600 nm with the maximum at ~500 nm. The recommended absorption cross sections in Table 4H-11 are taken from Seery and Britton [96].

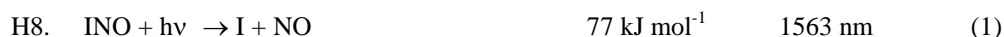
Photolysis Quantum Yield and Product Studies: Absolute quantum yields for Br^* formation, $\Phi(\text{Br}^*)$, were measured by Haugen et al. [44] over the wavelength range 450 – 530 nm. $\Phi(\text{Br}^*)$ increases from a value of 0.28 at 450 nm to a maximum of 0.73 near 500 nm. Peterson and Smith [78] reported the ratio of the Br atom spin-state quantum yields, $\Phi(\text{Br}^*)/(\Phi(\text{Br}^*) + \Phi(\text{Br}))$, to vary from ~0.3 at 444 nm to a maximum of unity near 520 nm followed by a decline to ~0.1 at 670 nm. Wrede et al. [115] reported a similar trend over the wavelength range 440 – 544 nm. Kim et al. [56] measured the relative quantum yields for the photolysis channels $\Phi(\text{I} + \text{Br})$, $\Phi(\text{I} + \text{Br}^*)$ and $\Phi(\text{I}^* + \text{Br})$ to be 0.23, 0.35 and 0.42, respectively, at 267 nm.

Table 4H-11. Absorption Cross Sections of IBr at 298 K

λ (nm)	$10^{20} \sigma$ (cm ²)	λ (nm)	$10^{20} \sigma$ (cm ²)	λ (nm)	$10^{20} \sigma$ (cm ²)
220	3.59	350	1.45	480	111
230	5.70	360	1.52	490	120
240	10.2	370	2.37	500	122
250	16.7	380	4.17	510	116
260	21.4	390	6.96	520	103
270	23.1	400	12.0	530	85.8
280	21.1	410	20.5	540	67.5
290	16.8	420	31.7	550	52.3
300	12.4	430	44.8	560	36.6
310	7.95	440	58.7	570	27.2
320	5.39	450	71.9	580	19.9
330	3.36	460	85.2	590	14.6
340	2.14	470	98.5	600	11.3

Note:

220 – 600 nm: Seery and Britton [96]



(Recommendation: 06-2, Note: 10-6, Evaluated: 10-6)

Absorption Cross Sections: The absorption cross sections of nitrosyl iodide, INO, have been measured at room temperature by Porter et al. [83] (390 – 470 nm), van den Bergh and Troe [112] (around 265 and 410 nm), Basco and Hunt [9] (220 – 460 nm), and Forte et al. [35] (223 – 300 nm and around 410 nm). The spectrum shows two absorption bands, a strong and asymmetric band in the UV between 220 and 300 nm with the maximum at 238 nm, and a second weaker band, weaker by two orders of magnitude, between 355 and 470 nm with a maximum near 410 nm. The results for the UV band are in good agreement except for the region around 250 nm, where the absorption curve reported by Basco and Hunt [9] shows a hump and an absorption cross section larger by a factor of ~1.5 than that reported by Forte et al. [35]. The absorption curve in the near UV and visible reported by Porter et al. [83] is shifted to longer wavelengths by ~20 nm and the absorption cross sections are smaller by 50-30% at 400 – 430 nm compared to the results of Basco and Hunt [9].

The recommended absorption cross sections in Table 4H-12 are the mean of the data from Basco and Hunt [9] and Forte et al. [35] for the wavelength range 223 – 290 nm and the data from Basco and Hunt [9] at 300 and 310 nm. For the absorption band in the near UV and visible the IUPAC (1982-2000) [12], [7], [6], [5] recommendation which is the mean of the data from van den Berg and Troe [112], Basco and Hunt [9], and Forte et al. [35] is adopted after correcting the errors in the values at 400 and 410 nm.

Photolysis Quantum Yield and Product Studies: The photolysis quantum yield is expected to be unity at wavelengths above the dissociation threshold.

Table 4H-12. Absorption Cross Sections of INO at 298 K

λ (nm)	$10^{20} \sigma$ (cm ²)	λ (nm)	$10^{20} \sigma$ (cm ²)
223	225	360	45
230	1690	370	59
235	5640	380	65
238	6850	390	78
245	6000	400	92*
251	4880	410	110*
260	2270	420	100
270	1040	430	94
280	500	440	80
290	187	450	60
300	92	460	40
310	41		

Note:

223 – 290 nm: mean of data from Basco and Hunt [9] and Forte et al. [35]

300, 310 nm: Basco and Hunt [9]

360 – 460 nm: IUPAC-1982-2000 recommendation (* corrected) [12], [7], [6], [5]



(Recommendation: 06-2, Note: 10-6, Evaluated: 10-6)

Absorption Cross Sections: The UV absorption spectrum of iodine nitrite, IONO, has been measured at room temperature by Bröske [19] over the wavelength range 210 – 390 nm. The spectrum consists of three broad absorption bands with cross section maxima of 4.20×10^{-18} , 9.6×10^{-19} , and 3.9×10^{-19} cm² molecule⁻¹ at 240, 282, and 342 nm, respectively. These values were obtained assuming the stoichiometric conversion of NO₂ to IONO in the photolysis of I₂ – NO₂ mixtures. The recommended absorption cross section values in Table 4H-13 are taken from the evaluation by Atkinson et al. [5].

Photolysis Quantum Yield and Product Studies: No studies are available.

Table 4H-13. Absorption Cross Sections of IONO at 298 K

λ (nm)	$10^{20} \sigma$ (cm ²)	λ (nm)	$10^{20} \sigma$ (cm ²)	λ (nm)	$10^{20} \sigma$ (cm ²)	λ (nm)	$10^{20} \sigma$ (cm ²)
210	236	255	234	300	37.3	345	37.3
215	187	260	162	305	30.8	350	29.8
220	196	265	99.6	310	24.7	355	29.5
225	279	270	87.1	315	25.1	360	27.1
230	347	275	89.8	320	27.5	365	20.7
235	399	280	99.6	325	32.5	370	14.9
240	422	285	92.2	330	31.2	375	7.40
245	400	290	81.0	335	34.9	380	2.40
250	330	295	62.0	340	37.3		

Note:

210 – 380 nm: Bröske [19] from Atkinson et al. [5]



(Recommendation: 06-2, Note: 10-6, Evaluated: JPL10-6)

Absorption Cross Sections: The UV absorption spectrum of iodine nitrate, IONO₂, has been reported by Mössinger et al. [71] (245 – 415 nm) and Joseph et al. [52] (240 – 370 nm). Both studies used pulsed laser photolysis of NO₂/CF₃I/N₂ mixtures to produce IONO₂ in the gas-phase. The IONO₂ spectrum consists of a broad continuous absorption band over this wavelength range. There are, however, significant discrepancies between the two studies for the wavelength dependence and absolute absorption cross sections. The reason for the discrepancies in these two very similar studies is not known. The recommended cross section values given in Table 4H-14 are taken from Mössinger et al. [71] and are unchanged from JPL 02-25[93].

Photolysis Quantum Yield and Product Studies: The photoproducts of IONO₂ are not well characterized. In the only quantum yield study to date, Joseph et al. [52] report IO and NO₃ quantum yields of $\Phi(\text{IO}) \leq 0.02$ and $\Phi(\text{NO}_3) = 0.21 \pm 0.09$ at 248 nm. Photolysis is most likely the major daytime loss process for IONO₂ even considering the current large uncertainty in the UV absorption cross sections.

Table 4H-14. Absorption Cross Sections of IONO₂ at 298 K

λ (nm)	$10^{20} \sigma$ (cm ²)	λ (nm)	$10^{20} \sigma$ (cm ²)	λ (nm)	$10^{20} \sigma$ (cm ²)	λ (nm)	$10^{20} \sigma$ (cm ²)
245	1210	290	631	335	374	380	184
250	1170	295	577	340	360	385	153
255	1060	300	525	345	348	390	130
260	946	305	495	350	334	395	103
265	880	310	462	355	316	400	78.0
270	797	315	441	360	294	405	60.5
275	772	320	404	365	270	410	49.6
280	741	325	396	370	242	415	41.6
285	691	330	380	375	213		

Note:

245 – 415 nm: Mössinger et al. [71], values in the range 335 – 385 nm were obtained from an interpolation of the experimental data.



(Recommendation: 02-25, Note: 10-6, Evaluated: 10-6)

Absorption Cross Sections: The UV absorption spectrum of methyl iodide, CH₃I, has been measured at room temperature by Rebbert et al. [86] (147 nm), Porret and Goodeve [81] (200 – 360 nm), Baughcum and Leone [11] (200 – 310 nm), Pence et al. [77] (180 – 400 nm), Felps et al. [34] (257.7 nm), Jenkin et al. [50] (205 – 335 nm), Man et al. [67] (205 – 360 nm), Kwok and Phillips [63] (192 – 225 nm) and Eden et al. [29] (115 – 315 nm). Kwok and Phillips [63] also measured the CH₃I spectrum in cyclohexane solution. Fahr et al. [31] also measured the absorption cross sections in the range 330 – 400 nm in the liquid phase and used a wavelength shift procedure to derive gas-phase cross section values. The temperature dependence of the absorption spectrum has been reported by Fahr et al. [31] (223 – 333 K), Rattigan et al. [85] (243 – 333 K), and Roehl et al. [87] (210 – 298 K). The room temperature cross section data for the wavelength range 210 – 305 nm are in reasonable to good agreement with Rattigan et al. [85] reporting the smallest and Fahr et al. [31] the largest values. The agreement is generally better than 15% except for the region around the absorption maximum where the spread is ~30%. Rattigan et al. [85] and Fahr et al. [31] report values of $1.07 \times 10^{-18} \text{ cm}^2 \text{ molecule}^{-1}$ and $1.4 \times 10^{-18} \text{ cm}^2 \text{ molecule}^{-1}$, respectively, for the maximum at ~260 nm. The peak cross section values from the other studies range from $1.15 \times 10^{-18} \text{ cm}^2 \text{ molecule}^{-1}$ to $1.22 \times 10^{-18} \text{ cm}^2 \text{ molecule}^{-1}$. In the wavelength range 305 – 330 nm, the agreement is within 20%. At wavelengths below 210 nm, the data reported by Jenkin et al. [50], Roehl et al. [87] and Kwok and Phillips [62] fit into the strong and highly structured band system reported by Fahr et al. [31] and Eden et al. [29]. However, the absorption cross sections reported by Eden et al. [29] in this wavelength range are significantly larger, ~x10. The recommended room temperature absorption cross sections for the wavelength range above 210 nm in Table 4H-15 are the mean of the values reported by Jenkin et al. [50], Fahr et al. [31], and Roehl et al. [87] for the range 210 – 230 nm, the mean of the values reported by Jenkin et al. [50], Fahr et al. [31], Rattigan et al. [85], and Roehl et al. [87] for the range 235 – 330 nm; the mean of the values reported by Fahr et al. [31], Rattigan

et al. [85], and Roehl et al. [87] for the range 335 – 350 nm, and the values of Rattigan et al. [85] for the range 355 – 365 nm.

Studies of the spectrum temperature dependence are in qualitative agreement with an increase in the peak absorption cross section and decrease in the long wavelength tail cross sections with decreasing temperature. Roehl et al. [87] and Rattigan et al. [85] parameterized the cross section temperature dependence using the empirical expressions

$$\sigma(\lambda, T) = \sigma(298 \text{ K}) [1 + a_1(\lambda)(T - 298) + a_2(\lambda)(T - 298)^2] \quad (\text{Roehl et al. [87]})$$

$$\ln \sigma(\lambda, T) = \ln \sigma(\lambda, 298 \text{ K}) + B(\lambda)(T - 298) \quad (\text{Rattigan et al. [85]})$$

Both expressions reproduce the experimental data well and the $a_1(\lambda)$, $a_2(\lambda)$, and $B(\lambda)$ parameters are included in Table 4H-15.

Photolysis Quantum Yield and Product Studies: The photolysis quantum yield for CH_3I is expected to be unity for wavelengths above the dissociation threshold. Quantum yields for $\text{I}^*(^2\text{P}_{1/2})$ atom formation, $\Phi(\text{I}^*)$, have been reported by several groups for photolysis between 222 and 333.5 nm. Uma and Das [109], [110], [111] reported $\Phi(\text{I}^*)$ values of 0.63 ± 0.02 , 0.79 ± 0.02 , 0.69 ± 0.02 , and 0.43 ± 0.02 for 222, 266, 280, and ~305 nm, respectively. Gedanken [111] reported $\Phi(\text{I}^*) = 0.72 \pm 0.08$ at 248 nm. Pence et al. [77] reported $\Phi(\text{I}^*) = 0.81 \pm 0.03$ and ~ 0.05 at 248 and 308 nm, respectively. Kang et al. [54] reported $\Phi(\text{I}^*) = 0.30$ at 304 nm. Ogorzalek Loo et al. [76] reported $\Phi(\text{I}^*) = 0.47$, 0.77, and 0.92 at 325.8, 329.4, and 333.5, respectively. Ogorzalek Loo et al. [76] and Brewer et al. [17] have also reported I^* quantum yields for the photolysis of CD_3I . Quantum yields for $\text{I}^*(^2\text{P}_{3/2})$ atom formation, $\Phi(\text{I})$, can be derived from $\Phi(\text{I}) = 1 - \Phi(\text{I}^*)$.

Table 4H-15. Absorption Cross Sections of CH_3I at 298 K and Temperature Coefficients

λ (nm)	$10^{20} \sigma$ (cm^2)	$10^3 a_1$ (K^{-1})	$10^5 a_2$ (K^{-2})	$10^3 B$ (K^{-1})	λ (nm)	$10^{20} \sigma$ (cm^2)	$10^3 a_1$ (K^{-1})	$10^5 a_2$ (K^{-2})	$10^3 B$ (K^{-1})
210	3.62	3.07	2.42	—	290	8.04	6.14	2.57	4.98
215	5.08	2.61	2.28	—	295	4.00	7.27	2.91	6.38
220	6.90	1.06	1.22	—	300	2.06	7.82	3.53	6.97
225	9.11	1.74	1.96	—	305	1.10	7.82	3.85	6.84
230	12.6	1.47	1.67	—	310	0.621	7.37	3.71	6.78
235	20.5	1.91	2.04	0.67	315	0.359	6.98	3.47	6.75
240	38.1	1.74	2.06	0.61	320	0.221	7.39	3.54	6.53
245	65.6	1.52	2.15	0.34	325	0.126	7.23	2.82	6.79
250	96.3	1.20	2.11	0.08	330	0.0684	8.93	3.74	7.82
255	117.7	0.890	1.95	-0.10	335	0.0388	10.88	4.88	9.34
260	119.7	0.882	1.93	-0.12	340	0.0212	11.30	4.46	10.95
265	102.9	1.21	2.00	0.10	345	0.0114	15.68	8.44	13.58
270	75.9	1.77	2.11	0.54	350	0.00609	15.94	8.22	16.83
275	49.6	2.52	2.12	1.33	355	0.00320	—	—	18.91
280	29.2	3.62	2.24	2.43	360	0.00190	—	—	17.28
285	15.6	4.84	2.38	3.74	365	0.00090	—	—	23.63

Note:

Absorption cross sections (σ)

210 – 230 nm: mean of data from Jenkin et al. [50], Fahr et al. [31], and Roehl et al. [87]

235 – 330 nm: mean of data from Jenkin et al. [50], Fahr et al. [31], Rattigan et al. [85], and Roehl et al. [87]

335 – 350 nm: mean of data from Fahr et al. [31], Rattigan et al. [85], and Roehl et al. [87]

355 – 365 nm: Rattigan et al. [85]

Temperature coefficients

a_1 and a_2 : Roehl et al. [87] (210 – 298 K), $\sigma(\lambda, T) = \sigma(298 \text{ K}) [1 + a_1(T - 298) + a_2(T - 298)^2]$

B: Rattigan et al. [85] (243 – 333 K), $\ln \sigma(\lambda, T) = \ln \sigma(\lambda, 298 \text{ K}) + B(\lambda)(T - 298)$



(Recommendation: 02-25, Note: 10-6, Evaluated: 10-6)

Absorption Cross Sections: The UV absorption spectrum of diiodomethane, CH_2I_2 , has been measured at room temperature by Pence et al. [77] (180 – 400 nm), Schmitt and Comes [94] (220 – 360 nm), Baughcum and Leone [11] (200 – 360 nm), Koffend and Leone [59] (265 – 341 nm), Kwok and Phillips [61] (220 – 400 nm), Roehl et al. [87] (215 – 385 nm), and Mössinger et al. [72] (215 – 385 nm). Kwok and Phillips [61] also measured the CH_2I_2 spectrum in methanol and cyclohexane solvents. The temperature dependence of the absorption spectrum has been reported by Roehl et al. [87] (273 and 298 K) and Mössinger et al. [72] (273, 298, 348 K).

The absorption spectrum shows clear evidence for multiple transitions in the wavelength range 200 – 400 nm with absorption maxima at ~215, 250 and 290 nm. The room temperature cross section data from the various groups are in very good agreement with the exception of Kwok and Phillips [61]. The reported cross sections are within 5 to 10% between 230 and 380 nm. The data from Schmitt and Comes [94] and Koffend and Leone [59] near the 290 nm peak are higher than those of Roehl et al. [87] and Mössinger et al. [72]. The values of Kwok and Phillips [61] are lower by 15–20% near 290 nm. The recommended room temperature absorption cross sections in Table 4H-16 are the values from Roehl et al. [87] for the range 205 – 215 nm, the mean of the values reported by Roehl et al. [87] and Mössinger et al. [72] for the range 220 – 380 nm, and the value of Mössinger et al. [72] at 385 nm.

The studies of the spectrum temperature dependence are in good agreement with a slight increase in the peak absorption cross section and decrease in the long wavelength tail cross section with decreasing temperature. Mössinger et al. [72] parameterized the cross section temperature dependence between 273 and 348 K using the expression

$$\ln \sigma(\lambda, T) = \ln \sigma(\lambda, 298\text{K}) + B(\lambda)(T - 298)$$

The $B(\lambda)$ coefficients are listed in Table 4H-16. (Note: an erroneous B value at 305 nm was corrected via a personal communication with Dr. Mössinger).

Photolysis Quantum Yield and Product Studies: The photolysis quantum yield for CH_2I_2 is expected to be unity for wavelengths above the dissociation threshold. Pence et al. [77] have reported quantum yields for $\text{I}^*(^2\text{P}_{1/2})$ atom formation, $\Phi(\text{I}^*)$, at 193, 248, and 308 nm of ~0.05, 0.46 ± 0.04 , and 0.25 ± 0.02 , respectively. Quantum yields for $\text{I}(^2\text{P}_{3/2})$ atom formation, $\Phi(\text{I})$, can be derived from $\Phi(\text{I}) = 1 - \Phi(\text{I}^*)$.

Table 4H-16. Absorption Cross Sections of CH_2I_2 at 298 K

λ (nm)	$10^{20} \sigma$ (cm ²)	$10^3 B$ (K ⁻¹)	λ (nm)	$10^{20} \sigma$ (cm ²)	$10^3 B$ (K ⁻¹)
205	407.0	–	300	357.0	–0.37
210	404.0	–	305	338.5	–0.16
215	366.0	0.15	310	313.5	0.07
220	260.0	0.14	315	280.0	0.15
225	197.5	0.19	320	244.0	0.27
230	133.0	0.51	325	203.0	0.27
235	109.0	0.56	330	161.5	0.51
240	122.5	0.15	335	120.5	0.55
245	150.0	0.18	340	83.3	1.36
250	157.0	0.67	345	53.7	1.99
255	139.5	1.58	350	32.6	3.19
260	120.5	2.04	355	19.2	4.09
265	130.0	1.30	360	10.9	5.39
270	178.5	0.00	365	6.05	6.77
275	255.0	–0.71	370	3.45	8.25
280	328.5	–1.24	375	1.93	11.3
285	371.5	–1.21	380	1.17	–
290	380.5	–0.94	385	0.769	–
295	371.5	–0.58			

Note:

Absorption cross sections

205 – 215 nm: Roehl et al. [87]

220 – 380 nm: mean of data from Roehl et al. [87] and Mössinger et al. [72]

385 nm: Mössinger et al. [72]

Temperature coefficients

$B(\lambda)$: Mössinger et al. [72] (273 – 348 K), $\ln \sigma(\lambda, T) = \ln \sigma(\lambda, 298 \text{ K}) + B(\lambda)(T - 298)$



(Recommendation: 02-25, Note: 10-6, Evaluated: 10-6)

Absorption Cross Sections: The UV absorption spectrum of iodoethane, $\text{C}_2\text{H}_5\text{I}$, has been measured at room temperature by Rebbert et al. [86] (147 nm, $\sigma = 1.48 \times 10^{-17} \text{ cm}^2$), Porret and Goodeve [82] (205 – 360 nm), Roehl et al. [87] (205 – 365 nm), and Rattigan et al. [85] (235 – 355 nm). The temperature dependence of the absorption spectrum has been reported by Roehl et al. [87] (223 – 298 K), Rattigan et al. [85] (243 – 333 K), and Zhang et al. [116] (323 K, 220 – 320 nm). The room temperature data are in good agreement with the values of Roehl et al. [87] being larger by 5 – 15% over the wavelength range 235 – 325 nm and 125% at 355 nm than the values from Rattigan et al. [85]. The Rattigan et al. [85] values agree to within 10 – 15% with the values from Porret and Goodeve [82]. The recommended absorption cross sections in Table 4H-17 are the mean of the values reported by Roehl et al. [87] and Rattigan et al. [85] for the wavelength range 235 – 355 nm and the data from Roehl et al. [87] in the range 215 – 230 nm.

Studies of the spectrum temperature dependence by Roehl et al. [87] and Rattigan et al. [85] show that the peak absorption cross section increases with decreasing temperature. The absorption cross sections in the long wavelength tail of the spectrum decrease with decreasing temperature. The data reported by Zhang et al. [116] for 323 K are 10 – 40% larger around the absorption maximum and as much as 200% larger in the long wavelength tail than the data for 313 and 333 K reported by Rattigan et al. [85]. Roehl et al. [87] and Rattigan et al. [85] parameterized the cross section temperature dependence using the empirical expressions

$$\sigma(\lambda, T) = \sigma(298 \text{ K}) [(1 + a_1(\lambda)(T - 298) + a_2(\lambda)(T - 298)^2)] \quad (\text{Roehl et al. [87]})$$

$$\ln \sigma(\lambda, T) = \ln \sigma(\lambda, 298 \text{ K}) + B(\lambda)(T - 298) \quad (\text{Rattigan et al. [85]})$$

Both expressions reproduce the experimental data well and the $a_1(\lambda)$, $a_2(\lambda)$, and $B(\lambda)$ parameters are included in Table 4H-17.

Photolysis Quantum Yield and Product Studies: The photolysis quantum yield for $\text{C}_2\text{H}_5\text{I}$ is expected to be unity for wavelengths above the dissociation threshold. Uma and Das [109], [110], [111] have reported quantum yields for $\text{I}^*(^2\text{P}_{1/2})$ atom formation, $\Phi(\text{I}^*)$, at wavelengths between 222 and 305 nm to be 0.57 ± 0.02 , 0.72 ± 0.02 , 0.60 ± 0.02 , and 0.39 ± 0.02 at 222, 266, 280, and ~305 nm, respectively. Gedanken [37] report $\Phi(\text{I}^*) = 0.78 \pm 0.07$ at 248 nm. Brewer et al. [17] report $\Phi(\text{I}^*) = 0.68 \pm 0.02$ at 248 nm. Kang et al. [54] report $\Phi(\text{I}^*) = 0.22$ at 304 nm. Quantum yields for $\text{I}(^2\text{P}_{3/2})$ atom formation, $\Phi(\text{I})$, can be derived from $\Phi(\text{I}) = 1 - \Phi(\text{I}^*)$. Rebbert et al. [86] report that the quantum yield at 147 nm for the overall process $\text{C}_2\text{H}_5\text{I} + h\nu \rightarrow \text{C}_2\text{H}_4 + \text{H} + \text{I}$ to be 0.75.

Table 4H-17. Absorption Cross Sections of C₂H₅I at 298 K and Temperature Coefficients

λ (nm)	$10^{20} \sigma$ (cm ²)	$10^3 a_1$ (K ⁻¹)	$10^5 a_2$ (K ⁻²)	$10^3 B$ (K ⁻¹)	λ (nm)	$10^{20} \sigma$ (cm ²)	$10^3 a_1$ (K ⁻¹)	$10^5 a_2$ (K ⁻²)	$10^3 B$ (K ⁻¹)
205	11.9	6.38	3.15	—	285	19.1	3.85	0.926	3.61
210	4.22	4.07	6.28	—	290	10.3	5.47	1.65	4.83
215	4.56	4.93	6.75	—	295	5.38	7.00	2.52	6.33
220	6.18	4.06	5.70	—	300	2.78	8.56	4.11	7.48
225	9.09	2.81	3.81	—	305	1.44	9.31	4.89	8.08
230	14.3	2.62	3.83	—	310	0.777	10.56	6.87	7.55
235	23.2	1.28	2.17	-0.27	315	0.416	10.83	6.81	7.92
240	41.7	0.876	1.96	-0.40	320	0.227	11.98	9.76	8.27
245	69.3	0.233	1.62	-0.62	325	0.127	12.98	11.3	8.81
250	99.3	-0.111	1.58	-0.79	330	0.0743	14.56	17.5	9.30
255	119.7	-1.03	0.606	-0.82	335	0.0403	18.81	24.6	10.20
260	121.8	-1.48	-0.0332	-0.75	340	0.0246	13.90	9.08	11.16
265	105.9	-1.09	1.2 ×	-0.44	345	0.0133	18.86	22.1	12.41
270	80.6	-0.538	-0.257	0.36	350	0.00840	20.19	20.1	11.28
275	54.4	0.770	0.0299	1.23	355	0.00488	-7.04	-40.5	12.20
280	33.5	2.01	0.110	2.36					

Note:

Absorption cross sections

205 – 230 nm: Roehl et al. [87]

235 – 355 nm: mean of data from Roehl et al. [87] and Rattigan et al. [85]

Temperature coefficients

$a_1(\lambda)$ and $a_2(\lambda)$: Roehl et al. [87] (223 – 298 K), $\sigma(\lambda, T) = \sigma(298 \text{ K}) [1 + a_1(\lambda)(T - 298) + a_2(\lambda)(T - 298)^2]$

$B(\lambda)$: Rattigan et al. [85] (243 – 333 K), $\ln \sigma(\lambda, T) = \ln \sigma(\lambda, 298 \text{ K}) + B(\lambda)(T - 298)$

H14. CH₃CHI₂ + hν → Products

(Recommendation: 02-25, Note: 10-6, Evaluated: 10-6)

Absorption Cross Sections: The UV absorption spectrum of 1,1-diiodoethane, CH₃CHI₂, has been measured at 298 K by Schmitt and Comes [94] over the wavelength range 220 – 360 nm. The continuous spectrum consists of several overlapping transitions with maxima at <220 nm and peaks at 250 and 290 nm. A weaker band appears as a shoulder in the spectrum near 320 nm. The recommended cross sections in Table 4H-18 are taken from Schmitt and Comes [94]

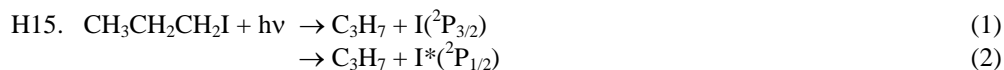
Photolysis Quantum Yield and Product Studies: The photolysis quantum yield for CH₃CHI₂ is expected to be unity for wavelengths above the dissociation threshold. There is no quantum yield data available.

Table 4H-18. Absorption Cross Sections of CH₃CHI₂ at 298 K

λ (nm)	$10^{20} \sigma$ (cm ²)	λ (nm)	$10^{20} \sigma$ (cm ²)	λ (nm)	$10^{20} \sigma$ (cm ²)
220	304	270	183	320	222
225	240	275	243	325	201
230	181	280	304	330	175
235	144	285	352	335	138
240	138	290	374	340	107
245	151	295	366	345	75.7
250	157	300	339	350	49.3
255	143	305	305	355	31.7
260	133	310	273	360	19.1
265	145	315	247		

Note:

220 – 360 nm: Schmitt and Comes [94]



(Recommendation: 02-25, Note: 10-6, Evaluated: 10-6)

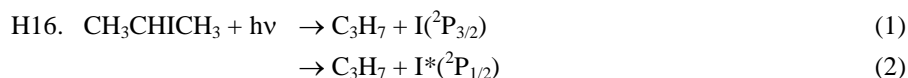
Absorption Cross Sections: The UV absorption spectrum of 1-iodopropane, 1-C₃H₇I, has been measured over the wavelength range 205 – 335 nm by Roehl et al. [87] for temperatures between 223 and 298 K. The continuous absorption spectrum peaks at 255 nm with evidence for another absorption band at wavelengths <205 nm. A VUV absorption cross section of $7 \times 10^{-18} \text{ cm}^2 \text{ molecule}^{-1}$ at 147 nm has been reported by Rebbert et al. [86]. The recommended room temperature cross sections for 1-C₃H₇I in Table 4H-19 are taken from Roehl et al. [87].

The absorption cross section near the peak increases with decreasing temperature. The cross sections in the long wavelength tail decrease with decreasing temperature. Roehl et al. [87] parameterized the temperature dependence using the empirical expression

$$\sigma(\lambda, T) = \sigma(298 \text{ K}) [1 + a_1(\lambda)(T - 298) + a_2(\lambda)(T - 298)^2]$$

The $a_1(\lambda)$ and $a_2(\lambda)$ parameters are included in Table 4H-19.

Photolysis Quantum Yield and Product Studies: The photolysis quantum yield for 1-C₃H₇I is expected to be unity for wavelengths above the dissociation threshold. Uma and Das [109], [111] report quantum yields for I*({}^2P_{1/2}) atom formation, $\Phi(\text{I}^*)$, at several photolysis wavelengths to be 0.54 ± 0.02 , 0.66 ± 0.02 , 0.56 ± 0.02 , and 0.35 ± 0.02 at 222, 266, 280, and ~305 nm, respectively. Brewer et al. [17] report $\Phi(\text{I}^*) = 0.60 \pm 0.02$ at 248 nm. Kang et al. [54] report $\Phi(\text{I}^*) = 0.20$ at 304 nm. Quantum yields for I({}^2P_{3/2}) atom formation, $\Phi(\text{I})$, can be derived from $\Phi(\text{I}) = 1 - \Phi(\text{I}^*)$. At 147 nm, Rebbert et al. [86] report quantum yields for the overall processes $1\text{-C}_3\text{H}_7\text{I} + h\nu \rightarrow \text{C}_3\text{H}_6 + \text{H} + \text{I}$ and $1\text{-C}_3\text{H}_7\text{I} + h\nu \rightarrow \text{CH}_3 + \text{C}_2\text{H}_4 + \text{I}$ to be 0.38 and 0.47, respectively.



(Recommendation: 02-25, Note: 10-6, Evaluated: 10-6)

Absorption Cross Sections: The UV absorption spectrum of 2-iodopropane, 2-C₃H₇I, has been measured by Roehl et al. [87] (223 – 298 K and 205 – 380 nm) and Phillips et al. [80] (298 K, 235 – 305 nm). Phillips et al. [80] also report an absorption spectrum of 2-C₃H₇I in a cyclohexane solution. The continuous absorption spectrum peaks at 260 nm with evidence for another absorption band at wavelengths <205 nm. The gas-phase data reported by Phillips et al. [80] are larger by 30–70% over the entire absorption band than the data from Roehl et al. [87]. A room temperature cross section of $7.59 \times 10^{-17} \text{ cm}^2 \text{ molecule}^{-1}$ at 147 nm has been reported by Rebbert et al. [86]. The recommended room temperature values for 2-C₃H₇I in Table 4H-19 are taken from Roehl et al. [87].

The absorption cross section near the peak increases with decreasing temperature. The cross sections in the long-wavelength tail decrease with decreasing temperature. Roehl et al. [87] parameterized the temperature dependence using the empirical expression

$$\sigma(\lambda, T) = \sigma(298 \text{ K}) [1 + a_1(\lambda)(T - 298) + a_2(\lambda)(T - 298)^2]$$

The $a_1(\lambda)$ and $a_2(\lambda)$ parameters are included in Table 4H-19.

Photolysis Quantum Yield and Product Studies: The photolysis quantum yield for 2-C₃H₇I is expected to be unity for wavelengths above the dissociation threshold. Uma and Das [110] report quantum yields for I*(²P_{1/2}) atom formation, $\Phi(I^*)$, at several wavelengths to be 0.40 ± 0.02 , 0.44 ± 0.03 , and 0.19 ± 0.02 at 222, 266, and ~305 nm, respectively. Brewer et al. [17] report $\Phi(I^*) = 0.26 \pm 0.02$ at 248 nm. Quantum yields for I(²P_{3/2}) atom formation, $\Phi(I)$, can be derived from $\Phi(I) = 1 - \Phi(I^*)$. At 147 nm, Rebbert et al. [86] report quantum yields for the overall processes $2\text{-C}_3\text{H}_7\text{I} + h\nu \rightarrow \text{C}_3\text{H}_6 + \text{H} + \text{I}$ and $2\text{-C}_3\text{H}_7\text{I} + h\nu \rightarrow \text{CH}_3 + \text{C}_2\text{H}_4 + \text{I}$ to be 0.80 and 0.07.

Table 4H-19. Absorption Cross Sections of C₃H₇I at 298 K and Temperature Coefficients

λ (nm)	1-C ₃ H ₇ I			2-C ₃ H ₇ I		
	$10^{20} \sigma$ (cm ²)	$10^3 a_1$ (K ⁻¹)	$10^5 a_2$ (K ⁻²)	$10^{20} \sigma$ (cm ²)	$10^3 a_1$ (K ⁻¹)	$10^5 a_2$ (K ⁻²)
205	15.6	7.60	4.37	44.9	15.14	8.46
210	5.05	0.283	1.57	4.53	7.84	7.23
215	5.14	-1.49	-2.46	3.57	4.96	5.08
220	6.84	-1.59	-2.97	4.20	1.55	1.27
225	10.4	-0.891	-2.14	6.45	2.21	1.99
230	17.7	-0.375	-1.26	11.0	1.60	1.80
235	32.8	-0.311	-1.04	20.4	0.480	0.681
240	58.1	-0.611	-0.804	38.2	-0.333	0.121
245	91.9	-0.949	-0.609	66.7	-0.680	0.0947
250	124	-1.22	-0.611	102	-0.795	0.289
255	141	-1.55	-0.776	133	-0.966	0.570
260	136	-1.44	-0.867	148	-1.14	0.512
265	113	-1.02	-1.04	143	-0.589	0.824
270	82.2	-0.306	-1.16	120	-0.439,	0.281
275	53.4	0.524	-1.50	90.2	0.792	0.873
280	32.0	1.68	-1.66	61.4	1.65	0.466
285	18.1	3.08	-1.44	38.6	2.88	0.534
290	9.96	5.56	0.812	22.6	4.13	0.559
295	5.42	6.76	2.05	12.8	5.71	1.04
300	2.96	7.16	2.90,	6.94	7.20	1.93
305	1.63	6.90	3.20	3.73	8.19	2.33
310	0.945	7.10	4.01	2.04	8.75	2.81
315	0.532	5.59	2.78	1.09	8.49	2.25
320	0.301	3.68	0.0140	0.627	10.79	4.36
325	0.177	4.23	0.0238	0.348	9.54	2.76
330	0.110	11.40	12.3	0.202	10.99	5.94
335	0.0627	15.76	25.8	0.115	12.37	7.58
340	—	—	—	0.0688	13.69	12.2
345	—	—	—	0.0402	16.32	17.1
350	—	—	—	0.0253	18.50	24.7
355	—	—	—	0.0150	19.41	24.3
360	—	—	—	0.0105	18.61	13.9
365	—	—	—	0.00666	29.85	50.9
370	—	—	—	0.00479	37.24	76.8
375	—	—	—	0.00535	36.71	80.7
380	—	—	—	0.00530	22.00	40.0

Note:

Absorption cross sections

205 – 380 nm: Roehl et al. [87]

Temperature coefficients

$a_1(\lambda)$ and $a_2(\lambda)$: Roehl et al. [87] (223 – 298 K)

$$\sigma(\lambda, T) = \sigma(298 \text{ K}) [1 + a_1(\lambda)(T - 298) + a_2(\lambda)(T - 298)^2]$$

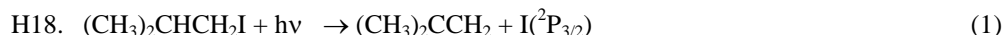


(Recommendation: 02-25, Note: 10-6, Evaluated: 10-6)

Absorption Cross Sections: Absorption cross sections for *n*-C₄H₉I are not available.

Photolysis Quantum Yield and Product Studies: The quantum yield of *n*-C₄H₉I for UV photolysis is expected to be unity. Quantum yields for I*(²P_{1/2}) atom formation has been reported by Uma and Das [109] [111] to be 0.51 ± 0.02 , 0.64 ± 0.03 , 0.50 ± 0.03 , and 0.30 ± 0.02 at 222, 266, 280, and ~305 nm, respectively.

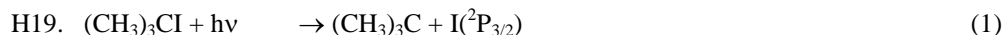
Brewer et al. [17] and Kang et al. [54] have reported quantum yields for I*(²P_{1/2}) of 0.53 ± 0.03 and $= 0.14$ at 248 nm and 304 nm, respectively.



(Recommendation: 02-25, Note: 10-6, Evaluated: 10-6)

Absorption Cross Sections: Absorption cross sections for *iso*-C₄H₉I are not available.

Photolysis Quantum Yield and Product Studies: The quantum yield of *iso*-C₄H₉I for UV photolysis is expected to be unity. The I*(²P_{1/2}) atom quantum yield, $\Phi(\text{I}^*(^2\text{P}_{1/2}))$, has been shown to be wavelength dependent with lower yields at longer photolysis wavelengths. Uma and Das [111] reported $\Phi(\text{I}^*(^2\text{P}_{1/2}))$ values of 0.71 ± 0.01 , 0.56 ± 0.03 , and 0.35 ± 0.02 , at 266, 280, and ~305 nm, respectively. Brewer et al. [17], however, reported a significantly lower value of $\Phi(\text{I}^*(^2\text{P}_{1/2}))$ at 248 nm, 0.20 ± 0.02 .



(Recommendation: 02-25, Note: 10-6, Evaluated: 10-6)

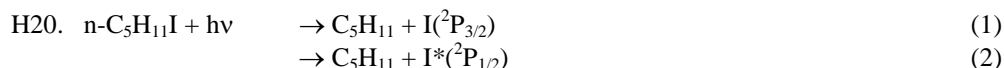
Absorption Cross Sections: The UV absorption spectrum of *tert*-butyl iodide, *tert*-C₄H₉I, at 323 K has been reported by Phillips et al. [80] (230 – 310 nm). The spectrum is continuous and shows a single absorption band with a peak cross section of $\sim 2.1 \times 10^{-18} \text{ cm}^2$ at ~268 nm. The recommended absorption cross sections in Table 4H-20 were taken from a figure given in Phillips et al. [80].

Photolysis Quantum Yield and Product Studies: Quantum yields for I atom formation in the photolysis of *tert*-C₄H₉I have been reported by Kim et al. [58] to be $\Phi(\text{I}(^2\text{P}_{3/2}) + \text{I}^*(^2\text{P}_{1/2})) = 0.93$ and 0.92 at 277 and 304 nm, respectively. On the basis of this study a *tert*-C₄H₉I photolysis quantum yield of unity is recommended for wavelengths <310 nm. The I*(²P_{1/2}) atom quantum yield, $\Phi(\text{I}^*(^2\text{P}_{1/2}))$, has been shown to be wavelength dependent with lower yields for photolysis at the longer wavelengths. Uma and Das [110] reported values for $\Phi(\text{I}^*(^2\text{P}_{1/2}))$ of 0.33 ± 0.03 , 0.20 ± 0.03 , and 0.12 ± 0.03 at 222, 266, and ~305 nm, respectively. Gedanken [37] reported $\Phi(\text{I}^*(^2\text{P}_{1/2})) = 0.41 \pm 0.10$ for 248 nm photolysis. Brewer et al. [17] reported a much lower value, 0.03 ± 0.02 , for photolysis at 248 nm in disagreement with the other studies.

Table 4H-20. Absorption Cross Sections of (CH₃)₃CI at 298 K

λ (nm)	$10^{20} \sigma$ (cm ²)	λ (nm)	$10^{20} \sigma$ (cm ²)	λ (nm)	$10^{20} \sigma$ (cm ²)
235	28.5	265	209	295	54.0
240	42.5	270	211	300	34.0
245	64.8	275	186	305	21.5
250	98.0	280	150	310	14.0
255	140	285	116		
260	180	290	83.0		

Note:
Phillips et al. [80]



(Recommendation: 02-25, Note: 10-6, Evaluated: 10-6)

Absorption Cross Sections: Absorption cross sections for $n\text{-C}_5\text{H}_{11}\text{I}$ are not available.

Photolysis Quantum Yield and Product Studies: By analogy with other alkyl iodides the photolysis quantum yield of $n\text{-C}_5\text{H}_{11}\text{I}$ in the UV is expected to be unity. A quantum yield for $\text{I}^*(^2\text{P}_{1/2})$ atom formation in the photolysis of $n\text{-C}_5\text{H}_{11}\text{I}$ at 222 nm, $\Phi(\text{I}^*(^2\text{P}_{1/2}))$ of 0.50 ± 0.03 has been reported by Uma and Das [109].



(Recommendation: 02-25, Note: 10-6, Evaluated: 10-6)

Absorption Cross Sections: The UV absorption spectrum of trifluoroiodomethane, CF_3I , has been reported in a number of studies as summarized in Table 4H-21. The spectrum is continuous between 180 and 400 nm with a strong band centered at 267 nm with a long wavelength tail and a strong band evident at wavelengths <200 nm. The agreement among the room temperature cross section values at wavelengths >200 nm is better than 20% near the absorption maximum. At wavelengths <255 nm and in the range 280 – 350 nm the agreement is better than 15%. Fahr et al. [30] report the largest peak cross section and Rattigan et al. [85] the smallest. The cross section data from Solomon et al. [99] become increasingly greater than those of Rattigan et al. [85] at the longer wavelengths. The cross section data from Limão-Vieira et al. [66] lies between the data of Solomon et al. [99] and Fahr et al. [30]. For wavelengths <230 nm and >310 nm the Limão-Vieira et al. [66] data shows systematic deviations from the other studies. The recommended absorption cross sections in Table 4H-22 are taken from the data of Fahr et al. [30] in the range 180 – 215 nm, the mean of the values reported by Brouwer and Troe [20], Solomon et al. [99], and Fahr et al. [30] in the range 220 – 230 nm, the mean of the values reported by Brouwer and Troe [20], Solomon et al. [99], Fahr et al. [30], and Rattigan et al. [85], in the range 235 – 310 nm, the mean of the values reported by Solomon et al. [99], Fahr et al. [30], and Rattigan et al. [85] in the range 315 – 350 nm, and the values from Rattigan et al. [85] in the range 355 – 385 nm.

Table 4H-21. Summary of CF_3I Absorption Cross Section Studies

Study	Year	Temperature (K)	Wavelength (nm)	$10^{20} \sigma(267 \text{ nm})$ (cm^2)
Roxlo and Mandl [90]	1980	298	170 – 230	–
Brouwer and Troe [20]	1981	298, 625, 1050	220 – 360	~60.5
Bagratashvili et al. [8] and Abel et al. [1, 2]	1985	~4000 *	450	–
Solomon et al. [99]	1994	200 – 298	216 – 370	64.4
Fahr et al. [30]	1995	218 – 333	160 – 350	~70
Rattigan et al. [85]	1997	243 – 333	235 – 390	59.5
Limão-Vieira et al. [66]	2003	298	205 – 325 113 – 181	66.9

* CF_3I molecules excited by infrared laser absorption

Fahr et al. [30] (160 – 350 nm) and Limão-Vieira et al. [66] (113 – 181 nm) reported spectra with pronounced band structure and large absorption cross sections in the short wavelength region. The maximum absorption cross section reported was $\sim 1 \times 10^{-16} \text{ cm}^2 \text{ molecule}^{-1}$ at ~160 nm. The spectrum reported by Roxlo and Mandl [90] (170 – 230 nm) is in poor agreement with the results of Fahr et al. [30] and Limão-Vieira et al. [66].

Studies of the spectrum temperature dependence by Solomon et al. [99], Fahr et al. [30], and Rattigan et al. [85] are in qualitative agreement with an increase in the peak absorption cross section and decrease in the long wavelength tail cross sections (>280 nm) with decreasing temperature. The ratio $\sigma(298 \text{ K})/\sigma(\sim 240 \text{ K})$ at the peak is ~0.9 and the ratio $\sigma(333 \text{ K})/\sigma(298 \text{ K})$ is ~1. Solomon et al. [99] report a further increase of the

peak cross section down to 200 K whereas Fahr et al. [30] report a slight decrease between 253 and 218 K. The ratio $\sigma(298 \text{ K})/\sigma(\sim 240 \text{ K})$ increases from ~ 1.0 to ~ 1.9 between 280 and 340 nm and the ratio $\sigma(333 \text{ K})/\sigma(298 \text{ K})$ is nearly constant at ~ 1.3 . In the wavelength region 160 – 180 nm, Fahr et al. [30] report a decrease in the absorption cross sections with decreasing temperature. Solomon et al. [99] and Rattigan et al. [85] parameterized the cross section temperature dependence using the empirical expression

$$\ln \sigma(\lambda, T) = \ln \sigma(\lambda, 298 \text{ K}) + B(\lambda)(T - 298)$$

which reproduces the experimental data reasonably well. Fahr et al. [30] parameterized their measured cross section wavelength dependence using the empirical expression

$$\sigma(\lambda) = \sigma_0(\lambda) \exp(-L/\lambda) \text{ for } \lambda > 320 \text{ nm}$$

and the temperature dependence at 300, 310, 320, 330, 340, and 350 using

$$\sigma(T) = \sigma_0(T) \exp(-\theta/T)$$

Their paper should be consulted for the optimized $\sigma_0(\lambda)$, L , $\sigma_0(T)$ and θ parameters. There are some systematic differences in the $B(\lambda)$ coefficients reported by Solomon et al. [99] and Rattigan et al. [85]. The $B(\lambda)$ coefficients reported by Rattigan et al. [85] are recommended and listed in Table 4H-22.

Photolysis Quantum Yield and Product Studies: The photolysis quantum yield for CF_3I is expected to be unity for wavelengths above the dissociation threshold. CF_3I serves as a model system for the study of the photodynamics of $\text{I}^*(^2\text{P}_{1/2})$ atom production following UV photolysis of iodine containing molecules. There has been a number of studies reporting iodine spin-state quantum yields, $\Phi(\text{I}^*(^2\text{P}_{1/2}))$ and $\Phi(\text{I}(^2\text{P}_{3/2}))$. A summary of the quantum yield studies for photolysis in the wavelength range 248 – 308 nm is given in Table 4H-23. Quantum yields for $\text{I}(^2\text{P}_{3/2})$ atom formation, $\Phi(\text{I})$, can be derived from $\Phi(\text{I}) = 1 - \Phi(\text{I}^*)$.

Table 4H-22. Absorption Cross Sections of CF_3I at 298 K

λ (nm)	$10^{20} \sigma$ (cm^2)	$10^3 B$ (K^{-1})	λ (nm)	$10^{20} \sigma$ (cm^2)	$10^3 B$ (K^{-1})
180	3.11	—	285	33.4	0.55
185	0.75	—	290	22.7	1.65
190	0.28	—	295	14.3	2.98
195	0.16	—	300	8.6	4.22
200	0.15	—	305	5.06	5.61
205	0.19	—	310	2.82	6.84
210	0.34	—	315	1.62	7.68
215	0.68	—	320	0.905	8.27
220	1.52	—	325	0.485	8.74
225	2.88	—	330	0.262	9.25
230	5.03	—	335	0.142	9.92
235	8.21	0.16	340	0.0750	10.27
240	13.6	-0.16	345	0.0407	11.71
245	21.8	-0.52	350	0.0210	12.85
250	32.4	-0.86	355	0.0115	13.26
255	45.2	-1.17	360	0.0064	14.65
260	56.9	-1.37	365	0.0036	14.63
265	63.4	-1.43	370	0.002	15.49
270	63.1	-1.30	375	0.0011	17.14
275	56.1	-0.94	380	0.0007	17.66
280	45.1	-0.62	385	0.0004	19.71

Note:

Absorption cross sections

180 – 215 nm: Fahr et al. [30]

220 – 230 nm: mean of data from Brouwer and Troe [20], Solomon et al. [99], and Fahr et al. [30]

235 – 310 nm: mean of data from Brouwer and Troe [20], Solomon et al. [99], Fahr et al. [30], and Rattigan et al. [85],

315 – 350 nm: mean of data from Solomon et al. [99], Fahr et al. [30], and Rattigan et al. [85]

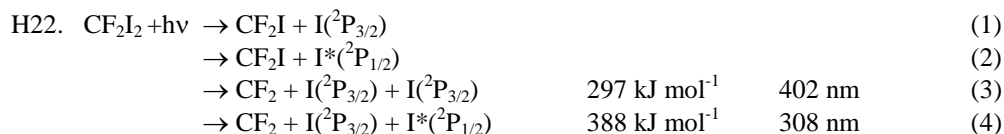
355 – 385 nm: Rattigan et al. [85]

Temperature coefficients

$B(\lambda)$: Rattigan et al. [85]; $\ln \sigma(\lambda, T) = \ln \sigma(\lambda, 298 \text{ K}) + B(\lambda)(T - 298)$, (243 – 333 K)

Table 4H-23. Summary of CF₃I Quantum Yield Studies

Study	Year	Photolysis Wavelength (nm)	$\Phi(I^*)$
Brewer et al. [17]	1983	248	0.89 ± 0.01
Gedanken et al. [37]	1987	248	0.87 ± 0.04
Felder [32]	1991	248	0.88
Furlan et al. [36]	1996	275	0.99 ± 0.01
Kim et al. [57]	1996	277	0.87
Furlan et al. [36]	1996	279	0.91 ± 0.01
		283	0.89 ± 0.01
		290	0.84 ± 0.01
		293	0.81 ± 0.01
		295	0.69 ± 0.01
		296	0.68 ± 0.01
		297	0.63 ± 0.02
		298	0.61 ± 0.02
		300	0.47 ± 0.01
		302	0.41 ± 0.0
		303	0.37 ± 0.01
Kang et al. [54]	1996	304	0.69
Felder [33]	1992	308	0.21



(Recommendation: 02-25, Note: 10-6, Evaluated: 10-6)

Absorption Cross Sections: The room temperature UV absorption spectrum of difluorodiodomethane, CF₂I₂, has been measured by Wannenmacher et al. [114] and Baum et al. [13] over the wavelength range 190 – 420 nm. The spectrum consists of a strong band that peaks at ~195 nm and several weaker overlapping absorption bands between 230 and 400 nm. The overlapping bands suggest transitions corresponding to the different dissociation processes. Numerical cross section data was obtained from Pfister and Huber [79]. The recommended absorption cross sections in Table 4H-24 are from Pfister and Huber [79] and were normalized to a peak value of 2.929×10^{-18} cm² molecule⁻¹ at 300 nm. The peak cross section was derived from five different spectra and has an uncertainty of $\pm 16\%$.

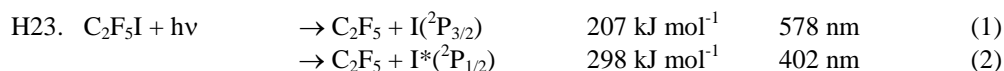
Photolysis Quantum Yield and Product Studies: The photodissociation of CF₂I₂ has been studied at room temperature and wavelengths 248, 308, 337, and 351 nm by Wannenmacher et al. [114] and Baum et al. [13].

Table 4H-24. Absorption Cross Sections of CF₂I₂ at 294 K

λ (nm)	$10^{20} \sigma$ (cm ²)	λ (nm)	$10^{20} \sigma$ (cm ²)	λ (nm)	$10^{20} \sigma$ (cm ²)
190	3163	270	203.1	350	66.24
195	4616	275	215.7	355	57.76
200	4070	280	224.3	360	49.81
205	2285	285	236.4	365	41.51
210	837.0	290	259.5	370	33.92
215	238.1	295	281.9	375	26.85
220	75.78	300	292.9	380	18.90
225	36.39	305	288.5	385	13.60
230	29.50	310	266.7	390	9.892
235	35.51	315	235.6	395	6.713
240	47.34	320	198.6	400	4.240
245	66.07	325	163.9	405	3.356
250	89.21	330	135.5	410	1.943
255	118.0	335	111.6	415	1.413
260	150.1	340	91.33	420	0.7066
265	180.5	345	78.25		

Note:

190 – 420 nm: Wannenmacher et al. [114] and Baum et al. [13] from Pfister and Huber [79]



(Recommendation: 02-25, Note: 10-6, Evaluated: 10-6)

Absorption Cross Sections: The UV absorption spectrum of pentafluoroiodoethane, C₂F₅I, was measured at 323 K by Zhang et al. [116] over the wavelength range 220 – 320 nm. The continuous absorption band has a maximum at ~269 nm with a cross section of $\sim 6.7 \times 10^{-19}$ cm² molecule⁻¹. Pence et al. [77] report a slightly smaller cross section of 6.39×10^{-19} cm² molecule⁻¹ at 268 nm and 295 K. The recommended values in Table 4H-25 were obtained from a figure in Zhang et al. [116].

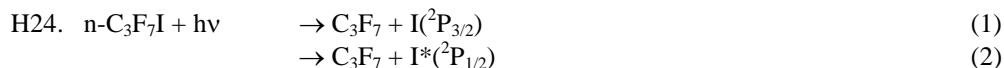
Photolysis Quantum Yield and Product Studies: The photolysis quantum yield for C₂H₅I is expected to be unity for wavelengths above the dissociation threshold. Kavita and Das [55] reported quantum yields for I*(²P_{1/2}) atom formation, $\Phi(I^*)$, at 266, 288, and ~305 nm to be 0.97 ± 0.03 , 0.75 ± 0.03 , and 0.83 ± 0.05 , respectively. Quantum yields for I(²P_{3/2}) atom formation, $\Phi(I)$, can be derived from $\Phi(I) = 1 - \Phi(I^*)$.

Table 4H-25. Absorption Cross Sections of C₂F₅I at 323 K

λ (nm)	$10^{20} \sigma$ (cm ²)	λ (nm)	$10^{20} \sigma$ (cm ²)	λ (nm)	$10^{20} \sigma$ (cm ²)
220	1.95	255	49.8	290	35.3
225	3.27	260	60.0	295	25.0
230	5.60	265	65.5	300	16.3
235	9.40	270	66.8	305	10.4
240	16.0	275	63.2	310	6.4
245	25.3	280	56.1	315	3.9
250	37.5	285	46.5	320	2.3

Note:

220 – 310 nm: Zhang et al. [116]



(Recommendation: 02-25, Note: 10-6, Evaluated: 10-6)

Absorption Cross Sections: The UV absorption spectrum of heptafluoropropyl iodide, $n\text{-C}_3\text{F}_7\text{I}$, has been measured at room temperature by Koffend and Leone [59] (265 – 341 nm) and Pence et al. [77] (180 – 400 nm). Pence et al. [77] report a plot (in arbitrary units) that shows an absorption band between ~220 and 340 nm with the maximum at ~268 nm. They report absolute absorption cross sections for 248, 268, and 308 nm. The data for 268 and 308 nm are in good agreement with the corresponding data reported by Koffend and Leone. The recommended absorption cross sections in Table 4H-26 include the value at 248 nm reported by Pence et al. [77], the mean of the values from Pence et al. and Koffend and Leone at 268 nm, and values from Koffend and Leone for the wavelength range 270 – 340 nm (values obtained by interpolation and extrapolation).

Photolysis Quantum Yield and Product Studies: The quantum yield for $n\text{-C}_3\text{F}_7\text{I}$ at wavelengths above the dissociation threshold is expected to be unity. Kavita and Das [55] reported quantum yields for $\text{I}^*({}^2\text{P}_{1/2})$ atom formation, $\Phi(\text{I}^*)$, of 0.83 ± 0.02 , 0.89 ± 0.03 , and 0.90 ± 0.05 at 266, 288, and ~305 nm, respectively. They also report $\Phi(\text{I}^*) = 0.83 \pm 0.01$, 0.80 ± 0.03 , and 0.89 ± 0.02 for $2\text{-C}_3\text{F}_7\text{I}$ at 266, 288, and ~305 nm, respectively. Quantum yields for $\text{I}({}^2\text{P}_{3/2})$ atom formation, $\Phi(\text{I})$, can be derived from $\Phi(\text{I}) = 1 - \Phi(\text{I}^*)$.

Table 4H-26. Absorption Cross Sections of $n\text{-C}_3\text{F}_7\text{I}$ at 298 K

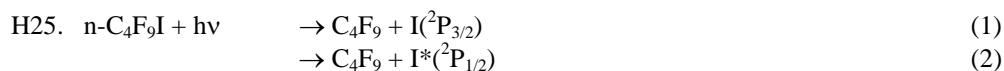
λ (nm)	$10^{20} \sigma$ (cm ²)	λ (nm)	$10^{20} \sigma$ (cm ²)	λ (nm)	$10^{20} \sigma$ (cm ²)
248	31.0	290	43.7	320	3.3
268	77.3	295	31.8	325	2.0
270	77.0	300	21.3	330	1.2
275	74.0	305	14.2	335	0.70
280	66.5	310	9.2	340	0.42
285	56.2	315	5.5		

Note:

248 nm: Pence et al. [77]

268 nm: mean of data from Pence et al. [77] and Koffend and Leone [59]

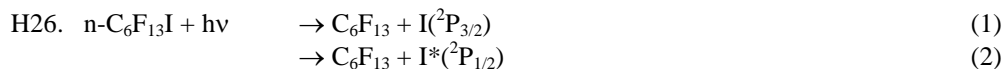
270 – 340 nm: Koffend and Leone [59] (Interpolation and extrapolation)



(Recommendation: 02-25, Note: 10-6, Evaluated: 10-6)

Absorption Cross Sections: Absorption cross sections for perfluorobutyl iodide, $n\text{-C}_4\text{F}_9\text{I}$, are not available.

Photolysis Quantum Yield and Product Studies: The quantum yield for $n\text{-C}_4\text{F}_9\text{I}$ at wavelengths above the dissociation threshold is expected to be unity. Kavita and Das [55] report quantum yields for $\text{I}^*({}^2\text{P}_{1/2})$ atom formation, $\Phi(\text{I}^*)$, of 0.75 ± 0.03 , 0.80 ± 0.03 , and 0.87 ± 0.02 at 266, 288, and ~305 nm, respectively. Quantum yields for $\text{I}({}^2\text{P}_{3/2})$ atom formation, $\Phi(\text{I})$, can be derived from $\Phi(\text{I}) = 1 - \Phi(\text{I}^*)$.



(Recommendation: 02-25, Note: 10-6, Evaluated: 10-6)

Absorption Cross Sections: Absorption cross sections for perfluorohexyl iodide, $n\text{-C}_6\text{F}_{13}\text{I}$, are not available.

Photolysis Quantum Yield and Product Studies: The quantum yield for $n\text{-C}_6\text{F}_{13}\text{I}$ at wavelengths above the dissociation threshold is expected to be unity. Kavita and Das [55] report quantum yields for $\text{I}^*({}^2\text{P}_{1/2})$ atom formation, $\Phi(\text{I}^*)$, of 0.82 ± 0.02 , 0.74 ± 0.03 , and 0.82 ± 0.01 at 266, 288, and ~305 nm, respectively. Quantum yields for $\text{I}({}^2\text{P}_{3/2})$ atom formation, $\Phi(\text{I})$, can be derived from $\Phi(\text{I}) = 1 - \Phi(\text{I}^*)$.



(Recommendation: 02-25, Note: 10-6, Evaluated: 10-6)

Absorption Cross Sections: The UV absorption spectrum of chloriodomethane, CH_2ICl , at room temperature has been reported by Schmitt and Comes [95] (205 – 330 nm), Kwok and Phillips [62, 63] (192 – 225 nm and 215 – 400 nm), Roehl et al. [87] (205 – 355 nm), and Rattigan et al. (235 – 390 nm) [85]. Kwok and Phillips also measured the CH_2ICl spectrum in cyclohexane solution. Schmitt and Comes [95] and Kwok and Phillips [62, 63] have only given their data as plots and are not considered further in this evaluation. Roehl et al. [87] (223 – 298 K) and Rattigan et al. [85] (243 – 333 K) have also reported cross section data over a range of temperatures. The room temperature data of Roehl et al. and Rattigan et al. are in good agreement with the values from Rattigan et al. being lower by $\leq 10\%$ between 240 and 345 nm. The recommended absorption cross sections in Table 4H-27 are from Roehl et al. for the wavelength range 205 – 230 nm, the mean of the values reported by Roehl et al. and Rattigan et al. for the range 235 – 355 nm, and from Rattigan et al. [85] for the range 360 – 390 nm.

The cross section data from Roehl et al. and Rattigan et al. show an increase in absorption cross sections around the absorption peak (~250 – 285 nm) with decreasing temperature. An opposite effect was reported for wavelengths >285 nm. The peak cross section at ~250 K reported in the two studies agree to within 15%. Roehl et al. and Rattigan et al. parameterized the cross section temperature dependence using different empirical expressions

$$\sigma(\lambda, T) = \sigma(298 \text{ K}) [1 + a_1(\lambda)(T - 298) + a_2(\lambda)(T - 298)^2] \text{ (Roehl et al.)}$$

$$\ln \sigma(\lambda, T) = \ln \sigma(\lambda, 298 \text{ K}) + B(\lambda)(T - 298) \text{ (Rattigan et al.)}$$

Both expressions reproduce the experimental data well and the $a_1(\lambda)$, $a_2(\lambda)$, and $B(\lambda)$ coefficients are given in Table 4H-27.

Photolysis Quantum Yield and Product Studies: The photolysis quantum yield for CH_2ICl is expected to be unity for wavelengths above the dissociation threshold. The quantum yield branching ratio $\text{I}^*(^2\text{P}_{1/2})/(\text{I}^*(^2\text{P}_{3/2}) + \text{I}^*(^2\text{P}_{1/2}))$ has been reported by Senapati et al. [98] at 5 wavelengths to be 0.47 ± 0.02 at 222 nm, 0.51 ± 0.01 at 236 nm, 0.51 ± 0.02 at 266 nm, 0.55 ± 0.03 at 280 nm, and 0.38 ± 0.01 at 304 nm. The quantum yield branching ratio $\text{Cl}^*(^2\text{P}_{1/2})/(\text{Cl}^*(^2\text{P}_{3/2}) + \text{Cl}^*(^2\text{P}_{1/2}))$ was reported by Senapati and Das [97] at 4 wavelengths to be 0.44 at 222 nm, 0.44 at 266 nm, 0.30 at 280 nm, and 0.22 at 304 nm.

Table 4H-27. Absorption Cross Sections of CH₂ICl at 298 K and Temperature Coefficients

λ (nm)	$10^{20} \sigma$ (cm ²)	$10^3 a_1$ (K ⁻¹)	$10^5 a_2$ (K ⁻²)	$10^3 B$ (K ⁻¹)	λ (nm)	$10^{20} \sigma$ (cm ²)	$10^3 a_1$ (K ⁻¹)	$10^5 a_2$ (K ⁻²)	$10^3 B$ (K ⁻¹)
205	132	-1.59	-3.83	—	300	25.9	2.38	-0.0473	2.56
210	42.1	8.47	3.76	—	305	16.7	3.13	0.394	3.08
215	11.1	6.12	4.30	—	310	10.9	3.13	0.303	3.50
220	7.50	0.232	0.129	—	315	7.16	2.74	-0.317	3.56
225	9.76	-0.0938	0.660	—	320	4.79	2.44	-0.533	3.46
230	14.9	-0.268	—	—	325	3.23	2.87	0.140	3.44
235	21.2	-0.512	-0.388	0.24	330	2.14	8.52	-4.21	3.72
240	32.1	-0.793	-0.664	0.12	335	1.40	2.02	-2.25	4.09
245	45.9	-0.929	-0.758	-0.02	340	0.906	5.20	4.54	4.87
250	63.3	-1.22	-1.13	-0.11	345	0.569	7.05	6.88	5.69
255	84.5	-1.25	-0.998	-0.28	350	0.350	9.12	11.7	6.88
260	106	-1.56	-1.14	-0.44	355	0.225	12.27	18.9	8.16
265	122	-1.05	-0.294	-0.55	360	0.133	—	—	9.01
270	128	-1.33	-0.593	-0.59	365	0.081	—	—	11.06
275	121	-1.07	-0.298	-0.47	370	0.048	—	—	11.47
280	104	-0.618	-0.309	-0.18	375	0.027	—	—	12.77
285	81.1	-0.326	-0.554	0.32	380	0.017	—	—	15.14
290	58.5	0.300	-0.711	0.99	385	0.008	—	—	19.12
295	39.9	1.55	-0.245	1.73	390	0.006	—	—	20.48

Note:

Absorption cross sections (σ)

205 – 230 nm : Roehl et al. [87]

235 – 355 nm: mean of data from Roehl et al. [87] and Rattigan et al. [85]

360 – 390 nm: Rattigan et al. [85]

Temperature coefficients

$a_1(\lambda)$ and $a_2(\lambda)$: Roehl et al. [87] ; $\sigma(\lambda, T) = \sigma(298 \text{ K}) [1 + a_1(\lambda)(T - 298) + a_2(\lambda)(T - 298)^2]$

$B(\lambda)$: Rattigan et al. [85] ; $\ln \sigma(\lambda, T) = \ln \sigma(\lambda, 298 \text{ K}) + B(\lambda)(T - 298)$



(Recommendation: 02-25, Note: 10-6, Evaluated: 10-6)

Absorption Cross Sections: The UV absorption cross sections of bromiodomethane, CH₂BrI, have been measured at room temperature by Man et al. [67] (180 – 360 nm) and at 273, 298, and 348 K by Mössinger et al. [72] (215 – 390 nm). The spectrum exhibits two absorption bands with maxima near 210 and 267 nm that can be assigned to electronic transitions to repulsive states anti-bonding in C–Br and C–I, respectively. The results from the two studies are not in quantitative agreement. Mössinger et al. report room temperature absorption cross sections of 5.7×10^{-18} and 2.3×10^{-18} cm² at 215 and 270 nm whereas Man et al. give larger values of $\sim 1 \times 10^{-17}$ and 3.5×10^{-18} cm² at these wavelengths (values extracted from a figure in their paper), respectively. The recommended room temperature cross sections in Table 4H-28 are taken from Mössinger et al. The absorption cross sections increase with decreasing temperature around the band maxima and decrease in the long-wavelength tails at 220 – 240 nm and above 290 nm. Mössinger et al. parameterized the temperature dependence using the empirical relation

$$\ln \sigma(\lambda, T) = \ln \sigma(\lambda, 298 \text{ K}) + B(\lambda)(T - 298)$$

The $B(\lambda)$ coefficients are listed in Table 4H-28 (an erroneous B value at 280 nm has been corrected).

Photolysis Quantum Yield and Product Studies: There are no quantum yield studies available. However, the photolysis quantum yield for wavelengths above the dissociation threshold is expected to be unity.

Table 4H-28. Absorption Cross Sections of CH₂BrI at 298 K and Temperature Coefficients

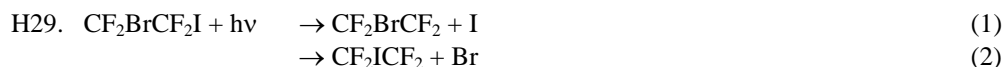
λ (nm)	$10^{20} \sigma$ (cm ²)	$10^3 B$ (K ⁻¹)	λ (nm)	$10^{20} \sigma$ (cm ²)	$10^3 B$ (K ⁻¹)
215	567	-2.16	305	42.9	1.13
220	423	-0.12	310	31.4	1.41
225	269	1.34	315	23.1	1.52
230	155	2.06	320	16.8	1.71
235	97.9	2.05	325	11.5	2.36
240	80.9	1.01	330	8.02	2.99
245	93.7	0.00	335	5.52	3.89
250	125	-0.58	340	3.50	4.79
255	170	-1.16	345	2.24	5.74
260	207	-1.29	350	1.41	6.73
265	228	-1.45	355	0.817	9.47
270	229	-1.73	360	0.498	11.5
275	214	-1.22	365	0.303	11.6
280	184	-0.94	370	0.165	14.3
285	150	-0.53	375	0.098	17.4
290	110	0.10	380	0.070	—
295	82.5	0.63	385	0.039	—
300	60.6	1.03	390	0.025	—

Note:

Mössinger et al. [72]

Temperature coefficients $B(\lambda)$ valid for the range 273 – 348 K

$$\ln \sigma(\lambda, T) = \ln \sigma(\lambda, 298 \text{ K}) + B(\lambda)(T - 298)$$



(Recommendation: 02-25, Note: 10-6, Evaluated: 10-6)

Absorption Cross Sections: The absorption spectrum of 1,1,2,2-tetrafluoro-1,2-bromoiodoethane, $\text{CF}_2\text{BrCF}_2\text{I}$, has been measured at room temperature over the wavelength range 190 – 350 nm by Pence et al. [77]. The absorption spectrum shows two distinct bands with a maxima near 268 nm corresponding to excitation in the C–I bond and below 193 nm corresponding to excitation in the C–Br bond. An absorption cross section of $2.36 \times 10^{-18} \text{ cm}^2$ at 193 nm was reported. The recommended cross sections in Table 4H-29 were taken from a figure in Pence et al. [77] and normalized to the quoted 193 nm cross section value.

Photolysis Quantum Yield and Product Studies: The quantum yield for $\text{CF}_2\text{BrCF}_2\text{I}$ photolysis is assumed to be unity for wavelengths <350 nm. A quantum yield for Br atom formation in the excited ($^2\text{P}_{1/2}$) spin state of 0.07 ± 0.05 at 193 nm was reported by Pence et al. [77].

Table 4H-29. Absorption Cross Sections of CF₂BrCF₂I at 298 K

λ (nm)	$10^{20} \sigma$ (cm ²)	λ (nm)	$10^{20} \sigma$ (cm ²)
190	256	265	114
195	219	270	119
200	181	275	117
205	138	280	107
210	105	285	92.0
215	72.7	290	73.0
220	53.4	295	54.6
225	42.5	300	39.5
230	37.3	305	27.8
235	37.3	310	18.4
240	42.9	315	11.4
245	50.2	320	5.77
250	63.2	325	3.61
255	80.3	330	1.34
260	98.0		

Note:

Pence et al. [77]

References for Section 4H

1. Abel, B., B. Herzog, H. Hippler and J. Troe, 1989, *J. Chem. Phys.*, 91, 890-899, 900-905.
2. Abel, B., H. Hippler and J. Troe, 1992, *J. Chem. Phys.*, 96, 8863-8871.
3. Ashworth, S. H., B. J. Allan and J. M. C. Plane, 2002, *Geophys. Res. Lett.*, 29, 65-1 - 65-4.
4. Atkinson, D. B., J. W. Hudjens and A. J. Orr-Ewing, 1999, *J. Phys. Chem. A*, 103, 6173-6180.
5. Atkinson, R., D. L. Baulch, R. A. Cox, R. F. Hampson, Jr., J. A. Kerr, M. J. Rossi and J. Troe, 2000, *J. Phys. Chem. Ref. Data*, 29, 167-266.
6. Atkinson, R., D. L. Baulch, R. A. Cox, R. F. Hampson, J. A. Kerr, M. J. Rossi and J. Troe, 1997, *J. Phys. Chem. Ref. Data*, 26, 521-1011.
7. Atkinson, R., D. L. Baulch, R. A. Cox, R. F. Hampson, J. A. Kerr and J. Troe, 1992, *J. Phys. Chem. Ref. Data*, 21, 1125-1568.
8. Bagratashvili, V. N., S. I. Ionov, G. V. Mishakov and V. A. Semchishen, 1985, *Chem. Phys. Lett.*, 115, 144-148.
9. Basco, N. and J. E. Hunt, 1978, *Int. J. Chem Kinet.*, 10, 733-743.
10. Bauer, D., T. Ingham, S. A. Carl, G. K. Moortgat and J. N. Crowley, 1998, *J. Phys. Chem.*, 102, 2857-2864.
11. Baughum, S. L. and S. R. Leone, 1980, *J. Chem. Phys.*, 72, 6531-6545.
12. Baulch, D. L., R. A. Cox, P. J. Crutzen, R. F. Hampson, Jr., J. A. Kerr, J. Troe and R. T. Watson, 1982, *J. Phys. Chem. Ref. Data*, 11, 327-496.
13. Baum, G. P., P. Felder and R. J. Huber, 1993, *J. Chem. Phys.*, 98, 1999-2010.
14. Binder, J. L., 1938, *Phys. Rev.*, 54, 114-117.
15. Bloss, W. J., D. M. Rowley, R. A. Cox and R. L. Jones, 2001, *J. Phys. Chem. A*, 105, 7840-7854.
16. Brewer, L. and J. Tellinghuisen, 1972, *J. Chem. Phys.*, 56, 3929-3938.
17. Brewer, P., P. Das, G. Ondrey and R. Bersohn, 1983, *J. Chem. Phys.*, 79, 720-723.
18. Bridges, L. and J. M. White, 1973, *J. Phys. Chem.*, 77, 295-298.
19. Broske, R. Ph.D. Thesis, University of Wuppertal, Germany, 1999.
20. Brouwer, L. and J. Troe, 1981, *Chem. Phys. Lett.*, 82, 1-4.
21. Calvert, J. G. and J. N. Pitts Jr. New York, 1966.
22. Campuzano-Jost, P. and J. N. Crowley, 1999, *J. Phys. Chem. A*, 103, 2712-2719.
23. Chichinin, A. I., 1993, *Chem. Phys. Lett.*, 209, 459-463.
24. Chichinin, A. I., S. A. Chasovnikov and L. N. Krasnoperov, 1987, *Chem. Phys. Lett.*, 138, 371-376.
25. Cox, R. A., W. J. Bloss, R. L. Jones and D. M. Rowley, 1999, *Geophys. Res. Lett.*, 26, 1857-1860.
26. Cox, R. A. and G. B. Coker, 1983, *J. Phys. Chem.*, 87, 4478-4484.
27. Dillon, T. J., M. E. Tucceri, D. Holscher and J. N. Crowley, 2005, *J. Photochem. Photobiol. A: Chem.*, 176, 3-14.
28. Donohue, T. and J. R. Wiesenfeld, 1975, *J. Chem. Phys.*, 63, 3130-3135.
29. Eden, S., P. Limão-Vieira, S. V. Hoffmann and N. J. Mason, 2006, *Chem. Phys.*, 331, 232-244.
30. Fahr, A., A. K. Nayak and R. E. Huie, 1995, *Chem. Phys.*, 199, 275-284.
31. Fahr, A., A. K. Nayak and M. J. Kurylo, 1995, *Chem. Phys.*, 197, 195-203.
32. Felder, P., 1991, *Chem. Phys.*, 155, 435-445.
33. Felder, P., 1992, *Chem. Phys. Lett.*, 197, 425-432.
34. Felps, W. S., K. Rupnik and S. P. McGlynn, 1991, *J. Phys. Chem.*, 95, 639-656.
35. Forte, E., H. Hippler and H. van den Bergh, 1981, *Int. J. Chem. Kinet.*, 13, 1227-1233.
36. Furlan, A., T. Gejo and R. J. Huber, 1996, *J. Phys. Chem.*, 100, 7956-7961.
37. Gedanken, A., 1987, *Chem. Phys. Lett.*, 137, 462-466.
38. Gibson, G. E. and H. C. Ramsperger, 1927, *Phys. Rev.*, 30, 598-600.
39. Gómez Martín, J. C., S. H. Ashworth, A. S. Mahajan and J. M. C. Plane, 2009, *Geophys. Res. Lett.*, 36, L09802.

40. Gómez Martín, J. C. and J. M. C. Plane, 2009, *Chem. Phys. Lett.*, 474, 79-83.
41. Gómez Martín, J. C., P. Spietz and J. P. Burrows, 2005, *J. Photochem. Photobiol. A: Chem.*, 176, 15-38.
42. Goodeve, C. F. and A. W. C. Taylor, 1936, *Proc. Roy. Soc. London, A* 154, 181-187.
43. Harwood, M. H., J. B. Burkholder, M. Hunter, R. W. Fox and A. R. Ravishankara, 1997, *J. Phys. Chem. A*, 101, 853-863.
44. Haugen, H. K., E. Weitz and S. R. Leone, 1964, *J. Chem. Phys.*, 83, 3402-3412.
45. Himmelmann, S., J. Orphal, H. Bovensmann, A. Richter, A. Ladstätter-Weissenmayer and J. P. Burrows, 1996, *Chem. Phys. Lett.*, 251, 330-334.
46. Huebert, B. J. and R. M. Martin, 1968, *J. Phys. Chem.*, 72, 3046-3048.
47. Ingham, T., M. Cameron and J. N. Crowley, 2000, *J. Phys. Chem. A*, 104, 8001-8010.
48. Jenkin, M. E. and R. A. Cox, 1985, *J. Phys. Chem.*, 89, 192-199.
49. Jenkin, M. E., R. A. Cox, A. Mellouki, G. Le Bras and G. Poulet, 1990, *J. Phys. Chem.*, 94, 2927-2934.
50. Jenkin, M. E., T. P. Murrells, S. J. Shalliker and G. D. Hayman, 1993, *J. Chem. Soc. Faraday Trans.*, 89, 433-446.
51. Joseph, D. M., S. H. Ashworth and J. M. C. Plane, 2005, *J. Photochem. Photobiol. A: Chem.*, 176, 68-77.
52. Joseph, D. M., S. H. Ashworth and J. M. C. Plane, 2007, *Phys. Chem. Chem. Phys.*, 9, 5599 - 5607.
53. Jung, K.-W., T. S. Ahmadi and M. A. El-Sayed, 1997, *J. Phys. Chem. A*, 101, 6562-6567.
54. Kang, W. K., K. W. Jung, D.-C. Kim and K.-H. Jung, 1996, *J. Chem. Phys.*, 104, 5815-5820.
55. Kavita, K. and P. K. Das, 2000, *J. Chem. Phys.*, 112, 8426-8431.
56. Kim, Y. S., Y. J. Jung and K.-H. Jung, 1997, *J. Chem. Phys.*, 107, 3805-3812.
57. Kim, Y. S., W. K. Kang and K.-H. Jung, 1996, *J. Chem. Phys.*, 105, 551-557.
58. Kim, Y. S., W. K. Kang, D.-C. Kim and K.-H. Jung, 1997, *J. Phys. Chem. A*, 101, 7576-7581.
59. Koffend, J. B. and S. R. Leone, 1981, *Chem. Phys. Lett.*, 81, 136-141.
60. Kortüm, G. and G. Friedheim, 1947, *Z. Naturforsch.*, 2a, 20-27.
61. Kwok, W. M. and D. L. Phillips, 1996, *J. Chem. Phys.*, 104, 2529-2540.
62. Kwok, W. M. and D. L. Phillips, 1997, *Mol. Phys.*, 90, 315-326.
63. Kwok, W. M. and D. L. Phillips, 1997, *Chem. Phys. Lett.*, 270, 506-516.
64. Langford, S. R., P. M. Regan, A. J. Orr-Ewing and N. M. R. Ashfold, 1998, *Chem. Phys.*, 231, 245-260.
65. Laszlo, B., M. J. Kurylo and R. E. Huie, 1995, *J. Phys. Chem.*, 99, 11701-11707.
66. Limão-Vieira, P., S. Eden and N. J. Mason, 2003, *Radiation Phys. Chem.*, 68, 187-192.
67. Man, S.-Q., W. M. Kwok, D. L. Phillips and A. E. Johnson, 1996, *J. Chem. Phys.*, 105, 5842-5857.
68. Martin, R. M. and J. E. Willard, 1964, *J. Chem. Phys.*, 40, 2999-3007.
69. Mashnin, T. S., A. V. Cheryshev and L. N. Krasnoperov, 1993, *Chem. Phys. Lett.*, 207, 105-109.
70. Mathieson, L. and A. L. G. Rees, 1956, *J. Chem. Phys.*, 25, 753-761.
71. Mössinger, J. C., D. M. Rowley and R. A. Cox, 2002, *Atmos. Chem. Phys.*, 2, 227-234.
72. Mossinger, J. C., D. E. Shallcross and R. A. Cox, 1998, *J. Chem. Soc. Faraday Trans.*, 94, 1391-1396.
73. Myer, J. A. and J. A. R. Samson, 1970, *J. Chem. Phys.*, 52, 716-718.
74. Ni, C.-K. and G. W. Flynn, 1993, *Chem. Phys. Lett.*, 210, 333-339.
75. Ogilvie, J. F., 1971, *Trans. Faraday Soc.*, 67, 2205-2215.
76. Ogorzalek Loo, R., H.-P. Haerri, G. E. Hall and P. L. Houston, 1989, *J. Chem. Phys.*, 90, 4222-4236.
77. Pence, W., S. Baughum and S. Leone, 1981, *J. Phys. Chem.*, 85, 3844-3851.
78. Petersen, A. B. and I. W. M. Smith, 1978, *Chem. Phys.*, 30, 407-413.
79. Pfister, R. and R. J. Huber, 2002, personal communication.
80. Phillips, D. L., A. B. Myers and J. J. Valentini, 1992, *J. Phys. Chem.*, 96, 2039-2044.
81. Porret, D. and C. F. Goodeve, 1937, *Trans. Faraday Soc.*, 33, 690-693.
82. Porret, D. and C. F. Goodeve, 1938, *Proc. Roy. Soc. London A*, 165, 31-42.
83. Porter, G., Z. G. Szabo and M. G. Townsend, 1962, *Proc. Roy. Soc. London, A* 270, 493-500.
84. Rabinowitch, E. and W. C. Wood, 1936, *Trans. Faraday Soc.*, 32, 540-546.

85. Rattigan, O. V., D. E. Shallcross and R. A. Cox, 1997, *J. Chem. Soc. Soc. Faraday Trans.*, 93, 2839-2846.
86. Rebbert, R. E., S. G. Lias and P. Ausloos, 1973, *Int. J. Chem. Kinet.*, 5, 893-908.
87. Roehl, C. M., J. B. Burkholder, G. K. Moortgat, A. R. Ravishankara and P. J. Crutzen, 1997, *J. Geophys. Res.*, 102, 12819-12829.
88. Romand, J., 1949, *Ann. Phys. (Paris)*, 4, 529-590.
89. Rowley, D. M., J. C. Mössinger, R. A. Cox and R. L. Jones, 1999, *J. Atmos. Chem.*, 34, 137-151.
90. Roxlo, C. and A. Mandl, 1980, *J. Appl. Phys.*, 51, 2969-2972.
91. Saiz-Lopez, A., R. W. Saunders, D. M. Joseph, S. H. Ashworth and J. M. C. Plane, 2004, *Atmos. Chem. Phys.*, 4, 1443-1450.
92. Sander, S. P., 1986, *J. Phys. Chem.*, 90, 2194-2199.
93. Sander, S. P., B. J. Finlayson-Pitts, R. R. Friedl, D. M. Golden, R. E. Huie, C. E. Kolb, M. J. Kurylo, M. J. Molina, G. K. Moortgat, V. L. Orkin and A. R. Ravishankara "Chemical Kinetics and Photochemical Data for Use in Atmospheric Studies, Evaluation Number 14," JPL Publication 02-25, Jet Propulsion Laboratory, Pasadena, 2002 <http://jpldataeval.jpl.nasa.gov>.
94. Schmitt, G. and F. J. Comes, 1980, *J. Photochem.*, 14, 107-123.
95. Schmitt, G. and F. J. Comes, 1987, *J. Photochem. Photobiol. A*, 41, 13-30.
96. Seery, D. J. and D. Britton, 1964, *J. Phys. Chem.*, 68, 2263-2266.
97. Senapati, D. and P. K. Das, 2004, *Chem. Phys. Lett.*, 393, 535-538.
98. Senapati, D., K. Kavita and P. K. Das, 2002, *J. Phys. Chem. A*, 106, 8479-8482.
99. Solomon, S., J. B. Burkholder, A. R. Ravishankara and R. R. Garcia, 1994, *J. Geophys. Res.*, 99, 20929-20935.
100. Spietz, P., 2005, PhD-Thesis, Univ. of Bremen, Germany.
101. Spietz, P., J. C. G. Martin and J. P. Burrows, 2005, *J. Photochem. Photobiol. A: Chem.*, 176, 50-67.
102. Spietz, P., J. G. Martín and J. P. Burrows, 2006, *Atmos. Chem. Phys.*, 6, 2177-2191.
103. Stickel, R. E., A. J. Hynes, J. D. Bradshaw, W. L. Chameides and D. D. Davis, 1988, *J. Phys. Chem.*, 92, 1862-1864.
104. Sulzer, P. and K. Wieland, 1952, *Helv. Phys. Acta*, 25, 653-676.
105. Tellinghuisen, J., 1973, *J. Chem. Phys.*, 58, 2821-2834.
106. Tonokura, K., Y. Matsumi, M. Kawasaki, H. L. Kim, S. Yabushita, S. Fujimura and K. Saito, 1993, *J. Chem. Phys.*, 99, 3461-3467.
107. Tucceri, M. E., D. Hölscher, A. Rodriguez, T. J. Dillon and J. N. Crowley, 2006, *Phys. Chem. Chem. Phys.*, 8, 834-846.
108. Turnipseed, A. A., M. K. Gilles, J. B. Burkholder and A. R. Ravishankara, 1995, *Chem. Phys. Lett.*, 242, 427-434.
109. Uma, S. and P. K. Das, 1994, *Can. J. Chem.*, 72, 865-869.
110. Uma, S. and P. K. Das, 1995, *Chem. Phys. Lett.*, 241, 335-338.
111. Uma, S. and P. K. Das, 1996, *J. Chem. Phys.*, 104, 4470-4474.
112. Van den Bergh, H. and J. Troe, 1976, *J. Chem. Phys.*, 64, 736-742.
113. Vogt, K. and J. Koenigsberger, 1923, *Z. Physik*, 13, 292-310.
114. Wannenmacher, E. A. J., P. Felder and R. J. Huber, 1991, *J. Chem. Phys.*, 95, 986-997.
115. Wrede, E., S. Laubach, S. Schulenburg, A. Brown, E. R. Wouters, A. J. Orr-Ewing and N. M. R. Ashfold, 2001, *J. Chem. Phys.*, 114, 2629-2646.
116. Zhang, L., W. Fuss and K. L. Kompa, 1990, *Chem. Phys.*, 144, 289-297.

SECTION 4I. SO_x PHOTOCHEMISTRY



(Recommendation: 79, Note: 10-6, Evaluated: 10-6)

Absorption Cross Sections: The UV absorption spectrum of sulfur dioxide, SO₂, is highly structured with a very weak absorption band in the 340 – 390 nm region, a weak absorption band in the 260 – 340 nm region, and a strong absorption band extending from 180 to 235 nm. For the wavelength region commonly used for atmospheric monitoring, 300 – 324 nm, there are numerous reports of room temperature absorption cross sections. Manatt and Lane [22] have compiled and evaluated SO₂ cross section measurements prior to 1993 that cover the wavelength range 106 – 403 nm. Since 1993 there have been additional studies including Bogumil et al. [2] (239 – 395 nm), Feng et al. [8] (7.7 – 248 nm), Hermans et al. [13] (227 – 416 nm), Prahlad and Kumar [28] (188 – 219 nm), Rufus et al. [31] (220 – 325 nm), Sprague and Joens [32] (352 – 396 nm), Vandaele et al. [34] (250 – 333 nm), Vattulainen et al. [36] (195 – 350 nm) and Wu et al. [42] (170 – 297 nm). The temperature dependence of the absorption spectrum has been measured by McGee and Burris [23] (295 and 210 K), Bogumil et al. [2] (203 – 293 K), Hicks [14] (199 – 300 K), Hermans et al. [13] (298 – 358 K), Leroy et al. [19] (218 – 296 K), Prahlad and Kumar [28] (220 – 300 K), Vattulainen et al. [36] (293 – 1073 K), and Wu et al. [42] (200 – 400 K). Absorption cross sections are not recommended due to the highly structured nature of the spectrum and should be obtained from the original literature.

Photolysis Quantum Yield and Product Studies: The atmospheric photochemistry of SO₂ has been reviewed by Hecklen et al. [12] and Calvert and Stockwell [6]. Photo-oxidation at $\lambda > \sim 300$ nm by way of the electronically excited states of SO₂ appears to be relatively unimportant.



(Table: 10-6, Note: 10-6, Evaluated: 10-6)

Absorption Cross Sections: The VUV/UV absorption spectrum of sulfur trioxide, SO₃, is continuous between 140 and 330 nm with weak vibrational band structure superimposed between 222 and 285 nm. Absorption cross sections have been reported by Leroy et al. [18] (240 – 264 nm), Burkholder and McKeen [4] (196 – 330 nm), and Hintze et al. [15] (140 – 194 nm). The cross section values are in good agreement in the regions of overlap and the recommended cross sections between 180 and 330 nm in Table 4I-1 are taken from Burkholder et al. [4] and Hintze et al. [15].

Photolysis Quantum Yield and Product Studies: No studies are available.

Table 4I-1. Absorption Cross Sections of SO₃ at 298 K

λ (nm)	$10^{20} \sigma$ (cm ²)	λ (nm)	$10^{20} \sigma$ (cm ²)	λ (nm)	$10^{20} \sigma$ (cm ²)	λ (nm)	$10^{20} \sigma$ (cm ²)
180	114	220	19.1	256	1.16	296	0.0574
182	108	218	23.3	258	1	298	0.0496
184	102	220	19.1	260	0.867	300	0.0424
186	97.3	222	15.6	262	0.75	302	0.0361
188	91.4	224	12.8	264	0.648	304	0.0308
190	87.8	226	10.6	266	0.559	306	0.0263
192	80.2	228	8.88	268	0.482	308	0.0224
194	75	230	7.49	270	0.416	310	0.0192
196	79.4	232	6.51	272	0.358	312	0.0163
198	76.8	234	5.62	274	0.308	314	0.014
200	73.2	236	4.87	276	0.265	316	0.0119
202	69.1	238	4.24	278	0.228	318	0.00976
204	64.5	240	3.69	280	0.195	320	0.00809
206	58.8	242	3.21	282	0.167	322	0.00693
208	52.6	244	2.79	284	0.143	324	0.0059
210	46.4	246	2.41	286	0.123	326	0.00502
212	40	248	2.09	288	0.106	328	0.00427
214	33.9	250	1.8	290	0.0907	330	0.00363
216	28.3	252	1.56	292	0.0774		
218	23.3	254	1.34	294	0.0664		

Note:

140 – 194 nm: Hintze et al. [15]

196 – 330 nm: Burkholder et al. [4]



(Recommendation: 78, Note: 10-6, Evaluated: 10-6)

Absorption Cross Sections: The UV absorption spectrum of hydrogen sulfide, H₂S, is weak at wavelengths >250 nm. H₂S has a strong absorption band with diffuse structure centered near 200 nm and a broad VUV spectrum. The H₂S absorption cross section at 184.9 nm has been measured by Wine et al. [39] to be 3.82 x 10⁻¹⁸ cm² molecule⁻¹ and at 121.6 nm by Watanabe and Jursa [37] and Vatsa and Volpp [35], to be 2.65 x 10⁻¹⁷ cm² molecule⁻¹ (average value). The recommended absorption cross sections in Table 4I-2 are taken from Wu and Chen [40]. Note that the values given here do not reproduce the full detail of the diffuse band structure.

Photolysis Quantum Yield and Product Studies: Photolysis is a minor atmospheric loss process for H₂S throughout the troposphere and stratosphere.

Table 4I-2. Absorption Cross Sections of H₂S at 298 K

λ (nm)	$10^{20} \sigma$ (cm ²)	λ (nm)	$10^{20} \sigma$ (cm ²)
180	189	216	187
182	242	218	155
184	302	220	129
186	382	222	106
188	452	224	86.4
190	534	226	69.6
192	616	228	55.3
194	636	230	43.2
196	724	232	33.3
198	667	234	25.5
200	670	236	19.3
202	623	238	14.3
204	512	240	10.4
206	423	242	7.55
208	359	244	5.38
210	307	246	3.75
212	260	248	2.55
214	223	250	1.69

Note:

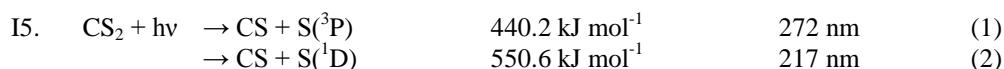
180 – 250 nm: Wu and Chen [40]



(Recommendation: 10-6, Note: 10-6, Evaluated: 10-6)

Absorption Cross Sections: The gas-phase absorption spectrum of sulfuric acid, H₂SO₄, was reported by Burkholder et al. [5](195-330 nm) at 473 K using diode array spectroscopy to have cross sections <1 x 10⁻²¹ cm² molecule⁻¹. Hintze et al. [15] studied the spectrum of H₂SO₄ vapor at 403-423 K and reported an upper limit of 1 x 10⁻¹⁸ cm² molecule⁻¹ for the absorption cross sections between 140 and 170 nm and an upper limit of 1 x 10⁻¹⁹ cm² molecule⁻¹ in the wavelength range 170-195 nm.

Photolysis Quantum Yield and Product Studies: No studies are available.



(Recommendation: 10-6, Note: 10-6, Evaluated: 10-6)

Absorption Cross Sections: The UV absorption spectrum of carbon disulfide, CS₂, has two distinct highly structured bands with a strong absorption extending from 185 to 230 nm and a weaker band in the 290 – 380 nm range. The absorption cross sections have been measured in several studies which are in reasonable agreement. Due to the high degree of structure in the absorption spectrum absorption cross sections at specific wavelengths should be obtained from the original literature. The absorption cross sections in Table 4I-3 were obtained by averaging the data from Hearn and Joens [11] over 1 nm intervals.

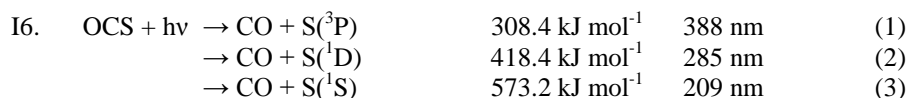
Photolysis Quantum Yield and Product Studies: The photochemistry of CS₂ has been reviewed by Okabe [25] and discussed by Wine et al. [38]. Wine et al. report that electronically excited CS₂ may react with O₂ to yield OCS.

Table 4I-3. Absorption cross sections of CS₂ at 298 K

λ (nm)	$10^{20} \sigma$ (cm ²)	λ (nm)	$10^{20} \sigma$ (cm ²)	λ (nm)	$10^{20} \sigma$ (cm ²)	λ (nm)	$10^{20} \sigma$ (cm ²)
275	0.017	299	2.017	323	5.180	347	0.328
276	0.020	300	1.879	324	3.517	348	0.109
277	0.027	301	3.269	325	8.628	349	0.368
278	0.043	302	3.166	326	5.023	350	0.239
279	0.050	303	3.131	327	3.481	351	0.127
280	0.053	304	4.438	328	2.849	352	0.255
281	0.062	305	4.461	329	2.848	353	0.066
282	0.080	306	3.658	330	3.802	354	0.172
283	0.103	307	5.122	331	1.301	355	0.247
284	0.122	308	7.101	332	3.057	356	0.052
285	0.158	309	4.930	333	1.552	357	0.133
286	0.209	310	8.838	334	1.506	358	0.055
287	0.254	311	5.611	335	1.375	359	0.059
288	0.309	312	6.692	336	0.861	360	0.119
289	0.445	313	8.148	337	1.377	361	0.042
290	0.438	314	7.842	338	0.591	362	0.048
291	0.635	315	9.440	339	1.121	363	0.021
292	0.640	316	7.039	340	0.489	364	0.037
293	0.878	317	9.462	341	0.386	365	0.012
294	0.801	318	7.159	342	0.573	366	0.036
295	1.137	319	9.803	343	0.387	367	0.023
296	1.134	320	4.518	344	0.556	368	0.020
297	1.861	321	6.122	345	0.353	369	0.011
298	2.287	322	4.221	346	0.350	370	0.018

Note:

275 – 370 nm: Hearn and Joens [11], average values



(Note: 10-6, Evaluated: 10-6)

Absorption Cross Sections: The UV absorption spectrum of carbonyl sulfide, OCS, peaks near 222 nm with weak diffuse structure near the peak and in the long wavelength tail that is superimposed on a stronger continuum. The absorption cross sections of OCS have been measured at room temperature by Breckenridge and Taube [3] (200 – 260 nm), Rudolph and Inn [30] (200 – 270 nm), Leroy et al. [18] (210 – 260 nm), Ferro and Ruben [9] (210 – 250 nm), Wu [41] (200 – 252 nm), and Molina et al. [24] (185 – 300 nm). The reported peak absorption cross sections agree to within 15%. The absorption spectrum temperature dependence has been measured by Wu [41] (170 – 370 K), Rudolph and Inn [30] (195 K), and Molina et al. [24] (225 K). The OCS spectrum shows a decrease in absolute cross section with decreasing temperature at all wavelengths between 210 – 300 nm. The recommended cross sections in Table 4I-4 are the values averaged over the wavelength intervals used in solar photolysis calculations taken from Molina et al. [24]. Using the recommended cross sections, solar photodissociation rate coefficients of OCS in the troposphere are negligible.

Photolysis Quantum Yield and Product Studies: Rudolph and Inn [30] measured the CO quantum yield following the photolysis of OCS at 220, 225.8, 230, 253.7 nm (Hg lines) and 214 nm (Zn line). The CO quantum yield was found to be independent of the photolysis wavelength, within the precision of the measurement, with an average value of 0.72 ± 0.08 . In a more direct CO quantum yield study, Zhao et al. [44] reported a CO quantum yield of >0.95 at 248 nm. A unit CO quantum yield is recommended over the wavelength range 220 – 254 nm.

Table 4I-4. Absorption Cross Sections of OCS at 225 and 295 K

λ (nm)	$10^{20} \sigma$ (cm ²)		λ (nm)	$10^{20} \sigma$ (cm ²)	
	295 K	225 K		295 K	225 K
186.1	18.9	13.0	231.2	22.1	18.8
187.8	8.33	5.63	233.9	17.1	14.0
189.6	3.75	2.50	236.7	12.5	9.72
191.4	2.21	1.61	239.5	8.54	6.24
193.2	1.79	1.53	242.5	5.61	3.89
195.1	1.94	1.84	245.4	3.51	2.29
197.0	2.48	2.44	248.5	2.11	1.29
199.0	3.30	3.30	251.6	1.21	0.679
201.0	4.48	4.50	254.6	0.674	0.353
203.1	6.12	6.17	258.1	0.361	0.178
205.1	8.19	8.27	261.4	0.193	0.0900
207.3	10.8	10.9	264.9	0.0941	0.0419
209.4	14.1	14.2	268.5	0.0486	0.0199
211.6	17.6	17.6	272.1	0.0248	0.0101
213.9	21.8	21.8	275.9	0.0119	0.0048
216.2	25.5	25.3	279.7	0.0584	0.0021
218.6	28.2	27.7	283.7	0.0264	0.0009
221.5	30.5	29.4	287.8	0.0012	0.0005
223.5	31.9	29.5	292.0	0.0005	0.0002
226.0	30.2	27.4	296.3	0.0002	–
228.6	26.8	23.7			

Note:

Molina et al. [24]

17. $\text{SF}_6 + h\nu \rightarrow \text{SF}_5 + \text{F}$ $391.6 \text{ kJ mol}^{-1}$ 305 nm (1)
 $\rightarrow \text{SF}_4 + \text{F}_2$ $458.1 \text{ kJ mol}^{-1}$ 261 nm (2)

(Note: 10-6, Evaluated: 10-6)

Absorption Cross Sections: Sulfur hexafluoride, SF_6 , has weak absorption at wavelengths $>130 \text{ nm}$ and its atmospheric photolysis occurs primarily at Lyman- α (121.6 nm). The absorption cross section at Lyman- α has been reported by Ravishankara et al. [29]. Bertrand et al. [1], Hitchcock and van der Weil [16], and Zetzsch [43] have reported cross sections near Lyman- α that are within a factor of two of the Ravishankara et al. value. The recommended Lyman- α cross section of $1.76 \times 10^{-18} \text{ cm}^2 \text{ molecule}^{-1}$ is taken from Ravishankara et al. [29]. The atmospheric residence time of SF_6 is estimated to be thousands of years (Ravishankara et al. [29]; Ko et al. [17]).

Photolysis Quantum Yield and Product Studies: No data are available.

18. $\text{SF}_5\text{CF}_3 + h\nu \rightarrow \text{SF}_5 + \text{CF}_3$ $347.3 \text{ kJ mol}^{-1}$ 344 nm (1)

(Recommendation: 10-6, Note: 10-6, Evaluated: 10-6)

Absorption Cross Sections: SF_5CF_3 does not absorb significantly at wavelengths $>160 \text{ nm}$. The VUV absorption cross sections have been measured in several studies [7, 10, 20, 21, 33] and photodissociation at Lyman- α (121.6 nm) accounts for the majority of SF_5CF_3 atmospheric photolysis rate. Chim et al. [7] reported $\sigma(121.6 \text{ nm}) = 1.3 \times 10^{-17} \text{ cm}^2 \text{ molecule}^{-1}$. The absorption cross sections reported by Takahashi et al. [33] and Limão-Vieira et al. [20, 21] are significantly smaller but agree to within 20% with each other. An average of the Takahashi et al. and Limão-Vieira et al. cross section values, $7.1 \times 10^{-18} \text{ cm}^2 \text{ molecule}^{-1}$ is recommended.

Photolysis Quantum Yield and Product Studies: No studies are available.

- I9. $\text{SO}_2\text{F}_2 + h\nu \rightarrow \text{SO}_2\text{F} + \text{F}$ 452.7 kJ mol⁻¹ 264 nm (1)
 $\rightarrow \text{SO}_2 + \text{F}_2$ 462.3 kJ mol⁻¹ 258 nm (2)

(Recommendation: 10-6, Note: 10-6, Evaluated: 10-6)

Absorption Cross Sections: The UV and VUV absorption spectrum of sulfuryl fluoride, SO_2F_2 , has been measured at room temperature by Pradayrol et al. [27] over the wavelength range 120 – 210 nm and Papadimitriou et al. [26] at 184.9, 193, and 213.9 nm, Table 4I-5. The agreement between these two studies is ~10% at 184.9 nm but large deviations exist at longer wavelengths.

Photolysis Quantum Yield and Product Studies: Papadimitriou et al. [26] reported the photodissociation quantum yield of SO_2F_2 at 193 nm to be <0.02. This upper limit is recommended for wavelengths >193 nm. No photolysis product studies are currently available.

Table 4I-5. Absorption Cross Sections of SO_2F_2 at 298 K

λ (nm)	$10^{20} \sigma$ (cm ²)
184.9	0.717
193	0.40
213.9	0.0208

Note:

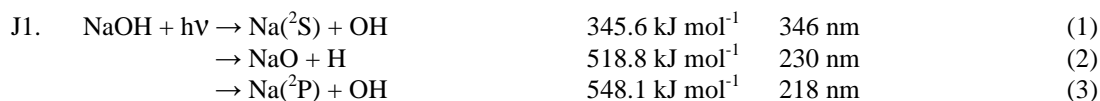
Papadimitriou et al. [26]

References for Section 4I

1. Bertrand, C., G. J. Collin and H. Gagnon, 1975, J. Chim. Phys., **72**, 719-723.
2. Bogumil, K., J. Orphal, T. Homann, S. Voigt, P. Spietz, O. C. Fleischmann, A. Vogel, M. Hartmann, H. Bovensmann, J. Frerick and J. P. Burrows, 2003, J. Photochem. Photobiol. A: Chem., **157**, 167-184.
3. Breckenridge, W. and H. H. Taube, 1970, J. Chem. Phys., **52**, 1713-1715.
4. Burkholder, J. B. and S. A. McKeen, 1997, Geophys. Res. Lett., **24**, 3201-3204.
5. Burkholder, J. B., M. Mills and S. McKeen, 2000, Geophys. Res. Lett., **27**, 2493-2496.
6. Calvert, J. G. and W. R. Stockwell. In *Acid Precipitation: SO₂, NO, NO₂ Oxidation Mechanisms: Atmospheric Considerations*; Ann Arbor Sci. Publishers: Ann Arbor, Michigan, 1983.
7. Chim, R. Y. L., R. A. Kennedy and R. P. Tuckett, 2003, Chem. Phys. Lett., **367**, 697-703.
8. Feng, R., G. Cooper, G. R. Burton, C. E. Brion and L. Avaldi, 1999, Chem. Phys., **240**, 371-386.
9. Ferro, B. M. and B. G. Reuben, 1971, Trans. Faraday Soc., **67**, 2847-2851.
10. Hatherly, P. A. and A. J. Flaxman, 2003, Chem. Phys. Lett., **380**, 512-515.
11. Hearn, C. H. and J. A. Joens, 1991, J. Quant. Spectrosc. Radiat. Transfer, **45**, 69 - 75.
12. Heicklen, J., N. Kelly and K. Partymiller, 1980, Rev. Chem. Intermediates, **3**, 315-404.
13. Hermans, C., A. C. Vandaele and S. Fally, 2009, J. Quant. Spectrosc. Radiat. Transfer, **110**, 756-765.
14. Hicks, E., B. Leroy, P. Rigaud, J.-L. Joudain and G. L. Bras, 1979, J. Chim. Phys., **76**, 693-698.
15. Hintze, P. E., H. G. Kjaergaard, V. Vaida and J. B. Burkholder, 2003, J. Phys. Chem. A, **107**, 1112-1118.
16. Hitchcock, A. P. and M. J. Van der Wiel, 1979, J. Phys. B: Atom. Mol. Phys., **12**, 2153-2169.
17. Ko, M. K. W., D. S. Nien, W. C. Wang, G. Shia, A. Goldman, F. J. Murcray, D. G. Murcray and C. P. Rinsland, 1993, J. Geophys. Res., **98**, 10499-10507.
18. Leroy, B., G. L. Bras and P. Rigaud, 1981, Ann. Geophys., **37**, 297-302.
19. Leroy, B., P. Rigaud, J. L. Jourdain and G. L. Bras, 1983, Moon Planets, **29**, 177-183.
20. Limão-Vieira, P., S. Eden, P. A. Kendall, N. J. Mason, A. Giuliani, J. Heinesch, M.-J. Hubin-Franskin, J. Delwiche and S. V. Hoffmann, 2004, Int. J. Mass Spectrom., **233**, 335-341.
21. Limão-Vieira, P., P. A. Kendall, S. Eden, N. J. Mason, J. Heinesch, M. J. Hubin-Franskin, J. Delwiche and A. Giuliani, 2003, Radiation Phys.Chem., **68**, 193-197.
22. Manatt, S. L. and A. L. Lane, 1993, J. Quant. Spectrosc. Radiat. Transfer, **50**, 267-276.
23. McGee, T. J. and J. Burris, 1987, J. Quant. Spectrosc. Radiat. Transfer, **37**, 165-182.
24. Molina, L. T., J. J. Lamb and M. J. Molina, 1981, Geophys. Res. Lett., **8**, 1008-1011.
25. Okabe, H. *Photochemistry of Small Molecules*; John Wiley and Sons Inc.: New York, 1978.
26. Papadimitriou, V. C., R. W. Portmann, D. W. Fahey, J. Muhle, R. F. Weiss and J. B. Burkholder, 2008, J. Phys. Chem. A, **112**, 12657-12666.
27. Pradayrol, C., A. M. Casanovas, I. Deharo, J. P. Geuelfucci and J. Casanovas, 1996, J. Phys. III France, **6**, 603-612.
28. Prahlad, V. and V. Kumar, 1997, J. Quant. Spectrosc. Radiat. Transfer, **57**, 719-723.
29. Ravishankara, A. R., S. Solomon, A. A. Turnipseed and R. F. Warren, 1993, Science, **259**, 194-199.
30. Rudolph, R. N. and E. C. Y. Inn, 1981, J. Geophys. Res., **86**, 9891-9894.

31. Rufus, J., G. Stark, P. L. Smith, J. C. Pickering and A. P. Thorne, 2003, *J. Geophys. Research -Planets*, **108**, 5011.
32. Sprague, K. E. and J. A. Joens, 1995, *J. Quant. Spectrosc. Radiat. Transfer*, **53**, 349-352.
33. Takahashi, K., T. Nakayama, Y. Matsumi, S. Solomon, T. Gejo, E. Shigemasa and T. J. Wallington, 2002, *Geophys. Res. Lett.*, **29**.
34. Vandaele, A. C., P. C. Simon, G. M., M. Carleer and R. Colin, 1994, *J. Geophys. Res.*, **99**, 25599-25605.
35. Vatsa, R. K. and H.-R. Volpp, 2001, *Chem. Phys. Lett.*, **340**, 289-295.
36. Vattulainen, J., L. Wallenius, J. Stenberg, R. Hernberg and V. Linna, 1997, *Appl. Spectrosc.*, **57**, 1311-1315.
37. Watanabe, K. and A. S. Jursa, 1964, *J. Chem. Phys.*, **41**, 1650-1653.
38. Wine, P. H., W. L. Chameides and A. R. Ravishankara, 1981, *Geophys. Res. Lett.*, **8**, 543-546.
39. Wine, P. H., N. M. Kreutter, C. A. Gump and A. R. Ravishankara, 1981, *J. Phys. Chem.*, **85**, 2660-2665.
40. Wu, C. Y. R. and F. Z. Chen, 1998, *J. Quant. Spectrosc. Radiat. Transfer*, **60**, 17-23.
41. Wu, C. Y. R., F. Z. Chen and D. L. Judge, 1999, *J. Quant. Spectrosc. Radiat. Transfer*, **61**, 265-271.
42. Wu, C. Y. R., B. W. Yang, F. Z. Chen, D. L. Judge, J. Caldwell and L. M. Trafton, 2000, *Icarus*, **145**, 289-296.
43. Zetzsch, C. UV absorption cross sections of sulfur hexafluoride and acetonitrile. In *Ozone in the Atmosphere*; R. D. Boikov and P. Fabian, Eds.; DEEPAK, 1989; pp 685-689.
44. Zhao, Z., R. E. Stickel and P. H. Wine, 1995, *Geophys. Res. Lett.*, **22**, 615-618.

SECTION 4J. METAL PHOTOCHEMISTRY



(Recommendation: 10-6, Note: 10-6, Evaluated: 10-6)

Absorption Cross Sections: The spectrum of sodium hydroxide, NaOH, has been reported by Rowland and Makide [4] (200 – 400 nm) and Self and Plane [6] (193 – 395 nm). Rowland and Makide inferred absorption cross section values and the average solar photodissociation rate from the flame measurements of Daidoji [1]. Self and Plane [6] used laser photofragment spectroscopy to measure absorption cross sections at 200 and 300 K from the production of Na atoms. The reported cross sections at the lower temperature are systematically smaller at all wavelengths but fall within the limits of the measurement precision for the room temperature values. The results from the Rowland and Makide [4] and Self and Plane [6] studies are in reasonable agreement. The recommended cross sections in Table 4J-1 are taken from Self and Plane [6].

Photolysis Quantum Yield and Product Studies: The quantum yield for photodissociation at wavelengths <346 nm is expected to be unity.

Table 4J-1. Absorption Cross Sections of NaOH at 298 K

λ (nm)	$10^{20} \sigma$ (cm ²)	λ (nm)	$10^{20} \sigma$ (cm ²)	λ (nm)	$10^{20} \sigma$ (cm ²)
193.4	551	234	1680	313	585
205.7	867	248.4	173	319.6	510
205.9	563	254.8	115	353.4	53.9
210.3	185	265.9	48	354.6	57
216.3	489	268.3	41.8	359.8	41.4
218.7	696	277	19.1	395.2	51.2
225.2	1430	285	7.1		
230.6	1820	291.8	43.8		

Note:

Self and Plane [6], reported negative values are not included



(Recommendation: 87-41; Note: 10-6; Evaluated: 10-6)

Absorption Cross Sections: There are several studies of the UV absorption spectra of sodium chloride, NaCl, vapor. For a review of work prior to 1982, which was carried out at high temperatures, see Rowland and Rogers [5]. The study of Davidovitz and Brodhead [2] is particularly noteworthy. They report a NaCl absorption spectrum over the wavelength range 200 – 300 nm for temperatures between 1123 – 1223 K with a cross section of $(3.5 \pm 0.3) \times 10^{-17} \text{ cm}^2 \text{ molecule}^{-1}$ at 238 nm. The recommended cross sections in Table 4J-2 are taken from the work of Silver et al. [7], who measured a spectrum of gas-phase NaCl at room temperature over the wavelength range 189 – 360 nm by directly monitoring Na atoms produced in the photolysis of NaCl.

Photolysis Quantum Yield and Product Studies: The photolysis quantum yield for NaCl is expected to be unity for absorption above the dissociation threshold.

Table 4J-2. Absorption Cross Sections of NaCl at 300 K

λ (nm)	$10^{20} \sigma$ (cm ²)	λ (nm)	$10^{20} \sigma$ (cm ²)
189.7	612	234.0	1300
193.4	556	237.6	638
203.1	148	241.4	674
205.3	90.6	248.4	129
205.9	89.6	251.6	251
210.3	73.6	254.8	424
216.3	151	260.2	433
218.7	46.3	268.3	174
225.2	146	277.0	40
230.4	512	291.8	0.8
231.2	947		

Note:

Silver et al. [7]



(Recommendation: 10-6, Note: 10-6, Evaluated: 10-6)

Absorption Cross Sections: The UV absorption spectrum of sodium oxide, NaO, has been reported by Self and Plane [6] at 200 and 300 K at wavelengths between 193 and 423 nm. Absorption cross sections were determined using pulsed laser photolysis of NaO combined with detection of Na atoms using laser induced fluorescence. A systematic decrease in absorption cross section at lower temperature was reported for all wavelengths included in their study. The recommended absorption cross sections in Table 4J-3 are taken from Self and Plane [6], which is the only study available.

Photolysis Quantum Yield and Product Studies: The photolysis quantum yield for NaO is expected to be unity for absorption above the dissociation threshold.

Table 4J-3. Absorption Cross Sections of NaO at 200 and 300 K

λ (nm)	$10^{20} \sigma$ (cm ²) 300 K	$10^{20} \sigma$ (cm ²) 200 K	λ (nm)	$10^{20} \sigma$ (cm ²) 300 K	$10^{20} \sigma$ (cm ²) 200 K
193.4	501	–	291.8	102	95.5
216.3	1490	515	313	1250	–
225.2	1100	–	319.6	1070	703
231.2	1170	353	353.4	276	119
248.4	206	93.7	354.6	280	–
265.9	180	–	359.8	174	–
268.3	160	24.6	395.2	244	155
277	46.3	–	423	52.2	–

Note:

Self and Plane [6]



(Recommendation: 10-6, Note: 10-6, Evaluated: 10-6)

Absorption Cross Sections: The UV absorption spectrum of sodium superoxide, NaO₂, has been reported by Rajasekhar et al. [3] and Self and Plane [6] at wavelengths between 193 and 423 nm at 200, 230, and 300 K.

Photolysis Quantum Yield and Product Studies: The photolysis quantum yield for NaO₂ is expected to be unity for absorption above the dissociation threshold.

λ (nm)	$10^{20} \sigma$ (cm ²)	λ (nm)	$10^{20} \sigma$ (cm ²)
193.4	383	285	73.4
205.9	146	291.8	168
210.3	542	313	127
216.3	511	319.6	12.1
225.2	235	353.4	16.2
230.8	935	354.6	35
248.4	414	359.8	61
254.8	550	395.2	108
268.3	458	423	42.8
277	181		

J5. $\text{NaO}_3 + h\nu \rightarrow \text{NaO} + \text{O}_2$ 141 kJ mol^{-1} 849 nm (1)
 $\rightarrow \text{NaO}_2 + \text{O}$ 252 kJ mol^{-1} 474 nm (2)

Absorption Cross Sections: The UV absorption spectrum of sodium trioxide, NaO_3 , at 300 K has been reported by Self and Plane [6] for wavelengths between 216 and 396 nm. The recommended absorption cross sections in Table 4J-5 are taken from Self and Plane [6], which is the only study available.

Photolysis Quantum Yield and Product Studies: The photolysis quantum yield for NaO_3 is expected to be unity for absorption above the dissociation threshold.

λ (nm)	$10^{20} \sigma$ (cm ²)
216.3	1310
231.2	228
248.4	119
268.3	94.9
291.8	145
319.6	345
353.4	55.6
395.2	71.7

4J-3

J6. $\text{NaHCO}_3 + h\nu \rightarrow \text{Products}$

(Recommendation: 10-6, Note: 10-6, Evaluated: 10-6)

Absorption Cross Sections: The UV absorption spectrum of sodium bicarbonate, NaHCO_3 , at 200 and 300 K has been reported by Self and Plane [6] for wavelengths between 193 and 277 nm. Absorption cross sections were determined using pulsed laser photolysis of NaHCO_3 combined with detection of Na atoms using laser induced fluorescence. No significant difference in absorption cross section with temperature was reported. The recommended absorption cross sections in Table 4J-6 are taken from Self and Plane [6], which is the only study available.

Photolysis Quantum Yield and Product Studies: The photolysis quantum yield for NaHCO_3 is expected to be unity for absorption above the dissociation threshold.

Table 4J-6. Absorption Cross Sections of NaHCO_3 at 200 and 300 K

λ (nm)	$10^{20} \sigma$ (cm^2) 300 K	$10^{20} \sigma$ (cm^2) 200 K
193.4	113	73.5
205.9	48.7	–
210.3	116	94.7
216.3	120	–
225.2	77.3	98.7
230.9	54.7	57.8
248.4	4.01	3.55
268.3	0.95	–
277	1.09	5.49

Note:

Self and Plane [6] reported negative values which are not included

References for Section 4J

1. Daidoji, H., 1979, Bunseki Kagaku, 28, 77.
2. Davidovits, P. and D. C. Brodhead, 1967, J. Chem. Phys., 46, 2968-2973.
3. Rajasekhar, B., J. M. C. Plane and L. Bartolotti, 1989, J. Phys. Chem., 93, 7399-7404.
4. Rowland, F. S. and Y. Makide, 1982, Geophys. Res. Lett., 9, 473-475.
5. Rowland, F. S. and P. J. Rogers, 1982, Proc. Natl. Acad. Sci. USA, 79, 2737-2739.
6. Self, D. E. and J. M. C. Plane, 2002, Phys. Chem. Chem. Phys., 4, 16-23.
7. Silver, J. A., D. R. Worsnop, A. Freedman and C. E. Kolb, 1986, J. Chem. Phys., 84, 4378-4384.

SECTION 5. HETEROGENEOUS CHEMISTRY

Table of Contents

SECTION 5. HETEROGENEOUS CHEMISTRY	5-1
5.1 Introduction	5-1
5.2 Surface Types—Acid/Water, Liquids and Solids	5-2
5.3 Surface Types—Soot and Alumina	5-3
5.4 Surface Types—Solid Alkali Halide Salts and Aqueous Salt Solutions	5-4
5.5 Surface Composition and Morphology	5-4
5.6 Surface Porosity	5-5
5.7 Temperature Dependences of Parameters	5-5
5.8 Solubility Limitations	5-6
5.9 Data Organization	5-6
5.10 Parameter Definitions	5-6
5.11 Mass Accommodation Coefficients for Surfaces Other Than Soot	5-12
5.12 Notes to Table 5-1	5-15
5.13 Gas/Surface Reaction Probabilities for Surfaces Other Than Soot	5-28
5.14 Notes to Table 5-2	5-34
5.15 Soot Surface Uptake Coefficients	5-63
5.16 Notes to Table 5-3	5-63
5.17 Henry's Law Constants for Pure Water	5-66
5.18 Notes to Table 5-4	5-70
5.19 Ion-Specific Schumpe Parameters	5-77
5.20 Henry's Law Constants for Acids	5-78
5.21 Notes to Table 5-6	5-79
5.22 References	5-83

Tables

Table 5-1. Mass Accommodation Coefficients (α) and Reversible Uptake Data	5-12
for Surfaces Other Than Soot	5-12
Table 5-2. Gas/Surface Reaction Probabilities (γ) for Surfaces Other Than Soot	5-28
Table 5-3. Soot Surface Uptake Coefficients	5-63
Table 5-4. Henry's Law Constants for Pure Water	5-66
Table 5-5. Ion-Specific Schumpe Parameters	5-77
Table 5-6. Henry's Law Constants for Acids	5-78

Figures

Figure 5-1. Recommended reactive uptake coefficients as a function of temperature for key stratospheric heterogeneous processes on sulfuric acid aerosols. For ClONO ₂ and HOCl species, the aerosol radius used in the calculation is 10 ⁻⁵ cm, a typical value in the stratosphere. Because the current uptake models for N ₂ O ₅ and BrONO ₂ hydrolysis do not provide the information about the reacto-diffusive length (ℓ), the aerosol radius used in the calculation is assumed to be much larger than their reacto-diffusive length (i.e. ℓ for N ₂ O ₅ and BrONO ₂ are set to zero.)	5-11
---	------

5.1 Introduction

We have evaluated and tabulated the currently available information on heterogeneous stratospheric processes. In addition, because of the increasing level of interest in tropospheric processes with a direct bearing on the fluxes of reactive species into the stratosphere, such as heterogeneous loss processes for partially oxidized degradation products of hydrohalocarbons and heterogeneous contrail and cloud processing of exhaust species from aircraft, we have included kinetic data for selected heterogeneous interactions relevant to modeling cloud droplet and aqueous aerosol chemistry in the free troposphere. However, both stratospheric and tropospheric heterogeneous chemistry are relatively new and rapidly developing fields, and further results can be expected to change our quantitative and even our qualitative understanding on a regular basis. The complexity is compounded

by the difficulty of characterizing the chemical and physical properties of atmospheric heterogeneous surfaces and then reproducing suitable simulations in the laboratory [349].

Uptake studies of volatile organic species (VOCs) on water ice surfaces have been included in this evaluation for the first time and uptake of acid gases and their precursors on ice have been updated. Several groups have investigated the interaction of small oxygenated organic compounds (alcohols, aldehydes, acids, and ketones) with ice surfaces, measuring equilibrium uptakes at temperatures relevant to the upper troposphere. The amounts taken up are relatively small compared to inorganic acids. The uptake process is fully reversible on the time scale of the experiments, and thus may have little consequences for upper tropospheric chemistry. More information on the interaction of small oxygenated organic compounds (alcohols, aldehydes, organic acids, and ketones) and inorganic acidic gases with ice surfaces is available in the reviews by Abbatt [5] and Huthwelker et al. [281].

Some important uptake processes occurring on alumina, liquid water, sulfuric acid solutions, solid salt, and salt solutions have also been added or updated. The compilation of Henry's law parameters for pure water has been extended to include a number of additional oxygenated organic and halo-organic compounds. The compilation of Henry's law parameters for sulfuric acid solutions has also been extended.

5.2 Surface Types—Acid/Water, Liquids and Solids

To a first approximation there are three major types of surfaces believed to be present at significant levels in the stratosphere. They are: (1) Type I polar stratospheric clouds (PSCs), nominally composed of nitric acid trihydrate ($\text{HNO}_3 \cdot 3\text{H}_2\text{O}$); (2) crystals of relatively pure water ice, designated as Type II PSCs because they form at lower temperatures than Type I and are believed to be nucleated by Type I (similar surfaces may form as contrails behind high-altitude aircraft under some stratospheric conditions); and (3) sulfuric acid aerosol, which is nominally a liquid phase surface generally composed of 60–80 weight percent H_2SO_4 and, concomitantly, 40–20 weight percent H_2O . While PSCs, as their name suggests, are formed primarily in the cold winter stratosphere at high latitudes, sulfuric acid aerosol is present year round at all latitudes and may influence stratospheric chemistry on a global basis, particularly after large injections of volcanic sulfur episodically increase their abundance and surface area. There is also increasing evidence that ternary $\text{H}_2\text{SO}_4/\text{HNO}_3/\text{H}_2\text{O}$ liquid solutions may play a significant role in PSC formation.

In addition to the major stratospheric surface types noted above, several other types of heterogeneous surfaces are found in the stratosphere and may play a significant role in some stratospheric processes. For instance, laboratory work has indicated that nitric acid dihydrate (NAD) may play an important role in the nucleation of Type I PSCs (Worsnop et al. [609], Fox et al. [190]) and that mixtures of solid nitric acid hydrates and sulfuric acid tetrahydrate (SAT) (Molina et al. [416], Zhang et al. [633]) and/or a more complex sulfuric acid/nitric acid hydrate (Fox et al. [190]) may also be key to understanding Type I PSC nucleation and evolution. Analyses of the range of atmospheric conditions possible in the polar stratosphere have also led to interest in solid SAT surfaces and possibly other forms of frozen sulfuric acid aerosols (Toon et al. [566], Middlebrook et al. [406]), as well as liquid sulfuric acid aerosols significantly more dilute than the 60–80 weight percent normally present at lower latitudes (Wolff and Mulvaney [607], Hofmann and Oltmans [268], Toon et al. [566]).

In the free troposphere the heterogeneous surfaces of interest include liquid or solid water (cloud droplets and crystals, contrails), and sulfate particles. Uptake data are compiled for liquid water for several reasons. First this surface is one asymptote of the aqueous acid aerosol continuum; second, the interactions of some trace species with liquid water and water ice (Type II PSC) surfaces are often similar, and third, the uptake of some trace species by liquid water surfaces in the troposphere can play a key role in understanding their tropospheric chemical lifetimes and thus, the fraction that may be transported into the stratosphere. The nature of the sulfate-bearing aerosol is complex. Field measurements by single-particle mass spectrometry show that the particles contain organic species to some degree. The chemical nature of the organics has not been quantified, although it is likely that they are highly oxidized having had long residence times in the atmosphere. Similarly, the inorganic composition is not clear. Most particles of continental origin are fully neutralized with ammonium, and there is some evidence from the free troposphere that this remains true far above the ground. However, in regions away from ammonia sources, there is the potential for the aerosol to be acidic. The phase of the particles may be either solid, or supercooled liquid. Low relative humidities and full neutralization with ammonia promotes crystallization, whereas higher relative humidities and acidic content are more frequently associated with liquid particles. The phase of the organics is not known.

5.3 Surface Types—Soot and Alumina

Aircraft at cruise altitudes and rocket exhausts contribute small but measurable amounts of carbonaceous “soot” (Pueschel et al. [456]) and aluminized solid propellant rocket exhausts and spacecraft debris produce increasing levels of alumina (Al_2O_3) and similar metal oxide particles (Zolensky et al. [638]) in the stratosphere and upper troposphere. Soot lofted above from surface combustion sources may also be present in the upper troposphere, and to a lesser extent in the lower stratosphere. Alumina from rocket exhausts is generally emitted as liquid droplets from the rocket nozzle and deposited in the alpha or metastable gamma phases as it quickly solidifies in the exhaust plume. “Soot” refers to a material that is a combination of elemental and organic carbon, with proportions varying depending on the source material and the combustion conditions. In studies of soot directed to understanding the interaction with atmospheric gases, two types of soot have been used: carbon blacks having relatively small hydrogen and oxygen contents (e.g. Degussa FW2, Cabot Monarch 1000, ground charcoal and spark-generated soot) and organic combustion soots having higher hydrogen, oxygen and nitrogen content (e.g. soots from the combustion of *n*-hexane, methane, propane, decane, ethylene, acetylene, toluene, stearic candles). In the case of organic combustion soots, even different fuels used to generate the soot have been reported to affect the chemistry; for example, the yields of HONO from the reaction of NO_2 with acetylene, toluene, ethylene and decane soots were observed to vary with the fuel used [21, 203].

Polycyclic aromatic hydrocarbons (PAH) and oxygenated polycyclic aromatic compounds (O-PAC) are major constituents of soots formed from the combustion of liquid fuels [16-18, 92, 183, 213, 525]. The bulk composition of soot can have varying amounts of C, H, and O. For example, Chughtai et al. [116] report that the composition (in weight %) of *n*-hexane soot varies from 87 to 92 % C, 1.2 to 1.6 % H, and 11 to 6% oxygen. Stadler and Rossi [534] showed that the elemental composition of the soot as well as its surface area depended on whether the flame was rich or lean; in the case of the rich flame giving a grey-colored soot, the composition (weight %) was 97.3% C, 0.83% H, 1.65% O, and 0.20% N while the lean flame gave a black soot comprised of 96.4% C, 0.19% H, 3.2% O, and 0.27% N.

The functional groups on the soot surface are expected to be important in terms of the uptake and reaction of gases on the surface. X-ray photoelectron spectroscopy (XPS) studies of *n*-hexane soot show surface carbon and oxygen, although the specific nature of the bonding could not be determined (Akhter et al. [18]). The surface functional groups on soot vary, depending on the fuel composition, method of generation and the post-treatment of the soot. For example, Degussa FW2 carbon black, which has been used in a number of studies of uptake and reactions of gases on soots, is post-treated with NO_2 by the manufacturer and Cabot Monarch 1000 is post-treated with aqueous HNO_3 . There may be sufficient NO and NO_2 concentrations generated under some conditions during the formation of soots by spark generators that these may also have been reacted with these gases prior to collection and uptake studies. Studies of a number of gases interacting with soot surfaces suggest there are at least two and likely more, types of reactive surface sites; one type reacts very rapidly, e.g. with O_3 , while others react more slowly. The first type may be most relevant to the reactions of soot particles in exhaust plumes from combustion sources, while the latter is most relevant to soot diluted in air.

Fourier transform infrared (FTIR), Raman and electron paramagnetic resonance (EPR) spectroscopic studies of *n*-hexane soot show C–O functionalities assigned to anhydrides and aryl ethers, alkyl ketones, as well as $\text{C}=\text{C}-\text{H}$, highly substituted aromatics and conjugated carbonyl-aromatic groups [16, 525]. Kirchner et al. [337] measured the FTIR spectra of soots from the combustion of diesel fuel and *n*-hexane (described as “flame deposited”) and soots collected from a commercial spark generator in Ar, from the emissions of a diesel automobile and Degussa FW2 soot (described as “filter deposited”). In all cases, absorption peaks due to $\text{C}-\text{C}$ -, $\text{C}=\text{C}$ -, $\text{C}-\text{O}$, aromatic $\text{C}=\text{O}$, and carboxylic $\text{C}=\text{O}$ groups (both aromatic and aliphatic) were observed. However, the flame-deposited soot showed bands due to substituted aromatics while the filter-collected samples did not. The filter-deposited samples had bands due to aliphatic $\text{C}-\text{H}$ groups that were not observed for the flame-deposited soots. Only the spark-generated soot showed bands due to both $\text{C}=\text{C}-\text{H}$ and to $\text{O}-\text{H}$.

For soot formed from the combustion of liquid fuels, the location in the flame at which the soot is collected also changes the surface enough to alter its reactions. For example, Akhter et al. [16] showed that the functional groups as well as particle size depend on the height of collection of soot from the base of the flame. Such changes appear to also alter the reactions of soot; for example, Gerecke et al. [203] measured HONO and NO yields from the reaction of NO_2 with ethylene soot and found that the HONO yield decreased with distance from the bottom of the flame that the soot was collected from, while the yield of NO increased. Kirchner et al. [337] reported much stronger infrared absorption bands due to substituted aromatics in soot samples collected from the combustion of *n*-hexane near the bottom of the flame compared to the top; in addition, absorption bands due to the $\text{O}-\text{H}$ group were only observed in samples collected at the bottom of the flame.

Not only can the surface groups directly affect its interaction with gases, but they determine the hygroscopic properties of the soot surface. Chughtai et al. [122, 125] have shown that the hydration of soot surfaces depends on the fuel composition (particularly sulfur and trace metal content) and combustion conditions, as well as the extent of surface oxidation. A highly hygroscopic surface holding significant amounts of water may behave differently than a “dry” surface with respect to the interaction with gases; for example, black carbon suspended in aqueous solutions with ozone and irradiated to generate OH has been shown to help assist in the initiation of bulk solution phase OH chemistry [299]. There are also free radical sites on soot surfaces whose EPR signals are strongly affected by the adsorption of paramagnetic species such as NO₂ (e.g. see Chughtai et al. [116]). These unpaired electrons in soot may contribute to the surface reactivity.

The *International Steering Committee for Black Carbon Reference Materials* (<http://www.du.edu/~dwsmith/bcsteer.html>) has issued preliminary recommendations for representative black carbon reference materials. They recommend that soot formed from the combustion of saturated hydrocarbons, preferably *n*-hexane, be used for soot black carbon. For aerosol black carbon, they recommend the use of Urban Dust Reference Material (SRM) 1649a, which is a sample collected in Washington, D.C. in a baghouse in 1976–1977. However, for studies of the uptake and reactions of gases in the atmosphere with combustion-generated soots, organic combustion generated soots, particularly *n*-hexane soot, appear to be the most reasonable surrogate.

5.4 Surface Types—Solid Alkali Halide Salts and Aqueous Salt Solutions

Some modeling studies also suggest that certain types of major volcanic eruptions transport significant levels of sodium chloride and associated alkali halide salts into the stratosphere (Michelangeli et al. [403]), so studies of stratospheric trace species interacting with solid NaCl or similar alkali halide salts, as well as salt solutions, have also been included. Sea salt aerosols are, of course, much more abundant in the troposphere, and have their largest influence on the chemistry of the marine boundary layer.

The heterogeneous chemistry of salt surfaces is very complex. For example; the uptake and reaction of gases with NaCl and NaBr have been shown to be very sensitive to the presence of small amounts of strongly adsorbed water (SAW) on the salt surface. Because water is not taken up on the 100 crystal surface of NaCl at room temperature, the SAW is thought to be concentrated at steps and edges where one water molecule can interact with two ions, resulting in a larger enthalpy of adsorption. This means that powders of salt, which have a larger surface-to-volume than single crystals, also have more SAW because of the relatively larger numbers of steps and edges. In addition, the amount of SAW on sprayed films is affected by the solvent used, with more SAW when water is used as the solvent. This SAW plays a key role in facilitating the reorganization of the surface during the reaction; thus, it appears to mobilize the product ions and allow them to recrystallize into 3-D microcrystallites of product on the surface, exposing fresh salt and allowing the reaction to continue well beyond the point that the surface would normally passivate. While the overall features of this process are reasonably well understood, the exact nature of the SAW and the molecular level interactions and processes are not. The overall effect, however, is a time-dependent uptake coefficient.

Salt particles may also exist as aqueous solutions, if the relative humidities are sufficiently high. Chemistry may then occur both on the surface of the liquid droplets and in the bulk. The surface composition is not necessarily the same as the bulk. In particular, it is believed that the more polarizable anions (such as bromide and iodide) partition to the surface of such particles, perhaps affecting their reactivity. When salt aerosols freeze, the resulting particle will be composed of ice and the vast majority of the solutes will be excluded into a brine that will exist on the surface of the particles and at any grain boundaries and crystal-crystal interfaces that exist. At sufficiently low temperatures, the sodium chloride component will crystallize but other components, such as bromide, are expected to remain in an increasingly concentrated brine [350].

5.5 Surface Composition and Morphology

The detailed composition and morphology of each surface type are uncertain and probably subject to a significant range of natural variability. Certain chemical and physical properties of these surfaces, such as their ability to absorb and/or solvate HCl and HNO₃, are known to be strongly dependent on their detailed chemical composition. Moreover, most heterogeneous processes studied under laboratory conditions (and in some cases proceeding under atmospheric conditions) can change the chemical composition of the surface in ways that significantly affect the kinetic or thermodynamic processes of interest. Thus, a careful analysis of the time-dependent nature of the active surface is required in the evaluation of measured uptake kinetics experiments.

Experimental techniques which allow the measurement of mass accommodation or surface reaction kinetics with high time resolution and/or with low trace gas fluxes are often more credible in establishing that measured kinetic parameters are not seriously compromised by surface saturation or changing surface chemical composition.

The relevant kinetic uptake parameters: mass accommodation coefficients and surface reaction probabilities, are separately documented for relevant atmospheric trace gas species for the major and, where available, the minor stratospheric and upper tropospheric surfaces noted above. Since these parameters can vary significantly with surface composition (e.g., the $\text{H}_2\text{SO}_4/\text{H}_2\text{O}$ ratio for sulfate aerosol or the $\text{HNO}_3/\text{H}_2\text{O}$ ratio for Type I PSC) the dependence of these parameters on surface composition is reviewed where sufficient data are available. In addition, in the notes to Table 5.1, we summarize the thermodynamic information that is now available to describe the non-reactive partitioning of species to a variety of surfaces, especially ice. Due to its chemical and morphological complexity, uptake values for soot are documented in a separate table.

5.6 Surface Porosity

The experimental techniques utilized to measure mass accommodation, heterogeneous reaction, and other uptake coefficients generally require knowledge of the surface area under study. For solid surfaces, and most particularly for water and acid ice surfaces formed *in situ*, the determination of how the molecular scale ice surface differs from the geometrical surface of the supporting substrate is not easy. Keyser, Leu, and coworkers have investigated the structure of water and nitric acid ice films prepared under conditions similar to those used in their flow reactor for uptake studies [331, 332, 334]. They have demonstrated that ice films grown *in situ* from the vapor can have a considerably larger available surface than that represented by the geometry of the substrate; they have also developed a simple model to attempt to correct measured uptake rates for this effect [333, 334]. This model predicts that correction factors are largest for small uptake coefficients and thick films. The application of the model to experimental uptake data remains controversial (Keyser et al. [333], Hanson and Ravishankara [249], Kolb et al. [349]). Some experimenters prefer to attempt growing ice surfaces as smooth as possible and to demonstrate that their measured uptake coefficients are only weakly dependent on surface thickness (Hanson and Ravishankara [248]). For the case of ice surfaces, it has been demonstrated that freezing thin films of liquid water leads to ice films that are smooth at the molecular level [6].

Similar issues arise for uptake experiments performed on powdered, fused and single crystal salt or oxide surfaces (Fenter et al. [173]; Hanning-Lee et al. [231]). There are two issues here. First, the molecular level Brunauer, Emmett, Teller (BET) surface area that is commonly measured by determining the mass of a gas such as N_2 adsorbed by a given sample mass is, for many atmospheric solids, larger than the geometric surface area. However, determining the BET surface area of porous materials does not necessarily reflect the available surface area for molecules larger than that used in the BET measurement. Second, many experimental studies have used samples consisting of multiple layers of particles in order to increase the amount of gas that is taken up and hence improve the accuracy of the measurement. However, there is considerable uncertainty in how to accurately assess the fraction of the total sample that is available for reaction. When recommendations are made for uptake coefficients on solid alkali salts in this assessment, the values have generally been obtained using at least two different sample types (e.g., powders, single crystals and spray-deposited films) and/or two different techniques (e.g., flow tubes and Knudsen cells).

The issue of surface area available for uptake is also important for interpreting uptake measurements on soot and soot surrogate surfaces. The degree to which measured uptake parameters must be corrected for porosity effects will remain in some doubt until a method is devised for accurately determining the effective surface area for the surfaces actually used in uptake studies.

Some studies evaluated in this review assume that the effective ice or salt surface area is the geometrical area, but more recent studies on solid surfaces generally attempt to assess the available surface area by employing BET measurements and porosity models. However, uncertainty in true reactive surface area for heterogeneous uptake on solids is often the dominant systematic error in reporting uptake coefficient values for these systems and makes evaluation of these data across laboratories and techniques difficult.

5.7 Temperature Dependences of Parameters

A number of laboratory studies have shown that mass accommodation coefficients and, to some extent, surface reaction probabilities can be temperature dependent. While these dependencies have not been characterized for many systems of interest, temperature effects on kinetic data are noted where available. More

work that fully separates heterogeneous kinetic temperature effects from temperature controlled surface composition is obviously needed.

5.8 Solubility Limitations

The uptake of certain trace gases by atmospherically relevant surfaces is usually governed by solubility limitations rather than kinetic processes. In these cases properly analyzed data can yield measurements of trace gas solubility parameters relevant to stratospheric conditions. In general, such parameters can be strongly dependent on both condensed phase composition and temperature. Such parameters may be very important in stratospheric models, since they can govern the availability of a reactant for a bimolecular heterogeneous process (e.g., the concentration of HCl available for the $\text{HCl} + \text{ClONO}_2$ reaction on sulfuric acid aerosols) or the gas/condensed phase partitioning of a heterogeneous reaction product (e.g., the HNO_3 formed by the reaction of N_2O_5 on sulfuric acid aerosols). Surface saturation limitations have also been observed in experimental uptake studies on solid surfaces, including water and water/acid ice surfaces.

5.9 Data Organization

Data for trace-gas heterogeneous interactions with relevant condensed-phase surfaces are tabulated in Tables 5-1 through 5-6. These are organized into:

Table 5-1—Mass Accommodation Coefficients and Reversible Uptake Data for Surfaces Other than Soot

Table 5-2—Surface Reaction Probabilities (γ) for Surfaces Other Than Soot

Table 5-3—Soot-Surface Uptake Coefficients

Table 5-4—Solubility Data for Pure Water

Table 5-5—Ion Specific Schumpe Parameters

Table 5-6—Solubility Data for Acids

5.10 Parameter Definitions

Mass accommodation coefficients (α), represent the probability of reversible uptake of a gaseous species colliding with the condensed surface of interest. For liquid surfaces this process is associated with interfacial (gas-to-liquid) transport and is generally followed by bulk liquid phase solvation. Examples include: simple surface absorption, absorption followed by ionic dissociation and solvation (e.g., $\text{HCl} + n\text{H}_2\text{O} \leftrightarrow \text{H}^+(\text{aq}) + \text{Cl}^-(\text{aq})$), and absorption followed by a reversible chemical reaction with a condensed phase substituent (e.g., $\text{SO}_2 + \text{H}_2\text{O} \leftrightarrow \text{H}^+ + \text{HSO}_3^-$ or $\text{CH}_2\text{O} + \text{H}_2\text{O} \leftrightarrow \text{CH}_2(\text{OH})_2$).

The term “sticking coefficient” is often used for mass accommodation on solid surfaces where physisorption or chemisorption takes the place of true interfacial mass transport.

Processes involving liquid surfaces are subject to Henry’s law, which limits the fractional uptake of a gas phase species into a liquid. The distribution of a substance between the gas and liquid phase is controlled, at equilibrium, by the Henry’s Law constant for that substance, which relates the concentration of the substance in solution to the partial pressure of the substance in the gas phase. In these tables, we present the Henry’s Law constants as solubility values:

$$H = [\text{solution}]/P(\text{gas})$$

The units are molar (M) for solution concentration and atmosphere (atm) for the partial pressure in the gas phase. In many studies and other compilations, volatility values are presented, which are the inverse of solubility values. Often, other concentration units are used, sometimes the same unit for both phases. This leads to a dimensionless value, with no indication from the units if it pertains to solubility or to volatility.

Henry’s Law is a limiting law, strictly valid only at the limit of zero concentration. For most gasses at concentrations of interest, deviations from this law are not significant. The value of the Henry’s Law constant, H , depends strongly upon temperature. For a typical gas, it decreases with increasing temperature at lower

temperatures, at least down to 0°C. At higher temperatures, typically well above 298 K, the value will increase with temperature. Over limited temperature ranges, the value is well represented by a linear relationship between the logarithm of H and the reciprocal of temperature.

$$\ln(H) = A + B/T$$

For a number of gasses, the experimental data are sufficient to display the expected curvature in a plot of $\ln H$ vs. $1/T$. In this review, we have represented these results by the three-parameter equation

$$\ln(H) = A + B/T + C \ln(T)$$

Below 0°C, measurements in strong acid solutions have suggested that the Henry's Law constant for a substrate would continue to increase as the temperature is lowered. A study on the solubility of benzene and alkyl benzenes, and methyl and ethyl *tert*-butyl ether, however, indicate that this is not the case [523]. In this study, the values were found to decrease with temperature in supercooled water. Indeed, the results from 25°C to -25°C are almost symmetrical around 0°C. Additional studies on this phenomenon are clearly needed, particularly for smaller solutes.

If the gas phase species is simply solvated, a physical Henry's law constraint holds; if the gas phase species reacts with a condensed phase substituent, as in the sulfur dioxide or formaldehyde hydrolysis cases noted above, a "chemically modified" or "effective" Henry's law constraint holds (Clegg and Brimblecombe [127], Schwartz [503], Watson et al. [595]). This value will typically involve an equilibrium constant for the chemical phenomenon, along with the physical Henry's law constant.

The solubility of a gas also depends upon the presence of other substances in the solution. The best known effect is that of an added salt. In most cases, the addition of a salt to the solution results in a lowering of the solubility of the gas. This effect is usually described by the Sechenov equation:

$$\text{Log}(c^0/c) = \text{Log}(H^0/H) = K_S c_s$$

which relates the ratio of the concentrations of gas dissolved for a given pressure in the absence, c^0 , and presence, c , of a given concentration of salt, c_s . The proportionality constant is the Sechenov coefficient, K_S . The Sechenov coefficient is specific to both the gas and the specific salt. Thus, in general, one needs a new value for any particular gas-salt combination, a tremendous amount of data. For this reason, models have been developed to extend measurements of K_S to systems for which no measurements have been made. Schumpe and co-workers [497, 598] developed the particular procedure adopted in this review. It assumes that K_S is composed of ion- and gas-specific constants:

$$K_S = \sum (h_i + h_G) n_i$$

Where h_i is the ion-specific constant, h_G is the gas-specific constant, and n_i is the ion index. For a mixed electrolyte solution,

$$\text{Log}(H^0/H) = \sum (h_i + h_G) c_i$$

The small temperature dependence of K_S is assumed to lie completely in h_G . Thus

$$h_G = h_{G,0} + h_T (T - 298.15 \text{ K})$$

Weisenberger and Schumpe [598] analyzed 892 Sechenov constants for various gases in salt solutions over the temperature range 273 K to 363 K. They derived an optimum set of h_i , $h_{G,0}$, and h_T parameters for a diverse set of ions and gases. Values for O_2 and H^+ were set to zero to make the set unique. The standard deviation in the predicted Sechenov constants is 0.026. We have included their values for the ion-specific parameters in Table 5-5.

Available gas-specific constants, $h_{G,0}$ and h_T , are included in Table 5-4, along with the Henry's law constants for pure water. In Table 5-4, we present those "salting out" parameters included in the optimum set derived by Weisenberger and Schumpe, along with some parameters derived from other studies. In the latter cases, the ion parameters are considered fixed and we solve for the gas-specific parameters.

Available Henry's law parameters for sulfuric acid/water, and in a few cases, sulfuric acid/nitric acid/water solutions are presented in Table 5-6. Effective Henry's law constants are designated H^* , while simple physical Henry's law constants are represented by H . Effective Henry's law constants are also employed to represent decreased trace gas solubilities in moderate ionic strength acid solutions via a Sechenov coefficient formulation which relates H^* to the concentration of the acid [282]. Available Henry's law constants for reactive upper tropospheric/stratospheric species in binary sulfuric acid/water solutions, and for a few cases of ternary sulfuric acid/nitric acid/water solutions, are tabulated as a function of acid weight percent and temperature. It is presently unclear whether "surface solubility" effects govern the uptake on nominally solid water ice or $\text{HNO}_3/\text{H}_2\text{O}$ ice surfaces in a manner analogous to bulk solubility effects for liquid substrates and no solubility parameters for these "ice" systems are presented; the reader is referred to the ice uptake studies in Table 5.1.

For some trace species on some surfaces, experimental data suggest that mass accommodation coefficients untainted by experimental saturation limitations have been obtained. These are tabulated in Table 5-1. In other cases experimental data can be shown to be subject to Henry's law constraints, and Henry's law constants, or at least their upper limits, can be determined. Some experimental data sets are insufficient to determine if measured "uptake" coefficients are true mass accommodation coefficients or if the measurement values are lower limits compromised by saturation effects. These are currently tabulated, with suitable caveats, in Table 5-1.

Also included in the specific notes by Table 5-1 are parameters relating to the non-reactive uptake of gases to solid atmospheric surfaces, such as ice. These quantities are useful for determining the likelihood that gas-phase species will be scavenged to the condensed phase, and to interpret the rates of surface-phase reactions. Many experimental approaches that can measure reactive uptake or mass accommodation coefficients can also assess the degree of non-reactive uptake, so these data are reported in the same Table. Experimental studies usually measure a total uptake (i.e. molecules or moles of adsorbate per unit surface area) at a specific temperature and gas-phase partial pressure or concentration.

By varying the gas-phase amounts, an adsorption isotherm is measured. For surfaces such as ice, simple isotherms such as the Langmuir form have been utilized. While this isotherm neglects adsorbate-adsorbate interactions and assumes that all adsorption sites are equivalent, these may be reasonable assumptions for ice surfaces which are highly dynamic and where adsorbate molecules are likely to be strongly hydrated. From the isotherm, the saturated surface coverage at high gas-phase concentrations and the gas-surface partition coefficient can be assessed:

$$\theta \equiv \text{fractional surface coverage} = K_{\text{conc}} [\text{gas}] / (1 + K_{\text{conc}} [\text{gas}]) = K_p P_{\text{gas}} / (1 + K_p P_{\text{gas}})$$

where K_{conc} and K_p are the adsorption coefficients, depending on whether concentration or pressure units are used for the gas phase. For consistency with the rest of the evaluation and to match the approach typically used in the literature, surface uptakes will be reported in units of molecules/cm². Correspondingly, adsorption coefficients will be converted into K_{conc} units, i.e. cm³ molecules⁻¹. Note that a partitioning coefficient (K_{part} , units molecules cm⁻² / molecules cm⁻³) can also be derived by taking the slope of a plot of uptake to gas-phase concentration in the surface-unsaturated regime. The relationship between a K_{conc} value derived from a Langmuir adsorption isotherm to a partition coefficient (K_{part}) is:

$$K_{\text{part}} = K_{\text{conc}} N_{\text{sat}}$$

where N_{sat} is the saturated surface coverage in units of molecules cm⁻².

By varying the temperature in uptake studies, the heat of adsorption can be derived in a van't Hoff analysis from the temperature dependence of the partition or adsorption coefficients. This approach is most accurate at low surface coverages where adsorbate-adsorbate interactions are likely to be fewest. While we report such values from the literature, care should be taken in their interpretation because an assumption of this approach is that the surface structure and the strength of the adsorbate-surface interactions remain constant as a function of temperature. Also, as the temperature changes, the degree of adsorbate-adsorbate interactions may change as well.

Surface reaction probabilities (γ) are kinetic values for generally irreversible reactive uptake of trace gas species on condensed surfaces. The rates of such processes may not be limited by Henry's law constraints; however, the fate of the uptake reaction products may be subject to saturation limitations. For example, N_2O_5 has been shown to react with sulfuric acid aerosol surfaces. However, if the $\text{H}_2\text{SO}_4/\text{H}_2\text{O}$ ratio is too high, the product HNO_3 will be insoluble, and a large fraction will be expelled back into the gas phase. Surface reaction

probabilities for substantially irreversible processes are presented in Table 5-2. Reaction products are identified where known.

Surface reaction probabilities on crystalline and non-ice amorphous solid surfaces, such as alumina and alkali salts are particularly susceptible to surface saturation effects, especially when exposed to the relatively high trace gas concentrations sometimes employed in laboratory experiments. In the case of gaseous HNO_3 reacting with NaCl for example, there is a rapid initial uptake of HNO_3 and formation of nitrate on the surface, followed by a decrease to a relatively constant (but slowly declining) value. When they are available, we tabulate the initial uptake coefficient, γ_0 , in Table 5-2, since that value often sets the upper limit for atmospheric uptake. In the corresponding note we may also site the reactive uptake coefficient appropriate to longer time exposure when the uptake appears to have reached an approximate steady-state, γ_{ss} .

The total experimental uptake coefficient measured in laboratory heterogeneous kinetic experiments are also often represented by the symbol γ . In those cases where surface and/or bulk reaction dominate the uptake, the total uptake coefficient (γ_{total}) and reactive uptake coefficient (γ_{rxn}) may well be identical. More formally, for cases where bulk liquid phase reaction is facile and there are no gas phase diffusion constraints, the total uptake coefficient for aerosol or cloud droplets can be approximated in terms of γ_{rxn} and γ_{sol} as [349]:

$$\frac{1}{\gamma_{total}} = \frac{1}{\alpha} + \frac{1}{\gamma_{sol} + \gamma_{rxn}}$$

where

$$\gamma_{sol} = \frac{8HRT}{\pi^{1/2}\bar{c}} \left(\frac{D}{t} \right)^{1/2}$$

and

$$\gamma_{rxn} = \frac{4HRT}{\bar{c}} (Dk_{rxn})^{1/2}$$

where t is the time integrated exposure of the trace gas to the liquid surface, R is the gas constant, D is the liquid phase diffusion coefficient, and \bar{c} is the mean trace gas molecular speed. In the limit of low solubility or long exposure time γ_{sol} becomes negligible and

$$\frac{1}{\gamma_{total}} = \frac{1}{\alpha} + \frac{1}{\gamma_{rxn}}$$

Discussion of how to use this approach to model chemical reactions in liquid stratospheric aerosols can be found in Hanson et al. [254] and Kolb et al. [349]. Note that these formulations are approximate. In cases where separate terms are competitive, more rigorous solution of the kinetic differential equations may be appropriate.

For solid surfaces, bulk diffusion is generally too slow to allow bulk solubility or bulk kinetic processes to dominate uptake. For solids, reactive uptake is driven by chemisorption/chemical reaction at the interface, a process that can also influence trace gas uptake on liquids. For liquids, surface reaction (γ_{surf}) occurs in parallel, rather than in series with mass accommodation, thus:

$$\gamma_{total} = \gamma_{surf} + \left[\frac{1}{\alpha} + \frac{1}{\gamma_{sol} + \gamma_{rxn}} \right]^{-1}$$

Examples where this more complex situation holds for liquid surfaces can be found in Hu et al. [272] and Jayne et al. [304]. In such cases γ may be significantly larger than α .

Uptake of gases on soot may occur due to three different processes: (1) physisorption (e.g. SO_2 or HNO_3 at room temperature and low nitric acid pressures); (2) reaction with the surface (e.g. NO_2), and (3) catalytic decomposition/reactions of the gas on the surface. All three processes may occur in parallel, and the relative contributions of each of these three may vary during the course of the reaction as the surface “ages.” As discussed above, there are different types of reactive sites on soot, leading in some cases to a rapid initial uptake

followed by a slower uptake; these are often characterized as reactions on “fresh” and “aged” surfaces respectively. Another complexity is that in some cases the geometric surface areas were used to calculate the uptake coefficients from the experimental data while in others, the available reactive surface area was estimated and used.

Because of these complexities with soot heterogeneous chemistry, uptake coefficients for soot interactions with gases have been broken out into a separate Table 5-3 rather than being included with the other surfaces in Table 5-1 and Table 5-2. When the uncertainty is more than an order of magnitude, a recommendation is not given in Table 5-3 and the range of reported values is given in the Notes. In most cases, the available reactive surface area rather than the geometric areas have been used in obtaining the uptake coefficients; in those cases where the geometric area was used but a higher available surface area was involved in the measured uptake, the uptake coefficient is given as an upper limit. Data are most commonly available for room temperature or there are very limited data at lower temperatures characteristic of the upper troposphere.

The data in Table 5-1 and Table 5-2 for uptake on non-soot surfaces are organized by trace gas species, since some systematic variation may be expected for surface accommodation or reaction as the surface composition and/or phase is varied. Data presented for one surface may be judged for “reasonableness” by comparing with data for a “similar” surface. In some cases it is not yet clear if surface uptake is truly reversible (accommodation) or irreversibly reactive in nature. In such cases the available uptake coefficients are generally tabulated in Table 5-1 as accommodation coefficients, a judgment that will be subject to change if more definitive data become available.

Where a specific evaluated value for an accommodation coefficient or reaction probability has been obtained, an estimated uncertainty factor is also tabulated. However, when the data evaluation yielded only a lower or upper limit, no uncertainty factor can be reliably estimated and none is presented.

Description of and reference citations to many of the laboratory techniques used to obtain the data in the following tables can be found in Kolb et al. [349].

Reactions of N_2O_5 , ClONO_2 , HOCl and BrONO_2 on/in sulfuric acid are generally dependent on the species’ Henry’s law solubility and liquid phase diffusion coefficient in the liquid acid as well as the surface and/or liquid phase reaction rate parameters. All of these processes are generally functions of the acid composition and temperature (Hanson et al. [254], Robinson et al. [471] Shi et al. [519]). Thus, these reactions’ reactive uptake coefficients must be represented by a complex phenomenological or empirical models that defy simple entry into Table 5-2. The notes in Table 5-2 for these reactions discuss and present the models adopted.

To aid in visualizing the resulting reactive uptake parameters the results for several reactions have been plotted in Figure 5.1 as a function of temperature for a background pressure of 50 mbar and background water vapor and HCl mixing ratios of 5 ppmv and 2 ppbv, respectively. These calculations are presented for monodisperse background sulfate aerosol particles with a radius of 1×10^{-5} cm (0.1 μm).

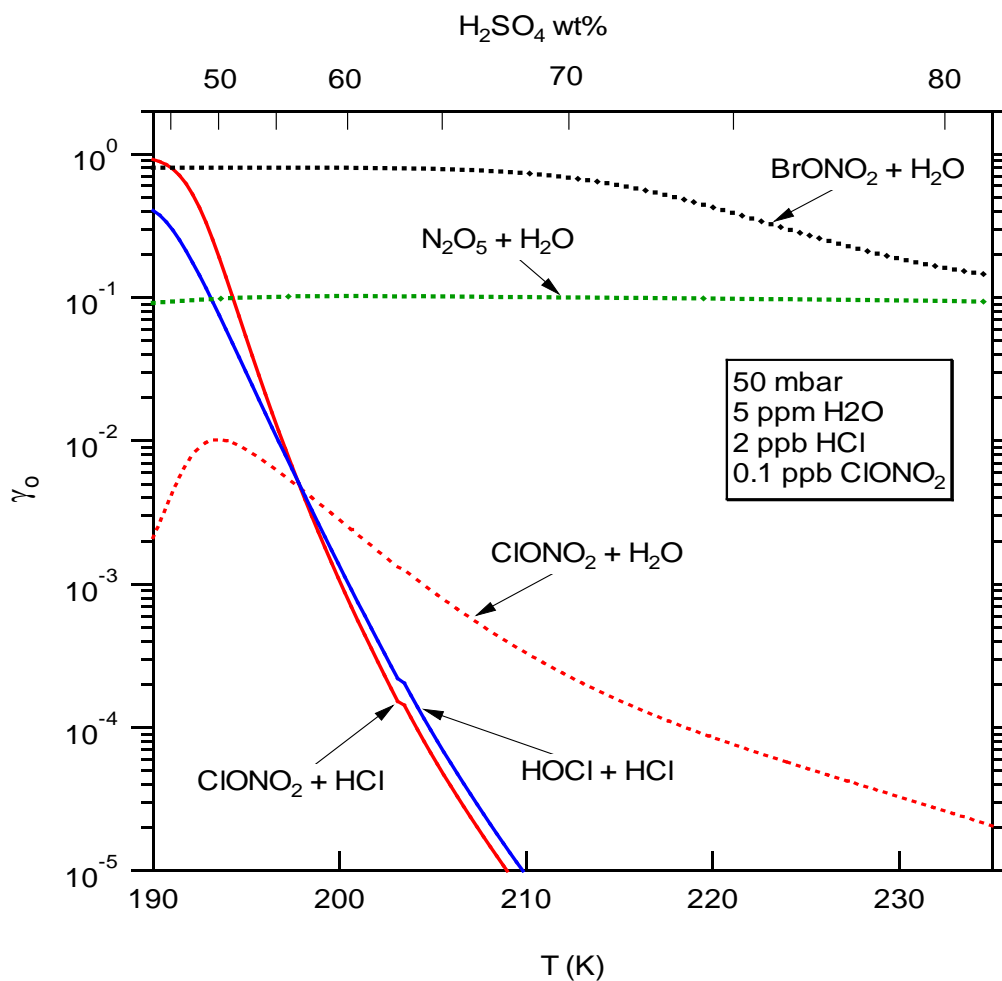


Figure 5-1. Recommended reactive uptake coefficients as a function of temperature for key stratospheric heterogeneous processes on sulfuric acid aerosols. For ClONO_2 and HOCl species, the aerosol radius used in the calculation is 10^{-5} cm, a typical value in the stratosphere. Because the current uptake models for N_2O_5 and BrONO_2 hydrolysis do not provide the information about the reacto-diffusive length (ℓ), the aerosol radius used in the calculation is assumed to be much larger than their reacto-diffusive length (i.e. ℓ for N_2O_5 and BrONO_2 are set to zero.)

5.11 Mass Accommodation Coefficients for Surfaces Other Than Soot

Table 5-1. Mass Accommodation Coefficients (α) and Reversible Uptake Data for Surfaces Other Than Soot

Gaseous Species	Surface Type	Surface Composition	T(K)	α	Uncertainty Factor	Notes
O	Water Ice Sulfuric Acid	H ₂ O(s) H ₂ SO ₄ • nH ₂ O(l) (97 wt.% H ₂ SO ₄)	See Note 298	See Note See Note		<u>1</u> <u>2</u>
O ₃	Water Ice Liquid Water Nitric Acid Ice Sulfuric Acid	H ₂ O(s) H ₂ O(l) HNO ₃ • 3H ₂ O(s) H ₂ SO ₄ • nH ₂ O(l) (50–98 wt.% H ₂ SO ₄)	195–262 275–300 195 193–295	>0.04 $\geq 1 \times 10^{-2*}$ $2.5 \times 10^{-4†}$ See Note	3	<u>3</u> <u>4</u> <u>3</u> <u>5</u>
OH	Water Ice Liquid Water	H ₂ O(s) H ₂ O(l)	205–253 275–300	>0.1 $\geq 1 \times 10^{-2*}$		<u>6</u> <u>7</u>
HO ₂	Liquid Water Aqueous Salts and Sulfuric Acid	H ₂ O(l) NH ₄ HSO ₄ (aq), LiNO ₃ (aq), H ₂ SO ₄ • nH ₂ O, NaCl (aq), (NH ₄) ₂ SO ₄ (aq), KCl(aq)	275 293	> 0.02 > 0.4		<u>8</u> <u>8</u>
H ₂ O	Water Ice Liquid Water Liquid Nitric Acid Nitric Acid Ice Sulfuric Acid Sodium Chloride	H ₂ O(s) H ₂ O(l) HNO ₃ • nH ₂ O(l) HNO ₃ • 3H ₂ O(s) H ₂ SO ₄ • nH ₂ O (96 wt.% H ₂ SO ₄) (50 wt.% H ₂ SO ₄) (70 wt.% H ₂ SO ₄) (82 wt.% H ₂ SO ₄) NaCl(s) NaCl(aq)	<200 250–290 278 197 298 250–280 250–295 270–300 ~298 ~299	>0.4 $\geq 0.1^*$ >0.3 See Note $> 2 \times 10^{-3†}$ 0.5 0.6 0.85 See Note See Note	1.3 1.3 1.3	<u>9</u> <u>10</u> <u>11</u> <u>12</u> <u>13</u> <u>13</u> <u>13</u> <u>14</u> <u>15</u>
H ₂ O ₂	Water Ice Liquid Water Sulfuric Acid	H ₂ O(s) H ₂ O(l) H ₂ SO ₄ • nH ₂ O(l) (96 wt.% H ₂ SO ₄)	213–238 273 298	See Note 0.18* $> 8 \times 10^{-4†}$	2	<u>16</u> <u>17</u> <u>18</u>
NO	Water Ice Sulfuric Acid	H ₂ O(s) H ₂ SO ₄ • nH ₂ O (70 wt.% H ₂ SO ₄) (97 wt.% H ₂ SO ₄)	195 193–243 298	See Note See Note See Note See Note		<u>19</u> <u>20</u> <u>20</u>
NO ₂	Water Ice	H ₂ O(s)	195	See Note		<u>21</u>
NO ₃	Liquid Water	H ₂ O(l)	273–293	$\geq 2 \times 10^{-3}$		<u>22</u>
HONO	Water Ice	H ₂ O(s)	180–200	See Note		<u>23</u>
HNO ₃	Water Ice Liquid Water Nitric Acid Ice Liquid Nitric Acid Sulfuric Acid Sulfuric Acid Tetrahydrate	H ₂ O(s) H ₂ O(l) HNO ₃ • 3H ₂ O(s) HNO ₃ • nH ₂ O(l) H ₂ SO ₄ • nH ₂ O(l) (57.7 wt.% H ₂ SO ₄) (73 wt.% H ₂ SO ₄) (75 wt.% H ₂ SO ₄) (97 wt.% H ₂ SO ₄) H ₂ SO ₄ • 4 H ₂ O(s)	<200 250–300 191–200 278 191–200 283 230 295 ~192	>0.1 $\geq 0.05^*$ 0.4 0.6 >0.3 0.1 $> 2 \times 10^{-3}$ $> 2.4 \times 10^{-3}$ >0.02*	2 2 2	<u>24</u> <u>25</u> <u>26</u> <u>27</u> <u>28</u> <u>28</u> <u>28</u> <u>28</u> <u>28</u>
HO ₂ NO ₂	Water Ice Sulfuric Acid	H ₂ O(s) H ₂ SO ₄ • nH ₂ O(l) (97 wt.% H ₂ SO ₄)	200 298	0.1† See Note	3	<u>29</u> <u>30</u>
NH ₃	Water Ice Liquid Water	H ₂ O(s) H ₂ O(l)	190 260–300	See Note $\geq 0.05^*$		<u>31</u> <u>32</u>
CO ₂	Water Ice Liquid Water	H ₂ O(s) H ₂ O(l)	209–263 290–300	See Note $\geq 5 \times 10^{-5}$		<u>33</u> <u>34</u>
CH ₃ OH	Water Ice Liquid Water	H ₂ O(s) H ₂ O(l)	150–213 260–291	See Note 0.12–0.02*	2	<u>35</u> <u>36</u>
CH ₃ CH ₂ OH	Water Ice Liquid Water	H ₂ O(s) H ₂ O(l)	193–243 260–292	See Note $\geq 2 \times 10^{-2*}$		<u>37</u> <u>38</u>
CH ₃ CH ₂ CH ₂ OH	Water Ice Liquid Water	H ₂ O(s) H ₂ O(l)	228 260–291	See Note 0.08–0.02*	2	<u>39</u> <u>40</u>
CH ₃ CH(OH)CH ₃	Liquid Water	H ₂ O(l)	260–291	0.10–0.02*	2	<u>40</u>

Gaseous Species	Surface Type	Surface Composition	T(K)	α	Uncertainty Factor	Notes
HOCH ₂ CH ₂ OH	Liquid Water	H ₂ O(l)	260–291	0.13–0.04*	2	<u>41</u>
CH ₃ O ₂	Sodium Chloride	NaCl(s)	296	$>4 \times 10^{-3}$		<u>42</u>
CH ₃ OOH	Liquid Water	H ₂ O(l)	260–282	$\geq 7 \times 10^{-3}$ *		<u>43</u>
CH ₂ O	Water Ice	H ₂ O(s)	198–268	See Note	3	<u>44</u>
	Liquid Water	H ₂ O(l)	260–270	0.04		<u>45</u>
	Sulfuric Acid	H ₂ O • mHNO ₃ • nH ₂ O(l)	235–300	0.04		<u>45</u>
CH ₃ CHO	Water Ice	H ₂ O(s)	120–233	See Note		<u>46</u>
	Liquid Water	H ₂ O(l)	267	>0.03 *		<u>47</u>
CH(O)CH(O)	Liquid Water	H ₂ O(l)	260–285	$\geq 1 \times 10^{-2}$ *		<u>48</u>
CH ₃ C(O)CH ₃	Water Ice	H ₂ O(s)	217–243	See Note		<u>49</u>
	Liquid Water	H ₂ O(l)	260–292	$\geq 2 \times 10^{-2}$ *		<u>50</u>
CH ₃ C(O)CHO	Liquid Water	H ₂ O(l)	260–293	$\geq 1 \times 10^{-4}$ *		<u>51</u>
CH ₃ OC(O)OCH ₃	Liquid Water	H ₂ O(l)	270–278	$\geq 2 \times 10^{-2}$ *		<u>52</u>
HC(O)OH	Water Ice	H ₂ O(s)	187–221	See Note	2	<u>53</u>
	Liquid Water	H ₂ O(l)	260–291	0.10–0.02*		<u>54</u>
CH ₃ C(O)OH	Water Ice	H ₂ O(s)	193–245	See Note		<u>55</u>
	Liquid Water	H ₂ O(l)	258–292	$\geq 2 \times 10^{-2}$ *		<u>56</u>
CH ₃ CO(O ₂)NO ₂	Water Ice	H ₂ O(s)	80–250	See Note		<u>57</u>
Cl ₂	Water Ice	H ₂ O(s)	200	See Note		<u>58</u>
OCIO	Water Ice	H ₂ O(s)	100, 189, 200	See Note		<u>59</u>
HCl	Water Ice	H ₂ O(s)	<u><205</u>	>0.1	2	<u>60</u>
	Liquid Water	H ₂ O(l)	260–295	≥ 0.05 *		<u>61</u>
	Nitric Acid Ice	HNO ₃ • 3H ₂ O(s)	191–211	>0.3		<u>62</u>
	Sulfuric Acid	H ₂ SO ₄ • nH ₂ O(l)				
		(n ≥ 8 , ≤ 40 wt.% H ₂ SO ₄)	284	0.15*		<u>63</u>
		(n < 8 , > 40 wt.% H ₂ SO ₄)	<u><243</u>	>0.1		<u>63</u>
	Sulfuric Acid Tetrahydrate	H ₂ SO ₄ • 4H ₂ O(s)	192–201	See Note		<u>64</u>
ClONO ₂	Liquid Water	H ₂ O(l)	260–280	≥ 0.05 *		<u>65</u>
CCl ₂ O	Liquid Water	H ₂ O(l)	260–290	See Note		<u>66</u>
CCl ₃ CClO	Liquid Water	H ₂ O(l)	260–290	See Note		<u>66</u>
HBr	Water Ice	H ₂ O(s)	200	>0.2		<u>67</u>
	Liquid Water	H ₂ O(l)	260–295	≥ 0.05 *		<u>68</u>
	Nitric Acid Ice	HNO ₃ • 3H ₂ O(s)	200	>0.3		<u>67</u>
	Sulfuric Acid	H ₂ SO ₄ • nH ₂ O(l) (55–70 wt.% H ₂ SO ₄)	<u>213</u>	≥ 0.1		<u>69</u>
HOBr	Water Ice	H ₂ O(s)	190–239	See Note	1.5	<u>70</u>
	Liquid Water	H ₂ O(l)	298	0.6		<u>71</u>
	Sulfuric Acid	H ₂ SO ₄ in H ₂ O(l) (58 wt.% H ₂ SO ₄)	228	>0.05 †		<u>72</u>
BrONO ₂	Liquid Water	H ₂ O(l)	260–280	≥ 0.03 *	1.5	<u>73</u>
	Sulfuric Acid	H ₂ SO ₄ in H ₂ O(l) (45–83 wt.% H ₂ SO ₄)	230–300	0.8		<u>74</u>
CHBr ₃	Water Ice	H ₂ O(l)	220	See Note		<u>75</u>
	Sulfuric Acid	H ₂ SO ₄ • nH ₂ O(l) (97 wt.% H ₂ SO ₄)	220	$>3 \times 10^{-3}$ †		<u>75</u>
BrCl	Liquid Water	H ₂ O(l)	270–285	≥ 0.15 *		<u>76</u>
I ₂	Liquid Water	H ₂ O(l)	270–293	≥ 0.01 *		<u>77</u>
HI	Water Ice	H ₂ O(s)	188–233	See Note		<u>78</u>
	Liquid Water	H ₂ O(l)	260–280	≥ 0.05 *		<u>79</u>
HOI	Sulfuric Acid	H ₂ SO ₄ • nH ₂ O(l)			3	<u>80</u>
		(40 wt.% H ₂ SO ₄)	195	0.07		
		(40 wt.% H ₂ SO ₄)	205	0.03		
		(40 wt.% H ₂ SO ₄)	212	0.04		
		(50 wt.% H ₂ SO ₄)	222–224	0.02		
		(70 wt.% H ₂ SO ₄)	230–232	0.02		
		(70 wt.% H ₂ SO ₄)	252	0.02	3	
HF	Water Ice	H ₂ O(s)	200	See Note		<u>81</u>
	Nitric Acid Ice	HNO ₃ • 3H ₂ O(s)	200	See Note		<u>81</u>
CF ₂ O	Water Ice	H ₂ O(s)	192	See Note		<u>82</u>
	Liquid Water	H ₂ O(l)	260–290	See Note		<u>66</u>
	Nitric Acid Ice	HNO ₃ • 3H ₂ O(s)	192	See Note		<u>82</u>
	Sulfuric Acid	H ₂ SO ₄ • nH ₂ O(l)	215–230			
		(40 wt.% H ₂ SO ₄)		$>3 \times 10^{-6}$ †		<u>82</u>
		(60 wt.% H ₂ SO ₄)		$>6 \times 10^{-5}$ †		<u>82</u>

Gaseous Species	Surface Type	Surface Composition	T(K)	α	Uncertainty Factor	Notes
CF ₃ CFO	Liquid Water	H ₂ O(l)	260–290	See Note		66
CF ₃ COOH	Liquid Water	H ₂ O(l)	263–288	0.2–0.1*	2	83
CF ₃ CClO	Liquid Water	H ₂ O(l)	260–290	See Note		66
SO ₂	Water Ice	H ₂ O(s)	190–238	See Note		84
	Liquid Water	H ₂ O(l)	260–298	≥0.12*	2	85
	Sulfuric Acid	H ₂ SO ₄ • nH ₂ O(l) (97 wt.% H ₂ SO ₄)	298	See Note		86
H ₂ S	Liquid Water	H ₂ O(l)	260–298	≥0.05*		87
H ₂ SO ₄	Sulfuric Acid	H ₂ SO ₄ • nH ₂ O(l) (50–98 wt.% H ₂ SO ₄)	200–300	0.7	1.4	88
CH ₃ S(O)CH ₃	Liquid Water	H ₂ O(l)	262–281	0.16–0.08*	2	89
CH ₃ S(O ₂)CH ₃	Liquid Water	H ₂ O(l)	262–281	0.27–0.08*	2	89
CH ₃ S(O ₂)OH	Liquid Water	H ₂ O(l)	260–283	≥0.1*		89

* Varies with T, see Notes

‡ May be affected by surface saturation

5.12 Notes to Table 5-1

1. O on H₂O(s). Murray and Plane [427] measured the uptake of O atoms on water ice at temperatures relevant to the upper mesosphere (112 -151 K), where noctilucent clouds are present. Their results indicate that in the absence of oxygen molecules the uptake coefficient α is small (7×10^{-6}). They recommend the following expression: $\alpha = 7 \times 10^{-6} + 1.5 \times 10^{-10} \exp(11.4 \text{ kJ/mol/RT})$, with an uncertainty of $\pm 24\%$. [Back to Table](#)
2. O on H₂SO₄ • nH₂O. Knudsen cell experiment of Baldwin and Golden [38] measured an uptake coefficient limit of $<10^{-6}$, this result probably cannot be equated with an accommodation coefficient due to surface saturation. [Back to Table](#)
3. O₃ on H₂O(s) and HNO₃ • nH₂O. Undoped ice surfaces saturate too quickly for reliable measurements. When ice is doped with Na₂SO₃ to chemically remove absorbed O₃ the apparent α increases to 1×10^{-2} (0.1M) or up to 4×10^{-2} (1M) (Dlugokencky and Ravishankara [155]). Limit of $\gamma < 10^{-6}$ for undoped ice is consistent with earlier measurement by Leu [360] of $\geq 1 \times 10^{-4}$ and with $< 6 \times 10^{-5}$ obtained by Kenner et al. [329]. Dlugokencky and Ravishankara also measured the tabulated value of an uptake coefficient for O₃ on a NAT “like” surface, but the data were difficult to reproduce and the surfaces were not well characterized. Kenner et al. also measured a lower limit for an uptake coefficient of 8×10^{-5} on NAT at 183 K, but this measurement is also certainly limited by surface saturation. [Back to Table](#)
4. O₃ on H₂O(l). Utter et al. [575] used a wetted wall flow tube technique with various chemical scavengers to measure a lower limit for α of 2×10^{-3} . The stopped flow measurement technique using an SO₃²⁻ scavenger (Tang and Lee [551]) is subject to saturation effects, so their quoted α of 5.3×10^{-4} is also taken as a lower limit. Using a droplet train flow reactor Hu et al. [272] measured a value of ~ 0.1 at 277 K with I⁻ as a reactive scavenger, consistent with a more extensive droplet train flow reactor measurement by Magi et al. [387] yielding a value of ≥ 0.1 also using I⁻ as a reactive scavenger. Schurath et al. [498] used a coaxial flow liquid jet to obtain a value of 4.5×10^{-3} at 298 K, probably limited by surface saturation although they also used I⁻ as a reactive scavenger. Müller and Heal [425] obtained a value of 4×10^{-2} at 293 K in a wetted wall flow tube with S₂O₃²⁻ as a reactive scavenger. Schütze and Herrmann [499] measured a lower limit of 2×10^{-2} at 298 K using a suspended droplet flow reactor method that also employed I⁻ as a reactive scavenger. It is highly likely that the mass accommodation coefficient for ozone on liquid water is ≥ 0.01 between ~ 275 and 300 K and may be significantly higher, although it is possible that interfacial reactions with near surface I⁻ bias some mass accommodation evaluations high because surface reactive uptake occurs in parallel with mass accommodation. Molecular dynamic simulations of O₃ uptake on water by Roeselová et al. [475] indicate a mass accommodation coefficient of order 0.1. [Back to Table](#)
5. O₃ on H₂SO₄ • nH₂O. Flow tube measurements (Dlugokencky and Ravishankara [155]) of an uptake coefficient limit of $<10^{-6}$ on both 50 and 97 wt.% H₂SO₄ surfaces are consistent with earlier, but probably less quantitative, static systems measurements of Olszyna et al. [433] and aerosol chamber measurements of Harker and Ho [255], who report uptake coefficients of the order 10^{-8} or less for a variety of sulfuric acid concentrations and temperatures. In these earlier experiments, doping the H₂SO₄ with Ni²⁺, Cr²⁺, Al³⁺, Fe³⁺, and NH₄⁺ (Olszyna et al. [433]) or Al₂O₃ or Fe₂O₃ (Harker and Ho [255]) did not significantly increase measured O₃ loss. An upper limit of 1×10^{-6} was also reported by Baldwin and Golden [37] for 97 wt.% H₂SO₄ at 295 K. Il'in et al. [287] performed static tube reactor measurements on 98 wt.% sulfuric acid at 239, 258, 273 K measuring uptake coefficients between 1.2 and 1.75×10^{-6} . Although these measurements are slightly larger than the limits in the other studies, uptake values this small are extremely hard to quantify and these measurements are not seen to be in serious disagreement with other studies finding slightly lower upper limits. All measurements are subject to solubility limitations and probably do not reflect true limits on mass accommodation. [Back to Table](#)
6. OH on H₂O(s). Cooper and Abbatt [132] analyzed uptake rates in a wall-coated flow tube to determine an initial $\gamma \sim 0.1$ over the temperature range of 205 – 230 K. Uptake coefficients decreased at longer exposure times, indicating surface saturation. These data indicate that α is at least 0.1 and possibly much larger. This is confirmed by an earlier experiment using a coated insert/flow tube technique by Gershenzon et al. [207], which yielded $\alpha > 0.4$ at 253 K. [Back to Table](#)
7. OH on H₂O(l). A lower limit of α on pure water of 3.5×10^{-3} at 275 K was determined by Hanson et al. [238] using a liquid-wall flow tube. Takami et al. [547] using a gas/liquid impinging flow technique

obtained a pure water value near pH 7 at 293 K of $(4.2 \pm 2.8) \times 10^{-3}$ while values 2 to 3 times higher were obtained for acid (pH=1) and basic (pH=10-13) aqueous solutions; a value of $(1.1 \pm 0.4) \times 10^{-2}$ was obtained when benzoic acid was added as a radical scavenger. Takami et al. also observed that uptake for pure water solutions decreased with gas/liquid contact times, indicating a saturation limitation and explaining the higher uptake values observed for solutions with H^+ , OH^- , or benzoic acid reactive scavengers. Based on these experimental results a value of $\alpha \geq 0.1$ is suggested. This recommendation is consistent with molecular dynamics calculations by Roeselová et al. [475, 476] who first published simulation values at room temperature 0.2 to 0.3, but later reported a value of 0.83 at 300 K using revised intermolecular potentials. [Back to Table](#)

8. HO_2 on $H_2O(l)$, aqueous salt solutions and $H_2SO_4 \cdot nH_2O$. Determination of α in liquid-wall flow tube (Hanson et al. [238]) is dependent on gas-phase diffusion corrections; measured limit ($\alpha > 0.02$) is consistent with $\alpha = 1$. In the aqueous salt aerosol measurements of Mozurkewich et al. [421], HO_2 was chemically scavenged by Cu^{++} from added $CuSO_4$ to avoid Henry's law constraints; the measured limit of >0.2 is also consistent with $\alpha = 1$. Thornton and Abbatt[555] and Taketani et al. ([549];[550]) have raised the upper limit to the mass accommodation coefficient to > 0.4 for Cu^{++} doped aqueous particles composed of sulfuric acid, ammonium sulfate, sodium chloride and potassium chloride, for relative humidities between 35 and 75% at room temperature. [Back to Table](#)
9. H_2O on $H_2O(s)$. Uptake coefficient measurements are available from Leu [359]293] ($0.3 (+0.7, -0.1)$) at 200 K, Haynes et al.[259] (1.06 ± 0.1 to 0.65 ± 0.08 from 20 to 185 K), Brown et al. [84] (0.99 ± 0.03 between 85 and 150 K and 0.97 ± 0.10 between 97 and 145 K), Fluckiger et al. [184] (0.43 at 200 K using D_2O^{18}), and Magee et al. [386] (0.006 at 223 K using levitated particles). Uptake coefficients measured by Delval et al. [151] and Pratte et al. [454], that should be viewed as lower limits to the mass accommodation coefficient, show a strong negative temperature dependence consistent with a precursor adsorption model; values are about 0.1 at 200 K. The lower value measured by Magee et al. at elevated temperatures could be important for modeling ice cloud growth rates and needs to be confirmed by another measurement approach. [Back to Table](#).
10. H_2O on $H_2O(l)$. Because the uptake of water vapor on and evaporation of water from liquid water are fundamental processes that are linked by microscopic reversibility and play extremely important roles in cloud physics, they have been the subject of over 75 published experimental studies spanning over eight decades. Many of these studies were reviewed by Marek and Staub [389], who note values of α deduced from these experiments range from ~ 0.001 to 1.0, with experiments involving growing water drops tending to higher values. Recently published experiments support values near the higher end of the range. Shaw and Lamb [518] used an electrodynamic droplet levitation cell to make simultaneous ice nucleation/water droplet evaporation rate observations to deduce a range of $0.04 < \alpha < 0.1$ at 237 K. Li et al. [366] used a droplet train flow reactor to measure the uptake of small excesses of $H_2^{17}O$ on water droplets that were in equilibrium with the surrounding normal water vapor, deducing a value of 0.17 ± 0.03 at 280K that increased to 0.32 ± 0.04 at 258K. Winkler et al. [604]; [604] used Mie scattering analyses of the growth of freshly nucleated droplets in an expansion chamber to deduce $0.4 < \alpha < 1.0$ over a temperature range of 270 to 290 K and $0.8 < \alpha < 1.0$ for 250-270 K. Voigtländer et al. [586] analyzed droplet growth in a laminar diffusion flow reactor to estimate $0.3 < \alpha < 1.0$ at 275-277 K. Saykally, Cohen and co-workers ([96]; [530]; [159]) performed a series of evaporation experiments from liquid jets and jet breakup droplet trains in very low-pressure reactors that approximate free evaporation conditions. Their studies of H/D isotope fraction in vapor from D_2O doped water jets yielded estimates of $\sim 0.15 < \alpha < \sim 0.3$ for the temperature range of 255-295 K [96]. Further experiments with jet break-up droplet trains produced an estimate of $\alpha = 0.62 \pm 0.09$ for H_2O between 245 and 298 K [530] and $\alpha = 0.57 \pm 0.06$ for D_2O between 255 and 295 K [159]. Maerefat and coworkers used a unique shock tube method to study the time resolved evolution of water film thickness on a window surface to estimate that $\alpha = 0.35$ over the temperature range 297.1-299.1K [385]. Jakubczyk and co-workers applied an atmospheric pressure single droplet evaporation electrodynamic trap technique ([298]; [636]; [637]) and a continuum vapor diffusion and heat transfer model, which they argue is more complete than that employed by Winkler et al. [605] and Voigtländer et al. [586]. When applied to temperature dependant data Jakubczyk and co-workers report $\alpha = 0.13 \pm 0.01$ at 293.1K increasing to 0.18 ± 0.05 at 273.1K [637], in close agreement with magnitude and temperature dependence reported by Li et al. [366]. Given the results from this wide range of experiments, it seems clear that mass accommodation values of water vapor on liquid water for temperatures below 295 K must exceed 0.1. The Li et al. and

- Winkler et al. experiments are further discussed in Davidovits et al. [143], which notes that reasons for the differences in their deduced values are not yet understood. [Back to Table](#)
11. H_2O on $\text{HNO}_3/\text{H}_2\text{O}(\text{l})$. Rudolf and Wagner[487] used aerosol expansion chamber techniques to illustrate that on liquid water/nitric acid aerosols α is greater than 0.3 and is consistent with 1.0 at 278 K. Experiments are similar to those at Winkler et al. [604]; supersaturated vapor may lead to a larger value of α than found for near equilibrium conditions. [Back to Table](#)
 12. H_2O on $\text{HNO}_3 \cdot n\text{H}_2\text{O}(\text{s})$. Middlebrook et al. [407] measured an uptake coefficient of 0.002 for water vapor co-depositing with nitric acid over NAT at 197 K. [Back to Table](#)
 13. H_2O on $\text{H}_2\text{SO}_4 \cdot n\text{H}_2\text{O}$. Baldwin and Golden [37] using a Knudsen cell measured $\alpha \sim 2 \times 10^{-3}$ at 96 wt.%, which is strongly affected by surface saturation (see Note for H_2O_2 on $\text{H}_2\text{SO}_4 \cdot n\text{H}_2\text{O}$). Gershenson et al. [204] used a droplet train flow reactor to measure the uptake of H_2^{17}O on 50 wt.% sulfuric acid from 250 to 278 K, on 70 wt.% from 250 to 295 K, and on 82 wt.% from 272 to 298 K. Measured mass accommodation coefficients range from 0.4 to 0.9, increasing with acid wt.% and decreasing temperature. [Back to Table](#)
 14. H_2O on $\text{NaCl}(\text{s})$. Fenter et al. [171] used Knudsen cell/mass spectrometry methods to measure $\gamma < 2 \times 10^{-4}$ for $\text{H}_2\text{O}(\text{g})$ uptake on NaCl powders, an observation confirmed by Beichert and Finlayson-Pitts [64], who found $\gamma < 1 \times 10^{-5}$. However, Dai et al. [138] used FTIR spectroscopy on NaCl crystallite films at 240 and 296 K to determine that a water adlayer does adhere to dry salt and that a small fraction of surface sites (<1%) cause H_2O dissociation. It is likely that the measurements of Fenter et al. and Beichert and Finlayson-Pitts were affected by surface saturation. [Back to Table](#)
 15. H_2O on $\text{NaCl}(\text{aq})$. Fung et al. [196] used Mie resonance scattering techniques to quantify aqueous NaCl droplet growth (5.8 to 7.8 μm), yielding fitted values of $\alpha > 0.5$ and consistent with 1.0. Such droplet growth measurements require modeling of heat and mass transfer and may not correspond to atmospheric conditions near vapor/liquid equilibrium. [Back to Table](#)
 16. H_2O_2 on $\text{H}_2\text{O}(\text{s})$. The uptake of H_2O_2 on ice surfaces has been studied by Clegg and Abbatt [130] who measured relatively small, reversible uptake between 213 and 238 K in a coated-wall flow tube experiment. The uptake scaled linearly with partial pressure and there was a weak temperature dependence, increasing with increasing temperature. By contrast, using the same flow tube technique but with a more direct H_2O_2 detection technique, values reported in by Crowley and co-workers in [452] are several orders of magnitude higher. A value of $K_{\text{part}} = 2.1 \times 10^{-5} \exp(3800/T)$ cm is reported. Although the source of discrepancy between these studies is not clear, the later study by Crowley and co-workers is preferred by virtue of the more direct detection technique. [Back to Table](#)
 17. H_2O_2 on $\text{H}_2\text{O}(\text{l})$. Measured accommodation coefficient (Worsnop et al. [611]) has a strong negative temperature dependence over the measured range of 260–292 K, with $\alpha = 0.3$ at 260 K decreasing to 0.1 at 292 K. [Back to Table](#)
 18. H_2O_2 on $\text{H}_2\text{SO}_4 \cdot n\text{H}_2\text{O}$. Knudsen cell uptake measurements are subject to surface saturation, thus uptake coefficient value of 7.8×10^{-4} quoted by Baldwin and Golden [37] is almost certainly a lower limit for α . This effect is probably also responsible for the lack of measured uptake ($\gamma < 10^{-6}$) for NO, NO_2 , SO_2 , Cl_2 , and other species reported in this reference and Baldwin and Golden [38]. [Back to Table](#)
 19. NO on $\text{H}_2\text{O}(\text{s})$. NO data (Leu [360], Saastad et al. [488]) are subject to the same concerns as NO_2 . See Note for NO_2 on $\text{H}_2\text{O}(\text{s})$. Using a radioactive tracer in a chromatographic technique, the adsorption enthalpy has been measured to be –20 kJ/mole by Bartels-Rausch et al. [44] [Back to Table](#)
 20. NO on $\text{H}_2\text{SO}_4 \cdot n\text{H}_2\text{O}$. See Notes for H_2O_2 on $\text{H}_2\text{SO}_4 \cdot n\text{H}_2\text{SO}_4$ and NO_2 on $\text{H}_2\text{SO}_4 \cdot n\text{H}_2\text{O}$. NO is subject to the same concerns as NO_2 for both reported measurements (Saastad et al. [488]; Baldwin and Golden [37]). [Back to Table](#)
 21. NO_2 on $\text{H}_2\text{O}(\text{s})$. In the absence of a chemical sink, Leu [360] measured no sustained uptake of NO_2 on ice yielding an apparent $\alpha \leq 1 \times 10^{-4}$. Saastad et al. [Saastad, 1993 #1795]; measured a lower limit of 5×10^{-5} for temperatures between 193 and 243 K. However these values are probably influenced by surface saturation. Using a radioactive tracer in a chromatographic technique, the adsorption enthalpy has been measured to be –22 kJ/mole by Bartels-Rausch et al. [44] [Back to Table](#)
 22. NO_3 on $\text{H}_2\text{O}(\text{l})$. Rudich et al. [485] analyzed uptake on KI solutions as a function of $[\text{I}^-]$ at 273 K. This work suggested that $\alpha > 0.04$, but this result may be biased due to reactive uptake by interfacial I^- .

Potentially smaller estimates of α were suggested by the work of Thomas et al. as quoted in Mihelcic et al. [408] at 293 K on pure water and Thomas et al., [554] on 293 K 0.1 M NaCl solutions, which reported uptake coefficients of 2.5×10^{-3} and 2×10^{-3} respectively. Schütze and Herrman [501] used a single suspended droplet flow reactor technique and the resistor model to analyze uptake data on aqueous Alizarin Red S dye and NaCl solutions to estimate a 293 K value of $\alpha = 4.2(+2.2, -1.7) \times 10^{-3}$, consistent with the limits suggested by Thomas and co-workers. However, their data do not rule out possible surface reactions with either interfacial Cl⁻ or Alizarin Red S. A lower limit of 2×10^{-3} for 273-293 K is recommended. [Back to Table](#)

23. HONO on H₂O(s). Fenter and Rossi [173] measured reversible uptake on water ice between 180 and 200 K using a Knudsen cell technique. An initial uptake coefficient of 1×10^{-3} suggests that α equals or exceeds this value. Chu et al. [109] used a cylindrical flow reactor to measure the uptake coefficient as a function of temperature, obtaining values ranging from 3.7×10^{-3} at 178 K to 6.4×10^{-4} at 200 K, in good agreement with the results of Fenter and Rossi. On the other hand, Chu et al. report significantly lower values after correction for the effects of surface porosity, i.e. 1.4×10^{-4} at 178 K and 1.3×10^{-5} at 200 K (see Keyser et al. [334]). The adsorption enthalpy has been measured to be -32 kJ/mole by Bartels-Rausch et al. [44]. [Back to Table](#)
24. HNO₃ on H₂O(s). Leu [359] report a lower limit of 0.2 at 195 K, Hanson [235] measured an uptake coefficient of greater than 0.3 at 191.5 and 200 K, and Aguzzi and Rossi [14] measured an uptake coefficient of 0.3 over the temperature range from 180 to 190 K with the value decreasing at T > 195 with an exponential temperature dependence of $-(3400 \pm 500)/T$. Aguzzi and Rossi attributed this change to an increasing evaporation rate, concluding that the accommodation coefficient most likely remains large. In a higher temperature regime, Hynes et al. [285] measured uptake coefficients as a function of temperature decreasing from 0.03 at 215 K to 0.006 at 235 K and Hudson et al. [275] report initial uptake coefficients ranging from 0.007 at 209 K to 0.003 at 220 K. On the other hand, Ullerstam et al. [568] report a temperature independent lower limit to the uptake coefficient of 0.1 from 200 K up to 239 K. It is unclear the extent to which the work of Aguzzi and Rossi, Hudson et al., and Hynes et al. are affected by outgassing of nitric acid from wall surfaces during uptake experiments at high temperatures, which would lead to apparently low uptake coefficients. Also, uptakes on surfaces that have already been exposed to nitric acid are smaller than those that are freshly exposed. Additional uncertainty is introduced by the effective ice surface area in the older fast-flow measurements (see Keyser et al. [334]) but these effects should be absent in the work of Hynes et al. and Ullerstam et al., which used smooth ice surfaces.

For low partial pressure experiments and temperatures above about 190 K, the uptake of nitric acid displays both reversible and irreversible components in amounts that do not exceed monolayer coverage ([4]; [639]; [568]). For high partial pressures and/or low temperatures, a different uptake regime is encountered where much larger uptakes can occur that are not necessarily atmospherically relevant. In particular, the ice surfaces may melt to form a thermodynamically stable nitric acid solution on the surface, or nitric acid hydrate layers may form. Focussing only on the sub-monolayer, atmospherically-relevant uptake regime, it is believed that the uptake proceeds initially via adsorption to the ice surface, with some degree of diffusion along grain boundaries and into the underlying ice bulk then proceeding. The relative fractions of adsorbed molecular nitric acid and dissociated nitric acid are not fully known, although it is likely that nitrate is present to a large degree [639]. For the initial exposure, uptakes are saturated at between 1 to 3×10^{14} molecules cm⁻² ([4]; [639]; [568]; [284]) when the gas phase concentrations are high (roughly 10^9 to 10^{10} molecules/cm³) for temperatures between roughly 200 and 230 K. At lower concentrations, the surface is unsaturated and the uptakes obey temperature-dependent Langmuir adsorption curves, with enhanced uptake at low temperatures [568]. In this regime, for temperatures between 214 to 239 K, the adsorption coefficient (converted to concentration units) for the initial uptake is $K_{\text{conc}} = -8.2 \times 10^{-12} T + 2.01 \times 10^{-9}$ cm³/molecule. The temperature dependence is qualitatively consistent with observations of nitric acid uptake to cirrus cloud particles, with more uptake at low temperature [568]. For repeated exposures, the amounts of nitric acid decrease relative to the initial uptake value. Cox et al. [136] have used a numerical model of the Ullerstam et al. [568] data to decouple adsorptive uptake from uptake arising by nitric acid diffusing into the upper layers of the ice. As a result, an effective temperature-dependent adsorption equilibrium constant has been deduced, which shows that roughly 85% of the uptake measured by Ullerstam et al. is adsorptive. The related enthalpy of adsorption is -31 kJ/mole. Using a radioactive tracer, chromatographic technique Bartels-Rausch et al. [44] have measured the adsorption enthalpy to be -44 kJ/mole, and Hynes et al. [284] report a value of -54 kJ/mole from a Van't Hoff analysis.

Note that uptake may be affected by co-adsorbed species. Studies by Hynes et al. [284] and Sokolov and Abbatt [533] involving co-adsorption of HCl indicate that HNO_3 binds more strongly than HCl, but that the presence of HCl does lead to suppressed HNO_3 uptake relative to behavior on bare ice surfaces. Also, enhanced uptake is observed if the ice surfaces are growing and not at equilibrium [567], probably arising through the formation of a metastable solution of HNO_3 in ice. The uptakes are larger under burial conditions than the amounts of nitric acid that are thermodynamically stable [553]. [Back to Table](#)

25. HNO_3 on $\text{H}_2\text{O}(\text{l})$. Measurements using a droplet train flow reactor show that α has a strong negative temperature dependence varying from 0.19 ± 0.02 at 268 K to 0.07 ± 0.02 at 293 K (Van Doren et al. [578]). Ponche et al. [448] measured a very consistent mass accommodation coefficient of 0.05 ± 0.01 at 297 K using the same technique. Schütze and Herrmann [499] measured a lower limit of 3×10^{-2} at 298 K using a suspended droplet flow reactor method, consistent with the droplet train flow reactor measurements. [Back to Table](#)
26. HNO_3 on $\text{HNO}_3 \cdot n\text{H}_2\text{O}(\text{s})$. Hanson [235] measured uptake coefficients of >0.3 and >0.2 on NAT surfaces at 191 K and 200 K, respectively. Middlebrook et al. [407] measured an uptake coefficient of 0.7 on NAT at 197 K under conditions where both nitric acid and water vapor were co-depositing. [Back to Table](#)
27. HNO_3 on $\text{HNO}_3 \cdot n\text{H}_2\text{O}(\text{l})$. Rudolf and Wagner [487] used an aerosol expansion chamber techniques to deduce that α for HNO_3 on 278 K $\text{H}_2\text{O}/\text{HNO}_3$ droplets is >0.3 and probably close to 1. The consistency of this value with smaller (~ 0.2) values measured for uptake on pure water by Van Doren et al. [578] is unclear, since the mechanism of co-condensation is unknown and the composition of the surface in the aerosol expansion chamber experiments may be kinetically controlled and has not been well determined. [Back to Table](#)
28. HNO_3 on $\text{H}_2\text{SO}_4 \cdot n\text{H}_2\text{O}$ and $\text{H}_2\text{SO}_4 \cdot 4\text{H}_2\text{O}(\text{s})$. Initial uptake at 73 wt.% H_2SO_4 allows a measurement of $\alpha = 0.11 \pm 0.01$ at 283 K (Van Doren et al. [578]). This value is expected to increase at lower temperatures, in a manner similar to $\text{H}_2\text{O}(\text{l})$ uptake (Van Doren et al. [577]). Total HNO_3 uptake is subject to Henry's law solubility constraints, even at stratospheric temperatures (Reihs et al. [459]). Solubility limitations also affected the earlier "sticking coefficient" measurements of Tolbert et al. [563] for 75 wt.% H_2SO_4 at 230 K. Hanson [235] measured an uptake coefficient of >0.3 for frozen 57.7 wt.% sulfuric acid at 191.5 and 200 K. Baldwin and Golden [37] reported a lower limit of 2.4×10^{-4} on 97 wt.% H_2SO_4 at 295 K, also reflecting solubility limits. Iraci et al. [293] monitored nitric acid trihydrate growth on sulfuric acid tetrahydrate with infrared techniques, measuring HNO_3 uptake coefficient limits of >0.03 at 192.5 K and >0.08 at 192 K. These measurements involved co-deposition of water vapor. [Back to Table](#)
29. HO_2NO_2 on $\text{H}_2\text{O}(\text{s})$. Li et al. [368] measured an uptake coefficient of 0.15 ± 0.10 ; uptake may be limited by surface saturation. Uptake appears to be reversible with no decomposition. [Back to Table](#)
30. HO_2NO_2 on $\text{H}_2\text{SO}_4 \cdot n\text{H}_2\text{O}(\text{l})$. Baldwin and Golden [37] measured $\gamma = 2.7 \times 10^{-5}$, which is probably solubility limited; see Note for H_2O_2 on $\text{H}_2\text{SO}_4 \cdot n\text{H}_2\text{O}$. [Back to Table](#)
31. NH_3 on $\text{H}_2\text{O}(\text{s})$. NH_3 interacts somewhat efficiently with ice surfaces according to the coated-wall flow tube results of Jin and Chu [309] at 190 K. The porosity-corrected uptake coefficients are 4×10^{-4} , with no evidence for surface saturation when partial pressures of 10^{-6} torr are used over hours of exposure time. This suggests that the surface is being substantially modified by the NH_3 exposure. [Back to Table](#)
32. NH_3 on $\text{H}_2\text{O}(\text{l})$. Ponche et al. [448] used a droplet train technique to obtain $\alpha = (9.7 \pm 0.9) \times 10^{-2}$ at 290 K, and Bongartz et al. [77] used a liquid jet technique to obtain $\alpha = 4.0 (+3.0, -0.05) \times 10^{-2}$ at the same temperature. These experiments were extended to other temperatures by Carstens et al. [102], demonstrating a negative temperature dependence. Ammonia uptake on liquid water as a function of both pH and temperature was investigated by Shi et al. [520] using a droplet train apparatus, yielding values that also demonstrated negative temperature dependence, varying between 0.08 at 290 K to 0.35 at 260 K. The data from these four studies are all in reasonable agreement and a temperature dependent data plot with a non-linear least squares fit to all of these measurements has been published by Worsnop et al. [610]. Earlier levitated droplet evaporation experiments [552] on NH_4Cl obtained a larger evaporation coefficient of $\alpha = 0.29 \pm 0.03$, which is discounted because of the indirect nature of the experiment. [Back to Table](#)
33. CO_2 on $\text{H}_2\text{O}(\text{s})$. The uptake of carbon dioxide on ice has been studied in a classical BET adsorption experiment from 209 to 263 K by Ocampo and Klinger [432]. The system is unusual in that the measured uptakes are higher at higher temperatures, unlike the behavior displayed by most gases that physically

adsorb to ice surfaces. Similar to SO_2 , the uptake may occur via formation and decomposition of H_2CO_3 in which case the ice surfaces may be somewhat acidified by this process. [Back to Table](#)

34. CO_2 on $\text{H}_2\text{O}(\text{l})$. Noyes et al. [430] used a dynamic stirring technique to monitor pressure decreases in a closed cylinder. They inferred $\alpha = (5.5 \pm 0.5) \times 10^{-8}$ at 293 K. This technique is uncalibrated against more widely used procedures and probably suffers from severe surface saturation effects. Schurath et al. [498] employed a coaxial jet flow technique to measure a 298K value of α of $1\text{--}2 \times 10^{-4}$, noting that its low Henry's law solubility in water made the measurement very difficult. For this reason the measurement probably also suffered from surface saturation even at their shortest gas/liquid contact times, so this value is most likely a lower limit. Boniface et al. [78] used a bubble train reactor to study the uptake by water as a function of pH. At high pH the reaction of CO_2 with OH^- partially relieves surface saturation allowing determination that the uptake coefficient, and therefore α , is $\geq 1 \times 10^{-5}$, consistent with the value measured by Schurath et al. and completely inconsistent with the much lower value obtained by Noyes et al. [430]. [Back to Table](#)
35. CH_3OH on $\text{H}_2\text{O}(\text{s})$. The uptake of methanol on ice has been measured in a coated-wall flow tube from 198 to 213 K ([603]; [306]) and in a Knudsen cell from 150 to 180 K [275]. Reversible uptakes are observed. Winkler et al. fit their data to a Langmuir adsorption isotherm and report $K_{\text{part}} = 6.24 \times 10^{-12} \exp(6178/T)$ cm and $N_{\text{sat}} = 3.2 \times 10^{14}$ molecules/cm². Hudson et al. measure the initial uptake coefficient and find it to be strongly temperature dependent, decreasing with increasing temperature to less than 0.01 at 180 K. [Back to Table](#)
36. CH_3OH on $\text{H}_2\text{O}(\text{l})$. Jayne et al. [301] measured uptake from 260–291 K and derived accommodation coefficients fitting $\alpha/(1-\alpha) = \exp(-\Delta G_{\text{obs}}^\ddagger/RT)$, where $\Delta G_{\text{obs}}^\ddagger = -8.0 \text{ kcal/mol} + 34.9 \text{ cal mol}^{-1} \text{ K}^{-1} T(\text{K})$. [Back to Table](#)
37. $\text{CH}_3\text{CH}_2\text{OH}$ on $\text{H}_2\text{O}(\text{s})$. The uptake of ethanol on ice has been measured in coated-wall flow tubes by Sokolov and Abbatt [532] from 217 to 236 K, by Peybernes et al. [445] from 193 to 223 K, and by Kerbrat et al. [330] from 213 to 243 K. In all cases, either BET or Langmuir adsorption isotherms are obeyed and saturated surface coverage is observed at $2 \text{ to } 3 \times 10^{14}$ molecules/cm², with reversible adsorption and desorption of ethanol displayed. Sokolov and Abbatt report an adsorption coefficient $K_{\text{conc}} = 2.88 \times 10^{-14}$ cm³/molecule at 228 K, and an adsorption enthalpy of -62 kJ/mole , which is similar to the values of Peybernes et al. (-57 kJ/mole) and Kerbrat et al. (-68 kJ/mole). [Back to Table](#)
38. $\text{CH}_3\text{CH}_2\text{OH}$ on $\text{H}_2\text{O}(\text{l})$. Jayne et al. [301] measured uptake from 260–291 K with a droplet train flow reactor and derived mass accommodation coefficients fitting $\alpha/(1-\alpha) = \exp(-\Delta G_{\text{obs}}^\ddagger/RT)$, where $\Delta G_{\text{obs}}^\ddagger = -11.0 \text{ kcal/mol} + 46.2 \text{ cal mol}^{-1} \text{ K}^{-1} T(\text{K})$. Similar, but somewhat larger values were reported for chloro-, bromo-, and iodo-ethanols. Shi et al. [521] used the same technique to measure the uptake of both normal and deuterated ethanol over the temperature range of 263–291 K as a function of pH. Normal ethanol uptake was not dependent on pH, while the uptake of the deuterated species was enhanced by surface isotopic exchange, especially at high and low pH. The mass accommodation values obtained for normal ethanol obtained by Shi et al. ranged from 0.128 ± 0.023 at 263 K to 0.057 ± 0.005 are consistent, within experimental error, with the lowest temperature value measured by Jayne et al., but are significantly higher above $\sim 275 \text{ K}$. Katrib et al. [327] also used the droplet train technique to measure the ethanol mass accommodation coefficient between ~ 266 and 281 K, obtaining lower values than those measured by Shi et al., [521] but agreeing with the higher temperature data of Jayne et al. [301]. Katrib et al. obtained mass accommodation coefficients fitting $\alpha/(1-\alpha) = \exp(-\Delta G_{\text{obs}}^\ddagger/RT)$, where $\Delta G_{\text{obs}}^\ddagger = -(5.6 \pm 1.5) \text{ kcal/mol} + (27.4 \pm 5.5) \text{ cal mol}^{-1} \text{ K}^{-1} T(\text{K})$. While the data of Shi et al. and Katrib et al. are off-set by about a factor of three, the negative temperature dependencies measure by the two groups are very similar. The differences among the three data sets are difficult to explain, given that all three used essentially the experimental same technique; the recommended lower limit is consistent with the lower values measured by Katrib et al. [327]. [Back to Table](#)
39. $\text{CH}_3\text{CH}_2\text{CH}_2\text{OH}$ on $\text{H}_2\text{O}(\text{s})$. The uptake of propanol by ice surfaces was studied in a coated-wall flow tube by Sokolov and Abbatt [532]. Uptake was well described by a Langmuir adsorption isotherm at 228 K, with a saturated surface coverage of 3.1×10^{14} molecules/cm² and an adsorption coefficient $K_{\text{conc}} = 8.3 \times 10^{-14}$ cm³/molecule. [Back to Table](#)
40. $\text{CH}_3\text{CH}_2\text{CH}_2\text{OH}$ and $\text{CH}_3\text{CH}(\text{OH})\text{CH}_3$ on $\text{H}_2\text{O}(\text{l})$. Jayne et al. [301] measured uptake coefficients between 260 and 291 K and derived accommodation coefficients fitting $\alpha/(1-\alpha) = \exp$

$(-\Delta G_{\text{obs}}^{\ddagger}/RT)$, where $\Delta G_{\text{obs}}^{\ddagger} = -9.2 \text{ kcal mol}^{-1} + 40.9 \text{ cal mol}^{-1} \text{ K}^{-1} T(\text{K})$ for 1-propanol and $-9.1 \text{ kcal mol}^{-1} + 43.0 \text{ cal mol}^{-1} \text{ K}^{-1} T(\text{K})$ for 2-propanol. Similar data for t-butanol were also reported. [Back to Table](#)

41. HOCH₂CH₂OH on H₂O(l). Jayne et al. [301] measured uptake coefficients for ethylene glycol between 260 and 291 K and derived accommodation coefficients fitting $\alpha/(1 - \alpha) = \exp(-\Delta G_{\text{obs}}^{\ddagger}/RT)$, where $\Delta G_{\text{obs}}^{\ddagger} = -5.3 \text{ kcal mol}^{-1} + 24.5 \text{ cal mol}^{-1} \text{ K}^{-1} T(\text{K})$. [Back to Table](#)
42. CH₃O₂ on NaCl(s). Gershenzon et al. [206] measured the uptake of CH₃O₂ on crystalline NaCl(s) in a central rod flow apparatus. They determined a value of $\gamma = (4 \pm 1) \times 10^{-3}$ at 296 K, suggesting that $\alpha \geq 4 \times 10^{-3}$. [Back to Table](#)
43. CH₃OOH on H₂O(l). Magi et al. [387] used a droplet train flow reactor to measure α over a temperature range of 261–281 K, showing a negative temperature dependence with values ranging from 9.2×10^{-3} at 281 to 20.8×10^{-3} at 261 K. Allowing for measurement uncertainty produces a recommendation that $\alpha \geq 7 \times 10^{-3}$ from 260 to 282 K. [Back to Table](#)
44. CH₂O on H₂O(s). The uptake of formaldehyde on ice in a coated-wall flow tube has been measured by Winkler et al., [603]. They report reversible uptake behavior with a partition coefficient of $K_{\text{part}} = 0.7 \text{ cm}$, temperature independent between 198 and 208 K. At much higher temperatures (238 to 268 K), the partitioning to ice was studied by Burkhart et al. [88] using artificial snow. It was found that the partitioning increased at lower temperatures, in accord with Winkler et al. Although there is also likely to be a significant surface component, the partition coefficients in this work are expressed in bulk solubility format, ranging from 56 to 245 M/atm from 268 to 238 K. [Back to Table](#)
45. CH₂O on H₂O(l) and H₂SO₄ • mHNO₃ • nH₂O(l). Jayne et al. [304] report uptake measurements for 0 – 85 wt.% H₂SO₄ and 0 – 54 wt.% HNO₃ over a temperature range of 241–300 K. Measured uptake coefficients vary from 0.0027–0.027, increasing with H⁺ activity (Jayne et al. [304]; Tolbert et al., [561]), and with increasing pH above 7 (Jayne et al., [302]). Reversible uptake is solubility limited through reactions to form H₂C(OH)₂ and CH₃O⁺. A model of uptake kinetics (Jayne et al., [304]) is consistent with $\gamma = 0.04 \pm 0.01$ for all compositions. A chemisorbed surface complex dominates uptake at 10 – 20 wt.% H₂SO₄, and CH₃O⁺ formation dominates above 20 wt.% (Tolbert et al., [561]; Jayne et al. [304], Iraci and Tolbert [295]). Low temperature (197–214 K) uptake studies by Iraci and Tolbert [295] confirm that uptake is solubility limited for uptake coefficients in the 10^{-3} to 10^{-2} range even at low temperatures. These chemical mechanisms allow γ to greatly exceed α for strong acidic and basic solutions. A full uptake model for acid solutions is presented in Jayne et al. [304], and for basic solutions in Jayne et al. [302]. XPS surface analysis by Fairbrother and Somorjai [168] failed to see CH₃O⁺ surface species reported by Jayne et al.; however, their sensitivity of 1% of surface coverage is too poor to see the predicted amounts of the surface species. [Back to Table](#)
46. CH₃CHO on H₂O(s). The uptake of acetaldehyde to ice surfaces was measured in a Knudsen Cell from 120 to 160 K by Hudson et al. [275] finding the uptake to decrease with increasing temperature. Fitting the results to a Langmuir adsorption model and extrapolating to 210 K, the authors conclude that there will be low surface coverages under upper tropospheric conditions of $< 5 \times 10^9$ molecules/cm². Hudson et al. report the initial uptake coefficient and find it to be strongly temperature dependent, decreasing with increasing temperature to less than 0.01 at 160 K. Petitjean et al. [444] have used a coated-wall flow tube to measure relatively small reversible uptakes. They report saturated surface coverages of between 1 and 2×10^{14} molecules/cm² and a heat of adsorption of -16 kJ/mole from 203 to 233 K. A higher heat of adsorption is calculated if the entropy of adsorption is fixed according to Trouton's rule. Larger uptakes are observed on mixed ice and nitric acid solution surfaces. [Back to Table](#)
47. CH₃CHO on H₂O(l). Jayne et al. [302] measured a lower accommodation coefficient limit of > 0.03 at 267 K. Uptake can be limited by Henry's law and hydrolysis kinetics effects—see reference. [Back to Table](#)
48. CH(O)CH(O) on H₂O (l). Schweitzer et al. [506] used a droplet train flow reactor to investigate the uptake of glyoxyl by water droplets over a temperature range of 263–283 K; measured uptake was near their detection limit. They reported an average α over their experimental temperature range of $2.3 (+1.1/-0.7) \times 10^{-2}$. [Back to Table](#)
49. CH₃C(O)CH₃ on H₂O(s). The uptake of acetone to ice surfaces has been measured in both coated-wall flow tubes ([603]; [446]; [45]; [63]) and in a Knudsen cell [275]. Reversible uptake that is described by the

simple Langmuir adsorption isotherm is demonstrated. Winkler et al. report a partition coefficient $K_{\text{part}} = 1.25 \times 10^{-10} \exp(5575/T) \text{ cm}$, an enthalpy of adsorption of -46 kJ/mole , and a saturated surface coverage of $3 \times 10^{14} \text{ molecules/cm}^2$, for temperatures between 198 and 218 K. Between 193 to 223 K, Peybernes et al. [446] report an adsorption enthalpy of -49 kJ/mole with a smaller saturated surface coverage of $1.3 \times 10^{14} \text{ molecules/cm}^2$. By fitting observed adsorption and desorption profiles at 190 to 220 K, Behr et al. conclude that a two-site model best represents their observations. Total adsorbed species are close to $3 \times 10^{14} \text{ molecules/cm}^2$ at saturation but the modeling suggests the presence of two crystallographic surfaces, one which binds acetone more strongly than the other. The relative proportion of the sites changes with ice film age, and adsorption energies are between -32 and -49 kJ/mole . Bartels-Rausch et al. report very similar adsorption enthalpies ($-51 \pm 2 \text{ kJ/mole}$) on a range of ice surfaces, including single and polycrystalline laboratory crystal ice, and snow from the field, at 198 to 223 K. Hudson et al. report somewhat smaller adsorption enthalpies at low temperatures (140 to 170 K) ranging from -28 to -39 kJ/mole . They also measure the initial uptake coefficient and find it to be strongly temperature dependent, decreasing with increasing temperature to less than 0.1 at 170 K. [Back to Table](#)

50. $\text{CH}_3\text{C(O)CH}_3$ on $\text{H}_2\text{O(l)}$. Duan et al. [160] measured uptake between 260 and 285 K, deriving $\alpha = 0.066$ at the lower temperature and 0.013 at the higher, with several values measured in between. Measured values fit $\alpha/(1-\alpha) = \exp(-\Delta G_{\text{obs}}^\ddagger/RT)$, where $\Delta G_{\text{obs}}^\ddagger = -12.7 \text{ kcal/mol} + 53.6 \text{ cal mol}^{-1} \text{ K}^{-1} \text{ T(K)}$. Schütze, M. and H. Herrmann [500] used a single suspended droplet flow reactor to measure the uptake of acetone and several larger carbonyl compounds at 293 K; their value for acetone of $\alpha = 5.4(+4.5/-2.6) \times 10^{-3}$ agrees well with the values of Duan et al. extrapolated to 293 K. [Back to Table](#)
51. $\text{CH}_3\text{C(O)CHO}$ on $\text{H}_2\text{O(l)}$. Schütze and Herrmann [500] used a single suspended droplet flow reactor to measure the uptake of 2-oxypropynal at 293 K, their value of $\alpha = (1.5 \pm 0.5) \times 10^{-4}$ is lower than those measured for acetone and acetaldehyde. [Back to Table](#)
52. $\text{CH}_3\text{OC(O)OCH}_3$ on $\text{H}_2\text{O(l)}$. Katrib et al. [326] measured the uptake of dimethyl carbonate on pure water and 0.1M aqueous NaOH over a temperature range of 270-278 K using a droplet train flow reactor. Uptake was not obviously dependent on $[\text{OH}^-]$ and displayed a negative temperature dependence with individual measurements varying from $(11 \pm 2) \times 10^{-2}$ at 270 K to $(1.2 \pm 0.9) \times 10^{-2}$ at 276 K. Although the data are fairly noisy the authors derived a mass accommodation coefficient fitting of $\alpha/(1-\alpha) = \exp(-\Delta G_{\text{obs}}^\ddagger/RT)$, where $\Delta G_{\text{obs}}^\ddagger = -(26 \pm 9) \text{ kcal mol}^{-1} + (99 \pm 35) \text{ cal mol}^{-1} \text{ K}^{-1} \text{ T(K)}$. Similar mass accommodation data for diethyl carbonate are also presented. [Back to Table](#)
53. HC(O)OH on $\text{H}_2\text{O(s)}$. The uptake of formic acid on ice has been measured in coated-wall flow tube from 187 to 221 K by Von Hessberg et al. [587] and Jedlovsky et al. [305]. Reversible uptakes are observed. Von Hessberg et al. fit their data to the Langmuir adsorption isotherm and report the adsorption constant to be $K_{\text{conc}} = 1.54 \times 10^{-24} \exp(6150/T) \text{ cm}^3/\text{molecule}$, for a saturated surface coverage of $2.2 \times 10^{14} \text{ molecules/cm}^2$. [Back to Table](#)
54. HC(O)OH on $\text{H}_2\text{O(l)}$. Jayne et al. [301] measured uptake coefficients for formic acid between 260 and 291 K and derived accommodation coefficients fitting $\alpha/(1-\alpha) = \exp(-\Delta G_{\text{obs}}^\ddagger/RT)$, where $\Delta G_{\text{obs}}^\ddagger = -7.9 \text{ kcal mol}^{-1} + 34.9 \text{ cal mol}^{-1} \text{ K}^{-1} \text{ T(K)}$. [Back to Table](#)
55. $\text{CH}_3\text{C(O)OH}$ on $\text{H}_2\text{O(s)}$. The uptake of acetic acid on ice has been measured in coated-wall flow tubes by Sokolov and Abbatt [532] from 222 to 245 K, by Picaud et al. [447] from 193 to 223 K, and by von Hessberg et al. [587] from 197 to 227 K. In all cases, either BET or Langmuir adsorption isotherms are demonstrated and saturated surface coverage is observed with between 2 to $3 \times 10^{14} \text{ molecules/cm}^2$. The values of the partition coefficients between the Sokolov and Abbatt and von Hessberg et al. studies agree to within roughly a factor of two, whereas the Picaud et al. results are one to two orders of magnitude smaller at low temperatures. The overall adsorption coefficient expressions from the Sokolov and Abbatt data, and von Hessberg et al. are $K_{\text{conc}} = 8.3 \times 10^{-28} \exp(7825/T) \text{ cm}^3/\text{molecule}$ and $K_{\text{conc}} = 6.55 \times 10^{-25} \exp(6610/T) \text{ cm}^3/\text{molecule}$, respectively. [Back to Table](#)
56. $\text{CH}_3\text{C(O)OH}$ on $\text{H}_2\text{O(l)}$. Jayne et al. [301] using a droplet train flow reactor measured uptake coefficients for acetic acid between 260 and 291 K and derived a mass accommodation coefficient fitting $\alpha/(1-\alpha) = \exp(-\Delta G_{\text{obs}}^\ddagger/RT)$, where $\Delta G_{\text{obs}}^\ddagger = -8.1 \text{ kcal mol}^{-1} + 34.9 \text{ cal mol}^{-1} \text{ K}^{-1} \text{ T(K)}$. Shi et al. [521] used the same technique to measure the uptake of both normal and deuterated acetic acid at 258 K and pH=7. They

obtained $\alpha = 0.19 (\pm 0.03)$ for normal acetic acid, while the uptake coefficient of the deuterated species was enhanced by surface isotopic exchange, equaling $0.96 (\pm 0.21)$. [Back to Table](#)

57. $\text{CH}_3\text{CO}(\text{O}_2)\text{NO}_2$ on $\text{H}_2\text{O}(\text{s})$. The adsorption enthalpy has been measured to be -30 kJ/mole by Bartels-Rausch et al. [44]. [Back to Table](#)
58. Cl_2 on $\text{H}_2\text{O}(\text{s})$. Measurement of Leu [359] yielded a limit of $<1 \times 10^{-4}$ for Cl_2 and is subject to same concern as NO_2 (see note). A similar limit of $<5 \times 10^{-5}$ has been measured by Kenner et al. [329], which is also probably limited by surface saturation. [Back to Table](#)
59. $\text{OCIO} + \text{H}_2\text{O}(\text{s})$. Brown et al. [85] and Graham et al. [218] used complementary ultra high-vacuum (UHV) and coated-wall flow tube techniques to show sub-monolayer reversible absorption of OCIO on water ice at 100 K (UHV) and 189 and 200 K (flow tube). No kinetic data are available at stratospheric temperatures but the mass accommodation coefficient for 100 K ice surfaces is near unity, with values of 0.8 ± 0.2 reported for amorphous ice and 0.6 ± 0.2 for crystalline ice [218]. [Back to Table](#)
60. HCl on $\text{H}_2\text{O}(\text{s})$. The uptake coefficients of Leu [359] (0.4; +0.6, -0.2) and Hanson and Ravishankara, [245] (≥ 0.3) are in reasonable agreement at stratospheric ice temperatures. At somewhat higher temperatures (205 K), Hynes et al. [286] measured slightly lower values (0.1) which decreased at higher temperatures. At very low temperatures (80 to 120 K), Rieley et al. [463] measured $\alpha = 0.95 \pm 0.05$.

A great deal of experimental effort (Abbatt et al. [7]; [4] ; Barone et al. [43]; Koehler et al. [347]; Chu et al. [115]; Foster et al. [189]; Graham and Roberts [216]; Graham and Roberts [217]; Hanson and Ravishankara, [245]; Henson et al. [262]; Hynes et al. [286]; Leu et al. [362]; Marti et al. [390]; McNeil et al. [396]; McNeil et al. [395]) has gone into understanding the magnitude and nature of the uptake of HCl by ice surfaces under stratospheric and upper tropospheric conditions. A general observation is that water ice at stratospheric temperatures can take up a significant, but sub-monolayer, amount of HCl even at HCl partial pressures typical of the stratosphere. However, quantitative agreement in the size of the uptake is lacking, with a range of close to three orders of magnitude for partial pressures of 10^{-7} torr at roughly 200 K. One issue is that the specific surface area of the ice was not measured in a number of early studies. Because the ice surface may have some roughness, depending on how it is prepared, a number of these uptakes may be biased high, if the surfaces were assumed to be smooth. Another issue is the partial pressure dependence of the uptake. In accord with a number of uptake measurements of other species on ice, saturated surface coverages are observed at about 2 to 3×10^{14} molecules/cm² in experiments where the specific surface area of the ice is well known (e.g. Henson et al. [262], Hynes et al. [286], McNeil et al. [395]). The drop-off into the unsaturated part of the adsorption isotherm appears to vary from experiment to experiment, as the HCl partial pressure is lowered. For example, Hanson and Ravishankara, [245] do not observe a drop off down to partial pressures well below 10^{-7} torr, whereas others (e.g. Henson et al. [262], McNeil et al. [395]) see a significant drop-off at higher partial pressures. And so, at the very low partial pressures of the upper troposphere, the surface coverage may be quite unsaturated; even in the stratospheric regime, there may not exist a full monolayer coverage. Some of the most thorough studies have been performed recently. For example, in a coated-wall flow tube study on a variety of ice surfaces at close to 200 K McNeil et al. [395] show that uptakes obeyed conventional Langmuir adsorption isotherms, and that they did not scale as well with the dissociative Langmuir isotherm. A weak adsorption enthalpy of -15 kJ/mole was derived, but the accuracy of this value may be impacted by measurements made at three relatively close temperatures; the true value is likely much higher. Langmuir adsorption constants, $K_{\text{conc}} = 3.1 \times 10^{-11}$, 8.4×10^{-11} and 3.9×10^{-11} cm³/molecule, were obtained at 213, 203 and 196 K, respectively. By contrast the work of Henson et al. [262] using a static adsorption technique yields a much lower (one to two orders of magnitude) surface coverage for the same HCl partial pressures and temperatures.

Note that for the same experimental conditions, the uptake may be affected by co-adsorbed species. Studies by Hynes et al. [284] and Sokolov and Abbatt [533] involving co-adsorption of HNO_3 indicate that HNO_3 binds more strongly than HCl, but that the presence of HCl does lead to suppressed HNO_3 uptake relative to behavior on bare ice surfaces. Fernandez et al. [176] also show that HCl uptake is significantly suppressed on a surface that has been exposed to HNO_3 .

Both the thermodynamic and spectroscopic properties of adsorbed HCl suggest that a large fraction dissociates to ions, forms ionic hydrates (especially at low temperatures), and is highly reactive (with ClONO_2 , HOBr and HOCl). Also, adsorption and desorption profiles in flow tubes suggest that uptake occurs via both reversible and irreversible processes, probably related to partitioning to different surface

sites such as the ice faces or grain boundaries. These experimental results contrast with initial theoretical calculations that predicted undissociated HCl hydrogen bonded to the ice surface and a very small adsorption probability at stratospheric temperatures (Kroes and Clary [351]); more recent simulations result in higher adsorption energies and theoretical accommodation coefficients of one for 190-K surfaces (Wang and Clary [592]). Molecular dynamics calculations by Gertner and Hynes [209] also show that ionic absorption is thermodynamically favorable by about 5 kcal/mole, facilitated by the role of mobile water molecules on the ice surface that can hydrate the ions. Using ellipsometry McNeil et al. [396] have experimentally shown the presence of a disordered layer on the ice surface, sometimes referred to as the quasi liquid layer, arising from HCl adsorption at low temperatures and partial pressures. By contrast, at HCl partial pressures significantly above those typical of the stratosphere, a thermodynamically stable liquid surface layer forms on the ice, greatly enhancing the total amount of HCl that the surface can absorb (Abbatt et al. [7]). These conditions should be avoided for lab studies as they are not atmospherically appropriate. [Back to Table](#)

61. HCl on H₂O(l). Recommendation is based on Van Doren et al. [577] and Schweitzer et al. [509]. Using a droplet train flow reactor, Van Doren et al. [577] measured α 's decrease from 0.18 ± 0.02 at 274 K to 0.064 ± 0.01 at 294 K, demonstrating strong negative temperature dependence. Schweitzer et al. [509] used the same technique over a temperature range of 262 to 281 K obtaining values decreasing from 0.24 to 0.13 that agree very well with the Van Doren et al. data. Tang and Munkelwitz [552] have measured a larger (0.45 ± 0.4) HCl evaporation coefficient for an aqueous NH₄Cl droplet at 299 K. [Back to Table](#)
62. HCl on HNO₃ • nH₂O. There was previously severe disagreement between Hanson and Ravishankara [245] ($\alpha \geq 0.3$) for NAT (54 wt.% HNO₃), and Leu and coworkers (Moore et al. [417], Leu et al. [361]). However, subsequent experiments at lower HCl concentrations by Leu and coworkers [115] as well as Abbatt and Molina [8] are generally consistent with Hanson and Ravishankara. The measurements of Hanson and Ravishankara are consistent with $\alpha = 1$. The experiments at stratospherically representative HCl concentrations show that HNO₃-rich NAT surfaces adsorb significantly less HCl than H₂O-rich surfaces, with the uptake at a fixed temperature determined by the partial pressure of water [8]. [Back to Table](#)
63. HCl on H₂SO₄ • nH₂O. Measurements by Watson et al. [595] at 284 K show $\alpha = 0.15 \pm 0.01$ independent of n for $n \geq 8$. Experimental uptake and, therefore, apparent α falls off for $n \leq 8$ (≥ 40 wt.% H₂SO₄). This behavior is also observed at a stratospheric temperature (218 K) by Hanson and Ravishankara [245]. Hanson and Lovejoy [241] reported a value of 0.75 ± 0.2 for 26 wt. % H₂SO₄ at 272K. More extensive measurements performed by Robinson et al. [472] at lower temperatures, also yielded higher values, reaching 1.03 ± 0.10 for 39 wt.% H₂SO₄ at 230 K; they also observed enhanced uptake for 69 wt.% H₂SO₄ that was attributed to the formation of chlorosulfonic acid. Solubility constraints also controlled earlier low temperature uptake measurements of Tolbert et al. [563]. A review of the most recent solubility data is presented in Table 5-6.

Molecular beam measurements of HCl impingement on liquid deuterated sulfuric acid surfaces determine the fraction of HCl scattered with no reaction and the fraction that is reactively converted and emitted as DCl. The fraction converted to DCl is assumed to have undergone interfacial transport, representing a lower limit to the mass accommodation coefficient, which varies from ~0.7 at 53-55 wt.% D₂SO₄ to ~0.1 near 70 wt.% Behr et al. [61]. More recent measurements indicate that the conversion fraction is relatively insensitive to HCl kinetic energy over the range of 6 to 140 kJmol⁻¹, and that the conversion fraction for 72 wt.% D₂SO₄ varies less dramatically, from ~0.33 at 213 K to ~0.47 at 243K Behr et al. [62]. The basic technique and analysis rationale are reviewed by Nathanson [429]. The impact of organic surfactants on mass accommodation sulfuric acid, including the surprising fact that a surface layer of butanol actually significantly enhances HCl uptake in 213K, 56-68 wt.% D₂SO₄ is reviewed in Park et al. [439]. These studies strongly indicate that the mass accommodation coefficient for 50-72 wt.% sulfuric acid surfaces for temperatures below 243 K is >0.1. [Back to Table](#)

64. HCl on H₂SO₄ • 4H₂O(s). Uptake is a strong function of temperature and water vapor partial pressure (relative humidity) (Zhang et al. [633]), both of which affect adsorbed surface water. [Back to Table](#)
65. ClONO₂ on H₂O(l). Dieber et al. [150] used a droplet train apparatus to measure the uptake of ClONO₂ on NaBr aqueous solutions to deduce the mass accommodation coefficient of 0.108 ± 0.011 at 274.5 K. This value may be affected by the reaction with interfacial Br⁻. [Back to Table](#)
66. Halocarbonyls on H₂O(l). Uptake is limited by Henry's law solubility and hydrolysis rate constants (De Bruyn et al. [145, 147] and Georg et al. [200, 202]). [Back to Table](#)

67. HBr on H₂O(s) and HNO₃•nH₂O. Hanson and Ravishankara [246, 247] have reported large uptake coefficients for HBr on 200-K ice and NAT. Lower limits of >0.3 and >0.2 for ice are reported in the two referenced publications, respectively, and a limit of >0.3 is reported for NAT. No surface saturation was observed, leading to the supposition that HBr, like HCl, dissociates to ions on ice surfaces at stratospheric temperatures. Abbatt [1] measured an uptake coefficient lower limit of >0.03 on water ice at 228 K consistent with Hanson and Ravishankara. Rieley et al. [463] measured an α of 1.0 ± 0.05 for water ice at 80–120 K. Flückiger et al. [185] report α values of ~0.2 at 210 K, increasing to ~0.3 at 190 K, while Percival et al. [442] measured an α of 0.03 ± 0.005 for water ice at $T > 212$ K, and $\alpha > 0.1$ at $T < 212$ K, attributing the apparent increase in the uptake coefficient to an increase in the surface area of the ice. Hudson et al. [274] report $\alpha = 0.61 \pm 0.06$ at 140 K, and $\alpha = 0.24 \pm 0.05$ at 100 K, for HBr pressures ranging from 3×10^{-8} to 1.4×10^{-7} Torr. Equilibrium HBr coverages for ice are reported by Chu and Heron [113] at 188 and 195 K, and by Chu and Chu [107] at 180–220 K. The latter authors also report the formation of various solid HBr hydrates. Given that no surface saturation is observed in the kinetics experiments leads to the supposition that HBr, like HCl, dissociates to ions. In addition to hydrate formation, it is likely that bulk melting of the ice surfaces may occur at stratospheric temperatures and the partial pressures used in the lab, to form thermodynamically stable HBr-H₂O solutions. Such behavior may not occur in the atmosphere where partial pressures of HBr are typically much lower than those used in the lab. [Back to Table](#)
68. HBr on H₂O(l). Schweitzer et al. [509] used the droplet train flow reactor technique over a temperature range of 262 to 281 K obtaining values decreasing from 0.16 to 0.068. Li et al. [367] and Zhang et al. [625] used the same technique to measure higher values of 0.14 ± 0.02 at 283 K and 0.21 ± 0.3 at 273 K, respectively. Given the good agreement between the two groups for HCl mass accommodation coefficients on water, there is no obvious reason for the discrepancy of a factor of 2-3 for HBr. [Back to Table](#)
69. HBr on H₂SO₄•nH₂O. Molecular beam measurements of HBr impingement on liquid deuterated sulfuric acid surfaces determine the fraction of HBr scattered with no reaction and the fraction that reacts, exchanging H for D, and is emitted as DBr. The fraction converted to DBr is assumed to have undergone interfacial transport, representing a lower limit to the mass accommodation coefficient, which varies from ~0.7 at 55 wt.% D₂SO₄ to ~0.2 near 70 wt.% Behr et al. [61]. This strongly indicates that the mass accommodation coefficient for HBr is >0.1 for 55-72 wt.% H₂SO₄ at 213K. [Back to Table](#)
70. HOBr on H₂O(s). Abbatt [1] measured an uptake coefficient for water ice of 2×10^{-3} at 228 K. Chu and Chu [107] report an uptake coefficient corrected for porosity effects in the range 0.11 to 0.007 at 190–218 K, with an exponential temperature dependence of $(3809 \pm 76)/T$, and in the range 2×10^{-3} to 6×10^{-4} at 223-239 K, with an exponential temperature dependence of $(4658 \pm 456)/T$. Chaix et al. [103] measured the uptake coefficient as a function of temperature on three different types of water-ice, obtaining values ranging from ~0.3 at 185 K to ~0.03 at 205 K, with an exponential temperature dependence of $(4900 \pm 500)/T$. Mössinger et al. [419] report an uptake coefficient value of 0.003 at 227 K increasing to 0.040 at 205 K. The four sets of results are in reasonable agreement with each other, and the temperature dependence of the uptake coefficient is attributed predominantly to changes in the evaporation rate. The results indicate that the uptake of HOBr on ice cannot be explained with Langmuir-type adsorption isotherms and that the process is not reversible, probably proceeding via the self-reaction of HOBr to form Br₂O, or possibly by formation of hydrates. Using a common precursor model, Flückiger and Rossi [184] have estimated accommodation coefficients α which are considerably larger than the measured uptake coefficients, with α values ranging from 0.18 at 215 K to 0.46 at 190K. [Back to Table](#)
71. HOBr on H₂O(l). See Note on HOBr + KBr and NaBr in reactive uptake table. [Back to Table](#)
72. HOBr on H₂SO₄•nH₂O(l). Abbatt [1] measured an uptake coefficient of 0.06 ± 0.02 by measuring HOBr gas phase loss at 228 K. This result may well be a lower limit due to surface saturation effects and the uptake may have been due to Br₂O formation. [Back to Table](#)
73. BrONO₂ on H₂O(l). Dieber et al. [150] used a droplet train apparatus to measure the uptake of BrONO₂ on NaBr aqueous solutions to deduce the mass accommodation coefficient of 0.063 ± 0.021 at 274.5 K. This value may be affected by the reaction with interfacial Br⁻. [Back to Table](#)
74. BrONO₂ on H₂SO₄•nH₂O. Hanson [232] modeled wetted-wall flow reactor data and aerosol flow reactor data to estimate $\alpha = 0.80$ over a wide range of temperatures and acid concentrations. [Back to Table](#)

75. CHBr_3 on $\text{H}_2\text{O}(\text{s})$ and $\text{H}_2\text{SO}_4 \cdot n\text{H}_2\text{O}(\text{l})$. Hanson and Ravishankara [247] investigated the uptake of bromoform on ice and 58 wt.% sulfuric acid at 220 K. No uptake on ice was observed, with a measured uptake coefficient of $<6 \times 10^{-5}$. Reversible uptake by the sulfuric acid surface was observed with an initial uptake coefficient of $>3 \times 10^{-3}$; both measurements are probably limited by surface saturation. [Back to Table](#)
76. BrCl on $\text{H}_2\text{O}(\text{l})$. Katrib et al. [325] used a droplet train flow reactor to measure the uptake of BrCl as a function of NaOH concentration over the temperature range of 270-285 K. Data were too noisy to assign a clear temperature dependence, but an average over measurements at 270, 274, 280 and 285 K for higher $[\text{NaOH}]$ where reactive scavenging relieved solubility constraints yielded $\alpha = 0.33 \pm 0.18$. The recommended lower limit is consistent with this value. [Back to Table](#)
77. I_2 on $\text{H}_2\text{O}(\text{l})$. Takami et al. [548] used the impinging flow technique to investigate the uptake of I_2 at 293 K as a function of pH. While solubility constraints prevented a clear measure of mass accommodation, they modeled high pH data where solubility constraints were relaxed by reactive scavenging by OH^- to determine that $\alpha \geq 0.1$. [Back to Table](#)
78. HI on $\text{H}_2\text{O}(\text{s})$. The uptake of HI has been studied by Chu and Chu in a coated-wall flow tube [111] to be large between 188 and 195 K, in the multi-layer coverage regime. Under their experimental conditions, it is likely that the surface is melting to form a bulk solution and/or hydrates are forming. Percival et al. [442] also report efficient uptake with the same technique between 200 and 233 K, with the uptake coefficient of 0.02 ± 0.004 above 212 K and larger than 0.1 for temperatures below 212 K. [Back to Table](#)
79. HI on $\text{H}_2\text{O}(\text{l})$. Schweitzer et al. [509] used the droplet train flow reactor technique over a temperature range of 262 to 281 K, obtaining values decreasing from 0.19 to 0.079. Zhang et al. [625] used the same technique to obtain a value of 0.17 ± 0.02 at 273 K, which is a little less than a factor of two higher than indicated by the Schweitzer et al. measurements for that temperature. [Back to Table](#)
80. HOI on $\text{H}_2\text{SO}_4 \cdot n\text{H}_2\text{O}$. Knudsen cell studies by Allanic and Rossi [26] measured uptake at several temperatures for 40, 50, and 70 acid wt.%. Time dependent studies show no sign of saturation, so uptake coefficients should correspond to mass accommodation coefficients. Some acid concentration data in the table have been averaged for similar temperatures and rounded to one significant figure. An uncertainty factor of three has been assigned due to the relatively small number of temperature/concentration points studied and a lack of confirming studies from other laboratories. The authors note evidence of HOI disproportionation to form I_2 , however, this second order reaction is unlikely to occur under atmospheric conditions. [Back to Table](#)
81. HF on $\text{H}_2\text{O}(\text{s})$ and $\text{HNO}_3 \cdot n\text{H}_2\text{O}(\text{s})$. Hanson and Ravishankara [246] attempted to measure the uptake of HF by 200 K water ice and NAT surfaces but were unable to observe measurable adsorption. They surmise that, unlike HCl and HBr , HF does not dissociate to ions on ice or NAT surfaces at 200 K. Lack of measurable uptake is probably due to surface saturation. [Back to Table](#)
82. CF_2O on $\text{H}_2\text{O}(\text{s})$, $\text{HNO}_3 \cdot n\text{H}_2\text{O}$ and $\text{H}_2\text{SO}_4 \cdot n\text{H}_2\text{O}$. Uptake coefficient measurements by Hanson and Ravishankara [244] on stratospheric surfaces are probably subject to surface and/or bulk saturation effects and may not represent accommodation coefficient measurements, particularly the lower limits of $>3 \times 10^{-6}$ reported for water and nitric acid ices. [Back to Table](#)
83. $\text{CF}_3\text{C}(\text{O})\text{OH}$ on $\text{H}_2\text{O}(\text{l})$. Hu et al. [273] measured mass accommodation coefficients for five haloacetic acids, including trifluoroacetic acid (TFA); the others were mono-, di-, trichloro-, and chlorodifluoro-acetic acids. All displayed negative temperature dependence and values for α of about 0.1 at 273 K. [Back to Table](#)
84. SO_2 on $\text{H}_2\text{O}(\text{s})$. Uptake experiments in coated-wall flow tubes have been conducted by Chu et al. [110] and by Clegg and Abbatt [130] who observe sub-monolayer reversible uptakes for temperatures between 190-211 K and 213-233 K, respectively. Chu et al. report an uptake coefficient of 1×10^{-5} at 191 K. Earlier studies from Clappsaddle and Lamb [126] using chromatographic-like uptake experiments with small ice spheres packed into a column, are in good quantitative agreement with those of Clegg and Abbatt. Both studies report that uptake increases with increasing temperature, unlike most other species that demonstrate more adsorption at lower temperatures. From the partial pressure dependence of the uptake and from the behavior on basic and acidic surfaces, Clegg and Abbatt infer the uptake occurs by formation of bisulfite on the surface, in the quasi-liquid layer on the surface of ice. [Back to Table](#)

85. SO₂ on H₂O(l). Using a droplet train flow reactor Worsnop et al. measured an α of 0.11 ± 0.02 with no significant temperature variation over a temperature range of 260–292 K (Worsnop et al. [611]). Ponche et al. [448] measured 0.13 ± 0.01 at 298 K, in agreement with the earlier measurement. Shimono and Koda [522] estimated an α of 0.2 at 293.5 K from analysis of pH-dependent uptake coefficients in a liquid impingement technique. Schurath et al. [498] used a coaxial flow liquid jet to obtain a value of 0.1 at 298 K. Boniface et al. [78] performed more extensive droplet train flow reactor measurements at high pH to relieve solubility constraints, obtaining a negative temperature dependence with α values ranging from 0.43 ± 0.4 at 264 K to 0.175 ± 0.015 at 291 K, their data can be fit to $\alpha/(1-\alpha) = \exp(-\Delta G_{\text{obs}}^{\ddagger}/RT)$, where $\Delta G_{\text{obs}}^{\ddagger} = -(7.6 \pm 0.6) \text{ kcal/mol} + (29.2 \pm 2.1) \text{ cal mol}^{-1} \text{ K}^{-1} \text{ T(K)}$. Donaldson et al. [157] have used second harmonic generation spectroscopy to detect a chemisorbed SO₂ surface species which was predicted from earlier uptake measurements by Jayne et al. [300]; this surface complex may play a role in SO₂ heterogeneous reactions on aqueous surfaces. [Back to Table](#)
86. SO₂ on H₂SO₄ • nH₂O. See Note for H₂O₂ on H₂SO₄ • nH₂O. [Back to Table](#)
87. H₂S on H₂O(l). Boniface et al. [78] performed droplet train flow reactor measurements over at 260–298 K at high pH to relieve solubility constraints, measured uptake coefficients were consistent with $\alpha \geq 0.05$. [Back to Table](#)
88. H₂SO₄ on H₂SO₄•nH₂O. Poschl et al. [449] measured $0.43 < \alpha < 1.0$ for 73–98 wt.% H₂SO₄ at 303 K in a wetted wall flow tube. Lower temperatures and acid concentrations would be expected to lead to larger values of α . As discussed in Poschl et al. [449] this contradicts an indirect measurement of $0.02 < \alpha < 0.09$ at 42.5 wt.% at 298 K by Van Dingenen and Raes [576] in a photochemical aerosol reactor. The Poschl et al. [449] result is consistent with room temperature α values very near that measured for (NH₄)₂SO₄ particles in an aerosol flow reactor by Jefferson et al. [307]. [Back to Table](#)
89. CH₃S(O)CH₃, CH₃S(O₂)CH₃ and CH₃S(O₂)OH on H₂O(l). De Bruyn et al. [146] measured uptake over the temperature range ~262–281 K and derived accommodation coefficients fitting $\alpha / (1 - \alpha) = \exp(-\Delta G_{\text{obs}}^{\ddagger}/RT)$, where $\Delta G_{\text{obs}}^{\ddagger} =$
 - $-0.12 \text{ kcal mole}^{-1} + 23.1 \text{ cal mole}^{-1} \text{ K}^{-1} \text{ T(K)}$ for dimethylsulfoxide
 - $-10.7 \text{ kcal mole}^{-1} + 43.0 \text{ cal mole}^{-1} \text{ K}^{-1} \text{ T(K)}$ for dimethylsulfone
 - $-3.50 \text{ kcal mole}^{-1} + 16.7 \text{ cal mole}^{-1} \text{ K}^{-1} \text{ T(K)}$ for methanesulfonic acid.

Schweitzer et al. [506] used a droplet train flow reactor to investigate the uptake of CH₃S(O₂)OH by water over a temperature range of 262–281 K, obtaining mass accommodation coefficient values decreasing from 0.17 to 0.11, in excellent agreement with those obtained by De Bruyn et al. [146]. [Back to Table](#)

5.13 Gas/Surface Reaction Probabilities for Surfaces Other Than Soot

Table 5-2. Gas/Surface Reaction Probabilities (γ) for Surfaces Other Than Soot

Gaseous Species	Surface Type	Surface Composition	T(K)	γ	Uncertainty Factor	Notes
O₃ + Surface → Products						
O ₃	Water Ice	H ₂ O(s)	223-258	$<10^{-8}$		<u>1</u>
	Alumina	Al ₂ O ₃ (s)	210-300	$\gamma_0 < 2 \times 10^{-4}$		<u>2</u>
	Sodium Chloride	NaCl(s)	223-300	$\gamma_0 < 10^{-4}$		<u>3</u>
		NaCl(aq)	298	$\gamma_0 < 10^{-4}$		<u>3</u>
	Sodium Bromide	NaBr(s)	300	$\gamma_0 < 10^{-4}$		<u>4</u>
		NaBr(aq)	298	See Note		<u>4</u>
	Potassium Bromide	KBr(s)	300	$\gamma_0 < 10^{-4}$		<u>4</u>
	Potassium Iodide	KI(s)	~298	See Note		<u>5</u>
	Sea Salt	See Note	300	$\gamma_0 < 2 \times 10^{-2}$		<u>6</u>
OH + Surface → Products						
OH	Water Ice	H ₂ O(s)	205-230	>0.01		<u>7</u>
	Hydrochloric Acid	HCl • nH ₂ O(l)	220	>0.2		<u>8</u>
	Nitric Acid Ice	HNO ₃ • 3H ₂ O(s)	200-228	>0.2		<u>9</u>
	Sulfuric Acid	H ₂ SO ₄ • nH ₂ O(l)	200-298	>0.2		<u>10</u>
	Sodium Chloride	NaCl(s)	245-300	$\gamma_0 \sim 10^{-2}$	3	<u>11</u>
		NaCl(aq)	298	≥ 0.1		<u>11</u>
	Alumina	Al ₂ O ₃ (s)	250-300	$\gamma_0 < 0.1$		<u>12</u>
HO₂ + Surface → Products						
	Water Ice	H ₂ O(s)	223	0.025	3	<u>13</u>
	Sulfuric Acid	H ₂ SO ₄ • nH ₂ O(l)		See Note		<u>13</u>
		(28 wt. %)	275			
		(47-50 wt. %)	293			
		(55 wt. %)	223			
		(80-96 wt. %)	243			
	Aqueous Salt	(NH ₄) ₂ SO ₄ (aq) and NaCl(aq)	298	≤ 0.1		<u>14</u>
	Sodium Chloride	NaCl(s)	245-300	See Note		<u>15</u>
	Potassium Chloride	KCl(s)	295	See Note		<u>15</u>
H₂O + Surface → Products						
H ₂ O	Alumina	α -Al ₂ O ₃	295-300	$\gamma_0 < 0.2$		<u>16</u>
2NO₂ + H₂O(l) → HONO + HNO₃						
NO ₂	Liquid Water	H ₂ O(l)	270-295	$<1 \times 10^{-3}$	3	<u>17</u>
	Sulfuric Acid	H ₂ SO ₄ • nH ₂ O (40-98 wt. %)	250-325	5×10^{-7}		<u>18</u>
	Alumina	γ -Al ₂ O ₃ (s)	298	$\gamma_0 < 1 \times 10^{-7}$		<u>19</u>
		α -Al ₂ O ₃ (s)	298	$\gamma_0 < 5 \times 10^{-5}$		<u>19</u>
2NO₂ (N₂O₄) + MX → Products						
NO ₂ /N ₂ O ₄	Sodium Chloride	NaCl(s)	298	See Note		<u>20</u>
		NaCl(aq)	298	$<1 \times 10^{-4}$		<u>20</u>
	Sodium Bromide	NaBr(s)	298	See Note		<u>21</u>
	Sea Salt	See Note for O ₃ + Sea Salt	298	See Note		<u>22</u>
NO₃ + H₂O → HNO₃ + OH						
NO ₃	Water Ice	H ₂ O(s)	170-200	$<10^{-3}$		<u>23</u>
	Liquid Water	H ₂ O(l)	273	$\geq 2 \times 10^{-3}$		<u>24</u>
NO₃ + NaX → Products						
NO ₃	Sodium Chloride	NaCl(s)	293	$\gamma_0 < 6 \times 10^{-2}$		<u>25</u>
		NaCl(aq)	273-293	See Note		<u>25</u>
	Sodium Bromide	NaBr(s)	293	$\gamma_0 = 0.2 \pm 0.1$	2	<u>26</u>
		NaBr(aq)	273	See Note		<u>26</u>
	Sodium Iodide	NaI(aq)	273	See Note		<u>26</u>
N₂O₅ + H₂O → 2HNO₃						

Gaseous Species	Surface Type	Surface Composition	T(K)	γ	Uncertainty Factor	Notes
N ₂ O ₅	Water Ice	H ₂ O(s)	188–195	0.02	2	27
	Liquid Water/Solutions	H ₂ O(l)/(NH ₄) ₂ SO ₄ (aq)	260–295	See Note	See Note	28
	Nitric Acid Ice					
	Sulfuric Acid	HNO ₃ • 3H ₂ O(s)	200	4 × 10 ⁻⁴	3	29
	Sulfuric Acid Monohydrate	H ₂ SO ₄ • nH ₂ O(l)	195–300	See Note*	See Note	30
	Sulfuric Acid Tetrahydrate	H ₂ SO ₄ • H ₂ O(s)	200–300	See Note	3	31
	Ternary Acid	H ₂ SO ₄ • 4H ₂ O(s)	195–207	0.006	2	32
		H ₂ SO ₄ • nHNO ₃ • nH ₂ O(l)	195–218	See Note		30
N ₂ O ₅ + HCl → ClNO ₂ + HNO ₃						
N ₂ O ₅	Water Ice	H ₂ O(s) • HCl(s)	190–220	0.03	See Note	33
	Nitric Acid Ice	HNO ₃ • 3H ₂ O(s) • HCl(s)	200	0.003	2	34
	Sulfuric Acid Monohydrate	H ₂ SO ₄ • H ₂ O(s)	195	<1 × 10 ⁻⁴		35
N ₂ O ₅ + HBr → BrNO ₂ + HNO ₃						
N ₂ O ₅	Water Ice	H ₂ O	180–200	See Note		36
	Nitric Acid Ice	HNO ₃ • 3H ₂ O(s)	200	0.005	10	37
N ₂ O ₅ + MX → Products						
N ₂ O ₅	Sodium Chloride	NaCl(s)	295	γ_0 <5x10 ⁻³		38
		NaCl(aq)	262-291	γ_0 <0.05		38
	Potassium Bromide	KBr(s)	298	γ_0 <5x10 ⁻³		39
	Sodium Bromide	NaBr(aq)	270-277	γ_0 <0.05		39
	Sodium Iodide	NaI(aq)	262-278	γ_0 <0.05		39
	Sea Salt	See Note for O ₃ + Sea Salt	295	See Note		40
HONO + H ₂ O → Products						
HONO	Liquid Water	H ₂ O(l)	245-295	0.03	5	41
HONO + H ₂ SO ₄ → Products						
HONO	Sulfuric Acid	H ₂ SO ₄ • nH ₂ O(l)	180–200	See Note		42
HONO + HCl → ClNO + H ₂ O						
HONO	Water Ice	H ₂ O(s)	180–200	0.05	3	43
	Sulfuric Acid	H ₂ SO ₄ • nH ₂ O(l)		See Note	See Note	44
HONO + HBr → BrNO + H ₂ O						
HONO	Water Ice	H ₂ O(s)	180-200	See Note		45
HONO + NaCl → Products						
HONO	Sodium Chloride	NaCl(s)	~300	<1 × 10 ⁻⁴		46
HNO ₃ + NaX(s) → HX + NaNO ₃						
HNO ₃	Sodium Chloride	NaCl(s)	295–298	γ_0 = 2x10 ⁻³	2	47
		NaCl(aq)	298	γ_0 >0.2		47
	Sodium Bromide	NaBr(s)	298	γ_0 <3x10 ⁻²		48
	Potassium Bromide	KBr(s)	298	γ_0 <3x10 ⁻²		48
	Sea Salt	See Note for O ₃ + Sea Salt	298	γ_0 =0.5	3	49
HNO ₃ + Al ₂ O ₃ (s) → Products						
HNO ₃	Alumina	αAl ₂ O ₃	295-300	γ_0 <0.2		50
HO ₂ NO ₂ + HCl → Products						
HO ₂ NO ₂	Sulfuric Acid	H ₂ SO ₄ • nH ₂ O (50–75 wt.%)	200–225	<1 × 10 ⁻⁴		51
NH ₃ + H ₂ SO ₄ → NH ₄ HSO ₄						
NH ₃	Sulfuric Acid	H ₂ SO ₄ • nH ₂ O	260-300	See Note		52
		< 50 wt. %	260-300	1.0	1.2	
		50-70 wt. %	260-300			
H ₂ CO + Al ₂ O ₃ → Products						
H ₂ CO	Alumina	Al ₂ O ₃	290-300	γ_0 <2x10 ⁻⁵		53
CH ₃ OH + H ₂ SO ₄ and H ₂ SO ₄ + HNO ₃ → Products						54
CH ₃ OH	Sulfuric Acid	H ₂ SO ₄ • nH ₂ O	293	See Note		55
	Ternary Acid	H ₂ SO ₄ • mHNO ₃ • nH ₂ O	283-329	See Note		
CH ₃ OH + Al ₂ O ₃ → Products						

Gaseous Species	Surface Type	Surface Composition	T(K)	γ	Uncertainty Factor	Notes
CH ₃ OH	Alumina	Al ₂ O ₃	290-300	$\gamma_0 < 3 \times 10^{-4}$		53
CH ₃ CH ₂ OH + H ₂ SO ₄ • nH ₂ O → Products						
CH ₃ CH ₂ OH	Sulfuric Acid	H ₂ SO ₄ • nH ₂ O(l)	193-273	See Note		55
CH ₃ COOH + Al ₂ O ₃ → Products						
CH ₃ COOH	Alumina	Al ₂ O ₃	290-300	$\gamma_0 < 1 \times 10^{-2}$		53
CH ₃ CHO + H ₂ SO ₄ • nH ₂ O → Products						
CH ₃ CHO	Sulfuric Acid	H ₂ SO ₄ • nH ₂ O(l)	211-298	See Note		56
CH ₃ CHO + Al ₂ O ₃ → Products						
CH ₃ CHO	Alumina	Al ₂ O ₃	290-300	$\gamma_0 < 6 \times 10^{-5}$		53
CH ₃ CH ₂ CHO + Al ₂ O ₃ → Products						
CH ₃ CH ₂ CHO	Alumina	Al ₂ O ₃	290-300	$\gamma_0 < 9 \times 10^{-5}$		53
CH ₃ C(O)CH ₃ + H ₂ SO ₄ • nH ₂ O → Products						
CH ₃ C(O)CH ₃	Sulfuric Acid	H ₂ SO ₄ • nH ₂ O	198-298	See Note		57
CH ₃ C(O)CH ₃ + Al ₂ O ₃ → Products						
CH ₃ C(O)CH ₃	Alumina	Al ₂ O ₃	290-300	$\gamma_0 < 4 \times 10^{-5}$		53
CH ₃ C(O)O ₂ + H ₂ O → CH ₃ C(O)OH + HO ₂						
CH ₃ C(O)O ₂	Liquid Water Sulfuric Acid	H ₂ O(l)	225	4×10^{-3}	3	57
		H ₂ SO ₄ • nH ₂ O (84 wt.% H ₂ SO ₄)	246	3×10^{-3}	3	58
		(51 wt.% H ₂ SO ₄)	223	1×10^{-3}	3	
		(71 wt.% H ₂ SO ₄)	298	1×10^{-3}	3	
CH ₃ C(O)O ₂ NO ₂ + HCl, Cl, ClO, and OClO → Products						
CH ₃ C(O)O ₂ NO ₂	Sulfuric Acid	H ₂ SO ₄ • nH ₂ O (40–70 wt.%)	200–225	$< 1 \times 10^{-4}$		59
Cl + Surface → Products						
Cl	Sulfuric Acid	H ₂ SO ₄ • nH ₂ O(l)	221–296	2×10^{-4}	10	60
Cl ₂ + HBr → BrCl + HCl						
Cl ₂ /HBr	Water Ice	H ₂ O(s)	200	>0.2		61
Cl ₂ + MX → Products						
Cl ₂	Sodium Chloride	NaCl(s)	298	$\gamma_0 < 1 \times 10^{-3}$		62
	Sodium Bromide	NaBr(s)	298	0.02		63
				$\gamma_0 < 0.2$; See Note		
	Sodium Iodide	NaBr(aq)	263-293	$\gamma_0 < 0.3$		63
	Potassium Bromide	NaI(aq)	263-293	$\gamma_0 < 0.3$		63
		KBr(s)	298	0.02		64
	Sea Salt	See Note for O ₃ + Sea Salt	298	$< \gamma_0 < 0.2$; See Note		65
ClO + Surface → Products						
ClO	Water Ice	H ₂ O(s)	183-213K	$< 10^{-4}$		66
	Nitric Acid Ice	HNO ₃ • 3H ₂ O(s)	183	See Note		66
	Sulfuric Acid	H ₂ SO ₄ • nH ₂ O(l) (60 to 95 wt.% H ₂ SO ₄)	221–296	See Note		67
HCl + HNO ₃ → Products						
HCl + HNO ₃	Sulfuric Acid	H ₂ SO ₄ • mHNO ₃ • nH ₂ O(l)		See Note	See Note	68
HOCl + HCl → Cl ₂ + H ₂ O						
HOCl/HCl	Water Ice	H ₂ O(s) • HCl(s)	195–200	0.2	2	69
	Nitric Acid Ice	HNO ₃ • 3H ₂ O(s) • HCl(s)	195–200	0.1	2	69
	Sulfuric Acid	H ₂ SO ₄ • nH ₂ O(l)	198–209	See Note	See Note	70
HOCl + HBr → BrCl + H ₂ O						

Gaseous Species	Surface Type	Surface Composition	T(K)	γ	Uncertainty Factor	Notes
HOCl/HBr	Water Ice Sulfuric Acid	H ₂ O(s) H ₂ SO ₄ •nH ₂ O(l)	189–220 228	See Note See Note	See Note	<u>71</u> <u>72</u>
HOCl + NaBr and KBr → Products						
HOCl	Sodium Bromide Potassium Bromide	NaBr(aq) Ice KBr(s)	233 300	0.03 $\gamma_0 > 5 \times 10^{-3}$	3	<u>73</u> 73
ClNO + Surface → Products						
ClNO	Liquid Water Sodium Chloride	H ₂ O(l) NaCl(s)	270–295 298	$\geq 4 \times 10^{-3}$ * $< 1 \times 10^{-5}$		<u>74</u> <u>75</u>
ClNO ₂ + H ₂ O → Products HCl + HNO ₃						
ClNO ₂	Liquid Water	H ₂ O(l)	275–295	4×10^{-6}	2	<u>76</u>
ClNO ₂ + MX → Products						
ClNO ₂	Potassium Bromides Sodium Chloride Sodium Bromide Sodium Iodide	KBr(s) NaCl(aq) NaBr(aq) NaI(aq)	300 291 275–293 275–293	1×10^{-4} See Note See Note See Note	2	<u>77</u> <u>77</u> 77 77
ClONO ₂ + H ₂ O → HOCl + HNO ₃						
ClONO ₂	Water Ice Liquid Water Nitric Acid Ice Sulfuric Acid Sulfuric Acid Monohydrate Sulfuric Acid Tetrahydrate	H ₂ O(s) H ₂ O(l) HNO ₃ • 3H ₂ O(s) H ₂ SO ₄ • nH ₂ O(l) H ₂ SO ₄ • H ₂ O(s) H ₂ SO ₄ • 4H ₂ O(s)	180–200 270–290 200–202 200–265 195 196–206	0.3 2.5×10^{-2} 0.004 See Note* $< 1 \times 10^{-3}$ See Note	3 4 3 See Note	<u>78</u> <u>79</u> <u>80</u> <u>81</u> <u>82</u> <u>82</u>
ClONO ₂ + HCl → Cl ₂ + HNO ₃						
ClONO ₂ /HCl	Water Ice Nitric Acid Ice Sulfuric Acid Sulfuric Acid Monohydrate Sulfuric Acid Tetrahydrate Alumina	H ₂ O(s) HNO ₃ •3H ₂ O•HCl H ₂ SO ₄ •nH ₂ O(l)•HCl(l) H ₂ SO ₄ •H ₂ O(s) H ₂ SO ₄ • 4H ₂ O(s) Al ₂ O ₃	180–200 185–210 195–235 195 195–206 180–200	0.3 0.2 See Note $< 1 \times 10^{-4}$ See Note 0.3	2 2 See Note 3	<u>83</u> <u>84</u> <u>85</u> <u>86</u> 86 <u>87</u>
ClONO ₂ + MX → Products						
ClONO ₂	Sodium Chloride Potassium Bromide Sodium Bromide Sea Salt	NaCl(s) NaCl(aq) KBr(s) NaBr(aq) See Note for O ₃ + Sea Salt	295 272–280 298 272–280 298	0.005 $< \gamma_0 < 0.2$: See Note > 0.1 See Note > 0.1		<u>88</u> 88 <u>89</u> 89 <u>90</u>
ClONO ₂ + HBr → BrCl + HNO ₃						
ClONO ₂ /HBr	Water Ice Nitric Acid Ice	H ₂ O(s) • HBr(s) HNO ₃ •3H ₂ O(s)•HBr(s)	200 200	> 0.3 > 0.3		<u>91</u> 91
ClONO ₂ + HF → Products						
ClONO ₂ /HF	Water Ice Nitric Acid Ice	H ₂ O(s) • HF(s) H ₂ O(s)•HNO ₃ (s)•HF(s)	200 200	See Note See Note		<u>92</u> 92
CF ₃ Cl _y + Al ₂ O ₃ → Products						
CCl ₄	Alumina	Al ₂ O ₃ (s)	120–300	1×10^{-5}	10	<u>93</u>
CFCl ₃	Alumina	Al ₂ O ₃ (s)	120–300	1×10^{-5}	10	93
CF ₂ Cl ₂	Alumina	Al ₂ O ₃ (s)	120–300	1×10^{-5}	10	93
CF ₃ Cl	Alumina	Al ₂ O ₃ (s)	120–300	1×10^{-5}	10	93
BrCl + MX → Products						
BrCl	Sodium Chloride Potassium Bromide Sodium Iodide Alkali Bromides	NaCl(s) KBr(s) NaI(aq) MBr(aq) Ice	298 298 273–288 233	See Note See Note See Note 0.03		<u>94</u> 94 94 <u>94</u>
Br ₂ + MX → Products						
Br ₂	Sodium Chloride Potassium Bromide Sodium Iodide	NaCl(s) KBr(s) NaI(aq)	298 298 263–293	See Note See Note $\gamma_0 < 0.5$		<u>95</u> 95 95
2BrO → Br ₂ + O ₂						

Gaseous Species	Surface Type	Surface Composition	T(K)	γ	Uncertainty Factor	Notes
BrO	Water Ice Sulfuric Acid	H ₂ O(s)	213	$<1 \times 10^{-3}$	3	96
		H ₂ SO ₄ • nH ₂ O (60 wt.% H ₂ SO ₄)	213	7×10^{-4}	3	96
	Aqueous Sodium Chloride	(70 wt.% H ₂ SO ₄)	213	5×10^{-4}	3	96
		NaCl(aq) (23 wt.% NaCl)	253	$<10^{-3}$		96
HOBr + H ₂ SO ₄ • nH ₂ O → Products						
HOBr	Sulfuric Acid	H ₂ SO ₄ • nH ₂ O	201-270	See Note		97
HOBr + HCl → BrCl + H ₂ O						
HOBr/HCl	Water Ice	H ₂ O(s) • HCl(s)	180–228	0.3	3	98
	Sulfuric Acid	H ₂ SO ₄ • nH ₂ O (60–69 wt.% H ₂ SO ₄)	198–218	See Note		99
HOBr + HBr → Br ₂ + H ₂ O						
HOBr/HBr	Water Ice	H ₂ O(s) • HBr(s)	180-228	>0.1		100
	Sulfuric Acid	H ₂ SO ₄ • nH ₂ O	228	See Note		100
HOBr + MX → Products						
HOBr	Sodium Chloride	NaCl(s)	298	$\gamma_o < 10^{-2}$	1.5	101
	Alkali Bromides	NaCl(aq)	298	$\gamma_o > 0.2$		101
		NaCl → NaCl(aq) Ice	~238	See Note		102
		KBr(s)	298	$\gamma_o \leq 0.2$		102
		NaBr(s)	250	See Note		102
		NaBr(aq)	298	$\gamma_o = 0.6$		102
		NaBr → NaBr(aq) Ice	~233	See Note		102
BrNO ₂ + H ₂ O → Products						
BrNO ₂	Liquid Water	H ₂ O(l)	275-300	2×10^{-6}	2	103
BrNO ₂ + MX → Products						
BrNO ₂	Potassium Chloride	KCL(s)	298	See Note		104
	Sodium Chloride	NaCl(aq)	277-293	$\gamma_o > 10^{-6}$		104
	Potassium Bromide	KBr(s)	298	$\gamma_o > 0.1$		105
	Sodium Bromide	NaBr(aq)	277-293	See Note		105
	Sodium Iodide	NaI(aq)	262-278	See Note		105
BrONO ₂ + H ₂ O → HOBr + HNO ₃						
BrONO ₂	Water Ice	H ₂ O(s)	190–200	>0.2	4	106
	Liquid Water	H ₂ O(l)	270-280	3×10^{-2}		107
	Sulfuric Acid	H ₂ SO ₄ • nH ₂ O	210–300	See Note		108
BrONO ₂ + HCl → BrCl + HNO ₃						
BrONO ₂ /HCl	Water Ice	H ₂ O(s)	200	See Note	2	106
	Sulfuric Acid	H ₂ SO ₄ • nH ₂ O	229	0.9		108
BrONO ₂ + HBrI						
BrONO ₂ /HBr	Water Ice_	H ₂ O(s)	180-210	$\gamma_o > 0.1$		109
BrONO ₂ + MX → Products						
BrONO ₂	Sodium Chloride	NaCl(s)	298	$\gamma_o > 0.2$		110
	Potassium Bromide Sodium Bromide	NaCl(aq)	278-280	See Note		110
		KBr(s)	298	$\gamma_o > 0.2$		110
		NaBr(aq)	272-280	See Note		111
ICl + NaCl and NaBr → Products						
	Sodium Chloride	NaCl(aq)	274-298	See Note		112
	Sodium Bromide	NaBr(aq)	274-298	See Note		112
HOI + NaCl and NaBr → Products						
HOI	Sodium Chloride	NaCl(s)	243-298	>0.01		113
	Sodium Bromide	NaCl(aq)	274	$>2 \times 10^{-3}$		113
		NaBr(s)	243-298	>0.01		113
		NaBr(aq)	274	$>2 \times 10^{-3}$		113
CF ₂ Br ₂ + Al ₂ O ₃ → Products						
CF ₂ Br ₂	Alumina	Al ₂ O ₃	210, 315	2×10^{-5}	10	93

Gaseous Species	Surface Type	Surface Composition	T(K)	γ	Uncertainty Factor	Notes
CF ₃ OH + H ₂ O → Products						
CF ₃ OH	Water Ice Sulfuric Acid	H ₂ O(l)	274	>0.01		114
		H ₂ SO ₄ • nH ₂ O				
		(40 wt.% H ₂ SO ₄)	210–250	0.07	3	114
		(45 wt.% H ₂ SO ₄)	210–250	0.04	3	114
		(50 wt.% H ₂ SO ₄)	210–250	0.01	3	114
(50 wt.% H ₂ SO ₄)	210–250	0.001	3	114		
SO ₂ + O ₃ → Products						
SO ₂ /O ₃		Al ₂ O ₃	See Note	See Note		115
SO ₂ + H ₂ O(s) → Products						
SO ₂	Water Ice	HOOH/H ₂ O(s)	200–228	See Note		116
SO ₂ + H ₂ O ₂ , O ₃ , HONO, NO ₂ and HNO ₃ → Products						
SO ₂ /H ₂ O ₂ , etc.	Sulfuric Acid	H ₂ SO ₄ • nH ₂ O (20–60 wt.% H ₂ SO ₄)	293	See Note		117
SO ₂ + Al ₂ O ₃ → Products						
SO ₂	Alumina	Al ₂ O ₃	295–300	$\gamma_0 > 1 \times 10^{-4}$ (γ -alumina) $\gamma_0 > 5 \times 10^{-3}$ (γ -alumina)		118
SO ₂ + MX → Products						
SO ₂	Sodium Chloride Sea Salt	NaCl(s)	298	$\gamma_0 < 1 \times 10^{-4}$		119
		See Note for O ₃ + Sea Salt	298	$\gamma_0 < 0.1$		119
SO ₃ + H ₂ O → Products						
SO ₃	Sulfuric Acid	H ₂ SO ₄ • nH ₂ O (78–92 wt.% H ₂ SO ₄)	300	1.0	+0.0, –0.3	120
OCS + Al ₂ O ₃ → Products						
OCS	Alumina	Al ₂ O ₃	298	See Note		121

* γ is temperature dependent

5.14 Notes to Table 5-2

1. O_3 on $H_2O(s)$. Ozone loss on pure ice is highly inefficient, with uptake coefficients in the range of 10^{-8} to 10^{-9} for partial pressures between 2×10^{-8} and 10^{-6} atm at 223 and 258 K, as measured in an ice-coated column. The uptake coefficients are dependent on the ozone partial pressure, increasing at low partial pressures Langenberg et al. [355]. [Back to Table](#)
2. $O_3 + Al_2O_3(s)$. Very low ozone decomposition efficiencies for reaction on coarse (3 μm dia.) and fine (0.1 μm dia., partially hydroxylated) γ -alumina and coarse (3 μm dia.) α -alumina were measured in flowing and static systems by Hanning-Lee et al. [231] at temperatures ranging between 212 and 473 K. Based on measured BET surface areas, γ_s ranged from 2×10^{-11} to 4×10^{-10} over the 212 to 298 K temperature range. γ_s for γ -alumina at lower temperatures exceeded those for α -alumina. Results are roughly consistent with earlier, unpublished flow tube data from L. F. Keyser and from fluidized bed reactor studies of Alebić-Juretić et al. [22]. Note that γ_s based on geometric surface particle surface areas would be significantly (10^4 – 10^7) larger. Additional fluidized bed reactor studies by Alebić-Juretić et al. [23] demonstrated that room temperature uptake are initially first order in O_3 , but change to a slower second order reaction at longer exposure times. Klimovskii et al. [342] reported an initial uptake coefficient (γ_o) of 1×10^{-4} on a γ -alumina surface at 293K assuming a geometric surface area, BET surface correction presumably would have yielded a lower value. Michel et al. [401, 402] reported Knudsen cell uptake studies at 296K on α -alumina particles that yielded γ_o values of $(8 \pm 5) \times 10^{-5}$ and $(1.4 \pm 0.3) \times 10^{-4}$ after BET surface area corrections. Sullivan et al. [540] used a coated wall flow reactor to obtain 298K γ_o values of 7×10^{-6} to 1.6×10^{-5} for α -alumina powder films exposed to no more than $[O_3]$ of 10^{13} cm^{-3} after BET surface area correction. Higher $[O_3]$ yielded lower apparent γ_o s. Usher et al. [574] demonstrated the pretreatment of α -alumina with HNO_3 vapor reduced O_3 Knudsen cell γ_o values by $\sim 70\%$. Mogili et al. [413] measured O_3 uptake on α -alumina particles in a room temperature environmental chamber obtaining an uptake coefficient of $(3.5 \pm 0.9) \times 10^{-8}$ for dry ($RH \leq 1\%$) particles that fell to $(4.5 \pm 1.1) \times 10^{-9}$ for measurements at 19% RH. Roscoe and Abbatt [479] demonstrated spectroscopically that there is a competition for surface sites when gas phase ozone and water vapor are exposed to the alumina surface. [Back to Table](#)
3. $O_3 + NaCl$. The reaction of O_3 with NaCl is slow. Il'in et al. [287] measured the loss of O_3 in a coated reactor over the temperature range 223 - 305 K, and found the same uptake coefficients, $\gamma \sim 10^{-6}$, independent of temperature, for NaCl and NH_4NO_3 and $(NH_4)_2SO_4$, suggesting that even the small uptake is not due to reaction with the chloride. Alebić-Juretić [22] did not observe any uptake on NaCl powders using a fluidized bed reactor but did not report an upper limit to the uptake coefficient. Akimoto and coworkers [411, 492], reported an upper limit of $\gamma_o < 1 \times 10^{-5}$ on NaCl. When the NaCl was mixed with 0.5 - 1% w:w $FeCl_3$, γ_o increased to 3×10^{-2} and production of gaseous Cl_2 was observed with yields from 25 - 50% of the ozone taken up. With 0.1 % $FeCl_3$, no production of Cl_2 was observed but the initial uptake coefficient was still 3×10^{-2} . These experiments were carried out with a Knudsen cell using multiple salt layers and the measured initial uptake coefficients were converted to the reported values using the pore diffusion model of Keyser et al. [333, 334].

Abbatt and Waschewsky [11] followed O_3 in a flow tube containing deliquesced 1 - 5 μm NaCl particles (75% RH); no significant loss was observed on unbuffered particles or particles buffered at pH of 7.2. An upper limit of $\gamma_o < 1 \times 10^{-4}$ was derived from these measurements. [Back to Table](#)
4. $O_3 + NaBr$ and KBr . Mochida et al. [411] did not observe any uptake of O_3 on NaBr or KBr powders, from which they derived an upper limit of $\gamma < 1 \times 10^{-5}$. Hirokawa et al. [264] reported production of gas phase Br_2 from the reaction of O_3 with NaBr only when water vapor was added so that the salt was near deliquescence.

Uptake of O_3 and production of gas phase Br_2 has been observed for deliquesced NaBr salt on a glass surface [31]. Production of Br_2 has also been measured by Hunt et al. [279] in the reaction of O_3 with deliquesced NaBr particles in the dark in an aerosol chamber; the production of Br_2 exceeded that from known aqueous phase chemistry by about an order of magnitude, suggesting that a surface reaction of O_3 with bromide at the air-solution interface was occurring with a reaction probability of $\gamma_o = (1.9 \pm 0.8) \times 10^{-6}$ (2 σ). [Back to Table](#)

5. $O_3 + KI$. Brown et al. ([86]; [87]) report that KIO_3 forms on single crystal, water-free KI surfaces with a reaction probability of 1.4×10^{-4} . On room temperature KI solutions, Sakamoto et al. [490] report that ozone exposure yields gas-phase I_2 and small amounts of IO (ratio of I_2 to IO >100). The reaction kinetics are indicative of a Langmuir-Hinshelwood mechanism, exhibiting saturation in the gas-phase yields as both ozone and iodide concentrations are increased. The reaction forming I_2 proceeds more rapidly with increasing acidity for $pH < 4$, but there is a pH-independent pathway operative to pH 11. [Back to Table](#)

6. $O_3 + \text{sea salt}$. Akimoto and coworkers [411, 492], reported uptake coefficients for O_3 on synthetic and natural sea salt powders of $\sim 1 \times 10^{-3}$ using a Knudsen cell with multiple salt layers. Similar uptake coefficients were reported for the hydrates of $MgBr_2$ and $CaBr_2$. These are the initial uptake coefficients after correction for the available surface area using the pore diffusion model of Keyser et al. [333, 334]. The measured values before this correction was applied were about a factor of 20 larger. Given the uncertainty associated with these corrections, the final values derived have a large uncertainty associated with them as well. When $FeCl_3$ was added to synthetic sea salt (Fe/Na weight ratio of 1%), the uptake coefficient increased by an order of magnitude to $(3.2 \pm 1.1) \times 10^{-2}$. Br_2 was the gas phase product, with variable yields up to 100% of the O_3 lost. The enhanced reactivity of sea salt compared to NaCl and NaBr is due to the significant amounts of surface-adsorbed water (SAW) present on sea salt; the component of sea salt present in the second highest concentration is magnesium chloride which forms a stable hydrate and is quite hygroscopic. Reactions with powders of $MgCl_2 \cdot 6H_2O$ and sea salt are often observed to be similar to reaction with aqueous salt solutions (see note on SO_2 uptake). The formation of Br_2 is favored over Cl_2 by a number of factors: (1) surface segregation of bromide ions [211, 212, 620] in mixed solid crystals of NaCl and NaBr; (2) higher solubility of NaBr which increases its concentration in the surface layer as a mixture of NaCl and NaBr crystallizes; (3) faster oxidation of Br^- compared to Cl^- ; [180, 224, 225, 480], (4) solution phase chemistry of chloride and bromide ion mixtures that favors the production of gas phase bromine compounds; [180, 480], (5) enhanced interfacial bromide ion concentrations compared to chloride ions at the air-water interface of aqueous solutions of mixed salts [311, 312]. On frozen sea-salt solutions, gas phase Br_2 was formed by exposure of O_3 (44 ppbv to 2.9 ppmv) to frozen sea salt solutions, at temperatures below 272 K [436]. No other products were reported and the production of Br_2 scaled with increasing O_3 . [Back to Table](#)

7. $OH + H_2O(s)$. Cooper and Abbatt [132] measured initial irreversible OH uptake coefficients of ~ 0.1 for water ice between 205–230 K; these decayed to $\gamma = 0.03 \pm 0.02$ after repeated exposure to OH. Self-reaction to form H_2O or H_2O_2 was indicated by the lack of observable gas phase products despite observation of first-order OH loss. It can not be ruled out that contamination of the ice surface drove the initial reactivity. [Back to Table](#)

8. $OH + HCl \cdot nH_2O(l)$. Cooper and Abbatt [132] demonstrated significant enhancement of OH uptake (to $\gamma > 0.2$) after HCl doping of 220 K ice surfaces sufficient to melt the surface layer. It is unclear whether OH is lost to self-reaction or reaction with hydrated Cl^- ions. [Back to Table](#)

9. $OH + HNO_3 \cdot 3H_2O$. Cooper and Abbatt [132] measured $\gamma > 0.2$ for nitric acid-doped ice surfaces under conditions suitable for NAT formation at 200 and 228 K. Increase over pure ice uptake rates is probably due to $HNO_3 + OH \rightarrow H_2O + NO_3$ reaction. [Back to Table](#)

10. $OH + H_2SO_4 \cdot nH_2O$. Lower limits of 0.2 for uptake coefficients on 45–65 wt.% H_2SO_4 between 220 and 230 K and for 96 wt.% H_2SO_4 at 230 and 298 K by Cooper and Abbatt [132] are consistent with a lower limit of 0.07 on 28 wt.% H_2SO_4 at 275 K in similar experiments by Hanson et al. [238] and a probable surface saturated value of $(4.9 \pm 0.5) \times 10^{-4}$ from Knudsen cell measurements by Baldwin and Golden [38] and an estimate of $\gamma = 1$ on ~96 wt.% H_2SO_4 at 298 K by Gerhenzon et al. [207] using a coated insert flow tube technique. Uptake is probably reactive with $OH + HSO_4^- \rightarrow H_2O + SO_4^-$ the hypothesized process. [Back to Table](#)

11. $OH + NaCl$. Ivanov et al. [296] measured the uptake of OH on solid NaCl and on NH_4NO_3 over the temperature range from 245 - 340 K using a fast flow discharge reactor with a coated rod along the axis and EPR detection of OH. The initial values of the uptake coefficient approached 10^{-2} . The OH was generated from the reaction of H atoms with excess NO_2 ; it is not clear whether NO_2 might have also reacted with the salt surface. Given that the uptake coefficients were similar for NaCl and NH_4NO_3 , the uptake likely does not reflect oxidation of the chloride. The pseudo-steady state value, γ_{ss} , was measured to be 4×10^{-3} at 298 K and the temperature dependence was described by $\gamma_{ss} = (1.2 \pm 0.7) \times 10^{-5} \exp[(1750 \pm 200)/T]$. This value is quite close to later measurements by Park et al. [437] who see little dependence of the uptake

coefficient on relative humidity, up to 38% at room temperature. Product studies have been performed by Sjostedt and Abbatt [524] who have exposed desiccated NaCl salts to gas-phase OH in a coated-wall flow tube at 298 and 253 K. Gas-phase Br₂ is formed with a yield of 0.6, relative to the loss of OH. The source of the Br₂ is the trace Br⁻ impurity in commercial, high purity NaCl_(s). BrCl was formed at a considerably smaller yield, 0.008. Humidification of the salt surface led to more sustained production but somewhat smaller yields.

Aerosol chamber studies by Finlayson-Pitts and coworkers showed that there was no Cl₂ production from NaCl particles when OH was generated by reaction of O(¹D) from photolysis of O₃ at relative humidities below the deliquescence point of NaCl; above the deliquescence point, however, a rapid reaction of OH with Cl⁻ at the interface to generate gas phase Cl₂ is observed [343, 435]. Because the mechanism is uncertain, and clearly must involve multiple steps, a unique value of the reaction probability for this interface reaction could not be obtained. At 269 K Frinak and Abbatt [195] have exposed acidic solutions containing molar levels of NaCl to gas-phase OH. The gas-phase product observed is Br₂, unless considerable OH exposure has reduced Br⁻ levels in the solution, in which case the product is Cl₂. The source of the Br₂ is the trace Br⁻ impurity in commercial, high purity NaCl_(s). At neutral pH, the products were below detection limit. Shaka et al. [517] and Laskin et al. [357] have both exposed chloride solutions to gas-phase OH, observing changes in solution alkalinity and chloride concentrations, respectively. This is another indication that chloride ions in solution are readily heterogeneously oxidized by OH. Laskin et al. report an uptake coefficient of ≥ 0.1 at room temperature. However, the OH concentrations were not measured which may lead to uncertainty in this value. [Back to Table](#)

12. OH + Al₂O₃(s). Measured value is from flow tube experiment with native oxide on aluminum as the active surface. An uptake coefficient of 0.04 ± 0.02 independent of temperature over the range of 253–348 K was recommended by (Gershenson et al. based on three measured values ranging unsystematically from 0.02 to 0.06 at 253, 298 and 348 K [207]). [Back to Table](#)
13. HO₂ + H₂O(s) and H₂SO₄ • nH₂O(l). Uptake of HO₂ on ice and super-cooled 55 wt.% sulfuric acid at 223 K has been demonstrated to be limited by HO₂ surface saturation by Cooper and Abbatt [132]. They argue that self-reaction, presumably $2\text{HO}_2 \rightarrow \text{H}_2\text{O}_2 + \text{O}_2$ is controlling measured uptake coefficients of 0.025 ± 0.005 for ice and 0.055 ± 0.020 for 55 wt.% H₂SO₄. Thornton and Abbatt [555] report room temperature aerosol flow reactor submicron droplet measurements on 47–50 wt% H₂SO₄, without HO₂ scavenger species, yielding $\gamma < 0.01$. Gershenson et al. [206] measured $\gamma > 0.2$ for 80 and 96 wt.% H₂SO₄ at 243 K and Hanson et al. [238] measured a lower limit for 28 wt.% H₂SO₄ at 275 K of 0.07. However, large gas phase diffusion corrections mean these values are consistent with $\gamma = 1$. Thornton et al. [558] have used available experimental data to develop a parameterized HO₂ self-reaction uptake model valid for pH < 6 aqueous droplets and gas phase HO₂ generation rates exceeding $1 \times 10^5 \text{ cm}^{-3} \text{ s}^{-1}$. They also assess the relative role of Cu⁺⁺ catalyzed oxidation of HO₂ in aqueous aerosols. [Back to Table](#)
14. HO₂ + (NH₄)₂SO₄(aq) and NaCl(aq). HO₂ uptake on aerosol particles has been studied in aerosol flow tubes. At high HO₂ concentrations detected by CIMS, Thornton and Abbatt [555] observed loss of HO₂ on aqueous ammonium sulphate particles, buffered to pH 5.1 at RH 42% and room temperature. An uptake coefficient of 0.1 could describe the kinetics, but the HO₂ decays were best fit by second-order kinetics consistent with a bulk-phase reaction between dissolved HO₂ species, when using literature HO₂ solubility and bulk liquid-phase rate constants. Because of the second-order kinetics, it was inferred that the uptake coefficient would be substantially smaller at lower (atmospheric) HO₂ gas-phase concentrations [558]. More recent studies using LIF by Taketani et al. ([549]; [550]) observed similar loss kinetics on aqueous particles of ammonium sulphate (0.11 to 0.19, 45 to 75% RH), sodium chloride (0.1, 50 to 75% RH) and sea salt (0.1, 35 to 75% RH) at atmospheric HO₂ concentrations about two orders of magnitude lower ($< 10^8 \text{ molecules/cm}^3$) than those of Thornton and Abbatt. Thus, the observed kinetics between the two research groups are very similar to each other but the interpretation of the results is not, if bulk phase kinetics between dissolved HO₂ species indeed drive the reactivity. In the absence of transition metal impurities such as iron or copper ions, there is no known reactive chemistry that will deplete HO₂ as rapidly as observed in the Taketani et al. experiments; it is possible that an unidentified surface process is prevalent. [Back to Table](#)
15. HO₂ + NaCl(s) and KCl(s). Gershenson and coworkers [206, 460] used a combination of matrix isolation EPR and gas phase EPR with a fast flow tube to measure the uptake of HO₂ on NaCl from 245 - 335 K. Early studies by Gershenson et al. [206] measured values of $\gamma = 1.8 \times 10^{-2}$ for KCl and 1.6×10^{-2} for NaCl, both at 295 K, supplementing an even earlier value of $\gamma \sim 8 \times 10^{-3}$ measured by Gershenson and Purmal

[208]. In later studies on NaCl [460] the uptake was reported to remain constant for at least 30 min, so this is likely to be a steady-state value, $\gamma_{ss} = 1.2 \times 10^{-2}$ at 295 K. The temperature dependence is given by $\gamma_{ss} = (5.7 \pm 3.6) \times 10^{-5} \exp[(1560 \pm 140)/T]$. Above 330 K, the uptake coefficient was significantly smaller than expected from this temperature dependence. The data are indistinguishable, within experimental error, from the uptake of HO₂ on NH₄NO₃, suggesting that the uptake of HO₂ likely involves recombination on the surface rather than oxidation of the chloride. The surface recombination was interpreted in terms of a combined Eley-Rideal and Langmuir-Hinshelwood mechanism. The addition of small amounts of water vapor decreased the uptake coefficient for HO₂; the authors attributed this to water adsorption on the active sites. Another possibility is formation of HO₂-H₂O complexes whose uptake and recombination on the surface is not as fast as for uncomplexed HO₂. A recent study by Loukhovitskaya et al. (2009) using a coated-wall flow tube finds temperature dependent uptake coefficients on salt surfaces, reporting uptake coefficient between 10^{-3} and 10^{-2} at room temperature. They report that gas-phase H₂O₂ was observed as a product, indicative of self-reaction. [Back to Table](#)

16. H₂O (g) + Al₂O₃ (s). Isotopic thermal programmed desorption studies at 300K by Elam et al. [164] show that H₂O dissociatively absorbs on α -alumina surfaces and that initial uptake coefficient (γ_0) is ~0.1. Pre-hydroxylation or long term exposure to water vapor decreases the H₂O uptake coefficient nearly exponentially. Al-Abadleh et al. [20] used FTIR techniques to study water vapor uptake at 296K on α -alumina crystal 0001 surfaces as a function of relative humidity (RH). Below 10% RH uptake is dissociative, but molecular absorption dominates uptake between 10 and 70% RH. FTIR spectra of water absorbed on both α -alumina and γ -alumina powder surfaces are similar to those on 0001 crystal surfaces. Goodman et al. [214] used FTIR to show that α -alumina surfaces saturated with HNO₃ vapor has the same water absorption isotherm as untreated samples at 296 K. [Back to Table](#)
17. NO₂ + H₂O(l). Value for γ of $(6.3 \pm 0.7) \times 10^{-4}$ at 273 K (Tang and Lee, [551]) was achieved by chemical consumption of NO₂ by SO₃²⁻; their stopped-flow measurement was probably still affected by surface saturation, leading to the measurement of a lower limit. Ponche et al. [448] measured an uptake coefficient of $(1.5 \pm 0.6) \times 10^{-3}$ at 298 K, which was also probably subject to saturation limitations. Mertes and Wahner [400] used a liquid jet technique to measure a lower limit of $\gamma \geq 2 \times 10^{-4}$ at 278 K, and they observed partial conversion of the absorbed NO₂ to HONO. Msibi et al. [423] used a cylindrical/annular flow reactor to derive $\gamma = (8.7 \pm 0.6) \times 10^{-5}$ on pH = 7 deionized water surfaces and $(4.2 \pm 0.9) \times 10^{-4}$ on pH = 9.3 wet ascorbate surfaces; it seems likely that these results are also subject to surface saturation given the gas/surface interaction times involved in the experiment. Harrison and Collins [256] performed aerosol flow reactor experiments on deliquescent sodium chloride and ammonium sulfate droplets at 279 K obtaining reactive uptake coefficients in the range of $(2.8-10) \times 10^{-4}$, probably with some surface saturation constraints. Cheung et al. [105] used a droplet train flow reactor to show that the reactive uptake coefficient for NO₂ at number densities between 10^{13} and 10^{16} on pure water at 273 K is $<5 \times 10^{-4}$, contradicting many of the earlier experiments. Cheung et al. also used a bubble train reactor to demonstrate that the reactive uptake of NO₂ is second order, so that experimental uptake coefficients will be dependent on gas phase NO₂ concentrations. Data are consistent with a reactive uptake coefficient of $<1 \times 10^{-3}$ for 270–295 K and a liquid-phase second-order hydrolysis of NO₂ to HONO and HNO₃ which depends on temperature and pH. However, the interplay between accommodation, possible surface reaction, and bulk reaction may be complex. [Back to Table](#)
18. NO₂ + H₂SO₄ • nH₂O. Kleffman et al. [341] performed bubble tube reactor uptake measurements for 0–98 wt.% acid at 298 K and for 44.6 and 56.1 wt.% from 250–325 K. At 298 K, measured uptake coefficients varied between 6 and 3×10^{-7} with a minimum near 70 wt.%. Most measurements at 44.6 and 56.1 wt.% overlapped within their error limits and showed little temperature dependence although there is evidence that uptake increases at the lowest temperatures. The data can all be captured with a recommended value of 5×10^{-7} with an uncertainty factor of three.

This recommendation is consistent with earlier upper limits of 1×10^{-6} by Baldwin and Golden [37] for 96 wt.% at 295 K and 5×10^{-6} for 70 wt.% between 193 and 243 K by Saastad et al. [488]. Kleffman et al. [341] conclude that their uptake measurements are mass accommodation limited; however, it is not clear that their values are not influenced by bulk or surface reaction of two NO₂ with H₂O to form HONO and HNO₃ at lower acid wt.% values and the formation of nitrosyl sulfuric acid at higher acid concentrations. Kleffman et al. [341] did perform separate static wetted wall reactor studies showing the formation of gas phase HONO at acid concentrations below 60 wt.%. It is more likely that reactive uptake is a controlling

factor and the measured uptakes are solubility and/or reaction rate limited. Thus, the mass accommodation coefficient may be much larger than the recommended uptake values. [Back to Table](#)

19. $\text{NO}_2 + \text{Al}_2\text{O}_3$. Miller and Grassian [409] observed NO_2 absorbed reactively on γ -alumina using FTIR and UV spectroscopy to observe surface nitrite and nitrate. Szanyi et al [543] used FTIR and thermal programmed desorption/mass spectrometry to determine products formed on γ -alumina surfaces at 300K, observing nitrites and nitrates (at higher NO_2 only nitrate). Exposure to water vapor converted most bridging nitrates to bidentate and monodentate nitrates. Baltrusaitis et al. [40] also used FTIR to observe monodentate, bidentate and bridging nitrates products on both α -alumina and γ -alumina particles at 296K. They also observed that co-absorbed water solvates surface nitrates. Underwood et al. [570-572] report Knudsen cell studies measuring γ_0 values on γ -alumina particles of 2×10^{-8} , 2.0×10^{-8} , and 2.2×10^{-8} at 298K based on BET surface area corrections and either KML [332] or linear mass dependent (LMD) corrections for porosity, with the KML and LMD corrections leading to very similar values [570]. They also report larger γ_0 values for α -alumina of 9.3×10^{-6} and 9.1×10^{-6} [570, 572]. Underwood et al. [572] also suggest a final “multiple collision” that would raise the γ_0 values for γ -alumina by factor of 1,1 and α -alumina by 9.4. This proposed correction is not included in the recommended upper limits. Börensén et al. [79] report diffuse reflectance FTIR measurements of uptake on γ -alumina showing that the reaction order is 1.86 ± 0.1 in NO_2 . They report BET corrected γ_0 values varying linearly from 7.3×10^{-10} to 1.3×10^{-8} as $[\text{NO}_2]$ was increased from 2.5×10^{13} to 8.5×10^{14} . Rubasinghege and Grassian [483] irradiated nitrate absorbed on γ -alumina particles with broad band light ($>300\text{nm}$) as a function of RH (at ~1, 20, 45 and 80% and with and without gas phase O_2) observing photolytic production of gas phase NO (primary product), NO_2 and N_2O . [Back to Table](#)
20. $\text{NO}_2/\text{N}_2\text{O}_4 + \text{NaCl}$. Schroeder and Urone reported that NO_2 at Torr concentrations reacted with NaCl to form ClNO [496]. Subsequently, Finlayson-Pitts [179] showed that the reaction continued at ppm concentrations of NO_2 and estimated a lower limit to the uptake coefficient for NO_2 of 5×10^{-8} , assuming the reaction was first order in NO_2 . Winkler et al. [606] used XPS to follow the increase in nitrate during the reaction of NO_2 with NaCl and reported that the rate was proportional to the square of the NaCl surface sites and the square root of NO_2 . Vogt and Finlayson-Pitts [583-585] used diffuse reflectance Fourier transform infrared spectrometry (DRIFTS) to follow the formation of nitrate and showed that the reaction was second order in NO_2 ; assuming that N_2O_4 was the reactant, the uptake coefficient was measured to be $(1.3 \pm 0.6) \times 10^{-4}$ (1 σ). Peters and Ewing [443] followed the formation of nitrate on single crystal NaCl(100) and also found the reaction was second order in NO_2 . Assuming that N_2O_4 is the reactant, the uptake coefficient was $(1.3 \pm 0.3) \times 10^{-6}$, two orders of magnitude less than reported by Vogt and Finlayson-Pitts. However, in the presence of 9.5 mbar water vapor, the uptake coefficient increased by a factor of about 100. It is likely that the difference is that their single crystals did not hold significant amounts of surface adsorbed water, whereas the powders used by Vogt and Finlayson-Pitts are known to hold significant amounts of SAW [64] which enhances the reactivity through mobilization of the nitrate ions and exposure of fresh NaCl during the reaction. Caloz et al. [93] measured using a Knudsen cell an upper limit of $<10^{-7}$ for uptake of NO_2 on NaCl and $<2 \times 10^{-7}$ for uptake on KBr, with the reaction being first order in NO_2 . Yoshitake [615] also used DRIFTS to study this reaction and reported that for “dry” NaCl, the reaction was second order in NO_2 with an uptake coefficient assuming the reactant is N_2O_4 of $(4 \pm 2) \times 10^{-5}$. However, if the NaCl had been pretreated with water vapor, the uptake was first order in NO_2 with $\gamma = (1.5 \pm 0.2) \times 10^{-8}$. Karlsson and Ljungström [324] generated NaCl particles and measured the loss of chloride and formation of nitrate using ion chromatography on particles collected on filters; they obtained a lower limit for the reaction probability of 3×10^{-4} . Surprisingly, the conversion of NO_2 to nitrate decreased as the relative humidity increased from 9 to 79%. These reactions are sufficiently slow that they are unlikely to be important in the atmosphere.

Abbatt and Waschewsky [11] measured the loss of NO_2 in a flow tube containing deliquesced 1 - 5 μm NaCl particles (75% RH); no significant loss was observed on unbuffered particles or particles buffered at pH of 7.2 or having pH of 0.3 using HCl. An upper limit of $\gamma_0 < 1 \times 10^{-4}$ for the uptake of NO_2 was derived from these measurements. Yabushita et al. [613] have recently shown using ESI-MS that uptake of NO_2 to aqueous droplets, yielding the nitrate anion, is facilitated by the presence of halide anions, perhaps through the formation of a complex with NO_2 on the surface. [Back to Table](#)

21. $\text{NO}_2 + \text{NaBr(s)}$. Vogt et al. [582] used diffuse reflectance infrared spectroscopy to study $\text{NO}_2 + \text{NaBr(s)}$ at 298 K. The reaction was determined to be approximately second order in NO_2 . Assuming that adsorbed N_2O_4 is the reactant leads to $\gamma = 2 (+4, -1.3) \times 10^{-4}$. [Back to Table](#)
22. $\text{NO}_2/\text{N}_2\text{O}_4 + \text{sea salt}$. Sverdrup and Kuhlman [541] measured the uptake of NO_2 on artificial sea salt using the NO_2 loss measured in a flow tube lined with the salt. The uptake coefficient was reported to increase from 10^{-7} to 10^{-6} as the relative humidity increased from 44% to 88%. Langer et al. [356] used diffuse reflectance Fourier transform infrared spectrometry to follow nitrate formation on synthetic sea salt and found the reaction was approximately second order (1.8 ± 0.2) in NO_2 in He carrier gas but approximately first order (1.2 ± 0.2) in NO_2 in air. Assuming that N_2O_4 was the reactant in He, $\gamma_{\text{ss}} = 1 \times 10^{-4}$, and assuming NO_2 is the reactant in air, $\gamma_{\text{ss}} = 1 \times 10^{-8}$. These reactions are sufficiently slow that they are unlikely to be important in the atmosphere. [Back to Table](#)
23. $\text{NO}_3 + \text{H}_2\text{O(s)}$. Fenter and Rossi [174] measured an upper limit for γ of 10^{-3} over the range from 170 to 200 K. [Back to Table](#)
24. $\text{NO}_3 + \text{H}_2\text{O(l)}$. Rudich et al. [485, 486] used wetted-wall flow tube techniques to measure uptake coefficients for NO_3 on pure water and aqueous NaCl, NaBr, NaI, and NaNO_2 solutions. These studies were extended to other aqueous solutions by Imamura et al. [289]. Uptake on pure water was consistent with reaction of NO_3 to produce HNO_3 and OH. Uptake coefficients with solutions containing I^- , Cl^- , Br^- , NO_2^- and other anions were larger and scaled with anion concentration, indicating electron transfer reactions to produce NO_3^- . Reactions with these anions and/or adsorbed organic contaminants may well dominate the reactive uptake of NO_3 by real atmospheric aqueous surfaces. The γ of $(2.0 \pm 1.0) \times 10^{-4}$ at 273 K determined for pure water by Rudich et al. is significantly lower than the lower limit of 2.5×10^{-3} from Thomas and co-workers as quoted by Mihelcic et al. [408] and further discussed in Thomas et al. [554], who also dispute that reactive uptake coefficient on pure water reported by Rudich et al. is due to nitric acid production. A detailed analysis of uptake coefficients for KI aqueous solutions by Rudich et al. [485] indicated that the NO_3 mass accommodation coefficient is >0.04 [485], but this result may be biased due to reactive uptake by interfacial I $^-$. Single droplet uptake results on Alizarin Red S dye and NaCl solutions at 293 K by Schütze and Herrman [501] suggest a value an order of magnitude smaller (see Table 5.1). [Back to Table](#)
25. $\text{NO}_3 + \text{NaCl}$. Also see note for $\text{NO}_3 + \text{H}_2\text{O(l)}$. Recommended value for the initial uptake coefficient on solid NaCl is based on work of Seisel et al. [511, 512] Gershenzon and coworkers [205] and Gratpanche and Sawerysyn [219]. Seisel et al. [511, 512] used a Knudsen cell with mass spectrometric and laser-induced fluorescence detection of the NO_3 . Salt powders from 60 - 630 μm in size were used, as well as spray-deposited samples; no dependence on the sample mass for powders or between powders and the spray-deposited samples was observed so no corrections for diffusion into underlying layers were applied. They obtained values for γ_0 of $(4.9 \pm 3) \times 10^{-2}$ and $(4.6 \pm 4) \times 10^{-2}$ (1 σ), respectively. Gershenzon and coworkers used flow reactors with ESR and MS detection and measured the loss of NO_3 on an axially located rod coated with salt; they interpret their results, and the associated value of γ_0 derived from their data based on a multi-step mechanism involving adsorption and then reaction of NO_3 on the salt. The value for γ_0 is sensitive to several unknown parameters in the model, and they give a range from $(0.2 - 3.9) \times 10^{-2}$. Gratpanche and Sawerysyn [219] used a flow tube coated with NaCl and ESR detection of NO_3 , and reported a value of $(1.7 \pm 1.2) \times 10^{-2}$ (1 σ); on very dry NaCl, no uptake was observed, again indicating the importance of small amounts of water for the reaction. Gershenzon et al. [205] reported that the uptake coefficient decreased by about a factor of 20 over about half an hour, suggesting that the steady state value of γ_{ss} is approximately 1.5×10^{-3} . Zelenov et al. reported that the uptake coefficient for NO_3 on NaCl (and NaBr; see next note) [621, 622] could be fit by a time-dependent term and a time-independent term: $\gamma(t) = \gamma_0 \exp(-t/\tau) + \gamma_{\text{ss}}$. They observed that γ_{ss} depends on the type of salt, as well as the NO_3 and water concentrations, while γ_0 depended only on the type of salt and NO_3 concentration. They concluded that the products are chemisorbed Cl atoms. No temperature dependence has been observed over the temperature range 258 - 301 K by Gratpanche and Sawerysyn, [219] consistent with only an $\sim 10\%$ change in the uptake coefficient from 293 to 373 K observed by Gershenzon et al. [205].

The uptake of NO_3 on aqueous solutions of NaCl has been measured at 273 K by Rudich et al. [486] and at 293 K by Thomas et al. [554]. NO_3 reacts in solutions with the halide ions. The measured uptake coefficients varied from $(0.8 - 6) \times 10^{-3}$ for solutions of activity ranging from 0.008 to 0.45 at 273 K [486] and was reported to be $> 2 \times 10^{-3}$ on 0.1 M NaCl at 293 K [554]. [Back to Table](#)

26. $\text{NO}_3 + \text{NaBr}$ and NaI . Also see notes for $\text{NO}_3 + \text{NaCl}$ and $\text{NO}_3 + \text{H}_2\text{O(l)}$. Recommended value of γ_0 for the reaction with solid NaBr is based on reported values of 0.16 ± 0.08 , [511] 0.20 ± 0.10 , [512] a range of 0.1 to 0.3 [205] and 0.11 ± 0.06 [219] (all errors cited are 1 σ). Gershenzon et al. [205] observed a decrease of about a factor of two with time, suggesting that $\gamma_{ss} \sim 0.05$. Gratpanche and Sawerysyn [219] found a slight negative temperature dependence, $\gamma_0 = (1.6^{+1.8}_{-0.9} \times 10^{-3}) \exp[(1210 \pm 200)/T]$ over the range from 243 - 293 K. Gershenzon et al. [205] also reported a small (30%) decrease in γ_0 from 293 to 373 K. Zelenov et al. [621, 622] reported that the uptake coefficient for NO_3 on NaBr (and NaCl ; see preceding note) could be fit by a time-dependent term and a time-independent term: $\gamma(t) = \gamma_0 \exp(-t/\tau) + \gamma_{ss}$. They observed that γ_{ss} depends on the type of salt, as well as the NO_3 and water concentrations, while γ_0 depended only on the type of salt and NO_3 concentration. They concluded that the products are bromine atoms in agreement with the observations of the branching ratio as well as the mass balance by Seisel et al. [511, 512].

Rudich et al. [485] measured the uptake of NO_3 on aqueous KI solutions; NO_3 is taken up and reacts with I^- in solution. Uptake coefficients increased with the concentration of I^- ranging from $\gamma = 0.9 \times 10^{-3}$ at $5 \times 10^{-6} \text{ M KI}$ to 3.2×10^{-3} at a concentration of $8 \times 10^{-5} \text{ M}$. [Back to Table](#)

27. $\text{N}_2\text{O}_5 + \text{H}_2\text{O(s)}$. Leu [359] and Hanson and Ravishankara [242] measured nearly identical values of 0.028 (± 0.011) and 0.024 ($\pm 30\%$) in the 195–202 K range on relatively thick ice films in coated wall flow tubes. Quinlan et al. [457] measured a maximum value for γ on ice surfaces at 188 K of 0.03 in a Knudsen cell reactor. The average of these three studies is 0.027 with a standard deviation of 0.003. Hanson and Ravishankara [245, 248] presented new and re-analyzed data as a function of ice thickness, with a value of ~ 0.008 for the thinnest ice sample, rising to 0.024 for the thickest. From these data there would appear to be no strong dependence on temperature, at least over the 188–195 K range. It is unclear whether the measured dependence on ice film thickness is due to added porosity surface area in the thicker films or decreased ice film integrity in thinner films. The error estimate in the table is driven by the possible systematic error due to unresolved film thickness effects rather than the small statistical error among the “thick film” values from the three groups.

Zondlo et al. [640] report the formation of a supercooled $\text{H}_2\text{O}/\text{HNO}_3$ liquid layer at 185 K as a reaction product, forming NAT or NAD only after decreasing the relative humidity below the ice frost point. This effect is similar to that resulting from the interaction of gaseous HNO_3 or ClONO_2 with the ice surface. These authors measured $\gamma = (7 \pm 3) \times 10^{-4}$ at 185 K for the reaction of N_2O_5 with this supercooled liquid layer. [Back to Table](#)

28. $\text{N}_2\text{O}_5 + \text{H}_2\text{O(l)}$. This reaction has now been studied widely on both pure water and on aqueous surfaces. The kinetics of the reaction are dependent on a number of conditions, as described below.

On pure water, Van Doren et al. [577] measured γ s of 0.057 ± 0.003 at 271 K and 0.036 ± 0.004 at 282 K using a droplet train uptake technique, indicating that the reaction has a negative temperature dependence. George et al. [201] also used a droplet train technique to measure γ s of $(3.0 \pm 0.2) \times 10^{-2}$ (262 K), $(2.9 \pm 1.2) \times 10^{-2}$ (267 K), $(2.0 \pm 0.2) \times 10^{-2}$ (273 K), $(1.6 \pm 0.8) \times 10^{-2}$ (276 K), and $(1.3 \pm 0.8) \times 10^{-2}$ (277 K) on pure water, while Schweitzer et al. [507] used the same approach for pure water and salt solutions between 262 and 278 K, obtaining similar results. Msibi et al. [422] measured a smaller γ of 2.5×10^{-3} for water adsorbed on a denuder flow tube well under 66–96% relative humidity conditions at room temperature, making the nature of the surface unclear. After correction for gas-phase diffusion effects, Schütze and Herrmann [499] measured a γ of 1.1×10^{-2} at 293 K using a single suspended droplet flow reactor method that was probably constrained by nitrate build-up in the droplet's surface layer.

A number of other groups have measured the uptake coefficients of N_2O_5 on aqueous solutions, where the reactivity of the N_2O_5 is with the water solvent molecules. These studies include: Mozurkewich and Calvert [420] on $\text{NH}_3/\text{H}_2\text{SO}_4/\text{H}_2\text{O}$ aerosols in an aerosol flow tube, Hu and Abbatt [271] on $(\text{NH}_4)_2\text{SO}_4$ aerosols at 297 K in an aerosol flow tube, Mentel and co-workers [591] and [399] on sodium sulfate and sodium nitrate particles in a large aerosol chamber, Thornton et al. [557] measured uptake on malonic acid aerosols in an aerosol flow tube, Hallquist et al. [228] studied ammonium sulfate and sodium nitrate particles, and Griffiths et al. [220] measured uptake on a variety of soluble organic acids with and without ammonium sulfate present. Note that the studies conducted with sodium chloride or sea salt as the solute are listed in the $\text{N}_2\text{O}_5 + \text{NaCl}$ note below.

Overall, the γ values measured at high relative humidity by Van Doren et al., Mozurkewich and Calvert, Hu and Abbatt, Thornton et al., Hallquist et al., and Griffiths et al., and those from experiments with NaCl at high relative humidity (Benke et al. [58] and Thornton and Abbatt [556]) are quite consistent when temperature and RH effects are factored in, yielding uptake coefficients in the 0.02 to 0.04 range at room temperature. The lower values from the Louis Pasteur (George et al.; Schweitzer et al.) and Birmingham (Msibi et al.) groups appear to have much less pronounced temperature dependence and are inconsistent with the other measurements. The same function used to fit the N_2O_5 uptake on sulfuric acid as a function of temperature and concentration, discussed below, has been extended to the Van Doren et al. and Hu and Abbatt data for pure water and very high RH aerosols. See note on $\text{N}_2\text{O}_5 + \text{H}_2\text{SO}_4 \cdot n\text{H}_2\text{O(l)}$ for the functional fit and its error discussion.

However, other factors that affect the uptake coefficient include: 1. At low relative humidities, the γ values are reduced from the values close to water saturation, with the uptake coefficient scaling linearly with the water content of the aerosol below a specific relative humidity (roughly 50% RH). This is indicative of a competition for water of a reactive intermediate formed via N_2O_5 initial uptake (see in particular Thornton et al. [557], Thornton and Abbatt [556], Hallquist et al. [228], Griffiths et al. [220]). 2. At high aerosol nitrate concentrations the kinetics are slower, falling below 0.001 in some cases, indicative that a reactive intermediate along the reaction pathway is less stable under such conditions (see Mentel and co-workers [591] and [399]; and Hallquist et al. [228]). Note that high nitrate levels may develop in laboratory experiments where high N_2O_5 concentrations are used, potentially biasing the uptake coefficients to lower values than are atmospherically significant. This may be manifest as an uptake coefficient that is dependent on the concentration of N_2O_5 used [557]. 3. By varying particle diameters, the reacto-diffusive length has been measured to be 48 nm at 50% RH on malonic acid aqueous particles, indicating that this process is not fully occurring at the surface of the particle and that there might be a particle-size dependence to the uptake coefficient [557]. 4. The uptake coefficients can be substantially suppressed when large organic molecules, such as those formed by the reaction of ozone with alpha-pinene or those present in humic-like materials are present in/on aqueous inorganic aerosol ([188]; [33]). The uptake coefficients in these systems can be substantially below 0.01, with only a few weight percent of organic present. Also, monolayers of surfactant organics on aqueous particles can have the same effect (Thornton and Abbatt [556]; McNeill et al. [397]). In studies of ambient particles, where decays of N_2O_5 were directly measured, it has been observed that the uptake coefficients are smallest (< 0.005) when the organic content of the particles is high [71]. Uptake coefficients of 0.03 were measured, but only on some occasions and when the sulphate/organic content of the particles was highest. 5. Finally, as observed with pure water by Van Doren et al. [577], there is a negative temperature dependence to the uptake coefficient over the small temperature range that has been studied ([228]; [220]). For example, the most recent measurements by Griffiths et al. [221] show the uptake coefficient changing from 0.035 to 0.005 from 263 to 303 K at 50% RH.

A new parameterization of laboratory kinetics that takes into account the water, nitrate, dissolved organic, and chloride concentrations has been published by Bertram and Thornton, [70]. [Back to Table](#)

29. $\text{N}_2\text{O}_5 + \text{HNO}_3 \cdot 3\text{H}_2\text{O(s)}$. Hanson and Ravishankara [243] have measured $\gamma = 0.0006 (\pm 30\%)$ near 200 K. They re-analyzed their results and give additional data as a function of ice thickness (Hanson and Ravishankara [245]; [248]), deriving a value of 3×10^{-4} for the thinnest NAT covered ice layer, with values up to three times higher for thicker NAT-covered ice layers. As in the case of uptake on water ice this may be due to increased surface area from porosity in the thicker films, or less integrity in the thinner films. The uncertainty listed in the Table is driven by this observed effect. All of the Hanson et al. data are in poor agreement with the $\gamma = 0.015 \pm 0.006$ reported by Quinlan et al. [457] from their Knudsen cell measurements; this measurement may have been biased by formation of a super-cooled aqueous nitric acid surface and is judged to be unreliable. It is possible that the uptake coefficients will be affected by whether the NAT surfaces are water-rich or poor. [Back to Table](#)
30. $\text{N}_2\text{O}_5 + \text{H}_2\text{SO}_4 \cdot n\text{H}_2\text{O(l)}$. This reaction has been intensively studied between 195 and 296 K for a wide range of H_2SO_4 wt.% values using four complementary experimental techniques. Data are available from aerosol flow tube studies (Fried et al. [194], Hanson and Lovejoy [239], Hu and Abbatt [271], and Hallquist et al. [227]), coated wall flow tube studies (Hanson and Ravishankara [243], Zhang et al. [628]), a stirred Knudsen cell (Manion et al. [388]) and droplet train studies (Van Doren et al. [577], Robinson et al. [471]). All studies have yielded γ s between ~ 0.05 and 0.20 with modest dependence on surface H_2SO_4 wt.% and temperature. The Knudsen cell studies, aerosol flow tube studies at higher N_2O_5 exposure and the ternary $\text{H}_2\text{SO}_4/\text{HNO}_3/\text{H}_2\text{O}$ studies of Zhang et al. [628] all illustrate that significant levels of HNO_3 in

the H₂SO₄/H₂O solutions will reduce γ measurably; this fact explains some of the scatter in aerosol flow tube studies and the surface saturation evident in the Knudsen cell studies. The “nitrate effect” reduction of γ was also studied in extensive aerosol chamber studies at 193.6 K by Wagner et al. [590]. The effect of 5.0×10^{-7} Torr HNO₃ on γ as a function of temperature at two water vapor concentrations are plotted in Zhang et al. [628]; the decrease in γ is greatest at low temperatures, approaching a factor of 2–5 between 200 and 195 K.

Experimental data on sulfuric acid surfaces between 40 and 80 wt.% sulfuric acid deemed to be free of saturation effects, plus the pure water uptake data of Van Doren et al. [577] and high relative humidity ammonium sulfate aerosol uptake data of Hu and Abbatt [271] were all fit to a polynomial expression to yield a single model describing γ for N₂O₅ uptake valid between 0 and 80 wt.% H₂SO₄ and 180 to 300 K (Robinson et al. [471]). The form of this function is: $\gamma_0 = \exp(k_0 + k_1/T + k_2/T^2)$, where T is the temperature in K. The parameters k_0 , k_1 , and k_2 obtained from the best-fit are:

$$k_0 = -25.5265 - 0.133188\text{wt} + 0.00930846\text{wt}^2 - 9.0194 \times 10^{-5}\text{wt}^3$$

$$k_1 = 9283.76 + 115.345\text{wt} - 5.19258\text{wt}^2 + 0.0483464\text{wt}^3$$

$$k_2 = -851801 - 22191.2\text{wt} + 766.916\text{wt}^2 - 6.85427\text{wt}^3$$

where wt is the weight percentage of H₂SO₄.

The overall error of applying the uptake function provided here consists of two components. One is the standard deviation of the model-calculated value with respect to measured data, σ_m , which is given by

$$\sigma_m = \sqrt{\frac{\sum_{i=1}^N \left(1 - \frac{\gamma_i}{\gamma_{\text{model}}}\right)^2}{N-1}}.$$

The other is the standard deviation of relative experimental measurement error from the mean, σ_d , which is given by

$$\sigma_d = \sqrt{\frac{\sum_{i=1}^N \left(\frac{\Delta\gamma_i}{\gamma_i}\right)^2}{N(N-1)}}.$$

The overall error is

$$\sigma = \sqrt{\sigma_m^2 + \sigma_d^2}.$$

(These formulations are also applied below in the error estimation for the ClONO₂ + H₂O and HCl, BrONO₂ + H₂O, and HOCl + HCl reaction system. For N₂O₅, the error is estimated to be 15% (one sigma), with $\sigma_m=14.7\%$ and $\sigma_d=2.9\%$).

Liquid trough flow reactor studies on 60-80 wt.% H₂SO₄ at 273-280 K by Bertram and co-workers demonstrated that adsorbed single and dual component coatings of organics like 1-hexadecanal, 1-octadecanal and stearic acid could reduce γ by well over a factor of 10, while coatings of phytanic acid had little effect. Even 0.75 monolayer coatings of 1-octadecanal reduced γ by a factor of 10 ([344]; [134]; [133]). Park et al. [438] impinged a molecular beam of N₂O₅ on 72 wt% H₂SO₄ at 216K, observing that sub-monolayer coverage of 1-butanol and 1-hexanol reduced bare acid reactive uptake coefficients from ~ 0.15 to ~ 0.10 and 0.06, respectively. [Back to Table](#)

31. N₂O₅ + H₂SO₄ • H₂O(s). Zhang et al. [629] used coated flow tube techniques to measure the uptake of N₂O₅ on solid sulfuric acid monohydrate over a temperature range of 200 to 225 K. The measurement values of γ were significantly higher at 200 K ($\gamma \sim 1 \times 10^{-3}$) than at 225 K ($\gamma \sim 10^{-4}$) and were well fit by $\log \gamma = [4.78 - 0.0386T(K)]$. Acid-rich H₂SO₄ • H₂O surfaces had a lower γ than water rich surfaces ($\log \gamma =$

[$0.162 - 0.789 \times \log p_{\text{H}_2\text{O}}$] where $p_{\text{H}_2\text{O}}$ is their experimental water vapor partial pressure in Torr). [Back to Table](#)

32. $\text{N}_2\text{O}_5 + \text{H}_2\text{SO}_4 \cdot 4\text{H}_2\text{O}(\text{s})$. Hanson and Ravishankara [249] studied N_2O_5 uptake by frozen 57.5 and 60 wt.% H_2SO_4 as a function of temperature and relative humidity. The 57.5 wt.% surface was not sensitive to relative humidity and was slightly more reactive ($\gamma = 0.008$ vs 0.005) at 205 K than at 195 K. Reaction probabilities on the 60 wt.% surface dropped off with temperature and relative humidity. [Back to Table](#)
33. $\text{N}_2\text{O}_5 + \text{HCl}$ on $\text{H}_2\text{O}(\text{s})$. Leu [360] measured $\gamma = 0.028 \pm 0.011$ at 195 K, while Tolbert et al. [562] measured a lower limit of 1×10^{-3} at 185 K. Seisel et al. [513] measured $\gamma \sim 0.03$ at 200 K using a Knudsen flow reactor with a range of HCl flows. The uptake coefficient at low HCl flows is only slightly enhanced compared to the uptake on a pure ice surface. ClNO_2 was observed as the product in these studies. These experiments were done at high HCl levels probably leading to a liquid water/acid surface solution (Abbatt et al. [7]). Indeed, Hanson and Ravishankara [243] point out that a pure ice surface is readily converted to one with a thin NAT coating even with low N_2O_5 partial pressures, making this reaction difficult to study on pure ice surfaces. [Back to Table](#)
34. $\text{N}_2\text{O}_5 + \text{HCl}$ on $\text{HNO}_3 \cdot 3\text{H}_2\text{O}(\text{s})$. Hanson and Ravishankara [243] measured $\gamma = 0.0032 (\pm 30\%)$ near 200 K. [Back to Table](#)
35. $\text{N}_2\text{O}_5 + \text{HCl}$ on $\text{H}_2\text{SO}_4 \cdot \text{H}_2\text{O}(\text{s})$. Zhang et al. [629] saw no increase in N_2O_5 uptake on sulfuric acid monohydrate at 195 K upon exposure to HCl, setting $\gamma < 10^{-4}$. [Back to Table](#)
36. $\text{N}_2\text{O}_5 + \text{HBr}$ on $\text{H}_2\text{O}(\text{s})$. Seisel et al. [513] report γ values ranging from $\sim 3 \times 10^{-3}$ to 0.1, depending on the HBr concentrations employed; the measurements were conducted at 180 and 200 K. These authors report Br_2 and HONO in 80% yield as products with respect to N_2O_5 taken up, generated presumably by the secondary reaction of the primary product BrNO_2 with HBr. [Back to Table](#)
37. $\text{N}_2\text{O}_5 + \text{HBr}$ on $\text{HNO}_3 \cdot 3\text{H}_2\text{O}(\text{s})$. This reaction, yielding $\gamma \sim 0.005$, was investigated on NAT surfaces near 200 K by Hanson and Ravishankara [246]. Under some conditions a much higher reaction coefficient of ~ 0.04 was observed. [Back to Table](#)
38. $\text{N}_2\text{O}_5 + \text{NaCl}$. This reaction has been studied on both solid NaCl and on aqueous solutions. The uptake of N_2O_5 on solid NaCl has been studied using Knudsen cells [172, 266], flow reactors [363, 376], annular reactors [422] and diffusion tubes [346]. The reaction has two possible channels if there is water available on the surface: $\text{N}_2\text{O}_5 + \text{NaCl} \rightarrow \text{ClNO}_2 + \text{NaNO}_3$ (1) and $\text{N}_2\text{O}_5 + \text{H}_2\text{O}/\text{NaCl} \rightarrow 2 \text{HNO}_3$ (2). The presence of the two channels is supported by measured yields of ClNO_2 (relative to N_2O_5 lost) that vary from 60 - 100% [172, 266, 346, 376] and by the observation of gaseous HCl as a reaction product [266]. Because hydrolysis on the surface occurs in addition to the reaction with Cl^- , the net uptake coefficient for N_2O_5 is particularly sensitive to the presence of surface-adsorbed water (SAW), with higher values for powders where there are more steps and edges that hold SAW. For example, Leu et al. [363] measured an upper limit of $\gamma < 1.0 \times 10^{-4}$ for salt powders that had been heated overnight in a vacuum, but $\sim 4.5 \times 10^{-4}$ for samples that were only pumped on for about an hour. Fenter et al. [172] reported a preferred value for the uptake coefficient of $(5 \pm 2) \times 10^{-4}$; however, the measured values varied from 2×10^{-3} for monodisperse powders (after correction for pore diffusion by factors of ~ 5 to 30) to $< 1.0 \times 10^{-4}$ for a polished window face. Hoffman et al. [266] report a steady state value of $\gamma_{\text{ss}} = 3 \times 10^{-3}$ based on Knudsen cell studies of powders using less than a layer of salt where corrections to the available surface area due to diffusion into the salt are not necessary; the branching ratio for reaction (1) was measured to be 0.73 ± 0.28 (2σ).

The uptake of N_2O_5 on NaCl solutions or aqueous particles has been measured by a number of techniques ([58]; [59]; [199] [423, 539, 556] [624]). Overall, the reported values of γ for relative humidities between 45 and 100% are between 1.5×10^{-2} to 5.0×10^{-2} and temperatures between 263 K and room temperature. Zetzsch and coworkers ([58]; [59]) used an aerosol chamber to measure the uptake of N_2O_5 on deliquesced NaCl particles from 71 - 94% RH, and obtained a value of $\gamma = 3.2 \times 10^{-2}$. Behnke et al. [58] measured ClNO_2 in a yield of $66 \pm 7\%$ from aerosol particle experiments. In a wetted wall flow tube, the yield was observed to increase to 100% at concentrations of NaCl of 1 M and above. Thornton and Abbatt [556] report a yield of at least 50% ClNO_2 at 50% RH, using an aerosol flow tube technique. It is proposed by both groups that a mechanism involving a competition between the reaction of NO_2^+ (or H_2ONO_2^+) with water to form HNO_3 or with Cl^- to form ClNO_2 determines the product yield. George et al. [199] used a

droplet train and measured the formation of NO_3^- in the droplets; the value of γ decreased from 0.039 ± 0.013 at 263 K to 0.014 ± 0.008 at 278 K. Stewart et al. [539] measured the uptake of N_2O_5 on NaCl particles in a flow tube; after correction for diffusion/particle size effects, an uptake coefficient of 3×10^{-2} was derived at relative humidities 30% and above. Schweitzer et al. [507] used a droplet train apparatus to measure the uptake of N_2O_5 on water and on solutions of NaCl, NaBr and NaI with concentrations ranging from 0.1 to 1 M over a temperature range from 262 to 278 K. Within experimental error, all of the uptake coefficients were the same, with an average value of $\gamma = 0.018 \pm 0.003$. For 1 M NaCl, the ClNO_2 yield was 100%.

Note that the uptake kinetics can be suppressed by the presence of an organic monolayer on the aqueous particles ([556] ; [397]). Also, the product yield can change to Cl_2 , when the acidity of the surface is taken below 2 and for chloride concentrations as low as 0.05 M (Roberts et al., [467]). [Back to Table](#)

39. $\text{N}_2\text{O}_5 + \text{KBr}, \text{NaBr}, \text{NaI}$. Fenter et al. [172] and Koch et al. [346] measured the uptake coefficient for N_2O_5 on KBr at ambient temperature using a Knudsen cell and molecular diffusion tube respectively. The Knudsen cell experiments gave a value of $(4 \pm 2) \times 10^{-3}$ after correction (by factors of 6-16) for pore diffusion, and the molecular diffusion tube a value of $(2.5 \pm 1) \times 10^{-3}$. In the Knudsen cell studies, the uptake coefficient was larger for powders and a depolished window face (both 4×10^{-3}) than for a polished window face ($< 1 \times 10^{-4}$), similar to the observations for the NaCl reaction ($\text{N}_2\text{O}_5 + \text{NaCl}$); this again suggests the importance of surface-adsorbed water and possibly surface defects created by roughening (which, however, also hold water) for the reaction. The initial product of the reaction is BrNO_2 , identified by Finlayson-Pitts et al. [182] by FTIR but this can react further with the salt to generate Br_2 , the product observed by Fenter et al. [172].

Schweitzer et al. [507] used a droplet train apparatus to measure the uptake of N_2O_5 on water and on solutions of NaBr and NaI, as well as NaCl, with concentrations ranging from 0.1 to 1 M over a temperature range from 262 to 278 K. Within experimental error, all of the uptake coefficients were the same, with an average value of $\gamma = 0.018 \pm 0.003$. For the NaBr reaction, the gas phase products were BrNO_2 , Br_2 and HONO . For the NaI reaction, the only gas phase product observed was I_2 . [Back to Table](#)

40. $\text{N}_2\text{O}_5 + \text{sea salt}$. The uptake of N_2O_5 on solid synthetic sea salt was measured to be $\gamma = (3.4 \pm 0.8) \times 10^{-2}$ (2σ) by Hoffman et al. [266]. This will be an upper limit as 1-2 layers of salt were used and no correction was made for diffusion into the bottom layer. However, it is clear that the reaction is at least an order of magnitude faster than that for NaCl; the yield of ClNO_2 is 100%.

Stewart and Cox [539] measured the uptake of N_2O_5 on submicron synthetic sea salt aerosols in a flow tube; after correction for diffusion/particle size effects, a value of $\gamma = 2.5 \times 10^{-2}$ was derived, independent of relative humidity above 30%. Similar results are reported for the same substrate by Thornton and Abbatt [556], with the uptake coefficient changing from 0.02 to 0.03 from 43 to 70% RH. For partially crystallized artificial sea salt, the uptake coefficient was 0.005 at 30% RH. [Back to Table](#)

41. $\text{HONO} + \text{H}_2\text{O(l)}$. Bongartz et al. [76] present uptake measurements by two independent techniques, the liquid jet technique of Schurath and co-workers and the droplet train/flow tube technique of Mirabel and co-workers (Ponche et al. [448]). With a surface temperature of ~ 245 K the droplet train techniques yielded $0.045 < \gamma < 0.09$, while the liquid jet operating with a surface temperature of 297 K obtained $0.03 < \gamma < 0.15$. Mertes and Wahner [400] used a liquid jet technique to measure $4 \times 10^{-3} < \gamma < 4 \times 10^{-2}$ at 278 K. Harrison and Collins [256] performed aerosol flow reactor experiments on deliquescent sodium chloride and ammonium sulfate droplets at 279 K obtaining reactive uptake coefficients of 0.0028 ± 0.0015 and 0.0028 ± 0.0006 , for 85% relative humidity conditions, respectively; these measurements are probably subject to significant surface saturation. Since HONO uptake by liquid water probably involves hydrolysis, an increase in Henry's law solubility with decreasing temperature may be offset by a decreasing hydrolysis rate constant, leaving the uptake coefficient's temperature trend uncertain. Measured uptake coefficients will not correspond to the mass accommodation coefficient. [Back to Table](#)
42. $\text{HONO} + \text{H}_2\text{SO}_4 \cdot n\text{H}_2\text{O(l)}$. Zhang et al. [631] measured uptake coefficients for HONO on sulfuric acid that increased from $(1.6 \pm 0.1) \times 10^{-2}$ for 65.3 wt.% H_2SO_4 (214 K) to $(9.1 \pm 1.6) \times 10^{-2}$ for 73 wt.% H_2SO_4 (226 K). Fenter and Rossi [173] measured uptake coefficients rising from 1.8×10^{-4} for 55 wt.% H_2SO_4 (220 K) to 3.1×10^{-1} for 95 wt.% H_2SO_4 (220 K and 273 K). Baker et al. [35] measured much smaller uptake coefficients for 60 wt.% at 298 K. In general, the values measured by Zhang et al. [631] are a factor of 2 to 5 higher than those of Fenter et al. [173] for comparable acid concentrations. Since the reaction

probably depends on both temperature and acid concentration and since the data scatter is high in both experiments, further independent data will be required to define γ as a function of acid concentration and temperature. These data are generally consistent with the effective Henry' law constant measurements of Becker et al. [57] who illustrate that HONO solubility decreases exponentially with H₂SO₄ concentration until ~53 wt.%, at which point reaction to form nitrosyl sulfuric acid increases H* dramatically as H₂SO₄ concentration increases. Baker et al. [35] invoke surface decomposition of HONO to explain their room temperature data, since they separately determine that the bulk second-order disproportionation rate for HONO is too slow to account for even their small uptake coefficients. It is possible that surface formation of nitrosyl sulfuric acid and not HONO disproportionation is responsible for much of their measured uptake. The Zhang et al. [631] and Fenter and Rossi [173] data have been combined and fit with a four-term polynomial as a function of acid wt.% (these data did not show an obvious temperature dependence):

$$\ln \gamma = a + b \text{ wt} + c \text{ wt}^2 + d \text{ wt}^3$$

where wt is the H₂SO₄ wt.%, and

$$a = -155.7 \pm 29.7$$

$$b = 5.663 \pm 1.232$$

$$c = -0.07061 \pm 0.01679$$

$$d = 0.000297 \pm 0.000076$$

This parameterization should be used only within the 55–95-wt.-%-H₂SO₄ range and the 214-to-273-K temperature range. [Back to Table](#)

43. HONO + HCl + H₂O(s). Knudsen cell uptake studies for HONO/HCl co-deposited on ice (180–200 K) and for HONO on 0.1 to 10 M HCl frozen solutions (~190 K) by Fenter and Rossi [173] showed HONO uptake coefficients in the 0.02 to 0.12 range as long as surface HCl concentrations significantly exceed HONO concentrations. ClNO was evolved quantitatively with HONO consumption. In a coated wall flow tube Diao and Chu [152] observed orders of magnitude lower uptake coefficients, even though low partial pressures of HONO were used. Some of the HCl partial pressures will have been large enough to melt the ice surface (Abbatt et al. [7]). [Back to Table](#)
44. HONO + HCl on H₂SO₄ • nH₂O(l). Fenter and Rossi [173] saw no reaction for acid wt.% > 65. They measured $\gamma = 2.0 \pm 0.7 \times 10^{-3}$ for 60 wt.% acid saturated with HONO at 230 K. Zhang et al. [631] also measured the uptake of HCl after exposure to HONO, they observed HCl uptake with γ s between 0.01–0.02 over an acid wt.% range of 60.8–71.3 (T = 207.9–222.6 K). The reaction was also studied by Longfellow et al. [377] using both HCl doped and HONO doped sulfuric acid aerosols. Their uptake measurements confirmed reaction at higher acid wt.%, but by using lower HONO partial pressures they measured smaller γ s. The reverse reaction, ClNO hydrolysis, was also studied in a wetted wall flow reactor and in the aerosol flow reactor by Longfellow et al. [377] and in a Knudsen cell reactor by Fenter and Rossi [173]. Data show clear evidence of both surface and bulk kinetics for the forward reaction. Longfellow et al. [377] report k^{II} values for the bulk reaction (in units of $10^4 \text{ M}^{-1} \text{ s}^{-1}$) for 50 wt.%: 81 at 250 K and 15 at 205 K; for 60 wt.%: 9.4 at 250 K, 6.9 at 230 K and 5.0 at 219 K; for 67 wt.%: 3.9 at 250 K; and for 70 wt.%: 5.8 at 269 K and 0.35 at 215 K. The reaction is clearly complex and will require a comprehensive model of both the surface and bulk processes to arrive at an appropriate parameterization for γ . [Back to Table](#)
45. HONO + HBr + H₂O(s). HONO reacts with HBr on ice films (Seisel and Rossi [515]; Diao and Chu [152]), but note that the HBr partial pressures used are generally higher than those prevalent in the atmosphere and so melting of the ice film may have occurred in these experiments. Diao and Chu observe BrNO as a product in a coated-wall flow tube. [Back to Table](#)
46. HONO + NaCl(s). Diffuse reflectance experiments by Vogt and Finlayson-Pitt [584] on room temperature NaCl(s) and Knudsen cell uptake experiments by Fenter and Rossi on room temperature NaCl(s) and frozen 0.1 M NaCl aqueous solutions, all failed to show HONO uptake [173]. The latter results yield $\gamma < 1 \times 10^{-4}$. HONO + NaCl. Junkermann and Ibusuki [313] reported that HONO reacts with NaCl to form nitrite on the surface. However, subsequent studies [584] showed that the infrared bands assigned to NO₂⁻ were due to nitrate, likely from the reaction of gas phase NO₂ and perhaps HNO₃ present in the HONO. There is no evidence at the present time for a reaction between HONO and NaCl. [Back to Table](#)

47. $\text{HNO}_3 + \text{NaCl(s)}$ and NaCl(aq) . Recommendation is based on an average of the values of Hoffman et al. [267], Ghosal and Hemminger [210], the data of Davies and Cox [144] as revised by Ghosal and Hemminger [210] using their model for surface reactivation, and the single crystal data of Leu et al. [363]. Hoffman et al. [267] used less than a single layer of particles so that diffusion into the underlying layers is not a factor to obtain an initial value of $\gamma_0 = (2.3 \pm 1.9) \times 10^{-3}$ (2σ). This is consistent within the combined experimental errors with a value of $(1.3 \pm 0.6) \times 10^{-3}$ determined from the formation of nitrate on the surface of single crystal (100) NaCl by Ghosal and Hemminger [210], and with a value of 1.1×10^{-3} from application of the Ghosal and Hemminger model to the Davis and Cox data [144]. Ghosal and Hemminger suggest that the value could be as high as 5×10^{-3} for NaCl powders that have more steps and edges that hold SAW [211]. At longer reaction times, the steady-state value [267] is a factor of two smaller, $\gamma = 1 \times 10^{-3}$. The reaction is hypothesized to occur both on dry terraces, which saturate rapidly, and on steps and edges that hold surface-adsorbed water. The water acts to recrystallize the product NaNO_3 so that the surface does not passivate during the reaction at atmospherically relevant HNO_3 pressures. This model, developed and modified by several research groups [64, 144, 210, 267] brings together most of the seemingly disparate measurements of the reaction probability made using a variety of techniques including flow tubes [144], Knudsen cells [64, 171, 172, 267], and XPS studies of nitrate formation on single crystals [210, 211, 584]. The only gas phase product observed is HCl, with a yield that is within experimental error of 100%. The higher value of $(1.3 \pm 0.4) \times 10^{-2}$ of Leu et al. [363] was obtained by correcting even larger measured values using a pore diffusion model [333, 334]; the corrections were typically in the range of a factor of 4-6. On single crystal NaCl where such corrections were not necessary, Leu et al. [363] measured a value of $(2.4 \pm 0.6) \times 10^{-3}$. A value of $(4 \pm 1) \times 10^{-2}$ was measured using a molecular diffusion tube technique by Koch et al. [346]. The corrected value of $(8.7 \pm 1.4) \times 10^{-5}$ reported by Zangmeister and Pemberton [618, 619] using Raman spectroscopy to follow the nitrate formed on the surface is lower than the other values likely because a much higher HNO_3 concentration was used ($\sim 10^{18} \text{ cm}^{-3}$), which would lead to a larger coverage of the surface by the recrystallized NaNO_3 product and passivation of much of the NaCl surface.

Abbatt and Waschewsky [11] measured the loss of gas-phase HNO_3 in a flow tube containing deliquesced 1 - 5 μm NaCl particles (75% RH) and obtained a lower limit to the uptake coefficient for HNO_3 of 0.2 on unbuffered NaCl. Stemmler et al. [537] report a value of 0.5 ± 0.2 for the initial uptake coefficient on deliquesced particles at 60% RH. Tolocka et al. [565] followed the reaction of HNO_3 with 100 - 220 nm NaCl particles at 80% RH using single particle MS to measure the $\text{Cl}^-/\text{NO}_3^-$ ratio; the uptake coefficient for 100 nm particles was $(4.9 \pm 2.7) \times 10^{-3}$ and increased with droplet size. Saul et al. [494] have extended the Tolocka et al. work, by studying the reaction over a wide range of relative humidities, both above and below the efflorescence point. Uptake coefficients on the mixed nitrate-chloride particles reach a maximum of 0.12 or so at 50% RH, decreasing at both higher and lower RHs. The presence of hygroscopic MgCl_2 increases the uptake coefficient at low RHs, where the particles may remain liquid. Liu et al. [373] using static particles probed spectroscopically determine the maximum uptake coefficients to be 0.2 (uncertainty a factor of three), also close to 50% RH, decreasing at higher and lower RHs. The combination of these studies shows that the initial uptake of HNO_3 into solution is fast, with $\gamma_0 > 0.2$; as the solution becomes acidified, HCl is expelled as the gaseous product. The uptake coefficient may decrease when the reaction proceeds on processed particles, where a large amount of nitrate has built up. In such cases, the maximum reactivity is at close to 50% RH. Note that the Stemmler et al. [537] study illustrated that monolayer coverages of long-chain surfactants can reduce the initial uptake coefficient by over an order of magnitude. [Back to Table](#)

48. $\text{HNO}_3 + \text{NaBr}$ and KBr . Fenter et al. [171] reported that the value of γ for uptake of HNO_3 on NaCl, NaBr, KBr and KCl was the same, $(2.8 \pm 0.3) \times 10^{-2}$, independent of sample mass. Koch et al. [346] reported an uptake coefficient of HNO_3 on KBr of $(2 \pm 1) \times 10^{-2}$ using a molecular diffusion tube technique. As discussed in Note 7, integration of the results of an extensive series of studies in different laboratories using different techniques, uptake coefficients for HNO_3 on NaCl give a value for the HNO_3 -NaCl reaction that is smaller than measured in the Fenter et al. [171] and Koch et al. [346] studies. These values for KBr may therefore be upper limits. Leu et al. [362] reported a value that is an order of magnitude smaller, $(2.8 \pm 0.5) \times 10^{-3}$ after applying large corrections (about an order of magnitude) for pore diffusion; the average uncorrected value using the geometric area was 0.027. [Back to Table](#)
49. $\text{HNO}_3 + \text{sea salt}$. The uptake coefficient for HNO_3 on synthetic sea salt [149] is much larger than that on NaCl, which is attributed to the very hygroscopic nature of sea salt due to such components as the

magnesium chloride and its hydrates (see Note on O_3 + sea salt). De Haan and Finlayson-Pitts [149] reported initial uptake coefficients of γ_0 in the range of 0.07 to 0.75 and steady state values in the range of 0.03 to 0.25; these were measured using salt layers from 2 layers to 10^3 layers. The initial uptake coefficient on $MgCl_2 \cdot 6H_2O$ was ≥ 0.4 and the steady-state value > 0.1 . At these high uptake values, the correction for diffusion into underlying layers is expected to be small. The large uptake coefficient on sea salt is consistent with the values measured for uptake on concentrated aqueous solutions of NaCl and the high water content of the surface of sea salt (see O_3 + seasalt Note above). The yield of HCl was within experimental error of 100%.

Guimbaud et al. [222] measured the uptake coefficient of HNO_3 on 70 nm supersaturated sea-salt particles (deliquesced particles held at 55% RH) to be 0.50 ± 0.20 ; they concluded that this was the mass accommodation coefficient. [Back to Table](#)

50. $HNO_3 + Al_2O_3$. Börensén et al. [79] used diffuse reflectance FTIR observations to show that HNO_3 reacts with surface hydroxyl groups on γ -alumina at 299 K to produce surface bonded nitrate, while Goodman et al. reported similar observations for α -alumina at 296 K [214]. Goodman et al. [214] also observed that higher relative humidity lead to higher HNO_3 uptake. They integrated their nitrate absorbance feature to yield a time averaged uptake coefficient of $(4 \pm 1) \times 10^{-8}$ [214]. Underwood et al. [569] report a linear mass dependent, BET corrected γ_0 for α -alumina at 295 K of $(9.7 \pm 0.5) \times 10^{-5}$. Hanisch and Crowley also measured liner mass dependent γ_0 s on α -alumina (at 298 K) for four particle sizes, which yielded an average value of 0.133 ± 0.033 [230]. They argue that the lack of variance of γ_0 s on a large range of particle sizes and masses indicate that the BET correction to the geometrical surface area is not required. They also measured γ_0 for an unpolished single crystal of $(1.6 \pm 1.4) \times 10^{-3}$ and smaller values on polished single crystals, showing the higher density of surface defect sites on small amorphous particle are critical for their high reactive active uptake coefficients. The recommendation is based on the Hanisch and Crowley data and analyses for particulate samples [230]. Seisel et al., [510] used Knudsen cell uptake experiments at 298 K to measure an initial uptake (γ_0) value of 0.13 ± 0.02 for γ -alumina with HNO_3 vapor concentrations of $\sim 10^{11} \text{ cm}^{-3}$. Lower values of γ were observed for higher nitric acid partial pressures; water vapor was observed as a product. They also performed DRIFTS experiments that yielded a mean uptake coefficient for surface nitrate formation of $(7.7 \pm 0.8) \times 10^{-3}$ at 298 K. [Back to Table](#)
51. $HO_2NO_2 + HCl$ on $H_2SO_4 \cdot nH_2O(l)$. Zhang et al. [632] performed wetted-wall flow-reactor studies with HCl and HO_2NO_2 partial pressures in the 10^{-6} to 10^{-7} Torr range. Using chemical ionization mass spectrometry (CIMS) to detect expected reaction products, no Cl_2 (using SF_4^- as an analyte ion) or $HOCl$ (using F^-) was detected over a temperature range of 200–225 K and an acid concentration range of 50–70 wt.% H_2SO_4 . An upper limit for the reactive uptake coefficient for HO_2NO_2 reacting with HCl of $\gamma < 1 \times 10^{-4}$ was deduced. [Back to Table](#)
52. $NH_3 + H_2SO_4 \cdot nH_2O$. Robbins and Cadle [466], Huntzicker et al. [280], McMurry et al. [394], and Daumer et al. [142] all studied NH_3 uptake by sulfuric acid aerosols in near room temperature flow reactors ($T = 281\text{--}300 \text{ K}$). Uptake coefficients varied between 0.1 and 0.5. Rubel and Gentry [484] used levitated H_3PO_4 acid droplets to show that heterogeneous reaction does control the initial NH_3 uptake on strong acid solutions. Both Rubel and Gentry and Däumer et al. also explored the effect of organic surface coatings. Swartz et al. [542] used a droplet train flow reactor to measure reactive uptake coefficients on 20 to 70 wt.% acid over a temperature range from 248 to 288 K. Measured uptake coefficients varied from 1.0 at 55 wt.% and above to 0.3 at 20 wt.% and drop off smoothly to the pure water results reported by the same group, as well as other droplet train flow reactor and coaxial jet uptake studies [610]. Hanson and Kosciuch [233] used an aerosol flow reactor to measure reactive uptake coefficients at room temperature (287 to 297 K) from 15 to 65 wt.%. While the data have a fair amount of scatter, taken as a whole they are consistent with $\gamma=1$ over the whole range of acid concentrations. There is no obvious reason for the discrepancy between the 15 to ~45 wt.% results from Swartz et al. [542] and Hanson and Kosciuch [233], the two groups have discussed conceivable issues at length in print [610] and Hanson and Kosciuch [234]. [Back to Table](#)
53. VOCs on Al_2O_3 . Carlos-Cueller et al. [98] and Li et al. [365] have reported Knudsen cell studies that determined γ_0 values for oxygenated volatile organic compounds (VOCs) at 295 and 298 K, respectively. Carlos-Cueller [98] measured γ_0 s on α -alumina for formaldehyde, $(7.7 \pm 0.3) \times 10^{-5}$, methanol, $(1.0 \pm 0.7) \times 10^{-4}$, and acetic acid, $(2 \pm 1) \times 10^{-3}$ based on BET surface areas and the KML [332] correction for porosity; the reported value for the relatively “sticky” acetic acid may not require the full BET and porosity

corrections and thus may be underestimated. Li et al. [365] measured BET corrected γ_0 s on α -alumina for acetaldehyde, 3.2×10^{-5} , propionaldehyde, 4.7×10^{-5} , and acetone, 2.0×10^{-5} . The recommended upper limits are factors higher than the measured values since all the measurements are from a single laboratory using a single experimental technique. BET may overcorrect. [Back to Table](#)

54. $\text{CH}_3\text{OH} + \text{H}_2\text{SO}_4 \cdot n\text{H}_2\text{O(l)}$ and $\text{H}_2\text{SO}_4 \cdot m\text{HNO}_3 \cdot n\text{H}_2\text{O(l)}$. Van Loon and Allen [579] report spectroscopic observations at 293 K for 0 to 96.5 wt.% H_2SO_4 exposed to methanol vapor. They observed rapid surface adsorption and saturation, followed by slower bulk absorption. For acid concentrations between 47.1 and 63.3 wt.% they observed surface reaction between methanol and sulfuric acid that formed methyl hydrogen sulfate, $\text{CH}_3\text{SO}_4\text{H}$. Iraci et al. [294] used infrared spectroscopy to monitor the production of gas phase methyl nitrate, CH_3ONO_2 , from the bulk reaction of ternary sulfuric acid/nitric acid/water solutions with 0.00005-0.005 M CH_3OH in 50.5 to 63.6 wt.% H_2SO_4 with 0.03-0.21 M HNO_3 between 278.2 and 328.6 K. Within this range methyl nitrate production increased linearly with methanol and nitric acid concentration and exponentially with sulfuric acid concentration. At high acid concentrations nitric acid reacts with protons to form water and the nitronium ion, NO_2^+ ; methyl nitrate production was observed to be proportional to the NO_2^+ concentration indicating it was the nitrating agent. [Back to Table](#)
55. $\text{CH}_3\text{CH}_2\text{OH} + \text{H}_2\text{SO}_4 \cdot n\text{H}_2\text{O}$. Timonen and Leu [560] used a trough flow reactor to measure uptake coefficients for ethanol on 41.1 to 79.3 wt.% H_2SO_4 , for selected temperatures between 193 to 273 K, but primarily for temperatures from 203 to 258 K. Uptake coefficients for 70.3 – 79.3 wt.% acid showed little temperature variation, starting at ~ 0.07 for 203 K and falling to 0.05 to 0.06 above 250K, while uptake coefficients for 41.1 to 64.1 wt.% started at ~ 0.07 at 203 K and decreased to about 0.02 at 233K for 41.1 wt.% 1, to ~ 0.03 at 243K for 54.4 wt.% and ~ 0.035 at 253K for 64.1 wt.%. Uptake was only partially reversible, so it was attributed to both physical and reactive processes, making the reported uptake coefficients as upper limits for γ . The authors attributed the reactive portion of the uptake to esterification reactions, forming ethyl hydrogen sulfate and diethyl sulfate, and saw some mass spectral evidence for these products when they mixed ethanol with 80 wt.% acid in their reactor at 296K. Michelsen et al. [405] found no evidence for ethyl hydrogen sulfate in Knudsen cell ethanol uptake experiments for 39-76 wt.% H_2SO_4 over a 209-237K temperature range, so the extent of reaction for low temperature acid solutions remains uncertain. Timonen and Leu suggest that at low ethanol vapor fluxes surface reactivity may be important. [Back to Table](#)
56. $\text{CH}_3\text{CHO} + \text{H}_2\text{SO}_4 \cdot n\text{H}_2\text{O}$. Knudsen cell uptake measurements are reported by Michelsen et al. [404] for 38.5-76.2 wt.% H_2SO_4 over a temperature range of 211-241K, with evidence of reactive uptake for some temperatures in the 38.5-66.3 wt.% H_2SO_4 range. Using a rotating wetted-wall flow reactor Esteve and Nozière [167] measured small, probably solubility constrained, uptake coefficients at $298 \pm 3\text{K}$ for 96 wt.% and 89.4 wt.% of 9.4×10^{-6} and 4.2×10^{-7} , respectively. Michelsen et al. found uptake over the 211-241K temperature range was controlled by Henry's law solubility, and had a complex dependence on acid concentration due to competition among the reversible bulk phase processes of physical dissolution, hydration to form the gem diol, protonation and enolization, all of which affect H^+ . They also saw evidence for aldol condensation at some temperatures for acid concentrations of 66.3 wt.% and below. Drawing on the complex aldol condensation mechanism presented to explain the bulk kinetic studies of Baigrie et al. [34], Michelsen et al. present plausible arguments why non-reversible condensation reactions might have the complex dependence on acid concentrations and temperature that they observed. Given its relatively small rate constant, they suggest that aldol condensation bulk reactions will play a negligible role for typical aldehyde concentrations in the atmosphere. [Back to Table](#)
57. $\text{CH}_3\text{C(O)CH}_3 + \text{H}_2\text{SO}_4 \cdot n\text{H}_2\text{O}$. Duncan et al. [161, 162] used IR spectra of thin sulfuric acid films to establish that acetone is absorbed as the protonated species. Above 70 wt.% protonated acetone undergoes a self condensation/dehydration reaction to form protonated mesityl oxide, which can, in turn, react with an additional protonated acetone to form trimethyl benzene. Kane et al. [322] Henry's law uptake measurements diverged above 80 wt.%, which they attribute to reactive uptake as suggested by Duncan et al. Using a rotating wetted-wall flow reactor Esteve and Nozière [167] measured small, probably solubility constrained, uptake coefficients at $298 \pm 3\text{K}$ for 89.4, 85, 80.8 and 73.9 wt.% H_2SO_4 of 5.2×10^{-5} , 5.6×10^{-6} , 4.7×10^{-6} and 1.6×10^{-6} , respectively. [Back to Table](#)
58. $\text{CH}_3\text{C(O)O}_2 + \text{H}_2\text{O(l)}$ and $\text{H}_2\text{SO}_4 \cdot n\text{H}_2\text{O}$. Villalta et al. [580] used wetted-wall flow tube techniques to measure $\gamma = 4.3 (+ 2.4 / -1.5) \times 10^{-3}$ for water at $274 \pm 3\text{K}$. They also measured uptake for 34 wt.% H_2SO_4 at 246 K ($\gamma = (2.7 \pm 1.5) \times 10^{-3}$), 51 wt.% at 273 K ($\gamma = (0.9 \pm 0.5) \times 10^{-3}$), and 71 wt.% at 298 K ($\gamma = (1.4$

- $\pm 0.7) \times 10^{-3}$). They suggest that products subsequent to hydrolysis are HO_2 and $\text{CH}_3\text{C}(\text{O})\text{OH}$. [Back to Table](#)
59. $\text{CH}_3\text{C}(\text{O})\text{O}_2\text{NO}_2 + \text{HCl}$, Cl , ClO , and OClO on $\text{H}_2\text{SO}_4 \cdot n\text{H}_2\text{O}(\text{l})$. Zhang and Leu [627] performed wetted wall flow reactor studies with Cl species partial pressures in the 10^{-6} to 10^{-7} Torr range and $\text{CH}_3\text{C}(\text{O})\text{O}_2\text{NO}_2$ at 3×10^{-6} Torr after equilibrating the acid surfaces (42, 51, and 69 wt.% at 202 and 224 K) with $\text{CH}_3\text{C}(\text{O})\text{O}_2\text{NO}_2$. Also uptake studies with 5×10^{-7} Torr $\text{CH}_3\text{C}(\text{O})\text{O}_2\text{NO}_2$ were performed after exposing the acid surface to the Cl species. No Cl species or $\text{CH}_3\text{C}(\text{O})\text{O}_2\text{NO}_2$ uptake enhancements were observed under either condition and an upper limit for the reactive uptake coefficient of $\gamma < 1 \times 10^{-4}$ of $\text{CH}_3\text{C}(\text{O})\text{O}_2\text{NO}_2$ was deduced. No gas phase reaction products were observed using CIMS after 42 wt.% H_2SO_4 at 210 K was exposed to $\text{CH}_3\text{C}(\text{O})\text{O}_2\text{NO}_2$ and each Cl species for 20 minutes. [Back to Table](#)
 60. $\text{Cl} + \text{H}_2\text{SO}_4 \cdot n\text{H}_2\text{O}(\text{l})$. Measured reaction probability (Martin et al. [391]) varies between 3×10^{-5} and 7×10^{-4} as H_2O and T co-vary. Reaction product is claimed to be HCl . [Back to Table](#)
 61. $\text{Cl}_2 + \text{HBr} + \text{H}_2\text{O}(\text{s})$. Hanson and Ravishankara [246] measured a reaction probability of > 0.2 on water ice near 200 K. BrCl was not detected, presumably due to rapid reaction with excess HBr . [Back to Table](#)
 62. $\text{Cl}_2 + \text{NaCl}$. Mochida et al. [410] used salt powders and spray-deposited films of NaCl and reported an initial uptake coefficient of 1.0×10^{-3} . Aguzzi and Rossi [13] reported no measurable uptake of Cl_2 on NaCl . [Back to Table](#)
 63. $\text{Cl}_2 + \text{NaBr}$ and NaI . Mochida et al. [410] used salt powders and spray-deposited films to obtain a value for the initial uptake coefficient of 2×10^{-2} . The measured uptake coefficients for the salt powders were a factor of six larger, but application of the pore diffusion model of Keyser et al. [333, 334] gave this value, which is in agreement with that for a spray-deposited film. Br_2 was generated in a yield of 100%, within experimental error.

Hu et al. [272] measured the uptake of Cl_2 on aqueous solutions of NaBr and NaI over the temperature range of 263 - 293 K using a droplet train flow reactor. Measured values of the uptake coefficients on NaBr solutions ranged from 0.16 at 263 K to 0.05 at 293 K, and there was evidence of a surface reaction between Cl_2 and Br^- at the air-particle interface. Similarly, the uptake coefficients for Cl_2 on NaI solutions ranged from 0.20 to 0.07 over the same temperature range, again with evidence for a contribution from an interface reaction. Huff and Abbatt [276] have studied the reaction of Cl_2 with films formed by freezing NaBr solutions at 233 K, observing Br_2 as the reaction product and that the maximum reaction probability is 0.1 when the surface is saturated with bromide ions. [Back to Table](#)
 64. $\text{Cl}_2 + \text{KBr}$. Mochida et al. [410] used salt powders and spray-deposited films to obtain a value for the initial uptake coefficients. The value measured for salt powders was 0.176, but after correction for pore diffusion, this became 3.7×10^{-2} , similar to a value of 2.3×10^{-2} measured for spray-deposited films. Br_2 was generated in a yield of 100%, within experimental error. Aguzzi and Rossi [13] measured a similar value, 2.7×10^{-2} , using a Knudsen cell. Santschi and Rossi [493] reported an initial value of $\gamma_0 = 0.11$ for the uptake of Cl_2 on thin spray-deposited films of KBr that had not been extensively pumped on; this initial value was 4×10^{-2} for films that had been pumped on for hours. They attributed the difference to the removal of surface-adsorbed water (SAW) by extensive pumping. [Back to Table](#)
 65. $\text{Cl}_2 + \text{sea salt}$. Mochida et al. [410] used a synthetic sea salt and a "natural" seasoning sea salt in Knudsen cell studies of the uptake of Cl_2 . The synthetic sea salt value of $(2.2 \pm 0.3) \times 10^{-2}$ is the value reported after correction of the measured value of 0.138 using the pore diffusion model. For the "natural" seasoning salt, the measured value was 0.11 which after correction for diffusion into the underlying layers became $(3.1 \pm 1.1) \times 10^{-2}$. Br_2 was the major gas phase product, with small mass spectrometric signals also seen for BrCl . [Back to Table](#)
 66. $\text{ClO} + \text{H}_2\text{O}(\text{s})$ and $\text{HNO}_3 \cdot n\text{H}_2\text{O}(\text{s})$. Proposed reaction (Leu [360]) is $2 \text{ClO} \rightarrow \text{Cl}_2 + \text{O}_2$; reactive uptake may depend on ClO surface coverage, which in turn may depend on gas phase ClO concentrations. Kenner et al. [329] measured reaction probabilities of $(8 \pm 2) \times 10^{-5}$ for ice at 183 K which is far lower than the limit of $> 1 \times 10^{-3}$ obtained by Leu [360]. Abbatt [3], using nearly the same low levels of ClO as Kenner et al., obtained $\gamma < 1 \times 10^{-5}$ at 213 K. The difference may lie in the level of ClO or other adsorbable reactive species present. The lower value of Abbatt is probably closer to the expected reactivity under stratospheric conditions. Kenner et al. also measured a reaction probability limit of $< (8 \pm 4) \times 10^{-5}$ for NAT at 183 K. [Back to Table](#)

67. $\text{ClO} + \text{H}_2\text{SO}_4 \cdot n\text{H}_2\text{O}$. Measured reaction probability (Martin et al. [391]) varies between 2×10^{-5} and 2×10^{-4} as H_2O content is varied by changing wall temperature. Reaction product is claimed to be HCl , not Cl_2 . Abbatt [3] measured $\gamma < 1 \times 10^{-5}$ for 60 and 70 wt.% H_2SO_4 at 213 K. [Back to Table](#)
68. $\text{HCl} + \text{HNO}_3$ on $\text{H}_2\text{SO}_4 \cdot m\text{HNO}_3 \cdot n\text{H}_2\text{O}(\text{l})$. Two studies have noted HCl activation in concentrated ternary $\text{H}_2\text{SO}_4/\text{HNO}_3/\text{H}_2\text{O}$ solutions or ice slurries. Luick et al. [381] saw only gas phase HCl in 64.6 wt.% H_2SO_4 / 4.8 wt.% HNO_3 at 200 K, but saw a vapor phase Cl partitioning of 50% HCl and 50% $\text{ClNO}/\text{ClNO}_2$ for a 76.6/20.1 wt.% solution (an ice slurry) at 200 K. Cappa et al. [97] saw substantial yields of ClNO , ClNO_2 , and Cl_2 at 273 K for a range of solution compositions; e.g. 32.6%, 9.8% and 44.4% respectively for a total HCl conversion of 86.9% in a 35% H_2SO_4 /45% HNO_3 solution and 20.2%, 6.9%, 27.9% for a 60/25 wt.% solution. While no kinetic coefficients or detailed mechanisms are available, these studies do show the potential for HCl activation in strong $\text{H}_2\text{SO}_4/\text{HNO}_3/\text{H}_2\text{O}$ solutions. [Back to Table](#)
69. $\text{HOCl} + \text{HCl} + \text{H}_2\text{O}(\text{s})$ and $\text{HNO}_3 \cdot 3\text{H}_2\text{O}(\text{s})$. Hanson and Ravishankara [245] and Abbatt and Molina [8] have investigated the $\text{HOCl} + \text{HCl}$ reaction on water ice and NAT-like surfaces, and Chu et al. [114]; [108] studied the reaction on water ice. Product yield measurements support the identification of Cl_2 and H_2O as the sole products. The measured yield of product Cl_2 is 0.87 ± 0.20 and was stated to be similar on both surfaces according to Abbatt and Molina. Within the accuracy of the experiments, the reaction probability does not depend on the gas phase HCl and HOCl densities. Only Abbatt and Molina investigated at more than one temperature, their data indicates that γ increases at lower temperatures. A plot of data from the three studies does show a weak temperature trend, with γ increasing about a factor of two as the temperature drops from 202 to 188 K. However, the data are too sparse to assign a definitive temperature dependence. The average of all three studies yields $\gamma = 0.26 \pm 0.08$ for data based on the geometrical area of the flow tube surfaces. Chu et al. [108] indicate that a porosity correction for their data would reduce their value by a factor of 3 to 4. The real uncertainty would appear to be dominated by systematic uncertainties in porosity corrections and a potential temperature dependence. Given the fact that any porosity correction must reduce the value, a central value of 0.2 is adopted with an uncertainty factor of 2. The high reaction probabilities measured for water ice indicate that this reaction may play a significant role in release of reactive chlorine from the HCl reservoir.

Two studies (Hanson and Ravishankara [245]; Abbatt and Molina [8]) have measured the reaction probability of $\text{HOCl} + \text{HCl}$ on NAT surfaces. These data show γ increases as the ambient water pressure increases and then reaches a plateau. At relatively high water pressure, the two studies averaged $\gamma = 0.135 \pm 0.049$, with no porosity correction. The reaction probability on water poor NAT-like surfaces falls off dramatically (a factor of 10). A recommendation of 0.1 with an uncertainty factor of 2 is shown in Table 5-2. Carslaw and Peter [100] have published a model of this reaction and its dependence on HCl uptake.

[Back to Table](#)

70. $\text{HOCl} + \text{HCl} + \text{H}_2\text{SO}_4 \cdot n\text{H}_2\text{O}(\text{l})$. This process has been studied in coated flow tubes over ~200–260 K by Zhang et al. [626], Hanson and Ravishankara [250], Donaldson et al. [158], and Hanson and Lovejoy [241]. Hanson and Lovejoy also made measurements in an aerosol flow tube from 251 to 276 K. A model of this and related sulfuric acid aerosol reactions tailored to stratospheric conditions has been published by Hanson et al. [254]. Zhang et al. held the water vapor partial pressure at 3.8×10^{-4} Torr and showed γ increased by a factor of 50 as the temperature was lowered from 209 to 198 K increasing the water mole fraction, showing that the reaction rate is strongly dependent on water activity.

A detailed kinetic uptake model has been developed to fit the experimental data [519]. The formulation for γ is given as:

$$\frac{1}{\gamma} = \frac{1}{\alpha} + \frac{1}{\Gamma_{\text{HOCl}}^{\text{rxn}}}$$

where

$$\Gamma_{\text{HOCl}}^{\text{rxn}} = \frac{4H_{\text{HOCl}}RT}{\bar{c}} \left(D_{\text{HOCl}} k_{\text{HOCl-HCl}} \right)^{1/2}$$

At the low temperatures of interest, α for HOCl was assumed to be unity consistent with the value for HCl measured at 240 K and below (Robinson et al. [472]). The individual formulations for H_{HOCl} , D_{HOCl} and $k_{\text{HOCl-HCl}}$ are given in Table A-4 in Shi et al. [519]. Reaction of HOCl with HCl is considered to be acid

catalyzed. It is known that the reaction rate for HOCl + HCl in pure water is low (Donaldson et al. [158]). Experimental data noted above indicated that the reaction rate of HOCl + HCl increases with acidity of H₂SO₄ solution. The data from the experimental studies noted above were fit to the model without bias. Using the same error analysis discussed in the note for N₂O₅ uptake on sulfuric acid, a detailed kinetic model yields a 33.4% error (one sigma fit to the available data set, with $\sigma_m=33.3\%$ and $\sigma_d=3.0\%$).

In the cold stratosphere where T<190 K, the reaction of ClONO₂ + HCl is so fast that HCl is depleted which slows down the reaction of HOCl + HCl. As shown in Table A-4 in Shi et al., the effect of HCl depletion on the HOCl reactive uptake coefficient (due to reaction with ClONO₂ inside/on the surface of particles) is taken into account via the factor F_{HCl} (also see the note on chlorine nitrate/hydrochloric acid reactive uptake on sulfuric acid surfaces). [Back to Table](#)

71. HOCl + HBr on H₂O(s). Chu and Chu [108] measured γ at 189 K to be in the range from 0.06 to 0.38 for HBr partial pressures ranging from 1.1×10^{-7} to 6.6×10^{-5} Torr. At 220 K they measured γ in the range from 0.01 to 0.07 for HBr partial pressures in the range from 7.2×10^{-7} to 1.3×10^{-5} Torr. These γ values were estimated assuming the area of the ice surface to be equal to the geometric area of the cylindrical flow reactor; corrections for surface porosity effects range from a factor of 3 to 10 lower. [Back to Table](#)
72. HOCl + HBr on H₂SO₄ · nH₂O(l). Abbatt and Nowak [10] measured uptake of HOCl in the presence of excess HBr on a 69.3 wt.% sulfuric acid solution in a wetted wall flow reactor at 228 K. A second order bulk reaction rate constant, k^{II} , of $2 \times 10^6 \text{ M}^{-1}\text{s}^{-1}$ was derived; this is a factor of ~10 faster than HOBr + HCl under the same conditions. Since HOCl and HBr have variable solubilities under stratospheric conditions, characterizing this reaction with a simple uptake coefficient is not appropriate. A full reaction/solubility/liquid phase diffusion model will require further data. [Back to Table](#)
73. HOCl + NaBr and KBr. Rossi [480] reported studies of the uptake of HOCl in a Knudsen cell using KBr powders and spray-deposited thin films. Values for the initial uptake coefficients covered a wide range, from 5×10^{-3} to 0.2, due to changes in the surface from adsorbed reaction products. The major product initially was Br₂, and subsequently BrCl and HOBr, with much smaller amounts of BrOCl and Br₂O. The mechanism was interpreted as the formation of small amounts of HBr on the surface from hydrolysis of KBr, followed by the reaction of HOCl with adsorbed HBr to form BrCl which then reacts with KBr to form Br₂. On frozen solutions of NaBr, Huff and Abbatt [276] observe reactivity of HOCl with uptake coefficients between 0.02 and 0.04 at 233 K in a coated-wall flow tube. Br₂ is the gas-phase product, thought to arise from the intermediate BrCl reacting with the bromide film. Although the kinetics are faster on the most acidic films (pH 2), there is no dependence of the acidity of the solution from pH 4 to 10. [Back to Table](#)
74. ClNO + H₂O(l). Scheer et al. [495] used droplet train and wetted wall flow reactor measurements to determine reactive uptake coefficients for ClNO over a temperature range of 273-293 K. Measured values show a weak negative temperature dependence ranging from 0.12 at 273 K to 0.0058 at 293K. The reaction was shown to be base catalyzed producing HONO. [Back to Table](#)
75. ClNO + NaCl(s). Using a Knudsen cell technique Beichart and Finlayson-Pitts [64] set upper limits of $\gamma < \sim 10^{-5}$ for reactive uptake of ClNO on NaCl(s) powders at 298 K. [Back to Table](#)
76. ClNO₂ + H₂O(l). Behnke, George and co-workers have used droplet train and wetted wall flow reactor techniques to investigate the reactive uptake of ClNO₂ on aqueous solutions [58, 175, 199, 507]. Droplet train flow reactor experiments from 268-279 K demonstrated that the reactive uptake coefficient on pure water is $< 1 \times 10^{-5}$ [199]. Wetted wall flow reactor studies from 279 to 292 K on pure water and very low concentration sodium halide solutions all yielded reactive uptake coefficients in the 10^{-6} range, with typical values of $(4.84 \pm 0.13) \times 10^{-6}$ at 291 K [58], and 3.41×10^{-6} at 276.6 K, 4.27×10^{-6} at 282.2 K, and 4.48×10^{-6} at 287.4 K [175]. There is apparently no significant temperature dependence. [Back to Table](#)
77. ClNO₂ + KBr, NaBr, NaI and NaCl. Caloz et al. [95] measured the uptake of ClNO₂ on solid KBr at room temperature using a Knudsen cell and salt samples in the form of powders, spray-deposited films, polished windows and depolished windows. The uptake coefficient increased with the number of layers of salt powders; correction of the uptake coefficients using the pore diffusion model gave initial uptake coefficients of $(1.0 - 1.3) \times 10^{-4}$, in agreement with values measured for the spray-deposited film (1.0×10^{-4}) and depolished window (1.0×10^{-4}). The value for the polished window was an order of magnitude smaller, as expected since this has much less surface-adsorbed water (SAW) that assists in keeping the surface from becoming passivated. The yield of Br₂ relative to ClNO₂ lost was 0.55 ± 0.2 . Using a

diffusion tube method, Koch and Rossi [345] measured an uptake coefficient of 2.0×10^{-4} , in reasonable agreement with the Knudsen cell results.

The uptake of ClONO_2 on aqueous solutions of NaBr has been shown to increase with the concentration of NaBr. Frenzel et al. [192] measured the uptake of ClONO_2 on $(0.5 - 5) \times 10^{-3}$ M NaBr solutions from 275–291 K using a wetted wall flow tube apparatus; the values of γ increased from 1.2×10^{-5} to 4.0×10^{-5} over this range of NaBr concentrations. Schweitzer et al. [507] used a droplet train apparatus from 275 - 288 K; γ increased from 8.6×10^{-6} to 9.4×10^{-4} as the NaBr concentration increased from 10^{-4} to 1.0 M. The main product was Br_2 , with traces of BrNO_2 and BrCl . In a subsequent study [508], they applied a wetted wall flow tube method from 275–293 K and reported uptake coefficients that were independent of temperature over this range, but again increased with the concentration of NaBr: γ increased from 7.1×10^{-6} at 10^{-4} M NaBr to 9.2×10^{-4} at 1.0 M. Fickert et al. [178] used a wetted wall flow tube at 274 K and measured an uptake coefficient of 1.1×10^{-5} for 10^{-4} M NaBr, increasing to 1.1×10^{-4} for 10^{-2} M NaBr. The major gas phase products were Br_2 and BrNO_2 , with the yield of BrNO_2 decreasing as the initial bromide ion concentration in solution increased. The mass accommodation coefficient for ClONO_2 on aqueous solutions at 275 K was measured to be $(9 \pm 4) \times 10^{-3}$. A Knudsen cell study by Beichart and Finlayson-Pitts [64] found $\gamma < \sim 10^{-5}$ on NaCl powders at 298 K.

The uptake of ClONO_2 on solutions of NaI was studied by George et al. [199] and by Schweitzer et al. [507, 508]. The uptake coefficient increases with the concentration of NaI. For example, George et al. [199] reported that γ_0 increased from 1.1×10^{-3} to 6.6×10^{-3} as the iodide concentration increased from 10^{-3} M to 10^{-2} M at 280 K. This is consistent with the results of Schweitzer et al. [507, 508] who reported that γ_0 increased from 3.1×10^{-5} to 4.5×10^{-3} as the iodide concentration increased from 10^{-4} M to 10^{-2} M at 275 K.

The uptake of ClONO_2 on solutions of NaCl is much slower than on NaBr or NaI solutions. Behnke et al. [58] reported uptake of ClONO_2 at 291 K using a wetted wall flow tube, with uptake coefficients decreasing as the NaCl concentration increased. At 0.1 M NaCl, $\gamma_0 = (3.1 \pm 0.3) \times 10^{-6}$ but at 4.6 M NaCl, the value was about an order of magnitude smaller, $\gamma_0 = (0.27 \pm 0.02) \times 10^{-6}$. They proposed that this was due to the common ion effect owing to the reversible hydrolysis of ClONO_2 to $\text{Cl}^- + \text{NO}_2^+$.

Roberts et al. [467] report that ClONO_2 produces Cl_2 when exposed to solutions of chloride with concentrations as low as 0.05 M, when the pH is less than 2. [Back to Table](#)

78. $\text{ClONO}_2 + \text{H}_2\text{O}(\text{s})$. Measurement of $\gamma = 0.3 (+0.7, -0.1)$ (Hanson and Ravishankara [243]) significantly exceeds early measurements of Molina et al. [415], Tolbert et al. [564], Leu [359] and Moore et al. [417] but agrees reasonably well with subsequent measurements by Chu et al. [114], Zhang et al. [628] and Fernandez et al. [176] when geometrical surface areas are assumed for analysis. Previous measurements were probably complicated by NAT formation on the surface (Hanson and Ravishankara [245]; Chu et al. [114]). Lower levels of ClONO_2 (g) used by Hanson and Ravishankara [243] minimized this surface saturation problem. Also, using lower ClONO_2 concentrations, Zhang et al. obtained a reaction probability of 0.08 ± 0.02 at 195 K, Fernandez et al. (2005) measured 0.1, and values were 0.03 to 0.13 from Chu et al. Subsequent Knudsen cell measurements at 180 and 200 K by Oppliger et al. [434] showed initial uptake γ s in the 0.2 to 0.4 range. Measured reaction products were HNO_3 and HOCl . All of the HNO_3 and much of the HOCl is retained on the surface under polar stratospheric conditions (Hanson and Ravishankara [243, 245]). Hanson [236] deposited ClONO_2 on H_2^{18}O enriched ice and detected H^{18}OCl showing the $\text{Cl}-\text{ONO}_2$ bond is broken at 191 K.

Data plots confirm a trend showing that at a high density of ClONO_2 , the product HNO_3 covers the ice surface preventing the further reaction of ClONO_2 with H_2O molecules on the surface. Therefore, data obtained at high ClONO_2 densities ($>10^{14}$ molecules/ cm^3) are excluded from further evaluation. An experiment (Berland et al. [69]) using a laser-induced thermal desorption technique yielded a much lower value of ClONO_2 reaction probability at 190 K (about 3 orders of magnitude lower) after extrapolating the results obtained at temperatures of 140 K and below. We also exclude this point in the averaging of data since the physical characteristics of ice surfaces at these very low temperatures may not be very representative of those found at stratospheric temperatures. Selected data show no temperature dependence between $T=180$ and 200 K and averaged $\gamma_0 = 0.28 \pm 0.25$. Again, within the experimental accuracy, the Hanson and Ravishankara [245, 248] and Chu et al. [114] data show that uptake measurements are nearly independent of ice substrate thickness. See Henson et al. [261] for discussion of a model which accounts for the effect of HNO_3 on the reaction ClONO_2 on water and nitric acid ice surfaces.

Zondlo et al. [640] report the formation of a supercooled H₂O/HNO₃ liquid layer at 185 K as a reaction product, forming NAT or NAD only after decreasing the relative humidity below the ice frost point. This effect is similar to that resulting from the interaction of gaseous HNO₃ or N₂O₅ with the ice surface. These authors measured $\gamma = (3 \pm 2) \times 10^{-3}$ at 185 K for the reaction of ClONO₂ with this supercooled liquid layer. [Back to Table](#)

79. ClONO₂ + H₂O(l). Deiber et al [150] used a droplet train reactor to measure uptake of ClONO₂ on pure water between 274 and 285 K. No apparent temperature dependence was observed with all three temperatures measured resulting in reactive uptake measurements near 0.025. [Back to Table](#)

80. ClONO₂ + HNO₃•nH₂O(s). Hanson and Ravishankara [243] report a γ value of 0.006 at 201 K for the ClONO₂ reaction with the water on NAT (HNO₃•nH₂O). However, these authors present re-analyzed and additional data with $\gamma \approx 0.001$ at 191 K in Hanson and Ravishankara [245, 248]. Similar experiments (Moore et al. [417], Leu et al. [361]) report a larger value of 0.02 ± 0.01 which falls very rapidly as slight excesses of H₂O above the 3/1 H₂O/HNO₃ ratio for NAT are removed. In general, it is difficult to know that only NAT is formed when freezing from solution; it is likely that the high value reflects the reactivity on water ice that will form when the solution stoichiometry is water rich. They measured γ of less than 1×10^{-6} for slightly water-poor NAT surfaces. Abbatt and Molina [9] report γ values reaching 0.002 at 202 K and high RH. Hanson and Ravishankara [245] reported that γ for this reaction increases by a factor of 4 as the surface temperature increases from 191 to 211 K. However, Knudsen cell measurements at 185 K by Barone et al. [42] reported $\gamma = 0.004$ at a relative humidity (RH) of 100%, rising to 0.007 near RH = 120%, indicating a possible mild negative temperature dependence when high RH values from this and other studies are compared. Excluding the JPL data, the other data obtained at high RH (~90%) were averaged, assuming no temperature dependence, to yield $\gamma = 0.0043 \pm 0.0021$. The strong dependence on RH and the possible temperature dependence suggest that systematic error probably exceeds the calculated statistical error. Within the experimental accuracy, the data of Hanson and Ravishankara [245, 248] show that measured uptake coefficients are independent of ice substrate thickness. Barone et al. report very similar uptake coefficients for nitric acid dihydrate (NAD) as for NAT as a function of RH at 202 K. See Henson et al. [261] for discussion of a model which accounts for the effect of HNO₃ on the reaction of ClONO₂ on water and nitric acid ice surfaces. [Back to Table](#)

81. ClONO₂ + H₂SO₄•nH₂O(l). Results from wetted-wall flow tube (Hanson and Ravishankara [251]) Knudsen cell reactor (Manion et al. [388]), aerosol flow tube (Hanson and Lovejoy [240]), and droplet train uptake (Robinson et al. [471]) experiments supplement older wetted-wall flow tube (Hanson and Ravishankara, [242]) and Knudsen cell measurements (Rossi et al. [482], Tolbert et al [563]). Although earlier Knudsen cell measurements probably suffered from surface saturation, more recent results compare well with those from other techniques. Saturation free results, available over a temperature range of 200–265 K and a H₂SO₄ concentration range of 39 to 75 wt.%, were fit to a phenomenological model developed by Robinson et al. [471]. Measured γ values depend strongly on H₂SO₄ concentration and vary modestly with temperature, with a trend to somewhat higher values for the 210–220 K temperature range. The temperature-dependent uptake model takes into account the temperature and composition dependence of the effective Henry's Law constant, liquid phase diffusion coefficient, and the liquid phase hydrolysis rate constant. The hydrolysis reaction was treated by modeling two reaction channels, a direct hydrolysis process dominating reaction at low H₂SO₄ concentrations with a reaction rate proportional to water activity and a proton-catalyzed reaction with a rate proportional to H⁺ activity, which dominates at higher acid concentrations.

The data fit to the original Robinson et al. model have been supplemented by additional wetted-wall flow tube and aerosol flow tube data from Hanson [237] and aerosol flow tube data from Ball et al. [39]. A revised kinetic model (Shi et al. [519]) incorporating these data has been developed that is based on the earlier work of Robinson et al. [471]. In this model, γ is calculated using the expression

$$\frac{1}{\gamma} = \frac{1}{\alpha} + \frac{1}{\Gamma_b^{H_2O}}$$

where,

$$\Gamma_b^{H_2O} = \frac{4H_{ClONO_2}RT}{\bar{c}} \left(D_{ClONO_2} k_{hydr} \right)^{1/2}$$

The detailed parameterizations for H_{ClONO_2} , D_{ClONO_2} , and k_{hydr} are given in the Appendix in Shi et al. [519]. As was the case for N_2O_5 hydrolysis k_{hydr} is seen to have a direct and an acid catalyzed channel. Using the same error analysis approach as in the note on N_2O_5 uptake, the model error is about 32.4% (one sigma), with $\sigma_m=32.2\%$ and $\sigma_d=4.0\%$.

In the calculation of the chlorine activation (Cl_2 production) rate under stratospheric conditions, one needs to take into account the competition between the reactions of $\text{ClONO}_2 + \text{H}_2\text{O}$ and $\text{ClONO}_2 + \text{HCl}$. The presence of HCl will depress the reaction probability of ClONO_2 with H_2O . [Back to Table](#)

82. $\text{ClONO}_2 + \text{H}_2\text{SO}_4 \cdot \text{H}_2\text{O(s)}$ and $\text{H}_2\text{SO}_4 \cdot 4\text{H}_2\text{O(s)}$. Measurements by Hanson and Ravishankara [249] and Zhang et al. [626] demonstrate that the reaction probability on the tetrahydrate is a strong function of both temperature and relative humidity, both of which affect the level of adsorbed H_2O . Both groups covered the temperature range of 192–205 K. The reaction is slowest at higher temperatures and lower relative humidities. Zhang et al. [626] have parameterized their data in the form of $\log \gamma = a_1 + a_2 \log x + a_3 \log^2 x$; for 195 K and x = water partial pressure in Torr: $a_1 = 10.12$, $a_2 = 5.75$ and $a_3 = 0.62$; for a water partial pressure of 3.4×10^{-4} Torr and $x = T(\text{K})$ between 182 and 206: $a_1 = 318.67$, $a_2 = -3.13$ and $a_3 = 0.0076$. Zhang et al. [630] have also measured a low value of $\gamma \sim 2 \times 10^{-4}$ on sulfuric acid monohydrate at 195 K. [Back to Table](#)
83. $\text{ClONO}_2 + \text{HCl} + \text{H}_2\text{O(s)}$. Reaction probabilities of 0.27 (+0.73, -0.13) (Leu [359]) and 0.05 to 0.1 (Molina et al. [415]) were reported at 195 and 185 K, respectively. Abbatt and Molina [9] and Hanson and Ravishankara [242] report that a portion of the reaction may be due to $\text{HOCl} + \text{HCl} \rightarrow \text{Cl}_2 + \text{H}_2\text{O}$, with HOCl formed from $\text{ClONO}_2 + \text{H}_2\text{O(s)} \rightarrow \text{HOCl} + \text{HNO}_3(\text{s})$. Hanson and Ravishankara [243] saw no enhancement of the ClONO_2 reaction probability when $\text{H}_2\text{O(s)}$ is doped with HCl . Their preferred value at 192 K is $\gamma = 0.3$, but this is consistent with $\gamma = 1$. Chu et al. [114] also report a value of 0.27 (± 0.19) at 188 K, assuming no correction for porosity, but suggest the true value is 0.10 (± 0.08). Using a Knudsen cell technique and looking at initial uptake, Oppliger et al. [434] measured $\gamma = 0.7$ at 180 K and 0.2 at 200 K with HCl in excess, and both Fernandez et al. [176] and McNeil et al. [396] report a value of > 0.1 at close to 200 K. McNeil et al. report that this value is substantially smaller at 218 K. Eliminating the Molina et al. points, which were taken at much higher ClONO_2 concentrations than the others, plots of the remaining data show no obvious bias when plotted as a function of reactant concentration or temperature (180–200 K). Their average value $\gamma = 0.26 \pm 0.06$. The Oppliger et al. data were presented for two HCl concentrations, differing by a factor of three. All points from both HCl concentrations were included since all the data were generally consistent with previous measurements, although the higher HCl concentrations did tend to produce modestly higher uptake coefficients. Until a fuller model is available, a single temperature independent value with a moderate uncertainty due to surface porosity seems appropriate. [Back to Table](#)
84. $\text{ClONO}_2 + \text{HCl} + \text{HNO}_3 \cdot 3\text{H}_2\text{O}$. Measurements by Hanson and Ravishankara [243, 245], Leu and co-workers in Moore et al. [417] and Leu et al. [361], and Abbatt and Molina [9] all report high γ values (> 0.1) on NAT for temperatures between 192 and 202 K on water-rich NAT. Hanson and Ravishankara indicate that reaction probabilities on NAD are similar to those on NAT. The most recent NAT studies (Abbatt and Molina [9]) show a strong fall-off with relative humidity from $\gamma > 0.2$ at 90% RH to 0.002 at 20% RH, indicating the necessity of sufficient water to solvate reactants. Within the limited measurements, data plots show no indication that the reaction probability of $\text{ClONO}_2 + \text{HCl}$ depends on HCl and ClONO_2 gas phase concentrations or temperature between 191 and 202 K for water-rich NAT, but for nitric acid-rich NAT, there is a strong dependence on the partial pressure of HCl indicating that HCl is a limiting reagent on the surface under those conditions (Abbatt and Molina [9]). Averaged data yield $\gamma = 0.23 \pm 0.10$ for the water-rich case. Carslaw and Peter [100] have published a model of this reaction and its dependence on HCl uptake. [Back to Table](#)
85. $\text{ClONO}_2 + \text{HCl} + \text{H}_2\text{SO}_4 \cdot n\text{H}_2\text{O(l)}$. Early work by Tolbert et al. [563] and Hanson and Ravishankara [242] indicated that the presence of HCl had little effect on the reaction of ClONO_2 with concentrated sulfuric acid (> 65 wt.% H_2SO_4). Subsequent realization that HCl would be more soluble, and therefore a more potent reactant, in the colder, more dilute sulfuric acid aerosols characteristic of the polar stratosphere led to additional investigations by Hanson and Ravishankara [251], Zhang et al. [626], Elrod et al. [166] and Hanson [237]. All these measurements show a strong dependence of reactivity on HCl solubility, which in turn depends on water activity. The solubility of HCl in a wide range of sulfuric acid solutions has been experimentally determined by a range of techniques that agree well with current thermodynamic models.

See Robinson et al. [472] for a review. Hanson and Lovejoy [240] measured a reacto-diffusive length, ℓ , of only $0.009 \pm 0.005 \mu\text{m}$ for 60 wt.% H_2SO_4 in an aerosol flow reactor. (See Hanson et al. [254] for a definition of ℓ .) This is a factor of four lower than the value for the hydrolysis reaction of ClONO_2 showing the significant enhancement of ClONO_2 uptake due to HCl .

The $\text{ClONO}_2 + \text{HCl}$ reaction on sulfuric acid has been modeled in Shi et al. [519] using the same phenomenological model for ClONO_2 hydrolysis driven uptake by sulfuric acid. Since the effect of HCl on the ClONO_2 uptake is to increase the ClONO_2 pseudo-first-order reaction rate, the model of ClONO_2 uptake (see note on ClONO_2 uptake on sulfuric acid) should include the pseudo first order reaction rate, k_{HCl} . The formulation of k_{HCl} is found in the Appendix in Shi et al. [519]. It is likely that the ClONO_2 reaction with HCl , like the ClONO_2 hydrolysis reaction, is acid catalyzed via protonated HClONO_2^+ , where Cl^+ is activated as in the case of $\text{HOCl} + \text{HCl}$. For the $\text{ClONO}_2 + \text{HCl}$ reaction, there is also a surface reaction (Hanson [237]). Hanson proposed that Γ_s is linearly proportional to water activity; however, the calculated value of γ_o at 250 K and 60 wt.% H_2SO_4 using his formulation is 0.02 (here $\gamma_o \sim \Gamma_s$), which is contradictory to his aerosol flow reactor result, which yielded $\gamma_o = 0.0079$ (here $\gamma_o \sim \Gamma_b$) (Hanson and Lovejoy [240]). In the model presented in the Shi et al. appendix, it is assumed that Γ_s is linearly proportional to Henry's law constant of ClONO_2 , rather than the water activity. The temperature dependence of Γ_s is determined, based on two measured values of Γ_s at 203 K (Hanson, [237]) and 250 K (Hanson and Lovejoy, [240]). The model yields a value of $\gamma_o \sim 0.011$ (here $\gamma_o \sim \Gamma_s$), which is close to the measured value.

In the stratosphere, when the reaction rate of ClONO_2 with HCl exceeds the flux of HCl to the particle surface, HCl is depleted. This, in turn, will depress the rate of both the ClONO_2 and $\text{HOCl} + \text{HCl}$ reactions, and increase the ClONO_2 hydrolysis rate. Shi et al. [519] have proposed a model in which this effect is taken into account by including a factor F_{HCl} (see Table A-3 in Shi et al.). The formulation of F_{HCl} is based on scaling HCl reaction and accommodation fluxes. This flux correction is not exact (i.e. it does not rigorously calculate the HCl surface or bulk concentration) but provides a good approximation to the expected reduction in $\text{HCl} + \text{ClONO}_2/\text{HOCl}$ reactivity and, just as importantly, the effective increase in $\text{ClONO}_2 + \text{H}_2\text{O}$ reactivity when $p_{\text{ClONO}_2} > p_{\text{HCl}}$. This is particularly relevant during cold Cl activation events when HCl can be removed almost completely (i.e., see Jaegle et al. [297]).

Using the same error analysis approach as in the note on N_2O_5 uptake by sulfuric acid, the error of using the model in the Appendix is about 40.0% (one sigma), with $\sigma_m = 39.8\%$ and $\sigma_d = 4.0\%$. [Back to Table](#)

86. $\text{ClONO}_2 + \text{HCl} + \text{H}_2\text{SO}_4 \cdot \text{H}_2\text{O}(\text{s})$ and $\text{H}_2\text{SO}_4 \cdot 4\text{H}_2\text{O}(\text{s})$. This reaction has been studied by Hanson and Ravishankara [249] and Zhang et al. [626]. The reaction probability is strongly dependent on the thermodynamic state of the SAT surface, which is controlled by the temperature and the water vapor partial pressure. At a water vapor pressure of 5.6×10^{-4} Torr the measured γ drops by over two orders of magnitude as the SAT surface temperature rises from 195 to 206 K. The results from the two groups are in qualitative agreement, but sample different H_2O and HCl partial pressures. Zhang et al. have parameterized their data as a function of water partial pressure (at 195 K) and temperature (both at an HCl partial pressure of 4 to 8×10^{-7} Torr) in the form $\log \gamma = a_1 + a_2 \log x + a_3 (\log x)^2$. For H_2O partial pressure, $a_1 = 5.25$, $a_2 = 1.91$, and $a_3 = 0.0$; for $T(\text{K})$, $a_1 = 175.74$, $a_2 = -1.59$, and $a_3 = 0.0035$. Care must be taken in extrapolating either data set to lower HCl concentrations. Zhang et al. [630] measured no enhancement of ClONO_2 uptake on sulfuric acid monohydrate at 195 K with $(2-8) \times 10^{-7}$ Torr of HCl present, implying $\gamma < 1 \times 10^{-4}$. [Back to Table](#)
87. $\text{ClONO}_2 + \text{HCl} + \text{Al}_2\text{O}_3(\text{s})$. Molina et al. [414] used flow tube techniques to measure $\gamma = 0.020 \pm 0.005$ on α -alumina at 195–230 K with stratospheric (5 ppmV) water vapor levels. Measured γ was independent of T and was affected very little by 5 ppbv HNO_3 vapor. The same γ was measured for a Pyrex surface, indicating the absorbed water and not the inorganic substrate hosted the reaction. [Back to Table](#)
88. $\text{ClONO}_2 + \text{NaCl}$. Timonen et al. [559] studied the uptake of ClONO_2 on NaCl powders at 296 K and 225 K using a flow tube. Complete deactivation of the surface was observed at 225 K but not at 296 K. The uptake coefficients, after correction (typically by an order of magnitude) using the pore diffusion model of Keyser et al. [333, 334] were $\gamma_0 = (4.6 \pm 3.1) \times 10^{-3}$ (1 σ) at 296 K and $\gamma_0 = (6.7 \pm 3.2) \times 10^{-3}$ (1 σ) at 225 K. Similarly low values for the uptake coefficient are reported by Zelenov et al. [623] using a flow tube approach. On the other hand, Caloz et al. [94] used a Knudsen cell and found that the initial uptake coefficient was 0.23 ± 0.06 , independent of the type of salt used (powders, single crystals, deposited salt films) and without applying a correction for pore diffusion since no mass dependence for γ was observed;

in similar studies. Aguzzi and Rossi [13] measured a value of $\gamma_0 = 0.10 \pm 0.05$ for the uptake of ClONO_2 on NaCl and 0.27 ± 0.10 for uptake on the unreactive NaNO_3 and Na_2SO_4 salts. The Cl_2 yield was 100% for NaCl, in agreement with the earlier studies [94, 559] but $27 \pm 7\%$ on the unreactive salts. Koch and Rossi [345] used a diffusion tube technique to measure a value of 0.1 for the uptake coefficient. Gebel and Finlayson-Pitts [197] used a Knudsen cell and measured an initial value of $\gamma_0 = 0.14 \pm 0.11$ (2σ) and a steady-state value of $\gamma = (3.9 \pm 1.8) \times 10^{-2}$, but concluded that approximately two layers of salt were sampled in these multi-layer experiments. The use of a single or sub-single layer of NaCl gave a steady state value corrected using the model of Hoffman et al. of $\gamma = (2.4 \pm 1.2) \times 10^{-2}$ [266]. The source of the very disparate results from the different groups and techniques is not clear. All studies agree that the yield of Cl_2 is 100%, consistent with $\text{ClONO}_2 + \text{NaCl} \rightarrow \text{Cl}_2 + \text{NaNO}_3$ as observed earlier [181], with small amounts of HOCl from hydrolysis of ClONO_2 on the surface being observed in the presence of water.

Deiber et al. [150] studied the uptake of ClONO_2 on water, NaCl and NaBr solutions using a droplet train flow reactor. The uptake coefficient was the same on water and 0.1 M NaCl, and Cl_2 was observed as the gas phase product. [Back to Table](#)

89. $\text{ClONO}_2 + \text{KBr}$ and NaBr. Caloz et al. [94] and Aguzzi and Rossi [13] report a rapid uptake of ClONO_2 on KBr solid salts at room temperature, $\gamma_0 = 0.35 \pm 0.06$ and $\gamma_0 = 0.18 \pm 0.07$ respectively; corrections for pore diffusion were not applied but are not expected to be large at these high uptake coefficients (see Introduction). This is consistent with a value of 0.1 measured by Koch and Rossi [345] using a diffusion tube technique. The reaction products are BrCl , Br_2 and Cl_2 . BrCl is the initial reaction product formed from $\text{ClONO}_2 + \text{KBr} \rightarrow \text{BrCl} + \text{KNO}_3$. Br_2 is generated in a secondary reaction of BrCl with KBr: $\text{BrCl} + \text{KBr} \rightarrow \text{Br}_2 + \text{KCl}$. Cl_2 is then formed as the surface KBr is converted to KCl, which then reacts with ClONO_2 .

Deiber et al. [150] studied the uptake of ClONO_2 on water, NaCl and NaBr solutions using a droplet train flow reactor. On NaBr, the uptake increased from 0.041 at 0.01 M NaBr to 0.073 at 1 M NaBr. From the dependence on the NaBr concentration, a value for the mass accommodation coefficient for ClONO_2 of 0.108 ± 0.033 (2σ) was obtained. The gas phase products were BrCl and Br_2 , the latter formed by secondary reactions of BrCl with Br^\cdot . [Back to Table](#)

90. $\text{ClONO}_2 + \text{sea salt}$. Gebel and Finlayson-Pitts [197] reported a rapid reaction between ClONO_2 and synthetic sea salt, with initial values based on the geometric sample area of $\gamma_0 = 0.42$ and steady-state values of $\gamma = 0.16$ (2σ). These were measured with multiple salt layers (3 - 236) but corrections for diffusion into underlying layers for such high uptake coefficients are relatively small, less than a factor of three. The yield of Cl_2 was $78 \pm 13\%$; small amounts of HCl and HOCl were also observed as products. The recommended lower limit is based on these studies and the rapid uptake of other reactive species such as HNO_3 and N_2O_5 . [Back to Table](#)
91. $\text{ClONO}_2 + \text{HBr} + \text{H}_2\text{O}(\text{s})$ and $\text{HNO}_3 \cdot n\text{H}_2\text{O}(\text{s})$. This reaction was studied by Hanson and Ravishankara [246] on water ice and NAT near 200 K. A diffusion-limited reaction probability of >0.3 was observed. Allan et al. [25] measured $\gamma = 0.56 \pm 0.11$ at 200 K on water ice, observing Cl_2 and Br_2 to be formed in yields of 100% and 66 to 80%, respectively, in the range 180 to 200 K. [Back to Table](#)
92. $\text{ClONO}_2 + \text{HF} + \text{H}_2\text{O}(\text{s})$ and $\text{HNO}_3 \cdot n\text{H}_2\text{O}(\text{s})$. Hanson and Ravishankara [246] were not able to observe this reaction on water ice and NAT surfaces near 200 K. [Back to Table](#)
93. $\text{CF}_x\text{Cl}_{(4-x)}$ ($x=0-3$) and $\text{CF}_2\text{Br}_2 + \text{Al}_2\text{O}_3(\text{s})$. Robinson et al. [469] reported steady-state dissociative uptake of CF_2Cl_2 and CF_2Br_2 on α -alumina surfaces at 210 and 315 K. Reaction probabilities of about 1×10^{-3} at 210 K were measured by monitoring the amounts of surface species bonded to the Al_2O_3 substrate. A re-analysis (Robinson et al. [470]) lowered this value by about a factor of 50. Moderate surface dosage with water vapor did not quench the reaction. In addition, Dai et al. [139] and Robinson et al. [468] studied dissociative chemisorption of CF_3Cl , CF_2Cl_2 , CFCl_3 , and CCl_4 on dehydroxylated γ -alumina powders. The obtained reactive uptake probabilities ranging from 0.4×10^{-5} for CFCl_3 to 1.0×10^{-5} for CF_2Cl_2 over a temperature range of 120 to 300 K. HCl and halomethyl radicals were observed as desorption products. Loss of these products may point to somewhat higher γ s, since they were measured by integrating halogen bound to Al_2O_3 substrates. [Back to Table](#)
94. $\text{BrCl} + \text{NaCl}$, NaBr, KBr and NaI. The uptake of BrCl on solid NaCl and KBr using a Knudsen cell has been reported by Aguzzi and Rossi [13], yielding 298 K values of 6×10^{-2} for NaCl and 0.14 on KBr. An

earlier preliminary study from the same group reported a value at $\gamma > 0.1$ on KBr [94]. Insufficient data are available to make a recommendation.

Katrib et al. [325] measured the uptake of BrCl on aqueous solutions of NaI over the temperature range from 273 to 288 K; the uptake coefficient increased from 0.37×10^{-2} to 0.7 as the I^- concentration increased from 1×10^{-4} to 0.5 M NaI. The complex dependence on the I^- concentration indicated that a surface reaction was occurring at the air-solution interface.

Huff and Abbatt [276] studied the loss of BrCl on frozen bromide salt solutions at 233 K, finding that the uptake coefficients vary between 0.02 and 0.04 depending on the bromide concentration, independent of solution acidity. [Back to Table](#)

95. $Br_2 + NaCl$, KBr and NaI. Only one report of the uptake of Br_2 on solid NaCl and KBr using a Knudsen cell is available [13] as part of a study of $BrONO_2$ uptake on salts. The uptake coefficient for Br_2 was 4×10^{-3} on NaCl and 3×10^{-3} on KBr. Insufficient data are available to make a recommendation.

Hu et al. [272] measured the uptake of Br_2 on aqueous solutions of NaI using a droplet train flow reactor over the temperature range of 263 to 293 K. The measured uptake coefficients decreased from 0.33 at 263 K to 0.08 at 293 K, with evidence for a significant contribution from a reaction at the interface between Br_2 and I^- . [Back to Table](#)

96. $BrO + H_2O(s)$, $H_2SO_4 \cdot nH_2O(l)$ and $NaCl(aq)$. Abbatt [3] used a coated flow tube technique to measure heterogeneous uptake on water ice, 60 and 70 wt.% H_2SO_4 at 213 K, and 23 wt.% aqueous NaCl at 253 K. He obtained $\gamma(ice) = (1.0 \pm 0.4) \times 10^{-3}$, $\gamma(60 \text{ wt.\% } H_2SO_4) = (7 \pm 2) \times 10^{-4}$, $\gamma(70 \text{ wt.\% } H_2SO_4) = (5 \pm 2) \times 10^{-4}$ and $\gamma(23 \text{ wt.\% } NaCl) < 3 \times 10^{-3}$. He observed product Br_2 , indicating BrO self-reaction on both water ice and sulfuric acid solutions. Since reaction rate will depend on BrO concentrations, no recommendation is made for an atmospheric rate. [Back to Table](#)

97. $HOBr + H_2SO_4 \cdot nH_2O$. Hanson[232] reported that uptake of HOBr on 80wt.% H_2SO_4 , producing Br_2 . Br_2 and Br_2O production was also observed by Iraci et al. [292] during Knudsen cell studied of HOBr uptake on 70 wt.% uptake for temperatures below 228K. These products probably arise from HOBr self-reaction, although impurities in the acid solution might also play a role. Iraci et al. discuss methods to correct HOBr uptake data for the effects of self-reaction and secondary reactions with its products. The bulk phase self-reaction of HOBr noted above is not likely to be significant over the expected range of atmospheric concentrations. [Back to Table](#)

98. $HOBr + HCl + H_2O(s)$. Abbatt [1] measured $\gamma = 0.25 (+0.10/-0.05)$ for this reaction on ice at 228 K. Chaix et al. [103] measured $\gamma = 0.3$ on ice from 180 to 195 K, dropping to ~ 0.15 at 205 K. The BrCl product was observed by mass spectrometry. Allan et al. [24] report a faster rate for this reaction than for HOBr uptake on pure ice (which had an uptake coefficient of 0.15 at 200 K). Mossinger et al. [419] report a lower limit for γ of 0.1, under conditions with HCl concentration in excess of the HOBr concentration. No data on NAT surfaces is available. [Back to Table](#)

99. $HOBr + HCl + H_2SO_4 \cdot nH_2O$. For the sulfuric acid reaction, Abbatt [2] measured γ s of ~ 0.1 to 0.2 for $[HCl] > 1 \times 10^{12} \text{ cm}^{-3}$ over 68.8 wt.% H_2SO_4 at 228 K; yielding an estimated $k_{HCl+HOBr}^{II} = 1.4 \times 10^5 \text{ M}^{-1} \text{ s}^{-1}$ with a factor of 2 uncertainty. Hanson and Ravishankara [252] also measured $\gamma \leq 0.2 (+0.2, -0.1)$ for 60 wt.% H_2SO_4 at 210 K. However, both of these measurements were based on significant underestimation of the solubility of HOBr in the relevant sulfuric acid solutions. More recent measurements by Waschewsky and Abbatt [594] indicate that the Henry's law constant for HOBr varies slightly with acidity between 60 to 70 wt.% H_2SO_4 and more strongly with temperature between 208 and 238 K. (For 59.7 wt.% H_2SO_4 , H (M atm^{-1}) = 1.2×10^6 at 208 K and 2.2×10^5 at 228 K.) The $HOBr + HCl$ second order liquid phase rate constant, $k_{HCl+HOBr}^{II}$, varies between 2×10^5 and $3 \times 10^8 \text{ (M}^{-1} \text{ s}^{-1})$ between 213 and 238 K over the same composition range (60–70 wt.% H_2SO_4). Such a strong dependence on acid composition for the reaction rate of $HOBr + HCl$ and the very small acid composition dependence for HOBr solubility in H_2SO_4 solution might be partially due to the formation of H_2OBr^+ in the acidic solution as discussed in their paper. However, this acid catalyzed reaction, i.e. $H_2OBr^+ + HCl$, alone does not completely account for measured reaction rates over the acid composition range studied.

Using the Henry's Law data for HOBr reported by Waschewsky and Abbatt [594], the limiting reagent will vary depending on atmospheric temperature (H_2SO_4 wt.%) and the concentrations of HOBr and HCl. For stratospheric conditions where [HOBr] is 10 pptv and [HCl] 1 ppbv, they predict dissolved HOBr will be in

excess above 204 K and HCl in excess below 204 K for a H₂O vapor partial pressure of 3×10^{-7} atm. From their coated wall flow reactor uptake measurements, Waschewsky and Abbatt [594] derived expressions for $k_{\text{HCl+HOBr}}^{\text{II}}$ and predicted uptake coefficients. For temperature between 204 and 218 K where HOBr is likely to be in excess, they calculated HCl uptake coefficients, γ_{HCl} , which range between 7×10^{-5} and 9×10^{-5} . For temperatures in the 202–198 K range, where dissolved HCl is likely to be excess, the calculated uptake coefficients for HOBr, γ_{HOBr} , of $\sim 1 \times 10^{-2}$. Hanson has reported Henry's law solubility data for 58–70 wt.% sulfuric acid and reactive uptake coefficients for HCl on HOBr doped sulfuric acid surfaces using a wetted wall flow reactor [232]. Hanson's reported that H_{HOBr} was independent of acid concentration at 250 K, however, the heat of solvation for HOBr derived is significantly lower (-12.5 ± 3.7 versus -9 ± 1 kcal/mol reported at lower temperatures by Waschewsky and Abbatt) that the values of H^* based on Hanson's data, taken from 250 to 270 K, are much higher than the prior study's when extrapolated to their lower temperatures. Hanson's reported γ_{HCl} are strongly dependent on HOBr partial pressure and drop almost three orders of magnitude as the sulfuric acid concentration is raised from 58 to 95 wt.%, possibly because HCl may be reacting with sulfuric acid at higher acid concentrations. The higher temperature $k_{\text{HCl+HOBr}}^{\text{II}}$ values computed by Hanson for his data disagree, when extrapolated to lower temperatures with the values reported by Waschewsky and Abbatt as well as a prior lower temperature value reported by Hanson and Ravishankara [252]. Better agreement can be obtained if the solvation enthalpy reported by Hanson is used to adjust the H_{HOBr} values used in the earlier, lower temperature studies. Clearly, the HOBr + HCl reaction will be difficult to parameterize in a simple manner. Potential inconsistencies in their $k_{\text{HCl+HOBr}}^{\text{II}}$ values, as discussed by Waschewsky and Abbatt [594] and Hanson [232] indicate that further measurements are required before this reaction can be definitively modeled. Iraci et al. [292] subsequently measured HOBr uptake over both of the temperature ranges covered in the prior experiments. Their derived H^* values agreed well with data from Waschewsky and Abbatt [594] at lower temperatures but fell far below Hanson's higher temperature measurements. Thus, it appears that HOBr + HCl kinetic parameters developed from analyses based on the Hanson [232] data may need to be reanalyzed. [Back to Table](#)

100. HOBr + HBr + H₂O(s) and H₂SO₄ • nH₂O. Abbatt [1] measured $\gamma = 0.12 \pm (0.03)$ on ice at 228 K. Chai et al. [103] measured γ_0 values ranging from 0.44 at 180 K to 0.15 at 205 K. The Br₂ product was observed by mass spectrometry. The HBr concentrations were such that the ice surface had probably melted. Abbatt [2] measured $\gamma = 0.25$ for $[\text{HBr}] = 1 \times 10^{12} \text{ cm}^{-3}$ over 68.8 wt.% H₂SO₄ at 228 K; yielding an estimated $k_{\text{II}} > 5 \times 10^4 \text{ M}^{-1} \text{ s}^{-1}$. [Back to Table](#)
101. HOBr + NaCl. Studies have been done on solid salts and aqueous surfaces. On solids, Mochida et al. [412] studied the uptake of HOBr on NaCl using multi-layer powders (10 - 500 μm) in a Knudsen cell at room temperature. After correction (by about an order of magnitude) for diffusion into the underlying layers, they obtained values for the initial uptake coefficient in the range of $(0.97 - 6.5) \times 10^{-3}$, with the corrected values decreasing with increasing concentrations of HOBr. They attributed this to competition between the reaction of HOBr with NaCl and a self-reaction of HOBr on the surface: $2 \text{HOBr} \rightarrow \text{Br}_2 + \text{H}_2\text{O} + \frac{1}{2} \text{O}_2$. Their final value of $\leq 6.5 \times 10^{-3}$ is based on their extrapolation back to very low HOBr concentrations. Both Br₂ and BrCl were observed as products. Chu et al. [112] measured the uptake of HOBr on NaCl at 250 K over a range of RH from 1.5 to 22.5%. After correcting the measured loss of HOBr by a factor of ~ 30 for diffusion into the underlying salt layers using the pore diffusion model, they obtained a value $\gamma_0 = 5 \times 10^{-5}$. The smaller value compared to the Knudsen cell results of Mochida et al. [412] may be due to the much lower temperature they used; BrCl was the only gas phase product observed. Huff and Abbatt [277] report reactivity with frozen NaCl solutions in a coated-wall flow tube at 233 K. Uptake coefficients were dependent on the chloride concentration of the solution and on the acidity, with faster kinetics on the more acidic surfaces. BrCl was the only product observed.

Abbatt and Waschewsky [11] measured the uptake of HOBr on deliquesced 1 - 5 μm NaCl particles (75% RH); for particles at pH values of 0.3 and 7.2, a lower limit to the uptake coefficient of $\gamma_0 > 0.2$ was measured. On unbuffered particles, the upper limit for the uptake coefficient was $\gamma_0 < 1.5 \times 10^{-3}$ due to the limited availability of H^+ for the reaction between HOBr and Cl^- to form BrCl. Somewhat smaller values have been measured by Pratte and Rossi [453] in another aerosol flow tube experiment, using acidified NaCl particles. Acidification was necessary for the reaction to be observable. In general, the uptake coefficients varied from 1 to 10×10^{-3} from 70 to 90% relative humidity. The particles were acidified with quite large amounts of H₂SO₄, and the authors show that the reactivity on pure H₂SO₄ is less than that on

the acidified salts. This could be a reason for the disagreement between the lower limit of Abbatt and Waschewsky and the Pratte and Rossi results. [Back to Table](#)

102. HOBr + NaBr and KBr. Mochida et al. [412] studied the uptake of HOBr on solid KBr using multi-layer powders and spray-deposited films in a Knudsen cell. After correction (by factors of ~ 4-5) for diffusion into the underlying layers for the powders, they obtained values for the initial uptake coefficient in the range of $(1.3 - 8.4) \times 10^{-2}$, with the corrected values again decreasing with increasing concentrations of HOBr due to the self-reaction of HOBr on the surface: $2 \text{HOBr} \rightarrow \text{Br}_2 + \text{H}_2\text{O} + \frac{1}{2} \text{O}_2$. On spray-deposited films where correction for diffusion into the underlying layers is not necessary, a value of 0.18 ± 0.04 was measured. The recommended upper limit is based on their extrapolation back to very low HOBr concentrations for the powders, and the spray-deposited film results. Br₂ was the only product observed.

Chu et al. [112] measured the uptake of HOBr on NaBr at 250 K in a flow tube at RH from 0.5 to 12 %. After correction by approximately an order of magnitude for diffusion of HOBr into the underlying salt layers using a pore diffusion model, a value for γ_0 of 2.5×10^{-3} was obtained; the smaller value may be due to the much lower temperature at which these studies were carried out. Again, Br₂ was the only product observed.

The uptake of HOBr on aqueous solutions of NaBr has been measured by Wachsmuth et al. [588] and by Fickert et al. [177]. Wachsmuth et al. [588] report a rapid rate of uptake that is limited by mass accommodation; the mass accommodation coefficient was calculated to be 0.6 ± 0.2 . This is consistent with the studies of Fickert et al. [177] who reported a lower limit for the mass accommodation coefficient of 1×10^{-2} at 274 K and observed that Br₂ was released at 100% yield at pH < 6.5. The yield of Br₂ decreased rapidly with pH at higher pH values due to the declining ratio of HOBr to BrO⁻. Fickert et al. [177] also measured the uptake of HOBr on aqueous solutions containing mixtures of NaCl and NaBr. BrCl was the major product at small Br⁻ concentrations while Br₂ dominated as the bromide ion concentration in solution increased.

Finally, there have been a number of coated-wall flow tube studies of HOBr reactivity on frozen salt solutions containing both NaCl and NaBr (Kirchner et al., [336]; Huff and Abbatt[277]; Adams et al., [12]). HOBr uptake coefficients are in the 10^{-2} to 10^{-3} range at roughly 233 K. A general finding is that if the HOBr concentrations are too high, then only BrCl is seen as a gas-phase product from films composed of the (low) seawater ratios of bromide to chloride. The reason for this is that the small concentrations of bromide at the surface are rapidly depleted, leaving only chloride available for reaction. However, for low HOBr concentrations (10^9 to 10^{10} molecules/cm³), as used by Adams et al., Br₂ is observed as the initial product. [Back to Table](#)

103. BrNO₂ + H₂O(l). Behnke, George and co-workers have used wetted wall flow reactor techniques to investigate the reactive uptake of BrNO₂ on aqueous solutions from 276 to 298 K [507] and [175]. Measured reactive uptake coefficients range from 1 to 3.5×10^{-6} with a small positive temperature dependence. [Back to Table](#)
104. BrNO₂ + KCl and NaCl. Caloz et al. [95] measured an uptake coefficient for BrNO₂ on KCl of 5×10^{-2} , but concluded that it was due only to reaction with a small bromide impurity in the KCl; as expected if this is the case, only Br₂ was generated in the reaction.

The uptake of BrNO₂ on aqueous solutions of 0.5 M NaCl has been measured using a droplet train flow reactor by Schweitzer et al. [507] from 277 - 293 K yielding $\gamma_0 \sim 1 \times 10^{-5}$. Frenzel et al. [192] used a wetted wall flow tube to obtain a lower limit for the uptake coefficient of 3.8×10^{-5} at 291 K. [Back to Table](#)

105. BrNO₂ + KBr, NaBr and NaI. Caloz et al. [95] used a Knudsen cell to study the uptake of BrNO₂ on solid KBr powders. The uptake was fast, $\gamma_0 \geq 0.3$, with production of Br₂ as the gas phase product.

On aqueous solutions of NaBr, the uptake coefficient increases as the concentration of NaBr increases [192, 507, 508]. For example, at 278 K, γ_0 increased from 8.6×10^{-6} to 1.1×10^{-4} as the NaBr concentration increased from 5×10^{-4} to 5×10^{-2} , but was independent of temperature over the range from 275 - 293 K [508]. The major gas phase product is Br₂, with smaller amounts of BrNO₂ and only at the smaller concentrations of NaBr [507, 508].

The uptake of BrNO₂ on aqueous NaI solutions has been determined using a droplet train flow reactor [507] and a wetted wall flow tube [508]; the uptake coefficient from 4.4×10^{-5} to 4.4×10^{-4} as the iodide concentration increased from 10^{-4} M to 5×10^{-3} M [508]. [Back to Table](#)

106. BrONO₂ and BrONO₂ + HCl + H₂O(s). Hanson and Ravishankara [248] investigated these reactions in an ice-coated flow reactor at 200 (±10) K. The reaction of BrONO₂ with H₂O(s) proceeded at a rate indistinguishable from the gas phase diffusion limit, implying that the reaction probability may be as high as one; the product BrNO(g) was observed. Allan et al [24] used a Knudsen cell reactor to measure BrONO₂ uptake between 190-200 K. Values of initial γ's in the 0.2-0.3 range were observed. An average $\gamma = 0.26 \pm 0.05$ was obtained from all of the appropriate data from both experiments. Aguzzi and Rossi [15] studied the hydrolysis reaction on various types of ices, obtaining $\gamma = 0.34 \pm 0.03$ at 180 K and $\gamma = 0.15 \pm 0.01$ at 210 K. They observed HOBr as the main product and Br₂O as a secondary product. Hanson and Ravishankara [248] also codeposited HCl with BrONO₂ observing rapid production of BrCl. It is unclear whether BrCl is produced directly from BrONO₂ + HCl or via HOBr (from BrONO₂ hydrolysis) reacting with HCl. [Back to Table](#)

107. BrONO₂ + H₂O(l). Deiber et al. [150] used a droplet train reactor to measure the uptake of BrONO₂ on pure water between 272 and 280 K. An apparent positive temperature dependence was observed with measured reactive uptake measurements ranging from 0.024 ± 0.0008 at 272.5 K to 0.039 ± 0.0012 at 279.7 K. [Back to Table](#)

108. BrONO₂ and BrONO₂ + HCl + H₂SO₄·nH₂O(l). Hanson and co-workers used both coated flow tube and aerosol flow tube techniques to show that the reaction of BrONO₂ with 45–70 wt.% H₂SO₄ is extremely facile at temperatures from 210 to 298 K. Hanson and Ravishankara [252] measured γs of 0.5 (+0.5, -0.25) (45 wt.% H₂SO₄, 210 K, 0.4 (+0.6, -0.2) (60 wt.%, 210 K), and 0.3 (+0.7, -0.1) (70 wt.%, 220 K) in a coated-wall flow tube experiment. Hanson et al. [253], measured $\gamma \sim 0.8$ (20 to 40% error) for submicron aerosols at temperatures between 249 and 298 K and H₂SO₄ concentrations of 45 to 70 wt.%; there was a sharp fall off in γ for H₂SO₄ concentrations between 73 and 83 wt.%. Hanson also reported additional temperature dependent (230-295 K) coated flow reactor and room temperature (295-300 K) aerosol flow reactor studies extending measurements to higher acid wt.% values [232]. Hanson has analyzed these combined data sets, the data indicated that γ is a function of sulfuric acid concentration, but independent of temperature. After eliminating one previously reported anomalously low 83 wt.% data point Hanson has fit an empirical expression for measured γs for BrONO₂ + H₂O in the form of: $1/\gamma = 1/\alpha + 1/\gamma_{\text{rxn}}$, where $\gamma_{\text{rxn}} = \exp(a+b \cdot \text{wt.})$ and $\alpha = 0.80$, and $a = 29.2$, $b = -0.40$ [232]. Using the same approach as detailed in the note for N₂O₅ uptake on sulfuric acid, the error for BrONO₂ + H₂O is 27.3% (one sigma), with $\gamma_m = 26.6\%$ and $\gamma_d = 6.3\%$. Addition of excess HCl to 229 K, 40 and 60 wt.% H₂SO₄ aerosols caused an increase in γ to 1.0 and 0.9, respectively [253]. [Back to Table](#)

109. BrONO₂ + HBr. Aguzzi and Rossi [15] measured γ over the 180-210 K temperature range, with $\gamma = 0.3$ at 180 K and an activation energy of -1.2 ± 0.2 kcal/mol. [Back to Table](#)

110. BrONO₂ + NaCl. Aguzzi and Rossi [13] used a Knudsen cell and three types of NaCl samples (powders, spray-deposited and single crystal) to measure the uptake of BrONO₂ and obtained consistent results with $\gamma_0 = 0.31 \pm 0.12$. No correction for diffusion into the powders was made because of the high uptake coefficient (see Subsection 5.6). BrCl was the major product, $80 \pm 20\%$, with smaller amounts (~ 10%) of Br₂ and some HCl. Rapid uptake of BrONO₂ of the same magnitude was observed on the unreactive salts NaNO₃ and Na₂SO₄, with a Br₂ yield of $45 \pm 10\%$; this uptake and reaction was attributed to the self-reaction of BrONO₂ on the surface to generate Br₂O which decomposed to Br₂.

Deiber et al. [150] studied the uptake of BrONO₂ on water, NaCl and NaBr solutions using a droplet train apparatus from 272 - 280 K. The uptake coefficient was the same on water and 0.1 M NaCl, where BrCl was observed as the gas phase product. On NaBr, the uptake increased with the square root of the NaBr concentration, from which a value for the mass accommodation coefficient for BrONO₂ of 0.063 ± 0.021 (2 σ) was obtained. [Back to Table](#)

111. BrONO₂ + KBr and NaBr. Aguzzi and Rossi [13] used a Knudsen cell and three types of KBr samples (powders, spray-deposited and single crystal) to measure the uptake of BrONO₂ and obtained consistent results with $\gamma_0 = 0.33 \pm 0.12$. No correction for diffusion into the powders was made because of the high uptake coefficient (see Subsection 5.6). Br₂ was the major product, with its yield decreasing as the

concentration of BrONO₂ increased; this was attributed to a competition between the reaction of BrONO₂ with KBr and the self-reaction of BrONO₂ on the surface.

Deiber et al. [150] studied the uptake of BrONO₂ on water, NaCl and NaBr solutions using a droplet train flow reactor from 272 - 280 K. The uptake coefficient was the same on water and 0.1 M NaCl. On NaBr, the uptake increased with the square root of the NaBr concentration, from which a value for the mass accommodation coefficient for BrONO₂ of 0.063 ± 0.021 (2σ) was obtained. The gas phase product on the NaBr solution was Br₂. [Back to Table](#)

112. ICl on NaCl/NaBr. ICl uptake onto acidified and neutral NaCl/NaBr solutions at 274 to 298 K was studied in coated-wall flow tubes. The initial uptake coefficients were in the 0.6 to 3×10^{-3} range depending on the experimental system used, for solutions containing bromide; IBr was the gas-phase product observed. In an aerosol flow tube, uptake of ICl onto concentrated NaBr solutions showed uptake coefficients of 1 to 2×10^{-2} , which dropped to values of 10^{-4} on sea-salt solution aerosols. IBr was the product of the reaction on NaBr particles, with a yield of 0.6 (Braban et al. [82]). [Back to Table](#)
113. HOI on NaCl/NaBr. HOI uptake on acidified and neutral NaCl/NaBr solutions at 274 K in a wetted-wall flow tube indicate a lower limit for the uptake coefficient of 2.2×10^{-3} (Braban et al. [82]). IBr is identified as the major gas-phase product when the solutions contain bromide to chloride ratios of $1:200$, whereas ICl is the product from pure NaCl solutions. HOI uptake on dry and frozen solutions of NaCl and NaBr with chloride to bromide ratios equal to that of seawater were also studied in a coated wall-flow tube. The product ICl is only formed when the surface is depleted of bromide, otherwise IBr forms. Uptake coefficients are > 0.01 at 243 K on the frozen films, and > 0.01 at 243 K and 298 K on dry salts. Mossinger and Cox [418] report uptake of HOI onto dry films of NaCl, NaBr and sea salt from 278 to 298 K and measured uptake coefficients of 0.016 , 0.034 and 0.061 respectively. The products are ICl, IBr and IC/IBr, respectively. [Back to Table](#)
114. CF₃OH + H₂O + H₂O(l) and H₂SO₄ • nH₂O(l). Lovejoy et al. [380] used both wetted-wall and aerosol flow tube techniques to measure reactive uptake of CF₃OH on water at 274 K and 39–60 wt.% H₂SO₄ at various temperatures between 206 and 250 K. γ 's showed a strong dependence on water activity. Aerosol uptake studies yielded reacto-diffusive lengths of $> 0.4 \mu\text{m}$ for 40 wt.% H₂SO₄ and $1.0 \mu\text{m}$ for 50 wt.% H₂SO₄, both at 250 K. Recommended γ 's were estimated by averaging bulk uptake measurements at similar H₂SO₄ concentrations and ignoring temperature effects on water activity. [Back to Table](#)
115. O₃ + SO₂ + Al₂O₃(s). Usher et al. [574] present Knudsen cell data showing that pretreatment of α -alumina with SO₂ increases γ_o values for O₃ uptake by 30%; FTIR observations by the same group show that O₃ oxidized surface sulfite and bisulfite formed by SO₂ absorption to sulfate and bisulfate. [Back to Table](#)
116. SO₂ on H₂O₂/ice. SO₂ loss on ice surfaces has been observed to proceed when H₂O₂ is present, making the reaction of potential significance in ice clouds. Clegg and Abbatt [129] have observed this reaction when both SO₂ and H₂O₂ are delivered from the gas phase in a coated-wall flow tube at 228 K, with H₂O₂ in excess. For both SO₂ and H₂O₂ only small fractions of a monolayer are present on the surface during the reaction. It is inferred that the reaction proceeds through the HSO₃⁻ intermediate because the reaction rate declines as acidity builds up on the surface from the sulphuric acid product, i.e. because dissociation of adsorbed SO₂ to form HSO₃⁻ is becoming inhibited. At about 200 K, relative to the uptake on pure ice, Chu et al. [110] observe enhanced loss of SO₂ on ice films that have been doped with 3% H₂O₂ and they detect sulphate as a product. Uptake coefficients are reported in Clegg and Abbatt that are dependent on both the H₂O₂ and SO₂ partial pressure, so no single value prevails for atmospheric conditions. [Back to Table](#)
117. SO₂ + H₂O₂, O₃, HONO, NO₂, HNO₃ + H₂SO₄ • nH₂O(l). Rattigan et al. [458] used a bubble train reactor to measure the uptake of SO₂ in the presence of solvated oxidants at 293 K. For H₂O₂ the second order rate constant at 1 wt.% H₂SO₄ agreed well with previous bulk kinetics measurements and with previous droplet train/flow reactor measurements. Measurements at 20, 40, and 60 wt.% H₂SO₄ are the first reported for concentrated acid. Reaction rate data were fit to a two term (acid catalyzed and water catalyzed) bulk second order rate expression, which, in the limit of high acid activity ($a_{\text{H}^+} = \alpha_{\text{H}^+}[\text{H}^+]$, where α_{H^+} is the H⁺ activity coefficient) reduces to: $k_{\text{H}_2\text{O}_2}^{\text{II}} = 8.3 \times 10^4 (\alpha_{\text{H}_2\text{O}} / a_{\text{H}^+})$, where $\alpha_{\text{H}_2\text{O}}$ is the water activity coefficient. Both α_{H^+} and $\alpha_{\text{H}_2\text{O}}$ can be obtained from the sulfuric acid thermodynamic model of Carslaw et al. [99]. The high a_{H^+} approximation for $k_{\text{H}_2\text{O}_2}^{\text{II}}$ should be accurate to a factor of two between 40 and 70 wt.%.

Uptake of SO₂ in the presence of solvated O₃ was measured for 1–70 wt.% acid; the Henry's law expression for O₃ was determined in separate experiments. Measured second order rates agree reasonably

well with previous results measured below 18 wt.%. A three term fit for reaction with $\text{SO}_2(\text{aq})$, HSO_3^- , and SO_4^{2-} was fit to the data: $k_{\text{O}_3}^{\text{II}} = 6.6 \times 10^3 [\text{SO}_2(\text{aq})] + 3.2 \times 10^5 [\text{HSO}_3^-] + 1 \times 10^9 [\text{SO}_4^{2-}]$. This expression should be accurate to a factor of two between 20 and 70 wt.%.

The HONO reaction was studied by adding nitrosyl sulfuric acid to 20, 40, 60, and 70 wt.% acid. Measured second order rate constants were moderately consistent with previous measurements below 10 wt.%. A $k_{\text{HONO}}^{\text{II}} = 142[\text{H}^+]$ was fit to the full data set; it should be accurate to a factor of two for acid concentrations between 10 and 70 wt.%.

No enhanced SO_2 uptake was observed with added gas phase NO , NO_2 , or with 20 wt.% HNO_3 added to 50–60 wt.% sulfuric acid. [Back to Table](#)

118. $\text{SO}_2 + \text{Al}_2\text{O}_3$. Goodman et al. [215] used FTIR observations of SO_2 absorption on α -alumina to show that surface bound sulfite and bisulfite products are produced, they integrated these surface feature absorbencies to estimate a γ_0 of $(9.5 \pm 0.3) \times 10^{-5}$. Usher et al. [573] performed BET corrected room temperature studies on four α -alumina samples reporting an average γ_0 of $(1.6 \pm 0.5) \times 10^{-4}$. Seisel et al. [514] measured $\gamma_0 = (7.4 \pm 0.9) \times 10^{-3}$ on γ -alumina at 298K using a pulsed Knudsen cell method. FTIR studies of SO_2 uptake on commercial γ -alumina catalyst samples also show sulfite formation on non-hydroxylated surfaces [141, 323]. Ma et al. [384] co-deposited SO_2 and NO_2 on γ -alumina surfaces, using FTIR to observe that rather than forming adsorbed nitrite or nitrate, NO_2 dimerized and the dimer oxidized SO_2 to sulfate. [Back to Table](#)
119. $\text{SO}_2 + \text{NaCl}$ and sea salt. Gebel et al. [198] reported no measurable uptake of SO_2 on NaCl , yielding an upper limit of 1×10^{-4} for the uptake coefficient. The same was true for synthetic sea salt that had been heated while pumping. However, sea salt that had not been heated or pumped on extensively had a rapid uptake of SO_2 , with initial uptake coefficients as large as 0.09. The time dependence of the uptake coefficient was consistent with uptake of SO_2 into a liquid layer, likely due to large amounts of water adsorbed on the hygroscopic components of sea salt such as magnesium hydrate. No gas phase products were observed but sulfite formation in the salt was seen by FTIR, indicating that uptake was due to dissolution of SO_2 into the water film on the salt surface. [Back to Table](#)
120. $\text{SO}_3 + \text{H}_2\text{SO}_4 \cdot n\text{H}_2\text{O}(\text{l})$. Jayne et al. [303] measured the uptake coefficient in a wetted wall-flow reactor at 300 K over a composition range of 78–92 H_2SO_4 wt.%. The measured γ was indistinguishable from 1.0. Higher water concentrations and lower temperatures probably tend to increase γ , so a value near 1.0 probably holds for all atmospheric conditions. [Back to Table](#)
121. $\text{OCS} + \text{Al}_2\text{O}_3$. Liu and co-workers have measured OCS uptake on both α -alumina and γ -alumina surfaces at 298K using Knudsen cell techniques [374] and on α -alumina surfaces with controlled water vapor levels using both a Knudsen cell and a reaction chamber equipped with diffuse reflectance infrared Fourier transform spectroscopy (DRIFTS) [375]. The DRIFTS technique was also used to investigate heterogeneous reaction mechanisms, revealing that surface Al-OH plays a major role in oxidizing adsorbed OCS to CO_2 and that a number of surface adsorbed reactive intermediate anions, including HSCO_2^- , are formed. The overall reaction is essentially a surface catalyzed hydrolysis reaction producing both CO_2 and H_2S [[260]; [372]; [375]]. Liu et al. [374] report uptake of relatively dry OCS yielding rather small $\gamma_0 = (4.9 \pm 0.5) \times 10^{-7}$ and $\gamma_{\text{ss}} = (6.5 \pm 2.4) \times 10^{-8}$ values for α -alumina and $\gamma_0 = (1.0 \pm 0.2) \times 10^{-7}$ and $\gamma_{\text{ss}} = (1.8 \pm 0.4) \times 10^{-8}$ values for γ -alumina at 298K. The low steady-state uptake coefficients are probably due to consumption of most of the surface Al-OH sites and a low regeneration rate due to limited water vapor. OCS uptake experiments that provide controlled water vapor fluxes to α -alumina surfaces produce somewhat higher γ_{ss} values in the Knudsen apparatus, and the values obtained by integrating the DRIFTS spectra for RH values between 7 and 47% fall in the range of 7.4×10^{-6} to 3.3×10^{-6} [375]. Interestingly, the highest uptake values are not obtained for the highest RH values because water vapor can also occupy reactive alumina surface sites and block OCS adsorption. [Back to Table](#)

5.15 Soot Surface Uptake Coefficients

Table 5-3. Soot Surface Uptake Coefficients

Gaseous Species	Uptake Coefficient (γ)	Notes
SO ₂	See Note	<u>1, 2</u>
NH ₃	0, See Note	<u>1, 3</u>
O ₃	See Note	<u>1, 4</u>
HNO ₃	See Note	<u>1, 5</u>
N ₂ O ₅	See Note	<u>1, 6</u>
NO ₂	See Note	<u>1, 7</u>
NO ₃	See Note	<u>1, 8</u>
HO ₂	See Note	<u>1, 9</u>
HO ₂ NO ₂	See Note	<u>1, 10</u>
H ₂ O	See Note	<u>1, 11</u>

5.16 Notes to Table 5-3

- See also the sections on soot under “Surface Types” and “Parameter Definitions” for a description of some of the factors affecting the uptake and reaction of gases on soot surfaces. In most cases, the available reactive surface area rather than the geometric areas have been used in obtaining the uptake coefficients; in those cases where the geometric area was used but a higher available surface area was involved in the measured uptake, the uptake coefficient is given as an upper limit. Most data are available at room temperature or there are very limited data at lower temperatures characteristic of the upper troposphere. [Back to Table](#)
- SO₂ + soot. $\gamma \leq 3 \times 10^{-3}$ measured using Degussa FW2 carbon black by Rogaski et al. [477]. This is an upper limit since it is based on the geometric surface area. Koehler et al. [348] measured an average value of $(2 \pm 1) \times 10^{-3}$ over the first 10–30 s on n-hexane soot at -100°C (the initial uptake may be larger), but indicate that taking into account surface roughness would reduce this value. A number of studies [36, 116, 117, 131, 348, 369, 477] suggest that uptake is primarily due to physisorption on the surface; oxidation occurs in the presence of water, oxidants and metals. [Back to Table](#)
- NH₃ + soot. Chughtai et al. [116] and Muentert and Koehler [424] measured the uptake of NH₃ on soot. Based on Muentert and Koehler [424] where conditions are closest to atmospheric, NH₃ is not taken up by soot particles at temperatures above 173 K. [Back to Table](#)
- O₃ + soot. Many studies report a rapid, initial loss of O₃ followed by a slower loss that also occurs on aged soot or soot pre-exposed to ozone [121, 125, 154, 169, 170, 287, 320, 379, 477, 526, 529, 538]. Initial, rapid O₃ loss may be most applicable for soot as it comes out of aircraft exhaust, with $\gamma^{\text{init}} \sim 10^{-3}$ from most studies using both carbon black and organic combustion soots [169, 170, 287, 477, 538]. The second stage of the reaction is probably more applicable to soot dispersed in air; $\gamma^{\text{aged}} \sim 10^{-4}$ – 10^{-6} using both carbon black and organic combustion soots [169, 170, 287, 320, 379, 450, 538], but in the range of 10^{-4} to 10^{-5} based on organic combustion soot data alone [287, 379]. A few studies have been carried out at temperatures below room temperature [121, 287, 320, 379]; given the wide ranges measured even at room temperature, these values generally fall in the same range. Il’in et al. [287] report a temperature dependence for the initial uptake on fresh soot of $\gamma^{\text{fresh}} = 1.9 \times 10^{-3}(\exp-780/T)$ and for aged soots, $\gamma^{\text{aged}} = 1.8 \times 10^{-4}(\exp-1000/T)$. Both physisorption and reaction of ozone with the surface appear to take place. The studies of Fendel et al. [169] suggest that lower particle growth in size below 40 ppb O₃ is due to less than a monolayer of O₃ on the surface. Stephens et al. [538] proposed a Langmuir-type reversible adsorption of O₃, followed by a slower reaction with the surface. Pöschl et al. [450] proposed a similar scheme for uptake of ozone on spark-generated graphite soot coated with benzo[a]pyrene. Initial reversible physisorption occurred with $\gamma \sim 10^{-3}$, and “apparent reaction probabilities” for O₃ with BaP on soot of $\gamma \sim 10^{-5}$ – 10^{-6} were reported. The presence of water inhibited the reaction, which was postulated to be due to competitive adsorption between water and ozone on the surface; this is in contrast to the report of Chughtai et al. [120] in which the rate of ozone loss increased with RH. Pöschl et al. [450] report Langmuir adsorption equilibrium constants for O₃ and H₂O, and a second order surface reaction rate constant for the O₃-BaP reaction of $(2.6 \pm 0.8) \times 10^{-17} \text{ cm}^2 \text{ s}^{-1}$. Three possible paths have been proposed: (1)

chemisorption of O_3 ; (2) catalytic decomposition of O_3 : $2O_3 \rightarrow 3O_2$; (3) surface oxidation and formation of gas-phase carbon oxides. The studies of Fendel et al. [169] suggest that lower particle growth in size below 40 ppb O_3 is due to less than a monolayer of O_3 . Studies of Smith et al. [529] and Smith and Chughtai [526] suggest that catalytic decomposition occurs to some extent over the entire reaction sequence. CO_2 and H_2O are the major gas phase and surface oxidized functional groups on the surface such as carboxylic acids are observed [120-122, 154, 169, 320, 393, 526-528, 538]. [Back to Table](#)

5. HNO_3 + soot. Studies of the uptake of HNO_3 on soot have been carried out over a range of nitric acid pressures [106, 135, 153, 337, 379, 477, 481, 489, 491]. Measured values of γ at room temperature are typically in the range 10^{-1} – 10^{-5} , with smaller uptake coefficients measured at longer reaction times. Saathoff et al. [489] report an upper limit of 3×10^{-7} as a time-averaged value over two days. At lower concentrations characteristic of the atmosphere, uptake appears to be primarily due to physisorption while at higher concentrations, $> 2 \times 10^{12}$ molecule cm^{-3} , a surface reaction occurs. At 220 K, $\gamma \sim 0.1$ with irreversible uptake attributed to reaction with surface groups [106]. Reaction of HNO_3 at concentrations from $(1-9) \times 10^{12}$ molecule cm^{-3} with “grey” soot from a rich flame using hexane has been reported [491] to generate HONO as the major gaseous product with initial and steady-state reaction probabilities of $\gamma_o = 4.6 \times 10^{-3}$ and $\gamma_{ss} = 5.2 \times 10^{-4}$ respectively; reaction with “black” soot from a lean flame gave NO as the major gaseous product, with initial and steady-state reaction probabilities of $\gamma_o = 2.0 \times 10^{-2}$ and $\gamma_{ss} = 4.6 \times 10^{-3}$ respectively (based on geometric surface area of sample holder). The NO was hypothesized to result from secondary reactions of an initial HONO product. [Back to Table](#)
6. N_2O_5 + soot. Brouwer et al. [83], Longfellow et al. [379] and Saathoff et al. [489] studied the uptake of N_2O_5 at room temperature on a ground charcoal (carbon black) sample, on propane soot and on spark-generated graphite soot, respectively. Brouwer et al. and Longfellow et al. report uptake coefficients based on the geometric sample surface area, and therefore give upper limits. An upper limit of $\gamma \leq 0.02$ can be derived based on the larger value of 0.016 reported by Longfellow et al. As discussed below, much smaller values are reported by Saathoff et al.: 4×10^{-5} under dry conditions and 2×10^{-4} at 50% RH. Three possible reactions may occur: (1) Decomposition of N_2O_5 on the surface to generate $NO_2 + NO_3$; (2) reaction of N_2O_5 with the soot; (3) hydrolysis of N_2O_5 with water on the surface to generate HNO_3 . The studies of Longfellow et al. support the decomposition reaction, with yields of NO_2 within experimental error of 100%; the generation of NO_3 on the surface followed by its decomposition to NO_2 , may contribute to the observed production of NO_2 . The studies of Brouwer et al. suggest that a redox reaction with the soot surface to generate NO occurs in parallel with hydrolysis of N_2O_5 to generate HNO_3 . Saathoff et al. propose two independent, parallel reactions: (1) hydrolysis generating HNO_3 , $N_2O_5 + \text{soot} \rightarrow 2 HNO_3$ with $\gamma = (4 \pm 2) \times 10^{-5}$ under dry conditions (< 10 ppm H_2O) which increases to $(2 \pm 1) \times 10^{-4}$ at 50% RH. (2) decomposition to NO and NO_2 : $N_2O_5 + \text{soot} \rightarrow NO + NO_2 + \text{products}$, with $\gamma = (4 \pm 2) \times 10^{-6}$ under dry conditions. [Back to Table](#)
7. NO_2 + soot. A fast initial uptake of NO_2 is observed on fresh soots [19, 21, 29, 116, 119, 123, 124, 203, 315, 337, 378, 477, 534, 545, 546] with the initial uptake coefficient in studies involving both carbon blacks and organic combustion soots in the range of $\gamma^{init} \equiv 10^{-1}$ to 10^{-4} . For longer reaction times on carbon black soots, $\gamma^{aged} \sim 10^{-4}$ based on studies by Kalberer et al. [316] and Ammann et al. [29, 30]. However, Kleffmann et al. [340] report a lower uptake coefficient of $\sim 10^{-7}$ on carbon black over the first 5 minutes of reaction and Saathoff et al. [489] report an upper limit of $< 4 \times 10^{-8}$ averaged over 5 days under dry conditions (< 10 ppm H_2O) on spark-generated graphite. On organic combustion soots, γ^{aged} has been reported to be in the range of $\sim 10^{-4}$ – 10^{-6} [19, 30, 32, 378, 491, 534]. All studies were done at room temperature except those of Longfellow et al. [378] which were carried out at 262 K. The surface deactivates on continued exposure to NO_2 , suggesting a maximum amount of HONO that can be formed per cm^2 of soot area or mg of soot; this has been reported to be in the range of 10^{16} to 10^{18} HONO per mg of soot [32, 203, 314, 315, 340, 534]. However, reactivation on heating of the surface, exposure to water vapor and/or with time after the exposure is stopped has been observed [203, 378, 534, 545, 546]. A small portion (~ 10 – 20%) of the NO_2 taken up appears to be chemisorbed to the surface [19, 32, 119, 314, 315, 337, 340, 534, 545, 546]. Infrared studies [19, 337, 528] show that surface C–ONO, C–N– NO_2 , and C– NO_2 groups are formed. The remainder of NO_2 reacted appears as gaseous HONO and NO; Salgado and Rossi [491] report HONO as the major product for hexane soot from a flame at near stoichiometric ratio but NO as the major product for soot from an extremely lean flame. In addition, N_2O , CO, and CO_2 have been observed as products at higher temperatures [49, 50]. At lower NO_2 concentrations, the HONO yield can approach 100%; production of NO may be due to the bimolecular reaction of HONO on the surface at

higher concentrations to give $\text{NO} + \text{NO}_2 + \text{H}_2\text{O}$. The HONO yield at 262 K appears to be smaller than at room temperature [378]. Formation of HONO is due to reaction with a reduced surface site and not to NO_2 surface-catalyzed hydrolysis. The formation of HONO from the reaction of NO_2 with unspecified semi-volatile organics in diesel exhaust has been reported [223] and proposed to be a much larger source of HONO than the reaction with the soot itself. [Back to Table](#)

8. NO_3 + soot. Saathoff et al. [489] report an upper limit of $\gamma < 3 \times 10^{-4}$ on dry soot (< 10 ppm H_2O) and $\leq 10^{-3}$ at 50% RH based on measurements of NO_3 and N_2O_5 . [Back to Table](#)
9. HO_2 + soot. Saathoff et al. [489] report an upper limit of $\gamma < 10^{-2}$ on dry soot (<10 ppm H_2O) based on the decay of HO_2NO_2 (in equilibrium with HO_2 and NO_2) in the presence and absence of soot. [Back to Table](#)
10. HO_2NO_2 + soot. Saathoff et al. [489] report an upper limit of $\gamma < 10^{-5}$ on dry soot (<10 ppm H_2O) based on the decay of HO_2NO_2 in the presence and absence of soot. [Back to Table](#)
11. H_2O + soot. Alcalá-Jornod et al. [21] report an upper limit to the initial uptake coefficient of $\gamma < 2 \times 10^{-3}$, consistent with the earlier measurements of Rogaski et al. [477]. The uptake is most likely a reversible physisorption [21, 449] although based on water uptake isotherms, Chughtai et al. [116, 118, 122, 125] propose that at low relative humidities (< 25%) chemisorption occurs. While prior exposure of Degussa FW-2 to NO_2 and SO_2 was not found to increase the uptake coefficient for water, treatment with HNO_3 increased the measured uptake coefficient by a factor of 28 and with H_2SO_4 by a factor of 68 [477]. Water adsorption isotherms on soot have been measured in a number of studies, e.g. [116, 118, 120, 122, 125] and the amount of water taken up found to increase with the air/fuel ratio used to generate the soot, with the sulfur content, with aging and oxidation of the surface (e.g. by O_3) and with the presence of metals [116, 118, 120, 122, 125, 597]. [Back to Table](#)

5.17 Henry's Law Constants for Pure Water

Table 5.4. Henry's Law Constants for Pure Water.

Substance	Temperature Range, K	H (298 K) ^a	A	B	C	Uncertainty Range ^b	100 x $h_{G,0}$ M ⁻¹	1000 x h_T , M ⁻¹ K ⁻¹	Note
O ₂	273–348	1.27×10 ⁻³	-161.6	8160	22.39	I	≡ 0	-0.334	<u>1</u>
O ₃	273–333	1.03×10 ⁻²	-14.08	2830		II	0.396	1.79	<u>2</u>
H	273–298	2.6×10 ⁻⁴				IV			<u>3</u>
OH	298	39				III			<u>4</u>
HO ₂	298	690				IV			<u>5</u>
H ₂ O ₂	278–303	8.44×10 ⁴	-14.16	7600		III			<u>6</u>
N ₂	273–348	6.52×10 ⁻⁴	-177.1	8640	24.71	I	-0.10	-0.605	<u>7</u>
NH ₃	273–348	60.2	-9.84	4160		III	-4.81		<u>8</u>
NF ₃	283–323	7.96×10 ⁻⁴	-242.8	12100	34.236	II			<u>9</u>
N ₂ F ₄	288–318	8.53×10 ⁻⁴	-332.7	16610	47.370	III			<u>10</u>
NH ₂ Cl	293–313	87	-15.51	5960		IV			<u>11</u>
NHCl ₂	293–313	29	-10.68	4180		IV			<u>11</u>
NCl ₃	293–313	0.10	-16.17	4130		IV			<u>11</u>
NO	273–358	1.92×10 ⁻³	-157.1	7950	21.298	II	0.60		<u>12</u>
NO ₂	276–293	1.2×10 ⁻²	-12.32	2360		III			<u>13</u>
NO ₃	298	3.8×10 ⁻²				IV			<u>14</u>
N ₂ O	273–313	2.42×10 ⁻²	-148.1	8610	20.266	I	-0.85	-0.479	<u>15</u>
NOCl	273–293	>0.05							<u>16</u>
HN ₃	277–309	12.0	10.19	3780		III			<u>17</u>
CO	278–323	9.81×10 ⁻⁴	-178.0	8750	24.875	I			<u>18</u>
CO ₂	273–353	3.38×10 ⁻²	-145.1	8350	19.960	I	-1.72	-0.338	<u>19</u>
CH ₄	273–328	1.41×10 ⁻³	-194.7	9750	27.274	I	0.22	-0.524	<u>20</u>
C ₂ H ₆	273–323	1.88×10 ⁻³	-240.2	12420	33.744	I	1.20	-0.601	<u>21</u>
C ₃ H ₈	273–348	1.51×10 ⁻³	-281.1	14510	39.652	I	2.40	-0.702	<u>22</u>
n-C ₄ H ₁₀	273–348	1.24×10 ⁻³	-269.9	14330	37.734	I	2.97	-0.726	<u>23</u>
CH ₃ CH(CH ₃)CH ₃	278–318	9.18×10 ⁻⁴	-360.6	18020	51.444	II			<u>24</u>
C ₂ H ₄	288–348	5.96×10 ⁻³	-154.6	8540	21.202	II	0.37		<u>25</u>
C ₂ H ₂	273–343	4.14×10 ⁻²	-271.8	13430	39.237	II	-1.59		<u>26</u>
CH ₃ F	273–313	6.15×10 ⁻²	-9.478	1990		IV			<u>27</u>
CH ₃ Cl	273–313	0.127	-13.13	3270		III			<u>27</u>
CH ₃ Br	273–313	0.173	-12.16	3100		III			<u>27</u>
CH ₃ I	273–313	0.200	-13.52	3550		III			<u>27</u>

Substance	Temperature Range, K	H (298 K) ^a	<i>A</i>	<i>B</i>	<i>C</i>	Uncertainty Range ^b	100 x $h_{G,0}$ M ⁻¹	1000 x h_T , M ⁻¹ K ⁻¹	Note
CH ₂ Cl ₂	273-313	0.366	-14.68	4080		III			27
CHCl ₃	273-313	0.255	-16.48	4510		II			27
CHCl ₂ Br	273-313	0.409	-18.32	5200		III			27
CHClBr ₂	273-313	0.868	-18.67	5530		III			27
CHBr ₃	273-313	1.76	-16.79	5170		III			27
CF ₂ Cl ₂	273-313	3.09×10 ⁻³	-17.41	3470		III			27
CFCl ₃	273-313	1.07×10 ⁻²	-15.74	3340		III			27
CCl ₄	273-313	3.47×10 ⁻²	-17.38	4180		II			27
CHF ₃	298-348	0.0134	-15.25	3260		IV			28
CHClF ₂	297-352	0.0346	-300.2	16150	42.60	II			28
CF ₃ Cl	298-348	0.0010	-12.53	1660		IV			28
CF ₄	276-323	2.11×10 ⁻⁴	-313.47	15140	44.62	III			28
CH ₃ OH	273-373	203	-97.53	9240	12.16	II			29
CH ₃ CH ₂ OH	273-373	190	-162.9	12900	21.91	II			30
<i>n</i> -C ₃ H ₇ OH	273-373	142	-217.7	15800	29.76	III			31
<i>iso</i> -C ₃ H ₇ OH	273-298	130	-20.15	7450		IV			32
<i>n</i> -C ₄ H ₉ OH	273-373	123	-265.7	18400	36.64	III			33
<i>iso</i> -C ₄ H ₉ OH	298	102				IV			34
<i>sec</i> -C ₄ H ₉ OH	273-298	110	-19.65	7260		IV			34
<i>tert</i> -C ₄ H ₉ OH	273-298	70	-23.63	8310		IV			34
CH ₃ OOH	277-293	300	-11.99	5280		IV			35
HOCH ₂ OOH	278-293	1.7×10 ⁶	-18.79	9870		V			36
CH ₃ C(O)OOH	278-301	837	-11.07	5310		V			37
C ₂ H ₅ OOH	278-301	336	-14.28	5995		V			37
HCHO	288-318	3.23×10 ³	-15.73	7100		IV	-240	69	H* 38
CH ₃ CHO	273-313	12.9	-17.19	5890		IV	-3.0	-5.5	H* 39
C ₂ H ₅ CHO	273-313	10.0	-12.20	4330		V	2.2	-4.0	40
C ₃ H ₇ CHO	283-318	9.6	-18.59	6220		V	8.7	-0.06	41
CHOCHO	278-308	4.19×10 ⁵	-12.15	7480		IV			H* 42
CH ₃ COCH ₃	273-311	27.8	-15.23	5530		III	-5.2	-2.9	43
C ₂ H ₅ COCH ₃	273-298	18	-16.40	5740		IV	1.1	-0.9	44
CH ₃ C(O)C(O)CH ₃	288-318	74	-14.66	5650		IV			45
HC(O)OH	275-308	8.9×10 ³	-11.40	6100		IV			46
CH ₃ C(O)OH	275-308	4.1×10 ³	-12.50	6200		IV			47

Substance	Temperature Range, K	H (298 K) ^a	<i>A</i>	<i>B</i>	<i>C</i>	Uncertainty Range ^b	100 x $h_{G,0}$ M ⁻¹	1000 x $h_{T,1}$ M ⁻¹ K ⁻¹	Note
HC(OH)C(O)OH	278–308	2.83x10 ⁴	-3.26	4030		IV			H* 48
HC(O)C(O)OH	278–308	1.09x10 ⁴	-6.84	4810		IV			H* 49
CH ₃ C(O)C(O)OH	278–308	3.11x10 ⁵	-4.417	5090		V	9.0		50
CH ₃ OC(O)H	278–298	4.2	-11.88	3970					51
C ₂ H ₅ OC(O)H	278–298	3.4	-14.11	4570					52
n-C ₃ H ₇ OC(O)H	278–398	2.6	-15.99	5050					53
C ₂ H ₅ OC(O)CH ₃	278–398	6.0	-17.97	5890					54
CH ₃ C(O)O ₂	274	<0.1				III			55
CH ₃ CN	273–303	52.8	-9.35	3970		III	-0.049		56
CH ₃ NO ₂	293–323	34.6	-9.92	4010		IV			57
C ₂ H ₅ NO ₂	293–323	21.7	-11.80	4430		IV			57
C ₃ H ₇ NO ₂	293–323	13.1	-13.22	4710		IV			57
CH ₃ CH(NO ₂)CH ₃	293–323	8.42	-13.02	4520		IV			57
CH ₃ ONO ₂	273–298	2.0	-15.20	4740		IV			58
C ₂ H ₅ ONO ₂	273–298	1.59	-17.50	5360		IV			58
1-C ₃ H ₇ ONO ₂	273–298	1.10	-18.31	5490		IV			58
2-C ₃ H ₇ ONO ₂	273–298	0.791	-18.20	5360		IV			58
1-C ₄ H ₉ ONO ₂	273–298	1.01	-19.40	5790		IV			58
2-C ₄ H ₉ ONO ₂	273–298	0.648	-18.59	5410		IV			58
CH ₃ C(O)O ₂ NO ₂	274–297	2.8	-18.15	5730		IV	-6.5		59
O ₂ NOC ₂ H ₄ ONO ₂	293	640				IV			60
HOC ₂ H ₄ ONO ₂	293	3.99x10 ⁴				IV			60
HOCH ₂ CH(ONO ₂)CH ₃	293	7.3x10 ³				IV			60
CH ₃ CH(OH)CH ₂ ONO ₂	293	6.7x10 ³				IV			60
CH ₃ CH(ONO ₂)CH ₂ ONO ₂	293	175				IV			60
CH ₃ C(O)CH ₂ ONO ₂	293	1.01x10 ³				IV			60
CCl ₃ NO ₂	298	0.48				III			61
CF ₃ CH ₂ OH	276–299	47.7	-17.00	6220		III			62
CHF ₂ CF ₂ CH ₂ OH	275–299	141	-18.53	7000		III			62
CF ₃ CF ₂ CH ₂ OH	275–299	14.6	-11.71	4290		III			62
CF ₃ C(O)CH ₃	288–318	138	-24.92	8900		IV			63
CFH ₂ C(O)OH	298	8.1x10 ⁴				V			64
CF ₂ HC(O)OH	278–308	3.0x10 ⁴	-12.71	6870		IV			65
CF ₃ C(O)OH	278–308	9.0x10 ³	-22.20	9330		IV			66
CF ₃ C(O)OCH ₃	278–298	0.11	-20.16	5250		IV			67

Substance	Temperature Range, K	H (298 K) ^a	A	B	C	Uncertainty Range ^b	100 x $h_{G,0}$ M ⁻¹	1000 x h_T M ⁻¹ K ⁻¹	Note
CF ₃ CH ₂ OC(O)H	278-298	0.55	-16.33	4690		IV			68
CH ₃ C(O)OCH ₂ CF ₃	278-298	0.56	-18.15	5240		IV			69
C ₂ H ₅ OC(O)CF ₃	278-298	0.09	-18.95	4930		IV			70
CH ₂ ClC(O)CH ₃	288-318	59	-14.08	5410		IV			71
CClH ₂ C(O)OH	278-308	1.1x10 ⁵	-21.08	9740		IV			72
CCl ₂ HC(O)OH	298-308	1.2x10 ⁵	-15.18	8010		IV			72
CCl ₃ C(O)OH	298-308	7.4x10 ⁴	-17.83	8660		IV			73
CClF ₂ C(O)OH	278-308	2.5x10 ⁴	-24.26	10250		IV			74
CBrH ₂ C(O)OH	278-308	1.5x10 ⁵	-19.12	9260		IV			74
CBr ₂ HC(O)OH	298-308	2.3x10 ⁵	-17.64	8940		IV			74
CBr ₃ C(O)OH	298-308	3.0x10 ⁵	-17.6	9000		V			75
Cl	298	2.3				IV			76
Cl ₂	283-383	9.29x10 ⁻²	-134.4	7590	18.702	II			77
ClO	298	0.71				VI			78
Cl ₂ O	273-293	17	-3.23	1810		IV			79
ClO ₂	383-333	1.01	-11.65	3470		II			80
HOCl		660	-13.2	5880		IV			81
Br ₂	273-308	0.725	-15.05	4390		II			82
BrCl	279-299	0.98	-18.9	5630		III			83
HOBr	298	>1.3x10 ²				V			84
SO ₂	278-383	1.36	-39.72	4250	4.525	II	-6.07	0.275	85
H ₂ S	273-323	0.102	-145.2	8120	20.296	III	-3.33		86
CS ₂	274-305	0.062	-17.05	4250		IV	5.49	-4.65	87
COS	273-288	2.02x10 ⁻²	-15.68	3510		IV			88
CH ₃ SH	298-368	0.39	-12.42	3420		V	0.3		89
C ₂ H ₅ SH	298-368	0.28	-13.82	3740		V			90
CH ₃ SCH ₃	272-305	0.54	-12.19	3460		V	-3.1	-0.26	91
CH ₃ S(O)CH ₃	298	9.9x10 ⁴				V			92
CH ₃ NCS	298	17				V			93

a. $\ln H = A + B/T + C \ln(T)$ [M atm⁻¹]

b. Uncertainty Classes:

I—Better than 10%

II—10% to 50%

III—50% to 100%

IV—Factor of 2 to factor of 10

V—Factor of 10 to factor of 100

VI—Greater than a factor of 100

5.18 Notes to Table 5-4

Many of the data sets required various transformations to convert them to the units ($\text{mol L}^{-1} \text{ atm}^{-1}$) and form (solubility instead of volatility) used in this Table. The transformations often involve either the mass or molar density of water, which in all cases was taken from [358].

1. O_2 . The recommendation was taken from the studies of Benson [68] and Rettich [462]. The data show clear curvature in a plot of $\ln H$ v. $1/T$. A two parameter fit gives $A = -13.26$ and $B = 1950 \text{ K}$ for the temperature range 273–285 K. The salt effect parameter $h_{\text{G},0}$ is, by definition, zero (see text). The temperature dependent salt effect parameter is from the optimization of Weisenberger and Schumpe [598]. [Back to Table](#)
2. O_3 . The recommendation of Rischbieter [465] was accepted and refitted. Salt effect parameters were obtained from the effect of NaCl, KCl, Na_2SO_4 , and $\text{Ca}(\text{NO}_3)_2$ on H, combined with specific ion parameters. [Back to Table](#)
3. H. An average of estimates of the solubility of H based on two approaches: One is simply the assumption that the solubility of H is the same as the solubility of H_2 . [440, 441]. The second assumes that the solubility of H is what would be expected for a rare gas atom of the same radius [474]. The average value from 273 K to 298 K is 2.6×10^{-4} , with very small variation with temperature. Above room temperature the solubility increases. [Back to Table](#)
4. OH. Calculated from the reduction potential of the OH radical, $E^\circ(\text{OH}/\text{OH}^\cdot) = (1.90 \pm 0.02)\text{V}$, derived from an equilibrium with Ti^+ [505]. [Back to Table](#)
5. HO_2 . The recommendation was from a calculation by Schwartz [502] based on the gas phase constituents HO_2 , H^\cdot , and O_2^\cdot . Thermodynamic values were updated to those in our Thermodynamic tables, to $pK_a = (4.8 \pm 0.1)$, and to a reduction potential $E(\text{O}_2/\text{O}_2^\cdot) = -(0.35 \pm 0.01)\text{V}$. The reduction potential, referenced to one atmosphere O_2 , is based primarily on equilibria reported by Meisel and Czapski, [398] corrected for a revised duroquinone potential [593]. [Back to Table](#)
6. H_2O_2 . The data of Lind and Kok (corrected) [370, 371], Hwang and Dasgupta [283], Yoshizumi et al. [616], Staffellback and Kok [535], and O'Sullivan et al. [431] are all in good agreement. The recommendation is from a two-parameter fit to all the results. (Kok, et al. and Hwang and Dasgupta are represented by calculated endpoints). Previous recommendations were $A = -13.27$ and $B = 7310$. [Back to Table](#)
7. N_2 . The recommendation of Battino [49] was accepted and refitted to three-parameter equations. A two parameter fit gives $A = 12.81$ and $B = 1625 \text{ K}$ for the temperature range 273–293 K. Salt effect parameters taken from the optimization of Weisberger and Schumpe [598]. [Back to Table](#)
8. NH_3 . Based on the recommendation by Edwards et al. [163], refit to a two-parameter equation. Over the temperature range 273–348 K, there appears to be little curvature in the data. The more recent data of Dasgupta and Dong [140] are in quite good agreement with this recommendation, whereas the results of Hales and Drewes [226] are somewhat higher and those of Shi and Davidovits [520] (an uptake study) are significantly lower. The Hales and Drewes paper also included studies of the effect of dissolved CO_2 on the solubility of NH_3 . The solubility of NH_3 in solutions containing a wide variety of ions is discussed by Clegg and Brimblecombe [128]. Salt effect parameters taken from the optimization of Weisberger and Schumpe [598]. [Back to Table](#)
9. NF_3 . Refit to three- parameter equation from the recommendation of Wilhelm et al. [599]. [Back to Table](#)
10. N_2F_4 . Refit to three- parameter equation from the recommendation of Wilhelm et al. [599]. [Back to Table](#)
11. Chloramines. Derived from flashoff studies with glass sparging columns at 20°C and 40°C [270]. The data point for ammonia at 20°C is in exact agreement with the recommended value in this Table. [Back to Table](#)
12. NO. Three-parameter refit from the recommendation of Battino [47]. Two-parameter fit gives $A = -12.27$ and $B = 1790 \text{ K}$ for the temperature range 273–293 K. Salt effect parameters taken from the optimization of Weisberger and Schumpe [598]. [Back to Table](#)
13. NO_2 . Based on NO_2 uptake studies and an analysis of literature values. [105] A value of 0.014 was obtained from an analysis of studies of reactive dissolution of NO_2 by Schwartz and White [504]. [Back to Table](#)
14. NO_3 . From the reduction potential $E^\circ(\text{NO}_3/\text{NO}_3^\cdot) = (2.46 \pm 0.02)\text{V}$, which is an average based on determinations of equilibria with Cl^- [91, 451]. This value is in good agreement with that calculated from the

uptake of NO_3 into a wetted-wall flow reactor containing Cl^- [486]. It is in very poor agreement with the much higher value derived from a study of the uptake of NO_3 by a series of wetted denuders [554]. [Back to Table](#)

15. N_2O . Three-parameter refit to the recommendation of Battino [46]. Two parameter fit gives $A = 13.40$ and $B = 2880 \text{ K}$ for the temperature range 273–293 K. Salt effect parameters taken from the optimization of Weisberger and Schumpe [598]. [Back to Table](#)
16. NOCl . Uptake kinetics measured as function of temperature into water and solutions containing HCl , NaCl , and NaOH . Only the latter had an effect. The kinetics were consistent with an uptake coefficient of 0.03 [495]. [Back to Table](#)
17. HN_3 . Measured using a packed column technique at pH 1.8 ($\mu = 0.02 \text{ mol L}^{-1}$). The effective Henry's law constant can be calculated using $K_H^* = K_H(1 + K_a/[\text{H}^+])$, with $pK_a = 4.65$ [74]. [Back to Table](#)
18. CO . The recommendation is based on smoothed data from Rettich et al. [461] and refit to three-parameter equation. A two parameter fit gives $A = -12.72$ and $B = 1720 \text{ K}$ for the temperature range 273–293 K. [Back to Table](#)
19. CO_2 . Refit to three-parameter equation from the recommendation of Wilhelm et al. [599]. Two parameter fit gives $A = 12.49$ and $B = 2710 \text{ K}$ for the temperature range 273–293 K. Salt effect parameters taken from the optimization of Weisberger and Schumpe [598]. [Back to Table](#)
20. CH_4 . The recommendation is a three-parameter fit to the smoothed recommendation of Battino [56]. There is very good agreement with the more recent data of Ben-Naim and Battino [65]. A two parameter fit gives $A = -13.45$ and $B = 2040 \text{ K}$ for the temperature range 273–293 K. Salt effect parameters taken from the optimization of Weisberger and Schumpe [598]. [Back to Table](#)
21. C_2H_6 . The recommendation is a three-parameter fit to the smoothed recommendation of Battino [48]. There is very good agreement with the more recent data of Ben-Naim and Battino [65]. Two parameter fit gives $A = -15.95$ and $B = 2875 \text{ K}$ for the temperature range 273–293 K. Salt effect parameters taken from the optimization of Weisberger and Schumpe [598]. [Back to Table](#)
22. C_3H_8 . The recommendation is from a three-parameter fit to the smoothed recommendation of [55]. There is very good agreement with the more recent data of Ben-Naim and Battino [65]. A two parameter fit gives $A = 17.52$ and $B = 3275 \text{ K}$ for the temperature range 273–293 K. Salt effect parameters taken from the optimization of Weisberger and Schumpe [598]. [Back to Table](#)
23. $n\text{-C}_4\text{H}_{10}$. The recommendation is from a three-parameter fit to the smoothed recommendation of Battino [54]. There is very good agreement with the more recent data of Ben-Naim and Battino [65]. A two parameter fit gives $A = -19.28$ and $B = 3740 \text{ K}$ for the temperature range 273–288 K. Salt effect parameters taken from the optimization of Weisberger and Schumpe [598]. [Back to Table](#)
24. $\text{CH}_3\text{CH}(\text{CH}_3)\text{CH}_3$. The recommendation is from a three-parameter fit to the smoothed recommendation of Battino [53]. A two parameter fit gives $A = 18.22$ and $B = 3340 \text{ K}$ for the temperature range 278–293 K. [Back to Table](#)
25. C_2H_4 . The recommendation is from a three-parameter fit to the smoothed recommendation of Wilhelm [599]. A two parameter fit gives $A = -12.40$ and $B = 2170 \text{ K}$ for the temperature range 288–313 K. Salt effect parameters taken from the optimization of Weisberger and Schumpe [598]. [Back to Table](#)
26. C_2H_2 . Recommended three parameter fit has been converted from the evaluation of Fogg et al. [187]. A two parameter fit to the Fogg et al. data gives $A = -10.70$ and $B = 2230$ for the temperature range 272–298 K. Previous recommendation was from a three-parameter fit to the recommendation of Wilhelm [599]. The recommendation of Yaws et al. [614] generates similar results. [Back to Table](#)
27. Halomethanes. A refit to the evaluation of Staudinger and Roberts [536]. [Back to Table](#)
28. Halomethanes. A refit to the evaluation of Welhelm [599]. [Back to Table](#)
29. CH_3OH . The recommendation is from a three-parameter fit to the values derived through a comprehensive analysis of limiting activity coefficients, infinite-dilution partial molar excess enthalpies and heat capacities, and measured Henry's law constants [156]. A two-parameter fit up to 298 K gives $A = -13.61$ and $B = 5640$. The previous recommendation was $A = -12.08$ and $B = 5210$, which was based on the two data points of Snider and Dawson [531]. The 298 K result of Butler et al. [90] and a calculation based on the NBS

Thermodynamic tables, [589], are in very good agreement. The 298 K result of Altschuh et al. [28] is about 40% lower. [Back to Table](#)

30. C_2H_5OH . The recommendation is from a three-parameter fit to the values derived through a comprehensive analysis of limiting activity coefficients, infinite-dilution partial molar excess enthalpies and heat capacities, and measured Henry's law constants [156]. A two-parameter fit up to 298 K gives $A = -17.14$ and $B = 6660$. The previous recommendation was $A = -16.98$ and $B = 6630$, which was based on the two data points of Snider and Dawson [531]. The 298 K results of [90] and [478], and a calculation based on the NBS Thermodynamic tables, [589], are in very good agreement. The 298 K result of Altschuh [28] is about 50% lower. [Back to Table](#)
31. $n-C_3H_7OH$. The recommendation is from a three-parameter fit to the values derived through a comprehensive analysis of limiting activity coefficients, infinite-dilution partial molar excess enthalpies and heat capacities, and measured Henry's law constants [156]. A two-parameter fit up to 298 K gives $A = -19.80$ and $B = 7370$. The previous recommendation was $A = -20.16$ and $B = 7470$, which was based on two data points each from Snider and Dawson [531]. Room temperature data from other studies [89, Butler, 1935 #2881], and [28] support these results. [Back to Table](#)
32. $iso-C_3H_7OH$. Recommendation is based on two data points from Snider and Dawson [531]. Room temperature data from other studies ([89, 90], and [28]) support these results. [Back to Table](#)
33. $n-C_4H_9OH$. The recommendation is from a three-parameter fit to the values derived through a comprehensive analysis of limiting activity coefficients, infinite-dilution partial molar excess enthalpies and heat capacities, and measured Henry's law constants [156]. A two-parameter fit up to 298 K gives $A = -17.68$ and $B = 6725$. The previous recommendation was $A = -19.34$ and $B = 72.10$, which was based on two data points from Snider and Dawson [531]. Room temperature data from other studies ([89] and [28]) support these results. [Back to Table](#)
34. $iso-C_4H_9OH$, $sec-C_4H_9OH$ and $tert-C_4H_9OH$. The recommendations for C4 alcohols are based on two data points each from Snider and Dawson [531]. Room temperature data from Butler et al. [90] support these results. [Back to Table](#)
35. CH_3OOH . The data of Lind and Kok [370, 371] and O'Sullivan et al. [431] are in excellent agreement and were fit to a two-parameter expression. [Back to Table](#)
36. $HOCH_2OOH$. The results of O'Sullivan [431] and Staffelback and Kok [535] are very close and were fit to obtain the recommended values. The results of Zhou and Lee [634] are much lower and were not included. [Back to Table](#)
37. $CH_3C(O)OOH$ and C_2H_5OOH . Experimental results of O'Sullivan [431]. [Back to Table](#)
38. $HCHO$. The recommended value is the apparent Henry's law constant and includes a contribution due to hydrolysis $H^* = H(1 + K_{hyd})$. Data from Betterton and Hoffmann [73] and Zhou and Mopper [635] are in substantial agreement and were fit to a two-parameter expression. Betterton and Hoffmann have calculated $H = 2.5 \text{ M atm}^{-1}$ at 298 K for the physical solubility. A gas-stripping study over the temperature range 5-50 C agreed at room temperature, but was lower below and higher above room temperature.[516] Salt effect parameters derived from data on the effect of seawater concentration (0 to 100%) on the measured H [635]. For these calculations, the seawater was assumed to be a solution of pure NaCl, with 35% salinity equal to 0.6 M. [Back to Table](#)
39. CH_3CHO . The recommended value is the apparent Henry's law constant and includes a contribution due to hydrolysis $H^* = H(1 + K_{hyd})$. The results of Snider and Dawson [531], Benkelberg et al. [67], and Betterton and Hoffmann [73] are in excellent agreement and have been fit to a two-parameter expression for the recommendation. The results of Zhou and Mopper [635] curve off at higher temperatures and were not included in the fit. (Note the similar situation for acetone.) Betterton and Hoffmann have calculated $H = 4.8 \text{ M atm}^{-1}$ at 298 K for the physical solubility. Salt effect parameters derived from data on the effect of seawater concentration (0 to 100%) on the measured H [635]. For these calculations, the seawater was assumed to be a solution of pure NaCl, with 35% salinity equal to 0.6 M. [Back to Table](#)
40. C_2H_5CHO . Results of Zhou and Mopper [635] and Snider and Dawson [531] agree only to within about a factor of two. The two points from the former were weighted by 3 and combined with the five points of the latter to generate the recommendation. Salt effect parameters derived from data on the effect of seawater

concentration (0 to 100%) on the measured H [635]. For these calculations, the seawater was assumed to be a solution of pure NaCl, with 35% salinity equal to 0.6 M. [Back to Table](#)

41. C_3H_7CHO . The only results are from Zhou and Mopper [635], which have been fit to a two-parameter expression. Salt effect parameters derived from data on the effect of seawater concentration (0 to 100%) on the measured H [635]. For these calculations, the seawater was assumed to be a solution of pure NaCl, with 35% salinity equal to 0.6 M. [Back to Table](#)
42. Glyoxal. Measured using a bubble-column method. Validation measurements on formaldehyde and acetic acid gave results of 4.8×10^3 and 5.0×10^3 , slightly higher than the recommendations here. The recommended value is the apparent Henry's law constant and includes a contribution due to hydrolysis $H^* = H(1 + K_{hyd})$. An intrinsic $K_h = 1.90 \text{ M atm}^{-1}$ was calculated at 298 K [290]. The solubility increased by about a factor of three in 0.05 M NaCl, but dropped by ~50% when the concentration was increased to 5 M. Na_2SO_3 concentrations of 0.0003 M to 0.03 M increased the solubility, up to a factor of ~50. Even higher sulfate concentrations led to values too high to measure. [Back to Table](#)
43. CH_3COCH_3 . The recommendation is from a fit to the data of Snider and Dawson [531] and Benkelberg et al. [67]. Room temperature data points of Hoff et al. [265], Burnett [89] and Vitenberg et al. [581] are in very good agreement. Results of Zhou and Mopper [635] are somewhat higher, particularly at room temperature and above. The situation is similar for acetaldehyde. Salt effect parameters derived from data on the effect of seawater concentration (0 to 100%) on the measured H [635]. For these calculations, the seawater was assumed to be a solution of pure NaCl, with 35% salinity equal to 0.6 M. The K_s values from this work are somewhat different than those obtained by Benkelberg et al. [67], 0.089 vs 0.17 at 298 K and 0.17 vs 0.085 at 273 K. The magnitude of this difference is not too great, but the two studies predict a different sign for h_T . [Back to Table](#)
44. $C_2H_5COCH_3$. The recommendation is from the two points of Snider and Dawson [531]. The room temperature points of Vitenberg et al. [581] and Rohrschneider [478] are in good agreement. The higher temperature data of Zhou and Mopper [635] are somewhat higher and those of Friant and Suffet [193] are lower than the recommendation. Salt effect parameters derived from data on the effect of seawater concentration (0 to 100%) on the measured H [635]. For these calculations, the seawater was assumed to be a solution of pure NaCl, with 35% salinity equal to 0.6 M. [Back to Table](#)
45. 2,3-Butanedione. Measured by a bubble-columne technique [72]. [Back to Table](#)
46. $HC(O)OH$. The results of Johnson et al. [310] are accepted. The 298 K result of Khan et al. [335] are about 75% lower. [Back to Table](#)
47. $CH_3C(O)OH$. The results of Johnson et al. [310] are accepted. A value calculated from the NBS Thermodynamic tables [589] is about a factor of two higher. [Back to Table](#)
48. Glycolic acid. Measured using a bubble-column method with no pH control (measured ~3-3.1). Validation measurements on formaldehyde and acetic acid gave results of 4.8×10^3 and 5.0×10^3 , slightly higher than the recommendations here [290]. An intrinsic $K_h = 2.37 \times 10^4 \text{ M atm}^{-1}$ was calculated at 298 K. [Back to Table](#)
49. Glyoxylic acid. Measured using a bubble-column method with no pH control (measured ~2.6-2.8). Validation measurements on formaldehyde and acetic acid gave results of 4.8×10^3 and 5.0×10^3 , slightly higher than the recommendations here [290]. An intrinsic $K_h = 28.67 \text{ M atm}^{-1}$ was calculated at 298 K. [Back to Table](#)
50. $CH_3C(O)C(O)OH$. Taken from Khan et al. [335] Salt effect derived from effect of NaCl ($k_s = 0.236 \text{ M}^{-1}$) and KCl ($k_s = 0.235 \text{ M}^{-1}$) on partial pressure over 1.5 M solution of pyruvic acid at various salt concentrations. Much different values derived when other salts were used, suggesting complications due to specific interactions and, possibly, to the weakly buffered nature of the solution. [Back to Table](#)
51. Methyl formate. Measured using a column-stripping method [352]. [Back to Table](#)
52. Ethyl formate. Measured using a column-stripping method [352]. [Back to Table](#)
53. n-Propyl formate. Measured using a column-stripping method [352]. [Back to Table](#)
54. Ethyl acetate. Measured using a column-stripping method [352]. [Back to Table](#)
55. $CH_3C(O)O_2$. Villalta et al. [580] measured an upper limit for H of 0.2 M atm^{-1} in a coated-wall flow tube uptake experiment on aqueous sodium ascorbate solutions. [Back to Table](#)

56. CH_3CN . The values reported by Benkelberg [67], Snider and Dawson [531], Hamm et al. [229] are all in good agreement and have been fit to a two-parameter expression for the recommendation. The Hamm et al. paper includes a measurement with artificial seawater at 293 K. Salt effect derived from the effect of 0.6 mol L^{-1} NaCl on solubility at 293 K [67]. [Back to Table](#)
57. Nitroalkanes (CH_3NO_2 , $\text{C}_2\text{H}_5\text{NO}_2$, $\text{C}_3\text{H}_7\text{NO}_2$, and $\text{CH}_3\text{CH}(\text{NO}_2)\text{CH}_3$). The recommended values are all taken from the work of Benes and Dohnal [66]. For nitromethane, the 298 K value from Rohrschneider [478] is about 30% higher. [Back to Table](#)
58. Alkyl nitrates (CH_3ONO_2 , $\text{C}_2\text{H}_5\text{ONO}_2$, 1- $\text{C}_3\text{H}_7\text{ONO}_2$, 2- $\text{C}_3\text{H}_7\text{ONO}_2$, 1- $\text{C}_4\text{H}_9\text{ONO}_2$, 2- $\text{C}_4\text{H}_9\text{ONO}_2$). The recommended values are all taken from the work of Kames and Schurath [318]. The results of Luke et al. [382] are in very good agreement for 1-butyl and 2-butyl nitrates, but the values reported by Hauff [257] for 1- and 2-propyl and butyl nitrates by head-space chromatography are significantly (~50%) lower. [Back to Table](#)
59. $\text{CH}_3\text{C}(\text{O})\text{O}_2\text{NO}_2$. (PAN) The results of Kames and Schurath [318] and Frenzel et al. [191] are close, but somewhat higher (~60%) than the single temperature point of Holdren et al. [269]. The recommendation is a fit to the data of Kames and Schurath, and Frenzel et al. Frenzel et al., Kames and Schurath, and Holdren et al. also measured hydrolysis rate constants. $K_s = 0.0807 \text{ M}^{-1}$ for NaCl at 293.2 K based on solubility in artificial sea water (~0.7 M) [318]. [Back to Table](#)
60. Bifunctional alkyl nitrates. The recommended values (at 293 K) are taken from the work of Kames and Schurath [317]. [Back to Table](#)
61. Chloromethylnitrate (chloropicrin). Measured by a stripping technique in water, 0.1 M and 0.2 M NaCl, and at pH 4.0 and 8.0 (buffered). All values were within the stated margin of error (± 0.3) [612]. [Back to Table](#)
62. Fluorinated alcohols. Measured using the equilibrium headspace technique. Parameters derived through a linear fit to the reported data [104]. [Back to Table](#)
63. 1,1,1-Trifluoroacetone. Measured by a bubble-colume technique [72]. [Back to Table](#)
64. $\text{CF}_2\text{HC}(\text{O})\text{OH}$. Equilibrium partial pressure of the acid obtained using a stripping technique over a solution containing 0.15 mol kg^{-1} HBr to suppress dissociation. Reported values corrected for the effect on the activity of the solution [80]. Due to high toxicity, only a single determination was made for this acid. [Back to Table](#)
65. $\text{CF}_2\text{HC}(\text{O})\text{OH}$. Equilibrium partial pressure of the acid obtained using a stripping technique over a solution containing 0.15 to 6.0 mol kg^{-1} HBr to suppress dissociation. Reported values corrected for the effect on the activity of the solution [81]. [Back to Table](#)
66. $\text{CF}_3\text{C}(\text{O})\text{OH}$. Equilibrium partial pressure of the acid obtained using a stripping technique over a solution containing HBr to suppress dissociation. Reported values corrected for the effect on the activity of the solution [80]. [Back to Table](#)
67. Methyl trifluoroacetate. Parameters derived from a linear fit to the reported data from a column-stripping study. A hydrolysis rate constant of $10^{5.3 \pm 2.0} \exp[-(5.07 \pm 1.27) \times 10^3/T] \text{ s}^{-1}$ was also obtained [353]. [Back to Table](#)
68. 2,2,2-Trifluoroethyl acetate. Value measured using a column-stripping method [352]. [Back to Table](#)
69. 2,2,2-Trifluoroethyl acetate. Parameters derived from a linear fit to the reported data from a column-stripping study. The hydrolysis rate constant was too slow to measure [353]. [Back to Table](#)
70. Ethyl trifluoroacetate. Value measured using a column-stripping method [352]. [Back to Table](#)
71. Chloroacetone. Measured by a bubble-colume technique [72]. [Back to Table](#)
72. $\text{CCl}_2\text{HC}(\text{O})\text{OH}$ and $\text{CCl}_2\text{C}(\text{O})\text{OH}$. Equilibrium partial pressure of the acids obtained using a stripping technique over a solution containing 0.15 to 6.0 mol kg^{-1} HBr to suppress dissociation. Reported values corrected for the effect on the activity of the solution [81]. [Back to Table](#)
73. $\text{CCl}_3\text{C}(\text{O})\text{OH}$. Equilibrium partial pressure of the acid obtained using a stripping technique over a solution containing 0.25 to 6.0 mol kg^{-1} HBr to suppress dissociation. Reported values corrected for the effect on the activity of the solution [81]. [Back to Table](#)

74. $\text{CClF}_2\text{C}(\text{O})\text{OH}$, $\text{CBrH}_2\text{C}(\text{O})\text{OH}$ and $\text{CBr}_2\text{HC}(\text{O})\text{OH}$. Equilibrium partial pressure of the acids obtained using a stripping technique over a solution containing 0.15 to 6.0 mol kg^{-1} HBr to suppress dissociation. Reported values corrected for the effect on the activity of the solution [81]. [Back to Table](#)
75. $\text{CBr}_3\text{C}(\text{O})\text{OH}$. Equilibrium partial pressure of the acid obtained using a stripping technique over a solution containing 0.15 to 6.0 mol kg^{-1} HBr to suppress dissociation. Reported values corrected for the effect on the activity of the solution [81]. Only a few measurements at 308 K and one at 298 K were made. The reported value of B is the mean of those for $\text{CF}_3\text{C}(\text{O})\text{OH}$ and $\text{CCl}_3\text{C}(\text{O})\text{OH}$. [Back to Table](#)
76. Cl. $E^\circ(\text{Cl}/\text{Cl}^-) = (2.43 \pm 0.03)\text{V}$ from an analysis of the reaction of OH with Cl^- , yielding the equilibrium constant for $\text{OH} + \text{Cl}^- + \text{H}^+ \leftrightarrow \text{H}_2\text{O} + \text{Cl}$ ($K_{\text{eq}} = 1.1 \times 10^5 \text{ M}^{-2}$, corrected to a standard state of water at unit activity), [617] and the reduction potential $E^\circ(\text{OH}^-, \text{H}^+/\text{H}_2\text{O}) = (2.73 \pm 0.02)\text{V}$ [505]. [Back to Table](#)
77. Cl_2 . Three-parameter refit to the recommendation of Battino [51]. Two parameter fit gives $A = 9.38$ and $B = 2090 \text{ K}$ for the temperature range 283–313 K. [Back to Table](#)
78. ClO . From the reduction potential $E(\text{ClO}/\text{ClO}^-) = (1.41 \pm 0.02)\text{V}$, which is based on an equilibrium with carbonate at high pH and ionic strength [278]. Due to the high ionic strength, 3 M, it was not possible to correct this value and obtain a reduction potential for the standard state. Thus, the derived Henry's Law constant must be considered uncertain. [Back to Table](#)
79. Cl_2O . Fit to recommendation of Wilhelm et al. [599]. Data appear somewhat uncertain. [Back to Table](#)
80. ClO_2 . Two-parameter fit to the recommendation of Battino [50]. [Back to Table](#)
81. HOCl . Huthwelker et al. [282] analyzed the limited data for pure water from Blatchley et al. [75] and Holzwarth et al. [270] along with the more extensive data for uptake by sulfuric acid from Hanson and Ravishankara [250], along with thermodynamic information, and obtained a consistent expression for the solubility of HOCl . [Back to Table](#)
82. Br_2 . The results of Kelley and Tartar [328] and Jenkins and King [308] agree well below about 313 K, and with the 298 K point of Hill et al. [263]. Recommendation based on a two-parameter fit to all data at and below 308 K. [Back to Table](#)
83. BrCl . The recommendation is from the study of Barlett and Margerum [41]. [Back to Table](#)
84. HOBr . The Henry's law constant was estimated to be more than twice that of HOCl based on a study of the effective Henry's law constant for free bromine from a stripping column [75]. [Back to Table](#)
85. SO_2 . The recommendation of Battino [52] was accepted and refit to a three-parameter equation. The earlier recommendation of Edwards et al. [163] is slightly lower. A two parameter fit gives $A = -9.53$ and $B = 2930 \text{ K}$ for the temperature range 278–298 K. New value of $h_{\text{SO}_{2,0}}$ from absorption equilibria studies in aqueous HCl and NaCl solutions [473]. Temperature dependence from the optimization of Weisberger and Schumpe [598]. [Back to Table](#)
86. H_2S . In the recommendation of Fogg [186], two expressions were given, representing the results above and below 283 K. The predicted values from these expressions were calculated, with the points at 283 K averaged, converted to the desired units, and then fit with the two- and three-parameter expressions. These are the recommended values. More recent results of Rinker and Sandall [464] and Munder et al. [426] are slightly lower; in these studies, the physical solubility of H_2S was determined through measurements involving aqueous solutions of glycols or amines, neutralized with HCl. The reported values of De Bruyn et al. [148] are significantly (~30%) lower. The earlier recommendation of Edwards et al. [163] is very close to the recommendation of Fogg [186] as is the recommendation of Yaws et al. [614]. The room temperature point calculated from the NBS Thermodynamic tables Wagman et al. [589] is also slightly lower. The work of De Bruyn et al. [148] covered also a wide range of NaCl and $(\text{NH}_4)_2\text{SO}_4$ concentration and of pH. Salt effect parameters taken from the optimization of Weisberger and Schumpe [598]. [Back to Table](#)
87. CS_2 . The recommendation is from a fit to data of Elliott [165], who also present data in 0.5 mol L^{-1} NaCl. The results of De Bruyn et al. [148] are significantly (50%) lower. The work of De Bruyn et al. covered also a wide range of NaCl and $(\text{NH}_4)_2\text{SO}_4$ concentration and of pH. Salt effect parameters derived from the ratio of the solubility of CS_2 in water and 0.5 M NaCl [165]. At 278 K, $k_s = 0.184 \text{ M}^{-1}$, compared to 0.150 M^{-1} from the results of de Bruyn, et al. [148]. Note also De Bruyn et al. obtained $K_s = 0.410 \text{ M}^{-1}$ for $(\text{NH}_4)_2\text{SO}_4$, whereas these parameters would predict 0.261 M^{-1} . [Back to Table](#)

88. COS. The reviews by Wilhelm et al. [599] and Yaws et al. [614] result in identical results over the low temperature range (<303 K) and are combined to generate the recommendation. The results of De Bruyn et al. [148] are somewhat (~25%) lower at the lower temperature range. The work of De Bruyn et al. covered also a wide range of NaCl and (NH₄)₂SO₄ concentration and of pH. [Back to Table](#)
89. CH₃SH. The recommendation is based on the data of Przyjazny et al. [455]. Results of De Bruyn et al. [148] are about half the recommended value at 298 K. Similar low values were observed for other compounds in the work of De Bruyn et al. The work of De Bruyn et al. covered a wide range of pH and NaCl and (NH₄)₂SO₄ concentrations. At 298 K, De Bruyn et al. [148] obtained $K_s = 0.314 \text{ M}^{-1}$ for (NH₄)₂SO₄ and $K_s = 0.143 \text{ M}^{-1}$ for NaCl. From the latter, we calculate $h_G = 0.003 \text{ M}^{-1}$; the values for (NH₄)₂SO₄ from this work have tended to be high. [Back to Table](#)
90. C₂H₅SH. The recommendation is based on the data of Przyjazny et al. [455]. The results of Vitenberg [581] are slightly lower than the extrapolated value at 293 K. [Back to Table](#)
91. CH₃SCH₃. The recommendation is based on the values of Dacey et al. [137]. The single temperature point of Wong and Wang [608] and the higher temperature results of Przyjazny et al. [455] are in good agreement. The results of De Bruyn et al. [148] are about 30% lower. The studies of Dacey et al. [137] and Wong and Wang [608] were also carried out with seawater. The work of De Bruyn et al. [148] covered also a wide range of NaCl and (NH₄)₂SO₄ concentration and of pH. Salt effect parameters based on the values of Dacey et al. [137] for Sargasso sea water from 0 to 29 C. The values for K_H obtained by Wong and Wang [608] for sea water from 18 to 44 C are in good agreement. Dacey et al. also measured K_H at 18 C for NaCl solutions up to 32%. For the 10 – 32% data, a value of $K_s = 0.117 \text{ M}^{-1}$ can be derived, in good agreement with the predicted value of 0.113 M^{-1} . The 278 K value of $K_s = 0.180 \text{ M}^{-1}$ obtained by De Bruyn et al. [148] is somewhat larger. Note also the de Bruyn, et al. obtained $K_s = 0.332 \text{ M}^{-1}$ for (NH₄)₂SO₄, whereas the recommended parameters would predict 0.223. [Back to Table](#)
92. CH₃S(O)CH₃. The recommendation is from Watts and Brimblecombe [596], cited by Allen et al. [27]. [Back to Table](#)
93. Methyl isothiocyanate. Measured by stripping technique in pure water. Measurements in NaCl and buffer solutions tended to be lower (0.1 M NaCl, 9; 0.2 M, 7) [612]. [Back to Table](#)

5.19 Ion-Specific Schumpe Parameters

Table 5-5. Ion-Specific Schumpe Parameters

Cation	h_i^c		Anion	h_i^a
H ⁺	0		OH ⁻	0.0839
Li ⁺	0.0754		HS ⁻	0.0851
Na ⁺	0.1143		F ⁻	0.092
K ⁺	0.0922		Cl ⁻	0.0318
Rb ⁺	0.0839		Br ⁻	0.0269
Cs ⁺	0.0759		I ⁻	0.0039
NH ₄ ⁺	0.0556		NO ₂ ⁻	0.0795
Mg ²⁺	0.1694		NO ₃ ⁻	0.0128
Ca ²⁺	0.1762		ClO ₃ ⁻	0.1348
Sr ²⁺	0.1881		BrO ₃ ⁻	0.1116
Ba ²⁺	0.2168		IO ₃ ⁻	0.0913
Mn ²⁺	0.1463		ClO ₄ ⁻	0.0492
Fe ²⁺	0.1523		IO ₄ ⁻	0.1464
Co ²⁺	0.168		CN ⁻	0.0679
Ni ²⁺	0.1654		SCN ⁻	0.0627
Cu ²⁺	0.1675		HCrO ₄ ⁻	0.0401
Zn ²⁺	0.1537		HCO ₃ ⁻	0.0549
Cd ²⁺	0.1869		CO ₃ ²⁻	0.1423
Al ³⁺	0.2174		HPO ₄ ²⁻	0.1499
Cr ³⁺	0.0648		SO ₃ ²⁻	0.127
Fe ³⁺	0.1161		SO ₄ ²⁻	0.1117
La ³⁺	0.2297		S ₂ O ₃ ²⁻	0.1149
Ce ³⁺	0.2406		PO ₄ ³⁻	0.2119
Th ⁴⁺	0.2709		Fe(CN) ₆ ⁴⁻	0.3574

The values in this table can be used to estimate the solubility of a gas in various mixed electrolyte solutions, even if these data have not been obtained experimentally for all of the ions. For example, the solubility of ozone in a solution of 0.8 M HCl and 1.2 M Na₂SO₄ at 273 K would be estimated as follows:

First, $H^0 = 0.024 \text{ M atm}^{-1}$ at 273 K, from the Henry's Law Table; from the same Table, the gas-specific parameters for ozone are $h_{G,0} = 0.00396 \text{ M}^{-1}$ and $h_T = 1.79 \times 10^{-3} \text{ M}^{-1} \text{ K}^{-1}$, thus:

$$k_G = 0.00396 + 1.79 \times 10^{-3}(273 - 298) = -0.0408 \text{ M}^{-1}$$

The specific ion parameters from Table 5-4 are corrected by this value to calculate the change in the logarithm of the Henry's law constant

$$\log (H^0/H^{273}) = 2 \times 1.2 \text{ M} \times (0.1143 - 0.0408) \text{ M}^{-1} + 1.2 \text{ M} \times 0.1117 - 0.0408) \text{ M}^{-1} +$$

$$0.8 \text{ M} \times (0 - 0.0408) \text{ M}^{-1} + 0.8 \text{ M} \times (0.0318 - 0.0408) \text{ M}^{-1} = 0.181$$

$$\text{Thus, } (H^0/H^{273}) = 1.517$$

$$H = 0.024 \text{ M atm}^{-1}/1.517 = 0.016 \text{ M atm}^{-1} \text{ for O}_3 \text{ in this salt solution at 273 K.}$$

5.20 Henry's Law Constants for Acids

Table 5-6. Henry's Law Constants for Acids

	T(K)	Wt.% H ₂ SO ₄	H or H* (M/atm)	Notes
O ₃ in H ₂ SO ₄ • nH ₂ O(l)	293	1–70	$\ln(H_0/H) = (4.08 \pm 0.2) \times 10^{-3} \times \text{wt}$ $H_0 = 0.012 \text{ M atm}^{-1}$ wt is the H ₂ SO ₄ wt. %	<u>1</u>
NO ₂ in H ₂ SO ₄ • nH ₂ O(l)	203–343	39–68	See Note	<u>2</u>
HONO in H ₂ SO ₄ • nH ₂ O(l)	248–298	>60	$\ln H^* = a_1 + a_2 \text{ wt} + a_3 \text{ wt}^2 + (b_1 + b_2 \text{ wt})/T$ $a_1 = 26.1 \pm 9.4$, $a_2 = -1.095 \pm 0.21$, $a_3 = 0.00732 \pm 0.00121$ $b_1 = -5792 \pm 1610$, $b_2 = 181.3 \pm 24$	<u>3</u>
HNO ₃ in H ₂ SO ₄ • nH ₂ O(l)	~195–300	0–80	See Note	<u>4</u>
HNO ₃ and HCl in H ₂ SO ₄ • nHNO ₃ • mH ₂ O(l)	~195–300	0–80	See Note	4
HO ₂ NO ₂ in H ₂ SO ₄ • nH ₂ O(l)	201–230	50–75	$\ln H = 3.69 - m\text{H}_2\text{SO}_4 \times (-0.25 + 65/T) - 8400 \times (1/T_0 - 1/T)$ mH ₂ SO ₄ is the molality of the H ₂ SO ₄ solution, T ₀ = 298.15 K	<u>5</u>
CH ₂ O in H ₂ SO ₄ • mHNO ₃ • nH ₂ O(l)	240–300	10–85 also 8–40 wt. % HNO ₃	See Note	<u>6</u>
CH ₃ OH in H ₂ SO ₄ • nH ₂ O(l)	197–223		See Note	<u>7</u>
CH ₃ CH ₂ OH in H ₂ SO ₄ • mH ₂ O(l)	209–237	39–76	See Note	<u>8</u>
CH ₃ C(O)CH ₃ in H ₂ SO ₄ • nH ₂ O(l)	198–298	10–80	$\ln H^* = a_1 + a_2 \text{ wt} + a_3 \text{ wt}^2 + (b_1 + b_2 \text{ wt} + b_3 \text{ wt}^2)/T$ wt is the H ₂ SO ₄ wt. %, $a_1 = -21.438 \pm 4.31$, $a_2 = -0.32163 \pm 0.207$, $a_3 = 0.0072935 \pm 0.00235$ $b_1 = 7292 \pm 1220$, $b_2 = 33.524 \pm 53.42$, $b_3 = -0.975 \pm 0.571$	<u>9</u>
CH ₃ C(O)O ₂ NO ₂ in H ₂ O(l), H ₂ SO ₄ • nH ₂ O(l)	199–295	0–75	$\ln H^* = 1.07 - m\text{H}_2\text{SO}_4 \times (0.69 - 152/T) - 5810 \times (1/T_0 - 1/T)$, mH ₂ SO ₄ = molality of the H ₂ SO ₄ solution T ₀ = 298.15 K	<u>10</u>
CF ₂ O in H ₂ SO ₄ • nH ₂ O(l)	215–230	60	< 5	<u>11</u>
CF ₃ OH in H ₂ SO ₄ • nH ₂ O(l)	250	40 50	> 240 210	<u>12</u>
HOCl in H ₂ SO ₄ • nH ₂ O(l)	200–300	46–80	$H_{\text{HOCl}} = 1.91 \times 10^{-6} \times \exp(5862.4/T) \times \exp(-S_{\text{HOCl}} M_{\text{H}_2\text{SO}_4}) \text{ M atm}^{-1}$ where: $S_{\text{HOCl}} = 0.0776 + 59.18/T \text{ M}^{-1}$, $M_{\text{H}_2\text{SO}_4} = \text{H}_2\text{SO}_4 \text{ molar conc}$	<u>13</u>
ClONO ₂ in H ₂ SO ₄ • nH ₂ O(l)	200–265	40–75	$H_{\text{ClONO}_2} = 1.6 \times 10^{-6} \times \exp(4710/T) \times \exp(-S_{\text{HOCl}} M_{\text{H}_2\text{SO}_4}) \text{ M atm}^{-1}$ where: $S_{\text{ClONO}_2} = 0.306 + 24.0/T \text{ M}^{-1}$, $M_{\text{H}_2\text{SO}_4} = \text{H}_2\text{SO}_4 \text{ molar conc.}$	<u>14</u>
HBr in H ₂ SO ₄ • nH ₂ O • H ₂ O(l) and H ₂ SO ₄ • nHNO ₃ • mH ₂ O(l)	200–240	40–72	$\ln H^* = a_1 + (b_1 + b_2 \text{ wt})/T$ $a_1 = -11.695 \pm 0.537$, $b_1 = 11,101 \pm 163$, $b_2 = -90.7 \pm 1.2$	<u>15</u>
HOBr in H ₂ SO ₄ • nH ₂ O(l)	201–252	45–252	See Note	<u>16</u>
SO ₂ in H ₂ O (l), H ₂ SO ₄ • nH ₂ O(l)	193–242	0–97	$\ln H^* = a_1 + a_2 \text{ wt} + a_3 \text{ wt}^2 + (b_1 + b_2 \text{ wt} + b_3 \text{ wt}^2)/T$, where: wt is the H ₂ SO ₄ wt. %, $a_1 = -10.778 \pm 2.07$, $a_2 = -0.11541 \pm 0.0827$, $a_3 = 0.0012506 \pm 0.000811$ $b_1 = 3310 \pm 578$, $b_2 = 30.581 \pm 22.2$, $b_3 = -0.35469 \pm 0.209$	<u>17</u>

5.21 Notes to Table 5-6

1. O_3 in $\text{H}_2\text{SO}_4 \cdot n\text{H}_2\text{O}(\text{l})$. Bubble train uptake measurements were performed by Rattigan et al. [458] at 293 K for 1–70 wt.% H_2SO_4 . Recommended expression is a Sechenov coefficient formulation where $H_0 = 0.012 \text{ M atm}^{-1}$ is the 293 K value of H for pure water from Wilhelm et al. [599]. In the measurement, account was taken of the loss of O_3 due to reaction with H^+ . [Back to Table](#)
2. NO_2 in $\text{H}_2\text{SO}_4 \cdot n\text{H}_2\text{O}(\text{l})$. Langenberg et al. [354] present novel capillary gas chromatography measurements for 39, 59, and 68 wt.% H_2SO_4 over the temperature range of 203 to 243 K. However, NO_2 solubility must be derived from chromatographic waveforms which are contorted by much higher N_2O_4 solubility. The resulting values for H_{NO_2} are in the 1 to 10^2 range, but show inconsistent trends with temperature and concentration, indicating possibly large systematic error. [Back to Table](#)
3. HONO in $\text{H}_2\text{SO}_4 \cdot n\text{H}_2\text{O}(\text{l})$. Becker et al. [57] measured HONO partial pressure, P_{HONO} , over bulk solutions in a temperature range of 248–298 K and a H_2SO_4 concentration range of 0–67 wt.%. Longfellow et al. [377] measured P_{HONO} in a wetted wall flow reactor over a temperature range of 218–295 K and an acid concentration range of 60–83 wt.%. Agreement between these two data sets is excellent. H^* decreases from 0 wt.% to 53 wt.% due to physical solubility, then increases above 53 wt.% due to protonation and/or association with H_2SO_4 to make nitrosyl sulfuric acid. Becker et al. parameterize their data as a function of sulfuric acid wt.% and temperature. However, the Becker et al. parameterization is not able to fit the combined sets of Becker et al. [57] and Longfellow et al. [377] data, particularly at the lower temperatures and higher wt.% most relevant to the stratosphere. Therefore, the recommended functional form was used to fit the data for >60 wt.%. This function fits both sets of data very well. It is important to note that this function is only valid for H_2SO_4 concentrations near 60 wt.% and above. The parameterization in Becker et al. [57] should be used to calculate H for H_2SO_4 concentrations <60 wt.%. (Note that the units for H are mol/kg-bar in Becker et al. [57]. The density parameterization of Myhre et al. [428] was used to convert to M/atm units.) [Back to Table](#)
4. HNO_3 and HCl in $\text{H}_2\text{SO}_4 \cdot n\text{H}_2\text{O}(\text{l})$ and $\text{H}_2\text{SO}_4 \cdot n\text{HNO}_3 \cdot m\text{H}_2\text{O}(\text{l})$. Effective Henry's law coefficients, H^* , for HNO_3 , and HCl in binary $\text{H}_2\text{SO}_4/\text{H}_2\text{O}$ and ternary $\text{H}_2\text{SO}_4/\text{HNO}_3/\text{H}_2\text{O}$ solutions over the temperature range 195 to 300 K are required to model the composition and heterogeneous chemistry of stratospheric and upper tropospheric aerosols. Solubility data can be obtained from analysis of heterogeneous uptake experiments with the liquid phase diffusion coefficient estimated from acid solution viscosity (Williams and Long [602]). Solubilities can also be obtained from equilibrium or from vapor pressure data.

Experimental solubility data for HNO_3 is provided by Van Doren et al. [578], Reihs et al. [459] and Zhang et al. [633]. Data for HCl solubility is provided by Watson et al. [595], Hanson and Ravishankara [245, 250], Zhang et al. [633], Williams and Golden [600], Abbatt [2], Elrod et al. [166] and Robinson et al. [472].

These studies all show that trace species solubility in $\text{H}_2\text{SO}_4/\text{H}_2\text{O}$ and $\text{H}_2\text{SO}_4/\text{HNO}_3/\text{H}_2\text{O}$ solutions is a strong function of water activity, which, in turn, depends on both temperature and acid concentrations. Prediction of HNO_3 and HCl H^* values for atmospheric compositions requires a sophisticated model. Comprehensive thermodynamic models of acid solutions for a range of atmospheric conditions have been published by Carslaw et al. [99], Tabazadeh et al. [544] and Luo et al. [383] and reviewed by Carslaw and Peter [101]. These models do an excellent job of reproducing the available experimental data, even for ternary $\text{H}_2\text{SO}_4/\text{HNO}_3/\text{H}_2\text{O}$ solutions (Elrod et al. [166]). These models and the Carslaw review should be consulted for plots/predictions of H^* for HNO_3 and HCl in strong acid solutions over the atmospheric temperature range. The most widely used model of Carslaw et al. [99] was revised in Massucci et al. [392]. [Back to Table](#)

5. HO_2NO_2 in $\text{H}_2\text{SO}_4 \cdot n\text{H}_2\text{O}(\text{l})$. Zhang et al. [632] performed wetted wall flow reactor studies using CIMS to detect HO_2NO_2 uptake over a temperature range of 201–230 K and an acid concentration range of 52.9–74 wt.% H_2SO_4 . $\text{HD}_1^{1/2}$ values were determined for 52.9, 58.3/59.1, 66.4 and 73.8/74 wt.%, with 5 to 15 data points per temperature or temperature pair. All uptake appeared to be reversible with the variation in H strongly temperature dependent, but only moderately dependent on H_2SO_4 wt.%. D_1 values were calculated from a cubic cell model to derive H . Uncertainties in measured H values were estimated by authors to be 25% for $H < 1 \times 10^6 \text{ M atm}^{-1}$ and 50% for $H > 1 \times 10^6 \text{ M atm}^{-1}$. These data were parameterized by Leu and

Zhang [364] in the Sechenov coefficient form adopted by Huthwelker for HOCl [282], and their formulation is recommended. [Back to Table](#)

6. CH_2O in $\text{H}_2\text{SO}_4 \cdot m\text{HNO}_3 \cdot n\text{H}_2\text{O(l)}$. The recommended Henry's Law relationship is:

$$H^* = H(1 + K_2 a_{\text{H}_2\text{O}} + K_3 a_{\text{H}^+})$$

where: $H = 3.4 \times 10^{-5} \exp[-(-0.0456 + 55.5/T)(0.46 m_{\text{H}_2\text{SO}_4} + 0.13 m_{\text{HNO}_3})] \text{ M atm}^{-1}$, T is the temperature in K, and $m_{\text{H}_2\text{SO}_4}$ and m_{HNO_3} are the respective acid molalities; $K_2 = \exp(4020/T - 5.83) \text{ M}^{-1}$, $K_3 = 0.56 \exp[8.84 - (T - 260/T)] \text{ M}^{-1}$, and $a_{\text{H}_2\text{O}}$ and a_{H^+} are the water and H^+ activities which are obtained from a thermodynamic model of the solution, e.g. Carslaw et al. [99]. Valid for 10–85 wt.% H_2SO_4 , 8–40 wt.% HNO_3 , $T = 240\text{--}300 \text{ K}$.

Knudsen cell studies by Tolbert et al. [561] and Iraci and Tolbert [295] and droplet train/flow reactor studies by Jayne et al. [304] all yield data showing that CH_2O is strongly absorbed by sulfuric acid solutions, and Jayne et al. also provide data for ternary acid solutions. The Jayne et al. [304] studies included H_2SO_4 concentrations from 10 to 85 wt.% and HNO_3 concentration between 8 and 40 wt.% with temperature variations from 241 to 300 K. These data were parameterized with three terms, representing physical CH_2O solubility, reversible hydrolysis to $\text{CH}_2(\text{OH})_2$, important in more dilute solutions, and reversible formation of CH_3O^+ , dominant at high acidities. The Jayne et al. [304] parameterization is recommended above. The H^* data from Iraci and Tolbert [295] cover 49 to 95 wt.% H_2SO_4 and a temperature range of 197 to 214.5 K and are in fair agreement with extrapolation of H^* expression from Jayne et al. [304] for concentrations below ~75 wt.%. However, the Iraci and Tolbert data are taken on such thin acid films that initial uptake slopes are difficult to determine accurately and the data scatter is large. While the Iraci and Tolbert data do indicate significantly larger H^* values for H_2SO_4 concentrations above 75 wt.%, the data do not compel a reformulation of the Jayne et al. parameterization. [Back to Table](#)

7. CH_3OH in $\text{H}_2\text{SO}_4 \cdot n\text{H}_2\text{O(l)}$. H^* data from Kane and Leu [321], taken over 40–85 wt.% H_2SO_4 and from 210–235 K, indicate soluble uptake below 65 wt.% and predominately reactive uptake to form methanesulfonic acid and dimethylsulfate above 65 wt.%. Uptake decreased slightly with temperature below 65 wt.% and increases slightly with temperature above. Data yield $H^*k^{1/2}$ at high acid concentrations. Weakly temperature dependent γ s of ~0.15 were measured for 65, 75, and 80 wt.%. However, Knudsen cell studies by Iraci et al. [291] at 45, 61 and 72 wt.% over a 197–223 K temperature range show only well behaved reversible uptake. They argue that low vapor pressures explain the lack of CH_3OH recovery for the short observation times used by Kane and Leu. They also cite three older literature studies on the reaction of methanol and ethanol at room temperature in sulfuric acid which report reaction rate constants much lower than those deduced by Kane and Leu [291]. Iraci et al. present the following parameterization of their data plus data for water:

$$\log H^* = A + 1000B/T$$

where $A = 7.00 + \log M_{\text{H}_2\text{O}}$, $B = 0.000619 m^2 + 0.00544 m + 2.267$, $M_{\text{H}_2\text{O}}$ is the molarity of water in the solution (mol L^{-1}) and m is the molality of the H_2SO_4 (moles H_2SO_4 per kg H_2O).

Note that this parameterization is based only on the Iraci et al. data. A reanalysis of the Kane and Leu [321] results to provide additional data in the 40–72 wt.% range, and H^* values for higher wt.% should be undertaken to validate and extend the Iraci et al. data.

Iraci et al. [294] used infrared spectroscopy to monitor the production of gas phase methyl nitrate, CH_3ONO_2 , from the bulk reaction of ternary sulfuric acid/nitric acid/water solutions with 0.00005–0.005 M CH_3OH in 50.5 to 63.6 wt.% H_2SO_4 with 0.03–0.21 M HNO_3 between 278.2 and 328.6 K. This reaction may complicate determinations of Henry's law solubility of methanol in ternary acid solutions when sulfuric acid concentrations are high enough (probably >70 wt.%) to produce high levels of NO_2^+ , the assumed nitrating agent. [Back to Table](#)

8. $\text{CH}_3\text{CH}_2\text{OH}$ in $\text{H}_2\text{SO}_4 \cdot n\text{H}_2\text{O(l)}$. Michelsen et al. [405] reported Knudsen cell ethanol uptake experiments for 36–76 wt.% H_2SO_4 over a 209–237 K temperature range as well as equilibrium methanol vapor pressure measurements for 0.5 M ethanol in 59.1 wt.% acid between 214.3 and 230.8 K and 0.1 M ethanol in 38.5 wt.% acid between 214.0 and 223.9 K. Henry's law solubility parameters from the two methods agreed well. Solubility increased dramatically with increasing acid wt.% and decreasing temperature. Michelsen et al. present the following parameterization of their data:

$$\log H^* = A + 1000B/T$$

where $A = \Delta S^\circ/2.303R + \log M_{H_2O}$, $B = 5.319 (\chi_{acid})^2 + 0.812 (\chi_{acid}) + 2.647$, and ΔS° is $-174 \text{ mol}^{-1}\text{K}^{-1}$, M_{H_2O} is the molarity of water in the solution calculated at 220K (mol L^{-1}) and χ_{acid} is the mole fraction of sulfuric acid in the solution. Representative values of these parameters are presented in Table 2 of [405].

Timonen and Leu [560] calculated H^* values from their uptake coefficients on 41.1 wt% H_2SO_4 that are in moderate agreement with the Michelsen et al. parameterization. [Back to Table](#)

9. $CH_3C(O)CH_3$ in $H_2SO_4 \cdot nH_2O(l)$. Duncan et al. [161, 162] used IR spectra of thin sulfuric acid films to establish that acetone is absorbed as the protonated species. Above 70 wt.% protonated acetone undergoes a self-condensation/dehydration reaction to form protonated mesityl oxide, which, in turn, reacts with an additional protonated acetone to form trimethyl benzene. Duncan et al. [162] measured reversible uptake and derived Henry's law constants for 70 wt.% H_2SO_4 at 180, 187 and 195 K and a value at 201 K for 76 wt.%. Kane et al. [322] measured uptake in a wetted wall flow reactor and derived H^* parameters for 40, 50, 65, and 75 wt.% over a much wider temperature range than Duncan et al. [162]. Their data diverge above 80 wt.% which they attribute to reactive uptake as suggested by Duncan et al. [161, 162]. Klassen et al. [338] provide Knudsen cell uptake derived data for 48.7 to 78.3 H_2SO_4 wt.% between 210 and 240 K that are generally consistent with that of Kane et al. [322]. Imamura and Akiyoshi [288] report wetted wall flow reactor H^* measurements at 230 K for 50 and 60 wt.%, 250 K for 60, 69 and 76 wt.%, and 270 K for 76 and 79 wt.%; their data diverges a factor of 2 to 4 from that of Kane et al. [322] and Klassen et al. [338].

Equally weighted data sets from Kane et al. [322] and Klassen et al. [338] were combined and fit to generate the recommended parameterization. Two points for the solubility of acetone in water at 298 K and 273 K (Benkelberg et al. [67]) were included to improve the extrapolation to low wt.% solutions. The data points from Imamura and Akiyoshi [288] were not included because they were inconsistent with the other data and have a very different temperature dependence. The few data points from Duncan et al. [161, 162] are also inconsistent with the other data and were not included in the parameterization. Using a rotating wetted-wall flow reactor Esteve and Nozière [167] measured H^* coefficients at 298 ± 3 K for 89.4, 85, 80.8 73.9 and 70 wt.% H_2SO_4 , reporting values of 840, 650, 500, and 320 M atm^{-1} , respectively. These data are not included in the recommended parameterization since the temperature/wt.% range they cover are unlikely to occur in the atmosphere. [Back to Table](#)

10. $CH_3C(O)O_2NO_2$ in H_2O and $H_2SO_4 \cdot nH_2O(l)$. Zhang and Leu [627] performed wetted wall flow reactor studies using CIMS to detect $CH_3C(O)O_2NO_2$ uptake over a temperature range of 199 to 226 K. Uptake studies were performed at 46, 54, 59, and 72 wt.% H_2SO_4 to yield $H^* D_1^{1/2}$ values. D_1 values were calculated from a cubic cell model to derive H^* . Leu and Zhang [364] fit their data from Zhang and Leu [627], including water data from Kames and Schurath [318] and Kames et al. [319], using the Sechenov coefficient form adopted by Huthwelker for HOCl [282]. This formulation is recommended for both water and sulfuric acid solutions. [Back to Table](#)
11. CF_2O in $H_2SO_4 \cdot nH_2O(l)$. Hanson and Ravishankara [244] calculate an upper limit for H of CF_2O based on assumed solubility limit resulting in lack of measurable uptake into 60 wt.% H_2SO_4 . [Back to Table](#)
12. CF_3OH in $H_2SO_4 \cdot nH_2O(l)$. Lovejoy et al. [380] determined reacto-diffusive lengths of $> 0.4 \mu\text{m}$ and $1.0 \mu\text{m}$ for CF_3OH uptake at 250 K on 40 and 50 wt.% H_2SO_4 aerosols, respectively. This leads to H^* estimates of > 240 and 210 M atm^{-1} , respectively. [Back to Table](#)
13. HOCl in $H_2SO_4 \cdot nH_2O(l)$. Recommendation is from the model of Shi et al. [519] which is based on wetted wall flow tube data from Hanson and Ravishankara [249] and Hanson and Lovejoy [241], and uptake by stirred and static solutions by Donaldson et al. [158]. This model incorporates newer, higher temperature data and replaces earlier recommended formulation by Huthwelker et al. [282]. [Back to Table](#)
14. $ClONO_2$ in $H_2SO_4 \cdot nH_2O(l)$. Recommendation is from the model of Shi et al. [519] who used a measurement of the hydrolysis reaction's reacto-diffusive length by Hanson and Lovejoy [240] on 60 wt.% H_2SO_4 at 250 K to derive the hydrolysis rate constant, k_{hyd} , and constrain H_{ClONO_2} at 250 K. Shi et al. fit the $Hk^{1/2}$ dependence of the $ClONO_2$ uptake coefficients for a variety of $ClONO_2$ hydrolysis and $ClONO_2 + HCl$ data to derive a parameterization for H as a function of wt.% and T. [Back to Table](#)

15. HBr in $\text{H}_2\text{SO}_4 \cdot m\text{HNO}_3 \cdot n\text{H}_2\text{O(l)}$. Experimental data for HBr solubility is provided by Williams et al. [601], Abbatt [2], Abbatt and Nowak [10], Kleffman et al. [339], and Behr et al. [60]. Data from time-dependent uptake measurements and from vapor pressure measurements is in good agreement after correcting for the fact that for some of the vapor pressure measurements the HBr concentration in solution was high enough to increase the acidity and thereby decrease the HBr solubility. By comparing pairs of data points with different HBr concentrations (from the same experiment), an average correction factor was obtained. The correction factor was used to correct the vapor pressure data of Williams et al. [601], Abbatt and Nowak [10] and Kleffmann et al. to zero effective HBr concentration. (This is different than the approach taken in Kleffmann et al. of using a “corrected” H_2SO_4 wt.%. However, the resulting parameterization is very similar to the one in Kleffmann et al. [339].) The time-dependent uptake data of Williams et al. [601] and Abbatt [2], and the molecular beam uptake data of Behr et al. [60] did not require correction. All of the experimental data have been fit to obtain the recommended parameterization as a function of H_2SO_4 wt.% and temperature.

Agreement between this parameterization and the updated activity coefficient model of Massucci et al. [392] (and <http://www.hpc1.uea.ac.uk/~e770/aim.html>) is good for > 60 wt.%, but not very good at lower H_2SO_4 wt.%, particularly at low temperatures. Therefore, this parameterization is recommended for calculating HBr Henry’s law solubilities.

The only data for HBr solubilities in ternary solutions is from Kleffmann et al. [339]. The data do not agree well with the updated activity coefficient in Massucci et al. [339] or with the older activity coefficient model in Luo et al. [383]. Until further information becomes available, the recommendation is to use the parameterization for ternary solutions given in Kleffmann et al. [339]. [Back to Table](#)

16. HOBr in $\text{H}_2\text{SO}_4 \cdot n\text{H}_2\text{O(l)}$. HOBr solubility measurements have been reported from coated wall flow reactor uptake studies by Waschewsky and Abbatt[594] and Hanson [232] and from Knudsen cell uptake studies from Iraci et al. [292]. Although they were performed in different temperature ranges, extrapolations of Hanson’s higher temperature data to the temperature range investigated by Waschewsky and Abbatt predicted much higher HOBr solubility than they measured. Iraci et al. subsequently measured HOBr uptake over both of the temperature ranges covered in the prior experiments. Their data agreed well with data from Waschewsky and Abbatt[594] at lower temperatures (213-238 K) but fall far below Hanson’s higher (250-270 K) temperature measurements. The Iraci et al. measurements were performed at ~45, 55, 61 and 70 wt.% H_2SO_4 and investigated over the temperature range from 201 to 252K. Their results, like the earlier studies, indicate that the dependence of H^* on acid concentration is relatively weak. For H_2SO_4 acid wt.% from 55 to 75, H^* is well described by: $\log \text{H}^* = (2349 \pm 280)/T - (5.27 \pm 1.24)$ Their ~45 wt.% data are fit by: $\log \text{H}^* = (3665 \pm 270)/T - (10.63 \pm 1.23)$. [Back to Table](#)
17. SO_2 in $\text{H}_2\text{SO}_4 \cdot n\text{H}_2\text{O(l)}$. Room temperature vapor pressure measurements reviewed by Hayduk et al. [258] and bubble train reactor uptake measurements by Rattigan et al. [458] for 0–70 wt.% H_2SO_4 agree very well. Langenberg et al. [354] used a novel capillary gas chromatography technique to deduce H^* values for 41–83 wt.% H_2SO_4 over a temperature range of 193–242 K. The recommended parameterization is a fair fit to the Rattigan et al. and Langenberg et al. data sets and allows reasonable extrapolation over the full range of atmospheric temperatures. Note that the Langenberg et al. [354] data is in mol/kg-bar units and was converted to mole/l units using the density parameterization of Myhre et al. [428]. [Back to Table](#)

5.22 References

1. Abbatt, J. P. D., 1994, *Geophys. Res. Lett.*, **21**, 665-668.
2. Abbatt, J. P. D., 1995, *J. Geophys. Res.*, **100**, 14009-14017.
3. Abbatt, J. P. D., 1996, *Geophys. Res. Lett.*, **23**, 1681-1684.
4. Abbatt, J. P. D., 1997, *Geophysical Research Letters*, **24**, 1479-1482.
5. Abbatt, J. P. D., 2003, *Chem. Rev.*, **103**, 4783-4800.
6. Abbatt, J. P. D., T. Bartels-Rausch, M. Ullerstam and T. J. Ye, 2008, *Env. Res. Lett.*, **3**, doi:10.1088/1748-9326/3/4/045008.
7. Abbatt, J. P. D., K. D. Beyer, A. F. Fucaloro, J. R. McMahon, P. J. Wooldridge, R. Zhong and M. J. Molina, 1992, *J. Geophys. Res.*, **97**, 15819-15826.
8. Abbatt, J. P. D. and M. J. Molina, 1992, *Geophys. Res. Lett.*, **19**, 461-464.
9. Abbatt, J. P. D. and M. J. Molina, 1992, *J. Phys. Chem.*, **96**, 7674-7679.
10. Abbatt, J. P. D. and J. B. Nowak, 1997, *J. Phys. Chem. A*, **101**, 2131-2137.
11. Abbatt, J. P. D. and G. C. G. Waschewsky, 1998, *J. Phys. Chem. A*, **102**, 3719-3725.
12. Adams, J. W., N. S. Holmes and J. N. Crowley, 2002, *Atmos. Chem. Phys.*, **2**, 79-91.
13. Aguzzi, A. and M. J. Rossi, 1999, *Phys. Chem. Chem. Phys.*, **1**, 4337-4346.
14. Aguzzi, A. and M. J. Rossi, 2001, *Phys. Chem. Chem. Phys.*, **3**, 3707-3716.
15. Aguzzi, A. and M. J. Rossi, 2002, *J. Phys. Chem. A*, **106**, 5891-5901.
16. Akhter, M. S., A. R. Chughtai and D. M. Smith, 1985, *Appl. Spectrosc.*, **39**, 143-153.
17. Akhter, M. S., A. R. Chughtai and D. M. Smith, 1985, *Appl. Spectrosc.*, **39**, 154-167.
18. Akhter, M. S., A. R. Chughtai and D. M. Smith, 1991, *Appl. Spectrosc.*, **45**, 653-665.
19. Al-Abadleh, H. A. and V. H. Grassian, 2000, *J. Phys. Chem. A*, **104**, 11926-11933.
20. Al-Abadleh, H. A. and V. H. Grassian, 2003, *Langmuir*, **19**, 341-347.
21. Alcalá-Jornod, C., H. Van den Bergh and M. J. Rossi, 2000, *Phys. Chem. Chem. Phys.*, **2**, 5584-5593.
22. Alebić-Juretić, A., T. Cvitas and L. Klasinc, 1992, *Ber. Bunsenges Phys. Chem.*, **96**, 493-495.
23. Alebić-Juretić, A., T. Cvitas and L. Klasinc, 2000, *Chemosphere*, **41**, 667-670.
24. Allanic, A., R. Oppliger and M. J. Rossi, 1997, *Journal of Geophysical Research-Atmospheres*, **102**, 23529-23541.
25. Allanic, A., R. Oppliger, H. Van den Bergh and M. J. Rossi, 2000, *Zeitschrift für Physikalische Chemie*, **214**, 11, 1479-1500.
26. Allanic, A. and M. J. Rossi, 1999, *J. Geophys. Res.*, **104**, 18,689-18,696.
27. Allen, H. C., D. E. Gragson and G. L. Richmond, 1999, *J. Phys. Chem. B*, **103**, 660-666.
28. Altschuh, J., R. Bruggemann, H. Santl, G. Eichinger and O. G. Piringier, 1999, *Chemosphere*, **39**, 1871-1887.
29. Ammann, M., M. Kalberer, D. T. Jost, L. Tobler, E. Rossler, D. Piguet, H. W. Gaggeler and U. Baltensperger, 1998, *Nature*, **395**, 157-160.
30. Ammann, M., M. Kalberer, K. Tabor, K. Tobler, C. Zellweger, E. Weingartner, S. Nyeki, Y. Parrat, F. Li, D. Piguet, E. Rossler, D. T. Jost, H. W. Gaggeler and U. Baltensperger. "Proc. 7th Euro. Symp. on Physico-Chem. Behav. of Atmos. Poll.", 1996, 683-687.
31. Anastasio, C. and M. Mozurkewich, 2002, *J. Atmos. Chem.*, **41**, 135-162.
32. Arens, F., L. Gutzwiller, U. Baltensperger, H. Gaggeler and M. Ammann, 2001, *Environ. Sci. Technol.*, **35**, 2191-2199.
33. Badger, C. L., P. T. Griffiths, I. George, J. P. D. Abbatt and R. A. Cox, 2006, *Journal of Physical Chemistry A*, **110**, 6986-6994.
34. Baigrie, L. M., R. A. Cox, H. Slebocka-Tilk, M. Tencer and T. T. Tidwell, 1985, *Journal of the American Chemical Society*, **107**, 3640-3645.
35. Baker, J., S. F. M. Ashbourn and R. A. Cox, 1999, *Phys. Chem. Chem. Phys.*, **1**, 683-690.
36. Baldwin, A. C., 1982, *Int. J. Chem. Kin.*, **14**, 269-277.
37. Baldwin, A. C. and D. M. Golden, 1979, *Science*, **206**, 562.
38. Baldwin, A. C. and D. M. Golden, 1980, *J. Geophys. Res.*, **85**, 2888-2889.
39. Ball, S. M., A. Fried, B. E. Henry and M. Mozurkewich, 1998, *Geophys. Res. Lett.*, **25**, 3339-3342.
40. Baltrusaitis, J., J. Schuttlefield, J. H. Jensen and V. H. Grassian, 2007, *Phys. Chem. Chem. Phys.*, **9**, 4970-4980.
41. Barlett, W. P. and D. W. Margerum, 1999, *Environmental Science and Technology*, **33**, 3410-3414.
42. Barone, S. B., M. A. Zondlo and M. A. Tolbert, 1997, *J. Phys. Chem. A*, **101**, 8643-8652.
43. Barone, S. B., M. A. Zondlo and M. A. Tolbert, 1999, *Journal of Physical Chemistry A*, **103**, 9717-9730.

44. Bartels-Rausch, T., B. Eichler, P. Zimmermann, H. W. Gaggeler and M. Ammann, 2002, *Atmospheric Chemistry and Physics*, **2**, 235-247.
45. Bartels-Rausch, T., C. Guimbaud, H. W. Gaggeler and M. Ammann, 2004, *Geophysical Research Letters*, **31**, 4432.
46. Battino, R. Nitrous oxide in water. In *Oxides of Nitrogen*; C. L. Young, Ed.; Pergamon: Oxford, 1981; Vol. 8; pp 1-22.
47. Battino, R. Oxygen in water. In *Oxygen and Ozone*; R. Battino, Ed.; Pergamon: Oxford, 1981; Vol. 7; pp 1-5.
48. Battino, R. Ethane in water. In *Ethane*; W. Hayduk, Ed.; Pergamon: Oxford, 1982; Vol. 9; pp 1-26.
49. Battino, R. Nitrogen in water. In *Nitrogen and Air*; R. Battino, Ed.; Pergamon: Oxford, 1982; Vol. 10; pp 1-29.
50. Battino, R. Chlorine dioxide in water. In *Sulfur Dioxide, Chlorine, Fluorine and Chlorine Oxides*; C. L. Young, Ed.; Pergamon: Oxford, 1983; Vol. 12; pp 454-456.
51. Battino, R. Chlorine in water. In *Sulfur Dioxide, Chlorine, Fluorine and Chlorine Oxides*; C. L. Young, Ed.; Pergamon: Oxford, 1983; Vol. 12; pp 333-347.
52. Battino, R. Sulfur dioxide in water. In *Sulfur Dioxide, Chlorine, Fluorine and Chlorine Oxides*; C. L. Young, Ed.; Pergamon: Oxford, 1983; Vol. 12; pp 3-33.
53. Battino, R. 2-Methylpropane in water. In *Propane, Butane and 2-Methylpropane*; W. Hayduk, Ed.; Pergamon: Oxford, 1986; Vol. 24; pp 34-37.
54. Battino, R. Butane in water. In *Propane, Butane and 2-Methylpropane*; W. Hayduk, Ed.; Pergamon: Oxford, 1986; Vol. 24; pp 16-32.
55. Battino, R. Propane in water. In *Propane, Butane and 2-Methylpropane*; W. Hayduk, Ed.; Pergamon: Oxford, 1986; Vol. 24; pp 1-15.
56. Battino, R. Methane in water. In *Methane*; H. L. Clever and C. L. Young, Eds.; Pergamon: Oxford, 1987; Vol. 27/28; pp 1-44.
57. Becker, K. H., J. Kleffman, R. Kurtenbach and P. Wiesen, 1996, *J. Phys. Chem.*, **100**, 14,984-14,990.
58. Behnke, W., C. George, V. Scheer and C. Zetsch, 1997, *J. Geophys. Res.*, **102**, 3795-3804.
59. Behnke, W., H.-U. Kruger, V. Scheer and C. Zetzsch, 1991, *J. Aerosol Sci.*, **22**, S609-S612.
60. Behr, P., J. R. Morris, M. D. Antman, B. R. Ringeisen, J. Splan and G. M. Nathanson, 2001, *Geophys. Res. Lett.*, **28**, 1961-1964.
61. Behr, P., J. R. Morris, M. D. Antman, B. R. Ringeisen, J. R. Splan and G. M. Nathanson, 2001, *Geophys. Res. Lett.*, **28**, 1961-1964.
62. Behr, P., U. Scharfenort, K. Ataya and R. Zellner, 2009, *Physical Chemistry Chemical Physics*, **11**, 8048-8055.
63. Behr, P., A. Terziyski and R. Zellner, 2006, *Journal of Physical Chemistry A*, **110**, 8098-8107.
64. Beichert, P. and B. J. Finlayson-Pitts, 1996, *J. Phys. Chem.*, **100**, 15218-15228.
65. Ben-Naim, A. and R. Battino, 1985, *J. Sol. Chem.*, **14**, 245-253.
66. Benes, M. and V. Dohnal, 1999, *J. Chem. Eng. Data*, **44**, 1097-1102.
67. Benkelberg, H. J., S. Hamm and P. Warneck, 1995, *J. Atmos. Chem.*, **20**, 17-34.
68. Benson, B. B., D. Krause and M. A. Peterson, 1979, *J. Sol. Chem.*, **8**, 655-690.
69. Berland, B. S., M. A. Tolbert and S. M. George, 1997, *J. Phys. Chem. A*, **101**, 9954-9963.
70. Bertram, T. H. and J. A. Thornton, 2009, *Atmospheric Chemistry and Physics*, **9**, 8351-8363.
71. Bertram, T. H., J. A. Thornton, T. P. Riedel, A. M. Middlebrook, R. Bahreini, T. S. Bates, P. K. Quinn and D. J. Coffman, 2009, *Geophysical Research Letters*, **36**, L19803.
72. Betterton, E. A., 1991, *Atmos. Environ.*, **25A**, 1473-1477.
73. Betterton, E. A. and M. R. Hoffmann, 1988, *Environ. Sci. Technol.*, **22**, 1415-1418.
74. Betterton, E. A. and J. L. Robinson, 1997, *Journal of the Air and Waste Management Association*, **47**, 1216-1219.
75. Blatchley, E. R., R. W. Johnson, J. E. Alleman and W. F. McCoy, 1991, *Water Research*, **26**, 99-106.
76. Bongartz, A., J. Kames, U. Schurath, C. George, P. Mirabel and J. L. Ponche, 1994, *J. Atmos. Chem.*, **18**, 149-169.
77. Bongartz, A., S. Schweighoefer, C. Roose and U. Schurath, 1995, *J. Atmos. Chem.*, **20**, 35-58.
78. Boniface, J., Q. Shi, Y. Q. Li, J. L. Chueng, O. V. Rattigan, P. Davidovits, D. R. Worsnop, J. T. Jayne and C. E. Kolb, 2000, *J. Phys. Chem. A*, **104**, 7502-7510.
79. Borensen, C., U. Kirchner, V. Scheer, R. Vogt and R. Zellner, 2000, *J. Phys. Chem. A*, **104**, 5036-5045.
80. Bowden, D. J., S. L. Clegg and P. Brimblecombe, 1996, *Chemosphere*, **32**, 405-420.
81. Bowden, D. J., S. L. Clegg and P. Brimblecombe, 1998, *Journal of Atmospheric Chemistry*, **29**, 85-107.

82. Braban, C. F., J. W. Adams, D. Rodriguez, R. A. Cox, J. N. Crowley and G. Schuster, 2007, *Physical Chemistry Chemical Physics*, **9**, 3136-3148.
83. Brouwer, L., M. J. Rossi and D. M. Golden, 1986, *J. Phys. Chem.*, **90**, 4599-4603.
84. Brown, D. E., S. M. George, C. Huang, E. K. L. Wong, K. B. Rider, R. S. Smith and B. D. Kay, 1996, *J. Phys. Chem.*, **100**, 4988-4995.
85. Brown, L. A., V. Vaida, D. R. Hanson, J. D. Graham and J. T. Roberts, 1996, *J. Phys. Chem.*, **100**, 3121-3125.
86. Brown, M. A., P. D. Ashby, D. F. Ogletree, M. Salmeron and J. C. Hemminger, 2008a, *Journal of Physical Chemistry C*, **112**, 8110-8113.
87. Brown, M. A., J. T. Newberg, M. J. Krisch, B. S. Mun and J. C. Hemminger, 2008b, *Journal of Physical Chemistry C*, **112**, 5520-5525.
88. Burkhart, J. F., M. A. Hutterli and R. C. Bales, 2002, *Atmospheric Environment*, **36**, 2157-2163.
89. Burnett, M. G., 1963, *Anal. Chem.*, **35**, 1567-1570.
90. Butler, J. V. A., C. N. Ramchandani and D. W. Thomson, 1935, *J. Chem. Soc.*, 280285.
91. Buxton, G. V., G. A. Salmon and J. Wang, 1999, *Phys. Chem. Chem. Phys.*, **1**, 3589-3593.
92. Cachier, H. Carbonaceous Combustion Aerosols. In *Atmospheric Particles*; R. M. Harrison and R. VanGrieken, Eds.; Wiley: New York, 1998.
93. Caloz, F., F. F. Fenter, K. D. Tabor and M. J. Rossi, 1997, *Rev. Sci. Instrum.*, **68**, 3172-3179.
94. Caloz, F., F. F. Fentner and M. J. Rossi, 1996, *J. Phys. Chem.*, **100**, 7494-7501.
95. Caloz, F., S. Seisel, F. F. Fenter and M. J. Rossi, 1998, *J. Phys. Chem. A*, **102**, 7470-7479.
96. Cappa, C. D., W. S. Drisdell, J. D. Smith, R. J. Saykally and R. C. Cohen, 2005, *Journal of Physical Chemistry B*, **109**, 24391 - 24400.
97. Cappa, C. D., S. E. Kuipers, J. M. Roberts, A. S. Gilbert and M. J. Elrod, 2000, *J. Phys. Chem. A*, **104**, 4449-4457.
98. Carlos-Cuellar, S., P. Li, A. P. Christensen, B. J. Krueger, C. Burrichter and V. H. Grassian, 2003, *J. Phys. Chem. A*, **107**, 4250-4261.
99. Carslaw, K. S., S. L. Clegg and P. Brimblecombe, 1995, *J. Phys. Chem.*, **99**, 11,557-11,574.
100. Carslaw, K. S. and T. Peter, 1997, *Geophys. Res. Lett.*, **24**, 1743-1746.
101. Carslaw, K. S., T. Peter and S. L. Clegg, 1997, *Rev. Geophys.*, **35**, 125-154.
102. Carstens, T., C. Wunderlich and U. Schurath. "*Proceedings EUROTRAC Symposium '96*", 1996, Southampton, U. K., 345-348.
103. Chaix, L., A. Allan and M. J. Rossi, 2000, *J. Phys. Chem. A*, **104**, 7268-7277.
104. Chen, L., N. Takenaka, H. Bandow and Y. Maeda, 2003, *Atmos. Environ.*, **37**, 4817-4822.
105. Cheung, J. L., Y. Q. Li, J. Boniface, Q. Shi, P. Davidovits, D. Worsnop, J. T. Jayne and C. E. Kolb, 2000, *J. Phys. Chem. A*, **104**, 2655-2662.
106. Choi, W. and M. T. Leu, 1998, *J. Phys. Chem A*, **102**, 7618-7630.
107. Chu, L. and L. T. Chu, 1999, *J. Phys. Chem. A*, **103**, 8640-8649.
108. Chu, L. and L. T. Chu, 1999, *J. Phys. Chem. A*, **103**, 691-699.
109. Chu, L., G. Diao and L. T. Chu, 2000, *J. Phys. Chem. A*, **104**, 3150-3158.
110. Chu, L., G. W. Diao and L. T. Chu, 2000, *Journal of Physical Chemistry A*, **104**, 7565-7573.
111. Chu, L. T. and L. Chu, 1997, *Journal of Physical Chemistry B*, **101**, 6271-6275.
112. Chu, L. T., G. Diao and L. Chu, 2002, *J. Phys Chem. B*, **106**, 5679-5688.
113. Chu, L. T. and J. W. Heron, 1995, *Geophys. Res. Lett.*, **22**, 3211-3214.
114. Chu, L. T., M.-T. Leu and L. F. Keyser, 1993, *J. Phys. Chem.*, **97**, 12798-12804.
115. Chu, L. T., M.-T. Leu and L. F. Keyser, 1993, *J. Phys. Chem.*, **97**, 7779-7785.
116. Chughtai, A. R., M. M. O. Atteya, J. Kim, B. K. Konowalchuck and D. M. Smith, 1998, *Carbon*, **36**, 1573-1589.
117. Chughtai, A. R., M. E. Brooks and D. M. Smith, 1993, *Aerosol Science and Technology*, **19**, 121-132.
118. Chughtai, A. R., M. E. Brooks and D. M. Smith, 1996, *J. Geophys. Res.*, **101**, 19505-19514.
119. Chughtai, A. R., S. A. Gordon and D. M. Smith, 1994, *Carbon*, **32**, 405-416.
120. Chughtai, A. R., J. M. Kim and D. M. Smith, 2002, *J. Atmos. Chem.*, **43**, 21-43.
121. Chughtai, A. R., J. M. Kim and D. M. Smith, 2002, *J. Atmos. Chem.*, **45**, 231-243.
122. Chughtai, A. R., N. J. Miller, D. M. Smith and J. R. Pitts, 1999, *J. Atmos. Chem.*, **34**, 259-279.
123. Chughtai, A. R., W. F. Welch, M. S. Akhter and D. M. Smith, 1990, *Appl. Spectrosc.*, **44**, 294-298.
124. Chughtai, A. R., W. F. Welch and D. M. Smith, 1990, *Carbon*, **28**, 411-421.
125. Chughtai, A. R., G. R. Williams, M. M. O. Atteya, N. J. Miller and D. M. Smith, 1999, *Atmos. Environ.*, **33**, 2679-2687.

126. Clappsaddle, C. and D. Lamb, 1989, *Geophys. Res. Lett.*, **16**, 1173-1176.
127. Clegg, S. L. and P. Brimblecombe, 1986, *Atmos. Environ.*, **20**, 2483.
128. Clegg, S. L. and P. Brimblecombe, 1989, *J. Phys. Chem.*, **93**, 7237-7248.
129. Clegg, S. M. and J. P. D. Abbatt, 2001, *Atmos. Chem. and Phys.*, **1**, 73-78.
130. Clegg, S. M. and J. P. D. Abbatt, 2001, *J. Phys. Chem. A*, **105**, 6630-6636.
131. Cofer, W. R., D. R. Schryer and R. S. Rogowski, 1981, *Atmospheric Environment*, **15**, 1281-1286.
132. Cooper, P. L. and J. P. D. Abbatt, 1996, *J. Phys. Chem.*, **100**, 2249-2254.
133. Cosman, L. M. and A. K. Bertram, 2008, *J. Phys. Chem. A*, **112**, 4625-4635.
134. Cosman, L. M., D. A. Knopf and A. K. Bertram, 2008, *J. Phys. Chem. A*, **112**, 2386-2396.
135. Cowin, J. P., personal comm.
136. Cox, R. A., M. A. Fernandez, A. Symington, M. Ullerstam and J. P. D. Abbatt, 2005, *Physical Chemistry Chemical Physics*, **7**, 3434-3442.
137. Dacey, J. W. H., S. G. Wakeham and B. L. Howes, 1984, *Geophys. Res. Lett.*, **11**, 991-994.
138. Dai, D. J., S. J. Peters and G. E. Ewing, 1995, *J. Phys. Chem.*, **99**, 10,299-10,304.
139. Dai, Q., G. N. Robinson and A. Freedman, 1997, *J. Phys. Chem.*, **101**, 4940-4946.
140. Dasgupta, P. K. and S. Dong, 1986, *Atmos. Environ.*, **20**, 565-570.
141. Datta, A., R. G. Cavell, R. W. Tower and Z. M. George, 1985, *J. Phys. Chem.*, **89**, 443-449.
142. Daumer, R. Nissner and D. Klockow, *J. Aerosol Sci.*, **23**, 315-325.
143. Davidovits, P., D. R. Worsnop, J. T. Jayne, C. E. Kolb, P. Winkler, A. Vrtala, P. E. Wagner, M. Kulmala, K. E. J. Lehtinen, T. Vessala and M. Mozurkewich, 2004, *Geophys. Res. Lett.*, **31**, L22111.
144. Davies, J. A. and R. A. Cox, 1998, *J. Phys. Chem. A*, **102**, 7631-7642.
145. De Bruyn, W. J., S. X. Duan, X. Q. Shi, P. Davidovits, D. R. Worsnop, M. S. Zahniser and C. E. Kolb, 1992, *Geophys. Res. Lett.*, **19**, 1939-1942.
146. De Bruyn, W. J., J. A. Shorter, P. Davidovits, D. R. Worsnop, M. S. Zahniser and C. E. Kolb, 1994, *J. Geophys. Res.*, **99**, 16927-16932.
147. De Bruyn, W. J., J. A. Shorter, P. Davidovits, D. R. Worsnop, M. S. Zahniser and C. E. Kolb, 1995, *Environ. Sci Technol.*, **29**, 1179-1185.
148. De Bruyn, W. J., E. Swartz, J. H. Hu, J. A. Shorter, P. Davidovits, D. R. Worsnop and M. S. Zahniser, 1995, *J. Geophys. Res.*, **100**, 7245-7251.
149. DeHaan, D. O. and B. J. Finlayson-Pitts, 1997, *J. Phys. Chem. A*, **101**, 9993-9999.
150. Deiber, G., C. George, S. Le Calve, F. Schweitzer and P. Mirabel, 2004, *Atmos. Chem. Phys.*, **4**, 1291-1299.
151. Delval, C. and M. J. Rossi, 2004, *Physical Chemistry Chemical Physics*, **6**, 4665-4676.
152. Diao, G. W. and L. T. Chu, 2005, *Journal of Physical Chemistry A*, **109**, 1364-1373.
153. Disselkamp, R. S., M. A. Carpenter and J. P. Cowin, 2000, *J. Atmos. Chem.*, **37**, 113-123.
154. Disselkamp, R. S., M. A. Carpenter, J. P. Cowin, C. M. Berkowitz, E. G. Chapman, R. A. Zaveri and N. S. Laulainen, 2000, *J. Geophys. Res.*, **105**, 9767-9771.
155. Dlugokencky, E. J. and A. R. Ravishankara, 1992, *Geophys. Res. Lett.*, **19**, 41-44.
156. Dohnal, V., D. Fenclova and P. Vrbka, 2006, *J. Phys. Chem. Ref. Data*, **35**, 1621-1651.
157. Donaldson, D. J., J. A. Guest and M. C. Goh, 1995, *J. Phys. Chem.*, **99**, 9313-9315.
158. Donaldson, D. J., A. R. Ravishankara and D. R. Hanson, 1997, *J. Phys. Chem. A*, **101**, 4717-4725.
159. Drisdell, W. S., C. D. Cappa, J. D. Smith, R. J. Saykally and R. C. Cohen, 2008, *Atmos. Chem. and Phys.*, **8**, 6699-6706.
160. Duan, S. X., J. T. Jayne, P. Davidovits, D. R. Worsnop, M. S. Zahniser and C. E. Kolb, 1993, *J. Phys. Chem.*, **97**, 2284-2288.
161. Duncan, J. L., L. R. Schindler and J. T. Roberts, 1998, *Geophys. Res. Lett.*, **25**, 631-634.
162. Duncan, J. L., L. R. Schindler and J. T. Roberts, 1999, *J. Phys. Chem. B*, **103**, 7247-7259.
163. Edwards, T. J., G. Maurer, J. Newman and J. M. Prausnitz, 1978, *AIChE Journal*, **24**, 966-976.
164. Elam, J. W., C. E. Nelson, M. A. Cameron, M. A. Tolbert and S. M. George, 1998, *J. Phys. Chem. B*, **102**, 7008-7015.
165. Elliott, S., 1989, *Atmos. Environ.*, **23**, 1977-1980.
166. Elrod, M. J., R. E. Koch, J. E. Kim and M. S. Molina, 1995, *Faraday Discuss*, **100**, 269-278.
167. Esteve, W. and B. Nozière, 2005, *Journal of Physical Chemistry A*, **109**, 10920 - 10928.
168. Fairbrother, D. H. and G. Somorjai, 2000, *J. Phys. Chem. B*, **104**, 4649-4652.
169. Fendel, W., D. Matter, H. Bartscher and A. Schimdt-Ott, 1995, *Atmos. Environ.*, **29**, 967-973.
170. Fendel, W. and A. Schmidt-Ott, 1993, *J. Aerosol Sci.*, **24**, S317-S318.
171. Fenter, F. F., F. Caloz and M. J. Rossi, 1994, *J. Phys. Chem.*, **98**, 9801-9810.

172. Fenter, F. F., F. Caloz and M. J. Rossi, 1996, J. Phys. Chem., **100**, 1008-1019.
173. Fenter, F. F. and M. J. Rossi, 1996, J. Phys. Chem., **100**, 13765-13775.
174. Fenter, F. F. and M. J. Rossi, 1997, J. Phys. Chem. A, **101**, 4110-4113.
175. Fenzel, A., V. Scheer, R. Sikorski, C. George, W. Behnke and C. Zetsch, 1998, J. Phys. Chem. A, **102**, 1329-1337.
176. Fernandez, M. A., R. G. Hynes and R. A. Cox, 2005, Journal of Physical Chemistry A, **109**, 9986-9996.
177. Fickert, S., J. W. Adams and J. N. Crowley, 1999, J. Geophys. Res., **104**, 23719-23727.
178. Fickert, S., F. Helleis, J. W. Adams, G. K. Moortgat and J. N. Crowley, 1998, J. Phys. Chem. A, **102**, 10689-10696.
179. Finlayson-Pitts, B. J., 1983, Nature, **306**, 676-677.
180. Finlayson-Pitts, B. J., 2003, Chemical Reviews (Washington, D. C.), **103**, 4801-4822.
181. Finlayson-Pitts, B. J., M. J. Ezell and J. N. Pitts, Jr., 1989, Nature, **337**, 241-244.
182. Finlayson-Pitts, B. J., F. E. Livingston and H. N. Berko, 1989, J. Phys. Chem., **93**, 4397-4400.
183. Finlayson-Pitts, B. J. and J. N. Pitts *Chemistry of the Upper and Lower Atmosphere: Theory, Experiments and Applications*; Academic: San Diego, 2000.
184. Fluckiger, B. and M. J. Rossi, 2003, Journal of Physical Chemistry A, **107**, 4103-4115.
185. Flückiger, B., A. Thielmann, L. Gutzwiller and M. J. Rossi, 1998, Ber. Bunsenges. Phys. Chem., **102**, 915-928.
186. Fogg, P. G. T. Hydrogen sulfide in water. In *Hydrogen Sulfide, Deuterium Sulfide and Hydrogen Selenide*; P. G. T. Fogg and C. L. Young, Eds.; Pergamon: Oxford, 1988; Vol. 32; pp 1-19.
187. Fogg, P. G. T., S. A. Bligh, M. E. Derrick, Y. P. Yampol'skii, H. L. Clever, A. Skrzecz and C. L. Young, 2002, J. Phys. Chem. Ref. Data, **30**, 1693-1876.
188. Folkers, M., T. F. Mentel and A. Wahner, 2003, Geophysical Research Letters, **30**, 1644.
189. Foster, K. L., M. A. Tolbert and S. M. George, 1997, Journal of Physical Chemistry A, **101**, 4979-4986.
190. Fox, L. E., D. R. Worsnop, M. S. Zahniser and S. C. Wofsy, 1994, Science, **267**, 351-355.
191. Frenzel, A., S. Kutsuna, K. Takeuchi and T. Ibusuki, 2000, Atmos. Environ., **34**, 3641-3544.
192. Frenzel, A., V. Scheer, R. Sikorski, C. George, W. Behnke and C. Zetsch, 1998, J. Phys. Chem. A, **102**, 1329-1337.
193. Friant, S. L. and I. H. Suffet, 1979, Anal. Chem., **51**, 2167-2176.
194. Fried, A., B. E. Henry, J. G. Calvert and M. Mozukewich, 1994, J. Geophys. Res., **99**, 3517-3532.
195. Frinak, E. K. and J. P. D. Abbatt, 2006, Journal of Physical Chemistry A, **110**, 10456-10464.
196. Fung, K. N., I. N. Tang and H. R. Munkelwitz, 1987, Appl. Optics, **26**, 1282-1287.
197. Gebel, M. E. and B. J. Finlayson-Pitts, 2001, J. Phys. Chem. A, **105**, 5178-5187.
198. Gebel, M. E., B. J. Finlayson-Pitts and J. S. Ganske, 2000, Geophys. Res. Lett., **27**, 887-890.
199. George, C., W. Behnke, V. Scheer, C. Zetsch, L. Magi, J. L. Ponche and P. Mirabel, 1995, Geophys. Res. Lett., **22**, 1505-1508.
200. George, C., J. Lagrange, P. Lagrange, P. Mirabel, C. Pallares and J. L. Ponche, 1994, J. Geophys. Res., **99**, 1255-1262.
201. George, C., J. L. Ponche, P. Mirabel, W. Behnke, V. Sheer and C. Zetsch, 1994, J. Phys. Chem., **98**, 8780-8784.
202. George, C., J. Y. Saison, J. L. Ponche and P. Mirabel, 1994, J. Phys. Chem., **98**, 10857-10862.
203. Gerecke, A., A. Thielmann, L. Gutzwiller and M. J. Rossi, 1998, Geophys. Res. Lett., **25**, 2453-2456.
204. Gershenzon, M., P. Davidovits, L. R. Williams, Q. Shi, J. T. Jayne, C. E. Kolb and D. Worsnop, 2004, J. Phys. Chem. A, **106**, 1567-1573.
205. Gershenzon, M. Y., S. Il'in, N. G. Fedotov, Y. M. Gershenzon, E. V. Aparina and V. V. Zelenov, 1999, J. Atmos. Chem., **34**, 119-135.
206. Gershenzon, Y. M., V. M. Grigorieva, A. V. Ivanov and R. G. Remorov, 1995, Faraday Discuss, **100**, 83-100.
207. Gershenzon, Y. M., A. V. Ivanov, S. I. Kucheryavyy and V. B. Rozenshtein, 1986, Kinet. Katal., **27**, 1069-1074.
208. Gershenzon, Y. M. and A. P. Purmal, 1990, Russ. Chem. Rev., **59**, 1007-1023.
209. Gertner, B. J. and J. T. Hynes, 1996, Science, **271**, 1563-1566.
210. Ghosal, S. and J. C. Hemminger, 1999, J. Phys. Chem. A, **103**, 4777-4781.
211. Ghosal, S. and J. C. Hemminger, 2004, Journal of Physical Chemistry B, **108**, 14102-14108.
212. Ghosal, S., A. Shbeeb and J. C. Hemminger, 2000, Geophys. Res. Lett., **27**, 1879.
213. Goldberg, E. D. *Black Carbon in the Environment*; Wiley: New York, 1985.
214. Goodman, A. L., E. T. Bernard and V. H. Grassian, 2001, J. Phys. Chem. A, **105**, 6443-6457.

215. Goodman, A. L., P. Li, C. R. Usher and V. H. Grassian, 2002, J. Phys. Chem. A, **105**, 6109-6120.
216. Graham, J. D. and J. T. Roberts, 1994, J. Phys. Chem., **98**, 5974-5983.
217. Graham, J. D. and J. T. Roberts, 1995, Geophys. Res. Lett., **22**, 251-254.
218. Graham, J. D., J. T. Roberts, L. A. Brown and V. Vaida, 1996, J. Phys. Chem., **100**, 3115-3120.
219. Gratpanche, F. and J.-P. Sawerysyn, 1999, J. Chim. Phys., **96**, 213-231.
220. Griffiths, P. T., C. L. Badger, R. A. Cox, M. Folkers, H. H. Henk and T. F. Mentel, 2009, Journal of Physical Chemistry A, **113**, 5082-5090.
221. Griffiths, P. T. and R. A. Cox, 2009, Atmospheric Science Letters, **10**, 159-163.
222. Guimbaud, C., F. Arens, L. Gutzwiller, H. W. Gäggeler and M. Ammann, 2002, Atmos. Chem. Phys., **2**, 249-257.
223. Gutzwiller, L., F. Arens, U. Baltensperger, H. W. Gäggeler and M. Ammann, 2002, Environ. Sci. Technol., **36**, 677-682.
224. Haag, W. R. and J. Hoigné, 1983, Environ. Sci. Technol., **17**, 261-267.
225. Haag, W. R. and J. Hoigné, 1983, Water Research, **17**, 1397-1402.
226. Hales, J. M. and D. R. Drewes, 1979, Atmos. Environ., **13**, 1133-1147.
227. Hallquist, M., D. J. Stewart, J. Baker and R. A. Cox, 2000, J. Phys. Chem. A, **104**, 3984.
228. Hallquist, M., D. J. Stewart, S. K. Stephenson and R. A. Cox, 2003, Physical Chemistry Chemical Physics, **5**, 3453-3463.
229. Hamm, S., J. Hahn, G. Helas and P. Warneck, 1984, Geophys. Res. Lett., **11**, 1207-1210.
230. Hanisch, F. and J. N. Crowley, 2001, J. Phys. Chem. A, **105**, 3096-3106.
231. Hanning-Lee, M. A., B. B. Brady, L. R. Martin and J. A. Syage, 1996, Geophys. Res. Lett., **23**, 1961-1964.
232. Hanson, D., 2003, J. Geophys. Res., **108**, doi:10.1029/2002JD002519.
233. Hanson, D. and E. Kosciuch, 2003, J. Phys. Chem. A, **107**, 2199-2208.
234. Hanson, D. and E. Kosciuch, 2003, J. Phys. Chem. A, **108**, 5849-5851.
235. Hanson, D. R., 1992, Geophys. Res. Lett., **19**, 2063-2066.
236. Hanson, D. R., 1995, J. Phys. Chem., **99**, 13,059-13,061.
237. Hanson, D. R., 1998, J. Phys. Chem. A, **102**, 4794-4807.
238. Hanson, D. R., J. B. Burkholder, C. J. Howard and A. R. Ravishankara, 1992, J. Phys. Chem., **96**, 4979-4985.
239. Hanson, D. R. and E. R. Lovejoy, 1994, Geophys. Res. Lett., **21**, 2401-2404.
240. Hanson, D. R. and E. R. Lovejoy, 1995, Science, **267**, 1326-1329.
241. Hanson, D. R. and E. R. Lovejoy, 1996, J. Phys. Chem., **100**, 6397-6405.
242. Hanson, D. R. and A. R. Ravishankara, 1991, J. Geophys. Res., **96**, 17307-17314.
243. Hanson, D. R. and A. R. Ravishankara, 1991, J. Geophys. Res., **96**, 5081-5090.
244. Hanson, D. R. and A. R. Ravishankara, 1991, Geophys. Res. Lett., **18**, 1699-1701.
245. Hanson, D. R. and A. R. Ravishankara, 1992, J. Phys. Chem., **96**, 2682-2691.
246. Hanson, D. R. and A. R. Ravishankara, 1992, J. Phys. Chem., **96**, 9441-9446.
247. Hanson, D. R. and A. R. Ravishankara. In *The Tropospheric Chemistry of Ozone in the Polar Regions*; H. Niki and K. H. Becker, Eds.; NATO, 1993; pp 17281-17290.
248. Hanson, D. R. and A. R. Ravishankara, 1993, J. Phys. Chem., **97**, 2802-2803.
249. Hanson, D. R. and A. R. Ravishankara, 1993, J. Geophys. Res., **98**, 22931-22936.
250. Hanson, D. R. and A. R. Ravishankara, 1993, J. Phys. Chem., **97**, 12309-12319.
251. Hanson, D. R. and A. R. Ravishankara, 1994, J. Phys. Chem., **98**, 5728-5735.
252. Hanson, D. R. and A. R. Ravishankara, 1995, Geophys. Res. Lett., **22**, 385-388.
253. Hanson, D. R., A. R. Ravishankara and E. R. Lovejoy, 1996, J. Geophys. Res., **101**, 9063-9069.
254. Hanson, D. R., A. R. Ravishankara and S. Solomon, 1994, J. Geophys. Res., **99**, 3615-3629.
255. Harker, A. B. and W. W. Ho, 1979, Atmos. Environ., **13**, 1005-1010.
256. Harrison, R. M. and G. M. Collins, 1998, J. Atmos. Chem., **30**, 397-406.
257. Hauff, K., R. G. Fischer and K. Ballschmiter, 1998, Chemosphere, **37**, 2599-2615.
258. Hayduk, W., H. Asatani and B. C. Y. Lu, 1988, J. Chem. Eng. Data, **33**, 506-509.
259. Haynes, D. R., N. J. Tro and S. M. George, 1992, J. Phys. Chem., **96**, 8502-8509.
260. He, H., J. Liu, Y. Mu, Y. Yu and M. Chen, 2005, Environmental Science and Technology, **39**, 9637 - 9642.
261. Henson, B. F., K. R. Wilson and J. M. Robinson, 1996, Geophys. Res. Lett., **23**, 1021-1024.
262. Henson, B. F., K. R. Wilson, J. M. Robinson, C. A. Noble, J. L. Casson and D. R. Worsnop, 2004, Journal of Chemical Physics, **121**, 8486-8499.
263. Hill, J. O., I. G. Worsley and L. G. Helper, 1968, J. Phys. Chem., **72**, 3695-3697.
264. Hirokawa, J., K. Onaka, Y. Kajii and H. Akimoto, 1998, Geophys. Res. Lett., **25**, 2449-2452.

265. Hoff, J. T., D. Mackay, R. Gillham and W. Y. Shiu, 1993, *Environ. Sci. Tehcnol.*, **27**, 2174-2180.
266. Hoffman, R. C., M. E. Gebel, B. S. Fox and B. J. Finlayson-Pitts, 2003, *Phys. Chem. Chem. Phys.*, **5**, 1780-1789.
267. Hoffman, R. C., M. Kaleuati and B. J. Finlayson-Pitts, 2003, *J. Phys. Chem. A*, **107**, 7818-7826.
268. Hofmann, D. J. and S. J. Oltmans, 1992, *Geophys. Res. Lett.*, **22**, 2211-2214.
269. Holdren, M. W., C. W. Spicer and J. M. Hales, 1984, *Atmos. Environ.*, **18**, 1171-1173.
270. Holzwarth, G., R. G. Balmer and L. Soni, 1984, *Water Research*, **18**, 1421-1427.
271. Hu, J. H. and J. P. D. Abbatt, 1997, *J. Phys. Chem. A*, **101**, 871-878.
272. Hu, J. H., Q. Shi, P. Davidovits, D. R. Worsnop, M. S. Zahniser and C. E. Kolb, 1995, *J. Phys. Chem.*, **99**, 8768-8776.
273. Hu, J. H., J. A. Shorter, P. Davidovits, D. R. Worsnop, M. S. Zahniser and C. E. Kolb, 1993, *J. Phys. Chem.*, **97**, 11037-11042.
274. Hudson, P. K., K. L. Foster, M. A. Tolbert, S. M. George, S. R. Carlo and V. H. Grassian, 2001, *J. Phys. Chem. A*, **105**, 694-702.
275. Hudson, P. K., J. E. Shilling, M. A. Tolbert and O. B. Toon, 2002, *J. Phys. Chem. A*, **106**, 9874-9882.
276. Huff, A. K. and J. P. D. Abbatt, 2000, *Journal of Physical Chemistry A*, **104**, 7284-7293.
277. Huff, A. K. and J. P. D. Abbatt, 2002, *Journal of Physical Chemistry A*, **106**, 5279-5287.
278. Huie, R. E., C. L. Clifton and P. Neta, 1991, *Radiat. Phys. Chem.*, **38**, 477-481.
279. Hunt, S. W., M. Roesolová, W. Wang, L. M. Wingen, E. M. Knipping, D. J. Tobias, D. Dabdub and B. J. Finlayson-Pitts, 2004, *J. Phys. Chem. A*, **108**, 11559-11572.
280. Huntzicker, J. J., R. A. Cary and C.-S. Ling, 1980, *Environ. Sci. Technol.*, **14**, 819-824.
281. Huthwelker, T., M. Ammann and T. Peter, 2006, *Chem. Rev.*, **106**, 1375-1444.
282. Huthwelker, T., T. Peter, B. P. Juo, S. L. Clegg, K. S. Carshaw and P. Brimblecombe, 1995, *J. Atmos. Chem.*, **21**, 81-95.
283. Hwang, H. and P. K. Dasgupta, 1985, *Environ. Sci. Technol.*, **19**, 255-258.
284. Hynes, A. J., M. A. Fernandez and R. A. Cox, 2002, *J. Geophys. Res.*, **107**, 4797.
285. Hynes, R. G., M. A. Fernandez and R. A. Cox, 2002, *Journal of Geophysical Research-Atmospheres*, **107**.
286. Hynes, R. G., J. C. Mossinger and R. A. Cox, 2001, *Geophysical Research Letters*, **28**, 2827-2830.
287. Il'in, S. D., V. V. Selikhonovich, Y. M. Gershenson and V. B. Rozenshtein, 1991, *Sov. J. Chem. Phys.*, **8**, 1858-1880.
288. Imamura, T. and H. Akiyoshi, 2000, *Geophys. Res. Lett.*, **27**, 1419-1422.
289. Imamura, T., Y. Rudich, R. K. Talukdar, R. W. Fox and A. R. Ravishankara, 1997, *J. Phys. Chem.*, **101**, 2316-2322.
290. Ip, H. S. S., X. H. H. Huang and J. Z. Yu, 2009, *Geophysical Research Letters*, **36**, L01802.
291. Iraci, L. T., A. M. Essin and D. M. Golden, 2002, *J. Phys. Chem. A*, **106**, 4054-4060.
292. Iraci, L. T., R. R. Michelsen, S. F. M. Ashbourn, T. A. Rammer and D. M. Golden, 2005, *Atmospheric Chemistry and Physics*, **5**, 1577-1587.
293. Iraci, L. T., A. M. Middlebrook, M. A. Wilson and M. A. Tolbert, 1994, *Geophys. Res. Lett.*, **21**, 867-870.
294. Iraci, L. T., B. G. Riffel, C. B. Robinson, R. R. Michelsen and R. M. Stephenson, 2007, *Journal of Atmospheric Chemistry*, **58**, 253-266.
295. Iraci, L. T. and M. A. Tolbert, 1997, *J. Geophys. Res.*, **102**, 16,099-16,107.
296. Ivanov, A. V., Y. M. Gershenson, F. Gratpanche, P. Devolder and J.-P. Savarysyn, 1996, *Ann. Geophys.*, **14**, 659-664.
297. Jaegle, L., C. R. Webster, R. D. May, D. C. Scott, R. M. Stimpfle, D. W. Kohn, P. O. Wennberg, T. F. Hansico, R. C. Cohen, M. H. Proffitt, K. K. Kelly, J. Elkins, D. Baumgardner, J. E. Dye, J. C. Wilson, R. F. Pueschel, K. R. Chan, R. J. Salawitch, A. F. Tuck, S. J. Hovde and Y. L. Yung, 1997, *J. Geophys. Res.*, **102**, 13,235-13,253.
298. Jakubczyk, D., M. Zientara, K. Kolwas and M. Kolwas, 2007, *Journal of Atmospheric Science*, **64**, 996-1004.
299. Jans, U. and J. Hoigne, 2000, *Atmos. Environ.*, **34**, 1069-1085.
300. Jayne, J. T., P. Davidovits, D. R. Worsnop, M. S. Zahniser and C. E. Kolb, 1990, *J. Phys. Chem.*, **94**, 6041-6048.
301. Jayne, J. T., S. X. Duan, P. Davidovits, D. R. Worsnop, M. S. Zahniser and C. E. Kolb, 1991, *J. Phys. Chem.*, **95**, 6329-6336.
302. Jayne, J. T., S. X. Duan, P. Davidovits, D. R. Worsnop, M. S. Zahniser and C. E. Kolb, 1992, *J. Phys. Chem.*, **96**, 5452-5460.

303. Jayne, J. T., U. Poschl, Y. Chen, D. Dai, L. T. Molina, D. R. Worsnop, C. E. Kolb and M. J. Molina, 1997, *J. Phys. Chem. A*, **101**, 10,000-10,011.
304. Jayne, J. T., D. R. Worsnop, C. E. Kolb, E. Swartz and P. Davidovits, 1996, *J. Phys. Chem.*, **100**, 8015-8022.
305. Jedlovszky, P., G. Hantal, K. Neurohr, S. Picaud, P. N. M. Hoang, P. von Hessberg and J. N. Crowley, 2008, *Journal of Physical Chemistry C*, **112**, 8976-8987.
306. Jedlovszky, P., L. Partay, P. N. M. Hoang, S. Picaud, P. von Hessberg and J. N. Crowley, 2006, *Journal of the American Chemical Society*, **128**, 15300-15309.
307. Jefferson, A., F. L. Eisele, P. J. Ziemann, R. J. Weber, J. J. Marti and P. H. McMurry, 1997, *J. Geophys. Res.*, **102**, 19,021-19,028.
308. Jenkins, J. and M. B. King, 1965, *Chem. Engin. Sci.*, **20**, 921-922.
309. Jin, R. H. and L. T. Chu, 2007, *Journal of Physical Chemistry A*, **111**, 7833-7840.
310. Johnson, B. J., E. A. Betterton and D. Craig, 1996, *J. Atmos. Chem.*, **24**, 113-119.
311. Jungwirth, P. and D. Tobias, 2001, *J. Phys. Chem. B.*, **105**, 10468-10472.
312. Jungwirth, P. and D. J. Tobias, 2002, *J. Phys. Chem. B*, **106**, 6361-6373.
313. Junkermann, W. and T. Ibusuki, 1992, *Atmos. Environ.*, **26A**, 3099-3103.
314. Kalberer, M., M. Ammann, F. Arens, H. W. Gaggeler and U. Baltensperger, 1999, *J. Geophys. Res.*, **104**, 13825-13832.
315. Kalberer, M., M. Ammann, H. W. Gaggeler and U. Baltensperger, 1999, *Atmos. Environ.*, **33**, 2815-2822.
316. Kalberer, M., K. Tabor, M. Ammann, Y. Parrat, E. Weingartner, D. Piguet, E. Rossler, D. T. Jost, A. Turler, H. W. Gaggeler and U. Baltensperger, 1996, *J. Phys. Chem.*, **100**, 15487-15493.
317. Kames, J. and U. Schurath, 1992, *J. Atmos. Chem.*, **15**, 79-95.
318. Kames, J. and U. Schurath, 1995, *J. Atmos. Chem.*, **21**, 151-164.
319. Kames, J., S. Schweighoefer and U. Schurath, 1991, *J. Atmos. Chem.*, **12**, 169-180.
320. Kamm, S., O. Mohler, K.-H. Naumann, H. Saathoff and U. Schurath, 1999, *Atmos. Environ.*, **33**, 4651-4661.
321. Kane, S. M. and M.-T. Leu, 2001, *J. Phys. Chem. A*, **105**, 1411-1415.
322. Kane, S. M., R. S. Timonen and M. T. Leu, 1999, *J. Phys. Chem. A*, **103**, 9259-9265.
323. Karge, H. G. and I. G. Dalla Lana, 1984, *J. Phys. Chem.*, **88**, 1538-1543.
324. Karlsson, R. and E. Ljungstrom, 1995, *J. Aerosol Sci.*, **26**, 39-50.
325. Katrib, Y., G. Deiber, F. Schweitzer, P. Mirabel and C. George, 2001, *J. Aerosol Sci.*, **32**, 893-911.
326. Katrib, Y., Y. Deiber, P. Mirabel, S. Le Calve, C. George, A. Mellouki and G. Le Bras, 2002, *J. Atmos. Chem.*, **43**, 151-174.
327. Katrib, Y., P. Mirabel, S. Le Calve, G. Weck and E. Kochanski, 2002, *J. Phys. Chem. B.*, **106**, 7237-7245.
328. Kelley, C. M. and H. V. Tartar, 1956, *J. Amer. Chem. Soc.*, **78**, 5752-5756.
329. Kenner, R. D., I. C. Plumb and K. R. Ryan, 1993, *Geophys. Res. Lett.*, **20**, 193-196.
330. Kerbrat, M., S. Le Calve and P. Mirabel, 2007, *Journal of Physical Chemistry A*, **111**, 925-931.
331. Keyser, L. F. and M.-T. Leu, 1993, *Micros. Res. Technol.*, **25**, 434-438.
332. Keyser, L. F. and M.-T. Leu, 1993, *J. Colloid Interface Sci.*, **155**, 137-145.
333. Keyser, L. F., M.-T. Leu and S. B. Moore, 1993, *J. Phys. Chem.*, **97**, 2800-2801.
334. Keyser, L. F., S. B. Moore and M. T. Leu, 1991, *J. Phys. Chem.*, **95**, 5496-5502.
335. Khan, I., P. Brimblecombe and S. L. Clegg, 1995, *J. Atmos. Chem.*, **22**, 285-302.
336. Kirchner, U., T. Benter and R. N. Schindler, 1997, *Phys. Chem. Chem. Phys.*, **101**, 975-977.
337. Kirchner, U., V. Scheer and R. Vogt, 2000, *J. Phys. Chem. A*, **104**, 8908-8915.
338. Klassen, J. K., J. Lynton, D. M. Golden and L. R. Williams, 1999, *J. Geophys. Res.*, **104**, 26,355-26,361.
339. Kleffman, J., K. H. Becker, R. Broske, D. Rothe and P. Wiesen, 2000, *J. Phys. Chem. A*, **104**, 8489-8495.
340. Kleffman, J., K. H. Becker, M. Lackhoff and P. Wiesen, 1999, *Phys. Chem. Chem. Phys.*, **1**, 5443-5450.
341. Kleffman, J., K. H. Becker and P. Wiesen, 1998, *Atmos. Environ.*, **32**, 3129-3137.
342. Klimovskii, A. O., A. V. Bavin, V. S. Tkalic and A. A. Lisachenko, 1983, *React. Kinet. Catal. Lett.*, **23**, 95-98.
343. Knipping, E. M., M. J. Lakin, K. L. Foster, P. Jungwirth, D. J. Tobias, R. B. Gerber, D. Dabdub and B. J. Finlayson-Pitts, 2000, *Science*, **288**, 301-306.
344. Knopf, D. A., L. M. Cosman, P. Mousavi, S. Mokamati and A. K. Bertram, 2007, *J. Phys. Chem. A*, **111**, 11021-11032.
345. Koch, T. G. and M. J. Rossi, 1998, *J. Phys. Chem. A*, **102**, 9193-9201.
346. Koch, T. G., H. vandenBergh and M. J. Rossi, 1999, *Phys. Chem. Chem. Phys.*, **1**, 2687-2694.

347. Koehler, B. G., L. S. McNeill, A. M. Middlebrook and M. A. Tolbert, 1993, *J. Geophys. Res.*, **98**, 10563-10571.
348. Koehler, B. G., V. T. Nicholson, H. G. Roe and E. S. Whitney, 1999, *J. Geophys. Res.*, **104**, 5507-5514.
349. Kolb, C. E., D. R. Worsnop, M. S. Zahniser, P. Davidovits, L. F. Keyser, M.-T. Leu, M. J. Molina, D. R. Hanson, A. R. Ravishankara, L. R. Williams and M. A. Tolbert. Progress and Problems in Atmospheric Chemistry. In *Adv. Phys. Chem. Series*, 3; J. R. Barker, Ed., 1994; pp 771-875.
350. Koop, T., A. Kapilashrami, L. T. Molina and M. J. Molina, 2000, *Journal of Geophysical Research-Atmospheres*, **105**, 26393-26402.
351. Kroes, G.-J. and D. C. Clary, 1992, *J. Phys. Chem.*, **96**, 7079-7088.
352. Kutsuna, S., L. Chen, T. Abe, J. Mizukado, T. Uchimaru, K. Tokuhashi and A. Sekiya, 2005, *Atmos. Environ.*, **39**, 5884-5892.
353. Kutsuna, S., L. Chen, K. Ohno, K. Tokuhashi and A. Sekiya, 2004, *Atmos. Environ.*, **38**, 725-732.
354. Langenberg, S., V. Proksch and U. Schurath, 1998, *Atm. Environ.*, **32**, 3129-3137.
355. Langenberg, S. and U. Schurath, 1999, *Geophysical Research Letters*, **26**, 1695-1698.
356. Langer, S., R. S. Pemberton and B. J. Finlayson-Pitts, 1997, *J. Phys. Chem. A*, **101**, 1277-1286.
357. Laskin, A., H. Wang, W. H. Robertson, J. P. Cowin, M. J. Ezell and B. J. Finlayson-Pitts, 2006, *Journal of Physical Chemistry A*, **110**, 10619-10627.
358. Lemmon, E. W., M. O. McLinden and D. G. Friend. Thermophysical properties of fluid systems. In *NIST Chemistry WebBook; NIST Standard Reference Database No. 69*; W. G. Mallard and P. J. Linstrom, Eds.; National Institute of Standards and Technology: Gaithersburg, MD, 2000.
359. Leu, M.-T., 1988, *Geophys. Res. Lett.*, **15**, 17-20.
360. Leu, M.-T., 1988, *Geophys. Res. Lett.*, **15**, 851-854.
361. Leu, M.-T., S. B. Moore and L. F. Keyser, 1991, *J. Phys. Chem.*, **95**, 7763-7771.
362. Leu, M.-T., R. S. Timonen and L. F. Keyser, 1997, *J. Phys. Chem. A*, **101**, 278-282.
363. Leu, M.-T., R. S. Timonen, L. F. Keyser and Y. L. Yung, 1995, *J. Phys. Chem.*, **99**, 13203-13212.
364. Leu, M.-T. and R. Zhang, 1999, *Geophys. Res. Lett.*, **26**, 1129-1132.
365. Li, P., K. A. Perreau, E. Covington, C. H. Song, G. R. Carmichael and V. H. Grassian, 2001, *J. Geophys. Res.*, **106**, 5517-5529.
366. Li, Y. Q., P. Davidovits, Q. Shi, J. T. Jayne, C. E. Kolb and D. R. Worsnop, 2001, *J. Phys. Chem. A*, **105**, 10623-10634.
367. Li, Y. Q., H. Z. Zhang, P. Davidovits, J. T. Jayne, C. E. Kolb and D. R. Worsnop, 2002, *J. Phys. Chem. A*, **106**, 1220-1227.
368. Li, Z., R. R. Friedl, S. B. Moore and S. P. Sander, 1996, *J. Geophys. Res.*, **101**, 6795-6802.
369. Liberti, A., D. Brocco and M. Possanzini, 1978, *Atmos. Environ.*, **12**, 255-261.
370. Lind, J. A. and G. L. Kok, 1986, *Journal of Geophysical Research*, **91**, 7889-7895.
371. Lind, J. A. and G. L. Kok, 1994, *J. Geophys. Res.*, **99**, 21119.
372. Liu, J., Y. Yu, Y. Mu and H. He, 2006, *Journal of Physical Chemistry B*, **110**, 3225-3230.
373. Liu, Y., J. P. Cain, H. Wang and A. Laskin, 2007, *Journal of Physical Chemistry A*, **111**, 10026-10043.
374. Liu, Y., H. He and Y. Mu, 2008, *Atmospheric Environment*, **42**, 960-969.
375. Liu, Y., Q. Ma and H. He, 2009, *Atmos. Chem. Phys.*, **9**, 6273-6286.
376. Livingston, F. E. and B. J. Finlayson-Pitts, 1991, *Geophys. Res. Lett.*, **18**, 17-21.
377. Longfellow, C. A., T. Imamura, A. R. Ravishankara and D. R. Hanson, 1998, *J. Phys. Chem. A*, **102**, 3323-3332.
378. Longfellow, C. A., A. R. Ravishankara and D. R. Hanson, 1999, *J. Geophys. Res.*, **104**, 13833.
379. Longfellow, C. A., A. R. Ravishankara and D. R. Hanson, 2000, *J. Geophys. Res.*, **105**, 24,345-24,350.
380. Lovejoy, E. R., L. G. Huey and D. R. Hanson, 1995, *J. Geophys. Res.*, **100**, 18,775-18,780.
381. Luick, T. J., R. W. Heckbert, K. Schultz and R. S. Disselkamp, 1999, *J. Atmos. Chem.*, **32**, 315-325.
382. Luke, W. T., R. R. Dickerson and L. J. Nunnermacker, 1989, *J. Geophys. Res.*, **94**, 14905-14921.
383. Luo, B., K. S. Carslaw, T. Peter and S. L. Clegg, 1995, *Geophys. Res. Lett.*, **22**, 247-250.
384. Ma, Q., Y. Liu and H. He, 2008, *Journal of Physical Chemistry A*, **112**, 6630-6635.
385. Maerefat, M., T. Akamatsu and S. Fujikawa, 1990, *Experiments in Fluids*, **9**, 345.
386. Magee, N., A. M. Moyle and D. Lamb, 2006, *Geophysical Research Letters*, **33**, 4403.
387. Magi, L., F. Schweitzer, C. Pallares, S. Cherif, P. Mirabel and C. George, 1997, *J. Phys. Chem. A*, **4**, 4943-4948.
388. Manion, J. A., C. M. Fittschen, D. M. Golden, L. R. Williams and M. A. Tolbert, 1994, *Israel J. Chem.*, **34**, 355-363.
389. Marek, R. and J. Straub, 2001, *Int. J. Heat Mass Transfer*, **44**, 39-53.

390. Marti, J., K. Mauersberger and D. Hanson, 1991, *Geophysical Research Letters*, **18**, 1861-1864.
391. Martin, L. R., H. S. Judeikis and M. Wun, 1980, *J. Geophys. Res.*, **85**, 5511-5518.
392. Massucci, M., S. L. Clegg and P. Brimblecombe, 1999, *J. Phys. Chem. A*, **103**, 4209-4226.
393. Mawhinney, D. B. and J. J. T. Yates, 2001, *Carbon*, **39**, 1167-1173.
394. McMurry, P. H., H. Takano and G. R. Anderson, 1983, *Environ. Sci. Technol.*, **17**, 347-357.
395. McNeill, V. F., F. M. Geiger, T. Loerting, B. L. Trout, L. T. Molina and M. J. Molina, 2007, *Journal of Physical Chemistry A*, **111**, 6274-6284.
396. McNeill, V. F., T. Loerting, F. M. Geiger, B. L. Trout and M. J. Molina, 2006, *Proceedings of the National Academy of Sciences of the United States of America*, **103**, 9422-9427.
397. McNeill, V. F., J. Patterson, G. M. Wolfe and J. A. Thornton, 2006, *Atmospheric Chemistry and Physics*, **6**, 1635-1644.
398. Meisel, D. and G. Czapski, 1975, *J. Phys. Chem.*, **79**, 1503-1509.
399. Mental, T. F., M. Sohn and A. Wahner, 1999, *Phys. Chem. Chem. Phys.*, **1**, 5451-5457.
400. Mertes, S. and A. Wahner, 1995, *J. Phys. Chem.*, **99**, 14000-14006.
401. Michel, A. E., C. R. Usher and V. H. Grassian, 2002, *Geophys. Res. Lett.*, **29**, 3249.
402. Michel, A. E., C. R. Usher and V. H. Grassian, 2003, *Atmos. Environ.*, **37**, 3201-3211.
403. Michelangeli, D. V., M. Allen and Y. L. Yung, 1991, *Geophys. Res. Lett.*, **18**, 673-676.
404. Michelsen, R. R., S. F. M. Ashbourn and L. T. Iraci, 2004, *Journal of Geophysical Research, D: Atmospheres*, **109**, D23205.
405. Michelsen, R. R., S. J. R. Staton and L. T. Iraci, 2006, *Journal of Physical Chemistry A*, **110**, 6711 - 6717.
406. Middlebrook, A. M., L. T. Iraci, L. S. McNeil, B. G. Koehler, M. A. Wilson, O. W. Saastad and M. A. Tolbert, 1993, *J. Geophys. Res.*, **98**, 20473-20481.
407. Middlebrook, A. M., B. G. Koehler, L. S. McNeill and M. A. Tolbert, 1992, *Geophys. Res. Lett.*, **19**, 2417-2420.
408. Mihelcic, D., D. Klemp, P. Megen, H. W. Ptz and A. Volz-Thomas, 1993, *J. Atmos. Chem.*, **16**, 313-335.
409. Miller, T. M. and V. H. Grassian, 1998, *Geophys. Res. Lett.*, **25**, 3835-3838.
410. Mochida, M., H. Akimoto, H. v. d. Bergh and M. J. Rossi, 1998, *J. Phys. Chem. A*, **102**, 4819-4828.
411. Mochida, M., J. Hirokawa and H. Akimoto, 2000, *Geophys. Res. Lett.*, **27**, 2629-2632.
412. Mochida, M., J. Hirokawa, Y. Kajii and H. Akimoto, 1998, *Geophys. Res. Lett.*, **25**, 3927-3930.
413. Mogili, P. K., P. D. Kleiber, M. A. Young and V. H. Grassian, 2006, *Journal of Physical Chemistry A*, **110**, 13799-13807.
414. Molina, M. J., R. F. Meads, D. D. Spencer and L. T. Molina, 1997, *Geophys. Res. Lett.*, **24**, 1619-1622.
415. Molina, M. J., T. L. Tso, L. T. Molina and F. C. Wang, 1987, *Science*, **238**, 1253-1259.
416. Molina, M. J., R. Zhang, P. J. Woolridge, J. R. McMahon, J. E. Kim, H. Y. Chang and K. D. Beyer, 1993, *Science*, **261**, 1418-1423.
417. Moore, S. B., L. F. Keyser, M. T. Leu, R. P. Turco and R. H. Smith, 1990, *Nature*, **345**, 333-335.
418. Mossinger, J. C. and R. A. Cox, 2001, *Journal of Physical Chemistry A*, **105**, 5165-5177.
419. Mossinger, J. C., R. G. Hynes and R. A. Cox, 2002, *J. Geophys. Res.*, **107**, 4740.
420. Mozurkewich, M. and J. Calvert, 1988, *J. Geophys. Res.*, **93**, 15882-15896.
421. Mozurkewich, M., P. H. McMurray, A. Gupta and J. G. Calvert, 1987, *J. Geophys. Res.*, **92**, 4163-4170.
422. Msibi, I. M., Y. Li, J. P. Shi and R. M. Harrison, 1994, *J. Atmos. Chem.*, **18**, 291-300.
423. Msibi, I. M., J. P. Shi and R. M. Harrison, 1993, *J. Atmos. Chem.*, 17339-17351.
424. Muentert, A. H. and B. G. Koehler, 2000, *J. Phys. Chem. A*, **104**, 8527-8534.
425. Müller, B. and M. R. Heal, 2002, *Phys. Chem. Chem. Phys.*, **4**, 3365-3369.
426. Munder, B., H. Lidal and O. C. Sandall, 2000, *J. Chem. Eng. Data*, **45**, 1201-1204.
427. Murray, B. J. and M. C. Plane, 2003, *Phys. Chem. Chem. Phys.*, **107**, 4129-4138.
428. Myhre, C. E. L., C. J. Nielsen and O. W. Saastad, 1998, *J. Chem. Eng. Data*, **43**, 617-622.
429. Nathanson, G. M., 2004, *Annual Review of Physical Chemistry*, **55**, 231-255.
430. Noyes, R. M., M. B. Rubin and P. G. Bowers, 1996, *J. Phys. Chem.*, **100**, 4167-4172.
431. O'Sullivan, D. W., M. Lee, B. C. Noone and B. G. Heikes, 1996, *J. Phys. Chem.*, **100**, 3241-3247.
432. Ocampo, J. and J. Klinger, 1982, *Journal of Colloid and Interface Science*, **86**, 377-383.
433. Olszyna, K., R. D. Cadle and R. G. dePena, 1979, *J. Geophys. Res.*, **84**, 1771-1775.
434. Oppliger, R., A. Allan and M. J. Rossi, 1997, *J. Phys. Chem. A*, **101**, 1903-1911.
435. Oum, K. W., M. J. Lakin, D. O. DeHaan, T. Brauers and B. J. Finlayson-Pitts, 1998, *Science*, **297**, 74-76.
436. Oum, K. W., M. J. Lakin and B. J. Finlayson-Pitts, 1998, *Geophysical Research Letters*, **25**, 3923-3926.
437. Park, J. H., A. V. Ivanov and M. J. Molina, 2008, *Journal of Physical Chemistry A*, **112**, 6968-6977.

438. Park, S.-C., D. K. Burden and G. M. Nathanson, 2007, *The Journal of Physical Chemistry A*, **111**, 2921-2929.
439. Park, S.-C., D. K. Burden and G. M. Nathanson, 2009, *Accounts of Chemical Research*, **42**, 379-387.
440. Parker, V. D., 1992, *J. Am. Chem. Soc.*, **114**, 7458-7462.
441. Parker, V. D., 1992, *Acta Chem. Scan.*, **45**, 692-694.
442. Percival, C. J., J. C. Mossinger and R. A. Cox, 1999, *Physical Chemistry Chemical Physics*, **1**, 4565-4570.
443. Peters, S. J. and G. E. Ewing, 1996, *J. Phys. Chem.*, **100**, 14093-14102.
444. Petitjean, M., P. Mirabel and S. Le Calve, 2009, *Journal of Physical Chemistry A*, **113**, 5091-5098.
445. Peybernes, N., S. Le Calve, P. Mirabel, S. Picaud and P. N. M. Hoang, 2004, *Journal of Physical Chemistry B*, **108**, 17425-17432.
446. Peybernes, N., C. Marchand, S. Le Calve and P. Mirabel, 2004, *Physical Chemistry Chemical Physics*, **6**, 1277-1284.
447. Picaud, S., P. N. M. Hoang, N. Peybernes, S. Le Calve and P. Mirabel, 2005, *Journal of Chemical Physics*, **122**.
448. Ponche, J. L., C. George and P. Mirabel, 1993, *J. Atmos. Chem.*, **16**, 1-21.
449. Poschl, U., M. Canagaratna, J. T. Jayne, L. T. Molina, D. R. Worsnop, C. E. Kolb and M. J. Molina, 1998, *J. Phys. Chem. A*, **102**, 10,082-10,089.
450. Pöschl, U., T. Letzel, C. Schauer and R. Niessner, 2001, *J. Phys. Chem. A*, **105**, 4029-4041.
451. Poskrebyshev, G. A., R. E. Huie and P. Neta, 2003, *J. Phys. Chem. A*, **107**, 1964-1970.
452. Pouvesle, N., M. Kippenberger, G. Schuster and J. N. Crowley, 2010, *Physical Chemistry Chemical Physics*, **12**, 15544-15550.
453. Pratte, P. and M. J. Rossi, 2006b, *Physical Chemistry Chemical Physics*, **8**, 3988-4001.
454. Pratte, P., H. van den Bergh and M. J. Rossi, 2006a, *Journal of Physical Chemistry A*, **110**, 3042-3058.
455. Przyjazny, A., W. Janicki, W. Chrzanowski and R. Staszewski, 1984, *J. Chromatogr.*, **280**, 249-260.
456. Pueschel, R. F., D. F. Blake, A. G. Suetsinger, A. D. A. Hansen, S. Verma and K. Kato, 1992, *Geophys. Res. Lett.*, **19**, 1659-1662.
457. Quinlan, M. A., C. M. Reihls, D. M. Golden and M. A. Tolbert, 1990, *J. Phys. Chem.*, **94**, 3255-3260.
458. Rattigan, O. V., J. Boniface, E. Swartz, P. Davidovits, J. T. Jayne, C. E. Kolb and D. R. Worsnop, 2000, *J. Geophys. Res.*, **105**, 29,065-29,078.
459. Reihls, C. M., D. M. Golden and M. A. Tolbert, 1990, *J. Geophys. Res.*, **95**, 16,545-16,550.
460. Remorov, R. G., Y. M. Gershenzon, L. T. Molina and M. J. Molina, 2002, *J. Phys. Chem. A*, **106**, 4558-4565.
461. Rettich, T. R., R. Battino and E. Wilhelm, 1982, *Ber. Bunsen. Phys. Chem.*, **86**, 1128-1132.
462. Rettich, T. R., R. Battino and E. Wilhelm, 2000, *J. Chem. Thermo.*, **32**, 1145-1156.
463. Rieley, H., H. D. Aslin and S. Haq, 1995, *J. Chem. Soc. Faraday Trans.*, **91**, 2349-2351.
464. Rinker, E. B. and O. C. Sandall, 2000, *Can. J. Chem. Eng.*, **78**, 232-236.
465. Rischbieter, E., H. Stein and A. Schumpe, 2000, *J. Chem. Eng. Data*, **45**, 338-340.
466. Robbins, R. C. and R. D. Cadle, 1958, *J. Phys. Chem.*, **62**, 469-471.
467. Roberts, J. M., H. D. Osthoff, S. S. Brown and A. R. Ravishankara, 2008, *Science*, **321**, 1059-1059.
468. Robinson, G. N., Q. Dai and A. Freedman, 1997, *J. Phys. Chem.*, **101**, 4947-4953.
469. Robinson, G. N., A. Freedman, C. E. Kolb and D. R. Worsnop, 1994, *Geophys. Res. Lett.*, **21**, 377-380.
470. Robinson, G. N., A. Freedman, C. E. Kolb and D. R. Worsnop, 1996, *Geophys. Res. Lett.*, **23**, 317.
471. Robinson, G. N., D. R. Worsnop, J. T. Jayne, C. E. Kolb and P. Davidovits, 1997, *J. Geophys. Res.*, **102**, 3583-3601.
472. Robinson, G. N., D. R. Worsnop, J. T. Jayne, C. E. Kolb, E. Swartz and P. Davidovits, 1998, *J. Geophys. Res.*, **103**, 25371-25381.
473. Rodriguez-Sevilla, J., M. Alvarez, G. Liminana and M. C. Diaz, 2002, *J. Chem. Engineer. Data*, **47**, 1339-1345.
474. Roduner, E. and D. M. Bartels, 1992, *Ber. Bunsenges. Phys. Chem.*, **96**, 1037-1042.
475. Roeselová, M., P. Jungwirth, D. J. Tobias and R. B. Gerber, 2003, *J. Phys. Chem. B.*, **107**, 12690-12699.
476. Roeselová, M., J. Vieceli, L. X. Dang, B. C. Garrett and D. J. Tobias, 2004, *J. Am. Chem. Soc.*, **126**, 16308-16309.
477. Rogaski, C. A., D. M. Golden and L. R. Williams, 1997, *Geophys. Res. Lett.*, **24**, 381-384.
478. Rohrschneider, L., 1973, *Anal. Chem.*, **45**, 1241-1247.
479. Roscoe, J. M. and J. P. D. Abbatt, 2005, *Journal of Physical Chemistry A*, **109**, 9028-9034.
480. Rossi, M. J., 2003, *Chemical Reviews (Washington, D. C.)*, **103**, 4823-4882.

481. Rossi, M. J., F. F. Fenter, K. Tabor, F. Caloz and L. Gutzwiller. In *Heterogeneous and Liquid Phase Processes. Transport and Chemical Transformation of Pollutants in the Troposphere*; P. Warneck, Ed.; Springer-Verlag: Berlin, 1996; pp 213-220.
482. Rossi, M. J., R. Malhotra and D. M. Golden, 1987, *Geophys. Res. Lett.*, **14**, 127-130.
483. Rubasinghege, G. and V. H. Grassian, 2009, *The Journal of Physical Chemistry A*, **113**, 7818-7825.
484. Rubel, G. O. and J. W. Gentry, 1984, *J. Aerosol Sci.*, **15**, 661-671.
485. Rudich, Y., R. K. Talukdar, T. Imamura, R. W. Fox and A. R. Ravishankara, 1996, *Chem. Phys. Lett.*, **261**, 467-473.
486. Rudich, Y., R. K. Talukdar, A. R. Ravishankara and R. W. Fox, 1996, *J. Geophys. Res.*, **101**, 21023-21031.
487. Rudolf, R. and P. E. Wagner, 1994, *J. Aerosol Sci.*, **25**, 597-598.
488. Saastad, O. W., T. Ellerman and C. J. Nielson, 1993, *Geophys. Res. Lett.*, **20**, 1191-1193.
489. Saathoff, H., K.-H. Naumann, N. Riemer, S. Kamm, O. Möhler, U. Schurath, H. Vogel and B. Vogel, 2001, *Geophys. Res. Lett.*, **28**, 1957-1960.
490. Sakamoto, Y., A. Yabushita, M. Kawasaki and S. Enami, 2009, *The Journal of Physical Chemistry A*, **113**, 7707-7713.
491. Salgado-Muñoz, M. S. and M. J. Rossi, 2002, *Phys. Chem. Chem. Phys.*, **4**, 5110-5118.
492. Sandanaga, Y., J. Hirokawa and H. Akimoto, 2001, *Geophys. Res. Lett.*, **28**, 4433-4436.
493. Santschi, C. and M. J. Rossi, 2004, *Phys. Chem. Chem. Phys.*, **6**, 3447-3460.
494. Saul, T. D., M. P. Tolocka and M. V. Johnston, 2006, *Journal of Physical Chemistry A*, **110**, 7614-7620.
495. Scheer, V., A. Frenzel, W. Behnke, C. Zetsch, L. Magi, C. George and P. Mirabel, 1997, *J. Phys. Chem. A*, **101**, 9359-9366.
496. Schroeder, W. H. and P. Urone, 1974, *Environ. Sci. Technol.*, **8**, 756-758.
497. Schumpe, A., 1993, *Chem. Engineer. Sci.*, **48**, 153-158.
498. Schurath, U., A. Bongartz, J. Kames, C. Wunderlich and T. Carstens. In *Heterogeneous and Liquid Phase Processes. Transport and Chemical Transformation of Pollutants in the Troposphere*; P. Warneck, Ed.; Springer-Verlag: Berlin, 1996; Vol. 2; pp 182-189.
499. Schütze, M. and H. Herrmann, 2002, *Phys. Chem. Chem. Phys.*, **4**, 60-67.
500. Schütze, M. and H. Herrmann, 2004, *Phys. Chem. Chem. Phys.*, **6**, 965-971.
501. Schütze, M. and H. Herrmann, 2005, *Journal of Atmospheric Chemistry*, **52**, 1 - 18.
502. Schwartz, S. E., 1984, *J. Geophys. Res.*, **89**, 11589-11598.
503. Schwartz, S. E., 1988, *Atmos. Environ.*, **22**, 2331.
504. Schwartz, S. E. and W. H. White. In *Trace Atmospheric Species. Properties, Transformations and Fates*; S. E. Schwartz, Ed.; John Wiley & Sons: New York, 1983; Vol. 12; pp 1-116.
505. Schwarz, H. A. and R. W. Dodson, 1984, *J. Phys. Chem.*, **88**, 3643-3647.
506. Schweitzer, F., L. Magi, P. Mirabel and C. George, 1998, *J. Phys. Chem. A*, **102**, 593-600.
507. Schweitzer, F., P. Mirabel and C. George, 1998, *J. Phys. Chem. A*, **102**, 3942-3952.
508. Schweitzer, F., P. Mirabel and C. George, 1999, *J. Atmos. Chem.*, **34**, 101-117.
509. Schweitzer, F., P. Mirabel and C. George, 2000, *J. Phys. Chem. A*, **104**, 72-76.
510. Seisel, S., C. Börensens, R. Vogt and R. Zellner, 2004, *Physical Chemistry Chemical Physics*, **6**, 5498-5508.
511. Seisel, S., F. Caloz, F. F. Fenter, H. vandenBergh and M. J. Rossi, 1997, *Geophys. Res. Lett.*, **24**, 2757-2760.
512. Seisel, S., B. Fluckiger, F. Caloz and M. J. Rossi, 1999, *Phys. Chem. Chem. Phys.*, **1**, 2257-2266.
513. Seisel, S., B. Fluckiger and M. J. Rossi, 1998, *Ber. Bunsenges. Phys. Chem.*, **102**, 811-820.
514. Seisel, S., T. Keil, Y. Lian and R. Zellner, 2006, *International Journal of Chemical Kinetics*, **38**, 242-249.
515. Seisel, S. and M. J. Rossi, 1997, *Berichte der Bunsen-Gesellschaft Physical Chemistry Chemical Physics*, **101**, 943-955.
516. Seyfioglu, R. and M. Odabasi, 2007, *Environ. Monit. Assess.*, **128**, 343-349.
517. Shaka, H., W. H. Robertson and B. J. Finlayson-Pitts, 2007, *Physical Chemistry Chemical Physics*, **9**, 1980-1990.
518. Shaw, R. A. and D. Lamb, 1999, *J. Chem. Phys.*, **111**, 10659-10663.
519. Shi, Q., P. Davidovits, J. T. Jayne, C. E. Kolb and D. R. Worsnop, 2001, *J. Geophys. Res.*, **106**, 24259-24274.
520. Shi, Q., P. Davidovits, J. T. Jayne, D. R. Worsnop and C. E. Kolb, 1999, *J. Phys. Chem. A*, **103**, 8812-8823.
521. Shi, Q., Y. Q. Li, P. Davidovits, J. T. Jayne, D. R. Worsnop, M. Mozurkewich and C. E. Kolb, 1999, *J. Phys. Chem. B.*, **103**, 2418-2430.
522. Shimono, A. and S. Koda, 1996, *J. Phys. Chem.*, **100**, 10,269-10,276.

523. Sieg, K., E. Starokozhev, M. U. Schmidt and W. Puttmann, 2009, *Chemosphere*, **77**, 8-14.
524. Sjostedt, S. J. and J. P. D. Abbatt, 2008, *Environmental Research Letters*, **3**, doi:10.1088/1748-9326/3/4/045007.
525. Smith, D. M. and A. R. Chughtai, 1995, *Colloids and Surfaces*, **105**, 47-77.
526. Smith, D. M. and A. R. Chughtai, 1996, *J. Geophys. Res.*, **101**, 19607-19620.
527. Smith, D. M. and A. R. Chughtai, 1997, *J. Atmos. Chem.*, **26**, 77-91.
528. Smith, D. M., W. F. Welch, S. M. Graham, A. R. Chughtai, B. G. Wicke and K. A. Grady, 1988, *Applied Spectroscopy*, **42**, 674-680.
529. Smith, D. M., W. F. Welch, J. A. Jassim, A. R. Chughtai and D. H. Stedman, 1988, *Applied Spectroscopy*, **42**, 1473-1482.
530. Smith, J. D., C. D. Cappa, W. S. Drisdell, R. C. Cohen and R. J. Saykally, 2006, *Journal of the American Chemical Society*, **128**, 12892 - 12898.
531. Snider, J. R. and G. A. Dawson, 1985, *J. Geophys. Res.*, **90**, 3797-3805.
532. Sokolov, O. and J. P. D. Abbatt, 2002, *Journal of Physical Chemistry A*, **106**, 775-782.
533. Sokolov, O. and J. P. D. Abbatt, 2002, *Geophysical Research Letters*, **29**.
534. Stadler, D. and M. J. Rossi, 2000, *Phys. Chem. Chem. Phys.*, **2**, 5420-5429.
535. Staffelbach, T. A. and G. L. Kok, 1993, *J. Geophys. Res.*, **98**, 12713-12717.
536. Staudinger, J. and P. V. Roberts, 2001, *Chemosphere*, **44**, 561-576.
537. Stemmler, K., A. Vlasenko, C. Guimbaud and M. Ammann, 2008, *Atmospheric Chemistry and Physics*, **8**, 5127-5141.
538. Stephens, S., M. J. Rossi and D. M. Golden, 1986, *Int. J. Chem. Kinetics*, **18**, 1133-1149.
539. Stewart, D. J., P. T. Griffiths and R. A. Cox, 2004, *Atmos. Chem. Phys.*, **4**, 1381-1388.
540. Sullivan, R. C., T. Thornberry and J. P. D. Abbatt, 2004, *Atmos. Chem. Phys.*, **4**, 1301-1310.
541. Sverdrup, G. M. and M. R. Kuhlman. "Heterogeneous Nitrogen Oxide-Particle Reactions"; 14th International Colloquium on Atmospheric Pollution, 1980, Paris, 245-248.
542. Swartz, E., Q. Shi, P. Davidovits, J. T. Jayne, D. Worsnop and C. E. Kolb, 1999, *J. Phys. Chem. A*, **103**, 8824-8833.
543. Szanyi, J., J. H. Kwak, R. J. Chimentao and C. H. F. Peden, 2007, *J. Phys. Chem. C*, **111**, 2661-2669.
544. Tabazadeh, A., R. P. Turco and M. Z. Jacobson, 1994, *J. Geophys. Res.*, **99**, 12,897-12,914.
545. Tabor, K., L. Gutzwiller and M. J. Rossi, 1993, *Geophys. Res. Lett.*, **20**, 1431-1434.
546. Tabor, K., L. Gutzwiller and M. J. Rossi, 1994, *J. Phys. Chem.*, **98**, 6172-7186.
547. Takami, A., S. Kato, A. Shimono and S. Koda, 1998, *Chem. Phys.*, **231**, 215-227.
548. Takami, A., T. Kondo, A. Kado and S. Koda, 2001, *J. Atmos. Chem.*, **39**, 139-153.
549. Taketani, F., Y. Kanaya and H. Akimoto, 2008, *Journal of Physical Chemistry A*, **112**, 2370-2377.
550. Taketani, F., Y. Kanaya and H. Akimoto, 2009, *Atmospheric Environment*, **43**, 1660-1665.
551. Tang, I. N. and J. H. Lee. In *The Chemistry of Acid Rain*; G. E. Gordon and R. W. Johnson, Eds.; Am. Chem. Soc. Symp. Series, 1987; pp 109-117.
552. Tang, I. N. and H. R. Munkelwitz, 1989, *J. Colloid Interface Sci.*, **128**, 289-295.
553. Thibert, E. and F. Domine, 1998, *Journal of Physical Chemistry B*, **102**, 4432-4439.
554. Thomas, K., A. Volz-Thomas, D. Mihelcic, H. G. J. Smit and D. Kley, 1998, *J. Atmos. Chem.*, **29**, 17-43.
555. Thornton, J. A. and J. P. D. Abbatt, 2005, *Journal of Geophysical Research, D: Atmospheres*, **110**, D08309.
556. Thornton, J. A. and J. P. D. Abbatt, 2005, *Journal of Physical Chemistry A*, **109**, 10004-10012.
557. Thornton, J. A., C. F. Braban and J. P. D. Abbatt, 2003, *Physical Chemistry Chemical Physics*, **5**, 4593-4603.
558. Thornton, J. A., L. Jaeglé and V. F. McNeil, 2008, *Journal of Geophysical Research, D: Atmospheres*, **113**, D05303.
559. Timonen, R. S., L. T. Chu, M.-T. Leu and L. F. Keyser, 1994, *J. Phys. Chem.*, **98**, 9509-9517.
560. Timonen, R. S. and M.-T. Leu, 2006, *Journal of Physical Chemistry A*, **110**, 6660 - 6666.
561. Tolbert, M. A., J. Praff, I. Jayaweera and M. J. Prather, 1993, *J. Geophys. Res.*, **98**, 2957-2962.
562. Tolbert, M. A., M. J. Rossi and D. M. Golden, 1988, *Science*, **240**, 1018-1021.
563. Tolbert, M. A., M. J. Rossi and D. M. Golden, 1988, *Geophys. Res. Lett.*, **15**, 847-850.
564. Tolbert, M. A., M. J. Rossi, R. Malhotra and D. M. Golden, 1987, *Science*, **238**, 1258-1260.
565. Tollock, M., T. D. Saul and M. V. Johnston, 2004, *J. Phys. Chem. A*, **108**, 2659-2665.
566. Toon, O., E. Browell, B. Gray, L. Lait, J. Livingston, P. Newman, R. Russell, P. P., M. Schoeberl, G. Toon, W. Traub, F. P. J. Valero, H. Selkirk and J. Jordan, 1993, *Science*, **261**, 1136-1140.
567. Ullerstam, M. and J. P. D. Abbatt, 2005, *Physical Chemistry Chemical Physics*, **7**, 3596-3600.
568. Ullerstam, M., T. Thornberry and J. P. D. Abbatt, 2005, *Faraday Discussions*, **130**, 211-226.

569. Underwood, G. M., P. Li, H. A. Al-Abadleh and V. H. Grassian, 2001, *J. Phys. Chem. A*, **105**, 6609-6620.
570. Underwood, G. M., P. Li, C. R. Usher and V. H. Grassian, 2000, *J. Phys. Chem. A*, **104**, 819-829.
571. Underwood, G. M., T. M. Miller and V. H. Grassian, 1999, *J. Phys. Chem. A*, **103**, 6184-6190.
572. Underwood, G. M., C. H. Song, M. Phadnis, G. R. Carmichael and V. H. Grassian, 2001, *J. Geophys. Res.*, **106**, 18055-18066.
573. Usher, C. R., H. Al-Hosney, S. Carlos-Cuellar and V. H. Grassian, 2002, *J. Geophys. Res.*, **107**, 4713.
574. Usher, C. R., A. E. Michel, D. Stec and V. H. Grassian, 2003, *Atmos. Environ.*, **37**, 5337-5347.
575. Utter, R. G., J. B. Burkholder, C. J. Howard and A. R. Ravishankara, 1992, *J. Phys. Chem.*, **96**, 4973-4979.
576. Van Dingenen, R. and F. Raes, 1991, *Aerosol Sci. Technol.*, **15**, 93-106.
577. Van Doren, J. M., L. R. Watson, P. Davidovits, D. R. Worsnop, M. S. Zahniser and C. E. Kolb, 1990, *J. Phys. Chem.*, **94**, 3265-3269.
578. Van Doren, J. M., L. R. Watson, P. Davidovits, D. R. Worsnop, M. S. Zahniser and C. E. Kolb, 1991, *J. Phys. Chem.*, **95**, 1684-1689.
579. Van Loon, L. and H. C. Allen, 2008, *J. Phys. Chem. A*, **112**, 7873 (8).
580. Villalta, P. W., E. R. Lovejoy and D. R. Hanson, 1996, *Geophys. Res. Lett.*, **23**, 1765-1768.
581. Vitenberg, A. G., B. V. Ioffe, Z. S. Dimitrova and I. L. Butaeva, 1975, *J. Chromatog.*, **112**, 319-327.
582. Vogt, R., C. Elliott, H. C. Allen, J. M. Laux, J. C. Hemminger and B. J. Finlayson-Pitts, 1996, *Atmos. Environ.*, **30**, 1729-1737.
583. Vogt, R. and B. Finlayson-Pitts, 1994, *J. Phys. Chem.*, **98**, 3747-3755.
584. Vogt, R. and B. F. Finlayson-Pitts, 1994, *Geophys. Res. Lett.*, **21**, 2291-2294.
585. Vogt, R. and B. J. Finlayson-Pitts, 1995, *J. Phys. Chem.*, **99**, 13,052.
586. Voigtländer, J., F. Stratmann, D. Niedermeier, H. Wex and A. Kiselev, 2007, *Journal of Geophysical Research*, **112**, D20208.
587. von Hessberg, P., N. Pouvesle, A. K. Winkler, G. Schuster and J. N. Crowley, 2008, *Physical Chemistry Chemical Physics*, **10**, 2345-2355.
588. Wachsmuth, M., H. W. Gäggeler, R. v. Glasow and M. Ammann, 2002, *Atmos. Chem. Phys.*, **2**, 121-131.
589. Wagman, D. D., W. H. Evans, V. B. Parker, R. H. Schumm, I. Halow, S. M. Bailey, K. L. Churney and R. L. Nutall, 1982, *J. Phys. Chem. Ref. Data*, **11**, , Suppl. No. 1.
590. Wagner, R., K.-H. Naumann, A. Mangold, O. Möhler, H. Saathoff and U. Schurath, 2005, *Journal of Physical Chemistry A*, **109**, 8140 - 8148.
591. Wahner, A., T. F. Mental, M. Sohn and J. Stier, 1998, *J. Geophys. Res.*, **103**, 31103-31112.
592. Wang, L. and D. C. Clary, 1996, *J. Chem. Phys.*, **104**, 5663-5673.
593. Wardman, P., 1991, *Free Rad. Res. Comm.*, **14**, 57-67.
594. Waschewsky, G. C. G. and J. P. D. Abbatt, 1999, *J. Phys. Chem. A*, **103**, 5312-5320.
595. Watson, L. R., J. M. V. Doren, P. Davidovits, D. R. Worsnop, M. S. Zahniser and C. E. Kolb, 1990, *J. Geophys. Res.*, **95**, 5631-5638.
596. Watts, S. F. and P. Brimblecombe, 1987, *Environ. Technol. Lett.*, **8**, 483-486.
597. Weingartner, E., H. Bartscher and U. Baltensperger, 1997, *Atmos. Environ.*, **31**, 2311-2327.
598. Weisenberger, S. and A. Schumpe, 1996, *AIChE Journal*, **42**, 298-300.
599. Wilhelm, E., R. Battino and R. J. Wilcock, 1977, *Chem. Rev.*, **77**, 219-262.
600. Williams, L. R. and D. M. Golden, 1993, *Geophys. Res. Lett.*, **20**, 2227-2230.
601. Williams, L. R., D. M. Golden and D. L. Huestis, 1995, *J. Geophys. Res.*, **100**, 7329-7335.
602. Williams, L. R. and F. S. Long, 1995, *J. Phys. Chem.*, **99**, 3748-3751.
603. Winkler, A. K., N. S. Holmes and J. N. Crowley, 2002, *Phys. Chem. Chem. Phys.*, **4**, 5270-5275.
604. Winkler, P., A. Vrtala, P. E. Wagner, M. Kulmala, K. E. J. Lehtinen and T. Vesala, 2004, *Phys. Rev. Lett.*, **93**, doi: 10.1103/Phys.Rev.Lett93.075701.
605. Winkler, P. M., A. Vrtala, R. Rudolf, P. E. Wagner, I. Riipinen, T. Vesala, K. E. J. Lehtinen, Y. Viisanen and M. Kulmala, 2006, *Journal of Geophysical Research*, **111**, D19202.
606. Winkler, T., J. Goschnick and H. J. Ache, 1991, *J. Aerosol Sci.*, **22**, S605-S608.
607. Wolff, E. W. and R. Mulvaney, 1991, *Geophys. Res. Lett.*, **18**, 1007-1010.
608. Wong, P. K. and Y. H. Wang, 1997, *Chemosphere*, **35**, 535-544.
609. Worsnop, D. R., L. E. Fox, M. S. Zahniser and S. C. Wofsy, 1993, *Science*, **259**, 71-74.
610. Worsnop, D. R., L. R. Williams, C. E. Kolb, M. Mozurkewich, M. Gershenson and P. Davidovits, 2004, *J. Phys. Chem. A*, **108**, 5846-5848.
611. Worsnop, D. R., M. S. Zahniser, C. E. Kolb, J. A. Gardner, L. R. Watson, J. M. V. Doren, J. T. Jayne and P. Davidovits, 1989, *J. Phys. Chem.*, **93**, 1159-1172.
612. Worthington, E. K. and E. A. Wade, 2007, *Atmospheric Environment*, **41**, 5510-5515.

613. Yabushita, A., S. Enami, Y. Sakamoto, M. Kawasaki, M. R. Hoffmann and A. J. Colussi, 2009, *Journal of Physical Chemistry A*, **113**, 4844-4848.
614. Yaws, C. L., J. R. Hopper, X. Wang and A. K. Rathinsamy, 1999, *Chem. Eng.*, 102-105.
615. Yoshitake, H., 2000, *Atmos. Environ.*, **34**, 2571-2580.
616. Yoshizumi, K., K. Aoki, I. Nouchi, T. Okita, T. Kobayashi, S. Kamakura and M. Tajima, 1984, *Atmos. Environ.*, **18**, 395-401.
617. Yu, X. Y. and J. R. Barker, 2003, *J. Phys. Chem. A*, **107**, 1313-1324.
618. Zangmeister, C. D. and J. E. Pemberton, 2001, *J. Phys. Chem. A*, **105**, 3788-3795.
619. Zangmeister, C. D. and J. E. Pemberton, 2004, *J. Phys. Chem. A*, **108**, 236-236.
620. Zangmeister, C. D., J. A. Turner and J. E. Pemberton, 2001, *Geophys. Res. Lett.*, **28**, 995.
621. Zelenov, V. V., E. V. Aparina, M. Y. Gershenson, S. D. Il'in and Y. M. Gershenson, 2003, *Khim. Fiz.*, **22**, 58-70.
622. Zelenov, V. V., E. V. Aparina, M. Y. Gershenson, S. D. Il'in and Y. M. Gershenson, 2003, *Khim. Fiz.*, **22**, 37-48.
623. Zelenov, V. V., E. V. Aparina, S. A. Kashtanov, D. V. Shestakov and Y. M. Gershenson, 2006, *Journal of Physical Chemistry A*, **110**, 6771-6780.
624. Zetzsch, C. and W. Behnke, 1992, *Ber. Bunsenges. Phys. Chem.*, **96**, 488-493.
625. Zhang, H. Z., Y. Q. Li, P. Davidovits, W. L. R., J. T. Jayne, C. E. Kolb and D. R. Worsnop, 2003, *J. Phys. Chem. A*, **107**, 6398-6407.
626. Zhang, R., J. T. Jayne and M. J. Molina, 1994, *J. Phys. Chem.*, **98**, 867-874.
627. Zhang, R. and M.-T. Leu, 1997, *J. Geophys. Res.*, **102**, 8837-8843.
628. Zhang, R., M.-T. Leu and L. F. Keyser, 1994, *J. Phys. Chem.*, **98**, 13,563-13,574.
629. Zhang, R., M.-T. Leu and L. F. Keyser, 1995, *Geophys. Res. Lett.*, **22**, 1493-1496.
630. Zhang, R., M.-T. Leu and L. F. Keyser, 1995, *J. Geophys. Res.*, **100**, 18,845-18,854.
631. Zhang, R., M.-T. Leu and L. F. Keyser, 1996, *J. Phys. Chem.*, **100**, 339-345.
632. Zhang, R., M.-T. Leu and L. F. Keyser, 1997, *J. Phys. Chem. A*, **101**, 3324-3330.
633. Zhang, R., P. J. Wooldridge and M. J. Molina, 1993, *J. Phys. Chem.*, **97**, 8541-8548.
634. Zhou, X. and Y. N. Lee, 1992, *J. Phys. Chem.*, **96**, 265-272.
635. Zhou, X. and K. Mopper, 1990, *Environ. Sci. Technol.*, **24**, 1864-1869.
636. Zientara, M., D. Jakubczyk, G. Derkachov, K. Kolwas and M. Kolwas, 2005, *Journal of Physics D: Applied Physics*, **38**, 1978-1983.
637. Zientara, M., D. Jakubczyk, K. Kolwas and M. Kolwas, 2008, *J. Phys. Chem. A*, **112**, 5152-5158.
638. Zolensky, M. E., D. S. McKay and L. A. Kaczor, 1989, *J. Geophys. Res.*, **94**, 1047-1056.
639. Zondlo, M. A., S. B. Barone and M. A. Tolbert, 1997, *Geophysical Research Letters*, **24**, 1391-1394.
640. Zondlo, M. A., S. B. Barone and M. A. Tolbert, 1998, *J. Phys. Chem. A*, **102**, 5735-5748.

APPENDIX A. THERMODYNAMIC PARAMETERS

Table of Contents

APPENDIX A. THERMODYNAMIC PARAMETERS	1
A.1 Gas-phase entropy and enthalpy values	1
A.2 Notes to Appendix A.....	17
A.3 References	48

Tables

Table A-1. Gas-phase entropy and enthalpy values for selected species at 298.15 K and 100 kPa.....	2
--	---

A.1 Gas-phase entropy and enthalpy values

Table A-1 lists selected entropy and enthalpy of formation values for a number of atmospheric species. As much as possible, the values were taken from primary evaluations that develop a recommended value from the original studies. Otherwise, the values were selected from the original literature, which is referenced in the table. Often, the enthalpy of formation and the entropy values are taken from different sources, usually due to a more recent value for the enthalpy of formation. The cited error limits are from the original references and therefore reflect often widely varying criteria. Some enthalpy values have been corrected to reflect the value of a reference compound selected for this table; these are mentioned in the Notes. Values that are calculated or estimated are also indicated in the Notes, along with information on the level of theory. Results other than those recommended are also often mentioned in the Notes, including recommendations from previous versions of this Table. These should provide a better perspective on the selected value.

Table A-1. Gas-phase entropy and enthalpy values for selected species at 298.15 K and 100 kPa.

SPECIES	$\Delta_f H(298\text{ K})$ kJ mol^{-1}	$\Delta_f H(0\text{ K})$ kJ mol^{-1}	$S(298\text{ K})$ $\text{J K}^{-1} \text{mol}^{-1}$	Notes
H	217.998±0.001	216.034±0.0001	114.717±0.001	1
H ₂	0.00	0.00	130.680±0.003	2
O(³ P)	249.229±0.002	246.844±0.002	161.059±0.003	3
O(¹ D)	438.05±0.1			4
O ₂	0.00		205.152±0.005	5
O ₂ (¹ Δ _g)	94.29±0.01			6
O ₂ (¹ Σ _g ⁺)	156.96±0.01			"
O ₃	141.732±0.039	144.386±0.039	239.01	7
OH	37.36±0.13	37.11±0.13	183.737	8
H ₂ O	-241.826±0.040	-238.923±0.033	188.835±0.010	9
HO ₂	12.30±0.25	15.22±0.25	229.1	10
HO ₂ •H ₂ O	-268.0±3	-259.6±3	308.9	11
H ₂ O ₂	-135.9±0.2	-129.9±0.2	234.5±0.1	12
HO ₃	18.1±6.2	21.8±6.3		13
HOOOH	-90.0	-81.1		14
HOOOOH	-44.4	-33.5		15
N(⁴ S)	472.420±0.050	470.570±0.050	153.301±0.003	16
N ₂	0.00	0.00	191.609±0.004	17
NH	357±1	357±1	181.25±0.04	18
NH ₂	186.2±1.0	189.1±1.0	194.868	19
NH ₃	-45.94±0.35	-38.95±0.35	192.77±0.05	20
N ₂ H	251	254	156.77	21
<i>trans</i> -N ₂ H ₂	201	209	218.20	22
<i>cis</i> -N ₂ H ₂	223	230	218.45	23
N ₂ H ₃	225	235	237.27	24
N ₂ H ₄	95.2±0.5	109.3±0.5	238.165	25
NO	91.04±0.08	90.54±0.08	210.76	26
N ₂ O	81.6±0.5	85.3±0.5	220.01	27
NO ₂	33.97±0.08	36.78±0.08	240.17	28
NO ₃	74.7±1.1	79.9±1.1	258.4±1.0	29
N ₂ O ₃	86.6±1	91.2±1	314.74	30
N ₂ O ₄	11.1±1	20.4±1	304.45	31
N ₂ O ₅	13.3±1.5	22.9±1.5	355.7±7	32
HNO	109.2±2.1	112.1±2.1	220.914	33
HON	217.1±2.1	220.0±2.1		34
NH ₂ O	66.9±3.3	72.4±3.3		35
NH ₂ OH	-47.7±2.5		236.18	36
HNOH	96.7±3.3	103.8±3.3		37
NH ₂ NO ₂	-26±10	-12.3±10	268.54	38
HONO	-78.45±0.8	-72.80±0.8	254.07	39
<i>trans</i> -HONO	-78.94±0.6	-72.80±0.6	249.109	40
<i>cis</i> -HONO	-77.45±0.7	-71.1±0.7	266.876	41
HNO ₂	-45.61±0.2		232.46	42
HONO ₂	-134.3±0.5	-124.6±0.5	266.88±0.7	43

SPECIES	$\Delta_f H(298\text{ K})$ kJ mol ⁻¹	$\Delta_f H(0\text{ K})$ kJ mol ⁻¹	$S(298\text{ K})$ J K ⁻¹ mol ⁻¹	Notes
<i>cis,cis</i> -HOONO	-14.9	-7.6	279	44
<i>trans,perp</i> -HOONO	-0.5	6.1	291	45
HO ₂ NO ₂	-54.0		297±4	46
C	716.68±0.45	711.19±0.45	158.100±0.001	47
CH	595.8±0.6	592.5±0.6	183.04	48
CH ₂ (³ B ₁)	391.2±1.6	390.7±1.6	194.436	49
CH ₂ (¹ A ₁)	428.8±1.6	428.3±1.6	189.220	50
CH ₃	146.7±0.3	150.0±0.3	194.008	51
CH ₄	-74.549±0.060	-66.580±0.060	186.38	52
CO	-110.53±0.17	-113.81±0.17	197.660±0.004	53
CO ₂	-393.51±0.13	-393.14±0.13	213.785±0.010	54
HCO	44.15±0.43		224.34	55
CH ₂ O	-108.7±0.50	-104.86±0.50	218.76	56
CH ₂ O•H ₂ O	-380			57
<i>trans</i> -HOCO	-187.9±2.1	-183.7±2.1		58
<i>cis</i> -HOCO	-175.7±2.1	-171.5±2.1		59
HC(O)O	-126.6±1.7	-123.0±1.7	244.7	60
C(O)OH	-193		251.6	61
HC(O)OH	-378.6±0.7		248.2	62
HC(O)OOH	-285.3±2.5	-290.8±2.5		63
CH ₂ OO	110	118		64
CH ₂ O ₂	5.0	12.6		65
CH ₃ O	21.0±2.1	28.4±2.1	234.278	66
CH ₃ O ₂	9.0±5.1			67
CH ₂ OH	-17.0±0.7	-10.7±0.7	244.170±0.018	68
CH ₃ OH	-201.00±0.6	-190.12±0.6	239.865	69
CH ₃ OH•HO ₂	179.3		381	70
CH ₂ OOH	67.20		270.4	71
CH ₃ OOH	-132.2		273.4	72
CN	440±5	437±5	202.64	73
HCN	132±4	132.4±4	201.82	"
C ₂ N ₂	309.1±0.8	307.15±0.8	242.20	"
CH ₂ NH ₂	149±8			74
CH ₃ NH ₂	-23.4±1.0		242.89	75
CH ₂ CN	252.6±4	255.2±4		76
CH ₃ CN	74.0±0.4	81.0±0.4	245.12±0.8	77
CH ₂ NO	157±4			78
NH ₂ CO	-15.1±4			79
NCO	151±14		232.38	80
HNCO	-104±12		237.97±0.8	81
HCONH ₂	-193.9±2.0			82
CH ₂ N ₂	273.2	279.1		83
CH ₂ NO ₂	147.3		272.48	84
CH ₃ NO ₂	-74.3±0.6		275.2	85
CH ₃ ONO	-64.0		284.3	86
CH ₃ ONO ₂	-122.2±4.3		301.9	87

SPECIES	$\Delta_f H(298\text{ K})$ kJ mol^{-1}	$\Delta_f H(0\text{ K})$ kJ mol^{-1}	$S(298\text{ K})$ $\text{J K}^{-1} \text{mol}^{-1}$	Notes
$\text{CH}_2\text{N(O)OH}$	-13.0			88
$\text{CH(NO}_2)_2$	169			"
$\text{CH}_2(\text{NO}_2)_2$	-42.7			"
$\text{CH}_2(\text{NO}_2)\text{ONO}$	-75.7			"
$\text{CH(NO}_2)\text{N(O)OH}$	-1.26			"
$\text{CH(NO}_2)_3$	7.1			"
$\text{CH(NO}_2)_2\text{ONO}$	-50.2			"
$\text{C(NO}_2)_2(\text{NOOH})$	68.6			"
$\text{C(NO}_2)_4$	82.0			89
$(\text{NH}_2)_2\text{CO}$	-245.8±2.0			90
C_2H	565.3±2.9	561.1±2.9	209.73	91
C_2H_2	227.4±0.8	227.96±0.8	200.93	92
H_2CC	428±17	427±17		93
C_2H_3	295.4±1.7		233.0	94
C_2H_4	52.4±0.5	60.99±0.5	219.316	95
C_2H_5	120.9±1.7	131.8±1.7	250.52	96
C_2H_6	-83.85±0.29		229.162	97
$\text{C}_2\text{H}_2\text{OH}$	121±11			98
CHCO	173.0±9.6			99
CH_2CO	-49.58±0.88	-46.44±0.88		100
CH_3CO	-10.3±1.8	-3.6±1.8	267.448	101
$\text{CH}_2\text{C(O)H}$	13±3		259.52	102
$\text{CH}_3\text{C(O)H}$	-166.1±0.5		263.95	103
CH_3OCO	-173.8±2.4		290.1	104
$\text{CH}_2\text{OC(O)H}$	-155.2		289.7	105
$\text{CH}_3\text{OC(O)H}$	-357.4±0.7		287.1	106
$(\text{CHO})_2$	-212±0.8	-206.4±0.5		107
cy-($\text{C}_2\text{H}_2\text{O}$) _n	-190±10			108
CH_3CHOOH	26.40		314.8	109
$\text{C}_2\text{H}_5\text{O}_2$	-27.4±9.9			110
$\text{C}_2\text{H}_5\text{OOH}$	-166.9		311.5	111
$\text{CH}_3\text{CH}_2\text{O}$	-13.6±4.0	-0.2±4.0	277.642	112
$\text{CH}_2\text{CH}_2\text{OH}$	-31±7			113
CH_3CHOH	-53.22		282.2	114
$\text{C}_2\text{H}_5\text{OH}$	-234.8±0.5	-217.08±0.5	281.622	115
CH_3COO	-190		284.9	116
$\text{CH}_2(\text{OH})\text{C(O)}$	-154			117
CH(OH)C(O)H	-207			-
$\text{CH}_2(\text{OH})\text{C(O)H}$	-318			118
$\text{CH}_2\text{C(O)OH}$	-253±13		283.4	119
$\text{CH}_3\text{C(O)O}$	-192.5			120
$\text{CH}_3\text{C(O)OH}$	-432.8±0.5		332.67	121
$\text{CH}_3\text{C(O)O}_2$	-154.4			122
$\text{CH}_2(\text{OH})\text{COOH}$	-583±10	-568±10	318.6±5.0	123
CH_3OCH_2	3.8		278.2	124
CH_3OCH_3	-184.1±0.5		267.34	125
$\text{CH}_2\text{C(OH)}_2$	-309.2±1.3			126

SPECIES	$\Delta_f H(298\text{ K})$ kJ mol^{-1}	$\Delta_f H(0\text{ K})$ kJ mol^{-1}	$S(298\text{ K})$ $\text{J K}^{-1} \text{mol}^{-1}$	Notes
$\text{CH}_2(\text{OH})\text{CH}_2\text{OH}$	-392.2 ± 4.0		303.81	127
$\text{C}(\text{OH})_2\text{C}(\text{O})\text{H}$	-400 ± 1			128
$\text{CH}(\text{OH})_2\text{C}(\text{O})\text{H}$	-496 ± 0.4			129
$\text{C}(\text{O})\text{HC}(\text{O})\text{H}$	-212.0 ± 0.7			130
CH_2OOCH_3	71.42		303.8	131
CH_3OOCH_3	-125.5 ± 5.0	-106.5 ± 5.0	308.4 ± 3.0	132
$\text{CH}_2(\text{OH})\text{OOCH}_2\text{OH}$	-571.7 ± 6.6			133
$(\text{HOCO})_2$	-731.8 ± 2.0	-721.2 ± 2.0	320.6 ± 5.0	134
$\text{C}_2\text{H}_5\text{NO}_2$	-105.56 ± 0.29			135
$\text{C}_2\text{H}_5\text{ONO}$	-99.37 ± 0.50			136
$\text{CH}_3\text{C}(\text{O})\text{O}_2\text{NO}_2$	-240.1			137
$\text{CH}_3\text{CHN}(\text{O})\text{OH}$	-54.4			138
$\text{C}_2\text{H}_5\text{NH}_2$	-47.5 ± 0.6			139
CH_3NHCH_3	-18.8 ± 1.5			140
CH_3CONH_2	-238.3 ± 0.8			141
C_3H_4	190.5 ± 1.1			142
C_3H_4	184.9 ± 0.7			143
<i>cy</i> - C_3H_4	277.1 ± 2.5			144
C_3H_5	166.1 ± 4.3		248 ± 15	145
C_3H_6	20.0 ± 0.7		266.6	146
<i>n</i> - C_3H_7	101.3 ± 1.0	119.1 ± 1.0		147
<i>i</i> - C_3H_7	86.6 ± 2.0		281 ± 5	148
C_3H_8	-104.68 ± 0.50		270.20	149
1- $\text{C}_3\text{H}_7\text{OH}$	-255.1 ± 0.4			150
2- $\text{C}_3\text{H}_7\text{OH}$	-272.6 ± 0.5			"
$\text{CH}_3\text{CH}(\text{OH})\text{CH}_2\text{OH}$	-429.8 ± 4.1			151
$\text{C}_2\text{H}_5\text{CO}$	-36.4 ± 2.9		298.3	152
$\text{C}_2\text{H}_5\text{C}(\text{O})\text{H}$	-185.6 ± 0.8		304.51	153
$\text{CH}_3\text{C}(\text{O})\text{CH}_2$	-34 ± 3		303.99	154
$\text{CH}_3\text{C}(\text{O})\text{CH}_3$	-217.1 ± 0.7		295.46	155
$\text{CH}_3\text{CHOCH}_3$	-37.2		313.7	156
$\text{CH}_3\text{CH}_2\text{OCH}_2$	-31.3		315.1	"
$\text{CH}_3\text{CH}_2\text{OCH}_3$	-216.4 ± 0.6		305.9	157
$\text{CH}_2\text{CC}(\text{O})\text{H}$	177.8 ± 1.7			158
CH_2CHCO	100 ± 13		279.5	159
$\text{CH}_2\text{CHC}(\text{O})\text{H}$	-74.3 ± 1.7			160
$\text{CH}_2\text{OC}(\text{O})\text{CH}_3$	-210.6		323.5	161
$\text{CH}_3\text{OC}(\text{O})\text{CH}_3$	-413.0		320.9	"
$\text{CH}_3\text{OCH}_2\text{OCH}_3$	-348.5 ± 0.8			162
$\text{CH}_3\text{CH}_2\text{OC}(\text{O})$	-194.6		325.8	163
$\text{CH}_3\text{CHOC}(\text{O})\text{H}$	-197.2		327.6	"
$\text{CH}_3\text{CH}_2\text{OC}(\text{O})\text{H}$	-392.8		323.5	"
$\text{CH}_2(\text{OH})\text{C}(\text{O})\text{CH}_3$	-373			164
$\text{CH}_3\text{CHOOCH}_3$	31.5		347.52	165
$\text{CH}_3\text{CH}_2\text{OOCH}_3$	-154.5		344.4	166
$(\text{CH}_3)_2\text{CHOO}$	-65.4 ± 11.3			167

SPECIES	$\Delta_f H(298\text{ K})$ kJ mol^{-1}	$\Delta_f H(0\text{ K})$ kJ mol^{-1}	$S(298\text{ K})$ $\text{J K}^{-1} \text{mol}^{-1}$	Notes
$(\text{CH}_3)_2\text{COOH}$	-14.2		349.9	168
$(\text{CH}_3)_2\text{CHOOH}$	-204.2		340.0	169
$\text{CH}_3\text{C}(\text{OH})_2\text{C}(\text{O})\text{H}$	-550.8 \pm 7.1			170
$\text{CH}_2(\text{OH})\text{CH}(\text{OH})\text{CH}_2\text{O}$ H	-577.9 \pm 1.1			171
$\text{C}_3\text{H}_7\text{NH}_2$	-70.8 \pm 1.5	-43.3 \pm 1.5		172
$(\text{CH}_3)_3\text{N}$	-23.6 \pm 1.3			173
$(\text{CH}_3)_3\text{NO}$	80 \pm 5			174
$\text{NCC}(\text{O})\text{CN}$	247.5 \pm 6.4	246.5 \pm 6.4	310.0 \pm 1.0	175
n-C ₄ H ₁₀	-125.65 \pm 0.67		309.91	176
$(\text{CH}_3)_3\text{COO}$	-101.5 \pm 9.2			177
$(\text{CH}_3)_3\text{COOH}$	-239 \pm 18			178
$(\text{CH}_3\text{COO})_2$	-500 \pm 10	-477 \pm 10	390.7 \pm 6.0	179
F	79.38 \pm 0.30	77.27 \pm 0.30	158.751 \pm 0.004	180
F ₂	0.00	0.00	202.791 \pm 0.005	181
HF	-273.30 \pm 0.70	273.25 \pm 0.70	173.799 \pm 0.003	182
HO ₂ F	-98.3 \pm 4.2	-95.4 \pm 4.2	226.77 \pm 0.21	183
FO	109 \pm 10	108 \pm 10	216.40 \pm 0.3	184
FOF	24.5 \pm 2	26.8 \pm 2	247.46 \pm 0.4	185
OFO	380 \pm 20	381 \pm 20	251 \pm 1	186
FOO	25.6 \pm 2		259.5 \pm 0.2	187
HOOF	-42.7 \pm 4	-36.8 \pm 4		188
FOOF	19.2 \pm 2.0	22.9 \pm 2.0	277.2 \pm 0.2	189
FONO	67			190
FNO	-65.7		248.0	191
FNO ₂	-79		277.1	"
FONO ₂	15 \pm 3	22 \pm 3	293.165	192
CF	244.1 \pm 10	240.5 \pm 10	213.03	193
CHF	149.8 \pm 2.1	149.8 \pm 2.1	223.09	194
CH ₂ F	-32 \pm 8		236.52	195
CH ₃ F	-238.9 \pm 0.8		222.78	196
CF ₂	-192.0 \pm 3.3	-192.5 \pm 3.3	240.66	197
CHF ₂	-239 \pm 4		258.50	198
CH ₂ F ₂	-452.7 \pm 0.8		246.59	199
CF ₃	-465.7 \pm 2.1	-462.8 \pm 2.1	264.56	200
CHF ₃	-692.9 \pm 2.1	-685.8 \pm 2.1	259.67	201
CF ₄	-933.20 \pm 0.75	-927.20 \pm 0.75	261.454	202
CFH ₂ O	-210			203
CFH ₂ OH	-433			"
FCO	-174.1 \pm 2	-174.5 \pm 2	248.78	204
FCO ₂	-362.8 \pm 2.5			205
CHFO	-381.2 \pm 2	-377.8 \pm 2	246.69	206
CF ₂ HO	-417			207
CF ₂ HOH	-682			"
CF ₂ O	-623.8 \pm 5.9	-620.9 \pm 5.9	258.97	208

SPECIES	$\Delta_f H(298\text{ K})$ kJ mol^{-1}	$\Delta_f H(0\text{ K})$ kJ mol^{-1}	$S(298\text{ K})$ $\text{J K}^{-1} \text{mol}^{-1}$	Notes
CF ₃ O	-635±7			209
CF ₂ O ₂	-427±6			210
CF ₃ O ₂	-614±15			211
CF ₃ OH	-908.8±3.8			212
CF ₃ OF	-740.1±7.5			213
CF ₃ CN	-495.4±1.7	-491.6±1.7		214
CH ₂ CHF	-138.8±1.7			215
CH ₂ CH ₂ F	-59.4±8		279.7	216
CH ₃ CHF	-70.3±8		274.0	217
CH ₃ CH ₂ F	-278.2±1.7	-263.3±1.7	265.1	218
CH ₂ CF ₂	-335.0±4.5			219
CH ₃ CHF ₂	-497.0±8.3			220
CH ₂ FCH ₂ F	-432±25			221
CH ₂ FCHF	235.5		293.3	222
CHF ₂ CH ₂	-277		297.8	223
CH ₃ CF ₂	-302.5±8.4		290.3	224
CH ₃ CHF ₂	-500.8±6.3	-486.9±6.3	282.4	225
CH ₂ FCHF ₂	-665±4			226
CH ₂ CF ₃	-517.1±5		306.8	227
CH ₃ CF ₃	-745.6±1.7	-732.8±1.7	287.3	228
CF ₂ CF ₂	-658.9±4.9			229
CHF ₂ CHF ₂	-860±24		320.3	230
CHFCF ₃	-697		326.2	231
CH ₂ FCF ₃	-896±8	-885±8	316.2	232
CF ₂ CF ₃	-891±5			233
CHF ₂ CF ₃	-1105±5	-1095±5	333.7	234
C ₂ F ₆	-1344.3±3.4	-1335.9±3.4	331.8	235
CF ₃ CO	-605±2		325.5	236
CF ₃ C(O)H	-810.4		317.6	237
CH ₃ C(O)F	-442.1±3.3			238
CF ₃ C(O)OH	-1031±1.7			239
CF ₃ OCO ₂	-958±16			240
CF ₃ OOCF ₃	-1471±21			241
<i>iso</i> -C ₃ H ₇ F	-315.5±2.1			242
<i>tert</i> -C ₄ H ₉ F	-360±8			243
Cl	121.303±0.002	119.622±0.0002	165.190±0.004	244
Cl ₂	0.0		223.081±0.010	245
HCl	-92.31±0.10	-92.13±0.10	186.902±0.005	246
ClO	101.681±0.040	101.086±0.040	224.96±0.1	247
OCI•OH ₂	-130			248
ClO•HOH	-125			249
ClOO	98.3±2.1	99.8±2.1	270.3	250
ClOOH	0.8±4			251
OCIO	99.4±0.6		263.52	252
ClO ₃	194±12	200±10	270.75±0.5	253

SPECIES	$\Delta_f H(298\text{ K})$ kJ mol^{-1}	$\Delta_f H(0\text{ K})$ kJ mol^{-1}	$S(298\text{ K})$ $\text{J K}^{-1} \text{mol}^{-1}$	Notes
CICIO	133.5	134.7	277.6	254
CIOCI	81.3±1.8	83.1±1.8		255
CIOOCI	129.0±2	132.4±2	301.1	256
CICIO ₂	114±5	118±5	294.4±6	257
CIOCIO	164±5	166±5	312.3±6	258
Cl ₂ O ₃	139±5	144±5	337.8±6	259
HOCl	-74.8±1.2		236.50±0.42	260
CICO	21.8±2.5			261
CINO	52.7±0.5	54.6±0.5	261.58	262
CINO ₂	12.5±1.0	17.9±1	272.23	263
<i>cis</i> -CIONO	64.4			264
<i>trans</i> -CIONO	75.3			"
<i>cis, perp</i> -ClO ₂ NO	102		315.9	265
<i>trans, perp</i> -ClO ₂ NO	108		318.8	266
CIONO ₂	22.9±2.0		302.38	267
<i>cis, perp</i> -ClOONO	132	136		268
<i>trans, perp</i> -ClOONO	139	144		269
<i>trans, perp</i> -OCIONO	179	183		270
O ₂ CIONO ₂	92±17			271
FCI	-55.70±0.31	-55.605±0.31	217.94	272
CHCl	319.4±0.8		234.88	273
CH ₂ Cl	117.3±3.1		271±7	274
CH ₃ Cl	-81.9±0.6		227.15	275
CClH ₂ O	-18.4			276
CClH ₂ OH	-246			"
CCl ₂	229.4±0.8		265.03	277
CHCl ₂	89.0±3.0		280±7	278
CH ₂ Cl ₂	-95.1±2.5		270.31	279
CCl ₃	71.1±2.5		303.24	280
CHCl ₃	-102.9±2.5		295.51	281
CCl ₄	-95.6±2.5		309.90	282
CClO	-24.9±4.2		266.0	283
CHClO	-164±20		259.07	284
CH ₂ OCI	135.5		279.7	285
CH ₃ OCI	-64.5		272.8	286
CH ₂ ClO ₂	-5.1±13.6			287
CH ₂ ClOOH	-173.3±6.1		303.09	288
CCl ₂ O	-220.9		283.8	289
CCl ₂ HO	-27.6			290
CCl ₂ HOH	-277			"
CHCl ₂ O ₂	-19.2±11.2			291
CH ₂ ClOCI	-92.3		311.8	292
CHCl ₂ OOH	-187.2±13.6		330.75	293
CHCl ₂ OCI	-109.4		339.1	294
CCl ₃ O	-43.5±20			295
CCl ₃ OH	-293			296

SPECIES	$\Delta_f H(298\text{ K})$ kJ mol ⁻¹	$\Delta_f H(0\text{ K})$ kJ mol ⁻¹	$S(298\text{ K})$ J K ⁻¹ mol ⁻¹	Notes
CCl ₃ O ₂	-20.9±8.9			297
CCl ₃ OOH	-190.9±13.1		346.64	298
CCl ₃ OCI	-111.8		357.2	299
CHFCI	-61±10			300
CH ₂ FCI	-264±8		264.3	301
CFCl	31±13		259.03	302
CF ₂ Cl	-279±8			303
CFCl ₂	-89.1±10.0			304
CHFCI ₂	-285±9		293.0	305
CHF ₂ Cl	-482.6±3.2		280.8	306
CFCI ₃	-285.3		309.9	307
CF ₂ Cl ₂	-494.1		300.7	308
CF ₃ Cl	-709.2±2.9	-704.2±2.9	285.2	309
CFCIO	-429±20		276.70	310
CF ₃ OCI	-734.7±4.2			311
CCl ₃ OF	-158.1			312
<i>cis</i> -FC(O)OCI	-418	-414		313
<i>trans</i> -FC(O)OCI	-429	-425		314
C ₂ HCl	226±10			315
C ₂ H ₃ Cl	22±3			316
CH ₂ CH ₂ Cl	93.0±2.4		271±7	317
CH ₃ CHCl	76.5±1.6		279±6	318
CH ₃ CH ₂ Cl	-112.1±0.7		275.78	319
C ₂ Cl ₂	227±14			320
CH ₂ CCl ₂	2.4±2.0			321
<i>cis</i> -CHClCHCl	-3±2			322
<i>trans</i> -CHClCHCl	-0.5±2.0			323
CH ₃ CCl ₂	42.5±1.7		288±5	324
CH ₃ CHCl ₂	-132.5±3.5		305.05	325
CHCl ₂ CH ₂	90.1			326
CH ₂ ClCH ₂ Cl	-132.0±3.5			327
C ₂ HCl ₃	-17.5±3.0		325.20	328
CH ₂ ClCHCl ₂	-148.0±4.0			329
CH ₂ CCl ₃	71.5±8			330
CH ₃ CCl ₃	-144.6±2.0		320.03	331
C ₂ Cl ₄	-24.2±4		341.03	332
CHCl ₂ CHCl ₂	-156.7±3.5			333
CH ₂ ClCCl ₃	-152.3±2.4			334
C ₂ Cl ₅	-21.3±5.4			335
C ₂ HCl ₅	-155.9±4.3			336
C ₂ Cl ₆	-148.2±5.7		398.62	337
CH ₃ CHFCI	-313.4±2.6			338
CH ₂ CF ₂ Cl	-316.2		322.08	339
CH ₃ CF ₂ Cl	-536.2±5.2		307.1	340
CH ₃ CFCl ₂	-347.0			341
CF ₂ CFCl	-505.5±4.7			342

SPECIES	$\Delta_f H(298\text{ K})$ kJ mol^{-1}	$\Delta_f H(0\text{ K})$ kJ mol^{-1}	$S(298\text{ K})$ $\text{J K}^{-1} \text{mol}^{-1}$	Notes
CF ₃ CHFCl	-690.4±4.9			"
CF ₃ CH ₂ Cl	-746.4			343
CF ₃ CHCl ₂	-749.7			"
CF ₃ CCl ₃	-754.0			"
CF ₂ ClCF ₂ Cl	-937.0±7.3			344
CF ₂ ClCFCl ₂	-716.8±4.3			"
C ₂ F ₅ Cl	-1118.8±4.1			"
CH ₃ CHClO ₂	-54.7±3.4			345
CH ₃ C(O)Cl	-242.8±0.8			346
CH ₂ ClC(O)OH	-427.6±1.0	-416.0±1.0	325.9±5.0	347
CH ₂ ClCH ₂ OOH	-191±5		373.38	348
CH ₃ CHClOOH	-226		331	349
CH ₃ CCl ₂ OOH	-244		362	350
CH ₂ ClC(O)Cl	-244.8±8.6			351
Cl(O)CC(O)Cl	-335.8±6.2			352
CHCl ₂ C(O)Cl	-241.0±8.6			353
CCl ₃ CH ₂ OOH	-210±6		405.26	354
CCl ₃ CO	-62.8		359.4	355
CCl ₃ C(O)H	-236		346.4	356
CCl ₃ C(O)Cl	-240±9			357
CH ₃ CCl ₂ O ₂	-69.7±4			358
CHCl ₂ CH ₂ OOH	-205±6		386.31	359
Br	111.87±0.12	117.93±0.12	175.018±0.004	360
Br ₂ (g)	30.91±0.11	45.71±0.11	245.468±0.005	361
HBr	-36.29±0.16	-28.44±0.16	198.700±0.004	362
BrO	123.4±0.4	131.0±0.4	232.97±0.1	363
OBBr•OH ₂	-133			364
BrO•HOH	-126			365
OBBrO	163.9±4.4	171.1±4.3	271±2	366
BrOO	119.8±6	128.2±6	289±3	367
HOBr	-60.5±1.1	-50.0±1.1	248.0	368
BrOOH	24.3±4			369
HOBrO	42.3			370
HBrO ₂	249			"
BrO ₃	221±50	233±50	285±2	371
BrOBr	107.6±3.5	124.1±3.5	290.8±2	372
BrBrO	168.2±6	184.1±6	313±2	373
BrOOBr	166.1±6	184.5±6		374
BrOBrO	205.0±6	222.2±6		375
OBBrBrO	303			376
BrBrO ₂	201.7±6	219.7±6		377
BrOF	52.9			378
ClOBr	94.1±6	103.3±6		379
ClBrO	145.2±6	154.0±6		380
BrClO	159.4±6	168.2±6		381

SPECIES	$\Delta_f H(298\text{ K})$ kJ mol^{-1}	$\Delta_f H(0\text{ K})$ kJ mol^{-1}	$S(298\text{ K})$ $\text{J K}^{-1} \text{mol}^{-1}$	Notes
CIOOBr	151.5±6	162.3±6		382
CIOBrO	192.5±6	202.5±6		"
BrOCIO	186.2±6	196.2±6		"
ClBrO ₂	171.1±6	182.0±6		"
BrClO ₂	158.2±6	169.5±6		"
BrNO	82.17±0.8	91.46±0.8	273.66±0.8	383
<i>cis</i> -BrONO	71.9			384
<i>trans</i> -BrONO	88.3			385
BrNO ₂	45.2			386
BrONO ₂	42.7±8			387
OBronO ₂	153.6±8			388
O ₂ BrONO ₂	161.9±8			"
BrF	-58.85±1.0	-51.2±1.0	228.985	389
BrCl	14.79±0.16	22.23±0.16	240.046	390
CBr	498.3±2.1	501.7±2.1	230.9	391
CHBr	378.7±2.9	386.4±2.9	252.9	392
CH ₂ Br	172.8±2.7			393
CH ₃ Br	-36.36±0.4		245.85±0.25	394
CBr ₂	350.2±0.4	363.7±0.4	288.7	395
CHBr ₂	188.9±9		298.6	396
CH ₂ Br ₂	3.6±3.4	24.9±3.4	294	397
CBr ₃	224±9		334.57	398
CHBr ₃	55.4±3.3		330.67	399
CBr ₄	83.9±3.4		358.06	400
CFBr	89.1			401
CH ₂ FBr	-214.2		276.19	402
CHF ₂ Br	-424.9±1.0		295.17	403
CF ₃ Br	-641.4±2.3	-637.6±2.3	297.49	404
CClBr	285			405
CHClBr	143±6			406
CH ₂ ClBr	-43.7±1.9	-43.3±1.9		407
CHFCIBr	-229.8		304.74	408
CF ₂ ClBr	-589.5		318.70	409
CFCl ₂ Br	-230.1		330.48	"
CCl ₂ Br	124			410
CHCl ₂ Br	-48.8	-36.8	316.18	411
CHFBr ₂	-191.6	-171.8	316.98	"
CCl ₃ Br	-41.1±2.0	-32.0±2.0	332.92	412
CF ₂ Br ₂	-386.6	-368.4	325.24	413
CClBr ₂	163			414
CHClBr ₂	-9.0	10.1	327.79	415
CFCIBr ₂	-183.0	-165.9	342.82	"
CCl ₂ Br ₂	9.3	25.5	348.30	"
CFBr ₃	-143.5	-119.5	345.87	416

SPECIES	$\Delta_f H(298\text{ K})$ kJ mol^{-1}	$\Delta_f H(0\text{ K})$ kJ mol^{-1}	$S(298\text{ K})$ $\text{J K}^{-1} \text{mol}^{-1}$	Notes
CClBr ₃	48.7	71.6	357.69	417
CBr ₂ O	-27.1±0.6			418
CBr ₃ O	93.4			419
CBr ₃ OH	-125.0			"
CBr ₃ OF	11.5			"
CBr ₃ OCl	24.7			"
CBr ₃ OBr	38.7			"
CF ₃ OBr	-755.6			420
CCl ₃ OBr	-132.6			421
C ₂ Br	623.7		295.0	422
C ₂ HBr	296±6	298±6	252.7	423
CH ₂ CHBr	79.2±1.9			424
CH ₂ CH ₂ Br	135.6±6.7			425
CH ₃ CHBr	127±8			426
CH ₃ CH ₂ Br	-61.5±1.0		287.3±0.4	427
C ₂ Br ₂	335.3		294.5	428
<i>trans</i> -CHBrCBr	333.6		326.7	429
CH ₃ CBr ₂	140.2±5.4			430
CH ₃ CBr ₂ H	-26.7±1.9			431
CHBrCBr ₂	144.2		360.0	432
CH ₂ BrCH ₂ Br	-71.6±1.1			433
C ₂ Br ₃	385.4		369.9	434
CH ₂ BrCHBr ₂	53.5±4.3			435
CH ₃ CBr ₃	-4.6	27.2	354.1	436
C ₂ Br ₄	190.1		387.4	437
CHBr ₂ CBr ₂	218.8		419.0	438
CBr ₃ CHBr	243.6		416.9	"
C ₂ Br ₅	183.3		444.7	"
C ₂ HBr ₅	113.1		439.2	"
C ₂ Br ₆	165.5		459.1	"
CF ₃ CH ₂ Br	-694.5±2.0			439
CF ₂ HCF ₂ Br	-833.4±4.9			"
CF ₃ CF ₂ Br	-1064.4±4.1			"
CF ₂ BrCF ₂ Br	-789.1±5.7			"
CHFClCF ₂ Br	-644.8±6.4			"
CHClBrCHClBr	-36.9±8.4			"
CF ₂ BrCFClBr	-656.6±20.7			"
CH ₃ C(O)Br	-190.4±0.6			440
CH ₂ BrCOOH	-383.5±3.1	-364.6±4	337.0±5.0	441
I	106.760±0.04	107.161±0.04	180.787±0.004	442
I ₂	62.42±0.08	65.50±0.08	260.687±0.005	443
HI	26.50±0.10		206.590±0.004	444
IO	125.1±2.5	127.2±2.5	239.6±0.1	445
OIO	119.7±6	123.4±6	279.9	446
IOO	86.3±6	87.6±6	308.4	447
IO ₃	154.0	164.0	293±4	448

SPECIES	$\Delta_f H(298\text{ K})$ kJ mol^{-1}	$\Delta_f H(0\text{ K})$ kJ mol^{-1}	$S(298\text{ K})$ $\text{J K}^{-1} \text{mol}^{-1}$	Notes
IOI	107.5±6	114.2±6	306.5	449
IIO	158.2±6	164.0±6	317.8	450
IOOI	177.8±6	186.2±6	337.0	451
IIO ₂	138.5±6	147.7±6	339.9	452
IOIO	152.3±6	161.5±6	349.7	453
OIO	259.4±6	263.2±6	356.3	454
IOIO ₂	71.2	84.8		455
OIOIO ₂	125.7	145.9		456
O ₂ IOIO ₂	46.4	78.0		457
HOI	−69.6±5.4	−64.9±5.4	255.0±0.1	458
HIO	143.3	148.0		459
HOIO	−17.4	−11.0		460
HOOI	36.9	43.6		461
ClIO	95.0±6	97.5±6		462
ClOI	94.1±6	97.5±6		463
ICIO	180.7±6	183.3±6		464
ClIO ₂	56.9±6	61.5±6		465
ClOIO	143.1±6	149.0±6		466
ClOOI	154.4±6	161.1±6		467
IOClO	182.4±6	188.7±6		468
IClO ₂	191.6±6	196.6±6		469
BrOI	107.1±6	118.0±6		470
BrIO	122.2±6	133.9±6		471
IBrO	192.5±6	204.2±6		472
BrOOI	169.9±6	184.1±6		"
BrOIO	152.3±6	166.9±6		"
IOBrO	202.5±6	216.3±6		"
BrIO ₂	92.5±6	105.9±6		"
IBrO ₂	239.7±6	253.1±6		"
OIBrO	273.6±6	292.5±6		"
INO	121±4		282.8±4	473
INO ₂	60.2±4		294±6	474
IONO ₂	37.5	46.1		475
ICl	17.393±0.040	19.026±0.040	247.572	476
IBr	40.807±0.14	49.754±0.14	258.809	477
CHI	425			478
CH ₂ I	217.2±3			479
CH ₃ I	13.22±0.5		253.70±0.25	480
Cl ₂	450			481
CHI ₂	290.4±6			482
CH ₂ I ₂	107.9±4.5	117.4±4.5	309.41±1.34	483
CHI ₃	251.0±1.4			484
Cl ₃	369±9			485

SPECIES	$\Delta_f H(298\text{ K})$ kJ mol^{-1}	$\Delta_f H(0\text{ K})$ kJ mol^{-1}	$S(298\text{ K})$ $\text{J K}^{-1} \text{mol}^{-1}$	Notes
Cl ₄	474±13			486
CH ₃ OIO ₂	−73±12			487
CFI	154			488
CF ₃ I	−586.2±2.1	−580.3±2.1	307.78	489
CF ₂ I ₂	−274.8	−269.3	346.34	490
CClI	343			491
CH ₂ ClI	11.1±1.9	19.2±1.9		492
CCl ₃ I	9.0	12.1	340.31	493
CHBrI	242±6			494
CH ₂ BrI	55.4±3.4	70.8±3.4		495
CBr ₂ I	272±9			496
CHBr ₂ I	105±9			"
CBrI	395			497
CBrI ₂	321±9			498
CHBrI ₂	158±9			"
<i>cis</i> -CHICHI	207.4±0.8			499
<i>trans</i> -CHICHI	207.4±0.8			"
CH ₃ CH ₂ I	−7.5±0.9		295.52±0.42	500
CF ₃ CH ₂ I	−644.5±2.8			501
CF ₃ CF ₂ I	−1000.2±4.1			"
CH ₃ C(O)I	−126.4±2.7			502
CH ₂ ICH ₂ I	75.0±4.0			503
ICH ₂ CN	172.5±4.0			504
S	277.17±0.15	274.92±0.15	167.829±0.006	505
S ₂	128.60±0.3	128.29±0.3	228.167±0.010	506
HS	142.92±0.78	142.47±0.78	195.552	507
H ₂ S	−20.60±0.5	−17.68±0.5	205.81±0.05	508
HSS	105±4			509
HSSH	15.5		252.40	510
HSSS	110±4	129±4		511
HSSSH	22±4	28.9±4		512
SO	4.78±0.25	4.73±0.25	221.94	513
SOO	205±4	207±4		514
SO ₂	−296.81±0.20	−294.30±0.20	248.223±0.050	515
SO ₃	−395.9±0.7	−390.16±0.7	256.541	516
SSO	−55.39±1.10	−53.35±1.10	266.961	517
SOS	224±4	226±4		518
HSO	−6.1±2.9	−3.8±2.9		519
HSO ₂	−178±8			520
HOSO	−247±4	−243±4		521
HOO	113±6	118±6		522
HOSH	−117±4	−111±4		523
HOOS	59±6	64±6		524
HOOSH	−31.0±4	−23.4±4		525
HOSOH	−285±4	−276±4		526

SPECIES	$\Delta_f H(298\text{ K})$ kJ mol^{-1}	$\Delta_f H(0\text{ K})$ kJ mol^{-1}	$S(298\text{ K})$ $\text{J K}^{-1} \text{mol}^{-1}$	Notes
HOSO ₂	-373±6			527
H ₂ SO ₄	-732.7±2	-720.8±2.0	311.3±1.5	528
HOSS	-67±4	-63±4		529
HSSO	-40±4	-36±4		530
HSOS	105±6	109±6		531
HOSSH	-128±4	-120±4		532
HSOSH	-0.4±4	6.3±4		533
HSNO	95			534
FSH	-128.2			535
NS	283±24	283±24	222.093	536
PS	152±10	153±10	234.065	537
CS	279.775±0.75	276.529±0.75	210.55	538
CS ₂	116.70±1.0	115.91±1.0	237.882	539
CS ₂ OH	108.4±5.4		321±20	540
HCS	300.4±8.4	300.0±8.4		541
CH ₂ S	114.6±8.4	118.4±8.4		542
CH ₃ S	124.7±1.8			543
CH ₂ SH	151.9±9.2			544
CH ₃ SH	-22.9±0.7		255.14	545
CH ₂ SO	-30			546
CH ₂ S(O)O	-144.7			547
CH ₃ SO	-70.3			548
CH ₃ S(O)O	-211			549
CH ₃ OSO	-230			550
CH ₃ SOO	75.7±5.4			551
CH ₃ SCH ₂	136.3±8.2			552
CH ₃ SCH ₃	-37.4±0.6		285.96	553
CH ₃ S(O)CH ₃	-151.3±0.8			554
CH ₃ SSCH ₃	-24.7±1.0		336.80	555
C ₂ H ₅ SH	-46.1±0.6			556
HSCH ₂ CH ₂ SH	-9.7±1.2			557
CH ₃ C(O)SH	-175.1±8.4			558
OCS	-141.7±2	-141.8±2	231.644	559
Li	159.3±1	157.7±1	138.78	560
Li ₂	215.9±3.0	215.5±3.0	197.00	561
LiH	140.624±0.04	140.794±0.04	170.909	562
LiF	-341±4	-341±8	200.278±0.008	563
LiCl	-196±4	-196±12	212.92	564
LiBr	-154±13	-146±13	224.35	565
LiOH	-229.0±5	-227.1±5	214.66	566
LiO	53.1±4	53.6±4	210.96	567
LiO ₂	-94.6±4	-92.5±4		568
LiO ₃	-77.8±4	-73.6±4		"
Li ₂ O	-158.6±4	-157.7±4	229.11	569
Li ₂ SO ₄	-1042±84	-1030±84	332.82±42	570
Na	107.5±0.7	107.8±0.7	153.72	571
Na ₂	142.07±1.2	144.56±1.2	230.243±0.030	572

SPECIES	$\Delta_f H(298\text{ K})$ kJ mol^{-1}	$\Delta_f H(0\text{ K})$ kJ mol^{-1}	$S(298\text{ K})$ $\text{J K}^{-1} \text{mol}^{-1}$	Notes
NaH	124.3±19	126.2±19	188.39	573
NaF	−290±2	−289±2	217.61	574
NaCl	−181±2	−180±2	229.79	575
NaBr	−143.9±2.1	−135.0±2.2	241.22	576
NaOH	−191.0±8	−187.4±8	229.27	577
NaO	90.4±4	92.0±4	229.13±2.1	578
NaO ₂	−47.7±4	−44.4±4		579
NaO ₃	−51.5±4	−46.0±4		"
Na ₂ O	−21.8±4	−18.8±4	260.66±6.24	580
Na ₂ SO ₄	−1034±25	−1020±25	346.85±16.7	581
K	89.0±0.8	89.9±0.8	160.22	582
KH	123.0±15	125.5±15	198.02	583
KF	−326.8±2	−324.7±2	226.612±0.04	584
KCl	−214.7±0.4	−212.9±0.4	239.09	585
KBr	−180.1±2.1	−170.9±2.1	250.53	586
KOH	−232±3	−228±3	238.59	587
KO	62.3±4	64.0±4	238.027±2.1	588
KO ₂	−86.6±4	−83.3±4		589
KO ₃	−77.0±4	−72.0±4		"
K ₂ O	−61.0±4	−57.3±4	284.11±6.24	590
K ₂ SO ₄	−1094±17	−1081±17	366.15±17	591

A.2 Notes to Appendix A

¹ Enthalpy value is from the optimization of Ruscic, et al.[198] and is the same as the CODATA Key Value, [52] but with a smaller error limit. Entropy value from CODATA.

² CODATA Key Value [52]

³ Enthalpy value is from the optimization of Ruscic, et al.[198] CODATA Key Value [52] of $\Delta_f H_{298}^\circ = 249.18 \pm 0.10 \text{ kJ mol}^{-1}$ was used in previous evaluation. Entropy value is from CODATA.

⁴ Based on a transition to the weighted midpoint of the O³P J-levels. [157]

⁵ CODATA Key Value. [52]

⁶ Spectroscopic value from Huber and Herzberg. [96]

⁷ Enthalpy value is from the optimization of Ruscic, et al.[198] Entropy from Gurvich review, which also gave the previously-listed enthalpy of $141.8 \pm 2 \text{ kJ mol}^{-1}$ [91]

⁸ Enthalpy value is an update [197] to the recommendation of the IUPAC Task Group. [198] It is an optimization, based on photoionization measurements. Values based on Birge-Sponer extrapolations of OH vibrational levels are 2.1 kJ mol^{-1} higher. The entropy is taken from Gurvich. [91]

⁹ CODATA Key Value [52] The active thermochemical tables optimization gives an enthalpy of $-241.818 \pm 0.033 \text{ kJ mol}^{-1}$. [198]

¹⁰ The enthalpy value is from an optimization based on both experimental and theoretical data. [197] Previous enthalpy value at 298K of $13.4 \pm 2.1 \text{ kJ mol}^{-1}$ was based upon a negative ion thermodynamic cycle,[185] which was in good agreement with the photoionization result of $13.8 \pm 3.3 \text{ kJ mol}^{-1}$. [136]

¹¹ Derived from the recommended equilibrium constant for the formation of the complex (Table 3-1, Note 3).

¹² Enthalpy value based on the enthalpy of formation of liquid H₂O₂ and the enthalpy of vaporization. [66] A CCSD(T) calculation of the atomization energy, employing the cc-pVnZ basis sets (n=T,Q,5,6) led to $\Delta_f H_{298}^\circ = -32.28 \text{ kcal mol}^{-1}$ and $\Delta_f H_0^\circ = -30.83 \text{ kcal mol}^{-1}$. [60]

¹³ Enthalpy for the reaction $\text{HOOOH} + \text{FOO} \rightarrow \text{HOOF} + \text{HOOO}$ at the CCSD(T)/CBS(Q5) level of theory is $9.50 \text{ kcal mol}^{-1}$. Adjusted for the Table reference values, this gives the cited enthalpy of formation. The minimum was found to be the *trans* configuration at the CCSD(T)/CBS(Q5) level of theory, with the *cis* configuration $0.5 \text{ kcal mol}^{-1}$ higher in energy. [87] Note that the enthalpy values obtained from the atomization energy were higher, due, apparently, to higher order correlation effects. [87] The selected value is supported by another analysis using the isodesmic reaction $\text{HO}_2 + \text{FOO} \rightarrow \text{HO}_3 + \text{FO}$ which leads to a value of $\Delta_f H_{298}^\circ = 6.3 \text{ kcal mol}^{-1}$. [60] An older theoretical study, using both atomization energies and the reaction $\text{HOOO} + \text{HOH} = \text{HOOOH} + \text{OH}$, resulted in $\Delta_f H_{298}^\circ = 7.1 \pm 2 \text{ kcal mol}^{-1}$ (not adjusted). [59] The enthalpy of formation derived from an estimate of the ionization energy of HO₃, which comes from a study of the electron transfer reactions between HO₃⁺ and a series of neutral substrates, was $\Delta_f H_{298}^\circ = -1 \pm 5 \text{ kcal mol}^{-1}$. [219] The stability of HO₃ has been supported by a neutralization-reionization mass spectrometry experiment, which led to a lifetime of $>1 \mu\text{s}$, [36] and an infrared action spectrum, which leads to an upper limit for the HO-O₂ bond strength of $6.12 \text{ kcal mol}^{-1}$. [158]

¹⁴ CCSD(T) calculation of the atomization energy, employing the cc-pVnZ basis sets (n=T,Q,5,6). [60] Reaction enthalpy for the reaction $2 \text{HOOH} = \text{HOOOH} + \text{HOH}$ was calculated to be $-15.5 \text{ kcal mol}^{-1}$ using the G2 method, leading to $\Delta_f H_{298}^\circ = -22.7 \text{ kcal mol}^{-1}$. [124] Atomization energy calculated by the CCSD(T) extrapolated to the CBS limit, with geometry optimized at the CCSD(T)/aV(n+d)Z (n = D,T,Q,5) level gives $\Delta_f H_{298}^\circ = -21.3 \text{ kcal mol}^{-1}$ and $\Delta_f H_0^\circ = -19.2 \pm 1 \text{ kcal mol}^{-1}$. [87]

¹⁵ CCSD(T) calculation of the atomization energy, employing the cc-pVnZ basis sets (n=T,Q,5,6). [60]

¹⁶ Derived from a PFI-PEPICO TOF study. [228] Entropy and previous enthalpy value ($472.68 \pm 0.40 \text{ kJ mol}^{-1}$) CODATA Key Values [52]

¹⁷ CODATA Key Values [52]

¹⁸ Enthalpy from review of Anderson. [7] Entropy and enthalpy difference (0.05 kJ mol^{-1}) from JANAF. [45]

¹⁹ Recommended values from the IUPAC Task Group.[193] Enthalpy is a weighted average of four measurements since 1982. Previous recommendation was $186 \pm 1 \text{ kJ mol}^{-1}$. [7] Entropy was taken from a

computed anharmonic potential surface, [141] and is close to the JANAF value of $194.71 \pm 0.05 \text{ kJ mol}^{-1}$. [45]

²⁰ CODATA Key Value [52] The JANAF Tables give $\Delta_f H_0^\circ = -38.91 \text{ kJ mol}^{-1}$, $\Delta_f H_{298}^\circ = -45.90 \text{ kJ mol}^{-1}$, and $S^\circ = 192.774 \text{ J mol}^{-1}$. [45]

²¹ Geometry optimized at the frozen core CCSD(T) level of theory with aug-cc-pVDZ and aug-cc-pVTZ basis sets; the CCSD(T) energy extrapolated to the CBS limit. [142]

²² Geometry optimized at the frozen core CCSD(T) level of theory with aug-cc-pVDZ and aug-cc-pVTZ basis sets; the CCSD(T) energy extrapolated to the CBS limit. [142] Previous value, $212 \pm 10 \text{ kJ mol}^{-1}$, taken from the Gurvich review. [91] (The same value was used for the equilibrium mixture.)

²³ Geometry optimized at the frozen core CCSD(T) level of theory with aug-cc-pVDZ and aug-cc-pVTZ basis sets; the CCSD(T) energy extrapolated to the CBS limit. [142] Previous enthalpy value, $248 \pm 12 \text{ kJ mol}^{-1}$, based on enthalpy of conversion of the *trans* to *cis* isomers, $36 \pm 12 \text{ kJ mol}^{-1}$. [91]

²⁴ Geometry optimized at the frozen core CCSD(T) level of theory with aug-cc-pVDZ and aug-cc-pVTZ basis sets; the CCSD(T) energy extrapolated to the CBS limit. [142]

²⁵ Taken from review of Gurvich. [91] An enthalpy value of $23.1 \text{ kcal mol}^{-1}$ was obtained using a geometry optimized at the frozen core CCSD(T) level of theory with aug-cc-pVDZ and aug-cc-pVTZ basis sets; the CCSD(T) energy extrapolated to the CBS limit. [142]

²⁶ The enthalpy value is from an optimization based on experimental data. [197] $\Delta_f H_0^\circ = 21.64 \pm 0.02 \text{ kcal mol}^{-1}$. Previous enthalpy value, $91.29 \pm 0.17 \text{ kJ mol}^{-1}$ from review of Anderson. [7] Much of the difference can be ascribed to the change in the enthalpy for N. Entropy from JANAF. [45]

²⁷ Taken from review of Gurvich, et al. [91] The JANAF Tables give $\Delta_f H_0^\circ = 85.48 \text{ kJ mol}^{-1}$, $\Delta_f H_{298}^\circ = 82.05 \text{ kJ mol}^{-1}$, and $S^\circ = 219.957 \text{ J mol}^{-1}$. [45]

²⁸ The enthalpy value is from an optimization based on experimental data. [197] Entropy from [91].

²⁹ Enthalpy derived from a molecular beam photofragmentation translational spectroscopic study, adjusted to Table values for O and NO₂. [54] Entropy from review of Abramowitz, et al. [1]

³⁰ Taken from review of Gurvich, et al. [91] The JANAF Tables give $\Delta_f H_0^\circ = 89.6 \text{ kJ mol}^{-1}$, $\Delta_f H_{298}^\circ = 82.8 \text{ kJ mol}^{-1}$, and $S^\circ = 308.539 \text{ J mol}^{-1}$. [45]

³¹ Taken from review of Gurvich, et al. [91] The JANAF Tables give $\Delta_f H_0^\circ = 18.7 \text{ kJ mol}^{-1}$, $\Delta_f H_{298}^\circ = 9.1 \text{ kJ mol}^{-1}$, and $S^\circ = 304.376 \text{ J mol}^{-1}$. [45]

³² Taken from review of Gurvich, et al. [91]. The JANAF Tables give $\Delta_f H_0^\circ = 12.7 \text{ kJ mol}^{-1}$, $\Delta_f H_{298}^\circ = 11.3 \text{ kJ mol}^{-1}$, and $S^\circ = 346.548 \text{ J mol}^{-1}$. [45]

³³ Geometry optimized at the frozen core CCSD(T) level of theory with aug-cc-pVDZ and aug-cc-pVTZ basis sets; the CCSD(T) energy extrapolated to the CBS limit. [64] Previous enthalpy, $107.1 \pm 2.5 \text{ kJ mol}^{-1}$, from review of Anderson. [8] Entropy from Gurvich, who cites an enthalpy of 102 kJ mol^{-1} . [91]

³⁴ Geometry optimized at the frozen core CCSD(T) level of theory with aug-cc-pVDZ and aug-cc-pVTZ basis sets; the CCSD(T) energy extrapolated to the CBS limit. [64]

³⁵ Geometry optimized at the frozen core CCSD(T) level of theory with aug-cc-pVDZ and aug-cc-pVTZ basis sets; the CCSD(T) energy extrapolated to the CBS limit. [64]

³⁶ Calculated using isodesmic reactions at several levels of theory and several basis sets. [201] Previous value of $-9.6 \pm 2.2 \text{ kcal mol}^{-1}$ based on average of theoretical and experimental values. [8] Entropy from Gurvich. [91]

³⁷ Geometry optimized at the frozen core CCSD(T) level of theory with aug-cc-pVDZ and aug-cc-pVTZ basis sets; the CCSD(T) energy extrapolated to the CBS limit. [64]

³⁸ Enthalpy value based on measurements of the enthalpy of formation of the crystalline substance and an estimated value of the enthalpy of sublimation, $60.7 \pm 10 \text{ kJ mol}^{-1}$. [91]

³⁹ Thermodynamic properties for the equilibrium mixtures of isomers, from Gurvich review. [91]

⁴⁰ Taken from review of Gurvich, et al. [91] Values calculated using G3, CBS-QB3, and CBS-APNO methods applied to atomization, isomerization, and work reactions are $\Delta_f H_{298}^\circ = -18.90 \pm 0.05 \text{ kcal mol}^{-1}$ and $S^\circ = 57.89 \text{ cal K}^{-1} \text{ mol}^{-1}$. [9]

⁴¹ Enthalpy value obtained on basis of enthalpy of conversion of *trans*-HONO into *cis*-HONO, $1.7 \pm 0.4 \text{ kJ mol}^{-1}$. [91] Values calculated using G3, CBS-QB3, and CBS-APNO methods applied to atomization, isomerization, and work reactions are $\Delta_f H_{298}^\circ = -18.40 \pm 0.05 \text{ kcal mol}^{-1}$ and $S^\circ = 57.64 \text{ cal K}^{-1} \text{ mol}^{-1}$. [9]

⁴² Nitryl hydride. Calculated using G3, CBS-QB3, and CBS-APNO methods applied to atomization, isomerization, and work reactions. [9]

- ⁴³ Extensive review.[66]
- ⁴⁴ Derived from a third-law analysis of the equilibrium constant for $\text{HO} + \text{NO}_2 \leftrightarrow c,c\text{-HOONO}$ (Table 3-1, Note 1). Previous enthalpy value of $-5.7 \text{ kcal mol}^{-1}$ and values for the *cis,perp*- and *trans,perp*-HOONO calculated at the MP2 level of theory.[146]
- ⁴⁵ Derived from the dissociation energy for *t,p*-HOONO and reported molecular constants (Table 3-1, Note 1). Enthalpy values for the *cis,cis*-, *cis,perp*-, and *trans,perp*-HOONO have also been calculated at the MP2 level of theory.[146]
- ⁴⁶ Derived from a third-law analysis of the equilibrium constant for $\text{HO}_2\text{NO}_2 \leftrightarrow \text{HO}_2 + \text{NO}_2$. [84] Previous recommended enthalpy value of $-12.7 \pm 0.6 \text{ kcal mol}^{-1}$ from [186]
- ⁴⁷ CODATA Key Value [52] The JANAF Tables give $\Delta_f H_0^\circ = 711.2 \text{ kJ mol}^{-1}$, $\Delta_f H_{298}^\circ = 716.7 \text{ kJ mol}^{-1}$, and $S^\circ = 158.100 \text{ J mol}^{-1}$. [45]
- ⁴⁸ Recommendation taken from IUPAC Task Group.[193] Previous recommendations of $\Delta H_f(298 \text{ K}) = 597.37 \pm 1.3 \text{ kJ mol}^{-1}$ was from Gurvich. [91] The preferred value corresponds to the theoretical value of Császár et al., [53] which is in agreement with the experimental values but of considered higher accuracy. The entropy was taken from Gurvich. [91]
- ⁴⁹ Recommendation taken from IUPAC Task Group.[193] Previous recommendations of $\Delta H_f(298 \text{ K}) = 390.4 \pm 0.8 \text{ kJ mol}^{-1}$ and $S(298 \text{ K}) = 194.90 \text{ J K}^{-1} \text{ mol}^{-1}$ were from experiments of Ruscic, et al. [195] The present enthalpy recommendation represents a weighted average of this and other experimental results; the higher uncertainty reflects this and the differences between measurements that relate methylene to methyl and those derived from the dissociation of ketene.
- ⁵⁰ Recommendation taken from IUPAC Task Group.[193] Previous recommendations of $\Delta H_f(298 \text{ K}) = 428.0 \pm 0.8 \text{ kJ mol}^{-1}$ was from Jacox. [98] The preferred value is based on the enthalpy of formation of triplet methylene and a separation between the singlet and triplet states of $3147 \pm 5 \text{ cm}^{-1}$.
- ⁵¹ Recommendation taken from IUPAC Task Group.[193] Entropy value differs only slightly from previously recommended value of $193.96 \text{ J K}^{-1} \text{ mol}^{-1}$ from Gurvich.
- ⁵² Enthalpy from an active thermochemical tables optimization. [198] Enthalpy from flame calorimetry $-74.48 \pm 0.41 \text{ kJ mol}^{-1}$ used previously.[182] Entropy from Frenkel et al. [79]
- ⁵³ CODATA Key Value [52]. Atomization energies calculated using CCSD(T) with aug cc-pVnZ (n=D - 7) basis sets, using frozen-core CCSD(T) optimized geometries and extrapolated to the complete basis set limit, led to enthalpies of $\Delta_f H_0^\circ = -27.0 \pm 0.2 \text{ kcal mol}^{-1}$ and $\Delta_f H_{298}^\circ = -26.2 \pm 0.2 \text{ kcal mol}^{-1}$. [76]
- ⁵⁴ CODATA Key Value [52] The active thermochemical tables optimization gives an enthalpy value of $-393.473 \pm 0.014 \text{ kJ mol}^{-1}$. [198] Atomization energies calculated using CCSD(T) with aug cc-pVnZ (n=D - 7) basis sets, using frozen-core CCSD(T) optimized geometries and extrapolated to the complete basis set limit, led to enthalpies of $\Delta_f H_0^\circ = -93.7 \pm 0.2 \text{ kcal mol}^{-1}$ and $\Delta_f H_{298}^\circ = -93.8 \pm 0.2 \text{ kcal mol}^{-1}$. [76]
- ⁵⁵ Enthalpy from reversible reactions of I and Br with CH_2O , [19] using present values for HI and HBr. Entropy taken from [91]. Atomization energies calculated using CCSD(T) with aug cc-pVnZ (n=D - 7) basis sets, using frozen-core CCSD(T) optimized geometries and extrapolated to the complete basis set limit, led to enthalpies of $\Delta_f H_0^\circ = 10.4 \pm 0.2 \text{ kcal mol}^{-1}$ and $\Delta_f H_{298}^\circ = 10.5 \pm 0.2 \text{ kcal mol}^{-1}$. [76]
- ⁵⁶ Taken from review of Gurvich, et al. [91] A CCSD(T) calculation with the aug-cc-pVnZ (n=D,T,Q,5) basis set extrapolated to the CBS limit gave $\Delta_f H_0^\circ = -24.9 \pm 0.5 \text{ kcal mol}^{-1}$, $\Delta_f H_{298}^\circ = -25.8 \pm 0.5 \text{ kcal mol}^{-1}$, and $S = 52.24 \text{ cal K}^{-1} \text{ mol}^{-1}$. [144]
- ⁵⁷ Binding energy of $7.1 \text{ kcal mol}^{-1}$ calculated at the B3LYP/6-311++G(3df,3pd) level of theory. [4]
- ⁵⁸ Enthalpy obtained from atomization energies calculated using CCSD(T) with aug cc-pVnZ (n=D - 7) basis sets, using frozen-core CCSD(T) optimized geometries and extrapolated to the complete basis set limit. [76] An earlier computational study using G3 and CBS-Qb3 methods gave $\Delta_f H_{298}^\circ = -43.3 \pm 2 \text{ kcal mol}^{-1}$. [69] These results are in agreement with photoionization lower limit of $-46.5 \text{ kcal mol}^{-1}$. [194]
- ⁵⁹ Enthalpy obtained from atomization energies calculated using CCSD(T) with aug cc-pVnZ (n=D - 7) basis sets, using frozen-core CCSD(T) optimized geometries and extrapolated to the complete basis set limit; $\Delta_f H_0^\circ = -41.0 \pm 0.5 \text{ kcal mol}^{-1}$. (Result presented in text as an energy difference of $2.9 \text{ kcal mol}^{-1}$ over the *trans* form.)[76] An earlier computational study using G3 and CBS-Qb3 methods gave $\Delta_f H_{298}^\circ = -41.4 \pm 2 \text{ kcal mol}^{-1}$. [69]
- ⁶⁰ Enthalpy obtained from atomization energies calculated using CCSD(T) with aug cc-pVnZ (n=D - 7) basis sets, using frozen-core CCSD(T) optimized geometries and extrapolated to the complete basis set

limit. [76] An earlier study using vibrational frequencies calculated at the HF/6-31G(D) level and total energies evaluated at the G2(MP2) level, also making use of isodesmic reactions, gave $\Delta_f H_{298}^\circ = -30 \text{ kcal mol}^{-1}$ and the quoted entropy value. [245] A CCSD(T)-CBS (W1U) calculation gives $\Delta_f H_{298}^\circ = -129.4 \pm 12.6 \text{ kJ mol}^{-1}$. [73]

⁶¹ Vibrational frequencies calculated at the HF/6-31G(D) level and total energies evaluated at the G2(MP2) level, also making use of isodesmic reactions. [245] Enthalpy calculated using the atomization energy method at the CBS-Q level gave $-41.62 \text{ kcal mol}^{-1}$. [224]

⁶² Enthalpy taken from NBS Tables [237]; entropy calculated based on structure optimized at MP2/6-31G(D) and frequencies calculated at HF/6-31G(D) level. [245] See also discussion of enthalpy in [245]. $\Delta_f H_{298}^\circ = -90.5 \text{ kcal mol}^{-1}$ also obtained by calculating optimized geometry at the CCSD(T) level with the aug-cc-pVTZ basis set; CCSD(T) energy extrapolated to the CBS limit. [160] Atomization energies calculated using CCSD(T) with aug cc-pVnZ (n=D - 7) basis sets, using frozen-core CCSD(T) optimized geometries and extrapolated to the complete basis set limit, led to enthalpies of $\Delta_f H_0^\circ = -88.9 \pm 0.4 \text{ kcal mol}^{-1}$ and $\Delta_f H_{298}^\circ = -90.7 \pm 0.4 \text{ kcal mol}^{-1}$. [76]

⁶³ Enthalpy obtained from atomization energies calculated using CCSD(T) with aug cc-pVnZ (n=D - 7) basis sets, using frozen-core CCSD(T) optimized geometries and extrapolated to the complete basis set limit; $\Delta_f H_0^\circ = -65.9 \pm 0.6 \text{ kcal mol}^{-1}$. [76]

⁶⁴ Formaldehyde O-oxide (Criegee intermediate). Optimized geometry calculated at the CCSD(T) level with the aug-cc-pVTZ basis set; CCSD(T) energy extrapolated to the CBS limit. [160]

⁶⁵ Dioxirane. Optimized geometry calculated at the CCSD(T)/aVTZ level with the aug-cc-pVTZ basis set; CCSD(T) energy extrapolated to the CBS limit. [160]

⁶⁶ Selection taken from IUPAC Task Group.[193] The recommended enthalpy is a weighted average of the experimental determinations, with an amplified uncertainty for the older gas-phase acidity determinations. The recommendation is supported by one recent high-level theoretical study. This value is significantly higher than that recommended here previously, $17.15 \pm 3.8 \text{ kJ mol}^{-1}$ from the evaluation of Berkowitz et al. [23] and most other previous recommendations. The recommended entropy is also somewhat different than the previously recommended value of $232.86 \text{ J K}^{-1} \text{ mol}^{-1}$. [91] Atomization energies calculated using CCSD(T) with cc-pVnZ (n=D, T, and Q) basis sets, using (U)MP2/aug-cc-pVTZ optimized geometries and extrapolated to the complete basis set limit, led to enthalpies of $\Delta_f H_0^\circ = 7.4 \text{ kcal mol}^{-1}$ and $\Delta_f H_{298}^\circ = 5.5 \text{ kcal mol}^{-1}$. [143]

⁶⁷ Based on a re-analysis of previous equilibrium data on $\text{R} + \text{O}_2 \leftrightarrow \text{RO}_2$ from the same laboratory. [113]

⁶⁸ Recommendation taken from IUPAC Task Group.[193] Enthalpy is a weighted average of the most recent experimental studies and a theoretical study, and is in good agreement with all the previous experimental results. (Note that the previous value listed in this Table, $\Delta_f H_0^\circ = -11.5 \pm 1.3 \text{ kJ mol}^{-1}$, was inadvertently for OK.) The entropy value reported by Johnson and Hudgens was accepted and is included here with their error limits. [102] Results of Dóbe, et al. [65] give $-16.6 \pm 1.3 \text{ kJ mol}^{-1}$. Atomization energies calculated using CCSD(T) with cc-pVnZ (n=D, T, and Q) basis sets, using (U)MP2/aug-cc-pVTZ optimized geometries and extrapolated to the complete basis set limit, led to enthalpies of $\Delta_f H_0^\circ = -2.3 \text{ kcal mol}^{-1}$ and $\Delta_f H_{298}^\circ = -3.8 \text{ kcal mol}^{-1}$. [143]

⁶⁹ Taken from review of Gurvich, et al. [91] Atomization energies calculated using CCSD(T) with cc-pVnZ (n=D, T, and Q) basis sets, using (U)MP2/aug-cc-pVTZ optimized geometries and extrapolated to the complete basis set limit, led to enthalpies of $\Delta_f H_0^\circ = -45.7 \text{ kcal mol}^{-1}$ and $\Delta_f H_{298}^\circ = -48.3 \text{ kcal mol}^{-1}$. [143]

⁷⁰ Estimated from a K_{eq} expression from studies on the decay of HO_2 in the presence of CH_3OH over the temperature range 231 to 261 K, with supporting *ab initio* calculations (Table 3-1, Note 4).

⁷¹ Calculated using the complete basis set method, CBS-Q. Enthalpies calculated using the atomization energy method. Entropy based on geometric properties optimized at the MP2/6-31G(d') level and vibrational frequencies at the HF/6-31G(d') level.[224] This radical is unstable to decomposition to $\text{CH}_2\text{O} + \text{OH}$.

⁷² Reaction enthalpies determined using the G2 method indicated $DH_{298}^\circ(\text{CH}_3\text{OO-H})$ is $1.6 \text{ kcal mol}^{-1}$ lower than $DH_{298}^\circ(\text{HOO-H})$, or $85.9 \text{ kcal mol}^{-1}$. [124] Previous enthalpy value ($-139.0 \pm 8.1 \text{ kJ mol}^{-1}$) was computed on the assumption that the dissociation energy for ROO-H is $366 \pm 3 \text{ kJ mol}^{-1}$ (Stocker & Pilling, unpublished work). [113] Enthalpy calculated using the atomization energy method at the CBS-Q

level gave $-30.75 \text{ kcal mol}^{-1}$. [224] Entropy based on geometric properties optimized at the MP2/6-31G(d') level and vibrational frequencies at the HF/6-31G(d') level. [224]

⁷³ From the review of Gurvich. [91]

⁷⁴ Based on recommendation of [148], adjusted for enthalpy for CH_3NH_2 used here ($-5.6 \text{ kcal mol}^{-1}$, vs. $-5.5 \text{ kcal mol}^{-1}$). Calculations at the G2(MP2) level lead to an enthalpy of 147 kJ mol^{-1} . [239]

⁷⁵ Enthalpy from review of Pedley [176]; entropy value from TRC Data Series. [79]. Values of $\Delta_f H_{298}^\circ = -21.8 \pm 1.5 \text{ kJ mol}^{-1}$ and $\Delta_f H_0^\circ = -7.0 \pm 1.5 \text{ kJ mol}^{-1}$ have been derived from a threshold PEPICO study of alkyl amines and the use of two isodesmic reaction networks, connected through the TPEPICO dissociation energies, and with reaction heats calculated at the CBS-APNO and W1U levels of theory. [28]

⁷⁶ Based on an analysis of the negative ion cycle. [121]

⁷⁷ Enthalpy at 298K by combustion calorimetry; [5] 0 K value based on measured vibrational frequencies. [121] Entropy from NBS Tables. [237]

⁷⁸ From computed G2 heats of reaction. [215]

⁷⁹ This is the more stable isomer of CH_2NO , which is formed by the association of CH_2 with NO . From computed G2 heats of reaction. [215]

⁸⁰ Enthalpy from $\text{D}(\text{H-NCO}) = 4.9 \pm 0.01 \text{ eV}$ [165], using present value for HNCO . Entropy from [91]

⁸¹ Isocyanic. Enthalpy from photodissociation of HNCO by measuring $\text{NH}(a^1\Delta)$ threshold and fragment energy. Adjusted for the present enthalpy of NH . [220] Entropy from [237].

⁸² Formamide. From review of Pedley, et al. [176]

⁸³ Enthalpy from a CCSD(T) calculation of the atomization energy. [63]

⁸⁴ Recommendation from the TRC Data Series. [79] A calculation of the atomization energy at the G3 level of theory leads to $\Delta_f H_{298}^\circ = 31.5 \text{ kcal mol}^{-1}$. Calculations also carried out at the G2, G2M(CC5), B3LYP, MW1B95, and MPWB1K levels. [109]

⁸⁵ Enthalpy from Pedley, [176] entropy from Frenkel et al. [79] Enthalpy value calculated using G3, CBS-QB3, and CBS-APNO methods applied to atomization, isomerization, and work reactions is $\Delta_f H_{298}^\circ = -17.67 \pm 0.27 \text{ kcal mol}^{-1}$, which becomes $-17.73 \pm 0.27 \text{ kcal mol}^{-1}$ using the reference enthalpy for *cis*-HONO from this Table. [10] A calculation of the atomization energy at the G3 level of theory leads to $\Delta_f H_{298}^\circ = -17.5 \text{ kcal mol}^{-1}$. Calculations also carried out at the G2, G2M(CC5), B3LYP, MW1B95, and MPWB1K levels. [109]

⁸⁶ Taken from review of Stull, et al. [221] Enthalpy value calculated using G3, CBS-QB3, and CBS-APNO methods applied to atomization, isomerization, and work reactions is $\Delta_f H_{298}^\circ = -15.64 \pm 0.10 \text{ kcal mol}^{-1}$, which becomes $-15.81 \pm 0.10 \text{ kcal mol}^{-1}$ using the reference enthalpy for *cis*-HONO from this Table. [10] A calculation of the atomization energy at the G3 level of theory leads to $\Delta_f H_{298}^\circ = -15.4 \text{ kcal mol}^{-1}$. Calculations also carried out at the G2, G2M(CC5), B3LYP, MW1B95, and MPWB1K levels. [109]

⁸⁷ Enthalpy from Pedley, [176] entropy from Stull et al. [221]

⁸⁸ Enthalpy value calculated from the atomization energy at the G3 level of theory. Calculations also carried out at the G2, G2M(CC5), B3LYP, MW1B95, and MPWB1K levels. [109]

⁸⁹ Enthalpy value calculated from the atomization energy at the G3 level of theory. Calculations also carried out at the G2, G2M(CC5), B3LYP, MW1B95, and MPWB1K levels. (see addition and corrections) [109]

⁹⁰ Urea. From review of Pedley, et al. [176]

⁹¹ Enthalpy from review of Berkowitz, Ellison, and Gutman. [23] $\Delta_f H_0^\circ = 134.1 \pm 0.7 \text{ kcal mol}^{-1}$. Entropy from Gurvich. [91] High level *ab initio* calculations result in an enthalpy value of $567.4 \pm 1.5 \text{ kJ mol}^{-1}$. [227]

⁹² From the review of Gurvich. [91] Pedley gives the enthalpy as $228.2 \pm 0.7 \text{ kJ mol}^{-1}$. [176] The JANAF Tables give $\Delta_f H_0^\circ = 227.3 \text{ kJ mol}^{-1}$, $\Delta_f H_{298}^\circ = 226.7 \text{ kJ mol}^{-1}$, and $S^\circ = 200.958 \text{ J mol}^{-1}$. [45]

⁹³ Vinylidene. Based on a series of negative ion photoelectron spectroscopic measurements combined with proton-transfer kinetics. [71] CCSD(T) calculations, extrapolated to the CBS level, lead to $\Delta_f H_0^\circ = 98.6 \text{ kcal mol}^{-1}$ and $\Delta_f H_{298}^\circ = 98.8 \text{ kcal mol}^{-1}$. [159]

⁹⁴ Enthalpy derived from a third-law analysis of the reaction $\text{Cl} + \text{C}_2\text{H}_4 \leftrightarrow \text{HCl} + \text{C}_2\text{H}_3$. [104] A second-law analysis gives $69.1 \pm 1.6 \text{ kcal mol}^{-1}$. The recommendation of Tsang is $71.5 \pm 1 \text{ kcal mol}^{-1}$. [230] See also discussion by Lago and Baer. [24] Negative ion photoelectron spectroscopy combined with proton-transfer

kinetics leads to a value of $\Delta_f H_{298}^\circ = 71.6 \pm 0.8 \text{ kcal mol}^{-1}$. [71] The entropy value was provided by Tsang. [104]

⁹⁵ From the review of Gurvich. [91] The JANAF Tables give $\Delta_f H_0^\circ = 60.0 \text{ kJ mol}^{-1}$, $\Delta_f H_{298}^\circ = 52.5 \text{ kJ mol}^{-1}$, and $S^\circ = 219.330 \text{ J mol}^{-1}$. [45]

⁹⁶ Enthalpy from review of Berkowitz, Ellison, and Gutman. [23] Entropy from Gurvich. [91] Enthalpy of $120.7 \pm 1.0 \text{ kJ mol}^{-1}$ has been derived from a threshold PEPICO study of alkyl amines and the use of two isodesmic reaction networks, connected through the TPEPICO dissociation energies, and with reaction heats calculated at the CBS-APNO and W1U levels of theory. $\Delta_f H_0^\circ = 132.3 \pm 1.0 \text{ kJ mol}^{-1}$. [28]

⁹⁷ Enthalpy from flame calorimetry measurement. [182] Entropy from Gurvich, et al. [91], who gives $\Delta_f H_{298}^\circ = -84.00 \pm 0.40 \text{ kJ mol}^{-1}$ and $\Delta_f H_0^\circ = 68.38 \pm 0.40 \text{ kJ mol}^{-1}$.

⁹⁸ Calculated from the heat of reactions for $\text{OH} + \text{C}_2\text{H}_2$ of $-146 \pm 10 \text{ kJ mol}^{-1}$. [81]

⁹⁹ Based on the recommended dissociation energy for CH_2CO of $105.3 \pm 2.1 \text{ kcal mol}^{-1}$. [23] High level *ab initio* calculations result in an enthalpy of $173.8 \pm 1.5 \text{ kJ mol}^{-1}$. [227]

¹⁰⁰ From photoionization of CH_2CO and a subsequent optimization of a local thermochemical network. [195]

¹⁰¹ Recommendation taken from IUPAC Task Group. [193] Enthalpy is a weighted average of the experimental results, with amplified uncertainties assigned to the most negative values. This recommendation is only slightly lower than the value $-10.0 \pm 1.2 \text{ kJ mol}^{-1}$ previously recommended here. [23]

¹⁰² Enthalpy value an average of the a value obtained from the gas-phase basicity and proton affinity determined by a kinetic method ($9.9 \pm 3.9 \text{ kJ mol}^{-1}$) and a reexamination of the results of Holmes, et al. [95] on the dissociation of ethyl acetate after electron ionization ($15.9 \pm 5.6 \text{ kJ mol}^{-1}$). [29] This value is supported by several computational studies. [94],[99],[93],[70] Previous recommendation, $10.5 \pm 9.2 \text{ kJ mol}^{-1}$, was from an analysis of gas-phase acidity and electron affinity studies. [23] The entropy value is from G3MP2B3 calculation. [99]

¹⁰³ Enthalpy from Pedley, [176] entropy from Frenkel et al. [79]

¹⁰⁴ Radical from methyl formate. An average of two isodesmic reactions calculated at the G3MP2//B3LYP/6-31G(d) level. [206] Enthalpy calculated using the atomization energy method at the CBS-Q level gave $\Delta_f H_{298}^\circ = -37.87 \text{ kcal mol}^{-1}$. [224] Entropy based on geometric properties optimized at the MP2/6-31G(d') level and vibrational frequencies at the HF/6-31G(d') level. [224]

¹⁰⁵ Calculated using the complete basis set method, CBS-Q. Enthalpies calculated using the atomization energy method. Entropy based on geometric properties optimized at the MP2/6-31G(d') level and vibrational frequencies at the HF/6-31G(d') level. [224]

¹⁰⁶ Methyl formate. [176] An average of three isodesmic reactions calculated at the G3MP2//B3LYP/6-31G(d) level, supported by G3 and B3LYP calculations gives $\Delta_f H_{298}^\circ = -82.3 \pm 0.49 \text{ kcal mol}^{-1}$. [206] Enthalpy calculated using the atomization energy method at the CBS-Q level gave $\Delta_f H_{298}^\circ = -85.87 \text{ kcal mol}^{-1}$. [224] Entropy based on geometric properties optimized at the MP2/6-31G(d') level and vibrational frequencies at the HF/6-31G(d') level. [224]

¹⁰⁷ Glyoxal. The lowest energy conformer is the *trans* isomer. From the updated JANAF Tables, based on measurements of the heat of combustion. [67]

¹⁰⁸ Oxiranone (an α -lactone of ethylene oxide). *Ab initio* calculations utilizing isodesmic reactions. [191]

¹⁰⁹ Calculated using the complete basis set method, CBS-Q. Enthalpies calculated using the atomization energy method. Entropy based on geometric properties optimized at the MP2/6-31G(d') level and vibrational frequencies at the HF/6-31G(d') level. [224] This radical is unstable towards dissociation.

¹¹⁰ Based on a re-analysis of previous equilibrium data on $\text{R} + \text{O}_2 \leftrightarrow \text{RO}_2$ from the same laboratory. [113]

¹¹¹ Reaction enthalpy for the reaction $\text{CH}_3\text{CH}_2\text{OO} + \text{CH}_3\text{OOH} = \text{CH}_3\text{CH}_2\text{OOH} + \text{CH}_3\text{OO}$ calculated to be $0.5 \text{ kcal mol}^{-1}$ using the QCISD(T)/6-31G**// MP2/6-31G* method. [124] Previous enthalpy value ($-175.4 \pm 12.9 \text{ kJ mol}^{-1}$) was computed on the assumption that the dissociation energy for ROO-H is $366 \pm 3 \text{ kJ mol}^{-1}$ (Stocker & Pilling, unpublished work). [113] Pedley gives a value of $-198.9 \pm 58.7 \text{ kJ mol}^{-1}$. [176] Enthalpy calculated using the atomization energy method at the CBS-Q level gave $-38.78 \text{ kcal mol}^{-1}$. [224] Entropy based on geometric properties optimized at the MP2/6-31G(d') level and vibrational frequencies at the HF/6-31G(d') level. [224]

¹¹² Recommendation taken from IUPAC Task Group. [193] Enthalpy is based on a collision-induced dissociation measurement, which lies between the theoretical results and most of the previous

recommendations, including that previously included here, $\Delta_f H_{298}^\circ = -15.5 \pm 3.3 \text{ kJ mol}^{-1}$. [23] Ruscic, et al. note that their new preferred value corresponds to an O–H bond dissociation energy for ethanol more in line with that in methanol. Atomization energies calculated using CCSD(T) with cc-pVnZ (n=D, T, and Q) basis sets, using (U)MP2/aug-cc-pVTZ optimized geometries and extrapolated to the complete basis set limit, led to enthalpies of $\Delta_f H_0^\circ = 0.8 \text{ kcal mol}^{-1}$ and $\Delta_f H_{298}^\circ = -2.7 \text{ kcal mol}^{-1}$. [143]

¹¹³ Calculated from the heat of reaction for the addition of OH to C₂H₄ of $-123 \pm 6 \text{ kJ mol}^{-1}$. [81]

Atomization energies calculated using CCSD(T) with cc-pVnZ (n=D, T, and Q) basis sets, using (U)MP2/aug-cc-pVTZ optimized geometries and extrapolated to the complete basis set limit, led to enthalpies of $\Delta_f H_0^\circ = -3.1 \text{ kcal mol}^{-1}$ and $\Delta_f H_{298}^\circ = -6.2 \text{ kcal mol}^{-1}$. [143]

¹¹⁴ Calculated using the complete basis set method, CBS-Q. Enthalpies calculated using the atomization energy method. Entropy based on geometric properties optimized at the MP2/6-31G(d') level and vibrational frequencies at the HF/6-31G(d') level. [224] Enthalpy recommended in the review of McMillen and Golden is $-15.2 \pm 1 \text{ kcal mol}^{-1}$. [148] Atomization energies calculated using CCSD(T) with cc-pVnZ (n=D, T, and Q) basis sets, using (U)MP2/aug-cc-pVTZ optimized geometries and extrapolated to the complete basis set limit, led to enthalpies of $\Delta_f H_0^\circ = -9.8 \text{ kcal mol}^{-1}$ and $\Delta_f H_{298}^\circ = -13.1 \text{ kcal mol}^{-1}$. [143]

¹¹⁵ Taken from review of Gurvich, et al. [91] Atomization energies calculated using CCSD(T) with cc-pVnZ (n=D, T, and Q) basis sets, using (U)MP2/aug-cc-pVTZ optimized geometries and extrapolated to the complete basis set limit, led to enthalpies of $\Delta_f H_0^\circ = -52.1 \text{ kcal mol}^{-1}$ and $\Delta_f H_{298}^\circ = -56.4 \text{ kcal mol}^{-1}$. [143]

¹¹⁶ Vibrational frequencies calculated at the HF/6-31G(D) level and total energies evaluated at the G2(MP2) level, also making use of isodesmic reactions. [245]

¹¹⁷ Enthalpy derived from isodesmic reactions calculated by the B3LYP/6-31G(d,p) and G3 methods. Reported results were adjusted for enthalpy values of reference compounds in this Table. [72]

¹¹⁸ Glycoaldehyde. Enthalpy derived from isodesmic reactions calculated by the B3LYP/6-31G(d,p) and G3 methods. Reported results were adjusted for enthalpy values of reference compounds in this Table. [72]

¹¹⁹ Enthalpy based on CID studies of the acetate radical anion yielding D(H-CH₂COOH) = $95.3 \pm 2.9 \text{ kcal mol}^{-1}$. [240] Entropy based on vibrational frequencies calculated at the HF/6-31G(D) level. [245] Isodesmic reactions at the G2(MP2) level give -243 kJ mol^{-1} .

¹²⁰ Derived from a hybrid experimental/CBS-Q approach. [149]

¹²¹ Enthalpy from Pedley [176], entropy from Chao. [41]

¹²² Derived from a hybrid experimental/CBS-Q approach. [149]

¹²³ Glycolic acid. From the updated JANAF Tables, estimated based on additivity methods. [67]

¹²⁴ Calculated using the complete basis set method, CBS-Q. Enthalpies calculated using the atomization energy method. Entropy based on geometric properties optimized at the MP2/6-31G(d') level and vibrational frequencies at the HF/6-31G(d') level. [224] Recommendation in the review of McMillen and Golden, adjusted to allow for present enthalpy of CH₃COCH₃, is $-3 \pm 1 \text{ kcal mol}^{-1}$. [148]

¹²⁵ Enthalpy from Pedley, [176] entropy from Frenkel et al. [79] Enthalpy calculated using the atomization energy method at the CBS-Q level gave $-43.98 \text{ kcal mol}^{-1}$. [224]

¹²⁶ Ethene, 1-diol. Enthalpy obtained from three isodesmic reactions at the G3MP2//B3LYP/6-31G(d) level of theory. [206]

¹²⁷ 1,2-Ethanediol. Enthalpy from Pedley, [176] entropy from Frenkel et al. [79]

¹²⁸ Radical from ethanal, 2-diol. Calculated from two isodesmic reactions at the G3MP2//B3LYP/6-31G(d) level of theory. [206]

¹²⁹ Ethanal, 2-diol. Calculated from two isodesmic reactions at the G3MP2//B3LYP/6-31G(d) level of theory. [206]

¹³⁰ Ethanedial (glyoxal). From review of Pedley. [176]

¹³¹ Calculated using the complete basis set method, CBS-Q. Enthalpies calculated using the atomization energy method. Entropy based on geometric properties optimized at the MP2/6-31G(d') level and vibrational frequencies at the HF/6-31G(d') level. [224] This radical is unstable towards decomposition.

¹³² Enthalpy from updated JANAF Tables, based on calorimetric measurements. [67] Enthalpy calculated using the atomization energy method at the CBS-Q level gave $\Delta_f H_{298}^\circ = -29.17 \text{ kcal mol}^{-1}$. [224] Entropy based on geometric properties optimized at the MP2/6-31G(d') level and vibrational frequencies at the HF/6-31G(d') level. [224]

- ¹³³ Dioxybismethanol. From review of Pedley. [176]
- ¹³⁴ Oxalic acid. Updated JANAF Tables, based on the enthalpy of combustion of the solid and the enthalpy of vaporization. [67]
- ¹³⁵ Calculated using G3, CBS-QB3, and CBS-APNO methods applied to atomization, isomerization, and work reactions, Value reported is $\Delta_f H_{298}^\circ = -25.06 \pm 0.07 \text{ kcal mol}^{-1}$, which is adjusted using the reference enthalpy for *cis*-HONO from this Table. [10] A calculation of the atomization energy at the G3 level of theory leads to $\Delta_f H_{298}^\circ = -24.7 \text{ kcal mol}^{-1}$. Calculations also carried out at the G2, G2M(CC5), B3LYP, MW1B95, and MPWB1K levels. [109]
- ¹³⁶ Calculated using G3, CBS-QB3, and CBS-APNO methods applied to atomization, isomerization, and work reactions, Value reported is $\Delta_f H_{298}^\circ = -23.58 \pm 0.12 \text{ kcal mol}^{-1}$, which is adjusted using the reference enthalpy for *cis*-HONO from this Table. [10] A calculation of the atomization energy at the G3 level of theory leads to $\Delta_f H_{298}^\circ = -22.9 \text{ kcal mol}^{-1}$. Calculations also carried out at the G2, G2M(CC5), B3LYP, MW1B95, and MPWB1K levels. [109]
- ¹³⁷ Derived from a hybrid experimental/CBS-Q approach. [149]
- ¹³⁸ Enthalpy value calculated from the atomization energy at the G3 level of theory. Calculations also carried out at the G2, G2M(CC5), B3LYP, MW1B95, and MPWB1K levels. [109]
- ¹³⁹ Ethylamine. [176] Values of $\Delta_f H_{298}^\circ = -50.1 \pm 1.5 \text{ kJ mol}^{-1}$ and $\Delta_f H_0^\circ = -28.6 \pm 1.5 \text{ kJ mol}^{-1}$ have been derived from a threshold PEPICO study of alkyl amines and the use of two isodesmic reaction networks, connected through the TPEPICO dissociation energies, and with reaction heats calculated at the CBS-APNO and W1U levels of theory. [28]
- ¹⁴⁰ Dimethylamine. From review of Pedley. [176]
- ¹⁴¹ Acetamide. From review of Pedley. [176]
- ¹⁴² Propadiene. Enthalpy from Pedley. [176]
- ¹⁴³ Propyne. Enthalpy from Pedley. [176]
- ¹⁴⁴ Cyclopropene. Enthalpy from Pedley. [176]
- ¹⁴⁵ From a second-law analysis of $\text{C}_3\text{H}_5 + \text{HBr} \leftrightarrow \text{C}_3\text{H}_6 + \text{Br}$. [209]
- ¹⁴⁶ Enthalpy from Pedley[176], entropy from Chao. [40]
- ¹⁴⁷ Enthalpy derived from a threshold PEPICO study of alkyl amines and the use of two isodesmic reaction networks, connected through the TPEPICO dissociation energies, and with reaction heats calculated at the CBS-APNO and W1U levels of theory. [28] Previous value of $\Delta_f H_{298}^\circ = 100 \pm 2 \text{ kJ mol}^{-1}$ estimated by Tsang. [230]
- ¹⁴⁸ From a second-law analysis of $\text{iso-C}_3\text{H}_7 + \text{HBr} \leftrightarrow \text{iso-C}_3\text{H}_8 + \text{Br}$. [213] An enthalpy of $\Delta_f H_{298}^\circ = 88.5 \pm 1.0 \text{ kJ mol}^{-1}$ and $\Delta_f H_0^\circ = 106.2 \pm 1.0 \text{ kJ mol}^{-1}$ has been derived from a threshold PEPICO study of alkyl amines and the use of two isodesmic reaction networks, connected through the TPEPICO dissociation energies, and with reaction heats calculated at the CBS-APNO and W1U levels of theory. [28]
- ¹⁴⁹ Enthalpy by combustion calorimetry. [182] Entropy by ideal gas properties calculations. [39]
- ¹⁵⁰ From review of Pedely, et al. [176]
- ¹⁵¹ 1,2-Propanediol. From review of Pedley, et al. [176]
- ¹⁵² CBS-4 and G2(MP2,SVP) methods used to obtain thermodynamic properties. Value listed is recommendation based on theoretical and experimental results. Entropy at the G2(MP2(full))/MP2(full)/6-31G(d) level treating internal rotations as harmonic oscillators.[236]
- ¹⁵³ Enthalpy from Pedley, [176] entropy from Frenkel et al. [79]
- ¹⁵⁴ Enthalpy value an average of the a value obtained from the gas-phase basicity and proton affinity determined by a kinetic method ($-34.6 \pm 8.4 \text{ kJ mol}^{-1}$) and a reexamination of the results of Holmes, et al. [95] on the dissociation of 2-propenyl acetate and acetylacetone after electron ionization (-33.1 and $-30.3 \text{ kJ mol}^{-1}$). [29] This value is supported by several computational studies. [100],[30],[70] The previous recommendation, $-28.1 \pm 3.1 \text{ kJ mol}^{-1}$, was derived from forward and reverse rate constants for the reaction $\text{CH}_3\text{C}(\text{O})\text{CH}_2 + \text{HBr} \leftrightarrow \text{CH}_3\text{C}(\text{O})\text{CH}_3 + \text{Br}$. [74] The reverse rate constant requires an extrapolation from high temperature for the reference reaction. An earlier photobromination determination of the reverse reaction results in an enthalpy value of $-24.3 \pm 5.8 \text{ kJ mol}^{-1}$. [108] Density functional and ab initio calculations at the CBS-QB3 level of theory, using a series of isodesmic reactions, led to $\Delta_f H_{298}^\circ = -24.3 \pm 5.8 \text{ kJ mol}^{-1}$. [70] The entropy value is from G3MP2B3 calculation. [100] The equilibrium constant values recommended in Table 3 are more consistent with $\Delta_f H_{298}^\circ = -32.9 \pm 2.0 \text{ kJ mol}^{-1}$.
- ¹⁵⁵ Enthalpy from review of Pedley [176]; entropy value from Frenkel [79].

- ¹⁵⁶ Calculated using the complete basis set method, CBS-Q. Enthalpies calculated using the atomization energy method. Entropy based on geometric properties optimized at the MP2/6-31G(d') level and vibrational frequencies at the HF/6-31G(d') level.[224]
- ¹⁵⁷ Methoxyethane (methyl ethyl ether). Enthalpy from Pedley, et al.[176]. Enthalpy calculated using the atomization energy method at the CBS-Q level gave $-52.20 \text{ kcal mol}^{-1}$. [224] Entropy based on geometric properties optimized at the MP2/6-31G(d') level and vibrational frequencies at the HF/6-31G(d') level.[224]
- ¹⁵⁸ Radical from propenal. Enthalpy obtained from four isodesmic reactions at the G3MP2//B3LYP/6-31G(d) level of theory. [206]
- ¹⁵⁹ CBS-4 and G2(MP2,SVP) methods used to obtain thermodynamic properties. Value listed is recommendation based on theoretical and experimental results. Entropy at the G2(MP2(full))/MP2(full)/6-31G(d) level treating internal rotations as harmonic oscillators.[236]
- ¹⁶⁰ Propenal. Enthalpy obtained from two isodesmic reactions at the G3MP2//B3LYP/6-31G(d) level of theory. [206]
- ¹⁶¹ Calculated using the complete basis set method, CBS-Q. Enthalpies calculated using the atomization energy method. Entropy based on geometric properties optimized at the MP2/6-31G(d') level and vibrational frequencies at the HF/6-31G(d') level.[224]
- ¹⁶² Dimethoxymethane. From review of Pedely, et al. [176]
- ¹⁶³ Calculated using the complete basis set method, CBS-Q. Enthalpies calculated using the atomization energy method. Entropy based on geometric properties optimized at the MP2/6-31G(d') level and vibrational frequencies at the HF/6-31G(d') level.[224]
- ¹⁶⁴ Hydroxyacetone. Enthalpy derived from isodesmic reactions calculated by the B3LYP/6-31G(d,p) and G3 methods. Reported results were adjusted for enthalpy values of reference compounds in this Table. [72]
- ¹⁶⁵ Calculated using the complete basis set method, CBS-Q. Enthalpies calculated using the atomization energy method. Entropy based on geometric properties optimized at the MP2/6-31G(d') level and vibrational frequencies at the HF/6-31G(d') level.[224] This radical is unstable towards dissociation
- ¹⁶⁶ Calculated using the complete basis set method, CBS-Q. Enthalpies calculated using the atomization energy method. Entropy based on geometric properties optimized at the MP2/6-31G(d') level and vibrational frequencies at the HF/6-31G(d') level.[224]
- ¹⁶⁷ Based on a re-analysis of previous equilibrium data on $R + O_2 \leftrightarrow RO_2$ from the same laboratory. [113]
- ¹⁶⁸ Calculated using the complete basis set method, CBS-Q. Enthalpies calculated using the atomization energy method. Entropy based on geometric properties optimized at the MP2/6-31G(d') level and vibrational frequencies at the HF/6-31G(d') level.[224]
- ¹⁶⁹ Reaction enthalpy for the reaction $(CH_3)_2CHOO + CH_3OOH = (CH_3)_2CHOOH + CH_3OO$ calculated to be $0.6 \text{ kcal mol}^{-1}$ using the QCISD(T)/6-31G**// MP2/6-31G* method. [124] Enthalpy calculated using the atomization energy method at the CBS-Q level gave $-48.1 \text{ kcal mol}^{-1}$. [224] Entropy based on geometric properties optimized at the MP2/6-31G(d') level and vibrational frequencies at the HF/6-31G(d') level.[224]
- ¹⁷⁰ Propanol, 2-diol. Enthalpy obtained from three isodesmic reactions at the G3MP2//B3LYP/6-31G(d) level of theory. [206]
- ¹⁷¹ 1,2,3-Propanetriol. From review of Pedely, et al. [176]
- ¹⁷² Enthalpy derived from a threshold PEPICO study of alkyl amines and the use of two isodesmic reaction networks, connected through the TPEPICO dissociation energies, and with reaction heats calculated at the CBS-APNO and W1U levels of theory. [28]
- ¹⁷³ Trimethylamine. From review of Pedely, et al. [176]
- ¹⁷⁴ Trimethylene-N-oxide enthalpy from heat of combustion of solid and estimated sublimation enthalpy. [2]
- ¹⁷⁵ Oxopropanedinitrile. From the updated JANAF Tables, based on calorimetric measurements. [67]
- ¹⁷⁶ Enthalpy by combustion calorimetry. [182] Entropy by ideal gas properties calculations. [79]
- ¹⁷⁷ Based on a re-analysis of previous equilibrium data on $R + O_2 \leftrightarrow RO_2$ from the same laboratory. [113]
- ¹⁷⁸ Enthalpy based on the gas-phase acidity and electron affinity from a negative ion photoelectron spectral study, leading to a BDE(O-H) of $85 \pm 2 \text{ kcal mol}^{-1}$ ($83 \pm 2 \text{ kcal mol}^{-1}$ at 0 K). [51] Reaction enthalpy for the reaction $(CH_3)_3COO + CH_3OOH = (CH_3)_3COOH + CH_3OO$ was calculated to be $1.3 \text{ kcal mol}^{-1}$ using the QCISD(T)/6-31G**// MP2/6-31G* method, leading to $\Delta_f H_{298}^\circ = -56.8 \text{ kcal mol}^{-1}$. [124]

- ¹⁷⁹ Diacetyl peroxide. From updated JANAF Tables, based on a calorimetric measurement on the liquid and an assumed enthalpy of vaporization. [67]
- ¹⁸⁰ CODATA Key Value [52] $\Delta_f H_o^\circ = 77.3 \text{ kJ mol}^{-1}$. The active thermochemical tables optimization gives an enthalpy value of $79.313 \pm 0.24 \text{ kJ mol}^{-1}$. [198]
- ¹⁸¹ CODATA Key Value [52]
- ¹⁸² CODATA Key Value [52] The active thermochemical tables optimization gives an enthalpy value of $-272.775 \pm 0.24 \text{ kJ mol}^{-1}$. [198] The most recent NIST-JANAF review gives an enthalpy of $-273.3000 \pm 0.70 \text{ kJ mol}^{-1}$ and an entropy of $173.778 \pm 0.005 \text{ J K}^{-1} \text{ mol}^{-1}$. [216]
- ¹⁸³ JANAF review from 1972. [45]
- ¹⁸⁴ NIST-JANAF thermochemical tables for the oxygen fluorides. [44] Enthalpy based on mass spectrometric and thermal decomposition studies of FOF. The atomization energy calculated with CCSD(T) using aug-cc-pVnZ (n=D-6) basis sets, approaching the complete basis set limit, resulted in $\Delta_f H_{298}^\circ = 27.9 \pm 0.4 \text{ kcal mol}^{-1}$ and $\Delta_f H_o^\circ = 27.6 \pm 0.4 \text{ kcal mol}^{-1}$. [75]
- ¹⁸⁵ NIST-JANAF thermochemical tables for the oxygen fluorides. [44] Enthalpy based on a series of calorimetric studies. The atomization energy calculated with CCSD(T) using aug-cc-pVnZ (n=D-6) basis sets, approaching the complete basis set limit, resulted in $\Delta_f H_{298}^\circ = 6.6 \pm 0.5 \text{ kcal mol}^{-1}$ and $\Delta_f H_o^\circ = 7.1 \pm 0.5 \text{ kcal mol}^{-1}$. [75]
- ¹⁸⁶ NIST-JANAF thermochemical tables for the oxygen fluorides. [44] Calculated value of enthalpy difference between OFO and FOO at 0 K of 356 kJ mol^{-1} .
- ¹⁸⁷ From an analysis of studies of the equilibrium $F + O_2 \leftrightarrow FOO$ (Table 3-1, Note 10). NIST-JANAF thermochemical tables for the oxygen fluorides, based on several experimental values, primarily from kinetic studies recommends $\Delta_f H_{298}^\circ = 25.4 \pm 2 \text{ kJ mol}^{-1}$ and $\Delta_f H_o^\circ = 27.2 \pm 2 \text{ kJ mol}^{-1}$. [44] This is also the source of the entropy value. A determination of the atomization energy gave $\Delta_f H_{298}^\circ = 5.8 \pm 0.3 \text{ kcal mol}^{-1}$, [77] whereas a UCCSDT calculation led to $\Delta_f H_{298}^\circ = 6.5 \pm 1 \text{ kcal mol}^{-1}$. [58]
- ¹⁸⁸ Atomization energy calculated by the CCSD(T) extrapolated to the CBS limit, with geometry optimized through the CCSD(T)/aV(T+d)Z level. [87]
- ¹⁸⁹ NIST-JANAF thermochemical tables for the oxygen fluorides. [44] Value adopted for enthalpy is that recommended by Lyman (J. Phys. Chem. Ref. Data **18** 799 (1989)) based on a calorimetric measurement on the decomposition into O_2 and F_2 . The atomization energy calculated with CCSD(T) using aug-cc-pVnZ (n=D-6) basis sets, approaching the complete basis set limit, resulted in $\Delta_f H_{298}^\circ = 40.2 \pm 3.8 \text{ kJ mol}^{-1}$ and $\Delta_f H_o^\circ = 43.9 \pm 3.8 \text{ kJ mol}^{-1}$. [75]
- ¹⁹⁰ Estimated value. [13]
- ¹⁹¹ Taken from review of Stull, et al. [221] The JANAF Tables give $\Delta_f H_o^\circ = -63.3 \text{ kJ mol}^{-1}$, $\Delta_f H_{298}^\circ = -65.7 \text{ kJ mol}^{-1}$, and $S^\circ = 248.082 \text{ J mol}^{-1}$. [45]
- ¹⁹² Taken from review of Gurvich, et al. [91] The JANAF estimate from 1963 gave an enthalpy of $10 \pm 2 \text{ kJ mol}^{-1}$. [45]
- ¹⁹³ Thermodynamic properties from Gurvich review. [91]
- ¹⁹⁴ Calculated for the X^1A' state. Enthalpy from a CCSD(T) calculation with the aug-cc-pVnZ (n=D,T,Q,5) basis set extrapolated to the CBS limit and entropy from a MP2/aVTZ calculation. [144] Enthalpy obtained using the computed enthalpy of a reaction of the type: $CH_2(^1A_1) + CH_2F_2 + 2CH_3Y = CFY(^1A_1) + 3CH_4$ results in $\Delta_f H_{298}^\circ = 146 \text{ kJ mol}^{-1}$ at the QCISD(T)/6-311+G(3df,2p)//QCISD/6-311G(d,p) level of theory. Calculations also done at the G2 level. [204] Previous recommendation, $\Delta_f H_{298}^\circ = 143 \pm 13.0 \text{ kJ mol}^{-1}$, based on combining experimental chloride dissociation energies from the parent anion, prior experimental measurements, and G2 calculations. [184]
- ¹⁹⁵ Derived from the kinetics and equilibria of the iodination reaction $CH_3F + I_2 \leftrightarrow CH_2FI + HI$. [181] A QCISD(T)/6-311+G(3df,2p) isodesmic study resulted in an enthalpy of $-29.0 \pm 4.1 \text{ kJ mol}^{-1}$. [205]
- ¹⁹⁶ Enthalpies of reaction calculated at the MCG3/MCQCISD level of theory (up to 6-311++G(3d2f,2df,2p) basis set) for the homolytic fragmentation to the alkyl radical and fluoride atom, and for the atomization reaction and averaged. Enthalpy also calculated for the heterolytic fragmentation into the alkyl cation and fluoride anion for support. [115] Previous value, $\Delta_f H_{298}^\circ = -238 \pm 8 \text{ kJ mol}^{-1}$, estimated in review of Rodgers et al. [189] Luo and Benson recommend $-55.9 \pm 1 \text{ kcal/mol}$. [138]
- ¹⁹⁷ Calculated for the X^1A' state. Enthalpy from a CCSD(T) calculation with the aug-cc-pVnZ (n=D,T,Q,5) basis set extrapolated to the CBS limit and entropy from a MP2/aVTZ calculation. [144] $\Delta_f H_o^\circ =$

- 46.0±0.8 kcal mol⁻¹. Enthalpy obtained using the computed enthalpy of a reaction of the type: CH₂(¹A₁) + CH₂F₂ + 2CH₃Y = CFY(¹A₁) + 3CH₄ results in $\Delta_f H_{298}^{\circ} = -196 \text{ kJ mol}^{-1}$ at the QCISD(T)/6-311+G(3df,2p)//QCISD/6-311G(d,p) level of theory. Calculations also done at the G2 level. [204]
Previous recommendation, –44.0±2 kcal mol⁻¹, based on combining experimental chloride dissociation energies from the parent anion, prior experimental measurements, and G2 calculations. [184]
- ¹⁹⁸ Derived from the kinetics and equilibria of the iodination reaction CH₃F + I₂ ↔ CH₂FI + HI. [181] A QCISD(T)/6-311+G(3df,2p) isodesmic study resulted in an enthalpy of –241.2±4.1 kJ mol⁻¹. [205]
- ¹⁹⁹ From review by Rodgers, et al. [189] Pedley gives –452.3±0.9 kJ mol⁻¹. [176]
- ²⁰⁰ Enthalpy from a simultaneous solution of a thermochemical network for the CF₃X species, where X = nil, H, Cl, Br, I, CF₃, CN. [196] Entropy from recommendation of Gurvich. [91] A QCISD(T)/6-311+G(3df,2p) isodesmic study resulted in an enthalpy of –465.9±4.1 kJ mol⁻¹. [205]
- ²⁰¹ Enthalpy from a simultaneous solution of a thermochemical network for the CF₃X species, where X = nil, H, Cl, Br, I, CF₃, CN. [196] Entropy from recommendation of Gurvich. [91] An enthalpy calculation from the atomization energy was obtained starting with a ‘best estimated’ structure from extensive calculations and analysis, followed by CCST with aug-cc-pVQZ and aug-cc-pV5Z basis sets, and CCSD(T) with aug-cc-pVTZ and aug-cc-pVQZ basis sets. Values of $\Delta_f H_0^{\circ} = -165.18 \text{ kJ mol}^{-1}$ and $\Delta_f H_{298}^{\circ} = -166.86 \text{ kJ mol}^{-1}$ were obtained. [31]
- ²⁰² CODATA Key Value [52] The JANAF Tables give $\Delta_f H_0^{\circ} = -927.2 \pm \text{kJ mol}^{-1}$, $\Delta_f H_{298}^{\circ} = -933.2 \pm \text{kJ mol}^{-1}$, and $S^{\circ} = 261.419 \text{ J mol}^{-1}$. [45]
- ²⁰³ The enthalpy of formation based on an isodesmic reaction calculated at the MP2/6-31G(d,p) level of theory. [202]
- ²⁰⁴ Enthalpy from a CCSD(T) calculation with the aug-cc-pVnZ (n=D,T,Q,5) basis set extrapolated to the CBS limit and entropy from a MP2/aVTZ calculation. [144] The decomposition rate constant for FCO → F + CO [111], combined with the rate constant $k = 2.4 \times 10^{22} \text{ cm}^6 \text{ s}^{-1}$ [214] for the reverse reaction, results in an upper limit of $\Delta_f H_{298}^{\circ} < -153.1 \text{ kJ mol}^{-1}$. [111] A. CCSD(T) calculation gives $\Delta_f H_{298}^{\circ} = -42.0 \pm 0.5 \text{ kcal/mol}$. [32]
- ²⁰⁵ Fluoroformyloxyl radical. Calculated at the CCSD(T) level of theory. CFO value from same work is –42.0±0.5 kcal/mol, which differs from value in Table.[32]
- ²⁰⁶ Enthalpy from a CCSD(T) calculation with the aug-cc-pVnZ (n=D,T,Q,5) basis set extrapolated to the CBS limit and entropy from a MP2/aVTZ calculation. [144] $\Delta_f H_0^{\circ} = -90.3 \pm 0.5 \text{ kcal mol}^{-1}$. Previous enthalpy, –91.6 kcal mol⁻¹, from an ab initio calculation [203] and entropy from Gurvich. [91]
- ²⁰⁷ The enthalpy of formation based on an isodesmic reaction calculated at the MP2/6-31G(d,p) level of theory. [202]
- ²⁰⁸ Based on photoionization study. Enthalpy presented as lower limit; [11] Entropy from Gurvich. [91] Pedley review gives an enthalpy value of –639.8±1.4 kJ mol⁻¹. [176] A CCSD(T) calculation with the aug-cc-pVnZ (n=D,T,Q,5) basis set extrapolated to the CBS limit gave $\Delta_f H_0^{\circ} = -143.9 \pm 0.5 \text{ kcal mol}^{-1}$, $\Delta_f H_{298}^{\circ} = -144.7 \pm 0.5 \text{ kcal mol}^{-1}$, and $S = 61.87 \text{ cal K}^{-1} \text{ mol}^{-1}$. [144]
- ²⁰⁹ Re-analysis of data of Batt and Walsh, using new value for CF₂O, [11] The enthalpy of formation, $\Delta_f H_{298}^{\circ} = -154.5 \text{ kcal mol}^{-1}$, based on an isodesmic reaction calculated at the MP2/6-31G(d,p) level of theory. [202]
- ²¹⁰ Determined on the basis of extensive ab initio calculations. [116] Isomeric forms F₂COO and FC(=O)OF are calculated to have enthalpies of –60 and –104 kcal/mole, respectively.
- ²¹¹ Two values for the C-O bond dissociation energy in CF₃O₂ are given in Lightfoot, et al., –144±3.3 and –141±10 kJ mol⁻¹ at 0 K and adjusted to 298 K. [134] The value given is an average of the two resulting enthalpies.
- ²¹² Based on photoionization study. Enthalpy presented as lower limit. [12] The enthalpy of formation, $\Delta_f H_{298}^{\circ} = -220.7 \text{ kcal mol}^{-1}$, based on an isodesmic reaction calculated at the MP2/6-31G(d,p) level of theory. [202]
- ²¹³ Based on photoionization of CF₃OF and an analysis of the CF₃⁺ and CF₂O⁺ fragments. [12] A G2 calculation led to an enthalpy of –774.5 kJ mol⁻¹. [34]
- ²¹⁴ Enthalpy from a simultaneous solution of a thermochemical network for the CF₃X species, where X = nil, H, Cl, Br, I, CF₃, CN. [196] Entropy from recommendation of Chen, et al. [46]
- ²¹⁵ Enthalpy from review of Pedley. [176]

- ²¹⁶ Enthalpy from photobromination studies. [153] Entropy determined at the UHF/6-31G* level of theory. [48]
- ²¹⁷ Enthalpy from photobromination studies. [153] Entropy determined at the UHF/6-31G* level of theory. [48]
- ²¹⁸ Enthalpies of reaction calculated at the MCG3/MCQCISD level of theory (up to 6-311++G(3d2f,2df,2p) basis set) for the homolytic fragmentation to the alkyl radical and fluoride atom, and for the atomization reaction and averaged. Enthalpy also calculated for the heterolytic fragmentation into the alkyl cation and fluoride anion for support. [115] Previous value, $\Delta_f H_{298}^\circ = -227.4 \pm 4.2$, estimated by Luo and Benson. [138] Entropy from Gurvich review. [91] Enthalpy difference from TRC review. [46]
- ²¹⁹ Enthalpy from review of Pedley. [176]
- ²²⁰ 1,1-Difluoroethane. From review of Pedley. [176]
- ²²¹ An analysis of the thermal elimination of HF from $\text{CH}_2\text{FCH}_2\text{F}$ led to a C-C bond dissociation energy of $88 \pm 2 \text{ kcal mol}^{-1}$. [106] This was combined with the present enthalpy value for CH_2F .
- ²²² Thermodynamic properties determined at the UHF/6-31G* level, utilizing isodesmic/homodesmotic reactions for enthalpy of formation. [50]
- ²²³ Thermodynamic properties determined at the UHF/6-31G* level, utilizing isodesmic/homodesmotic reactions for enthalpy of formation. [48]
- ²²⁴ The dissociation energy of $\text{CH}_3\text{CF}_2\text{-H}$ of $99.5 \pm 1 \text{ kcal mol}^{-1}$ was derived from a study of the equilibrium $\text{CH}_3\text{CF}_2\text{H} + \text{I}_2 \leftrightarrow \text{CH}_3\text{CF}_2\text{I} + \text{HI}$. [180] Entropy calculated from molecular properties computed at the UHF/6-31* level of theory. [49]
- ²²⁵ TRC review. [46]
- ²²⁶ Enthalpy of formation based on the heat of hydrogenation of CF_2CFCl . [120] Pedley gives an enthalpy value of $-730.7 \pm 20.8 \text{ kJ mol}^{-1}$. [176]
- ²²⁷ The dissociation energy of $\text{CF}_3\text{CH}_2\text{-H}$ was derived from a study of the equilibrium $\text{CF}_3\text{CH}_3 + \text{I}_2 \leftrightarrow \text{CF}_3\text{CH}_2\text{I} + \text{HI}$. [243] Entropy calculated from molecular properties computed at the UHF/6-31* level of theory. [48]
- ²²⁸ TRC review. [46] Pedley review gives $-744.6 \pm 1.7 \text{ kJ mol}^{-1}$. [176]
- ²²⁹ Enthalpy from review of Pedley. [176]
- ²³⁰ Enthalpy calculated based on the C-C bond strength estimate of $91.4 \pm 3.7 \text{ kcal mol}^{-1}$. [150] Entropy from TRC review. [79]
- ²³¹ Entropy calculated from molecular properties computed at the UHF/6-31* level of theory. Enthalpy derived from isodesmic reactions and adjusted up by 2 kcal mol^{-1} to reflect the enthalpy value for CH_2FCF_3 in this Table. [50]
- ²³² TRC review. [46] Enthalpy estimated.
- ²³³ The dissociation energy of $\text{C}_2\text{F}_5\text{-I}$ of $52.5 \pm 1 \text{ kcal mol}^{-1}$ was derived from a study of the reaction of pentafluoroethyl iodide with HI. [244]
- ²³⁴ TRC review. [46] Pedley review gives an enthalpy value of $-1100.4 \pm 4.1 \text{ kJ mol}^{-1}$. [176]
- ²³⁵ Enthalpy from a simultaneous solution of a thermochemical network for the CF_3X species, where X = nil, H, Cl, Br, I, CF_3 , CN. [196] Entropy from recommendation of Chen, et al. [46]
- ²³⁶ CBS-4 and G2(MP2,SVP) methods used to obtain thermodynamic properties. In addition, enthalpy was derived from isodesmic reaction calculations. Value listed is recommendation based on theoretical and experimental results. Entropy at the G2(MP2(full))/MP2(full)/6-31G(d) level treating internal rotations as harmonic oscillators. [236]
- ²³⁷ Thermodynamic properties calculated at the G2(MP2(full))/MP2(full)/6-31G(d) level of theory. Enthalpy from atomization energy and entropy calculated treating internal rotations as harmonic oscillators. Similar values obtained at the CBS-4//HF/3021G* level. [236]
- ²³⁸ Acetyl fluoride. Enthalpy from review of Pedley. [176]
- ²³⁹ Trifluoroacetic acid. Enthalpy from review of Pedley. [176]
- ²⁴⁰ An average of a result from an isodesmic reaction and an atomization energy, both calculated at the CBS-4 level of theory. [170]
- ²⁴¹ A thermal decomposition study from 575 to 900 K led to a BDE(O-O) of $47.5 \pm 0.5 \text{ kcal mol}^{-1}$. [187] An MP2//6-31G(d,p) calculation utilizing isodesmic and isogyric reactions resulted in $-343 \pm 3 \text{ kcal mol}^{-1}$. [203] A CBS-QB3 calculation led to a BDE(O-O) of $209.4 \text{ kJ mol}^{-1}$, and thus an enthalpy of $-1479 \text{ kJ mol}^{-1}$. [3]

- ²⁴² Enthalpies of reaction calculated at the MCG3/MCQCISD level of theory (up to 6-311++G(3d2f,2df,2p) basis set) for the homolytic fragmentation to the alkyl radical and fluoride atom, and for the atomization reaction and averaged. Enthalpy also calculated for the heterolytic fragmentation into the alkyl cation and fluoride anion for support. [115] $\Delta_f H_{298}^\circ = -318.8 \pm 4.2$ estimated by Luo and Benson. [138]
- ²⁴³ Enthalpies of reaction calculated at the MCG3/MCQCISD level of theory (up to 6-311++G(3d2f,2df,2p) basis set) for the homolytic fragmentation to the alkyl radical and fluoride atom, and for the atomization reaction and averaged. Enthalpy also calculated for the heterolytic fragmentation into the alkyl cation and fluoride anion for support. [115] $\Delta_f H_{298}^\circ = -363.6 \pm 4.2$ estimated by Luo and Benson. [138]
- ²⁴⁴ Enthalpy value is from the optimization of Ruscic, et al. [198]. Entropy is a CODATA Key Value [52] as was the previous enthalpy value of $\Delta_f H_{298}^\circ = 121.301 \pm 0.008$ kJ mol⁻¹.
- ²⁴⁵ CODATA Key Value [52]
- ²⁴⁶ CODATA Key Value [52] The active thermochemical tables optimization gives an enthalpy value of -92.1763 ± 0.0063 kJ mol⁻¹. [198] The most recent NIST-JANAF review gives an enthalpy of -92.31 ± 0.10 kJ mol⁻¹ and an entropy of 186.901 ± 0.005 J K⁻¹ mol⁻¹. [216]
- ²⁴⁷ Both JANAF [45] and Gurvich [91] use the dissociation energy from Coxan and Ramsay of 265.380 ± 0.036 kJ mol⁻¹. The present recommendation is a recalculation using reference values from this Table. The entropy is a statistical mechanical calculation [18] using data from JANAF. The previous value of 101.63 ± 0.1 kJ mol⁻¹ was from the JANAF recommendation. [45] A CCSD(T) calculation, extrapolated to the complete basis set limit, for the atomization energy leads to an enthalpy of formation of 24.8 kcal mol⁻¹ at both 0 K and at 298 K. [145] Another CCSD(T) calculation of the dissociation energy, both directly and thorough a negative ion thermochemical cycle, led to enthalpy values of $\Delta_f H_0^\circ = 24.1 \pm 0.3$ and $\Delta_f H_{298}^\circ = 24.1 \pm 0.3$ and 24.2 ± 0.3 kcal mol⁻¹. [179]
- ²⁴⁸ Obtained from a dissociation energy of 2.70 kcal mol⁻¹, calculated at the MP2//aug-cc-pVTZ level of theory with a quadruple- ζ basic set. Values of 1.70 - 1.79 kcal mol⁻¹ were calculated using B3LYP with triple to quintuple- ζ bases sets. B3LYP//aug-cc-pVTZ was also used to calculate BDEs for hydrates with up to six water molecules. [82]
- ²⁴⁹ Obtained from a dissociation energy of 1.55 kcal mol⁻¹, calculated at the MP2//aug-cc-pVTZ level of theory with a quadruple- ζ basic set. Value of 1.06 - 1.23 kcal mol⁻¹ were calculated using B3LYP with triple to quintuple- ζ bases sets. B3LYP//aug-cc-pVTZ was also used to calculate BDEs for hydrates with up to six water molecules. [82]
- ²⁵⁰ Enthalpy and entropy values are from an analysis of equilibrium constant measurements (see Table 3-1, Note 13). More recent measurements over the temperature range 212 - 245 K [223], support these values. Previous enthalpy value of 98 ± 4 kJ mol⁻¹ and entropy value of 269.32 ± 0.5 J K⁻¹ mol⁻¹ from JANAF. Enthalpy for the reaction $\text{HOOC} + \text{FOO} \rightarrow \text{HOOF} + \text{ClOO}$ at the CCSD(T)/CBS(Q5) level of theory, adjusted for the Table value for FOO, leads to $\Delta_f H_{298}^\circ = 103.9 \pm 6$ kJ mol⁻¹ and $\Delta_f H_0^\circ = 104.7 \pm 6$ kJ mol⁻¹. [88]
- ²⁵¹ Isodesmic reaction calculations done at MP2, CCSD, and CCSD(T) level with ANO basis sets to determine enthalpy of formation. [130]
- ²⁵² Near-threshold fragmentation studies led to a dissociation energy to $\text{O} + \text{ClO}$ of 247.3 ± 0.5 kJ mol⁻¹. [55] This leads to an enthalpy of formation at 0 K of 100.6 ± 0.6 kJ mol⁻¹. A computational study gives, at 0 K, 102.2 ± 6.5 kJ/mol. [126] Previous 298 K enthalpy of formation, 94.6 ± 1.2 , derived from equilibrium constant for $\text{ClO} + \text{ClO} \leftrightarrow \text{Cl} + \text{OClO}$. [161] Entropy and enthalpy function are from a statistical mechanical calculation (see Table 3.1, Note 15) A CCSD(T), extrapolated to the complete basis set limit, for the atomization energy leads to an enthalpy of formation of 24.5 kcal mol⁻¹ at 0 K and 23.9 at 298 K. [145]
- ²⁵³ JANAF recommendation based on experimental and theoretical studies. [45] A more recent density functional/G3 calculation led to a 298 K enthalpy of 43.1 kcal mol⁻¹. [217]
- ²⁵⁴ A CCSD(T), extrapolated to the complete basis set limit, for the atomization energy leads to the recommended enthalpy of formation and a value of 32.2 kcal mol⁻¹ at 0 K. For the ¹A' state. $\Delta_f H_{298}^\circ = 52.4 \pm 1$ kcal mol⁻¹ for the ³A" state. [145] The previous recommendation, 90 ± 30 kJ mol⁻¹, from the JANAF evaluation [45], was based on an interpretation of the infrared spectrum and suggested that ClClO was less

stable than ClOCl by $\sim 9 \text{ kJ mol}^{-1}$. Several computational studies cited in the JANAF review indicated that the stability difference was considerably greater, typically about 60 kJ mol^{-1} . The present recommendation leads to a stability difference of 52 kJ mol^{-1} . Entropy and enthalpy difference calculated by a statistical mechanical calculation using vibrational frequencies from the WebBook and PM3 rotational moments. [18]

²⁵⁵ Enthalpy value based on experimental reports on the equilibrium constant for the reaction $\text{H}_2\text{O} + \text{Cl}_2\text{O} \leftrightarrow 2\text{HOCl}$ and the recommended enthalpy of formation for HOCl. [92] Gurvich recommended an enthalpy of formation at 298 K of $79 \pm 10 \text{ kJ mol}^{-1}$. [91] A CCSD(T) calculation, extrapolated to the complete basis set limit, for the atomization energy leads to an enthalpy of formation of $19.3 \text{ kcal mol}^{-1}$ at 0 K and 18.9 at 298 K. [145]

²⁵⁶ Selected enthalpy value derived from a third-law calculation on the equilibrium constant for the dimerization reaction, $\text{ClO} + \text{ClO} \leftrightarrow \text{ClOOC}$, presented in Table 3-1, note 14. Entropy value calculation is also discussed in Table 3-1. Previous Table value of $\Delta_f H_{298}^\circ$, $127.6 \pm 2.9 \text{ kJ mol}^{-1}$, was from the equilibrium constant of [161] and the entropy was the JANAF recommendation. [45] A study of the fragmentation threshold of ClO^+ from the photoionization of ClOOC yielded a 0 K enthalpy of $134.07 \pm 2.8 \text{ kJ mol}^{-1}$ and a 298 K value of $130.87 \pm 2.8 \text{ kJ mol}^{-1}$. [183] A CCSD(T) calculation, extrapolated to the complete basis set limit, for the atomization energy leads to an enthalpy of formation of $32.9 \text{ kcal mol}^{-1}$ at 0 K and 31.6 at 298 K. [145]

²⁵⁷ Derived from a CCSD(T) calculation, extrapolated to the complete basis set limit, for the atomization energy. [145] See Table 3-1, note 17 for a more complete discussion. The previous value, $154.2 \text{ kJ mol}^{-1}$ ($36.9 \text{ kcal mol}^{-1}$), was calculated at Gaussian-2 level of theory. [133] Entropy from JANAF evaluation. [45] The same value resulted from a statistical mechanical calculation.

²⁵⁸ Derived from a CCSD(T) calculation, extrapolated to the complete basis set limit, for the atomization energy [145]. See Table 3-1, note 14b for a more complete discussion. The previous value, $175.5 \text{ kJ mol}^{-1}$ ($41.9 \text{ kcal mol}^{-1}$), was calculated at Gaussian-2 level of theory [133] and the previous entropy ($309 \pm 2 \text{ kJ mol}^{-1}$) was from the JANAF evaluation. [45]

²⁵⁹ Selected enthalpy and entropy values derived from a third-law calculation on the equilibrium constant for the reaction, $\text{ClO} + \text{OCIO} \leftrightarrow \text{Cl}_2\text{O}_3$, presented in Table 3-1, note 15. Previous values in Table, $\Delta_f H^\circ = 35.8 \pm 1.5 \text{ kcal/mol}$ and $\Delta S = 94 \pm 5 \text{ cal/K mol}$, were taken from a single study. [35] The most stable structure among the Cl_2O_3 isomers is calculated to be ClOCl(O)O. [246] A density functional/G3 calculation led to a 298 K enthalpy of $31.7 \text{ kcal mol}^{-1}$. [217]

²⁶⁰ Enthalpy value from an evaluation of the experimental data. [92] Entropy from JANAF evaluation. [45] An enthalpy value of $-18.1 \pm 0.3 \text{ kcal mol}^{-1}$ has been calculated by coupled-cluster theory with correlation consistent basis sets and corrections for core-valence, relativistic, and anharmonic effects. [57]

²⁶¹ Second- and third-law analyses of the equilibration kinetics for the reaction $\text{Cl} + \text{CO} = \text{ClCO}$ led to $\Delta_f H_{298}^\circ = -7.7 \pm 0.6 \text{ kcal mol}^{-1}$, $\Delta_f H_0^\circ = -6.9 \pm 0.7 \text{ kcal mol}^{-1}$, and $\Delta_f S_{298}^\circ = -23.8 \pm 2.0 \text{ cal mol}^{-1} \text{ K}^{-1}$. [163] See also Table 3-1, Note 12.

²⁶² Taken from review of Gurvich, et al. [91] The JANAF Tables give $\Delta_f H_0^\circ = 53.6 \text{ kJ mol}^{-1}$, $\Delta_f H_{298}^\circ = 51.7 \text{ kJ mol}^{-1}$, and $S^\circ = 261.680 \text{ J mol}^{-1}$. [45]

²⁶³ Taken from review of Gurvich, et al. [91] The JANAF Tables give $\Delta_f H_0^\circ = 17.5 \text{ kJ mol}^{-1}$, $\Delta_f H_{298}^\circ = 12.1 \text{ kJ mol}^{-1}$, and $S^\circ = 272.187 \text{ J mol}^{-1}$. [45]

²⁶⁴ Predicted based on isodesmic reactions at the CCSD(T) level of theory. [127]

²⁶⁵ Enthalpy calculated at MP2 level of theory using basis sets ranging from 6-31G(d) to 6-311G(2df,2p). [146] A G3//B3LYP study gave enthalpies at 0 K and 298 K of 32.5 and $31.5 \text{ kcal mol}^{-1}$, respectively. [131]

²⁶⁶ Enthalpy calculated at MP2 level of theory using basis sets ranging from 6-31G(d) to 6-311G(2df,2p). [146] A G3//B3LYP study gave enthalpies at 0 K and 298 K of 34.4 and $33.2 \text{ kcal mol}^{-1}$, respectively. [131]

²⁶⁷ Derived from a study of the thermal dissociation of ClONO₂. [6] Enthalpy values obtained from the atomization energy obtained using the G3//B3LYP level of theory are $\Delta_f H_0^\circ = 7.0 \text{ kcal mol}^{-1}$ and $\Delta_f H_{298}^\circ = 5.5 \text{ kcal mol}^{-1}$. [131]

²⁶⁸ Value obtained from the atomization energy obtained using the G3//B3LYP level of theory. [131]

²⁶⁹ Value obtained from the atomization energy obtained using the G3//B3LYP level of theory. [131]

²⁷⁰ Value obtained from the atomization energy obtained using the G3//B3LYP level of theory. [131]

- ²⁷¹ Based on a study of the recombination of OCIO and NO₃, leading to a bond strength of 18±3 kcal mol⁻¹. [80]
- ²⁷² Taken from review of Gurvich, et al. [91] The JANAF Tables give $\Delta_f H_o^\circ = -50.2 \pm 0.4$ kJ mol⁻¹, $\Delta_f H_{298}^\circ = -50.3 \pm 0.4$ kJ mol⁻¹, and $S^\circ = 217.938$ J mol⁻¹. [45]
- ²⁷³ Calculated for the X¹A' state. The triplet-singlet energy gap is estimated to be 2170±40 cm⁻¹. Enthalpy determined by calculating the enthalpy of the reaction CH₂ + HCl → HCCl + H₂. Calculations involved the focal-point approach, based on methods up to CCSDTQ and basis sets ranging from aug-cc-pVDZ to aug-cc-pV6Z, extrapolated to the complete basis set limit. [229] Enthalpy obtained using the computed enthalpy of a reaction of the type: CH₂(¹A₁) + CH₃X + CH₃Y = CXY(¹A₁) + 2CH₄ results in $\Delta_f H_{298}^\circ = 320$ kJ mol⁻¹ at the QCISD(T)/6-311+G(3df,2p)//QCISD/6-311G(d,p) level of theory. Calculations also done at the G2 level. [204] Previous recommendation was based on combining experimental chloride dissociation energies from the parent anion, prior experimental measurements, and G2 calculations. [184] Entropy values from Gurvich review. [91]
- ²⁷⁴ Measured rate constant for the reaction of the radical with HBr, combined with previous measurements on the reverse reaction, with thermodynamic values obtained through a second-law analysis. [207] A QCISD(T)/6-311+G(3df,2p) isodesmic study resulted in an enthalpy of 117.0±4.1 kJ mol⁻¹. [205] A dissociative photoionization study of CH₂ClBr results in an enthalpy of 110.7 kJ mol⁻¹. [132]
- ²⁷⁵ Enthalpy from Manion evaluation. [139] Entropy from TRC evaluation. [189]
- ²⁷⁶ The enthalpy of formation based on an isodesmic reaction calculated at the MP2/6-31G(d,p) level of theory. [202]
- ²⁷⁷ Calculated for the X¹A' state. The triplet-singlet energy gap is estimated to be 7045±60 cm⁻¹. Enthalpy determined by calculating the enthalpy of the reaction CH₂ + 2HCl → CCl₂ + 2H₂. Calculations involved the focal-point approach, based on methods up to CCSDTQ and basis sets ranging from aug-cc-pVDZ to aug-cc-pV6Z, extrapolated to the complete basis set limit. [229] Enthalpy obtained using the computed enthalpy of a reaction of the type: CH₂(¹A₁) + CH₃X + CH₃Y = CXY(¹A₁) + 2CH₄ results in $\Delta_f H_{298}^\circ = 230$ kJ mol⁻¹ at the QCISD(T)/6-311+G(3df,2p)//QCISD/6-311G(d,p) level of theory. Calculations also done at the G2 level. [204] Previous recommendation (55.0±2.0 kcal mol⁻¹) based on combining experimental chloride dissociation energies from the parent anion, prior experimental measurements, and G2 calculations. [184] Entropy values from Gurvich review. [91]
- ²⁷⁸ Measured rate constant for the reaction of the radical with HBr, combined with previous measurements on the reverse reaction, with thermodynamic values obtained through a second-law analysis. [207] A QCISD(T)/6-311+G(3df,2p) isodesmic study resulted in an enthalpy of 91.1±4.1 kJ mol⁻¹. [205]
- ²⁷⁹ Enthalpy from Manion evaluation. [139] Entropy from TRC evaluation. [189]
- ²⁸⁰ A third-law determination based on the reaction CCl₃ + Br₂ ↔ CCl₃Br + Br, re-evaluating the kinetics of the reverse reaction and using spectroscopic data to calculate the entropy. [97] A QCISD(T)/6-311+G(3df,2p) isodesmic study resulted in an enthalpy of 72.2±4.1 kJ mol⁻¹. [205]
- ²⁸¹ Enthalpy from Manion evaluation. [139] Entropy from TRC evaluation. [189]
- ²⁸² Enthalpy from Manion evaluation. [139] Entropy from TRC evaluation. [189]
- ²⁸³ Enthalpy derived from the kinetics of the thermal decomposition of COCl₂. [135] Entropy from the JANAF tables. [45]
- ²⁸⁴ Thermodynamic values from Gurvich review; [91] enthalpy estimated.
- ²⁸⁵ Molecular properties determined at the MP2/6-31G(p,d), B3LYP/6-31G(d,p), and MP2/6-31G(d) level with single-point energy calculations at B3LYP/6-311+G(3df,2p) levels. Enthalpy based on four isodesmic reactions calculated at the CBS-Q//MP2/6-31(G(d,p)) level. [30]
- ²⁸⁶ Molecular properties determined at the B3LYP/6-31G(d,p) level, with single-point calculations at this and the B3LYP/6-311+G(3df,2p), QCISD(T)/6-31G(d,p), and CBS-Q levels. Enthalpies determined using several non-isodesmic reactions. [103]
- ²⁸⁷ Based on a re-analysis of previous equilibrium data on R + O₂ ↔ RO₂ from the same laboratory. [113]
- ²⁸⁸ Molecular geometries determined at the B3LYP/6-31G(d,p) level of theory and electronic energies obtained through single-point calculations at the CBSQ level. Enthalpy of formation determined using five reaction schemes, three of which were isodesmic. [226]
- ²⁸⁹ Taken from "The Chemical Thermodynamics of Organic Compounds". [221] Pedley review gives an enthalpy value of -219.1±0.5 kJ mol⁻¹. [176]

- ²⁹⁰ The enthalpy of formation based on an isodesmic reaction calculated at the MP2/6-31G(d,p) level of theory. [202]
- ²⁹¹ Based on a re-analysis of previous equilibrium data on $R + O_2 \leftrightarrow RO_2$ from the same laboratory. [113]
- ²⁹² Molecular properties determined at the B3LYP/6-31G(d,p) level, with single-point calculations at this and the B3LYP/6-311+G(3df,2p), QCISD(T)/6-31G(d,p), and CBS-Q levels. Enthalpies determined using several non-isodesmic reactions. [103]
- ²⁹³ Molecular geometries determined at the B3LYP/6-31G(d,p) level of theory and electronic energies obtained through single-point calculations at the CBSQ level. Enthalpy of formation determined using five reaction schemes, three of which were isodesmic. [226]
- ²⁹⁴ Molecular properties determined at the B3LYP/6-31G(d,p) level, with single-point calculations at this and the B3LYP/6-311+G(3df,2p), QCISD(T)/6-31G(d,p), and CBS-Q levels. Enthalpies determined using several non-isodesmic reactions. [103]
- ²⁹⁵ Enthalpy of formation based on an isodesmic reaction calculated at the MP2/6-31G(d,p) level of theory. [202]
- ²⁹⁶ Enthalpy of formation based on an isodesmic reaction calculated at the MP2/6-31G(d,p) level of theory. [202]
- ²⁹⁷ Based on a re-analysis of previous equilibrium data on $R + O_2 \leftrightarrow RO_2$ from the same laboratory. [113]
- ²⁹⁸ Molecular geometries determined at the B3LYP/6-31G(d,p) level of theory and electronic energies obtained through single-point calculations at the CBSQ level. Enthalpy of formation determined using five reaction schemes, three of which were isodesmic. [226]
- ²⁹⁹ Molecular properties determined at the B3LYP/6-31G(d,p) level, with single-point calculations at this and the B3LYP/6-311+G(3df,2p), QCISD(T)/6-31G(d,p), and CBS-Q levels. Enthalpies determined using several non-isodesmic reactions. [103] $\Delta_f H_{298}^\circ = -146.6 \text{ kJ mol}^{-1}$ from a G2 calculation of the total energy of formation from the gas-phase elements. [33]
- ³⁰⁰ Enthalpy derived from an analysis of thermochemical and kinetic data on the bromination of CH_2FCl . [231] A QCISD(T)/6-311+G(3df,2p) isodesmic study resulted in an enthalpy of $-63.8 \pm 4.1 \text{ kJ mol}^{-1}$. [205]
- ³⁰¹ TRC review. [46] Enthalpy estimated.
- ³⁰² Recommendation based on combining experimental chloride dissociation energies from the parent anion, prior experimental measurements, and G2 calculations. [184] Enthalpy obtained using the computed enthalpy of a reaction of the type: $CH_2(^1A_1) + CH_3X + CH_3Y = CXY(^1A_1) + 2CH_4$ results in $\Delta_f H_{298}^\circ = 29.4 \text{ kJ mol}^{-1}$ at the QCISD(T)/6-311+G(3df,2p)/QCISD/6-311G(d,p) level of theory. Calculations also done at the G2 level. [204] Entropy values from Gurvich review. [91]
- ³⁰³ A photobromination study leads to $D(CClF_2-H) = 100.7 \pm 2 \text{ kcal mol}^{-1}$. [155] Note that the enthalpy of the parent is estimated. A QCISD(T)/6-311+G(3df,2p) isodesmic study resulted in an enthalpy of $-274.7 \pm 4.1 \text{ kJ mol}^{-1}$. [205]
- ³⁰⁴ Enthalpy derived from an analysis of thermochemical and kinetic data on the bromination of CH_2FCl . [231] A QCISD(T)/6-311+G(3df,2p) isodesmic study resulted in an enthalpy of $-94.3 \pm 4.1 \text{ kJ mol}^{-1}$. [205]
- ³⁰⁵ TRC review. [46] Enthalpy estimated.
- ³⁰⁶ Enthalpy from Pedley review. [176] Entropy from TRC review. [46]
- ³⁰⁷ Enthalpy based on equilibrium measurements for the reaction $CClF_3 + 2CCl_4 \leftrightarrow 3CCl_2F$ leading to a heat of reaction of $10.59 \text{ kcal mol}^{-1}$, changed to reflect present enthalpy values. [47] Pedley review gives an enthalpy value of $-268.3 \pm 8.4 \text{ kJ mol}^{-1}$. [176]
- ³⁰⁸ Enthalpy based on equilibrium measurements for the reaction $2CClF_3 + CCl_4 \leftrightarrow 3CCl_2F_2$ leading to a heat of reaction of $7.59 \text{ kcal mol}^{-1}$, changed to reflect present enthalpy values. [47] Pedley review gives an enthalpy value of $-477.4 \pm 7.2 \text{ kJ mol}^{-1}$. [176]
- ³⁰⁹ Enthalpy from a simultaneous solution of a thermochemical network for the CF_3X species, where X = nil, H, Cl, Br, I, CF_3 , CN. [196] Entropy from recommendation of TRC. [47]
- ³¹⁰ Thermodynamic values from Gurvich review. [91]
- ³¹¹ Based on photoionization study. Enthalpy presented as lower limit. [12] A G2 calculation led to an enthalpy of $-768.3 \text{ kJ mol}^{-1}$. [34]
- ³¹² Derived from a G2 calculation of the total energy of formation from the gas-phase elements. [33]
- ³¹³ Enthalpy computed at the G3/B3LYP/6-311++G(3df,3pd) level of theory with both atomization energies and isodesmic reactions. [14]

- ³¹⁴ Enthalpy computed at the G3//B3LYP/6-311++G(3df,3pd) level of theory with both atomization energies and isodesmic reactions. [14]
- ³¹⁵ Enthalpy from Manion evaluation based on calculations involving isodesmic reactions. [139]
- ³¹⁶ Enthalpy from Manion evaluation. [139] Pedley review gives an enthalpy value of 37.2 ± 1.2 kJ mol⁻¹. [176]
- ³¹⁷ Measured rate constant for the reaction of the radical with HBr, combined with previous measurements on the reverse reaction, with thermodynamic values obtained through a second-law analysis. [208]
- ³¹⁸ Measured rate constant for the reaction of the radical with HBr, combined with previous measurements on the reverse reaction, with thermodynamic values obtained through a second-law analysis. [207]
- ³¹⁹ Enthalpy from Manion evaluation. [139] Entropy from TRC evaluation. [38]
- ³²⁰ Enthalpy from Manion evaluation based on calculations involving isodesmic reactions. [139]
- ³²¹ Enthalpy from Manion evaluation. [139] Pedley review gives an enthalpy value of 2.8 ± 1.3 kJ mol⁻¹. [176]
- ³²² Enthalpy from Manion evaluation. [139] Pedley review gives an enthalpy value of 4.6 ± 8.4 kJ mol⁻¹. [176]
- ³²³ Enthalpy from Manion evaluation. [139] Pedley review gives an enthalpy value of 5.0 ± 8.4 kJ mol⁻¹. [176]
- ³²⁴ Measured rate constant for the reaction of the radical with HBr, combined with previous measurements on the reverse reaction, with thermodynamic values obtained through a second-law analysis. [207]
- ³²⁵ Enthalpy from Manion evaluation. [139] Entropy from TRC evaluation. [38] Pedley review gives an enthalpy value of -127.7 ± 1.4 kJ mol⁻¹. [176]
- ³²⁶ Measured rate constant for the reaction of the radical with HBr, combined with calculated (MP2(fc)/6-31G(d,p)) values for the reverse reaction, leading to thermodynamic values obtained through a second-law analysis. [210]
- ³²⁷ Enthalpy from Manion evaluation. [139] Pedley review gives an enthalpy value of -126.4 ± 2.3 kJ mol⁻¹. [176]
- ³²⁸ Enthalpy from Manion evaluation. [139] Previous enthalpy from the heat of combustion of trichloroethene, $\Delta_f H_{298}^\circ = -19.1 \pm 3.0$ kJ mol⁻¹. [173] Entropy from review of Frenkel. [79] Pedley review gives an enthalpy value of -9.0 ± 8.8 kJ mol⁻¹. [176]
- ³²⁹ Enthalpy from Manion evaluation. [139]
- ³³⁰ An analysis of the kinetic data from the bromine-catalyzed elimination of HCl from CH₃CCl₃ resulted in a C-H bond strength of 103.8 ± 2 kcal mol⁻¹. [190]
- ³³¹ Enthalpy from Manion evaluation. [139] Entropy from TRC evaluation. [38] Pedley review gives an enthalpy value of -144.4 ± 1.7 kJ mol⁻¹. [176]
- ³³² Enthalpy from Manion evaluation. [139] Pedley review gives an enthalpy value of -10.9 ± 8.3 kJ mol⁻¹. [176] Entropy from Gurvich. [91]
- ³³³ Enthalpy from Manion evaluation. [139] Pedley review gives an enthalpy value of -149.3 ± 8.4 kJ mol⁻¹. [176]
- ³³⁴ Enthalpy from Manion evaluation. [139]
- ³³⁵ Derived from both second- and third-law analyses of the equilibrium data for the reaction $\text{Cl} + \text{C}_2\text{Cl}_4 \leftrightarrow \text{C}_2\text{Cl}_5$, with the enthalpy adjusted for present reference values. [164] $\Delta_f H_o^\circ = 5.2 \pm 1.5$ kcal mol⁻¹
- ³³⁶ Enthalpy from Manion evaluation. [139] Pedley review gives an enthalpy value of -142.0 ± 9.0 kJ mol⁻¹. [176]
- ³³⁷ Enthalpy from Manion evaluation. [139] Entropy from Gurvich. [91] Pedley review gives an enthalpy value of -143.6 ± 9.1 kJ mol⁻¹. [176]
- ³³⁸ Review of the literature. [114]
- ³³⁹ Derived from an exothermicity of 3.69 kcal mol⁻¹ for the isodesmic reaction $\text{CH}_3\text{CF}_2\text{Cl} + \text{CH}_3\text{CH}_2 \rightarrow \text{CH}_2\text{CF}_2\text{Cl} + \text{CH}_3\text{CH}_3$, calculated at the HF/6-31G* level. [172]
- ³⁴⁰ Enthalpy from literature review. [114] Entropy calculated from experimental frequencies. [172] Enthalpy calculated at the MP2/6-311G** level of theory, -128.41 kcal mol⁻¹. [167]
- ³⁴¹ Enthalpy calculated at the MP2/6-311G** level of theory. [167]
- ³⁴² Enthalpy from review of Pedley. [176]
- ³⁴³ Enthalpy calculated at the MP2/6-311G** level of theory. [167]
- ³⁴⁴ Enthalpy from review of Pedley. [176]

- ³⁴⁵ Based on a re-analysis of previous equilibrium data on $R + O_2 \leftrightarrow RO_2$ from the same laboratory. [113]
- ³⁴⁶ Acetyl chloride. Enthalpy from review of Pedley. [176]
- ³⁴⁷ Review of the literature. [67] Pedley review gives an enthalpy value of $-435.2 \pm 9.3 \text{ kJ mol}^{-1}$. [176]
- ³⁴⁸ Geometries and frequencies calculated at the B3LYP/6-31G(d,p) level of theory. Enthalpy calculated from three isodesmic reactions at the CBSQ//B3LYP/6-31(Gd,p) level and corrected for mixing of rotational conformers. [225]
- ³⁴⁹ Geometric parameters calculated at the RHF/6-31G* and MP2/6-31G* levels of theory, and the entropy obtained using the rigid-rotor/harmonic-oscillator approximation. Enthalpy calculated using the isodesmic reaction $CH_3OOH + C_2H_5Cl = CH_3CHClOOH + CH_4$, adjusted with reference values from the present Table. [125]
- ³⁵⁰ Geometric parameters calculated at the RHF/6-31G* and MP2/6-31G* levels of theory, and the entropy obtained using the rigid-rotor/harmonic-oscillator approximation. Enthalpy calculated using the isodesmic reaction $CH_3OOH + 1,1-C_2H_4Cl_2 = CH_3CCl_2OOH + CH_4$, adjusted with reference values from the present Table. [125]
- ³⁵¹ Chloroacetyl chloride. Enthalpy from review of Pedley. [176]
- ³⁵² Ethanedioyl dichloride (oxalyl chloride). Enthalpy from review of Pedley. [176]
- ³⁵³ Dichloroacetyl chloride. Enthalpy from review of Pedley. [176]
- ³⁵⁴ Geometries and frequencies calculated at the B3LYP/6-31G(d,p) level of theory. Enthalpy calculated from three isodesmic reactions at the CBSQ//B3LYP/6-31(Gd,p) level and corrected for mixing of rotational conformers. [225]
- ³⁵⁵ Enthalpy is an average of values obtained at the CBS-4//HF/3-21G* and G2(MP2(full)//MP2(full)/6-31G(d) levels of theory, using both atomization energies and formation from molecular species. Entropy at the G2(MP2(full)//MP2(full)/6-31G(d) level treating internal rotations as harmonic oscillators.[236]
- ³⁵⁶ Thermodynamic properties calculated at the G2(MP2(full)//MP2(full)/6-31G(d) level of theory. Enthalpy from atomization energy and entropy calculated treating internal rotations as harmonic oscillators. Similar values obtained at the CBS-4//HF/3021G* level.[236]
- ³⁵⁷ Trichloroacetyl chloride. Enthalpy from review of Pedley. [176]
- ³⁵⁸ Based on the equilibrium study using laser photolysis/PI mass spectrometry [112], adjusted by using the enthalpy for CH_3CCl_2 cited in this Table.
- ³⁵⁹ Geometries and frequencies calculated at the B3LYP/6-31G(d,p) level of theory. Enthalpy calculated from three isodesmic reactions at the CBSQ//B3LYP/6-31(Gd,p) level and corrected for mixing of rotational conformers. [225]
- ³⁶⁰ CODATA Key Value. [52]
- ³⁶¹ CODATA Key Value. [52] A calculation of the atomization energy at the CCSD(T) level, extrapolated to the CBS limit, leads to $\Delta_f H_{298}^\circ = 33.1 \pm 4 \text{ kJ mol}^{-1}$ and $\Delta_f H_0^\circ = 47.7 \pm 4 \text{ kJ mol}^{-1}$. [88]
- ³⁶² CODATA Key Value [52] The most recent NIST-JANAF review gives an enthalpy of $-36.29 \pm 0.16 \text{ kJ mol}^{-1}$ and an entropy of $198.699 \pm 0.005 \text{ J K}^{-1} \text{ mol}^{-1}$. [216]
- ³⁶³ Enthalpy derived from a photodissociation dynamics study using velocity map ion imaging. [107] Previous enthalpy value of $30.2 \pm 0.4 \text{ kcal mol}^{-1}$ based on a Birge-Sponer extrapolation. [242] Entropy from the JANAF table for bromine oxides. [42] A CCSD(T) calculation of the dissociation energy, both directly and through a negative ion thermochemical cycle, led to enthalpy values of $\Delta_f H_0^\circ = 31.4 \pm 0.4$ and $\Delta_f H_{298}^\circ = 29.6 \pm 0.4 \text{ kcal mol}^{-1}$. [179] A calculation of the atomization energy at the CCSD(T) level, extrapolated to the CBS limit, leads to $\Delta_f H_{298}^\circ = 128 \pm 6 \text{ kJ mol}^{-1}$ and $\Delta_f H_0^\circ = 136 \pm 6 \text{ kJ mol}^{-1}$. [88]
- ³⁶⁴ Obtained from a dissociation energy of $3.48 \text{ kcal mol}^{-1}$, calculated at the MP2//aug-cc-pVTZ level of theory. A value of $2.54 \text{ kcal mol}^{-1}$ was calculated using B3LYP, which was also used to calculate BDEs for hydrates with up to four water molecules. [83]
- ³⁶⁵ Obtained from dissociation energy of $1.70 \text{ kcal mol}^{-1}$, calculated at the MP2//aug-cc-pVTZ level of theory. A value of $1.58 \text{ kcal mol}^{-1}$ was calculated using B3LYP, which was also used to calculate BDEs for hydrates with up to four water molecules. [83]
- ³⁶⁶ Enthalpy based on the photoionization appearance energy of BrO^+ from $OBrO$, recalculated using the Table enthalpy for BrO . [110] A newer computational study gives an enthalpy at 0 K of $163.9 \pm 7.1 \text{ kJ mol}^{-1}$. [126] Entropy taken from the JANAF table for bromine oxides. [42] A calculation of the atomization energy at the CCSD(T) level, extrapolated to the CBS limit, leads to $\Delta_f H_{298}^\circ = 169.9 \pm 6 \text{ kJ mol}^{-1}$ and $\Delta_f H_0^\circ = 179.5 \pm 6 \text{ kJ mol}^{-1}$. [88]

- ³⁶⁷ Enthalpy for the reaction $\text{HOBr} + \text{FOO} \rightarrow \text{HOOF} + \text{BrOO}$ at the CCSD(T)/CBS(Q5) level of theory, adjusted for the Table value for FOO, leads to the cited enthalpy. [88] An estimate based on recombination rate constants for bromine atoms and subsequent calculations of interaction potentials, leads to a bond strength of about 1 kcal mol^{-1} and $\Delta_f H_{298}^\circ = 108 \pm 40 \text{ kJ mol}^{-1}$ and $\Delta_f H_0^\circ = 116 \pm 10 \text{ kJ mol}^{-1}$. [42] These results have been supported by other computational studies. [171, 222] CCSD(T)/AREP calculations predict, however, that BrOO lies below OBrO by about 5 kcal mol^{-1} , which appears to be inconsistent with these results. [171] Entropy from NIST-JANAF thermochemical tables for bromine oxides. [42]
- ³⁶⁸ Enthalpy value from an evaluation of the experimental data. [92] An enthalpy value of $-15.3 \pm 0.6 \text{ kcal mol}^{-1}$ has been calculated by coupled-cluster theory with correlation consistent basis sets and corrections for core-valence, relativistic, and anharmonic effects. [57] Entropy value calculated from the experimental structure and vibrational frequencies. [147]
- ³⁶⁹ CCSD(T) calculation with spdfg one-particle basis set, using isodesmic reaction and present values of reference enthalpies. [129]
- ³⁷⁰ Isomerization energy calculated at CCSD(T)/ANO4 level of theory, corrected for zero-point energy and to 298 K. BrOOH energy from present table. [129]
- ³⁷¹ NIST-JANAF thermochemical tables for bromine oxides. [42] Estimated values.
- ³⁷² Enthalpy derived from a photoionization study. This value was accepted by the NIST-JANAF thermochemical tables for bromine oxides, which also discussed three related studies and recommended the entropy value. [42] A CCSD(T)/ANO4 result based on the isodesmic reaction $2\text{HOBr} \rightarrow \text{H}_2\text{O} + \text{Br}_2\text{O}$, adjusted for the present enthalpy values for the references, gives $26.9 \pm 1.6 \text{ kcal mol}^{-1}$. [128] A calculation of the atomization energy at the CCSD(T) level, extrapolated to the CBS limit, leads to $\Delta_f H_{298}^\circ = 108.4 \pm 6 \text{ kJ mol}^{-1}$ and $\Delta_f H_0^\circ = 124.7 \pm 6 \text{ kJ mol}^{-1}$. [88]
- ³⁷³ The enthalpy is from a calculation of the atomization energy at the CCSD(T) level, extrapolated to the CBS limit. For the $^1\text{A}'$ state. $\Delta_f H_{298}^\circ = 236.0 \pm 6 \text{ kJ mol}^{-1}$ for the $^3\text{A}''$ state and $\Delta_f H_{298}^\circ = 251.5 \pm 6 \text{ kJ mol}^{-1}$ for the $^3\text{A}'$ state. [88] Entropy from the NIST-JANAF thermochemical tables for bromine oxides, which estimated the enthalpy as $168 \pm 20 \text{ kJ mol}^{-1}$. [42]
- ³⁷⁴ The enthalpy is from a calculation of the atomization energy at the CCSD(T) level, extrapolated to the CBS limit. [88] Calculated enthalpy for the reaction $\text{BrO} + \text{BrO} \rightarrow \text{BrOOBr}$, $\Delta E = -16.93 \text{ kcal/mol}$ by the B3LYP/aug-cc-pVTZ method, leads to $\Delta_f H_{298}^\circ = 42.1 \text{ kcal mol}^{-1}$. [83] The dominant product observed in the matrix isolation/infrared spectroscopy study was BrOBrO.
- ³⁷⁵ The enthalpy is from a calculation of the atomization energy at the CCSD(T) level, extrapolated to the CBS limit. [88] Calculated enthalpy for the reaction $\text{BrO} + \text{BrO} \rightarrow \text{BrOBrO}$, $\Delta E = -6.08 \text{ kcal/mol}$ by B3LYP/aug-cc-pVTZ method, leads to $\Delta_f H_{298}^\circ = 52.9 \text{ kcal mol}^{-1}$. [83] The dominant product observed in the matrix isolation/infrared spectroscopy study was BrOBrO.
- ³⁷⁶ Calculated enthalpy for the reaction $\text{BrO} + \text{BrO} \rightarrow \text{OBrBrO}$, $\Delta E = +13.44 \text{ kcal/mol}$ by the $\beta\text{B3LYP/aug-cc-pVTZ}$ method. [83] The dominant product observed in the matrix isolation/infrared spectroscopy study was BrOBrO
- ³⁷⁷ The enthalpy is from a calculation of the atomization energy at the CCSD(T) level, extrapolated to the CBS limit. [88]
- ³⁷⁸ Derived from the O-F BDE for BrOF, calculated by four selected DFT and H-F/DFT methods. Calculations also done for BrOF_n ($n=2-5$). [86] A CCSD(T)/ANO4 result based on the isodesmic reaction $\text{Br}_2\text{O} + \text{HOF} \rightarrow \text{HOBr} + \text{FOBr}$, adjusted for the present enthalpy values for the references, gives $14.0 \pm 3.1 \text{ kcal mol}^{-1}$. [128]
- ³⁷⁹ The enthalpy is from a calculation of the atomization energy at the CCSD(T) level, extrapolated to the CBS limit. [88] A CCSD(T)/ANO4 study, based on the isodesmic reaction $\text{HOBr} + \text{HOCl} \rightarrow \text{H}_2\text{O} + \text{ClOBr}$, adjusted for the present enthalpy values for the references, led to $\Delta_f H_{298}^\circ = 98 \pm 7 \text{ kJ mol}^{-1}$. [128]
- ³⁸⁰ The enthalpy is from a calculation of the atomization energy at the CCSD(T) level, extrapolated to the CBS limit for the $^1\text{A}'$ state. $\Delta_f H_{298}^\circ = 145.2 \pm 6 \text{ kJ mol}^{-1}$ for the $^3\text{A}''$ state and $\Delta_f H_{298}^\circ = 252.7 \pm 6 \text{ kJ mol}^{-1}$ for the $^3\text{A}'$ state. [88]
- ³⁸¹ The enthalpy is from a calculation of the atomization energy at the CCSD(T) level, extrapolated to the CBS limit. For the $^1\text{A}'$ state. $\Delta_f H_{298}^\circ = 226.4 \pm 6 \text{ kcal mol}^{-1}$ for the $^3\text{A}'$ state. [88]
- ³⁸² The enthalpy is from a calculation of the atomization energy at the CCSD(T) level, extrapolated to the CBS limit. [88]

- ³⁸³ NBS thermochemical tables. [237] A CCSD(T)/ANO4 result based on the homodesmotic reaction $\text{BrNO} + \text{H}_2\text{O} \rightarrow \text{HNO} + \text{HOBr}$, adjusted for the present enthalpy values for the references, gives $22.7 \pm 1.9 \text{ kcal mol}^{-1}$. [128]
- ³⁸⁴ Calculated using the isodesmotic reaction $\text{H}_2\text{O} + \text{cis-BrONO} \rightarrow \text{cis-HONO} + \text{HOBr}$ at several levels of theory, leading to a reaction enthalpy of $7.6 \text{ kcal mol}^{-1}$. [129]
- ³⁸⁵ Based on a calculated energy difference above BrNO_3 of $10.3 \text{ kcal mol}^{-1}$ from calculations at several levels of theory. [129]
- ³⁸⁶ Based on a calculated energy difference below cis-BrONO of $6.4 \text{ kcal mol}^{-1}$ from calculations at several levels of theory. [129]
- ³⁸⁷ The study of the thermal decomposition of BrONO_2 is used to obtain a reaction enthalpy of $28.2 \pm 1.5 \text{ kcal mol}^{-1}$. [169]
- ³⁸⁸ Enthalpy from isodesmotic reactions calculated at the CCSD(T) level of theory. [175]
- ³⁸⁹ Review of the literature. [91]
- ³⁹⁰ Review of the literature. [91] A calculation of the atomization energy at the CCSD(T) level, extrapolated to the CBS limit, leads to $\Delta_f H_{298}^\circ = 15.9 \pm 6 \text{ kJ mol}^{-1}$ and $\Delta_f H_0^\circ = 23.4 \pm 6 \text{ kJ mol}^{-1}$. [88]
- ³⁹¹ Enthalpy from a CCSD(T) calculation extrapolated to the CBS limit. [199] A calculation at the W2DK level of theory gave an enthalpy of $118.51 \text{ kcal mol}^{-1}$. [168] Entropy obtained from the same study, using a DFT approach (B97-1/aug-cc-pVTZ) for geometry optimization and frequency calculations.
- ³⁹² Enthalpy from a CCSD(T) calculation extrapolated to the CBS limit. [62] A calculation at the DK-CCSD(T)/aug-VTZ level, utilizing methyl bromide in an isodesmotic reaction, resulted in an enthalpy value of $90.12 \text{ kcal mol}^{-1}$. [168] Entropy obtained from the same study, using a DFT approach (B97-1/aug-cc-pVTZ) for geometry optimization and frequency calculations. Enthalpy obtained using the computed enthalpy of a reaction of the type: $\text{CH}_2(^1\text{A}_1) + \text{CH}_3\text{X} + \text{CH}_3\text{Y} = \text{CH}_2\text{XY}(^1\text{A}_1) + 2\text{CH}_4$ results in $\Delta_f H_{298}^\circ = 380 \text{ kJ mol}^{-1}$ at the QCISD(T)/6-311+G(3df,2p)/QCISD/6-311G(d,p) level of theory. Calculations also done at the G2 level. [204]
- ³⁹³ Measured rate constant for the reaction of the radical with HBr , combined with previous measurements on the reverse reaction, with thermodynamic values obtained through a second-law analysis. [212] Recalculated from C-H bond strength of $427.2 \text{ kJ mol}^{-1}$ and enthalpy for CH_3Br and H from this Table. Statistical thermodynamic methods also utilized. *Ab initio* calculations at the QCISD(T)/6-311+G(3df,2p) level of theory, utilizing an isodesmotic reaction with methyl bromide, resulted in an enthalpy value of $166.6 \pm 3 \text{ kJ mol}^{-1}$. [140]
- ³⁹⁴ Calculated from the dissociation of energy-selected CH_3Br^+ and its adiabatic ionization energy. [218] Enthalpy from Gurvich review is $-36.4 \pm 0.5 \text{ kJ mol}^{-1}$. [91] Entropy taken from Ideal Gas Thermodynamic Properties, which gives an enthalpy of $-37.7 \pm 1.5 \text{ kJ mol}^{-1}$. [117] Pedley review gives an enthalpy of $-35.4 \pm 1.1 \text{ kJ mol}^{-1}$. [176]
- ³⁹⁵ Enthalpy from a CCSD(T) calculation extrapolated to the CBS limit. [62] Enthalpy obtained using the computed enthalpy of a reaction of the type: $\text{CH}_2(^1\text{A}_1) + \text{CH}_3\text{X} + \text{CH}_3\text{Y} = \text{CH}_2\text{XY}(^1\text{A}_1) + 2\text{CH}_4$ results in $\Delta_f H_{298}^\circ = 339 \text{ kJ mol}^{-1}$ at the QCISD(T)/6-311+G(3df,2p)/QCISD/6-311G(d,p) level of theory. Calculations also done at the G2 level. [204] A calculation at the W2DK level of theory gave an enthalpy of $82.10 \text{ kcal mol}^{-1}$. [168] Entropy obtained from the same study, using a DFT approach (B97-1/aug-cc-pVTZ) for geometry optimization and frequency calculations.
- ³⁹⁶ Enthalpy derived from an analysis of thermochemical and kinetic data on the bromination of CH_2FCl . [231] *Ab initio* calculations at the QCISD(T)/6-311+G(3df,2p) level of theory, utilizing an isodesmotic reaction with methyl bromide, resulted in an enthalpy value of $191.7 \pm 6 \text{ kJ mol}^{-1}$. [140] A calculation at the DK-CCSD(T)/aug-VTZ level, again utilizing methyl bromide in an isodesmotic reaction, resulted in an enthalpy value of $47.44 \text{ kcal mol}^{-1}$. [168] Entropy obtained from the same study, using a DFT approach (B97-1/aug-cc-pVTZ) for geometry optimization and frequency calculations.
- ³⁹⁷ Enthalpy taken from a dissociative photoionization study of a series of dihalomethanes, normalized using the experimental enthalpy of dichloromethane. [122] The reported value has been adjusted by $+0.4 \text{ kJ mol}^{-1}$ to agree with the present enthalpy for CH_2Cl_2 . Previous value of $-11.1 \text{ kJ mol}^{-1}$ from Allen bond-energy scheme. [25]. *Ab initio* calculations at the QCISD(T)/6-311+G(3df,2p) level of theory, utilizing an isodesmotic reaction with methyl bromide, resulted in an enthalpy value of $4.3 \pm 6 \text{ kJ mol}^{-1}$. [140] Entropy from evaluation of Gurvich. [91]

- ³⁹⁸ Enthalpy value from *ab initio* calculations at the QCISD(T)/6-311+G(3df,2p) level of theory, utilizing an isodesmic reaction with methyl bromide. [140] A calculation at the DK-CCSD(T)/aug-VTZ level, again utilizing methyl bromide in an isodesmic reaction, resulted in an enthalpy value of 55.50 kcal mol⁻¹. [168] This same study, using a DFT approach for geometry optimization and frequency calculations, reported an entropy value of 80.60 cal K⁻¹. Gurvich review has 235±25 kJ mol⁻¹. Entropy from Gurvich. [91]
- ³⁹⁹ Enthalpy of formation derived from the heat of combustion of the liquid of 545.1±3.3 kJ mol⁻¹ measured by bomb calorimetry. [174] An enthalpy value of 51.6±9 kJ mol⁻¹ was obtained from *ab initio* calculations at the QCISD(T)/6-311+G(3df,2p) level of theory, utilizing an isodesmic reaction with methyl bromide. [140] A calculation at the DK-CCSD(T)/aug-VTZ level, again utilizing methyl bromide in an isodesmic reaction, resulted in an enthalpy value of 12.97 kcal mol⁻¹. [168] This same study, using a DFT approach for geometry optimization and frequency calculations, reported an entropy value of 78.93 cal K⁻¹. Previous value of 5.7 kcal mol⁻¹ from Allen bond-energy scheme. [25]. Entropy from evaluation of Gurvich. [91] Pedley gives enthalpy as 23.8±4.5 kJ mol⁻¹. [176]
- ⁴⁰⁰ Enthalpy from rotation-bomb calorimetry. [25] *Ab initio* calculations at the QCISD(T)/6-311+G(3df,2p) level of theory, utilizing an isodesmic reaction with methyl bromide, resulted in an enthalpy value of 110.6±12 kJ mol⁻¹. [140] A calculation at the DK-CCSD(T)/aug-VTZ level, again utilizing methyl bromide in an isodesmic reaction, resulted in an enthalpy value of 28.49 kcal mol⁻¹. [168] This same study, using a DFT approach for geometry optimization and frequency calculations, reported an entropy value of 85.61 cal K⁻¹. Entropy from Gurvich. [91]
- ⁴⁰¹ Enthalpy obtained using the computed enthalpy of a reaction of the type: CH₂(¹A₁) + CH₂F₂ + 2CH₃Y = CFY(¹A₁) + 3CH₄ at the QCISD(T)/6-311+G(3df,2p)//QCISD/6-311G(d,p) level of theory. Calculations also done at the G2 level. [204]
- ⁴⁰² Taken from review of Kudchadker and Kudchadker. Enthalpy estimated. [118]
- ⁴⁰³ Enthalpy from review of Pedley. [176] Entropy from review of Kudchadker and Kudchadker, who also estimate an enthalpy of -102.66 kcal mol⁻¹. [118]
- ⁴⁰⁴ Enthalpy from a simultaneous solution of a thermochemical network for the CF₃X species, where X = nil, H, Cl, Br, I, CF₃, CN. [196] Entropy from review of Kudchadker and Kudchadker. [118]
- ⁴⁰⁵ Enthalpy obtained using the computed enthalpy of a reaction of the type: CH₂(¹A₁) + CH₃X + CH₃Y = CXY(¹A₁) + 2CH₄ at the QCISD(T)/6-311+G(3df,2p)//QCISD/6-311G(d,p) level of theory. Calculations also done at the G2 level. [204]
- ⁴⁰⁶ Measured rate constant for the reaction of the radical with HBr, combined with previous measurements on the reverse reaction, with thermodynamic values obtained through a second-law analysis. [212]
- ⁴⁰⁷ Enthalpy taken from a dissociative photoionization study of a series of dihalomethanes, normalized using the experimental enthalpy of dichloromethane. [122] The reported value has been adjusted by +0.4 kJ mol⁻¹ to agree with the present enthalpy for CH₂Cl₂.
- ⁴⁰⁸ Taken from review of Kudchadker and Kudchadker. Enthalpy estimated. [118]
- ⁴⁰⁹ Taken from review of Kudchadker and Kudchadker. All parameters estimated. [118]
- ⁴¹⁰ Measured rate constant for the reaction of the radical with HBr, combined with calculated (MP2(fc)/6-31G(d,p)) values for the reverse reaction, leading to thermodynamic values obtained through a second-law analysis. [210]
- ⁴¹¹ Taken from review of Kudchadker and Kudchadker. All parameters estimated. [118]
- ⁴¹² Enthalpy from review of Pedley. [176] Entropy and enthalpy difference from review of Kudchadker and Kudchadker. [118]
- ⁴¹³ Taken from review of Kudchadker and Kudchadker. All parameters estimated. [118]
- ⁴¹⁴ Measured rate constant for the reaction of the radical with HBr, combined with calculated (MP2(fc)/6-31G(d,p)) values for the reverse reaction, leading to thermodynamic values obtained through a second-law analysis. [210]
- ⁴¹⁵ Taken from review of Kudchadker and Kudchadker. All parameters estimated. [118]
- ⁴¹⁶ Taken from review of Kudchadker and Kudchadker. Enthalpy estimated. [118]
- ⁴¹⁷ Taken from review of Kudchadker and Kudchadker. All parameters estimated. [118]
- ⁴¹⁸ Carbonyl bromide. Enthalpy from review of Pedley. [176]
- ⁴¹⁹ Derived from a G2 calculation of the total energy of formation from the gas-phase elements. [33]
- ⁴²⁰ Derived from a G2 calculation of the total energy of formation from the gas-phase elements. [34]
- ⁴²¹ Derived from a G2 calculation of the total energy of formation from the gas-phase elements. [33]

- ⁴²² An *ab initio* calculation at the W2DK level of theory. [168] Entropy obtained from the same study, using a DFT approach (B97-1/aug-cc-pVTZ) for geometry optimization and frequency calculations.
- ⁴²³ Bromoacetylene. Enthalpy from measurements of the photodissociation of bromoacetylene, leading to dissociation energy of 91.0 ± 1.2 kcal mol⁻¹. [166] $\Delta_f H_o^\circ = 71.3 \pm 1.5$ kcal mol⁻¹. A calculation at the W2DK level of theory gave an enthalpy of 67.50 kcal mol⁻¹. [168] Entropy obtained from the same study, using a DFT approach (B97-1/aug-cc-pVTZ) for geometry optimization and frequency calculations.
- ⁴²⁴ Enthalpy from review of Pedley, et al. [176] An enthalpy of 74.1 ± 3.1 kJ mol⁻¹ has been derived from a dissociative photoionization study of CH₂BrCHBr₂ with a computed vinyl cation enthalpy. [24]
- ⁴²⁵ An experimental study of the reaction $\text{Br} + \text{C}_2\text{H}_4 \leftrightarrow \text{C}_2\text{H}_4\text{Br}$ led to an enthalpy of reaction of 6.8 ± 1.6 kcal mol⁻¹. [21]
- ⁴²⁶ A photobromination study leads to $D(\text{CH}_3\text{CHBr-H}) = 97.2 \pm 1$ kcal mol⁻¹. [154]
- ⁴²⁷ Enthalpy from review of the literature. [114] Pedley gives -61.9 ± 1.6 kcal mol⁻¹ [176]. Entropy calculated by Kudchadker & Kudchadker. [119]
- ⁴²⁸ An *ab initio* calculation at the W2DK level of theory. [168] Entropy obtained from the same study, using a DFT approach (B97-1/aug-cc-pVTZ) for geometry optimization and frequency calculations.
- ⁴²⁹ *Trans*-dibromovinyl radical. A calculation at the DK-CCSD(T)/aug-VTZ level, utilizing methyl bromide in an isodesmic reaction. [168] Entropy obtained from the same study, using a DFT approach (B97-1/aug-cc-pVTZ) for geometry optimization and frequency calculations.
- ⁴³⁰ A photobromination study leads to $D(\text{CClF}_2\text{-H}) = 94.9 \pm 1.2$ kcal mol⁻¹. [156]
- ⁴³¹ Review of the literature. [114]
- ⁴³² Tribromoethene. A calculation at the DK-CCSD(T)/aug-VTZ level, utilizing methyl bromide in an isodesmic reaction. [168] Entropy obtained from the same study, using a DFT approach (B97-1/aug-cc-pVTZ) for geometry optimization and frequency calculations.
- ⁴³³ Enthalpy from review of Pedley. [176]
- ⁴³⁴ A calculation at the DK-CCSD(T)/aug-VTZ level, utilizing methyl bromide in an isodesmic reaction. [168] Entropy obtained from the same study, using a DFT approach (B97-1/aug-cc-pVTZ) for geometry optimization and frequency calculations.
- ⁴³⁵ Enthalpy derived from a dissociative photoionization study of CH₂BrCHBr₂ and a computed vinyl cation enthalpy. [190]
- ⁴³⁶ Taken from TRC review. Enthalpy estimated. [119]
- ⁴³⁷ A calculation at the DK-CCSD(T)/aug-VTZ level, utilizing methyl bromide in an isodesmic reaction. [168] Entropy obtained from the same study, using a DFT approach (B97-1/aug-cc-pVTZ) for geometry optimization and frequency calculations.
- ⁴³⁸ A calculation at the DK-CCSD(T)/aug-VTZ level, utilizing methyl bromide in an isodesmic reaction. [168] Entropy obtained from the same study, using a DFT approach (B97-1/aug-cc-pVTZ) for geometry optimization and frequency calculations.
- ⁴³⁹ Enthalpy from review of Pedley, et al. [176]
- ⁴⁴⁰ Acetyl bromide. Enthalpy from review of Pedley, et al. [176]
- ⁴⁴¹ Review of the literature. [67]
- ⁴⁴² CODATA Key Value [52] The JANAF values are $\Delta_f H_{298}^\circ = 106.76$ kJ mol⁻¹, $\Delta_f H_o^\circ = 107.16$ kJ mol⁻¹, and $S = 180.786$ J K⁻¹ mol⁻¹. [45]
- ⁴⁴³ CODATA Key Value [52] The JANAF values are $\Delta_f H_{298}^\circ = 62.42$ kJ mol⁻¹, $\Delta_f H_o^\circ = 65.50$ kJ mol⁻¹, and $S = 260.685$ J K⁻¹ mol⁻¹. [45] A calculation of the atomization energy at the CCSD(T) level, extrapolated to the CBS limit, leads to $\Delta_f H_{298}^\circ = 61.9 \pm 6$ kJ mol⁻¹ and $\Delta_f H_o^\circ = 65.3 \pm 6$ kJ mol⁻¹. [88]
- ⁴⁴⁴ CODATA Key Value [52] The most recent NIST-JANAF review gives an enthalpy of 26.50 ± 0.10 kJ mol⁻¹ and an entropy of 206.589 ± 0.005 J K⁻¹ mol⁻¹. [216]
- ⁴⁴⁵ Derived from a CCSD(T) calculation of the dissociation energy, both directly and thorough a negative ion thermochemical cycle. [179] The NIST-JANAF thermochemical tables for iodine oxides recommends $\Delta_f H_{298}^\circ = 126 \pm 18$ kJ/mol and $\Delta_f H_o^\circ = 128 \pm 18$ kJ/mol, based on molecular beam studies. [43] The earlier spectroscopic studies are also discussed here. An equilibrium constant derived from the forward and reverse rate constants for $\text{IO} + \text{ClO} \leftrightarrow \text{I} + \text{OClO}$ leads to an enthalpy at 298 K of about 28.6 kcal/mol (using reference values from this table) and 27.5 kcal/mol from the equilibrium $\text{Cl} + \text{IO} \leftrightarrow \text{I} + \text{ClO}$. [20] Enthalpy of reaction obtained using CCSD(T) calculations at B3LYP geometries, with corrections for spin-orbit coupling, for $\text{I} + \text{O} \rightarrow \text{IO}$, using Table reference values, leads to $\Delta_f H_{298}^\circ = 117.3$ kJ mol⁻¹. [105] A

calculation of the atomization energy at the CCSD(T) level, extrapolated to the CBS limit, leads to $\Delta_f H_{298}^\circ = 128.0 \pm 6 \text{ kJ mol}^{-1}$ and $\Delta_f H_0^\circ = 130.1 \pm 6 \text{ kJ mol}^{-1}$. [88] Entropy based on extensive calculations. [92]

⁴⁴⁶ The enthalpy is from a calculation of the atomization energy at the CCSD(T) level, extrapolated to the CBS limit. [88] Molecular properties calculated at the MP2/6-31G(d) and MP2/6-311+G(3df) levels of theory provided the entropy and, with this information, an enthalpy of $\Delta_f H_{298}^\circ = 75 \text{ kJ mol}^{-1}$ was derived using approximate QCISD(T)/6-311+G93df energies coupled with isodesmic reactions. [152] A more recent computational study gives an enthalpy at 0 K of $113.9 \pm 10.3 \text{ kJ/mol}$. [126] Enthalpy of reaction obtained using CCSD(T) calculations at B3LYP geometries, with corrections for spin-orbit coupling, for $2\text{IO} \rightarrow \text{OIO} + \text{I}$, using Table reference values, leads to a 298 K enthalpy of 127 kJ mol^{-1} . [105]

⁴⁴⁷ Enthalpy for the reaction $\text{HOOI} + \text{FOO} \rightarrow \text{HOO} + \text{IOO}$ at the CCSD(T)/CBS(DTQ) level of theory, adjusted for the Table value for FOO, leads the cited enthalpy. [88] Entropy from molecular properties calculated at the MP2/6-31G(d) and MP2/6-311+G(3df) levels of theory and, with this information, an enthalpy of $\Delta_f H_{298}^\circ = 96 \text{ kJ mol}^{-1}$ was derived using approximate QCISD(T)/6-311+G93df energies coupled with isodesmic reactions. [152]

⁴⁴⁸ Enthalpy of reaction obtained using CCSD(T) calculations at B3LYP geometries, with corrections for spin-orbit coupling, for $\text{OIO} + \text{IO}_3 \rightarrow \text{I}_2\text{O}_5$, using Table reference values. Enthalpy at 0 K is $164.0 \text{ kJ mol}^{-1}$. [105] Entropy from NIST-JANAF thermochemical tables for iodine oxides. [43] Previous enthalpy value of 242 kJ mol^{-1} was estimated.

⁴⁴⁹ The enthalpy is from a calculation of the atomization energy at the CCSD(T) level, extrapolated to the CBS limit. [88] Entropy from molecular properties calculated at the MP2/6-31G(d) and MP2/6-311+G(3df) levels of theory and, with this information, an enthalpy of $\Delta_f H_{298}^\circ = 92.5 \pm 17 \text{ kJ mol}^{-1}$ was derived using approximate QCISD(T)/6-311+G93df energies coupled with isodesmic reactions. [152] Enthalpy of reaction obtained using CCSD(T) calculations at B3LYP geometries, with corrections for spin-orbit coupling, for $\text{I} + \text{IO} \rightarrow \text{IOI}$, using Table reference values, leads to a 298 K enthalpy of $114.3 \text{ kJ mol}^{-1}$. [105]

⁴⁵⁰ The enthalpy is from a calculation of the atomization energy at the CCSD(T) level, extrapolated to the CBS limit. For the $^1\text{A}'$ state. $\Delta_f H_{298}^\circ = 234.3 \pm 6 \text{ kJ mol}^{-1}$ for the $^3\text{A}_2$ state. [88] Entropy from molecular properties calculated at the MP2/6-31G(d) and MP2/6-311+G(3df) levels of theory and, with this information, an enthalpy of $\Delta_f H_{298}^\circ = 134 \pm 17 \text{ kJ mol}^{-1}$ was derived using approximate QCISD(T)/6-311+G93df energies coupled with isodesmic reactions. [152]

⁴⁵¹ The enthalpy is from a calculation of the atomization energy at the CCSD(T) level, extrapolated to the CBS limit. [88] Entropy from molecular properties calculated at the MP2/6-31G(d) and MP2/6-311+G(3df) levels of theory and, with this information, an enthalpy of $\Delta_f H_{298}^\circ = 157 \text{ kJ mol}^{-1}$ was derived using approximate QCISD(T)/6-311+G93df energies coupled with isodesmic reactions. [152] Enthalpy of reaction obtained using CCSD(T) calculations at B3LYP geometries, with corrections for spin-orbit coupling, for $\text{IO} + \text{IO} \rightarrow \text{IOOI}$, using Table reference values, leads to a 298 K enthalpy of $187.1 \text{ kJ mol}^{-1}$. [105]

⁴⁵² The enthalpy is from a calculation of the atomization energy at the CCSD(T) level, extrapolated to the CBS limit. [88] Entropy from molecular properties calculated at the MP2/6-31G(d) and MP2/6-311+G(3df) levels of theory and, with this information, an enthalpy of $\Delta_f H_{298}^\circ = 103 \text{ kJ mol}^{-1}$ was derived using approximate QCISD(T)/6-311+G(3df) energies coupled with isodesmic reactions. [152] Enthalpy of reaction obtained using CCSD(T) calculations at B3LYP geometries, with corrections for spin-orbit coupling, for $\text{IO} + \text{IO} \rightarrow \text{IIO}_2$, using Table reference values, leads to a 298 K enthalpy of $165.1 \text{ kJ mol}^{-1}$. [105]

⁴⁵³ The enthalpy is from a calculation of the atomization energy at the CCSD(T) level, extrapolated to the CBS limit. [88] Entropy from molecular properties calculated at the MP2/6-31G(d) and MP2/6-311+G(3df) levels of theory and, with this information, an enthalpy of $\Delta_f H_{298}^\circ = 124 \text{ kJ mol}^{-1}$ was derived using approximate QCISD(T)/6-311+G93df energies coupled with isodesmic reactions. [152] Enthalpy of reaction obtained using CCSD(T) calculations at B3LYP geometries, with corrections for spin-orbit coupling, for $\text{IO} + \text{IO} \rightarrow \text{IOIO}$, using Table reference values, leads to a 298 K enthalpy of $148.5 \text{ kJ mol}^{-1}$. [105]

⁴⁵⁴ The enthalpy is from a calculation of the atomization energy at the CCSD(T) level, extrapolated to the CBS limit. [88] Molecular properties calculated at the MP2/6-31G(d) and MP2/6-311+G(3df) levels of

theory. Enthalpy derived using approximate QCISD(T)/6-311+G93df) energies coupled with isodesmic reactions gives $\Delta_f H_{298}^0 = 224 \text{ kJ mol}^{-1}$. [152]

⁴⁵⁵ Enthalpy of reaction obtained using CCSD(T) calculations at B3LYP geometries, with corrections for spin-orbit coupling, for $\text{IO} + \text{OIO} \rightarrow \text{I}_2\text{O}_3$, using Table reference values. [105]

⁴⁵⁶ Enthalpy of reaction obtained using CCSD(T) calculations at B3LYP geometries, with corrections for spin-orbit coupling, for $2\text{OIO} \rightarrow \text{I}_2\text{O}_4$, using Table reference values. [105]

⁴⁵⁷ Enthalpy of reaction obtained using CCSD(T) calculations at B3LYP geometries, with corrections for spin-orbit coupling, for $\text{I}_2\text{O}_4 + \text{O}_3 \rightarrow \text{I}_2\text{O}_5 + \text{O}_2$, using Table reference values. [105]

⁴⁵⁸ Enthalpy based on the measured activation energy of the reaction $\text{OH} + \text{CF}_3\text{I} \rightarrow \text{CF}_3 + \text{HOI}$ and G2(MP2) calculation indicating a negligible barrier for the reverse reaction. [24] Entropy based on extensive calculations. [92] Enthalpy values have also been calculated using the isogyric reaction $\text{HOOH} + \text{IO} \rightarrow \text{HOO} + \text{HOI}$ with density functional theory (GP96PW91 level), leading to $-58.6 \text{ kJ mol}^{-1}$ and $-63.3 \text{ kJ mol}^{-1}$ at 0 and 298 K, employing reference enthalpies from this Table. [22] Enthalpy of reaction obtained using CCSD(T) calculations at B3LYP geometries, with corrections for spin-orbit coupling, for $\text{OH} + \text{I} \rightarrow \text{HOI}$, using Table reference values, leads to a 298 K enthalpy of $-61.2 \text{ kJ mol}^{-1}$. [105]

⁴⁵⁹ Enthalpy difference calculated $\text{HOI} \rightarrow \text{HIO}$ with density functional theory (GP96PW91 level). [22]

⁴⁶⁰ Enthalpy difference calculated $\text{HOOI} \rightarrow \text{HOIO}$ with density functional theory (GP96PW91 level). $\Delta_f H_0^0 = -11.0 \text{ kJ mol}^{-1}$. [22]

⁴⁶¹ Enthalpy values calculated using the isogyric reaction $\text{HOOH} + \text{IO} \rightarrow \text{HO} + \text{HOOI}$ with density functional theory (GP96PW91 level), employing reference enthalpies from this Table. [22]

⁴⁶² The enthalpy is from a calculation of the atomization energy at the CCSD(T) level, extrapolated to the CBS limit. For the $^1\text{A}'$ state. $\Delta_f H_{298}^0 = 164.0 \pm 6 \text{ kJ mol}^{-1}$ for the $^3\text{A}''$ state. [88] Enthalpy derived using molecular properties calculated at the MP2/6-311+G(3df) level of theory, with Gaussian-2 energies coupled with isodesmic reactions, $\Delta_f H_{298}^0 = 68.2 \text{ kJ mol}^{-1}$. Reference enthalpies changed to correspond to values in this Table. [151]

⁴⁶³ The enthalpy is from a calculation of the atomization energy at the CCSD(T) level, extrapolated to the CBS limit. [88] Enthalpy derived using molecular properties calculated at the MP2/6-311+G(3df) level of theory, with Gaussian-2 energies coupled with isodesmic reactions, $\Delta_f H_{298}^0 = 76.1 \text{ kJ mol}^{-1}$. Reference enthalpies changed to correspond to values in this Table. [151]

⁴⁶⁴ The enthalpy is from a calculation of the atomization energy at the CCSD(T) level, extrapolated to the CBS limit. [88] Enthalpy derived using molecular properties calculated at the MP2/6-311+G(3df) level of theory, with Gaussian-2 energies coupled with isodesmic reactions, $\Delta_f H_{298}^0 = 166 \text{ kJ mol}^{-1}$. Reference enthalpies changed to correspond to values in this Table. [151]

⁴⁶⁵ The enthalpy is from a calculation of the atomization energy at the CCSD(T) level, extrapolated to the CBS limit. [88] Enthalpy derived using molecular properties calculated at the MP2/6-311+G(3df) level of theory, with Gaussian-2 energies coupled with isodesmic reactions, $\Delta_f H_{298}^0 = 10.9 \text{ kJ mol}^{-1}$. Reference enthalpies changed to correspond to values in this Table. [151]

⁴⁶⁶ The enthalpy is from a calculation of the atomization energy at the CCSD(T) level, extrapolated to the CBS limit. [88] Enthalpy derived using molecular properties calculated at the MP2/6-311+G(3df) level of theory, with Gaussian-2 energies coupled with isodesmic reactions, $\Delta_f H_{298}^0 = 107 \text{ kJ mol}^{-1}$. Reference enthalpies changed to correspond to values in this Table. [151]

⁴⁶⁷ The enthalpy is from a calculation of the atomization energy at the CCSD(T) level, extrapolated to the CBS limit. [88] Enthalpy derived using molecular properties calculated at the MP2/6-311+G(3df) level of theory, with Gaussian-2 energies coupled with isodesmic reactions, $\Delta_f H_{298}^0 = 126 \text{ kJ mol}^{-1}$. Reference enthalpies changed to correspond to values in this Table. [151]

⁴⁶⁸ The enthalpy is from a calculation of the atomization energy at the CCSD(T) level, extrapolated to the CBS limit. [88] Enthalpy derived using molecular properties calculated at the MP2/6-311+G(3df) level of theory, with Gaussian-2 energies coupled with isodesmic reactions, $\Delta_f H_{298}^0 = 154 \text{ kJ mol}^{-1}$. Reference enthalpies changed to correspond to values in this Table. [151]

⁴⁶⁹ The enthalpy is from a calculation of the atomization energy at the CCSD(T) level, extrapolated to the CBS limit. [88] Enthalpy derived using molecular properties calculated at the MP2/6-311+G(3df) level of theory, with Gaussian-2 energies coupled with isodesmic reactions, $\Delta_f H_{298}^0 = 188 \text{ kJ mol}^{-1}$. Reference enthalpies changed to correspond to values in this Table. [151]

- ⁴⁷⁰ The enthalpy is from a calculation of the atomization energy at the CCSD(T) level, extrapolated to the CBS limit. [88]
- ⁴⁷¹ The enthalpy is from a calculation of the atomization energy at the CCSD(T) level, extrapolated to the CBS limit. For the ¹A' state. $\Delta_f H_{298}^\circ = 190.0 \pm 6 \text{ kJ mol}^{-1}$ for the ³A" state. [88]
- ⁴⁷² The enthalpy is from a calculation of the atomization energy at the CCSD(T) level, extrapolated to the CBS limit. [88]
- ⁴⁷³ Thermodynamic parameters from a third-law analysis of the equilibrium reaction $\text{I} + \text{NO} (+\text{He}) \leftrightarrow \text{INO} (+\text{He})$. [233] Enthalpy of reaction obtained using CCSD(T) calculations at B3LYP geometries, with corrections for spin-orbit coupling, for $\text{I} + \text{NO} \rightarrow \text{INO}$, using Table reference values, leads to a 298 K enthalpy of $134.2 \text{ kJ mol}^{-1}$. [105]
- ⁴⁷⁴ Thermodynamic parameters from a third-law analysis of the equilibrium reaction $\text{I} + \text{NO}_2 (+\text{He}) \leftrightarrow \text{INO}_2 (+\text{He})$. [233]
- ⁴⁷⁵ Enthalpy of reaction obtained using CCSD(T) calculations at B3LYP geometries, with corrections for spin-orbit coupling, for $\text{IO} + \text{NO}_2 \rightarrow \text{IONO}_2$, using Table reference values. [105] From the same study, the reaction $\text{I} + \text{IONO}_2 \rightarrow \text{NO}_3 + \text{I}_2$ leads to $\Delta_f H_{298}^\circ = 50.1 \text{ kJ mol}^{-1}$ and $\Delta_f H_0^\circ = 65.65 \text{ kJ mol}^{-1}$. An evaluation of the pressure dependence of the reaction $\text{IO} + \text{NO}_2 \rightarrow \text{IONO}_2$ lead to an IO-NO₂ bond strength of about 150 kJ mol^{-1} . [85] This implies an enthalpy of formation of about 9 kJ mol^{-1} .
- ⁴⁷⁶ Taken from review of Gurvich, et al. [91] The JANAF Tables give $\Delta_f H_0^\circ = 19.141 \pm 0.105 \text{ kJ mol}^{-1}$, $\Delta_f H_{298}^\circ = 17.506 \pm 0.105 \text{ kJ mol}^{-1}$, and $S^\circ = 247.567 \text{ J mol}^{-1}$. [45] A calculation of the atomization energy at the CCSD(T) level, extrapolated to the CBS limit, leads to $\Delta_f H_{298}^\circ = 18.8 \pm 4 \text{ kJ mol}^{-1}$ and $\Delta_f H_0^\circ = 20.5 \pm 4 \text{ kJ mol}^{-1}$. [88]
- ⁴⁷⁷ Taken from review of Gurvich, et al. [91] The JANAF Tables give $\Delta_f H_0^\circ = 49.815 \pm 0.08 \text{ kJ mol}^{-1}$, $\Delta_f H_{298}^\circ = 40.878 \pm 0.08 \text{ kJ mol}^{-1}$, and $S^\circ = 258.95 \text{ J mol}^{-1}$. [45] A calculation of the atomization energy at the CCSD(T) level, extrapolated to the CBS limit, leads to $\Delta_f H_{298}^\circ = 41.4 \pm 4 \text{ kJ mol}^{-1}$ and $\Delta_f H_0^\circ = 50.2 \pm 4 \text{ kJ mol}^{-1}$. [88]
- ⁴⁷⁸ Enthalpy obtained using the computed enthalpy of a reaction of the type: $\text{CH}_2(^1\text{A}_1) + \text{CH}_3\text{X} + \text{CH}_3\text{Y} = \text{CXY}(^1\text{A}_1) + 2\text{CH}_4$ at the QCISD(T)/6-311+G(3df,2p)//QCISD/6-311G(d,p) level of theory. Calculations also done at the G2 level. [204]
- ⁴⁷⁹ Enthalpy value from ab initio calculations at the QCISD(T)/6-311+G(3df,2p) level of theory, utilizing an isodesmic reaction with methyl bromide. [140] Previous enthalpy value of $228.0 \pm 2.8 \text{ kJ mol}^{-1}$ from ab initio calculations used to determine the entropies of the reactants and the transition state for $\text{Br} + \text{CH}_3\text{I} \rightarrow \text{HBr} + \text{CH}_2\text{I}$. Arrhenius parameters were then calculated by transition state theory. The kinetics of the reverse reactions were measured in a flow system. The enthalpy value was obtained from a second-law analysis. [211] Entropy value also from [211]
- ⁴⁸⁰ Calculated from the dissociation of energy-selected CH_3I^+ and its adiabatic ionization energy. [218] Enthalpy from rotating combustion calorimetry is $14.4 \pm 1.4 \text{ kJ mol}^{-1}$. [37] Entropy from ideal gas thermodynamic properties. [117]
- ⁴⁸¹ Enthalpy obtained using the computed enthalpy of a reaction of the type: $\text{CH}_2(^1\text{A}_1) + \text{CH}_3\text{X} + \text{CH}_3\text{Y} = \text{CXY}(^1\text{A}_1) + 2\text{CH}_4$ at the QCISD(T)/6-311+G(3df,2p)//QCISD/6-311G(d,p) level of theory. Calculations also done at the G2 level. [204]
- ⁴⁸² Enthalpy value from ab initio calculations at the QCISD(T)/6-311+G(3df,2p) level of theory, utilizing an isodesmic reaction with methyl bromide. [140] Previous enthalpy value of $314.4 \pm 3.3 \text{ kJ mol}^{-1}$ from ab initio calculations used to determine the entropies of the reactants and the transition state for $\text{Br} + \text{CH}_2\text{I}_2 \rightarrow \text{HBr} + \text{CHI}_2$. Arrhenius parameters were then calculated by transition state theory. The kinetics of the reverse reactions were estimated. The enthalpy value was obtained from a second-law analysis. [211] Entropy value also from this study.
- ⁴⁸³ Enthalpy taken from a dissociative photoionization study of a series of dihalomethanes, normalized using the experimental enthalpy of dichloromethane. [122] The reported value has been adjusted by $+0.4 \text{ kJ mol}^{-1}$ to agree with the present enthalpy for CH_2Cl_2 . Previous value of $119.5 \pm 2.2 \text{ kJ mol}^{-1}$ from rotating combustion calorimetry. [37] Ab initio calculations at the QCISD(T)/6-311+G(3df,2p) level of theory, utilizing an isodesmic reaction with methyl iodide, resulted in an enthalpy value of $108.1 \pm 6 \text{ kJ mol}^{-1}$. [140] Entropy from ideal gas thermodynamic properties. [117]

- ⁴⁸⁴ Enthalpy from rotating combustion calorimetry. [37] Ab initio calculations at the QCISD(T)/6-311+G(3df,2p) level of theory, utilizing an isodesmic reaction with methyl iodide, resulted in an enthalpy value of $208.5 \pm 9 \text{ kJ mol}^{-1}$. [140]
- ⁴⁸⁵ Enthalpy value from ab initio calculations at the QCISD(T)/6-311+G(3df,2p) level of theory, utilizing an isodesmic reaction with methyl bromide. [140] Previous enthalpy value of $424.9 \pm 2.8 \text{ kJ mol}^{-1}$ from ab initio calculations used to determine the entropies of the reactants and the transition state for $\text{Br} + \text{CH}_2\text{I}_2 \rightarrow \text{HBr} + \text{CHI}_2$. Arrhenius parameters were then calculated by transition state theory. The kinetics of the reverse reactions were estimated. The enthalpy value was obtained from a second-law analysis. [211] Entropy value also from this study.
- ⁴⁸⁶ Enthalpy from rotating combustion calorimetry. [37] Ab initio calculations at the QCISD(T)/6-311+G(3df,2p) level of theory, utilizing an isodesmic reaction with methyl iodide, resulted in an enthalpy value of $321.3 \pm 12 \text{ kJ mol}^{-1}$. [140]
- ⁴⁸⁷ Enthalpy from the calculated reaction energy for dissociation into $\text{CH}_3\text{O}_2 + \text{IO}$ at the CCSD(T) level of theory using the average from both the Sadlej-PVTZ and LANL2DZspdf basis sets. [68]
- ⁴⁸⁸ Enthalpy obtained using the computed enthalpy of a reaction of the type: $\text{CH}_2(^1\text{A}_1) + \text{CH}_2\text{F}_2 + 2\text{CH}_3\text{Y} = \text{CFY}(^1\text{A}_1) + 3\text{CH}_4$ at the QCISD(T)/6-311+G(3df,2p)//QCISD/6-311G(d,p) level of theory. Calculations also done at the G2 level. [204]
- ⁴⁸⁹ Enthalpy from a simultaneous solution of a thermochemical network for the CF_3X species, where X = nil, H, Cl, Br, I, CF_3 , CN. [196] Entropy from recommendation of Gurvich. [91]
- ⁴⁹⁰ Taken from review of Kudchadker and Kudchadker. All parameters estimated. [118]
- ⁴⁹¹ Enthalpy obtained using the computed enthalpy of a reaction of the type: $\text{CH}_2(^1\text{A}_1) + \text{CH}_3\text{X} + \text{CH}_3\text{Y} = \text{CXY}(^1\text{A}_1) + 2\text{CH}_4$ at the QCISD(T)/6-311+G(3df,2p)//QCISD/6-311G(d,p) level of theory. Calculations also done at the G2 level. [204]
- ⁴⁹² Enthalpy taken from a dissociative photoionization study of a series of dihalomethanes, normalized using the experimental enthalpy of dichloromethane. [122] The reported value has been adjusted by $+0.4 \text{ kJ mol}^{-1}$ to agree with the present enthalpy for CH_2Cl_2 .
- ⁴⁹³ Taken from review of Kudchadker and Kudchadker. All parameters estimated. [118]
- ⁴⁹⁴ Enthalpy value from ab initio calculations at the QCISD(T)/6-311+G(3df,2p) level of theory, utilizing an isodesmic reaction with methyl bromide and methyl iodide. [140]
- ⁴⁹⁵ Enthalpy taken from a dissociative photoionization study of a series of dihalomethanes, normalized using the experimental enthalpy of dichloromethane. [122] The reported value has been adjusted by $+0.4 \text{ kJ mol}^{-1}$ to agree with the present enthalpy for CH_2Cl_2 . Ab initio calculations at the QCISD(T)/6-311+G(3df,2p) level of theory, utilizing an isodesmic reaction with methyl bromide and methyl iodide, resulted in an enthalpy value of $56.8 \pm 6 \text{ kJ mol}^{-1}$. [140]
- ⁴⁹⁶ Enthalpy value from ab initio calculations at the QCISD(T)/6-311+G(3df,2p) level of theory, utilizing an isodesmic reaction with methyl bromide and methyl iodide. [140]
- ⁴⁹⁷ Enthalpy obtained using the computed enthalpy of a reaction of the type: $\text{CH}_2(^1\text{A}_1) + \text{CH}_3\text{X} + \text{CH}_3\text{Y} = \text{CXY}(^1\text{A}_1) + 2\text{CH}_4$ at the QCISD(T)/6-311+G(3df,2p)//QCISD/6-311G(d,p) level of theory. Calculations also done at the G2 level. [204]
- ⁴⁹⁸ Enthalpy value from ab initio calculations at the QCISD(T)/6-311+G(3df,2p) level of theory, utilizing an isodesmic reaction with methyl bromide and methyl iodide. [140]
- ⁴⁹⁹ Enthalpy from review of Pedley. [176]
- ⁵⁰⁰ Enthalpy from review of the literature. [114] Pedley gives $-8.1 \pm 2.2 \text{ kJ mol}^{-1}$. [176] Entropy calculated by Kudchadker & Kudchadker. [119]
- ⁵⁰¹ Enthalpy from review of Pedley, et al. [176]
- ⁵⁰² Acetyl iodide. Enthalpy from review of Pedley. [176]
- ⁵⁰³ Enthalpy from review of Pedley, et al. [176]
- ⁵⁰⁴ From a PEPICO study of the neutral using the known enthalpy of CH_3CN . [121]
- ⁵⁰⁵ CODATA Key Value [52] The JANAF Tables give $\Delta_f H_0^\circ = 274.735 \text{ kJ mol}^{-1}$, $\Delta_f H_{298}^\circ = 276.98 \text{ kJ mol}^{-1}$, and $S^\circ = 167.828 \text{ J mol}^{-1}$. [45]
- ⁵⁰⁶ CODATA Key Value [52] The JANAF Tables give $\Delta_f H_0^\circ = 128.3 \text{ kJ mol}^{-1}$, $\Delta_f H_{298}^\circ = 128.6 \text{ kJ mol}^{-1}$, and $S^\circ = 228.165 \text{ J mol}^{-1}$. [45]
- ⁵⁰⁷ Updated and corrected NIST-JANAF thermochemical tables. [137] Enthalpy calculated at the CCSD(T)/CBS level of theory is $34.4 \text{ kcal mol}^{-1}$. [188]

- ⁵⁰⁸ CODATA Key Value [52] The JANAF Tables give $\Delta_f H_0^\circ = -17.58 \text{ kJ mol}^{-1}$, $\Delta_f H_{298}^\circ = -20.50 \text{ kJ mol}^{-1}$, and $S^\circ = 205.757 \text{ J mol}^{-1}$. [45]
- ⁵⁰⁹ A UCCSD(T)/cc-pV(n+d)Z(n=D,T,Q,5) calculation with correlation-consistent basis sets results in $3.63 \pm 1.0 \text{ kcal mol}^{-1}$. [56] Atomization energy calculated by the CCSD(T) extrapolated to the CBS limit, with geometry optimized at the CCSD(T)/aV(n+d)Z (n = D,T,Q,5) level gives $\Delta_f H_{298}^\circ = 24.3 \pm 1 \text{ kcal mol}^{-1}$ and $\Delta_f H_0^\circ = -25.0 \pm 1 \text{ kcal mol}^{-1}$. [87]
- ⁵¹⁰ TRC recommendation. [79] A UCCSD(T) calculation with correlation-consistent basis sets results in $3.63 \pm 1.0 \text{ kcal mol}^{-1}$. [56] The atomization energy calculated by the CCSD(T) extrapolated to the CBS limit, with geometry optimized at the CCSD(T)/aV(n+d)Z (n = D,T,Q,5) level, gives $\Delta_f H_{298}^\circ = 3.4 \pm 1 \text{ kcal mol}^{-1}$ and $\Delta_f H_0^\circ = 4.8 \pm 1 \text{ kcal mol}^{-1}$. [87] Lowest energy configuration is the *syn* isomer. Values for the *trans* isomer are $\Delta_f H_{298}^\circ = 7.8 \pm 1 \text{ kcal mol}^{-1}$ and $\Delta_f H_0^\circ = 9.3 \pm 1 \text{ kcal mol}^{-1}$ and for the *cis* isomer $\Delta_f H_{298}^\circ = 10.0 \pm 1 \text{ kcal mol}^{-1}$ and $\Delta_f H_0^\circ = 11.5 \pm 1 \text{ kcal mol}^{-1}$.
- ⁵¹¹ Atomization energy calculated by the CCSD(T) extrapolated to the CBS limit, with geometry optimized at the CCSD(T)/aV(n+d)Z (n = D,T,Q,5) level. [87] Lowest energy configuration is the *syn* isomer. Values for the *cis* isomer are $\Delta_f H_{298}^\circ = 27.0 \pm 1 \text{ kcal mol}^{-1}$ and $\Delta_f H_0^\circ = 28.1 \pm 1 \text{ kcal mol}^{-1}$ and for the *trans* isomer $\Delta_f H_{298}^\circ = 27.0 \pm 1 \text{ kcal mol}^{-1}$ and $\Delta_f H_0^\circ = 27.7 \pm 1 \text{ kcal mol}^{-1}$.
- ⁵¹² Atomization energy calculated by the CCSD(T) extrapolated to the CBS limit, with geometry optimized at the CCSD(T)/aV(T+d)Z level. [87] Lowest energy configuration is the *syn* isomer.
- ⁵¹³ Enthalpy value based on the dissociation energy of SO. [91]
- ⁵¹⁴ Atomization energy calculated by the CCSD(T) extrapolated to the CBS limit, with geometry optimized at the CCSD(T)/aV(n+d)Z (n = D,T,Q,5) level. $\Delta_f H_0^\circ = 49.5 \pm 1 \text{ kcal mol}^{-1}$. [87]
- ⁵¹⁵ CODATA Key Value [52] The JANAF Tables give $\Delta_f H_0^\circ = -294.3 \text{ kJ mol}^{-1}$, $\Delta_f H_{298}^\circ = -296.8 \text{ kJ mol}^{-1}$, and $S^\circ = 248.212 \text{ J mol}^{-1}$. [45]
- ⁵¹⁶ Review of the literature. [91] The JANAF Tables give $\Delta_f H_0^\circ = -390.0 \text{ kJ mol}^{-1}$, $\Delta_f H_{298}^\circ = -395.8 \text{ kJ mol}^{-1}$, and $S^\circ = 256.769 \text{ J mol}^{-1}$. [45]
- ⁵¹⁷ Updated and corrected NIST-JANAF thermochemical tables. [137] Atomization energy calculated by the CCSD(T) extrapolated to the CBS limit, with geometry optimized at the CCSD(T)/aV(n+d)Z (n = D,T,Q,5) level gives $\Delta_f H_{298}^\circ = -13.1 \pm 1 \text{ kcal mol}^{-1}$ and $\Delta_f H_0^\circ = -13.1 \pm 1 \text{ kcal mol}^{-1}$. [87]
- ⁵¹⁸ Atomization energy calculated by the CCSD(T) extrapolated to the CBS limit, with geometry optimized at the CCSD(T)/aV(n+d)Z (n = D,T,Q,5) level. [87]
- ⁵¹⁹ Enthalpy at 0 K determined to be $-0.9 \pm 0.7 \text{ kcal mol}^{-1}$ from crossed beam reactive scattering of O + H₂S. [16] Assuming the enthalpy of reaction does not change significantly with temperature, this leads to the value in the Table. In a more recent study, the authors suggested that the lower bound to the uncertainty could be as much as -3 kcal mol^{-1} , but confirmed the upper bound as $0.7 \text{ kcal mol}^{-1}$. [17] Atomization energy calculated by the CCSD(T) extrapolated to the CBS limit, with geometry optimized at the CCSD(T)/aV(n+d)Z (n = D,T,Q,5) level gives $\Delta_f H_{298}^\circ = -5.9 \pm 1 \text{ kcal mol}^{-1}$ and $\Delta_f H_0^\circ = -5.2 \pm 1 \text{ kcal mol}^{-1}$. [87] In the same study, the enthalpy for HOS was calculated to be $\Delta_f H_{298}^\circ = -1.8 \pm 1 \text{ kcal mol}^{-1}$ and $\Delta_f H_0^\circ = -1.1 \pm 1 \text{ kcal mol}^{-1}$, in what appears to be much better agreement with the experimental results for HSO.
- ⁵²⁰ Enthalpy obtained with DFT calculations on dissociation, atomization, and isodesmic reactions. [61] Value supported by a calculation of the H + SO₂ dissociation asymptote. [15] The latter study shows that HOSO is the more stable configuration, with HSO(O) as a local minimum.
- ⁵²¹ Atomization energy calculated by the CCSD(T) extrapolated to the CBS limit, with geometry optimized at the CCSD(T)/aV(n+d)Z (n = D,T,Q,5) level. [87] Lowest energy configuration is the *cis* isomer. Values for the *trans* isomer are $\Delta_f H_{298}^\circ = -56.2 \pm 1 \text{ kcal mol}^{-1}$ and $\Delta_f H_0^\circ = -55.1 \pm 1 \text{ kcal mol}^{-1}$. Another CCSD(T) calculation to the CBS limit, with additional corrections, including correlation through the the CBSDT(Q) level, resulted in values for these isomers (identified as the *syn* and *anti* isomers) of $\Delta_f H_0^\circ = -58.0 \text{ kcal mol}^{-1}$ and $\Delta_f H_0^\circ = -55.7 \text{ kcal mol}^{-1}$, respectively. [241]
- ⁵²² Enthalpy for the reaction HOOSH + FOO \rightarrow HOOH + HSOO at the CCSD(T)/CBS(Q,5) level of theory is $18.00 \text{ kcal mol}^{-1}$. Adjusted for the Table reference values, this gives the cited enthalpy of formation. [87] Lowest energy configuration is the *syn* isomer. Values for the *cis* isomer are $\Delta_f H_{298}^\circ = 29.9 \pm 1 \text{ kcal mol}^{-1}$ and $\Delta_f H_0^\circ = 31.3 \pm 1 \text{ kcal mol}^{-1}$ and for the *trans* isomer $\Delta_f H_{298}^\circ = 29.8 \pm 1 \text{ kcal mol}^{-1}$ and $\Delta_f H_0^\circ = 31.2 \pm 1 \text{ kcal mol}^{-1}$.

- ⁵²³ Atomization energy calculated by the CCSD(T) extrapolated to the CBS limit, with geometry optimized at the CCSD(T)/aV(n+d)Z (n = D,T,Q,5) level. $\Delta_f H_0^\circ = -26.5 \pm 1$ kcal mol⁻¹. [87] Lowest energy configuration is the *syn* isomer. Values for the *trans* isomer are $\Delta_f H_{298}^\circ = -24.3 \pm 1$ kcal mol⁻¹ and $\Delta_f H_0^\circ = -22.7 \pm 1$ kcal mol⁻¹ and for the *cis* isomer $\Delta_f H_{298}^\circ = -22.6 \pm 1$ kcal mol⁻¹ and $\Delta_f H_0^\circ = -21.0 \pm 1$ kcal mol⁻¹.
- ⁵²⁴ Enthalpy for the reaction HOOSH + FOO → HOOF + HOOS at the CCSD(T)/CBS(Q,5) level of theory is 5.14 kcal mol⁻¹. Adjusted for the Table reference values, this gives the cited enthalpy of formation. $\Delta_f H_0^\circ = 15.3 \pm 1.5$ kcal mol⁻¹. [87]
- ⁵²⁵ Atomization energy calculated by the CCSD(T) extrapolated to the CBS limit, with geometry optimized at the CCSD(T)/aV(T+d)Z level. [87] Lowest energy configuration is the *syn* isomer.
- ⁵²⁶ Atomization energy calculated by the CCSD(T) extrapolated to the CBS limit, with geometry optimized at the CCSD(T)/aV(T+d)Z level. [87] Lowest energy configuration is the *syn* isomer.
- ⁵²⁷ A third-law analysis of equilibrium data for the reaction OH + SO₂ ↔ HOSO₂ (extrapolated from data over the temperature range 523 to 603 K). [27]
- ⁵²⁸ Taken from review of Dorofeeva, et al. [66]
- ⁵²⁹ Atomization energy calculated by the CCSD(T) extrapolated to the CBS limit, with geometry optimized at the CCSD(T)/aV(T+d)Z level. [87] Lowest energy configuration is the *cis* isomer. Values for the *trans* isomer are $\Delta_f H_{298}^\circ = -13.6 \pm 1$ kcal mol⁻¹ and $\Delta_f H_0^\circ = -12.7 \pm 1$ kcal mol⁻¹.
- ⁵³⁰ Atomization energy calculated by the CCSD(T) extrapolated to the CBS limit, with geometry optimized at the CCSD(T)/aV(T+d)Z level. [87] Lowest energy configuration is the *syn* isomer. Values for the *cis* isomer are $\Delta_f H_{298}^\circ = -9.1 \pm 1$ kcal mol⁻¹ and $\Delta_f H_0^\circ = -7.8 \pm 1$ kcal mol⁻¹ and for the *trans* isomer $\Delta_f H_{298}^\circ = -8.7 \pm 1$ kcal mol⁻¹ and $\Delta_f H_0^\circ = -7.8 \pm 1$ kcal mol⁻¹.
- ⁵³¹ Enthalpy for the reaction HSOSH + FOO → HOOF + HSOS at the CCSD(T)/CBS(Q,5) level of theory is 8.81 kcal mol⁻¹. Adjusted for the Table reference values, this gives the cited enthalpy of formation. [87] Lowest energy configuration is the *syn* isomer. Values for the *cis* isomer are $\Delta_f H_{298}^\circ = 27.5 \pm 1$ kcal mol⁻¹ and $\Delta_f H_0^\circ = 28.9 \pm 1$ kcal mol⁻¹ and for the *trans* isomer $\Delta_f H_{298}^\circ = 28.1 \pm 1$ kcal mol⁻¹ and $\Delta_f H_0^\circ = 28.9 \pm 1$ kcal mol⁻¹.
- ⁵³² Atomization energy calculated by the CCSD(T) extrapolated to the CBS limit, with geometry optimized at the CCSD(T)/aV(T+d)Z level. [87] Lowest energy configuration is the *syn* isomer.
- ⁵³³ Atomization energy calculated by the CCSD(T) extrapolated to the CBS limit, with geometry optimized at the CCSD(T)/aV(T+d)Z level. [87] Lowest energy configuration is the *syn* isomer.
- ⁵³⁴ In an analysis of the fall-off curve for HS + NO → HSNO, a bond strength of 139 kJ mol⁻¹ was required to match the experimental data. [26]
- ⁵³⁵ Enthalpy from isodesmic reactions calculated at the MPW1K/6-311G(d,p) with single-point calculations at QCISD(T)/6-311G(3df,2dp). [238]
- ⁵³⁶ Updated and corrected NIST-JANAF thermochemical tables. [137] $\Delta_f H_0^\circ = 277.3 \pm 2$ kJ mol⁻¹ and $\Delta_f H_{298}^\circ = 278.0 \pm 2$ kJ mol⁻¹ calculated from three working reactions at the CCSD(T) level of theory, extrapolated to CBS limit, with corrections for anharmonic ZPE, scalar and vector relativistic terms, and core-valence electron correlation. [178]
- ⁵³⁷ Updated and corrected NIST-JANAF thermochemical tables. [137]
- ⁵³⁸ Taken from review of Gurvich, et al. [91] The JANAF Tables give $\Delta_f H_0^\circ = 277.1$ kJ mol⁻¹, $\Delta_f H_{298}^\circ = 280.3$ kJ mol⁻¹, and $S^\circ = 210.554$ J mol⁻¹. [45]
- ⁵³⁹ Taken from review of Gurvich, et al. [91] The JANAF Tables give $\Delta_f H_0^\circ = 116.1$ kJ mol⁻¹, $\Delta_f H_{298}^\circ = 116.9$ kJ mol⁻¹, and $S^\circ = 237.977$ J mol⁻¹. [45]
- ⁵⁴⁰ The temperature dependence of the equilibrium constant for the reaction OH + CS₂ ↔ CS₂OH resulted in a heat of reaction of -10.9 ± 1.0 kcal mol⁻¹ and an entropy change of -24.0 ± 4.4 cal K⁻¹ mol⁻¹ Murrells, 1990 #960]
- ⁵⁴¹ Enthalpy $\Delta_f H_0^\circ = 71.7 \pm 2.0$ kcal mol⁻¹ obtained from a photoionization study of CH₂S and CHS, obtained by sequential abstraction from CH₃SH. [192] 298K value from [23].
- ⁵⁴² Enthalpy $\Delta_f H_0^\circ = 28.3 \pm 2.0$ kcal mol⁻¹ obtained from a photoionization study of CH₂S and CHS, obtained by sequential abstraction from CH₃SH. [192] Integrated heat capacity from [23].

- ⁵⁴³ Second- and third-law analysis were utilized to obtain an enthalpy of reaction of -0.14 ± 0.28 kcal mol⁻¹ for the reaction $\text{Br} + \text{CH}_3\text{SH} \leftrightarrow \text{HBr} + \text{CH}_3\text{S}$. [162] Enthalpy calculated at the CCSD(T)/CBS level of theory is 29.7 kcal mol⁻¹. [188] DFT calculations support an enthalpy value of 29.78 ± 0.44 kcal mol⁻¹. [61]
- ⁵⁴⁴ A photoionization study [192] leads to a recommended value for H-CH₂SH of 93.9 ± 2.0 kcal mol⁻¹. [23] The enthalpy is from this and the present values for H and CH₃SH.
- Enthalpy from Pedley, [176] entropy from Frenkel et al. [79] Enthalpy calculated at the CCSD(T)/CBS level of theory is -5.31 kcal mol⁻¹. [188]
- ⁵⁴⁶ Enthalpy derived from OBS-QB3 calculations on 10 reactions (one isodesmic). [200]
- ⁵⁴⁷ Enthalpy derived from B3PW91 and OBS-QB3 calculations on 3 reactions (one isodesmic). [235]
- ⁵⁴⁸ Derived from an reaction enthalpy of -22.88 kcal mol⁻¹ for the isodesmic reaction $\text{CH}_3\text{S} + \text{SO}_3 \rightarrow \text{CH}_3\text{SO} + \text{SO}_2$ calculated at the CCSD(T) level extrapolated to the CBS limit.[188]
- ⁵⁴⁹ Heat of atomization, dissociation, and three isodesmic reactions calculated at the G2(MP2) level of theory to yield the enthalpy of formation. [78] Enthalpy calculated at the CCSD(T)/CBS level of theory is -52.2 kcal mol⁻¹. [188] A DFT estimate gives -56.3 kcal mol⁻¹. [61]
- ⁵⁵⁰ Heat of atomization, dissociation, and two isodesmic reactions calculated at the G2(MP2) level of theory to yield the enthalpy of formation. [78]
- ⁵⁵¹ The equilibrium constant for the reaction $\text{CH}_3\text{S} + \text{O}_2 \leftrightarrow \text{CH}_3\text{SOO}$ was measured between 216 to 258 K and resulted in a bond strength of 11.7 ± 0.9 kcal mol⁻¹. [232]
- ⁵⁵² An analysis of the equilibrium constant for the reaction $\text{Br} + \text{CH}_3\text{SCH}_3 \leftrightarrow \text{HBr} + \text{CH}_3\text{SCH}_2$ resulted in a heat of reaction of 6.11 ± 1.37 kcal mol⁻¹, [101] which was combined with present enthalpy values.
- ⁵⁵³ Enthalpy from Pedley, [176] entropy from Frenkel et al. [79]
- ⁵⁵⁴ Dimethyl sulfoxide. [176]
- ⁵⁵⁵ Enthalpy from Pedley, [176] entropy from Frenkel et al. [79]
- ⁵⁵⁶ Enthalpy from review of Pedley, et al. [176]
- ⁵⁵⁷ 1,2-Ethanedithiol. Enthalpy from review of Pedley, et al. [176]
- ⁵⁵⁸ Ethanethioic acid. Enthalpy from review of Pedley, et al. [176]
- ⁵⁵⁹ Taken from review of Gurvich, et al. [91] The JANAF Tables give $\Delta_f H_0^\circ = -138.5$ kJ mol⁻¹, $\Delta_f H_{298}^\circ = -138.4$ kJ mol⁻¹, and $S^\circ = 231.581$ J mol⁻¹. [45]
- ⁵⁶⁰ CODATA Key Value [52] The Lamoreaux and Hildenbrand review gives $\Delta_f H_{298}^\circ = 159.4 \pm 0.4$ kJ mol⁻¹ and $S^\circ = 138.69$ J mol⁻¹. [123]
- ⁵⁶¹ Enthalpy and entropy values from the JANAF tables, adopting the $\Delta_f H_{298}^\circ$ value from the NBS table. [45]. The Lamoreaux and Hildenbrand review gives $\Delta_f H_{298}^\circ = 214.9 \pm 1.2$ kJ mol⁻¹ and $S^\circ = 196.89$ J mol⁻¹. [123]
- ⁵⁶² Enthalpy and entropy values from the JANAF tables. A calculation of the atomization energy at the CCSD(T) level, extrapolated to the CBS limit, leads to $\Delta_f H_{298}^\circ = 138.9 \pm 4$ kJ mol⁻¹ and $\Delta_f H_0^\circ = 139.3 \pm 4$ kJ mol⁻¹. [234]
- ⁵⁶³ Enthalpy and entropy values from the JANAF tables. [45] A calculation of the atomization energy at the CCSD(T) level, extrapolated to the CBS limit, leads to $\Delta_f H_{298}^\circ = -340.6 \pm 4$ kJ mol⁻¹ and $\Delta_f H_0^\circ = -340.6 \pm 4$ kJ mol⁻¹. [234]
- ⁵⁶⁴ Enthalpy and entropy values from the JANAF tables. [45] A calculation of the atomization energy at the CCSD(T) level, extrapolated to the CBS limit, leads to $\Delta_f H_{298}^\circ = -192.9 \pm 4$ kJ mol⁻¹ and $\Delta_f H_0^\circ = -192.9 \pm 1$ kJ mol⁻¹. [234]
- ⁵⁶⁵ Enthalpy and entropy values from the JANAF tables.
- ⁵⁶⁶ From an extensive evaluation from the Thermocenter of the Russian Academy of Science. [89] The JANAF Tables give $\Delta_f H_0^\circ = -234 \pm 6$ kJ mol⁻¹, $\Delta_f H_{298}^\circ = -234 \pm 4$ kJ mol⁻¹, and $S^\circ = 210.66 \pm 2.1$ J mol⁻¹. [45] A calculation of the atomization energy at the CCSD(T) level, extrapolated to the CBS limit, leads to $\Delta_f H_{298}^\circ = -239.7 \pm 4$ kJ mol⁻¹ and $\Delta_f H_0^\circ = -237.7 \pm 1$ kJ mol⁻¹ [234]
- ⁵⁶⁷ The enthalpy is from a calculation of the atomization energy at the CCSD(T) level, extrapolated to the CBS limit. Cited values are for the ²Π state. Enthalpy at both 0K and 298K for the ²Σ⁺ state is 89.5 ± 4 kJ mol⁻¹ [234] The JANAF values are $\Delta_f H_{298}^\circ = 84 \pm 21$ kJ mol⁻¹ and $\Delta_f H_0^\circ = 84 \pm 21$ kJ mol⁻¹, and the cited entropy. [45] The Pedley and Marshall review gives $\Delta_f H_{298}^\circ = 75 \pm 8$ kJ mol⁻¹. [177] The Lamoreaux and Hildenbrand review gives $\Delta_f H_{298}^\circ = 69.0 \pm 4.2$ kJ mol⁻¹ and $S^\circ = 211.11$ J mol⁻¹. [123]
- ⁵⁶⁸ Atomization energy calculated by the CCSD(T) extrapolated to the CBS limit. [234]

- ⁵⁶⁹ The enthalpy is from a calculation of the atomization energy at the CCSD(T) level, extrapolated to the CBS limit. [234] The JANAF values, calculated from the enthalpy of the crystal and the enthalpy of sublimation, are $\Delta_f H_{298}^\circ = -167 \pm 10 \text{ kJ mol}^{-1}$ and $\Delta_f H_0^\circ = -166 \pm 10 \text{ kJ mol}^{-1}$, and the cited entropy. [45] The Lamoreaux and Hildenbrand review gives $\Delta_f H_{298}^\circ = -172.8 \pm 3.7 \text{ kJ mol}^{-1}$ and $S^\circ = 229.15 \text{ J mol}^{-1}$. [123]
- ⁵⁷⁰ Enthalpy and entropy values from the JANAF tables. [45]
- ⁵⁷¹ CODATA Key Value [52] The Lamoreaux and Hildenbrand review gives $\Delta_f H_{298}^\circ = 107.1 \pm 0.4 \text{ kJ mol}^{-1}$ and $S^\circ = 153.57 \text{ J mol}^{-1}$. [123]
- ⁵⁷² Enthalpy and entropy values from the JANAF tables. [45]
- ⁵⁷³ Enthalpy and entropy values from the JANAF tables. $\Delta_f H_{298}^\circ = -84 \pm 40 \text{ kJ mol}^{-1}$ and $\Delta_f H_0^\circ = -85 \pm 40 \text{ kJ mol}^{-1}$
- ⁵⁷⁴ Enthalpy and entropy values from the JANAF tables. [45]. A calculation of the atomization energy at the CCSD(T) level, extrapolated to the CBS limit, leads to $\Delta_f H_{298}^\circ = -291.6 \pm 4 \text{ kJ mol}^{-1}$ and $\Delta_f H_0^\circ = -290.0 \pm 4 \text{ kJ mol}^{-1}$. [234]
- ⁵⁷⁵ Enthalpy and entropy values from the JANAF tables. [45]. A calculation of the atomization energy at the CCSD(T) level, extrapolated to the CBS limit, leads to $\Delta_f H_{298}^\circ = -180.3 \pm 4 \text{ kJ mol}^{-1}$ and $\Delta_f H_0^\circ = -178.7 \pm 4 \text{ kJ mol}^{-1}$. [234]
- ⁵⁷⁶ Enthalpy and entropy values from the JANAF tables.
- ⁵⁷⁷ From an extensive evaluation from the Thermocenter of the Russian Academy of Science. [89] The JANAF Tables give $\Delta_f H_{298}^\circ = -198 \pm 12 \text{ J mol}^{-1}$ and $\Delta_f H_0^\circ = -194 \pm 12 \text{ J mol}^{-1}$, and $S^\circ = 228.44 \pm 1 \text{ J mol}^{-1}$. [45] A calculation of the atomization energy at the CCSD(T) level, extrapolated to the CBS limit, leads to $\Delta_f H_{298}^\circ = -187.0 \pm 4 \text{ kJ mol}^{-1}$ and $\Delta_f H_0^\circ = -184.1 \pm 4 \text{ kJ mol}^{-1}$. [234]
- ⁵⁷⁸ The enthalpy is from a calculation of the atomization energy at the CCSD(T) level, extrapolated to the CBS limit. [234] Cited values are for the $^2\Pi$ state. For the $^2\Sigma^+$ state $\Delta_f H_{298}^\circ = 113.8 \pm 4 \text{ kJ mol}^{-1}$ and $\Delta_f H_0^\circ = 115.5 \pm 4 \text{ kJ mol}^{-1}$. The JANAF values are $\Delta_f H_{298}^\circ = -84 \pm 40 \text{ kJ mol}^{-1}$ and $\Delta_f H_0^\circ = -85 \pm 40 \text{ kJ mol}^{-1}$, and the cited entropy. [45] The Pedley and Marshall review gives $\Delta_f H_{298}^\circ = 100 \pm 17 \text{ kJ mol}^{-1}$. [177] The Lamoreaux and Hildenbrand review gives $\Delta_f H_{298}^\circ = 104.6 \pm 4.2 \text{ kJ mol}^{-1}$ and $S^\circ = 228.48 \text{ J mol}^{-1}$. [123]
- ⁵⁷⁹ Atomization energy calculated by the CCSD(T) extrapolated to the CBS limit. [234]
- ⁵⁸⁰ Atomization energy calculated by the CCSD(T) extrapolated to the CBS limit. [234] The Lamoreaux and Hildenbrand review gives $\Delta_f H_{298}^\circ = -31.8 \pm 3.7 \text{ kJ mol}^{-1}$ and the cited entropy. [123]
- ⁵⁸¹ Enthalpy and entropy values from the JANAF tables. [45]
- ⁵⁸² CODATA Key Value [52] The Lamoreaux and Hildenbrand review gives $\Delta_f H_{298}^\circ = 89.2 \pm 0.2 \text{ kJ mol}^{-1}$ and the cited entropy. [123]
- ⁵⁸³ Enthalpy and entropy values from the JANAF tables. [45] A calculation of the atomization energy at the CCSD(T) level, extrapolated to the CBS limit, leads to $\Delta_f H_{298}^\circ = 132.2 \pm 4 \text{ kJ mol}^{-1}$ and $\Delta_f H_0^\circ = 134.7 \pm 4 \text{ kJ mol}^{-1}$. [234]
- ⁵⁸⁴ Enthalpy and entropy values from the JANAF tables. [45] A calculation of the atomization energy at the CCSD(T) level, extrapolated to the CBS limit, leads to $\Delta_f H_{298}^\circ = -326.8 \pm 4 \text{ kJ mol}^{-1}$ and $\Delta_f H_0^\circ = -324.7 \pm 4 \text{ kJ mol}^{-1}$. [234]
- ⁵⁸⁵ Enthalpy and entropy values from the JANAF tables. [45] A calculation of the atomization energy at the CCSD(T) level, extrapolated to the CBS limit, leads to $\Delta_f H_{298}^\circ = -215.5 \pm 4 \text{ kJ mol}^{-1}$ and $\Delta_f H_0^\circ = -213.4 \pm 4 \text{ kJ mol}^{-1}$. [234]
- ⁵⁸⁶ Enthalpy and entropy values from the JANAF tables.
- ⁵⁸⁷ From an extensive evaluation from the Thermocenter of the Russian Academy of Science. [90] The JANAF Tables give $\Delta_f H_{298}^\circ = -233 \pm 12 \text{ J mol}^{-1}$ and $\Delta_f H_0^\circ = -228 \pm 12 \text{ J mol}^{-1}$, and $S^\circ = 236.379 \pm 1.3 \text{ J mol}^{-1}$. [45] A calculation of the atomization energy at the CCSD(T) level, extrapolated to the CBS limit, leads to $\Delta_f H_{298}^\circ = -221.8 \pm 4 \text{ kJ mol}^{-1}$ and $\Delta_f H_0^\circ = -218.0 \pm 4 \text{ kJ mol}^{-1}$. [234]
- ⁵⁸⁸ The enthalpy is from a calculation of the atomization energy at the CCSD(T) level, extrapolated to the CBS limit. [234] Cited values are for the $^2\Pi$ state. For the $^2\Sigma^+$ state $\Delta_f H_{298}^\circ = 59.8 \pm 4 \text{ kJ mol}^{-1}$ and $\Delta_f H_0^\circ = 61.9 \pm 4 \text{ kJ mol}^{-1}$. The JANAF values are $\Delta_f H_{298}^\circ = 71 \pm 40 \text{ kJ mol}^{-1}$ and $\Delta_f H_0^\circ = 73 \pm 40 \text{ kJ mol}^{-1}$, and the cited entropy. [45] The Pedley and Marshall review gives $\Delta_f H_{298}^\circ = 61 \pm 21 \text{ kJ mol}^{-1}$. [177] The Lamoreaux and Hildenbrand review gives $\Delta_f H_{298}^\circ = 59.9 \pm 4.2 \text{ kJ mol}^{-1}$ and $S^\circ = 237.88 \text{ J mol}^{-1}$. [123]

⁵⁸⁹ Atomization energy calculated by the CCSD(T) extrapolated to the CBS limit. [234]

⁵⁹⁰ Atomization energy calculated by the CCSD(T) extrapolated to the CBS limit. [234] The Lamoreaux and Hildenbrand review gives $\Delta_f H_{298}^\circ = -58.61 \pm 2.2 \text{ kJ mol}^{-1}$ and the cited entropy.[123]

⁵⁹¹ Enthalpy and entropy values from the JANAF tables. [45]

A.3 References

1. Abramowitz, S. and M. W. Chase, 1991, *Pure App. Chem.*, **63**, 1449-1454.
2. Acree, W. E., G. Pilcher and M. da Silva, 2005, *J. Phys. Chem. Ref. Data*, **34**, 553-572.
3. Agapito, F., B. J. C. Cabral and J. A. M. Simoes, 2005, *J. Mol. Struct. - Theochem*, **729**, 223-227.
4. Aloisio, S. and J. S. Francisco, 2000, *J. Phys. Chem. A*, **104**, 404-407.
5. An, X. W. and M. Mansson, 1983, *J. Chem. Thermo.*, **15**, 287-293.
6. Anderson, L. C. and D. W. Fahey, 1990, *J. Phys. Chem.*, **94**, 644-652.
7. Anderson, W. R., 1989, *J. Phys. Chem.*, **93**, 530-536.
8. Anderson, W. R., 1999, *Comb. Flame*, **117**, 394-403.
9. Asatryan, R., J. W. Bozzelli and J. M. Simmie, 2007, *Int. J. Chem. Kinet.*, **39**, 378-398.
10. Asatryan, R., J. W. Bozzelli and J. M. Simmie, 2008, *J. Phys. Chem. A*, **112**, 3172-3185.
11. Asher, R. L., E. H. Appelman and B. Ruscic, 1996, *J. Chem. Phys.*, **105**, 9781-9795.
12. Asher, R. L., E. H. Appelman, J. L. Tilson, M. Litorja, J. Berkowitz and B. Ruscic, 1997, *J. Chem. Phys.*, **106**, 9111-9121.
13. Atkinson, R., D. L. Baulch, R. A. Cox, R. F. Hampson, J. A. Kerr, M. J. Rossi and J. Troe, 1997, *J. Phys. Chem. Ref. Data*, **26**, 521-1011.
14. Badenes, M. P., A. E. Croce and C. J. Cobos, 2006, *J. Phys. Chem. A*, **110**, 3186-3196.
15. Ballester, M. Y. and A. J. C. Varandas, 2005, *Phys. Chem. Chem. Phys.*, **7**, 2305-2317.
16. Balucani, N., P. Casavecchia, D. Stranges and G. G. Volpi, 1993, *Chem. Phys. Lett.*, **211**, 469-472.
17. Balucani, N., D. Stranges, P. Casavecchia and G. G. Volpi, 2004, *J. Chem. Phys.*, **120**, 9571-9582.
18. Barker, J. R., N. F. Ortiz, J. M. Preses, L. L. Lohr, Maranzana, P. J. Stimac and L. T. Nguyen. MultiWell; 2009.1 ed.; University of Michigan. Ann Arbor, MI, 2009.
19. Becerra, R., I. W. Carpenter and R. Walsh, 1997, *J. Phys. Chem.*, **101**, 4185-4190.
20. Bedjanian, Y., G. Le Bras and G. Poulet, 1997, *J. Phys. Chem. A*, **101**, 4088-4096.
21. Bedjanian, Y., G. Poulet and G. Le Bras, 1999, *J. Phys. Chem. A*, **103**, 4026-4033.
22. Begović, N., Z. Marković, S. Anić and L. Kolar-Anić, 2004, *J. Phys. Chem. A*, **108**, 651-657.
23. Berkowitz, J., G. B. Ellison and D. Gutman, 1994, *J. Phys. Chem.*, **98**, 2744-2765.
24. Berry, R. J., Y. Yuan, A. Misra and P. Marshall, 1998, *J. Phys. Chem. A*, **102**, 5182-5188.
25. Bickerton, J., M. E. M. da Piedade and G. Pilcher, 1984, *J. Chem. Thermo.*, **16**, 661-668.
26. Black, G., R. Patrick, L. E. Jusinski and T. G. Slanger, 1984, *J. Chem. Phys.*, **80**, 4065-4070.
27. Blitz, M. A., K. J. Huges and M. J. Pilling, 2003, *J. Phys. Chem. A*, **107**, 1971-1978.
28. Bodi, A., J. P. Kercher, C. Bond, P. Meteesatien, B. Sztaray and T. Baer, 2006, *J. Phys. Chem. A*, **110**, 13425-13433.
29. Bouchoux, G., J. Chamot-Rooke, D. Leblanc, P. Mourgues and M. Sablier, 2001, *ChemPhysChem*, **2**, 235-241.
30. Bozzelli, J. W. and D. Jung, 2001, *J. Phys. Chem. A*, **105**, 3941-3946.
31. Breidung, J., J. Cosleou, J. Demaison, K. Sarka and W. Thiel, 2004, *Mol. Phys.*, **102**, 1827-1841.
32. Breidung, J. and W. Thiel, 2006, *J. Phys. Chem. A*, **110**, 1575-1585.
33. Brudnik, K., J. T. Jodkowski, A. Nowek and J. Leszczynski, 2007, *Chem. Phys. Lett.*, **435**, 194-200.
34. Brudnik, K., J. T. Jodkowski and E. Ratajczak, 2003, *J. Mol. Struct.*, **656**, 333-339.
35. Burkholder, J. B., R. K. Talukdar, A. R. Ravishankara and S. Solomon, 1993, *J. Geophys. Res.*, **98**, 22937-22948.
36. Cacace, F., G. de Petris, F. Pepi and A. Troiani, 1999, *Science*, **285**, 81-82.
37. Carson, A. S., P. G. Laye, J. B. Pendley and A. M. Welsby, 1993, *J. Chem. Thermo.*, **25**, 261-269.
38. Chao, J., A. S. Rodgers, R. C. Wilhoit and B. J. Zwolinski, 1974, *J. Phys. Chem. Ref. Data*, **3**, 141-162.
39. Chao, J., R. C. Wilhoit and B. J. Zwolinski, 1973, *J. Phys. Chem. Ref. Data*, **2**, 427-437.
40. Chao, J. and B. J. Zwolinski, 1975, *J. Phys. Chem. Ref. Data*, **4**, 251-261.
41. Chao, J. and B. J. Zwolinski, 1978, *J. Phys. Chem. Ref. Data*, **7**, 363-377.
42. Chase, M. W., 1996, *J. Phys. Chem. Ref. Data*, **25**, 1069-1111.
43. Chase, M. W., 1996, *J. Phys. Chem. Ref. Data*, **25**, 1297-1340.
44. Chase, M. W., 1996, *J. Phys. Chem. Ref. Data*, **25**, 551-603.
45. Chase, M. W., 1998, *J. Phys. Chem. Ref. Data*, **Monograph 9**.

46. Chen, S. S., A. S. Rodgers, J. Chao, R. C. Wilhoit and B. J. Zwolinski, 1975, J. Phys. Chem. Ref. Data, **4**, 441-456.
47. Chen, S. S., R. C. Wilhoit and B. J. Zwolinski, 1976, J. Phys. Chem. Ref. Data, **5**, 571-580.
48. Chen, Y., A. Rauk and E. Tschuikow-Roux, 1990, J. Chem. Phys., **93**, 6620-6629.
49. Chen, Y., A. Rauk and E. Tschuikow-Roux, 1990, J. Chem. Phys., **93**, 1187-1195.
50. Chen, Y., A. Rauk and E. Tschuikow-Roux, 1991, J. Chem. Phys., **94**, 7299-7310.
51. Clifford, E. P., P. G. Wenthold, R. Gareyev, W. C. Lineberger, C. H. DePuy, V. M. Bierbaum and G. B. Ellison, 1998, J. Chem. Phys., **109**, 10293-10310.
52. Cox, J. D., D. D. Wagman and V. A. Medvedev *CODATA Key Values for Thermodynamics*; Hemisphere Publishing Corp.: New York, 1989.
53. Császár, A. G., P. G. Szalay and M. L. Leininger, 2002, Mol. Phys., **100**, 3879-3883.
54. Davis, H. F., B. Kim, H. S. Johnston and Y.-T. Lee, 1993, J. Phys. Chem., **97**, 2172-2180.
55. Delmdahl, R. F., D. H. Parker and A. T. J. B. Eppink, 2001, J. Chem. Phys., **114**, 8339-8346.
56. Denis, P. A., 2006, Chem. Phys. Lett., **422**, 434-438.
57. Denis, P. A., 2006, J. Phys. Chem. A, **110**, 5887-5892.
58. Denis, P. A., and O. N. Ventura, 2004, Chem. Phys. Lett., **385**, 292-297.
59. Denis, P. A., M. Kieniger, O. N. Ventura, R. E. Cachau and G. H. F. Dierksen, 2002, Chem. Phys. Lett., **365**, 440-449.
60. Denis, P. A. and F. R. Ornellas, 2009, J. Phys. Chem. A, **113**, 199-506.
61. Denis, P. A. and O. N. Ventura, 2001, Chem. Phys. Lett., **344**, 221-228.
62. Dixon, D. A., W. A. de Jong, K. A. Peterson and J. S. Francisco, 2002, J. Phys. Chem. A, **106**, 4724-4728.
63. Dixon, D. A., W. A. de Jong, K. A. Peterson and T. B. McMahon, 2005, J. Phys. Chem. A, **109**, 4073-4080.
64. Dixon, D. A., J. S. Francisco and Y. Alexeev, 2006, J. Phys. Chem. A, **110**.
65. Dóbbé, S., T. Bérces, T. Turányi, F. Márta, J. Grussdorf, F. Temps and H. G. Wagner, 1996, J. Phys. Chem., **100**, 19864-19873.
66. Dorofeeva, O., V. S. Iorish, V. P. Novikov and D. B. Neumann, 2003, J. Phys. Chem. Ref. Data, **32**, 879-901.
67. Dorofeeva, O., V. P. Novikov and D. B. Neumann, 2001, J. Phys. Chem. Ref. Data, **30**, 475-513.
68. Drougas, E. and A. M. Kosmas, 2007, J. Phys. Chem. A, **111**, 3402-3408.
69. Duncan, T. V. and C. E. Miller, 2000, J. Chem. Phys., **113**, 5138-5140.
70. El-Nahas, A. M., J. W. Bozzelli, J. M. Simmie, M. V. Navarro, G. Black and H. J. Curran, 2006, J. Phys. Chem. A, **110**, 13618-13623.
71. Ervin, K. M., S. Gronert, E. E. Barlow, M. K. Gilles, A. G. Harrison, V. M. Bierbaum, C. H. DePuy, W. C. Lineberger and G. B. Ellison, 1990, J. Am. Chem. Soc., **112**, 5750-5759.
72. Espinosa-Garcia, J. and S. Dobe, 2005, J. Mol. Struct. - Theochem, **713**, 119-125.
73. Fabian, W. M. F. and R. Janoschek, 2005, J. Mol. Struct. - Theochem, **713**, 227-234.
74. Farkas, E., G. Kovács, I. Szilágyi, S. Dóbbé, T. Bérces and F. Márta, 2006, Int. J. Chem. Kinet., **38**, 32-37.
75. Feller, D. and D. A. Dixon, 2003, J. Phys. Chem. A, **107**, 9641-9651.
76. Feller, D., D. A. Dixon and J. S. Francisco, 2003, J. Phys. Chem. A, **107**, 1604-1617.
77. Feller, D., K. A. Peterson and D. A. Dixon, 2008, J. Chem. Phys., **129**, 204105-32.
78. Frank, A. J. and F. Turecek, 1999, J. Phys. Chem. A, **103**, 5348-5361.
79. Frenkel, M., G. J. Kabo, K. N. Marsh, G. N. Roganov and R. C. Wilhoit *Thermodynamics of organic compounds in the gas state*; Thermodynamics Research Center: College Station, TX, 1994; Vol. I.
80. Friedl, R. R., S. P. Sander and Y. L. Yung, 1992, J. Phys. Chem., **96**, 7490-7493.
81. Fulle, D., H. F. Hamann, H. Hippler and C. P. Jansch, 1997, Ber. Bunsenges. Phys. Chem., **101**, 1433-1442.
82. Gálvez, O. and P. C. Gómez, 2007, Chem. Phys. Lett., **448**, 16-23.
83. Gálvez, O., A. Zoerner and H. Grothe, 2006, J. Phys. Chem. A, **110**, 8818-8825.
84. Gierczak, T., J. Jimenez, V. Riffault, J. B. Burkholder and A. R. Ravishankara, 2005, J. Phys. Chem. A, **109**, 586-596.
85. Golden, D. M., 2006, J. Phys. Chem. A, **110**, 2940-2943.
86. Gong, L., Q. Li, Y. X. and H. F. Schaefer, 2005, Mol. Phys., **103**, 1995-2008.

87. Grant, D. J., D. A. Dixon, J. S. Francisco, D. Feller and K. A. Peterson, 2009, *J. Phys. Chem. A*, **113**, 11343-11353.
88. Grant, D. J., E. B. Garner, M. H. Matus, M. T. Nguyen, K. A. Peterson, J. S. Francisco and D. A. Dixon, 2010, *J. Phys. Chem. A*, **114**, 4254-4265.
89. Gurvich, L. V., G. A. Bergman, L. N. Borokhov, V. S. Iorish, V. Y. Leonidov and V. S. Yungman, 1996, *J. Phys. Chem. Ref. Data*, **25**, 1211-.
90. Gurvich, L. V., G. A. Bergman, L. N. Borokhov, V. S. Iorish, V. Y. Leonidov and V. S. Yungman, 1997, *J. Phys. Chem. Ref. Data*, **26**, 1031-.
91. Gurvich, L. V., I. V. Veyts and C. B. Alcock *Thermodynamic Properties of Individual Substances*, Fourth ed.; Hemisphere Publishing Corp.: New York, 1991; Vol. 2.
92. Hassanzadeh, P. and K. K. Irikura, 1997, *J. Phys. Chem. A*, **101**, 1580-1587.
93. Hassouna, M., E. Delbos, P. Devolder, B. Viskolcz and C. Fittschen, 2006, *J. Phys. Chem. A*, **110**, 6667-6672.
94. Henry, D. J., C. J. Parkinson, P. M. Mayer and L. Radom, 2001, *J. Phys. Chem. A*, **105**, 6750-6756.
95. Holmes, J. L., F. P. Lossing and J. K. Terlouw, 1986, *J. Am. Chem. Soc.*, **108**, 1086-1087.
96. *Constants of Diatomic Molecules*; Huber, K. P. and G. Herzberg, Eds.; National Institute of Standards and Technology, 1998.
97. Hudgens, J. W., R. D. Johnson, R. S. Timonen, J. A. Seetula and D. Gutman, 1991, *J. Phys. Chem.*, **95**, 4400-4405.
98. Jacox, M. E. *Vibrational and Electronic Energy Levels of Polyatomic Transient Molecules*; National Institute of Standards and Technology, 1998.
99. Janoschek, R. and M. J. Rossi, 2002, *Int. J. Chem. Kinet.*, **34**, 550-560.
100. Janoschek, R. and M. J. Rossi, 2004, *Int. J. Chem. Kinet.*, **36**, 661-686.
101. Jefferson, A., J. M. Nicovich and P. H. Wine, 1994, *J. Phys. Chem.*, **98**, 7128-7135.
102. Johnson, R. D. and J. W. Hudgens, 1996, *J. Phys. Chem.*, **100**, 19874-19890.
103. Jung, D., C. J. Chen and J. W. Bozzelli, 2000, *J. Phys. Chem. A*, **104**.
104. Kaiser, E. W. and T. J. Wallington, 1996, *J. Phys. Chem.*, **100**, 4111-4119.
105. Kaltsoyannis, N. and J. M. C. Plane, 2008, *Phys. Chem. Chem. Phys.*, **10**, 1723-1733.
106. Kerr, J. A. and D. M. Timlin, 1971, *Int. J. Chem. Kinet.*, **3**, 427-441.
107. Kim, H., J. S. Dooley, E. R. Johnson and S. W. North, 2006, *J. Chem. Phys.*, **124**, 134304.
108. King, K. D., D. M. Golden and S. W. Benson, 1970, *J. Am. Chem. Soc.*, **92**, 5541-6.
109. Kiselev, V. G. and N. P. Gritsan, 2008, *J. Phys. Chem. A*, **112**, 4458-4464.
110. Klemm, R. B., R. P. Thorn, L. J. Stief, T. J. Buckley and R. D. Johnson, 2001, *J. Phys. Chem. A*, **105**, 1638-1642.
111. Knyazev, V. D., A. Bencsura and I. R. Slagle, 1997, *J. Phys. Chem. A*, **101**, 849-852.
112. Knyazev, V. D., A. Bencsura and I. R. Slagle, 1998, *J. Phys. Chem. A*, **102**, 1760-1769.
113. Knyazev, V. D. and I. R. Slagle, 1998, *J. Phys. Chem. A*, **102**, 1770-1778.
114. Kolesov, V. P. and T. S. Papina, 1983, *Russ. Chem. Rev.*, **52**, 425-439.
115. Kormos, B. L., J. F. Liebman and C. J. Cramer, 2004, *J. Phys. Org. Chem.*, **17**, 656-664.
116. Kraka, E., Z. Konkoli, D. Cremer, J. Fowler and H. F. Schaefer, 1996, *J. Amer. Chem. Soc.*, **118**, 10595-10608.
117. Kudchadker, S. A. and A. P. Kudchadker, 1975, *J. Chem. Phys. Ref. Data*, **4**, 457-470.
118. Kudchadker, S. A. and A. P. Kudchadker, 1978, *J. Phys. Chem. Ref. Data*, **7**, 1285-1307.
119. Kudchadker, S. A. and A. P. Kudchadker, 1979, *J. Phys. Chem. Ref. Data*, **8**, 519-526.
120. Lacher, J. R. and H. A. Skinner, 1968, *J. Chem. Soc. A*, 1034-1038.
121. Lafleur, R. D., B. Szatary and T. Baer, 2000, *J. Phys. Chem. A*, **104**, 1450-1455.
122. Lago, A. F., J. P. Kercher, A. Bödi, B. Sztáray, B. Miller, D. Wurzelmann and T. Baer, 2005, *J. Phys. Chem. A*, **109**, 1802-1809.
123. Lamoreaux, R. H. and D. L. Hildenbrand, 1984, *J. Phys. Chem. Ref. Data*, **13**, 151-.
124. Lay, T. H. and J. W. Bozzelli, 1997, *J. Phys. Chem. A*, **101**, 9505-9510.
125. Lay, T. H., L. N. Krasnoperov, C. A. Venanzi, J. W. Bozzelli and N. V. Shokhirev, 1996, *J. Phys. Chem.*, **100**, 8240-8249.
126. Lee, S. Y., 2004, *J. Phys. Chem. A*, **108**, 10754-10761.
127. Lee, T. J., 1994, *J. Phys. Chem.*, **98**, 111-115.
128. Lee, T. J., 1995, *J. Phys. Chem.*, **99**, 15074-15080.

129. Lee, T. J., 1996, *J. Phys. Chem.*, **100**, 19847-19852.
130. Lee, T. J. and A. P. Rendell, 1993, *J. Phys. Chem.*, **97**, 6999-7002.
131. Lesar, A., S. Prebil and M. Hodošček, 2003, *J. Phys. Chem. A*, **107**, 9168-9174.
132. Li, J., J. Yang, Y. X. Mo, K. C. Lau, X. M. Qian, Y. Song, J. B. Liu and C. Y. Ng, 2007, *J. Chem. Phys.*, **126**, 184304.
133. Li, W. K. and C. Y. Ng, 1997, *J. Phys. Chem. A*, **101**, 113-115.
134. Lightfoot, P. D., R. A. Cox, J. N. Crowley, M. Destriau, G. D. Hayman, M. E. Jenkin, G. K. Moortgat and F. Zabel, 1992, *Atmos. Environ.*, **26A**, 1805-1961.
135. Lim, K. P. and J. V. Michael, 1994, *J. Phys. Chem.*, **98**, 211-215.
136. Litorja, M. and B. Ruscic, 1998, *J. Chem. Phys.*, **108**, 6748-6755.
137. Lodders, K., 2004, *J. Chem. Phys. Ref. Data*, **33**, 357-367.
138. Luo, Y. R. and S. W. Benson, 1997, *J. Phys. Chem. A*, **101**, 3042-3044.
139. Manion, J. A., 2002, *J. Phys. Chem. Ref. Data*, **31**, 123-172.
140. Marshall, P., G. N. Srinivas and M. Schwartz, 2005, *J. Phys. Chem. A*, **109**, 6371-6379.
141. Martin, J. M. L., J. P. François and R. Gijbels, 1992, *J. Chem. Phys.*, **97**.
142. Matus, M. H., A. J. Arduengo and D. A. Dixon, 2006, *J. Phys. Chem. A*, **110**, 10116-10121.
143. Matus, M. H., M. T. Nguyen and D. A. Dixon, 2007, *J. Phys. Chem. A*, **111**, 113-126.
144. Matus, M. H., M. T. Nguyen, D. A. Dixon and K. O. Christe, 2008, *J. Phys. Chem. A*, **112**, 4973-4981.
145. Matus, M. H., M. T. Nguyen, D. A. Dixon, K. A. Peterson and J. S. Francisco, 2008, *J. Phys. Chem. A*, **112**, 9623-9627.
146. McGrath, M. P. and F. S. Rowland, 1994, *J. Phys. Chem.*, **98**, 1060-1067.
147. McGrath, M. P. and F. S. Rowland, 1994, *J. Phys. Chem.*, **98**, 4773-4775.
148. McMillen, D. F. and D. M. Golden, 1982, *Ann. Rev. Phys. Chem.*, **33**, 493-532.
149. Miller, C. E., J. I. Lynton, D. M. Keevil and J. S. Francisco, 1999, *J. Phys. Chem. A*, **103**, 11451-11459.
150. Millward, G. E., R. Hartig and E. Tschuikow-Roux, 1971, *J. Phys. Chem.*, **75**, 3195-3201.
151. Misra, A. and P. Marshall, 1997, *J. Chem. Soc. Faraday*, **93**, 3301-3304.
152. Misra, A. and P. Marshall, 1998, *J. Phys. Chem. A*, **102**, 9056-9060.
153. Miyokawa, K., S. Ozaki and T. Yano, 1996, *Bull. Chem. Soc. Jpn.*, **69**, 869-873.
154. Miyokawa, K. and E. Tschuikow-Roux, 1990, *J. Phys. Chem.*, **94**, 715-717.
155. Miyokawa, K. and E. Tschuikow-Roux, 1992, *J. Phys. Chem.*, **96**, 7328-7331.
156. Miyokawa, K. and E. Tschuikow-Roux, 1999, *Bull. Chem. Soc. Jpn.*, **72**, 1-5.
157. Moore, C. E. *Atomic Energy Levels*; NSRDS: Washington. DC, 1971; Vol. 1.
158. Murray, C., E. L. Derro, T. D. Sechler and M. I. Lester, 2007, *J. Phys. Chem. A*, **111**, 4727-4730.
159. Nguyen, M. T., M. H. Matus, W. A. Lester, Jr. and D. A. Dixon, 2008, *J. Phys. Chem. A*, **112**, 2082-2087.
160. Nguyen, M. T., T. L. Nguyen, V. T. Ngan and H. M. T. Nguyen, 2007, *Chem. Phys. Lett.*, **448**, 183-188.
161. Nickolaissen, S. L., R. R. Friedl and S. P. Sander, 1994, *J. Phys. Chem.*, **98**, 155-169.
162. Nicovich, J. M., K. D. Kreutter, C. A. van Dijk and P. H. Wine, 1992, *J. Phys. Chem.*, **96**, 2518-2528.
163. Nicovich, J. M., K. D. Kreutter and P. H. Wine, 1990, *J. Chem. Phys.*, **92**, 3539-3544.
164. Nicovich, J. M., L. Wang, M. L. McKee and P. H. Wine, 1996, *J. Phys. Chem.*, **100**, 680-688.
165. Okabe, H., 1970, *J. Chem. Phys.*, **53**, 3507-3515.
166. Okabe, H., 1975, *J. Chem. Phys.*, **62**, 2782-2787.
167. Olleta, A. C. and S. I. Lane, 2001, *Phys. Chem. Chem. Phys.*, **3**, 811-818.
168. Oren, M., M. A. Iron, A. Burcat and J. M. L. Martin, 2004, *J. Phys. Chem. A*, **108**, 7752-7761.
169. Orlando, J. J. and G. S. Tyndall, 1996, *J. Phys. Chem.*, **100**, 19398-19405.
170. Paci, M. A. B., G. A. Argüello, P. García and H. Willner, 2005, *J. Phys. Chem. A*, **109**, 7481-7488.
171. Pacios, L. F. and P. C. Gómez, 1997, *J. Phys. Chem. A*, **101**, 1767-1773.
172. Paddison, S. J., Y. H. Chen and E. Tschuikow-Roux, 1994, *Can. J. Chem.*, **72**, 561-567.
173. Papina, T. S. and V. P. Kolesov, 1985, *Russ. J. Phys. Chem.*, **59**, 1289-1292.
174. Papina, T. S., V. P. Kolesov and Y. G. Golovanova, 1982, *Russ. J. Phys. Chem.*, **56**, 1666-1668.
175. Parthiban, S. and T. J. Lee, 2000, *J. Chem. Phys.*, **113**, 145-152.

176. Pedley, J. B. *Thermochemical Data and Structures of Organic Compounds*; Thermodynamics Data Center: College Station, TX, 1994.
177. Pedley, J. B. and E. M. Marshall, 1983, *J. Phys. Chem. Ref. Data*, **12**.
178. Peebles, L. R. and P. Marshall, 2002, *Chem. Phys. Lett.*, **366**, 520-524.
179. Peterson, K. A., B. C. Shepler, D. Figgen and H. Stoll, 2006, *J. Phys. Chem. A*, **110**, 13877-13883.
180. Pickard, J. M. and A. S. Rodgers, 1977, *J. Amer. Chem. Soc.*, **99**, 691-694.
181. Pickard, J. M. and A. S. Rodgers, 1983, *Int. J. Chem. Kinet.*, **15**, 569-577.
182. Pittam, D. A. and G. Pilcher, 1972, *J. Chem. Soc. Farad. Trans 1*, **68**, 2224-2229.
183. Plenge, J., S. Kühl, B. Vogel, R. Müller, F. Stroh, M. von Hobe, R. Flesch and E. Rühl, 2005, *J. Phys. Chem. A*, **109**, 6730-6734.
184. Poutsma, J. C., J. A. Paulino and R. R. Squires, 1997, *J. Phys. Chem. A*, **101**, 5327-5336.
185. Ramond, T. M., S. J. Blanksby, S. Kato, V. M. Bierbaum, G. E. Davico, R. L. Schwartz, W. C. Lineberger and G. B. Ellison, 2002, *J. Phys. Chem. A*, **106**, 9641-9647.
186. Regimbal, J. M. and M. Mozurkewich, 1997, *J. Phys. Chem. A*, **101**, 8822-8820.
187. Reints, W., D. A. Pratt, H. G. Korth and P. Mulder, 2000, *J. Phys. Chem. A*, **104**, 10713-70720.
188. Resende, S. M. and F. R. Ornellas, 2003, *Chem. Phys. Lett.*, **367**, 489-494.
189. Rodgers, A. S., J. Chao, R. C. Wilhoit and B. J. Zwolinski, 1974, *J. Phys. Chem. Ref. Data*, **3**, 117-140.
190. Rodgers, A. S. and P. Jerus, 1988, *Int. J. Chem. Kinet.*, **20**, 565-575.
191. Rodriguez, C. F. and I. H. Williams, 1997, *Journal of the Chemical Society-Perkin Transactions 2*, 953-957.
192. Ruscic, B. and J. Berkowitz, 1993, *J. Chem. Phys.*, **98**, 2568-2579.
193. Ruscic, B., J. E. Boggs, A. Burcat, A. G. Csaszar, J. Demaison, R. Janoschek, J. M. L. Martin, M. L. Morton, M. J. Rossi, J. F. Stanton, P. G. Szalay, P. R. Westmoreland, F. Zabel and T. Berces, 2005, *J. Phys. Chem. Ref. Data*, **34**, 573-656.
194. Ruscic, B. and M. Litorja, 2000, *Chem. Phys. Lett.*, **316**, 45-50.
195. Ruscic, B., M. Litorja and R. L. Asher, 1999, *J. Phys. Chem. A*, **103**, 8625-8633.
196. Ruscic, B., J. V. Michael, P. C. Redfern, L. A. Curtiss and K. Raghavachari, 1998, *J. Phys. Chem. A*, **102**, 10889-10899.
197. Ruscic, B., R. E. Pinzon, M. L. Morton, N. K. Srinivasan, M.-C. Su, J. W. Sutherland and J. V. Michael, 2006, *J. Phys. Chem. A*, **110**, 6592-6601.
198. Ruscic, B., R. E. Pinzon, M. L. Morton, G. von Laszewski, S. J. Bittner, S. G. Nijsure, K. A. Amin, M. Minkoff and A. F. Wagner, 2004, *J. Phys. Chem. A*, **108**, 9979-9997.
199. Ruscic, B., A. F. Wagner, L. B. Harding, R. L. Asher, D. Feller, D. A. Dixon, K. A. Peterson, Y. Song, X. M. Qian, C. Y. Ng, J. B. Liu and W. W. Chen, 2002, *J. Phys. Chem. A*, **106**, 2727-2747.
200. Ruttink, P. J. A., P. C. Burgers, M. A. Trikoupi and J. K. Terlouw, 2001, *Chem. Phys. Lett.*, **342**, 447-451.
201. Saraf, S. R., W. J. Rogers, M. S. Mannan, M. B. Hall and L. M. Thomson, 2003, *J. Phys. Chem. A*, **107**, 1077-1081.
202. Schneider, W. F., B. I. Nance and T. J. Wallington, 1995, *J. Amer. Chem. Soc.*, **117**, 478-485.
203. Schneider, W. F. and T. J. Wallington, 1994, *J. Phys. Chem.*, **98**, 7448-7451.
204. Schwartz, M. and P. Marshall, 1999, *J. Phys. Chem. A*, **103**, 7900-7906.
205. Schwartz, M., L. R. Peebles, R. J. Berry and P. Marshall, 2003, *J. Chem. Phys.*, **118**, 557-564.
206. Sebban, N., H. Brockhorn and J. W. Bozzelli, 2005, *J. Phys. Chem. A*, **109**, 2233-2253.
207. Seetula, J. A., 1996, *J. Chem. Soc. Faraday Trans.*, **92**, 3069-3078.
208. Seetula, J. A., 1998, *J. Chem. Soc. Faraday Trans.*, **94**, 891-898.
209. Seetula, J. A., 1999, *Phys. Chem. Chem. Phys.*, **1**, 4727-4731.
210. Seetula, J. A., 2000, *Phys. Chem. Chem. Phys.*, **2**, 3807-3812.
211. Seetula, J. A., 2002, *Phys. Chem. Chem. Phys.*, **4**, 455-460.
212. Seetula, J. A., 2003, *Phys. Chem. Chem. Phys.*, **5**, 849-855.
213. Seetula, J. A. and I. R. Slagel, 1997, *J. Chem. Soc. Faraday Trans.*, **93**, 1709-1719.
214. Sehested, J., T. Ellermann, O. J. Nielsen, T. J. Wallington and M. D. Hurley, 1993, *Int. J. Chem. Kinet.*, **25**, 701-717.
215. Shapley, W. A. and G. B. Bacskay, 1999, *J. Phys. Chem. A*, **103**, 4505-4513.
216. Shenyavskaya, E. A. and V. S. Yungman, 2004, *J. Phys. Chem. Ref. Data*, **33**, 923-957.

217. Sicre, J. E. and C. J. Cobos, 2003, J. Mol. Struct. THEOCHEM, **620**, 215-226.
218. Song, Y., X. M. Qian, K. C. Lau, C. Y. Ng, J. B. Liu and W. W. Chen, 2001, J. Chem. Phys., **115**, 4095-4104.
219. Speranza, M., 1996, Inorg. Chem., **35**, 6140-6151.
220. Spiglanin, T. A., R. A. Pery and D. W. Chandler, 1986, J. Phys. Chem., **90**, 6184-6189.
221. Stull, D. R., E. F. Westrum and G. C. Sinke *The Chemical Thermodynamics of Organic Compounds*; John Wiley & Sons: New York, 1969.
222. Suma, K., Y. Sumiyoshi and Y. Endo, 2005, J. Chem. Phys., **123**, 024312.
223. Suma, K., Y. Sumiyoshi, Y. Endo, S. Enami, S. Aloisio, S. Hashimoto, M. Kawasaki, S. Nishida and Y. Matsumi, 2004, J. Phys. Chem. A, **108**, 8096-8099.
224. Sumathi, R. and W. H. Green, 2003, Phys. Chem. Chem. Phys., **5**.
225. Sun, H. and J. W. Bozzelli, 2003, J. Phys. Chem. A, **107**, 1018-1024.
226. Sun, H., C. J. Chen and J. W. Bozzelli, 2000, J. Phys. Chem. A, **104**, 8270-8282.
227. Szalay, P. G., A. Tajti and J. F. Stanton, 2005, Mol. Phys., **103**, 2159-2168.
228. Tang, X., Y. Hou, C. Y. Ng and B. Ruscic, 2005, J. Chem. Phys., **123**, 074330.
229. Tarczay, G., T. A. Miller, G. Czako and A. G. Császár, 2005, Phys. Chem. Chem. Phys., **7**, 2881-2893.
230. Tsang, W. Heats of formation of organic free radicals by kinetic methods. In *Energetics of Free Radicals*; J. A. M. Simoes, A. Greenberg and J. F. Liebman, Eds.; Blackie Academic & Professional: London, 1996; pp 22-58.
231. Tschuikow-Roux, E. and S. Paddison, 1987, Int. J. Chem. Kinet., **19**, 15-24.
232. Turnipseed, A. A., S. B. Barone and A. R. Ravishankara, 1992, J. Phys. Chem., **96**, 7502-7505.
233. Van den Bergh, H. and J. Troe, 1976, J. Chem. Phys., **64**, 736-742.
234. Vasilu, M., S. G. Li, K. A. Peterson, D. Feller, J. L. Gole and D. A. Dixon, 2010, J. Phys. Chem. A, **114**, 4272-4281.
235. Ventura, O. N., M. Kieninger and P. A. Denis, 2003, J. Phys. Chem. A, **107**, 518-521.
236. Viskolcz, B. and T. Berces, 2000, Phys. Chem. Chem. Phys., **2**, 5430-6436.
237. Wagman, D. D., W. H. Evans, V. B. Parker, R. H. Schumm, I. Halow, S. M. Bailey, K. L. Churney and R. L. Nutall, 1982, J. Phys. Chem. Ref. Data, **11**, , Suppl. No. 1.
238. Wang, L., J. Y. Liu, Z. S. Li and C. C. Sun, 2005, Int. J. Chem. Kinet., **37**, 710-716.
239. Wayner, D. D. M., K. B. Clark, A. Rauk, D. Yu and D. A. Armstrong, 1997, J. Am. Chem. Soc., **119**, 8925-8932.
240. Wenthold, P. G. and R. R. Squires, 1994, J. Am. Chem. Soc., **116**, 11890-11897.
241. Wheeler, S. E. and H. F. Schaefer, 2009, J. Phys. Chem. A, **113**, 6779-6788.
242. Wilmouth, D. M., T. F. Hanisco, N. M. Donahue and J. G. Anderson, 1999, J. Phys. Chem A, **103**, 8935-8945.
243. Wu, E. C. and A. S. Rodgers, 1974, J. Phys. Chem., **78**, 2315-2317.
244. Wu, E. C. and A. S. Rodgers, 1976, J. Amer. Chem. Soc., **98**, 6112-6115.
245. Yu, D., A. Rauk and D. A. Armstrong, 1994, J. Chem. Soc. Perkin Trans 2, 2207-2215.
246. Zhu, R. S. and M. C. Lin, 2003, J. Chem. Phys., **118**, 8645-8655.